THE JOURNAL
OF
CHEMICAL PHYSICS

VOLUME 34, NUMBER 4 APRIL, 1961

Normal Coordinate Treatments and Calculated Thermodynamic Properties of Phosphoryl Chloride, Thiophosphoryl Chloride, and Phosphoryl Fluoride*

JOSEPH S. ZIOMEK AND EDWARD A. PIOTROWSKI†

Chemistry Department, De Paul University, Chicago 14, Illinois

(Received September 16, 1960)

The infrared and Raman spectra for phosphoryl chloride, thiophosphoryl chloride, and phosphoryl fluoride were collected and examined for the most probable values for the wave numbers, intensities, and depolarization factors. The data are as follows: The Raman displacements $\Delta\sigma$ in cm^{-1}, the relative intensities I, and the depolarization factors ρ are for $POCl_3$: $\Delta\sigma(1)\rho=192.85$ (8) 0.83, 267.39 (6) 0.64, 337.44 (7) 0.81, 486.24 (10) 0.05, 581.2 (3) 6/7, and 1289.9 (5) 0.04; for $PSCl_3$: 172 (5) 6/7, 247 (7) 6/7, 247 (calculated) 430 (10) 0.1, 538 (1) 6/7, and 753 (1) P; and for POF_3: 337 (w) 6/7, 476 (m) 6/7, 483 (from infrared) P, 875 (s) 0.05, 982 (vw) 6/7, and 1395 (m) 0.1. As for the infrared spectral data, those of G. Cilento *et al.*, were used for $PSCl_3$, and those of Gutowsky and Liehr were used for POF_3. No published infrared spectral data were found for $POCl_3$. Also normal coordinate treatments were conducted for $POCl_3$, $PSCl_3$, POF_3, and PSF_3 on the basis of a model having C_{3v} symmetry. The normal coordinate treatments gave the listed wave numbers as fundamentals and lend support for the 247 cm^{-1} band for $PSCl_3$ and 483 cm^{-1} band (observed in the infrared and assigned as fundamental by Gutowsky and Liehr) for POF_3 as the missing Raman bands. Moreover, the F matrix elements obtained for these molecules were determined in such a manner that those potential constants for the PCl_3 group had nearly the same values in both $POCl_3$ and $PSCl_3$, those for the PF_3 group had nearly the same values in both POF_3 and PSF_3, the one for the PO group had nearly the same value in both $POCl_3$ and POF_3, and the one for the PS group had nearly the same value in both PSF_3 and $PSCl_3$. The potential constants determined had the following values in md/A: For $POCl_3$, $f_{PO}=9.890$, $f_{PCl}=2.466$, $f_{PClPCl}=0.399$, for $PSCl_3$, $f_{PS}=0.030$, $f_{PCl}=2.466$, $f_{PClPCl}=0.399$; for POF_3, $f_{PO}=9.890$, $f_{PF}=5.633$, $f_{PFPF}=0.483$, and for PSF_3, $f_{PS}=2.9694$, $f_{PF}=5.333$, $f_{PFPF}=0.183$. Finally, the values of the thermodynamic properties for these substances were computed for the ideal gaseous state using the rigid rotor harmonic oscillator approximation at 1 atm from 200° to 1000°K.

INTRODUCTION

AN examination of the literature for the Raman and infrared spectra of phosphoryl chloride, thiophosphoryl chloride, and phosphoryl fluoride revealed the absence of the normal coordinate treatments for the first two substances and only a partial one for the third. In an attempt to fill in this gap the normal coordinate treatments for these substances were undertaken on the basis of the most probable model and the thermodynamic properties of these substances were computed up to a rigid rotator harmonic oscillator approximation.

* Based in part on a thesis in partial fulfillment of the requirements for the Masters Degree in Chemistry by Mr. E. A. Piotrowski.

† Present address: Illinois Institute of Technology, Department of Physics, Chicago, Illinois.

Phosphoryl Chloride ($POCl_3$, Phosphorus Oxychloride)

Seven separate investigations[1–7] have included Raman displacements for $POCl_3$ and seven investigators[4–6] have measured depolarization factors. These data are summarized in Table I. The most probable data for the Raman spectrum were taken as follows: displacements and relative intensities of Langseth[2] (obtained under a high dispersion) and the depolarization factors of Cabannes and Rousset.[4]

[1] H. Nisi, Japan. J. Phys. **6**, 1 (1930).
[2] A. Langseth, Z. Physik. **72**, 350 (1931).
[3] S. Venkateswaran, Indian J. Phys. **6**, 275 (1931).
[4] J. Cabannes and A. Rousset, Ann. Phys. **19**, 229 (1933).
[5] H. Moureau, M. Magat, and G. Wetroff, Proc. Indian Acad. Sci. **8A**, 356 (1938).
[6] H. Gerding and R. Westrick, Rec. trav. chim. **61**, 842 (1942).
[7] M. Delwaulle and F. Francois, Compt. rend. **220**, 817 (1945).

Copyright © 1961 by the American Institute of Physics

TABLE I. Raman spectral data for $POCl_3$.[a]

M.P.			G.W.			A.L.		C.R.		
$\Delta\sigma$	I	ρ	$\Delta\sigma$	I	ρ	$\Delta\sigma$	I	$\Delta\sigma$	I	ρ
192.85	8	0.83	193	8	0.83	192.85	8	193	—	0.83
267.39	6	0.64	267	4	0.64	267.39	6	268		0.64
337.44	7	0.81	337	7	0.81	337.44	7	337		0.81
486.24	10	0.05	486	10	0.05	486.24	10	486		0.05
581.2	3	6/7	581	1	D	581.2	3	581		6/7
1289.9	5	0.04	1290	10	0.04	1289.9	5	1290		0.04

M.M.W.			H.N.	S.V.	D.F.		
$\Delta\sigma$	I	ρ	$\Delta\sigma$	$\Delta\sigma$	$\Delta\sigma$	I	ρ
193	8	6/7	192	191	193	8	0.83
267	6	P	270	269	267.4	6	0.64
337	7	6/7	337	338	337.4	7	0.81
486	10	P	486	485	486.2	10	0.05
581	3	6/7	581	585	581.2	3	6/7
1290	5	P	1295	1290	1290	5	0.40

[a] $\Delta\sigma$ is the Raman displacement, I is the relative intensity, ρ is the depolarization factor, H.N. = Nisi, footnote 1, A.L. = Langseth, footnote 2, C.R. = Cabannes and Rousset, footnote 4, M.M.W. = Moureau, Magat, and Wetroff, footnote 5, D.F. = Delwaulle and Francois, footnote 7, G.W. = Gerding and Westrick, footnote 6, and S.V. = Venkateswaran, footnote 3. M.P. = most probable data selected from those that are listed.

TABLE II. Raman and infrared spectral data for $PSCl_3$.[a]

Infrared spectrum			Raman spectrum										
			SS	T	GW			DF			MP		
$\sigma(g)$	$\sigma(l)$	I_e	$\Delta\sigma$	$\Delta\sigma$	$\Delta\sigma$	I	ρ	$\Delta\sigma$	I	ρ	$\Delta\sigma$	I	ρ
			168	171	167	5	(1.00)	172	5	6/7	169	5	6/7
			244	246	250	7	0.91	247	7	6/7	247	7	6/7
			382	382									
433	430	s	429	432	435	10	0.11	430	10	0.1	431	10	0.10
441													
	500sh	w											
	540	vs	536	543	542	1–2	0.85	538	1	6/7	540	1	6/7
550													
593	590												
684	680												
715	710	s											
	751		747	750	753	1–2	0.31	753	1	D	751	1	D
762													
768.5													
775													
793sh													
865	860	w											
934	922	w											
977	964	w											
	984	w											
	1011	vw											
1089	1076	w											
1197	1183	w											
1321	1301	w											
1530	1503	w											

[a] $\Delta\sigma$ = Raman displacement in cm^{-1}, I = relative intensity, ρ = depolarization factor, I_e = estimated intensity, SS = Simon and Schulze, footnote 9, T = Thatte, footnote 8, GW = Gerding and Westrick, footnote 6, DF = Delwaulle and Francois, footnote 7, MP = most probable values, s = strong, vs = very strong, m = medium, w = weak, vw = very weak, sh = shoulder, br = broad. $\sigma(l)$ and $\sigma(g)$ = wave numbers in K for liquid and gas, respectively.

TABLE III. Raman and infrared spectral data for POF_3[a] and PSF_3.

POF_3					PSF_3		
Raman spectrum			Infrared spectrum		Raman spectrum		
$\Delta\sigma$	I	ρ	(g)	I_e	$\Delta\sigma$	I	ρ
337	w	6/7			276	35	6/7
476	m	6/7	473	s	402	7	6/7
			485	ms			
			690	vw	440	15	0.3
			830	w			
875	s	0.05	873	ms	695	70	0.15
			946	w	894	10	0.1
			957	w			
982	vw	6/7	990	vs	940	*W*	6/7
			1275	w			
			1330	m			
			1345	m			
			1360	w			
1395	m	0.1	1415	ms			
			1462	w			
			1472	w			
			1740	vw			
			1855	m			
			2295	w			
			2815	vw			

[a] See Tables I and II for definition of the symbols.

Thiophosphoryl Chloride ($PSCl_3$, Phosphorus Thiochloride)

Seven investigators[6–9] reported the Raman spectrum of this phosphoryl chloride. First Thatte[8] and Simon *et al.*[9] reported six displacements. Later Gerding and Westrick[6] repeated this work and found only five. By comparing the spectrum of $PSCl_3$ with that of $POCl_3$ they estimated the missing displacement to be near 240 cm^{-1} and claimed that this band could be obscured by the one at 250 cm^{-1} which they observed. This observation was later confirmed by Delwaulle and Francois.[7] As for depolarization factors, four investigators[6,7] reported the overlap of the 167 cm^{-1} band with the exciting line. The large value for the 247 cm^{-1} Raman band (reported by Gerding *et al.*) could be due to the missing band overlapping with the 247 cm^{-1} band. All these data along with the report of the infrared spectrum by Cilento[10] are summarized in Table II. An examination of Table II indicates that the band at 382 cm^{-1} was taken as a band due to the presence of an impurity. As may be seen from Table II, there is general agreement with respect to the displacements, relative intensities, and depolarization factors. The average values of the Raman displacements as reported in Table II were taken as the most favorable values of the fundamental frequencies.

The most probable values for the relative intensities and depolarization factors were taken as those reported by Delwaulle and Francois.[7]

[8] V. N. Thatte, Nature **138**, 468 (1936).
[9] A. Simon and G. Schulze, Naturwissenschaften **25**, 669 (1937).
[10] G. Cilento, D. A. Ramsey, and R. N. Jones, J. Am. Chem. Soc. **71**, 2753 (1949).

Phosphoryl Fluoride (POF_3, Phosphorus Oxyfluoride)

Delwaulle and Francois[7] reported only five Raman displacements for POF_3 in the liquid state along with values for the relative intensities and depolarization factors. Recently Gutowsky and Liehr[11] have reported infrared spectral data. These data were taken as most probable and are listed in Table III.

Thiophosphoryl Fluoride (PSF_3, Phosphorus Thiofluoride)

Delwaulle and Francois[7] reported the Raman displacements for PSF_3 along with values for the relative intensities and depolarization factors. These data were taken as most probable and are listed in Table III. No infrared data were found.

Most Probable Model

Previous nonspectroscopic investigations indicated the tetrahedral structure for the phosphoryl halides. The electron diffraction data of Brockway and Beach[12] and those of Beach and Stevenson[13] for $PSCl_3$ indicate that the most probable structure has C_{3v} symmetry. This is in agreement with the report of Weisenheimer and Lichtenstadt that the enantiomorphs of organophosphorus compounds of the type $R_1R_2R_3PO$ can be resolved. Furthermore, the results of dipole moment

[11] H. S. Gutowsky and A. D. Liehr, J. Chem. Phys. **20**, 1652 (1952).
[12] L. O. Brockway and J. Y. Beach, J. Am. Chem. Soc. **60**, 1836 (1938).
[13] J. Y. Beach and D. P. Stevenson, J. Chem. Phys. **6**, 75 (1938).

TABLE IV. Potential constants for XY_3P.[a]

	δD	δd_1	δd_2	δd_3	δa_{12}	δa_{13}	δa_{23}	δb_1	δb_2	δb_3
δD	f_D	f_{Dd}	f_{Dd}	f_{Dd}	f_{Da}	f_{Da}	f_{Da}	f_{Db}	f_{Db}	f_{Db}
δd_1		f_d	f_{dd}	f_{dd}	f_{da}	f_{da}	f_{da}	f_{db}	f_{db}	f_{db}
δd_2			f_d	f_{dd}	f_{da}	f'_{da}	f_{da}	f'_{db}	f_{db}	f'_{db}
δd_3				f_d	f'_{da}	f_{da}	f_{da}	f'_{db}	f'_{db}	f_{db}
δa_{12}					f_a	f_{aa}	f_{aa}	f_{ab}	f_{ab}	f'_{ab}
δa_{13}						f_a	f_{aa}	f_{ab}	f'_{ab}	f_{ab}
δa_{23}							f_a	f'_{ab}	f_{ab}	f_{ab}
δb_1								f_b	f_{bb}	f_{bb}
δb_2									f_b	f_{bb}
δb_3										f_b

[a] $f_{ij}=f_{ji}$.

determination[14] lend support to this evidence. Moreover, Williams, Sheridan, and Gordy[15] reported microwave data for $POCl_3$, POF_3, $PSCl_3$, and PSF_3 on the basis of the same model and the results for PSF_3 and POF_3 were confirmed by Hawkins, Cohen, and Koski.[16] Then according to the group theory methods this model, $Y_3PX(C_{3v})$, should have six fundamental frequencies, all allowed in both the infrared and Raman spectra. Also, the Raman spectrum of each substance should contain at least three depolarized lines and at least three polarized lines. An examination of the Raman spectrum of all three phosphoryl halides reveals that there are at least three depolarized lines in each case. As for the polarized lines, three are found for $POCl_3$ and two are found for POF_3 and $PSCl_3$. Hence, the most probable model is the one that has symmetry belonging to the point group C_{3v}.

NORMAL COORDINATE TREATMENT

In order to establish the fundamental frequencies of POF_3, $POCl_3$, and $PSCl_3$, normal coordinate treatments (*FG* matrix method) were carried out on the basis of the C_{3v} model. The equilibrium configuration along with the bond distances and bond angles is given in Fig. 1.

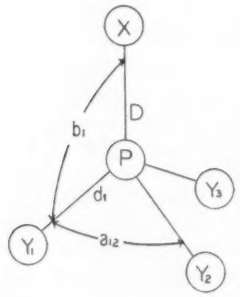

FIG. 1. Equilibrium configuration for the XY_3P molecule.

The changes in the bond distances and interbond angles as depicted in Fig. 1 were taken as internal coordinates. According to the selection rules, there are three fundamental frequencies of the a_1 type and three fundamental frequencies of the e type. Then the following set of linear combinations of internal coordinates was chosen as the symmetry coordinates (orthonormal) set): for the type a_1,

$$R_1=\delta D,$$

$$R_2=3^{-\frac{1}{2}}(\delta d_1+\delta d_2+\delta d_3),$$

$$R_3=6^{-\frac{1}{2}}(\delta a_{12}+\delta a_{23}+\delta a_{13}-\delta b_1-\delta b_2-\delta b_3),$$

$$R_4=6^{-\frac{1}{2}}(\delta a_{12}+\delta a_{23}+\delta a_{13}+\delta b_1+\delta b_2+\delta b_3)\equiv 0$$

(a redundant coordinate);

and, for type e,

$$R_{1a}=6^{-\frac{1}{2}}(2\delta d_1-\delta d_2-\delta d_3),$$

$$R_{1b}=2^{-\frac{1}{2}}(\delta d_2-\delta d_3),$$

$$R_{2a}=6^{-\frac{1}{2}}(2\delta b_1-\delta b_2-\delta b_3),$$

$$R_{2b}=2^{-\frac{1}{2}}(\delta b_2-\delta b_3),$$

$$R_{3a}=6^{-\frac{1}{2}}(2\delta a_{23}-\delta a_{12}-\delta a_{13}),$$

$$R_{3b}=2^{-\frac{1}{2}}(\delta a_{13}-\delta a_{12}).$$

The symmetry coordinates $R_3(a_1)$ and $R_4(a_1)$ are valid only for angles which to a sufficiently good approximation are tetrahedral. However, for small deviation from tetrahedral angles, it is found that the symmetry coordinates as given are still adequate for a satisfactory normal coordinate treatment.

The potential function had the coefficients given in Table IV. From the potential energy matrix and the

[14] C. P. Smyth, G. L. Lewis, A. J. Grossman, and F. B. Jennings, J. Am. Chem. Soc. **62**, 1219 (1940).
[15] Q. Williams, J. Sheridan, and W. Gordy, J. Chem. Phys. **20**, 164 (1952).
[16] N. J. Hawkins, V. W. Cohen, and W. S. Koski, J. Chem. Phys. **20**, 528 (1952).

TABLE V. F matrix elements for $POCl_3$, POF_3, $PSCl_3$, and PSF_3.[a]

Element	$POCl_3$	POF_3	$PSCl_3$	PSF_3	$POCl_3$ calc	$POCl_3$ obs	POF_3 calc	POF_3 obs	$PSCl_3$ calc	$PSCl_3$ obs	PSF_3 calc	PSF_3 obs
F_{11}^a	9.8900[b]	9.8900	3.0300	2.9694	1288.4	1290	1404.9	1395	759.6	753	877.7	874
					488.4	486	874.3	875	426.2	430	694.5	695
F_{12}^a	0.2000	0.5000	0.4800	0.5500	265.2	267	469.6	473	248.2	247	439.3	440
F_{13}^a	0.0770	0.5000	0.3500	−0.2300								
F_{22}^a	3.2640	6.6000	3.2640	5.7000								
F_{23}^a	0.0000	0.7500	−0.3000	0.7070								
F_{33}^a	1.1985	1.8500	1.7050	2.5500								
F_{11}^e	2.0678	5.1500	2.0678	5.1500	580.3	581	979.2	982	538.0	538	940.6	940
					337.7	337	489.5	485	246.3	(247)	400.5	402
F_{12}^e	0.0800	−0.1400	−0.0500	−0.1450	193.1	193	334.2	337	172.4	172	276.8	276
F_{13}^e	−0.2900	−0.0500	−0.2900	−0.1400								
F_{22}^e	1.3800	1.6366	1.2000	1.3320								
F_{23}^e	−0.1900	−0.3300	−0.2300	−0.4444								
F_{33}^e	1.0470	1.1730	1.0470	1.1730								

[a] F_{11}^a, F_{12}^a, F_{22}^a, and F_{11}^e are given in md/A, F_{13}^a, F_{23}^a, F_{13}^e, and F_{12}^e are given in md/rad, and F_{22}^a, F_{22}^e, F_{23}^e, and F_{33}^e are given in md A/rad^2.

[b] This number of significant figures is not justified except that they are necessary to give the best reproduction of the observed wave numbers and to secure internal consistency in the calculations.

matrix formed from the coefficients contained in the symmetry coordinates, the following F matrix elements were obtained:

for type a_1,

$$F_{11}=f_D,$$

$$F_{12}=3^{\frac{1}{2}}f_{Dd}$$

$$F_{13}=(\tfrac{3}{2})^{\frac{1}{2}}d(f_{Da}-f_{Db}),$$

$$F_{22}=f_d+2f_{dd},$$

$$F_{23}=2^{-\frac{1}{2}}d(f'_{da}+2f_{da})-(f_{db}+2f'_{db}),$$

$$F_{33}=d^2[(f_a+2f_{aa})+(f_b+f_{bb})-2(f'_{ab}+2f_{ab})]/2;$$

and, for type e,

$$F_{11}=f_d-f_{dd},$$

$$F_{12}=d(f_{ab}-f'_{ab}),$$

$$F_{13}=d(f'_{da}-f_{da}),$$

$$F_{22}=d^2(f_b-f_{bb}),$$

$$F_{23}=d^2(f'_{ab}-f_{ab}),$$

$$F_{33}=d(f_a-f_{aa}).$$

The elements of the G matrix were obtained from relations given by Wilson.[17]

[17] E. B. Wilson, Jr., J. Chem. Phys. **7**, 1047 (1939), **9**, 76 (1941).

They are:

for type a_1,

$$G_{11}^a=u_V+u_P$$

$$G_{12}^a=3^{\frac{1}{2}}u_P\cos b$$

$$G_{13}^a=(\tfrac{3}{2})^{\frac{1}{2}}u_P[(A)\ (\cos b)+B]$$

$$G_{22}^a=u_X+u_P(1+2\cos a)$$

$$G_{23}^a=2^{-\frac{1}{2}}u_P[(A)(1+2\cos a)-3(B)\ (\cos b)]$$

$$G_{33}^a=(\tfrac{1}{2})\epsilon^2u_X(2C-4D+1)$$

$$+u_P[(\tfrac{1}{2})(1+2\cos a)(2E-F)^2+(\tfrac{3}{2})(B)^2+3AB(\cos b)]$$

$$+(u_Yr^2/2\sin^2 b)(1+2\cos b-3\cos^2 b)$$

$$G_{11}^e=u_X+u_P(1-\cos a)$$

$$G_{12}^e=u_P(F)\ (\cos a-1)$$

$$G_{13}^e=u_P(E)(1-\cos a)$$

$$G_{22}^e=u_X^2+u_P(F)^2(1-\cos a)+(u_Y^2/\sin^2 b)(1-\cos a)$$

$$G_{23}^e=u_PEF(\cos a-1)-u_X\epsilon^2(1-\cos a)(\cos b)/\sin a\sin b$$

$$G_{33}^e=u_X\epsilon^2(2-\cos a-\cos^2 a)/\sin^2 a+u_PE^2(1-\cos a),$$

TABLE VI. Heat content, free energy, entropy, and heat capacity of $POCl_3$, $PSCl_3$, and POF_3 for the ideal gaseous state at 1 atm pressure.

	$POCl_3$				POF_3				$PSCl_3$			
T°K	$\frac{(H^\circ-E_0^\circ)}{T}$	$-\frac{(F^\circ-E_0^\circ)}{T}$	S°	C°_p	$\frac{H^\circ-E_0^\circ}{T}$	$-\frac{(F^\circ-E_0^\circ)}{T}$	S°	C°_p	$\frac{H^\circ-E_0^\circ}{T}$	$-\frac{(F^\circ-E_0^\circ)}{T}$	S°	C°_p
200	11.85[a]	58.04	69.89	17.20	9.622	52.71	62.33	13.20	12.78	59.48	72.53	18.57
250	13.10	60.82	73.93	18.94	10.52	54.95	65.48	15.01	14.12	62.75	76.87	20.28
273.16	13.63	62.01	75.63	19.57	10.94	55.90	66.84	15.76	14.67	64.02	78.69	20.90
298.16	14.15	63.22	77.37	20.16	11.37	56.88	68.25	16.50	15.22	65.33	80.55	21.47
300	14.19	63.31	77.50	20.20	11.40	56.95	68.35	16.55	15.26	65.43	80.68	21.51
400	15.92	67.64	83.56	21.90	13.01	60.46	74.47	18.97	17.03	70.07	87.11	23.07
500	17.23	71.34	88.57	22.95	14.38	63.51	77.89	20.66	18.34	74.02	92.36	23.94
600	18.24	74.58	92.82	23.65	15.53	66.24	81.77	21.86	19.32	77.45	96.77	24.47
700	19.05	77.45	96.50	24.13	16.50	68.71	85.21	22.71	20.08	80.50	100.59	24.80
800	19.71	80.08	99.79	24.48	17.32	70.96	88.28	23.33	20.68	83.21	103.90	25.03
900	20.25	82.40	102.65	24.73	18.01	73.05	91.06	23.78	21.18	85.68	106.86	25.19
1000	20.71	84.55	105.26	24.92	18.61	74.97	93.58	24.13	21.58	87.95	109.54	25.31

[a] All quantities in this table have units of cal deg^{-1} mole^{-1}.

where

$$A=(\tau-\epsilon\cos b)/(\sin b)-2\epsilon(1-\cos a)/\sin a$$

$$B=(\epsilon-\tau\cos b)/(\sin b)$$

$$C=(1-2\cos^2 a+\cos a)/\sin^2 a$$

$$D=(\cos b-\cos a\cos b)/\sin a\sin b$$

$$E=(\epsilon-\epsilon\cos a)/\sin a$$

$$F=(\tau-\epsilon\cos b)/\sin b$$

and

$$\epsilon=1/d \qquad \tau=1/D.$$

The equilibrium values of the bond distances and interbond angles taken from Gordy *et al.*,[16] were:

for $POCl_3$,

$$d(\text{P–O})=1.45\pm0.03\text{A},$$

$$d(\text{P—Cl})=1.99\pm0.02\text{ A}, \quad \text{and} \quad a=103.6\pm2°;$$

for $PSCl_3$,

$$d(\text{P—S})=1.85\pm0.02\text{ A},$$

$$d(\text{P—Cl})=2.02\pm0.01\text{ A}, \quad \text{and} \quad a=105\pm1°;$$

for POF_3,

$$d(\text{P—O})=1.45\pm0.03\text{ A},$$

$$d(\text{P—F})=1.53\pm0.02\text{ A}, \quad \text{and} \quad a=102.5\pm2°;$$

and for PSF_3,

$$d(\text{P—S})=1.87\pm0.03\text{ A},$$

$$d(\text{P—F})=1.53\pm0.02\text{ A}, \quad \text{and} \quad a=100.3\pm2°.$$

The values for the u_i

$$u_{Cl}=1.69943\times10^{22}; \quad u_F=3.17140\times10^{22},$$

$$u_P=1.94533\times10^{22},$$

$$u_O=3.76604\times10^{22}; \quad u_S=1.87914\times10^{22}.$$

Calculations

The F matrix elements of the two types (F_{ij}^a and F_{ij}^e) for each molecule were estimated from the values of the potential constants for similar molecules. For $POCl_3$ and $PSCl_3$ the values of the potential constants for PCl_3 as given by Howard and Wilson[18] and those of Gore[19] for the P—O and P—S bonds were used as a first approximation. For POF_3 the values of the F_{ij}^a and F_{ij}^e as reported by Gutowsky and Liehr[11] and the F_{ij}^e and F_{ij}^e of Wilson and Polo[20] for PF_3 were used, together with the constants for the PO and PS bonds as given by Gore.[20] First, for each molecule the

[18] J. B. Howard and E. B. Wilson, Jr., J. Chem. Phys. **2**, 630 (1934).
[19] R. C. Gore, Discussions Faraday Soc. **9**, 138 (1950).
[20] M. K. Wilson and S. R. Polo, J. Chem. Phys. **20**, 1716 (1952).

F_{ij}^a were estimated and then modified to give calculated wave numbers to within 1% of those observed. Then these were used as a first approximation for the F_{ij}^e as a test of their validity. Once their validity was established the F_{ij}^e were then modified to give calculated wave numbers of the e type to within 1% of those observed. Then the values of whatever potential constants that could be calculated from linear combinations of the F_{ij}^a and F_{ij}^e were obtained and compared with those reported for similar molecules. If the comparison was favorable then these values of the potential constants would be used in the estimation of the F_{ij} of the common part of another molecule. Thus the F_{ij}^a and F_{ij}^e for the PCl_3 group were used for $POCl_3$ and $PSCl_3$, those F_{ij}^a and F_{ij}^e for the PF_3 group were used for POF_3 and PSF_3, and f_{PS} was used for both PSF_3 and $PSCl_3$. PSF_3 was included here for the purpose of establishing the potential constant for the P—S bond. Since only the values of f_{P-Cl}, $f_{P-Cl\ P-Cl}$, f_{P-F}, f_{FPF}, and f_{P-S} could be computed, it was decided to report only the F_{ij}^a and F_{ij}^e which are given in Table V along with the calculated and observed wave numbers. An examination of Table V reveals that the values of the potential constants computed from the linear combinations of F_{ij}^a and F_{ij}^e for the foregoing molecules are in agreement with those reported by Wilson and Polo[21] for PF_3, Howard and Wilson[19] for PCl_3, and that by Gore[20] for the PO group. As for the PS group in PSF_3, the value of the potential constant was taken as 2.9694 md/A in order that the values of the potential constants for PF_3 group be near those of Wilson and Polo[21] and obtain calculated wave numbers to within 1% of those observed. As evidence in favor of this value for the PS group, it was found that if in $PSCl_3$ the PS group had a value of 3.030 md/A while the values of potential constants for the PCl_3 group were nearly the same as those for the PCl_3 group in $POCl_3$, the calculated wave numbers of $PSCl_3$ were within 1% of those observed.

THERMODYNAMIC PROPERTIES

The probable values of the wave numbers in Tables I, II, and III were used to calculate values of the heat content, entropy, free energy, and heat capacity for the ideal gaseous state at 1 atm pressure using the rigid rotator, harmonic oscillator approximation. The previously given bond distances and interbond angles were used to calculate the product of the principal moments of inertia. The symmetry number was 3 in each case and the molecular weights were computed from the following atomic weights: For P=30.975, F=19.000, O=16.000, Cl=35.457, and S=32.066. Nuclear spins and isotopic mixing were neglected. The values so computed are listed in Table VI, for the temperature range from 200° to 1000°K.

ACKNOWLEDGMENTS

The authors greatly appreciate the support of this work by a contract with the office of Ordnance Research, U.S. Army, and the suggestion and aid received from Professor F. F. Cleveland in the preparation of this manuscript.

NMR Spectra of Propyl Derivatives*

JAMES R. CAVANAUGH† AND B. P. DAILEY

Department of Chemistry, Columbia University, New York, New York

(Received August 11, 1960)

A perturbation treatment, carried to third order in the energies and first order in the intensities of the analysis of the propyl group spectra, is presented. Accurate values are given for the coupling constants and the chemical shifts of the common propyl derivatives, both for the pure compound and as extrapolated to infinite dilution in carbon tetrachloride.

INTRODUCTION

THE NMR spectra of the alkyl derivatives might be expected to display interesting regularities with respect to the variables which determine the chemical shift. Within this group of molecules the propyl derivatives play an important role. The methyl and ethyl derivatives of most of the common occurring functional groups have been investigated in detail, but to date few accurate chemical shift data for the propyl derivatives have been available. The spectra of most propyl derivatives observed at frequencies of 30 or 40 Mc are quite complicated and while, at 60 Mc, the multiplet patterns of the three chemically distinct groups of protons are clearly delineated, the analysis of the spectrum cannot be successfully approximated by a simple first-order treatment. An exact analysis of the spectrum, including the solution of the secular equations as a function of the chemical shift and spin-spin coupling parameters, would be tedious and time consuming. However, since the coupling constants J have values ranging from 6 to 8 Mc and the minimum value of the chemical shift δ observed in this series is of the order of 25 cps at 60 Mc, the corresponding values of J/δ (less than 0.4) make it appear that the spectra might be safely analyzed using perturbation methods.

SOLUTION OF THE SPIN HAMILTONIAN

The method of setting up and solving the spin Hamiltonian follows that of Bernstein, Schneider, and Pople.[1] The propyl group may be designated as an $A_2B_2C_3$ system, where A, B, and C refer to the α-methylene, β-methylene, and methyl groups, respectively. Since only mono-substituted propanes are being studied, there will be sufficient internal rotation about the two carbon-carbon bonds so that the protons in each group will be chemically equivalent. Consequently, at most five parameters will be needed to describe the system, two internal shifts, and three coupling constants, as shown in Fig. 1.

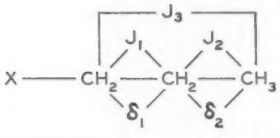

FIG. 1. Chemical shift and spin-spin coupling parameters for propyl derivatives.

The coupling between the protons within the groups may be equated to zero since one is unable to observe experimentally the coupling between equivalent protons. Also, let us assume that the coupling between the α-CH_2 protons and the CH_3 protons will be negligible and the coupling constant J_3 may be set equal to zero. Hence the system may be described by just four parameters: δ_1, δ_2, J_1, and J_2.

The Hamiltonian for the system is

$$\mathbf{H}=\mathbf{H}^0+\mathbf{H}'. \tag{1}$$

Here $\mathbf{H}^0$ is the zero-order Hamiltonian and may be written

$$H^0=\sum_i \eta_i H_i I_z(i), \tag{2}$$

where $2\pi\eta_i$ is the gyromagnetic ratio of nucleus i. Since we are dealing only with the proton, η will be the same for all nuclei, H_i is the total field of resonance of nucleus i in the absence of spin-spin coupling, $I_z(i)$ is the z component of the nuclear spin $\mathbf{I}$ of nucleus i. The sum is over all nuclei in the system.

Here $\mathbf{H}'$ is the perturbing Hamiltonian, given by

$$H'=\sum_{i<j}\sum J_{ij}\mathbf{I}(i)\cdot\mathbf{I}(j), \tag{3}$$

where J_{ij} is the coupling constant between nuclei i and j. The sum is over all pairs of nuclei in the system.

In numbering the nuclei, let 1 and 2 be the protons in group A, 3 and 4 the protons in group B, and 5, 6, and 7 will be the protons in group C. Then,

$$\begin{aligned} H_1&=H_2=H_0(1-\sigma_A)\\ H_3&=H_4=H_0(1-\sigma_B)\\ H_5&=H_6=H_7=H_0(1-\sigma_C), \end{aligned} \tag{4}$$

where σ_A, σ_B, and σ_C are the shielding constants for protons A, B, and C, respectively, and H_0 is the applied

* Supported by grants from the National Science Foundation, the Office of Scientific Research, Air Research and Development Command, U. S. Air Force, and the Alfred P. Sloan Foundation.

† Present Address: Socony Research Laboratories, Paulsboro, New Jersey.

[1] J. A. Pople, W. G. Schneider, and H. J. Bernstein, *High Resolution Nuclear Magnetic Resonance* (McGraw-Hill Book Company, Inc., New York, 1959), Chap. 6.

field. Also,

$$\delta_1=\eta H_0(\sigma_A-\sigma_B)$$
$$\delta_2=\eta H_0(\sigma_B-\sigma_C) \qquad (5)$$
$$J_{13}=J_{14}=J_{23}=J_{24}=J_1$$
$$J_{35}=J_{36}=J_{37}=J_{45}=J_{46}=J_{47}=J_2$$
$$J_{12}=J_{34}=J_{56}=J_{57}=J_{67}=0$$
$$J_{15}=J_{16}=J_{17}=J_{25}=J_{26}=J_{27}=0.$$

Next it is necessary to choose a set of basis functions for the Hamiltonian. A simple product wave function for the molecule will be formed from a product of the individual wave functions for each nucleus, where these will be either α or β, the eigenfunctions of I_z with eigenvalues $+\hbar/2$ and $-\hbar/2$, respectively.

However, one may first form a set of wave functions for each of the three groups and from these form a set of wave functions for the molecule. Since there are 2, 2, and 3 nuclei, respectively, in groups A, B, and C, there will be 4, 4, and 8 simple product wave functions for these three groups, respectively, as follows:

A	B	C	
$\alpha\alpha$	$\alpha\alpha$	$\alpha\alpha\alpha$	$\alpha\beta\beta$
$\alpha\beta$	$\alpha\beta$	$\alpha\alpha\beta$	$\beta\alpha\beta$
$\beta\alpha$	$\beta\alpha$	$\alpha\beta\alpha$	$\beta\beta\alpha$
$\beta\beta$	$\beta\beta$	$\beta\alpha\alpha$	$\beta\beta\beta$.

Now, from the four functions for A, symmetric and antisymmetric wave functions will be formed, similarly, for group B. From the eight functions in the group C, functions are formed which are a basis for a proper representation of the symmetry group C_3. This will yield the following:

A	B	C
Symmetric		
$\alpha\alpha$	$\alpha\alpha$	$\alpha\alpha\alpha$
$1/\sqrt{2}(\alpha\beta+\beta\alpha)$	$1/\sqrt{2}(\alpha\beta+\beta\alpha)$	$1/\sqrt{3}(\alpha\alpha\beta+\alpha\beta\alpha+\beta\alpha\alpha)$
$\beta\beta$	$\beta\beta$	$1/\sqrt{3}(\beta\beta\alpha+\beta\alpha\beta+\alpha\beta\beta)$
		$\beta\beta\beta$
A	B	C
Antisymmetric		
$1/\sqrt{2}(\alpha\beta-\beta\alpha)$	$1/\sqrt{2}(\alpha\beta-\beta\alpha)$	
E Representation		
		$1/(6)^{\frac{1}{2}}(2\beta\alpha\alpha-\alpha\beta\alpha-\alpha\alpha\beta)$
		$1/\sqrt{2}(\alpha\beta\alpha-\alpha\alpha\beta)$
		$1/(6)^{\frac{1}{2}}(2\alpha\beta\beta-\beta\alpha\beta-\beta\beta\alpha)$
		$1/\sqrt{2}(\beta\alpha\beta-\beta\beta\alpha)$.

Forming products of the wave functions from each group as a wave function for the molecule, products of the following eight types may be formed:

A	B	C	No.
S	S	S	36
S	S	E	36
A	S	S	12
A	S	E	12
S	A	S	12
S	A	E	12
A	A	S	4
A	A	E	4.

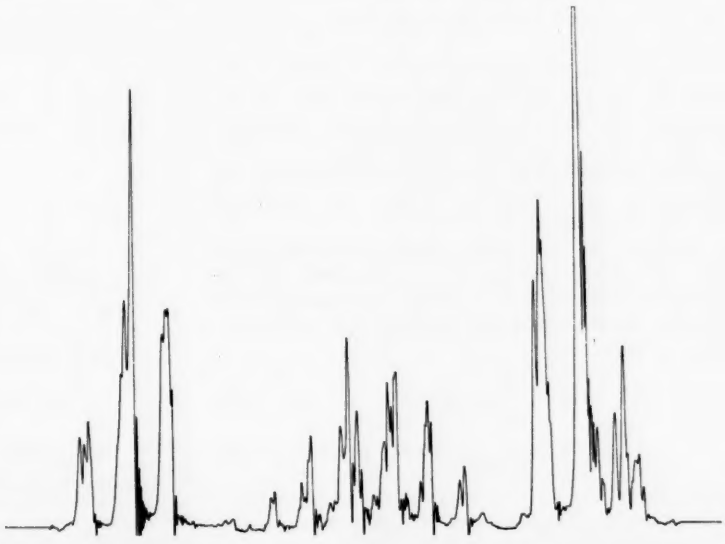

FIG. 2. Spectrum of butyronitrile at 60 Mc.

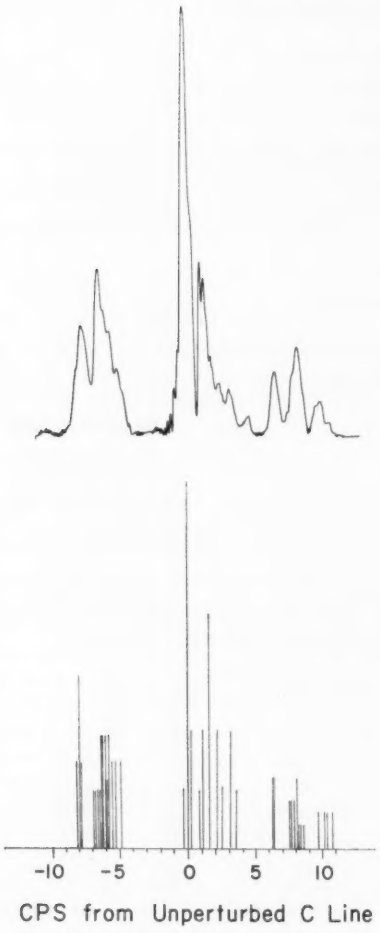

FIG. 3. CH_3 group, butyronitrile.

Using this set of wave functions as a basis for the Hamiltonian, the matrix elements may then be calculated. If the wave functions are chosen in this way, it may be shown that there is no mixing, i.e., no connecting off-diagonal elements, between states of one designation with states of a different designation of the above eight types.

Applying the usual perturbation formulas,[2,3] the corrected energy states and wave functions may be calculated. The result is a power series expansion in J/δ for the stationary-state energies and wave functions, as follows:

$$E_n=\sum_{m=0}^{\infty}a_{nm}(J^m/\delta^{m-1}) \tag{6}$$

$$\psi_n=\sum_p[\sum_{m=0}a_{npm}(J/\delta)^m]\psi_p(0), \tag{7}$$

where J and δ stand symbolically for all the J's and δ's needed to describe the system. In the present case, the energies were corrected to third order and the wave functions to first order. Transition energies and intensities were calculated. Again, it may be shown that transitions occurring between states of different designation, as given above, are forbidden. Transitions were labeled A, B, or C, depending on the way the transition may be described in the limit of the vanishing value of J. Combination transitions, in which all three groups change spin simultaneously, were not considered. Detailed results are available as a supplementary document from the American Documentation Institute.[4]

The groups A and C both contain an unperturbed line. They are the right and left lines, respectively, of the center of the α-CH_2 and CH_3 triplet resonances. A comparison of the predicted and observed spectra for

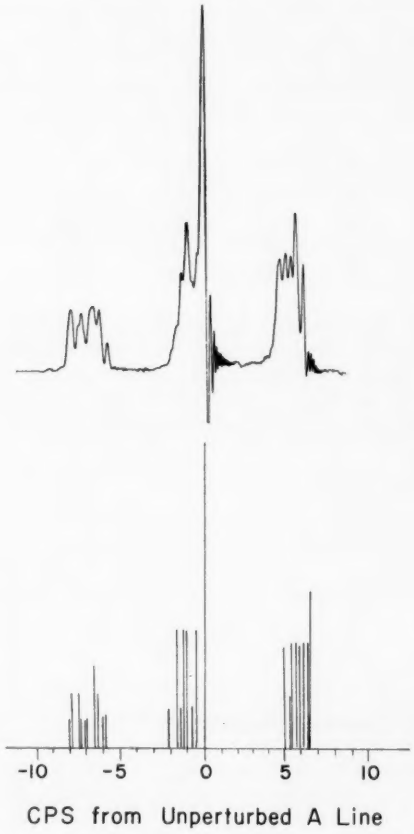

FIG. 4. αCH_2 group, butyronitrile.

[2] W. A. Anderson, Phys. Rev. **102**, 151 (1956).
[3] P. L. Corio, Chem. Revs. (to be published).

[4] For supplementary material, order Document 6607 from American Documentation Institute, 1719 N Street, N. W., Washington 6, D. C., remitting $1.25 for microfilm (images 1 in. high on standard 35 mm motion picture film readable in microfilm reader or under low-power microscope) or $7.25 for photocopies (6×8 in. readable without optical aid.)

butyronitrile is given in Figs. 2 to 5. The predicted spectrum is based on the following values of the parameters: $J_1=6.7$, $J_2=7.7$, $\delta_1=42.2$, $\delta_2=36.3$ in cps at 60 Mc.

In order to investigate the upper limit of the validity of the perturbation method carried to third order, the energies calculated by the perturbation method were compared to the energies as calculated by an exact solution for two sets of parameters with J/δ equal to 0.2 and 0.4. The two sets of parameters and the agreement of the exact and the perturbation energies are shown in Table I.

As seen from Table I for a value of 0.4 for the ratio of J/δ, the third-order perturbation calculation is a poor approximation. Higher-order terms would have to be included when the value of J/δ becomes this large. However, for a value of 0.2 for J/δ, the method is reasonably accurate. Hence the upper limit of the validity of the perturbation method carried to third order will fall in the region, $0.2<J/\delta<0.4$. Since, in the compounds studied, the ratio of J/δ never becomes larger than 0.3, it can be assumed that the perturbation method sufficiently approximates the exact solution for these cases.

TABLE I. Comparison perturbation and exact energies for $J/\delta=0.2$, 0.4.

Agreement to within (in cps)	% Transitions	Agreement to within (in cps)	% Transitions
Exact	66	Exact	20
0.1	82	0.5	54
0.2	92	1.0	81
0.4	99	2.0	89
0.6	100	6.0	95
		10.0	100
Set No. 1		Set No. 2	
$J_1=4.0$ $J_2=6.0$ $\delta_1=20.0$ $\delta_2=30.0$		$J_1=4.0$ $J_2=8.0$ $\delta_1=10.0$ $\delta_2=20.0$	
$J/\delta=0.2$		$J/\delta=0.4$	

EXPERIMENTAL RESULTS

The measurements were made on a Varian Associates high-resolution nuclear magnetic resonance spectrometer, operating at a fixed frequency of 60 Mc. The frequency separations between lines were measured using the usual audio-modulation side-band technique, employing a method similar to that of Tiers.[5] The audio-modulation frequency was counted directly using a Hewlett-Packard frequency counter model No. 521 A, equipped with a 10-kc crystal-controlled time base and a 10-sec gate. Frequency separations so measured could be reproduced to within ± 0.2 cps.

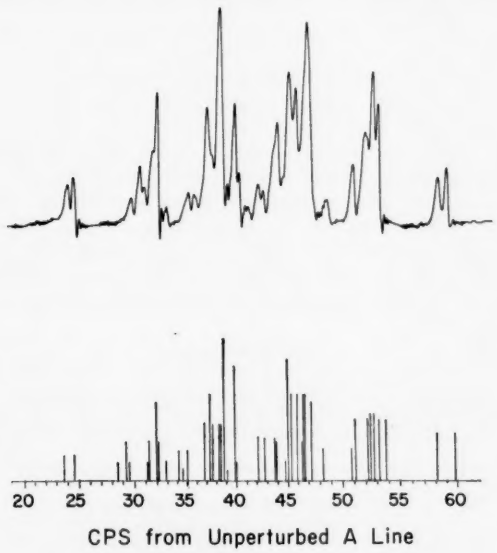

FIG. 5. βCH_2 group, butyronitrile.

The samples were contained in cylindrical sample tubes of 3 mm, i.d. Benzene, sealed in a capillary tube, was then inserted into the sample tube and used as an external reference. Samples were obtained from commercial sources and were of the highest purity.

Measurements were taken on the pure compound and a set of parameters where chosen for J_1, J_2, δ_1, and δ_2 that best fit the perturbation analysis to the measured lines. On the basis of the fit obtained for the predicted spectra to the observed spectra, the accuracies of the assignments made are estimated to be: J_1, J_2, δ_A, $\delta_C=0.2$ cps; $\delta_B=0.3$ cps. Measurements were then taken on 20% and 10% concentrations by volume in carbon tetrachloride and the chemical shifts were calculated on the basis of the assignments made on the pure compound. The results were then linearly extrapolated to zero concentration in carbon tetrachloride. In all cases, the three points fell on the extrapolation line within their experimental accuracy.

It is to be noted that the extrapolation lines for the α, β, and γ protons have different slopes, i.e., the internal shifts in these compounds vary with the concentration in carbon tetrachloride. While the shifts at infinite dilution are to be regarded as the true shifts, the measurements made on the pure compounds will be added for completeness. The results are given in Table II. All values are given in cycles per second at 60 Mc relative to benzene as an external standard.

It should also be pointed out that in some of these compounds several small lines were observed to lie between the β-CH_2 and CH group resonances that could not be accounted for by an analysis of the spectra. It is assumed that these anomalous lines are due to the presence of small amounts of impurities in the sample.

[5] G. V. D. Tiers, J. Phys. Chem. **62**, 1151 (1958).

TABLE II. Data on propyl derivatives.[a]

Substituent	J_1	J_2	Pure compound α-CH_2	Pure compound β-CH_2	Pure compound CH_3	Infinitely dilute in CCl_4 α-CH_2	Infinitely dilute in CCl_4 β-CH_2	Infinitely dilute in CCl_4 CH_3
CH	6.5	7.5	196.1	314.5	351.5	180.3	297.6	334.4
CN	6.7	7.7	266.1	308.3	344.6	252.4	286.5	323.6
COOH	7.5	7.0	272.6	314.0	354.0	251.4	289.4	329.6
C_6H_5	7.5	7.5	271.8	326.4	267.2	234.3	290.6	332.5
$-O-$	6.3	7.5	213.8	319.1	356.9	192.7	297.2	334.2
NO_3^-	6.5	7.6	152.2	312.8	357.9	126.7	283.3	326.7
Br	6.5	7.3	187.3	277.5	328.3	188.6	275.5	325.6
$-S_2-$	7.2	7.5	234.2	290.8	333.7	232.2	287.2	328.4
$-S-$	7.0	7.3	252.4	304.1	340.8	243.9	293.9	329.2
CHO[c] $J_0 \pm 1.6$	7.1	7.6	278.9	324.4	365.9	248.7	290.9	331.1
NH_2	7.0	7.5	252.4	323.8	354.1	232.9	304.4	334.1
NO_2	6.8	7.5	158.4	301.6	362.7	133.3	268.7	327.9
I	7.0	7.2	181.9	262.0	313.2	200.4	277.4	327.5
Cl	6.3	7.4	194.0	295.6	341.8	181.3	281.0	326.3

[a] All values for the chemical shifts are given in cps at 60 Mc relative to benzene as an external standard.
[b] $\delta_1 = (\beta - CH_2) - (\alpha - CH_2)$, $\delta_2 = (CH_3) - (\beta - CH_2)$.
[c] The CHO and $\alpha - CH_2$ protons couple in butyraldehyde. The chemical shift between them is sufficiently large that a first-order approximation to the splitting is accurate. The $\alpha - CH_2$ analysis was made by splitting each transition calculated from the perturbation method into two transitions which were 1.6 cps apart.

DISCUSSION

Certain obvious regularities are present in the chemical shift data for propyl derivatives. The shifts for the α protons are quite similar to those observed for the corresponding α-ethyl protons. The chemical shift of the γ protons is relatively insensitive to the presence of different functional groups at the other end of the chain. The β-propyl shifts are all consistently larger than the β-ethyl shifts.

These points are discussed at greater length in the following paper on the chemical shifts of the alkyl derivatives.

Proton Chemical Shifts for the Alkyl Derivatives*

JAMES R. CAVANAUGH† AND B. P. DAILEY

Department of Chemistry, Columbia University, New York, New York

(Received August 11, 1960)

The chemical shifts of a series of methyl, ethyl, propyl, and isopropyl derivatives have been studied in an effort to determine the distance and angular dependence of any contribution to the chemical shift arising from magnetically anisotropic substituent groups. It was found that electron withdrawal effects play a dominant role in determining the chemical shifts for methyl derivatives. The nearly exactly linear relation of the methyl shifts to electronegativity for the methyl halides seems to rule out any large influence due to magnetic anisotropy. The ethyl shifts were found to be determined by electron withdrawal effects plus a factor which acted equally at the α and β positions. It was found that this factor arises from the carbon-carbon bond. By assigning a chemical shift due to the presence of the C−C bond, which is dependent in size on the substituent attached to the α carbon, the apparently anomalous frequencies observed for the alkyl derivatives can be accounted for. A possible explanation for the C−C bond shift may be regular changes in the paramagnetic term in the Ramsey equation due to changes in the excitation energy denominator when a C−C bond replaces a C−H bond.

INTRODUCTION

UP to now, at least, rather disappointing progress has been made in understanding the chemical shifts, $(-\mathbf{H}\cdot\boldsymbol{\sigma}_N)_N$ observed in high-resolution nuclear magnetic resonance spectra. A general theory of nuclear shielding has been given by Ramsey,[1,2] leading to the equation in approximate form

$$\sigma_N=(e^2/3mc^2)\,V(0)-(4/3\Delta E)\times[0\,|\sum_{jk}\mathbf{m}_j{}^0\cdot(\mathbf{m}_k{}^0/\mathbf{r}_k{}^3)\,|\,0]. \quad (1)$$

In this equation, σ_N is the nuclear magnetic shielding constant at nucleus N, averaged over all molecular orientations, $V(0)$ is the electrostatic potential produced at the nucleus N by all of the molecular electrons, ΔE is an average electronic excitation energy, $\mathbf{m}_j{}^0$ is the angular momentum of electron j about an origin centered on nucleus N. Unfortunately, it is quite difficult to apply this equation to most molecules and while numerous approximate calculations have been made not all of them have been completely successful.

McConnell[3] and Pople[3a] have attempted to divide the contributions to σ_N into those arising from one-center integrals centered on N and proportional to Z_N, the effective nuclear charge of N; and into terms arising from various magnetic anisotropies. It would appear that an equation of the following from

$$\sigma_N=\sigma_{ed}+\sigma_{ep}+\sigma_{an} \quad (2)$$

might be found to describe the behavior of chemical shifts in related series of molecules. Here σ_{ed} is a term proportional to the electron density (and therefore to the effective nuclear charge) of the atom to which the proton N is bounded; σ_{ep} is the paramagnetic term involving electrons surrounding this nucleus, σ_{an} is the long range shielding term dependent on the anisotropy of neighboring groups.

σ_{ep} includes terms arising from the second-order paramagnetic term in the Ramsey equation and from what Pople refers to as the paramagnetic part of the neighbor-anisotropy effect. In Eq. (2) it is assumed that ring current effects for alkyl chains are negligible.

Numerous attempts have been made to fit an equation of the foregoing form to data obtained for series of molecules. In certain cases, correlations have been made between the chemical shift and electron densities, emphasizing the role of the first term in the equation. Dailey and Shoolery[4] have shown the direct dependence of the proton chemical shift as measured in benzene solution of the methyl derivatives and the internal shift of the ethyl derivatives on the electronegativity of the substituent. The methyl derivative shifts, as measured in the infinitely dilute solution of carbon tetrachloride, also have been shown by Allred and Rochow[5] to correlate with the electronegativity of the substituent. However, cases in which there is this agreement appear to be small in number.

The present study represents an attempt to investigate the role of the other two terms in Eq. (2) in a simple series of compounds, namely, the alkyl derivatives. In particular this series offers an opportunity to investigate the distance and angular dependence of any chemical shifts arising from anisotropic substituent groups.

* Supported by grants from the National Science Foundation, the Alfred P. Sloan Foundation, and by the office of Scientific Research, Air Research and Development Command, U. S. Air Force.

† Present Address: Socony Research Laboratories, Paulsboro, New Jersey.

[1] N. F. Ramsey, Phys. Rev. **78**, 699 (1950).

[2] N. F. Ramsey, Phys. Rev. **86**, 243 (1952).

[3] H. M. McConnell, J. Chem. Phys. **27**, 226 (1957); (a) J. A. Pople, W. G. Schneider, and H. J. Bernstein, *High Resolution Nuclear Magnetic Resonance* (McGraw-Hill Book Company, Inc., New York, 1959), pp. 175–183.

[4] B. P. Dailey and J. N. Shoolery, J. Am. Chem. Soc. **77**, 3977 (1956).

[5] A. L. Allred and E. G. Rochow, J. Am. Chem. Soc. **79**, 5361 (1957); (b) Varian Associates, Technical Information Bulletin from the Radio-Frequency Spectroscopy Laboratories of the Instrument Division of Varian Associates, Vol. 2, No. 3.

TABLE I. Chemical shifts of some alkyl derivatives. Shifts to lower field in cps at 60 Mc reference methane.

Substituent	Methyl	Ethyl		Isopropyl		Propyl		
	α	α	β	α	β	α	β	γ
Cl	170*	195**	66**	235*	79*	195	95	50
Br	148*	189*	86*	239*	90*	187	100	50
I	116*	176*	99*	241*	100*	176	99	48
OH	190*	202*	57*	223	56	196	78	42
CN	105*	127	65	147	67	124	89	53
COOH	111*	128	56	140	59	125	87	46
C_6H_5	127*	144*	59*	160*	61*	142	85	44
—O—	181*	189*	55*	200	51	183	79	42
—S—	112*	136	61	162	61	132	82	45
CHO	117*	134	54	130*	54*	127	85	45
NH_2	134	151	52	171*	48*	143	72	42
$—S_2—$		147	67			144	89	48
NO_3^-		256	70	296	69	249	93	49
NO_2	244*	249	81	150*	78*	243	107	48
F	243*							
H	0	38					67	41

EXPERIMENTAL

Details concerning methods of measurement are given in the preceeding paper on the analysis of the propyl group spectra. Included in this paper are data on the ethyl and isopropyl derivatives, some from this laboratory and some collected from other sources.

Ethyl Derivatives

The assignments made for the chemical shifts of the ethyl derivatives were usually made on the basis of a first order approximation, i.e., the center line of the methyl triplet and the average of the two center lines of the CH_2 quartet were chosen as the chemical shifts for the CH_3 and CH_2 groups respectively. In those cases in which these lines were split, the average of the high field lines of the center lines of the CH_2 quartet and the low field line of the center of the methyl triplet were chosen. The results are shown in Table I. These measurements are estimated to be accurate to within ± 0.4 cps. All values are given in cps at 60 Mc with benzene as an external standard. As in the previous paper, the data for both the pure compound and for extrapolation to infinite dilution in carbon tetrachloride are given.

Isopropyl Derivatives

The assignments for the isopropyl derivatives were also made on the basis of a first-order approximation. The center line of the CH septet and the center of the CH_3 doublet were chosen as the chemical shifts of the CH and CH_3 groups respectively. In three cases, only the CH group chemical shift was measured as the CH_3 data were obtained from other sources. These results are given in Table I. All values are given in cps at 60 Mc with benzene as an external standard.

Methyl and Ethyl Amine

Since these compounds were gases at room temperature, the measurements could not be made in the usual way. Also, it was found that the amines reacted with carbon tetrachloride. Therefore, measurements were taken on these compounds as solutions in cyclohexane, with 2% benzene by weight added as an internal standard. In order to conform to the present scale, measurements of several compounds were taken in solutions in cyclohexane and compared to the results in carbon tetrachloride. Though the results vary slightly, depending on what compounds were being compared, the value of -22 cps at 60 Mc was taken as the correction from C_6H_{12} to CCl_4.

Also, the benzene resonance had to be measured as a function of concentration in carbon tetrachloride, in order to relate the internal to the external standard. The extrapolated value is -27.6 cps and the value for 2% is -27.0 cps. The final results for the methyl and ethyl amine are given in Table I. Because of the uncertainties involved, the results are probably no better than ± 2 cps.

Other Data

The data on several hydrocarbons, as measured in solutions in carbon tetrachloride with benzene as external standard are from Varian Associates.[5a] The results are given in Table I.

In the text of the discussion, all data will be given in reference to the chemical shift for methane. In Table I is a complete tabulation of all data used. All values have been rounded off to the nearest cps. The values marked with an asterisk (*) are taken from Tiers.[6] The data of Tiers are converted to the present scale by expressing the results in cps at 60 Mc and subtracting 211 cps. The average deviation of 14 measurements in both scales was 1.1 cps.

The value for ethyl chloride (**) is taken from the data of Bothner-By *et al.*[7] Their data are converted to the present scale by subtracting 997 cps and multiplying by 1.5.

DISCUSSION

Chemical Shifts and Electron Densities

The correlation of the chemical shifts of the methyl derivatives and of the internal shifts of the ethyl derivatives with the electronegativity of the substituent has been demonstrated by Dailey and Shoolery. Their empirically derived formula relates the internal shift of the ethyl derivatives, i.e., $\delta\,CH_3-\delta\,CH_2$, with the Huggin's electronegativity[8] of first atom of the substituent bound to the carbon atom, in the following equation:

$$\text{Electronegativity}=0.01158\delta_{\text{Internal}}+1.71, \qquad (3)$$

where δ is given in cps at 60 Mc.

However, their measurements were carried out on benzene solutions, with the benzene resonance as an internal standard. Consequently, since benzene has been shown to have anomalous dilution effects, their results must be reviewed in the light of measurements made on dilute solutions of these compounds in carbon tetrachloride or as extrapolated to zero concentration in carbon tetrachloride. The methyl derivatives, as measured by Allred and Rochow in the infinitely dilute solution in carbon tetrachloride, still show this excellent correlation. The nitro group is anomalous. The low-frequency position is perhaps due to contributions from resonance structures of the following kind, leading to decreased electron density about the α proton:

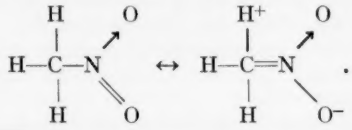

[6] G. V. D. Tiers, "Tables of τ values for a variety of organic compounds" (1958) (privately circulated).

[7] A. A. Bothner-By and C. Naar-Colin, J. Am. Chem. Soc. **80**, 1728 (1958).

[8] M. L. Huggins, J. Am. Chem. Soc. **75**, 4123 (1953).

TABLE II. Internal chemical shift of ethyl derivatives in C_6H_6 and CCl_4 solutions.

Substituent	Internal chemical shift of ethyl group in benzene[a]	Internal chemical shift of ethyl group in CCl_4[a]
Cl	128	129
Br	106	103
I	84	77
OH	154	145
CN	70	62
COOH	74	72
C_6H_5	86	85
—S—	80	75
CHO	78	80
NH_2	110	99
NO_3^-	190	186
NO_2	182	168

[a] Shifts are in cycles per second at 60 Mc between α and β protons in ethyl derivatives.

The proton resonances of the other nitro-alkanes are also anomalous. Since the cause of the deviation is probably due to the double-bond character of the C—N bond, it will not be pertinent to discuss the nitro group in relation to the other derivatives.

The internal shifts of the ethyl derivatives as measured in carbon tetrachloride differ slightly from those measured in benzene. A comparison of the two sets of data is given in Table II. However, the correlation of the internal shifts with the electronegativity of the substitutent is still apparent. A revised Dailey and Shoolery equation may be set up using the new data

$$\text{Electronegativity}=0.0114\delta_{\text{Internal}}+1.78, \qquad (4)$$

where δ is in cps at 60 Mc.

A tabulation of the calculated electronegativities of the substituents is given in Table III and may be compared to the electronegativity values as found from the previous data.

Using this scale of electronegativities, one may set up a relation for the methyl shifts to the electronegativities of the substituent. The following equation relates the chemical shift of the methyl derivatives, using methane as a reference, to the previously found electronegativities:

$$\text{Methyl shift}=100\times\text{electronegativity}-151, \qquad (5)$$

where the shifts are in cps at 60 Mc.

The frequencies calculated from this equation may be compared to the observed frequencies in Table IV. The agreement is excellent.

TABLE III. Electronegativity of substituent groups.

Substituent	Electronegativity this study (calc)	Electronegativity Dailey and Shoolery
Cl	3.25	3.19
Br	2.96	2.94
I	2.66	2.68
OH	3.43	3.51
CN	2.49	2.52
COOH	2.60	2.57
C_6H_5	2.75	2.70
—O—	3.31	...
—S—	2.64	2.64
CHO	2.69	2.61
NH_2	2.91	2.99
$—S_2—$	2.69	...
NO_3	3.90	3.91

Chemical Shift and Magnetic Anisotropy

Equation 2 suggests that in addition to the electron density effects discussed in the preceding section there could also be present long-range effects due to magnetically anisotropic groups. For axially symmetric groups sufficiently distant to permit use of the dipolar approximation, this term has been given by McConnell[3] as

$$\delta_{an}=(\Delta\chi/3R^3)(1-3\cos^2\theta), \qquad (5a)$$

where R is the distance between the nucleus N and the center of the anisotropic group, $\Delta\chi=\chi_{\parallel}-\chi_{\perp}$, and $\chi_{\parallel}$ and $\chi_{\perp}$ are the components of the magnetic susceptibility tensor parallel and perpendicular to the bond axis.

θ is the angle between R and the axis of axial symmetry. For the methyl halides McConnell estimated shifts of ±6(CH_3F), ±18, (CH_3Cl), ±18 (CH_3Br), and ±24 cycles (CH_3I). The presence of an effect, due to magnetic anisotropy, of this size seems unlikely when examining the results of the preceding discussion. Chemical shifts calculated from Eq. (5) for the methyl halides agree with observed shifts to within two or three cycles at most. Since the expected change in anisotropy shift in going from F to I is in the opposite direction to the electronegativity shift and is probably far from linear, the observed linear relation would seem to place, for these molecules, a rather low limit on the shift due to magnetic anisotropy. However in comparing toluene to methyl cyanide, which has the lowest shift of the observed carbon compounds, it is conceivable that the shift of 26 cycles in the methyl resonance does reflect a sizeable anisotropy for the benzene ring.

TABLE IV. Chemical shifts of methyl derivatives calculated from derived electronegativities.

Substituent	Methyl shift calc	Methyl shift obs	Difference
Cl	174	170	+4
Br	145	148	−3
I	115	116	−1
OH	192	190	+2
CN	98	105	−7
COOH	109	111	−2
C_6H_5	124	127	−3
—O—	180	181	−1
—S—	113	112	+1
CHO	118	117	+1
NH_2	140	134	+6
F	239	243	+4

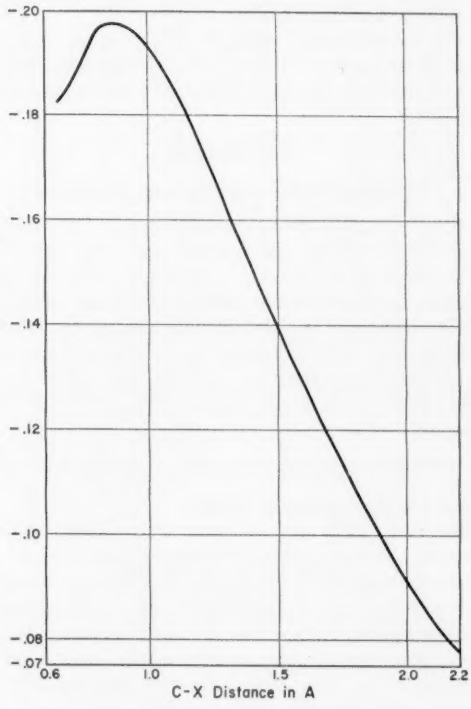

FIG. 1. Geometric factor α proton.

Despite the fact that the internal shifts of the ethyl derivatives correlate very well with the electronegativity of the substituent, the absolute shifts of the α and β protons cannot be explained on this basis alone. Indeed, a plot of the α proton shift vs the electro-

negativity of the substituent shows large deviations from a linear scale. The β proton shifts show no obvious regularities and in fact, the halides show a reversal of the expected trend, i.e., the β proton resonance of ethyl iodide is at the lowest field in the halide series.

In order to evaluate the effect of a magnetically anisotropic distribution in the substituent on the alkyl chain, the value of the geometric factor, $(1-3\cos^2\theta)/R^3$, must be evaluated for the α, β, and γ protons. Figures 1–3 show the results of such calculations for the α, β, and γ protons. It was assumed that the center of the anisotropy could be placed along the carbon-substituent bond and that it was axially symmetric, coaxial with the bond. This assumption is true for the halogens, but not for many of the other

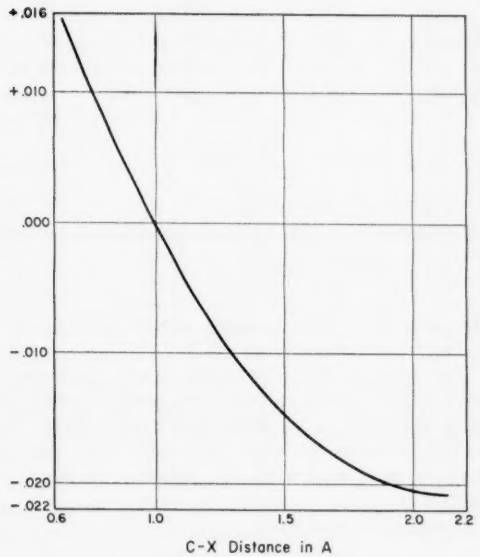

FIG. 2. Geometric factor β proton.

derivatives. The C–X distance is the distance from the α carbon atom to the center of the anisotropy along the carbon-substituent bond. The values are in A^{-3}.

For the β and γ protons, the geometric factor was averaged over the appropriate internal rotations of the molecule, using the freely rotating model. However, for the case of hindered rotation it can be shown that the values for the β proton as shown do not change appreciably. For the γ proton, on the other hand, the values given decrease towards zero as the rotation becomes more and more hindered.

The geometric factors for the α and β protons of ethyl chloride, bromide, and iodide are given in Table V. The three halogens all have electronegativities lower than oxygen and therefore we can assume for the moment that the extra β proton shift in the ethyl halides over diethyl ether is not due to electron with-

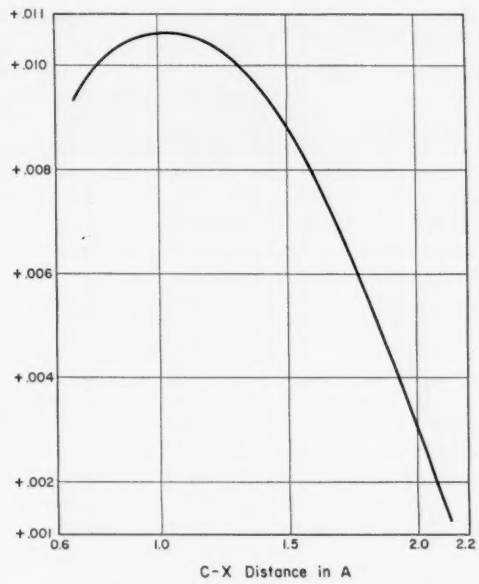

FIG. 3. Geometric factor γ proton.

drawal and may be due to magnetic anisotropy effects. The shifts with respect to β ethyl in diethyl ether are given in column I and the corresponding calculated α proton shifts due to anisotropy are given in column IV. If the methyl shifts of the three halides are corrected by the amounts indicated in column IV, the electron withdrawal shifts for I and Br become negative, while for Cl it is still a sizeable positive quantity. This result is in very poor agreement with the observed linear dependence of the total shift on electronegativity. If the anisotropy of the oxygen in diethyl ether is not negligible as was assumed above, the agreement with experiment becomes even poorer.

It may be objected that the α/β ratio is exaggerated by the use of the dipolar approximation. But since the observed deviation from a linear dependence on electronegativity is less than three cycles, it seems safe to conclude that the behavior of the β proton shifts in these molecules cannot be accounted for solely by

TABLE V. Anisotropy calculations for ethyl halides.

Substituent	I Anisotropy shift for β proton (shift in excess of 55 cycles)	II Geometric factor for β proton	III Geometric factor for α proton	IV Corrections for α proton (I×III/II)
Cl	11	−0.0188	−0.112	66
Br	31	−0.0201	−0.0985	152
I	44	−0.02075	−0.0840	178

TABLE VI. C—C bond shifts.[a]

Substituent	I C—C bond shift in ethyl (α ethyl-α methyl)	II Residual β ethyl shift (β ethyl-*I*)	III (α Isopropyl-α methyl)	IV C—C bond shift in isopropyl (III/2)	V Residual isopropyl shift (β isopropyl-IV)	VI Extra C—C bond shift in β propyl (β propyl-β ethyl)
Cl	25	41	65	33	46	29
Br	41	45	91	46	44	14
I	60	39	125	63	37	0
OH	12	45	33	16	40	21
CN	22	43	42	21	46	24
COOH	17	39	29	15	44	31
C_6H_5	17	42	33	16	45	26
—O—	8	47	19	10	41	24
—S—	24	37	50	25	36	21
CHO	17	37	13	7	47	31
NH_2	17	35	37	18	30	20
$—NO_2$						23
$—S_2—$						22
Av					41	24[b]

[a] All shifts are in cycles per second at 60 Mc.
[b] Does not include iodine value.

involving the electron density and substituent anisotropy terms in Eq. (2).

Chemical Shift and the Carbon—Carbon Bond

One would expect to find for the α-proton shifts in the ethyl derivatives a close correlation with the corresponding methyl shifts. The substitution of a methyl group for a hydrogen should make a roughly constant difference in electron density. The anisotropy shifts, at least on the basis of the above model, should be the same for methyl and α-ethyl protons. Actually, the difference in chemical shift between methyl and α-ethyl as seen in Table VI, is found to be far from constant, ranging from 60 cps for the iodides to 8 cps for the others.

If we make the hypothesis that the extra shift experienced by the α proton arises from the carbon-carbon bond, then the β protons should to first order be equally affected, since the α and β protons are symmetrically placed with respect to the carbon-carbon bond. Assuming that the difference in the methyl and α-ethyl shifts is due to the carbon-carbon bond, in Table VI we present the result of subtracting this difference from the β proton shift. This second difference varies over a moderate range, but its average value for all substituents is 41 cycles, while the corresponding shift for ethane itself is 38 cycles. The implication here is that, when corrected for the extra shift due to the carbon-carbon bond as affected by the various substituents, all of these β-methyl groups have a similar electronic environment.

The chemical shift of both the α and β protons appears to arise from at least two distinct terms, one which includes an electron withdrawal effect (and possibly includes an anisotropy shift also) and one which is associated with the presence of the C—C bond.

Therefore we may write

$$\delta\alpha \text{ ethyl}X = \delta(\text{elect.}\alpha)_X + \delta(\text{C—C})_X,$$

$$\delta\beta \text{ ethyl}X = \delta(\text{elect.}\beta)_X + \delta(\text{C—C})_X. \qquad (6)$$

From this it is obvious why there is the excellent correlation between the methyl derivative shifts and the internal shifts of the ethyl derivatives since there is a contribution from the C—C bond which equally affects both the α and β protons.

If this interpretation is correct, then for the case of the isotropyl derivatives, the change in the α proton in going from methyl to isopropyl should be twice that in going from methyl to ethyl since, now there are two carbon-carbon bonds adjacent to the α proton. That is;

$$\delta\alpha \text{ isopropyl}X - \delta \text{ methyl}X = 2\delta(\text{C—C})_X. \qquad (7)$$

This is exactly what is observed, namely that the change in the α proton in going from methyl to isopropyl is approximately twice the change in going from methyl to ethyl, as can be seen from Table VI. Also, in

Table VI note that the β proton resonances of the ethyl and isopropyl derivatives are approximately the same. This is what is to be expected if the source of the shift is at the carbon-carbon bond, since the β proton is β to the other carbon-carbon bond and would not be expected to change appreciably.

The data on the propyl derivatives can also be explained on this basis. The α proton propyl resonance is approximately the same as for the α proton of the ethyl derivatives, indicating that the addition of a methyl group to the β carbon does not greatly affect the α position. Also, the γ proton resonances of all the substituents are at approximately the same frequency, as is expected since the γ proton is three bond lengths removed from the substituent. On the other hand, the β proton experiences a down-field shift that is roughly constant for all substituents, the average value of which is 24 cps. The value for the iodide is anomalous. These results are also shown in Table VI.

Thus, the shift for the β proton in the propyl derivatives may be written

$$\delta\beta \text{ propyl}X = \delta \text{ ethane} + \delta(\text{C—C})_X + \delta(\text{C—C})_{\text{const}}, \quad (8)$$

where $\delta(\text{C—C})_{\text{const}}$ is an extra contribution from the added C—C bond, which is the same for all substituents. That the value for the contribution from this carbon-carbon bond is constant for all substituents is consistent with this interpretation since the "substituent" at the β carbon is in all cases the α carbon of the propyl chain. The value of 24 cps for this (C—C) bond shift is to be compared to the 26 cps for the internal shift in propane. In that case, the β proton sees the effect of two carbon-carbon bonds, whereas the α protons see only one.

It is probably true that the C—C bond shifts obtained above include effects due to changes in electron density. The effective formal charge on the α carbon of an ethyl derivative should be somewhat smaller than for the corresponding methyl derivative and because of a small electron withdrawal effect the effective charge on the β carbon should be larger than in ethane. In general these changes are difficult to estimate but a procedure is available for doing so approximately in the alkyl halides. Smith *et al.*[9,10] have derived a set of empirical parameters which reproduce the molecular dipole moments in terms of the effective charges calculated for the various atomic positions. The effective charges for the carbon atoms in the ethyl, isopropyl and propyl halides are given in Table VII, as calculated by Dailey.[11]

The assumptions necessary to obtain this set of charges are such as to give little reason to believe that they are correct and accurate in detail. However, their agreement with dipole moment and nuclear quadrupole coupling data is excellent and it seems probable that they give a correct qualitative picture of the charge distribution in these molecules.

Using the ratio of the methyl chemical shift to the methyl effective charge the effective charge data can be used to calculate shifts due to the electron density term alone. Subtracting these from the observed shifts should give the corrected C—C bond shift for these molecules, which should be approximately constant for all molecules containing the same halogen substituent. An inspection of Table VII shows that with one or two exceptions the derived C—C bond shifts are reasonably constant.

Also, there is probably a small residual electron withdrawal effect present at the γ carbon in the propyl derivatives. From the effective charge data for the halides, 8, 7, and 5 cps are estimated to be the effect for the γ protons in the propyl chloride, bromide, and iodide respectively. Note that the average shift of the γ proton resonances for all substituents is 6 cps from the methyl resonance in propane.

Origin of the C—C Bond Shift

It has been suggested by Bothner-By[12] that the C—C bond shifts observed in hydrocarbon spectra were due to the magnetic anisotropy of the bond. It was shown that the chemical shifts observed in cyclopentane, cyclohexane and numerous other hydrocarbons could be accounted for in terms of a large anisotropy for the C—C bond. Narasimhan and Rogers[13] have made calculations on the internal chemical shift in propane which indicate that a molar anisotropy of at least 4.1 ppm for the C—C bond would be required. Since the theoretical results of Tillieu[14] gave a value for the C—C bond of 1.2 ppm they rejected this explanation as implausible. It would be even more difficult to account for the very large increase in the C—C bond shift due to the presence of an iodine atom. It would appear that some factor other than magnetic anisotropy is making a major contribution to the C—C bond shift.

It is interesting to point out that the effect of the carbon-carbon bond in changing from methyl to ethyl as dependent on the substituent group can be related to the size of the substituent. In Table VIII the cube of the van der Waals radius for the first atom in the substituent group has been multiplied by the constant 5.4. The results for all substituents yield values that are very nearly equal to the α proton shift in changing from the methyl to the ethyl derivative.

Because of their similar direction and dependence on distance along the chain it does not seem possible to

[9] R. P. Smith, T. Ree, J. L. Magee, and H. Eyring, J. Am. Chem. Soc. **73,** 2263 (1951).
[10] R. P. Smith and E. M. Mortensen, J. Am. Chem. Soc. **78,** 3932 (1956).
[11] B. P. Dailey, J. Chem. Phys. **33,** 1641 (1960).
[12] A. A. Bothner-By and C. Naar-Colin, Ann. N. Y. Acad. Sci. **70,** 833 (1958).
[13] P. J. Narasimhan and M. J. Rogers, J. Chem. Phys. **31,** 1302 (1959).
[14] J. Tillieu and J. Guy, J. Chem. Phys. **24,** 1117 (1956).

TABLE VII. Effective charges and chemical shifts for alkyl halides.

I		II	III	IV	V
Ratio methyl shift to effective charge	Derivative	Effective charge (statcoulombs $\times 10^{-10}$) on adjacent carbon	Electron withdrawal shift (I×II)	Actual Shift	C—C bond shift (IV–III)
Cl 239	α proton ethyl	+0.65	155	195	40
	β proton ethyl	+0.15	36	66	30
	α proton propyl	+0.65	155	195	40
	α proton isopropyl	+0.60	143	235	(92)46
	β proton isopropyl	+0.14	33	79	46
	β proton propyl	+0.14	33		
	γ proton propyl	+0.03	8		
Br 235	α ethyl	+0.58	136	189	53
	β ethyl	+0.14	33	86	53
	α propyl	+0.57	134	187	53
	α isopropyl	+0.53	125	239	(114)57
	β isopropyl	+0.13	31	90	59
	β proton propyl	+0.13	31		
	γ proton propyl	+0.03	7		
I 219	α ethyl	+0.51	112	176	64
	β ethyl	+0.12	26	99	73
	α propyl	+0.49	107	176	69
	α isopropyl	+0.46	101	241	(140)70
	β isopropyl	+0.11	24	100	76
	β proton propyl	+0.11	24		
	γ proton propyl	+0.02	5		

TABLE VIII. C—C bond shift calculated from van der Waals radius.

Substituent	van der Waals Radius in A	5.4 R^3	Change in α proton methyl-ethyl	Difference
Cl	1.80	31	25	−6
Br	1.95	39	41	−2
I	2.15	54	61	−7
OH	1.40	15	12	+3
CN	1.6	22	25	−3
COOH	1.6	22	17	+5
C_6H_5	1.6	22	17	+5
—O—	1.40	15	8	+7
—S—	1.85	33	24	+9
CNO	1.6	22	17	+5
NH_2	1.5	18	17	+1
CH_2X	1.6	22	25	−3

separate electron withdrawal effects from the residual influence of magnetic anisotropy. Still, the question of the size of this anisotropic shift is of great interest. The calculations of the distance and angular dependence of the anisotropic shifts reported here may be criticized because use was made of the dipolar approximation. The calculations of Johnson and Bovey[15] are not subject to this criticism although in applying their results to alkyl chains they had some difficulty with averaging over hindered internal rotation. They obtained a ratio of α to β shifts of 2.4 with a calculated ring current shift of 48 cycles for a proton α to a benzene ring and 20 cycles for a proton β to a benzene ring.

The chemical shift data for the α protons in ethyl and isopropyl benzene seem to clearly indicate the presence of a C—C bond shift. If the β-proton shifts for these two molecules are corrected for the C—C bond shift they become 42 cycles for ethyl benzene and 45

[15] C. E. Johnson, Jr., and F. A. Bovey, J. Chem. Phys. **29**, 1012 (1958).

cycles for isopropyl benzene (cumene). These figures allow a maximum of 5 cycles for the anisotropy "ring current" shift which is only one-fourth the calculated amount. Similar results are obtained for the β position in propyl benzene.

This makes it appear now that the supposed agreement of Johnson and Bovey's results with the observed data on alkyl benzenes is no longer valid and suggests that their calculations represent an appreciable overestimate of the ring current effect.

CONCLUSIONS

There can be little doubt that electron withdrawal effects play a dominant role in the chemical shifts of the methyl derivatives. The correlation of these shifts with electronegativities is almost within experimental error. This nearly exactly linear relation for the methyl halide chemical shifts as a function of electronegativity seems to rule out any large influence due to the magnetic anisotropy of the carbon-halogen bond since this would have the opposite trend with increasing atomic size. The excellent correlation of the internal shifts of the ethyl derivatives with the electronegativity of the substituents and with the methyl derivative shifts seems to indicate that the α and β shifts in the ethyl derivatives are determined by electron withdrawal effects plus some effect which acts equally at both positions.

The results of this study indicate that this factor arises from the carbon-carbon bond. By attributing a chemical shift arising in some fashion from the presence of the C—C bond, which is dependent in size on the substituent attached to the α carbon, the apparently anomalous frequencies of both the α and β protons of the ethyl derivatives can be accounted for. The analogous role of the C—C bond in the propyl and isopropyl derivatives is also indicated by the data obtained for these compounds. It does not seem possible to account for these chemical shifts simply in terms of electron withdrawal and the magnetic anisotropy of the substituent. It is unlikely that this conclusion would be changed if more elaborate calculations of the anisotrophy shift were to be made.

The question of the origin of the C—C bond shift and the role of the substituent in determining its magnitude remains to be answered. It has been suggested that the C—C bond shift arises in the magnetic anisotropy of the bond and it has been shown that this is in agreement with the spectra of the hydrocarbons. However it is difficult to reconcile this idea and the large values for the C—C bond shift observed for the halide substituents, with the small theoretically calculated value for the C—C bond magnetic anisotropy, and the apparently small role of anisotropy in determining the shifts of the methyl derivatives.

Another possible explanation might be a change in the paramagnetic term in the chemical shift σ_{ep} in Eq. (2) involving the excitation energy denominator caused by the substitution of a C—C bond for a C—H bond. This is a change which could be strongly influenced by the presence of a substituent and yet which might display most of the regularities observed in this study for the C—C bond shift.

Regardless of the correct theoretical explanation, the results of this study seem to establish the C—C bond shift as a new empirical regularity in the study of chemical shifts in NMR spectra.

Calculation of Complex Equilibrium with an Unknown Number of Phases

R. H. Boll

The Babcock & Wilcox Company, Research Center, Alliance, Ohio

(Received September 12, 1960)

An extension of Brinkley's generalized procedure is proposed for calculating the equilibrium compositions of complex systems in which several phases are possible but their actual number and identities at equilibrium are not known *a priori*. In contrast to other methods, the present method eliminates the trial and error associated with presence or absence of phases. Thus, little computational effort is required beyond that expended when the number and identities of all phases are known. The essential equations are given together with a description of the computational procedure.

INTRODUCTION

A NUMBER of methods [1–10] are available for calculating the equilibrium composition of a gas containing many constituents. Most of them might be extended to include the presence of condensed phases, and several [2,4,7,9,10] have been. However, the extensions require an initial assumption as to which phases are present. The correctness of this assumption is determined only after an iterative computation has been converged. If wrong, a new assumption must be made and the computation repeated.

Such procedures encounter one or both of two difficulties when applied to cases where several condensed phases are possible but the actual presence of each is not known *a priori*. The first is the expenditure of considerable computer time and programming effort, for the number of different initial assumptions increases very rapidly with the number of possible condensed phases. The second is that a change in the identity of the phases assumed to be present may demand a change in the set-up of the problem,[2,4,7] which is at least awkward and, on some machines, time consuming or impossible. The present purpose is to describe a simple modification of Brinkley's method[1,2] which surmounts both of these difficulties, yet requires very little additional computation.

METHOD

The present method is built upon Brinkley's derivations[1,2] and most of its equations are his. The essential departure lies in writing one set of equilibrium conditions as inequalities rather than equalities. Except where new symbols are needed for the modification, Brinkley's[2] nomenclature is used throughout. A complete tabulation is provided at the end of the text.

If the kth phase in an equilibrium mixture is correctly assumed to be absent, then the equilibrium composition will lead to

$$\sum_{j=1}^{c} N_j^{(k)} + \sum_{i=c+1}^{s} N_i^{(k)} = \sum_{j=1}^{c} x_j a_{jk} + \sum_{i=c+1}^{s} x_i a_{ik} < 1. \quad (1)$$

If the kth phase is incorrectly assumed to be absent, then

$$\sum_{j=1}^{c} x_j a_{jk} + \sum_{i=c+1}^{s} x_i a_{ik} > 1. \quad (2)$$

Account may be taken of this circumstance by writing the G_k-equilibrium condition as

$$1 - \sum_{j=1}^{c} x_j a_{jk} - \sum_{i=c+1}^{s} x_i a_{ik} = G_k(x_1, \cdots x_j, \cdots x_c) \geq 0, \quad (3)$$

instead of $G_k = 0$ as Brinkley has it.

The problem is set up as though all p phases were to be present. Since the value of $G_k^{(r)}$ depends only upon the rth set of values x_j it is a relatively simple matter to temporarily eliminate (in effect) any phase (k) on the $(r+1)$ approximation if $G_k^{(r)} > 0$. If $G_k^{(r)} \leq 0$, the kth phase is present, at least for the $(r+1)$th approximation, and the treatment proceeds according to Brinkley. Thus, tests for the presence of the various phases may be included within the secondary (Newton-Raphson) iteration loop, and the final composition will then include the correct phases.

Exactly how this procedure works is indicated by the following equations and outline of computational steps. The relationships and steps which differ from Brinkley[2] are indicated by an asterisk.

Equilibrium Conditions

$$F_j(x_j; n^{(k)}) = 0, \qquad j = 1, 2, \cdots c, \quad (4)$$

$$G_k(x_j) \geq 0, \qquad k = 1, 2, \cdots p. \quad (5)^*$$

[1] S. R. Brinkley, Jr., J. Chem. Phys. **14**, 563 (1946).
[2] S. R. Brinkley, Jr., J. Chem. Phys. **15**, 107 (1947).
[3] F. J. Krieger and W. B. White, J. Chem. Phys. **16**, 358 (1958).
[4] H. J. Kandiner and S. W. Brinkley, Jr., Ind. Eng. Chem. **42**, 850 (1950).
[5] V. N. Huff, S. Gordon, and V. E. Morrell, Natl. Advisory Comm. Aeronaut. Rept. 1037 (1951).
[6] W. B. White, S. M. Johnson, and G. B. Dantzig, J. Chem. Phys. **28**, 751 (1958).
[7] D. S. Villars, J. Phys. Chem. **63**, 521 (1959).
[8] S. R. Goldwasser, Ind. Eng. Chem. **51**, 595 (1959).
[9] R. L. Potter and W. Vanderkulk, J. Chem. Phys. **32**, 1304 (1960).
[10] F. P. Boynton, J. Chem. Phys. **32**, 1880 (1960).

Definitions

$$F_j = q_j - x_j \sum_{k=1}^{p} a_{jk} n^{(k)} - \sum_{i=c+1}^{s} \nu_{ij} x_i \sum_{k=1}^{p} a_{ik} n^{(k)}, \tag{6}$$

$$G_k = 1 - \sum_{j=1}^{c} x_j a_{jk} - \sum_{i=c+1}^{s} x_i a_{ik}, \tag{7}$$

$$a_{jk} = K_j^{(k,k_j)} f_i^{(k_j)} / f_j^{(k)}, \tag{8}$$

$$a_{ik} = K_i^{(k,k_i)} f_i^{(k_i)} / f_i^{(k)}, \tag{9}$$

$$x_i = b_i \prod_{j=1}^{c} x_j^{\nu_{ij}}, \tag{10}$$

$$b_i = K_i \prod_{j=1}^{c} [f_j^{(k_j)}]^{\nu_{ij}} / f_i^{(k_i)}, \tag{11}$$

$$N_j^{(k)} = a_{jk} x_j, \tag{12}$$

and

$$N_i^{(k)} = a_{ik} x_i. \tag{13}$$

Newton-Raphson Linearization

$$\left[\begin{array}{c|c} A_{jj'}^{(r)} & B_{jk'}^{(r)} \\ \hline \bar{B}_{kj'}^{(r)} & C_{kk'}^{(r)} \end{array}\right] \left[\begin{array}{c} h_{j'}^{(r)} \\ \hline g_{k'}^{(r)} \end{array}\right] = \left[\begin{array}{c} F_j^{(r)} \\ \hline G_k^{(r)} \end{array}\right] \tag{14}*$$

$$A_{jj'} = x_j \delta_{jj'} \sum_{k=1}^{p} a_{jk} n^{(k)} + \sum_{i=c+1}^{s} \nu_{ij} \nu_{ij'} x_i \sum_{k=1}^{p} a_{ik} n^{(k)}, \tag{15}$$

$$B_{jk'} = B_{jk}, \tag{16}$$

$$B_{jk} = x_j a_{jk} + \sum_{i=c+1}^{s} \nu_{ij} x_i a_{ik}, \tag{17}$$

$$\left.\begin{array}{lll} \bar{B}_{kj'} = B_{jk}, & & k = 1, 2, \cdots p_0 \\ \bar{B}_{kj'} = 0, & G_k > 0 & \\ \bar{B}_{kj'} = B_{jk}, & G_k \leq 0 & \end{array}\right\}, \quad k = p_0+1, p_0+2, \cdots p \tag{18}*$$

$$\left.\begin{array}{lll} C_{kk'} = 0, & & k = 1, 2, \cdots p_0 \\ C_{kk'} = \delta_{kk'}, & G_k > 0 & \\ C_{kk'} = 0, & G_k \leq 0 & \end{array}\right\}, \quad k = p_0+1, p_0+2, \cdots p$$

$$k, k' = 1, 2, \cdots p; \quad j, j' = 1, 2, \cdots c. \tag{19}*$$

$$x_j^{(r+1)} = x_j^{(r)} (1 + \lambda h_j^{(r)}), \tag{20}$$

and

$$[n^{(k)}]^{(r+1)} = [n^{(k)}]^{(r)} + \lambda g_k^{(r)}. \tag{21}$$

Outline of Computational Procedure

In the following it is understood that the indices, j, i, and k, take on their full range of values: $j = 1, 2, \cdots c$; $i = c+1, c+2, \cdots s$; $k = 1, 2, \cdots p$, except as noted.

(1) Read in data: q_j, ν_{ik}, $K_j^{(k,k_j)}$, $K_i^{(k,k_i)}$, K_i, $f_j^{(k)}$, $f_i^{(k)}$.

(2) Read in initial assumption: x_j, $n^{(k)}$.

(3) Calculate: $N_j^{(k)}$, $N_i^{(k)}$ via Eqs. (8)–(13).

(4) Calculate: F_j, G_k via Eqs. (6) and (7).

(5)* Test: $G_k > 0$?, $k = p_0+1$, p_0+2, $\cdots p$; if yes, set $n^{(k)} \leftarrow 0$, $G_k \leftarrow 0$.

(6) Test convergence; if converged, print $N_j^{(k)}$, $N_i^{(k)}$, $n^{(k)}$ and stop.

(7)* Calculate: $A_{jj'}$, $B_{jk'}$, $\bar{B}_{kj'}$, $C_{kk'}$ via Eqs. (15)–(19).

(8) Solve Eqs. (14) for: $h_{j'}^{(r)}$, $g_{k'}^{(r)}$.

(9)* Set $\lambda \leftarrow 1$.

(10) Calculate: $x_j^{(r+1)}$, $[n^{(k)}]^{(r+1)}$ via Eqs. (20) and (21).

(11)* Test: is any $x_j^{(r+1)}$ or $[n^{(k)}]^{(r+1)}$ negative? If yes, set $\lambda \leftarrow \frac{1}{2}\lambda$ and return to step (10). If no, return to step (3).

DISCUSSION

Equations (18) and (19) and steps (5) and (7) have the effect of eliminating from consideration the phases whose absence is indicated. Excluding the phases known to be present ($k = 1, 2, \cdots p_0$) from the G_k tests and conditions, Eqs. (18) and (19), may not be essential, for even if a k_j phase were eliminated ($n^{(k_j)} = 0$), there would be no reason why a fictitious value for the corresponding x_j might not be computed and used in the continuing computation. As is, however, there is no possibility that a known phase will be even temporarily eliminated, and faster convergence should result.

The linear Eqs. (14) may be solved by several procedures.[11] Computing time might be shortened in some cases if the equations corresponding to absent phases were completely, instead of only partially, eliminated. However, the partial elimination, Eqs. (18) and (19) and step (5), has the advantage that exactly the same procedure can be applied regardless of the number of identity of phases considered present on any given iteration. Thus, the detailed machine program is shortened.

The factor λ in Eqs. (20) and (21) and steps (9) and (11) is introduced to guard against negative values of x_j in case any x_j becomes small in comparison with the corresponding q_j. Negative values, x_j can cause the computation to diverge or, if free-energy values and $\ln x_j$ are used to calculate the x_i, to stop.

The computational procedure outlined here embraces Brinkley's[2] "secondary iteration" only. Where activity coefficients, $f_j^{(k)}$ and $f_i^{(k)}$, vary with concentration, his "primary iteration" can be superimposed.

We have successfully used a specialized version of this general procedure to obtain the equilibrium concentrations of minor constituents in the combustion gas

[11] K. S. Kunz, *Numerical Analysis* (McGraw-Hill Book Company, Inc., New York, 1957), Chap. 10.

of power boilers.[12] The system amounted to the seven-component COHNSClNa system. The gas phase contained about 30 constituents (including components) and five possible condensed phases, Na_2O, NaCl, NaOH, Na_2SO_4, and Na_2CO_3, were considered. The gas was assumed to be ideal and the condensed phases pure. The detailed program was written for an IBM–650. It required 15 to 30 min running time per case, depending upon the temperature and fuel-air ratio.

NOMENCLATURE

$A_{jj'}$ = element of matrix = $x_{j'}(\partial F_j/\partial x_{j'})$
a_{jk} = modified phase equilibrium constant for the distribution of jth component between the kth phase and the representative, k_jth, phase
a_{ik} = same as a_{jk} but for the ith constituent
$B_{jk'}$ = element of matrix
$B_{kj'}$ = element of matrix.
$B_{jk} = \partial F_j/\partial n^{(k')} = x_{j'}(\partial G_k/\partial x_{j'})$
b_i = modified chemical equilibrium constant for the reaction forming the ith constituent in its representative phase (k_ith) from components in their respective (k_jth) phases.
$C_{kk'}$ = element of matrix. When $G_k \leq 0$, is equal to $\partial G_k/\partial n^{(k')} = 0$,
c = number of components.
F_j = function defined by Eq. (6).
$f_i^{(k)}$ = activity coefficient for ith constituent in kth phase.
$f_j^{(k)}$ = same as $f_i^{(k)}$, but for jth component.
G_k = function defined by Eq. (7).
$g_k^{(r)}$ = correction to be applied to $[n^{(k)}]^{(r)}$ to obtain $[n^{(k)}]^{(r+1)}$.
$h_j^{(r)}$ = correction to be applied to $x_j^{(r)}$ to obtain $x_j^{(r+1)}$.
i = index for constituents; ranges from $c+1$ to s.
j, j' = index for components; ranges from 1 to c.
$K_j^{(k,k_j)}$ = phase equilibrium constant for the reaction forming the jth component in the kth phase from the jth component in the k_jth phase = $\exp(-\Delta F^0/RT)$.
$K_i^{(k,k_i)}$ = same as $K_j^{(k,k_j)}$, but for the ith constituent.
K_i = chemical equilibrium constant for the reaction forming the ith constituent in its representative phase (k_ith) from components in their representative phases (k_jth) = $\exp(-\Delta F^\circ/RT)$.
k, k' = index for phases; ranges from 1 to p.
$N_j^{(k)}$ = mole fraction of jth component in kth phase.
$N_i^{(k)}$ = mole fraction of ith constituent in kth phase.
$n^{(k)}$ = total number of moles in kth phase.
p = number of possible phases.
p_0 = number of phases whose presence is certain.
q_j = number of moles of the jth component if the mixture were to contain only components.
R = universal gas constant.
s = number of molecular species in equilibrium mixture.
T = temperature.
$x_i = N_i^{(k_i)}$ = mole fraction of ith constituent in its representative phase.
$x_j = N_j^{(k_j)}$ = mole fraction of jth component in its representative phase.
ν_{ij} = coefficient of the jth component in the chemical reaction forming one mole of the ith constituent from components.
$\delta_{jj'}$, $\delta_{kk'}$ = Kronecker delta.
λ = "overshoot" protection parameter.

Superscripts

(k) = kth phase.
(k_i) = representative phase for the ith constituent.
(k_j) = representative phase for the jth component.
(r) = evaluated according to the rth approximation to the equilibrium composition.
$(r+1)$ = pertaining to the $(r+1)$th approximation to the equilibrium composition.

[12] R. H. Boll and H. C. Patel, "The Role of Chemical Thermodynamics in Analyzing Gas-Side Problems in Boilers. Part I. Minor Constituents of Gas", presented at the Winter Annual Meeting of the ASME, New York, November 27–December 2, 1960.

Changes in the Electronic Transitions of Aromatic Hydrocarbons on Chemical Substitution. I. Perturbation Theory for Substituted Cyclic Polyenes* †

JOHN PETRUSKA‡

Laboratory of Molecular Structure and Spectra, University of Chicago, Chicago, Illinois

(Received October 24, 1960)

General formulas are derived by first- and second-order perturbation theory for the changes in the transition moment, transition probability, and frequency of aromatic cyclic-polyene transitions produced by ideal chemical substitutions. The changes are described in terms of the interactions of three kinds of prototype electronic states: *carbon-ring* states, *substituent* states, and *charge-transfer* states. The interaction of the ring states with one another is regarded as an inductive effect of substitution; the interaction with the substituent and charge-transfer states, as a conjugative effect. Using the symmetry properties of the prototype states and assuming that the interactions are caused by a sum of perturbation operators for the individual of substituents, it is shown how the changes depend on the nature, the number, and the positions of the substituents on the ring. Formulas pertaining to the singlet-singlet pi-electronic transitions in benzene are given.

INTRODUCTION

THIS series of studies concerns the effects of chemical substitution in aromatic hydrocarbons on the electronic transitions associated with the visible and near-ultraviolet absorptions. As is well known from comparisons of the absorption spectra of aromatic-hydrocarbon derivatives, each transition of the parent hydrocarbon changes in intensity and shifts in frequency in a characteristic manner as a function of the nature, the number, and the positions of the substituents. The purpose of these studies is to show how the behavior of the intensity changes and frequency shifts may be described and interpreted for certain types of aromatics on the basis of some theoretical properties of the electronic states involved.

Incorporating ideas of Sklar,[1] Platt,[2] Moffitt,[3] and Murrell and Longuet-Higgins,[4] we assume that in general three kinds of prototype electronic states are involved in the transitions in the substituted hydrocarbon: (a) *carbon-framework* states characteristic of the carbon framework in the parent hydrocarbon, (b) *substitutent* states characteristic of the substituents in their hydrides, and (c) *charge-transfer* states resulting from electron transfer between the carbon framework and the substituents. The parent-hydrocarbon transitions, which initially occur between the ground and excited carbon-framework states, are considered to change as a result of certain interactions of the carbon-framework states with one another and with the substituent and charge-transfer states.

In the event of relatively weak interactions a perturbation-type approach is adopted; it is supposed that the cause of the interactions is some substituent perturbation operator P associated with the difference between the carbon-substituent bonds and the original carbon-hydrogen bonds. To the extent that the carbon-substituent bonds are independent of one another, P for polysubstitution is regarded as a sum of perturbation operators for monosubstitution.

Paper I deals with weak interactions in the case of highly symmetrical, aromatic *cyclic polyenes* of general formula $C_{4N+2}H_{4N+2}$ (where N is an integer). The main objectives here are twofold: (a) to show how for ideal substituted cyclic polyenes, the perturbation matrix elements for polysubstitution are related to those for monosubstitution as a consequence of the symmetry properties of the prototype states and (b) to derive the resultant general first- and second-order perturbation formulas for the changes in the transition moment, the transition probability (intensity), and the frequency of the cyclic-polyene transitions.

In paper II[5] the perturbation formulas are applied to the near-ultraviolet absorption spectra of benzene ($N=1$) derivatives. Here the chief aims are (a) to show which terms in the formulas are important for the 2600-, 2050-, and 1850-A transitions of benzene, (b) to determine for which range of chemical substitution in benzene the formulas are applicable, (c) to evaluate some substituent perturbation parameters from the observed intensity changes and frequency shifts, and (d) to interpret the empirical values in the light of theoretical expectations.

Paper III[6] extends these considerations to the aromatic ring systems of general formula $C_{4N+2}H_{2N+4}$, known as *catacondensed* hydrocarbons, which include the polyacenes and their isomers. These hydrocarbons, having the same number of carbons as the cyclic poly-

* This work was supported by a Shell Oil Fellowship.

† Part of a Ph.D. dissertation presented to the University of Chicago, 1960.

‡ Present address: California Institute of Technology, Pasadena, California.

[1] A. L. Sklar, J. Chem. Phys. **7**, 984 (1939); **10**, 135 (1942); Revs. Modern Phys. **14**, 232 (1942).

[2] J. R. Platt, J. Chem. Phys. **19**, 263 (1951).

[3] W. Moffitt, J. Chem. Phys. **22**, 320 (1954).

[4] J. N. Murrell and H. C. Longuet-Higgins, Proc. Phys. Soc. (London) **A68**, 329, 601, 969 (1955).

[5] J. Petruska, J. Chem. Phys. **34**, 1120 (1961).

[6] J. Petruska, J. Chem. Phys. **34**, (to be published).

enes of paper I, are regarded as *crosslinked* derivatives of the cyclic polyenes obtained by replacing $N-1$ pairs of hydrogens by $N-1$ carbon-carbon bonds. Following Platt[7] and Moffitt,[3] it is assumed that their carbon-framework states are derived from the carbon-ring states of the parent cyclic polyenes. The changes in the catacondensed-hydrocarbon transitions on chemical substitution are then treated as changes in the parent cyclic-polyene transitions produced by substituent *plus* crosslink perturbations.

Strong interactions, for which the first- and, second-order perturbation formulas break down, are discussed in paper IV.[8]

BASIC THEORETICAL CONSIDERATIONS

In the hypothetical aromatic cyclic polyenes of general formula $C_{4N+2}H_{4N+2}$ the $4N+2$ carbons may be considered to lie equally spaced on the circumference of a circle; the $4N+2$ hydrogens, to lie on the same radii as the carbons, equally spaced on the circumference of a somewhat larger concentric circle. For convenience, let the carbons and symmetry axes of the carbon ring be labeled as shown for the one real cyclic polyene of this type, benzene ($N=1$), in Fig. 1. Then, $m=0, 1, \cdots, 4N+1$ numbers the carbons in order on going clockwise around the ring; X is the twofold axis passing through carbons 0 and $2N+1$; Y is the twofold axis bisecting the bond between carbons N and $N+1$ and the bond between carbons $3N+1$ and $3N+2$; Z is the $(4N+2)$ fold axis normal to the plane of the ring; and X_m is the twofold axis through m corresponding to X rotated clockwise about Z by the angle $m\rho$, where $\rho=\pi/(2N+1)$.

In *ideal* substituted derivatives of these cyclic polyenes let it be assumed that the carbon ring remains undistorted and that the substituent replacing the hydrogen at m is symmetric with respect to (w.r.t.) reflection in the XY and X_mZ planes. Also, suppose that the carbon-substituent bonds are the same for polysubstitution as for monosubstitution, i.e., there is no interaction between the substituents. Then, regarding the prototype state functions and the substituent perturbation operator P for polysubstitution, we note that (a) the state functions have certain properties associated with the symmetries of the carbon ring and the substituents and (b) the operator P is of the form

$$P=\sum_m P_m, \tag{1}$$

where P_m, the monosubstitution perturbation operator for the substituent at m, is symmetric w.r.t. reflection in XY and X_mZ.

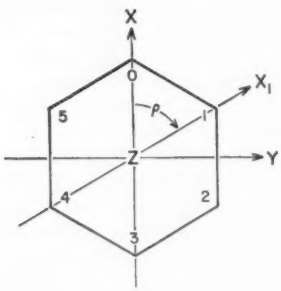

FIG. 1. Labeling of carbons and symmetry axes for the benzene ring.

Symmetry Properties of the Prototype States

Consider the prototype state functions $\mathfrak{R}$ describing the various electronic states of the carbon ring. The ring being symmetric w.r.t. reflection in XZ, rotation about Z by $m\rho$, and reflection in XY, these functions have the following properties in accordance with group theory[9]: (a) they are expressible in (real) forms $\mathfrak{R}_a$ and $\mathfrak{R}_b$ that are symmetric and antisymmetric, respectively, w.r.t. reflection of the ring in XZ; (b) they are also expressible in equivalent "rotated" forms $\mathfrak{R}_{m,a}$ and $\mathfrak{R}_{m,b}$ (corresponding to $\mathfrak{R}_a$ and $\mathfrak{R}_b$ rotated clockwise about Z by $m\rho$) that are symmetric and antisymmetric, respectively, w.r.t. reflection of the ring in X_mZ; and (c) they are either symmetric or antisymmetric w.r.t. reflection in XY.

From group theory it is known that $\mathfrak{R}_{m,a}$ and $\mathfrak{R}_{m,b}$ are related to $\mathfrak{R}_a$ and $\mathfrak{R}_b$ by

$$\begin{vmatrix}\mathfrak{R}_{m,a}\\ \mathfrak{R}_{m,b}\end{vmatrix}=\begin{vmatrix}\cos(M m\rho) & \sin(M m\rho)\\ -\sin(M m\rho) & \cos(M m\rho)\end{vmatrix}\begin{vmatrix}\mathfrak{R}_a\\ \mathfrak{R}_b\end{vmatrix}, \tag{2}$$

where M is a whole number in the range 0 to $2N+1$. The value of M is determined by the number of *radial* nodal planes normal to the ring in $\mathfrak{R}_a$ and $\mathfrak{R}_b$, i.e., by the ring quantum number for $\mathfrak{R}_a$ and $\mathfrak{R}_b$. Specifically, $M=0, 1, 2, \cdots, 2N+1$ when there are $(4N+2)n$, $|(4N+2)n\pm1|$, $|(4N+2)n\pm2|$, $\cdots$, $|(4N+2)n\pm(2N+1)|$ radial nodal planes, respectively (where n may have the values 0, 1, 2, $\cdots$). From Eq. (2) it is apparent that the ring states are *nondegenerate* if $M=0$ or $2N+1$ but *twofold degenerate* if $M=1, 2, \cdots, 2N$. In the latter cases the ring states each have two components of equal energy; the two components being describable by an $\mathfrak{R}_a$ and $\mathfrak{R}_b$ pair of functions or by an equivalent $\mathfrak{R}_{m,a}$ and $\mathfrak{R}_{m,b}$ pair or by any other orthogonal linear combination of the $\mathfrak{R}_a$ and $\mathfrak{R}_b$ pair.

In particular for the ring states of interest here (those involved in the visible and near-ultraviolet absorptions) it may be assumed that the functions are *symmetric* w.r.t. reflection in XY, in accordance with molecular orbital theory.[3,4] The ground state may be considered to be described by a function $\mathfrak{R}_a^0$, with $M=M^0=0$, that is of symmetry type A_{1g} in conventional group theoretical notation. The excited states may be considered to be described by functions $\mathfrak{R}_a^\kappa$ and $\mathfrak{R}_b^\kappa$ that, for $M=M^\kappa=0, 1, 2, \cdots, 2N, 2N+1$,

[7] J. R. Platt, J. Chem. Phys. **17**, 484 (1949).
[8] J. Petruska, J. Chem. Phys. (to be published).
[9] H. Eyring, J. Walter, and G. E. Kimball, *Quantum Chemistry* (John Wiley & Sons, Inc., New York, 1944), pp. 172–189.

are of symmetry type (in the case of $\mathfrak{R}_a^\kappa$) A_{1g}, E_{1ua}, E_{2ga}, $\cdots$, E_{2Nga}, B_{1u}, respectively, and (in the case of $\mathfrak{R}_b^\kappa$) A_{2g}, E_{1ub}, E_{2gb}, $\cdots$, E_{2Ngb}, B_{2u}, respectively. These symmetry types are illustrated for benzene ($N=1$) in Fig. 2.

Now consider the prototype state functions $\mathfrak{S}_m$ describing the various excited electronic states of the substituent at m and charge-transfer states obtained by transferring electrons from the carbon ring to this substituent or vice versa. With the substituent and the ring both being symmetric w.r.t. reflection in X_mZ and XY, these functions have the following properties: (a) they are either symmetric or antisymmetric w.r.t. reflection of the substituent and the ring in X_mZ and (b) they are either symmetric or antisymmetric w.r.t. reflection in XY.

Of the various possible $\mathfrak{S}_m$ only those, labeled $\mathfrak{S}_m^\mu$, that are *symmetric* w.r.t. reflection in XY will interact with $\mathfrak{R}^0$ and $\mathfrak{R}^\kappa$; the perturbation operator P being also symmetric w.r.t. this reflection, all matrix elements of P between $\mathfrak{R}^0$ and $\mathfrak{R}^\kappa$ and the antisymmetric $\mathfrak{S}_m$ are necessarily zero on symmetry grounds. Following the notation for the ring state functions, one may designate the $\mathfrak{S}_m^\mu$ as $\mathfrak{S}_{m,a}^\mu$ or $\mathfrak{S}_{m,b}^\mu$ according as they are symmetric or antisymmetric, respectively, w.r.t. reflection in X_mZ.

Perturbation Matrix Elements

Let us examine the matrix elements of P that contribute to the first- and second-order perturbations of $\mathfrak{R}^\kappa$. To begin with, suppose that the most important interactions are those with the various ring state functions $\mathfrak{R}^\lambda$ (where λ includes, 0, κ, and all the other ring states symmetric w.r.t. reflection in XY) and the various substituent or charge-transfer functions $\mathfrak{S}_m^\mu$. Charge-transfer state functions $\mathfrak{S}_{mn}$ resulting from electron transfer between the substituents at m and n are also theoretically possible, but suppose for the time being that the interactions with these are not very important. Then, within the framework of first- and second-order perturbation theory, the matrix elements to be considered are $\langle\mathfrak{R}^\kappa|P|\mathfrak{R}^\lambda\rangle$ and $\langle\mathfrak{R}^\kappa|P|\mathfrak{S}_m^\mu\rangle$. How these depend on the individual substituents may be determined simply by examining the matrix elements of P_m and applying Eq. (2).

Taking into account the "a" and "b" character of the state functions, we note that the matrix elements of P_m between functions of different character w.r.t. reflection in X_mZ are zero on symmetry grounds, i.e.,

$$\langle\mathfrak{R}_{m,a}^\kappa|P_m|\mathfrak{R}_{m,b}^\lambda\rangle=\langle\mathfrak{R}_{m,b}^\kappa|P_m|\mathfrak{R}_{m,a}^\lambda\rangle=0 \quad \text{for all } \lambda$$

$$\langle\mathfrak{R}_{m,a}^\kappa|P_m|\mathfrak{S}_{m,b}^\mu\rangle=\langle\mathfrak{R}_{m,b}^\kappa|P_m|\mathfrak{S}_{m,a}^\mu\rangle=0 \quad \text{for all } \mu. \tag{3}$$

Further, on the grounds that the ring-substituent bonds are independent of one another, we may set

$$\langle\mathfrak{R}^\kappa|P_m|\mathfrak{S}_n^\mu\rangle=0 \quad \text{for} \quad m\neq n, \tag{4}$$

regardless of the "a" and "b" classification of the states. The other matrix elements of P_m, between

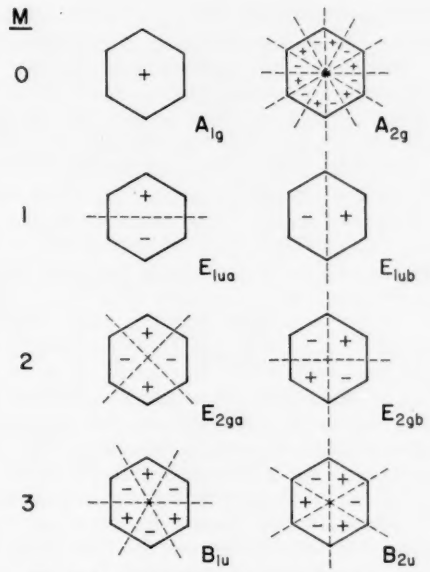

FIG. 2. Symmetry types of benzene ring states.

state functions of the *same* character w.r.t. reflection in X_mZ, however, are nonzero in general:

$$\begin{aligned}
&\langle\mathfrak{R}_{m,a}^\kappa|P_m|\mathfrak{R}_{m,a}^\lambda\rangle\equiv a_m^{\kappa\lambda}\\
&\langle\mathfrak{R}_{m,b}^\kappa|P_m|\mathfrak{R}_{m,b}^\lambda\rangle\equiv b_m^{\kappa\lambda}\\
&\langle\mathfrak{R}_{m,a}^\kappa|P_m|\mathfrak{S}_{m,a}^\mu\rangle\equiv A_m^{\kappa\mu}\\
&\langle\mathfrak{R}_{m,b}^\kappa|P_m|\mathfrak{S}_{m,b}^\mu\rangle\equiv B_m^{\kappa\mu}.
\end{aligned} \tag{5}$$

These will have values characteristic of the substituent at m. Applying the linear transformations given by Eq. (2) for $\mathfrak{R}^\kappa$ and $\mathfrak{R}^\lambda$ we find the following general expressions for the matrix elements of $P=\sum_m P_m$:

$$\begin{aligned}
\langle\mathfrak{R}_a^\kappa|P|\mathfrak{R}_a^\lambda\rangle&=\sum_m\{a_m^{\kappa\lambda}\cos(M^\kappa m\rho)\cos(M^\lambda m\rho)\\
&\quad+b_m^{\kappa\lambda}\sin(M^\kappa m\rho)\sin(M^\lambda m\rho)\}\\
\langle\mathfrak{R}_a^\kappa|P|\mathfrak{R}_b^\lambda\rangle&=\sum_m\{a_m^{\kappa\lambda}\cos(M^\kappa m\rho)\sin(M^\lambda m\rho)\\
&\quad-b_m^{\kappa\lambda}\sin(M^\kappa m\rho)\cos(M^\lambda m\rho)\}\\
\langle\mathfrak{R}_b^\kappa|P|\mathfrak{R}_a^\lambda\rangle&=\sum_m\{a_m^{\kappa\lambda}\sin(M^\kappa m\rho)\cos(M^\lambda m\rho)\\
&\quad-b_m^{\kappa\lambda}\cos(M^\kappa m\rho)\sin(M^\lambda m\rho)\}\\
\langle\mathfrak{R}_b^\kappa|P|\mathfrak{R}_b^\lambda\rangle&=\sum_m\{a_m^{\kappa\lambda}\sin(M^\kappa m\rho)\sin(M^\lambda m\rho)\\
&\quad+b_m^{\kappa\lambda}\cos(M^\kappa m\rho)\sin(M^\lambda m\rho)\}
\end{aligned} \tag{6a}$$

$$\begin{aligned}
&\langle\mathfrak{R}_a^\kappa|P|\mathfrak{S}_{m,a}^\mu\rangle=A_m^{\kappa\mu}\cos(M^\kappa m\rho)\\
&\langle\mathfrak{R}_a^\kappa|P|\mathfrak{S}_{m,b}^\mu\rangle=-B_m^{\kappa\mu}\sin(M^\kappa m\rho)\\
&\langle\mathfrak{R}_b^\kappa|P|\mathfrak{S}_{m,a}^\mu\rangle=A_m^{\kappa\mu}\sin(M^\kappa m\rho)\\
&\langle\mathfrak{R}_b^\kappa|P|\mathfrak{S}_{m,b}^\mu\rangle=B_m^{\kappa\mu}\cos(M^\kappa m\rho).
\end{aligned} \tag{6b}$$

The matrix elements in Eqs. (6a) may be considered to represent *inductive* perturbations of the substituents; those in Eqs. (6b), *conjugative* perturbations. The inductive effect of substitution in aromatic hydrocarbons, as defined in molecular orbital (MO) theory,[3,4] refers to the change in the "core" potential acting on the *pi* orbitals of the carbon framework. In linear combinations of atomic orbitals (LCAO) MO theory this is expressed in terms of changes in the one-electron coulomb (α) and resonance-bond (β) integrals for the $2p\pi$ atomic orbitals of the carbons. By describing the prototype state functions in terms of configurations of LCAO MO's,[3,4] one finds that the matrix elements designated by a_m and b_m are linearly related to the changes produced by the substituent at m in the coulomb integral for the carbon m and in the resonance-bond integrals between this carbon and the neighboring carbons in the ring. The conjugative effect, on the other hand, refers to the resonance interactions of the *pi* orbitals of the substituents with the *pi* orbitals of the carbon framework.[4] This leads to the formation of new resonance-bond integrals between the substituents and the carbons to which they are attached. It can be shown that the matrix elements designated by A_m and B_m are linearly related to the resonance-bond integral for the substituent at m.[4]

DERIVATION OF PERTURBATION FORMULAS

Transition-Moment and Transition-Probability Changes

We are now in a position to describe the changes produced by ideal weak substituent perturbations in the transition dipole moment and transition probability of the original cyclic-polyene transitions. Consider the electric dipole transition from the ground ring state described by $\mathfrak{R}^0$ to the excited state described by $\mathfrak{R}^\kappa$. Before substitution the transition dipole moment is $\mathbf{Q}^{0\kappa}=\langle\mathfrak{R}^0|\,\mathbf{r}\,|\mathfrak{R}^\kappa\rangle$ where $\mathbf{r}$ represents the sum of the position vectors for the individual electrons. The corresponding transition probability or dipole strength,[10] measuring the intensity of the transition is $D^{0\kappa}=|Q^{0\kappa}|^2$. After substitution, when $\mathfrak{R}^0$ and $\mathfrak{R}^\kappa$ have been changed by small amounts $\Delta\mathfrak{R}^0$ and $\Delta\mathfrak{R}^\kappa$, the transition moment is changed (to first order) by

$$\Delta Q^{0\kappa}=\langle\Delta\mathfrak{R}^0|\,\mathbf{r}\,|\mathfrak{R}^\kappa\rangle+\langle\mathfrak{R}^0|\,\mathbf{r}\,|\Delta\mathfrak{R}^\kappa\rangle, \tag{7}$$

and the transition probability by

$$\begin{aligned}\Delta D^{0\kappa}&=|\mathbf{Q}^{0\kappa}+\Delta\mathbf{Q}^{0\kappa}|^2-|Q^{0\kappa}|^2\\&=2\mathbf{Q}^{0\kappa}\cdot\Delta\mathbf{Q}^{0\kappa}+|\Delta Q^{0\kappa}|^2.\end{aligned} \tag{8}$$

Upon taking as the criterion for weak perturbations of $\mathfrak{R}^\kappa$

$$\begin{aligned}&|\langle\mathfrak{R}^\kappa|\,P\,|\mathfrak{R}^\lambda\rangle|\ll|E^\kappa-E^\lambda| \quad \text{for} \quad \lambda\neq\kappa\\&|\langle\mathfrak{R}^\kappa|\,P\,|\mathbb{S}_m{}^\mu\rangle|\ll|E^\kappa-E_m{}^\mu| \quad \text{for all } \mu,\end{aligned} \tag{9}$$

where E^κ, E^λ, and $E_m{}^\mu$ are (unperturbed) excitation energies of $\mathfrak{R}^\kappa$, $\mathfrak{R}^\lambda$, and $\mathbb{S}_m{}^\mu$, we have the following general expression for $\Delta\mathfrak{R}^\kappa$ from perturbation theory (assuming the prototype states are orthogonal),

$$\Delta\mathfrak{R}^\kappa=-\gamma^\kappa\mathfrak{R}^\kappa+\sum_{\lambda\neq\kappa}\delta^{\kappa\lambda}\mathfrak{R}^\lambda+\sum_m\sum_\mu\delta_m{}^{\kappa\mu}\mathbb{S}_m{}^\mu, \tag{10}$$

where

$$\delta^{\kappa\lambda}=\langle\mathfrak{R}^\kappa|\,P\,|\mathfrak{R}^\lambda\rangle/(E^\kappa-E^\lambda),$$

$$\delta_m{}^{\kappa\mu}=\langle\mathfrak{R}^\kappa|\,P\,|\mathbb{S}_m{}^\mu\rangle/(E^\kappa-E_m{}^\mu),$$

and

$$\gamma^\kappa=\tfrac{1}{2}\{\sum_{\lambda\neq\kappa}|\delta^{\kappa\lambda}|^2+\sum_m\sum_\mu|\delta_m{}^{\kappa\mu}|^2\}.$$

Writing a similar expression for $\Delta\mathfrak{R}^0$ and substituting in Eq. (7), we have for the transition-moment change

$$\begin{aligned}\Delta\mathbf{Q}^{0\kappa}=&-(\gamma^0+\gamma^\kappa)\mathbf{Q}^{0\kappa}+\sum_{\lambda\neq0}\delta^{0\lambda}\mathbf{Q}^{\kappa\lambda}+\sum_{\lambda\neq\kappa}\delta^{\kappa\lambda}\mathbf{Q}^{0\lambda}\\&+\sum_m\sum_\mu(\delta_m{}^{0\mu}\mathbf{Q}_m{}^{\kappa\mu}+\delta_m{}^{\kappa\mu}\mathbf{Q}_m{}^{0\mu}),\end{aligned} \tag{11}$$

where $\mathbf{Q}^{\kappa\lambda}=\langle\mathfrak{R}^\kappa|\,\mathbf{r}\,|\mathfrak{R}^\lambda\rangle$, $\mathbf{Q}_m{}^{\kappa\mu}=\langle\mathfrak{R}^\kappa|\,\mathbf{r}\,|\mathbb{S}_m{}^\mu\rangle$, etc. From Eq. (11), using the expressions for the perturbation matrix elements given by Eqs. (6a) and (6b), one can derive formulas for $\Delta\mathbf{Q}^{0\kappa}$ in terms of the individual substituents. These, along with the corresponding formulas for $\Delta D^{0\kappa}$, are derived below assuming that $\mathfrak{R}^\kappa$, like $\mathfrak{R}^0$, is a singlet state (in which the total electron spin is zero). Three types of transitions are distinguished: (a) nondegenerate and symmetry-forbidden, (b) twofold-degenerate and symmetry-forbidden, and (b) twofold-degenerate and symmetry-allowed.

Nondegenerate, Symmetry-Forbidden Transitions

If M^κ is equal to 0 or $2N+1$, the transition is nondegenerate and symmetry-forbidden since $\mathfrak{R}^\kappa$, like $\mathfrak{R}^0$, is nondegenerate and $\mathbf{Q}^{0\kappa}$ is zero (in accordance with the selection rule for electric dipole transitions that ΔM must be equal to 1 for the transition moment to be nonzero[11]). Setting $|Q^{0\kappa}|=0$ in Eq. (11) along with $|Q^{\kappa\lambda}|=0$ when $|M^\kappa-M^\lambda|\neq1$ and $|Q^{0\lambda}|=0$ when $M^\lambda\neq1$, we have as the transition moment arising on substitution

$$\begin{aligned}\Delta\mathbf{Q}^{0\kappa}=&\sum_{\lambda'}\delta^{\kappa\lambda'}\mathbf{Q}^{0\lambda'}+\sum_{\lambda''}\delta^{0\lambda''}\mathbf{Q}^{\kappa\lambda''}\\&+\sum_m\sum_\mu(\delta_m{}^{\kappa\mu}\mathbf{Q}_m{}^{0\mu}+\delta_m{}^{0\mu}\mathbf{Q}_m{}^{\kappa\mu}),\end{aligned} \tag{12}$$

where λ' and λ'' are those of the ring states λ with M^λ equal to 1 and $|M^\kappa\pm1|$, respectively. The directions of the contributing moments are readily determined after taking into account the "a" and "b" character of the state functions. For example, in the case of $\mathbf{Q}^{\kappa\lambda}$ with

[10] R. S. Mulliken and C. A. Rieke, Repts. Progr. Phys. **8**, 231 (1941).

[11] H. Sponer and E. Teller, Revs. Modern Phys. **13**, 75 (1941).

$M^\lambda = M^\kappa + 1$, it is easily verified that

$$\mathbf{Q}^{\kappa\lambda}/|Q^{\kappa\lambda}| = \begin{cases} \mathbf{i} & \text{for } \mathfrak{R}_a{}^\kappa,\ \mathfrak{R}_a{}^\lambda \text{ and for } \mathfrak{R}_b{}^\kappa,\ \mathfrak{R}_b{}^\lambda \\ \mathbf{j} & \text{for } \mathfrak{R}_a{}^\kappa,\ \mathfrak{R}_b{}^\lambda \\ -\mathbf{j} & \text{for } \mathfrak{R}_b{}^\kappa,\ \mathfrak{R}_a{}^\lambda) \end{cases} \tag{13}$$

and in the case of $\mathbf{Q}_m{}^{\kappa\mu}$

$$\mathbf{Q}_m{}^{\kappa\mu}/|Q_m{}^{\kappa\mu}| = \begin{cases} \mathbf{r}_m & \text{for } \mathfrak{R}_{m,a}{}^\kappa,\ \mathfrak{S}_{m,a}{}^\mu \text{ and for } \mathfrak{R}_{m,b}{}^\kappa,\ \mathfrak{S}_{m,b}{}^\mu \\ \mathbf{t}_m & \text{for } \mathfrak{R}_{m,a}{}^\kappa,\ \mathfrak{S}_{m,a}{}^\mu \text{ and for } \mathfrak{R}_{m,b}{}^\kappa,\ \mathfrak{S}_{m,a}{}^\mu, \end{cases} \tag{14}$$

where $\mathbf{i}$ and $\mathbf{j}$ are the unit vectors along the X and Y axes, respectively, and $\mathbf{r}_m$ and $\mathbf{t}_m$ are the unit radial and tangential vectors at m, respectively, defined by

$$\mathbf{r}_m = \mathbf{i}\cos(m\rho) + \mathbf{j}\sin(m\rho)$$
$$\mathbf{t}_m = \mathbf{j}\cos(m\rho) - \mathbf{i}\sin(m\rho). \tag{15}$$

After substituting for the matrix elements of P the expressions given by Eqs. (6a) and (6b) and collecting similar terms, it becomes apparent that $\Delta\mathbf{Q}^{0\kappa}$ of Eq. (12) may be written as follows for $\mathfrak{R}^\kappa = \mathfrak{R}_a{}^\kappa$,

$$\Delta\mathbf{Q}^{0\kappa} = \Delta\mathbf{Q}_a{}^{0\kappa} = \sum_m q_m{}^{0\kappa}\mathbf{r}_{(1-M^\kappa)m}, \tag{16}$$

where $q_m{}^{0\kappa}$ is the value of the transition moment induced by the substituent at m and

$$\mathbf{r}_{(1-M^\kappa)m} = \mathbf{i}\cos[(1-M^\kappa)m\rho] + \mathbf{j}\sin[(1-M^\kappa)m\rho], \tag{17}$$

is the unit transition moment vector for the position m. On the other hand, for $\mathfrak{R}^\kappa = \mathfrak{R}_b{}^\kappa$,

$$\Delta\mathbf{Q}^{0\kappa} = \Delta\mathbf{Q}_b{}^{0\kappa} = \sum_m q_m{}^{0\kappa}\mathbf{t}_{(1-M^\kappa)m}, \tag{18}$$

where

$$\mathbf{t}_{(1-M^\kappa)m} = \mathbf{j}\cos[(1-M^\kappa)m\rho] - \mathbf{i}\sin[(1-M^\kappa)m\rho] \tag{19}$$

is the unit transition moment vector for the position m.

The corresponding formula for $\Delta D^{0\kappa}$ in either case, $\mathfrak{R}_a{}^\kappa$ or $\mathfrak{R}_b{}^\kappa$, is

$$\Delta D^{0\kappa} = |\sum_m q_m{}^{0\kappa}\exp[i(1-M^\kappa)m\rho]|^2. \tag{20}$$

When $M^\kappa = 0$ this becomes simply

$$\Delta D^{0\kappa} = |\sum_m q_m{}^{0\kappa}\exp(im\rho)\ |^2, \tag{21a}$$

and when $M^\kappa = 2N+1$

$$\Delta D^{0\kappa} = |\sum_m q_m{}^{0\kappa}\exp(i2Nm\rho)\,|^2. \tag{21b}$$

Twofold-Degenerate, Symmetry-Forbidden Transitions

If M^κ is equal to 2, 3, $\cdots$, $2N-1$, or $2N$ the transition is not only symmetry-forbidden but also twofold-degenerate, since $\mathfrak{R}^\kappa$ is twofold-degenerate. There are now two components to $\Delta\mathbf{Q}^{0\kappa}$ corresponding to the two components of $\mathfrak{R}^\kappa$.

The two components of $\mathfrak{R}^\kappa$ are describable by $\mathfrak{R}_a{}^\kappa$ and $\mathfrak{R}_b{}^\kappa$ or by any orthogonal linear combinations of these two functions. The desired linear combinations for the perturbation problem at hand are those with a zero matrix element of P between them, namely,

$$\mathfrak{R}_+{}^\kappa = \mathfrak{R}_a{}^\kappa\cos\omega + \mathfrak{R}_b{}^\kappa\sin\omega \tag{22}$$
$$\mathfrak{R}_-{}^\kappa = \mathfrak{R}_b{}^\kappa\cos\omega - \mathfrak{R}_a{}^\kappa\sin\omega,$$

where ω, the angle making $\langle\mathfrak{R}_+{}^\kappa|\,P\,|\mathfrak{R}^\kappa\rangle = 0$, is given by

$$2\omega = \tan^{-1}\left[\frac{2\langle\mathfrak{R}_a{}^\kappa|\,P\,|\mathfrak{R}_b{}^\kappa\rangle}{\langle\mathfrak{R}_a{}^\kappa|\,P\,|\mathfrak{R}_a{}^\kappa\rangle - \langle\mathfrak{R}_b{}^\kappa|\,P\,|\mathfrak{R}_b{}^\kappa\rangle}\right]. \tag{23}$$

Substituting $\mathfrak{R}^\kappa = \mathfrak{R}_\pm{}^\kappa$ in Eq. (12) and proceding as in the case of the nondegenerate, symmetry-forbidden transitions, we arrive at the following formulas for the two components of the transition moment arising on substitution,

$$\Delta\mathbf{Q}_+{}^{0\kappa} = \sum_m\{q_m{}^{0\kappa}\mathbf{r}_{(1-M^\kappa)m+\omega/\rho} + \Delta q_m{}^{0\kappa}\mathbf{r}_{(1+M^\kappa)m-\omega/\rho}\}$$
$$\Delta\mathbf{Q}_-{}^{0\kappa} = \sum_m\{q_m{}^{0\kappa}\mathbf{t}_{(1-M^\kappa)m+\omega/\rho} - \Delta q_m{}^{0\kappa}\mathbf{t}_{(1+M^\kappa)m-\omega/\rho}\}, \tag{24}$$

where $q_m{}^{0\kappa} = \frac{1}{2}(q_{a,m}{}^{0\kappa} + q_{b,m}{}^{0\kappa})$ and $\Delta q_m{}^{0\kappa} = \frac{1}{2}(q_{a,m}{}^{0\kappa} - q_{b,m}{}^{0\kappa})$ are the values of two transition-moment parameters ($\Delta q \leq q$) for the substituent at m, and

$$\mathbf{r}_{(1\pm M^\kappa)m\pm\omega/\rho} = \mathbf{i}\cos[(1\pm M^\kappa)m\rho\pm\omega] + \mathbf{j}\sin[(1\pm M^\kappa)m\rho\pm\omega]$$
$$\mathbf{t}_{(1\pm M^\kappa)m\pm\omega/\rho} = \mathbf{j}\cos[(1\pm M^\kappa)m\rho\pm\omega] - \mathbf{i}\sin[(1\pm M^\kappa)m\rho\pm\omega], \tag{25}$$

are the unit transition-moment vectors for the position m.

The corresponding transition-probability formulas are

$$\Delta D_\pm{}^{0\kappa} = |\sum_m q_m{}^{0\kappa}\exp[i(1-M^\kappa)m\rho]|^2 + |\sum_m \Delta q_m{}^{0\kappa}\exp[i(1+M^\kappa)m\rho]|^2 \pm 2\sum_m\sum_p q_m{}^{0\kappa}\Delta q_p{}^{0\kappa}\cos[M^\kappa - 1)m\rho + (M^\kappa+1)p\rho - 2\omega]. \tag{26}$$

For the total transition probability induced, $\Delta D^{0\kappa} = \Delta D_+{}^{0\kappa} + \Delta D_-{}^{0\kappa}$, the resultant formula is

$$\Delta D^{0\kappa} = 2\{|\sum_m q_m{}^{0\kappa}\exp[i(1-M^\kappa)m\rho]|^2 + |\sum_m \Delta q_m{}^{0\kappa}\exp[i(1+M^\kappa)m\rho]|^2\}. \tag{27}$$

Twofold-Degenerate, Symmetry-Allowed Transitions

If $M^\kappa = 1$ the transition is twofold-degenerate but, unlike the transitions above, it is symmetry-allowed.

Now the initial moment $\mathbf{Q}^{0\kappa}$ is large and the principal contribution to $\Delta\mathbf{Q}^{0\kappa}$ is likely to come from the terms containing $\mathbf{Q}^{0\kappa}$ in Eq. (11). Keeping only such terms, we have

$$\Delta\mathbf{Q}^{0\kappa}=-\tfrac{1}{2}\mathbf{Q}^{0\kappa}\{\sum_m\sum_\mu(|\delta_m{}^{0\mu}|^2+|\delta_m{}^{\kappa\mu}|^2)+\sum_{\lambda\neq0}|\delta^{0\lambda}|^2+\sum_{\lambda\neq\kappa}|\delta^{\kappa\lambda}|^2\},\quad(28)$$

and to a first approximation

$$\Delta D^{0\kappa}=2\mathbf{Q}^{0\kappa}\cdot\Delta\mathbf{Q}^{0\kappa}.\quad(29)$$

Substituting $\mathfrak{R}^\kappa=\mathfrak{R}_\pm{}^\kappa$ in Eq. (28) and proceding as above we obtain

$$\begin{aligned}\Delta\mathbf{Q}_\pm{}^{0\kappa}=-\tfrac{1}{2}\mathbf{Q}_\pm{}^{0\kappa}[&\sum_m\{\gamma_m{}^{0\kappa}\pm\Delta\gamma_m{}^{0\kappa}\cos[2(m\rho-\omega)]\}\\&+\sum_{\lambda\neq0}|\sum_m\delta_m{}^{0\lambda}\exp(iM^\lambda m\rho)|^2\\&+\sum_{\lambda\neq\kappa}\{|\sum_m\delta_m{}^{\kappa\lambda}\exp[i(1-M^\lambda)m\rho]|^2\\&+|\sum_m\Delta\delta_m{}^{\kappa\lambda}\exp[i(1+M^\lambda)m\rho]|^2\}\\&\pm2\sum_m\sum_p\delta_m{}^{\kappa\lambda}\cdot\Delta\delta_p{}^{\kappa\lambda}\\&\times\cos[(1-M^\lambda)m\rho+(1+M^\lambda)p\rho-2\omega]\}],\end{aligned}\quad(30)$$

where

$$\delta_m{}^{0\lambda}=a_m{}^{0\lambda}/(E^0-E^\lambda),$$

$$\delta_m{}^{\kappa\lambda}=\tfrac{1}{2}(a_m{}^{\kappa\lambda}+b_m{}^{\kappa\lambda})/(E^\kappa-E^\lambda),$$

and

$$\Delta\delta_m{}^{\kappa\lambda}=\tfrac{1}{2}(a_m{}^{\kappa\lambda}-b_m{}^{\kappa\lambda})/(E^\kappa-E^\lambda)$$

are quantities arising from the *inductive* perturbations of the substituent at m;

$$\gamma_m{}^{0\kappa}=\tfrac{1}{2}\sum_\mu\{|A_m{}^{\kappa\mu}/(E^\kappa-E_m{}^\mu)|^2+|B_m{}^{\kappa\mu}/(E^\kappa-E_m{}^\mu)|^2+2|A_m{}^{0\mu}/(E^0-E_m{}^\mu)|^2\}$$

and

$$\Delta\gamma_m{}^{0\kappa}=\tfrac{1}{2}\sum_\mu\{|A_m{}^{\kappa\mu}/(E^\kappa-E_m{}^\mu)|^2-|B_m{}^{\kappa\mu}/(E^\kappa-E_m{}^\mu)|^2\}$$

are quantities arising from its *conjugative* perturbations. The changes $\Delta\mathbf{Q}_\pm{}^{0\kappa}$ lie in the directions of $\mathbf{Q}_\pm{}^{0\kappa}$, where

$$\begin{aligned}\mathbf{Q}_+{}^{0\kappa}&=|Q_+{}^{0\kappa}|(\mathbf{i}\cos\omega+\mathbf{j}\sin\omega)\\\mathbf{Q}^{0\kappa}&=|Q_-{}^{0\kappa}|(\mathbf{j}\cos\omega-i\sin\omega),\end{aligned}\quad(31)$$

with $|Q_+{}^{0\kappa}|=|Q_-{}^{0\kappa}|=|Q_a{}^{0\kappa}|=|Q_b{}^{0\kappa}|$ being the magnitude of the initial transition moment for each component.

From Eq. (29) similar formulas are obtained for $\Delta D_\pm{}^{0\kappa}$. The resultant formula for $\Delta D^{+\kappa}=\Delta D_+{}^{0\kappa}+\Delta D_-{}^{0\kappa}$ is

$$\begin{aligned}\Delta D^{0\kappa}=-D^{0\kappa}[&\sum_m\gamma_m{}^{0\kappa}+\sum_{\lambda\neq0}|\sum_m\delta_m{}^{0\lambda}\exp(iM^\lambda m_\rho)|^2\\&+\sum_{\lambda\neq\kappa}\{|\sum_m\delta_m{}^{\kappa\lambda}\exp i(1-M^\lambda)m\rho|^2\\&+|\sum_m\Delta\delta_m{}^{\kappa\lambda}\exp[i(1+M^\lambda)m\rho]|^2\}],\end{aligned}\quad(32)$$

where $D^{0\kappa}=|Q_+{}^{0\kappa}|^2+|Q_-{}^{0\kappa}|^2$ is the initial transition probability for the two components together. This formula may be simplified by assuming that the inductive perturbations are proportional to a single parameter δ as indicated by simple LCAO MO theory.[3,4] On setting $\delta_m{}^{0\lambda}=f^{0\lambda}\delta_m$, $\delta_m{}^{\kappa\lambda}=f^{\kappa\lambda}\delta_m$, $\Delta\delta_m{}^{\kappa\lambda}=\Delta f^{\kappa\lambda}\delta_m$ where $f^{0\lambda}$, $f^{\kappa\lambda}$, $\Delta f^{\kappa\lambda}$ are constants for the transition, the formula becomes

$$\Delta D^{0\kappa}=-D^{0\kappa}[\sum_m\gamma_m{}^{0\kappa}+\sum_{M=0}^{2N+1}C_M{}^{0\kappa}|\sum_m\delta_m\exp(iMm\rho)|^2],\quad(33)$$

in which $C_M{}^{0\kappa}$ are coefficients characteristic of the transition given by

$$C_M{}^{0\kappa}=\sum_{\lambda'}(f^{0\lambda'})^2+\sum_{\lambda''}(f^{\kappa\lambda''})^2+\sum_{\lambda'''}(\Delta f^{\kappa\lambda'''})^2,\quad(34)$$

where λ', λ'', and λ''' are those of the ring states λ with M^λ equal to M, $|1\pm M|$, and $M-1$, respectively.

Frequency Shifts

Let us now examine the frequency shifts that accompany the changes described above. Initially, the transition from $\mathfrak{R}^0$ to $\mathfrak{R}^\kappa$ has a frequency (in units of energy) $\nu^{0\kappa}=E^\kappa-E^0$. After substitution, when E^0 and E^κ are changed by small amounts ΔE^0 and ΔE^κ, the frequency is shifted by the amount $\Delta\nu^{0\kappa}=\Delta E^\kappa-\Delta E^0$. Corresponding to the general expression for $\Delta\mathfrak{R}^\kappa$ given by Eq. (10), we have the following expression for ΔE^κ (to second order),

$$\Delta E^\kappa=d^\kappa+\sum_{\lambda\neq\kappa}(v^{\kappa\lambda})^2+\sum_m\sum_\mu(v_m{}^{\kappa\mu})^2,\quad(35)$$

where $d^\kappa=\langle\mathfrak{R}^\kappa|P|\mathfrak{R}^\kappa\rangle$, $v^{\kappa\lambda}=\langle\mathfrak{R}^\kappa|P|\mathfrak{R}^\lambda\rangle/(E^\kappa-E^\lambda)^{\frac{1}{2}}$, and $v_m{}^{\kappa\mu}=\langle\mathfrak{R}^\kappa|P|\mathfrak{S}_m{}^\mu\rangle/(E^\kappa-E_m{}^\mu)^{\frac{1}{2}}$. Writing a similar expression for ΔE^0, we obtain for the frequency shift (toward the red),

$$-\Delta\nu^{0\kappa}=d^0-d^\kappa+\sum_{\lambda\neq0}(v^{0\lambda})^2-\sum_{\lambda\neq\kappa}(v^{\kappa\lambda})^2+\sum_m\sum_\mu\{(v_m{}^{0\mu})^2-(v_m{}^{\kappa\mu})^2\}.\quad(36)$$

The dependence of the frequency shift on the individual substituents is described below for the nondegenerate and twofold-degenerate transitions.

Nondegenerate Transitions

For the nondegenerate transitions, with M^κ equal to 0 or $2N+1$, after substituting in Eq. (36) the expressions for the matrix elements of P given by Eqs. (6a) and (6b) and collecting similar terms, we find that the frequency shift may be expressed as follows,

$$-\Delta\nu^{0\kappa}=\sum_m l_m{}^{0\kappa}+\sum_{\lambda\neq 0}\left|\sum_m v_m{}^{0\lambda}\exp(iM^\lambda m\rho)\right|^2 -\sum_{\lambda\neq\kappa}\left|\sum_m v_m{}^{\kappa\lambda}\exp[i(M^\kappa-M^\lambda)m\rho]\right|^2, \quad (37)$$

where $l_m{}^{0\kappa}$ comes from the first-order *inductive* and second-order *conjugative* energy changes produced by the substituent at m; $v_m{}^{0\lambda}$ and $v_m{}^{\kappa\lambda}$, from the second-order *inductive* energy changes. If we assume that $v_m{}^{0\lambda}$ and $v_m{}^{\kappa\lambda}$ are proportional to a single parameter, i.e., $v_m{}^{0\lambda}=g^{0\lambda}v_m$ and $v_m{}^{\kappa\lambda}=g^{\kappa\lambda}v_m$ where $g^{0\lambda}$ and $g^{\kappa\lambda}$ are constants for the transitions, then we obtain the formula

$$-\Delta\nu^{0\kappa}=\sum_m l_m{}^{0\kappa}+\sum_{M=0}^{2N+1}C_M{}^{0\kappa}\left|\sum_m v_m\exp(iMm\rho)\right|^2, \quad (38)$$

in which $C_M{}^{0\kappa}$ are constants for each transition determined by

$$C_M{}^{0\kappa}=\sum_{\lambda'}(g^{0\lambda'})^2-\sum_{\lambda''}(g^{\kappa\lambda''})^2, \quad (39)$$

where λ' and λ'' are those of the ring states λ for which M^λ is equal to M and $|M^\kappa\pm M|$, respectively.

Twofold-Degenerate Transitions

For the twofold-degenerate transitions, with $M^\kappa=1, 2, \cdots, 2N$, there are two components to the frequency shift corresponding to the two components of $\mathfrak{R}^\kappa$. After substituting in Eq. (36) the expressions for $\mathfrak{R}_\pm{}^\kappa$ given by Eqs. (22), the matrix elements given by Eqs. (6a) and (6b), etc., we obtain

$$\begin{aligned}-\Delta\nu_\pm{}^{0\kappa}=&\sum_m\{l_m{}^{0\kappa}\pm\Delta l_m{}^{0\kappa}\cos 2(M^\kappa m\rho-\omega)\}\\&+\sum_{\lambda\neq 0}\left|\sum_m v_m{}^{0\lambda}\exp(iM^\lambda m\rho)\right|^2\\&-\sum_{\lambda\neq\kappa}\{\left|\sum_m v_m{}^{\kappa\lambda}\exp[i(M^\kappa-M^\lambda)m\rho]\right|^2\\&+\left|\sum_m\Delta v_m{}^{\kappa\lambda}\exp[i(M^\kappa+M^\lambda)m\rho]\right|^2\\&\pm 2\sum_m\sum_p v_m{}^{\kappa\lambda}\cdot\Delta v_p{}^{\kappa\lambda}\\&\times\cos[(M^\kappa-M^\lambda)m\rho+(M^\kappa+M^\lambda)p\rho-2\omega]\}, \quad (40)\end{aligned}$$

where $l_m{}^{0\kappa}=\frac{1}{2}(l_{a,m}{}^{0\kappa}+l_{b,m}{}^{0\kappa})$ and $\Delta l_m{}^{0\kappa}=\frac{1}{2}(l_{a,m}{}^{0\kappa}-l_{b,m}{}^{0\kappa})$ arise from the first-order *inductive* and second-order *conjugative* energy changes; $v_m{}^{\kappa\lambda}=\frac{1}{2}(v_{a,m}{}^{\kappa\lambda}+v_{b,m}{}^{\kappa\lambda})$, $\Delta v_m{}^{\kappa\lambda}=\frac{1}{2}(v_{a,m}{}^{\kappa\lambda}-v_{b,m}{}^{\kappa\lambda})$, and $v_m{}^{0\lambda}=v_{a,m}{}^{0\lambda}$, from the second-order *inductive* energy changes. Thus for the *average* of the frequency shifts of the two components, $\Delta\nu^{0\kappa}=\frac{1}{2}(\Delta\nu_+{}^{0\kappa}+\Delta\nu_-{}^{0\kappa})$, we have

$$\begin{aligned}-\Delta\nu^{0\kappa}=&\sum_m l_m{}^{0\kappa}+\sum_{\lambda\neq 0}\left|\sum_m v_m{}^{0\lambda}\exp(iM^\lambda m\rho)\right|^2\\&-\sum_{\lambda\neq\kappa}\{\left|\sum_m v_m{}^{\kappa\lambda}\exp i(M^\kappa-M^\lambda)m\rho\right|^2\\&+\left|\sum_m\Delta v_m{}^{\kappa\lambda}\exp i(M^\kappa+M^\lambda)m\rho\right|^2\}, \quad (41)\end{aligned}$$

and for their *difference*, $\Delta(\Delta\nu^{0\kappa})=\Delta\nu_0{}^{0\kappa}-\Delta\nu_+{}^{0\kappa}$, which represents the frequency *splitting*,

$$\begin{aligned}\Delta(\Delta\nu^{0\kappa})=&\sum_m 2\Delta l_m{}^{0\kappa}\cos[2(M^\kappa m\rho-\omega)]\\&-\sum_m\sum_p 4v_m{}^{\kappa\lambda}\cdot\Delta v_p{}^{\kappa\lambda}\\&\times\cos[(M^\kappa-M^\lambda)m\rho+(M^\kappa+M^\lambda)p\rho-2\omega]. \quad (42)\end{aligned}$$

Assuming that $v_m{}^{0\lambda}=g^{0\lambda}v_m$, $v_m{}^{\kappa\lambda}=g^{\kappa\lambda}v_m$, and $\Delta v_m{}^{\kappa\lambda}=\Delta g^{\kappa\lambda}v_m$, we may write Eqs. (41) and (42) as follows,

$$-\Delta\nu^{0\kappa}=\sum_m l_m{}^{0\kappa}+\sum_{M=0}^{2N+1}C_M{}^{0\kappa}\left|\sum_m v_m\exp(iMm\rho)\right|^2 \quad (43)$$

$$\begin{aligned}\Delta(\Delta\nu^{0\kappa})=&\sum_m 2\Delta l_m{}^{0\kappa}\cos[2(M^\kappa m\rho-\omega)]\\&+\sum_{M=0}^{2N+1}C_M{}^{\kappa\lambda'}\sum_m\sum_p v_m v_p\\&\times\cos[(M^\kappa-M)m\rho+(M^\kappa+M)p\rho-2\omega], \quad (44)\end{aligned}$$

where $C_M{}^{0\kappa}$ and $C_M{}^{\kappa\lambda'}$ are coefficients determined by

$$C_M{}^{0\kappa}=\sum_{\lambda'}(g^{0\lambda'})^2-\sum_{\lambda''}(g^{\kappa\lambda''})^2-\sum_{\lambda'''}(\Delta g^{\kappa\lambda'''})^2 \quad (45)$$

$$C_M{}^{\kappa\lambda'}=-\sum_{\lambda'}4g^{\kappa\lambda'}\cdot\Delta g^{\kappa\lambda'},$$

with λ', λ'', and λ''' being those of the ring states λ having M^λ equal to M, $M^\kappa\pm M$, and $M-M^\kappa$, respectively.

FORMULAS FOR BENZENE

Setting $N=1$ and $\rho=\pi/3$ in the perturbation formulas derived above, one obtains formulas applying to the transitions in benzene from the singlet ground state, ${}^1A_{1g}(M=0)$, to the singlet excited states that, for $M=0, 1, 2, 3$, are of type ${}^1A_{1g}$ and ${}^1A_{2g}$, ${}^1E_{1u}$, ${}^1E_{2g}$, ${}^1B_{1u}$, and ${}^1B_{2u}$, respectively.

The formulas for the changes in the transition dipole moment ($\Delta\mathbf{Q}$) and transition probability (ΔD) are as follows:

(1) Nondegenerate, symmetry-forbidden transitions to excited state

$$^1A_{1g}: \quad \Delta\mathbf{Q}=\sum_m q_m\mathbf{r}_m \tag{46a}$$

$$\Delta D=|\sum_m q_m \exp(im\pi/3)|^2 \tag{46b}$$

$$^1A_{2g}: \quad \Delta\mathbf{Q}=\sum_m q_m\mathbf{t}_m \tag{47a}$$

$$\Delta D=|\sum_m q_m \exp(im\pi/3)|^2 \tag{47b}$$

$$^1B_{1u}: \quad \Delta\mathbf{Q}=\sum_m q_m\mathbf{r}_{-2m} \tag{48a}$$

$$\Delta D=|\sum_m q_m \exp(i2m\pi/3)|^2 \tag{48b}$$

$$^1B_{2u}: \quad \Delta\mathbf{Q}=\sum_m q_m\mathbf{t}_{-2m} \tag{49a}$$

$$\Delta D=|\sum_m q_m \exp(i2m\pi/3)|^2, \tag{49b}$$

where q_m is the value of a transition-moment parameter for the substituent at m and $\mathbf{r}_{km}$ and $\mathbf{t}_{km}$ are the unit transition-moment vectors

$$\mathbf{r}_{km}=\mathbf{i}\cos(km\pi/3)+\mathbf{j}\sin(km\pi/3)$$

$$\mathbf{t}_{km}=\mathbf{j}\cos(km\pi/3)-\mathbf{i}\sin(km\pi/3). \tag{50}$$

The vectors for $k=1, -2$ are shown in Fig. 3.

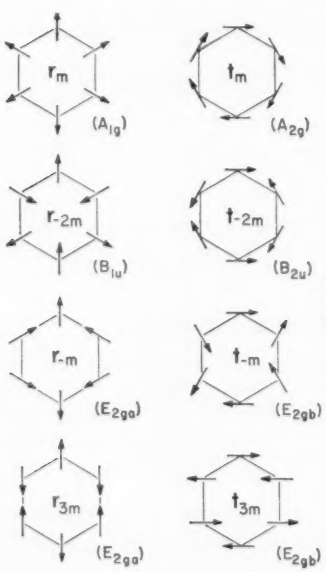

FIG. 3. Unit transition-moment vectors for the symmetry-forbidden transitions of benzene.

(2) Twofold-degenerate, symmetry-forbidden transitions to excited state $^1E_{2g}$:

$$\Delta\mathbf{Q}_+=\sum_m\{q_m\mathbf{r}_{-m+3\omega/\pi}+\Delta q_m\mathbf{r}_{3m-3\omega/\pi}\}$$

$$\Delta\mathbf{Q}_-=\sum_m\{q_m\mathbf{t}_{-m+3\omega/\pi}-\Delta q_m\mathbf{t}_{3m-3\omega/\pi}\} \tag{51a}$$

$$\Delta D=|\Delta Q_+|^2+|\Delta Q_-|^2$$

$$=2\{|\sum_m q_m \exp(im\pi/3)|^2+|\sum_m \Delta q_m(-1)^m|^2\}, \tag{51b}$$

where q_m and $\Delta q_m(\leq q_m)$ are the values of two transition-moment parameters for the substituent at m and $\mathbf{r}_{km\pm3\omega/\pi}$ and $\mathbf{t}_{km\pm3\omega/\pi}$ are the unit transition-moment vectors

$$\mathbf{r}_{km\pm3\omega/\pi}=\mathbf{i}\cos(km\pi/3\pm\omega)+\mathbf{j}\sin(km\pi/3\pm\omega)$$

$$\mathbf{t}_{km\pm3\omega/\pi}=\mathbf{j}\cos(km\pi/3\pm\omega)-\mathbf{i}\sin(km\pi/3\pm\omega). \tag{52}$$

The value of ω, in terms of the *diagonal* perturbation matrix elements a_m and b_m for the "a" and "b" components of the twofold degenerate excited state, is determined by

$$2\omega=\tan^{-1}\left[\frac{\sum_m(a_m-b_m)\sin(2m\pi/3)}{\sum_m(a_m-b_m)\cos(2m\pi/3)}\right]. \tag{53}$$

The directions of the unit transition-moment vectors for $k=-1, 3$ when $\omega=0$ are shown in Fig. 3.

(3) Twofold-degenerate symmetry-allowed transitions to excited state $^1E_{1u}$:

$$\Delta\mathbf{Q}_\pm=-\tfrac{1}{2}\mathbf{Q}_\pm[\sum_m\{\gamma_m\pm\Delta\gamma_m\cos(2m\pi/3-2\omega)\}$$

$$+\sum_{M=0}^{3}\{C_M|\sum_m\delta_m\exp(iMm\pi/3)|^2\pm C_M'\sum_m\sum_p\delta_m\delta_p$$

$$\times\cos[(1-M)m\pi/3+(1+M)p\pi/3-2\omega]\}] \tag{54a}$$

$$\Delta D=\Delta D_++\Delta D_-=2\{\mathbf{Q}_+\cdot\Delta\mathbf{Q}_++\mathbf{Q}_-\cdot\Delta\mathbf{Q}_-\}$$

$$=-D\{\sum_m\gamma_m+\sum_{M=0}^{3}C_M|\sum_m\delta_m$$

$$\times\exp(iMm\pi/3)|^2\}, \tag{54b}$$

where γ_m, $\Delta\gamma_m(\leq\gamma_m)$, and δ_m are the values of three parameters for the substituent at m; C_M and C_M' are coefficients characteristic of the transition; $\mathbf{Q}_\pm$ are the initial transition moments

$$\mathbf{Q}_+=|Q_+|(\mathbf{i}\cos\omega+\mathbf{j}\sin\omega)$$

$$\mathbf{Q}_-=|Q_-|(\mathbf{j}\cos\omega-\mathbf{i}\sin\omega), \tag{55}$$

and $D=|Q_+|^2+|Q_-|^2$ is the initial total transition probability.

For the frequency shifts ($-\Delta\nu$), on the other hand, the formulas are as follows:

(1) Nondegenerate transitions to excited state $^1A_{1g}$, $^1A_{2g}$, $^1B_{1u}$, or $^1B_{2u}$:

$$-\Delta\nu=\sum_m l_m+\sum_{M=0}^{3}C_M\left|\sum_m v_m\exp(iMm\pi/3)\right|^2, \quad (56)$$

where l_m and v_m are the values of two parameters for the substituent at m, and C_M are constants for the transition.

(2) Twofold-degenerate transitions to excited state $^1E_{1u}$ or $^1E_{2g}$:

$$-\Delta\nu=-\tfrac{1}{2}(\Delta\nu_+ +\Delta\nu_-)$$

$$=\sum_m l_m+\sum_{M=0}^{3}C_M\left|\sum_m v_m\exp(iMm\pi/3)\right|^2 \quad (57a)$$

$$|\Delta(\Delta\nu)|=|\Delta\nu_+-\Delta\nu_-|=\Big|\sum_m 2\Delta l_m\cos(2m\pi/3-2\omega)$$

$$+\sum_{M=0}^{3}C_M'\sum_m\sum_p v_m v_p F$$

$$\times\cos[(1-M)m\pi/3+(1+M)p\pi/3-2\omega]\Big|, \quad (57b)$$

where l_m, $\Delta l_m(\leq l_m)$, and v_m are the values of three parameters for the substituent at m; C_M and C_M' are constants for the transition; and $F=1$ for $^1E_{1u}$, $(-1)^{m+p}$ for $^1E_{2g}$.

Predictions for Homosubstitution

If the substituents are all the same the following predictions are made:

(1) The transition probabilities induced in a symmetry-forbidden transition, exhibit a characteristic pattern determined by the M value of the excited state. For the various types of excited states the transition probabilities relative to monosubstitution are given as follows:

$^1A_{1g}$, $^1A_{2g}(M=0)$:

$$\Delta D/\Delta D(1)=\left|\sum_m\exp(im\pi/3)\right|^2 \quad (58a)$$

$^1E_{2g}(M=2)$:

$$\Delta D/\Delta D(1)=(1+w)^{-1}\{\left|\sum_m{}'\exp(im\pi/3)\right|^2$$

$$+w\left|\sum_m(-1)^m\right|^2\} \quad (58b)$$

$^1B_{1u}$, $^1B_{2u}(M=3)$:

$$\Delta D/\Delta D(1)=\left|\sum_m\exp(i2m\pi/3)\right|^2, \quad (58c)$$

where $w=(\Delta q)^2/q^2\leq 1$. The resultant patterns for the twelve possible homosubstitutions in benzene are shown in Fig. 4.

(2) The changes in the total transition probability of a twofold-degenerate symmetry-allowed transition

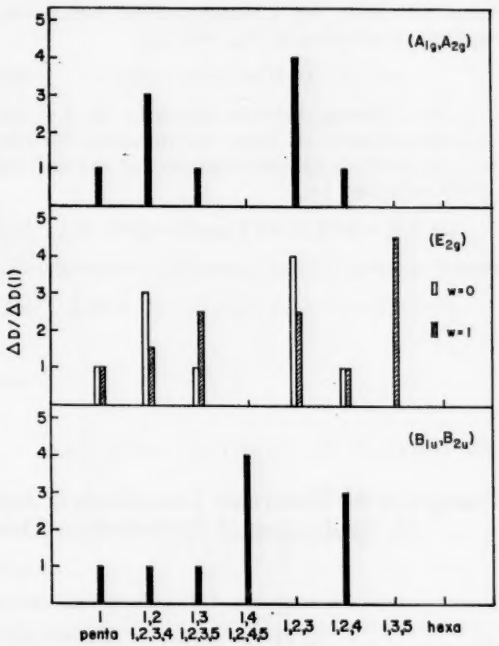

FIG. 4. Homosubstitution intensity patterns for the symmetry-forbidden transitions of benzene.

(excited state $^1E_{1u}$ with $M=1$) exhibit a pattern made up of two parts; one part being proportional to the *number* of substituents, the other varying in a characteristic manner with their *arrangement*,

$$-\Delta D/D=\gamma_n+\delta^2\sum_{M=0}^{3}C_M\left|\sum_m\exp(iMm\pi/3)\right|^2, \quad (59)$$

where n is the number of substituents. The variation with arrangement, determined by the coefficients C_M, depends upon the relative amounts of mixing of the parent ground and excited states with the various other benzene states.

(3) The frequency shifts of a nondegenerate transition or the *average* frequency shifts for two components of a twofold-degenerate transition also exhibit a pattern with two parts (one part proportional to the number of substituents, the other varying with their arrangement),

$$-\Delta\nu=l\text{n}+v^2\sum_{M=0}^{3}C_M\left|\sum_m\exp(iMm\pi/3)\right|^2. \quad (60)$$

Here the coefficients C_M, which determine how the frequency shift varies with the relative positions of the substituents, depend upon the magnitudes of the energy changes caused by the interactions with the various benzene states.

(4) Although the coefficients C_M may be different for different transitions, the frequency shift for 1,3,5-trisubstitution is always *three times* the difference be-

tween the shifts for 1,3-disubstitution and monosubstitution according to Eq. (60), i.e.,

$$\Delta\nu(1,3,5)=3[\Delta\nu(1,3)-\Delta\nu(1)]. \quad (61)$$

Also, the difference between the shifts for 1,4- and 1,3-disubstitution is *C times* the difference between twice the shift for monosubstitution and the shift for 1,3-disubstitution, i.e.,

$$\Delta\nu(1,4)-\Delta\nu(1,3)=C[2\Delta\nu(1)-\Delta\nu(1,3)], \quad (62)$$

where C, a constant for each transition, is determined by

$$C=(3C_2-C_1-4C_3)/(C_2+C_1-2C_3-2C_0). \quad (63)$$

Equivalent relationships are also predicted for the transition-probability changes by Eq. (59).

ACKNOWLEDGMENTS

The author is grateful to Professor J. R. Platt, who sponsored the research in this and the following two papers, for his kindly assistance, patience, and encouragement. He also thanks the other members of the Laboratory of Molecular Structure and Spectra, particularly Professor R. S. Mulliken, Professor C. C. J. Roothaan, and Dr. M. Gouterman, for many interesting and stimulating discussions.

THE JOURNAL OF CHEMICAL PHYSICS VOLUME 34, NUMBER 4 APRIL, 1961

Changes in the Electronic Transitions of Aromatic Hydrocarbons on Chemical Substitution. II. Application of Perturbation Theory to Substituted-Benzene Spectra* †

JOHN PETRUSKA‡

Laboratory of Molecular Structure and Spectra, University of Chicago, Chicago, Illinois

(Received October 24, 1960)

An analysis is made of the changes that occur in the 2600, 2050, and 1850 A transitions of benzene on chemical substitution. Formulas derived by first- and second-order perturbation theory, with coefficients evaluated by molecular orbital theory, are presented and applied to a large collection of intensity-change and frequency-shift data obtained from the literature. Most of these data pertain to the 2600 A transition. The first-order intensity formula derived for the 2600 A transition (taking the excited state to be $^1B_{2u}$) is found to hold quite well for substituents with monoshift (frequency shift on monosubstitution) less than 1500 cm^{-1}; the first- and second-order frequency-shift formula, for substituents with monoshift less than 2000 cm^{-1}. No attempt is made to analyze the intensity changes observed in the 2050 and 1850 A transitions as these changes are too small, relative to the initial intensity, to be reliably measured for weakly perturbing substituents from existing spectra. The frequency shifts, however, can be measured fairly reliably for these two transitions, and it is shown that the formulas derived on the basis of $^1B_{1u}$ and $^1E_{1u}$ excited states, respectively, hold for methyl substitution at least. Empirical values of the intensity and frequency perturbation parameters for the 2600 A transition are presented for over 30 substituents; values of the frequency perturbation parameters for the 2050 and 1850 A transitions for more than half of these are also presented. The meaning of the parametric values is discussed in the light of theoretical expectations.

INTRODUCTION

THE considerable amount of data in the literature on the near-ultraviolet absorptions of benzene derivatives affords an opportunity to test and apply the perturbation formulas derived in paper I.[1]

As is well known, benzene has three absorption systems in the 2700–1800 A near-ultraviolet region. These systems, shown in Fig. 1 for a solution of benzene in aliphatic-hydrocarbon solvent, are identified with transitions from the ground electronic state ($^1A_{1g}$) to different excited singlet electronic states that are symmetric with respect to reflection in the plane of the benzene ring.[2] The weak 2600 A and fairly intense 2050 A systems are identified with symmetry-forbidden transitions to $^1B_{2u}$ and $^1B_{1u}$ states, respectively; the very intense 1850 A system, with symmetry-allowed transitions to a twofold-degenerate, $^1E_{1u}$ state. In the labeling scheme devised by Platt,[3] these excited states are designated as ^1L_b, ^1L_a, and $^1B_{a,b}$ (or simply ^1B), respectively. The corresponding absorption systems in a substituted benzene, 1,4-dimethylbenzene, are shown in Fig. 2.

In this paper the observed intensity changes and frequency shifts of these systems on chemical substitution are analyzed in some detail, with the following

* This work was supported by a Shell Oil Fellowship.

† Part of a Ph.D. dissertation presented to the University of Chicago, 1960.

‡ Now at the California Institute of Technology, Pasadena, California.

[1] J. Petruska, J. Chem. Phys. **34**, 000 (1961).

[2] M. Goeppert-Mayer and A. L. Sklar, J. Chem. Phys. **6**, 645 (1938); C. C. J. Roothaan and R. S. Mulliken, *ibid.* **16**, 118 (1948); C. C. J. Roothaan and R. G. Parr, *ibid.* **17**, 1001 (1949); R. Pariser and R. G. Parr, *ibid.* **21**, 767 (1953).

[3] J. R. Platt, J. Chem. Phys. **17**, 484 (1949).

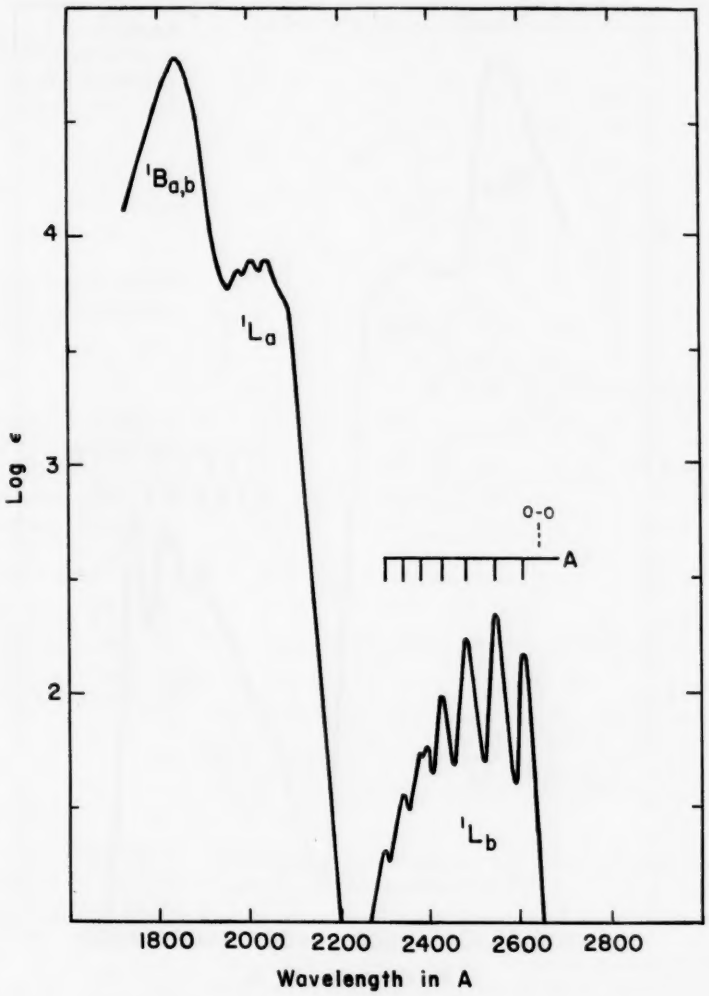

FIG. 1. Absorption spectrum of benzene in heptane or isooctane (according to Jones and Taylor and the American Petroleum Institute *Catalog of Ultraviolet Spectra*).

chief aims in mind: (a) to establish the kinds of substitution to which the formulas of paper I are applicable; (b) to determine which terms in the formulas are important for the 2600, 2050, and 1850 A benzene transitions; (c) to obtain empirical values for the intensity and frequency perturbation parameters for a variety of substituents; and (d) to interpret the empirical values in the light of theory.

THE 2600 A SYSTEM

The 2600 A (^1L_b) system in benzene is vibrationally induced; its intensity, $I^0=I_v{}^0(=0.0016$ in units of oscillator strength), being produced by ring-distorting vibrations of type e_{2g}.[4] The principal series of absorption peaks, labeled *A* in Fig. 1, represents transitions made allowed by a 520 cm^{-1} e_{2g} vibration in the excited state. These are the transitions from the ground-state zero-point vibrational level to the excited-state vibrational levels having $n=0, 1, 2, \cdots$ quanta of 920 cm^{-1} a_{1g} (totally-symmetric) vibration *plus* 1 quantum of 520 cm^{-1} e_{2g} vibration. There is no appreciable peak corresponding to 0–0 or any other transition in which only totally symmetric vibrations are involved. Such transitions are *symmetry-forbidden*. The 0–0 peak position, indicated by a broken line in Fig. 1, is expected to be at 38 089 cm^{-1} in vapor; 37 850 cm^{-1} in aliphatic-hydrocarbon solvent.

Intensity Changes

In a substituted benzene, like 1,4-dimethylbenzene (Fig. 2), the intensity has two components.[5] In addition

[4] H. Sponer, G. Nordheim, A. L. Sklar, and E. Teller, J. Chem. Phys. **7**, 207 (1939).

[5] A. L. Sklar, J. Chem. Phys. **10**, 135 (1942).

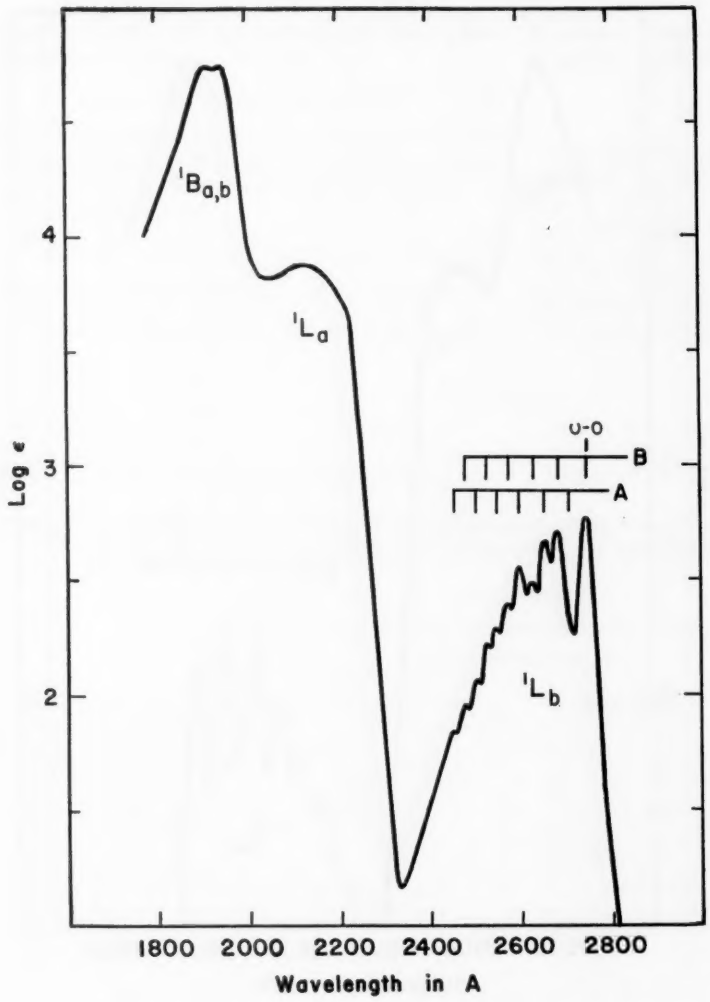

FIG. 2. Absorption spectrum of 1,4-dimethylbenzene in heptane or isooctane (according to Jones and Taylor and the American Petroleum Institute *Catalog of Ultraviolet Spectra*).

to a vibrationally induced component I_v, the counterpart of I_v^0, there is a substituent-induced component I_q.

The component I_q has as its principal series of peaks, that labeled B in Fig. 2, starting with the 0–0 transition. This series corresponds to the symmetry-forbidden transitions in benzene from the ground-state zero-point level to the excited-state levels having $n=0, 1, 2, \cdots$ quanta of 920 cm^{-1} a_{1g} vibration *alone*.[6] These transitions are made allowed to various extents by the substituent perturbations.

Evaluation of I_v and I_q

For three cases of homosubstitution (substitution involving identical substituents) $I_q=0$, as revealed by the *absence* of the B series of peaks (including 0–0). These are 1,2,3-, 1,3,5-, and hexa-, for which the transition moment induced by the substituents are predicted to cancel out when the excited state is $^1B_{2u}$.[1,5] In these cases, for which a direct measurement of I_v is possible, values of I_v in the range 1 to 3 times I_v^0 are found (Table I), with $I_v(1, 2, 3) \approx I_v(1, 3, 5) \leqslant I_v(\text{hexa})$. Assuming that I_v varies regularly with the *number* of substituents but is independent of their arrangement, as suggested by Sklar,[5] one may estimate its value for other substitutions from these $I_q \rightarrow 0$ homosubstitution values and the benzene value (I_v^0) by interpolation. Subtracting I_v from the total intensity I, one obtains I_q.

Values of I_v and I_q derived from spectra in the literature are presented in Table I for various substitutions. These are given as oscillator strengths, f_v and f_q, re-

[6] F. A. Matsen, W. W. Robertson, and R. L. Chuoke, Chem. Revs. **41**, 273 (1947).

spectively. The total oscillator strength f is evaluated by measuring the area under the absorption curve in units of $\epsilon\nu$, where ϵ is the molar extinction coefficient in liters/mole-cm and ν is the frequency in cm^{-1}, and applying the formula[7]

$$f=4.32\times10^{-9}\int \epsilon d\nu. \quad (1)$$

Values of ΔD

From f_q we can determine ΔD, the change in transition probability produced by the substituent perturbations. For this purpose we use the formula[7]

$$\Delta D=9.22\times10^{-12}f_q/(\nu^0+\Delta\nu),$$

where ν^0 is the frequency of the electronic transition in benzene and $\Delta\nu$ is the frequency shift in the derivative. As the value of ν^0 we take the frequency at the maximum of the envelope for the A series of peaks *minus* 520 cm^{-1} (the frequency of the e_{2g} vibration). This value, 39 000 cm^{-1} in vapor and 38 800 cm^{-1} in solution, represents the frequency of the Frank-Condon transition in the absence of ring-distorting vibrations. For $\Delta\nu$ we take the frequency shift of the 0–0 peak, which can be fairly accurately measured. The resultant values of ΔD, along with the values of $\Delta\nu$ found for the 0–0 peak, are included in Table I. For small $\Delta\nu$, ΔD is given approximately by

$$\Delta D=2.4\times10^{-16}f_q. \quad (3)$$

Comparison with Theory

On the grounds that the excited state of the 2600 A system in benzene is $^1B_{2u}$, we expect ΔD to obey the following formula, derived in paper I, as long as the substituent perturbations are small and independent of one another,

$$\Delta D=|\sum_m q_m \exp(i2m\pi/3)|^2, \quad (4)$$

where $m=0, 1, \cdots, 5$ labels the carbons in order on going clockwise around the ring, and q_m is the transition-moment constant for the substituent at m. The conventional carbon labels, which are used in Table I, correspond to $m+1$.

From the work of Sklar[5] and Platt[8] we already know that Eq. (4) is applicable for several different substitutions. Our analysis of the data in Table I reveals that it holds quite well for substituents whose monoshifts (frequency shifts on monosubstitution) are *less* than 1500 cm^{-1}. As the monoshift increases there is a more or less regular departure from the predictions of Eq. (4). This is to be expected on the grounds that increasing monoshift means increasing strength of perturbation. The departure for 1,2-, 1,3-, and 1,4-disubstitutions is shown in Fig. 3.

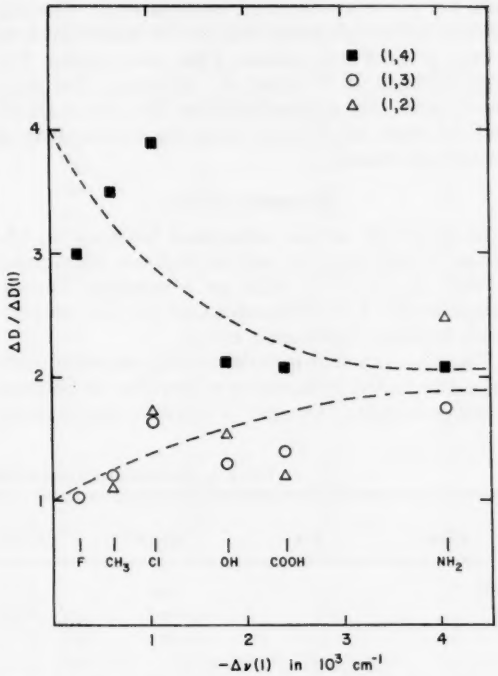

FIG. 3. Illustration of departure from Eq. (4) for the ^1L_b transition as strength of perturbation increases. Substituent-induced transition probability relative to monosubstitution, $\Delta D/\Delta D(1)$, for 1,2-, 1,3-, and 1,4-disubstitution is shown as a function of the monoshift, $-\Delta\nu(1)$. The predicted values are 1, 1, and 4, respectively.

Empirical q values

In Table II are presented empirical values of the transition-moment parameter q obtained from ΔD in Table I. For the substituents with monoshift *less* than 1500 cm^{-1}, Eq. (4) is considered to hold at least semi-quantitatively and is used in evaluating q. The values shown for F, Cl, Br, CH_3, CH_2CH_3, $CH(CH_3)_2$, $C(CH_3)_3$, CF_3, and aza (N) are the average values, with standard deviation 10% or less, obtained from the two or more homosubstitutions for which ΔD is known. Those for I, CH_2F, CHF_2, CH_2Cl, $CHCl_2$, CCl_3, CH_2OH, CH_2NH_2, CH_2COOH, and CH_2CHCH_2 are obtained from monosubstitution data alone; there being only such data available for these substituents.

For substituents with monoshift *greater* than 1500 cm^{-1}, Eq. (4) is considered to hold only qualitatively at best. The q values shown for OH, OCH_3, SH, NH_2, CHO, COOH, $COOCH_3$, CN, $CHCH_2$, and CCH are those obtained from monosubstitution in accordance with $\Delta D(1)=q^2$. These are included for comparison.

The *sign* of q is established as follows. For CH_3 it is taken to be *positive* arbitrarily. Then, in accordance

[7] R. S. Mulliken and C. A. Rieke, Repts. Progr. in Phys. **8**, 231 (1941).
[8] J. R. Platt, J. Chem. Phys. **19**, 263 (1951).

with Eq. (4), if a substituent in combination with CH_3 leads to ΔD for 1,4- *greater* than for 1,3- substitution, its q value is taken to be *positive*; if *less* than, *negative*. The signs enclosed in brackets are uncertain. For these substituents only monosubstitution data are available and the signs are inferred from the known signs of related substituents.

Frequency Shifts

In practically all the substituted benzenes the ^1L_b system is shifted to the red, i.e. to lower frequencies, so that the frequency shift $\Delta\nu$ is negative. Notable exceptions are 1,3,5-trifluorobenzene and the aza benzenes (pyridine, pyridazine, etc.).

The frequency shift is fairly precisely measured with respect to the 0–0 peak. One can determine the position of this peak within a few cm^{-1} in vapor and within about 30 cm^{-1} in solution. The 0–0 frequency in benzene is considered to be 38 089 cm^{-1} in vapor, 37 850 cm^{-1} in aliphatic-hydrocarbon solvents (hexane, heptane, or isooctane), 37 860 cm^{-1} in alcohol, and 37 980 cm^{-1} in water (Table I).

The values of the frequency shift recorded in Table I refer to the 0–0 peak except in cases where the vibrational structure is inadequately resolved. In these cases, for which the value is enclosed in brackets, the shift is measured with respect to the maximum of the envelope for the B transitions (the transitions made allowed by the substituent perturbations). This maximum for benzene is estimated to be at 39 000 cm^{-1} in vapor and 38 800 cm^{-1} in solution (aliphatic-hydrocarbon or alcohol), assuming that the intensity distribution for the B series would be the same as for the A series if the B transitions could be seen.

TABLE I. Intensity and frequency-shift data for the 2600 A (^1L_b) system.

Subst.	Pos.	Med.[a]	f_v ($\times 10^4$)	f_q ($\times 10^4$)	ΔD ($\times 10^{60}$)	$-\Delta\nu$ (cm^{-1})	Ref.[b]
None		vap	16	0	0	0	c
		iso	16.4	0	0	0	d
		alc	17	0	0	0	e
			Homosubstitution				
F	1	vap	17	72	171	270	c
		iso	17	70	167	270	f
	1, 3	vap	17	79	187	180	c
		iso	17	68	162	200	f
	1, 4	vap	17	207	507	1246	c
		iso	17	205	503	1290	f
	1, 2, 4	vap	17	175	423	966	c
		iso	17	170	414	950	f
	1, 3, 5	vap	20	0	0	−438	c
		iso	17	0	0	−440	f
	1, 2, 4, 5	vap				1484	c
Cl	1	vap	18	12	29	1037	c
		iso	18	12	29	1030	g
	1, 2	vap	20	20	50	1824	c
		iso	20	20	50	1850	g
	1, 3	vap	20	21	52	1903	c
		iso	20	18	45	1900	g
	1, 4	vap	20	48	120	2346	c
		iso	20	42	106	2340	g
	1, 2, 3	hex	21	0	0	2600	h
	1, 2, 4	vap	21	39	100	2981	c
		hex	21	32	82	3000	h
	1, 3, 5	vap	21	0	0	2591	c
		hex	21	0	0	2600	h
	1, 2, 3, 4	hex	22	22	57	3550	h
	1, 2, 3, 5	hex	22	20	52	3450	h
	1, 2, 4, 5	hex	22	58	154	3850	h
	penta	hex	23	21	56	4250	h
	hexa	hex	24	0	0	4850	h
		iso	24	0	0	4920	g

TABLE I.—*Continued.*

Subst.	Pos.	Med.[a]	f_p ($\times 10^4$)	f_q ($\times 10^4$)	ΔD ($\times 10^{20}$)	$-\Delta\nu$ (cm^{-1})	Ref.[b]
Br	1	vap				1093	i
		iso	18	10	24	1070	j
	1, 2	hex	20	14	35	1850	k
	1, 3	hex	20	24	60	1950	k
	1, 4	hex	20	32	79	2450	l
	1, 3, 5	hex	21	0	0	2800	m
I	1	iso	20	30	70	(1200)	n
OH	1	vap				1740	i
		iso	20	154	385	1800	o
	1, 2	hex	20	240	600	2700	p
	1, 3	hex	20	200	500	2600	p
	1, 4	hex	20	300	820	5400	p
	1, 3, 5	alc		0	0	(2100)	q
OCH_3	1	hex	20	180	450	1850	p
	1, 2	hex	20	260	650	2400	p
	1, 3	hex	20	220	560	2500	p
	1, 4	hex	20	300	800	4500	p
SH	1	hex	20	110	280	3280	r
NH_2	1	vap				4055	i
		iso	20	224	590	4000	s
		alc	20	220	580	(3800)	t
	1, 2	alc	20	540	1450	(4600)	t
	1, 3	alc	20	380	1020	(4600)	t
	1, 4	alc	20	460	1230	(4400)	t
$NHCH_3$	1	iso	20	280	760	5000	u
$N(CH_3)_2$	1	iso	20	300	830	5600	u
NC	1	hep	20	15	37	1550	v
CH_3	1	vap				605	w
		iso	21	10	24	610	x
	1, 2	vap				781	w
		iso	25	11	27	920	x
	1, 3	vap				1134	w
		iso	25	12	29	1150	x
	1, 4	vap				1356	w
		iso	25	34	84	1390	x
	1, 2, 3	iso	29	0	0	1260	x
	1, 2, 4	iso	29	30	75	1570	x
	1, 3, 5	iso	29	0	0	1520	x
		vap				1532	w
	1, 2, 3, 4	iso	32	13	32	1700	x
	1, 2, 3, 5	iso	32	10	25	1750	x
	1, 2, 4, 5	iso	32	50	120	1890	x
	penta	iso	34	10	25	2030	x
CH_2CH_3	1	iso	21	8	19	550	y
	1, 2	iso	25	9	22	1030	y
	1, 3	iso	25	9	22	1060	y
	1, 4	iso	25	28	69	1250	y
	1, 3, 5	iso	29	0	0	1350	y
$CH(CH_3)_2$	1	iso	21	7	17	470	z
	1, 2	iso	25	8	19	950	z
	1, 3	iso	25	8	19	900	z
	1, 4	iso	25	20	49	1050	z
	1, 3, 5	iso	29	0	0	1200	z

TABLE I.—*Continued.*

Subst.	Pos.	Med.[a]	f_σ ($\times 10^4$)	f_q ($\times 10^4$)	ΔD ($\times 10^{20}$)	$-\Delta\nu$ (cm^{-1})	Ref.[b]
$C(CH_3)_3$	1	iso	21	5	12	400	a′
	1, 3	iso	25	6	14	750	a′
	1, 4	iso	25	14	34	900	a′
	1, 3, 5	iso	29	0	0	1020	a′
CH_2F	1	iso	20	14	34	520	b′
CHF_2	1	iso	20	21	50	380	b′
CF_3	1	vap	20	50	120	270	c
		iso	20	33	80	260	b′
	1, 4	vap	20	100	240	629	c
		iso				620	c′
	1, 3, 5	vap	21	0	0	−10	c
CH_2Cl	1	iso	20	10	24	1000	d′
$CHCl_2$	1	iso	20	25	61	1130	d′
CCl_3	1	iso	20	43	105	1430	d′
CH_2OH	1	alc	20	10	24	550	e′
CH_2NH_2	1	iso	20	10	24	590	f′
CH_2COOH	1	alc	20	10	24	50	e′
$CH_2CH{=}CH_2$	1	alc	20	20	48	550	e′
CHO	1	vap				2895	i
		alc	20	160	410	2930	t
COOH	1	iso	20	125	315	2400	g′
		met	20	100	255	2140	g′
	1, 2	alc	25	120	300	2270	t
	1, 3	alc	25	140	360	3140	t
		wat				3440	h′
	1, 4	alc	25	200	530	3960	t
		wat				4090	h′
	1, 3, 5	wat		0	0	4400	h′
$COOCH_3$	1, 2	iso	25	150	380	2300	g′
	1, 3	iso	25	140	360	3060	g′
	1, 4	iso	25	200	530	3910	g′
$COOC_2H_5$	1	iso	20	110	280	2140	g′
CN	1	vap				1573	i
		iso	20	52	129	1640	i′
$CH{=}CH_2$	1	iso	20	85	220	3500	j′
$CH{=}CHCH_3$	1	iso	20	80	210	3700	j′
$C{\equiv}CH$	1	hex	20	20	50	2400	j′
(N)	1	iso	20	350	810	(−800)	k′
	1, 2	hep	20	180	410	(−1600)	l′
	1, 3	hep	20	500	1110	(−2600)	l′
	1, 4	hep	20	980	2320	(−100)	l′
	1, 3, 5	hep	20	0	0	(−5800)	m′

TABLE I.—*Continued.*

Subst.	Pos.	Med.[a]	f_v ($\times 10^4$)	f_q ($\times 10^4$)	ΔD ($\times 10^{20}$)	$-\Delta\nu$ (cm^{-1})	Ref.[b]
			Heterosubstitution				
F, CH_3	1, 2	vap				463	n′
		hex	20	60	145	600	o′
	1, 3	hex	20	70	170	700	o′
	1, 4	vap				1163	n′
		hex	20	140	350	1350	o′
F, CF_3	1, 3	vap				734	p′
		hep	20	120	290	800	q′
	1, 4	vap				223	p′
		hep	20	10	24	200	q′
Cl, CH_3	1, 2	iso	22	15	37	1270	r′
	1, 3	iso	22	14	34	1460	r′
	1, 4	iso	22	38	95	1790	r′
Br, CH_3	1, 2	hex	22	20	49	1300	o′
	1, 3	hex	22	18	44	1550	o′
	1, 4	hex	22	36	90	1850	o′
I, CH_3	1, 2	hex				1550	o′
	1, 3	hex				1600	o′
	1, 4	hex				2100	o′
OH, CH_3	1, 2	iso	22	200	500	1890	s′
	1, 3	iso	22	177	440	2100	s′
	1, 4	iso	22	196	500	2900	s′
SH, CH_3	1, 2	iso	22	90	230	2980	t′
	1, 3	iso	22	80	210	3370	t′
	1, 4	iso	22	90	240	4000	t′
NH_2, CH_3	1, 2	iso	23	270	710	(3700)	u′
	1, 3	iso	23	250	650	(4100)	u′
	1, 4	iso	23	260	700	(4800)	v′
NC, CH_3	1, 2	hep	23	90	225	2050	v
	1, 4	hep	23	5	12	1850	v
CH_3, CH_2CH_3	1, 2	iso	25	9	22	1000	w′
	1, 3	iso	25	10	24	1100	w′
	1, 4	iso	25	30	74	1320	w′
CH_3, $CH(CH_3)_2$	1, 2	iso	25	9	22	1060	x′
	1, 3	iso	25	10	24	1000	x′
	1, 4	iso	25	28	69	1220	x′
CH_3, $C(CH_3)_3$	1, 2	iso	25	7	17	900	y′
	1, 3	iso	25	8	20	960	y′
	1, 4	iso	25	22	61	1110	y′
CH_3, COOH	1, 2	alc	25	(110)	(280)	(3000)	z′
	1, 3	alc	25	(170)	(440)	(3000)	z′
	1, 4	alc	25	(50)	(125)	(2400)	z′
CH_3, CHO	1, 2	alc	25	(220)	(600)	(4800)	a″
	1, 3	alc	25	(180)	(480)	(4500)	a″
	1, 4	alc	25	(120)	(320)	(3900)	a″

TABLE I.—*Continued.*

Subst.	Pos.	Med.[a]	f_v ($\times 10^4$)	f_q ($\times 10^4$)	ΔD ($\times 10^{20}$)	$-\Delta\nu$ (cm^{-1})	Ref.[b]
CH_3, CN	1, 2	iso	25	112	285	2450	b″
	1, 3	iso	25	86	215	2380	b″
	1, 4	iso	25	30	75	1880	b″
CH_3, $CH{=}CH_2$	1, 3	iso	25	(95)	(250)	4200	c″
	1, 4	iso	25	(155)	(410)	4100	c″
CH_3, (N)	1, 2	iso	20	420	1190	(250)	d″
	1, 3	iso	20	400	950	(350)	d″
	1, 4	iso	20	260	610	(−500)	d″

[a] Medium: vap—vapor, hex—hexane, hep—heptane, iso—isooctane, met—methanol, alc—ethanol, wat—water.

[b] Abbreviations used in references:

API—American Petroleum Institute Research Project 44, *Catalog of Ultraviolet Spectrograms* (National Bureau of Standards, 1945–50, and Carnegie Institute of Technology, 1950–57). The number of the spectrogram is given.

FO—R. A. Friedel and M. Orchin, *Ultraviolet Spectra of Aromatic Compounds* (John Wiley & Sons, Inc., New York, 1951). The number of the spectrogram is given.

[c] H. Sponer, J. Chem. Phys. **22,** 234 (1954).

[d] API, 40; F. A. Matsen, W. W. Robertson, and R. L. Chuoke, Chem. Revs. **41,** 273 (1947).

[e] N. S. Bayliss and L. Hulme, Australian J. Chem. **6,** 257 (1953).

[f] API, 296, 492–5.

[g] API, 234, 300, 458–60.

[h] H. Conrad-Billroth, Z. physik. Chem. **B19,** 76 (1932).

[i] H. Sponer and E. Teller, Revs. Modern Phys. **13,** 76 (1941).

[j] API, 304.

[k] H. Conrad-Billroth and G. Forster, Z. physik. Chem. **B33,** 312 (1936).

[l] F. W. Klingstedt, Z. physik. Chem. **B20,** 125 (1933).

[m] P. Grammaticakis, Bull. soc. chim. France **5,** 762 (1949).

[n] API, 308.

[o] API, 99.

[p] A. Kiss, J. Molnar, and C. Sandorfy, Bull. soc. chim. France **5,** 275 (1949); FO 53–4.

[q] T. W. Campbell and G. M. Coppinger, J. Am. Chem. Soc. **73,** 2708 (1951).

[r] API, 586.

[s] API, 171.

[t] R. A. Morton and A. L. Stubbs, J. Chem. Soc. **1940,** 1347.

[u] API, 372–3.

[v] K. L. Wolf and O. Strasser, Z. physik. Chem. **B21,** 389 (1933).

[w] V. J. Hammond, W. C. Price, J. P. Teegan, and A. D. Walsh, Discussions Faraday Soc. **9,** 53 (1950).

[x] API, 42–5, 126–9, 162–4, 391–3.

[y] API, 20, 186–8, 618.

[z] API, 160, 189–91, 620.

[a′] API, 166, 236–7, 622.

[b′] API, 297–9.

[c′] C. D. Cooper and F. W. Noegel, J. Chem. Phys. **20,** 1903 (1952).

[d′] API, 301–3

[e′] T. W. Campbell, S. Linden, S. Godshalk, and W. G. Young, J. Am. Chem. Soc. **69,** 880 (1947).

[f′] FO, 19.

[g′] API, 354–5, 358, 380–2.

[h′] N. Berman, C. H. Ruof, and H. C. Howard, Anal. Chem. **23,** 1882 (1951).

[i′] API, 227.

[j′] API, 121, 168; R. A. Morton, A. Hassan, and T. C. Calloway, J. Chem. Soc. **1934,** 883.

[k′] API, 108.

[l′] H. B. Klevens and J. R. Platt, *Survey of Ultraviolet Spectra of Organic Compounds in Solution* (Reprinted from Technical Report 1953–4 Part One, Laboratory Molecular Structure and Spectra, University of Chicago).

[m′] R. C. Hirt, F. Halverson, and R. G. Schmitt, J. Chem. Phys. **22,** 1148 (1954).

[n′] H. Tentex, Bull. sect. sci. acd. roumaine **21,** 219 (1939); **22,** 16 (1939).

[o′] H. Conrad-Billroth, Z. physik. Chem. **B25,** 141 (1934).

[p′] W. T. Cave and H. W. Thompson, Discussions Faraday Soc. **9,** 35 (1950).

[q′] C. H. Miller and H. W. Thompson, J. Chem. Phys. **17,** 845 (1949).

[r′] API, 116–8.

[s′] API, 322, 429, 431.

[t′] API, 433, 435, 437.

[u′] FO, 84–5.

[v′] API, 107.

[w′] API, 63–4, 161.

[x′] API, 534–6.

[y′] API, 463–5.

[z′] C. M. Moser and A. I. Kohlenberg, J. Chem. Soc. **1951,** 804.

[a″] P. Grammaticakis, Bull. soc. chim. France **5,** 821 (1953).

[b″] API, 228–30.

[c″] K. C. Bryant, G. T. Kennedy, and E. M. Tanner, J. Chem. Soc. **1949,** 2389.

[d″] API, 478–81.

Comparison with Theory

Tables III and IV show how well two predictions for homosubstitution based on the general frequency-shift formula,

$$-\Delta\nu=\sum l_m+\sum_{M=0}^{3}C_M\,|\,\sum v_m\exp(iMm\pi/3)\,|^2, \quad (5)$$

derived in paper I are obeyed. The predictions are that

$$[-\Delta\nu(1,3,5)/3]=[\Delta\nu(1)-\Delta\nu(1,3)], \quad (6)$$

and that

$$[\Delta\nu(1,3)-\Delta\nu(1,4)]/[\Delta\nu(1,3)-2\Delta\nu(1)]=C, \quad (7)$$

a constant characteristic of the transition given by

$$C=(3C_2-C_1-4C_3)/(C_2+C_1-2C_3-2C_0). \quad (8)$$

From Table III is is apparent that Eq. (6) is obeyed quite well by substituents with monoshift *less* than 2000 cm^{-1}. Table IV reveals that C of Eq. (7) is very nearly constant for such substituents, with an average value 2.7±0.2.

TABLE II. Empirical q values for the ^1L_b transition.

Substituent	$q\times10^{10}$	Substituent	$q\times10^{10}$
Monoshift <1500 cm^{-1}		$CH_2CH{=}CH_2$	(−)7
F	12.5	(*N*)	−27
Cl	6.0	Monoshift >1500 cm^{-1}	
Br	6	OH	20
I	8	OCH_3	21
CH_3	5.0	SH	17
CH_2CH_3	4.5	NH_2	24
$CH(CH_3)_2$	4.0	$NHCH_3$	27
$C(CH_3)_3$	3.5	$N(CH_3)_2$	29
CH_2F	(−)6	NC	−6
CHF_2	(−)7	CHO	−20
CF_3	−9	COOH	−17
CH_2Cl	(−)5	$COOCH_3$	−17
$CHCl_2$	(−)8	CN	−11
CCl_3	(−)10	$CH{=}CH_2$	15
CH_2OH	(−)5	$CH{=}CHCH_3$	15
CH_2NH_2	(−)5	C≡CH	(+)7
CH_2COOH	(−)5		

On comparing ΔD and $-\Delta\nu$ in Table I one finds that apart from a linear term depending on the number of substituents, $-\Delta\nu$ varies much like ΔD. This similarity, which was first noted by Forster,[9] indicates that C_2 is the *most important* of the coefficients C_M for the ^1L_b transition. Setting $C_2=1$ and $C_0=C_1=C_3=0$, one obtains a two-term frequency-shift formula like that proposed by Forster[9] and used by Sponer[10]

$$-\Delta\nu=\sum l_m'+|\sum v_m'\exp(i2m\pi/3)\,|^2. \quad (9)$$

This gives $C=3$, which is in quite good agreement with the observed values in Table IV.

That a *positive* C_2 coefficient should be most important is predicted by molecular orbital theory, as shown by the work of Murrell and McEwen.[11] Of the second-order *inductive* energy changes in the parent $^1A_{1g}$ ground and $^1B_{2u}$ excited states, resulting from the interactions with the various benzene-ring states, that coming from the interaction of the excited state with the $^1E_{1u}$ state at 1850 A is predicted to be the *largest* for monosubstitution. This gives a positive contribution to the $M=2$ coefficient since the M values[1] of $^1B_{2u}$ and $^1E_{1u}$ (3 and 1, respectively) *differ* by 2 and the energy of the $^1B_{2u}$ excited state is *lowered* by the interaction. Part of this large positive contribution to C_2 (about one-half) is cancelled out by the negative contribution from the depression of the $^1A_{1g}$ ($M=0$) ground state by the two $^1E_{2g}$($M=2$) states expected around 1600 and 1100 A.[11,12]

The next most important coefficient is predicted to be C_3 with a value approximately-0.2C_2 according to the Murrell-McEwen results.[11,12] The $M=3$ coefficient has a fairly large *negative* contribution from the depression of the ground state by the $^1B_{1u}$ ($M=3$) state at 2050 A, which is about two-thirds cancelled out by the positive contribution from the depression of the excited state by the $^1A_{2g}$ ($M=0$) state expected around 1300 A. Upon taking $C_2=1$ and $C_3=-0.2$ (leaving

TABLE III. Comparison of $l_I'=[\Delta\nu(1)-\Delta\nu(1,3)]$ and $l_{II}'=-\Delta\nu(1,3,5)/3$ for the ^1L_b transition (in cm^{-1}).

Substituent	Medium	l_I'	l_{II}'	Average (l')
F	vap	−90	−146	−118±28
Cl	vap	866	864	865±1
Br	hex	880	930	905±25
OH	hex, alc	800	700	750±50
CH_3	vap	529	511	520±9
(N)	hep	−1800	−1930	−1865±65

TABLE IV. Evaluation of $C=[\Delta\nu(1,3)-\Delta\nu(1,4)]/[\Delta\nu(1,3)-2\Delta\nu(1)]$ for the ^1L_b transition.

Substituent	Medium	$[\Delta\nu(1,3)-\Delta\nu(1,4)]$	$[\Delta\nu(1,3)-2\Delta\nu(1)]$	C
F	vap	1066	360	3.0
Cl	vap	443	171	2.6
Br	hex	500	190	2.6
OH	hex	2800	1000	2.8
CH_3	vap	222	76	2.9
(N)	hep	2500	1000	2.5
			Av	2.7±0.2

[9] Th. Forster, Z. Naturforsch **2a,** 149 (1947).
[10] H. Sponer, J. Chem. Phys. **22,** 234 (1954).
[11] J. N. Murrell and K. Lenore McEwen, J. Chem. Phys. **25,** 1143 (1956).
[12] Murrell and McEwen calculated the depression of the ground state and $^1B_{2u}$ excited state by the various other benzene states in terms of $(\Delta\alpha)^2$, where $\Delta\alpha$ is the change in the coulomb integral for the carbon to which the substituent is attached. In units of $(\Delta\alpha)^2$ we find from their results for monosubstitution: C_2= (depression of the excited state by the $^1E_{1u}$ state) − (depression of the ground state by the two $^1E_{2g}$ states) = 0.0597 − 0.0257 − 0.0019 = 0.0321; C_3 = (depression of the excited state by the $^1A_{2g}$ state) − (depression of the ground state by the $^1B_{1u}$ state) = 0.0119 − 0.0181 = −0.0062. Hence $C_3/C_2=-0.2$.

TABLE V. Empirical l and v values for the ^1L_b transition.

Substituent	l (cm^{-1})	v (cm^{-1})
Monoshift <2000 cm^{-1}		
F	50	17.0
Cl	935	11.0
	840 ortho	
Br	975	11
I	1000	15
OH	1200	27.5
OCH_3	1100	26.0
CH_3	560	8.0
	405 ortho	
CH_2CH_3	515	7.5
$CH(CH_3)_2$	440	7.0
$C(CH_3)_3$	370	6.5
CH_2F	470	(−)8 est.
CHF_2	320	(−)9 est.
CF_3	100	−10
CH_2Cl	960	(−)7 est.
$CHCl_2$	1050	(−)10 est.
CCl_3	1300	(−)13 est.
CH_2OH	510	(−)7 est.
CH_2NH_2	550	(−)7 est.
CH_2COOH	0	(−)7 est.
CH_2CHCH_2	490	(−)9 est.
CN	1350	−15
NC	1400	−8
(N)	−1430	−27
Monoshift >2000 cm^{-1}		
SH	3000	19
NH_2	3550	21
COOH	2150	−18
CHO	2650	−18
$CHCH_2$	3500	(−3)

$C_0=C_1=0$) one has the three-term frequency-shift formula for the ^1L_b transition,

$$-\Delta\nu=\sum l_m+|\sum v_m \exp(i2m\pi/3)|^2 -0.2|\sum v_m(-1)^m|^2. \quad (10)$$

This gives $C=2.71$, which is in excellent agreement with the average value in Table IV.

For substituents with monoshift greater than 2000 cm^{-1} a frequency-shift formula of the general form of Eq. (5), such as Eq. (9) or (10), breaks down. With increasing monoshift there is a departure similar to that observed for the intensity changes (Fig. 3). The value of C, for instance, instead of remaining constant around 2.7, decreases rapidly with increasing monoshift beyond 2000 cm^{-1}; dropping to 0.9 for COOH (monoshift 2400 cm^{-1}) and to −0.1 for NH_2 (monoshift 4000 cm^{-1}).

Empirical l and v values

In Table V are presented values of l and v obtained by applying Eq. (10) to the observed frequency shifts in Table I. The corresponding values of l' and v' obtained by Eq. (9) are very nearly given by $l'=l-0.6v^2$ and $v'=1.16\,v$.

The values shown for F, Cl, Br, OH, OCH_3, CH_3, CH_2CH_3, $CH(CH_3)_2$, $C(CH_3)_3$ and aza (N) are derived from the 1-, 1,3-, 1,4-, and 1,3,5-homosubstitution shifts. For these substituents the monoshift is less than 2000 cm^{-1} and Eq. (10) holds satisfactorily. Taking the quantity in the last column of Table III as the value of $l'=l-0.6\,v^2$, we evaluate v from the following relation dictated by Eq. (10): $8v^2=-\Delta\nu(1)-\Delta\nu(1,3)-\Delta\nu(1,4)-5l'$; and l from the relation, $l=l'+0.6v^2$. The l value labeled ortho shown for CH_3 and Cl is obtained from the other homosubstitutions, in which there are two or more substituents in adjacent (ortho) positions on the ring; more will be said about this later in connection with the ortho effect.

For the other substituents with monoshift less than 2000 cm^{-1}, to which Eq. (10) is considered to be applicable, fewer homosubstitution data are available. The values shown for I, NC, CF_3, and CN are obtained with the aid of data for disubstitutions in which the substituent occurs with CH_3 or F (in the case of CF_3). Knowing the value of v for one substituent, v_1, we can determine the value for the other, v_2, from the difference between the shifts in the 1,3- and 1,4-derivatives, using the predicted relation 4.2 $v_1v_2=\Delta\nu(1,3)-\Delta\nu(1,4)$. Once v is known, the evaluation of l is straightforward, e.g., l can be evaluated from the monoshift by $l=-\Delta\nu(1)-0.8\,v^2$. The values of v shown for CH_2F, CHF_2, CH_2Cl, $CHCl_2$, CCl_3, CH_2OH, CH_2NH_2, CH_2COOH, and CH_2CHCH_2 are estimated from the values of q assuming that v/q for these substituents is approximately the average for CH_3 and CF_3, $v/q=1.3\times10^{10}$.

For the substituents with monoshift *greater* than 2000 cm^{-1} Eq. (10) no longer holds very well. The value of v shown is estimated from the difference between the 1,3- and 1,4-disubstitution shifts when the substituent occurs with the weakly perturbing CH_3 group. The value of l shown is obtained by subtracting the estimated v^2 from the monoshift.

The sign of v is determined in the same way as the sign of q in Table II. For CH_3 a *positive* sign is chosen arbitrarily, as was done for q. Then, if a substituent in combination with CH_3 yields $[\Delta\nu(1,3)-\Delta\nu(1,4)]$ positive, it is also given a positive sign; if negative, a negative sign; in accordance with Eq. (10). The signs enclosed in brackets are uncertain; there being insufficient data to establish them, these are taken to be the same as for q.

Correction for Ortho Effect

In all substitutions apart from 1-, 1,3- 1,4-, and 1,3,5- two or more substituents occupy adjacent positions on the ring. For these there are observed departures from theory that may be attributed to an ortho effect caused by an interaction, possibly steric, between adjacent substituents. In the case of CH_3 and Cl substitutions, especially, the frequency shifts calculated, using the l and v values obtained from the four nonortho substitutions, are *larger* than observed. The difference is approximately *proportional* to n_{ortho}

(the number of ortho substituents), which is taken to be 2 for 1,2- and 1,2,4-, 3 for 1,2,3- and 1,2,3,5-, 4 for 1,2,3,4- and 1,2,4,5-, 5 for penta-, and 6 for hexa-substitution. When Eq. (10) is used, the difference is approximately 155 n_{ortho} for CH_3 and 95 n_{ortho} for Cl (in cm^{-1}); when Eq. (9) is used, approximately 125 n_{ortho} and 40 n_{ortho}, respectively. This difference, being linear in n_{ortho}, may be removed by modifying the l and l' values. On taking in Eq. (10) $l_{ortho}=l-155$ and $l-95$ for CH_3 and Cl, respectively, and in Eq. (9) $l'_{ortho}=l-125$ and $l-40$, respectively, one obtains good agreement with all the observed shifts, as is shown in Fig. 4.

Relatively little difference is found between the shifts calculated by Eqs. (9) and (10) for CH_3 and Cl substitutions, because the v values are small. For substitutions involving F, however, where the v value is twice as large, the difference is quite appreciable. Included in Fig. 4 are the frequency shifts calculated by both equations for all the F substitutions (without any correction for the ortho effect, which for F is expected to be smaller than for Cl). While the shifts calculated for the four non-ortho substitutions agree, those for all the other substitutions differ by 100 to 1000 cm^{-1}. It is apparent that for the two ortho substitutions whose shifts are known, 1,2,4- and 1,2,4,5-, Eq. (10) gives much better agreement with the observed values.

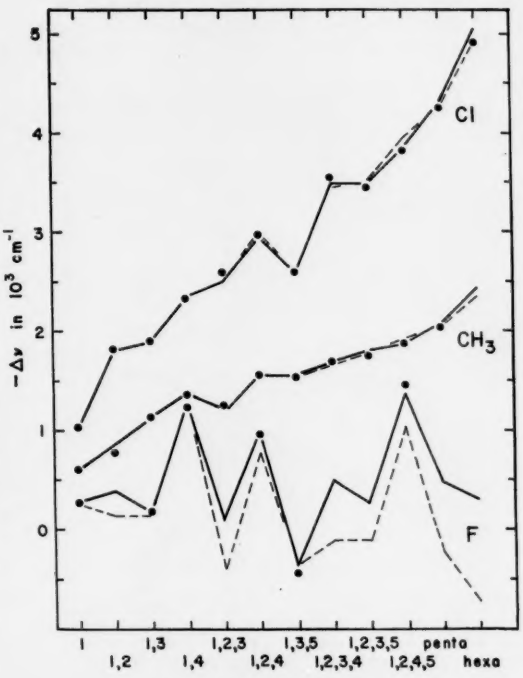

FIG. 4. Comparison of observed and calculated frequency shifts for the ^1L_b transition. The circles represent the observed shifts; the solid line, the shifts calculated by Eq. (10); the dashed line, the shifts calculated by Eq. (9). A correction for the ortho effect is included in the calculated shifts for CH_3 and Cl but not for F (see text).

THE 2050 A AND 1850 A SYSTEMS

Intensity Changes

The intensities of the 2050 A (^1L_a) and 1850 A (^1B) systems show relatively little change for substitutions that might be regarded as weakly perturbing, e.g., alkyl groups and halogens. For each of these systems the initial intensity is large, much larger than for ^1L_b. The symmetry-forbidden ^1L_a system has a vibrationally induced intensity I_v^0 some 60 times larger than ^1L_b. The symmetry-allowed ^1B system has an "allowed" intensity greater by another factor of 10. In each case absolute intensity changes comparable to those in the ^1L_b system, observed for such substituents as CH_3 and Cl, are too small relative to the initial intensity to be reliably measured from existing spectra. The uncertainty in the measured values makes it virtually impossible to make a meaningful comparison with theory.

If the intensity changes could be properly measured, however, we would expect Eq. (5) to hold for the transition-probability changes obtained for the ^1L_a system in the absence of ring-distorting vibrations, assuming that the excited state is initially $^1B_{1u}$.[1] Also, assuming the excited state to be initially twofold-degenerate $^1E_{1u}$, we would expect the following formula (derived in paper I[1]) to hold for the total transition-probability changes in the ^1B system,

$$\Delta D=-D\{\sum\gamma_m+\sum_{M=0}^{3}C_M\,|\delta_m\exp(iMm\pi/3)\,|^2\},\qquad(11)$$

with a positive C_2, determined by the interaction of $^1E_{1u}$ with the $^1B_{1u}$ and $^1B_{2u}$ states below it, being the most important of the coefficients C_M.

Frequency Shifts

While the intensities are little affected, the frequencies of the ^1L_a and ^1B transitions shift markedly. The frequency shifts are 2 to 3 times as large and in the same direction, generally, as those of ^1L_b. For the ^1L_a system, which has poorly defined vibrational structure and is undercut by the ^1B system, the frequency shift is best measured with respect to some point on the low-frequency side of the absorption curve. The point chosen here is that at which $\log\epsilon=3.5$ ($\epsilon=3160$). The frequency at this point in benzene is 48 700 cm^{-1} in vapor and 47 600 cm^{-1} in heptane.[13] For the ^1B system, which is essentially one fairly smooth, broad peak, the shift is best measured with respect to the peak maximum. The maximum in benzene is at 56 250 cm^{-1} in vapor and 54 400 cm^{-1} in heptane.[13,14] Frequency-shift measure-

[13] L. C. Jones, Jr., and L. W. Taylor, Anal. Chem. **27**, 235 (1955).

[14] L. W. Pickett, M. Muntz, and E. M. McPherson, J. Am. Chem. Soc. **73**, 4862 (1951); V. J. Hammond and W. C. Price, Trans. Faraday Soc. **51**, 605 (1955).

TABLE VI. Observed frequency shifts of the 2050 A (^1L_a) and 1850 A (^1B) systems (in hexane, heptane, or isooctane).

Substituent	Pos.	$-\Delta\nu(\text{cm}^{-1})$ ^1L_a	^1B	Ref.
		Homosubstitution		
F	1	200	−300	a
Cl	1	2500	1700	a, b
	1, 2	3700	3200	a
	1, 3	3600	3400	a
	1, 4	5000	2600	a
	1, 3, 5	4400	5000	a
	hexa	8000	8400	a, b
Br	1	3500	2000	a, b
I	1	5300	3000	a, b
OH	1	2100	1700	a, c
	1, 2	2800		c
	1, 3	3800		c
OCH_3	1	3400		c
SH	1	7800		b
NH_2	1	7000	3600	b
$NHCH_3$	1	8400		b
$N(CH_3)_2$	1	9900		b
CH_3	1	1400	1400	a, d
	1, 2	1900	2100	a, d
	1, 3	2500	2700	a, d
	1, 4	2900	2500	a, d
	1, 2, 3	2600	3000	b, d
	1, 2, 4	3200	3200	b, d
	1, 3, 5	3300	3800	b, d
	1, 2, 3, 4	3200		b
	1, 2, 3, 5	3600	4100	b, d
	1, 2, 4, 5	3500	3700	b, d
	penta	3900		b
CH_2Cl	1	3300		b
$CHCl_2$	1	4300		b
CCl_3	1	5100		b
COOH	1	6500	3400	a, b
CN	1	4500	2200	a, b
$CH{=}CH_2$	1	9600	5200	a, b
$C{\equiv}CH$	1	7800	4200	a
(N)	1	−1600	−2400	a
	1, 2	−2300		a
	1, 3	−4500 est.	−4600 est.	a
	1, 4	−1800	−5600 est.	a
		Heterosubstitution		
F, CH_3	1, 2	1200	1100	a
	1, 4	1600	800	a
OH, CH_3	1, 2	2400	2200	a, b
	1, 3	2900	2600	a, b
	1, 4	3600	2100	a, b
CN, CH_3	1, 2	5300		b
	1, 3	5100		b
	1, 4	6000		b
(N), CH_3	1, 2	−200		b
	1, 3	0		b
	1, 4	−1100		b

[a] H. B. Klevens and J. R. Platt, *Survey of Ultraviolet Spectra of Organic Compounds in Solution* (Reprinted from Technical Report 1953-4 Part One, Laboratory of Molecular Structure and Spectra, University of Chicago).

[b] American Petroleum Institute Research Project 44, *Catalog of Ultraviolet Spectrograms* (National Bureau of Standards, 1945-50, and Carnegie Institute of Technology, 1950-57).

[c] R. A. Friedel and M. Orchin, *Ultraviolet Spectra of Aromatic Compounds* (John Wiley & Sons, Inc., New York, 1951).

[d] L. C. Jones, Jr., and L. W. Taylor, Anal. Chem. **27**, 235 (1955).

ments so obtained from spectra in the literature, having a probable error of about 100 cm^{-1}, are presented in Table VI.

Comparison with Theory

For the ^1L_a transition, taking the excited state to be initially $^1B_{1u}$, we are led to the following frequency-shift formula by the results of molecular orbital theory,[11,15]

$$-\Delta\nu=\sum l_m-1.2\,|\sum v_m(-1)^m|^2. \qquad (12)$$

The most important of the coefficients C_M is now C_3. The coefficient C_2, which was most important for the ^1L_b transition, is expected to be quite small on the grounds that the $^1B_{1u}$ state interacts with the $^1E_{1u}$ state (at 1850 A) less than one-half as strongly as does the $^1B_{2u}$ state[15]; the positive contribution to C_2 from the depression of the $^1B_{1u}$ state by the $^1E_{1u}$ state is then very nearly cancelled out by the negative contribution from the depression of the ground state by the $^1E_{2g}$ states (expected around 1600 and 1100 A). On the other hand, the coefficient C_3 is about six times as large as for the ^1L_b transition. The negative contribution to C_3 from the depression of the ground state by the $^1B_{1u}$ state, which for the ^1L_b is two-thirds cancelled out by the positive contribution from the depression of the $^1B_{2u}$ state by the $^1A_{2g}$ state (expected around 1300 A), is now reinforced by an *equal* negative contribution from the concomitant elevation of the $^1B_{1u}$ excited state by the ground state. Thus, while C_3 is only −0.2 for ^1L_b, it becomes −1.2 for ^1L_a.

For the ^1B transition, on the other hand, taking the excited state to be initially $^1E_{1u}$, we arrive at the following formula for the *average* frequency shift of the two components,

$$-\Delta\nu=\sum l_m-2\,|\sum v_m\exp(i2m\pi/3)\,|^2 -0.6\,|\sum v_m(-1)^m|^2. \qquad (13)$$

The value of −2 for C_2 is found after averaging the negative contributions from the elevation of the $^1E_{1u}$ state by the $^1B_{1u}$ and $^1B_{2u}$ states below and adding the negative contribution from the depression of the ground state by the $^1E_{2g}$ states. The values of −0.6 for C_3 is just one-half that for the ^1L_a transition; this comes from the depression of the ground state by the $^1B_{1u}$ state.

Using Eqs. (12) and (13) and the values of v obtained for the ^1L_b transition (Table IV), we can evaluate l for the ^1L_a and ^1B transitions from the frequency shifts in Table VI. The values found are compared with the ^1L_b values in Table VII.

[15] W. Moffitt, J. Chem. Phys. **22**, 320 (1954). Among other things, this paper shows that the $^1B_{1u}-^1E_{1u}$ interaction depends on $\Delta\beta$, the change in the resonance-bond integral between adjacent carbons of the ring, while the $^1B_{2u}-^1E_{1u}$ interaction depends on $\Delta\alpha$, the change in the coulomb integral for the carbons. Making the reasonable assumption that $\Delta\beta/\Delta\alpha=-\frac{1}{2}(\beta/\alpha)$, we find the matrix element for the former interaction to be $\beta/\alpha=0.32$ times that for the latter.

How well Eqs. (12) and (13) hold for weakly perturbing substitutions is indicated by Fig. 5, which shows a comparison of the calculated shifts for methylbenzenes. In the calculated shifts the v value obtained for $^1L_b(v=8)$ is used along with the following l values: $l=1400$, $l_{ortho}=850$ for ^1L_a; $l=1460$, $l_{ortho}=1040$ for ^1B (in cm^{-1}). The agreement with the observed shifts is seen to be quite good.

Anomalies for donor-acceptor substituent pairs. It is noteworthy that for methylbenzonitriles (CH_3 and CN substitution) the ^1L_a frequency shift for 1,4- is *greater* than for 1,3-, while Eq. (12) predicts the *opposite* on the grounds that the v values for CH_3 and CN are opposite in sign. This anomaly we attribute to the fact that CH_3 and CN make up a donor-acceptor substituent pair for which there is a low-lying *charge-transfer* state resulting from *intersubstituent* charge-transfer; this state is obtained by transferring an electron from the highest filled π orbital of CH_3 (the donor) to the lowest vacant π orbital of the CN (the acceptor). Interactions between the benzene-ring states and such charge-transfer states have been neglected in the perturbation theory of paper I, upon which the formulas discussed here are based. These interactions need not be considered for the ^1L_b transition, because the $^1B_{2u}$ state has a nodal plane at each carbon-substituent bond and therefore can interact only very weakly, if at all, with these intersubstituent charge-transfer states. However, they should be considered for the ^1L_a transition, as the $^1B_{1u}$ state has an antinode at each carbon-substituent bond and can interact quite strongly. That the interaction with the $^1B_{1u}$ state for 1,4-substitution should be stronger than for 1,3- may be justified theoretically, as is done in paper IV.[16]

TABLE VII. Comparison of l values for the benzene transitions. Values in brackets are for ortho substitution.

Subst.	l (cm^{-1}) ^1L_b	^1L_a	^1B
F	50	550	450
Cl	935	2600	1900
	(840)	(1800)	(1600)
Br	975	3600	2300
I	1000	5600	3600
OH	1200	3000	3500
OCH_3	1100	4200	
SH	3000	8200	
NH_2	3550	7500	4800
CH_3	560	1400	1460
	(405)	(850)	(1040)
CH_2Cl	960	3400	
$CHCl_2$	1050	4400	
CCl_3	1300	5200	
COOH	2150	6900	4200
CN	1350	4700	2800
$CH{=}CH_2$	3500	9600	5200
CCH	2400	7800	4200
(N)	−1430	−800	−700

[16] J. Petruska, J. Chem. Phys. (to be published).

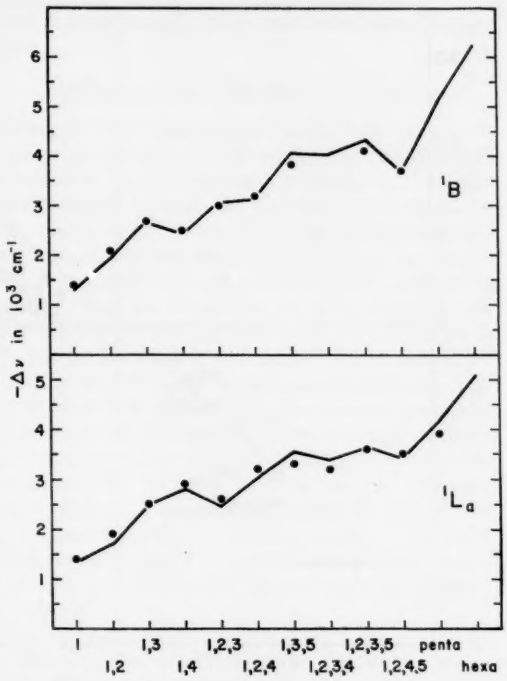

FIG. 5. Comparison of observed and calculated frequency shifts for the ^1L_a and ^1B transitions in methylbenzenes. The circles represent the observed shifts; the line, the calculated shifts (with correction for ortho effect included).

An alternate explanation for the anomaly has been suggested by Platt[17]; namely, that in 1,4-methylbenzonitrile one is looking at a perturbed $^1E_{2g}$ state that has been pushed below the perturbed $^1B_{1u}$ state. For this to be true the $^1E_{2g}$ state would have to be very close to the $^1B_{1u}$ state in benzene; in which case, a fairly large *positive* C_1 coefficient ($M=1$ term) should appear in the frequency-shift formulas for the ^1L_b and ^1L_a transitions and a fairly large *negative* C_1 in the formula for the ^1B transition. The fact that the formulas with $C_1=0$ hold satisfactorily for weakly perturbing substituents, such as CH_3 and Cl, seems to rule out this possibility; indeed, it provides support for the lowest $^1E_{2g}$ state being *higher* than the $^1E_{1u}$ state as indicated by the Murrell-McEwen calculations.[11]

DISCUSSION OF PERTURBATION PARAMETERS

Comparison of q and v

For the ^1L_b transition, at least, q is approximately proportional to v, as is shown in Fig. 6. This indicates that q arises principally from the perturbations that determine v, namely the *inductive* perturbations that mix the carbon-ring states.

[17] J. R. Platt, private communication.

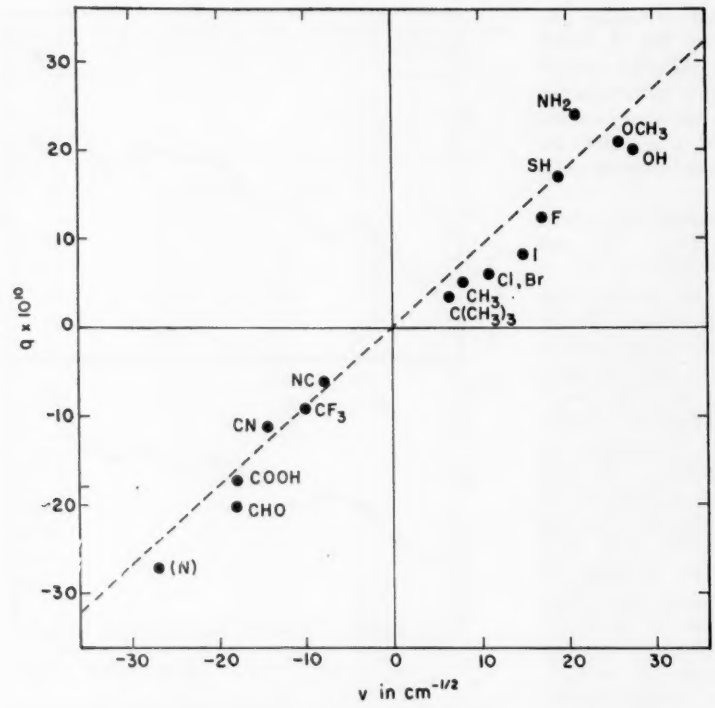

FIG. 6. Comparison of q and v for the ^1L_b transition. The dashed line represents $q=0.9\times10^{-10}v$, predicted from the $^1B_{2u}$-$^1E_{1u}$ interaction.

Two kinds of ring-state mixing contribute to q for the ^1L_b transition: (a) the mixing of the parent excited $^1B_{2u}$ state with the $^1E_{1u}$ state 1.7×10^4 cm^{-1} above it (at 1850 A) and (b) the mixing of the parent $^1A_{1g}$ ground state with the $^1E_{2g}$ states theoretically 5.6–8.8$\times10^4$ cm^{-1} above ground. Of these the former is certainly much more important. In accordance with the results of Murrell and McEwen,[11] we expect from this mixing alone $q=1.36\ vQ(\Delta E)^{-1}$, where Q is the transition moment between $^1B_{2u}$ and one component of $^1E_{1u}$ and ΔE is the difference in energy between the two states. Setting $Q=8.5\times10^{-9}$ and $\Delta E=1.74\times10^4$ cm^{-1}, as found from the benzene spectrum in vapor, we obtain $q=0.9\times10^{-10}v$. This falls right in the range of the observed q, 0.5–$1.2\times10^{-10}v$.

Mixing in terms of v

Using the values found for v we can estimate the contributions the various kinds of excited benzene states make to the ground state in substitute benzenes as a result of the *inductive* perturbations. The percent contribution of one benzene state to another is of the form $g^2\,|\sum v_m \exp(i\Delta M m\pi/3)\,|^2$, where ΔM is the difference between the M values for the two states and g^2 is a factor directly proportional to the square of the perturbation matrix element for monosubstitution and inversely proportional to the separation in energy between the states.[1] Taking the values of g^2 indicated by molecular orbital theory,[11] we have for the percent contribution to the initially $^1A_{1g}(M=0)$ ground state from

$$\begin{aligned}
&^1E_{1u}(M=1): \quad 0.0009\,|\sum v_m \exp(im\pi/3)\,|^2\\
&^1E_{2g}(M=2): \quad 0.0013\,|\sum v_m \exp(i2m\pi/3)\,|^2\\
&^1B_{1u}(M=3): \quad 0.0012\,|\sum v_m(-1)^m\,|^2. \qquad (14)
\end{aligned}$$

Similarly we find for the percent contribution to the initially $^1B_{2u}(M=3)$ excited state of the ^1L_b transition from

$$\begin{aligned}
&^1A_{2g}(M=0): \quad 0.0010\,|\sum v_m(-1)^m\,|^2\\
&^1E_{1u}(M=1): \quad 0.011\,|\sum v_m \exp(i2m\pi/3)\,|^2\\
&^1E_{2g}(M=2): \quad 0.0017\,|\sum v_m \exp(im\pi/3)\,|^2. \qquad (15)
\end{aligned}$$

Hence, the ground state in fluorobenzene ($v=17$), for example, has acquired 0.26% $^1E_{1u}$, 0.38% $^1E_{2g}$, and 0.35% $^1B_{1u}$ character; in 1,4-difluorobenzene, 1.5% $^1E_{2g}$ but no $^1E_{1u}$ or $^1B_{1u}$ character; in 4-fluoropyridine ($v=17$ and -27), 1.7% $^1E_{1u}$, 0.13% $^1E_{2g}$, and 2.3% $^1B_{1u}$ character. At the same time the ^1L_b excited state in fluorobenzene has acquired 0.29% $^1A_{2g}$, 3.2% $^1E_{1u}$, and 0.49% $^1E_{2g}$ character; in 1,4-difluorobenzene, 12.7% $^1E_{1u}$ but no $^1A_{2g}$ or $^1E_{2g}$ character; in 4-fluoropyridine, 1.9% $^1A_{2g}$, 1.1% $^1E_{1u}$, and 3.3% $^1E_{2g}$ character.

Meaning of l

There are at least three contributions to the empirical value of l, which may be designated as $l^{(0)}$, $l^{(1)}$, and $l^{(2)}$.

The components $l^{(1)}$ and $l^{(2)}$ have been taken into account in deriving the theoretical frequency-shift formulas: $l^{(1)}$ comes from the first-order *inductive* energy changes associated with the diagonal perturbation matrix elements, while $l^{(2)}$ comes from the second-order *conjugative* energy changes associated with the off-diagonal matrix elements between the carbon-ring states and the substituent and charge-transfer states. The component $l^{(0)}$, which has not been taken into account so far, comes from the change in zero-point vibrational energy.

Contribution from Change in Zero-Point Vibrational Energy

Some information regarding $l^{(0)}$ is provided by the spectra of deuterobenzenes. It is observed that on deuterosubstitution the 2600 A (^1L_b) system is shifted to the blue (higher frequency) by $33n$ cm^{-1}, where n is the number of deuteriums.[18] This shift has its origins in (a) the fact that the zero-point vibrational energy in the ^1L_b excited state of benzene is *smaller* than in the ground state and (b) the fact that on deuterosubstitution, while there is no change in the electronic energy, the zero-point vibrational energy of both states is *reduced* because of the increase in mass.

A general description of this shift, $\Delta\nu_{\text{vib}}$, may be given as follows. Let ϵ and ϵ' be the zero-point vibrational energies of the ground and excited states in benzene; $(1+d)\epsilon$ and $(1+d')\epsilon'$, the corresponding energies in a substituted benzene. Then,

$$\Delta\nu_{\text{vib}}=d'\epsilon'-d\epsilon. \tag{16}$$

Taking d and d' to be linearly dependent on the substituents, as is the case for deuterosubstitution, we may write

$$-\Delta\nu_{\text{vib}}=\sum l_m^{(0)}=\sum(\epsilon d_m-\epsilon' d_m') \tag{17}$$

In particular for the ^1L_b transition, with $\epsilon=21\,530$ cm^{-1} and $\epsilon'=20\,050$ cm^{-1} as found by Ingold and coworkers,[18] we have $l_m^{(0)}=21\,530d_m-20\,050d_m'$ cm^{-1}. Thus, for the substituent deuterium, where $d=-0.0317$ and $d'=-0.0324$, $l^{(0)}=-683+650=-33$ cm^{-1}.

As a rule, provided that ϵ' is smaller than ϵ as for the ^1L_b transition, $l^{(0)}$ will be *negative* for substituents that decrease the zero-point vibrational energy, i.e., for which d and d' are negative. In the case of the single-atom substituents, the halogens, the zero-point energy is definitely decreased because of the increase in mass. The negative values of $l^{(0)}$ are expected to increase in the order F<Cl<Br<I and reach 100 cm^{-1} or more judging by deuterium. For many-atom substituents like CH_3, however, the mass effect is bound to be offset to some degree by the addition of new vibrations. Compared to the halogens these substituents should have smaller negative values; if the new vibrational energy added is large enough, they may even have positive values.

Contribution from Inductive Perturbations

Going by molecular-orbital theory,[15] we expect $l^{(1)}$ to be proportional to v. On examining the diagonal perturbation matrix expressed in terms of integrals between atomic orbitals, we find that these contain a term linearly related to $\Delta\beta$, the change in the resonance-bond integral between the carbon to which the substituent is attached and each of the adjacent carbons of the ring. Since the separation in energy between the molecular orbitals depends essentially on β, this term is different for the ground and excited states. Hence, $l^{(1)}$ is linearly related to $\Delta\beta$. In particular for the ^1L_b, ^1L_a, and ^1B transition, we find from the expressions for the perturbation matrix elements given by simple molecular orbital theory, $l^{(1)}=\frac{2}{3}(\Delta\beta)$. Making the reasonable assumption that the ratio of $\Delta\beta$ to $\Delta\alpha$ (the coulomb-integral change) is approximately one-half the ratio of the original integrals, i.e., $\Delta\beta/\Delta\alpha=\frac{1}{2}(\beta/\alpha)=0.16$, and taking $\Delta\alpha=510\,v$ cm^{-1} (in accordance with the results of Murrell and McEwen[11]), we are led to the estimate $l^{(1)}=54v$ cm^{-1}.

This estimate agrees fairly well with the results for aza substitution (replacement of CH by N as in pyridine). For this substitution there is no conjugative perturbation, i.e., $l^{(2)}=0$. The observed l, apart from a small correction for $l^{(0)}$, is purely $l^{(1)}$. As found from the values for aza in Tables V and VII, $l^{(1)}/v=53$, 30, and 26 for the ^1L_b, ^1L_a, and ^1B transitions, respectively.

Contribution from Conjugative Perturbations

The value of $l^{(2)}$ is determined by the difference between the depression of the excited benzene state and the depression of the ground state by the substituent and charge-transfer states, particularly by the charge-transfer states. According to molecular orbital theory,[19] the matrix element for the interaction of the charge-transfer states with the ground state is $\sqrt{2}$ times that for the interaction with the ^1L_b, ^1L_a, and ^1B excited states. Thus, when the charge-transfer states are more than 80 000 cm^{-1} (10 ev) above the ground state, $l^{(2)}$ is small; it may even be negative, meaning that the ground state is depressed more than the excited state. However, when the charge-transfer states fall below 10 ev, the excited state is depressed more than the ground state, since the charge-transfer states are now so much closer to the excited state; $l^{(2)}$ then becomes positive and increases as the charge-transfer states decrease in energy. Bearing in mind that the energy required to transfer an electron from the substituent to the ring is directly related to the ionization potential of the substituent, we thus expect $l^{(2)}$ to *increase* as the ionization potential of the substituent *decreases*.

[18] F. M. Garforth, C. K. Ingold, and H. G. Poole, J. Chem. Soc. **1948**, 508.

[19] J. N. Murrell, Proc. Phys. Soc. (London) **A68**, 969 (1955).

An approximate value of $l^{(2)}$ (including $l^{(0)}$) may be obtained by subtracting from the observed l the reasonable estimate of the inductive contribution, $l^{(1)}=40v$. This value is shown in the following comparatively for three groups of substituents. In each group the substituents are listed in order of decreasing ionization potential for their hydrides. The value of the ionization potential is given in brackets beside the substituents.

(1) Halogens (positive v):

	^1L_b	^1L_a	^1B
F (17)	−600	−100	−200
Cl (12.8)	500	2200	1500
Br (12.0)	500	3200	1900
I (10.3)	400	5000	3000

(2) Saturated substituents in first row of periodic table (positive v):

F (17)	−600	−100	−200
CH_3 (12.9)	250	1100	1150
OH (12.6)	100	1100	1600
NH_2(10.3)	1600	6100	3400

(3) Unsaturated substituents (negative v):

CN (13.9)	2000	5300	3400
COOH (11.3)	2900	7600	4900
$CH{=}CH_2$ (10.5)	3500	9600	5200.

For the halogens and saturated substituents, which introduce no substituent states and only charge-transfer states of type R^-S^+ (where R is the ring and S the substituent), the estimated $l^{(2)}$ does indeed increase with decreasing ionization potential. A similar behavior is evident for the unsaturated substituents. However, for these the value is considerably larger for the same ionization potential. This may be attributed to the fact that, in addition to charge-transfer states of type R^-S^+, the unsaturated substituents introduce charge-transfer states of type R^+S^- and also substituent states that interact with the ring states.

The difference in $l^{(2)}$ for the three transitions is worth noting. We see that for ^1L_a and ^1B the value is considerably larger than that for ^1L_b. This is in accordance with the fact that the charge-transfer states are closer and thus interact more strongly with the higher states. However, we also see that the ^1L_a value tends to be larger than the ^1B value, even though the ^1B state is higher. To explain this we have to take into account the repulsion between the $^1B_{1u}$ and $^1E_{1u}$ ring states resulting from the interaction with the charge-transfer states. This repulsion, which emerges from higher order terms in perturbation theory, is discussed in paper IV.[16]

Platt's Spectroscopic Moment

The *spectroscopic moment* evaluated by Platt[7] for the ^1L_b transition is roughly proportional to our transition moment q. This moment is obtained from the change in the extinction coefficient at the maximum of the smooth curve drawn through the vibration structure, which is an approximate measure of the intensity I_q induced by the substituent perturbations. Its value is approximately $1.6\times10^{10}q$.

THE JOURNAL OF CHEMICAL PHYSICS VOLUME 34, NUMBER 4 APRIL 1961

Millimeter Wave Spectrum and Molecular Structure of Oxygen Difluoride

A. RAY HILTON, JR.,* ALBERT W. JACHE, JAMES B. BEAL, JR., WILLIAM D. HENDERSON, AND R. J. ROBINSON†

Department of Chemistry of The Agricultural and Mechanical College of Texas, College Station, Texas

(Received August 10, 1960)

The molecular structure of oxygen difluoride (OF_2) has been studied by microwave spectroscopy techniques. A video microwave spectrometer was used to find 13 rotational absorption lines. Klystron-driven crystal harmonic generators were used as energy sources for the spectrometer. The frequencies of the lines were measured with a precise frequency standard. Nine of the lines were assigned to rotational transitions of OF_2 using a graphical method. The three average rotational constants A, B, and C were determined from the exact energy solutions for the rotational transitions. The values for the rotational constants together with the effective moments of inertia calculated from them were $A=61\,567.71$ Mc, $I_A=8.21096$ amu, A^2; $B=11\,066.54$ Mc, $I_B=45.6809$; $C=9\,343.85$ Mc; $I_C=54.1088$ amu, A^2. The effective values for the oxygen fluorine interatomic distance and the apex angle 2θ calculated from I_A and I_B were $r=1.3896$ A, $2\theta=104.163$. The rotational inertial defect was found to be $+0.217$ amu, A^2.

INTRODUCTION

CONSIDERABLE data are available concerning the structure of oxygen difluoride (OF_2). The purpose of this investigation was to determine the structure of oxygen difluoride more precisely by using the frequencies of rotational absorption lines observed in the microwave region.

Oxygen difluoride has been studied using infrared spectroscopy and electron diffraction methods. Perhaps the best way to present the results is by the use of a table taken from one of the papers. Table I presents a comparison by Ibers and Schomaker[1] of their results and other values given in the literature.[2–4]

The structural parameters, O—F and 2θ, are chosen because oxygen difluoride is a nonlinear triatomic molecule with two equivalent oxygen fluorine bonds (O—F) which are separated by an apex angle 2θ.

Some comments should be made concerning the sources and reliability of the structural parameters given in Table I. The work of Sutton and Brockway[2] was carried out using early (1935) electron diffraction methods, as was the work of Boersch.[3] That early electron diffraction methods were not considered to be very reliable, is obvious from the large value of maximum error listed by these workers.

Bernstein and Powling[4] assigned the three principal infrared vibrational frequencies of OF_2. They determined rotational constants from the resolved fine structure by treating OF_2 as a symmetric-top molecule. Their structural values given in the table were calculated from these symmetric-top rotational constants.

The first values given by Ibers and Schomaker[1] are the results of a study of OF_2 using electron diffraction methods. Combining their results with the rotational constants given by Bernstein and Powling, they determined a most probable value for the oxygen fluorine distance and the apex angle 2θ. The most probable values are given in the table.

One must exercise some judgment in selecting structure parameters to use for calculation of approximate rotational transition frequencies. Beal[5] used the range of variable, 1.360–1.400 A° and 100.1–105.1°, for calculation of energy levels. Tolberg[6] accepted the bond distance from the infrared (1.380 A) and the latest electron diffraction angle ($2\theta=103.5$) and calculated the expected rotational frequencies of 66 lines found in the microwave region.

TABLE I. Structural parameters of OF_2 given in the literature.

O—F A	2θ°	Source
1.36±0.1	105±5	2
1.41±0.05	100±3	3
1.38±0.03	101.5±1.5	4
1.413±0.10	103.8±1.5	1
1.418	103.2	1

EXPERIMENTAL PROCEDURE

1. Preparation of Oxygen Difluoride

Oxygen difluoride was prepared by passing fluorine gas through a flowing cold dilute aqueous solution of sodium hydroxide. The resulting mixture of gases was passed through two traps containing a dilute, aqueous solution of sodium hydroxide to remove hydrogen fluoride and excess fluorine. To remove the water, the gas mixture was then passed through a third trap

* Present address: Texas Instruments, Inc., Dallas, Texas.

† Present address: Production Research, Humble Oil and Refining Company, Houston, Texas.

[1] J. A. Ibers and Verner Schomaker, J. Phys. Chem. **57**, 699 (1953).

[2] L. E. Sutton and L. O. Brockway, J. Am. Chem. Soc. **57**, 473 (1935).

[3] H. Boersch, Monatsh. Chem. **65**, 311 (1935).

[4] H. J. Bernstein and J. Powling, J. Chem. Phys. **18**, 685 (1950).

[5] James A. Beal, M.S. thesis, Texas A. and M. College, College Station, Texas (1959).

[6] Wesley E. Tolberg, Ph.D. dissertation, Texas A. and M. College, College Station, Texas (1958).

TABLE II. Klystron fundamental frequencies of observed lines.

Klystron frequencies	Mc
23 397.96	(*A*)
26 111.72	(*A*)
26 854.56	(*A*)
27 068.62	(*A*)
22 544.66	(*A*)
35 455.46	(*A*)
24 491.33	(*B*)
32 655.45	(*C*)
34 945.89	(*C*)
31 799.38	(*C*)
32 626.62	(*C*)
32 808.63	(*C*)
30 731.81	(*C*)

cooled with dry ice. The remaining sample was collected in a sample holder (cooled by liquid nitrogen) as a liquid solution containing approximately 50% OF_2 and 50% oxygen. Most of the oxygen could be removed by placing the sample under reduced pressure (below 1 mm Hg) while it was still cooled by liquid nitrogen. About two-thirds of the liquid sample was allowed to boil away.

A check on the gas composition was made by means of its infrared spectrum. All of the known bands of OF_2 were observed plus some bands from traces of carbon tetrafluoride. The sample was stored as a liquid at liquid nitrogen temperature.

2. Microwave Spectrometers

Two video-type spectrometers were used. Details of construction and operation can be found in standard texts.[7,8] The absorption cells (*K* band) of these spectrometers were fitted with transition sections. The transition sections for the cells were to *I* band (above 34 kMc); and to *G* band (above 79 kMc).

The energy source of the *I*-band cell (Duke designation[7]) was a klystron-driven *K*-band to *I*-band harmonic generator. Slotted IN26 crystals were utilized in this generator. The detector was made of *I*-band waveguide using a slotted IN26 crystal. Much more elaborate generators and detectors were used on the *G*-band absorption cell.[9] The energy sources were klystron-driven *K*-band to *G*-band harmonic generators. Three different detectors were used on this cell. These detectors were made of *G*, *J*, and *F* waveguide and used silicon crystals.

The absorption cells were always cooled with dry ice. The low temperature of dry ice increased the population of the gas molecules in the low *J* and ground vibrational states. Low-temperature operation also increased the amount of microwave energy available by lowering the electrical resistance of the cell.

3. Frequency Measurements

Frequency measurements were made using a precise frequency standard. The accuracy of the frequency standard is based on a 1-Mc oscillator (James Knights Company, FS–1000, model 1). The accuracy of the 1-Mc standard was verified by beating its frequency against the National Bureau of Standards WWV 20-Mc broadcast. The over-all accuracy of the frequency standard and the frequency determining procedure, was verified by measuring an OCS and several BrCN lines, and comparing the values with accepted values found in the literature.

4. Frequencies of Predicted Rotational Absorption Lines

The calculated values of Beal were used as guides in determining in what range to look for a given transition. Beal, using an IBM 650 digital computer, calculated values for rotational transitions by fixing the interatomic distances and then varying the apex angle 2θ in increments of 0.2°. He then changed the radius by 0.002 A and repeated the procedure. Beal also used $I_C=I_A+I_B$. In the present work, reasonable limits were selected in which a given transition would be expected from Beal's data.

RESULTS

1. Observed Rotational Absorption Lines

Thirteen rotational absorption lines of OF_2 were found. The measured frequency of the klystron fundamental of each line is shown in Table II.

The observed lines in group *A* were found using the *I* band absorption cell and the frequency doubler. The frequency of a line in this group is probably second, third, or fourth harmonic of the measured fundamental. Frequency doublers of this type have very little energy of higher than fourth harmonic.

The one line lettered (*B*) was found using the *K*-band to *G*-band harmonic generator and the *G*-band absorption cell. The frequency of the line must be fourth or above and up to about twelfth harmonic of the fundamental.

The lines lettered (*C*) were found using the *J*-band to *G*-band harmonic generator with the *G*-band absorption cell. The frequency of a line in the group must be third or above and up to about 14th harmonic

[7] Walter Gordy, W. V. Smith, and Ralph Trambarulo, *Microwave Spectroscopy* (John Wiley & Sons, Inc., New York, 1953).
[8] C. H. Townes and A. L. Schawlow, *Microwave Spectroscopy* (McGraw-Hill Book Company, Inc., New York, 1955).
[9] W. E. Tolberg, W. D. Henderson, and A. W. Jache, "New components for use in millimeter wave spectroscopy," 135th National American Chemical Society Meeting, Boston, Massachusetts, April, 1959.

of the fundamental. Two of the lines were observed by using an *F*-band detector. This would indicate that their frequencies are in excess of 130 kMc. The frequencies of the two lines observed while using the *F*-band detector have fundamental frequencies of 32 655.45 and 31 799.38 Mc.

Unfortunately, it is not possible to observe just any rotational line in the 20- to 400-kMc range. One is restricted to areas in which his particular set of generators, crystals, and klystrons function well. These 13 rotational lines represent our best combination of good energy and available transitions. Other rotational transitions which would have been of considerable help in our calculations were not available to us because of poor energy response in the region where the absorption line occurred.

2. Assignments

The initial J level of a transition can be determined by the Stark splitting. However, in OF_2, the electric dipole moment is small[10] and thus the observed lines are weak. When a weak line is split into several components, some of the components may not be visible. Attempts were made to identify some of the (A) group lines, using a Stark spectrometer. The absorption line of group A whose frequency has the klystron fundamental frequency of 27 068.62, was found to have two Stark components. The initial J level of this transition is thus indicated to be $J=1$ or $J=2$.

The absorption line whose frequency has the klystron fundamental frequency of 26 854.56 was found to have three Stark components. The initial J level of this transition is thus indicated to be $J=2$ or $J=3$. Stark splitting was observed for other lines in group A, but the results were inconclusive.

Often a molecule will have several lines for the same transition because of natural isotopes of one or more atoms in the molecule. Identification of these lines sometimes enables one to calculate the structure from one or two transitions. The major isotope lines must be strong in order for the minor, naturally occurring isotope lines, to be visible. Oxygen is 99.8% O^{16} and fluorine is 100% F^{19}. No minor isotope lines of OF_2 could be found and used to help determine the structure.

One method commonly used for identification of transitions involves use of Ray's asymmetry parameter κ and King, Hainer, and Cross, energy tables.[11] The rotational energy for an asymmetric molecule in a particular rotational state is given by

$$W/h=(A+C)J(J+1)/2+(A-C)E_{\lambda(\kappa)}/2, \quad (1)$$

where J is the principal angular momentum quantum number. Here, A and C are the rotation constants and

[10] J. W. Bransford, A. C. Kunkle, A. W. Jache, J. Inorg. & Nuclear Chem. **14**, 159 (1960).

[11] G. W. King, R. M. Hainer, and P. C. Cross, J. Chem. Phys. **11**, 27 (1943).

TABLE III. Centrifugal distortion constants of OF_2.

Constant	Value in Mc
A_1	-1.04×10^{-9}
A_2	$+1.45\times10^{-6}$
A_3	-5.76×10^{-2}
A_4	-2.91×10^{-1}
A_5	-1.43
A_6	$+5.74\times10^{-6}$

$E_{\lambda(\kappa)}$ is the value tabulated in the King, Hainer, Cross, tables for a particular level as a function of κ.

For a Q branch transition ($\Delta J=0$) the change in energy ($\Delta W/h$) is a function of $(A-C)$ and κ alone, not $(A+C)$,

$$\Delta E+(A-C)\Delta E_{\lambda(\kappa)}/2.$$

Values calculated for Q-branch transitions by Tolberg and Beal ($J\lesssim4$) were examined and possible values of a particular transition, were examined as a multiple of one of the frequencies listed in Table II. Possible values were selected over ranges of about 2000 Mc. A possible value for a particular Q-branch transition was solved for values of $A-C$ from the King, Hainer, Cross, tables as a function of the asymmetry parameter κ. A plot was prepared of all $(A-C)$ values vs κ for Q-branch transitions. An intersection point of two or more possible values for different transitions indicates a common value for $(A-C)$ and κ.

From intersection points, different possible values of $(A-C)$ were used to prepare other plots for transitions where $\Delta J=0$. The plots were prepared, again using the tables. From the accepted value of $(A-C)$ and possible values for a particular transition selected from Table II, relation (1) was solved for values of $(A+C)$ as a function of κ the asymmetry parameter. For a P- or R-branch transition the change in energy ΔE is given by

$$\Delta E=(A+C)\{\tfrac{1}{2}[J'(J+1)]-\tfrac{1}{2}[J(J+1)]\}$$
$$+\tfrac{1}{2}[(A-C)\Delta E_{\lambda_\kappa}],$$

where J and J' signify the initial and final total angular momentum quantum numbers.

In order for any solution found in this manner to be acceptable, the intersection of the plots of the possible values for different transitions must be at a common $(A+C)$ and at the same κ as that which determined $(A-C)$. Another test which the solution had to pass, was that the A, B, and C calculated from the data also had to fit the exact solutions of the energy equations taken from Gordy.[7] Only two values of $(A-C)$ and κ produced any common point of more than two values. These values are $(A-C)=52\,223.4$, $\kappa=-0.950$, and $\kappa=-0.934$. The finding of the $0_{00}-1_{11}$ transition confirmed the values $\kappa=-0.934$, $(A-C)=$

TABLE IV. Assignment of rotational levels of OF_2.

Transition	Klystron fundamental	Harmonic	Calculated	Observed	Centrifugal distortion correction
$0_{00}\rightarrow 1_{11}$	35 455.46	$X2$	70 909.24	70 910.92	1.32
$1_{01}\rightarrow 1_{10}$	26 111.72	$X2$	52 223.49	52 223.44	1.37
$2_{21}\rightarrow 3_{30}$	31 799.38	$X10$	317 985.97	317 993.80	84.95
$2_{02}\rightarrow 3_{13}$	26 854.56	$X4$	107 433.94	107 418.24	3.00
$5_{32}\rightarrow 5_{41}$	32 655.45	$X11$	359 176.42	359 209.95	222.88
$6_{16}\rightarrow 7_{07}$	34 945.82	$X3$	104 831.84	104 837.67	24.28
$8_{36}\rightarrow 8_{45}$	32 626.62	$X11$	358 872.21	358 892.82	235.67
$9_{28}\rightarrow 10_{19}$	23 397.96	$X4$	93 592.34	93 591.84	74.48
$11_{57}\rightarrow 12_{48}$	30 731.81	$X7$	215 121.98	215 122.67	363.53

52 223.4, and $(A+C)=70\,910.92$. These values produced several assignments which fit very well.

Further assignments could not be made until after the rotational levels were corrected for centrifugal distortion effects. From the value of $(A+C)$, $(A-C)$, and the asymmetry parameter, the rotational constants A, B, and C were calculated. Approximate values for the interatomic distance and the apex angle 2θ were calculated from the moments of inertia I_A and I_B obtained from their respective rotational constants.

3. Centrifugal Distortion Corrections

The rotational levels were corrected for the effect of centrifugal distortion by a method developed by Kivelson and Wilson.[12] In this method each unperturbed rotational level is calculated as a function of the equilibrium values of the rotational constants. This rotational level is then corrected to the real value by six constants used in the equation

$$W=W_0+A_1W_0^2+A_2W_0J(J+1)+A_3J^2(J+1)^2$$
$$+A_4J(J+1)\langle P_z^2\rangle_{Av}+A_5\langle P_z^4\rangle_{Av}+A_6W_0\langle P_z^2\rangle_{Av},$$

where W is the real energy of the level, W_0 is the unperturbed value, and the quantum numbers of the rotational state are designated by J and K_{-1}. For a near-symmetric top molecule, $\langle P_z^2\rangle_{Av}$ is about equal to K^2 and $\langle P_z^4\rangle_{Av}\approx K^4$.

TABLE V. Unassigned lines.

Klystron fundamental	Harmonic
27 068.62	$\geqslant 2$
22 544.66	$\geqslant 2$
24 491.33	$\geqslant 4$
32 808.63	$\geqslant 3$

A generalized program was written to calculate the six constants for OF_2. The method used was similar to the one outlined by Kivelson and Wilson[13] except that the results were not as exact. A nonlinear triatomic molecule such as OF_2 has four vibrational potential constants. These constants are necessary for an exact calculation of the centrifugal distortion constants. The three vibrational frequencies for OF_2[4] are not enough empirical data to enable determination of the four constants. No vibrational frequencies for OF_2 containing isotopes other than F^{19} and O^{16} are reported in the literature.

The six constants for OF_2 were calculated using valence force coordinates. The two force constants were calculated assuming that the vibrational frequencies V_1, V_2, V_3 were the same as the normal vibrational frequencies ω_1, ω_2, ω_3. For the first set the structural parameters were obtained from the initial assignments. From the structural parameters obtained from final assignments, the calculations were repeated until there was no appreciable change in the six constants. The final values are shown in Table III.

4. Final Assignments

A generalized program was written to use the six distortion constants to correct the rotational levels by the equation given above. The unperturbed level was calculated from the initial values of $(A+C)$, $(A-C)$, and the King, Hainer, and Cross tables. The real level was then calculated. Corrections were of the order of $-26\,000$ Mc for $J=12$. Over 500 transitions were considered for levels of $J\lesssim 12$. Intensity coefficients were calculated and compared when necessary. The final assignment of nine transitions for OF_2 are given in Table IV. These lines were fitted with some preference shown for the high J lines. The average deviation for the nine lines is ± 9.6 Mc with the greatest con-

[12] D. Kivelson E. B. Wilson, Jr., J. Chem. Phys. **20**, 1575 (1952).

[13] D. Kivelson and E. B. Wilson, Jr., J. Chem. Phys. **21**, 1229 (1953).

tribution to the deviation coming from the highest frequency transitions. The small deviation is probably due to inaccuracies in the distortion constants.

The unassigned lines are shown in Table V with only their klystron fundamentals listed. These lines are probably of higher J value than those considered here.

5. Structure

The effective values for the rotational constants and their respective moments of inertia are:

$A=61\,567.71$ Mc $\quad I_A=8.21096$ amu A^2

$B=11\,066.54$ Mc $\quad I_B=45.6809$

$C=\ 9\,342.85$ Mc $\quad I_C=54.1088.$

The asymmetry constant κ is found to be

$$\kappa=-0.93400.$$

The equations for I_A and I_B are easily solved for the interatomic distance r and the apex angle 2θ. The values are $r=1.3896$ A, $2\theta=104.16°$.

6. Inertial Defect

In a nonlinear triatomic molecule such as OF_2, the largest moment of inertia should be equal to the sum of the other two ($I_C=I_A+I_B$). The fact that it does not, is termed an inertial defect. This discrepancy is measured by the magnitude of the deviation ($\Delta=I_C-I_A-I_B$). The value for OF_2 calculated from our data is $+0.217$ amu A^2.

An explicit expression for the inertial defect for a nonlinear triatomic molecule of the C_{2v} type was derived by Darling and Dennison.[14] The calculation for OF_2 was carried out using the structural parameters from the assignments and assuming that the observed vibrational frequencies were equal to the normal frequencies. It was necessary to use displacement coordinates in the calculations. The potential constants used in the displacement coordinate treatment were obtained by linearly transforming a set of four potential constants obtained by Duchesne and Burnelle[15] using a graphical method. The calculated value was found to be $+0.165$ amu A^2. The discrepancy is due primarily to the assumption that the observed vibrational frequencies are equal to the normal frequencies. In OF_2, V_1 is larger than V_2 but about equal in magnitude, which should result in a great deal of interaction.

[14] B. T. Darling and D. M. Dennison, Phys. Rev. **57**, 128 (1940).

DISCUSSION OF RESULTS

Any large errors obtained in these data are not due to frequency measurements. The frequency measurements are all good at least to about 0.2 Mc. The main sources of error are the reliability in Planck's constant (1 part in 10 000), the error due to inaccuracies in the centrifugal distortion constants (1 part in 10 000 was maximum), and the error due to the inertial defect. Because of the necessary assumptions made in the calculation of the centrifugal distortion constants and the inertial defect, we are unable to determine a reliability figure that would properly represent the accuracy of the data. We report the structural parameters of OF_2 to be $r=1.3896$ A, $2\theta=104.16°$.

ACKNOWLEDGMENT

This investigation was supported by the Robert A. Welch Foundation.

[15] J. Duchesne and L. Burnelle, J. Chem. Phys. **19**, 1191 (1951).

Influence of the Molecular Environment on the Carbonyl Frequency. Electronic Calculation

S. BRATOŽ AND MME. S. BESNAINOU

Centre de Mécanique Ondulatoire Appliquée, Paris 15°, France

(Received June 2, 1960)

The $K_{\nu C=O}$ force constants of formaldehyde, acetaldehyde, acetone, glyoxal, *p*-benzoquinone, *o*-benzoquinone, and of chloroacetaldehyde have been determined by Pariser-Parr-Pople's SCF-MO procedure. The theoretical expression for the force constant corresponding to this theory is given. The $K_{\nu C=O}$ force constant is found to decrease in the order formaldehyde, chloroacetaldehyde, acetaldehyde, acetone; this is due to the corresponding decrease of the effective electronegativity of the carbonyl carbon atom. The $K_{\nu C=O}$ force constant decreases also in the series acetone, *o*-benzoquinone, *p*-benzoquinone, and in the series acetaldehyde, glyoxal; this is due to conjugation effects. The force constants calculated by this theory agree satisfactorily with the experimental values.

1. INTRODUCTION

A CONSIDERABLE interest has been manifested in the spectral behaviour of the carbonyl group.[1–4] It has been shown that the $\nu_{C=O}$ frequency associated with the C=O group is rather insensitive to changes in the molecular environment. The $\Delta\nu_{C=O}$ frequency shifts are small but characteristic of the type of compound being investigated. These spectral shifts are due: (a) to the variation from one molecule to another of the amount of the vibrational coupling between the $\nu_{C=O}$ vibrator and the vibrators associated with the rest of the molecule; (b) to the variation of the force constant $K_{\nu C=O}$ which results from the change of the electronic structure of the carbonyl group in passing from one molecule to another. The relative importance of the vibrational and electronic effects can be estimated either by performing a vibrational analysis of the infrared spectra of some typical carbonyl compounds or by calculating the force constant $K_{\nu C=O}$ of these molecules by the help of an electronic theory. The vibrational problem[5–11] has been recently treated in detail in a work, further referred to as (I).[11] In this paper the electronic problem will be studied (see also[12–21]). It will be shown that in the cases, where mass coupling effects are small, the $\Delta\nu_{C=O}$ frequency shifts are mainly determined by (a) the effective electronegativity of the carbonyl carbon atom and (b) by the conjugation effects.

2. THEORY

In this section the theoretical techniques necessary for the electronic calculation of the bond stretching force constants will be discussed. The molecules treated are given in Table I which also gives the geometrical (and other) parameters entering into the calculation. It would have been desirable to have included in this table the cyclanones and compounds like phosgene. This was not done, however, because of the mathematical difficulties to be discussed later.

The fundamental assumption upon which the calculation is based consists of supposing that the modifications of the $K_{\nu C=O}$ force constant when going from one carbonyl molecule to another, is due to π electrons.[16,19–21] In addition, the relatively large size of the molecules in question renders the use of an empirical method unavoidable. The Pariser-Parr-Pople[22–24] approximate SCF-MO procedure has finally been adopted in the form used by Sidman[25] in his work on the carbonyl group. Two problems arise when applying this procedure to the study of small variations of the carbonyl frequency: (a) a method must be given to evaluate the penetration integrals expressing the influence of the σ

[1] R. N. Jones, F. Herling, J. Org. Chem. **19**, 1252 (1954).
[2] J. Lecomte, Bull. soc. chim. France **1959**, 717.
[3] R. N. Jones and C. Sandorfy, *Chemical Applications of Spectroscopy* (Interscience Publishers, Inc., New York, 1956), pp. 443–509.
[4] L. T. Bellamy, *The Infra-Red Spectra of Complex Molecules* (Methuen and Company, Ltd., London, 1958).
[5] G. B. Bonino and P. Chiorboli, Atti accad. nazl. Lincei [8] **9**, 17 (1950).
[6] B. G. Bonino, E. Scrocco, P. Chiorboli, Atti accad. nazl. Lincei [8] **9**, 17 (1950).
[7] K. W. F. Kohlrausch and A. Pongratz, Z. physik. Chem. (Leipzig) **B27**, 176 (1934).
[8] R. C. Lord and F. A. Miller, Appl. Spectroscopy **10**, 115 (1956).
[9] J. O. Halford, J. Chem. Phys. **24**, 830 (1956).
[10] T. Miyazawa, J. Chem. Soc. Japan, Pure Chem. Sect. **77**, 366 (1956).
[11] S. Bratož and S. Besnaïnou, J. chim. phys. **56**, 555 (1959).
[12] E. T. Hartwell, R. E. Richards, and H. W. Thompson, J. Chem. Soc. **1948**, 1436.
[13] G. B. Bonino and E. Scrocco, Atti accad. nazl. Lincei [8] **4**, 421 (1949).
[14] E. Scrocco and P. Chiorboli, Atti accad. nazl. Lincei [8] **8**, 248 (1950).
[15] G. B. Bonino and P. Chiorboli, Mem. accad. sci. Bologna [10] **7**, 3 (1951).
[16] G. Berthier, B. Pullman, and J. Pontis, J. chim. phys. **49**, 365 (1952).
[17] E. Scrocco and O. Salvetti, Bull. sci. fac. chim. ind. Bologna **12**, 93 (1954).
[18] R. E. Kagarize, J. Am. Chem. Soc. **77**, 1377 (1957).
[19] M. L. Josien and J. Deschamps, J. chim. phys. **52**, 213 (1955).
[20] J. Deschamps, thesis, University of Bordeaux, 1956.
[21] J. Baudet, G. Berthier, and B. Pullman, J. chim. phys. **54**, 282 (1957).
[22] R. Pariser and R. G. Parr, J. Chem. Phys. **21**, 466 (1953).
[23] R. Pariser and R. G. Parr, J. Chem. Phys. **21**, 767 (1953).
[24] J. A. Pople, Trans. Faraday Soc. **49**, 1375 (1953).
[25] J. W. Sidman, J. Chem. Phys. **27**, 429 (1957).

substitution on the π electron system; (b) a theoretical expression for the force constant corresponding to the Pariser-Parr-Pople theory must be derived. Both these problems as well as others concerning the choice of parameters will be discussed. Here are the details.

The first stage of the work consists of the calculation of the π electron SCF-MO wave functions. This has been done using Sidman's values for the parameters $\beta_{C=O}$, β_{C-C} and his formulas for the bielectronic integrals (pp/qq).[26] However, Sidman's procedure could not be followed in calculating the α_p elements:

$$\alpha_p = \int \chi^* H_{\text{core}} \chi d\tau = W_p - \sum_{p \neq q} [(pp \mid qq) + (q{:}pp)] - \sum_r (r{:}pp) = U_p - \sum_{p \neq q} (pp \mid qq) \quad (1)$$

$$U_p = W_p - \sum_{p \neq q} (q{:}pp) - \sum_r (r{:}pp). \quad (2)$$

(The symbols have their usual significance[22]; the summation over r is relative to the noncharged core atoms and the summation over p to the charged core atoms. In Sidman's work the U_C and U_O values[27] are supposed to be equal for all carbon (or oxygen) atoms and for all molecules which have been investigated. This hypothesis is not useful in the present case where the influence of the σ substitution on the behavior of the π-electron system is investigated (e.g., comparing formaldehyde and acetaldehyde). In this work, the penetration integrals associated with the directly bonded atoms have been taken into account and U_p values have been calculated in the following way. For the (s^2p^4)[28] carbonyl oxygen atom, one has

$$U_O = W_{\pi O} - (C{:}\pi_O\pi_O). \quad (3)$$

As the nearest neighbor of the carbonyl oxygen is always the same (i.e., the carbonyl carbon), this equation is valid for all molecules investigated and Sidman's values -13.00 ev has been taken for U_O. The U_C values associated with the $(t^3\pi)$ carbonyl carbon atom depend, on the contrary, on the substituents R and R' attached to the carbonyl group C=O. Considering, as before, only the nearest-neighbor penetration integrals, one has

$$U_C = \begin{cases} W_{\pi C} - (O{:}\pi_C\pi_C) - 2(H{:}\pi_C\pi_C) = U^F & \text{for } H_2CO \quad (4) \\ W_{\pi C} - (O{:}\pi_C\pi_C) - (H{:}\pi_C\pi_C) - (C{:}\pi_C\pi_C) \\ = U^F - [(C{:}\pi_C\pi_C) - (H{:}\pi_C\pi_C)] & \text{for } HCH_3CO \quad (5) \\ W_{\pi C} - (O{:}\pi_C\pi_C) - 2(C{:}\pi_C\pi_C) \\ = U^F - 2[(C{:}\pi_C\pi_C) - (H{:}\pi_C\pi_C)] & \text{for } (CH_3)_2CO. \quad (6) \end{cases}$$

For formaldehyde, Sidman's value $U_C = U_C^F = -9.5$ ev has been taken. For other molecules the difference $(C{:}\pi_C\pi_C) - (H{:}\pi_C\pi_C)$ has been estimated by considering the π electron ionization potentials of the radicals $\dot{C}H_3$, $C_2H_5{\cdot}\dot{C}H_2$, and $(CH_3)_2{\cdot}\dot{C}H$; they are, respectively, equal to 9.95,[29] 8.69,[30] and 7.90[30] ev. If one supposes that the central carbon atom is always in the $(t^3\pi)$ state[31–33] and if one neglects the hyperconjugation effects, one has

$$I^\pi(\dot{C}H_3) - I^\pi(C_2H_5\dot{C}H_2) = 1.26 \text{ ev} = -[(C{:}\pi_C\pi_C) - (H{:}\pi_C\pi_C)] \quad (7)$$

$$I^\pi(\dot{C}H_3) - I^\pi[(CH_3)_2\dot{C}H] = 2.05 \text{ ev} = -2[(C{:}\pi_C\pi_C) - (H{:}\pi_C\pi_C)], \quad (8)$$

i.e., values, respectively, for the simple and double methyl substitution. The same procedure has been used to determine U_C in the case of chloroacetaldehyde. In this case, one has:

$$U_C = W_{\pi C} - (O{:}\pi_C\pi_C)_{C=O} - (H{:}\pi_C\pi_C) - (C{:}\pi_C\pi_C)_{C-CH_2Cl} = U^F - [(O{:}\pi_C\pi_C)_{C-CH_2Cl} - (H{:}\pi_C\pi_C)], \quad (9)$$

and one requires data on the $\dot{C}H_2{\cdot}CH_2Cl$ radical. Unfortunately, these data are lacking and the ionization potential of the chloro-ethyl radical has been estimated by the help of the appearance potential A of the $(CH_2CH_2Cl)^+$ ion from 1-chloropropane.[34] Using the formula

$$A(CH_2CH_2Cl)^+ = D(CH_3CH_2CH_2Cl \rightarrow \dot{C}H_3 + \dot{C}H_2CH_2Cl) + I^\pi(\dot{C}H_2CH_2Cl), \quad (10)$$

and putting D equal to the average CC single bond energy 62.2 kcal/mole,[35] one finds $I^\pi(C_2H_5Cl)$ equal to 9.13 ev; this value represents, of course, a rough estimation. Finally the $(C{:}\pi_C\pi_C)$ penetration integral of the group

is needed in order to determine, e.g., the U_C value of the atom C_2 of *p*-benzoquinone. It has been put equal to the integral $(O{:}\pi_C\pi_C)$ of the group C=O; this is con-

[26] Sidman's parameters have been chosen in the way to reproduce the uv spectra of some typical carbonyl compounds.

[27] Sidman's U's correspond to the quantities defined by the Eq. (2).

[28] This hypothesis, used by Sidman, is retained in this work.

[29] F. P. Lossing, K. U. Ingold, and I. H. S. Henderson, J. Chem. Phys. **22**, 621 (1959).

[30] F. P. Lossing and J. B. de Sousa, J. Am. Chem. Soc. **81**, 281 (1959).

[31] The radical CH_3 is, in fact, planar or nearly so.[32,33]

[32] G. Herzberg and J. Shoosmith, Can. J. Phys. **34**, 523 (1956).

[33] W. Gordy and C. G. McCormick, J. Am. Chem. Soc. **78**, 3243 (1956).

[34] D. P. Stevenson and J. A. Hipple, J. Am. Chem. Soc. **64**, 2766 (1942).

[35] E. U. Condon, *Handbook of Physics* (McGraw-Hill Book Company, Inc., New York, 1958).

TABLE I.

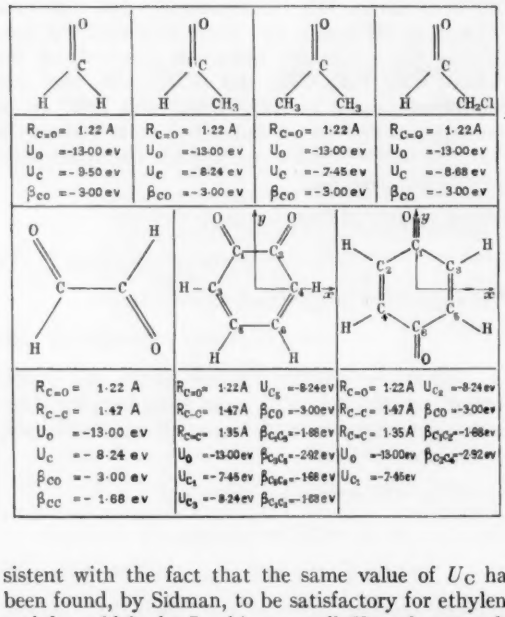

sistent with the fact that the same value of U_C has been found, by Sidman, to be satisfactory for ethylene and formaldehyde. In this way, all U_C values can be determined, they are reproduced in the Table I. The iteration procedure was performed by the help of Bull-AET electronic digital computer. The program used is based on a method proposed by Lefebvre and Moser[36] and was written by Dr. M. Salkoff. The SCF molecular orbitals which were finally obtained are given in Table II.

The SCF-MO wave functions once found, the second stage of the calculation, e.g., the calculation of the force constants, must be undertaken. One is tempted to use the well-known Coulson and Longuet-Higgins formula[37]

$$k_{12}=\{(1-p_{12})k_s+p_{12}k_d\}+\left\{\left[\frac{k_sk_d(s-d)}{k_s(1-p_{12})+k_dp_{12}}\right]^2\frac{\pi_{1212}}{2}\right\}. \tag{11}$$

(k_s and k_d are the force constants associated with pure simple and double bonds. p_{12} is the bond order and π_{1212} the self-polarizability of the bond 12 in question.) This expression is, however, valid only when the Hückel LCAO approximation is used. One is obliged, therefore, to derive an analogous expression appropriate to the Pariser-Parr-Pople approximation. A satisfactory procedure is to introduce into the exact SCF-MO expression for the energy the approximations contained in the Pariser-Parr-Pople method[22–24] and to derive it with respect to $R_{C=O}$. If this is done, one finds

$$E=E_\sigma+\sum_s p_{ss}[U_s+\tfrac{1}{4}p_{ss}(ss\mid ss)]+\sum_{s<t}2p_{st}\beta_{st}+\sum_{s<t}[p_{ss}p_{tt}-p_{ss}Z_t-p_{tt}Z_s-\tfrac{1}{2}p_{st}^2](ss\mid tt) \tag{12}$$

$$E^*=E_\sigma^*+\sum_s p_{ss}U_s^*+\sum_{s<t}2p_{st}\beta_{st}^*+\sum_{s<t}[p_{ss}p_{tt}-p_{ss}Z_t-p_{tt}Z_s-\tfrac{1}{2}p_{st}^2](ss\mid tt)^* \tag{13}$$

$$E^{**}=E_\sigma^{**}+\sum_s p_{ss}U_s^{**}+\sum_{s<t}2p_{st}\beta_{st}^{**}+\sum_{s<t}[p_{ss}p_{tt}-p_{ss}Z_t-p_{tt}Z_s-\tfrac{1}{2}p_{st}^2](ss\mid tt)^{**}+\sum_s p_{ss}^*U_s^*+\sum_{s<t}2p_{st}^*\beta_{st}^*+\sum_{s<t}[p_{ss}^*p_{tt}+p_{ss}p_{tt}^*-p_{ss}^*Z_t-p_{tt}^*Z_s-p_{st}^*p_{st}](ss\mid tt)^* \tag{14}$$

(p_{st} are Pople's charge—bond order operators

$$2\sum_i c_{is}c_{it},$$

E_σ is the core energy, Z_s is the net charge of the core atom s. The asterisk indicates the derivative with respect to $R_{C=O}$; the procedure to find p_{st}^* is described in the Appendix.

Equation (12) is identical with the one given by Pople.[24] Equation (13) is obtained by taking derivatives in (12), the integrals but not the charge-bond orders p_{st}. It has been shown[38] that the terms containing the derivatives of the LCAO coefficients can be put into the form

$$2\sum_{i\,st}c_{is}c_{it}\epsilon_i s_{st}^*;$$

they disappear in the Pariser-Parr-Pople approximation.[39] Finally, Eq. (14) is obtained by deriving Eq. (13). In order that Eqs. (13) and (14) may be used in a practical calculation, some additional hypotheses concerning the derivatives of E_σ, U_s, β_{st}, and (ss/tt) are still needed. All these quantities are considered in the Pariser-Parr-Pople theory as empirical quantities; their derivatives will be treated in this theory in the same way. The following hypotheses have been introduced: (a) If the atoms s and t are nonadjacent, the derivatives β_{st}^* and β_{st}^{**} are neglected. (b) The derivatives $(ss/tt)^*$ and $(ss/tt)^{**}$ are obtained by deriving the Pariser-Parr formulas.[40]

[36] R. Lefebvre and C. Moser, J. chim. phys. **53**, 393 (1956).

[37] C. A. Coulson and H. C. Longuet-Higgins, Proc. Roy. Soc. (London) **A193**, 456 (1948).

[38] S. Bratož, *Calcul des fonctions d'onde moléculaires* (Centre National de la Recherche Scientifique, Paris, 1958), p. 287.

[39] The result is closely related to the fact that the first-order perturbation energy is obtained by the help of the nonperturbed wave functions; no similar simplification can be expected for the second derivative.

[40] For $R\leqq 2.8$ A, one has $(ss/tt)=A+BR+\frac{1}{2}$ CR²; $(ss\,|\,tt)^*=B+CR$; $(ss/tt)^{**}=C$; for $R>2.8$ A the charged sphere approximation is used.

TABLE II.

Formaldehyde	$\pi_1=0.7596\chi_O+0.6504\chi_C$	$\epsilon_1=-12.03$ ev
	$\pi_2=-0.6504\chi_O+0.7596\chi_C$	$\epsilon_2=2.58$ ev
Acetaldehyde	$\pi_1=0.7976\chi_O+0.6032\chi_C$	$\epsilon_1=-11.37$ ev
	$\pi_2=-0.6032\chi_O+0.7976\chi_C$	$\epsilon_2=3.41$ ev
Acetone	$\pi_1=0.8194\chi_O+0.5732\chi_C$	$\epsilon_1=-10.98$ ev
	$\pi_2=-0.5732\chi_O+0.8194\chi_C$	$\epsilon_2=3.94$ ev
Chloro-acetaldehyde	$\pi_1=0.7847\chi_O+0.6198\chi_C$	$\epsilon_1=-11.59$ ev
	$\pi_2=-0.6198\chi_O+0.7847\chi_C$	$\epsilon_2=3.11$ ev
Glyoxal	$\pi(1a_u)=0.5239(\chi_O+\chi_{O'})+0.4749(\chi_C+\chi_{C'})$	$\epsilon_1=-12.59$ ev
	$\pi(1b_g)=0.5991(\chi_O-\chi_{O'})+0.3756(\chi_C-\chi_{C'})$	$\epsilon_2=-11.11$ ev
	$\pi(2a_u)=-0.4749(\chi_O+\chi_{O'})+0.5239(\chi_C+\chi_{C'})$	$\epsilon_3=1.85$ ev
	$\pi(2b_g)=-0.3756(\chi_O-\chi_{O'})+0.5991(\chi_C-\chi_{C'})$	$\epsilon_4=4.25$ ev
o-Benzoquinone	$\pi(1b_2)=0.3935(\chi_{O_1}+\chi_{O_2})+0.4011(\chi_{C_1}+\chi_{C_2})+0.3094(\chi_{C_3}+\chi_{C_4})+0.2975(\chi_{C_5}+\chi_{C_6})$	$\epsilon_1=-12.62$ ev
	$\pi(1a_2)=0.5087(\chi_{O_1}-\chi_{O_2})+0.3514(\chi_{C_1}-\chi_{C_2})+0.2906(\chi_{C_3}-\chi_{C_4})+0.1824(\chi_{C_5}-\chi_{C_6})$	$\epsilon_2=-11.09$ ev
	$\pi(2b_2)=-0.3542(\chi_{O_1}+\chi_{O_2})-0.2412(\chi_{C_1}+\chi_{C_2})+0.3148(\chi_{C_3}+\chi_{C_4})+0.4661(\chi_{C_5}+\chi_{C_6})$	$\epsilon_3=-10.88$ ev
	$\pi(2a_2)=-0.3379(\chi_{O_1}-\chi_{O_2})-0.1033(\chi_{C_1}-\chi_{C_2})+0.4701(\chi_{C_3}-\chi_{C_4})+0.3926(\chi_{C_5}-\chi_{C_6})$	$\epsilon_4=-9.15$ ev
	$\pi(3b_2)=-0.3374(\chi_{O_1}+\chi_{O_2})+0.2987(\chi_{C_1}+\chi_{C_2})+0.3989(\chi_{C_3}+\chi_{C_4})-0.3713(\chi_{C_5}+\chi_{C_6})$	$\epsilon_5=1.13$ ev
	$\pi(3a_2)=-0.2155(\chi_{O_1}-\chi_{O_2})+0.2991(\chi_{C_1}-\chi_{C_2})+0.3318(\chi_{C_3}-\chi_{C_4})-0.5040(\chi_{C_5}-\chi_{C_6})$	$\epsilon_6=3.36$ ev
	$\pi(4b_2)=-0.3254(\chi_{O_1}+\chi_{O_2})+0.4378(\chi_{C_1}+\chi_{C_2})-0.3822(\chi_{C_3}+\chi_{C_4})+0.2374(\chi_{C_5}+\chi_{C_6})$	$\epsilon_7=3.51$ ev
	$\pi(4a_2)=-0.2838(\chi_{O_1}-\chi_{O_2})+0.5257(\chi_{C_1}-\chi_{C_2})-0.2907(\chi_{C_3}-\chi_{C_4})+0.2420(\chi_{C_5}-\chi_{C_6})$	$\epsilon_8=5.68$ ev
p-Benzoquinone	$\pi(1b_{1u})=0.3735(\chi_O+\chi_{O'})+0.3778(\chi_{C1}+\chi_{C3})+0.3299(\chi_{C2}+\chi_{C3}+\chi_{C4}+\chi_{C5})$	$\epsilon_1=-12.68$ ev
	$\pi(1b_{3g})=0.5556(\chi_O-\chi_{O'})+0.4226(\chi_{C_1}-\chi_{C5})+0.0799(\chi_{C_2}+\chi_{C_3}-\chi_{C_4}-\chi_{C_5})$	$\epsilon_2=-11.50$ ev
	$\pi(1b_{2g})=0.5000(\chi_{C2}-\chi_{C3}+\chi_{C4}-\chi_{C5})$	$\epsilon_3=-10.38$ ev
	$\pi(2b_{1u})=-0.4632(\chi_O+\chi_{O'})-0.1682(\chi_{C_1}+\chi_{C_6})+0.3585(\chi_{C2}+\chi_{C3}+\chi_{C4}+\chi_{C5})$	$\epsilon_4=-9.37$ ev
	$\pi(2b_{3g})=-0.3564(\chi_O-\chi_{O'})+0.3315(\chi_{C_1}-\chi_{C_6})+0.3627(\chi_{C_2}+\chi_{C_3}-\chi_{C_4}-\chi_{C_5})$	$\epsilon_5=1.04$ ev
	$\pi(1a_u)=0.5000(\chi_{C2}-\chi_{C3}-\chi_{C4}+\chi_{C5})$	$\epsilon_6=2.84$ ev
	$\pi(3b_{1u})=-0.3819(\chi_O+\chi_{O'})+0.5735(\chi_{C_1}+\chi_{C_6})-0.1122(\chi_{C_2}+\chi_{C_3}+\chi_{C_4}+\chi_{C_5})$	$\epsilon_7=4.07$ ev
	$\pi(3b_{2g})=0.2536(\chi_O-\chi_{O'})-0.4599(\chi_{C_1}-\chi_{C_6})+0.3348(\chi_{C_2}+\chi_{C_3}-\chi_{C_4}-\chi_{C_5})$	$\epsilon_8=5.51$ ev

(c) The derivatives U_s^* and U_s^{**} are neglected. (d) The core energy is written as a sum of terms associated with all pairs st of atoms:

$$E_\sigma=\tfrac{1}{2}\sum_{st}\sigma_{st}. \tag{15}$$

If the atoms s and t are nonadjacent, one puts $\sigma_{st}=Z_sZ_t\ (ss/tt)$; $\sigma_{st}^*=Z_sZ_t(ss/tt)^*\cdots$; there is no contribution associated with nonadjacent noncharged pairs of core atoms. (e) If the atoms s and t are adjacent, the derivatives of σ_{st} and β_{st} are determined by the following procedure. The energy of a purely double bond E_d and the energy of a purely single bond E_s are first expressed by help of Eq. (12) putting $p_{11}=p_{12}=p_{22}=1$ for a double bond and $p_{11}=p_{22}=1$; $p_{12}=0$ for a single bond. On the other hand, one expressed the same energies by help of the force constants K_d, K_s and bond lengths d, s associated, respectively, with a purely double and a purely simple bond. This gives

$$E_d=\tfrac{1}{2}K_d(R_{12}-d)^2=\text{const}+\sigma_{12}+2\beta_{12}-\tfrac{3}{2}(11/22) \tag{16}$$

$$E_s=\tfrac{1}{2}K_s(R_{12}-s)^2=\text{const}'+\sigma_{12}-(11/22); \tag{17}$$

the constants contain the terms which do not depend on the bond distance. If one solves Eqs. (16) and (17) for σ_{12} and β_{12}, one finds

$$\sigma_{12}=\text{const}+\tfrac{1}{2}K_s(r_{12}-s)^2+(11/22) \tag{18}$$

$$2\beta_{12}=\text{const}'+\left[\tfrac{1}{2}K_d(R_{12}-d)^2-\tfrac{1}{2}K_s(R_{12}-s)^2\right]+\tfrac{1}{2}(11/22). \tag{19}$$

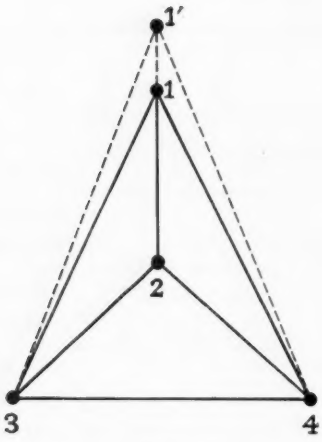

FIG. 1.

The value $K_d=66.50$ ev/A^2 ($=10.7\ 10^5$ d cm^{-1}), $K_s=31.00$ ev/A^2 ($=5.0\ 10^5$ d cm^{-1}), $d=1.22$ A and $s=1.43$ A have been used in this work. The final expression for the force constant is now easily obtained. If one supposes that the variation of the R_{12} distance (Fig. 1) is accomplished by deplacing the atom 1 and holding all other atoms fixed, only the distances between the atoms 1–2, 1–3$\cdots$etc., are effected by the deplacement of the atom 1 but not the distances between the atoms 2–3, 2–4, etc$\cdots$. On introducing into Eq. (14) the simplifications listed, one has finally[41]

$$K_{12}=\{(1-p_{12})K_s+p_{12}K_d+\sum_t q_{1t}(11/tt)^{**}\}$$

$$+\{p_{12}^{*}[K_d(r-d)-K_s(r-s)]+\sum_t{}' q_{1t}^{*}(11/tt)^{*}\} \quad (20)$$

with

$$q_{12}=1+p_{11}p_{22}-p_{11}Z_2-p_{22}Z_1+\tfrac{1}{2}p_{12}-\tfrac{1}{2}p_{12}^{2}$$

$$q_{1t}=Z_1Z_t+p_{11}p_{tt}-p_{11}Z_t-p_{tt}Z_1-\tfrac{1}{2}p_{1t}^{2} \quad (t\neq 2). \quad (20a)$$

Using these formulas, the force constant is easily calculated if the LCAO-MO coefficients as well as their derivatives are known (see the Appendix for this latter point). It is seen that a bond stretching force constant which is mainly determined by the π electrons (like $K_{\nu C=O}$ force constant) depends essentially on three factors: (a) the bond order p_{12}, (b) the atomic charges p_{tt}, and (c) the quantities p_{st}^{*} expressing the rearrangement of MO's during vibration. The general structure of the formula (20) is similar to that of the Coulson—Longuet-Higgins formula; the terms contained in a curly bracket of one of them correspond to the analogous terms of the other. The electron repulsion terms, neglected in the Hückel's theory, but accounted for on that of Pariser-Parr-Pople, are responsible for the difference between (11) and (20). This gives rise, in (20) to terms like $q_{1t}\ (11/tt)^{**}$ and prevent the second curly bracket to be reduced to the simple form it has in the Coulson—Longuet-Higgins Formula.[42] The terms of the first bracket have been found to be very much larger than these associated with the second bracket. In the case of glyoxal where the second bracket terms are particularly large, they do not contribute more than 0.15% to the total value of $K_{\nu C=O}$. The force constants have been calculated completely, i.e., including first and second bracket terms in the case of formaldehyde acetaldehyde, acetone, chloroacetaldehyde, and glyoxal. Only first bracket terms have been calculated in the case of *o*-benzoquinone and *p*-benzoquinone because of the mathematical difficulties encountered. It is not probable, however, that this simplification affects the results in any significant way.

3. RESULTS AND DISCUSSION

The principal results which have been established by extensive experimental work and which will be discussed in this paper, are the following.[1–4] If the ketones are saturated and contain, in α or α' no halogen atoms, one finds: (a) the ketones absorb in the neighborhood of 1710 cm^{-1}; (b) the aldehydes absorb at somewhat higher frequencies, in the neighborhood of 1730 cm^{-1}. This is true also for (c) the esters and monomeric acids, the typical $\nu_{C=O}$ values being 1740 and 1760 cm^{-1}; (d) the $\nu_{C=O}$ frequency is the largest for the cyclanones, if there are less than five atoms in the ring (1775 cm^{-1} in the case of cyclobutanone). The effect is inverse if the number of carbon atoms in the ring is larger than six; in this case the carbonyl frequency is smaller than that of the ketones. If the ketones are either nonsaturated or α (or α') halogenated, two additional effects superpose on the effects just cited. The presence of the nonsaturated groups in a carbonyl molecule gives rise to a low-frequency shift $\Delta\nu_{C=O}$ which becomes larger with increasing conjugation (it can be as large as 80 cm^{-1}).[43] The presence, in α, α' or α and α' of the halogen atoms has the opposite effect; it results in a high frequency $\Delta\nu_{C=O}$ shift of the order some tens of wave numbers. Taking the $\nu_{C=O}$ frequency of the saturated ketones ($\sim$1710 cm^{-1}) as reference, the problem to be resolved by the theory is to explain the origin of the shifts of the $\nu_{C=O}$ frequency of a given carbonyl molecule with respect to that of the saturated ketones.

[41] There is some difficulty in applying these formulas to the case of nonsymmetrical (heteropolar) double bonds as no purely double bonds ($p_{12}=1$) really exist in this case. A hypothetical molecule with a bond having this property can, however, be introduced; this confers upon K_d and K_s the character of empirical parameters. In the C=O case, one has $p_{12}=0.9881$ for formaldehyde (see the following).

[42] This simplification is due to the fact that, in Hückel's LCAO theory, E_π can be supposed to depend on R only through β; this can not be supposed in the Pariser-Parr-Pople theory, because of the existence of the electron repulsion integrals.

[43] We do not deal with the chelated compounds, like acetylacetone.

This problem has been treated in I, as a vibrational problem. It has been found that the vibrational coupling interaction is mainly responsible for the carbonyl frequency shifts of the cyclanones and that it gives an appreciable contribution to the frequency shifts of the aldehydes and quinones. In other cases the $\Delta\nu_{C=O}$ frequency shifts indicate the variation of the carbonyl force constant $K\nu_{C=O}$ with respect to that of the saturated ketones. In these cases the electronic perturbation is said to be predominant.

In this paper, the problem is reexamined using the inverse procedure, i.e., by help of techniques explained in the preceding section. The results are given in Table III where the values obtained by the electronic theory (column 1) may be compared with the experimental values obtained in I (column 2). The agreement is satisfactory. It is therefore probable that the procedure described in this paper represents a useful interpolation procedure although the quantitative agreement is not to be taken too literally. The frequency shifts in the cases of predominant, or nonnegligible electronic perturbation are now explained as follows. The carbonyl carbon U_C decreases in its absolute value, in the series formaldehyde, acetaldehyde, and acetone. This increases the asymmetry and the polarity of the carbonyl bond. Its results, among others, are a decrease of the carbonyl bond order (see Table II). From the other side, it is found that the bond order term $(1-p_{12})K_s+p_{12}K_d$ of the Eq. (20) gives, by far, the largest contribution to the $K_{\nu_{C=O}}$ force constant.[44] One concludes that the force constant of the carbonyl carbon bond decreases with increasing polarity of the C=O bond, i.e., in the foregoing series. If a halogen atom is introduced into the aldehyde methyl group, U_C becomes larger, the carbonyl bond less polar and $\nu_{C=O}$ shifts to higher values. The behavior of the carbonyl force constant is therefore governed, in these cases, by the variation of the effective electronegativity of the carbonyl carbon atom ("inductive effect").[4] This is certainly true also for the carboxylic acids and for the esters. Electronic perturbation of another type is observed in the series acetone, *o*-benzoquinone, *p*-benzoquinone and in the series acetaldehyde, glyoxal. In both cases, the carbonyl force constant decreases in the order cited, i.e., with increased conjugation. The conjugation, reducing the carbonyl bond order, influences the carbonyl force constant in the way to reduce it as the conjugation increases ("mesomeric effect").[4] All these results agree well with the conclusions reached by Berthier, Pullman and coll,[16,21] Josien and Deschamps,[19,20] Kagarize,[18] Bellamy,[4] and others. Unfortunately, it has not been possible to treat in this article a third different type of electronic perturbation found in the cases where the halogen atom is directly attached to the carbonyl group (e.g., phosgene). In these cases the lone pair oxygen electrons are no longer localized on the oxygen atom and the carbonyl bond has a partly triple bond character.[45-47] However, our method being adapted to a treatment of the π-electrons was not able to treat problems concerning the *n*-electrons without considerable modification of the theory.

[41] This explains the success of the Coulson Longuet-Higgins formula; these results suggest that the net charge contributions to a bond stretching constant are not very large.

TABLE III.

Molecule	$K\nu_{C=O}$[a] (Electronic theory)	$K\nu_{C=O}$[a] (Exptl.)
Formaldehyde	10.58	10.8[b]
Chloroacetaldehyde	10.49	?
Acetaldehyde	10.42	10.3–10.6
Glyoxal	10.33	?
Acetone	10.29	10.0–10.3
o-Benzoquinone	10.15	10.0[c]
p-Benzoquinone	10.11	9.8[c]

[a] All in 10^5 d cm^{-1}.
[b] S. Bratož and S. Besnaïnou (unpublished calculations).
[c] The calculations[11] situate the $K\nu_{C=O}$ of different *o*-quinones and *p*-quinones to the intervals 9.7–10.1 and 9.5–9.9, respectively, the values of the table are the estimated values for the special cases of *o*-benzoquinone and *p*-benzoquinone.

ACKNOWLEDGMENTS

The authors wish to thank Professor R. Daudel for a critical reading of the manuscript and Dr. M. Salkoff for the aid in the machine computation. They wish also to acknowledge the help of Professor R. de Possel who kindly permitted the use of the Bull-AET electronic digital computer of the Institute Blaise Pascal for the mathematical resolution of this problem.

APPENDIX

The derivatives of the LACO coefficients c_{kt}^* can be obtained by help of the following formulas:[38]

$$\sum_{st} S_{st}c_{ls}c_{kt}^* = \sum_{st}\frac{c_{ls}c_{kt}}{\epsilon_k-\epsilon_l}\Big[H_{st}^*-\epsilon_k S_{st}^* + \sum_{juv} c_{ju}c_{jv}(2\vartheta_{stuv}^*-\vartheta_{sutv}^*) + 2\sum_{juv} c_{ju}^*c_{jv}(2\vartheta_{stuv}-\vartheta_{sutv})\Big] \qquad (l\neq k)$$

$$\sum_{st} S_{st}c_{ls}c_{kt}^* = -\tfrac{1}{2}\sum_{st} c_{ls}c_{kt}S_{st}^*. \qquad (l=k)$$

The above equations represent a system linear in c_{kt}^*, thus permitting these quantities to be determined. This system is of the order 2×2 in the cases of formaldehyde, acetaldehyde, acetone and chloroacetaldehyde

[45] This is easily seen comparing the $R_{C=O}$ distance [(1.166 A)[46]] and force constant [(14.0 10^5 cm^{-1})[47]] of phosgene with those of acetone and carbon monoxide.
[46] G. W. Robinson, J. Chem. Phys. **21**, 1741 (1953).
[47] J. Duchesne, Nuovo cimento **3**, Suppl. 688 (1956).

and of the order 8×8 for glyoxal. In the case of the two benzoquinones it would be of the order 32×32 but the c_{kt}^{*}'s have not been calculated in these two cases. These equations have been simplified by introducing the hypotheses of Pariser-Parr-Pople as explained in the text. The 8×8 system was resolved using the 704 IBM digital computor. The p_{st}^{*} are easily obtained from the calculated values of the derivatives c_{kt}^{*}.

THE JOURNAL OF CHEMICAL PHYSICS VOLUME 34, NUMBER 4 APRIL, 1961

Thermoelectric Power of Silver Halides*

R. W. CHRISTY

Department of Physics, Dartmouth College, Hanover, New Hampshire

(Received September 12, 1960)

Thermoelectric power measurements have been made on the systems AgCl+$CdCl_2$, AgBr+Ag_2S, and AgBr+CdS, as well as the pure silver halides, in the temperature range from 100° to 400°C. Silver metal electrodes were used. The behavior of AgCl and $CdCl_2$ is similar to the previously investigated AgBr+$CdBr_2$ system, except that the effect of the impurity is more pronounced in AgCl. The results of Cd-doping of AgBr and AgCl are analyzed according to the theory of Howard and Lidiard to give the concentration of Frenkel defects, the ratio of mobilities, and the quantities $q_i^{*}+q_v^{*}$, $q_i^{*}+Ts_i'$, and $q_v^{*}+Ts_v'$, where q^{*} and s' are the heats of transport and entropies of formation for the interstitials and vacancies. The results are in agreement with conductivity data, but the heats of transport are surprisingly large and temperature dependent. It is concluded that association between Cd^{++} and Ag^{+} vacancies is negligible above 100°C, but that association between S^{--} and Ag^{+} interstitials, and between Cd^{++} and S^{--}, is significant even at 400°C.

I. INTRODUCTION

A PREVIOUS measurement of the thermoelectric power of silver bromide[1] was found to be in excellent agreement with the thermodynamical theory of Howard and Lidiard.[2] The theory applies to an ionic conductor containing Frenkel pairs of cation interstitials and vacancies, present in numbers which can be controlled by doping with divalent impurities. It is assumed that long-range interactions (Debye-Hückel theory) between the defects can be neglected, though the possibility of short-range interactions (association) with the impurities is admitted. In fitting the data to the theoretical expression, values derived from the conductivity measurements of Teltow[3] were used for the quantities ξ, the ratio of the concentration of free (unassociated) vacancies in the doped crystal to the concentration in a pure crystal at the same temperature, and ϕ, the ratio of the interstitial mobility to the vacancy mobility. It was possible to infer from the thermoelectric data values for the quantity $(q_i^{*}+q_v^{*}+h)$, where h is the heat of formation of a Frenkel pair of defects, and q_i^{*} and q_v^{*} are the heats of transport of interstitials and vacancies, respectively. An unexpected result was that $(q_i^{*}+q_v^{*})$ appeared to depend rather strongly on the absolute temperature T. This result is confirmed by Haga, who has independently developed the theory,[4] using data for silver chloride.[5]

In view of theoretical interest in a kinetic calculation of the heats of transport, which can elucidate the dynamics of defect motion in the crystal, the previous measurements are repeated for silver chloride in the present work, and accurate values for the heats of transport, as a function of temperature, are presented for both AgBr and AgCl. As a further check on the thermodynamic theory, measurements have also been made on the effect of a divalent anion (sulfide) impurity in AgBr, and the results will be reported. In addition, it will be argued that association between Cd^{++} impurities and silver vacancies can be neglected above 100°C, but that association is probably important in the case of S^{--} impurities even at 400°.

The theoretical expression for the total thermoelectric power θ derived by Howard and Lidiard[2] is

$$\theta=\frac{(q_v^{*}+h)\xi^2-\phi q_i^{*}}{eT(\xi^2+\phi)}-(k/e)\times\ln\xi-s_i/e+s_m/e+(k/e)\ln c_0-(k/e)\ln(N'/N),$$

where k is Boltzmann's constant and e is the magnitude of the electronic charge, s_i is the entropy of an interstitial, s_m is the entropy of a silver ion in the silver metal electrode, c_0 is the vacancy (or interstitial) concentration in the pure salt, and N' and N are, re-

* This work was supported by the Office of Naval Research.

[1] R. W. Christy, E. Fukushima, and H. T. Li, J. Chem. Phys. **30**, 136 (1959).

[2] R. E. Howard and A. B. Lidiard, Phil. Mag. **2**, 1462 (1957).

[3] J. Teltow, Ann. Physik **5**, 63, 71 (1949).

[4] E. Haga, J. Phys. Soc. Japan **13**, 1090 (1958).

[5] Y. Susuki, S. Endo, and E. Haga, J. Phys. Soc. Japan **14**, 729 (1959).

spectively, the number of interstitial sites and normal lattice sites per unit volume of the salt. The sign convention for θ is the same as that of Howard and Lidiard: θ is positive if the hotter end of the sample is at higher potential. To eliminate the entropies and c_0, the data can be compared with the difference between the values of θ for the doped crystal and for the pure crystal ($\xi=1$),

$$\Delta\theta=[(\xi^2-1)/(\xi^2+\phi)][(\phi Q^*)/eT(\phi+1)]-(k/e)\ln\xi, \tag{1}$$

where $Q^*=q_i^*+q_v^*+h$. From this expression Q^* can be determined.

If q_v^* is eliminated using the definition of Q^*, the foregoing expression for θ can be transformed to

$$e\theta T=Q^*/(1+\phi/\xi^2)+kT\ln(c_0/\xi)-kT \times\ln(N'/N)-q_i^*-T(s_i-s_m).$$

For the pure sample, $\xi=1$, this equation reduces to

$$e\theta T=Q^*/(1+\phi)+kT\ln c_0-kT \times\ln(N'/N)-q_i^*-T(s_i-s_m). \tag{2}$$

If c_0 is determined, Eq. (2) can be used to find the quantity $q_i^*+T(s_i-s_m)$.

By making use of

$$c_0^2=(N'/N)\exp[-(h-Ts)/kT], \quad s=s_i+s_v, \tag{3}$$

where s_v is the vacancy entropy, θ can also be expressed by

$$e\theta T=-Q^*/(1+\xi^2/\phi)-kT\ln(c_0\xi)+q_v^*+T(s_v+s_m). \tag{4}$$

Again, for the pure sample, Eq. (4) reduces to

$$e\theta T=-Q^*/(1+1/\phi)-kT\ln c_0+q_v^*+T(s_v+s_m), \tag{5}$$

and $q_v^*+T(s_v+s_m)$ can be found from Eq. (5).

The relations between ξ and c, the concentration of divalent cation impurity, are,[3] assuming no association,

$$(\xi-1/\xi)=c/c_0; \tag{6}$$

or, assuming association between the vacancies and impurities,

$$(\xi-1/\xi)(1+Kc_0\xi)=c/c_0, \tag{7}$$

where K is the equilibrium constant for the dissociation of the vacancy-impurity complexes. These relations are derived from the assumption of charge neutrality in the crystal.

If Eq. (6) holds, then for $\xi\gg1$, Eq. (4) reduces to

$$e\theta T=-kT\ln c+q_v^*+T(s_v+s_m). \tag{8}$$

This expression will be used to check the assumption regarding association.

In the following sections, new data will be reported for AgCl, and then these data and the previous data for AgBr will be analyzed to obtain values for the thermodynamic parameters.

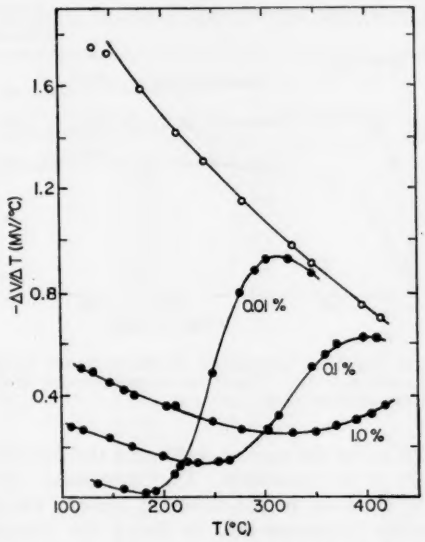

FIG. 1. Total thermoelectric power of pure AgCl (open circles) and AgCl containing $CdCl_2$, as a function of temperature.

II. THERMOELECTRIC POWER OF AgCl+$CdCl_2$

The experimental procedure was the same as that previously described,[1] except that the samples were cast in a Pyrex tube. The electrodes attached to the sample were silver in all cases. The pure sample reported was a specially purified AgCl single crystal, kindly supplied by Dr. F. Moser of the Eastman Kodak Research Laboratories. The doped samples were prepared from less pure material precipitated in our Laboratory, but the accidental impurity content of this material was more than an order of magnitude smaller than the least doping concentration (0.01 atom %).

The total thermoelectric power is shown in Fig. 1 as a function of temperature for the pure sample and for three different doping concentrations. The results are qualitatively the same as in AgBr. The effect of the impurity is more pronounced in AgCl, even relative to the melting temperature, which is about 30° higher than for AgBr, because in AgCl the equilibrium number of lattice defects is smaller.

The agreement with theory is illustrated by Fig. 2. The difference between the total thermoelectric power of doped samples and the pure sample is plotted on three different isotherms. The curves are obtained from Eq. (1), using values of ξ and ϕ calculated[6] from the conductivity data of Ebert and Teltow.[7] The agreement is within the experimental error, although it is not quite

[6] Calculations by K. Tharmalingam were kindly communicated by R. E. Howard.

[7] I. Ebert and J. Teltow, Ann. Physik **15**, 268 (1955).

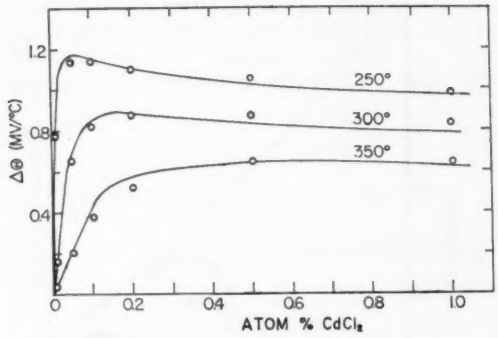

FIG. 2. The difference between the thermoelectric powers of doped and of pure AgCl. The circles are experimental points and the curves are theoretical.

so good as for the case of AgBr, and the discrepancy appears to be systematic. The discrepancy will be further discussed in the following section. The only adjustable parameter used in fitting the theoretical curves to the data is the quantity $Q^*=(q_i^*+q_v^*+h)$. The values derived for this parameter will be tabulated in Sec. IV.

III. DEGREE OF ASSOCIATION WITH Cd^{++}

A remarkable feature of the curves of total thermoelectric power θ versus temperature is that at low temperatures, in the impurity controlled region, all the curves appear to be parallel, for both AgCl (Fig. 1) and AgBr. This observation means that θ is the sum of a function of temperature only and a function of concentration only. It can be understood on the basis of Eq. (8), which applies to the simple no-association theory of vacancy concentration in the doped crystal. To test this equation, in Fig. 3 is plotted $e\theta T$ vs $kT \ln c$, at temperatures of 150° and 175°, where the condition $\xi \gg 1$ is satisfied for all the experimental values of c. The results are seen to lie on straight lines of slope 1, confirming Eq. (6) for the no-association theory. Similar results may be obtained from the AgBr data.

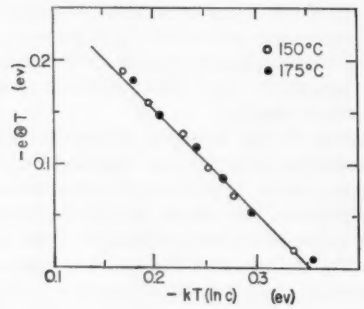

FIG. 3. Thermoelectric power of AgCl at low temperatures, as a function of $CdCl_2$ concentration c, plotted to test the association hypothesis.

If, on the contrary, association were important the slope would be ½ according to Eq. (7).

Teltow, on the other hand, concluded[3] that the assumption of the existence of interactions between the defects is necessary for the interpretation of his conductivity data, and this conclusion has usually been accepted. Therefore, in order to compare the conductivity data with the assumption of no interaction between the impurities and vacancies, in Fig. 4 values of $(\xi-1/\xi)$ are plotted versus the impurity concentration c, where the values of ξ are those calculated[6] from the conductivity. If Eq. (6) for no interaction applies, the points should lie on straight lines of slope 1 for all values of c. If the simple association theory of Eq. (7) applied, the points should lie on lines of slope ½ at

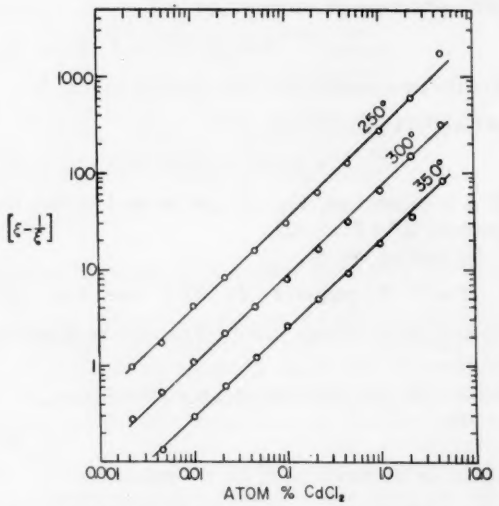

FIG. 4. Relation between relative vacancy concentration ξ and impurity concentration in AgCl, testing the association hypothesis. The lines have a slope of 0.9. (Values of ξ from conductivity, footnote 7.)

large values of c. In fact, the points lie on straight lines for all values of c, although the slope is about 0.9. The situation for AgBr is similar. One may conclude that, although the assumption of no interaction may not be quite correct, its simplicity recommends it over the other possibilities considered by Teltow, none of which is completely satisfactory.

The fact that Eq. (6) is confirmed by the thermoelectric data at low temperatures, and should hold *a fortiori* at high temperatures where association would be less, permits a direct comparison of the theory, Eqs. (1) and (6), with the experimentally determined quantities, θ, T, and c, without depending on values of ξ determined from the conductivity. Since there appears in Fig. 2 to be some systematic discrepancy between the data and the best fit which can be obtained with Eq. (1) using Ebert and Teltow's values[7] for ξ and ϕ

TABLE I. Ratio of mobilities ϕ and intrinsic vacancy concentration c_0, assuming no association with Cd^{++}; the heats of transport are expressed in electron volts.

Salt	Temperature (°C)	Conductivity[a] ϕ	Conductivity[a] c_0	Thermoelectric power ϕ	Thermoelectric power c_0	Q^*	$-q_v^*-T(s_v+s_m)$	$q_i^*+T(s_i-s_m)$
AgBr	150			11.9	0.142×10^{-4}	0.728	0.372	0.291
	175	7.26	0.38×10^{-4}	7.5	0.36	0.705	0.377	0.265
	200	6.35	0.96	5.9	0.94	0.670	0.383	0.268
	225	4.78	2.04	4.8	2.08	0.629	0.391	0.267
	250	3.74	3.9	3.8	4.4	0.587	0.406	0.264
	275	2.97	7.8	2.9	8.0	0.535	0.432	0.263
	300	2.48	14.7	2.53	15.4	0.470	0.451	0.247
	325	2.13	26	2.41	27	0.417	0.451	0.222
	350	2.01	42	2.12	42	0.346	0.476	0.195
	375			1.76	50	0.263	0.522	0.154
AgCl	150			(14.3)	(0.0038)	0.996	0.360	0.256
	175			(12.0)	(0.013)	0.953	0.377	0.256
	200			(10.6)	(0.042)	0.932	0.368	0.262
	225			(9.3)	(0.11)	0.902	0.371	0.264
	250	7.87	0.27	8.1	0.28	0.865	0.383	0.268
	275	7.27	0.50	7.5	0.56	0.816	0.394	0.252
	300	5.96	0.89	7.0	1.35	0.770	0.400	0.257
	325	4.76	1.72	6.3	2.33	0.720	0.416	0.236
	350	3.95	3.4	5.1	4.4	0.668	0.430	0.231
	375	3.06	6.3	4.1	7.9	0.614	0.449	0.225
	400	2.51	10.8	3.2	13.5	0.551	0.472	0.217
	425	2.21	18.9					

[a] For AgBr, J. Teltow, Ann. Physik **5**, 63 (1949); for AgCl, I. Ebert and J. Teltow, Ann. Physik **15**, 268 (1955).

and adjusting only Q^*, it seemed desirable to make an independent choice of parameters. Accordingly, a least-squares method has been used to fit Eqs. (1) and (6) to the thermoelectric data, with ϕ, c_0, and Q^* as adjustable parameters. The result is an improved fit at high temperatures, though some apparently systematic deviation remains. Below 250°C the improvement is negligible. The same procedure has also been used in the case of AgBr, although in this case the fit was already excellent.

IV. HEATS OF TRANSPORT

The primary purpose of the thermoelectric measurements is the determination of the heat of transport $Q^*=q_i^*+q_v^*+h$. This quantity has been computed by the least-squares fit referred to in the preceding section, for both AgBr and AgCl. The values are given as a function of temperature in Table I. These values are probably accurate to within 0.01 ev, and are essentially the same as the values for Q^* obtained when ξ and ϕ are taken from the conductivity data. The strong decrease of Q^* with increasing temperature previously observed[1,5] is seen here. The value at the melting point is about 0.3 ev larger for AgCl than for AgBr.

The least-squares fit also yields values for ϕ and c_0, which are included in Table I and compared with the values from conductivity assuming no association.[8] Only about 10% accuracy can be claimed for these values. That is, a change in ϕ of about this amount can be compensated by a corresponding change in c_0 without seriously affecting the fit to $\Delta\theta$. The value of Q^*, however, is not affected by more than 0.01 ev by such changes. At the highest temperatures the values of ϕ and c_0 become less reliable because of the small values of $\Delta\theta$. At lower temperatures, the values are in very good agreement with the conductivity values. At still lower temperatures (below 250°C in AgCl), where ξ is large for all concentrations of impurity used, they cannot be determined from the thermoelectric data; the values in Table I in parentheses are extrapolated from higher temperature.

In order to try to separate out the heats of transport q_i^* and q_v^*, the quantity $h-Ts$ has been computed from Eq. (3) using values of c_0 from Table I and $N'/N=2$. The results are plotted in Fig. 5. The points for AgBr lie on a straight line, and also the points for AgCl above 250°. From the intercept and slope of these lines are obtained the values of h and s given in Table II. These values of h are in reasonably good agreement with the conductivity values[3,7] namely 1.27 and 1.69 ev for AgBr and AgCl, respectively. Subtracting h from Q^* gives the values of $q_i^*+q_v^*$ plotted in Fig. 6. The predominant heat of transport (presumably q_v^*) is seen to be negative and strongly temperature dependent.

The heats of transport for interstitials and vacancies can be separated in another way by computing $q_i^*+T(s_i-s_m)$ and $q_v^*+T(s_v+s_m)$ from the total thermoelectric power of the pure sample, using Eqs. (2) and

[8] The least-squares values are not really completely independent of the conductivity values: The surface in (ϕ, c_0, Q^*) space seems to have many local minima, so that if one starts at a very different point the least-squares method may converge to an entirely different set of values. Since the conductivity values were used as starting point, the method gives the best fit in the neighborhood of these values.

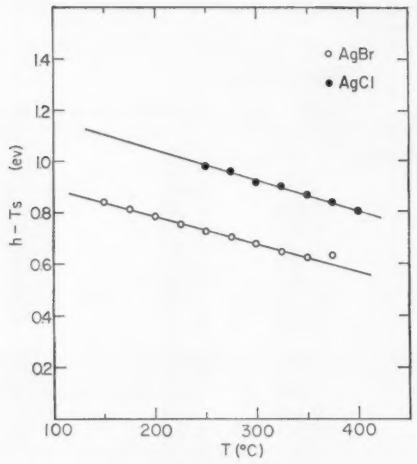

FIG. 5. Free energy of formation for Frenkel defects in AgBr and AgCl, from the thermoelectric power data.

(5) and the values of ϕ, c_0, and Q^* from Table I. The thermoelectric power of the leads to the sample must be subtracted from the values in Fig. 1. This contribution, which has been estimated[9] to be about 20 μv/°K, gives only a small correction. The corrected values of θ, inserted in Eqs. (2) and (5), yield the results given in Table I. These results are probably accurate to within about 0.01 ev except at the highest temperatures. They depend on the rather uncertain values of ϕ and c_0, but not very sensitively. Furthermore, at any temperature, $q_v^*+T(s_v+s_m)$, for example, can also be computed from Eq. (4) for the impure samples, and the results obtained for different values of impurity concentration c scatter by about 0.01 ev.

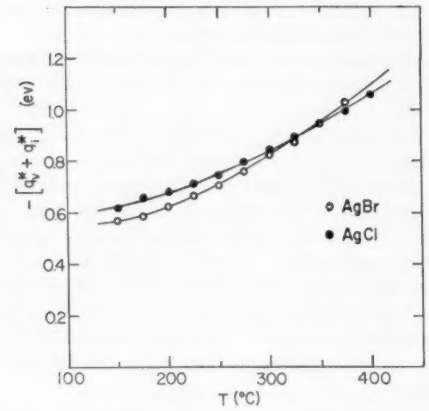

FIG. 6. Sum of the heats of transport for silver vacancies and interstitials in AgBr and AgCl, as a function of temperature.

[9] L. Patrick and A. W. Lawson, J. Chem. Phys. **22**, 1492 (1954).

To proceed further, it is necessary to make theoretical estimates of the entropies s_m, s_i, and s_v. The entropy s_m is identified with the entropy of lattice vibrations in silver metal.[2] This quantity can be calculated from the Debye specific heat theory. Values of entropy have been tabulated[10] in terms of T_D/T, where T_D is the Debye temperature. By using $T_D=229$°K for silver,[11] the values of s_m have been calculated between 150° and 400°C.

The change in entropy s_v produced by removing a Ag^+ ion from a lattice site in the silver halide to infinity can be decomposed into the entropy change on removing an ion from the interior to the surface, plus the change on removing it from the surface to infinity.[12] Thus $s_v=s_v'-\frac{1}{2}s_s$, where s_s is the entropy of the lattice vibrations of the salt and s_v' arises because of the change in frequency of the lattice vibrations on the production of a vacancy by removal of the ion to the surface. Similarly, $s_i=s_i'+\frac{1}{2}s_s$, where s_i' is the entropy change on taking an ion from the surface to an interstitial site. The entropy of the salt s_s was computed in the same way as the entropy of the metal s_m, using[11] as the Debye temperature 144°K for AgBr and 183°K for AgCl.

TABLE II. Enthalpy h and entropy s of formation of Frenkel defect pairs.

Salt	h (ev)	s/k
AgBr	1.29	12.5
AgCl	1.61	13.9

The quantities $q_i^*+Ts_i'$ and $q_v^*+Ts_v'$, calculated from the thermoelectric data using the Debye theory for the entropy of lattice vibrations, are tabulated versus temperature in Table III. These quantities are also thought to be reliable. The entropies of the salt s_s and metal s_m partly cancel, and in any case the Debye theory should give sufficiently accurate values.

Unfortunately, the present state of theory does not permit further resolution of the experimentally determined quantities. Calculation of changes in frequency of the normal modes when a vacancy or interstitial is introduced is a difficult problem, and attempts to solve it[13–16] have not given an unambiguous answer. A simple approximation, taking into account only nearest

[10] F. Simon, *Handbuch der Physik* (Springer-Verlag, Berlin, Germany, 1926), Vol. X, p. 350. Tables reprinted in *American Institute of Physics Handbook* (McGraw-Hill Book Company, Inc., New York, 1957), p. 46.

[11] *American Institute of Physics Handbook* (McGraw-Hill Book Company, Inc., 1957), pp. 4–47, 48.

[12] R. E. Howard and A. B. Lidiard, Discussions Faraday Soc. **23**, 113 (1957).

[13] G. H. Vineyard and G. J. Dienes, Phys. Rev. **93**, 265 (1954).

[14] H. B. Huntington, G. A. Shirn, and E. S. Wajda, Phys. Rev. **99**, 1085 (1955).

[15] E. W. Montroll and R. B. Potts, Phys. Rev. **100**, 525 (1955).

[16] A. W. Lawson, S. A. Rice, R. D. Corneliussen, and N. H. Nachtrieb, J. Chem. Phys. **32**, 447 (1960).

neighbors in the Einstein model,[13] gives $s_v' \approx 2k$, which value is consistent with conductivity data for NaCl (but not LiF). On the same model, s_i' would be expected to be negative. On the other hand, $s = s_i' + s_v'$ is very much larger in the silver halides (Table II), so that it seems probable that both s_i' and s_v' are large and positive. This fact probably would require dropping the assumptions of nearest neighbor interactions and perhaps the harmonic approximation (s' independent of temperature). A consideration of the normal mode frequencies indicates[16] that s_v' could very well be about $6k$.

V. ADDITIONS OF S^{--} TO AgBr

A. Addition of Ag_2S

As a further check on the validity of the thermodynamic theory of thermoelectric power as applied to the simple Frenkel defect model of the silver halides, it is of interest to consider the effects of adding a divalent anion impurity. If there is no association between the impurity and the silver interstitials, Eq. (6) shows that for an anion impurity (c negative) ξ must be replaced by $1/\xi$. This substitution in Eq. (1) merely changes the sign of $\Delta\theta$ for $\xi \approx 1$. That is, for small impurity concentrations an anion impurity should have just the opposite effect to that of a cation impurity.

Unfortunately, the solubility limits of most anion impurities seem to be rather small. Teltow has shown,[17] however, that Ag_2S is sufficiently soluble to influence the conductivity. According to his phase diagram, it should also be soluble enough to give small but perceptible changes in the thermoelectric power.

TABLE III. Heats of transport for silver vacancies and interstitials in electron volts.

Salt	Temperature (°C)	$-q_v^* - Ts_v'$	$q_i^* + Ts_i'$
AgBr	150	0.32	0.24
	175	0.32	0.21
	200	0.33	0.21
	225	0.33	0.21
	250	0.34	0.20
	275	0.37	0.20
	300	0.38	0.18
	325	0.38	0.15
	350	0.40	0.12
	375	0.44	0.08
AgCl	150	0.34	0.23
	175	0.35	0.23
	200	0.34	0.23
	225	0.34	0.23
	250	0.35	0.24
	275	0.36	0.22
	300	0.37	0.22
	325	0.38	0.20
	350	0.39	0.20
	375	0.41	0.19
	400	0.44	0.18

[17] J. Teltow, Z. physik. Chem. (Leipzig) **195**, 213 (1950).

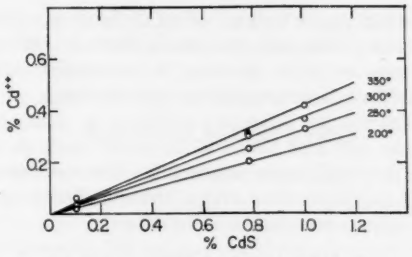

FIG. 7. Effective concentration of Cd^{++} in AgBr doped with CdS as a function of CdS concentration added, at four different temperatures.

The thermoelectric power of an AgBr sample containing 1.0 mole % of Ag_2S was measured. This amount of Ag_2S is soluble at 400°C, but may be expected to precipitate out progressively as the temperature is lowered. The measured thermoelectric power was the same as a pure sample at all temperatures, even though attempts were made to quench in excess Ag_2S by lowering the temperature from 400° as rapidly as possible.

The simplest explanation for the failure to observe any effect is that there is association between the Ag^+ interstitials and the S^{--} ion. On this basis, one concludes that at least 50% of the defects are associated even at 400°. This assumption is perhaps reasonable in view of the smaller radius of S^{--} compared with Br^-: The electrostatic attraction for the Ag^+ ion would be enhanced by a lower elastic energy when the interstitial was next to the S^{--}. If this suggestion is correct, the association could be expected to be less in AgCl. A similar consideration may help explain the absence of association between silver vacancies and Cd^{++}.

B. Addition of CdS

Another way to add S^{--} is to add CdS. If the dissolved S^{--} ion has no effect on the thermoelectric power, then the addition of CdS might be expected to have the same effect as an equal atom percent of $CdBr_2$.

Samples were measured containing 0.1, 0.78, and 1.0% of CdS. The results were qualitatively similar to those for $CdBr_2$ additions, except that the effect was less pronounced. In Fig. 7 is shown the effective amount of Cd^{++} in the crystal as a function of the amount of CdS added. The effective amount of Cd^{++} is obtained from the experimental isotherm for the system AgBr+$CdBr_2$ at a given temperature, as the concentration of $CdBr_2$ which would give the same thermoelectric power as the added concentration of CdS actually gives at that temperature. If, as suggested, the CdS had the same effect as $CdBr_2$, the points should all lie on a straight line of slope 1. The points in Fig. 7 do lie approximately on straight lines, thus eliminating the possibility that CdS precipitates out, but the slopes of the lines are less than 1 and dependent on temperature.

This effect can be understood on the basis of a chemical reaction in the solid solution. If there is some nonionic character to the bonds, it is meaningful to consider the dissociation reaction in the solution,

$$CdS+2\,AgBr\rightarrow CdBr_2+Ag_2S.$$

If K is the equilibrium constant for the reaction and s is the solubility limit for Ag_2S, the law of mass action gives for the concentration x of $CdBr_2$

$$x=[(1+4Kc)^{\frac{1}{2}}-1]/2K \qquad x\leq s$$
$$x=c/(1+Ks) \qquad x\geq s, \tag{9}$$

where c is the total concentration of Cd, i.e., the sum of the CdS and $CdBr_2$ concentrations. At concentrations greater than the very small solubility limit for Ag_2S, Eq. (9) predicts the linear relationship observed in Fig. 7. The slopes of the lines are determined by Ks. The lines drawn in the figure correspond to an exponential dependence of Ks on inverse temperature, with an activation energy of 4130 cal/mole. In taking s from the published phase diagram,[17] an activation energy of about 30 kcal/mole is found for K. This value contains a large uncertainty due to the uncertainty in s, but it is of the right order of magnitude for a chemical reaction.

VI. CONCLUSIONS

From the thermoelectric power measurements on AgBr and AgCl doped with Cd^{++}, it has been possible to derive accurate values for the heat of transport $Q^*=q_v^*+q_i^*+h$ as a function of temperature. Of all the thermodynamical parameters characterizing the formation and motion of defects in the crystal, the values of Q^* can probably provide the most certain experimental information for checking a theoretical calculation of the mechanics of point defects in the crystal. The derived values of Q^* depend insensitively on the choice of other parameters occurring in the thermodynamical theory, and do not depend on any assumption concerning association between impurities and vacancies. They may be expected to be only slightly modified by taking into account long-range Coulomb interactions between the defects.[18] The conclusion that Q^* is rather strongly temperature dependent appears inescapable and is confirmed by an independent measurement.[5]

The further analysis depends on the assumption that there is no association between Cd^{++} impurities and Ag^+ vacancies, which assumption is substantiated by the data, and on the derived values of ϕ and c_0. On this basis, values of $q_i^*+q_v^*$, $q_i^*+Ts_i'$, $q_v^*+Ts_v'$, and $s_i'+s_v'$ have been derived. If any one of these quantities could be ascertained, the others could be separated, though this resolution does not appear possible on the basis of present theory. Any plausible assumption concerning the entropies of the defects, however, seems to leave q_v^* and q_i^* strongly temperature dependent and probably greater in magnitude than the corresponding activation energies for mobility. These facts invite a refinement of the existing kinetic theory of the heats of transport.[19] It has been argued[20,21] that the heat of transport is equal to the activation energy for migration, but this relation seems to be in conflict with the present data and is not substantiated by such other measurements of thermal diffusion as have been made.[19,22] According to Wirtz,[19] the magnitude of the heat of transport should not be greater than the activation energy, although it could be less; this restriction was already violated by results on AgI and appears inconsistent with the present data. Wirtz commented that the assumption of temperature independence of the heat of transport was only a first approximation, and indeed the values of ϕ from conductivity indicate that the mobility activation energies are also temperature dependent. The activation energy for vacancy motion has been related to the normal vibrations,[23] the the temperature dependence to be expected is not clear.

The assumption that the Cd^{++} impurities and Ag^+ vacancies are unassociated above about 100°C is strongly indicated by the thermoelectric data. A reexamination of the conductivity data shows that the assumption, while not strictly consistent with the data, is at least much better than the prediction of the simple association theory. Therefore, it is concluded that the best simple approximation is to assume that Cd^{++} is unassociated.

On the other hand, the absence of any observable effect of the addition of Ag_2S implies that association of S^{--} and silver interstitials is significant even at 400°C. More complex relations in this system are also suggested by the difficulty of interpreting the corresponding conductivity measurements.[17] Additions of CdS also imply some association of Cd^{++} and S^{--} from the thermoelectric data, in contradiction with Teltow's qualitative conclusions from conductivity measurements.[17]

The agreement of thermoelectric power measurements in the silver halides with the thermodynamic theory is very satisfactory for the Cd-doped case, so that the simple model of unassociated Frenkel defects is apparently substantiated. The values of the thermodynamic parameters, however, do not appear to submit to simple mechanical calculation. The heat of formation h is reasonably constant, at least at high temperatures, but the magnitude of the entropy s and the magnitude and temperature dependence of the heats of transport q^* may require rather refined calculations for their explanation.

[18] E. Haga, J. Phys. Soc. Japan **14**, 992 (1959).

[19] K. Wirtz, Physik. Z. **44**, 221 (1943).
[20] A. D. LeClaire, Phys. Rev. **93**, 344 (1954).
[21] A. R. Allnatt and S. A. Rice J. Chem. Phys. **33**, 573 (1960).
[22] P. Shewmon, J. Chem. Phys. **29**, 1032 (1958).
[23] S. A. Rice, Phys. Rev. **112**, 804 (1958).

Alternatively, the temperature dependence of the heat of transport could perhaps be modified by changing the model on which the thermodynamic theory is based, since the derived values are obtained from a comparison between the result of the theoretical calculation and the experimental data. One modification which could be made would be to introduce some association between the Frenkel defects in the pure crystal. This modification would, however, have no effect on the thermoelectric power or the conductivity, since the associated pairs are uncharged and do not affect the equilibrium of unassociated defects if they are treated as a separate molecular species.

Another possible modification would be to assume the presence of some Schottky defects at high temperatures, in addition to the Frenkel defects. This assumption would modify the theory of both the thermoelectric power and the conductivity, and indeed there is other experimental evidence for the existence of some Schottky defects. Their presence also, however, does not affect the values of Q^* which are deduced. The contribution of the Schottky defects can be included in Eq. (1) if ϕ is replaced by ϕ', where $\phi'=\phi/(1+NK_S/N'K_F)$, K_S and K_F being the equilibrium constants for the formation of Schottky and Frenkel defects, respectively. The formula for the conductivity of a doped specimen relative to a pure one must be modified in just the same way, by replacing ϕ with ϕ'. Therefore, if the values of ϕ used in analyzing the thermoelectric data are those which are obtained from the minima of the relative conductivity isotherms, the presence of Schottky defects would affect both in the same way, and the derived values of Q^* would be unchanged.

In summary, the heats of transport for defects in the silver halides have been found to be surprisingly large and temperature dependent, from the standpoint of existing theories, and it seems difficult to escape this conclusion by modifying the assumed defect model for the salts.

ACKNOWLEDGMENTS

Most of the measurements reported here were performed by H. A. Ali. The calculations were carried out by W. E. Daniels, Jr., S. D. Merrill, and A. W. Bevan. Their assistance is gratefully acknowledged. We also wish to thank Dr. F. Moser of Eastman Kodak Research Laboratories for the gift of specially prepared pure single crystals.

Wave Functions and Correlation Energies for F, F^-, and Ne

LELAND C. ALLEN

Department of Chemistry, Princeton University, Princeton, New Jersey

(Received August 31, 1960)

Hartree-Fock solutions have been obtained by the finite expansion technique and a comparison is made with other computational methods and results. Total energies, correlation energies, and one-electron parameters are presented as well as a tabulation of the radial functions in analytic form. The correct sign and order of magnitude of the fluorine electron affinity is predicted.

I. INTRODUCTION AND METHOD OF SOLUTION

HARTREE-FOCK solutions for free atoms and ions continue to play a prominent role in the theory of atoms, molecules, and solids. The present set of calculations were specifically undertaken to provide basis functions and an estimate of the correlation energy for the hydrogen fluoride molecule.[1] However, the wave functions given here have already been used for a variety of other applications. These include the diamagnetic susceptibility of neon[2]; x-ray scattering factors for F^-, F, and Ne[3]; F^- basis orbitals for the calculation of both superexchange effects in transition metal fluorides,[4] and the V_K center in LiF.[5] Photoionization cross sections for neon have also been computed from Hartree-Fock solutions.[6]

Several other Hartree-Fock calculations for F, F^-, and Ne exist in the literature.[7–9] These, as well as almost all existing Hartree-Fock solutions, were obtained by direct numerical integration of the integro-differential equations. This method and the equations themselves have been discussed completely in an excellent book.[10] Our work has employed the finite expansion technique[11,12] generally referred to as the Roothaan procedure. In this scheme the energy of a determinantal wave function is minimized by the self-consistent evaluation of the linear coefficients in a finite, predetermined basis set. As in the standard Hartree-Fock technique, these basis functions are assumed to be a product of a radial function and a spherical harmonic. For our problem the radial function is a series of terms of the exponential type, $r^m e^{-kr}$ (m integral, $k>0$). Each final self-consistent one-electron orbital for a given l value is made from all exponential radial terms associated with that l. In practice the true Hartree-Fock solution is achieved by modification of the parameters m and k, and by increasing the size of the basis set until there is no further lowering of the energy.

The equations, formalism,[11,12] and applications[1] of the Roothaan procedure are adequately documented in the literature and will not be repeated here. Because it may be formulated as a matrix method, the scheme is especially well suited for use with a high-speed digital computer and at least two computer programs of it exist.[13] For our computations we employed a prior version of the M.I.T. program written for the Whirlwind I computer. The special advantage offered by these programs is the opportunity to utilize the arge number of significant figures that it is possible to carry through the calculations. This computational procedure enabled us to obtain highly accurate radial functions, total energies, and the electron affinity of fluorine. It is the lack of total energy values which is the greatest shortcoming of most existing Hartree-Fock solutions. Besides the work reported here,[14] relatively few attempts have been made to obtain Hartree-Fock solutions via the Roothaan scheme and these have been almost exclusively concerned with atoms containing only s electrons.[15–17]

The single determinant wave functions for F^- and Ne raise no special problems because these are closed shell structures and correspond to the Hartree-Fock equations in their simplest form. F, however, has a ^2P ground state and an open p shell. Open shells lead to off-diagonal Lagrangian multipliers in the Hartree-Fock equations and suitable methods of handling this problem have been developed by Shortley,[18]

[1] A. M. Karo and L. C. Allen, J. Chem. Phys. **31**, 968 (1959).
[2] M. Kårplus, University of Illinois (private communication).
[3] B. H. Worsley, Can. J. Physics **37**, 967 (1959); A. J. Freeman, Acta Cryst. **12**, 929 (1959).
[4] R. Stuart, Lawrence Radiation Laboratory, Livermore, California (private communication).
[5] T. P. Das and R. Knox, University of Rochester, Rochester, New York (private communication).
[6] M. J. Seaton, Proc. Roy. Soc. (London) **A208**, 408 (1951).
[7] F. W. Brown, Phys. Rev. **44**, 214 (1933).
[8] C. Froese, Proc. Cambridge Phil. Soc. **53**, 206 (1957).
[9] B. H. Worsley, Can. J. Phys. **36**, 289 (1958).
[10] D. R. Hartree, *The Calculation of Atomic Structures* (John Wiley & Sons, Inc., New York, 1957).
[11] C. A Coulson, Proc. Cambridge Phil. Soc. **34**, 204 (1938).
[12] C. C. J. Roothaan, Revs. Modern Phys. **23**, 69 (1951).
[13] (a) M.I.T. IBM 704, coded by R. K. Nesbet. Described in Mass. Inst. Technol. Solid State and Molecular Theory Group, Quart. Prog. Repts. 16–18 (1955). (b) Argonne National Laboratory, IBM 704, and University of Chicago, Remington-Rand 1103A (located at the Wright-Patterson Air Force Base), coded by C. C. J. Roothaan and L. M. Sacks.
[14] An account of many of the results obtained here has been given by the author previously in Mass. Inst. Technol. Solid State and Molecular Theory group, Quart. Prog. Repts. 25 and 26 (1957).
[15] C. C. J. Roothaan, L. M. Sacks, and A. W. Weiss, Revs. Modern Phys. **32**, 186 (1960).
[16] R. K. Nesbet and R. E. Watson, Phys. Rev. **110**, 1073 (1958); R. E. Watson, *ibid.* **119**, 170 (1960).
[17] R. E. Watson Phys. Rev. **118**, 1036 (1960) calculations for the iron group atoms.
[18] G. H. Shortley, Phys. Rev. **50**, 1072 (1936).

Hartree,[19] Nesbet,[20] Roothaan,[21] and Lefebvre.[22] We have used Nesbet's digital computer programs and in order to retain a single determinant representation for open shells he introduces an "equivalence restriction" which restricts the degenerate set of spinorbitals of the open shell to be orthonormal transforms of one another. In addition to the designation of some specific electron as the missing one in the p shell, a particular, though arbitrary, spin orbital is selected and the Hamiltonian matrix is constructed in terms of this choice.[23] It is possible to select a unique Hamiltonian which represents the *average* value of all possible choices,[24] and for the case where the closed and open shells have no symmetry in common (F atom) this averaged equivalence restriction and the methods of Shortley, Hartree, Roothaan, and Lefebvre are all identical. We have used this averaging scheme in our calculations.

II. CHOICE OF NONLINEAR PARAMETERS

The central problem in using the finite expansion method to obtain Hartree-Fock solutions is the choice of nonlinear parameters. The actual choice procedure is a "boot-strapping" process wherein we use available crude data to initially establish rules-of-thumb and then attempt successive refinements by experimentation. A number of years ago F. W. Brown constructed approximate Hartree-Fock solutions for F, F⁻, and Ne.[7] He omitted exchange effects in certain cases and employed relatively crude numerical techniques. He also devised analytic approximations of the exponential type for his numerical functions with a few terms and low accuracy. Löwdin on the other hand has carried through high-accuracy analytic fits (of exponential type) to a *Hartree* F⁻ function with his node removal scheme.[25] For each of the structures F, F⁻, and Ne, Brown used four s and two p basis functions. Löwdin's set comprises six s's and four p's. Our initial calculations employed Brown's original nonlinear parameters. The next calculations were performed using Löwdin's nonlinear F^- parameters for F, F^-, and Ne. We found that the self-consistent adjustment of the *linear* parameters by the Roothaan procedure produced remarkably good solutions for all *three* atomic structures. A relatively large improvement in the total energies over those obtained by use of Brown's parameters was realized. A first refinement of this single set was then developed by comparing Löwdin's and Brown's F⁻ parameters and establishing scaling rules between them. These rules were applied to Brown's F and Ne parameters and sets of six s and four p basis functions derived. Slightly improved energies for F and Ne resulted. A second refinement was the addition of an s and a p function. This further refinement was obtained by first noting the position of the maxima of Brown's numerical tables of $P(r)\equiv rR(r)$. The maxima of exponential basis functions, with m one greater than the principal quantum number of the second shell, were then matched to Brown's maxima positions. Thus for $r^m e^{-kr}$, $k=3/r_{\max}$. (The functions determined by this rule are the final s and final p parameters listed in Table II.) A final re-

TABLE I. Total energies of F atom for successive refinements in the basis set.[a]

Brown's parameters	99.25121
Löwdin's parameters	99.40609
Present work	99.40792

[a] Hartree units, all energies negative. 1 Hartree unit=27.20972 ev.

TABLE II. Nonlinear parameters.

$x\equiv r^m e^{-kr}$

s functions			p functions		
x	m	k	x	m	k
		F atom			
x_1	0	12.187	x_8	1	5.954
x_2	0	8.189	x_9	1	3.068
x_3	1	14.296	x_{10}	1	1.752
x_4	1	4.096	x_{11}	1	0.7863
x_5	1	2.767	x_{12}	2	4.17
x_6	1	1.716			
x_7	2	3.75			
		F⁻ ion			
x_1	0	12.187	x_8	1	5.9696
x_2	0	8.189	x_9	1	3.0759
x_3	1	14.296	x_{10}	1	1.4357
x_4	1	4.1211	x_{11}	1	0.64417
x_5	1	2.7178	x_{12}	2	4.05
x_6	1	1.6465			
x_7	2	3.75			
		Ne atom			
x_1	0	13.552	x_8	1	6.928
x_2	0	9.106	x_9	1	3.570
x_3	1	16.208	x_{10}	1	2.016
x_4	1	4.567	x_{11}	1	0.9048
x_5	1	3.044	x_{12}	2	4.69
x_6	1	1.863			
x_7	2	4.23			

[19] D. R. Hartree, Proc. Roy. Soc. (London) **A150,** 96 (1935). Also see the work cited in footnote 10.
[20] R. K. Nesbet, Proc. Roy. Soc. (London) **A230,** 312 (1955).
[21] C. C. J. Roothaan, Revs. Modern Phys. **32,** 179 (1960).
[22] R. Lefebvre, J. chim. phys. **54,** 168 (1957).
[23] Examples of the effect on the energy of different choices and further discussion can be found in R. K. Nesbet and R. E. Watson, Ann. Phys. **9,** 260 (1960), and also in the work cited in footnote 24.
[24] L. C. Allen, Mass. Inst. Technol. Solid State and Molecular Theory Group, Quart. Progr. Rept. 22 (1956).
[25] P. O. Löwdin, Phys. Rev. **90,** 120 (1953).

TABLE III. Coefficients, ij, for the SCF radial solutions, $Ui(r)=r\sum_j f_{ij}x_j$.

$U_1(r)\equiv P_{1s}(r)$		$U_2(r)\equiv P_{2s}(r)$		$U_8(r)\equiv P_{2p}(r)$	
		F atom			
f_{11}	0.1177113	f_{21}	0.0055334	f_{88}	0.1677057
f_{12}	0.8894719	f_{22}	−0.3572457	f_{89}	0.0636986
f_{13}	−0.0024849	f_{23}	0.0176802	$f_{8\,10}$	0.5802266
f_{14}	0.0061420	f_{24}	0.1303075	$f_{8\,11}$	0.0357962
f_{15}	−0.0148922	f_{25}	0.6776013	$f_{8\,12}$	0.2751730
f_{16}	0.0019636	f_{26}	0.2348418		
f_{17}	0.0116363	f_{27}	0.0481173		
		F^- ion			
f_{11}	0.1180129	f_{21}	0.0513805	f_{88}	0.0764172
f_{12}	0.8889146	f_{22}	−0.3435381	f_{89}	0.4744668
f_{13}	−0.0023635	f_{23}	0.0163459	$f_{8\,10}$	0.5135816
f_{14}	0.0052933	f_{24}	0.1871588	$f_{8\,11}$	0.0794088
f_{15}	−0.0120010	f_{25}	0.4786040	$f_{8\,12}$	0.0014772
f_{16}	0.00177573	f_{26}	0.3095857		
f_{17}	0.0099697	f_{27}	0.1314513		
		Ne atom			
f_{11}	0.1222399	f_{21}	0.0542633	f_{88}	0.0573562
f_{12}	0.8834132	f_{22}	−0.3595172	f_{89}	0.5641636
f_{13}	0.00003826	f_{23}	0.0158172	$f_{8\,10}$	0.5045485
f_{14}	0.0040082	f_{24}	0.1514835	$f_{8\,11}$	0.0713649
f_{15}	−0.0167735	f_{25}	0.6951764	$f_{8\,12}$	−0.0992280
f_{16}	0.0022717	f_{26}	0.2056376		
f_{17}	0.0147063	f_{27}	0.0416358		

finement consisted of doubling the power of r and doubling the exponent of the exponential for the third s function (see Table II) in our list. This retained the same position of the maximum but avoided the tendency toward linear dependence present in Löwdin's parameters. These last refinements produced only very minute energy changes as can be seen from Table I. Small variations in our final sets of seven s and five p basis functions convinced us that, at least within the broad framework of our choice procedure, no further energy improvement was to be obtained and thus Hartree-Fock solutions had been achieved.

III. RESULTS AND COMPARISONS

A. Analytic Expressions

Tables II and III give the nonlinear parameters and linear coefficients for analytic representation of our solutions.

B. Numerical Functions and Cusp Values

Tabulations of the normalized F, F^-, and Ne radial functions have been deposited with the American Documentation Institute.[26] The mesh employed was that required for evaluation of two-center molecular integrals in the application to hydrogen fluoride mentioned in the introduction. Initial mesh interval size is 0.003125. This is successively doubled at $r=0.05$, 0.1, 0.2, 0.4, 2.0, 2.4, 4.0, and 6.4 with values extending to 22.4. Table IV presents a comparison of our results with the best other numerical functions at representative mesh points. The calculations of Froese and Worsley were both performed on the University of Toronto FERUT computer (but using different programs) and both display the same accuracy. They deviate from ours by 3–5 in the fourth decimal place for most r values with the discrepancy increasing to about 1–2 in the third decimal for points in the tails of the functions.

In our tabulation of numerical functions we have retained the number of significant figures corresponding to the digital computer accuracy. It is to be noted, however, that we do not have a Hartree-Fock solution to this accuracy, but rather to about $3\frac{1}{2}$–4 decimal places. This is indicated by the small hump around

TABLE IV. Comparison of numerical functions.

	r	C. Froese[a]	Present work
		F^- ion	
P_{1s}	0.01	0.4726	0.4725762
	1.20	0.0049	0.0052129
P_{2s}	0.01	0.1065	0.1068846
	1.20	0.8022	0.8037476
P_{2p}	0.01	0.0018	0.0017528
	1.20	0.7335	0.7331340
		Ne atom	
	r	B. H. Worsley[b]	Present work
P_{1s}	0.0066402	0.3775	0.3774810
	0.098805	2.2664	2.266532
	0.73007	0.0506	0.0510637
P_{2s}	0.0066402	0.0886	0.0889318
	0.098805	0.4626	0.4625628
	0.73007	1.0825	1.081503
P_{2p}	0.006402	0.0011	0.00117423
	0.098805	0.1701	0.1706138
	0.73007	0.9535	0.9558809

[a] See work cited in footnote 8.
[b] See work cited in footnote 9.

[26] Document number 6608, ADI Auxiliary Publications Project, Photoduplication Service, Library of Congress, Washington 25, D. C. A copy may be secured by citing the document number and by remitting $1.25 for photoprints, or $1.25 for 35-mm microfilm. Advance payment is required. Make checks or money orders payable to: Chief, Photoduplicator Service Library of Congress.

$r=3.0$ in the tails of the $P_{1s}(r)$ for all three functions. The hump maximum is about 0.115×10^{-3} (or roughly 0.005% of the function maximum) above a smooth extrapolation. An almost identical situation has been found by Roothaan, Sacks, and Weiss for atoms containing s electrons.[15] Our 3½–4 decimal place accuracy implies seven significant figures in the energies.

For values approaching $r=0$ solutions to the Hartree-Fock equations must obey the relation[15,27]

$$[(1/g)(dg/dr)]_{r=0}=-z/(l+1)$$

$$z\equiv \text{atomic number}$$

$$g\equiv R(r)/r^l. \qquad (1)$$

Table V lists the cusp values defined by

$$[(1/g)(dg/dr)]_{r=0}$$

and compares them to the correct value (in parenthesis). The cusp relation has recently led Roothaan and co-workers[28] to investigate sets of analytic basis functions containing one term which reproduces Eq. (1) exactly plus additional terms making no contribution to it. This may become a useful rule for choosing nonlinear parameters. For example, a Hartree-Fock solution which does not satisfy Eq. (1) adequately will yield an inferior value for the quadrupole coupling constant [where one is concerned with the operator $(3\cos^2\theta-1)/r^3$]. However, the cusp value has little effect on the energy and other operators such as those representing magnetic properties.

C. Total Energies, Correlation Energies, and Relativistic Corrections

In Table VI we tabulate Hartree-Fock total energies, the best experimental values available, the difference between these two numbers and the correlation energy of F⁻. The difficulties in obtaining values for the relativistic contribution are well known. A discussion and summary of this problem which is particularly appropriate to our work is provided in two papers by Fröman.[29] His estimate for F⁻ is included in our table and subtracting this from the difference between the Hartree-Fock and experimental values gives a correlation energy of 10.61 ev. Fröman has performed similar calculations on the 10-electron system Al^{+3} yielding a correlation energy of 11.00 ev. For F, it is not easy to obtain a relativistic estimate because it is only for closed shell structures that several difficult to evaluate terms in the relativistic Hamiltonian are zero. For neon, the evaluation of a relativistic contribution has little significance because of the lack of accurate experimental data.

If we adopt the value of approximately ½ ev correlation energy per electron that is generally accepted for two and four particle structures of s electrons,[29,30] one is tempted to regard the correlation energy tied up in the s electrons of F⁻ and Al^{+3} as 2 ev. Of course, one can not separate the correlation energy into s electron and p electron contributions, but if each type acted independently we would have approximately 1½ ev correlation energy per p electron.

No discussion of F⁻ and neon would be complete without mention of the pioneering work of Bernal and Boys on these systems.[31] They set up many determinant wave functions and obtained total energies about halfway between the Hartree-Fock values and experiment. The total energies of the dominant single determinant have a percent error roughly twice that of the Hartree-Fock result. However, these relatively high energies arose because Bernal and Boys were not interested in an exploration for Hartree-Fock solutions but rather in establishing a good starting point for a configuration interaction treatment.

TABLE V. Cusp values, $|[(1/g)(dg/dr)]_{r=0}|$.

	F	F⁻	Ne
P_{1s}	8.647 (9)	8.665 (9)	9.657 (10)
P_{2s}	10.969 (9)	10.880 (9)	11.815 (10)
P_{2p}	2.317 (4.5)	2.363 (4.5)	3.000 (5)

TABLE VI. Total energies and the correlation of energy of F⁻.

	F	F⁻	Ne
Hartree-Fock	−99.40792[b]	−99.45891	−128.54318
Experimental	−99.8096[e]	−99.9426[d]	−129.0[e]
Difference (Exptl.-H.F.)	10.93 ev	13.16 ev	12.4 ev
Relativistic[a]		2.55 ev	
Correlation		10.61 ev	

[a] See the work cited in footnote 29.
[b] Hartree units unless otherwise stated.
[c] See footnote 29. The value was obtained from the first eight ionization potentials given by C. E. Moore, *Atomic Energy Levels*, Vol. 1, Natl. Bur. Standards (U.S.) Circ. No. 467, U. S. Dept. of Commerce (1949). The last ionization potential was calculated by Dirac theory.
[d] Using an electron affinity of 3.62 ev [L. M. Brauscomb and S. J. Smith, J. Chem. Phys. **25**, 598 (1956)].
[e] First six ionization potentials from C. E. Moore. Last four are extrapolated values determined by W. Finkelnburg [Phys. Rev. **77**, 304 (1950)].

D. One-Electron Energy Parameters

These parameters along with those for the other calculations are listed in Table VII.

E. Electron Affinity of Fluorine

For some time there has been a question as to whether or not the Hartree-Fock total energy of F⁻ would be

[27] P. O. Löwdin, Phys. Rev. **94**, 1600 (1954).
[28] Private communication.
[29] A. Fröman, Phys. Rev. **112**, 807 (1958); Revs. Modern Phys. **32**, 317 (1960).
[30] P. O. Löwdin, Advances in Phys. **5**, No. 17 (1956).
[31] M. J. M. Bernal and S. F. Boys, Phil. Trans. Roy. Soc. London **A245**, 139 (1952).

TABLE VII. One-electron energy parameters.[a]

	F. W. Brown[b]	Present work	
F atom			
ϵ_{1s}	26.54	26.38168	
ϵ_{2s}	1.20	1.570682	
ϵ_{2p}	0.55	0.7284173	
F^- ion			
	F. W. Brown[b]	C. Froese[c]	Present work
ϵ_{1s}	26.19	25.8225	25.82957
ϵ_{2s}	0.75	1.0765	1.074678
ϵ_{2p}	0.07	0.1815	0.1812090
Ne atom			
	F. W. Brown[b]	B. H. Worsley[d]	Present work
ϵ_{1s}	32.84	32.775	32.76755
ϵ_{2s}	1.37	1.933	1.925974
ϵ_{2p}	0.755	0.8525	0.8461500

[a] Hartree units, all values negative.
[b] See work cited in footnote 7.
[c] See work cited in footnote 8.
[d] See work cited in footnote 9.

less than that of F. The primary reason for this uncertainty is that use of a *single* exponential basis function per atomic orbital for F and F^- results in a *negative* electron affinity of about 8 ev.[1] Neither our final functions nor any of the preliminary trails showed this characteristic. Table VIII lists values obtained both from the difference in the total energies of F and F^- and from the ϵ_{2p} parameter of F^-. It is interesting to note that the electron affinity determined from the difference of total energies is a little over 2 ev too small. Two competing effects cause the calculated energy difference to deviate from the experimental value. First, configuration interaction effects will lower the energy of F^- less than F because F^- is a closed shell structure.

TABLE VIII. Electron affinity of fluorine.[a]

	Difference of total energies	One-electron parameter of F^-
F. W. Brown[b]		1.90
C. Froese[c]		4.94
Present work	1.39	4.93
Experimental value[d]	3.62	

[a] All values in ev. 1 Hartree unit=27.20972 ev.
[b] See work cited in footnote 7.
[c] See work cited in footnote 8.
[d] L. M. Brauscomb and S. J. Smith, J. Chem. Phys. **25**, 598 (1956).

Second, F^- has one more electron than F and thus a greater correlation energy. If configuration interaction effects were the same for both F and F^- and if we believe the value of $1\frac{1}{2}$ ev per p-electron mentioned in Sec. C, this would essentially account for the 2-ev discrepancy between the observed and calculated values.

Note added in proof. The author has just learned of some recent calculations performed by Dr. L. M. Sachs at the Argonne National Laboratories. They were carried out via the Roothaan procedure with the following total energies: F—99.40900; F^-—99.45921; Ne—128.54921. These are about $\frac{1}{20}$ ev lower than our values. A more complete account is to be given in a forthcoming Argonne Technical Report.

ACKNOWLEDGMENTS

I am indebted to Professor Robert K. Nesbet for use of his digital computer programs and helpful discussions concerning them. I also wish to thank Professor J. C. Slater for his interest and encouragement. The author held a National Science Foundation postdoctoral fellowship at the Department of Physics, University of California, and was a member of the Materials Research Laboratory, OMRO, Watertown, Massachusetts while part of this work was being carried out and the support of these organizations is gratefully acknowledged.

THE JOURNAL OF CHEMICAL PHYSICS VOLUME 34, NUMBER 4 APRIL, 1961

Anisotropic Hyperfine Interactions in the ESR Spectra of Alkyl Radicals*

E. L. COCHRAN, F. J. ADRIAN, AND V. A. BOWERS

Applied Physics Laboratory, The Johns Hopkins University, Silver Spring, Maryland

(Received August 29, 1960)

We have studied the effect of anisotropic hyperfine interactions on the electron spin resonance (ESR) spectra of alkyl radicals trapped in polycrystalline matrices. The anisotropy broadens some or all of the hfs components, thus complicating the spectra. In alkyl radicals one has both isotropic and anisotropic hfs interactions with the α protons, but only an isotropic interaction with the β protons. Computed and experimental line shapes for the ethyl and propyl radicals are in qualitative agreement, provided that the hfs interaction is averaged over the various equilibrium orientations of the $-CH_2\cdot$ group. This implies a rapid reorientation of the $-CH_2\cdot$ group. It is noteworthy that when the two α protons are antiparallel the hyperfine anisotropy cancels and sharp intense hfs components result, while parallel orientations of the α protons give broad weak hfs lines. In particular, if the broad weak lines associated with the α proton hfs interactions are overlooked, the propyl radical spectrum appears to be a triplet, implying hfs interactions with the β protons only. In radicals where there is an odd number of α hydrogens (e.g. $R'-\dot{C}H-R$) there is no possibility of cancellation, and all the lines will be broad and weak. Our attempts to observe radicals of this type have been unsuccessful, most likely for this reason.

I. INTRODUCTION

IN recent years extensive studies have been made of the electron spin resonance (ESR) spectra of free radicals trapped in various solid matrices. The value of these studies lies in the information they give on the magnetic hyperfine interactions between the unpaired electron and the various magnetic nuclei in the radical. These hyperfine interactions will split the ESR line into a multiline pattern which can often be used to identify the radical, or, in the case of a known radical, to obtain additional information about its structure and environment. In many cases, however, the hyperfine interaction experienced by some or all of the nuclei will be anisotropic, i.e., it will depend on the orientation of the external magnetic field with respect to a set of axes fixed in the radical. For the physically important case of radicals trapped in polycrystalline media, this anisotropy will produce a broadening of the ESR lines which may range from an obliteration of finer details of the spectrum to extreme broadening where the spectrum appears as a single broad, weak (or even undetectable) line.

In this paper we shall examine the effects of hyperfine anisotropy on the ESR spectra of alkyl radicals produced by photolysis of the corresponding alkyl iodides in solid argon at 4.2°K. These radicals have the general formulas

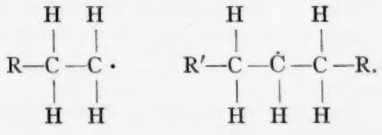

Primary Secondary

In the usual notation the carbon atom holding the unpaired electron is called an α carbon, and the hydrogen atoms bonded to it are called α hydrogens. The carbon atoms bonded to the α carbon are called β carbons, and the hydrogen atoms bonded to the β carbons are called β hydrogens. Theory and experiment indicate that in radicals of the foregoing type one will have isotropic hyperfine interactions of comparable magnitude with both the α and β hydrogen nuclei. The α hydrogen nuclei, however, will also experience an anisotropic hyperfine interaction of the same order of magnitude as the isotropic interaction, while the hyperfine anisotropy experienced by the β hydrogens will be considerably smaller.[1] The effect of the anisotropic hyperfine interactions with the α hydrogens will differ from one radical to another depending on the rotational freedom of the radical, the possibility of cancellation between two such α hydrogens, etc. It will be shown that many of the puzzling features of the ESR spectra of these radicals can be accounted for in terms of this hyperfine anisotropy.

In much of the past work on the ESR spectra of alkyl radicals, the paramagnetic species was produced by x- or γ-ray irradiation of relatively complex organic materials in the form of polycrystalline solids. In experiments of this type one has, in addition to the difficulties caused by magnetic anisotropy, the problem of potentially complex decomposition mechanisms. In this regard, the use of ultraviolet radiation has the distinct advantage that the number of possible decomposition products is somewhat more limited, and a number of such experiments has now been reported. Often, however, these investigations have suffered from the use of compounds whose photochemistry in the gas or liquid phases is either unknown or known to be complex. Even when the compounds irradiated have simple well-known dissociation mechanisms in fluid media, photolysis in the solid has been shown to be complicated by relatively low quantum yields and by

* This work supported by Bureau of Naval Weapons, Department of the Navy.

[1] C. Heller and H. M. McConnell, J. Chem. Phys. **32**, 1535 (1960).

secondary reactions of the primary photochemical products with the substrate.[2]

The photolysis of the alkyl iodides has been studied extensively in the gas and liquid phases and in solution.[3] The primary photochemical process has been almost universally assumed to be rupture of the carbon-iodine bond to form an alkyl radical and an iodine atom. Recent studies have elucidated the detailed mechanism of the photolysis and have pointed up the importance of hot radical reactions and of diffusion controlled disproportionation, but have confirmed earlier conclusions regarding the primary process.[4–6] The quantum yield for the primary process in fluid media is unity for actinic light of 2537 A, reduced quantum yields for ultimate decomposition being attributed to back reaction.[6] Reports have appeared on the photolysis of certain members of this series in the solid phase,[7,8] but the nature of the primary process has not been established.

Assuming that the primary process characteristic of fluid media is carried over to the solid phase, photolysis of the alkyl iodides should yield the corresponding alkyl radicals as primary products. The ESR of the second product of the photolysis, iodine atoms, is probably not observable in polycrystalline matrices.[9] In this work, a series of alkyl iodides was photolyzed at 2537 A at a temperature of 4.2°K. The iodides were diluted to a concentration of 1% by solid argon, to minimize secondary reactions. It was hoped by this technique to observe the ESR spectra of the aliphatic free radicals under conditions where only one resonance was present at a time, and thus to arrive at an unambiguous assignment of the ESR spectra of these free radicals. As will be seen, this objective was only partially achieved. Also, as a matter of some interest, the absolute quantum yields for radical trapping were determined.

II. EXPERIMENTAL

The liquid helium cryostat and microwave apparatus have been described elsewhere.[9] The gaseous 1% alkyl iodide-argon mixtures were deposited on a liquid helium-cooled sapphire rod at a rate predetermined to give a solid sample approximately 1 mm thick in 30 min. The lamp was a Hanovia SC2537 low-pressure mercury resonance lamp designed to fit into the 3-in. magnet gap in front of the window. When a quartz window was used, the 1849 A component from the lamp was filtered by 1 cm of a 1 *N* acetic acid solution. Photolysis times varied from one to a few hours.

Light intensity at the sample was determined using outgassed liquid ethyl iodide as actinometer (quantum yield for iodine atom production = 0.26),[10] in an experimental setup designed to simulate the cryostat geometry. Ethyl and *n*-propyl radical yields were measured by comparing integrated line intensities of their ESR spectra to that of a weighed sample of diphenyl picryl hydrazyl. Quantum yields determined in this manner are subject to considerable error, and should be regarded as approximate.

III. THEORY

A. Calculation of the Hyperfine Splittings

A general theory for calculating hyperfine splittings and line intensities has been given by Trammell, Zeldes, and Livingston.[11] Thus, we shall discuss only those features of the problem which are of special interest in the present study.

The magnetic interactions experienced by the unpaired electron and nuclei of a free radical in an external magnetic field $\mathbf{H}$ are described by the Hamiltonian,

$$\mathcal{H}=g\beta\mathbf{H}\cdot\mathbf{S}-\sum_i\gamma_i\hbar\mathbf{H}\cdot\mathbf{I}_i+\sum_i\gamma_i\hbar\mathbf{S}\cdot\mathfrak{T}_i\cdot\mathbf{I}_i. \quad (1)$$

The first term is the Zeeman energy of the electron, where β is the Bohr magneton, and the electron g factor g has been assumed to be isotropic.[12] The second term is the Zeeman energy of the nuclei, where γ_i is the gyromagnetic ratio of the ith nucleus. The third term describes the magnetic hyperfine interactions between the unpaired electron and the nuclei, where $\mathfrak{T}_i$ is the hyperfine interaction tensor

$$\mathfrak{T}_i=g\beta[(8\pi/3)\langle\delta(\mathbf{r}_i)\rangle_{Av}\mathfrak{I}+\langle 3\mathbf{r}_i\mathbf{r}_i/r_i^5-\mathfrak{I}/r_i^3\rangle_{Av}]. \quad (2)$$

The quantity $\mathbf{r}_i$ is the position vector of the unpaired electron measured from the ith nucleus as the origin, and the averages are taken over the charge distribution of the unpaired electron. The quantity $\mathfrak{I}$ is the unit tensor. The first term is, of course, the isotropic or contact term in the hyperfine interaction, and the second term is the anisotropic or dipole-dipole interaction.

---

[2] J. F. Gibson, D. J. E. Ingram, M. C. R. Symons, and M. G. Townsend, Trans. Faraday Soc. **53**, 914 (1957).

[3] E. W. R. Steacie, *Atomic and Free Radical Reactions* (Reinhold Publishing Corporation, New York, 1954), 2nd ed., p. 397 ff.

[4] G. R. McMillan and W. A. Noyes, J. Am. Chem. Soc. **80**, 2108 (1958).

[5] R. M. Harris and J. E. Willard, J. Am. Chem. Soc. **76**, 4678 (1954).

[6] D. L. Bunbury, R. R. Williams, and E. W. Hamill, J. Am. Chem. Soc. **78**, 6228 (1956).

[7] I. Norman and G. Porter, Proc. Roy. Soc. (London) **A230**, 399 (1955).

[8] T. O. Jones, R. H. Luebbe, J. R. Wilson, and J. E. Willard, J. Phys. Chem. **62**, 9 (1958).

[9] (a) S. N. Foner, E. L. Cochran, V. A. Bowers, and C. K. Jen, J. Chem. Phys. **32**, 963 (1960); (b) Phys. Rev. **112**, 1169 (1958).

[10] E. L. Cochran, W. H. Hamill, and R. R. Williams, J. Am. Chem. Soc. **76**, 2145 (1954).

[11] G. T. Trammell, H. Zeldes, and R. Livingston, Phys. Rev. **110**, 630 (1958).

[12] The g-factor shifts and resulting g-factor anisotropies are quite small in the simple alkyl radicals. For example the work cited in footnote 9 gives g-factor shifts of the order of 0.0003 for the methyl radical in a variety of matrices. Sands [R. H. Sands, Phys. Rev. **99**, 1222 (1955)] has shown that g-factor anisotropy and hyperfine anisotropy have quite similar effects on the ESR line shape.

The form of the hyperfine interaction tensor $\mathfrak{T}_i$ will depend on the coordinate system used. In many calculations, such as averaging the hyperfine interaction Hamiltonian over various rotational motions of the radical, it will be convenient to transform from one coordinate system to another.[13] Whenever possible we will use that coordinate system, called the principal axis system, which diagonalizes $\mathfrak{T}_i$. Then the hyperfine interaction Hamiltonian has the familiar form

$$\mathcal{H}_i^{hfs}=h(A_iS_zI_{iz}+B_iS_xI_{ix}+C_iS_yI_{iy}). \qquad (3)$$

The principal axis system is illustrated for an α hydrogen nucleus in Fig. 1. The work of McConnell *et al.* on the radical $CH(COOH)_2$ in a single crystal of malonic acid has shown that for such a hydrogen nucleus: $A=-29$ Mc; $B=-61$ Mc; and $C=-91$ Mc.[14]

In the usual ESR experiment the external magnetic field is sufficiently large that the projection of the electron spin on this field, which quantity we denote as M_S, is a good quantum number. One can then compute the net magnetic field acting on the ith nucleus as the vector sum of the external magnetic field and the magnetic field due to the unpaired electron. The Hamiltonian for the interaction of the ith nucleus with this field is

$$\mathcal{H}_i(M_S)=-\gamma_i\hbar[\mathbf{H}-M_S\boldsymbol{\tau}_H\cdot\mathfrak{T}_i]\cdot\mathbf{I}_i, \qquad (4)$$

where the second term in the bracket is the field at the ith nucleus due to the electron, and the quantity $\boldsymbol{\tau}_H$ is a unit vector in the direction of the external field.

By using Eq. (4) for the effective field acting on the ith nucleus, we can readily calculate the various energy levels and transition energies. However, the resulting expressions are rather complicated for the most general case. An approximation which is satisfactory in a majority of the cases encountered is to neglect the Zeeman energy of the nuclei.[15] This is a very good approximation for the treatment of hyperfine interactions with α hydrogen nuclei in alkyl radicals when the ESR experiment is carried out at X-band frequencies.[1,14] It becomes less satisfactory at higher frequencies (and correspondingly higher fields) where the nuclear Zeeman energy is greater, and for certain conjugated radicals such as the allyl radical where the unpaired electron charge density is spread over several atoms with a consequent reduction in the hyperfine interactions with the individual nuclei. Such simplifications will be useful, however, even in cases where they give only rough approximations, because the experimental line shapes are usually subject to some uncertainty, and it is impractical to attempt a highly detailed comparison of the experimental and theoretical line shapes. If the nuclear Zeeman energy is neglected in Eq. (4), then the following equation for the hyperfine splitting due to interaction with a given nucleus is readily obtained,

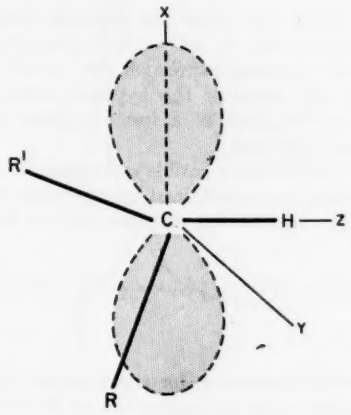

FIG. 1. The principal axis coordinate system for the magnetic hyperfine interaction tensor of an α proton.

$$\nu-\nu_e=M_I(A^2\cos^2\theta+B^2\sin^2\theta\cos^2\phi+C^2\sin^2\theta\sin^2\phi)^{\frac{1}{2}}. \qquad (5)$$

Here, ν_e is the transition frequency in the absence of hyperfine splitting, and M_I is the projection of the nuclear spin on the magnetic field due to the electron. The angles θ and ϕ are the polar and azimuthal angles specifying the orientation of the external magnetic field in the principal axis coordinate system.

The following modification of Eq. (5) will be convenient. Let us choose the X, Y, and Z axes of the principal axis system so that the conditions

$$|B^2-C^2|\leq|A^2-B^2|\leq|A^2-C^2| \qquad (6)$$

are fulfilled. Then Eq. (5) can be rewritten as

$$\nu-\nu_e=M_Ia[1+(b^2/a^2)(\tfrac{3}{2}\cos^2\theta-\tfrac{1}{2}-\tfrac{1}{2}\eta\sin^2\theta\cos2\phi]^{\frac{1}{2}}, \qquad (7)$$

where

$$a^2=(\tfrac{1}{3})(A^2+B^2+C^2); \qquad b^2=(\tfrac{1}{3})(2A^2-B^2-C^2) \qquad (8)$$

and

$$\eta=3(C^2-B^2)/(2A^2-B^2-C^2). \qquad (9)$$

The quantity η is a measure of the axial asymmetry of the hyperfine interaction. It ranges in value from -1

[13] For a discussion of coordinate transformations see Lloyd P. Smith, *Mathematical Methods for Scientists and Engineers* (Prentice-Hall, Inc., Englewood Cliffs, New Jersey, 1953), pp. 273–276.

[14] H. M. McConnell, C. Heller, T. Cole, and R. W. Fessenden, J. Am. Chem. Soc. **82**, 766 (1960).

[15] If this approximation is invalid the spectrum may be complicated by the presence of "forbidden" transitions in which a nuclear spin transition accompanies the electron spin transition. Such transitions become allowed when the hyperfine interaction is highly anisotropic, and is comparable in magnitude to the nuclear Zeeman energy. This situation is discussed in detail in the works cited in footnotes 1, 11, and 14. The problem of calculating line shapes under these conditions will be extremely difficult.

to $+1$, being zero when the hyperfine interaction is axially symmetric. It will be seen presently that by using the foregoing expression for $(\nu-\nu_e)$, one can compute the shape of the hyperfine broadened line using a modification of a formula given by Bloembergen and Rowland.[16]

A still simpler more flexible expression for the hyperfine splitting can be obtained by expanding the radical in Eq. (7) and retaining only the first two terms. This gives

$$\nu-\nu_e=M_I[a+(b^2/2a)(\tfrac{3}{2}\cos^2\theta-\tfrac{1}{2}-\tfrac{1}{2}\eta\sin^2\theta\cos 2\phi)]. \tag{10}$$

This familiar expression for the hyperfine splitting is rigorous only when the isotropic term in the hyperfine interaction is considerably larger than the anisotropic term. This expression has the advantages of being simpler, and of giving an expression for the line shape which is more readily understood. This is particularly true when the total hyperfine interaction is the result of two or more inequivalent nuclei. For these reasons it may be desirable to use Eq. (10) in qualitative calculations even though it may not be rigorously applicable.

B. Calculation of the Line Shape Resulting from Hyperfine Broadening

Any of the procedures described in the previous section gives the frequency of a given hyperfine component of the ESR spectrum as a function of magnetic field orientation. In a polycrystalline sample one has a random distribution of magnetic field orientations, and the probability of finding the magnetic field within an element of solid angle $d\Omega$, which probability we denote as $P(\Omega)d\Omega$, is given by the expression

$$P(\Omega)d\Omega=(1/4\pi)d\Omega=(1/4\pi)\sin\theta d\theta d\phi. \tag{11}$$

Now the result given by an ESR experiment is the absorption intensity (or its derivative) as a function of frequency. Thus, we must calculate the probability that the frequency of the given hyperfine component will lie in a region of frequency $d\nu$ centered around ν. This probability is denoted as $I_h(\nu)d\nu$, where $I_h(\nu)$ is the absorption intensity in the presence of hyperfine broadening only. To do this we first calculate the quantity $I_h(\nu,\theta)$ which is the absorption intensity as a function of frequency when θ is held fixed.[16] Provided that one and only one value of ϕ exists which gives the desired frequency for the chosen value of θ,[17] then $I_h(\nu,\theta)d\nu$ is simply equal to the probability of finding ϕ in a region $d\phi$, which is given by the expression

$$I_h(\nu,\theta)d\nu=(1/2\pi)d\phi=(1/2\pi)(\partial\phi/\partial\nu)d\nu. \tag{12}$$

To get the actual line intensity $I_h(\nu)$ we average the expression for $I_h(\nu,\theta)$ over the angle θ. This gives

$$I_h(\nu)=(1/4\pi)\int\sin\theta(\partial\phi/\partial\nu)d\theta. \tag{13}$$

Bloembergen and Rowland[16] have given an expression for $I_h(\nu)$ for the case where ν is given by Eq. (10). Their results as restated by Cohen and Reif[18] are as follows. From Eq. (10) we obtain the relation

$$x=(\nu-\nu_e-M_Ia)/(M_Ib^2/2a)=\tfrac{3}{2}\cos^2\theta-\tfrac{1}{2}-\tfrac{1}{2}\eta\sin^2\theta\cos 2\phi. \tag{14}$$

We now restrict η to be positive, i.e.,

$$0\leq\eta\leq 1.$$

This restriction involves no loss of generality since if η is negative, it can be made positive by changing the origin of the angle ϕ, i.e., $\phi=\phi'+\frac{1}{2}\pi$. Then the probability that x lies in a region dx centered about a given value of x is $F(x)dx$, where the function $F(x)$ is defined in the following equations:

$$F(x)=K(k)/\pi[\eta(1-x)]^{\frac{1}{2}};\quad -\tfrac{1}{2}(1+\eta)\leq x\leq-\tfrac{1}{2}(1-\eta), \tag{15a}$$

$$F(x)=2K(k^{-1})/\pi[(2x+1+\eta)(3-\eta)]^{\frac{1}{2}};\quad -\tfrac{1}{2}(1-\eta)\leq x\leq 1. \tag{15b}$$

Here, $K(k)$ denotes the complete elliptic integral[19] whose argument k is given by the equation

$$k=\tfrac{1}{2}[(2x+1+\eta)(3-\eta)/\eta(1-x)]^{\frac{1}{2}}. \tag{16}$$

From the relation between x and ν given in Eq. (14), we readily obtain the following expression for $I_h(\nu)$,

$$I_h(\nu)=F([\nu-\nu_e-M_Ia]/M_Ib^2/2a)(2a/M_Ib^2). \tag{17}$$

The properties of the function $F(x)$ are best noted from Fig. 2, which gives plots of this function for various values of η. The peak, which occurs at $x=-(\frac{1}{2})(1-\eta)$, is a logarithmic singularity which becomes less pronounced as η increases. The hyperfine broadened line shape is most unsymmetrical for $\eta=0$, and becomes symmetrical at $\eta=1$. Of course, there will be other sources of line broadening which will round off the sharp peak and discontinuous edges of the hyperfine broadened lines. Typical line shapes resulting from the combination of hyperfine broadening with other types of line broadening are illustrated by the dotted curves in Fig. 2. The problem of actually calculating the observed line shape is discussed in the next section.

When the hyperfine splitting is given by Eq. (7) an expression for the line shape is readily obtained in

[16] N. Bloembergen and T. J. Rowland, Acta Met. **1**, 731 (1953).
[17] This condition is achieved by placing suitable limits on the values of θ in the subsequent integration over this angle.
[18] M. H. Cohen and F. Reif, *Solid-State Physics*, edited by D. Turnbull and F. Seitz (Academic Press, Inc., New York, 1957), Vol. 5, p. 342.
[19] E. Jahnke and F. Emde, *Tables of Functions* (Dover Publications, New York, 1945), 4th ed., p. 73 ff.

terms of the function $F(x)$. We note that the function $[(\nu-\nu_e)^2-M_I^2a^2]/M_I^2b^2$ has the same form as the function x defined in Eq. (14), and thus the same distribution function $F(x)$. This leads to the following expression for the line intensity

$$I_h(\nu)=F[\{(\nu-\nu_e)^2-M_I^2a^2\}/M_I^2b^2][2(\nu-\nu_e)/M_I^2b^2]. \quad (18)$$

So long as the isotropic hyperfine interaction is larger than the anisotropic term, the line shapes given by the foregoing expression have much the same form as those given in Fig. 2. When the hyperfine anisotropy is comparable to or larger than the isotropic interaction, the line shapes become more complicated. Blinder has calculated the line shapes resulting from large hyperfine anisotropies for the axially symmetric ($\eta=0$) case.[20]

C. Observed Line Shape

The line shape which is actually observed is the result of a superposition of hyperfine broadening and all other types of broadening. These other sources of line broadening lead to symmetric absorption lines which are Gaussian or Lorentzian depending on the broadening mechanism. The chief source of Lorentzian broadening is dipole-dipole interactions between the paramagnetic species. In the work described here, the radical concentration is sufficiently low that this source of broadening may be neglected, and we may expect the free radical ESR line shapes to be Gaussian. Most observed radical line shapes are more nearly Gaussian than Lorentzian. Thus, we represent the line intensity resulting from all sources of broadening except hyperfine broadening, which quantity is denoted as $I_0(\nu-\nu_0)$, by the Gaussian

$$I_0(\nu-\nu_0)=[1/\sigma(2\pi)^{\frac{1}{2}}]\exp[-(\nu-\nu_0)^2/2\sigma^2]. \quad (19)$$

The parameter σ is the rms linewidth. It is also one-half the distance between maximum slope points of the absorption line. In many cases it will be possible to estimate the parameter σ from the width of those hyperfine components for which the hyperfine broadening is canceled out. In other cases σ may be estimated from the linewidths of similar radicals.

The combination of hyperfine broadening with the other sources of line broadening will give a line of intensity $I(\nu)$, where

$$I(\nu)=[1/\sigma(2\pi)^{\frac{1}{2}}]\int I_h(\nu')\exp[-(\nu-\nu')^2/2\sigma^2]d\nu'. \quad (20)$$

The derivative of the absorption line, which is the quantity usually observed in practice, is given by the expression

$$dI(\nu)/d\nu=[1/\sigma^3(2\pi)^{\frac{1}{2}}]\int(\nu-\nu')I_h(\nu')\times\exp[-(\nu-\nu')^2/2\sigma^2]d\nu'. \quad (21)$$

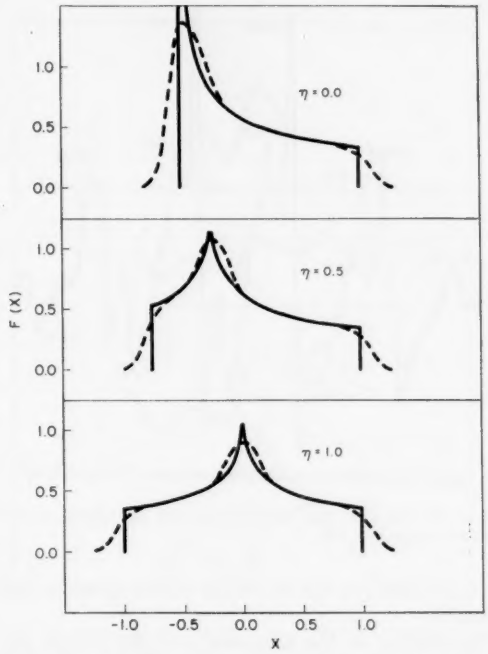

FIG. 2. ESR absorption lines resulting from anisotropic hyperfine broadening. The different curves correspond to varying degrees of axial asymmetry in the hyperfine interaction ranging from the axially symmetric case ($\eta=0$) to the maximum possible axial asymmetry ($\eta=1$). The solid curves are the line shapes due to hyperfine broadening only. The dotted curves are typical lines resulting from the combination of hyperfine broadening with other sources of line broadening.

In general the actual line shapes will have to be calculated by numerical integration of the right-hand side of Eq. (20) or Eq. (21). It is relatively easy, however, to get a qualitative picture of the effect of hyperfine broadening. We are interested mainly in cases where the hyperfine broadening is an order of magnitude greater than the other sources of line broadening. In such cases the line shape will be determined primarily by the hyperfine broadening with the other sources of line broadening serving to round off the sharp peak and edges of the pure hyperfine broadened line. The resulting line shapes have been illustrated in Fig. 2. The hyperfine broadened lines are quite unsymmetrical, except for the case of maximum axial asymmetry ($\eta=1$) in the hyperfine interaction. There is a marked tendency for such lines to resemble two or three poorly resolved lines. Moreover, these effects become more pronounced in the derivative of the absorption line.

[20] S. M. Blinder, J. Chem. Phys. **33**, 748 (1960).

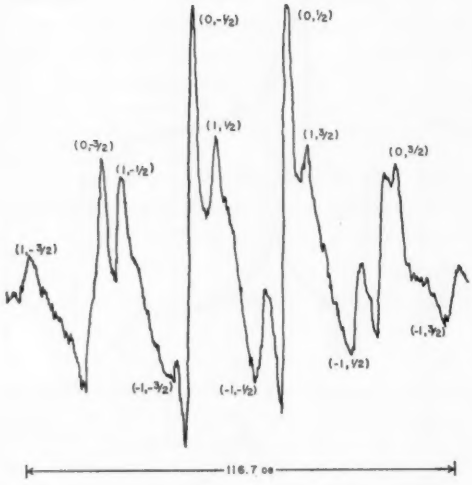

FIG. 3. ESR spectrum produced by the photolysis of ethyl iodide in argon at 4.2°K.

(See, for example, the derivative curves shown in Figs. 4 and 5.)

In addition to the unsymmetrical line shapes produced by the hyperfine anisotropy, there may be other complications. For one thing, the different hyperfine components in the ESR spectrum of a given radical will usually experience varying degrees of hyperfine broadening, because of the dependence of the hyperfine interaction on the nuclear magnetic quantum numbers M_I. Thus, some components of the spectrum will be intense, narrow, and symmetrical, while others will be weak, broad, and unsymmetrical. In many cases the hyperfine broadened lines will overlap. In such cases the individual hyperfine components will have to be synthesized from the observed spectrum, a process which will not always give an unambiguous result. In view of the many factors involved, it is to be expected that hyperfine broadening will produce very complicated ESR spectra. This is definitely the case in the alkyl radical spectra, which will be discussed in the next section.

IV. RESULTS AND DISCUSSION

A. Methyl Radical

A number of workers have observed the spectrum of the methyl radical, which is a quartet of sharp symmetrical lines.[9b,21,22] Judging from the sharp line spectrum obtained for this case, the methyl radical has almost complete rotational freedom within the matrix. This behavior is typical of the small radicals such as $CH_3\cdot$ and $NH_2\cdot$.[23] The larger more cumbersome radicals, which are the object of the present study, have insufficient rotational freedom to completely average out the hyperfine anisotropy. Thus, some or all of the hyperfine components in the ESR spectra of these radicals will be broadened by the hyperfine anisotropy.

B. Ethyl Radical

The spectrum obtained from the photolysis of ethyl iodide in solid argon is given in Fig. 3. This spectrum appears to be identical with that found by Smaller and Matheson[21] in γ-irradiated ethane, ethylene, or ethyl chloride. For convenience in discussion, the hyperfine components are denoted by the symbol (M_α, M_β) where M_α is the net magnetic quantum number of the α hydrogen nuclei, and M_β is the same quantity for the β hydrogen nuclei. In using this notation it should be noted that the high-frequency hyperfine components correspond to negative values of M_α because the α proton hyperfine interaction constants are negative.

It is readily noted from Fig. 3 that the lines for which $M_\alpha=0$ are sharper and more symmetrical than the other lines. A similar situation will be found in the propyl radical spectrum (cf. Fig. 7). This shows that when the two α protons are antiparallel the hyperfine anisotropy is canceled out. This cancellation can take place only if the two α protons are magnetically equivalent. In turn, this condition is fulfilled only if the $—CH_2\cdot$ group is reorienting between its various equilibrium positions sufficiently rapidly that the hyperfine interaction experienced by each α proton is an average over all the equilibrium orientations of the $—CH_2\cdot$ group. The $—CH_2\cdot$ group may reorient either by an external or an internal rotation about the carbon-carbon bond. Since external rotations are rather difficult for steric reasons in larger radicals such as the propyl radical, the reorientation process will most likely take place via internal rotation in these radicals. In the ethyl radical, internal and external rotations about the carbon-carbon bond are equally feasible. However, only the internal rotation of the $—CH_2\cdot$ group will cause the three β protons in the ethyl radical to have the same isotropic hyperfine interaction, in agreement with experiment.

From the previous qualitative discussion it is very likely that there is a rapid reorientation of the $—CH_2\cdot$ group in the alkyl radicals. It is interesting nonetheless to investigate the case where the $—CH_2\cdot$ group is rigidly fixed, and to calculate the resulting ESR line shapes. In this calculation, and for a number of other calculations in this paper, it is convenient to use a coordinate system in which the Z' axis lies along the carbon-carbon bond, the X' axis is perpendicular to the plane of the $—CH_2\cdot$ group, and the Y' axis lies in the plane of the $—CH_2\cdot$ group. The hyperfine interaction

[21] B. Smaller and M. Matheson, J. Chem. Phys. **28**, 1169 (1958).

[22] W. Gordy and C. G. McCormick, J. Am. Chem. Soc. **78**, 3243 (1956).

[23] S. N. Foner, E. L. Cochran, V. A. Bowers, and C. K. Jen, Phys. Rev. Letters **1**, 91 (1958).

tensors of the α protons are readily transferred from their respective principal axis systems to this coordinate system.[13] In this, and in all subsequent calculations, we will use the values of McConnell *et al.*[14] for the components of the α proton hyperfine interaction tensor in the principal axis system.

The results of this calculation are somewhat surprising since they show that the hyperfine broadening is greater when the two α protons are antiparallel. The total spread in hyperfine broadening is 18.5 oe when the α protons are antiparallel, and only 9.4 oe when they are parallel. This is in marked contradiction to the experimental results for the ethyl and propyl radicals where the lines corresponding to $M_\alpha=\pm 1$ are noticeably broader than the $M_\alpha=0$ lines. For the case where the two α protons are antiparallel, the hyperfine splitting can be represented approximately by the formula

$$\nu-\nu_e=17.9\sin\theta\cos\theta\sin\phi. \qquad (22)$$

Here, and in subsequent calculations, frequencies will be given in units of magnetic field, namely, oersteds.

The derivative line shape resulting from the combination of the above hyperfine broadening and all other sources of line broadening was calculated using Eq. (21).[24] The line shape in the absence of hyperfine broadening was taken to be a Gaussian having a root mean-square width σ, and the calculation was carried out for a range of typical values of σ. Also presented in Fig. 4 for comparison is the derivative of a Gaussian with $\sigma=1.67$ oe, which is the approximate shape of the $M_\alpha=0$ lines in the ethyl and propyl radical spectra. Each of the curves in Fig. 4 has been scaled so that the derivative of the corresponding unbroadened Gaussian line will have a maximum height of one unit. This scaling clearly shows the effect of hyperfine broadening on the line intensity. For the values of σ chosen the hyperfine broadening reduces the line intensity by factors ranging from 14 to 4 as σ varies from 1.00 to 2.76 oe.

Another interesting effect of the hyperfine broadening in this case is to give the line the appearance of being a triplet. This effect is most pronounced when the hyperfine broadening is large compared to all other sources of line broadening. The possibility of observing such spurious multiplets is marginal, however, because they are produced under conditions which also severely reduce the line intensity. It is more likely that lines which are hyperfine broadened, but still observable, will have a bumpy appearance, e.g., the line in Fig. 4 corresponding to $\sigma=2.76$, suggesting a poorly resolved multiplet structure. These complications should be considered when dealing with suspected hyperfine anisotropies in ESR spectra.

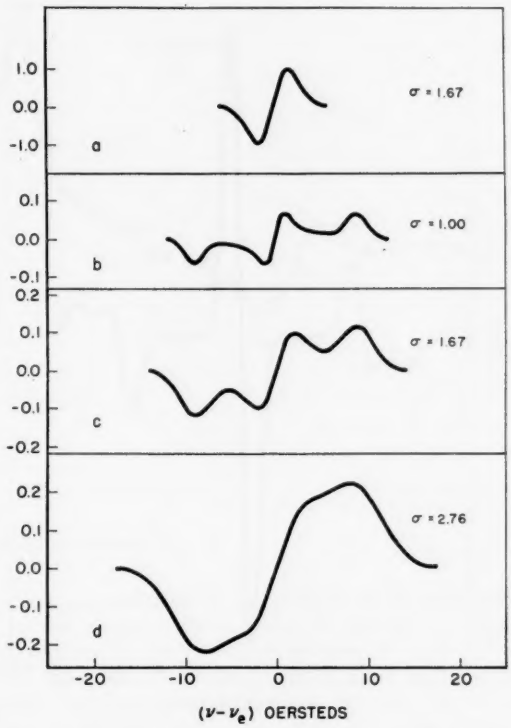

FIG. 4. Theoretical line shapes (derivative presentation) for the ESR hyperfine line corresponding to the antiparallel state of the two α protons in a rigid $-CH_2\cdot$ group. (a): An unbroadened Gaussian line with a root-mean-square linewidth σ of 1.67 oe. (b)–(d): Lines resulting from the superposition of the anisotropic hyperfine broadening on Gaussian lines of varying width σ. Each of these lines has been scaled so that the corresponding unbroadened Gaussian will have a maximum height of one unit.

It is clear that the hyperfine broadened lines given in Fig. 4 are incompatible with the observed spectra of the ethyl and propyl radicals. The lines corresponding to $\sigma=1.00$ and 2.76 do not have the correct separation between the inner maxima and minima. The line corresponding to $\sigma=1.67$ does have the correct separation between the inner maxima and minima, but has equally intense outer maxima and minima which cannot be reconciled with the observed spectra. Thus, the conclusion that the $-CH_2\cdot$ group is reorienting in these radicals is inescapable.

Accordingly, we have calculated the effect of hyperfine broadening on the $M_\alpha=\pm 1$ lines for the case where the $-CH_2\cdot$ group is reorienting between equilibrium positions. There will be at least three such equilibrium positions in the ethyl radical, and this gives just as complete an averaging of the hyperfine interaction as would unrestricted rotation about the carbon-carbon bond. The averaging is carried out by first transforming

[24] In this calculation a transformation of coordinates (the new coordinate system is obtained from the original one by a rotation of 45° about the X' axis, followed by an interchange of the X' and Y' axes) changes Eq. (22) into an expression having the form of Eq. (10) with $\eta=1$.

FIG. 5. Theoretical ESR spectrum of a triplet due to hyperfine interactions with the α protons in the ethyl radical.

from the principal axis system to the coordinate system in which the Z axis lies along the carbon-carbon bond, and then rotating about the new Z axis to obtain the hyperfine interaction tensor for the various orientations of the $-CH_2\cdot$ group. The calculation shows that the hyperfine splitting resulting from the interaction with the α protons is very well approximated by the formula

$$\nu(M_\alpha, M_\beta)-\nu(0, M_\beta) = -21.9M_\alpha[1+0.518(\tfrac{3}{2}\cos^2\theta-\tfrac{1}{2})]^{\frac{1}{2}}. \quad (23)$$

Figure 5 gives the calculated line shapes for the triplet $(1, M_\beta)$, $(0, M_\beta)$ and $(-1, M_\beta)$. The center unbroadened line is a Gaussian with $\sigma=1.67$ oe, which corresponds to the observed width of the $M_\alpha=0$ lines. The hyperfine anisotropy is axially symmetric in this radical, and therefore produces very unsymmetrical lines. One lobe of the derivative curve is virtually unchanged in shape although reduced in intensity by a factor of roughly 2, while the other lobe is broadened into a double humped curve with a somewhat greater reduction in intensity. It is to be noted that the negative lobe of the $(-1, M_\beta)$ line is the more intense, while the positive lobe is more intense in the $(+1, M_\beta)$ line, so that the entire triplet is symmetric with respect to inversion through the origin.

These results agree qualitatively with the observed ethyl radical spectrum. Each of the lines with $M_\alpha=\pm1$ appears as a single lobe, with the weaker double humped lobe either being obscured under a strong line or lost in the noise. Consider, for example, the triplet $(-1, \frac{1}{2})$, $(0, \frac{1}{2})$, and $(1, \frac{1}{2})$. Here, the line $(1, \frac{1}{2})$ is seen only as a positive lobe, the weaker negative lobe being lost under the line $(0, -\frac{1}{2})$, while for the line $(-1, \frac{1}{2})$ the negative lobe is the more intense, and the positive lobe falls under the line $(0, \frac{3}{2})$.

The rather compressed trace of the entire spectrum shown in Fig. 3 is not suitable for detailed comparison of theoretical and experimental line shapes, since in taking such compressed traces with our instrumentation, the magnetic field is swept rapidly, and this often leads to rapid passage effects which distort the line shapes and intensities. In Fig. 6 the high-frequency lines of the ethyl radical spectrum are shown on an expanded scale. The outer region of the spectrum was chosen to minimize the difficulty of overlapping lines. This advantage is offset somewhat by the reduced intensity of the outer lines.

We note from Fig. 6 that the upper half of the $(0, \frac{3}{2})$ line is badly distorted, having the appearance of a rather broad double peaked curve. We have tried to interpret this line shape as being inherent in the ethyl radical spectrum without success. One possibility considered was that the upper half of the $(-1, \frac{1}{2})$ line which lies partially under the $(0, \frac{3}{2})$ line might distort the latter line. Calculation shows, however, that the intensity of the upper half of the $(-1, \frac{1}{2})$ line will be only $\frac{1}{3}$ of the peak height of the undistorted $(0, \frac{3}{2})$ line, and this is insufficient to produce the observed distortion. Another possibility was an anisotropy in the β proton hyperfine interaction. In order to produce the observed double peaked curve, the line broadening resulting from the hyperfine anisotropy would have to be two or three times greater than the natural linewidth. Since the alkyl radicals have natural linewidths of the order of 3 oe between maximum slope points, the β proton hyperfine anisotropy would have to produce linewidths of 6 to 9 oe. This is comparable to the hyperfine broadening associated with the α protons, and is considerably larger than the value predicted for the β protons.[1] Thus, we have no satisfactory explanation of the distortion of the $(0, \frac{3}{2})$ line. It is possible that the distortion is the result of an additional unknown resonance which overlaps the $(0, \frac{3}{2})$ line so as to produce the observed distortion.

The other features of the spectrum are in good agreement with theory. The $(-1, \frac{3}{2})$ line is quite weak, and the lower half is more intense than the upper half. Indeed the upper half of this line is more or less lost in the noise, although there is a faint hint of the double peak predicted by theory. The lower half of the $(0, \frac{3}{2})$ line, which is presumably undistorted, is 3.7 times as intense as the lower half of the $(1, \frac{3}{2})$ line, in good agreement with the theoretical intensity ratio of 4 to 1. The

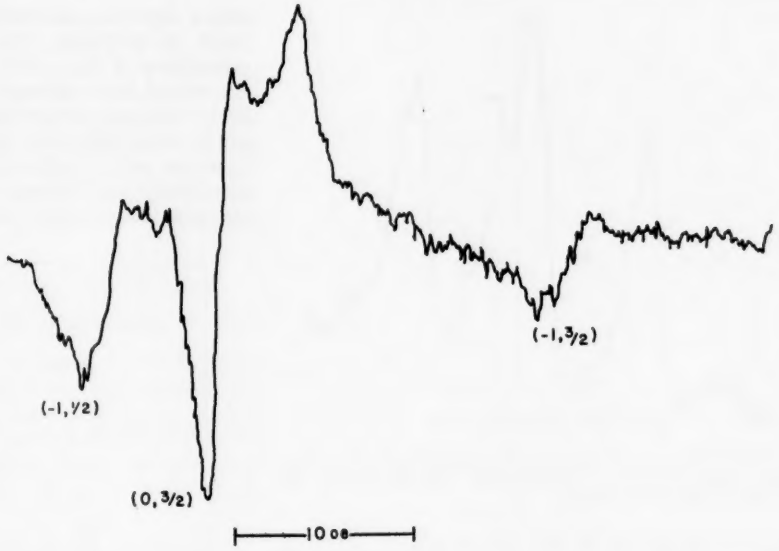

FIG. 6. High-frequency lines of the ESR spectrum produced by the photolysis of ethyl iodide in argon at 4.2°K.

separation between the $(0, \frac{3}{2})$ line and the $(1, \frac{3}{2})$ line is 19.9 oe, in agreement with the theoretical value of 20.4 oe. The β proton splitting is 26.5 oe.[24a]

C. *n*-Propyl Radical

The spectrum obtained from the photolysis of *n*-propyl iodide is shown in Fig. 7. This spectrum contains three strong lines and a number of weaker lines. The assignment of the three strong lines was made by studying the spectra obtained from photolysis of the α and β deuterated *n*-propyl iodides. The spectrum obtained from α deuterated *n*-propyl iodide, which is shown in Fig. 8, contains the same three strong lines, although they are now considerably broader. (The reason for this broadening will be discussed presently.) The β deuterated *n*-propyl iodide, however, gives a five line spectrum, shown in Fig. 9, with a line spacing reduced by a factor of 6.5 from the spacing of the triplet obtained previously. These results show that the three strong lines are *n*-propyl radical lines resulting from hyperfine interactions with the β protons. The splitting constant is 35.0 oe.

In the light of the present theory we may go further and say that the strong lines occur when the α protons are antiparallel, $M_\alpha = 0$, so that the hyperfine anisotropy is canceled. The *n*-propyl radical lines for which $M_\alpha = \pm 1$ will be greatly reduced in intensity by the hyperfine anisotropy, and must be sought among the weak lines in the spectrum. The central region of the spectrum is complicated by the presence of lines belonging to the methyl radical, which is produced in small quantities by the photolysis of *n*-propyl iodide. Thus we shall concentrate on two weak lines in the outer high- and low-field regions of the spectrum. These two

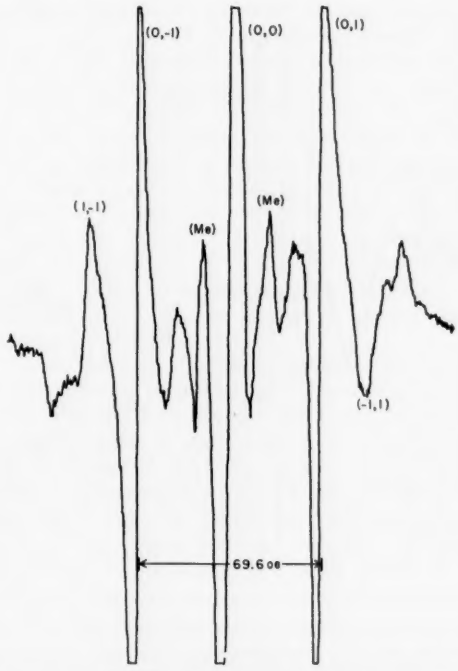

FIG. 7. ESR spectrum produced by the photolysis of *n*-propyl iodide in argon at 4.2°K. The lines labeled Me are due to the methyl radical.

[24a] Fessenden and Schuler [R. W. Fessenden and R. H. Schuler, J. Chem. Phys. **33**, 935 (1960)] have recently reported the ESR spectrum of the ethyl radical in liquid ethane. All components of the spectrum are very sharp indicating that the magnetic anistropies are completely averaged out in the liquid. Their values for the isotropic splitting constants are in agreement with the results of this work.

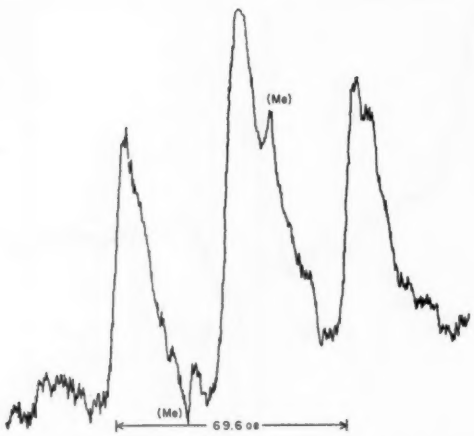

FIG. 8. ESR spectrum produced by the photolysis of α deuterated *n*-propyl iodide in argon at 4.2°K. The lines labeled Me are due to the methyl radical.

lines are assumed to be the $(-1, 1)$ and $(1, -1)$ lines of the *n*-propyl radical as indicated in Fig. 7. Comparison of the intensity and position of these lines with theoretical estimates will justify this assignment.

The treatment of the *n*-propyl radical, unlike the ethyl radical, is complicated by the fact that the effective hyperfine anisotropy, which quantity is the result of averaging over the various equilibrium orientations of the $—CH_2·$ group, is not completely determined from symmetry considerations. It is most likely that one configuration of the *n*-propyl radical will be more stable than any other. This optimum configuration will actually correspond to a pair of indistinguishable orientations of the $—CH_2·$ group. It is also possible, however, that the interactions of the $—CH_2·$ group with the β hydrogens and the methyl group are such as to give two or more distinct equilibrium configurations. These configurations would be analogous to the gauche forms of such molecules as the 1,2 dihalogenoethanes.[25] Thus, we have calculated the line shape resulting from a single equilibrium position for the $—CH_2·$ group (case I), and from a pair of equilibrium positions which differ in orientation by 120° (case II). If there are three or more distinct equilibrium configurations, the resulting line shape will be the same as that found for the ethyl radical.

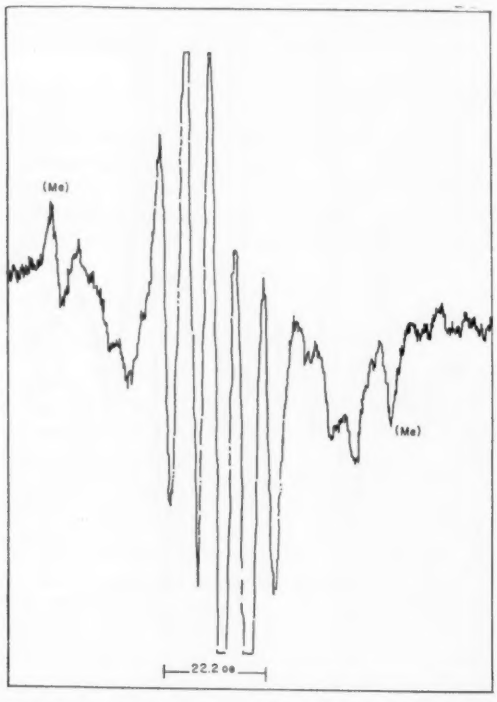

FIG. 9. ESR spectrum produced by the photolysis of β deuterated *n*-propyl iodide in argon at 4.2°K. The lines labeled Me are due to the methyl radical.

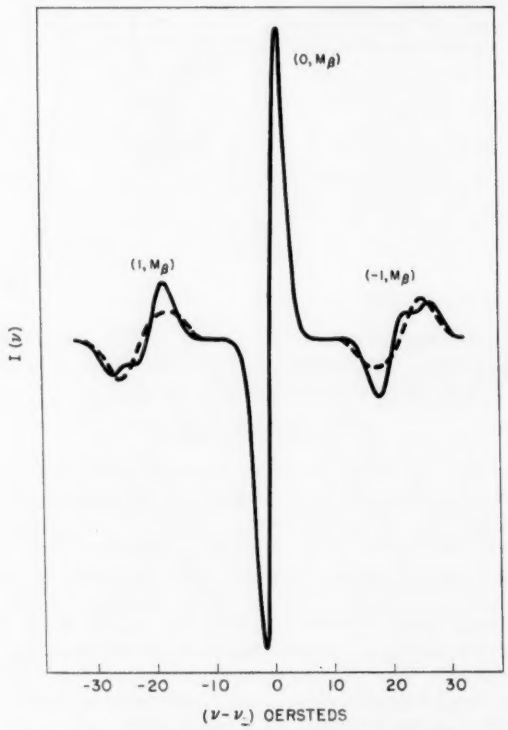

FIG. 10. Theoretical ESR spectra of a triplet due to hyperfine interactions with the α protons in the *n*-propyl radical. The dotted curve is for the case of a single equilibrium position for the $—CH_2·$ group in this radical. The solid curve is for the case of two equilibrium positions for the $—CH_2·$ group differing in orientation by 120°.

[25] S. Mizushima, *Structure of Molecules and Internal Rotation* (Academic Press, Inc., New York, 1954), p. 7 ff.

In calculating the hyperfine anisotropy the average over the various equilibrium orientations of the $-CH_2\cdot$ group is carried out by transforming to a coordinate system in which the Z axis is along the carbon-carbon bond. The various equilibrium orientations of the $-CH_2\cdot$ group are obtained by appropriate rotations about the Z axis of this coordinate system. For case I the azimuthal angles specifying the orientations of the $-CH_2\cdot$ group are taken to be $\pm 90°$. One then obtains the formula

$$\nu(M_\alpha, M_\beta)-\nu(0, M_\beta)=-22.0M_\alpha[1+0.500(\tfrac{3}{2}\cos^2\theta -\tfrac{1}{2}-(0.916/2)\sin^2\theta\cos 2\phi)]^{\frac{1}{2}}, \quad (23')$$

which is a very good approximation for the hyperfine splitting due to the interaction with the α protons. For case II the azimuthal angles specifying the orientations of the CH_2 group are taken to be $\pm 60°$ and $\pm 240°$. For this case the hyperfine splitting due to the interaction with the α protons is very well approximated by the formula

$$\nu(M_\alpha, M_\beta)-\nu(0, M_\beta)=-21.9M_\alpha[1+0.514(\tfrac{3}{2}\cos^2\theta -\tfrac{1}{2}-(0.453/2)\sin^2\theta\cos 2\phi)]^{\frac{1}{2}}. \quad (24)$$

The resulting line shapes have been calculated for each of these cases, and the results are given in Fig. 10. The line shape in the absence of hyperfine broadening is taken to be a Gaussian with $\sigma=1.67$ oe, which corresponds to the observed shape of the $M_\alpha=0$ lines.

In Fig. 11 we have presented an expanded trace of the high frequency lines of the spectrum obtained from the photolysis of n-propyl iodide. A similar spectrum has been found for the low-field region. The weak resonance at the high-field end of Fig. 11 has the appearance of two overlapping lines. It is tempting to regard this resonance as a single n-propyl radical line with the positive double-peaked lobe being due to hyperfine anisotropy. Comparison with the theoretical curves shows, however, that this explanation is untenable. One difficulty is that none of the possible theoretical curves for the $(-1, 1)$ line of the n-propyl radical has nearly so large a depression between the two positive peaks as does the experimental line. Even more damaging is the fact that the theoretical separation between the negative peak and the outer positive peak is at best 9 oe, while the observed separation is 14 oe.

We are thus forced to the conclusion that the high-field resonance is two partially overlapping lines. Since the outermost line does not correspond to any of the peaks in any of the possible theoretical line shapes it must be regarded as an unknown line. The inner line of this pair has been assigned as the $(-1, 1)$ line of the n-propyl radical from the following comparison of the experimental and theoretical line shapes. The observed separation between the $(0, 1)$ and $(-1, 1)$ lines is 19.5 oe, while the theoretical separations are 22.0, 20.9, and 20.4 oe depending on whether there are one, two, or three equilibrium positions for the $-CH_2\cdot$ group in the n-propyl radical. Comparison of the negative lobe of the $(0, 1)$ line with the negative lobe of the $(-1, 1)$ line gives an experimental intensity ratio of 5.7:1. The theoretical intensity ratios are 10.4:1, 5.2:1, and 4.0:1, depending on whether there are one, two, or three equilibrium positions for the $-CH_2\cdot$ group. We cannot, however, use these results to determine the configuration of the n-propyl radical, because the theoretical values obtained for the case of a single equilibrium configuration are rather sensitive to the values of the hyperfine interaction constants which enter the calculation. Changing the values of these constants within the assigned experimental errors[14] can improve considerably the agreement between theory and experiment for this case.

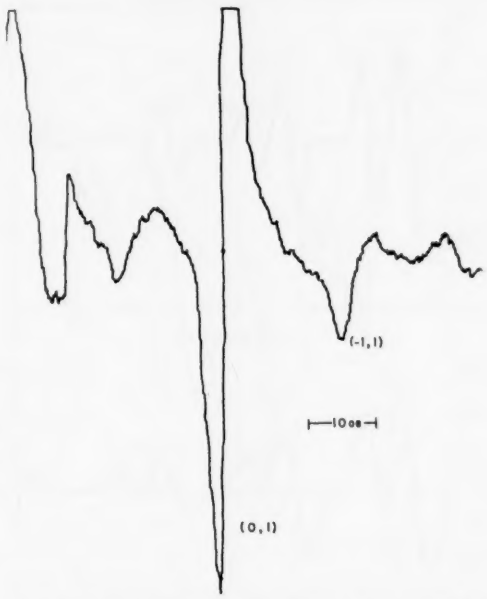

FIG. 11. High-frequency lines of the ESR spectrum produced by the photolysis of n-propyl iodide in argon at 4.2°K.

Further evidence for the existence of a hyperfine interaction with the α protons in the n-propyl radical comes from the experiments on the α and β deuterated n-propyl iodides. It was pointed out earlier that the individual lines of the triplet obtained from the photolysis of α deuterated n-propyl iodide, cf. Fig. 8, were relatively broad. This broadening can be explained in terms of hyperfine interactions with the α deuterons. These hyperfine splittings are quite small, the isotropic hyperfine interaction constant being roughly 3.4 oe. This isotropic hyperfine interaction would, in the absence of line broadening, give a five-line multiplet equally spaced at intervals of 3.4 oe, and with relative intensities of 1:2:3:2:1. The hyperfine anisotropy and other sources of line broadening are comparable in

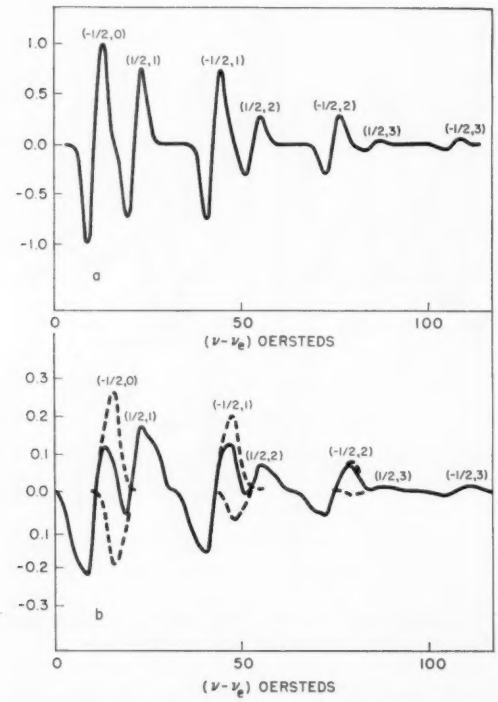

FIG. 12. The effect of anisotropic hyperfine broadening on the ESR spectrum of the isopropyl radical. (a): High-frequency half of the theoretical ESR spectrum of the isopropyl radical in the absence of hyperfine broadening. (b): High-frequency half of the theoretical ESR spectrum of the isopropyl radical with hyperfine broadening included. The dotted curves are the individual hyperfine components of the spectrum. The solid curve is the net spectrum.

magnitude to the multiplet splitting, and they will cause the deuterium multiplet to appear as a single, broad line whose shape will correspond approximately to the envelope of the multiplet pattern. The width of this envelope line at half-intensity will be roughly 10 oe. The observed lines have half-intensity widths of 10 to 15 oe.

In the spectrum of the β deuterated *n*-propyl radical shown in Fig. 9 there is a group of weak, poorly resolved lines in both the high- and the low-field regions of the spectrum. These lines are in addition to the lines labelled Me which are due to the methyl radical. The position and relative intensity of these lines are consistent with their assignment as the $M_\alpha=\pm 1$ lines of the $CH_3CD_2CH_2\cdot$ radical. No detailed analysis of the line shape was made for this case, however, since the spectrum resulting from the hyperfine broadening of the closely spaced deuterium multiplet will be extremely complicated. (The spectrum of the isopropyl radical, given in Fig. 12 is an example of the complicated spectrum which results when hyperfine broadening causes adjacent lines to overlap.)

D. Secondary Radicals

In secondary radicals there is only one α proton, and, consequently, all the hyperfine components of such radicals will be broadened equally. A secondary radical trapped in a solid matrix will not be able to undergo any rotations or reorientations which will reduce the hyperfine anisotropy of the α proton. Thus, the hyperfine interaction tensor is that of a fixed α proton, and the resultant hyperfine splitting is given by the approximate formula

$$\nu(M_\alpha M_\beta)-\nu(0, M_\beta)=-23.4M_\alpha[1+0.934(\tfrac{3}{2}\cos^2\theta -\tfrac{1}{2}-(0.72/2)\sin^2\theta\cos 2\phi)]^{\frac{1}{2}}. \quad (25)$$

The effect of this hyperfine broadening on a Gaussian line with $\sigma=1.67$ oe is shown in Fig. 12.

The effect of the α proton hyperfine anisotropy on the spectrum of the isopropyl radical is also given in Fig. 12. In this calculation the splitting resulting from the β protons was taken to be 32 oe, an estimate arrived at from the results obtained for the ethyl and propyl radicals. Part (a) of Fig. 12 is the isopropyl radical spectrum in the absence of hyperfine broadening. Part (b) of Fig. 12 is the theoretical spectrum for the isopropyl radical which shows that the hyperfine broadening causes each of the closely spaced pairs of lines to overlap, while reducing the individual line intensities by a factor of roughly four.

The spectrum observed from the photolysis of isopropyl iodide in argon at 4.2°K is shown in Fig. 13. The four strong lines labeled Me are the result of the methyl radical which is apparently a by-product of the photolysis. There is also a strong line in the center of the spectrum at the free electron value, which cannot belong to the isopropyl radical. Although there seem to be some other relatively weak lines in the spectrum, there is no evidence for the isopropyl radical. It would, however, be impossible to identify a weak,

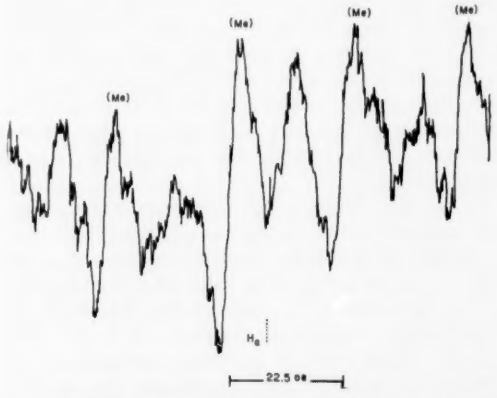

FIG. 13. ESR spectrum produced by the photolysis of isopropyl iodide in argon at 4.2°K. The lines labeled Me are due to the methyl radical.

broad, relatively complex spectrum such as is predicted for the isopropyl radical in the presence of lines resulting from other radicals. The presence of the methyl radical is especially damaging, because theory predicts that the innermost and strongest lines of the isopropyl radical would fall under the $M_\alpha = \pm\frac{1}{2}$ lines of the methyl radical. It will be necessary to devise some means of obtaining the isopropyl radical in the absence of other radicals before its spectrum can be established.

An experiment aimed at observing the cyclohexyl radical in the photolysis products of cyclohexyl iodide also failed. In this case no ESR spectrum whatsoever was observed. The theoretical calculation of the spectrum is somewhat more difficult for this case, because one does not have unrestricted reorientation of the β protons in this cyclic radical. Thus, some or all of the β protons may have different hyperfine interaction constants. There is, moreover, a certain amount of torsional freedom in the ring which would have a rather complicated effect on both the β proton hyperfine interaction constant, and the α proton hyperfine anisotropy. However, the hyperfine broadening should reduce the line intensities by roughly the same amount as it did in the isopropyl radical, and we may use this as a guide in our analysis. If one had only the cyclohexyl iodide photolysis experiment one could not eliminate the possibility that no radicals whatsoever were formed. However, when cyclohexane in solid argon was photolyzed using a hydrogen lamp and sapphire optics, good H-atom resonances were observed. In this experiment it is reasonable to assume that for each hydrogen atom there must be another free radical species. There are, however, three factors which will reduce the intensity of the cyclohexyl lines relative to the hydrogen atom lines. First, the hydrogen atom lines are considerably narrower ($\sigma \cong 1$ oe) than the narrowest alkyl radical lines ($\sigma \cong 3$ oe). Since under optimum conditions the minimum detectable signal varies inversely as σ,[26] this effect reduces one's ability to detect the cyclohexyl lines relative to the H atom lines by a factor of roughly $\frac{1}{3}$. Secondly, there are only two hyperfine components in a hydrogen atom resonance, whereas there is a much larger number of hyperfine components in the cyclohexyl radical. If we take the most favorable case where all the β protons are equivalent, this effect reduces the strongest cyclohexyl lines by a factor of $\frac{3}{8}$ relative to the H-atom lines. Finally, the α proton hyperfine anisotropy reduces the line intensity by a factor of roughly $\frac{1}{4}$. The combination of these factors leads to a prediction that even after optimizing all observational parameters the strongest cyclohexyl lines would be at best $\frac{1}{32}$ as intense as the observed hydrogen atom resonances. It is very unlikely that such resonances would be detected.

[26] D. J. E. Ingram, *Free Radicals as Studied by Electron Spin Resonance* (Butterworths Scientific Publications, Ltd., London, 1958), pp. 99–100.

FIG. 14. ESR spectrum produced by the photolysis of allyl iodide in argon at 4.2°K.

It will be necessary to repeat these experiments using techniques which will make it possible to build up observable concentrations of the alkyl radical species.

E. Allyl Radical

As a final example we shall consider the allyl radical. This radical which has the structural formula

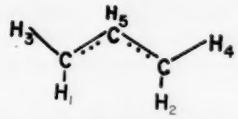

is the simplest conjugated radical. When allyl iodide is photolyzed at 4.2°K one obtains the spectrum shown in Fig. 14. This spectrum was also observed by Smaller and Matheson in γ-irradiated solid propylene.[21] It consists of five rather broad lines, whose intensity ratio suggests hyperfine interactions with four equivalent protons. Theory indicates that in the allyl radical the unpaired electron charge density will be concentrated mainly on the two end or α carbon atoms, giving a relatively large hyperfine interaction with the four α protons, and a smaller hyperfine interaction with the one β proton.[27] Thus, the observed spectrum is consistent with that expected for the allyl radical.

The unusual width of the observed lines is mainly due to anisotropic hyperfine interactions with the α protons, although unresolved isotropic hyperfine interaction with the β protons will also contribute to the

[27] H. M. McConnell, J. Chem. Phys. **29**, 244 (1958).

linewidth. The allyl radical presents a somewhat different case from the radicals studied previously, because in this radical each of the carbon-carbon bonds is a partial double bond so that the $-CH_2\cdot$ group cannot reorient by rotation about these bonds. Hence, only two of the α protons (labeled 1 and 2 in the structural formula) are magnetically equivalent, and complete cancellation of the hyperfine anisotropy is impossible, even for the $M_\alpha=0$ component. As a result all the lines in the allyl spectrum will be broad, in contrast to the mixture of narrow and broad lines observed in the ethyl and *n*-propyl radical spectra.

The detailed calculation of the hyperfine broadening in the allyl radical is considerably more complicated than it was in the case of the saturated alkyl radicals. The difficulty comes from the fact that the unpaired-electron charge density is spread out in the conjugated allyl radical, thereby reducing the hyperfine interaction with the individual nuclei. Consequently the α proton hyperfine interaction energy roughly equals the nuclear Zeeman energy for numerous orientations of the magnetic field. Under these circumstances there is no simple formula for the position of the various hyperfine lines as a function of magnetic field orientation. Indeed at many magnetic field orientations "forbidden" transitions where a proton spin flip accompanies the electron spin transition are allowed, and the hyperfine interaction with a given proton will give four lines instead of two.

The observed spectrum presents an additional problem since it is weak, and was taken under rapid-passage conditions. In consequence of the rapid passage condition the lines have the appearance of absorptions rather than the usual derivative presentations. Lines observed under rapid-passage conditions are almost certainly distorted, and the observed line shapes can have only a qualitative correspondence to the true line shapes.

In view of these difficulties we shall restrict our discussion of the allyl radical to a qualitative comparison of the observed spectrum with the total spread in hyperfine broadening predicted for the various hyperfine components of the spectrum. The separation of the lines in the allyl spectrum is roughly 15 oe. Theory shows that the isotropic hyperfine interaction with a given proton is proportional to the unpaired electron charge density on the adjacent carbon atom. Thus, the unpaired electron charge density on each of the α carbon atoms in the allyl radical is $\frac{2}{3}$, a value in agreement with theory.[27] This gives the following values in oersteds for the components of the α proton hyperfine interaction tensor in the principal axis system: $A=-6.9$; $B=-14.5$; $C=-21.7$. Here, A, B, and C are as defined in Eq. (3). If we use the principal axis system of protons 1 and 2 as our coordinate system, then the hyperfine splittings resulting from the various α protons can be represented by the formulas:

$$\Delta\nu_1=M_1[211.2\sin^2\theta\cos^2\phi+469.9\sin^2\theta\sin^2\phi+47.5\cos^2\theta]^{\frac{1}{2}}$$

$$\Delta\nu_2=M_2[211.2\sin^2\theta\cos^2\phi+469.9\sin^2\theta\sin^2\phi+47.5\cos^2\theta]^{\frac{1}{2}}$$

$$\Delta\nu_3=M_3[211.2\sin^2\theta\cos^2\phi+152.9\sin^2\theta\sin^2\phi+363.3\sin\theta\cos\theta\sin\phi+363.1\cos^2\theta]^{\frac{1}{2}}$$

$$\Delta\nu_4=M_4[211.2\sin^2\theta\cos^2\phi+152.9\sin^2\theta\sin^2\phi-363.3\sin\theta\cos\theta\sin\phi+363.1\cos^2\theta]^{\frac{1}{2}}, \quad (26)$$

where M_i is the projection of the ith proton on the magnetic field. For the reasons given previously these formulas are not correct over the entire range of magnetic field orientation. They break down in those regions where the "forbidden" transitions become allowed, so that the interaction with a single proton gives a four-line pattern instead of the customary two lines. In the region of breakdown the foregoing formulas do, however, give a splitting which is the root mean square of the individual splittings.[14] Thus, these formulas retain qualitative significance even in those regions where they are not strictly applicable.

In Table I we have given the spread in frequency of the hyperfine components corresponding to various ways of orienting the individual α protons. It is expected, though nonetheless noteworthy, that different orientations of the individual α protons which add up to the same value of M_α will be broadened differently by the hyperfine anisotropy. Some arrangements of these protons lead to very broad lines and may be neglected. In Table I the proton arrangements listed above the double space suffer the least broadening and will correspond to the observed lines. The proton arrangements listed below the space give much broader

TABLE I. Range of hyperfine broadening corresponding to various arrangements of the α protons in the allyl radical.

M_α	M_1	M_2	M_3	M_4	$(\nu-\nu_0)$ oe
	$\frac{1}{2}$	$-\frac{1}{2}$	$\frac{1}{2}$	$-\frac{1}{2}$	
0	$-\frac{1}{2}$	$\frac{1}{2}$	$\frac{1}{2}$	$-\frac{1}{2}$	-6.1 to 6.1
	$\frac{1}{2}$	$-\frac{1}{2}$	$-\frac{1}{2}$	$\frac{1}{2}$	
	$-\frac{1}{2}$	$\frac{1}{2}$	$-\frac{1}{2}$	$\frac{1}{2}$	
	$\frac{1}{2}$	$-\frac{1}{2}$	$\pm\frac{1}{2}$	$\pm\frac{1}{2}$	
±1	$-\frac{1}{2}$	$\frac{1}{2}$	$\pm\frac{1}{2}$	$\pm\frac{1}{2}$	±12.4 to ±19.0
±2	$\pm\frac{1}{2}$	$\pm\frac{1}{2}$	$\pm\frac{1}{2}$	$\pm\frac{1}{2}$	±26.0 to ±34.0
0	$\pm\frac{1}{2}$	$\pm\frac{1}{2}$	$\mp\frac{1}{2}$	$\mp\frac{1}{2}$	±9.3 to ∓12.2
±1	$\pm\frac{1}{2}$	$\pm\frac{1}{2}$	$-\frac{1}{2}$	$\frac{1}{2}$	±6.9 to ±21.7
	$\pm\frac{1}{2}$	$\pm\frac{1}{2}$	$\frac{1}{2}$	$-\frac{1}{2}$	

lines, and will not contribute significantly to the observed spectrum. Among the proton arrangements which give observable lines there are four such arrangements corresponding to $M_\alpha=0$, two arrangements each for $M_\alpha=\pm1$, and one each for $M_\alpha=\pm2$. These would be the observed intensity ratios were all the lines equally broadened. However, the $M_\alpha=0$ line has a spread of 12 oe, while the $M_\alpha=\pm1$ lines have a spread of only 6.8 oe. Thus, we may expect that the intensity of these lines will be considerably more than one-half the intensity of the $M_\alpha=0$ line, as is observed. Moreover, the $M_\alpha=\pm1$ lines appear as partially resolved doublets, whereas no such splitting is discernable in the other lines. It is reasonable to assume that this doublet is due to hyperfine interaction with the β proton which is unresolved in the other lines due to the more extreme anisotropic hyperfine broadening. This interpretation gives the β proton an isotropic hyperfine interaction constant of 4 oe, which is the same as the theoretical value.[27]

Quantum Yields

The quantum yield for ethyl and *n*-propyl radical trapping was roughly 10^{-3} radicals trapped per quantum of 2537 light absorbed. These yields are low, indicating that there is a pronounced cage effect. The cage effect would be expected to prevent the separation of the alkyl radical from the iodine atom, thus promoting recombination, and the ultimate transfer of the absorbed energy to the argon lattice. An alternate possibility, that the cage effect promotes the disproportionation reaction between the alkyl radical and iodine atom to form HI and olefin is suggested by the work of Bunbury, Williams and Hamill.[6] No effort was made in this work to detect molecular products. The presence of easily detectable methyl radical resonances in the products from the photolysis of the propyl iodides is presumably also due to the cage effect in the solid, since no significant cracking was found in careful studies of the photolysis of isopropyl iodide in the liquid phase.[28]

Photolysis of the Pure Alkyl Iodides

When the alkyl iodides were deposited and photolyzed at liquid helium temperature in the absence of a diluent, the sample was observed to become bright red. Under these conditions, no ESR spectrum was ever observed. Samples diluted with argon remained snow-white even after extended photolysis. When the red samples of photolyzed alkyl iodide were allowed to warm up to $-196°C$, they turned dark brown. These color changes were observed earlier by Mador,[29] who attributed the red color to trapped CH_3 and the brown color to I_2, formed by the recombination of trapped I atoms on warmup. Our failure to observe resonance in red samples does not necessarily rule out the possibility that alkyl radicals may be trapped in them, since in the pure alkyl iodides the actinic light would be absorbed in a very thin layer and the resulting resonances might be excessively broad due to dipolar interactions.

ACKNOWLEDGMENTS

The authors are indebted to Dr. S. M. Blinder for a number of stimulating discussions on the effects of anisotropic hyperfine interactions. They would also like to thank Dr. S. N. Foner and Dr. C. K. Jen for their interest and encouragement.

[28] C. E. McCauley, W. H. Hamill, and R. R. Williams, J. Am. Chem. Soc. **76**, 6263 (1954).
[29] I. L. Mador, J. Chem. Phys. **22**, 1617 (1954).

Microwave Spectrum, Structure, Dipole Moment, and Internal Barrier of Vinyl Silane*

JAMES M. O'REILLY† AND LOUIS PIERCE

Department of Chemistry, University of Notre Dame, Notre Dame, Indiana

(Received August 24, 1960)

The structure of vinyl silane has been determined by studying the microwave spectra of each of its singly substituted isotopic species. Using Kraitchman's equations the following structural parameters were calculated:

C=C	1.347 A	Si−C=C	122°53′
Si−H	1.475	H−Si−H	108°42′
C−H(*cis*)	1.097	C=C−H(*cis*)	120°18′
C−H(*trans*)	1.097 (assumed)	C=C−H(*trans*)	120°38′
C−H	1.094	C=C−H	117°59′
Si−C	1.853		

By studying the isotopic species containing an asymmetric silyl group the equilibrium conformation was found to be staggered, i.e., the silyl hydrogens are staggered with respect to the hydrogen on the central carbon. The symmetry axis of the silyl group was found to be tilted by an angle of 1°49′ from the Si−C bond axis towards the double bond. Comparison of the Si−C bond distance of vinyl silane with that of methyl silane indicates that recent estimates of the effect of changes in hybridization on the covalent radius of carbon are much too large. The barrier to internal rotation for vinyl silane has been calculated from splittings of ground-state rotational transitions of SiH_3CHCH_2 and splittings of first-excited state transitions of SiH_3CHCH_2 and SiD_3CHCH_2, and also from Stark effect measurements on the $K=1$, $J=2\leftarrow1$ transitions of SiH_3CHCH_2. The various calculations are all in good agreement, and the best value for the barrier is found to be 1500 ± 30 cal/mole. Quadratic Stark effect measurements on the $J=2\leftarrow1$ transitions gave $\mu_a=0.648D$, $\mu_b=0.133D$, and $\mu=0.66D$. The resultant dipole moment makes an angle of $11\pm2°$ with the a axis of SiH_3CHCH_2.

HYPERCONJUGATION, one of the many constructs of valence theory, has recently undergone serious reappraisal.[1,2] It has been suggested that[1] experimental data, e.g., bond lengths and dipole moments, usually accepted as criteria for the existence of hyperconjugation, are, in fact, inconclusive. Dewar and Schmeising[1] argue that bonds formed by sp^2 carbon atoms must be shorter than analogous bonds formed by sp^3 carbon, and thus that until the extent of this shortening is established, no conclusions can be made from lengths of single bonds in molecules such as propylene. The fact that a molecule like propylene has a sizeable dipole moment is considered to be inconclusive because the sp^2 carbon atom is thought to be more electronegative than sp^3 carbon.

The present microwave study of the structure, dipole moment, and internal barrier of vinyl silane, we believe, sheds some light on the "hyperconjugation problem." Since the SiC bond is considerably longer than the CC single bond, it seems reasonable to expect that hyperconjugation, even if it is important in propylene, is of minor importance in vinyl silane. Thus a comparison of SiC bond lengths and dipole moments, of methyl and vinyl silane may be used to estimate the order of magnitude of differences in covalent radius and electronegativity of sp^2 and sp^3 carbon. Interpretation of internal barrier heights is considerably more difficult since the origin of barriers to internal rotation is at present not clearly understood. Nonetheless, if hyperconjugation seriously affects the CC single bond of propylene, then one might reasonably expect that barrier heights of ethane and pyopylene, will not be simply related to the barrier heights of their silyl analogs.

1. EXPERIMENTAL

The microwave spectra of SiH_3CHCH_2, SiH_3CDCH_2, SiH_3CHCDH (*cis* and *trans*), SiH_2DCHCH_2, $SiHD_2$-$CHCH_2$, and SiD_3CHCH_2 were observed with a conventional 100 kc Stark modulated spectrometer at the Notre Dame laboratory. The spectra of $Si^{29}H_3CHCH_2$, $Si^{30}CHCH_2$, $SiH_3C^{13}HCH_2$, and $SiH_3CHC^{13}H_2$ were initially measured in natural abundance with the assistance of Dr. L. C. Krisher at the Harvard laboratory of Professor E. B. Wilson, Jr. The natural abundance measurements were subsequently repeated at this laboratory. Temperature dependence of absorption intensities and the Stark effect provided confirmation of the $Si^{29,30}$ and C^{13} assignments.

Vinyl trichlorosilane (Anderson Chemical Company) was reduced to vinyl silane with a slight excess of $LiAlH_4$ (Metal Hydrides Company) in dry ether. SiD_3CHCH_2 was prepared in the same manner using $LiAlD_4$ (Metal Hydrides Company). By using an equimolar mixture of $LiAlH_4$ and $LiAlD_4$, a mixture SiH_3-, SiH_2D-, $SiHD_2$-, SiD_3-$CHCH_2$ was prepared in the approximate ratio 1:3:3:1.

Acetic anhydride was reduced with $LiAlD_4$ to give CH_3CD_2OH. The alcohol was converted to the bromide using PBr_3.[3] An equal amount of C_2H_5Br was then added to the CH_3CD_2Br to facilitate handling in later steps and also to test the success of the reaction scheme by observing the spectrum of SiH_3CHCH_2. Grignard reagent prepared from the ethyl bromide mixture was

* This research was made possible by a grant from the National Science Foundation.

† Present Address: General Electric Research Laboratory, Schenectady, New York.

[1] M. J. S. Dewar and H. N. Schmeising, Tetrahedron **5**, 166 (1959).

[2] R. S. Mulliken, Tetrahedron **6**, 68 (1959).

[3] V. J. Shriner, Jr., J. Am. Chem. Soc. **75**, 2925 (1953).

slowly added to $SiCl_4$ to yield ethyl trichlorosilane. Ethyl trichlorosilane was chlorinated with SO_2Cl_2 and a catalytic amount of benzoyl peroxide to α and β chloro ethyl trichlorosilane,[4] which was dehydrochlorinated by heating with excess quinoline.[5] The resulting vinyl trichlorosilane was reduced with $LiAlH_4$ to a mixture of SiH_3CHCH_2 and SiH_3CDCH_2. Over-all yield 5–10%.

Partially deuterated acetic acid was prepared from malonic acid and D_2O.[6] Acetic acid was converted to acetyl chloride with phthalyl chloride.[7] Acetyl chloride was reduced to ethanol with $LiAlH_4$ in diethyl carbitol. A mixture of SiH_3CHCH_2, SiH_3CHCHD, (*cis* and *trans*) and SiH_3CHCD_2 was prepared from the ethanol by following the reaction scheme above. The over-all yield was less than 5%.

2. SPECTRA AND DIPOLE MOMENT

The rotational spectrum of vinyl silane is typical of that of a nearly symmetric prolate top. The *a*-type transitions are quite intense and were easily assigned. Because of the small *b* component of the dipole moment, *b*-type transitions are quite weak and were assigned only for the common isotopic species and SiD_3CHCH_2. The low J ground-state transitions and rotational constants of these two species are listed in Table I. Table II lists observed transitions and the rotational constants *b* and *c* for nine other isotopic species of vinyl silane.

The geometry and barrier height of vinyl silane are such that the low-J ground-state *a*-type transitions are not resolvably split by coupling of internal and over-all rotation. Information about internal rotation in vinyl silane was obtained from three experimental sources, (1) a series of weak *a*-type *Q*-branch transitions ($J=7$ to 10) which appear as doublets in the ground-state spectrum of SiH_3CHCH_2, (2) Stark effect (first-order) measurements on the $K=1$, $J=2\leftarrow1$ *a*-type transitions of SiH_3CHCH_2, (3) first-excited ($2\leftarrow1$) torsional state transitions of SiH_3CHCH_2 and SiD_3CHCH_2. These data are summarized and analyzed in Sec. 4.

TABLE I. Ground-state rotational constants and transition frequencies (Mc).[a]

	SiH_3CHCH_2	SiD_3CHCH_2
a	34 159	24 703.00
b	5 275.20	4 773.26
c	4 820.80	4 404.48
$1_{01}\leftarrow0_{00}$	10 095.99	9 177.78
2_{12} 1_{11}	19 737.64	17 986.70
2_{02} 1_{01}	20 186.62	18 350.34
2_{11} 1_{10}	20 646.43	18 724.23
1_{10} 1_{01}	29 337[b] *E* 29 343[b] *A*	20 298.50
2_{11} 2_{02}	29 784[b] *E* 29 789[b] *A*	20 672.34
3_{12} 3_{03}	...	21 242.54
4_{13} 4_{04}	...	22 020.31

[a] Estimated uncertainty in transition frequencies: ±0.05 Mc except where otherwise indicated.

[b] Wave meter measurements. Estimated uncertainty in absolute frequency: ±10 Mc. Estimated uncertainty in $A-E$ separation: ±1 Mc.

The dipole moment of vinyl silane was determined from Stark effect (quadratic) measurements on SiH_3CHCH_2. Theoretical Stark coefficients were calculated by the method of Golden and Wilson,[8] using interpolated line strengths.[9] Calculated and observed coefficients are listed in Table III. Although μ_a accounts for most of the Stark displacement, μ_b can be estimated. The resultant dipole moment, $\mu=0.662\pm0.012$ *D* makes an angle of $11°\pm2°$ with the *a* axis. In principle the sign of this angle could be determined by Stark effect measurements on another isotopic species. Unfortunately, for vinyl silane, the rotation of principal axes which results from isotopic substitution is too small to be of any value. The angle between the SiC bond axis and the *a* axis of SiH_3CHCH_2 is approximately 21°, so that μ makes an angle of either $10\pm2°$ or $32\pm2°$ with the SiC bond. The former value is probably the correct one since a bond moment calculation places μ along the SiC bond.

3. STRUCTURE AND CONFORMATION

The data of Tables I and II are sufficient in principle to allow the determination of the coordinates all atoms of vinyl silane from *changes* in moments of inertia with isotopic substitution.[10,11] The *a* and *b* coordinates (SiH_3CHCH_2 principal axes) of the carbon atoms, the *cis* hydrogen atom, the hydrogen of the central carbon atom, and the *a* coordinates of the silicon atom and the *trans* hydrogen were obtained using Kraitchman's equations.[12] Since I_a was experimentally determined for only two isotopic species, it was necessary in these calculations to assume that for in-plane isotopic substitution

$$\Delta I_a=\Delta I_c-\Delta I_b, \tag{1}$$

where ΔI_g is the change in I_g with isotopic substitution. Equation (1) is equivalent to the assumption that the inertial defect does not change with isotopic substitution.

The *b* coordinate of the *trans* hydrogen atom is a "near-axis" coordinate for which Kraitchman's equations give an imaginary value. It was necessary to fix

[4] L. H. Sommer and F. C. Whitmore, J. Am. Chem. Soc. **68**, 485 (1946).
[5] D. T. Hurd, J. Am. Chem. Soc. **67**, 1813 (1945).
[6] C. L. Wilson, J. Chem. Soc. **1935**, 492.
[7] J. D. Cox and H. S. Turner, J. Chem. Soc. **1950**, 3176.
[8] S. Golden and E. B. Wilson, Jr., J. Chem. Phys. **16**, 699 (1948).
[9] R. Schwendeman and V. W. Laurie, *Line Strengths for Rotational Transitions* (Pergamon Press, New York, 1958).
[10] C. C. Costain, J. Chem. Phys. **29**, 864 (1958).
[11] L. Pierce, J. Mol. Spectroscopy **3**, 575 (1959).
[12] J. Kraitchman, Am. J. Phys. **21**, 17 (1953).

TABLE II. Rotational constants and a-type transitions (Mc)[a].

	b	c	$1_{10}\leftarrow 0_{00}$	$2_{12}\leftarrow 1_{11}$	$2_{02}\leftarrow 1_{01}$	$2_{11}\leftarrow 1_{10}$
$Si^{29}H_3CHCH_2$	5214.40	4769.61	...	19 523.22	19 962.92	20 412.81
$Si^{30}H_3CHCH_2$	5156.96	4721.31	...	19 320.91	19 751.60	20 192.25
$SiH_3C^{13}HCH_2$	5249.80	4787.15	...	19 611.24	20 067.88	20 536.54
$SiH_3CHC^{13}H_2$	5114.83	4682.70	...	19 162.94	19 590.25	20 027.20
SiH_3CDCH_2	5232.29	4673.35	...	19 252.34	19 801.56	20 370.22
SiH_3CHCHD (cis)	5137.09	4625.41	...	19 013.32	19 517.07	20 036.68
SiH_3CHCHD (trans)	4888.84	4496.24	...	18 377.57	18 766.27	19 162.76
SiH_2DCHCH_2 (sym.)	5214.80	4666.31	9881.05	19 213.72	19 752.92	20 310.72
SiH_2DCHCH_2 (asym.)	5035.33	4669.87	9705.16	19 044.95	19 406.68	19 775.85
$SiHD_2CHCH_2$ (sym.)	4815.64	4539.21	9354.8	18 433.27	18 707.1	18 986.14
$SiHD_2CHCH_2$ (asym.)	4984.80	4526.28	9511.02	18 563.63	19 015.05	19 480.67

[a] Estimated uncertainty in transition frequencies: ±0.10 Mc.

this coordinate by other means. We chose to assume the *trans* CH distance to be equal to the *cis* CH distance.

The b coordinate of silicon is also a near-axis coordinate. Its value was initially fixed by Kraitchman's equations. Coordinates for the silyl hydrogens were then calculated from 10 observed changes in b and c moments of inertia (for deuterium substitution in the silyl group) by the method of least squares. The b coordinate of the silicon atom was then calculated from the center of mass condition (resulting in a change of only 0.003 A). Using this new value of b_{Si}, the least-squares calculation of the silyl hydrogen coordinates was repeated. Further iterations were not warranted since at this stage the center of mass condition could be fulfilled by a 0.0003 A adjustment of b_{Si}.

In locating the silyl hydrogens, the silyl group was assumed to be symmetric but not necessarily coaxial with the SiC bond axis. With this one condition the 10 observed and calculated ΔI's were found to differ on the average by only 0.01 amu A². The SiH_3 symmetry axis, however, was found to be tilted from the SiC bond axis by an angle of 1°49 (see Fig. 1). This tilt angle, we feel, is quite reliably determined. If the SiH_3 symmetry axis is forced to be coaxial with the SiC bond axis, the 10 observed and calculated (least squares) ΔI's differ on the average by ±0.06 amu A².

The coordinates of all atoms, in SiH_3CHCH_2 principal axes, are listed in Table IV. Bond distances and angles for vinyl silane are given in Table V. Since isotopic species containing an asymmetric (SiH_2D-, $SiHD_2$-) silyl group were studied, the equilibrium conformation of the silyl group can be determined. The conforma-

TABLE III. Stark coefficients of SiH_3CHCH_2.[a]

Transition	M	$\Delta\nu/E^{2}$[b] obs	calc
$2_{02}\leftarrow 1_{01}$	0	−1.61	−1.64
	1	1.33	1.31
$2_{12}\leftarrow 1_{11}$	0	1.10	1.10
	1	58.40	57.12
$2_{11}\leftarrow 1_{10}$	0	1.24	1.28
	1	−54.87	−55.51
	$\mu_a=0.648\pm0.008$ D		
	$\mu_b=0.133\pm0.027$ D		
	$\mu=0.662\pm0.012$ D		

[a] Apparatus calibrated with OCS [0.7124 D, S. A. Marshall and J. Weber, Phys. Rev. **105**, 1502 (1957)].
[b] Mc/(kv/cm)².

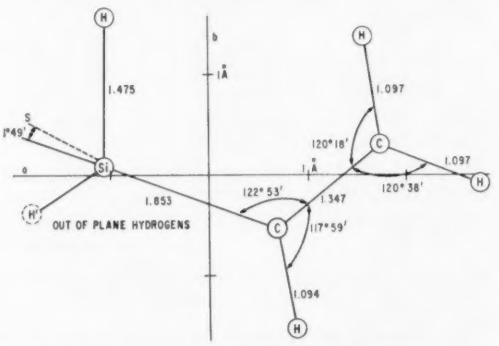

FIG. 1. The structure of vinyl silane. Except for two of the silyl hydrogens, the molecule is planar. Note that the symmetry axis of the silyl group (the dotted line S) is not coincident with the SiC bond axis. The axes marked a and b are the principal axes of the common isotopic species.

tion is found to be the staggered one, i.e., the silyl hydrogens stagger the CH bond of the central carbon (see Fig. 1). An identical conformation has been found for the methyl group of propylene.[13]

The b-type assignments for SiH_3CHCH_2 and SiD_3CHCH_2 were obtained after the described calculations were completed. Since all three moments of inertia are available for these species, an independent determination of the c coordinates of the silyl hydrogens is possible.[14] The moments for these two species yield $|c| = 1.201$ A which is in excellent agreement with the value of 1.198 A obtained from the least-squares calculation.

4. INTERNAL ROTATION

The analysis of fine structure, resulting from coupling of internal and over-all rotation, in the microwave spectrum of vinyl silane has been carried out using the "principal axis method."[15-17] According to this method, zero field (E) spectra arising from the vth torsional state are interpreted with the two Hamiltonians (see reference 17 for definitions):

$$H_{vA}=H_r+F\sum_n W_{vA}^{(n)}\mathcal{P}^n$$

$$H_{vE}=H_r+F\sum_n W_{vE}^{(n)}\mathcal{P}^n. \qquad (2)$$

The geometry and barrier height of vinyl silane are such that the summations in Eqs. (2) for the observed transitions can be approximated as

$$\sum_n W_{vA}^{(n)}\mathcal{P}^n \approx W_{vA}^{(2)}[\alpha^2 P_z^2+\beta^2 P_x^2]+W_{vA}^{(4)}\alpha^4 P_z^4$$

$$\sum_n W_{vE}^{(n)}\mathcal{P}^n \approx W_{vE}^{(2)}[\alpha^2 P_z^2+\beta^2 P_x^2]+W_{vE}^{(4)}\alpha^4 P_z^4$$

$$+\alpha W_{vE}^{(1)}P_z+\alpha^3 W_{vE}^{(3)}P_z^3, \qquad (3)$$

where $\alpha=\lambda_a I_a/I_a$, $\beta=\lambda_b I_a/I_b$, and the λ's are the direction cosines between the symmetry axis of the internal top and the principal axes of the entire molecule.

TABLE IV. Atom coordinates (SiH_3CHCH_2 principal axes) (A).

	a	b	c
Si	−1.0663	0.0785	0
C_1	0.6846	−0.5275	0
C_2	1.7441	0.3039	0
H (cis)	1.5948	1.3906	0
H (trans)	2.7666	−0.0933	0
H	0.8770	−1.6044	0
$H_s(SiH_3)$	−1.0492	1.5532	0
$H_a(SiH_3)$	−1.7898	−0.3860	±1.1985

TABLE V. Structure of vinyl silane.[a]

C=C	1.347±0.003 A	SiC=C	122°53′±15′
SiH	1.475±0.005 A	HSiH	108°42′±20′
CH (*cis*)	1.097±0.005 A	C=CH (*cis*)	120°18′±20′
CH (*trans*)	1.097 (assumed)	C=CH (*trans*)	120°38′±20′
CH	1.094±0.005 A	C=CH	117°59′±20′
SiC	1.853±0.003 A	θ[b]	121°4′±20′

Structural checks (SiH_3CHCH_2)

$\Sigma m_i b_i = -0.0092$ amu A

$\Sigma m_i a_i = -0.0787$ amu A

$\Sigma m_i a_i b_i = -0.0083$ amu A²

	calc	obs
I_a	14.8032	14.7993 amu A²
I_b	95.4925	95.8316 amu A²
I_c	104.5034	104.8645 amu A²

[a] Conversion factor: 505531 M_c amu A². Atomic masses taken from C. H. Townes and A. L. Shawlow, *Microwave Spectroscopy* (McGraw-Hill Book Company, Inc., New York, 1955).

[b] θ=angle between C=C bond axis and symmetry axis of silyl group.

Herschbach[17] has shown that the perturbation coefficients, $W_v^{(n)}$, are for sufficiently high barriers simply proportional to a quantity w_1, which is a measure of the energy difference between the vA and vE torsional sublevels. The barrier for vinyl silane is sufficiently high so that the reduced barrier s can be obtained by interpolation of tables of w_1 vs s, where $s=4V_3/9F$.

Doublet separations (~1 Mc) for the four $K=1$ a-type Q-branch transitions of SiH_3CHCH_2 are to an excellent approximation given by

$$\Delta\nu_E=F_{\beta^2}(W_{0E}^{(2)}-W_{0A}^{(2)})\Delta\langle P_x^2\rangle, \qquad (4)$$

where $\Delta\nu_E=\nu_E-\nu_A$ and $\Delta\langle P_x^2\rangle=\langle P_x^2\rangle_{\text{upper state}}-\langle P_x^2\rangle_{\text{lower state}}$. These four splittings yield a barrier height $V_3=1504\pm10$ cal/mole (see Table VI).

The odd powers of P_z in H_{vE} cause an appreciable first-order Stark effect in the $K=1$, $J=2\leftarrow1$ transitions of SiH_3CHCH_2. The $M=1$ lobes for these transitions appears as symmetric triplets, with triplet spacing proportional to the electric field E. The spacing $\Delta\nu$ between the outer components of the triplet is given by[18,19]

$$\Delta\nu/E=(16/9)[X\mu_a/(b-c)], \qquad (5)$$

where

$$X=F\sum_{n(\text{odd})}\alpha^n W_{0E}^{(n)}.$$

[13] D. R. Herschbach and L. C. Krisher, J. Chem. Phys. **28**, 728 (1958).

[14] V. W. Laurie, J. Chem. Phys. **28**, 704 (1958).

[15] R. W. Kilb, C. C. Lin, and E. B. Wilson, Jr., J. Chem. Phys. **26**, 1695 (1957).

[16] D. R. Herschbach, J. Chem. Phys. **27**, 1420 (1957).

[17] D. R. Herschbach, J. Chem. Phys. **31**, 91 (1959).

[18] J. D. Swalen and C. C. Lin, Revs. Modern Phys. **31**, 851 (1959).

[19] D. R. Lide, Jr., and D. E. Mann, J. Chem. Phys. **27**, 868 (1957).

The experimental value of X (Table VI) yields a barrier height $V_3=1500\pm15$ cal/mole, which is in excellent agreement with the value of V_3 obtained from ground-state Q-branch transitions. This agreement between first-order Stark effect (sensitive to λ_a) and Q-branch transitions (sensitive to λ_b) is dependent on the orientation of top and frame. The calculation summarized in Table VI were carried out using the "tilt" for the silyl group as determined from changes in moments of inertia (Sec. 3). The agreement is much less satisfactory if it is assumed that the symmetry axis of the silyl group is coincident with the SiC bond axis.

TABLE VI. Internal barrier from ground-state transitions of SiH_3CHCH_2

Transition	ν_A (obs)	$\Delta\nu_E$[a] (obs)	$\Delta\nu_E$ (calc)[b]
$7_{16}\leftarrow7_{17}$	12 715.13 Mc	−0.54 Mc	−0.56 Mc
$8_{17}\ 8_{18}$	16 339.47	−0.70	−0.72
$9_{18}\ 9_{19}$	20 409.38	−0.95	−0.90
$10_{1,9}\ 10_{1,10}$	24 920.20	−1.13	−1.11

First-order Stark effect ($2_{12}\leftarrow1_{11}$, $2_{11}\leftarrow1_{10}$)

$(\Delta\nu/E)_{obs}=5.03$ Mc/(kV/cm)

$X_{obs}=7.88$ Mc, $X_{calc}=7.90$ Mc

$I_a=5.7923$ amu A^2 $\quad\alpha=0.3656$

$F=133.9$ kMc $\quad\beta=0.02156$

$V_3=1500\pm15$ cal/mole

[a] $\Delta\nu_E=\nu_E-\nu_A$.
[b] Calculated for $V_3=1500$ cal/mole.

The torsional energy difference, $F(W_{vA}^{(0)}-W_{vE}^{(0)})$, increases about fifty fold in going from the ground- to the first-excited torsional state, and the perturbation coefficients and splittings, except for $K=1$ transitions, increase in the same proportion. Splittings for the $K=0$, $1\leftarrow0$, and $2\leftarrow1$ transitions can be fitted with Eq. (4) and yield a barrier height of $V_3=1563\pm15$ cal/mole. This value for V_3 is considerably higher than the value obtained from ground-state measurements. However, in terms of splittings, this represents a discrepancy of 0.4 Mc for the excited state $2\leftarrow1$ transition. It is quite possible that effects of nonrigidity of top and frame are this order of magnitude. For example, the $1\leftarrow0$, $v=1$ transition of CH_3SiH_3 is split by 0.7 Mc because of nonrigidity effects.[20]

In the first-excited torsional state of SiH_3CHCH_2 the $K=1$, $2\leftarrow1$ transitions exhibit very large splittings mainly because of the odd powers of P_z in H_{vE}. Eigenvalues of H_{vE} were calculated by formulas given in references 17 and 21. From the $K=1$ transitions V_3 is found to be 1498 ± 1 cal/mole. The $K=1$, $2\leftarrow1$ transitions of SiD_3CHCH_2 are also split mainly because of the odd powers of P_z in H_{vE} and yield a barrier height $V_3=1483\pm15$ cal/mole. The over-all good agreement between ground-state and first-excited state splittings is a good indication that deviation from a simple cosine barrier is quite small in vinyl silane. Calculations for excited state transitions are summarized in Table VII.

TABLE VII. Internal barrier from first-excited torsional state transitions of SiH_3CHCH_2 and SiD_3CHCH_2.

Transition	ν_A(obs)	$\Delta\nu_E$(obs)	$\Delta\nu_E$(calc)[a]	V_3(cal/mole)
		SiH_3CHCH_2		
$1_{01}\leftarrow0_{00}$	10 089.96 Mc	0.77 Mc	0.94	
$2_{02}\ 1_{01}$	20 174.75	1.45	1.88	1563±15
$2_{12}\ 1_{11}$	19 738.6	115.3	115.7	
$2_{11}\ 1_{10}$	20 621.8	−113.3	−112.0	1498±1
		SiD_3CHCH_2		
$1_{01}\leftarrow0_{00}$	9 174.9	b		
$2_{02}\ 1_{01}$	18 344.93	b		
$2_{12}\ 1_{10}$	17 996.71	1.12		1483±15
$2_{11}\ 1_{10}$	18 702.11	−0.91		

[a] Calculated for $V_3=1500$ cal/mole.
[b] Not resolved.

In the formulation of the "principal axis method"[15–17] the approximation is usually made that torsional energy differences are much greater than rotational energy differences. For molecules with high barriers and large moments of inertia the approximation is usually valid, but is inadequate for molecules with small moments of inertia and thus large rotational energy spacings. A better approximation is obtained if an expansion in terms of the ratio of rotational energy differences to torsional energy differences is made. This treatment adds terms to the effective rotational Hamiltonian which are referred to as denominator corrections.[17] Denominator corrections have little or no effect on the splittings used to calculate the barrier height but they do contribute to the effective rotational constants. In

TABLE VIII. Denominator corrections.

	$\beta^2W^{(d)}D$(Mc)	ΔI_c(corr-obs) (amu A^2)
SiH_3	0.61	0.013
SiH_2D (s)	0.89[a]	0.021
SiH_2D (a)	0.93[a]	0.022
$SiHD_2$ (s)	1.2[a]	0.03
$SiHD_2$ (a)	1.2[a]	0.03
SiD_3	1.56	0.041

[a] Approximate corrections—see text.

[20] D. Kivelson, J. Chem. Phys. **22**, 1733 (1954).
[21] R. W. Kilb and L. Pierce, J. Chem. Phys. **27**, 108 (1957).

the case of vinyl silane, they contribute because of the small a moment of inertia. The observed rotational constants are

$$a(\text{obs}) = a - D\beta^2 W_v^{(n)}$$
$$c(obs) = c + D\beta^2 W_v^{(n)}$$
$$b(\text{obs}) = b, \qquad (6)$$

where $D = a - \frac{1}{2}(b+c) + F(\alpha^2 - \beta^2/2)$ and $W_v^{(n)}$ = the barrier dependent perturbation coefficient defined and tabulated by Herschbach.[17]

For all isotopic species containing the unsubstituted silyl group, these corrections tend to cancel out because we are fitting differences in moments of inertia. In the most adverse case neglecting these terms would lead to an error of less than 0.001 A in a bond distance. In the other isotopic species, there is less cancellation and these terms were included in the structural analysis of the silyl group. For isotopic species containing an unsymmetric silyl group, the corrections applied were approximate since the theory applies to a symmetric internal rotor. For these species a value of F was calculated using the actual value of I_α, which is equivalent to assuming the difference in mass between hydrogen and deuterium is symmetrically distributed over the three silyl positions. Denominator corrections are listed in Table VIII.

5. DISCUSSION

Table IX compares certain molecular parameters of vinyl silane with parameters of methyl silane, ethane, propylene, and the methyl fluorosilanes. The most striking conclusion that can be drawn from the data is that while a difference of about 0.04 A in the covalent radii of sp^3 and sp^2 carbon accounts for the length of the CC single bond in propylene and many other sp^3-sp^2 CC single bonds, this difference is much too large to account for the length of the SiC bond of vinyl silane. In going from methyl silane to vinyl silane the SiC bond decreases by only 0.014 A. This result suggests that the covalent radii of sp^3 and sp^2 carbon differ at most by about 0.01 to 0.02 A. (This estimate, of course, assumes that hyperconjugation has no effect on the SiC bond of vinyl silane.) It is interesting to note that a recent theoretical calculation by Mulliken[2] sets the difference in covalent radii of sp^2 and sp^3 carbon at 0.02 A.

TABLE IX. Molecular parameters of vinyl silane and related molecules.

		μ (D)	V_3 (cal/mole)
	CC (A)		
CH_3CH_3	1.534[a]	0	2700–3000[b]
CH_3CHCH_2[c]	1.488	0.36	1980
	SiC (A)		
CH_3SiH_3[d]	1.867	0.73	1670
SiH_3CHCH_2[e]	1.853	0.66	1500
CH_3SiH_2F[f]	1.849	g	1560
CH_3SiHF_2[h]	1.840	g	1255

[a] H. C. Allen and E. K. Plyler, J. Chem. Phys. **31**, 1062 (1959).
[b] K. S. Pitzer, Discussions Faraday Soc. **10**, 66 (1951).
[c] Reference 19.
[d] References 21 and 17.
[e] This work.
[f] L. Pierce, J. Chem. Phys. **29**, 383 (1958); L. C. Krisher and L. Pierce, *ibid.* **32**, 1619 (1960).
[g] Not relevant to the discussion.
[h] J. D. Swalen and B. P. Stoicheff, J. Chem. Phys. **28**, 671 (1958); L. C. Krisher and L. Pierce, *ibid.* **32**, 1619 (1960).

Assuming that CH bond moments are identical for sp^2 and sp^3 carbon, the bond moment model then requires the dipole moments of ethane and propylene to be zero, and the dipole moments of methyl and vinyl silane to be equal. Assuming further that hyperconjugation effects are negligible in vinyl silane, comparison of its dipole moment with that of methyl silane shows that the order of magnitude of the difference in CH bond moments of sp^2 and sp^3 carbon is about 0.1 D; a value much to small to explain the dipole moment of 0.36 D for propylene. Thus, explanation of the data of Table IX would seem to require the construct "hyperconjugation" as well as the construct "hybridization."

Insofar as the barrier height of vinyl silane is concerned, it is difficult to attach significance to the fact that it is only 200 cal/mole less than the methyl silane barrier. However, it is interesting to note that (1) the barrier in propylene is considerably smaller (by 800 cal/mole) than the barrier in ethane and that bond distance and dipole moment data suggest hyperconjugation to be important in propylene, (2) both CH_3SiH_2F and CH_3SiHF_2 have a lower SiC distance and internal barrier than CH_3SiH_3, and that it has been suggested[22] that shortening of the SiC bond with fluorination of the silyl group results from the importance of nonclassical hyperconjugated structures such as

$$Me^+ = Si^- H_2F,$$

when silicon is attached to one or more highly electronegative elements. Thus the trends in the barriers listed in Table IX can qualitatively be explained by assuming that hyperconjugation in a molecule tends to favor the eclipsed conformation, while the primary, and as yet unidentified, cause for restricted internal rotation favors the staggered conformation.

ACKNOWLEDGMENTS

The authors are indebted to Professor E. Bright Wilson, Jr., for permission to use the Harvard microwave spectrometer. We are especially grateful to Dr. L. C. Krisher for his invaluable assistance in the difficult task of making the assignments of the spectra of the C^{13} and $Si^{29,30}$ isotopic species of vinyl silane.

[22] L. Pierce and D. H. Petersen, J. Chem. Phys. **33**, 907 (1960).

Analysis of the Absorption Spectrum and Zeeman Effect of Thulium Ethylsulphate*

EUGENE Y. WONG AND ISAAC RICHMAN

Physics Department, University of California, Los Angeles, California

(Received August 12, 1960)

The crystalline field interaction was calculated using first-order perturbation theory on intermediate coupling wave functions of Tm^{3+} in a D_{3h} field. Good agreement with experimental data of Tm^{3+} diluted with $La(C_2H_5SO_4)_3 \cdot 9H_2O$ was obtained. The following crystalline field parameters were chosen for best fit:

$A_2^0\langle r^2\rangle = 129.8\ \text{cm}^{-1}$, $A_4^0\langle r^4\rangle = -71.0\ \text{cm}^{-1}$, $A_6^0\langle r^6\rangle = -28.6\ \text{cm}^{-1}$, $A_6^6\langle r^6\rangle = 432.8\ \text{cm}^{-1}$.

INTRODUCTION

A RATHER complete absorption spectrum and Zeeman effect of $Tm(C_2H_5SO_4)_3 \cdot 9H_2O$ was reported by Johnsen.[1] A more complete spectrum together with an analysis was reported later by Gruber and Conway.[2,3] The identification of the multiplets agrees with the intermediate coupling calculations of f^{12} presented by Runciman and Wybourne,[4] Gruber and Conway,[2] and Margolis[5] very well. However, the analysis of the crystalline field interaction by Gruber and Conway is not as good as might be expected. The average deviation is about 18 cm^{-1}. The separation of different multiplets of Tm^{3+} is larger than those of Pr^{3+}. Hence one would expect a first-order calculation to be better than 5 cm^{-1} which is the average deviation obtained by Judd[6] in a first-order calculation for $PrCl_3$. Here we present an analysis of the spectrum of $La(C_2H_5SO_4)_3 \cdot 9H_2O$. The average deviation of the crystalline field splitting is 5 cm^{-1}. The Zeeman effect was also calculated and is in good agreement with Johnsen's results.

EXPERIMENT DETAILS

The rare earth ethylsulphate was prepared by hydrolysis of $(C_2H_5)_2SO_4$ in the presence of slightly excess rare earth oxide at a water bath temperature of 100°C. A 10 mole % of Tm^{3+} in $La(C_2H_5SO_4)_3 \cdot 9H_2O$ solution was then prepared from the pure earth ethylsulphates. The final crystals probably contain less than 10% Tm^{3+} because the ionic radius of Tm^{3+} is smaller than that of La^{3+}. The crystal was grown by slow evaporation of water at room temperature.

The spectrum was taken with a 21-ft grating spectrograph at both liquid-nitrogen and liquid-helium temperatures. In addition to this a liquid-air temperature spectrum was taken on a Cary recording spectrograph.

Photographic plates were used on the grating to cover the region from 2500 to 10 000 A. All the groups of lines reported by Johnsen were found. In addition, a new group of lines identified as 1_{D_2} was recorded. No lines due to the multiplets 1_{I_6}, 3_{P_2}, 3_{P_1}, 3_{P_0} were found even though they were expected to lie within the region recorded. Also not recorded were 3_{H_5}, 3_{H_4}, and 1_{S_0} but they were expected to lie outside the range of the photographable spectrum.

In the Cary all multiplets of f^{12} were recorded except 1_{S_0} and 1_{I_6}. The spectrum taken covered the range 20 000 to 2500 A. The Cary was able to detect lines not found on the photographic plates because it uses a balanced detector which results in higher contrast than the plates can achieve. No spectrum was taken on the Cary at liquid helium temperature.

The measurements from the grating spectra show deviations up to 1 cm^{-1}. The spectra taken with the Cary deviate as much as 10 cm^{-1} from the grating spectra.

CALCULATION OF CRYSTALLINE FIELD INTERACTION

Intermediate coupling wave functions and eigenvalues for f^{12} were calculated by Margolis. These wave functions were then used to compute the operator equivalent factors. These factors, together with the calculated and observed multiplet energy levels, are listed in Table I. The centers of gravity of the multiplets were computed from the Stark levels by assuming that the calculated crystal field splitting is correct. Also included in Table I are the operator equivalents of Gruber and Conway.[3] The number in parenthesis shows how much the authors differ from Gruber and Conway. It should be noted that the operator equivalents used here differ by less than 3% from those of Gruber and Conway except β for $^3F_2$, α for $^3F_4$, and α and γ for $^1G_4$, which differ by 4.6, 8, −8.2, and 12.3%, respectively. A difference of less than 3% will not affect the Stark splitting significantly. However, the difference in operator equivalents for $^1G_4$ may be the reason that Gruber and Conway were unable to obtain a good fit for that group.

* This work supported in part by the Office of Ordnance Research, U. S. Army.

[1] U. Johnsen, Z. Physik **152**, 454, 1958.

[2] J. B. Gruber and J. G. Conway, J. Chem. Phys. **32**, 1178 (1960).

[3] J. B. Gruber and J. G. Conway, J. Chem. Phys. **32**, 1531 (1960).

[4] W. A. Runciman and B. G. Wybourne, J. Chem. Phys. **31**, 1149 (1959).

[5] J. S. Margolis, Ph.D. dissertation, Physics Department, University of California at Los Angeles, Los Angeles, California, 1960.

[6] B. R. Judd, Proc. Roy. Soc. (London) **A241**, 414 (1957).

TABLE I. Calculated and observed multiplet energies and the operator equivalent factors of Tm^{3+}.

	Energy cm^{-1}				
	calc.	obs.	α	β	γ
$^3H_6$	0	0	1.0201×10^{-3}	1.5921×10^{-4}	-5.5284×10^{-6}
$^3H_4$	5634	5647	-2.1226×10^{-3}	7.2693×10^{-4}	6.8818×10^{-5}
$^3H_5$	8239	8061	1.3333×10^{-2}	2.5653×10^{-4}	-7.4000×10^{-6}
$^3F_4$	12 587	12 491	1.1755×10^{-2}	4.4426×10^{-4}	-7.0530×10^{-5}
$^3F_3$	14 478	14 313	-1.1111×10^{-2}	2.2447×10^{-4}	2.5900×10^{-4}
$^3F_2$	14 982	14 947	-4.1271×10^{-2}	-6.4127×10^{-3}	0
$^1G_4$	21 187	21 109	8.6361×10^{-3}	1.0589×10^{-3}	7.4142×10^{-5}
$^1D_2$	27 778	27 785	-4.7656×10^{-2}	2.2859×10^{-3}	0
$^1I_6$	32 686	...	2.0102×10^{-2}	-2.4083×10^{-4}	2.1647×10^{-6}
$^3P_0$	35 262	35 343	0	0	0
$^3P_1$	36 093	36 329	2.0000×10^{-1}	0	0
$^3P_2$	37 955	38 087	-7.2980×10^{-2}	-1.3510×10^{-2}	0
$^1S_0$			0	0	0

Operator equivalents of Gruber and Conway[a]

$^3H_6$	1.0202 (0.0%)	1.5933 (0.1%)	−5.5276 (0.0%)
$^3F_4$	1.0770 (8.0%)	4.4069 (0.8%)	−7.3322 (4.2%)
$^3F_3$	−1.1111 (0.0%)	2.2447 (0.0%)	2.5900 (0.0%)
$^3F_2$	−4.1549 (0.7%)	−6.5573 (4.6%)	
$^1G_4$	9.3454 (−8.2%)	1.0452 (1.3%)	6.5026 (12.3%)
$^1D_2$	−4.7352 (0.6%)	2.2222 (2.7%)	
$^3P_1$	2.0000 (0.0%)		
$^3P_2$	−7.3000 (0.0%)	−1.3312 (1.5%)	

[a] J. B. Gruber and J. C. Conway, work cited in footnote 3.

The crystal field parameters $A_2^0\langle r^2\rangle$ and $A_4^0\langle r^4\rangle$ were obtained from $^3F_2$ and $^1D_2$. $A_6^0\langle r^6\rangle$ was calculated from $^3F_3$, and $A_6^0\langle r^6\rangle$ from $^3F_3$ and $^3F_4$. The parameters obtained in this way are,

$$A_2^0\langle r^2\rangle = 129.8\ \text{cm}^{-1} \quad A_6^0\langle r^6\rangle = -28.6\ \text{cm}^{-1},$$

$$A_4^0\langle r^4\rangle = -71.0\ \text{cm}^{-1} \quad A_6^6\langle r^6\rangle = 432.8\ \text{cm}^{-1}.$$

The g_{11} listed in Table II were calculated by neglecting the mixing of the different Stark levels by the external magnetic field.

DISCUSSION

Three Stark levels were identified for this group. The experimental and calculated results are compared in Table II.

The calculated g_{11} for the lower energy $\mu=\pm1$ component is 1.09, about a factor of 2 smaller than Johnsen's reported value. To resolve this we measured the splitting shown in Fig. 3 of Johnsen's report. We accepted his value of $g=0.73$ for line three. From this the Zeeman splitting of the $\mu=\pm2$ component was calculated to be 3.59 cm^{-1}. Then taking the splitting of line one to be the sum of the $\mu=\pm2$ of $^3F_2$ and $\mu=\pm1$ of

TABLE II. Calculated Stark levels and g with observed values.

		Calculated		Experimental		
	μ	energy cm^{-1}	$g_\parallel$	energy cm^{-1}[a]	$g_\parallel$[b]	ΔE
	3	140.5	0			
	±2	114.8	6.64			
	0	53.0	0			
	0	46.6	0			
$^3H_6$	±1	38.0	10.4	24.1 (190.4)		13.9
	3	−4.2	0			
	±2	−53.0	1.98			
	±1	−134.2	1.09	−134.2 (32.1)	1.14	0.0
	0	−166.8	0	−166.3 (0.0)		−0.5
	±2	106.7	0.12	105.8 (12763.7)	0	0.9
	3	84.1	0	46.5 (12704.4)		44.7
$^3F_4$	±2	−15.7	3.69	−14.2 (12643.7)	3.14	−1.5
	±1	−40.4	1.91	−30.9 (12627.0)		−9.5
	3	−69.7	0	−69.7 (12588.2)		0.0
	0	−115.4	0			
	0	38.2	0			
	3	14.7	0	14.8 (14489.5)		−0.1
$^3F_3$	±2	14.7	4.33	14.3 (14489.0)	3.78	0.3
	±1	−8.0	2.17	−7.8 (14466.9)		−0.2
	3	−65.9	0	−69.5 (14408.8)		0.0
	0	64.9	0			
$^3F_2$	±1	−5.8	1.51	−5.8 (15103.4)		0.0
	±2	−26.7	3.02	−26.7 (15082.5)	3.08	0.0
	3	228.9	0	240.9 (21511.7)		−12.0
	3	67.1	0	72.2 (21343.0)		−5.1
$^1G_4$	±2	32.0	0.80	32.0 (21302.8)	0	0.0
	0	−50.2	0			
	±1	−62.3	1.92	−72.3 (21198.5)		10.0
	±2	−92.6	3.04	−98.9 (21171.9)	3.6	6.3
	±1	26.4	2.27	27.0 (27973.1)		−0.6
$^1D_2$	0	25.4	0			
	±2	−39.1	4.54	−39.1 (27907.0)		0.0

[a] The centers of gravity of the experimental value are adjusted to give the best fit to the calculated value. The value in the parentheses is the difference of energy from the ground state.

[b] Data obtained from Johnsen, see work cited in footnote 1.

$^3H_6$ we find a splitting factor for the latter: $g=1.14$ which is in fair agreement with our results.

The Stark level of 190 cm^{-1} above the ground state was identified as $\mu=\pm1$ of $^3H_6$ because of selection rules. This disagrees with the identification of Gruber and Conway. However in Figs. 3 and 4 of their report one could obtain a much better agreement with the selection rule if the present identification is used.

There were some more lines, possibly due to the excited states of the ground multiplet crystal, but there were not enough lines to give a positive identification. The quantum level of 231 cm^{-1} above the ground state reported by Gruber and Conway was not confirmed by this work.

$^3H_5$ and $^3H_4$

These two groups were recorded on the Cary at liquid-air temperature. Because of the number of vibronic lines present and the resolving power of the equipment it is difficult to identify the pure electronic lines. One $\mu=\pm2$ component of $^3H_5$ was identified at 8208 cm^{-1} above the ground state. For $^3H_4$ three Stark levels were identified, $\mu=3$ 5970 cm^{-1} $\mu=3$ 5865 cm^{-1} $\mu=\pm2$ 5703 cm^{-1}. These identifications may not be very reliable. The 10-wave number accuracy of the Cary is comparable to the crystal field splitting. For these reasons the data from the Cary was not used in the crystalline field calculations.

$^3F_4$

The liquid-helium temperature spectrum of this group has 10 lines showing σ polarization and six lines having π polarization. This is more than the pure electronic transitions can account for. Some of these lines may be due to vibrational levels superimposed on

the electronic levels. The present identification of the Stark levels agrees with Johnsen except for the $\mu=\pm1$ component. This level is found to be at 12 627.0 cm^{-1} above the ground state, and it gives a better fit to the calculated level. The line identified by Johnsen as $\mu=\pm1$ was also observed. The latter line may be due to a vibronic transition. The calculated g_{11} seems to be in fair agreement with Johnsen's value as shown in Table II.

The upper $\mu=3$ crystal quantum level alone contributed 42% of the average deviation. If this line is taken as a vibrational level superimposed on the lower $\mu=3$ state, the average deviation is then reduced to 3 cm^{-1}.

$^3F_2$ and $^3F_3$

The observed spectrum is almost the same as reported by Johnsen. The calculated g_{11} for the $\mu=\pm2$ component of $^3F_2$ is 3.02 compared to an observed value of 3.08. The calculated g_{11} value for $^3F_3$ is the same as reported by Johnsen.

$^1G_4$

The identification of the Stark components agrees with Johnsen and Gruber and Conway except for the higher energy $\mu=3$ component. Like the $^3F_4$ group there are definitely some lines due to vibrational plus electronic transitions. This makes identification difficult. It may be that the component identified by Johnsen as $\mu=3$ is such a level.

Gruber and Conway also report a $\mu=0$ Stark component. Although this line was also observed in this work it was not possible to make a reliable identification since such a transition is forbidden by selection rules.

$^1D_2$

The spectrum of this group consists of two lines having σ polarization and one with π polarization at liquid nitrogen temperature. At liquid-helium temperature only one line remains. It exhibits σ polarization. This spectrum is very similar to the $^3F_2$ group.

The calculated crystal quantum levels give a good fit to the observed lines because the crystal field parameters were chosen that way. Gruber and Conway had a very poor fit for this group simply because they chose a different set of parameters. The configuration interaction does not seem to be as important as claimed by them.

Gruber and Conway also identify a $\mu=0$ component. This identification is apparently based on the assignment of the $\mu=\pm2$ ground level component which the authors were unable to confirm.

$^3P_0$, $^3P_1$, and $^3P_2$

These three groups were recorded using the Cary spectrophotometer at liquid-nitrogen temperature only. The $^3P_1\mu=\pm1$ component is identified as 36 516 cm^{-1} above the lowest Stark component at the ground level, and the $^3P_2\mu=\pm2$ component is found to be 38 204 cm^{-1} above the ground level.

Here again since the data is from the Cary instrument it is not used in crystalline field calculations.

CONCLUSION

A good fit has been obtained to theoretical calculations with a deviation of the order expected. Although the authors observed all the lines reported by Johnsen and by Gruber and Conway some of their assignments could not be confirmed. It should be noted that Johnsen identified all his lines as pure electronic transitions. However, it can be seen from the discussion of $^3F_4$ that some lines must be due to vibronic transitions.

It should also be noted that a discrepancy in a few wave numbers between the data reported here and Johnsen's is to be expected. Johnsen diluted his crystals with ytterbium whereas the crystals used in this work were diluted with lanthanum.

ACKNOWLEDGMENTS

The authors wish to acknowledge the friendly encouragement and helpful discussion of Professor Robert A. Satten and Dr. J. S. Margolis.

Tests for Chemisorption of Nitrogen on a Clean (100) Nickel Surface

H. H. MADDEN AND H. E. FARNSWORTH

Barus Physics Laboratory, Brown University, Providence, Rhode Island

(Received October 28, 1960)

Tests have been made for chemisorption of nitrogen on the (100) surface of a nickel crystal, using low-energy electron diffraction and photoelectric work-function determinations. No chemisorption was observed after exposures as high as 10^{-3} mm Hg min at room temperature or at 350°C.

THE adsorption of nitrogen on a (111) nickel surface, using low-energy electron diffraction, has been reported by Germer and Hartman.[1] During investigations of gas adsorption on a (100) nickel surface now under way, using low-energy electron diffraction and photoelectric work-function determinations, we have searched for evidence of adsorption of nitrogen on this surface.

The experimental apparatus is such that both work-function and structure determinations can be made under the same conditions.[2] Mercury diffusion pumps and molybdenum getters are used, and nonlubricated ground glass valves separate the experimental tube from the pumping system and the getter tube. These valves are closed during exposures to nitrogen. The crystal surface is cleaned by the method of argon-ion bombardment and anneal[3] after the initial production of an ultra-high vacuum of the order of 10^{-10} mm Hg. The crystal is mounted on a solid molybdenum cylinder which had been preoutgassed at high temperatures in an auxiliary vacuum system. The crystal is heated by conduction from the mounting which in turn is heated by electron bombardment. All tungsten filaments have been outgassed previously until they liberate a negligible amount of contamination during the ion bombardment and anneal processes. The nitrogen from a 1-liter Pyrex flask with a breakoff tip passes into a storage volume at low pressure, through a calibrated adjustable porous porcelain leak, and through a liquid-nitrogen trap before it enters the experimental tube. Care has been taken to eliminate contaminating gases from the storage volume and connecting lines. No hot filaments are present during the exposure at room temperature. Tests were made to ensure that the nickel surface was clean before exposure to nitrogen. The surface received a small anneal subsequent to ion bombardment since this condition yields most pronounced adsorption effects in the case of oxygen.[4] A nitrogen exposure was made at room temperature at a pressure of 5×10^{-5} mm Hg for 20 min.

After evacuation of the nitrogen, the nature of the diffraction pattern and its intensity were found to be identical with those for the clean surface. Photoelectric measurements, using the Fowler method,[5] were made before and after exposure to nitrogen under the same conditions as were used in the diffraction measurements. The resulting values of work function before and after the nitrogen exposure were the same.

To test for the possibility of activated adsorption, nitrogen was admitted with the crystal at a temperature of 350°C. In 10 min the crystal cooled from 350° to 160°C in the presence of nitrogen at a pressure of 5×10^{-5} mm Hg. During the first minute of the exposure, a tungsten filament was heated in the vicinity of the crystal. The diffraction pattern from the surface following this treatment was again the same as that for a clean surface.

It must therefore be concluded that nitrogen does not chemisorb on a clean (100) nickel surface under the above conditions.

[1] L. H. Germer and C. D. Hartman, Second Conference on Semiconductor Surfaces, preprint q. White Oak, Maryland, December 2–4, 1959; L. H. Germer, E. J. Scheibner, and C. D. Hartman, Phil. Mag. **5**, 222 (1960). (This article contains the statement: "... it has not been established with certainty that the adsorbed gas is nitrogen rather than an impurity gas ....")

[2] H. E. Farnsworth and H. H. Madden (to be published).

[3] H. E. Farnsworth, R. E. Schlier, T. H. George, and R. M. Burger, J. Appl. Phys. **29**, 1150 (1958).

[4] H. E. Farnsworth and J. Tuul, J. Phys. Chem. Solids **9**, 48 (1959).

[5] R. H. Fowler, Phys. Rev. **38**, 45 (1931).

Three-Dimensional FE-MO Model. I. ΔH of Dissociation of Homonuclear Diatomic Molecules

SHELDON L. MATLOW

Hoffman Electronics Corporation, El Monte, California

(Received July 5, 1960)

By means of a three-dimensional FE–MO model, the ΔH's of dissociation for homonuclear diatomic molecules can be estimated. The atoms are represented by cubes, and the molecules by rectangular parallelepipeds. The parameters involved are the sizes of the boxes and the effective mass of the electrons. The spectroscopic terms for the ground states of both the atoms and the molecules are obtained from the model.

I. INTRODUCTION

THE FE–MO (free electron-molecular orbital) model has had considerable success in both the one[1]- and two[2]-dimensional forms. We, therefore, decided to investigate the applicability of using a three-dimensional model. In this and subsequent papers in this series, we shall report the results of our applying the model to various different types of problems. In this paper we shall discuss the calculation of ΔH for the reaction

$$A_2 \rightarrow 2A, \tag{1}$$

where A is any main group atom (at the time of this writing, we do not know how to apply the model to the transition elements).

The energy of the jth level of the three-dimensional model is given in rectangular coordinates by[1]

$$E_j=(h^2/8m)\left[(n_x^2/a^2)+(n_y^2/b^2)+(n_z^2/c^2)\right]_j, \tag{2}$$

where the subscript j on the bracket means that the values of the quantum numbers n_x, n_y, and n_z are given the values which apply to the jth energy level. Equation (2) can be rewritten so that it refers to the energy per gram atom or gram molecule and the size of the box is given in angstrom units. Thus,

$$E_j=k\left[(n_x^2/a^2)+(n_y^2/b^2)+(n_z^2/c^2)\right]_j, \tag{3}$$

where

$$k=868 \text{ kcal A}^2\text{/gram atom or gram molecule.} \tag{4}$$

Since this model assumes a constant potential everywhere in the box,[1] but the actual potential will be more negative or more positive in certain volume elements depending on whether the nuclear attraction or the "other electrons" repulsion predominates, it is not unreasonable to assume that the "effective" mass of the electron will not be that of the free electron. If the electron is bound more tightly in the real system than the electron in the model, the "effective" mass will have to be greater than the true electron mass. This is because a greater force has to be applied to the bound electron to give it a given acceleration. Thus, it has a greater inertia (or greater effective mass) than the free electron. In this case, k will have a value smaller than that given in Eq. (4). Similarly, if the electron in the real system is more loosely bound than the electron in the model, k will be greater than the value given in (4).

II. ATOMIC ENERGY LEVELS

If we approximate the atom by a cube, the electronic energy of the atom, Ea, will be given by

$$Ea=(k/s^2)\sum_j f_j, \tag{5}$$

where

$$f_j=(n_x^2+n_y^2+n_z^2)_j, \tag{6}$$

and where s is the length of an edge of the cube in angstrom units. The dimension s is a modified van der Waals diameter. It can be represented as

$$s=2\alpha r, \tag{7}$$

where r is the single bond covalent radius and α is the ratio of the van der Waals radius to the single bond covalent radius. The experimental values of α for various atoms are listed in Table I. Except for hydrogen the values of α range from about 1.5 to 2.0. Introducing Eq. (7) into (5), we have

$$Ea=(k/4\alpha^2r^2)\sum_j f_j. \tag{8}$$

The first seven energy levels are the 1,1,1 singlet ($f_j=3$), the 1,1,2−1, 2, 1–2, 1, 1, triplet ($f_j=6$) and the 1,2,2−2, 1, 2−2, 2, 1 triplet ($f_j=9$). Since the s and p levels are, respectively, singlets and triplets, we associate the 1, 1, 1, and s levels and the 1, 1, 2−1, 2, 1–2, 1, 1, and p levels. The d levels are quintuplets, but our next set of levels is a triplet. From this we conclude that the model in its simple form is applicable only to s and p levels, and that the model ignores all but the valence electrons.

[1] G. W. Wheland, *Resonance in Organic Chemistry* (John Wiley & Sons, Inc., New York, 1955), pp. 550–559 and 675–694, references to earlier works are given.

[2] J. R. Platt, J. Chem. Phys. **22**, 1448 (1954).

TABLE I. Experimental values of α[a].

Element	Van der Waal radius[b,c]	Single bond covalent[b,d] radius	α
H	1.2	0.37[d]	3.24
N	1.5	0.74	2.03
O	1.40	0.74	1.89
F	1.35	0.72	1.875
P	1.9	1.1	1.73
S	1.85	1.04	1.78
Cl	1.80	0.99	1.82
As	2.0	1.21	1.65
Se	2.00	1.17	1.71
Br	1.95	1.14	1.71
Sb	2.2	1.41	1.56
Te	2.20	1.37	1.61
I	2.15	1.33	1.62

[a] α is the ratio of the van der Waals radius to the single bond covalent radius.
[b] In angstrom units.
[c] Taken from L. Pauling, *The Nature of the Chemical Bond* (Cornell University Press, Ithaca, New York, 1948), 2nd ed., p. 189.
[d] Taken from C. A. Coulson, *Valence* (Oxford University Press, New York, 1952), pp. 87 and 180. The H value is one-half the equilibrium internuclear distance in H_2.

III. MOLECULAR ENERGY LEVELS

For the molecules we use a rectangular parallelepiped. We choose the x direction as that of the interatomic axis. The y and z dimensions of the box are taken as s, the van der Waals diameter. For the x dimension we take $s+2r$. The $2r$ term is, of course, the interatomic distance. We are assuming that the box extends one van der Waals radius on either side of the atoms. Thus, if Em is the electronic energy of the molecule,

$$Em=(k/4r^2)\sum_i g_i, \tag{9}$$

where

$$g_i=\{[n_x^2/(1+\alpha)^2]+(n_y^2+n_z^2)/\alpha^2\}_i. \tag{10}$$

Ignoring the $P\Delta V$ term, since it will be small at room temperature (about 600 cal/mole), ΔH for reaction (1) will be

$$\Delta H=2Ea-Em. \tag{11}$$

Combining Eqs. (8), (9), and (11) and rearranging terms, we have

$$4r^2\Delta H=k(2\sum_j f_j/\alpha^2-\sum_i g_i). \tag{12}$$

IV. THE CALCULATION OF k

Since r and ΔH are experimentally known values and $\sum_j f_j$ and $\sum_i g_i$ can be calculated easily, once a value for α is chosen, we will use the model to calculate k. The criterion for the utility of the model will be how closely the values of k for various elements agree. Before we do this, however, we must decide on a value for α. As we have indicated above, a reasonable value would be between 1.5 and 2.0. In Table II we have listed the values of the g_i's for the first ten energy levels for values of α from 1.0 to 2.0 in steps of 0.25. We have also listed the term symbols to be associated with these levels for the second period.

It has been recently shown that the ground state of the C_2 molecule is the $^1\Sigma_g{}^+$.[3] This means that the $\pi_y2p-\pi_z2p$ doublet must lie lower than the $\sigma2p$ level. This is the case for $\alpha=1.75$ and $\alpha=2.00$. The $\alpha=2.00$ case, however, introduces an unnamed doublet at a lower energy than the σ^*2p. Thus, of the values considered, $\alpha=1.75$ seems to be the best choice. Throughout the remainder of this discussion we shall use this value for α. Although we have no conclusive evidence one way or the other, it is our guess that the unnamed doublet is the $(d_z^2-d_x^2)$ and $(d_{x^2-y^2}-d_{x^2-y^2})$ orbitals.

TABLE II. Values of g_i for different α's.

Energy level			Term symbol	g_i				
n_x	n_y	n_z		$\alpha=1.00$	$\alpha=1.25$	$\alpha=1.50$	$\alpha=1.75$	$\alpha=2.00$
1	1	1	$\sigma2s$	2.250	1.480	1.049	0.786	0.611
2	1	1	σ^*2s	3.000	2.073	1.529	1.183	0.944
3	1	1	$\sigma2p$	4.250	3.061	2.329	1.844	1.500
1	2	1	π_y2p	5.250	3.403	2.382	1.766	1.361
1	1	2	π_z2p					
2	2	1	$\pi_y{}^*2p$	6.000	3.996	2.862	2.163	1.694
2	1	2	$\pi_z{}^*2p$					
4	1	1	σ^*2p	6.000	4.444	3.449	2.770	2.278
3	2	1	?	7.250	4.984	3.662	2.824	2.250
3	1	2	?					

[3] E. A. Ballik and D. A. Ramsey, J. Chem. Phys. **31**, 1128 (1959).

It is interesting to note that for all values of α, O_2 is paramagnetic.

Let us represent the factor in the parentheses in Eq. (12) by the symbol q. In Table III we have listed the values of q for different numbers of valence electrons per atom. It is obvious that the number of "valence" electrons per molecule is equal to twice the number of valence electrons per atom. Since, in Eq. (12), both k and $4r^2$ are positive quantities, the negative values of g for the 4 and 16 "valence" electron molecules indicate that ΔH for reaction (1) must be negative in these cases. Stating this conclusion differently, we would say that these molecules are unstable with respect to the monatomic states. It is a well-known chemical fact that the alkaline earths and the inert gases do not form diatomic molecules from atoms in the ground state. The significance of the third column in Table III will be discussed later.

We can now calculate k for the various molecules. The results of these calculations are listed in Table IV. As we pointed out in Sec. II, the degeneracies of the energy levels led us to believe that the model was applicable only to the second period. When one considers the extreme crudity of the model, it is rather surprising that the spread for k for the second period elements is so small. When we "blindly" attempted to apply the model to the other elements for which we had data, the spread was much greater. In fact, the extremes H_2 and I_2, differed in their values of k by an order of magnitude.

It should be pointed out that, for molecules with multiple bonds such as N_2 and O_2, we used the single bond radii. We did this for the convenience of using a single value of α. The correct procedure would have been to use as the dimensions of the box $2\alpha r_1 \times 2\alpha r_1 \times (2\alpha r_1 + 2r_{11})$, where r_1 is the single bond radius and r_{11} is the multiple bond radius. The effect of this change (from r_1 to r_{11}) would be small (of the order of 10%) and would involve considerably more work. We, therefore, chose to ignore this error in our calculations.

TABLE III. Values of q.

Number of "valence" electrons per molecule	q	q (with d-orbital perturbation)	Examples
2	0.388	0.388	H_2, Li_2, Na_2
4	−0.028	−0.028	He_2, Be_2, Mg_2
6	0.360	0.452	B_2, Al_2, Ga_2
8	0.748	0.840	C_2, Si_2, Ge_2
10	0.980	1.228	N_2, P_2, As_2
12	0.574	0.822	O_2, S_2, Se_2
14	0.168	0.416	F_2, Cl_2, Br_2
16	−1.452	−1.204	Ne_2, Ar_2, Kr_2

TABLE IV. The calculation of k.

Element	r[a]	ΔH[b]	$4r^2\Delta H$	k	
H	0.37	104.2	57.06	147.1	545.5[d]
Li	1.34	26.4	189.6	488.7	
C	0.77	141.8	336.3	449.6	
N	0.74	226.0	494.9	505.0	
O	0.74	119.1	260.8	454.4	
F	0.72	37.8	78.4	466.7	
Na	1.54	18.0	170.8	440.2	
Si	1.17	75.0[e]	410.7	549.1	488.9[e]
P	1.10	116.9	565.8	577.3	460.7[e]
S	1.04	83.0	359.1	625.6	436.9[e]
Cl	0.99	57.8	226.6	1348.8	543.8[e]
K	1.96	12.26	188.4	485.6	
As	1.21	90.0	527.1	537.9	429.2[e]
Se	1.17	64.7	354.3	617.2	431.0[e]
Br	1.14	46.1	239.6	1426.2	576.0[e]
Rb	2.11	11.65	207.5	534.8	
Sb	1.41	69.0	548.7	559.9	446.8[e]
Te	1.37	53.4	400.9	698.4	487.7[e]
I	1.33	36.1	255.4	1520.2	613.9[e]
Cs	2.25	10.71	216.9	559.0	

[a] Taken from C. A. Coulson, *Valence* (Oxford University Press, New York, 1952), pp. 87 and 180. The H value is one-half the equilibrium internuclear distance in H_2. The values are in angstrom units.

[b] Calculated from data given by D. R. Stull and G. C. Sinke, *Thermodynamic Properties of the Elements* (American Chemical Society, Washington, D. C., 1956). The values are in kcal/mole of the diatomic molecule.

[c] J. Drowart, G. DeMaria, and M. G. Inghram, J. Chem. Phys. **29**, 1015 (1958).

[d] Based on the corrected value of α of 2.93.

[e] d-Orbital perturbation included.

V. PERTURBATION CALCULATIONS

Since the model worked so well for the second period, we proceeded to investigate the factors which could explain the large deviations observed for the other periods. As we pointed out in the discussion of Table I, the ratio of the van der Waals radius to the single bond covalent radius for hydrogen is much larger than that for any other element studied. The average value of the ratio for the second period is 1.93. We, therefore, assumed that the correct value of α to use for H_2 is 1.75 times the fraction 3.24/1.93. This gives a value of 2.93 for the "corrected" α. Using this value for α, we obtained the value of 545.5 for k for H_2.

This "correction" cannot be the explanation for the other deviations observed. Aluminum, silicon, phosphorus, and sulfur have all been shown to use d orbitals for bonding. We then considered how a d-orbital perturbation would affect the system. If we are correct in assuming that the 3, 1, 2–3, 2, 1 doublet is a $\pi(d)$ doublet, then we would expect to find the largest perturbation effect on the 3, 1, 1 level. We, therefore, somewhat arbitrarily, decreased the value of the 3, 1, 1 level from 1.844 to 1.720. (This value was chosen to give a reasonable k for silicon. When this value was used, it was found that the values of k for the other elements agreed well.) This is the means by which the perturbed q's of Table III were obtained. These q's were used for the calculations of the perturbed k values of Table IV. It should be pointed out that this perturba-

tion makes the ground state of Si_2 the $^3\Sigma$ state. This agrees with the conclusion of Douglas.[4]

The extreme values of k, when both the α correction and the d-orbital perturbation are included, are 613.9 (I_2) and 429.2 (As_2). The average value is 492.2. Thus, the highest value is 25% greater than the average and the lowest value is 13% smaller than the average. If we assume that the I_2 value is poor because of an f-orbital perturbation and, therefore, ignore it, the average value of k is 458.8. The highest value then is that for Br_2 and is 19% greater than the average; and the lowest value is still that of As_2 and is 12% lower than the average. In either case, the agreement is better than could have been expected.

[4] A. E. Douglas, Can. J. Phys. **33**, 801 (1955).

VI. EFFECTIVE MASS CONSIDERATIONS

In the discussion of Eq. (4) the relationship between the value of k for the model and the error introduced by the assumption of a constant potential in the box was mentioned. Since our value of k is about one-half that of the expected value, this leads us to conclude that the atomic electrons and the electrons in the diatomic molecules considered are less mobile than the simple model would suggest.

ACKNOWLEDGMENT

We would like to take this opportunity to thank N. Yagol of the Hoffman Electronics Corporation for the helpful discussions during the time these calculations were being made.

Proton Magnetic Resonance Studies of Structure, Diffusion, and Resonance Shifts in Titanium Hydride*

B. STALINSKI,† C. K. COOGAN,‡ AND H. S. GUTOWSKY

Noyes Chemical Laboratory, University of Illinois, Urbana, Illinois

(Received October 27, 1960)

Measurements of the proton magnetic resonance at ~26.9 Mc in titanium hydride samples, ranging in composition from $TiH_{1.61}$ to $TiH_{1.97}$, have been made in the temperature range from −196° to about 200°C. The second moment of the proton resonance at the lower temperatures shows that the hydrogen atoms are randomly distributed among the lattice sites which are located tetrahedrally with respect to the titanium atoms. Self-diffusion of the hydrogen atoms narrows the proton resonance above room temperature. The temperature dependence of the correlation frequency for the proton motions, obtained from the linewidths, leads to diffusional activation energies which increase with hydrogen content from 9.4 kcal/g atom for $TiH_{1.607}$ to 10.2 for $TiH_{1.923}$. Moreover, the diffusion rate is directly proportional to the number of unfilled tetrahedral holes in the metallic lattice, which indicates that the self-diffusion takes place via a vacancy mechanism.

Proton resonance shifts to *higher* applied magnetic fields were observed. They were measured at room temperature for all specimens and were found to increase from 0.01% for $TiH_{1.607}$ to about 0.032% for $TiH_{1.969}$. For these two extreme compositions, the temperature dependence of the shift was measured between −95°C and 190°C and was found to be similar to the bulk susceptibility, the shifts for $TiH_{1.969}$ exhibiting an anomaly at about 13°C as does the susceptibility. These results are interpreted semiquantitatively in terms of exchange interactions which pair spins of electrons in the conduction band with those of electrons localized on the hydrogen. The results suggest that the hydrogen is held in the lattice by a combination of covalent and ionic bonding, the latter involving a net positive charge on the hydrogen. The general importance of exchange interactions in intermetallic compounds is commented upon.

I. INTRODUCTION

THE original purpose of these experiments was to investigate the nature of the anomalies observed near room temperature in the magnetic susceptibility[1,2] and in the specific heat[3] of titanium hydrides ranging in composition from about $TiH_{1.5}$ to TiH_2. X-ray[4,5] and neutron diffraction[6] studies have shown that in the region of these anomalies, the titanium hydrides undergo a small, continuous tetragonal deformation typical of a second-order transition. At temperatures above the anomalies, the hydrides have a face-centered cubic arrangement of titanium atoms, surrounded by hydrogen atoms apparently in the tetrahedrally located holes. That is, when the composition approaches the stoichiometric compound, TiH_2, it achieves the CaF_2 structure. Our particular interest was the possibility that hydrogen diffusion is connected with the structural transition and with the magnetic and specific heat anomalies.

Nuclear magnetic resonance methods are attractive for investigating self-diffusion in the solid state[8,7]. Hydrogen diffusion is especially difficult to measure in metal lattices by classical transport experiments, because gross errors result from grain boundaries, pores, cracks, and dislocations in the metals. For example, the data reviewed by Barrer[9] for hydrogen diffusion in palladium include activation energies ranging from 4.6 to 17.8 kcal/g atom. The most extensive prior study of hydrogen diffusion by proton magnetic resonance appears to be the work done on the palladium hydride system. Norberg[10] found narrow proton resonance lines in a series of samples up to $PdH_{0.8}$ and obtained activation energies for self diffusion by using rf pulse techniques to observe the temperature dependence of the spin-lattice relaxation time between 250° and 300°K. Similar results were reported by Torrey,[11] who also investigated the proton T_1 in $TiH_{1.77}$. A few scattered observations have been made of the proton resonance in other solid metal hydrides. Garstens[12] has looked at the proton resonance of NaH and CaH_2, finding broad lines typical of rigid-lattice solids. For tantalum hydride he found[13] a broad line at temperatures below 215°K with diffusional narrowing occuring at higher temperatures.

In the case of titanium hydride, Garstens[12] noted a broad room-temperature, proton linewidth of about 12 gauss for three samples of composition $TiH_{0.33}$, $TiH_{0.72}$,

* This work was supported in part by the Office of Naval Research.

† On leave of absence from the Institute of Technology and the Institute of Physical Chemistry of the Polish Academy of Sciences, Wroclaw, Poland.

‡ On leave of absence from the Division of Chemical Physics, C.S.I.R.O. Chemical Research Laboratories, Melbourne, Australia.

[1] W. Trzebiatowski and B. Stalinski, Bull. acad. polon. sci. Classe III **1**, 131 (1953).

[2] B. Stalinski, Zeszyty Nauk. Politech. Wroclaw. Chem. **4**, 25 (1957).

[3] B. Stalinski and Z. Biegański, Bull. acad. polon. sci. Serie sci. chim. geol. geogr. **8**, 243 (1960).

[4] B. Stalinski and B. Idziak (unpublished).

[5] H. L. Yakel, Acta Cryst. **11**, 46 (1958).

[6] S. S. Sidhu, L. Heaton, and D. D. Zauberis, Acta. Cryst. **9**, 607 (1956)

[7] H. S. Gutowsky, Phys. Rev. **83**, 1073 (1951).

[8] C. P. Slichter in *Report of the Bristol Conference on Defects in Crystalline Solids* (The Physical Society, London, 1955), p. 52.

[9] R. M. Barrer, *Diffusion in and through Solids* (Cambridge University Press, New York, 1951), 2nd ed.

[10] R. E. Norberg, Phys. Rev. **86**, 745 (1952).

[11] H. C. Torrey, Nuovo cimento Suppl. to **9**, Ser. **10**, 95 (1958).

[12] M. A. Garstens, Phys. Rev. **79**, 397 (1950).

[13] M. A. Garstens, Phys. Rev. **81**, 288 (1951).

and $TiH_{1.87}$. Similar results were obtained in the more recent room-temperature studies by Maluchkov and Finkelstein[14]; they also made some unsuccessful attempts to measure proton resonance shifts and to obtain the second moment of the proton absorption and compare it with the value calculated for the rigid lattice. Our more detailed studies which were outlined in a preliminary report,[15] failed to establish any direct connection between the hydrogen diffusion and the various anomalies which occur in the titanium hydrides. However, it proved possible to characterize the diffusion process in very interesting detail by observing the temperature dependence of the proton linewidth over a wide range of composition and temperature. Also, we have found large, negative Knight shifts[16] in the proton magnetic resonance position. The temperature and concentration dependences of the shift parallel the magnetic susceptibility and demonstrate that the anomalies are associated with the conduction electrons. The details of our various findings are presented here.

II. EXPERIMENTAL DETAILS

A. Preparation of Samples

The titanium hydride samples were of the composition $TiH_{1.607}$, $TiH_{1.719}$, $TiH_{1.775}$, $TiH_{1.845}$, $TiH_{1.933}$, and $TiH_{1.969}$. They were prepared by the absorption of known volumes of high purity hydrogen in the apparatus described previously.[17] The hydrogen was obtained by thermal decomposition of another sample of titanium hydride. The titanium was produced by E. I. du Pont de Nemours and Company. The purity was listed as better than 99.5%. Spectral analysis revealed the presence of the following impurities, in weight percent: $Si \sim 10^{-3}$, $Mg \sim 10^{-3}$, $Mn \sim 10^{-4}$, $Sn \sim 10^{-2}$, $Cu \sim 10^{-3}$, $Fe \sim 10^{-3}$. Moreover, bulk magnetic susceptibility measurements gave no evidence of ferromagnetic impurities.

The titanium metal powder used to prepare the samples was obtained by powdering some of the embrittled metal. The latter was made by saturating the original sponge metal with hydrogen and then degassing it by heating in a high vacuum for several hours at a temperature of about 820°C. This temperature should be somewhat lower than the α–β transition point of the metal to prevent sintering. All of the hydride samples, except $TiH_{1.969}$, were synthesized by slowly cooling 2.5 to 4 g of the metal powder, in contact with the hydrogen gas, from 450°C to a temperature at which essentially all of the gas had been absorbed. The sample was then held for 20 to 40 hr at this temperature, which was usually 250°C or somewhat higher. Of these five samples, all but $TiH_{1.933}$ showed a dissociation pressure of 10^{-2} mm Hg or less at 200°C. The $TiH_{1.933}$ showed a dissociation pressure as high as 1 mm Hg at 200°C, so its hydrogenation was completed at 150°C where the pressure dropped to about 10^{-2} mm Hg.

The sample of highest hydrogen content $TiH_{1.969}$ was prepared by gradually lowering the temperature from 450°C to room temperature, using an excess pressure of hydrogen. This sample was sealed under a hydrogen pressure of 431 mm Hg to prevent decomposition in the magnetic resonance experiments carried out above room temperature. At such pressures of hydrogen, the saturation of the metal with hydrogen is essentially complete at temperatures below 200°C. This is shown by the 5-mm drop observed in the hydrogen pressure upon cooling a sample from 300°C to room temperature. In the vacuum apparatus used, this pressure change corresponds to a composition change of $TiH_{1.957}$ to $TiH_{1.969}$.

Microscopic examination ($\times 100$) of the particles revealed, of course, a considerable apread in particle size, but it was apparent that no particles were larger than 10^{-3} cm in diameter. The samples actually used in the magnetic resonance experiments were about 1 cc in volume and, except as noted for $TiH_{1.967}$, they were sealed under their equilibrium pressure of H_2 in glass tubes whose outer diameter was about 9 mm.

B. Apparatus and Procedure

The broad-line regenerative spectrometer used in these experiments was similar to that described previously.[18] It was operated at a fixed radio frequency of about 26.92 Mc, and the derivative of the proton absorption was observed by automatically sweeping the field of the 6300-gauss permanent magnet. The 30-cps modulation amplitude was kept small to reduce its broadening of the absorption, and in cases where the modulation had to be large due to a low signal-to-noise ratio, the appropriate corrections were made.[19] Care was taken to prevent saturation of the lines, but in some cases it appeared that these efforts were not completely successful. The volume of the sample coil was about 1.5 cc. The high conductivity of the samples led to appreciable losses in the rf coil; this required the use of higher plate voltages and greater feedback than usual in the marginal oscillator stage of the spectrometer.

Measurements below room temperature were made with a Dewar-type cryostat,[18] using either liquid nitrogen or a dry-ice and alcohol slush as the refrigerant. Higher temperatures were obtained with a gas flow cryostat. The temperature of the sample was measured by means of a copper-constantan thermocouple at-

[14] O. T. Maluchkov and B. N. Finkelstein, Doklady Akad. Nauk S.S.S.R. **127**, 822 (1959).
[15] B. Stalinski, C. K. Coogan, and H. S. Gutowsky, J. Chem. Phys. **33**, 933 (1960).
[16] W. D. Knight, Solid State Phys. **2**, 93 (1956).
[17] W. Trzebiatowski, A. Sliwa, and B. Stalinski, Roczniki Chem. **28**, 12 (1954).
[18] H. S. Gutowsky, L. H. Meyer, and R. E. McClure, Rev. Sci. Instr. **24**, 644 (1953).
[19] E. R. Andrew, Phys. Rev. **91**, 425 (1953).

tached to the outside of the sample tube with a heat-resistant glass tape.

The resonance shifts were measured by comparing the magnetic field at the center of the proton absorption in the titanium hydrides with that in a silicone polymer, Dow-Corning Silastic Gum 400. Small pieces of the silicone gum were inserted between the turns of the rf coil, so that the spectrum recorded was that of the hydride with a small signal from the silicone superimposed. The proton linewidth in the silicone is about 2 cps at room temperature and it is narrow enough to be a good reference over a wide temperature range. In the case of the lowest temperatures, about −95°C, at which the shift was measured, tetramethyl silane was used as the reference. It was sealed into thin glass capillaries which were inserted in the rf coil beside the tube containing the hydride.

III. RESULTS AND DISCUSSION

Our presentation of the results is divided into three main sections: the low-temperature rigid-lattice second moments, the diffusional narrowing of the absorption at higher temperatures, and the resonance shifts. One feature common to all of the experiments is that the absorption lines are simple, bell-shaped curves with no evidence of structure. Moreover, although the lines narrow at higher temperature, their shape otherwise remains essentially the same.

A. Low-Temperature Second Moments

Experimental Results

The broad absorption lines observed at liquid nitrogen temperature do not begin to narrow appreciably until room temperature or above, depending upon hydrogen content. This suggests that the low temperature corresponds to a "rigid lattice" and that some structural information might be gained from a detailed analysis of the second moments.

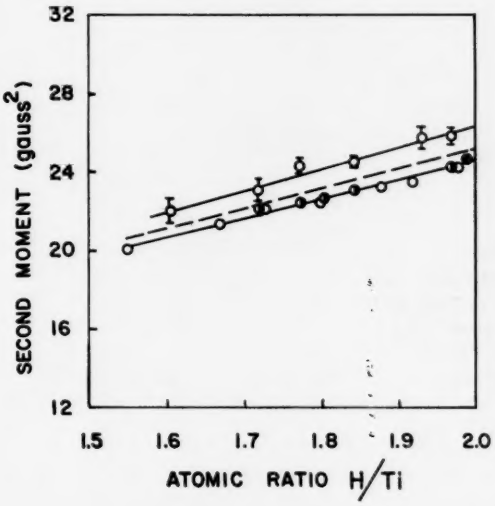

FIG. 1. The dependence of the proton second moment upon the hydrogen content of titanium hydride. The upper curve is a least-squares straight line fitted to the experimental points Φ for −196°C. The lower solid curve is a least-squares straight line fitted to second moments calculated for room temperature from the fcc lattice parameters of the following authors: ○ B. Stalinski [Zeszyty Nauk. Politech. Wroclaw. Chem. **4**, 25 (1957)]; ◑ B. Stalinski and B. Idziak, unpublished results; ● H. L. Yakel [Acta Cryst. **11**, 76 (1958)]. The calculations assume a random distribution of the protons among the tetrahedral sites. The dotted curve represents the conversion to −196°C of these room temperature theoretical values, by correcting for the tetragonal deformation and thermal contraction.

TABLE I. Linewidths and second moments of the proton magnetic resonance absorption in titanium hydride at −196°C.

Composition	Observed linewidth[a,b]	Observed second moment	Theoretical second moment[c]
$TiH_{1.607}$	12.1±0.1 gauss	22.0±0.7 gauss²	21.3 gauss²
$TiH_{1.719}$	12.4±0.2	23.1±0.6	22.4
$TiH_{1.775}$	12.7±0.2	24.3±0.45	23.0
$TiH_{1.845}$	13.1±0.1	24.5±0.15	23.7
$TiH_{1.933}$	13.5±0.15	25.7±0.55	24.6
$TiH_{1.969}$	13.5±0.2	25.8±0.45	24.9

[a] The full width between the maximum and minimum on the derivative curve.
[b] The errors are the standard deviations of from 5 to 10 measurements.
[c] These values assume that the protons are distributed, at random, in the tetrahedral sites only; they were obtained by applying corrections for the tetragonal deformation and thermal expansion to second moments calculated for the fcc structure at room temperature. The latter were taken from the straight line at the bottom of Fig. 1, drawn through the points calculated from the room-temperature lattice parameters of various authors for different hydrogen content.

Experimental values for the second moments were obtained by numerical integration of several derivative curves recorded at −196°C for each of the six samples. The results are summarized in Table I and show a systematic increase with hydrogen content, from 22.0 gauss² for $TiH_{1.607}$ to 25.8 gauss² for $TiH_{1.969}$. The linear extrapolation indicated in Fig. 1 gives a value of 26.3 gauss² for the second moment of the stoichiometric compound TiH_2 at −196°C. These values have been corrected for the magnetic-field modulation broadening which was of the order of 4% for all of the measurements. The linewidths, defined as the separation in gauss between the inflection points of the absorption, show an increase from 12.1 to 13.5 gauss paralleling that in the second moment. These values agree with that of 12 gauss reported by Garstens[12] for $TiH_{1.57}$ at room temperature. However, our linewidths and second moments are about 20% less than the values reported by Maluchkov and Finkelstein[14] for room temperature. The discrepancies may be due, at least in part, to the fact that the signal-to-noise ratio is much better at −196°C than at room temperature.

Theoretical Second Moments

Theoretical second moments of the proton absorption may be calculated from Van Vleck's results for the dipolar broadening in a rigid lattice. For a crystal powder, the relation is of the form[20]

$$\Delta H_2^2=(\tfrac{6}{5})I(I+1)g^2\mu_0^2N^{-1}\sum_{j>k}r_{jk}^{-6}, \qquad (1)$$

where, for our purposes, I and g are the proton spin and magnetogyric ratio, respectively, N is the number of protons in the crystal, and r_{jk} is the separation of protons j and k. There are similar terms[20] for the dipolar broadening of the proton resonance by the Ti^{47} and Ti^{49} nuclei; however, they constitute only about 0.5% of the total. Therefore, although they were included in the numerical results given, we shall not refer to them again.

In principle, the substitution into Eq. (1) of an experimentally observed second moment can lead to the determination of one structural parameter. However, there is also the observed, essentially linear dependence of the second moment on hydrogen content, and an additional structural feature might be inferred from it. The positions of the titanium atoms in the unit cell have been obtained quite accurately from x-ray diffraction studies.[4,5] However, the location of the protons is not known with any assurance.[5,6] In particular, there are two types of interstitial sites which the protons might occupy in the titanium lattice. One set is located in tetrahedral positions with respect to the titanium atoms; the other, in octahedral. There is also the question as to whether or not the sites occupied in the nonstoichiometric hydrides are located at random. The situation is favorable, inasmuch as there are two observed quantities and two structural questions.

Nonetheless there are some complications in comparing the experimental second moments with values calculated for various possible distributions of the protons. The experimental values are most accurate at liquid nitrogen temperatures because of the better signal-to-noise ratio at low temperatures. Moreover, at low temperatures the residual motional narrowing of the absorption will be less. However, most of the known structural parameters and their dependence upon hydrogen content have been determined at room temperature. Also, because of the second-order phase transition, the calculation of low-temperature second moments from these data must take into account not only the volume change at lower temperature but also the slight tetragonal deformation of the unit cell. Fortunately both effects are small and can be described with sufficient accuracy by a simple analytic expression so that the comparison of experimental and theoretical second moments for different temperatures can be readily made.

The lattice constants of the tetragonal unit cell are identified as $a=b\neq c$, where $c=a(1+\Delta)$; and the lattice constant of the cubic cell, as a_0. By comparing the sums of the contributions from the first and second nearest neighbors, which constitute about 90% of $\sum_{i>j}r_{ij}^{-6}$ in Eq. (1) for the tetragonal and cubic crystals, we find that the two total lattice sums are related by the following approximate equation,

$$a^6\sum_t\cong a_0^6(1-2\Delta+4\Delta^2)\sum_c. \qquad (2)$$

The subscripts t and c refer to the tetragonal and cubic crystals, respectively, and it is assumed that Δ is small compared to unity. Thermal expansion is incorporated into Eq. (2) by using the relations $V_t=a^3(1+\Delta)$ and $V_c=a_0^3$ to eliminate a^6 and a_0^6 in Eq. (2). This gives the final result

$$\sum_t\cong(1+\Delta^2)(V_c/V_t)^2\sum_c, \qquad (3)$$

which permits us to interconvert second moments at -196°C and at room temperature, providing we know the cubic lattice parameter at room temperature, the thermal expansion, and Δ.

The x-ray studies[4,5] show that the axial ratio c/a is about 0.945 at liquid nitrogen temperature. Hence, taking Δ to be -0.055 and introducing the observed change in molar volume with temperature,[5] Eq. (3) leads to a second moment at -196°C which is about 2% larger than at room temperature. This agrees well with the approximate 0.5-gauss[2] difference actually observed and suggests that there is no significant change in the motional effects on going from room temperature to -196°C.

Location of the Hydrogen Atoms

Let us now consider the question of the location of the hydrogen atoms. If octahedral as well as tetrahedral sites are occupied, the observed second moment will be the following average of the second moments for protons in each of the sites,

$$\Delta H_2^2=f_{oct}(\Delta H_2^2)_{oct}+f_{tet}(\Delta H_2^2)_{tet}, \qquad (4)$$

where the f's are the fractions of the protons in each type of site. We now assume a random distribution within each type of site and define the probability of an octahedral site being occupied as α and a tetrahedral site β. Bearing in mind that there are twice as many tetrahedral sites as octahedral, this gives

$$f_{oct}=\alpha/(2\beta+\alpha) \quad \text{and} \quad f_{tet}=2\beta/(2\beta+\alpha). \qquad (5)$$

Furthermore, in the compound $TiH_{2-\delta}$, α and β are related to δ as follows,

$$(2\beta+\alpha)=(2-\delta) \quad \text{or} \quad 2\beta=(2-\delta-\alpha). \qquad (6)$$

The second moments $(\Delta H_2^2)_{oct}$ and $(\Delta H_2^2)_{tet}$ in

[20] H. S. Gutowsky, G. B. Kistiakowsky, G. E. Pake, and E. M. Purcell, J. Chem. Phys. **17**, 972 (1949).

Eq. (4) require the computation of the lattice sums $N^{-1}\sum_{i>j} r_{ij}^{-6}$ of Eq. (1). However, the octahedral sites are equivalent, as are the tetrahedral. Therefore, we need only to pick a particular filled site of each kind, labeled o and t, and compute the sums $\frac{1}{2}\sum_j r_{oj}^{-6}$ and $\frac{1}{2}\sum_j r_{tj}^{-6}$ to all other filled sites j. The assumed random distribution of filled sites makes it easier to take the sums over all sites k, weighting each by the probability of its being occupied. For the protons in the octahedral sites, this approach gives

$$(\Delta H_2^2)_{oct}=(\tfrac{6}{5})I(I+1)g^2\mu_0^2\tfrac{1}{2}\sum_j r_{oj}^{-6}, \quad (7)$$

with

$$\sum_j r_{oj}^{-6}=\sum_k r_{ok}^{-6}p_k=\sum_l r_{ol}^{-6}\alpha+\sum_m r_{om}^{-6}\beta$$
$$=(115.6\alpha+1322\beta)a_0^{-6}. \quad (8)$$

The indices l and m designate all octahedral and all tetrahedral sites, respectively, surrounding the nucleus at the origin of the summation. Similarly, for the protons in the tetrahedral sites, one finds

$$\sum_j r_{tj}^{-6}=\sum_k r_{tk}^{-6}p_k=\sum_l r_{tl}^{-6}\alpha+\sum_m r_{tm}^{-6}\beta$$
$$=(660.5\alpha+537.7\beta)a_0^{-6}. \quad (9)$$

The numerical values for the sums in the fcc structure are from the literature[21]; they may be assigned by noting that the octahedral-tetrahedral spatial relationship is equivalent to that of Ca and F in CaF_2, and that the octahedral holes and tetrahedral holes lie on a fcc and a simple cubic lattice, respectively.

The appropriate substitution of Eqs. (5)–(9) in Eq. (4) gives the dependence of the second moment upon the probability α of an octahedral site being occupied,

$$\Delta H_2^2=[(2-2\delta+2.92\alpha-1.46\alpha\delta-1.74\alpha^2+0.5\delta^2)/(2-\delta)]$$
$$\times(\Delta H_2^2)_{tet}^\circ, \quad (10)$$

where $(\Delta H_2^2)_{tet}^\circ$ is the second moment for the stoichiometric hydride with only tetrahedral sites occupied. For the case $\delta=0$, or TiH_2, this becomes

$$\Delta H_2^2=(1+1.46\alpha-0.87\alpha^2)(\Delta H_2^2)_{tet}^\circ. \quad (11)$$

A value of 24.6 gauss^2 is obtained for $(\Delta H_2^2)_{tet}^\circ$ by extrapolating the theoretical values in Fig. 1 to $\delta=0$. This is to be compared with the experimental value of 25.7 gauss^2, which is the 26.3 gauss^2 observed at -196°C, corrected for thermal expansion and the lattice change. Thus the observed second moment is about 4% larger than that calculated for the fcc hydride with only tetrahedral sites occupied. It follows from Eq. (11) that $\alpha=0.025$ and that the proportion of *all* hydrogen atoms in octahedral sites is about 1.25%.

[21] H. S. Gutowsky and B. R. McGarvey, J. Chem. Phys. **20**, 1472 (1952).

Actually this is an upper limit to the fraction of protons occupying octahedral sites because there are several other factors which can give an increase in the second moment. One might expect the observed second moment to be low because of the residual motional narrowing effects. However, the symmetry of the lattice is such that for even moderately large amplitude oscillations, as many interproton distances are decreased as are increased and by about the same amount, so the net effect is very small. On the other hand, there are several possible broadening mechanisms, including spin-lattice relaxation, saturation, nonrandom distribution of the protons, and anisotropy in the tetragonal lattice of the large proton resonance shifts. The T_1 broadening could be as much as 0.3 gauss^2 if the proton T_1 were related to the resonance shift in the same fashion as found for pure metals[21]; but direct measurement of the proton T_1 gives somewhat longer times[11] ($\sim$0.3 sec) than predicted on this basis ($\sim$0.1 sec), and the probable broadening from this cause is correspondingly less. The T_1 is long enough for saturation broadening to occur and there was some evidence for it even though efforts were made to operate the experiments at very low rf levels. In Sec. III.B., it is pointed out in the discussion of the diffusion mechanism that about 1.25% of the tetrahedral sites are inaccessible to hydrogen. If these inaccessible sites are clustered, as indeed appears to be very likely, then the second moment of $TiH_{2-0.025}$ should be $(\Delta H_2^2)_{tet}^\circ$, which would account for about $\frac{1}{4}$ of the 4% discrepancy. The tetragonal deformation is about 5% at -196°C; if there were a corresponding anisotropy in the large proton shifts, it alone would account for the difference.

A final argument on this point also concerns the question of random versus nonrandom distribution of the hydrogen in the lattice. In principle, the latter question can be answered by the dependence of the second moment upon hydrogen content. If the protons were distributed at random among the tetrahedral sites, one would predict, for example, that the second moment would be given by

$$\Delta H_2^2=[(2-\delta)/2](\Delta H_2^2)_{tet}^\circ, \quad (12)$$

which is obtained by setting $\alpha=0$ in Eq. (10). At the other extreme, if the "clustering" of protons were complete so that the sample was a two-phase system of pure metal and pure stoichiometric hydride TiH_2 the second moment would be $(\Delta H_2^2)_{tet}^\circ$, independent of average composition. Less extensive clustering leads to a smaller second moment, but one still larger than that for a random distribution.

At first glance, Eq. (12) would seem to predict a straight line through the origin. However, $(\Delta H_2^2)_{tet}^\circ$ is itself a function of δ via the dependence of the unit cell size upon hydrogen content. The calculated values plotted in Fig. 1 include this dependence; the result over the composition range of $\delta=1.55$ to $\delta=1.98$ is

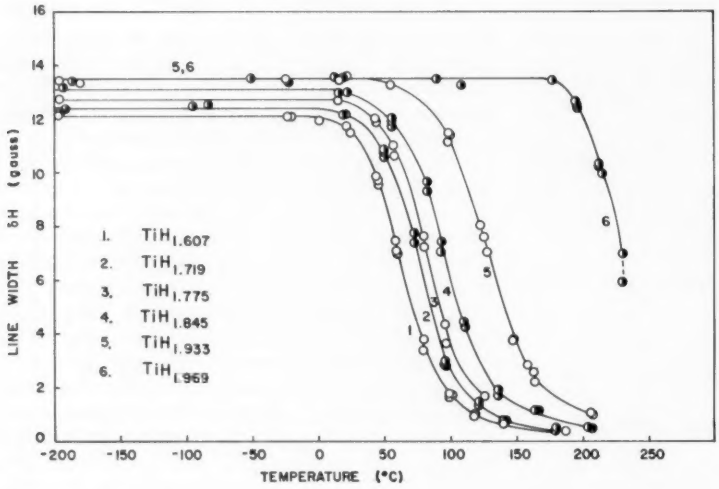

FIG. 2. The observed proton linewidth plotted as a function of temperature for the titanium hydride samples. Not all experimental points have been shown, to avoid confusion. The effect of decomposition in sample 6 at high temperature is shown by the dotted line.

nonetheless a good straight line, but it has a $\delta=0$ intercept of about 7 gauss[2] rather than zero. The experimental points agree quite well with this calculated line except for the 4% displacement already noted. Also, the experimental line has a slightly steeper slope than the theoretical, and the experimental points could be fitted somewhat better by a parabolic curve, concave downwards. This sort of nonlinear behavior, if real, could result from a small tendency for cluster formation. On the other hand, if the excess broadening is from anisotropy of the proton resonance shift, the strong concentration dependence of the latter would account for the difference in slope and shape of the theoretical and experimental curves. The latter explanation is favored.

B. Diffusional Narrowing

Experimental Results

Figure 2 shows the linewidth plotted as a function of temperature for each of the six samples. The linewidth is defined here as the full separation between the maximum and the minimum of the first derivative of the absorption. It can be seen that the linewidth is substantially constant at low temperatures but that the absorption narrows quite rapidly with increasing temperature starting near room temperature. Moreover, the temperature at which the linewidth reaches half its maximum value depends on the hydrogen content of the sample, increasing from 66°C for $TiH_{1.607}$ to 130°C for $TiH_{1.933}$, as listed in Table II. In the region

TABLE II. Summary of quantities obtained from the diffusional narrowing of the proton resonance observed in the nonstoichiometric hydrides $TiH_{2-\delta}$.

δ	$T_{\frac{1}{2}}$[a]	E_a	A[b]	ν_0[c]
0.393	66°C	9.4±0.5 kcal	1.69×10^{11} sec^{-1}	0.41×10^{12} sec^{-1}
0.281	88	9.85	2.08	0.80
0.225	86	9.85	1.64	0.80
0.155	97	10.45	2.35	1.74
0.067	130	10.2	0.56	1.23
0.031	232(?)	...	...	...

[a] $T_{\frac{1}{2}}$ is the temperature at the center of the linewidth change.
[b] A is the frequency factor obtained by fitting the $\log \nu_c$ vs $1/T$ plots with the equation $\nu_c=A\exp(-E_a/RT)$.
[c] ν_0 is the frequency factor corrected for the dependence of ν_c upon the probability that a hydrogen has a neighboring vacant site into which it can jump; see Eq. (15).

of rapidly changing linewidth, it was found to be important to "equilibrate" the sample for about an hour before making a measurement. Otherwise, thermal inhomogeneities could lead to appreciable errors.

Decomposition of a sample at higher temperatures also could lead to spurious results. If decomposition did occur, the sample would give results expected for a sample of lower hydrogen concentration, and the apparent linewidth change would be displaced to lower temperatures from the actual curve for the undecomposed specimen. Evidence for such decomposition was found only in the case of $TiH_{1.969}$, the sample containing the largest concentration of hydrogen. For this sample, decomposition at high temperatures led to a discontinuous decrease in linewidth. However, upon slow recooling, the sample reverted to its original composition, as shown by its linewidth and second moment. None of the other samples exhibited such behavior or any thermal hysteresis in the line shape, so it is believed that decomposition was important only in $TiH_{1.969}$ at high temperatures. This is consistent with the conditions under which the samples could be prepared.

Activation Energy for Hydrogen Diffusion

The only type of motion which can produce the observed averaging out of the dipolar broadening is self-diffusion of the hydrogen. The extent of the narrowing depends upon the rate at which the motions occur, as shown by the analyses of BPP[22] and of Kubo and Tomita.[23] The rate of the motions is described by the correlation frequency ν_c, which may be calculated from the width δH of the partially narrowed line by means of the following slightly modified form of the BPP equation

$$\nu_c = 2(2\ln 2)^{\frac{1}{2}}\Delta\nu/\tan[\pi(\delta H/\delta H_0)^2/2], \qquad (13)$$

where $\Delta\nu$ is the observed linewidth in cycles per second, and δH_0 is the observed rigid-lattice linewidth in gauss. This equation is applicable only to a line shape which is Gaussian in the low-temperature limit.

Fortunately, the proton line shapes observed in the hydrides are very nearly Gaussian, as borne out by the fact that the ratio of δH to the root second moment, ΔH_2, is approximately 2. In addition, the general shape of the absorption is preserved in the narrowed lines, so that any errors resulting from the slightly non-Gaussian character should be systematic. In any event, we have used Eq. (13) to calculate the temperature dependence of ν_c from the observed temperature dependence of δH. These calculations were made only for linewidths for which $\delta H/\delta H_0$ lies between about 0.1 and 0.85. For narrower linewidths, inhomogeneity and T_1 broadening introduces errors; while for broader lines, errors result from approximations in the BPP theory.

[22] N. Bloembergen, E. M. Purcell, and R. V. Pound, Phys. Rev. **73**, 679 (1948).

[23] R. Kubo and K. Tomita, J. Phys. Soc. Japan **9**, 888 (1954).

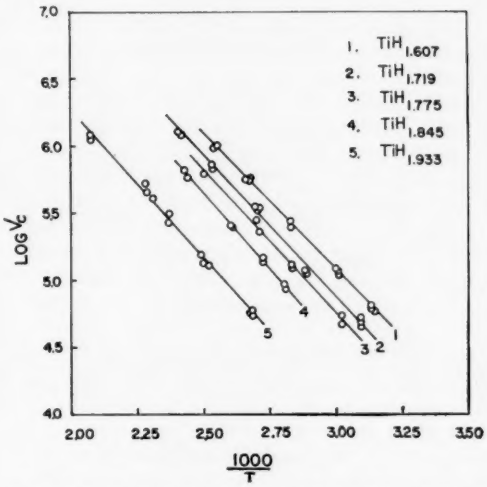

FIG. 3. The Arrhenius plot of the diffusional correlation frequency ν_c, for the five samples for which this plot was possible. The values for ν_c were obtained from the linewidths given in Fig. 2, using Eq. (13). The least-squares straight lines are drawn through the data for each sample.

The logarithm of ν_c has been plotted in Fig. 3 as a function of the inverse of the absolute temperature. It can be seen that these Arrhenius plots give a straight line for each of the samples. The straight lines in the figure were obtained by a least-squares fit of the data for each sample. The lines are very nearly parallel to one another. The activation energy E_a for self-diffusion of the hydrogen can be obtained from the slopes of the lines. The values range from 9.4±0.5 kcal/g atom for $TiH_{1.607}$ to 10.4±0.5 kcal/g atom for $TiH_{1.933}$. The results are listed in Table II and are plotted as a function of composition in Fig. 4. It appears that there is a small linear increase in E_a with hydrogen content; however, the increase is of the same order as the possible experimental error. The least-squares linear fit of the data gives an extrapolated value of 10.5 kcal/g atom for E_a in the stoichiometric hydride TiH_2. These results are considered in more detail in a subsequent paper.[24] It describes a very simple electrostatic model which leads to a semiquantitative explanation of the diffusional activation energy and the dependence upon hydrogen content.[24a]

[24] C. K. Coogan and H. S. Gutowsky, J. Chem. Phys. (to be published).

[24a] W. Spalthoff has recently investigated the proton magnetic resonance in a number of hydrides including one titanium hydride, of composition $TiH_{1.98}$. For this sample he reports a low-temperature (−190°C) linewidth of 11.8 gauss and the narrowing of the absorption at higher temperatures, centered at approx 150°C. In addition, his analysis of the linewidth change gives an activation energy for proton diffusion of 5.8±0.8 kcal/mole. These values are all significantly below those which we report. Discrepancies of this nature would result if his sample had suffered decomposition at the high temperatures 250–300°C which he used in his experiments. We wish to thank Dr. Spalthoff for making his manuscript available to us prior to its future publication in Z. physik. Chem.

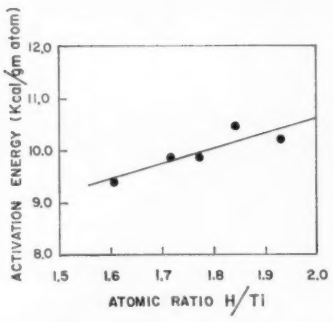

FIG. 4. The activation energy for hydrogen diffusion as a function of composition. The activation energies shown are determined from the least-squares analysis of the data given in Fig. 3.

Diffusion Mechanism

The nature of the diffusion mechanism in our samples is shown with remarkable clarity and directness by the dependence of the diffusional jump frequency ν_c upon the hydrogen content. This dependence is obtained in simple graphical form by taking the $\log\nu_c$ versus $1/T$ curves for the different compositions in Fig. 3 and constructing ν_c versus composition isotherms from them, as shown in Fig. 5. The points plotted on this diagram are averages in that they were taken from the least-squares straight lines of Fig. 3, for each specified temperature, and not directly from the experimental points because ν_c was not measured for all the samples for exactly the same temperatures. It may be seen in Fig. 5 that to a very good degree of approximation, ν_c is directly proportional to the stoichiometric defect

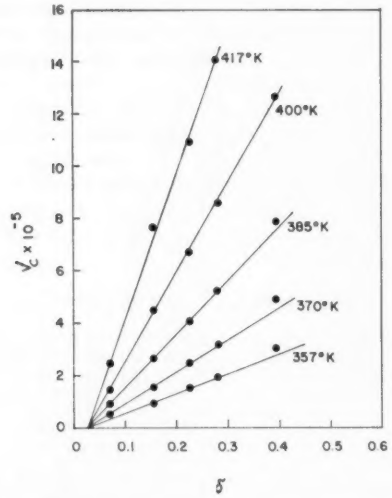

FIG. 5. Isotherms giving the dependence of ν_c upon the stoichiometric defect δ in the compounds $TiH_{2-\delta}$. The data plotted here are taken from the least-squares lines of Fig. 3.

δ. The latter describes the concentration of vacant tetrahedral sites. Therefore, it is clear that the diffusion occurs via a vacancy mechanism, i.e., a hydrogen atom can diffuse only by jumping into an unoccupied, neighboring tetrahedral site, at least for the temperatures over which δH changes rapidly.

Our results are fitted approximately by a single equation of the form

$$\nu_c=\nu_0 n(\delta/2)\exp(-E_a/RT), \tag{14}$$

where ν_0 is a frequency factor, n is the number of neighboring tetrahedral sites to which a proton can jump, and $(\delta/2)$ is the probability of a tetrahedral site being vacant. Equation (14) predicts that the isotherms will be a family of straight lines going through the origin. Scrutiny of Fig. 5 shows that this is essentially so. The most striking exception is that the curves converge at the point $\nu_c=0$, $\delta=0.025$ rather than at the origin. This requires that $(\delta/2)$ in Eq. (14) be replaced by $(\frac{1}{2})(\delta-\delta_0)$ where $\delta_0=0.025$.

Also, it may be seen that the experimental points for large δ fall above the straight line portion of the isotherms for smaller δ, and that this is more pronounced for the lower temperature isotherms. Deviations of this sort would be expected from the linear dependence of E_a upon δ. However, the deviations are actually much smaller than would be expected from this cause alone, because they are very largely compensated by the dependence of ν_0 upon δ. This dependence is also linear, as shown by the values summarized in Table II. So we can write $\nu_0\cong\nu_0^0(1-B\delta)$ and $E_a=E_a^0(1-C\delta)$, where ν_0^0 and E_a^0 refer to the stoichiometric compound TiH_2. With these revisions, Eq. (14) becomes

$$\nu_c=\nu_0^\circ(1-B\delta)n(\tfrac{1}{2})(\delta-\delta_0)\exp[-(E_a^\circ-C\delta)/RT]. \tag{15}$$

The δ-dependent term in the exponential can be approximated as $(1+C\delta/RT)$, for small δ and large T, giving

$$\nu_c=\nu_0^\circ(1-B\delta)n(\tfrac{1}{2})(\delta-\delta_0)(1+C\delta/RT)\times\exp(-E_a^\circ/RT). \tag{16}$$

The values of B and C/RT are nearly equal so that $(1-B\delta)(1+C\delta/RT\cong1$, at least for moderate values of δ, and our final result is

$$\nu_c\cong\nu_0^\circ n(\tfrac{1}{2})(\delta-\delta_0)\exp(-E_a^\circ/RT), \tag{17}$$

which describes the isotherms in Fig. 5 very well.

The "Frequency Factor" in the Diffusion Rate Law

Aspects of Eqs. (14)–(16) which merit further comment include n, the value of ν_0 and its dependence on δ, and the significance of δ_0. All of these affect the frequency factor in the rate expression for the diffusion of hydrogen. The value of n depends upon the type of path along which the hydrogen diffuses. The tetrahedral sites occupied by the hydrogen in the fcc titan-

ium hydride lattice are in a simple cubic arrangement with a cube edge of $a_0/2$. It appears that the most probable diffusion path is along the body diagonals of these cubes.[24] A given tetrahedral site has 8 such diagonals leading from it; however, four are blocked by the titanium atoms, so n is 4.

The experimental source of the frequency factors is Fig. 3. Extrapolation to infinite temperature of the $\log\nu_c$ vs $1/T$ plots gives an Arrhenius frequency factor which is the A in the equation $\nu_c = A\exp(-E_a/RT)$. These values, which are listed in Table II, include the dependence of ν_c upon the probable number, $n(\delta/\delta_0)/2$, of neighboring vacant sites to which the hydrogen can jump. The "true" frequency factor[25] ν_0 may be calculated from A by the relation, obtained from Eq. (15),

$$\nu_0 = A/n(\tfrac{1}{2})(\delta-\delta_0). \qquad (18)$$

The values which result are listed in Table II. It is found that they increase with decreasing δ. If this dependence upon δ is fitted by the linear relation $\nu_0 = \nu_0^\circ(1-B\delta)$, the values of ν_0 in Table II lead to a value for ν_0° of about 1.8×10^{12} and for B of about 2.

The frequency factor is a weighted mean[26,27] of the vibrational spectrum of the hydrogen atoms in the lattice. At first glance the numerical values of 10^{12} sec^{-1} may seem to be low, but they are compatible with the rather flat potential function calculated[24] for the hydrogen in the vicinity of the tetrahedral sites. Moreover, the steepness of the potential function and also the value of the vibrational frequency should increase with E_a; this agrees qualitatively with experiment. The difficulty in obtaining very accurate values of ν_0 renders a more detailed discussion profitless at this time.

As to the significance of δ_0, it does not seem probable that the passing of the isotherms in Fig. 5 through this point could arise from experimental error. Each of the isotherms is well defined and linear to a high degree in the region of interest, and all the lines intersect at the same point within very close limits. This nonzero intercept can be interpreted according to the vacancy mechanism as representing the nonavailability for the purpose of self-diffusion of a small fraction $\delta_0/2=0.013$ of the tetrahedral sites. Such an interpretation agrees with the experimental fact that it was not possible to produce titanium hydrides with more hydrogen than about $TiH_{1.98}$. The inaccessibility of this 1% of the tetrahedral sites could arise from several causes. One possibility is suggested by the work of Bevington, Martin, and Matthews,[28] who found that the addition of small amounts of O, N, and C to zirconium and titanium reduces the saturation concentration of hydrogen in the metal. The effects increase with the atomic radius of the impurity; one atom of oxygen inhibits the solution of one atom of hydrogen, while one atom of nitrogen inhibits 4 to 6 atoms of hydrogen. Thus, only 0.2% of the sites would need to be occupied by nitrogen to produce the observed effect, and this is not unlikely.

Another possibility is that δ_0 represents sites which are rendered inaccessible by edge dislocations. Cottrell[29] has shown, using a simple elastic stress model, that a considerable binding energy for interstitial atoms occurs on the stress-favored side of the dislocation. On the other side of the dislocation, the interstitials are squeezed out. In order to have 1% of the tetrahedral sites inaccessible from this cause, there would need to be about 10^{12} dislocations/cm^2, with about 20 sites affected per atom plane. These figures are reasonable as the metal was cold-worked in the preparation of the powder and was probably not annealed to a sufficiently high temperature subsequently to destroy the dislocations. Determination of the actual cause of δ_0 requires further experiments, preferably ones in which the value of δ_0 is changed reproducibly by cold-working and annealing of the metal or by the controlled introduction of impurities.

Relation of Diffusion to the Crystal Structure

Because of the neutron diffraction[6] and proton second-moment studies, it has been assumed in this discussion of the diffusion mechanism that only tetrahedral sites are occupied by hydrogen and that this occupation is random. In addition, the diffusion isotherms themselves afford very strong evidence for the first of these points. If the octahedral sites were occupied to a fractional extent d, then the concentration of tetrahedral vacancies would be $(d+\delta)$, the ν_c for diffusion would be approximately proportional[30] to $(d+\delta)$ and the intercept of the diffusion isotherms would be at approximately $\delta=-d$. The fact that the intercept is observed at $+0.025$ and that there is independent support for this being equal to the concentration of inaccessible vacancies is strong evidence that even though the protons go through the octahedral sites, they don't sit there long.

However, the diffusion data offer no conclusions on the question of random occupancy of the tetrahedral sites. If the vacancies coalesce to form vacancy pairs or groups of higher order, as do negative-ion

[25] In this discussion, ν_c should not be identified as precisely equal to the frequency with which a proton jumps from one site to another. They are related by a constant, of the order of unity, whose value depends upon the complex correlation function which describes the diffusional motions. See e.g., H. C. Torrey, Phys. Rev. **92**, 962 (1953) and the work cited in footnote 11.

[26] S. A. Rice, Phys. Rev. **112**, 804 (1958).

[27] D. Lazarus, Solid State Phys. **10**, 86 (1960).

[28] C. F. Bevington, S. L. Martin, and D. H. Matthews, Proc. 11th Int. Congress on Pure and Appl. Chem. **1**, 3 (1947).

[29] A. H. Cottrell, *Dislocations and Plastic Flow in Crystals* (Oxford University Press, New York, 1953).

[30] There would be some deviation from a linear relationship because occupation of an octahedral site would partially block diffusion to an adjacent tetrahedral site, if it were vacant; but this effect would approach zero as the tetrahedral vacancy concentration became small.

vacancies in alkali halides, the probability of there being a vacancy adjacent to a particular hydrogen atom will be reduced. The net result is that ν_e is reduced by a factor of the form $(1-k_2\delta-k_3\delta^2\cdots)$ where k_2, $k_3\cdots$ incorporate the association equilibrium constants and give the net effect of the association on the diffusion probability. Unfortunately, this functional form is indistinguishable from the dependence of ν_0 upon E_a, and thus upon δ, which was discussed in connection with Eq. (15).

Finally, there does not appear to be any direct relation between the diffusion of the hydrogen and the various structural anomalies which occur just below room temperature. In fact, the diffusion rate is too low at these temperatures to produce any significant narrowing of the dipolar broadening, so there is little hope of detecting any anomalous change in the diffusion rate in the vicinity of the other anomalies.

C. The Proton Resonance Shift

Experimental Results

It was found, by the method outlined in Sec. II.B, that the proton resonance is shifted upfield in the titanium hydride samples from its position in the silicone reference. That is, the shift is in the opposite direction to that of the Knight shift found in most metals.[16] The shifts are from 0.6 to 2 gauss out of 6300, which is very large for protons. However, because of the dipolar broadening, the shifts are a modest fraction of the linewidth, so considerable pains were taken to determine whether or not the shifts were real and, once this was apparent, to obtain accurate measurements of them.

Inasmuch as an external reference was used in the shift measurements, the effect of magnetic field inhomogeneities was checked by changing the relative positions in the rf coil of the sample and of the silicone. This caused small changes in the apparent shift, but they were, at most, less than $\frac{1}{10}$ of the observed shift. The magnetic field was swept from high to low fields, as well as from low to high, to ensure that magnetic hysteresis or lags associated with the integrating and recording system did not contribute to the apparent shift; but no differences were found.

None of the particles of titanium hydride were larger than 10^{-3} cm in diameter, so that one would predict[31] any skin effects upon the resonance position to be less than a part in 10^5, which is small compared to the observed shifts of several parts in 10^4. As a precaution against the possibility of larger effects being produced by aggregation of the small particles, a sample was mixed with carbon tetrachloride to break up surface contacts between particles. The same shift was obtained. Moreover, the absorption lines did not show any evidence of the asymmetry typical of skin effects.

Any correction for the bulk magnetic susceptibility is also small compared to the resonance shifts. If we assume that the sample approximates an infinite cylinder normal to the magnetic field, the measured bulk susceptibility[1] leads to a correction of the order of three parts in 10^5. However, this is a maximum because the reference was contiguous with the sample proper.

The results of all these experiments are consistent with the proton shifts being a real phenomenon, to be attributed to interactions at the atomic and nuclear levels, rather than to an instrumental or a bulk effect. Therefore, detailed measurements were made of the dependence of the shifts upon hydrogen content and temperature. Each shift reported is the mean of at least ten measurements; this number of measurements were made because the shifts are a small to moderate fraction of the linewidth and the signal-to-noise ratio left something to be desired. No effort was made to apply any corrections for bulk susceptibility effects because of their relative smallness and uncertainty.

The proton shift was measured at room temperature for all six samples. From the results plotted in Fig. 6, it can be seen that the shift is a definite function of hydrogen content. It is approximately constant at 0.01% between $TiH_{1.6}$ and $TiH_{1.85}$, but then increases sharply to 0.03% for $TiH_{1.97}$. The temperature dependence of the proton shift was measured for $TiH_{1.607}$ and $TiH_{1.969}$, which are the samples at the end of the composition range investigated. The results given in Fig. 7 show that the shift in $TiH_{1.607}$ is virtually independent of temperature while that in $TiH_{1.969}$ shows a pronounced anomaly at about 15°C.

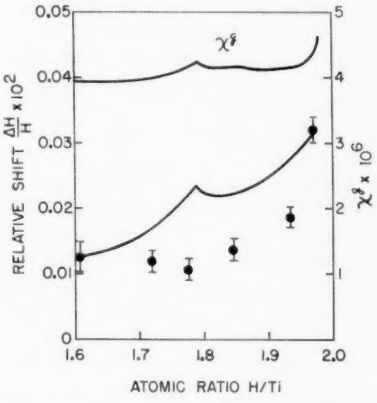

FIG. 6. The room-temperature shifts in the proton resonance, plotted as a function of hydrogen content. The errors shown are the standard deviations of ten or more measurements. All shifts are in the direction of higher applied magnetic fields. The curve fitted to the experimental points for $TiH_{1.607}$ and $TiH_{1.969}$ was calculated by means of Eq. (32). The curve at the top of the figure is the bulk susceptibility, in cgs units per gram, as reported in the work cited in footnote 1.

[31] A. C. Chapman, P. Rhodes, and E. F. Seymour, Proc. Phys. Soc. (London) **B70**, 345 (1957).

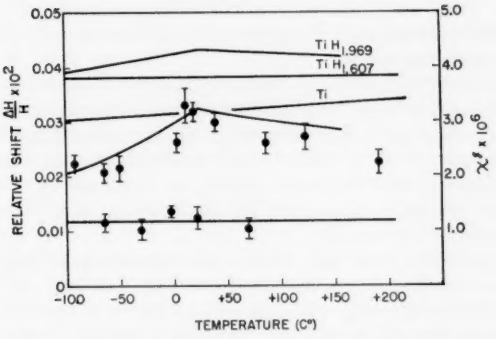

FIG. 7. The shifts in the proton resonance of $TiH_{1.607}$ and $TiH_{1.969}$, plotted as a function of temperature. The errors shown are the standard deviations of ten or more measurements. All shifts are in the direction of higher applied magnetic fields. The curve fitted to the experimental points for $TiH_{1.969}$ at −100° and 15°C and that for $TiH_{1.607}$ at room temperature were calculated by means of Eq. (32). The curves at the top of the figure are the bulk susceptibility, in cgs units per gram, as interpolated from the results reported in the work cited in footnote 1.

Comparison of the Shifts with Other Observations

The most striking aspects of the proton shifts are their large magnitude and their direction. The shifts observed in the titanium hydrides are an order of magnitude larger than the total range of 3 parts in 10^5 for proton shifts in ordinary diamagnetic compounds. For example, we searched for a shift in solid CaH_2, at room temperature, but without positive results, that is $|\Delta H/H| < 0.001\%$. Nor, apparently, is there a report for any of the other stoichiometric hydrides of a proton shift of the magnitude found for $TiH_{2-\delta}$. However, proton shifts have been found in two other nonstoichiometric hydrides. In the case of $VH_{0.66}$ Oriani *et al.*[32] found a relatively large upfield shift of 0.0095%, which is comparable with those reported here for the titanium hydrides of lower hydrogen content; but they also reported a negligible proton shift in $TaH_{0.33}$. On the other hand, in $PdH_{0.6}$, Norberg[10] found a small downfield shift of 0.0017%, which is the direction of the normal Knight shift.[16] Thus, it seems probable that large shifts are to be found only in the interstitial, metal hydrides, but not in all of them.

Except for their direction, the proton shifts in the titanium and vanadium hydrides are reminiscent of the Knight shift in metals. In fact, the hydrides exhibit electrical conductivity and bulk paramagnetism similar to the pure metals. The Knight shift in metals is well known[16] and arises from the interaction of the conduction electrons, near the Fermi surface of the metal, with the metal nuclei. In an externally applied magnetic field H, these unpaired electrons have a net spin polarization $\chi_p H$ which contributes a local magnetic field at the nucleus. This local field ΔH is proportional to the product of $\chi_p H$ and the density $\langle|\psi_M(0)|^2\rangle_{Av}$ of the conduction electrons at nucleus M. In particular, the local field shifts the resonance position by a fractional amount

$$\Delta H/H = (8\pi/3)\chi_p{}^a\langle|\psi_M(0)|^2\rangle_{Av}, \qquad (19)$$

where the superscript a on χ_p indicates that the Pauli or spin susceptibility is in atomic units. If the susceptibility is given in cgs units per gram, $\chi_p{}^g$, Eq. (19) becomes

$$\Delta H/H = (8\pi/3)M\chi_p{}^g\langle|\psi_M(0)|^2\rangle_{Av}, \qquad (20)$$

where M is the atomic or molecular weight of the sample.

In this expression, $\langle|\psi_M(0)|^2\rangle_{Av}$ is unknown and cannot be calculated for most metals, and so the assumption is made that an indication of its value can be obtained from the equivalent expression for the free atom, $|\psi_A(0)|^2$. There are several ways of obtaining the latter,[16] of which the most direct is from the experimental determination of the atomic hyperfine coupling constant, $a(s)$, which is given by

$$a(s) = (16\pi/3)(\mu_I/I)\mu_B|\psi_A(0)|^2, \qquad (21)$$

where μ_I and I are the nuclear magnetic moment and spin, respectively, and μ_B is the Bohr magneton. With the further definition of ξ as

$$\xi = \langle|\psi_M(0)|^2\rangle_{Av}/|\psi_A(0)|^2, \qquad (22)$$

which is of the order of unity, we can write Eq. (20) as

$$\Delta H/H = a(s)M\chi_p{}^g\xi/2g_I\mu_B, \qquad (23)$$

where g_I is the nuclear magnetogyric ratio. It is to be noted that the shift results from the contact part $\psi(0)$ of the electronic wave function and that, therefore, only s conduction electrons make a direct contribution.

The shifts predicted by this equation are opposite in sign to those observed for protons in the titanium hydrides; but the magnitudes can be comparable depending upon the values of ξ and $\chi_p{}^g$. In fact, both positive and negative proton shifts of the same magnitude as those in the titanium hydrides have been found in solid free radicals.[33] These shifts are proportional to the spin susceptibility and distribution in the radical of the unpaired electron and depend upon the electron-nucleus hyperfine interaction as do the Knight shifts. Therefore it is of interest to compare the proton shifts with the spin susceptibility of the titanium hydrides. Unfortunately, the latter is not directly available, as it is difficult to separate the spin and diamagnetic components from the bulk susceptibility χ. However, the spin susceptibility is of the same order as the bulk susceptibility, and for the transition metals it is a pretty fair approximation to take them as equal because the

[32] R. A. Oriani, E. McCliment, and J. F. Youngblood, J. Chem. Phys. **27**, 330 (1957).

[33] T. H. Brown, D. H. Anderson, and H. S. Gutowsky, J. Chem. Phys. **33**, 720 (1960); and earlier work cited therein.

effective mass m^* of the electron is large.[34,35] On this basis, Eq. (23) predicts that the proton shifts should be proportional to the bulk molar susceptibility, $\chi = M\chi^g$. However, the change in hydrogen content causes M to vary only from 49.5 to 49.9 g mole^{-1}, which can be neglected; therefore, our comparisons are given in terms of the χ^g values from the literature.

Figure 6 includes the dependence upon hydrogen content of χ^g as well as of the proton shift. It may be seen that both χ^g and the shift increase with increasing hydrogen content. However, χ^g has a small anomaly at $TiH_{1.79}$, for which there may be no counterpart in the shift, but more shifts would need to be measured in the vicinity of this composition to establish the point. Probably of more importance is the fact that over the range of hydrogen content investigated, the shift increases by a factor of three while χ^g increases by only about 15%. In Fig. 7, the temperature dependence of χ^g parallels that of the shift for the two samples investigated. Particularly striking is the correspondence between the anomaly in the shift and in χ^g at 15°C for $TiH_{1.969}$. This shows very clearly that the proton shifts are directly related to the magnetic susceptibility of the electrons in the hydrides. However, again the quantitative comparison is poor in that the shift at the anomaly is larger than that at −50°C by a factor of about 1.5 while χ^g is only about 5% larger.

It seems that there is no simple, direct link between the diffusional motion of the hydrogen and the proton shifts. The sample of $TiH_{1.969}$ exhibits an anomaly in the shift over a temperature range where there is negligible diffusion. On the other hand, for $TiH_{1.607}$ the ν_c for diffusion is of the order of 10^5 sec^{-1} at 50°C, ν_c changes considerably over the temperature range for which the proton shift was measured, and yet there are no anomalies in the shift. Of course, it is conceivable that there is an inverse relationship between the anomaly and the hydrogen diffusion; that is, the hydrogen diffusion disrupts the interactions producing the anomaly and reduces the magnitude of the anomaly in the samples of lower hydrogen content.

Origin of the Proton Shifts

From the results discussed in the foregoing section, we conclude that the proton shifts are related to some electronic interaction or property which makes an appreciable, but not dominant contribution to the bulk magnetic susceptibility of the titanium hydrides. There are several such possibilities. The diamagnetic or orbital effects of the conduction electrons produce shifts to higher fields. However, detailed calculations[35] have shown that these contributions are at most of the order of a few percent of the spin effects, so it seems reasonable at this stage to consider further only the latter.

There are three ways in which the spin polarization of the conduction electrons can lead to a shift in the proton resonance:

(a) The conduction electrons themselves can have a finite density at the protons. This, however, would give rise to a Knight shift which we have already noted is opposite to the observed shifts. Therefore, any contribution of this nature must be overcome by the mechanism(s) responsible for the negative sign of the observed proton shifts.

(b) There can be a direct bonding overlap between the conduction electrons and electrons localized in 1*s* orbitals centered on the protons. By the Pauli exclusion principle, this would pair the spin of the 1*s* electron antiparallel to that of the conduction electron, and there would result a proton shift opposite to the Knight shift. This type of effect we will denote as a "direct exchange" interaction.

(c) The conduction electron density on the titanium atoms can participate in an exchange interaction with the bonding electrons in atomic orbitals centered on the titanium atoms. This Hund's rule coupling tends to orient the spins of the bonding electrons parallel to those of the conduction electrons. The bonding electrons centered on the titanium atoms transmit the spin polarization, with a change in sign, to the protons via the exchange interaction in the covalent part of the Ti—H bond. The model is similar to that for the C—H fragment,[36] where a positive spin polarization of an odd electron in the π orbital on the carbon gives rise to an upfield shift of the proton resonance.[33] This mechanism will be called an "indirect exchange."

It is beyond the scope of this work to attempt a general *a priori* calculation of the various electron-electron, electron-nucleus, spin-spin interactions which we have divided in the fashion just described. For example, it is very difficult to estimate the indirect exchange to better than an order of magnitude in the simpler, isolated-fragment case.[36] Instead, we will present an *ad hoc* analysis which seeks to identify the factors responsible for the major features of the observed proton shifts. These include the sign and magnitude of the shifts and their dependence upon temperature and sample composition.

From a phenomenological viewpoint, we assume that the proton shift is proportional to $\chi_H{}^a$, where the latter is the spin susceptibility of electrons "on" the hydrogen atoms, expressed in gram atomic units. The effects of the direct and indirect exchange interactions between the conduction electrons, which presumably are concentrated on the titanium atoms, can be combined in the expression

$$\chi_H{}^a = -\eta\chi_{Ti}{}^a. \tag{24}$$

This means that there is a probability η for the spin

[34] C. Kittel, *Solid State Physics* (John Wiley & Sons, Inc., New York, 1956), 2nd ed., p. 295.

[35] T. P. Das and E. H. Sondheimer, Phil. Mag. **5**, 529 (1960).

[36] H. M. McConnell and D. B. Chesnut, J. Chem. Phys. **28**, 107 (1958); and prior work cited therein.

susceptibility $\chi_{Ti}{}^a$ of conduction electrons "on" the titanium atoms to be transmitted with a change of sign to electrons about the protons. As defined here, η includes the effects of both the degree of the spin exchange and the extent to which the orbital on the hydrogen is occupied. One might next be inclined to say that χ_p, the spin susceptibility of the conduction electrons, should equal $\chi_{Ti}{}^a$. However, this leads to the result that $\chi_{Ti}{}^a$ is directly proportional to χ^g, and that the proton shift is also directly proportional to χ^g. But this is incompatible with the observed temperature dependence of the proton shifts, unless the polarization exchange probability η in Eq. (24) is very sensitive to temperature. To be sure, one would expect some dependence of η upon temperature and hydrogen content; however, for simplicity we will assume it to be constant and explore the consequences.

A comment on notation may be helpful here. The symbol χ_p has been used to designate the Pauli susceptibility, which is the spin susceptibility of the conduction electrons. Titanium hydride differs from metals in that according to our atomic orbital model, χ_p is but one of several contributions to the total molar spin susceptibility χ_s. Nonetheless, one would still expect the latter to be approximately equal to the bulk susceptibility in the hydride, i.e., $\chi_s=M\chi^g$, just as $\chi_p=M\chi^g$ in the metals. The effective mass of conduction electrons is large in the transition metals, so their diamagnetic, orbital contributions to the bulk susceptibility are very small[34,35]; and one would expect this to apply to the titanium hydride as well, because the Ti-Ti distance in the hydride is not very different from that in the metal and the conductivity is of the same order. Moreover, in the hydride, the electrons centered on the protons contribute mainly to χ_s because they are s electrons.

With η constant, the temperature dependence of the proton shift can be fitted by assuming that there is a relatively large, constant component of χ_s which is not involved in the exchange interactions; that is

$$\chi_{s,ex}{}^M=\chi_s-\chi_0=M(\chi^g-\chi_0{}^g), \tag{25}$$

where χ_0 and $\chi_0{}^g$ are constants and $\chi_{s,ex}{}^M$ is the *net* component, in gram mole units, of the spin susceptibility of electrons associated with the exchange interactions. This latter quantity consists of opposing contributions from electrons centered on titanium and hydrogen atoms. For $TiH_{2-\delta}$, this approach leads to the relation

$$\chi_{s,ex}{}^M=\chi_{Ti}{}^a+(2-\delta)\chi_H{}^a, \tag{26}$$

which, upon substitution of Eq. (24) and rearrangement, becomes

$$\chi_H{}^a=-\eta\chi_{s,ex}{}^M/[1-(2-\delta)\eta]. \tag{27}$$

This can be related to the observed bulk susceptibility per gram χ^g via Eq. (25), giving

$$\chi_H{}^a=-M(\chi^g-\chi_0{}^g)/[1-(2-\delta)\eta]. \tag{28}$$

Equation (28) provides a basis for calculating from the bulk susceptibility the proton shift produced by the exchange interactions.

For this purpose, we modify Eq. (23) for the Knight shift by substituting $\chi_H{}^a$ for χ_p. This gives

$$(\Delta H/H)_{ex}=a(s)\chi_H{}^a\xi_H/2g_I\mu_B, \tag{29}$$

where ξ_H is the ratio of $|\psi(0)|_H{}^2$ for a $1s$ electron on a hydrogen atom in the titanium hydride solid to that for a free hydrogen atom. In addition to the exchange interaction, there is the possibility that the conduction electrons themselves have an appreciable density at the protons and thus makes a direct Knight-type contribution to the proton shift.[37] This requires a model similar to that applied with considerable success to the case of substitutional alloys,[16] except that allowance must be made for the difference in conduction electron density about the hydrogen *atom* compared to the titanium *atom*. A difficulty arises, however, in determining the value of the spin susceptibility to be associated with this direct Knight shift. Probably it is as reasonable a choice as any to use $\chi_{Ti}{}^a$ for this purpose On this basis one obtains

$$(\Delta H/H)_K=a(s)\chi_{Ti}{}^a\xi_{Ti}{}^H\xi_H/2g_I\mu_B, \tag{30}$$

where $\xi_{Ti}{}^H$ is defined as the ratio

$$\xi_{Ti}{}^H=\langle|\psi(H)|^2\rangle_{Av}/\langle|\psi(\mathrm{Ti})|^2\rangle_{Av}. \tag{31}$$

In both Eq. (29) and Eq. (30), $a(s)$ is the hyperfine interaction constant for the free hydrogen atom. The Knight-type contribution can be expressed in terms of the bulk susceptibility χ^g by elimination of $\chi_{Ti}{}^a$ with Eqs. (24) and (27). The final result is

$$\begin{aligned}\Delta H/H&=(\Delta H/H)_{ex}+(\Delta H/H)_K\\&=[a(s)\xi_H/2g_I\mu_B](1-\xi_{Ti}{}^H/\eta)\chi_H{}^a\\&=[a(s)\xi_H/2g_I\mu_B]\frac{(1-\xi_{Ti}{}^H/\eta)M(\chi^g-\chi_0{}^g)}{1-(2-\delta)\eta}.\end{aligned} \tag{32}$$

The various experimental observations of the proton shifts are fitted at least semiquantitatively by this equation with more or less reasonable values for the four adjustable parameters ξ_H, $\xi_{Ti}{}^H$, η, and $\chi_0{}^g$.

Comparison of the Exchange Interaction Model with Experiment

For the temperature dependence of the proton shift in a specific hydride, Eq. (32) reduces to the form

$$\Delta H/H=A_\delta(\chi^g-\chi_0{}^g), \tag{33}$$

[37] This contribution was not included in the preliminary analysis reported in work cited in footnote 24. However, if it is not included, an unreasonably low value of 0.125 is required for ξ_H in order to fit the data.

where the "constant" A_δ depends upon δ. A value of 3.25 is obtained for χ_0^g by fitting this equation to the experimental proton shifts and bulk susceptibilities at $-100°$ and 15°C for $TiH_{1.969}$. The solid curve drawn through the experimental shifts plotted in Fig. 7 for $TiH_{1.969}$ was calculated from the bulk susceptibility at the top of the figure by means of Eq. (33) with this value of 3.25 for χ_0^g. The parameter η can now be evaluated via Eqs. (32) and (33) from the ratio of A_δ for samples of two different compositions. In this manner a value of 0.37 is obtained for η from the room temperature proton shifts and bulk susceptibilities of $TiH_{1.607}$ and $TiH_{1.969}$. The temperature dependence of the proton shifts in $TiH_{1.607}$ has been calculated from the experimental bulk susceptibilities given at the top of Fig. 7, using Eq. (33) with $\eta=0.37$ and $\chi_0^g=3.25$. The solid curve at the bottom of the figure shows the results.

Thus far we have considered only the relative values of the proton shifts. The various constants in Eqs. (32) and (33), excepting η and χ_0^g but including ξ_H and $\xi_{Ti}{}^H$ have been treated as a scale factor. The latter two remaining parameters can now be evaluated by fitting Eq. (32) to the numerical values of the shift and bulk susceptibility at a point. For consistency, we have used the values for $TiH_{1.607}$ at room temperature. The result is not a unique value for both ξ_H and $\xi_{Ti}{}^H$ but a function relating one to the other, namely,

$$\xi_{Ti}{}^H=0.37-0.047\xi_H{}^{-1}. \tag{34}$$

By employing this condition in Eq. (32) along with $\eta=0.37$ and $\chi_0^g=3.25$, we have calculated the dependence of the proton shift upon sample composition from the bulk susceptibilities plotted at the top of Fig. 6. The result is the solid curve drawn at the bottom of the figure.

It can be seen that this and the other calculated curves agree reasonably well with experiment. The temperature dependence of the shifts is fitted very well. However, the observed dependence upon composition is nearly an exponential rise as the stoichiometric compound is approached, while the calculated curve is hyperbolic. In treating the dependence upon composition, one might argue about the effects of the inaccessible sites. For instance, should not the term in the denominator of Eq. (32) be $(2-\delta-\delta_0)$ rather than $(2-\delta)$? If the former is used, one obtains a slightly different value for η; however, the agreement between calculations and experiment is not affected materially. There is some slight evidence that the positive charge on the hydrogen increases with hydrogen content[24]; if true, this would decrease η and improve the fit between the calculated and experimental shifts.

The values of the various parameters obtained by fitting the experimental data with Eqs. (29)–(34) appear to be feasible. Although Eq. (34) does not provide a numerical value for either $\xi_{Ti}{}^H$ or ξ_H, an independent estimate can be made for ξ_H. Even here, there are a large number of factors which could affect the value, such as a van der Waals expansion of the electron orbital,[38] electrostatic effects of the surrounding titanium atoms, and reduction of orbital overlap by contraction of the hydrogen orbital. Hydrogen is most closely related to the alkali metals and for Li, Na, Rb, and Cs, ξ increases in the sequence[16] 0.43, 0.72, 1.00, and 1.3, respectively. Therefore, a value of about 0.4 seems appropriate for ξ_H; and, in any case, one would not expect ξ_H to be greater than unity. Accordingly, $\xi_{Ti}{}^H$ would be about 0.27 and no larger than 0.32. Returning to Eqs. (29) to (32), we note that this requires the Knight contribution to the proton shift to be nearly $\frac{3}{4}$ as large as the exchange contribution. Hence, the analysis suggests that the proton shifts result from a fractional difference in the opposing effects of the Knight and exchange contributions.

The value of $\xi_{Ti}{}^H$ itself seems feasible. It represents the decrease of the conduction electron wave function in the vicinity of a titanium atom, and the estimated value of 0.27 is certainly less than unity as would be expected. Moreover, a value as large as 0.3 is not out of the question because each hydrogen atom is surrounded by a tetrahedral first shell of titanium neighbors for which the H-Ti internuclear separation is only ~1.9 A. Of course, if χ_p were used, instead of the smaller quantity $\chi_{Ti}{}^a$, to calculate the Knight-type contribution, $\xi_{Ti}{}^H$ would be less by a reciprocal factor.

This raises the question of the significance of χ_0^g. It represents a large component of the spin susceptibility which does not participate in the exchange interactions. This is compatible with our use of $\chi_{Ti}{}^a$ in Eq. (30), which assumes that χ_0^g does not participate in the Knight-type contribution to the proton shift, because both involve the conduction electron distribution at the "exterior" of the titanium atoms. This suggests that χ_0^g be interpreted as a contribution to the spin susceptibility from the titanium "cores." The outer electron configuration of titanium is $3d^24s^2$ and it is possible that either the d or s electrons are involved preferentially in the exchange interactions. In principle, this could be checked by observing the titanium resonance shift in the hydrides. In this regard it is suggestive that χ_0^g is very nearly the same as χ^g for the pure metal. In fact, the experimental results can be fitted somewhat better by using χ^g for the pure metal in Eqs. (32) and (33) instead of $\chi_0^g=3.25$. This procedure gives a slightly lower value for η, 0.34 instead of 0.37, with a corresponding modification in Eq. (34) for the value of $\xi_{Ti}{}^H$.

The picture emerging is one in which each hydrogen atom donates some fraction of its 1s electron to the conduction band of the solid hydride. The proton shift and the change in bulk susceptibility of the hydride from that of the metal are determined largely by the electrons contributed to the conduction band and by

[38] F. J. Adrian, J. Chem. Phys. **32**, 972 (1960).

the electron density remaining localized in the hydrogen 1*s* orbital. Accordingly, the fact that η is less than unity results at least in part from incomplete occupancy of the hydrogen 1*s* orbital; and it would seem that the hydrogen has a net positive charge, counter to what would be expected from electronegativity arguments. The value of 0.37 found for η is acceptable insofar as we can judge. It equals the extent to which the hydrogen 1*s* orbital is occupied times the factor describing the extent of the spin coupling by the exchange mechanism(s). Thus, the value of 0.37 for η corresponds to a range in occupation number from unity to 0.37 while the reciprocal range for the coupling factor is 0.37 to unity. In the ·C-H radical fragment, for which the hydrogen 1*s* orbital is essentially fully occupied, a factor of about 0.05 describes transmission by the indirect exchange mechanism of the spin polarization of the unpaired π electron to the hydrogen 1*s* electron. This factor should be several fold larger for titanium because of its larger nuclear charge. However, it is unlikely to be as large as the required minimum value of 0.37, which suggests that the direct exchange interaction is important.

An entirely different approach to the nature of the shifts can be based upon the relation between the Knight shift and the spin-lattice relaxation time in metals. Korringa[39,40] has derived the following approximate expression for the metal nucleus,

$$T_1(\Delta H/H)^2=\hbar\mu_B^2/\pi kTg_I^2. \tag{35}$$

Experimental values of the proton T_1 are available[11] for $TiH_{1.77}$ from room temperature to 400°C. The T_1 value remains virtually constant over the lower 60°C of this range, decreasing from 0.39 sec at room temperature to 0.35 sec at 90°C. The effects of self-diffusion begin to be important at higher temperatures and the T_1 decreases sharply. However, the T_1 at lower temperatures is due presumably to the interactions with the conduction electrons. If Eq. (35) applies to the protons as one would expect for the model described, the room temperature shift of 0.01% corresponds with a T_1 of 0.09 sec. The factor of 4 between this value and experiment is within the approximations. Moreover, the temperature dependence observed for T_1 is in accord with Eq. (35). It is of interest that the net proton shift must be used in Eq. (35) to obtain agreement with experiment. If the Knight or the exchange contribution to the shift were used, or the sum of their absolute values, the observed T_1 would be 35, 65, and 200 times longer, respectively, than that calculated with Eq. (35).

[39] J. Korringa, Physica **16**, 601 (1950).

[40] N. Bloembergen and T. J. Rowland, Acta Met. **1**, 731 (1953). A recent careful study of the shifts in NaTl, by W. D. Knight and H. E. Schone, has substantiated that the shifts are −0.16% for Na and −0.5% for Tl, in qualitative agreement with Bloembergen and Rowland (private communication); H. E. Schone, Ph.D. thesis, University of California (1961).

Negative Knight Shifts in Other Systems

On the basis of the very limited information available on proton shifts in other nonstoichiometric hydrides, they appear to be related to the nuclear charge Z of the metal. Starting at low Z, the room-temperature proton shifts are −0.012% for $TiH_{1.607}$, −0.009$_5$% for $VH_{0.66}$,[32] 0.000$_6$% for $TaH_{0.33}$[32] and +0.0017% for $PdH_{0.66}$.[10] In view of the sensitive balance of opposing factors which govern the shifts, this apparent Z dependence could very well be accidental. Further study of these systems is needed to check the basic features of the model proposed before one can inquire, for example, whether the differences in the proton shifts of particular hydrides result mainly from the effects of the radius ratio and electronegativity of the metal on η or from other differences in the nature of the conduction band.

In our preliminary report,[15] there was included an attempt to evaluate η for $VH_{0.66}$ using the observed proton shift in combination with that for V^{51} in the hydride compared to that in the metal. It is now apparent that the situation is more complex than was then assumed. However, there are some qualitative features which illustrate what might be gained by detailed studies of the metal as well as of the proton resonance shifts. By combining Eqs. (24), (29), and (30), we can express the proton shift in vanadium hydride as

$$\Delta H/H=a_{\mathrm{H}}\xi_{\mathrm{H}}(\xi_{\mathrm{V}}{}^{\mathrm{H}}-\eta)\chi_{\mathrm{V}}{}^{a}/2g_{\mathrm{H}}\mu_B. \tag{36}$$

Also, Eq. (23) gives the Knight shift for the vanadium resonance in the hydride to be

$$k_{\mathrm{V}}=\Delta H/H=a_{\mathrm{V}}\xi_{\mathrm{V}}\chi_{k,\mathrm{V}}{}^{a}/2g_{\mathrm{V}}\mu_B, \tag{37}$$

where $\chi_{k,\mathrm{V}}{}^{a}$ is that portion of the Pauli spin susceptibility which contributes to the V^{51} Knight shift, and $\chi_{\mathrm{V}}{}^{a}$ is that involved in the exchange interactions.

A value of 0.72% is obtained for k_{V} in $VH_{0.66}$ by adding the 0.17% downfield shift observed for the V^{51} resonance in it compared to the metal,[32] and the 0.55% Knight shift for the metal itself.[16] Upon substitution of this and the other available experimental data into Eqs. (36) and (37) and dividing the latter, one finds

$$\eta=\xi_{\mathrm{V}}{}^{\mathrm{H}}+0.094(\xi_{\mathrm{V}}/\xi_{\mathrm{H}})(\chi_{k,\mathrm{V}}{}^{a}/\chi_{\mathrm{V}}{}^{a}). \tag{38}$$

If the same values, 0.3 and 0.4, are assumed for $\xi_{\mathrm{V}}{}^{\mathrm{H}}$ and ξ_{H} as were employed for titanium hydride, and a value of 2.7 for ξ_{V},[16] Eq. (38) becomes

$$\eta=0.3+0.63(\chi_{k,\mathrm{V}}{}^{a}/\chi_{\mathrm{V}}{}^{a}). \tag{39}$$

Even when allowance is made for the fact that 2.7 is probably too large a value for ξ_{V}, Eq. (39) gives a reasonable result for η only if $\chi_{k,\mathrm{V}}{}^{a}<\chi_{\mathrm{V}}{}^{a}$. That is, the spin susceptibility of conduction electrons contributing to k_{V} is less than that of the conduction electrons participating in the exchange interactions with the hydrogen atoms. However, even though this might be

explained by saying that the exchange interaction involves only the d electrons of the vanadium $3d^34s$ outer configuration, the 0.17% V^{51} shift between the hydride and the metal requires that the s electrons be affected as well. More detailed analyses of such questions can be based upon the bulk susceptibilities. Moreover, it would be helpful if the resonance of the conduction electrons could be observed.

The first report of negative Knight shifts was made by Bloembergen and Rowland,[40] who observed negative shifts for both components in an ordered intermetallic compound NaTl. There is some doubt about the Na^{23} shift, which is small (-0.016%) and may be due to a chemical shift or to uncertainty about the datum for shifts. The authors tentatively suggested that the effect may be due to configurational interaction,[41] in which an inner s electron is promoted to a higher s-type orbit in the conduction band. Negative Knight shifts have also been reported for the Al^{27} resonance in the magnetic rare earth intermetallic compounds[42] having the cubic Laves structure, for α and β Mn,[43] for Pt,[44] for Sn and Ga in the intermetallic compounds Nb_3X and V_3X,[45] and for the Pt, Ga, Sb, and Si resonances in the intermetallic vanadium compounds V_3X.[46] An exchange interaction between the f electrons localized on the rare earth atom, and the conduction electrons has been proposed as the origin of the negative aluminum shifts.[42] Our results for titanium hydride have been interpreted in terms of exchange interactions of somewhat different character, and it appears likely that the negative shifts in the intermetallic compounds also involve exchange interactions.

[41] A. Abragam and M. H. L. Pryce, Proc. Roy. Soc. (London) **A205**, 135 (1951).
[42] V. Jaccarino, B. T. Matthias, M. Peter, H. Suhl, and J. H. Wernick, Phys. Rev. Letters **5**, 251 (1960).
[43] V. Jaccarino, M. Peter, and J. H. Wernick, Phys. Rev. Letters **5**, 53 (1960).
[44] T. J. Rowland, J. Chem. Phys. Solids **7**, 95 (1958).
[45] R. G. Shulman, B. T. Wyluda, and B. T. Matthias, Phys. Rev. Letters **1**, 278 (1958).
[46] W. E. Blumberg, J. Eisinger, V. Jaccarino, and B. T. Matthias, Phys. Rev. Letters **5**, 149 (1960).

ACKNOWLEDGMENTS

One of us (B.S.) would like to thank the Institute of International Education and the Ford Foundation for a Visiting Senior Scholarship which made this work possible. Another (C.K.C.) would like to thank the C.S.I.R.O. for leave of absence and to acknowledge with gratitude the support given by the International Cooperation Administration under the Visiting Scientist Program administered by the National Academy of Sciences of the United States of America.

Approach to Thermodynamic Equilibrium

J. E. MAYER

Enrico Fermi Institute for Nuclear Studies, University of Chicago, Chicago, Illinois

(Received August 2, 1960)

The properties of a macroscopic classical system consisting of some 10^{20} molecules are determined by a probability density function W of the complete Γ space of moments and coordinates of all the molecules. This probability density function is that of the ensemble representing the totality of all experimental systems prepared according to the macroscopic specifications. The entropy is always to be defined as the negative of k times the integral over the distinguishable phase space of $W \ln W h^{\Gamma}$. However, the total probability density function W, even for a thermodynamically isolated system, does not obey the Liouville equation, $\partial W/\partial t = LW$, since small fluctuations due to its contact with the rest of the universe necessarily "smoothes" W, by smoothing the direct many-body correlations in its logarithm. This smoothing is the cause of the entropy increase, and in systems near room temperature and above, in which there is heat conduction or chemical species diffusion, the smoothing keeps the true entropy numerically equal to that inferred from the local temperatures, pressures, and compositions. This, however, is by no means necessarily general. The criterion of thermodynamic isolation is not that the complete probability density function W is unaffected by the surroundings, but that reduced probability density functions w_n in the Γ space of $n=2,3,\cdots$ molecules evolve in time as if the system were unaffected by the surroundings. This criterion is sufficient to give a mathematically definable method of "smoothing" the complete probability density function. The smoothing consists of replacing the direct many-body correlations in $\ln W$ by their average n-body values, $n=2,3,\cdots$, such that the smaller reduced probability density functions w_n are unaffected.

A. PHENOMENOLOGICAL DISCUSSION

I. Introduction

WE wish to discuss, from a statistical mechanical viewpoint, the approach of an isolated thermodynamic system to equilibrium. The object of the discussion is to point out, in some detail, a mathematical description of the ensemble distribution as a function of time, in which those terms of negative entropy which disappear in time are precisely formulated. The pure mathematics are, however, far more clearly presented if first the motivation for the description is given. In addition it is necessary to emphasize why the mathematical proofs presented, which themselves are almost trivial once the description is made, are apparently so limited in nature. Several theorems which one might expect to be correct are simply not true, as is evidenced by the existence of simple counter examples.

We therefore first discuss some well-known paradoxes, one of which particularly appears to us to have been given too little attention. In order to make the discussion as explicit as possible we restrict our attention to a particularly simple class of systems. The general features of our conclusion are applicable to a far wider variety of examples.

We discuss an isolated thermodynamic system of simple molecules in the absence of external forces other than those supplied by the retaining wall, which latter are assumed to exert only short range forces. The volume V, energy E, and number set $\mathbf{N}=N_a, N_b, \cdots$, etc., of molecules of species a, b, $\cdots$ are fixed for all times. Since we wish to discuss nonequilibrium states there must be at least one other parameter which we designate $x(t)$ that can vary with time. We assume that there is local thermodynamic equilibrium, so that the state at any time is described by thermodynamic parameters; in other words that $x(t)$ has a thermodynamic significance. We do this in order to be able to discuss a thermodynamic entropy $S(t)$; that is, we assume that a conceivable process of inserting insulating diaphragms which will stop all fluxes would be a reversible process, and that the thermodynamic entropy could then be analyzed by the usual thermodynamic methods on the separate parts of the system. On the other hand, we could also *infer* the temporary value of $S(t)$ by knowing the temperature, composition, and density, at t, in every part of the system. We shall later make a distinction between these two methods of determining $S(t)$.

In general $x(t)$ would be a function of the space coordinate $\mathbf{r}$ in the system, say the local temperature $T(\mathbf{r})$, or composition, or both, but in order to simplify the discussion we shall tacitly assume that a single number, such as the difference in temperature or composition at top and bottom is adequate. We choose x so that $x(t=\infty)=x_{eq}=0$ and in general that $x(t=0)=x_0>0$. The behavior of the system is that x decreases in time, approaching zero asymptotically, and, at least after long times, it presumably decreases exponentially. We assume the time constant to be of the order of minutes, so that, say $x(t=10^3 \text{ sec})=x_0/e$, Fig. 1.

The negative entropy $-S(t)$, also decreases with t,

and $$-\Delta S(t) = -S(t) + S(t=\infty) = -S(t) + S_{eq}$$

roughly parallels $x(t)$. The plot of Fig. 1 may be regarded, qualitatively, as being either for x or for the negative excess inferred thermodynamic entropy.

We remark here that if the value of $x(t)$ (or its functional dependence on the coordinate $\mathbf{r}$ at t) determines all properties of the system at t and for all future times, independently of past history, then the system is completely described at all times by the static thermo-

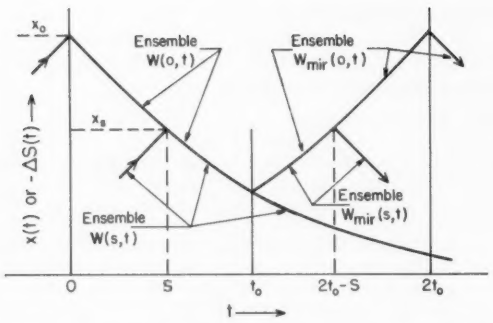

FIG. 1. The evolution with time of a physical variable $x(t)$ [or $-\Delta S(t)$] for an ensemble $W(0, t)$ started at $t=0$ and $x=x_0$, and for an ensemble $W(s, t)$ started at $t=s$, $x=x_s$, and also for two ensembled obtained by "mirroring" these at $t=t_0$.

dynamic variables. Many systems do not have this property. For instance, the state of certain glasses depend on the speed with which they have been cooled. Other systems, which go to an eventual equilibrium, appear to show hysteresis in certain phases of development, the properties at $t_0+\Delta t$ depending on the past history at $t<t_0$, as well as upon instantaneously measurable properties at t_0. We will discuss the significance of this later.

II. Mechanical Description

Since we prefer to talk about coordinates and momenta and the correlations between them, rather than phase relations between vector functions in Hilbert space, we assume that the system is purely classical. The mechanical state is specified by giving the coordinates and momenta

$$\gamma_{ia}=\mathbf{r}_{ia}, \mathbf{p}_{ia} \tag{2.1}$$

of every molecule $1a\leq i_a\leq Na$ for all species a. We will tacitly assume that there are no internal coordinates, $\mathbf{r}_{ia}=x_{ia}, y_{ia}, z_{ia}$, although this assumption is not explicitly used. The complete Γ space specification is then symbolized by

$$\{\mathbf{N}\}=\{N_a\}, \{N_b\}, \cdots, \tag{2.2}$$

$$\{N_a\}=\gamma_{ia}, \gamma_{2a}, \cdots, \gamma_{Na}, \tag{2.3}$$

and the symbol $d\{\mathbf{N}\}$ is used for the volume element.

The potential energy function $U_N\{\mathbf{N}\}$ is assumed to be a true potential, and to include only pair interactions plus singlet terms due to the walls,

$$U_N\{\mathbf{N}\}=\sum_a \sum_{ia=1a}^{ia=Na} u_a(\text{wall}, \mathbf{r}_{ia}) + \sum_a \sum_b \sum_{ia} \sum_{jb}{}' u_{ab}(r_{ia,jb}), \tag{2.4}$$

$$r_{ia,jb}=|\mathbf{r}_{ia}-\mathbf{r}_{jb}|. \tag{2.5}$$

This assumption is more essential to our argument than we would like it to be. The effect of violations of Eq. (2.4) are briefly discussed at the end.

For given initial thermodynamic parameters, $VE, \mathbf{N}$, x_0, etc., we define an initial ensemble consisting of the totality of all systems experimentally prepared according to these specifications, and define a probability density function, $W_0\{\mathbf{N}\}$, such that this function gives the probability density of finding a member of the ensemble at the fully determined Γ-space position $\{\mathbf{N}\}$ at $t=0$. The normalization used is that

$$\int d\{\mathbf{N}\}[\mathbf{N}!]^{-1}W_0\{\mathbf{N}\}=1, \tag{2.6}$$

$$\mathbf{N}!=N_a!N_b!\cdots, \tag{2.7}$$

so that $W_0\{\mathbf{N}\}$ represents the probability density of finding any molecule of species a at the position γ_{ia}, etc., rather than the probability density for finding a previously numbered set at the numbered positions.

If the Hamiltonian is fully time independent, namely, if there is a true time-independent potential such as that specified by Eq. (2.4), the time evolution of W is given by

$$\partial W(t, \mathbf{N})/\partial t=\mathrm{L}W(t, \{\mathbf{N}\}) \tag{2.8}$$

with L the Liouville operator (Sec. IX). Symbolically, we have then, at time t,

$$W^{(\mathrm{L})}(t, \{\mathbf{N}\})=e^{t\mathrm{L}}W_0\{\mathbf{N}\}. \tag{2.9}$$

The average value $\langle F\rangle$ in the ensemble of any function $F\{\mathbf{N}\}$, and hence of any instantaneously measureable physical quantity, is given by

$$\langle F\rangle=\int d\{\mathbf{N}\}[\mathbf{N}!]^{-1}F\{\mathbf{N}\}W\{\mathbf{N}\}, \tag{2.10}$$

and is therefore, by Eq. (2.9), determined for all time through W_0. Measurable macroscopic quantities $F\{\mathbf{N}\}$, however, always consist of a sum of functions each dependent only on the phase space, either of single molecules or at most on the Γ space, $\{\mathbf{n}\}_N$, of small subsets $\mathbf{n}=n_a, n_b, \cdots$ of molecules. We can formally write

$$F\{\mathbf{N}\}=\sum_{\mathbf{n}\geq 1}^{n\leq m} \sum_{\{\mathbf{n}\}\mathbf{N}} \mathbf{f}_n\{\mathbf{n}\}_N, \tag{2.11}$$

where the largest value, $n=n_a+n_b+\cdots$, of numbers of molecules whose Γ space appears in a single function is m, and the sum, for each set $\mathbf{n}$, runs over the $\mathbf{N}!/(\mathbf{N}-\mathbf{n})!\mathbf{n}!$ different possible subsets $\{\mathbf{n}\}_N$ for given $\mathbf{n}=n_a, n_b$, etc.

For instance, the kinetic energy in a sum only of singlet terms, $\mathbf{n}=a$ or b, etc., $\mathbf{p}_{ia}\cdot\mathbf{p}_{ia}/2m_a$. The potential energy of Eq. (2.4) depends on pair terms $u_{ab}(r_{ia,jb})$. The pressure, through the virial theorem, also depends on singlet and pair terms only. All thermodynamic properties are fully determined by functions up to $m=2$. Static properties involve only functions

which are even in the momenta, whereas flux variables have functions which are odd in the momenta.

At least one measurable instantaneous property, namely, slow neutron scattering does, in principle, involve functions up to $m=4$. The interference of only two scattering molecules determines the angular dependence of the scattering amplitude, but the momentum transfer is affected by the forces exerted on these molecules by their neighbors.

We define reduced probability density functions $w_n\{\mathbf{n}\}$ of the Γ space of small sets $\mathbf{n}$ of molecules. The integral operators

$$\mathcal{G}_N=\int[\mathbf{N}!]^{-1}d\{\mathbf{N}\},$$

$$\mathcal{G}_{N-n}=\int[\mathbf{N}-\mathbf{n}]^{!-1}d\{\mathbf{N}-\mathbf{n}\} \tag{2.12}$$

occur so often that we find it convenient to use the shortened symbolism. With this notation we have

$$w_n\{\mathbf{N}\}=\mathcal{G}_{N-n}W\{\mathbf{N}\} \tag{2.13}$$

and, since there are $\mathbf{N}!/(\mathbf{N}-\mathbf{n})!\mathbf{n}!$ subsets $\{\mathbf{n}\}_N$ for each $\mathbf{n}$, it is seen from Eqs. (2.10) and (2.11) that

$$\langle F\rangle=\sum_{n=1}^{n\leq m}\mathcal{G}^n f_n\{\mathbf{n}\}w_n\{\mathbf{n}\}. \tag{2.14}$$

We wish particularly to emphasize that all instantaneously measurable properties of a system depend only on those functions w_n for $\mathbf{n}$ up to some small value $n=m$, and that the pure thermodynamic properties depend on w_n only up to $n=2$.

III. Entropy and $\ln W$

The thermodynamic entropy S for a system in thermodynamic equilibrium is given by the equation

$$-S/k=\mathcal{G}_N W\{\mathbf{N}\}\ln(W\{\mathbf{N}\}h^{3N}), \tag{3.1}$$

where the $\ln h^{3N}$ is used to assure a value consistent with the third-law quantum mechanical absolute entropy.

The quantity $\ln(Wh^{3N})$ may be written as

$$\ln(Wh^{3N})=\sum_{n\geq 0}\Phi_n\{\mathbf{N}\}, \tag{3.2}$$

where Φ_0 is a constant. The other terms are the sums

$$\Phi_1\{\mathbf{N}\}=\sum_a\sum_{ia=1}^{ia=Na}\phi_a(\boldsymbol{\gamma}_{ia}),$$

$$\Phi_n\{\mathbf{N}\}=\sum_{\{n\}_N}\phi_n\{\mathbf{n}\}_N\Big(\sum_a n_a=n\Big), \tag{3.3}$$

the term Φ_n being a sum over the $\mathbf{N}!/(\mathbf{N}-\mathbf{n})!\mathbf{n}!$ different possible subsets of $\mathbf{n}=n_a, n_b,$ molecules, of functions ϕ_n of the Γ space $\{\mathbf{n}\}_N$ of these molecules. The functions ϕ_n would be uniquely defined *only if* we require that they, in turn, *do not* contain additive terms expressible as a sum of functions of smaller subsets of molecules.

For an equilibrium system

$$\Phi_0=-(PV/kT),$$

$$\phi_a(\boldsymbol{\gamma}_{ia})=(\mu_a/kT)-\mathbf{p}_{ia}\cdot\mathbf{p}_{ia}/2m_akT,$$

$$\phi_{ab}(\boldsymbol{\gamma}_{ia}\boldsymbol{\gamma}_{jb})=-u_{ab}(\mathbf{r}_{ia,jb})/kT,$$

$$\Phi_n\{\mathbf{N}\}=0,\qquad n\geq 3, \tag{3.4}$$

where μ_a in ϕ_a is the chemical potential of species a. For the equilibrium system we could obviously have added

$$\sum_a N_a\mu_a/kT=\mathbf{N}\cdot\mathbf{y}/kT \tag{3.5}$$

to the constant term Φ_0, and subtracted μ_a/kT from each of the N_a terms ϕ_a, writing $\Phi_0=A/kT$ with A the Helmholtz free energy. This is a more familiar form than Eq. (3.4) for the closed system.

We wrote the equations as in Eq. (3.4) to make the form for the initial nonequilibrium state with zero fluxes more obvious, namely,

$$\phi_a(\boldsymbol{\gamma}_{ia})=\mu_a(\mathbf{r}_{ia})/kT(\mathbf{r}_{ia})-\mathbf{p}_{ia}\cdot\mathbf{p}_{ia}/2m_akT(\mathbf{r}_{ia}),$$

$$\phi_{ab}=-u_{ab}(\mathbf{r}_{ia,jb})\{\tfrac{1}{2}[kT(\mathbf{r}_{ia})]^{-1}+\tfrac{1}{2}[kT(\mathbf{r}_{jb})]^{-1}\}, \tag{3.6}$$

which represents the function $\ln Wh^{3N}$ through Eqs. (3.3) and (3.2) for the local thermodynamic equilibrium of given $T(\mathbf{r})$ and $\mu_a(\mathbf{r})$. The constant Φ_0 must, in general, be determined by the normalization condition, Eq. (2.6). We discuss this later in Sec. X.

In general, then, if we use Eq. (3.6) with $\Phi_n=0$, $n\geq 3$, as initial states, the time evolution of $\ln W(t\{\mathbf{N}\})$ and hence of the functions Φ_n of Eq. (3.2) are determined by the Liouville equation. The nature of the equation is such that Φ_n for $n\gg 3$ becomes nonzero for $t>0$. We discuss this in more detail in Sec. IV.

For given functions $\phi_n\{\mathbf{n}\}$ using (Eq. 3.1) for the entropy, and Eq. (2.12) for w_n, we find

$$-S/k=\Phi_0+\sum_{n>1}\mathcal{G}_n\cdot w_n\{\mathbf{n}\}\phi_n\{\mathbf{n}\}. \tag{3.7}$$

IV. Three Paradoxes

There are three well-known paradoxes that follow from the assumption that the time evolution of a system is determined by the Liouville operator L through Eq. (2.9). These are as follows:

Paradox 1. If a proof is possible that $dS/dt>0$ for $t>0$ for an isolated system initially in a state of local thermodynamic equilibrium without flux [such as that determined by Eq. (3.6)] at $t=0$, then it is equally possible to prove that $dS/dt<0$ for $t<0$.

Paradox 2. For every ensemble characterized by a probability density distribution $W^{(L)}(t_0, \{\mathbf{N}\})$ given by Eq. (2.9) at t_0 from an initial distribution W_0 at $t=0$, there exists a "mirrored" ensemble $W_{\mathrm{mir},t_0}(t, \{\mathbf{N}\})$ obtained from W_0 by operating with $\exp[(t-t_0)\mathrm{L}-t_0\mathrm{L}]$

for which the gradients (in temperature or composition) at $t=t_0$ are the same as for $W^{(L)}(t_0)$, but for which the flows are in the opposite direction. Thus if the original system $W^{(L)}(t, \{\mathbf{N}\})$ has $dS/dt>0$ its mirror has $dS/dt<0$.

Paradox 3. If $-S/k$ is computed by Eq. (3.1) and $W^{(L)}$ given by the Liouville equation Eq. (2.9) then,

$$dS^{(L)}/dt=\dot{S}^{(L)}=0. \tag{4.1}$$

The first paradox follows simply from the fact that the Liouville operator is odd in the momenta. The initial state of static local thermodynamic equilibrium, with zero initial fluxes, is even in the momenta. The probability densities computed at t and $-t$ by Eq. (2.9) differ only in the replacement of each $\mathbf{p}_{ia}$ by $-\mathbf{p}_{ia}$. Since the static thermodynamic properties, and hence S are even in the momenta the statement of the paradox follows.

The second paradox is merely a restatement of the first, but in a form which is convenient for use as a counter example to many theorems that one would like to prove. For the present we content ourselves with a simple remark. A very usual experimental procedure is to start a system in some defined static thermodynamic state at $t=0$, let the flows settle to some quasi-stationary state at $t>0$, and start measurements. If Eq. (2.9) gives the correct $W^{(L)}(t, \{\mathbf{N}\})$ then this is the probability distribution appropriate to the description of an ensemble of systems so prepared. The only criterion by which we could judge $W_{mir}(t, \{\mathbf{N}\})$ to be less "probable" than $W^{(L)}(t, \{\mathbf{N}\})$ is just that $\dot{S}$ has the wrong sign. This augurs poorly for the possibility of rigorous proof that $\dot{S}\geq 0$.

The third paradox is well known. It follows rather trivially from the fact that the integral of L operating on any function which is zero at the limit of integration (as is $W \ln W$ for a closed system) is zero. The more physical interpretation is that every value $W_0\{\mathbf{N}_0\}$ at $t=0$, is transferred unchanged, and with unchanged volume element, to a new position $\{\mathbf{N}_t\}$ by the operation e^{tL}. The integral of $W^{(L)} \ln W^{(L)}$ thus remains unchanged in time.

The resolution of this last paradox is classical and well known.[1] We propose here that it is correct, but as classically given it is incomplete, and requires modification and amplification. The resolution long given is to define a "smoothed" probability density, $\bar{W}(t\{\mathbf{N}\})$, obtained by averaging $W^{(L)}$ in the neighborhood of the Γ-space point $\{\mathbf{N}\}$. With this function in Eq. (3.1) we define an entropy function $\bar{S}(t)$. One may then readily prove that

$$\bar{S}(t)\geq S^{(L)}(t). \tag{4.2}$$

The simplest argument for this procedure is by analogy, as originally given by Gibbs. The Liouville operator L acting on W_0 gives equations strikingly analogous to those for hydrodynamic flow in an incompressible medium. Consider a spherical globule of ink inserted in a still beaker of water by means of a medicine dropper. The composition of ink as a function of coordinate $\mathbf{r}$ is everywhere zero or unity, the abrupt rise occurring at the spherical surface of the globule. Smoothing this function over small distances makes little difference, since we "blur" only the small volume close to the surface. Now stir the mixture. The composition still remains zero or unity at all positions, with the volume in which it is unity unchanged. However, now the volume containing ink is strung out in long narrow filaments with a tremendous surface. Smoothing the composition function by averaging over the neighborhood at each position leads to the uniform low composition that we actually see, since all volume elements are close to some interface surface.

Analogously, the initial W_0, such as that of Eq. (3.6), is smooth. At $t=0$ we find $\bar{S}(t=0)=S^L(t=0)=S(\text{thermo. } t=0)$. At a later time the $W^{(L)}(t\{\mathbf{N}\})$ given by Eq. (2.9) using the Liouville operation on W_0 has the same values that occur in W_0, but intricately wound up in filaments in the $6N$-dimensional Γ space. "Smoothing" now alters the function radically. Since the integral of $W \ln W$ over Γ space has a minimum when W is constant in the allowable Γ space (restricted by the values of E and V), the smoothed negative entropy is lower than the initial value, $\bar{S}(t)>S(t=0)$.

There can be little doubt that this description holds at least much of the truth. However, as given, it is subject to several criticisms.

Firstly, the exact prescription for smoothing, that is, for obtaining $\bar{W}$ from $W^{(L)}$ is unclear. Any unrestricted averaging over all $\boldsymbol{\gamma}_{ia}$ independently, even over an extremely short range, alters the entropy for even the equilibrium function. That is, it is not correct to say that W_0 is microscopically smooth, since the necessary pair potential terms $-u_{ab}(r_{ia,jb})/kT$ in the exponent make it a rapidly varying function. The smoothing must be done by averaging in the Γ space near the point $\{\mathbf{N}\}$ *only over that portion of the* Γ *space for which the physical properties of the system are unaltered.* We shall come back to this criterion later.

The second objection to the smoothing prescription, as outlined, is more cogent to the logic. The validity of Eq. (4.2) does not suffice to prove that $d\bar{S}/dt>0$. An obvious counter example is given by the ensemble described by $W_{mir,t_0}(t, \{\mathbf{N}\})$ of our second paradox. This function at $t=t_0$ contains the intricately woven filaments of irregular W values, and $\bar{S}_{mir}(t_0)>S^{(L)}(t_0)$, indeed greater by a considerable amount. However at time $t=2t_0$ we have $W_{mir,t_0}(t=2t_0, \{\mathbf{N}\})=W_0\{\mathbf{N}\}$, namely, the initial "smooth" function, and $\bar{S}_{mir}(2t_0)=S^{(L)}(t=0)=S^{(L)}(t_0)$. If the existence of $W_{mir,t_0}(t, \{\mathbf{N}\})$ is acknowledged, the macroscopically inferred thermo-

[1] See, for instance, R. C. Tolman, *The Principles of Statistical Mechanics* (Oxford University Press, New York, 1938), for a rather complete analysis.

dynamic entropy actually decreases. Either the entropy is not that inferred from the static thermodynamic properties, or entropy can decrease with time.

At this stage the natural reaction is to deny the reality of W_{mir} and to state that the prescription of smoothing is indeed correct, but that there is merely needed an additional mathematical proof that W_{mir} cannot be attained. In other words that the ink sphere, once stirred into the water, cannot be would up again into a single globule. The proof is not only lacking, but an experimental gadget is purchasable in the magic shops which does wind up the ink ball!

The innocent spectator is shown a uniformly weakly dyed viscous fluid. The magician then proceeds to wind the dye into a neat intensely colored ball, leaving the rest of the solution clear.

The trick is accomplished by a modification of what is reported to be the even superior magic of G. I. Taylor. Taylor placed the Gibbs ink globule (in a less viscous fluid) between two cylinders, rather than in a beaker. By rotating the inner cylinder a prescribed number of turns at a prescribed rate (above the instability limit) the globule gives a uniform light color in a broad band encircling the anular space between the cylinders. On reversing the rotation of the inner cylinder by the same number of turns at the same rate, the ink is rewound into (almost) the original globule.

One may well object that this is argument only by analogy, and that the ink dispersion was in no sense molecular, so that the entropy, even if computed by smoothing W on the molecular scale, had not really increased significantly at any stage during the experiment.

The objection has been answered by John Blatt[2] who points out that the Hahn spin-echo experiment[3,4] shows a similar recovery of the inferred negative entropy loss, and on a truly molecular scale. The brief description of the experiment is as follows. Spins are aligned, and thereby given a high excess negative entropy. They are then caused to precess by a transverse magnetic field. The magnetic moment, whose magnitude is our $x(t)$, Fig. 1, then precesses in direction, but also decreases in magnitude since the individual spins do not all precess at exactly the same rate. The excess negative entropy inferred from the magnetic moment decreases towards its zero equilibrium value. In the course of the process at time t_0, by a clever pulsing technique on a field parallel to the original alignment, Hahn throws the spins into an alignment corresponding to our $W_{\text{mir},t_0}(t)$. The process is reversed, the magnetic moment magnitude starts to increase, and at $2t_0$ attains (almost) its original magnitude, and the negative entropy excess which was apparently lost is (almost) recovered.

The conclusion drawn by Blatt[2] is that which we also find obvious.[5] The smoothing of $W^{(L)}$ to $\bar{W}$ is unallowed as a pure mathematical artifice. It does, however, to a limited extent at least, always occur in every experiment. The mathematical reason is trivial. The $W^{(L)}$ computed from W_0 by the operation e^{tL} is correct only if the Hamiltonian is time independent. The Hamiltonian determined by the potential energy function Eq. (2.4) is not that of the experimental ensemble. Random time fluctuation in the wall potential occur, and it is these which "smooth" the probability density function W. No system within the universe is truly isolated in the sense implied by using the Liouville operator. Even if the walls are included within the system, fluctuations at the boundary due to radiation exchange with the surroundings necessarily occur.

In the case of the Hahn spin-echo experiment two circumstances minimize the smoothing. The phenomenon observed, the spin, is very loosely coupled to the surroundings, the experiment is carried out at an extremely low temperature, and the times involved are of the order of milliseconds, rather than of minutes as in our example. We will present reasons, which appear to us to be cogent, for believing that the recoverable negative entropy, in excess of the entropy to be inferred from the thermodynamic state, is negligible in the ordinary heat conduction or diffusion experiment carried out near room temperature and with time constants of the order of minutes. The point, however, is hardly important. We wish mainly to derive a more concise explanation and description of the smoothing process in nature, and of the "location" in W of that excess negative entropy above that of the inferred thermodynamic value.

V. Qualitative Nature of the Smoothing

We wish in this section, without recourse to a detailed mathematical description, to derive, on the basis of physical arguments, the nature of the negative entropy loss due to time dependent fluctuations at the walls. In the next section we give a more detailed mathematical formalism by which the process can be described.

Consider, first, a continuum of different probability distribution functions, $W(s, t, \{\mathbf{N}\})$ all giving the probability distribution as a function of $\{\mathbf{N}\}$ at time t, differing only in the time s at which they had started

[2] John Blatt, Progr. Theoret. Phys. (Kyoto) **22**, 745 (1959).
[3] E. L. Hahn, Phys. Rev. **80**, 580 (1950).
[4] E. L. Hahn, Phys. Today **6**, 4 (1953).

[5] This point of view is not revolutionary or new. It is, for instance, implied in many derivations of the relation between equilibrium statistical mechanics and thermodynamics, such as that in J. E. Mayer and M. G. Mayer, *Statistical Mechanics* (John Wiley & Sons, Inc., New York, 1940), and earlier by others. In these derivations the ergodicity is introduced as a perturbation on the idealized Hamiltonian of the system. As an explicit concept in the treatment of time dependent systems it has recently been used by Lebowitz and co-workers: P. G. Bergmann and J. L. Lebowitz, Phys. Rev. **99**, 578 (1955); E. P. Gross and J. L. Lebowitz, *ibid.* **104**, 1528 (1956); J. L. Lebowitz and H. L. Frisch, *ibid.* **107**, 917 (1957); and J. L. Lebowitz and P. G. Bergmann, Ann. Phys. **1**, 1 (1959). The article by Blatt discusses the logical philosophy of the concept, and does so with clarity.

on the curve $x(t)$, Fig. 1. The function $W(0, t, \{\mathbf{N}\})$ is given by

$$W(0, t, \{\mathbf{N}\}) = e^{t\mathrm{L}} W_0\{\mathbf{N}\}, \tag{5.1}$$

previously described by Eq. (2.9) for the system started at $t=0$, and at $x(t=0)=x_0$. The initial function for $W(s, t\{\mathbf{N}\})$ is then to be a function $W_s\{\mathbf{N}\}$, constructed similarly to the set of equations (3.6) but with the values of the local thermodynamic equilibrium $T(\mathbf{r})$ and $\mu_a(\mathbf{r})$ appropriate to $x(s)$, and

$$W(s, t, \{\mathbf{N}\}) = \exp[(t-s)\mathrm{L}] W_s\{\mathbf{N}\}. \tag{5.2}$$

If the systems of the ensemble are truly described by the static thermodynamic properties solely, as discussed at the end of the introduction, the systems for different values of s, in the interval $0 \leq s \leq t$, will all have identical behavior[6] for all times $t' \geq t$. Let us summarize this by the statement that the members of the ensembles described by $W(s, t\{\mathbf{N}\})$ for differing s values, $s<t$, have all identical macroscopic physical properties for all times $t'>t$.

Now consider the ensembles described by the functions $W_{\mathrm{mir}.t_0}(s, t, \{\mathbf{N}\})$ mirrored at t_0, i.e., $W_{\mathrm{mir}.t_0}(s, t) = \exp[(t-t_0)\mathrm{L} + (t_0-s)(-\mathrm{L})] W_s\{\mathbf{N}\}$ for different s values. There are two qualities of these ensembles which depend strongly on s. The first characteristic is shared with the ensembles $W(s, t\{\mathbf{N}\})$, namely, that

$$S^{(\mathrm{L})}(s, t) = S[\text{thermo.}, x(s)] \tag{5.3}$$

with

$$dS[\text{thermo. } x(s)]/ds > 0. \tag{5.4}$$

The second characteristic is that each of these ensembles will climb "uphill" on the $x(t)$ or $-\Delta S(t)$ curve (Fig. 1) until time $t=2t_0-s$, and then descend with "normal" behavior.

Now we ask what are the required built-in characteristics of the probability density that can cause the ensemble $W_{\mathrm{mir}}(s, t, \{\mathbf{N}\})$ to behave "abnormally" between times t_0 and $2t_0-s$. Consider the behavior of the systems, $W(s, t, \{\mathbf{N}\})$, on the "normal" branch of descending $x(t)$, say in the case of diffusion of molecules of species a from the top to bottom of the system. The collisions of a molecules with others are essentially random: as many are thrown up as down in each collision. However, since there are more above any horizontal plane than below, the net flux is downward. For the mirrored ensemble $W_{\mathrm{mir}}(s, t, \{\mathbf{N}\})$, there are still more a molecules above than below, but the collisions are such that an excess move up after collision: the net flow is reversed. Some abnormal property is built into the function $W_{\mathrm{mir}}(s, t_0, \{\mathbf{N}\})$ which determines this character in the collisions for all times until $2t_0-s$. The requirement that molecule ia when colliding with jb at $t_0+\Delta t$ shall take a peculiar course requires that not only the phase-space position of ia and jb were correlated at t_0, but that also these were correlated with all molecules kc, lc, etc., with which these had collided between t_0 and $t_0+\Delta t$, and also, in turn with all with which these had previously collided, etc.

The total number of molecules between which the correlations must be determined in order that the mirrored ensemble run uphill until $t_0+\Delta t$ may be estimated as the number in a sphere of radius $c\Delta t$, with c the sound velocity. Since sound velocities are of the order of centimeters per millisecond it follows that if t_0-s is of order much greater than milliseconds, the "abnormal" behavior of the mirrored ensemble is due to correlations between all the molecules in the system. On the other hand, if t_0-s is only of the order of some milliseconds, then for systems with time constants of the order of minutes, the excess negative entropy $S[\text{thermo. } x(s)] - S[\text{thermo. } x(t_0)]$ at t_0 is completely negligible.

We thus arrive at the following somewhat vague conclusions which motivate our subsequent analysis. Firstly, the original excess negative entropy of the initial system diffuses with time into terms associated with correlations between increasing numbers of molecules. In times of the order of milliseconds it reaches correlations between all molecules in the system. Secondly, for systems with time constants of the order of minutes the amount of negative entropy stored in correlations between numbers of molecules less than M, with $M \sim N^{1/3}$ is relatively negligible. Thirdly, the "smoothing" done by the random time dependent effect of the surroundings on the walls of the system occurs in the correlations between numbers of molecules M or greater, M of order $N^{1/3}$. We can hardly believe that such correlations can persist for appreciable times when the walls are subject to radiation exchange with the surroundings at temperatures near to room temperatures.

We proceed to formulate these considerations more precisely.

VI. Physically Insignificant Correlations

The most naïve reaction to the conclusions of the previous section, when applied to the equations for the entropy given in Sec. III, would be to assume that the terms $\phi_n\{\mathbf{n}\}$ with $M<n<N$ of Eq. (3.7) could be simply neglected. In other words the smoothing of nature might be to set $\phi_n=0$ for $n>M$.

A little consideration shows this to be erroneous. For instance, if only the singlet terms, $\phi_a(\boldsymbol{\gamma}_{ia})$ are retained, the equations correspond to the time evolution of a system with no interactions between molecules. Diffusion and temperature equalization would proceed with sound velocity. The high order ϕ_n's with $n \cong N$ are essential in determining the physical properties of the system.

[6] Since the initial states are always those of systems with zero fluxes, it will require several or more collision times, of order 10^{-12} sec, before those initially started at s "catch up" with those started earlier. It is partially for this reason that we limited our consideration to systems with long time constants.

The procedure that is required may be described in two alternate fashions. In any case the physical basis is the same. We have emphasized in the second section that the instantaneously measurable physical properties depend only on the reduced probability density functions, $w_n\{\mathbf{n}\}$, for small numerical values of n. By the definition of a thermodynamically isolated system these functions w_n for small n must be the same as those of the system obeying the exact Liouville relation, Eq. (2.9), since the isolated system is not influenced in its physical behavior by the surroundings. We thus always use Eq. (2.12) to define $w_n\{\mathbf{n}\}$ with the Liouville function for all molecules, $W^{(L)}(t, \{\mathbf{N}\})$ under the integrand on the right.

Now suppose that these functions, $w_n(t, \{\mathbf{n}\})$ are thus defined at t for all sets n with $n \leq m$, but not for higher n-values. This limited set of functions would not suffice to define a unique $W^{(m)}(t, \{\mathbf{N}\})$. However, a unique function, $W^{(m)}(t, \{\mathbf{N}\})$ can be defined from this set as follows. Require that

$$w_n(t, \{\mathbf{n}\}) = g_{N-n} W^{(m)}(t, \{\mathbf{N}\}) \quad \text{for} \quad n \leq m, \quad (6.1)$$

and that

$$\ln h^{3N} W^{(m)}(t, \{\mathbf{N}\}) = \sum_{\mathbf{n}\geq 1}^{\mathbf{n}\leq \mathbf{m}} \sum_{\{n\}_N} \psi_n^{(m)}(t, \{\mathbf{n}\}_N), \quad (6.2)$$

where the sum of Eq. (6.2) runs up to m only. We may make the functions ψ_n unique by requiring that each has no additive part which can be written as a sum of functions of the Γ space of a smaller subset, $\{\mathbf{v}\}_n$ except for the singlet terms, $\psi_a(\boldsymbol{\gamma}_a)$, in which we choose to include a constant to retain the normalization condition Eq. (2.6).

Equations (6.1) and (6.2) define, for each w_n, including $w_0 \equiv 1$, a corresponding function, $\psi_n^{(m)}$, of the same Γ space.

Carry this procedure out for all m values to $m = N$. We then have

$$W^{(N)}(t\{\mathbf{N}\}) = W^{(L)}(t, \{\mathbf{N}\}). \quad (6.3)$$

We have thus, for every time t, constructed a hierarchy of probability density distributions, $W^{(m)}(t, \{\mathbf{N}\})$ for $1 \leq m \leq N$, of increasing complexity with increasing m value. The function with $m = 2$ gives correctly the energy and pressure, and hence also the *inferred* thermodynamic entropy. More detailed instantaneous measurements made upon the system, such as slow neutron scattering, may require functions for higher m values, say up to $m = 4$, to correctly reproduce the experimental values. Let us arbitrarily choose some value m_0, and say that all instantaneously measurable properties depend on $w_n\{\mathbf{n}\}$ for $n \leq m_0$.

The function $W^{(m_0)}(t, \{\mathbf{N}\})$ is then a "smoothed" probability density function which correctly gives all measurable properties of the system. The function $W^{(2)}(t, \{\mathbf{N}\})$, if used in Eq. (3.1) for $-S/k$ gives correctly the *inferred* thermodynamic entropy. The function $W^{(N)}(t, \{\mathbf{N}\})$ gives the probability density for a hypothetical mathematically ideal system completely isolated by a time-independent Hamiltonian at the walls from any contact with the rest of the universe. The functions $W^{(m)}$ for $m_0 \leq m \leq N$ correspond to ensembles all having identical measurable physical properties. If used in Eq. (3.1) to compute $-S/k$ they lead to differing values $S^{(m)}$ of the entropy. In view of the remark that the "smoothest" function W consistent with a given restraint leads to the maximum value of the entropy from this equation, it is not surprising that we can readily prove (Sec. XIII) that

$$S^{(2)} \geq S^{(3)} \geq \cdots \geq S^{(m)} \geq S^{(m+1)} \geq \cdots \geq S^{(N)} = S^{(L)}. \quad (6.4)$$

Our picture is then the following. Experimental systems are always subject to time dependent fluctuations at the walls. The effect of these is to wipe out correlations for numbers of molecules greater than some value M. The *true* entropy is then that given by $S^{(M)}$. For any initial state of local thermodynamic equilibrium $S^{(2)}(t=0) = S^{(L)}(t=0)$. As t increases $S^{(L)} = S^{(N)}$ stays constant, but in a very short interval of time the difference $S^{(M)}(t) - S^{(N)}$, starts to increase. This time is usually of the order of that required for a sound wave in the medium to traverse the system. The *inferred* thermodynamic entropy $S^{(2)}(t)$ is greater than the *true* entropy $S^{(M)}(t)$. In ordinary classical experiments at room temperature or above, with time constants of the order minutes, this difference is negligible. However, as shown by the Hahn spin-echo, if the time constant is short, the temperature low, and the coupling of the phenomenon observed with the surrounding universe is small, then $S^{(2)}(t) - S^{(M)}(t)$ may become large. By sufficiently clever manipulation one may cause this difference to decrease, $dS^{(2)}(t)/dt < 0$, but always $dS^{(M)}(t)/dt \geq 0$.

Now, however, at any stage t_0 of experimentation, imagine that all transport is halted, for instance by the insertion of insulating and nonpermeable walls to "freeze" the system into a stationary thermodynamic state. In this state proceed to measure the thermodynamic entropy by a true thermodynamic heat cycle. The process necessarily destroys the correlations even below numbers M of molecules, and the true entropy rises to the inferred value, $S^{(2)}(t_0)$.

This concludes our discussion of the logic and method, referring the mathematical proofs to the later sections. We define an entropy for which $\dot{S} \geq 0$. We define a method for computing an *inferred* thermodynamic entropy, $S_{th} = S^{(2)}$, which may not always increase in time, but which will be the entropy measured if at any time the experiment is stopped and a thermal measurement made. We have not disposed of the first paradox.

The first paradox is essentially semantic. Thermodynamics never states that for a given system the entropy will increase, but that for the average system of an ensemble prepared in a given state, and *then left*

isolated, that $\dot{S} \geq 0$. We can equally well prove that for this ensemble, *if they have been isolated for all past time*, they must have originated as a fluctuation from equilibrium with a consequent decrease in entropy. This is extraordinarily unlikely. Our viewpoint of the past is biased by our biological memory, our knowledge of history. If we find a laboratory system markedly out of equilibrium, we assume something which is *a priori* even more unlikely than that it arise by a fluctuation, namely, that a more remarkable fluctuation of molecules produced a scientist who has previously prepared it out of equilibrium.

We must concede, however, that our logic precludes a discussion of the entropy of the finite universe, since this (if it is finite) is a single system, and we know only the entropy of a representative member of an ensemble.[2] On the other hand, we can measure local thermodynamic entropies of the parts of the universe in our reach, and there is no doubt that for these the entropy flow is in one time direction. That this time direction is necessarily coupled with that of biological memory has been discussed by Blum.[7]

B. MATHEMATICAL DETAILS

VII. Outline and the Equation for $W^{(m)}$

We have suppressed the discussion of mathematical derivations as far as seemed practical in the preceding sections, and have given no proofs of the more mathematical assertions. In this and the succeeding sections we develop some equations, and make one necessary proof.

First, in this section we show how, in principle at least, it is possible to compute $W^{(m)}$ from a knowledge of the reduced probability density functions $w_n\{\mathbf{n}\}$ for sets $\mathbf{n}$ of molecules for $n \leq m$; the requirement making $W^{(m)}$ unique is that $\ln W^{(m)}$ is expressible as a sum of functions $\psi_n\{\mathbf{n}\}$ for $n \leq m$, that is, it contains no correlation functions for sets of greater than m molecules. Second, in Sec. VIII we prove that the function $W^{(m)}$ so defined has a maximum entropy compared to all other functions W which lead to the *same* set of reduced probability density functions $w_n\{\mathbf{n}\}$ for $n \leq m$. We thus prove the assertion of Eq. (6.4).

In Sec. IX we discuss the Liouville operator and show that the first time derivative of $w_n\{\mathbf{n}\}$ depends only on functions w_n' for n' having one more molecule than the set $\mathbf{n}$. From this it follows that $\dot{w}_m$, and hence $\dot{W}^{(m)}$ is fully determined by $W^{(m+1)}$. In Sec. X we write the equations necessary for the definition of localized thermodynamic densities and their fluxes, particularly for the entropy. From this, in Sec. XI we show that our equations are consistent with the "irreversible thermodynamics" equations for localized entropy production in the steady state.

[7] Harold F. Blum, *Times Arrow and Evolution* (Princeton University Press, Princeton, New Jersey, 1951).

An explanation of the notation may be in order here, although we have attempted to make it as self-evident as seemed possible consistent with reasonable brevity.

In equations in which it is unnecessary to distinguish the types, a, b, $\cdots$ of molecules we number the molecules by i or j, $1 \leq i \leq N$, and use m_i for the mass of molecule i and $u_{ij}(r_{ij})$ for the pair potential. Where the distinction of the type of molecule is important we number ia, jb, $\cdots$ etc., $1a \leq ia \leq Na$, $1b \leq jb \leq Nb$, and use m_a, u_{aa}, u_{ab}, $\cdots$. If we wish to indicate that ia is a member of the subset $\{\mathbf{n}\}_N$ we write $ia \subset \{\mathbf{n}\}_N$ or more simply $ia \subset \mathbf{n}$.

The functions, $w_n\{\mathbf{n}\}$, $\psi_n\{\mathbf{n}\}$, etc., are written with the subscript $\mathbf{n}$ to indicate that the functional form of the dependence on the variable depends on the number set $\mathbf{n}=n_a, n_b, \cdots$, whereas the variable is the $6n$-dimensional Γ space $\{\mathbf{n}\}$ of the subset. When it is necessary to indicate that the set is a sum of two sets, $\mathbf{n}+\mathbf{m}$ we use $w_{n+m}\{\{\mathbf{n}\}+\{\mathbf{m}\}\}$. If $_n$ is now a single molecule of type a we use $w_{a+m}\{\gamma_{ia}+\{\mathbf{m}\}\}$. When the set contains one *less* molecule of type a than a set $\mathbf{n}$ (for which necessarily $n_a \geq 1$), we use $w_{n-a}\{\{\mathbf{n}\}-\gamma_{ia}\}$ where, of course, $ia \subset \{\mathbf{n}\}$, and we also will use $w_{n-\nu}\{\{\mathbf{n}\}-\{\nu\}_n\}$ for the set $\mathbf{n}$ less some subset $\nu \subset \mathbf{n}$.

The functions introduced so far are always symmetric in permutations of like molecules. When this is not the case, as in $K_{n,m}(\{\mathbf{n}\}, \{\mathbf{m}\})$ of Eq. (7.16), this is indicated by a comma, $\mathbf{n}, \mathbf{m}$, rather than by the sum sign, $\mathbf{n}+\mathbf{m}$. The function $K_{n,m}$ is symmetric in permutations of like molecules of the set $\mathbf{n}$ with each other, and in permutations of like molecules of $\mathbf{m}$ with each other, but not in permutations between the two sets.

The notation should be reasonably self-evident, except possibly in one case, Eq. (7.7′), where it is necessary to sum over subsets $\{\mathbf{\nu}\}_m$ of a set $\mathbf{m}$, but with the restriction that the subsets are identical to a set ν, $\mu_a=\nu_a$, $\mu_b=\nu_b$, $\cdots$. This is indicated by setting $\nu=\mathbf{\nu}$ under the summation.

We generally use ∇_{ri} for the three-dimensional vector operator of components $\partial/\partial x_i$, $\partial/\partial y_i$, $\partial/\partial z_i$, and ∇_{pi} for that of components $\partial/\partial p_{xi}$, $\partial/\partial p_{yi}$, $\partial/\partial p_{zi}$. In this section alone we find it convenient to use ∇_i for a *six*-dimensional vector operator of six *different* components, $\partial/\partial x_i \cdots \partial/\partial p_z$.

We turn now to the equations determining $W^{(m)}$. In general, if

$$\ln W h^{3N} = \sum_{n \geq 1} \sum_{\{n\}_N} \psi_n\{\mathbf{n}\}_N, \tag{7.1}$$

and

$$w_n\{\mathbf{n}\} = \vartheta_{N-n} W, \tag{7.2}$$

then, after operation on both sides of Eq. (7.2) with ∇_i (where $i \subset \mathbf{n}$) one has

$$\nabla_i w_n = \vartheta_{N-m} \sum_{\nu=0}^{\nu=n-1} \sum_{\{m\}N-n \geq 0} \sum_{\{\nu\}\, n-i} W \nabla_i \psi_{i+\nu+m}. \tag{7.3}$$

Since there are $(\mathbf{N}-\mathbf{n})!/\mathbf{m}!(\mathbf{N}-\mathbf{n}-\mathbf{m})!$ different

subsets $\{\mathbf{m}\}_{N-n}$ leading to the same integral, one finds

$$\nabla_{i\alpha}w_n=\sum_{\nu=0}^{\nu=n-1}\sum_{\{\nu\}_{n-i}}\sum_{m\geq 0}g_m w_{n+m}\{\{\mathbf{n}\}+\{\mathbf{m}\}\}\times\nabla_{i\alpha}\psi_{i+\nu+m}\{\{\nu\}_n+\{\mathbf{m}\}+\gamma_i\},\quad(7.4)$$

where the terms $m=0$ are simple products.

We now wish to simplify the appearance of Eq. (7.4) at the cost of introducing more complicated kernel integrators by collecting all terms of $\nu+\mathbf{m}=\mathbf{k}$ to arrive at the form

$$\nabla_{i\alpha}w_{a+n}\{\gamma_{i\alpha}+\{\mathbf{n}\}\}=\sum_{m\geq 0}g_m L_{a,n,m}(\gamma_{i\alpha},\{\mathbf{n}\},\{\mathbf{m}\})\nabla_{i\alpha}\psi_{a+m}\{\gamma_{i\alpha}+\{\mathbf{m}\}\},\quad(7.5)$$

where we now distinguish the species a of molecule for which the differential operator $\nabla_{i\alpha}$ is used.

To obtain Eq. (7.5) we define a sum of products of Dirac delta functions, $\Delta_{\nu,m}(\{\nu\},\{\mathbf{m}\})$, defined for any two sets ν, $\mathbf{m}$, including $\nu\equiv 0$ but for which $\nu\leq\mathbf{m}$, i.e., $\nu_a\leq m_a$ for all a. The function, $\Delta_{0,m}$, for $\nu\equiv 0$ is unity, that for $0<\nu\leq\mathbf{m}$ is a sum of $\mathbf{m}!/(\mathbf{m}-\nu)!$ different products of the $\nu=\sum\nu_a$ different possible products of six dimensional Dirac delta-functions between like molecules of ν and $\mathbf{m}$. That is, we define

$$\delta(\gamma_{i\alpha}-\gamma_{j\alpha})=\prod_{\alpha=1}^{\alpha=3}\delta(x_{\alpha i\alpha}-x_{\alpha i\alpha})\delta(p_{\alpha i\alpha}-p_{\alpha j\alpha})\quad(7.6)$$

and for two identical sets $\nu=\mu$, the sum of $\nu!$ products of such functions,

$$\delta(\{\nu\},\{\mu\})=\prod_a\sum_{p=1}^{p=\nu a!}\mathcal{P}_p(\nu a)\prod_{i\alpha\subset\nu,j\alpha\subset\mu}\delta(\gamma_{i\alpha}-\gamma_{j\alpha})\quad(7.6')$$

with $\mathcal{P}$ the permutation operator. We then define

$$\Delta_{0,m}=1\quad(7.7)$$

$$\Delta_{\nu,m}(\{\nu\},\{\mathbf{m}\})=\sum_{\mu\equiv\nu}\sum_{\{\mu\}_m}\delta(\{\nu\},\{\mu\}_m),\quad(7.7')$$

where the sum runs over the $\mathbf{m}!/(\mathbf{m}-\nu)!\nu!$ different subsets $\{\mu\}_m$ for which $\mu=\nu$.

The functions $\Delta_{\nu,m}$ obey the recursion formula

$$\Delta_{a+\nu,m}(\{\gamma_{i\alpha+\nu a}+\{\nu\}\},\{\mathbf{m}\})=\sum_{j\alpha\subset m}\delta(\gamma_{i\alpha+\nu a}-\gamma_{ja})\Delta_{\nu,m-a}(\{\nu\},\{\{\mathbf{m}\}-\gamma_{ja}\}),\quad(m_a\geq\nu_a+1)\quad(7.7'')$$

which suffices to define them with $\Delta_{0,m}=1$. Now define

$$\omega_{\nu+k,\nu,m}(\{\nu\},\{\mathbf{k}\},\{\mathbf{m}\})=w_{k+m}\{\{\mathbf{k}\}+\{\mathbf{m}\}\}\Delta_{\nu,m}(\{\nu\},\{\mathbf{m}\})\quad(7.8)$$

so that

$$g_m\omega_{a+n,\nu,m}(\{\nu\}_n,\{\gamma_{i\alpha}+\{\mathbf{n}\}-\{\nu_n\},\{\mathbf{m}\})\nabla_{i\alpha}\psi_{a+m}\{\gamma_{i\alpha}+\{\mathbf{m}\}\}=g_{m-\mu}(\nu=\mu)w_{a+n+m-\mu}\{\gamma_{i\alpha}+\{\mathbf{n}\}+\{\mathbf{m}\}-\{\mu\}_m\}\times\nabla_{i\alpha}\psi_{a+\nu-m-\mu}\{\gamma_{i\alpha}+\{\nu\}_n+\{\mathbf{m}\}-\{\mu\}_m\}.\quad(7.9)$$

Finally with the kernel function

$$L_{a,n'm}(\nu_{i\alpha},\{\mathbf{n}\},\{\mathbf{m}\})=\sum_{\nu=0}^{\nu=n,m}\sum_{\{\nu\}_n}\omega_{a+n,\nu,m}(\{\nu\}_n,\{\gamma_{i\alpha}+\{\mathbf{n}\}-\{\nu\}_n\},\{\mathbf{m}\}),\quad(7.10)$$

one sees from Eq. (7.9) that Eq. (7.5) follows directly from Eq. (7.4).

Equation (7.4) or (7.5) for a one component fluid at equilibrium, for which $\psi_1=-p^2/2mkT+\mu/kT-P/\rho kT$, $\psi_2=-u(r_{ij})/kT$, $\psi_m=0$, $m>2$, written for the three-dimensional operator ∇_{ri} operating on w_2, and integrated over the momenta, becomes

$$\nabla_{ri}\rho_2(r_{ij})=-\rho_2(r_{ij})\nabla_{ri}[u(r_{ij})/kT]-\int d\mathbf{r}_k\rho_3(\mathbf{r}_i,\mathbf{r}_j,\mathbf{r}_k)\nabla_{ri}[-u(r_{ik})/kT],\quad(7.11)$$

which is the Yvon[8] or Born-Green[9] integral equation for the pair probability density function $\rho_2(r_{ij})$. Equations (7.4) or (7.5) are simply generalizations of this.

Now our problem is as follows: We assume that the reduced probability density functions $w_n\{\mathbf{n}\}$ are known for $1\leq n\leq m$. For a one-component system there are m such functions, for a two-component system there are $(1/2)m\ (m+3)$ functions. In general, let us say, there are k different functions. We demand that the complete probability density function $W^{(m)}$ be such that the k equations (7.2) are satisfied for $n\leq m$, and that

$$\ln W^{(m)}=\sum_{n=1}^{n=m}\sum_{\{n\}_N}\psi_n^{(m)}\{\mathbf{n}\}_N,\quad(7.12)$$

so that there are only k nonzero functions ψ_n.

The k-coupled linear nonhomogeneous integro-differential equations (7.5) with appropriate boundary conditions then serve to determine the unknown functions ψ_n.

For $2\leq n\leq m$ the boundary conditions are that ψ_n be zero if any distance, r_{ij}, $i,j\subset\mathbf{n}$, approach infinite value.

For $\mathbf{n}=a,b,\cdots$, etc., one normalization condition, $w_0=g_N W=1$, gives one equation for the arbitrary additive constants of $\psi_a,\psi_b,\cdots$. These constants in the individual functions are otherwise arbitrary, since if a constant A is added to each of the N_a different func-

[8] J. Yvon, *Statistiques des Fluides et L'Equation D'Etat* (Hermann & Cie, Paris, France, 1935).

[9] M. Born and H. S. Green, *A General Kinetic Theory of Liquids* (Cambridge University Press, New York, 1949).

tions ψ_a, and $B=-(N_a/N_b)A$ added to each of the N_b functions ψ_b, the value of $\ln W$ is unchanged.

For the limiting case $m=1$ the solutions of Eq. (7.5) are $\psi_a^{(1)}(\gamma_a)=\ln w_a(\gamma_a)-\ln N_a$. For $m=2$, one has, from Eq. (7.4) or (7.5)

$$\nabla_a w_a(\gamma_a)=w_a(\gamma_a)\nabla_a\psi_a^{(2)}(\gamma_a)+\sum_c\int d\gamma_c w_{ac}(\gamma_a,\gamma_c)\nabla_a\psi_{ac}^{(2)}(\gamma_a,\gamma_c), \quad (7.13)$$

$$\nabla_a\psi_a^{(2)}(\gamma_a)=\nabla_a\ln w_a(\gamma_a)-\sum_c\int d\gamma_c\frac{w_{ac}(\gamma_a,\gamma_c)}{w_a(\gamma_a)}\nabla_a\psi_{ac}^{(2)}(\gamma_a,\gamma_c), \quad (7.13')$$

and

$$\nabla_a w_{ab}(\gamma_a,\gamma_b)=w_{ab}(\gamma_a,\gamma_b)[\nabla_a\psi_a^{(2)}(\gamma_a)+\nabla_a\psi_{ab}^{(2)}(\gamma_a,\gamma_b)]+\sum_c\int d\gamma_c w_{abc}(\gamma_a,\gamma_b,\gamma_c)\nabla_a\psi_{ac}^{(2)}(\gamma_a,\gamma_c), \quad (7.14)$$

which, with Eq. (7.13′) reduces to

$$\nabla_a\psi_{ab}^{(2)}(\gamma_a,\gamma_b)=\nabla_a\ln[w_{ab}(\gamma_a,\gamma_b)/w_a(\gamma_a)]-\sum_c\int d\gamma_c\left[\frac{w_{abc}(\gamma_a,\gamma_b,\gamma_c)}{w_{ab}(\gamma_a,\gamma_b)}-\frac{w_{ac}(\gamma_a,\gamma_c)}{w_a(\gamma_a)}\right]\times\nabla_a\psi_{ac}^{(2)}(\gamma_a,\gamma_c). \quad (7.14')$$

For a single-component system the summation over c disappears, the equation is a single linear nonhomogeneous Fredholm integral equation in $\nabla_a\psi_{aa}(\gamma_a,\gamma_a)$.

For sufficiently large distances r_{ab},

$$w_{ab}(\gamma_a,\gamma_b)/w_a(\gamma_a)\to w_b(\gamma_b), \qquad r_{ab}\to\infty$$

$$w_{abc}(\gamma_a,\gamma_b,\gamma_c)/w_{ab}(\gamma_a,\gamma_b)\to w_{ac}(\gamma_a,\gamma_c)/w_a(\gamma_a), \qquad r_{ab}\to\infty$$

so that $\nabla_a\psi_{ab}(\gamma_a,\gamma_b)\to 0$, $r_{ab}\to\infty$, and the boundary condition $\psi_{ab}\to 0$, $r_{ab}\to\infty$, can be used. This characteristic of the kernels remains for higher m values.

For the unsymmetrical kernels $L_{a,n,m}$ there are no general existence theorems that real solutions ψ_n can be found to the set of k-coupled equations (7.5). Indeed it is rather obvious that arbitrary reduced probability density functions $w_n\{\mathbf{n}\}$ which still obey the necessary condition,

$$\int d\gamma_a w_{a+n}\{\gamma_a+\{\mathbf{n}\}\}=(N_a-n_a)w_n\{\mathbf{n}\},$$

may be found for which no real solutions ψ_n exist. To show this, it suffices to consider the one-component case, and choose $w_2(\gamma_i,\gamma_j)=0$ for $r_{ij}<2r_0$, but with

$$\rho=N/V=V^{-1}\int_V d\gamma_i w_1(\gamma_i)>(4\sqrt{2}r_0^3)^{-1}.$$

For this case the pair-distribution function is assumed to be such that no molecule has a neighbor with center closer than $2r_0$, but the total density is greater than that of close packed spheres of radius r_0. Obviously no real positive definite probability density, $W\{N\}$, of all the molecules can correspond to such a pair distribution, and hence no real functions, $\psi_n\{n\}$, of Eq. (7.1) exist.

However, our assumptions are that the reduced probability density functions w_n are those computed by Eq. (7.2) from $W^{(L)}=e^{tL}W(t=0)$, and hence do actually correspond to at least one real positive definite function W, namely, $W^{(L)}$. In the next section we show that of the infinite continuum of functions W in the complete Γ space $\{\mathbf{N}\}$, which lead to the k functions w_n for $n\le m$, there is one unique function $W^{(m)}$ of maximum entropy. For that function $\psi_n\equiv 0$ for $n>m$. For $n\le m$ the functions $\psi_n\{n\}$ are the undetermined multipliers $\phi_n\{\mathbf{n}\}$ introduced into the variation in order to require that the functions $w_n\{\mathbf{n}\}$ be held constant at the position $\{\mathbf{n}\}$. This function $\phi_n\{\mathbf{n}\}$ is then the change of $-S/k$ per infinitesimal increment in w_n at $\{\mathbf{n}\}$, and hence real. Since, then, there are real functions $\psi_n\{\mathbf{n}\}$ for $1\le n\le m$, that lead to a positive $W\{\mathbf{N}\}$, indeed that of maximum entropy, and since these obey Eq. (7.5), it follows that there are solutions to Eq. (7.5) for those functions w_n that correspond to any real system.

There is, however, one comment that should be made about Eqs. (7.4) or (7.5). We assume knowledge of the functions w_n for $n\le m$, but not for $n\ge m$. In Eq. (7.14′) for $\nabla_a\psi_{ab}^{(2)}$ the function w_{abc} for three molecules enters into the kernel. The correct function w_{abc} to use is that obtained from $\vartheta_{N-a-b-c}W^{(2)}$. In practice one would presumably use the Kirkwood closure,

$$w_{abc}(\gamma_a,\gamma_b,\gamma_c)=w_{bc}(\gamma_b,\gamma_c)w_{ca}(\gamma_c,\gamma_a)w_{ab}(\gamma_a,\gamma_b)\times[w_a(\gamma_a)w_b(\gamma_b)w_c(\gamma_c)]^{-1}.$$

In principle, of course, having used this closure to obtain approximate $\psi_n^{(2)}$s one could use Eq. (7.2) to improve the kernel, and so iterate. In practice, for liquids, this is not feasible.

We conclude this section by recording the equations relating the time derivatives $\dot{w}_n=\partial w_n/\partial t$ and $\dot{\psi}_n=\partial\psi_n/\partial t$. Use Eq. (7.1) and operate by $\partial/\partial t$ on both sides of Eq. (7.2). One obtains

$$\dot{w}_n\{\mathbf{n}\}=\sum_{\nu=0}^{\nu=n}\sum_{\{\nu\}_n}\sum_{m\ge 0}\vartheta_m w_{n+m}\{\{\mathbf{n}\}+\{\mathbf{m}\}\}\psi_{\nu+m}\{\{\nu\}_n+\{\mathbf{m}\}\}. \quad (7.15)$$

If the kernel,

$$K_{n,m}(\{\mathbf{n}\},\{\mathbf{m}\})=\sum_{\nu=0}^{\nu=n,m}\sum_{\{\nu\}_n}\omega_{n,\nu,m}(\{\nu\}_n,\{\{\mathbf{n}\}-\{\nu\}_n,\{\mathbf{m}\}), \quad (7.16)$$

is defined, Eq. (7.15) becomes

$$\dot{w}_n\{\mathbf{n}\}=\sum_{m>1}\mathcal{g}_m K_{n,m}(\{\mathbf{n}\},\{\mathbf{m}\})\psi_m\{\mathbf{m}\}. \quad (7.17)$$

The set of k equations, (7.17), for $1\leq n\leq m$, with the boundary condition of given initial $\psi_n(t=0,\{\mathbf{n}\})$ are alternate to Eq. (7.5) for the determination of $\psi_n(t,\{\mathbf{n}\})$.

VIII. Entropies, $S^{(m)}$

We wish, in this section, to make the proof that, for fixed values of the reduced probability density functions w_n for $0\leq n\leq m$, of those functions W which lead to these w_n by the equation $\mathcal{g}_{N-n}W=w_n$, that of maximum entropy is the function $W^{(m)}$ whose logarithm given by Eq. (7.12) contains nonzero functions ψ_n only up to $n=m$. The general method is to use $\mathcal{g}_N W\ln(Wh^{3N})$ for $-S/k$, and, by the method of undetermined multipliers, to show that this is an extremum with $\psi_n=0$ for $n>m$, if the w_n for $n\leq m$ are fixed.

Make use of the delta-function $\Delta_{n,N}(\{\mathbf{n}\},\{\mathbf{N}\})$ defined by Eq. (7.7) to write

$$w_n\{\mathbf{n}\}=\mathcal{g}_N\Delta_{n,N}(\{\mathbf{n}\},\{\mathbf{N}\})W\{\mathbf{N}\}. \quad (8.1)$$

This must be multiplied by an undetermined multiplier $\phi_n\{\mathbf{n}\}$ and subtracted from the variation of $-S/k$, if $w_n\{\mathbf{n}\}$ is not to be allowed to vary at $\{\mathbf{n}\}$. Since, however, w_n is not to vary at *any* $\{\mathbf{n}\}$ we must subtract

$$\begin{aligned}\mathcal{g}_n\phi_n\{\mathbf{n}\}&=\mathcal{g}_n\mathcal{g}_N\phi_n\{\mathbf{n}\}\Delta_{n,N}(\{\mathbf{n}\},\{\mathbf{N}\})W\{\mathbf{N}\}\\&=\sum_{\{n\}_N}\mathcal{g}_N\phi_n\{\mathbf{n}\}_N W\{\mathbf{N}\} \quad (8.2)\end{aligned}$$

from $\delta(-S/k)$ for all $\mathbf{n}$ with $0\leq n\leq m$. With Eq. (7.1) for $\ln Wh^{3N}$ as a sum of functions, ψ_0 plus ψ_n, one has, at the extremum,

$$\begin{aligned}&\delta\mathcal{g}_N W\Big[\ln W-\sum_{n\geq 0}^{n\leq m}\sum_{\{n\}_N}\phi_n\{\mathbf{n}\}_N\Big]\\&=\mathcal{g}_N W\Big[(\psi_0+1-\phi_0)+\sum_{n\geq 0}^{n\leq m}\sum_{\{n\}_N}\psi_n\{\mathbf{n}\}_N-\phi_n\{\mathbf{n}\}_N)\\&\qquad+\sum_{n>m}\sum_{\{n\}_N}\psi_n\{\mathbf{n}\}_N\Big]\delta\ln W=0 \quad (8.3)\end{aligned}$$

for any variation in $\ln W$. The solutions are that $\psi_n\equiv 0$ for $n>m$, and that the functions ψ_n are the undetermined multipliers ϕ_n for $n\leq m$. One may arbitrarily set $\psi_0=0$ and absorb it into the ψ_n's maintaining the normalization.

We have described a hierarchy of functions, $W^{(m)}\{\mathbf{N}\}$ for all values of m in the range $1\leq m\leq N$. The logarithms of these functions are each a sum of functions $\psi_n^{(m)}\{\mathbf{n}\}_N$ of the Γ space of subsets $\{\mathbf{n}\}_N$ for $n\leq m$ only. We may describe a procedure to define these in an alternative fashion.

Suppose the true function representing an experimental ensemble at some time t is $W^{(M)}$ with M having some large value. The logarithm of this function is composed of a sum including terms $\psi_M{}^{(M)}\{\mathbf{M}\}_N$ depending on the Γ space of subsets $\{\mathbf{M}\}_N$ which cannot be broken down into a sum of functions of smaller subsets. These terms affect the values of all the reduced probability densities, w_n, for all n values, including those for $n<M$. However, in computing w_n for $n\leq M-1$ we could replace these terms, $\psi_M{}^{(M)}\{\mathbf{M}\}_N$, by a sum of functions, $-\Delta\psi_n{}^{(M)}\{\mathbf{n}\}_N$, of subsets for all values of n with $n\leq M-1$, such that each of these functions approach zero in value when the coordinates of any two or more subsets of $\{\mathbf{n}\}$ are at a great distance from each other. That is we find an averaged value

$$\Big\langle\sum_{\{M\}_N}\psi_M{}^{(M)}\{\mathbf{M}\}_N\Big\rangle=-\sum_{n=1}^{n=M-1}\sum_{\{n\}_N}\Delta\psi_n{}^{(M)}\{\mathbf{n}\}_N$$

of the sum of ψ_M's which can replace these functions in $\ln W^{(M)}$ without altering w_n for any $n\leq M-1$. The new function $W^{(M-1)}$, defined by

$$\ln W^{(M-1)}=\ln W^{(M)}-\Psi_M\{\mathbf{N}\}, \quad (8.4)$$

with

$$\psi_M\{\mathbf{N}\}=\sum_{\{M\}_N}\psi_M{}^{(M)}\{\mathbf{M}\}_N+\sum_{n=1}^{n=m-1}\sum_{\{n\}_N}\Delta\psi_n{}^{(M)}\{\mathbf{n}\}_N, \quad (8.4')$$

than has its logarithm given by a sum with

$$\psi_n{}^{(M-1)}=\psi_n{}^{(M)}-\Delta\psi_n{}^{(M)} \quad (8.5)$$

only up to $n=M-1$, and leads to the same reduced functions, w_n for $n\leq M-1$. The function $\Psi_M\{\mathbf{N}\}$ then has no affect on w_n for $n\leq M-1$. Repeating this step $(M-m)$ times to $m=1$ we find the complete hierarchy $W^{(M)}$ such that

$$\ln[h^{3N}W^{(m)}]=\sum_{\mu=1}^{\mu=m}\Psi_\mu\{\mathbf{N}\}, \quad (8.6)$$

with Ψ_μ given by (8.4'). From (8.5) we have our formerly defined functions $\psi_n{}^{(m)}$ as

$$\psi_n{}^{(m)}=\psi_n{}^{(M)}-\sum_{\mu=m+1}^{\mu=M}\Delta\psi_n{}^{(\mu)}.$$

We then have, if we extend M to $M=N$ for the Liouville ensemble $W^{(L)}=W^{(N)}$, for any member $W^{(n+m)}$ of the hierarchy

$$w_n\{\mathbf{n}\}=\mathcal{g}_{N-n}W^{(n+m)}0\leq m\leq N-n. \quad (8.7)$$

The entropy $S^{(m)}$ is given by

$$-S^{(m)}/k=\sum_{\mu=1}^{\mu=m}\mathcal{g}_N W^{(m)}\Psi_\mu\{\mathbf{N}\}. \quad (8.8)$$

In view of the fact, Eq. (8.5), that Ψ_μ contains no functions of sets of more than μ molecules, and from Eq. (8.7) that w_μ for $\mu<m$ is the same if computed

from $W^{(\mu)}$ or $W^{(m)}$ we may also write

$$-S^{(m)}/k=\sum_{\mu\geq 1}^{\mu=m}\mathcal{G}_N W^{(\mu)}\Psi_\mu\{\mathbf{N}\}. \tag{8.9}$$

Defining

$$\Delta S^{(m)}=S^{(m)}-S^{(m-1)}, \tag{8.10}$$

we have

$$-\Delta S^{(m)}/k=\mathcal{G}_N W^{(m)}\Psi_m\{\mathbf{N}\}$$
$$=\mathcal{G}_N W^{(m-1)}\Psi_m\{\mathbf{N}\}\exp\Psi_m\{\mathbf{N}\}. \tag{8.11}$$

If now Ψ_m is proportional to λ and we form the second derivative with respect to λ one finds, at $\lambda=0$,

$$[\partial^2(-\Delta S^{(m)}/k)/\partial\lambda^2]_{\lambda=0}=\mathcal{G}_N W^{(m-1)}[\Psi_m\{\mathbf{N}\}]^2>0, \tag{8.12}$$

since $W^{(m-1)}$ is positive. It follows that the extremum with $\Psi_m=0$ that we found in the entropy with fixed w_n, $n\leq m$, is indeed a maximum in S. The sequence $\Delta S^{(m)}\leq 0$, $S^{(m-1)}\geq S^{(m)}$, Eq. (6.4) is thus established. The equality $S^{(m-1)}=S^{(m)}$ holds only if $\Psi_m\{\mathbf{N}\}\equiv 0$.

IX. Liouville Operator and Time Dependence

The complete Liouville operator is

$$\mathrm{L}=\sum_{i=1}^{i=N}[-(\mathbf{p}_i/m_i)\cdot\boldsymbol{\nabla}_{ri}+\boldsymbol{\nabla}_{ri}U_N\{\mathbf{N}\}\cdot\boldsymbol{\nabla}_{pi}]. \tag{9.1}$$

For a closed system, $W\{\mathbf{N}\}$ is zero at the walls, and of course is also zero at the limits $-\infty$, $+\infty$ in any momentum component, p_{xi}. It follows that

$$\int_V d\mathbf{r}_i(\mathbf{p}_i/m_i)\cdot\boldsymbol{\nabla}_{ri}W=0, \tag{9.2}$$

and

$$\int_{-\infty}^{+\infty}d\mathbf{p}_i\boldsymbol{\nabla}_{ri}U_N\{\mathbf{N}\}\cdot\boldsymbol{\nabla}_{pi}W=0. \tag{9.3}$$

From this it follows trivially that the normalization $w_0=\mathcal{G}_N W=1$ is retained under the Liouville operation,

$$\dot{w}_0=\mathcal{G}_N\mathrm{L}W\{\mathbf{N}\}=0, \tag{9.4}$$

but also that in expressing the time dependence of w_n one need only retain the terms in the operator which operate on the Γ space of the set $\mathbf{n}$,

$$\dot{w}_n=\mathcal{G}_{N-n}\sum_{i=1}^{i=n}[-(\mathbf{p}_i/m_i)\cdot\boldsymbol{\nabla}_{ri}$$
$$+(\boldsymbol{\nabla}_{ri}U_N\{\mathbf{N}\})\cdot\boldsymbol{\nabla}_{pi}]W\{\mathbf{N}\}. \tag{9.5}$$

Since U_N is independent of the momenta we can write $\boldsymbol{\nabla}_{ri}U_N\{\mathbf{N}\}\cdot\boldsymbol{\nabla}_{pi}=\boldsymbol{\nabla}_{pi}\cdot(\boldsymbol{\nabla}_{ri}U_N)$, and take $\boldsymbol{\nabla}_{pi}$ in this term, and $\boldsymbol{\nabla}_{ri}$ of the first term outside of the integration, since they operate only on variables not under the integral. One has, then,

$$\dot{w}_n=\sum_{i=1}^{i=n}[-(\mathbf{p}_i/m_i)\cdot\boldsymbol{\nabla}_{ri}\mathcal{G}_{N-n}W+\boldsymbol{\nabla}_{pi}\cdot\mathcal{G}_{N-n}W\boldsymbol{\nabla}_{ri}U_N]. \tag{9.6}$$

Define the average vector force $\mathbf{f}_{i,n}(\boldsymbol{\gamma}_i,\{\{\mathbf{n}\}-\boldsymbol{\gamma}_i\})$, acting on the molecule $i\subset\mathbf{n}$ at $\boldsymbol{\gamma}_i$, when the set $\mathbf{n}$ is at the Γ-space position $\{\mathbf{n}\}$, averaged over all positions of the $N-n$ other molecules. From its definition this force is given by

$$\mathbf{f}_{i,n}(\boldsymbol{\gamma}_i,\{\{\mathbf{n}\}-\boldsymbol{\gamma}_i\})w_n\{\mathbf{n}\}=-\mathcal{G}_{N-n}W\{\mathbf{N}\}\boldsymbol{\nabla}_{ri}U_N\{\mathbf{N}\}. \tag{9.7}$$

One sees that Eq. (9.6) is then

$$\dot{w}_n\{\mathbf{n}\}=-\sum_{i=1}^{i=n}[(\mathbf{p}_i/m_i)\boldsymbol{\nabla}_{ri}w_n\{\mathbf{n}\}$$
$$+\boldsymbol{\nabla}_{pi}\cdot\mathbf{f}_{i,n}(\boldsymbol{\gamma}_i,\{\{\mathbf{n}\}-\boldsymbol{\gamma}_i\})w_n\{\mathbf{n}\}. \tag{9.8}$$

For the particular case that the potential is a sum of pair potentials we have from Eq. (9.7) that

$$\mathbf{f}_{i,n}(\boldsymbol{\gamma}_i,\{\{\mathbf{n}\}-\boldsymbol{\gamma}_i\})=-\sum_{j\subset n}{}'\boldsymbol{\nabla}_{ri}u(r_{ij})$$
$$-\sum_c\int d\boldsymbol{\gamma}_c\frac{w_{n+c}\{\{\mathbf{n}\}+\boldsymbol{\gamma}_c\}}{w_n\{\mathbf{n}\}}\boldsymbol{\nabla}_{ri}u(r_{ic}), \tag{9.9}$$

and depends on the functions w_{n+c} for only one more molecule than is in the set $\mathbf{n}$.

The expression Eq. (9.8) for $\dot{w}_n$ then looks formally almost identical to $\dot{W}=\mathrm{L}W$ with Eq. (9.1) for L. The formal difference is only in the order of writing $\boldsymbol{\nabla}_{pi}$ and $-\boldsymbol{\nabla}_{ri}U=\mathbf{f}_{i,N-i}$; that is, if we write, for a set $\mathbf{n}$ of molecules

$$\mathrm{L}^{(n)}=-\sum_{i=1}^{i=n}[(\mathbf{p}_i/m)\cdot\boldsymbol{\nabla}_{ri}+\boldsymbol{\nabla}_{pi}\cdot\mathbf{f}_{i,n}(\boldsymbol{\gamma}_i,\{\{\mathbf{n}-\boldsymbol{\gamma}_i\}) \tag{9.10}$$

with $\mathbf{f}_{i,n}$ the vector force on molecule i of the set $\mathbf{n}$, understanding that the $\boldsymbol{\nabla}_{pi}$ operator acts both on $\mathbf{f}_{i,n}$ *and* on the function operated upon by L, then

$$\dot{W}^L\{\mathbf{N}\}=\mathrm{L}^{(N)}W\{\mathbf{N}\}, \tag{9.11}$$

$$\dot{w}_n\{\mathbf{n}\}=\mathrm{L}^{(n)}w_n\{\mathbf{n}\}. \tag{9.12}$$

The important difference in the two cases of Eqs. (9.11) and (9.12) is that whereas for the set $\mathbf{N}$ of molecules which are the complete set of molecules in an isolated system, the force $\mathbf{f}_{i,N}$ is independent of the momenta, whereas for the *subset* $\mathbf{n}$ the force $\mathbf{f}_{i,n}$ is, in general, momentum dependent. That is, if one writes

$$\boldsymbol{\nabla}_{pi}\cdot\mathbf{f}_{i,n}=(\boldsymbol{\nabla}_{pi}\cdot\mathbf{f}_{in})+\mathbf{f}_{in}\cdot\boldsymbol{\nabla}_{pi}, \tag{9.13}$$

where the brackets $(\boldsymbol{\nabla}_{pi}\cdot\mathbf{f}_{in})$ indicate that this term is a simple product function in the operator, then this term $(\boldsymbol{\nabla}_{pi}\cdot\mathbf{f}_{in})$ is zero for the complete set $\mathbf{N}$, but generally not for the subset $\mathbf{n}$.

One other conclusion that we wish to draw from Eq. (9.12) is that since, for the system in which the potential U_N is a sum of pair terms, so that $\mathbf{f}_{i,n}$ is determined fully by the reduced probability density functions w_{n+c}, Eq. (9.9) then $\dot{w}_n$ is correctly given by integration of $LW^{(n+1)}$,

$$\dot{w}_n\{\mathbf{n}\}=g_{N-n}LW^{(n+1)}\{\mathbf{N}\}. \tag{9.14}$$

It follows that the first time derivatives of w_n for $n\leq 2$, which functions fully determine the thermodynamic properties, depend only on the functions $\psi_n^{(3)}$, and not on the detailed correlations between more than triples of molecules. The time derivatives $\dot{\psi}_n^{(3)}$, in turn, are determined by $\dot{w}_n$ for $n\leq 3$, and hence on the functions $\psi_n^{(4)}$, but not on higher correlation functions than those between quadruples of molecules.

Presumably in the time evolution of a system started at local thermodynamic equilibrium, with small gradients in composition or temperature, the functions $\psi_n^{(m)}$ for small values of $m=2$, 3, 4, etc., soon reach steady values, the slow secular changes of these functions for $m=2$, which represent the gradual changes due to fluxes of molecular species and of heat, being determined by their own values, and, probably to a less extent, by the steady values of $\Delta\psi_n^{(3)}$.

For a later interval of time, probably in many systems only of the order of that necessary for a sound wave to traverse the system, the functions $\Psi_m\{\mathbf{N}\}=\sum\Delta\psi_n^{(m)}$ keep successively building up to nonzero values, without affecting the time evolution of the physical properties. At some stage, probably of the order $M\cong N^{1/3}$, the development of these functions no longer follows the prediction of the Liouville operator, and the higher order correlation functions Ψ_M for $M>N^{1/3}$ are actually destroyed by fluctuation terms at the walls.

In the hypothetical mirror system the odd terms in the momenta in Ψ_m have the opposite sign. The fluxes represented in $\psi_n^{(2)}$ are reversed. The gradual time evolution of the functions w_n for $n\leq 2$ is in the opposite direction from the normal, and is maintained so by a "feedback" from the terms in $\Delta\psi_n^{(3)}$, which in turn are maintained by "feedback" from $\Delta\psi_n^{(4)}$, etc. If this hypothetical mirror system starts with nonzero functions Ψ_M up to $M=M_0$, since the symmetry of the operator L requires that the time evolution exactly reverse that of the "normal" system in the realm where the Liouville operator is valid, the terms Ψ_M for successively smaller M—values will go to zero values. When $\Psi_3=\sum\Delta\psi_n^{(3)}$ goes to zero, the time evolution will start to reverse, the fluxes become "normal" and the high order correlation functions start again to develop from the bottom up, with the "normal" sign of the odd order momentum terms.

X. Localized Thermodynamic Functions and Fluxes

The local number density $\rho_a(\mathbf{r})$ of molecules of species a per unit volume at $\mathbf{r}$ is

$$\rho_a(\mathbf{r})=g_N\sum_{i_a=1_a}^{i_a=N_a}\delta(\mathbf{r}-\mathbf{r}_{i_a})W\{\mathbf{N}\}$$

$$=\int d\mathbf{p}_a w_a(\mathbf{p}_a,\mathbf{r}). \tag{10.1}$$

The vector flux $\mathbf{J}_a(\mathbf{r})$ of molecules per unit area and per unit time at $\mathbf{r}$ is then

$$\mathbf{J}_a(\mathbf{r})=g_N\sum_{i_a=1_a}^{i_a=N_a}\delta(\mathbf{r}-\mathbf{r}_{i_a})(\mathbf{p}_{i_a}/m_a)W\{\mathbf{N}\}, \tag{10.2}$$

and the gradient, $\nabla_r\mathbf{J}_a(\mathbf{r})$, of this flux is the excess flow *out* of unit volume in unit time of molecules of species a at $\mathbf{r}$,

$$\nabla_r\mathbf{J}_a(\mathbf{r})=g_N\sum_{i_a=1_a}^{i_a=N_a}\delta(\mathbf{r}-\mathbf{r}_{i_a})(\mathbf{p}_{i_a}/m_a)\cdot\nabla_{r_i}W\{\mathbf{N}\}, \tag{10.3}$$

where the relation

$$\partial/\partial y\int dx\delta(y-x)f(x)=\int\delta(y-x)\partial f/\partial x$$

has been used. The change in number density per unit time is

$$\dot{\rho}_a(\mathbf{r})=g_N\sum_{i_a=1_a}^{i_a=N_a}\delta(\mathbf{r}-\mathbf{r}_{i_a})LW\{\mathbf{N}\}. \tag{10.4}$$

Using the fact that the integral of the additive contribution of any coordinate or momentum in LW is zero, only the single terms, $-\mathbf{p}_{i_a}/m_a\cdot\nabla_{r_i}$, survive the integration of Eq. (10.4) so that

$$\dot{\rho}_a(\mathbf{r})=-g_N\sum_{i_a=1_a}^{i_a/N_a}\delta(\mathbf{r}-\mathbf{r}_{i_a})(\mathbf{p}_{i_a}/m_a)\cdot\nabla_{r_i}W$$

$$=-\nabla_r\mathbf{J}_a(\mathbf{r}), \tag{10.5}$$

which expresses the conservation of molecules of species a in the flow.

Similarly, one may define an average kinetic energy $\epsilon_{ka}(\mathbf{r})$, of species a of molecules at $\mathbf{r}$ by

$$\rho_a(\mathbf{r})\epsilon_{ka}(\mathbf{r})=g_N\sum_{i_a=1_a}^{i_a=N_a}\delta(\mathbf{r}-\mathbf{r}_{i_a})[(\mathbf{p}_{i_a}\cdot\mathbf{p}_{i_a})/2m_a]W\{\mathbf{N}\}, \tag{10.6}$$

which includes that due to any mass motion of the total fluid. The vector flux $\mathbf{J}_{ka}(\mathbf{r})$ giving the flux of kinetic energy due to molecules of species a, in energy per unit area and per unit time, is

$$\mathbf{J}_{ka}(\mathbf{r})=g_N\sum_{i_a=1_a}^{i_a=N_a}\delta(\mathbf{r}-\mathbf{r}_{i_a})[(\mathbf{p}_{i_a}\cdot\mathbf{p}_{i_a})/2m_a](\mathbf{p}_{i_a}/m_a)$$

$$\times W\{\mathbf{N}\} \tag{10.7}$$

and the gradient of this, the net flow per unit volume and per unit time of kinetic energy *out* of $\mathbf{r}$ due to

molecules of species a, is

$$\nabla_r\cdot\mathbf{J}_{ka}(\mathbf{r})=\mathcal{G}_N\sum_{ia=1a}^{}\delta(\mathbf{r}-\mathbf{r}_{ia})[(\mathbf{p}_{ia}\cdot\mathbf{p}_{ia})/2m_a](\mathbf{p}_{ia}/m_a)\cdot\nabla_{ri}W\{\mathbf{N}\}. \quad (10.8)$$

The change with time, $(d/dt)\ \rho_a=\dot{\rho}_a\epsilon_{ka}+\rho_a\dot{\epsilon}_{ka}$, is found from Eq. (10.6) by operating on W with L. Only the terms $-(\mathbf{p}_{ia}/m_a)\cdot\nabla_{ri}$ and $\nabla_{pi}\cdot\nabla_{ri}U$ survive the integration. The former term is $-\nabla_r\cdot\mathbf{J}_{ka}$. The latter term can be integrated over $d\mathbf{p}_{ia}$ by parts. One has for $\dot{Q}_{ka}(\mathbf{r})$, the rate of production per unit volume per unit time, of kinetic energy due to molecules of species a at $\mathbf{r}$,

$$\dot{Q}_{ka}(\mathbf{r})=(d/\partial t)\rho_a(\mathbf{r})\epsilon_{ka}(\mathbf{r})+\nabla_r\cdot\mathbf{J}_{ia}(\mathbf{r})$$
$$=-\mathcal{G}_N\sum_{ia=1a}^{ia=Na}\delta(\mathbf{r}-\mathbf{r}_{ia})[(\mathbf{p}_{ia}/m_a)\cdot\nabla_{ri}U_N\{\mathbf{N}\}]W\{\mathbf{N}\}. \quad (10.9)$$

This term is recognizable as the work done on the molecules of species a at $\mathbf{r}$, per unit volume and per unit time, namely,

$$\dot{Q}_{ka}(\mathbf{r})=\langle\mathbf{v}_a\cdot\mathbf{f}_{a,a}(\mathbf{r})\rangle\rho_a(\mathbf{r}), \quad (10.9')$$

where $\langle\mathbf{v}_a\cdot f_{a,a}(\mathbf{r})\rangle$ is the average, per molecule of species a at $\mathbf{r}$, of the scalar product of velocity, $\mathbf{p}_a/m_a$, with the force, $\mathbf{f}_{a,a}$, acting on the molecule due to the other molecules of the system.

The definition of the local potential energy is somewhat arbitrary, arising from the fact that the potential energy is a sum of pair terms, $u_{ij}(r_{ij})$, each depending on two molecules, i and j, which necessarily are not at identical positions. The most obvious choice is to assign half of this pair potential to each of the two molecules, i and j, so as to write for $\epsilon_{ua}(r)$, the average potential energy per molecule of species a at $\mathbf{r}$, the equation,

$$\rho_a(\mathbf{r})\epsilon_{ua}(\mathbf{r})=\mathcal{G}_N\sum_{ia=1a}^{ia=Na}\delta(\mathbf{r}-\mathbf{r}_{ia})\tfrac{1}{2}\sum_{j=1}^{j=N}u_{aj}(r_{ia,j})W\{\mathbf{N}\}, \quad (10.10)$$

where the prime on the summation over j indicates omission of the term $j=ia$, and the subscript j in u_{aj} is used to indicate that the form of the function depends on the species to which j belongs.

The quantity $\rho_a(\mathbf{r})\epsilon_{ua}(\mathbf{r})$ defined by Eq. (10.10) if integrated over the volume of the system gives a term that could be written as $N_a\bar{\epsilon}_{ua}$. The total potential energy U is the sum of these terms over all species a. One is tempted to conclude that the quantity ϵ_{ua} corresponds to the partial molal potential energy of species a divided by Avogadro's number, namely, that for an equilibrium system where ϵ_{ua} were independent of $\mathbf{r}$ it would be this quantity. Actually it is *not*. The partial molecular energy of species a at equilibrium is given by a much more complicated expression.

The vector flux, $\mathbf{J}_{ua}(\mathbf{r})$, of the energy of Eq. (10.10) is

$$\mathbf{J}_{ua}(\mathbf{r})=\mathcal{G}_N\sum_{ia=1a}^{ia=Na}\delta(\mathbf{r}-\mathbf{r}_{ia})(\mathbf{p}_{ia}/m_a)\tfrac{1}{2}\sum_{j=1}^{j=N}u_{aj}(r_{ia,j})W\{\mathbf{N}\}. \quad (10.11)$$

On using

$$\sum_{j=1}^{j=N}\nabla_{ri}u_{aj}(r_{ia,j})=\nabla_{ri}U_N\{\mathbf{N}\}, \quad (10.12)$$

one finds for the gradient of $\mathbf{J}_{ua}$ two terms

$$\nabla_r\cdot\mathbf{J}_{ua}(\mathbf{r})=\mathcal{G}_N\sum_{ia=1a}^{ia=Na}\delta(\mathbf{r}-\mathbf{r}_{ia})\{\tfrac{1}{2}\sum_{j=1}^{j=N}{}'u_{aj}(r_{ia,j})(\mathbf{p}_{ia}/m_a)\cdot\nabla_{ri}W\{\mathbf{N}\}+\tfrac{1}{2}W\{\mathbf{N}\}[(\mathbf{p}_{ia}/m_a)\cdot\nabla_{ri}U_N\{\mathbf{N}\}]\}. \quad (10.13)$$

This is, then, the net flow of potential energy of molecules of type a out of an element of volume at $\mathbf{r}$, per unit volume and per unit time.

The time derivative $(\partial/\partial t)\rho_a\epsilon_{ua}$ is obtained by replacing W with LW in Eq. (10.10). In the term multiplied by u_{aj} only the two terms of L, $-(\mathbf{p}_{ia}/m_a)\cdot\nabla\mathbf{r}_{ia}W$ and $-(\mathbf{p}_j/m_j)\cdot\nabla_{rj}W$ survive integration. The first of these terms is just the negative of the first term in Eq. (10.13) for $\nabla_r\cdot\mathbf{J}_{ua}$. By partial integration the second term can be replaced by $+W(\mathbf{p}_j/m_j)\cdot\nabla_{rj}u_{aj}$. One has for, $\dot{Q}_{ua}(\mathbf{r})$, the production rate per unit volume of potential energy of species a at $\mathbf{r}$,

$$\dot{Q}_{ua}(\mathbf{r})=\tfrac{1}{2}\mathcal{G}_N\sum_{ia=1a}^{ia=Na}\delta(\mathbf{r}-\mathbf{r}_{ia})W\{\mathbf{N}\}\times[(\mathbf{p}_{ia}/m_a)\cdot\nabla_{ri}U_N\{\mathbf{N}\}+\sum_{j=1}^{j=N}{}'(\mathbf{p}_j/m_j)\cdot\nabla_{rj}u_{aj}]. \quad (10.14)$$

The first term of this is seen to be half the negative of $\dot{Q}_{ka}$, Eq. (10.9), namely, half the negative of the work done per unit time on molecules of species a at $\mathbf{r}$. The second term is the other complement of this, namely half the negative work done by the potential field of the molecules of a at $\mathbf{r}$ on the other molecules of the system.

The sum $\dot{Q}_{ea}$ the total change of energy of molecules of species a in a volume element at $\mathbf{r}$, per unit volume and unit time is then

$$\dot{Q}_{ea}(\mathbf{r})=\dot{Q}_{ua}(\mathbf{r})+\dot{Q}_{ka}(\mathbf{r})=\tfrac{1}{2}\mathcal{G}_N\sum_{ia=1a}^{ia=Na}\delta(\mathbf{r}-\mathbf{r}_{ia})W\{\mathbf{N}\}[-(\mathbf{p}_{ia}/m_a)\cdot\nabla_{ri}U_N\{\mathbf{N}\}+\sum_{j=1}^{j=N}(\mathbf{p}_j/m_j)\cdot\nabla_{rj}u_{aj}(r_{ai,j})]. \quad (10.15)$$

The sum over a and integral of this over $d\mathbf{r}$ in the total volume of the system is seen to be the difference

of two equal terms, and hence zero as it must be. The integral over a volume macroscopic in size, but not that of the whole system, differs from zero in surface terms only.

The localized entropy has the same ambiguity of definition that arises in the case of the potential energy. In the expression $-S/k=\vartheta_N W \ln(Wh^{3N})$ if $\ln(Wh^{3N})$ contains a sum of terms $\psi_n\{\mathbf{n}\}$ dependent on the Γ space of a set $\{\mathbf{n}\}_N$ of molecules we may arbitrarily assign the fraction $1/n$ of this term to each molecule of the set, and localize the corresponding part of the entropy at the position of this molecule. One therefore writes

$$\sigma(\mathbf{r})=-S(\mathbf{r})/k$$
$$=\vartheta_N W\{\mathbf{N}\}\sum_{n\geq 1} n^{-1}\sum_{\{n\}_N}\sum_{i\subset\{n\}_N}\delta(\mathbf{r}-\mathbf{r}_i)\psi_n\{\mathbf{n}\}_N, \quad (10.16)$$

for a density $\sigma(\mathbf{r})$ of negative entropy (divided by k) at the position $\mathbf{r}$.

However, we wish to emphasize one feature of this definition. As long as $\psi_n\equiv 0$ for $n>m$, with m some small number, the functions ψ_n will approach zero in value if any one of the coordinates of the set $\mathbf{n}$ is far from the position $\mathbf{r}$ at which the molecule $i\subset\mathbf{n}$ is located. The local negative entropy density, $\sigma(\mathbf{r})$, at $\mathbf{r}$, will then depend only on the properties of the system near $\mathbf{r}$, the range being of the order m times the range of the molecular forces. Now a thermodynamic treatment of a system is only of value if the properties of the system vary negligibly in many mean free paths, and in such a case the properties of the system near $\mathbf{r}$ can be inferred from those at $\mathbf{r}$, and the gradients and fluxes at $\mathbf{r}$. The localization of the entropy has then physical meaning, in that it is a property which can be inferred from the properties at $\mathbf{r}$.

If, however, $\psi_M\neq 0$ for M of the order $M=N^{1/3}$, then ψ_M will be nonzero with members of the set $\mathbf{M}$ separated by distances of the order of the diameter of the system. In this case the value of $\sigma(\mathbf{r})$ will depend on the properties of the whole system, and not solely on those close to $\mathbf{r}$. In such a case it has little or no physical sense to attempt to describe a local entropy density.

In addition, the assignment of the fraction $1/n$ of the term ψ_n to each molecule of $\mathbf{n}$ is arbitrary. One might as logically have assigned the fraction $m_a/\Sigma n_b m_b$ to each molecule of species a. As long as n is small, with ψ_n localized to be nonzero only when all molecules of $\mathbf{n}$ are close to $\mathbf{r}$, the values of $S(\mathbf{r})$ will be independent of this assignment whenever the properties of the system vary only slowly with $\mathbf{r}$, and a thermodynamic description of the state at $\mathbf{r}$ has value. This would no longer be true were ψ_M nonzero for $M\sim N^{1/3}$.

In all that follows we tacitly assume that the sum over n in Eq. (10.16) is limited to small values.

There is one other comment required about the use of Eq. (10.16). In discussing the solutions of the integro-differential equations for $\psi_n^{(m)}$, Eq. (7.5), it was pointed out that only one condition, the normalization condition $\vartheta_N W=1$, was available to fix the arbitrary constants in ψ_a for all components. This single condition is adequate to uniquely define W, and hence all *mechanical* properties of the system. However, for systems of more than one chemical component, if the composition at $\mathbf{r}$ differs from the average value in the system, the value of the local entropy, $S(\mathbf{r})$ given by Eq. (10.16) will depend on the assignment of these arbitrary constants to the different species.

For the system of local initial thermodynamic equilibrium, Eq. (3.6), there is a unique method of assigning the normalizing term, the term $-PV/kT=\Phi_0$ of Eq. (3.4) to the different species. This assignment is simply to add $P(\mathbf{r}_{ia})\bar{v}_a(\mathbf{r}_{ia})/kT(\mathbf{r}_{ia})$ with

$$\bar{v}_a=(\partial V/\partial N_a)_{p,T}, \quad (10.17)$$

the partial molecular volume of species a to the term ϕ_a of each molecule of species a, writing for ψ_a at $t=0$

$$\psi_a(t=0,\boldsymbol{\gamma}_{ia})=[kT(\mathbf{r}_{ia})]^{-1}$$
$$\times\left[-P(\mathbf{r}_{ia})\bar{v}_a(\mathbf{r}_{ia})+\mu_a(\mathbf{r}_{ia})-\frac{\mathbf{p}_{ia}\cdot\mathbf{p}_{ia}}{2m_a}\right], \quad (10.18)$$

which will now make Eq. (10.16) consistent with thermodynamic local values. If the original system has small gradients compared to the mean free path the later state will usually[10] be close to that of a local thermodynamic equilibrium, but with nonzero fluxes. We will then have $\psi_n^{(2)}$ in the form

$$\psi_a^{(2)}(\boldsymbol{\gamma}_{ia})$$
$$=[kT(\mathbf{r}_{ia})]^{-1}\left[-P(\mathbf{r}_{ia})\bar{v}_a(\mathbf{r}_{ia})+\mu_a(\mathbf{r}_{ia})-\frac{\mathbf{p}_{ia}\cdot\mathbf{p}_{ia}}{2m_a}\right.$$
$$\left.+\theta_a(\boldsymbol{\gamma}_{ia})\right], \quad (10.19)$$

$$\psi_{ab}^{(2)}(\boldsymbol{\gamma}_{ia},\boldsymbol{\gamma}_{jb})=[-u_{ab}(r_{ij})+\theta_{ab}(\boldsymbol{\gamma}_{ia},\boldsymbol{\gamma}_{jb})]$$
$$\times[\tfrac{1}{2}k(T(\mathbf{r}_{ia})+T(\mathbf{r}_{jb}))]^{-1}, \quad (10.20)$$

where the (small) terms θ_a, θ_{ab}, will contain terms odd in the momenta. The expression (10.16) will again be that consistent with the thermodynamic functions plus terms due to the fluxes arising from θ_a and θ_{ab}.

One may integrate, for each term $\{\mathbf{n}\}_N$ in Eq. (10.16), over the Γ space of the molecules not in the

[10] This is not necessarily so. One need only consider the case of a system capable of a slow chemical reaction prepared initially with a thermal and composition gradient, but with the reaction at local equilibrium. Obviously heat conduction and diffusion could bring the system to uniform temperature and composition before the chemical reaction had proceeded to the new equilibrium value. Many other cases are imaginable. No general proof is to be expected that once local thermodynamic equilibrium is reached it is always maintained between all degrees of freedom.

subset $\{\mathbf{n}\}_N$, and sum over the $\mathbf{N}!/(\mathbf{N}-\mathbf{n})!\mathbf{n}!$ different subsets for the same set $\mathbf{n}$, to define

$$\sigma_n(\mathbf{r}) = \mathcal{G}_N n^{-1} \sum_{i \subset n} \delta(\mathbf{r}-\mathbf{r}_i)\psi_n\{\mathbf{n}\}w_n\{\mathbf{n}\} \quad (10.21)$$

so that,

$$\sigma(\mathbf{r}) = \sum_{n \geq 1} \sigma_n(\mathbf{r}) = -S(\mathbf{r})/k. \quad (10.22)$$

One may now define fluxes

$$\mathbf{J}_{\sigma n}(\mathbf{r}) = \mathcal{G}_N n^{-1} \sum_{i \subset n} \delta(\mathbf{r}-\mathbf{r}_i)(\mathbf{p}_i/m_i)\psi_n\{\mathbf{n}\}w_n\{\mathbf{n}\} \quad (10.23)$$

and gradients of the fluxes,

$$\nabla_r \cdot \mathbf{J}_{\sigma n}(\mathbf{r}) = \mathcal{G}_n n^{-1} \sum_{i \subset n} \delta(\mathbf{r}-\mathbf{r}_i)[\psi_n\{\mathbf{n}\}(\mathbf{p}_i/m_i)\cdot\nabla_r w_n\{\mathbf{n}\} + w_n\{\mathbf{n}\}(\mathbf{p}_i/m_i)\cdot\nabla_r\psi_n\{\mathbf{n}\}. \quad (10.24)$$

The total entropy production, per unit volume and per unit time, $\theta(\mathbf{r})$, is then

$$\theta(\mathbf{r}) = -k\sum_{n \geq 1}[\dot{\sigma}_n(\mathbf{r}) + \nabla_r \cdot \mathbf{J}_{\sigma n}(\mathbf{r})], \quad (10.25)$$

$$\dot{\sigma}_n(\mathbf{r}) + \nabla_r \cdot \mathbf{J}_{\sigma n}(\mathbf{r}) = -\theta_n(\mathbf{r})/k = \mathcal{G}_N n^{-1} \sum_{i \subset n} \delta(\mathbf{r}-\mathbf{r}_i)[w_n\{\mathbf{n}\}\dot{\psi}_n\{\mathbf{n}\} + \psi_n\{\mathbf{n}\}\dot{w}_n\{\mathbf{n}\} + w_n\{\mathbf{n}\}(\mathbf{p}_i/m_i)\cdot\nabla_{ri}\cdot\psi_n\{\mathbf{n}\} + \psi_n\{\mathbf{n}\}(\mathbf{p}_i/m_i)\cdot\nabla_{ri}\{\mathbf{n}\}]. \quad (10.25')$$

This total entropy density production rate,

$$\theta(\mathbf{r}) = -k\mathcal{G}_N \sum_{n \geq 1} n^{-1} \sum_{\{\mathbf{n}\}_N} \sum_{i \subset n} \delta(\mathbf{r}-\mathbf{r}_i)\theta_{i,n}^*(\boldsymbol{\gamma}_i, \{\mathbf{n}\}_N\{\mathbf{N}\}) \quad (10.26)$$

$$\theta_{i,n}^*(\boldsymbol{\gamma}_i, \{\mathbf{n}\}, \{\mathbf{N}\}) = (\mathbf{p}_i/m_i)\cdot(\nabla_{ri}\psi_n\{\mathbf{n}\}W\{\mathbf{N}\} + (\partial/\partial t)(\psi_n\{\mathbf{n}\}W\{\mathbf{N}\}) \quad (10.27)$$

is, of course, zero if the Liouville operator is used to compute by $(\partial/\partial t)(\psi_n W) = \mathrm{L}(\psi_n W)$. This follows since the only term surviving the integration is exactly the negative of the first term on the right of Eq. (10.27).

The entropy density production rate given by Eqs. (10.26) or by (10.25) with (10.25′) is only nonzero if the sum over n is terminated at a definite value m, and the appropriate $\psi_n^{(m)}$ are used.

XI. Discussion

It is rather trivial that the expressions in the last section for the local entropy are consistent with the classical treatment of thermodynamics for a definite initial and final state.

Let us consider a system of known entropy, prepared out of equilibrium, then isolated and allowed to change for a time, t. At t imagine that insulating walls are adiabatically inserted to stop all fluxes, freezing the system into the state of local equilibrium found at t. In our description, consistent with the concept that the system behaves as if truly isolated from the surroundings, the Liouville operator is used to predict the secular changes, but with attention focused on the reduced probability density functions w_n for small n. The process of insertion of insulating walls, if *adiabatic*, changes these only by stopping the fluxes, removing the terms which are odd in the momenta, and by removing any high-order correlations in $\ln W$ which may have survived the influence of the surroundings during the actual transport processes. Any measurement of the thermodynamic entropy by heat cycles on the different parts of the system will, of course, measure the local equilibrium entropy, which is that computed by the use of our expression $S^{(2)}$.

However, the thermodynamic treatment of irreversible processes does not confine itself to the initial and final states, but expresses the local entropy flux and production during the transport, particularly for systems in a steady state. Now a complete "steady state" throughout all parts of an isolated system means only that no change at all occurs. But a local steady state in part of an isolated system is by no means inconsistent with isolation of the system. Consider, for example, two large heat reservoirs, α and β of masses M_α and M_β, of specific heats c_α and c_β, and of temperatures $T_\alpha > T_\beta$, respectively, connected by a member of small cross section. The total heat flow, $\dot{Q} = -M_\alpha c_\alpha \dot{T}_\alpha = M_\beta c_\beta \dot{T}_\beta$, out of α and into β may be finite, but $-\dot{T}_\alpha$ and T_β may be made less than any ϵ at constant $\dot{Q}$, by increasing the masses, M_α and M_β of the reservoirs. Similarly the average temperature gradients in the reservoirs may be reduced towards zero.

In the thermodynamic language there is no entropy *production* in either α or β. An entropy per unit time $-\dot{S}_\alpha = \dot{Q}/T_\alpha$ flows *out* of α, and a larger entropy, $S_\beta = Q/T_\alpha$ flows *into* β. The total entropy production, $\dot{S} = \dot{S}_\alpha + \dot{S}_\beta$ occurs in the connecting member, where there is a temperature gradient, but where the properties are stationary in time.

The fact that the local physically measurable properties near a position $\mathbf{r}$ are stationary means that the reduced probability density functions, $w_n\{\mathbf{n}\}$, near $\mathbf{r}$ for all small values of n do not change in time, $\dot{w}_n = 0$, $n \leq m$. Since the correlation functions $\psi_n^{(m)}$ of $W^{(m)}$ are uniquely determined by w_n for $n \leq m$ it follows that for small m values $\dot{\psi}_n^{(m)} = 0$. The corresponding entropy $S^{(m)}$ then has a production rate $\theta^{(m)}$ per unit volume and unit time which is just $\theta^{(m)} = k\nabla \cdot \mathbf{J}_\sigma^{(m)}$.

Were we to admit that the exact total probability distribution, W, for the system during transport were $W^{(L)}$ there would be no truly stationary state, even locally. As time proceeds the correlation functions ψ_n in $\ln W^{(L)}$ up to $n = N$ keep increasing in value. These functions, for $M \sim N^{1/3}$ or greater, have nonzero values for subsets of molecules extending in their coordinate values throughout the entire system. No sensible

definition of a localizable entropy is possible. The state of the system is continually changing in that the positions of molecules at any $\mathbf{r}$ become increasingly correlated directly with that of molecules throughout the whole system.

Under normal conditions, that the surroundings are not held close to 0°K, and for heat or molecular transport, for which the coupling of the transport with the walls, and hence with the surroundings is high, the negative entropy stored in the terms of ψ_n between $2 \leq n \leq N^{1/3}$ will be negligible. The true entropy will differ but little from that computed using $W^{(2)}$, and the transport and production rates will be adequately represented by $\mathbf{J}_e^{(2)}$ and $\theta^{(2)}$, respectively. In any case, these will represent the values which would be *inferred* by observing molecular and heat transports together with local concentrations and temperature gradients.

The whole discussion of this paper has been limited to a mathematical formalism suitable to the treatment of a classical liquid system, and indeed one in which the molecules have no integral degrees of freedom, and in which the potential is a sum of pair interactions. Clearly no other alteration than the insertion into $\gamma_{\dot{\omega}}$ of the internal coordinates and momenta would be required, were these to play a significant role. An essentially similar, although somewhat more complicated formalism is applicable to the coordinate representation of the density matrix for quantum systems.

There is no essential reason why the coordinate-momentum space used should be that of molecules. For crystals one would presumably prefer normal coordinates of vibration, which are now nearly independent. The (weak) cubic and quartic terms of the displacement potential lead to interactions between these normal coordinates, and the Liouville operator, in time, leads to many-body correlation functions in $\ln W$, which again will be replaced with their pair and triple, etc., averages by the fluctuations at the boundaries. The essential features of the discussion remain unaltered.

The limitation of pair potential interaction requires more careful discussion. Any potential $U_N\{\mathbf{N}\}$ can be written as a sum,

$$U_N\{\mathbf{N}\} = \sum_{n \geq 1} \sum_{\{n\}N} u_n\{\mathbf{n}\}_N, \tag{11.1}$$

and if U_N is defined for all $\mathbf{N}$, the analysis is unique, with

$$u_n\{\mathbf{n}\} = \sum_{\nu \geq 1} \sum_{\{\nu\}\, n} (-)^{n-\nu} U_\nu\{\mathbf{v}\}_n. \tag{11.2}$$

As long as the sums of Eq. (11.2) approach zero rapidly for large n values, $u_n \cong 0$, $n \geq m$, no drastic change is required for our treatment, except one of considerable numerical complication. The energy, and hence the thermodynamic properties, depend on w_n up to $n=m$, rather than only up to $n=2$. The inferred thermodynamic entropy will be $S^{(m)}$, and the first time derivative of $W^{(m)}$ will depend on $W^{(2m-1)}$.

However, it is not true that the development of Eq. (11.1) necessarily converges. For instance if hydrogen atoms, or any other chemical species which form saturated valence bonds, are chosen for the entities, the development does *not* converge. In such a case even the equilibrium $\ln W$ contains high-order direct correlations, namely, $-u_n/kT$, up to $n=N$, and, as in the case of the entropy $S^{(L)}$, one cannot even properly define a localizable energy density. The formal solution of reducing the entities treated to nuclei and electrons would indeed reduce Eq. (11.1) to a sum of pair terms, but at considerable expense of numerical complication to the calculation. The usual answer is to treat H_2 molecules as the entities, and if necessary in a many component system to include chemical reactions in the formalism. Nevertheless there exists a region of density and temperature where the composition may be said to be half-molecules and half-dissociated atoms, but where interactions between pairs of atoms could not be neglected.

The contemplation of the difficulties of treatment, even at equilibrium, of such hypothetical problems may possibly serve to make more cogent the argument that the general concept of the discussion given in this paper has general validity. Either in quantum mechanical or in classical treatments of many-body problems, the attempt is necessarily made to find a coordinate system in which the problem is at least nearly separable. The interactions between these, if important, are then pairwise.

Finally, we would like to comment on one important feature of our discussion. We have emphasized that physical measurements depend only on the simultaneous values of comparatively few coordinates and momenta, and, in the case of many-body systems, on sums of such functions for similar subsets of the identical molecules. The use made of this fact has *not* been such as to elevate it to a philosophical principle. The concept has been used only to select the reduced probability density functions w_n for small n values as the functions which fully characterize the instantaneously measurable properties of a system. The criterion that a system be thermodynamically isolated is then interpreted as meaning only that these functions evolve in time as if the surroundings had no effect on the system. One might possibly be tempted to speculate, however, that some kind of statement of the impossibility of simultaneous measurement of very many correlated coordinates or momenta is indeed fundamental. Presumably if so, the argument would have to make use of quantum mechanical concepts similar to those used in deriving the uncertainty principle for conjugated momentum coordinate pairs.

Theoretical Molecular Transition Probabilities. I. The V-N Transition in H_2†

S. EHRENSON AND P. E. PHILLIPSON

Laboratory of Molecular Structure and Spectra, Department of Physics, University of Chicago, Chicago, Illinois

(Received September 15, 1960)

Theoretical investigation of the oscillator strength of the $V-N$ transition in H_2 has been carried out employing the alternative length, velocity, and acceleration operator methods in the calculations. By successive improvements in the approximate molecular wave functions assumed for the two states, convergence of the results obtained by the three methods toward a unique f value is demonstrated. The best wave functions employed yield an f value of 0.27 for the V–N transition in H_2. Because in general the three methods weight different spatial portions of the wave functions in the dipole strength integrals, comparison of the alternative numerical f values is shown to provide some insight into the goodness, over-all and regional, of these wave functions. Agreement among the three values is also shown to be a more sensitive test of the goodness of the wave functions than are the usual energy criteria. All integrals necessary in these computations are shown to be expressible in terms of $C_{\alpha\beta}^{\gamma\delta\epsilon}$ functions which are to be found in the literature. A systematic scheme for computing the oscillator strengths of any $\Sigma-\Sigma$ transition involving one and two quantum-number Slater orbitals in terms of these C functions is outlined.

I. INTRODUCTION

THE transition probability calculations published to date have been motivated for the most part by the desire to predict as well as possible f values for given transitions, or to test wave functions by comparison with experimental oscillator strengths.[1] Although it is well known[2] that there are three equivalent dipole operators which yield identical transition moments when exact wave functions for the initial and final transition states are employed, little advantage has been taken of the possible comparisons of the three methods of computation when approximate wave functions are used.[3]

In this paper we shall show that the oscillator strengths computed by the dipole length, velocity, and acceleration operators may be quite useful in concert as criteria of the goodness of molecular wave functions alternative to the variationally obtained state energies. Emphasis is laid upon the greater sensitivity of the former compared to the latter results, dependent upon the pair of wave functions employed. As a specific example, the ${}^1\Sigma_g^+-{}^1\Sigma_u^+(V-N)$ vertical transition probability for H_2 is investigated employing various types of approximate molecular wave functions. Theory is reviewed showing that agreement among the oscillator strength values calculated by the alternative methods are not independent of the state function energies; the reported investigations indicate that convergence of the results of the three methods toward a unique f value occurs as substantially better wave functions (in the energy sense) are employed. In addition, a systematic procedure is outlined for such computations with any pair of molecular wave functions expressed in terms of Slater atomic orbital basis sets, and the appropriate integrals for $\Sigma-\Sigma$ transitions tabulated.

II. THEORY

The oscillator strength f for an electronic transition between two states I and F is given by

$$f=(8\pi^2mc/3h)\nu D=1.085\times10^{11}\nu D=6.667\times10^{-1}(\bar{\nu}\bar{D}), \tag{1}$$

where $\nu(\bar{\nu})$ is the transition frequency in cm^{-1} (a.u.), and $D(\bar{D})$, the dipole strength, in cm^2 (a.u.); f is dimensionless. The dipole strength is related to the transition moment Q by

$$D=G|Q|^2. \tag{2}$$

The quantity G effectively counts the number of independent final states to which transitions are made; further details may be found in the Mulliken and Rieke review.[3]

Three equivalent expressions for the transition moment Q, easily obtainable from matrix mechanics[2] are (in atomic units),

$$\text{dipole length:} \qquad Q^L=\int\psi_F^*\sum_i\mathbf{r}_i\psi_I d\tau_i, \tag{3}$$

$$\text{dipole velocity:} \quad Q^V=(E_I-E_F)^{-1}\int\psi_F^*\sum_i\boldsymbol{\nabla}_i\psi_I d\tau_i, \tag{4}$$

dipole acceleration:

$$Q^{A\infty}=(E_I-E_F)^{-2}\int\psi_F^*\sum_i(\boldsymbol{\nabla}V)_i\psi_I d\tau_i, \tag{5}$$

where the summations are over all the electrons involved in the transition from I to F. It should be noted that the length and acceleration operators are multiplicative operators, while the velocity operator involves the gradient of the wave function ψ_I.

† Work supported in part by the Office of Naval Research.

[1] For a review of work on atomic transition probabilities, see R. H. Garstang, Vistas in Astron. **1**, 268 (1955).

[2] H. A. Bethe and E. E. Salpeter, *Encyclopedia of Physics* (Springer-Verlag, Berlin, Germany, 1957), Vol. XXXV, p. 334; S. Chandrasekhar, Astrophys. J. **102**, 223 (1945).

[3] H. Shull [J. Chem. Phys. **20**, 18 (1952)] pointed out the value of such an approach, comparing dipole velocity results with the dipole length results of R. S. Mulliken and C. A. Rieke [Repts. Progr. in Phys. **8**, 231 (1941)].

The f values for which the experimentally determined energy difference is employed [in Eq. (1) as well as in (4) and (5)] will be differentiated by the label, *semi-theoretical*, from those where the theoretically determined energies for both states are used.

The $V-N$ transition, following the notation of Mulliken, is of the $^1\Sigma-{}^1\Sigma$ type for which G is unity and the operators in Eqs. (3), (4), and (5) reduce respectively, by virtue of zero x and y components, to z_i, $\partial/\partial z_i$ and $[(z_a/r_a^3)-(z_b/r_b^3)]_i$. The two terms of the last operator arise as an expression of the potential energy contributions of the two nuclei a and b; the negative sign is due to the arbitrary choice of the z_a and z_b axes pointed towards each other. Further details are to be found in the Appendix.

Additional specification is required for the H_2 calculations presented. In all cases we have computed the vertical or Franck-Condon transition probability from a single level of zero rotational and lowest vibrational energy. The transition is computed for the equilibrium internuclear separation of the N state (1.4 a.u.) to the lowest-lying excited singlet, or V, state. A completely meaningful comparison to the experimentally observed oscillator strength would require consideration of contributions involving all possible vibrational and rotational levels of the states considered. As Mulliken and Rieke have shown,[3] however, the approximation we have employed should be relatively good and, what is more important, will not affect the agreement criteria for our intertheoretical comparisons. Exact purely electronic wave functions for the N and V states would therefore produce exact agreement among the three methods, in approximate agreement with the true $V-N$ (Lyman band) f value.[4]

It is apparent then that the value of these computations as tests of the goodness of the electronic wave functions for the transition states involved should not be overshadowed by the numerical values of the oscillator strength obtained.

III. DETAILS OF THE COMPUTATIONS

For the hydrogen molecule, normalized single-particle wave functions of several types were employed. The N state was represented alternatively as $\psi_N=\sigma_g(1)\sigma_g(2)$, with $\sigma_g\sim(1s_a+1s_b)$, using both free atom ($\zeta=1$) and varied orbital exponents,[5] by an SCF function constructed out of a basis set including $1s$, $2s$, and $2p\sigma$ Slater functions,[6] and by the simple configuration interaction function of Weinbaum.[7] The V state wave functions were taken to have the general form $\psi=(1/\sqrt{2})[\sigma_g(1)\sigma_u(2)+\sigma_u(1)\sigma_g(2)]$. The cases considered were $\sigma_g=\sigma_g 1s\sim(1s_a+1s_b)$, $\sigma_u=\sigma_u 1s\sim(1s_a-1s_b)$, first with equal orbital exponents for σ_g and σ_u, then with orbital exponents optimized separately for σ_g and σ_u[8]; finally, with the σ_u orbital also taken to have the form $\sigma_u=\sigma_u 2p\sim(2p\sigma_a-2p\sigma_b)$. Further, an SCF virtual orbital representation (*vide infra*) of the V state was examined.

All integrals over the three operators when transformed to prolate spheroidal coordinates may be reduced to functions of the form,

$$C_{\alpha\beta\gamma\delta\epsilon}=(-1)^{\beta+\delta+\epsilon}(\tfrac{1}{2}\rho_b)^{\alpha+\beta+\gamma+\delta+2\epsilon+1}\int_1^\infty d\xi\int_{-1}^{+1}d\eta$$
$$\times\exp(-\rho\xi-\tau\rho\eta)(\xi+\eta)^\alpha(\xi-\eta)^\beta(1+\xi\eta)^\gamma(1-\xi\eta)^\delta$$
$$\times(\xi^2-1)^\epsilon(1-\eta^2)^\epsilon, \quad (6)$$

where the parameter indices α through ϵ are determined by the operator and orbital combinations employed. These C functions were originally introduced by Rudenberg, Roothaan, and Jaunzemis[9] for their analysis of one- and two-center Coulomb and hybrid integrals, but their utility is quite general: any spatial one-electron integral involving Slater atomic orbitals can be reduced to these C functions.[10] The necessary dipole length, velocity, and acceleration integrals using $1s$, $2s$, $2p\sigma$, and $2p\pi$ Slater orbitals in terms of these C functions are to be found in the Appendix.

IV. RESULTS AND DISCUSSION

The f number results for the H_2 ($V-N$) transition calculations employing the approximate molecular orbitals, $\psi_N=[\sigma_g 1s]^2$, $\psi_V=[(\sigma_g 1s)(\sigma_u 1s \text{ or } \sigma_u 2p)]$ with equal and with varied orbital exponents are presented in Table I. Reproduction of the semitheoretical results of Mulliken and Rieke,[3] and Shull[8] serve to check the discussed C function analysis. A comparison of these and the associated purely theoretical results indicates strongly how relative agreement among the alternative f values depends upon the energy difference adopted in the calculations. Particularly striking in their differences are the results for the "free-atom ζ" orbital exponent approximations. This is of course directly attributable in this case to the very poor theoretical energy difference, and generally to the fact that f_L, f_V,

[4] An experimental value for the $V-N$ transition in hydrogen is unavailable at present due to overlapping of the Lyman with the $^1\Sigma_g^+-{}^1\Pi_u$ (Werner) bands. The respective frequencies for the transition maxima lie at 99 000 and 104 000 cm^{-1} for which a total f of roughly 0.65 may be assigned, according to Mulliken and Rieke.[3] The latter value was determined from the dispersion formulas of K. L. Wolf and K. F. Herzfeld, Handbuch der Physik **20,** 492 (1928).

[5] C. A. Coulson, Trans. Faraday Soc. **33,** 1479 (1937).

[6] Private communication from B. J. Ransil of this laboratory. See also B. J. Ransil, Revs. Modern Phys. **32,** 245 (1960).

[7] S. Weinbaum, J. Chem. Phys. **11,** 593 (1933).

[8] P. E. Phillipson and R. S. Mulliken, J. Chem. Phys. **28,** 1248 (1958).

[9] K. Ruedenberg, C. C. J. Roothaan, and W. Jaunzemis, *Technical Report* (Laboratory of Molecular Structure and Spectra, University of Chicago, 1952–3), pp. 137–256+ii. (Copies available upon request.) An abridged presentation is given in J. Chem. Phys. **24,** 201 (1956).

[10] W. C. Hamilton [J. Chem. Phys. **26,** 1018 (1957)] has reduced the dipole length integrals for quantum number one and two orbitals to C function difference equations which may be converted by coordinate transformation to the simpler forms presented in the Appendix.

TABLE I. Oscillator Strengths for $H_2(V\text{-}N)$ Transition, for $\psi_N=[\sigma_g 1s_a]^2$ and $\psi_V=[(\sigma_g 1s_a \text{ or } \sigma_u 2p)]$. (Each block of four numbers represents f_L, f_V, f_{Acc} and (E_V-E_N), in ev in column order.)[a]

	N / V	$\zeta_g(1s)$ 1.00	1.197[b]	1.40
$\zeta_g(1s)$	$\zeta_u(1s)$	0.248	0.163	0.055
		0.128	0.118	0.122
	0.200	0.241	0.203	0.278
		(12.56)	(12.56)	(11.37)
		0.391	0.275	0.206
		0.154	0.215	0.231
	0.275[c]	0.503	0.429	0.534
1.450[d]		(11.39)	(12.38)	(11.19)
		0.634	0.493	0.321
		0.368	0.382	0.431
	0.425	0.946	0.840	1.179
		(12.06)	(13.06)	(11.87)
			0.688	
			0.449	
			0.938	
			(14.69)	
		1.120, **0.68**[e]		
		0.316, **0.52**[e]		
1.00	1.00	0.552, **2.46**		
		(20.18)		
	$\zeta_u(2p)$	0.482, **0.44**[e]	0.281	
		0.175, **0.19**[e]	0.144	
1.00	0.50	0.193, **0.28**	0.148	
		(13.60)	(14.59)	

[a] Boldface values were computed by the semitheoretical method.

ΔE (experimental) = 99 000 cm^{-1} = 12.27 ev.

[b] Optimum $\zeta_g{}^N=1.197$, $E_N=-3.47$ ev from work cited in footnote 5.

[c] Optimum $\zeta_g{}^V=1.450$, $\zeta_u{}^V=0.275$, $E_N=8.92$ ev from work cited in footnote 8.

[d] Values obtained with $\zeta_g=1.325$ regularly paralleled the results for the optimum value of this parameter within 5%.

[e] See works cited in footnote 3.

and f_{Acc} have explicit dependence upon ΔE, $1/\Delta E$ and $1/\Delta E^3$, respectively. Whether it is legitimate ever to use the semitheoretical energy difference alone is doubtful. Certainly when agreement among the alternative operator results is to be used as a criterion for goodness of various pairs of approximate wave functions it is not. The results of Green, *et al.*[11] are interesting in this regard. They find that the theoretical energies give closer agreement to the f sum rule for all operators than do the experimental energies in the particular cases of calcium atom transitions. Later use will be made of the semi- and purely theoretical results, side by side.

Returning to the main body of the table, attention is directed to the results obtained for the best wave function pair. Here $\zeta_g{}^V=1.450$, $\zeta_u{}^V=0.275$ with $E_V=$ 8.912 ev[8], and $\zeta_g{}^N=1.197$ with $E_N=3.470$ ev[5]. These and all other energies quoted in this paper are referred to zero for infinitely separated ground state hydrogen atoms. Although both state energies are poor (viz., E_N experimental $=-4.7466$ ev[12]) their errors almost cancel in ΔE. Both the theoretical and semitheoretical methods (latter not shown) indicate relatively good agreement between the length and velocity f values, but a much higher acceleration value. The disagreement of f_{Acc} with f_L and f_V along with the state energies suggests that both ψ_N and ψ_V are poor wave functions, a conclusion which would not be as forcibly demonstrated by comparison of f_L with f_V alone, or by comparison of the theoretical with the experimental ΔE. The other combinations of wave functions yield similar or even less satisfactory agreement among the alternative results. It may be concluded at this point that these simple wave functions are not capable of providing a reliable estimate of the oscillator strength and conversely show themselves, one or both, to be poor approximations for the states which they are intended to represent. Nor as a general conclusion may the agreement among the alternative values of f calculated be noticeably better when slight improvements in poor functions are made. In other words, agreement among f_L, f_V and f_{Acc} is more dependent in a complex way upon the wave function parameters than are the state energies or their difference.

The reason why approximate wave functions should yield so widely divergent results by the three operator methods is worthy of further examination. That such divergence should be expected was pointed out by Chandrasekhar[2] in a discussion of his oscillator strength calculations for H^-. It is simply that the Q operators emphasize different spatial portions of the wave functions in the integral weighting process. A simple graphical example of this point is afforded by the hydrogen atom transition $1s$ to $2p$ where the exact wave functions are readily available. Here Q^L, Q^V, and Q^{Acc} are identical so that after spherical coordinate integration of the θ and φ functions which are the same in all cases,

$$\left.\begin{aligned} Q^L &= \langle 1s|z|2p\rangle = [3^{-1}2^{-\frac{1}{2}}]\int_0^\infty \exp(-\tfrac{3}{2}r)r^4dr \\ Q^V &= \langle 1s|\partial/\partial z|2p\rangle = [3^{-1}2^{-\frac{1}{2}}/(3/8)]\int_0^\infty \exp(-\tfrac{3}{2}r)r^3dr \\ Q^{Acc} &= \langle 1s|z/r^3|2p\rangle = [3^{-1}2^{-\frac{1}{2}}/(9/64)]\int_0^\infty \exp(-\tfrac{3}{2}r)r\,dr \end{aligned}\right\} = 128\sqrt{2}/243. \quad (7)$$

[11] L. C. Green, N. E. Weber, and E. Krawitz, Astrophys. J. **113**, 690 (1951).

[12] G. Herzberg, *Spectra of Diatomic Molecules* (D. Van Nostrand Company, Inc., Princeton, New Jersey, 1950), p. 530.

The correct $1s$ and $2p$ orbital exponents are 1.0 and 0.5, respectively. In Fig. 1, the normalized integrands of Eqs. (7) are plotted versus r, the radius vector of the electron. The r values of the respective maxima for the length, velocity, and acceleration curves lie at $\frac{8}{3}$, 2, and $\frac{2}{3}$ a.u. The important insights afforded by this example are in two in number. First, while the length and velocity operators do indeed stress different spatial portions of the wave functions, a much greater difference is noted in comparison of either with the regions emphasized by the acceleration operator. The latter heavily weights the regions close to the nucleus, just the portion of space in which approximate atomic electronic wave functions are generally poorest. Second, excess electron density for both states in a particular region should be reflected in an increased integrand value by the method stressing this region (although not necessarily in the result obtained upon division by ΔE, or if the two states are in error in the opposite direction in this region). It should again be emphasized that these conclusions require care in application to molecular systems where the electron density distribution is anisotropic; however, qualitatively they are similar.[13]

We are now in a position to reexamine in somewhat more detail the results of Table I. For all the orbital representations in terms of $1s$ Slater orbitals, with one reasonable exception, the dipole acceleration f value is found to be considerably greater than the corresponding values obtained from the length and velocity methods. This conclusion holds, in many cases more strongly, upon comparison of the corresponding semitheoretical results. It is well known[14] that simple LCAO-MO wave functions are unable, by virtue of their construction, to properly weight ionic and covalent contributions by explicit variational means.

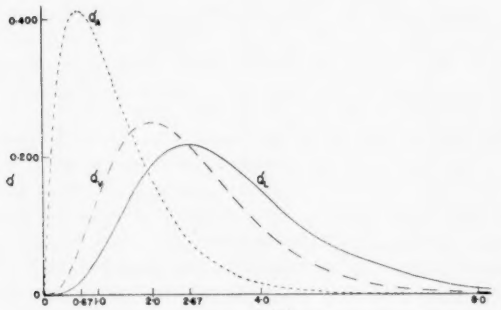

FIG. 1. Radial dependence of length, velocity, and acceleration oscillator strength integrands for hydrogen atom $1s-2p$ transition.

[13] Suggested by unpublished results from this laboratory. Work is presently underway to refine these considerations by examination of H_2^+ molecule transitions employing both exact and approximate wave functions in various combinations.

[14] C. A. Coulson, *Valence* (Oxford University Press, New York, 1952), Chap. VI.

This deficiency is of course more important in some cases than in others. For the ground state of hydrogen with $\psi_N=[\sigma_g 1s]^2$, the ionic and covalent contributions are equally weighted. However, as was demonstrated by Weinbaum[7] in his variational calculation, the energy minimum for the ground state represented as

$$\psi_N=C[1s_A(1)1s_B(2)+1s_B(1)1s_A(2)] +[1s_A(1)1s_A(2)+1s_B(1)1s_B(2)], \quad (8)$$

occurs when $\zeta(1s)=1.193$ and $C=3.9$ ($E_N=-4.024$ ev, an improvement of 0.5 ev over Coulson's value[9]). For this much improved representation, the covalent contribution is seen to be much more important than the ionic. Further, while the V state generally has been assumed dominantly ionic, the results of several computations have raised some questions about this.[15] The best V state functions examined here have departed from purely ionic character through gross variations in the orbital exponents ($\zeta_g^V>1$, $\zeta_u^V\ll 1$, where $\zeta_g^V=\zeta_u^V$ would give the purely ionic form, shown to be a very poor approximation[8]). Perhaps a Weinbaum-type treatment would further decrease the ionic contribution. Even assuming the V state to be properly pictured with regard to the weighting of these contributions, the ground state in the simple LCAO–MO approximation is overly ionic, and as a result regions near the nuclei should have an excess of electron density which would exaggerate the acceleration dipole value, Q^{Acc}. This implies, in general, that since there is too much charge density near the nuclei, regions farther out should be deficient in charge density. Therefore integrals over the dipole length and velcoity operators would tend to be too small, and integrals over the acceleration operator should be too large. This does not necessarily mean that f_{Acc} would always be too large, and f_L and f_V too small, since ΔE enters into these quantities in different powers. However, this conclusion fits well with the generally high values obtained from the acceleration calculations. In fact, the only parameters which result in reduction of the acceleration value to agreement with either of the values obtained by other methods also result in obviously incorrect diffuseness of charge (i.e., when $\zeta_g^N=1.00$, $\zeta_u^V=0.200$).

Where σ_u is approximated as $\sigma_u 2p$, the acceleration values are no longer higher than those computed by the other methods. This result is fully in agreement with the analysis presented when the spatial electron distributions in $2p\sigma$ and $1s$ orbitals are contrasted. The suggestion of Mulliken and Rieke,[3] to the effect that further improvement in the σ_u orbital, beyond minimization with respect to $\zeta_u(1s)$, might be accomplished by going over to the $2p\sigma_u$ Rydberg form, seems reasonable from these considerations. Further computations are in order, perhaps by including $2p\sigma$ orbitals in a Weinbaum-type treatment as discussed above.

[15] C. Zener and V. Guillemin, Jr., Phys. Rev. **34**, 999 (1929).

TABLE II. Oscillator strengths for $H_2(V-N)$ transition employing improved ground-state wave functions.

		Best $(\sigma_g 1s)^2$	SCF	Weinbaum
	L	0.275	0.273	0.242
f	V	0.215	0.225	0.287
	Acc	0.429	0.354	0.267
	E_N(ev)	−3.470	−3.595	−4.024

With these results noted, some improved wave functions were tried. Again taking the best simple V state wave function available ($\sigma_g 1s\,\sigma_u 1s$, with the optimum ζ's 1.450 and 0.275, respectively) we have examined the Weinbaum and SCF ground-state functions. The Weinbaum function has been described above; the SCF function[6] where $\psi_N = \sum c_j \varphi_j$, with φ_j including $1s$, $2s$ and $2p\sigma$ Slater orbitals, has all ζ's = 1.2313, and an energy of −3.595 ev. The coefficients c_{1s}, c_{2s}, and $c_{2p\sigma}$ are, respectively, equal to 0.4993, 0.0365, and 0.0408. Table II contains the results of these calculations with the values for the best wave function pair from Table I included for comparison.

Several interesting results emerge from consideration of Table II. The SCF function employed for the ground state has improved the agreement between the f values somewhat; however, the acceleration value, although the most improved, still remains quite high. This is perhaps not too surprising when the relatively small contributions of the $2s$ and $2p\sigma$ orbitals and the value of the single $\zeta(1.2313)$ are considered. Similar expression of the simple Coulson function reveals $c_{1s} = 0.535$ and $\zeta = 1.197$. Other SCF ground-state functions for H_2 have been constructed which should provide somewhat better results. In one of these which also employs a $1s$, $2s$, and $2p\sigma$ basis set, the orbital exponents and coefficients were variationally optimized to yield an energy of −3.632 ev.[6] The five-term SCF wave function of Coulson[16] would not seem to offer anything beyond this in as much as a single preset orbital exponent was employed. What is perhaps of more interest in this paper is the electron density comparison for the simple optimum $\zeta(1s)$ versus SCF functions. This shows a shift of charge from around the nuclear positions into the region between the nuclei in passing from the former to the latter.

Neither of these were examined however, attention being directed rather to another method of improvement of the approximate ground state representation, configuration interaction. The Weinbaum function, which has already been discussed, yielded the values found in the last column of Table II. Here the results of the three methods have converged well (to an average value of f equal to 0.265, spread over 0.045). While improvement was to be expected over the simple MO functions on the grounds of suppression of the ionic contribution, it is perhaps surprising that so much better agreement results. Besides the obvious shortcomings of as rough a V-state representation as was employed, the doubtlessly important effect of electron correlation has been completely overlooked in the V state. A possible reason for this improvement is that the decrease in the ionic portion of the N-state wave function has pulled charge away from the nuclei into regions further away, presumably between the nuclei, thus lowering f_{Acc}. These results indicate that at least in this case, the results are more sensitive to the N state than to the V state. This is because the electron correlation effects, which are partially accounted for in the Weinbaum function are far stronger in the N than in the V state. In the latter case, the two electrons are kept apart by the fact that they are in distinct orthogonal orbitals σ_g and σ_u.

Review of the discrepancies in the state energies and their difference as compared to experiment, however, leads to the interesting conclusion that the theoretical ΔE has provided a better picture of agreement than may in actuality be justified. The theoretical difference (12.94 ev) is over 5% greater than the experimentally measured value; employment of the latter yields the respective semitheoretical length, velocity, and acceleration values, 0.230, 0.301, and 0.309. Somewhat poorer agreement among these values and proximity of the velocity and acceleration results, both higher than that computed by the dipole length method, are noteworthy.

If the range 0.080 is roughly centered about the average theoretical value 0.265, all the results, both semitheoretical and purely theoretical, are encompassed. The best H_2 $(V-N)$ f-value estimate available then from this study is 0.27.

It was of interest to extend these calculations to examine the SCF V-state function generated as a by-product from variational optimization for the ground state SCF examined above. While there is no theoretical reason why a function of this sort (designated generally as a virtual orbital) should be a good representation of the actual symmetry state, several interesting points of rough agreement have been noted (i.e., slopes of potential curves and energy differences between excited states[6]). Since these functions are determined solely by the requirement that they be orthogonal within their symmetry to the ground state, it is surprising that they resemble the true picture at all. Calculation of the f numbers arising from use of this state provide another mode of comparison; most pertinent is the calculation of the transition probability from the SCF ground state, the determination of which is responsible for the virtual orbital representation. For the single ζ functions, the ground-state parameters are listed above. The virtual V-state function, with $E = 12.619$ ev, has the coefficients c_{1s}, c_{2s}, and $c_{2p\sigma}$

[16] C. A. Coulson, Proc. Cambridge Phil. Soc. **34**, 204 (1938).

TABLE III. Type I integrals $\langle a \mid Q_a \mid a' \rangle$.[a]

	Length: z_a	Velocity: $\partial/\partial z_a$	Acceleration: $\cos\theta_a/r_a^2$
$\langle 1s_a \mid Q_a \mid 2p\sigma_{a'} \rangle$	$\frac{32(\zeta_a^3\zeta_{a'}^5)^{\frac{1}{2}}}{(\zeta_a+\zeta_{a'})^5}$	$-\frac{8(\zeta_a\zeta_{a'})^{5/2}}{(\zeta_a+\zeta_{a'})^4}$	$\frac{4}{3}\frac{(\zeta_a^3\zeta_{a'}^5)^{\frac{1}{2}}}{(\zeta_a+\zeta_{a'})^2}$
$\langle 2s_a \mid Q_a \mid 2p\sigma_{a'} \rangle$	$\frac{160}{\sqrt{3}}\frac{(\zeta_a\zeta_{a'})^{5/2}}{(\zeta_a+\zeta_{a'})^6}$	$\frac{(\zeta_a\zeta_{a'})^{5/2}}{\sqrt{3}(\zeta_a+\zeta_{a'})^5}[24\zeta_a-8\zeta_{a'}]$	$\frac{8\sqrt{3}}{9}\frac{(\zeta_a\zeta_{a'})^{5/2}}{(\zeta_a+\zeta_{a'})^5}$

[a] For the dipole velocity: $\langle a \mid \partial/\partial z_a \mid a' \rangle = -\langle a' \mid \partial/\partial z_a \mid a \rangle$.

equal to 0.3460, 0.7826, and −0.2140. The respective length, velocity, and acceleration f values are 0.762, 0.538, and 0.607, in relatively poor agreement with each other and much higher than the estimated value of 0.27. The semitheoretical values are of course much worse (ΔE theoretical being 16.214 ev). From the viewpoint of the oscillator strength calculations then, in agreement with the energy, the only conclusion possible is that this virtual orbital V-state approximation is a very poor one.

V. CONCLUSIONS

The oscillator strength values calculated by the alternative dipole length, velocity, and acceleration methods for the $(V-N)$ transition in H_2 are found to exhibit improved internal agreement as the wave function representation of the participant states are grossly improved. Also, it appears that these values tend to converge toward a physically reasonable value. Both of these results are in agreement with theory. The effects of minor improvements as judged by the energies on very poor functions is, however, often not recognizable. The best functions considered here provide an f value for this transition of 0.27.

While it is still not possible to show unambiguously that *close* agreement between the alternative method results necessarily means that the correct f value is being approached, such a conclusion now seems more reasonable. The uncertainties voiced by Bates and Damgaard[17] on the possible fortuitous agreement obtainable for comparison of the length and velocity results are made less likely by the further and more stringent comparisons provided with the acceleration value. As an additional check, the semitheoretical values, where available, preclude apparent agreement through integral error cancellation by incorrect energy differences.

Extension of this investigation is suggested to further check the conclusions obtained from these results. Information on whether better, yet still approximate, wave functions would provide a more regular approach to convergence for the three methods would be of interest as would of course the exact value for the transition considered. For example, and in the degree of ultimate refinement the improved agreement accompanying the stepwise addition of terms in James and Coolidge[18] and Kolos and Roothaan[19] functions should provide, ignoring the attendant mathematical complexity, much valuable information in this regard.

[17] D. R. Bates and A. Damgaard, Phil. Trans. Roy. Soc. London **A242,** 101 (1949).

ACKNOWLEDGMENTS

The authors wish to thank Professor R. S. Mulliken and Professor C. C. J. Roothaan for their continued interest and suggestions on this work. The computational help of Tracy Kinyon is also acknowledged.

APPENDIX

Transition Moment Integrals in Terms of $C_{\alpha\beta}{}^{\gamma\delta\epsilon}$ Functions

For any atomic or molecular wave function constructed out of a Slater orbital basis set, all integrals over the three transition operators reduce to a linear combination of one-electron integrals of three types,

$$\begin{aligned} &\text{I} && \langle (nlm)_a \mid Q_a \mid (n'l'm')_{a'} \rangle \\ &\text{II} && \langle (nlm)_b \mid Q_a \mid (n'l'm')_{b'} \rangle \\ &\text{III} && \langle (nlm)_b \mid Q_a \mid (n'l'm')_a \rangle. \end{aligned} \tag{A1}$$

The dipole operators (in atomic units) are given by[20]

$$\begin{aligned} &Q_a{}^L = z_a = R - z_b \\ &Q_a{}^V = \partial/\partial z_a = -\partial/\partial z_b \\ &Q^{\text{Acc}} = (Z_a \cos\theta_a/r_a{}^2) - (Z_b \cos\theta_b/r_b{}^2) = Q_a{}^{\text{Acc}} - Q_b{}^{\text{Acc}}. \end{aligned} \tag{A2}$$

Here a and b refer to the two nuclei; the coordinate system is so chosen that the positive z_a and z_b axes point towards each other. Integrals of the form I are simply of the one-center one-electron type which may be

[18] H. James and A. Coolidge, J. Chem. Phys. **1,** 825 (1933).

[19] W. Kolos and C. C. J. Roothaan, Revs. Modern Phys. **32,** 219 (1960).

[20] In general these operators have x, y, and z components. In $\Sigma-\Sigma$ transitions of the type examined in this paper, only the z component yields nonvanishing integrals. Investigation will be limited here to these types. A fuller account will be published in the near future which will include dipole and quadrupole transition integrals for all components in terms of the $C_{\alpha\beta}{}^{\gamma\delta\epsilon}$ functions.

TABLE IV. Type II integrals $\langle b \mid Q_a \mid b' \rangle$.[a]

	Length: z_a	Acceleration: $\cos\theta_a/r_a^2$
$\langle 1s_b \mid Q_a \mid 1s_{b'} \rangle$	$\dfrac{8R(\zeta_b\zeta_{b'})^{3/2}}{(\zeta_b+\zeta_{b'})^3}$	$-\dfrac{2(\zeta_b\zeta_{b'})^{3/2}}{(\zeta_b+\zeta_{b'})}C_{-21}^{100}$
$\langle 1s_b \mid Q_a \mid 2s_{b'} \rangle$	$\dfrac{8R\sqrt{3}(\zeta_b^3\zeta_{b'}^5)^{1/2}}{(\zeta_b+\zeta_{b'})^4}$	$\dfrac{2}{\sqrt{3}}\dfrac{(\zeta_b^3\zeta_{b'}^5)^{1/2}}{(\zeta_b+\zeta_{b'})^2}C_{-22}^{100}$
$\langle 1s_b \mid Q_a \mid 2p\sigma_{b'} \rangle$	$-\dfrac{32(\zeta_b^3\zeta_{b'}^5)^{1/2}}{(\zeta_b+\zeta_{b'})^5}$	$\dfrac{2(\zeta_b^3\zeta_{b'}^5)^{1/2}}{(\zeta_b+\zeta_{b'})^2}C_{-21}^{110}$
$\langle 2s_b \mid Q_a \mid 2s_{b'} \rangle$	$\dfrac{32R(\zeta_b\zeta_{b'})^{5/2}}{(\zeta_b+\zeta_{b'})^5}$	$-\dfrac{2}{3}\dfrac{(\zeta_b\zeta_{b'})^{5/2}}{(\zeta_b+\zeta_{b'})^3}C_{-23}^{100}$
$\langle 2s_b \mid Q_a \mid 2p\sigma_{b'} \rangle$	$-\dfrac{160}{\sqrt{3}}\dfrac{(\zeta_b\zeta_{b'})^{5/2}}{(\zeta_b+\zeta_{b'})^6}$	$-\dfrac{2}{\sqrt{3}}\dfrac{(\zeta_b\zeta_{b'})^{5/2}}{(\zeta_b+\zeta_{b'})^3}C_{-22}^{110}$
$\langle 2p\sigma_b \mid Q_a \mid 2p\sigma_{b'} \rangle$	$\dfrac{32R(\zeta_b\zeta_{b'})^{5/2}}{(\zeta_b+\zeta_{b'})^5}$	$-\dfrac{2(\zeta_b\zeta_{b'})^{5/2}}{(\zeta_b+\zeta_{b'})^3}C_{-21}^{120}$
$\langle 2p\pi_b \mid Q_a \mid 2p\pi_{b'} \rangle$	$\dfrac{32R(\zeta_b\zeta_{b'})^{5/2}}{(\zeta_b+\zeta_{b'})^5}$	$\dfrac{(\zeta_b\zeta_{b'})^{5/2}}{(\zeta_b+\zeta_{b'})^3}C_{-21}^{101}$

[a] For the dipole velocity: $\langle b \mid \partial/\partial z_a \mid b' \rangle = -\langle b' \mid \partial/\partial z_a \mid b \rangle = -\langle a \mid \partial/\partial z_a \mid a' \rangle$; for the acceleration: $\langle b \mid \cos\theta_a/r_a \mid b' \rangle = \langle a \mid \cos\theta_a/r_a^2 \mid a' \rangle$.

TABLE V. Type III integrals $\langle b \mid Q_a \mid a \rangle$.[a]

	Length: z_a	Velocity: $\partial/\partial z_a$	Acceleration: $\cos\theta_a/r_a^2$
$\langle 1s_b \mid Q_a \mid 1s_a \rangle$	$-2(\zeta_a^3/\zeta_b^5)^{1/2}C_{11}^{100}$	$2(\zeta_a^5/\zeta_b^3)^{1/2}C_{01}^{100}$	$-2(\zeta_a^3\zeta_b)^{1/2}C_{-21}^{100}$
$\langle 1s_b \mid Q_a \mid 2s_a \rangle$	$-(2/\sqrt{3})(\zeta_a^5/\zeta_b^7)^{1/2}C_{21}^{100}$	$(2/\sqrt{3})[(\zeta_a^7/\zeta_b^5)^{1/2}C_{11}^{100}-(\zeta_a^5/\zeta_b^3)^{1/2}C_{01}^{100}]$	$-(2/\sqrt{3})(\zeta_a^5/\zeta_b)^{1/2}C_{-11}^{100}$
$\langle 2s_b \mid Q_a \mid 1s_a \rangle$	$(2/\sqrt{3})(\zeta_a^3/\zeta_b^5)^{1/2}C_{12}^{100}$	$-(2/\sqrt{3})(\zeta_a^5/\zeta_b^3)^{1/2}C_{02}^{100}$	$(2/\sqrt{3})(\zeta_a^3\zeta_b)^{1/2}C_{-22}^{100}$
$\langle 1s_b \mid Q_a \mid 2p\sigma_a \rangle$	$-2(\zeta_a^5/\zeta_b^7)^{1/2}C_{11}^{200}$	$2[(\zeta_a^7/\zeta_b^5)^{1/2}C_{01}^{200}-(\zeta_a^5/\zeta_b^3)^{1/2}C_{11}^{000}]$	$-2(\zeta_a^5/\zeta_b)^{1/2}C_{-21}^{200}$
$\langle 2p\sigma_b \mid Q_a \mid 1s_a \rangle$	$2(\zeta_a^3/\zeta_b^5)^{1/2}C_{11}^{110}$	$-2(\zeta_a^5/\zeta_b^3)^{1/2}C_{01}^{110}$	$2(\zeta_a^3\zeta_b)^{1/2}C_{-21}^{110}$
$\langle 2s_b \mid Q_a \mid 2s_a \rangle$	$\frac{2}{3}(\zeta_a^5/\zeta_b^7)^{1/2}C_{22}^{100}$	$\frac{2}{3}[(\zeta_a^5/\zeta_b^3)^{1/2}C_{02}^{100}-(\zeta_a^7/\zeta_b^5)^{1/2}C_{12}^{100}]$	$\frac{2}{3}(\zeta_a^5/\zeta_b)^{1/2}C_{-12}^{100}$
$\langle 2s_b \mid Q_a \mid 2p\sigma_a \rangle$	$(2/\sqrt{3})(\zeta_a^5/\zeta_b^7)^{1/2}C_{12}^{200}$	$(2/\sqrt{3})[(\zeta_a^5/\zeta_b^3)^{1/2}C_{12}^{000}-(\zeta_a^7/\zeta_b^5)^{1/2}C_{02}^{200}]$	$(2/\sqrt{3})(\zeta_a^5/\zeta_b)^{1/2}C_{-22}^{200}$
$\langle 2p\sigma_b \mid Q_a \mid 2s_a \rangle$	$(2/\sqrt{3})(\zeta_a^5/\zeta_b^7)^{1/2}C_{21}^{110}$	$(2/\sqrt{3})[(\zeta_a^5/\zeta_b^3)^{1/2}C_{01}^{110}-(\zeta_a^7/\zeta_b^5)^{1/2}C_{11}^{110}]$	$(2/\sqrt{3})(\zeta_a^5/\zeta_b)^{1/2}C_{-11}^{110}$
$\langle 2p\sigma_b \mid Q_a \mid 2p\sigma_a \rangle$	$2(\zeta_a^5/\zeta_b^7)^{1/2}C_{11}^{210}$	$2[(\zeta_a^5/\zeta_b^3)^{1/2}C_{11}^{010}-(\zeta_a^7/\zeta_b^5)^{1/2}C_{01}^{210}]$	$2(\zeta_a^5/\zeta_b)^{1/2}C_{-21}^{210}$
$\langle 2p\pi_b \mid Q_a \mid 2p\pi_a \rangle$	$(\zeta_a^5/\zeta_b^7)^{1/2}C_{11}^{101}$	$-(\zeta_a^7/\zeta_b^5)^{1/2}C_{01}^{101}$	$(\zeta_a^5/\zeta_b)^{1/2}C_{-21}^{101}$

[a] For the dipole velocity: $\langle b \mid \partial/\partial z_a \mid a \rangle = -\langle a \mid \partial/\partial z_a \mid b \rangle$, for the dipole acceleration: $\langle b \mid Z_a \cos\theta_a/r_a^2 \mid a \rangle \rightarrow \langle b \mid Z_b \cos\theta_b/r_b^2 \mid a \rangle$, as $\tau \rightarrow -\tau$, $\zeta_a \rightarrow \zeta_b$, $\zeta_b \rightarrow \zeta_a$, for example, $\langle 2p\sigma_b \mid Z_a \cos\theta_a/r_a^2 \mid 1s_a \rangle = 2Z_a(\zeta_a^3\zeta_b)^{1/2}C_{-21}^{110}(\tau) \rightarrow \langle 2p\sigma_b \mid Z_b \cos\theta_b/r_b^2 \mid 1s_a \rangle = -2Z_b(\zeta_b^5/\zeta_a)^{1/2}C_{-21}^{200}(-\tau)$.

easily evaluated in spherical coordinates. Integrals of the form II and III are of the two-center type most conveniently determined by first expressing them in prolate spheroidal coordinates defined by

$$r_{a,b}=\tfrac{1}{2}(\xi\pm\eta)R, \qquad \cos\theta_{a,b}=(1\pm\xi\eta)/(\xi\pm\eta),$$
$$\sin\theta_{a,b}=\frac{[(\xi^2-1)(1-\eta^2)]^{\frac{1}{2}}}{(\xi\pm\eta)}. \tag{A3}$$

The volume element is $(R^3/8)(\xi+\eta)(\xi-\eta)d\xi d\eta d\phi$, and the ranges of integrations are, $1\leq\xi\leq\infty$, $-1\leq\eta\leq+1$, $0\leq\phi\leq2\pi$. After the ϕ integration is carried out, integrals II and III assume the general form, ignoring the constants of normalization

$$\int_1^\infty d\eta\,\exp(-\rho\xi-\eta\tau\rho)$$
$$\times[(\xi+\eta)^\alpha(\xi-\eta)^\beta(1+\xi\eta)^\gamma(1-\xi\eta)^\delta(\xi^2-1)^\epsilon(1-\eta^2)^\epsilon]$$
$$=[(-1)^{\beta+\delta+\epsilon}(\tfrac{1}{2}\rho_b)^{\alpha+\beta+\gamma+\delta+2\epsilon+1}]^{-1}C_{\alpha\beta}{}^{\gamma\delta\epsilon}(\rho_a,\rho_b), \tag{A4}$$

where in general,

$$\rho=\tfrac{1}{2}(\zeta_a+\zeta_b)R, \qquad \tau=[(\zeta_a-\zeta_b)/(\zeta_a+\zeta_b)],$$
$$\rho_a=(1+\tau)\rho, \qquad \rho_b=(1-\tau)\rho. \tag{A5}$$

These conditions always hold for integrals of the form III. For II integrals these parameters assume the values

$$\rho=\tfrac{1}{2}(\zeta_b+\zeta_b')R, \qquad \tau=-1, \qquad \rho_a=0, \qquad \rho_b=2\rho.$$

The expressions for $C_{\alpha\beta}{}^{\gamma\delta\epsilon}(\rho_a,\rho_b)$ are tabulated by Rudenberg, Roothaan, and Jaunzemis[9] and are stated in terms of a parameter $\kappa=\frac{1}{2}(\tau+\tau^{-1})$; for II integrals $\kappa=-1$. Care must be exercised in taking the limits $\rho_a\to0$, $\kappa\to-1$ for integrals II. Cases for which $\tau=0$ ($\zeta_a=\zeta_b$) are already tabulated.

Nonvanishing integrals for 1- and 2-quantum Slater orbitals in terms of $C_{\alpha\beta}{}^{\gamma\delta\epsilon}(\rho_a,\rho_b)$ are tabulated in Tables III, IV, and V. These orbitals are:

$$(1s)=(\zeta^3/\pi)^{\frac{1}{2}}e^{-\zeta r}$$
$$(2s)=(\zeta^5/3\pi)^{\frac{1}{2}}re^{-\zeta r}$$
$$\left.\begin{array}{ll}(2p\sigma) & \\ (2p\pi)=(\zeta^5/\pi)^{\frac{1}{2}}re^{-\zeta r} & \\ (2p\pi) & \end{array}\right\}\begin{array}{l}\cos\theta\\ \sin\theta\cos\phi\\ \sin\theta\sin\phi.\end{array} \tag{A6}$$

The integrals are over the operators z_a, $\partial/\partial z_a$, and $Q^{A\infty}/Z_a=\cos\theta_a/r_a{}^2$. Any integrals over center b can be obtained using Eqs. (A3) and noting the comments at the bottom of each table.

THE JOURNAL OF CHEMICAL PHYSICS VOLUME 34, NUMBER 4 APRIL, 1961

The SPO (Split p-Orbital) Method and Its Application to Ethylene

MICHAEL J. S. DEWAR AND N. L. HOJVAT*

George Herbert Jones Laboratory, University of Chicago, Chicago 37, Illinois

(Received August 26, 1960)

Difficulties arise in the MO treatment of π-electron systems due to electron correlation. Current methods allow, explicitly to some extent, for horizontal correlation (i.e., correlation of electron motions parallel to the carbon skeleton) but not for vertical correlation, (i.e., correlation of electron interchange between the two π lobes). A method for doing this, first suggested by M. J. S. Dewar and C. E. Wulfman [J. Chem. Phys. **29,** 158, (1958)], is outlined and applied to ethylene with satisfactory results.

ONE major and unresolved problem in the molecular orbital method has been to find some adequate way of allowing for electron correlation,[1] using the term in a general sense to cover the correlation of electron motions due both to the exclusion principle and to their mutual Coulomb repulsions. Here we shall consider one specific aspect of the general problem; the inclusion of electron correlation in the treatment of the π electrons in conjugated systems, following the conventional Hückel approximation that the π electrons can be treated apart from the "core" of inner electrons and electrons forming σ bonds. We shall also make the approximation, unavoidable at present, of expressing the wave functions for the π electrons in terms of $2p$-AO's ϕ_i of the contributing atoms.

The wave function ψ for a π-electron system containing n electrons can be written in the form

$$\psi = \sum_m a_m \prod_{k=1}^{n} \phi_i^k \sigma^k, \tag{1}$$

where $\phi_i^k \sigma_i^k$ denotes electron k occupying the AO ϕ_i with spin function σ^k and the a_m are algebraic coefficients. The sum extends over all possible sets of such products of the ϕ_i; subject to the condition that no ϕ_i occur more than twice (and then only if the two corresponding spin functions differ). This notation represents the wave function Ψ as a linear combination or hybrid of a number of contributing structures, in each of which the n electrons are shared out in some definite way among the conjugated atoms; structures in which each ϕ_i appears once are described as covalent; structures in which at least one ϕ_i appears twice as ionic. The square of each coefficient a_m is a measure of the importance of the corresponding structure.

In the SCF LCAO MO treatment,[2] where electron correlation is neglected apart from antisymmetrization, the importance of ionic structures is overestimated; the importance of such structures is diminished by the strong mutual repulsion of two electrons occupying the same AO, an effect which is neglected in the SCF treatment. In the VB (valence bond) method the opposite approximation is made of assuming that the mutual repulsion of two electrons in the same AO is so great that ionic structures can be neglected; in the case of H_2, where accurate wave functions are available, the truth lies nearer the VB extreme. An intermediate course is taken in the SCF CI[3] method, where the value of the coefficients a_m in Eq. (1) are adjusted by writing the wave function Ψ of a molecule as a combination of individual LCAO MO functions,

$$\Psi = \sum_p A_p \Psi_p. \tag{2}$$

When this treatment is applied to simple diatomic molecules it leads to wave functions Ψ for the ground state that differ from the simple ground state SCF functions ψ_0; there are large contributions from excited SCF functions ψ_p. When the resulting function Ψ is expanded in products of AO's [cf. Eq. (1)] the terms corresponding to covalent structures predominate. Both these facts suggest that the SCF treatment is a very poor approximation, the true wave functions lying much closer to the VB extreme with very little participation from ionic structures.

Recent work[4–6] has shown, however, that the fault lies not with the MO method itself but with the neglect of electron correlation in calculating the mutual repulsion of electrons. These repulsions appear in the calculations as sums of terms $(ij;\ kl)$ defined by

$$(ij;\ kl) = \int \phi_i^a \phi_j^a (e^2/r_{ab}) \phi_k^b \phi_l^b d\tau, \tag{3}$$

where r_{ab} is the distance between electrons a, b. This integral represents the repulsion of two electron distributions without allowing for the fact that the two electrons will tend to correlate their motions in such a way as to reduce their mutual repulsion as much as possible. The estimated total electron repulsion, found by summing terms of the form $(ij;\ kl)$, is, therefore, too great. The error is greatest when the electrons a, b

* On leave of absence from Facultad de Ciencias Exactas, Universidad de Buenos Aires, Argentina.

[1] M. J. S. Dewar and C. E. Wulfman, J. Chem. Phys. **29,** 158 (1958).

[2] C. C. J. Roothaan, Revs. Modern Phys. **23,** 69 (1951).

[3] D. P. Craig, Proc. Roy. Soc. (London) **A200,** 474 (1950).

[4] R. Pariser, J. Chem. Phys. **21,** 568 (1953).

[5] R. Pariser and R. Parr, J. Chem. Phys. **21,** 466, 767 (1953).

[6] W. Moffitt and J. Scanlan, Proc. Roy. Soc. (London) **A218,** 464 (1953).

occupy the same AO, so that $i=j=k=l$ in Eq. (3); the overestimate of electron repulsions is, therefore, greatest for ionic structures and consequently, the SCF CI method underestimates their importance.

The errors so introduced may not be too large in the case of σ bonds formed by s- or hybrid orbitals; in such an AO there is only one region of high-orbital density. If two electrons occupy the AO, they are unable to keep apart unless one of them is pushed away into regions where the nuclear field is low; electron correlation cannot do much to lower their energy since any gain in reduced electron repulsion is lost in reduced nuclear attraction. Neglect of electron correlation will not, therefore, have too serious an effect in such cases. The situation is entirely different in the case of p-AO's where there are *two* equivalent regions or lobes of high-orbital density; two electrons occupying such an AO can greatly reduce their mutual repulsions by correlating their motions in such a way that at any instant they occupy different lobes; since their motions need not be otherwise affected their interaction with the nuclei need not be reduced. Correlation of this kind, therefore, greatly reduces the total energy and so the SCF CI method should be greatly in error when applied to MO's built up from p-AO's, i.e., when applied to π electrons. In such cases the SCF CI method should greatly underestimate the importance of ionic structures.

This argument is supported by a comparison of the calculated and observed values for the integral (11; 11) between two electrons occupying the same carbon $2p$-AO. This can be estimated from the energy required to transfer an electron from one neutral carbon atom to another,[4] i.e.,

$$\mathrm{C.}+\mathrm{C.}=\overset{-}{\mathrm{C}}:+\overset{+}{\mathrm{C}}, \qquad (4)$$

which is known from spectroscopic data to be 10.53 ev; this should be equal to the integral (11; 11) since the core potential for the two electrons indicated in Eq. (4) is the same in each case. The experimental value is much less than the theoretical one (16.93 ev) calculated from Eq. (3) using a Slater function for the AO.

Pariser and Parr[5] have met this difficulty in a frankly empirical way by setting the value of the integral (11;11) equal to the experimental value; they also modified certain other repulsion integrals in an analogous manner. Use of these values in a modified SCF calculation gives results in much better agreement with experiment than the SCF or SCF CI methods, while in the case of ethylene, interaction of the ground state with excited states becomes unimportant so that the SCF wave function represents the ground state well. Similar conclusions have been reached by Moffitt[6] by a method similar in principle to that of Pariser and Parr; here again experimental data were used to estimate the mutual repulsion of a pair of electrons attached to the same atom.

These treatments are essentially empirical. The Pariser-Parr method relies on the use of empirical values for the electron repulsion integrals, while Moffitt's atoms-in-molecules method uses empirical values for the energies of atoms, the energy of a molecule being found from the energies of the component atoms by a perturbation method. Dewar and Wulfman[1] suggested an alternative approach, based on the arguments given in the foregoing and avoiding any appeal to experiment. They argued that the *vertical correlation* of two electrons occupying a p-AO, i.e., their tendency to correlate their motions in such a way as to keep in separate lobes of the p-AO, might be almost complete, so that a good approximation might be obtained by assuming that it *is* complete and that the probability of finding both electrons simultaneously in the same p lobe is zero. They pointed out that the value ($\overline{11}$, 11) calculated on this basis for the (11; 11) integral, using a Slater function for the AO, is 10.37 ev, in almost exact agreement with experiment. This supports very strongly the suggestion that vertical correlation is almost complete for two electrons occupying the same $2p$-AO; it also suggests that vertical correlation should also be essentially complete for a pair of electrons occupying any orbital of p-type symmetry, i.e., any orbital where there are two equivalent regions of high-orbital density, such as the π orbital of ethylene. An obvious extension of this idea led to the suggestion that similar vertical correlation may occur in conjugated systems where a number of electrons occupy a set of π orbitals; vertical correlation in such cases should tend to keep the electrons evenly shared between the two lobes of the π orbitals, exactly half the electrons being at any instant on each side of the nodal plane. Preliminary calculations along these lines gave encouraging results. Snyder and Parr[7] independently used a similar treatment to calculate the ground state energy of the helium atom and pointed out that the same approach should be applicable to molecules containing π electrons.

Dewar and Schmeising[8] have carried the argument further in a qualitative way. They pointed out that vertical correlation in the case of a polyene should have an important effect on the electron distribution, tending to concentrate the electrons in pairs in the bonds written as double in the classical structure. Treatments in which vertical correlation is neglected must then overestimate the degree of delocalization of electrons in such molecules. The empirical adjustment of integrals adopted by Pariser and Parr[5] and Moffitt[6] does not help in this connection; these methods still attach too much weight to configurations in which there are more electrons on one side of the nodal plane than on the other.

Kolos[9] has described a method in which electron

[7] L. C. Snyder and R. G. Parr, J. Chem. Phys. **28**, 1250 (1958).
[8] M. J. S. Dewar and H. N. Schmeising, Tetrahedron **5**, 166 (1959).
[9] W. Kolos, Acta Phys. Polon. **16**, 257 (1957).

correlation is taken explicitly into account by including in the MO wave function terms in which the inter-electronic distances appear directly; it would, however, be extremely difficult to apply this method to any but very simple molecules; so far it has been applied to no π-electron systems other than those in ethylene and benzene where the MO's are determined by symmetry. Calculations even for butadiene would be very difficult to carry out.

The best hope seems to lie in the method outlined by Dewar and Wulfman[1] which we propose to call the SPO (split p-orbital) method. This paper describes the first steps in applying the SPO method to conjugated molecules; the method is described in detail and the results of its application to ethylene are presented.

SPO METHOD

The basic principle of the SPO method will be made clear by its application to the case of two electrons occupying a given p-AO, ϕ_i. Denote by χ_i, ω_i the upper and lower lobes (SPO's) of ϕ_i, respectively. It is assumed that ϕ_i, χ_i, ω_i are normalized; hence

$$\phi_i=(1/\sqrt{2})(\chi_i+\omega_i). \tag{5}$$

In the usual orbital picture, the space part of the two-electron wave function can be written

$$\phi_i^1\phi_i^2=\tfrac{1}{2}(\chi_i^1+\omega_i^1)(\chi_i^2+\omega_i^2) \tag{6}$$

$$=\tfrac{1}{2}(\chi_i^1\chi_i^2+\omega_i^1\omega_i^2)+\tfrac{1}{2}(\chi_i^1\omega_i^2+\chi_i^2\omega_i^1). \tag{7}$$

Here the first pair of terms in (7) represents states in which both electrons occupy the same lobe of the p-AO, while the second pair of terms represent states in which the electrons occupy different p-AO's. In the SPO method it is assumed that the electrons cannot occupy the same lobe simultaneously; the SPO wave function becomes

$$(1/\sqrt{2})(\chi_i^1\omega_i^2+\chi_i^2\omega_i^1). \tag{8}$$

Now the wave functions (7) and (8) are precisely analogous to the MO and VB wave functions for a homonuclear diatomic molecule (e.g., H_2); this provides a justification by analogy for the SPO approach. The neglect of terms such as χ_i^1, χ_i^2 in the SPO method corresponds to the neglect of ionic terms in the VB method; both represent attempts to allow for electron correlation by the extreme approximation that electron repulsion makes it impossible for electrons to be near each other in space.

The expressions (8) can be further simplified since the functions χ_i, ω_i are not merely orthogonal but do not overlap at all; this being so, one can equally well use a single product $\chi_i^1\omega_i^2$ or $\chi_i^2\omega_i^1$.

Two further points are worth mentioning. The individual SPO functions χ, ω are solutions of the atomic Schroedinger equation for a space bounded by the node of the p-AO on one side. The functions are therefore well behaved. Second, the kinetic energy of an electron occupying the SPO χ_i or ω_i is easily shown to be identical with that of an electron occupying the complete p-AO ϕ_i; use of SPO functions therefore introduces no difficulties either on the grounds that the functions are not well behaved or on the grounds that the kinetic energy is affected by limiting the electron to half-space.

These ideas can now easily be extended to molecules. Consider a set of $N\pi$-MO's, ψ_m, expressed in terms of component p-AO's ϕ_i by

$$\psi_m=\sum_i a_{mi}\phi_i. \tag{9}$$

These π-MO's can be divided into two sets of split π-MO's $\xi_m\eta_m$ given by

$$\psi_m=(1/\sqrt{2})(\xi_m+\eta_m) \tag{10}$$

with

$$\xi_m=\sum_i a_{mi}\chi_i \tag{11}$$

$$\eta_m=\sum_i a_{mi}\omega_i \tag{12}$$

[note that the coefficients a_{mi} are the same in Eqs. (9), (11), and (12)]. Consider a set of $2N$ electrons occupying the N MO's ψ_m. In the SPO approximation we assume that exactly half the electrons occupy ξ-type orbital, and the other half η-type orbitals. It can be shown[1] that there is no loss in generality in assuming that all the ξ electrons have similar (α) spin, and all the η electrons the opposite (β) spin. Since the ξ and η electrons occupy orbitals that do not overlap at all in space, the complete wave function can be written as a product of two independent N-electron functions Ξ_p, Ω_p, expressed as Slater determinants:

$$\Xi_p=\det|\xi_m{}^i\alpha^i|$$

$$\Omega_p=\det|\eta_m{}^i\beta^i|. \tag{13}$$

The calculations from this point are similar to those involved in a normal SCF treatment,[2] apart from the use of different values for the two electron integrals. The calculations are of course simplified considerably by the use of a $2N$-electron wave function which is a product of two N-row Slater determinants rather than a single 2 N-row determinant. The one-electron integrals have the same values as in the SCF treatment; thus for the one-electron resonance integrals:

$$\int\phi_iH_c\phi_j d\tau=\tfrac{1}{2}\int(\chi_i+\omega_i)H_c(\chi_j+\omega_j)d\tau$$

$$=\tfrac{1}{2}\left[\int\chi_iH_c\chi_j d\tau+\int\omega_iH_c\omega_j d\tau\right]$$

$$=\int\chi_iH_c\chi_j d\tau=\int\omega_iH_c\omega_j d\tau. \tag{14}$$

Note that integrals of the type $\int\chi_iH_c\omega_j d\tau$ vanish since there is no region where both χ_i and ω_j are nonvanish-

TABLE I. Values of integrals for ethylene (C—C bond length, 1.337 A).

Integral	$(\bar{1}\bar{1};11)$	$(\bar{1}\bar{1};22)$	$(\bar{1}\bar{1};12)$	$(\bar{1}\bar{2};12)$
Values (ev) for:				
Uniformly charged sphere approximation	10.02	7.61	2.58	0.81
Slater AO's	10.98	7.32	...	...

ing. Note also that the core Hamiltonian H_c is the same throughout. A similar argument shows that the overlap integrals $\int\phi_i\phi_j d\tau$, $\int\chi_i\chi_j d\tau$ and $\int\omega_i\omega_j d\tau$ all have the same value (S).

The electron repulsion integrals are of two types:

$$(\bar{i}j;\bar{k}\bar{l})\equiv\int\chi_i{}^a\chi_j{}^a(e^2/r_{ab})\chi_k{}^b\chi_l{}^b d\tau \qquad (15)$$

$$(\bar{i}j;kl)\equiv\int\chi_i{}^a\chi_j{}^a(e^2/r_{ab})\omega_k{}^b\omega_l{}^b d\tau. \qquad (16)$$

All the other integrals vanish by virtue of the fact that no χ orbital overlaps anywhere with any ω orbital. The bar notation in Eqs. (15), (16) is self-explanatory.

From Eqs. (3), (5), (15), and (16),

$$(ij;kl)=\tfrac{1}{2}[(\bar{i}j;\bar{k}\bar{l})+(\bar{i}j;kl)]. \qquad (17)$$

The integrals $(\bar{i}j;kl)$ can be estimated with sufficient accuracy by the uniformly charged sphere approximation[5] since they represent the mutual repulsions of noninterpenetrating electron distributions. The integrals $(\bar{i}j;\bar{k}\bar{l})$ can then be found from Eq. (17) using tabulated values for $(ij;kl)$.

Configuration interaction can be included in the usual[3] way, using appropriate values for the necessary one- and two-electron integrals.

RESULTS FOR ETHYLENE

The SPO method was applied to ethylene in the manner indicated in the foregoing; here the split π orbitals are determined by symmetry, being given by:

$$\xi_1=(2+2S)^{-\frac{1}{2}}(\chi_1+\chi_2);\quad \xi_2=(2-2S)^{-\frac{1}{2}}(\chi_1-\chi_2)$$

$$\eta_1=(2+2S)^{-\frac{1}{2}}(\omega_1+\omega_2);\quad \eta_2=(2-2S)^{-\frac{1}{2}}(\omega_1-\omega_2). \qquad (18)$$

The necessary two-electron integrals for a C—C bond length of 1.337 A[10] are listed in the first row of Table I; they were calculated by the uniformly charged sphere approximation.[5] The value for $(\bar{1}\bar{1};11)$ differs somewhat from that (10.37 ev) reported by Dewar and Wulfman,[1] due to the use of a slightly different value for the radius of the sphere. The second row of Table I shows values for the $(\bar{1}\bar{1};11)$ and $(\bar{1}\bar{1};22)$ integrals, calculated by Snyder[11] by direct quadrature using Slater orbitals. (The value for $(\bar{1}\bar{1};22)$ is interpolated.) The values given by the uniformly charged sphere approximation seem more satisfactory since the theoretical value for the $(\bar{1}\bar{1};11)$ integral should be less than the empirical one (10.53 ev). It would be interesting to have the corresponding integral for Hartree-Fock orbitals.

Table II compares the calculated and observed values for the $N-V$ and $N-T$ transition energies and for the separation of the singlet and triplet excited states. The calculated values are for the SCF,[12] SCF CI,[12] Pariser-Parr,[5] AIM,[6] Kolos,[9] and SPO methods. The two SPO values correspond to different values for the one-electron resonance integral β.

The experimental value for the $N-T$ transition has been somewhat uncertain; the value quoted is a recent determination by Evans.[14]

In the LCAO MO treatment of ethylene the ground state can interact only with the doubly excited state.[3]

TABLE II. Transition energies and separation of the singlet and triplet excited states for ethylene calculated by various methods; comparison with experiment. (Values in ev).

	Exper.	SCF[a]	SCF CI[b]	P.-P.[c]	AIM[d]	Kolos[e]	SPO[f]	SPO[g]
$N-T$	4.6	1.8	3.1	4.5	5.5	6.2	4.7	5.2
$N-V$[h]	7.6	10.2	11.5	7.6	7.3	7.6	7.1	7.6
$T-V$	1.7	8.4	8.4	3.1	1.8	1.4	2.4	2.4

[a] See footnote 12.
[b] See footnote 12.
[c] See footnote 5.
[d] See footnote 6.
[e] See footnote 9.
[f] SPO calculated with $\beta=2.85$ ev (see footnote 13).
[g] SPO calculated with $\beta=3.13$ ev (see footnote 5).
[h] P. G. Wilkinson and H. Johnston, J. Chem. Phys. **18**, 190 (1950).

[10] H. Allen, Jr., and E. K. Plyler, J. Am. Chem. Soc. **80**, 2673 (1958).
[11] L. C. Snyder, thesis, Carnegie Institute of Technology, Pittsburgh, Pennsylvania (1959).
[12] R. Parr and B. Crawford, J. Chem. Phys. **16**, 526 (1948).
[13] R. Parr and B. Crawford, J. Chem. Phys. **16**, 1049 (1948).
[14] D. F. Evans, J. Chem. Soc. **1960**, 1735.

TABLE III. Effect of configuration interaction in various approximate treatments of ethylene.

	SCF CI	P.-P.	SPO
C_1	0.96	0.992	0.994
C_2	0.30	0.118	0.106
% ionic structures	21	37	42
Lowering of ground state (ev)	1.3	0.18	0.17

The resulting wave function for the ground state can be written in the form:

$$\Psi = C_1 \text{ (ground-state function)} + C_2 \text{ (doubly excited function)}. \quad (19)$$

Table III lists values of the coefficients C_1, C_2 for the SCF CI method for the corresponding Pariser-Parr treatment, and for the SPO method, together with the corresponding weights of ionic structures and the lowering of the ground state energy. Configuration interaction has very little effect in the two latter cases. (Note that the simple MO method without configuration interaction corresponds to 50% contribution by ionic structures in the ground state.)

DISCUSSION

The results in Table II are very encouraging. The SPO method is at least as good as any method that could reasonably be applied to conjugated systems of any complexity and it avoids the empiricism of the Pariser-Parr method and Moffitt's atoms-in-molecules method.

Table III indicates that configuration interaction is even less important than in the Pariser-Parr method; it seems clear that the extensive configuration interaction in the SCF CI method is an artifact due to neglect of electron correlation and that the ground state of ethylene is well represented by a single LCAO MO wave function.

Even in this case the results differ from those given by the Pariser-Parr and AIM methods; the differences are likely to be greater in the case of molecules containing more π electrons, for two reasons. First, the other methods do not require the numbers of π electrons in the two π lobes to be approximately the same at any instant; secondly, they replace the $(ii;jj)$ integral by a lower value nelecting the fact that the lower value applies only to the SPO integral $(\bar{i}i;jj)$. The corresponding integral $(\bar{i}i;\bar{j}j)$ for two electrons in the *same* π lobe is much greater than the "classical" value. Thus the $(\bar{1}1;\bar{1}1)$ integral is very much larger (23.4 ev) than the usual (11; 11) integral (16.9 ev). The qualitative consequence of these approximations has been discussed elsewhere[8]; it seems fairly certain that they must make the Pariser-Parr and AIM methods overestimate the importance of electron delocalization in molecules such as polyenes for which only single classical structures can be written.

We are at present extending the SPO method to more complex molecules, in particular benzene and butadiene.

ACKNOWLEDGMENTS

One of us (N.L.H.) gratefully acknowledges the award of a Fellowship by the Consejo Nacional de Investigaciones de la Rep. Argentina. We are also grateful to Dr. L. C. Snyder for helpful discussion and for sending us his calculated values of integrals.

Relation of Perturbation Theory to Variation Method*

OKTAY SINANOĞLU

Sterling Chemistry Laboratory, Yale University, New Haven, Conecticut

(Received September 16, 1960)

The various order wave functions of the Rayleigh-Schrödinger perturbation theory can be obtained directly by solving certain differential equations or by minimizing equivalent variational expressions. These expressions are related to the ordinary variation method. The perturbation series is shown to result in a unique way from the minimization of larger and larger portions of $\langle\psi, H\psi\rangle/\langle\psi, \psi\rangle$. In addition to several orders of perturbation, each step gives the exact remainders and upper limits to the energy. The approach suggests several "variation-perturbation" schemes.

INTRODUCTION

PERTURBATION theory is especially useful in many-electron problems. It allows one to reduce a many-electron problem *rigorously* to fewer-electron problems[1,2] within given orders of perturbation. In contrast the variation method uses *arbitrary* trial functions. It has the advantage, however, of always providing upper limits to the energy.

In perturbation theory energies calculated to *odd* orders also yield upper limits[1,3] to the exact energy. Under certain conditions the *even* orders give lower limits.[4]

In the most common form of the perturbation method, various orders of the wave function and energy are written as infinite sums over a known complete set of basis functions. Because of large continuum contributions such sums can be obtained only very approximately. Instead, more general ways of solving the nonhomogeneous differential equations of the perturbation method may be used. Each of these differential equations can also be converted into variational principles. Hylleraas[5] devised such a "variation-perturbation" method for obtaining the first order W.F.'s of ground states. The method has been extended to excited states by the present writer.[6]

The purpose of this article is to examine the connection between such "variation-perturbation" methods and the ordinary variation method. It will be shown that the Rayleigh-Schrödinger (RS) perturbation series can be derived from the variation method in a rather unique way by minimizing larger and larger portions of $\langle\psi, H\psi\rangle/\langle\psi, \psi\rangle$. This derivation gives the exact remainders after each order of perturbation. The use of the remainders in conjunction with the perturbation method suggests several variation-perturbation schemes.

PERTURBATION METHOD

We first outline and comment on the properties of the RS perturbation method.

Let H of the eigenvalue problem, $H\Psi=E\Psi$, be split as H_0+H_1, and ϕ_0 be an exact unperturbed eigenfunction. For the state of interest, it is assumed that in the limit $H_1\to 0$, $\Psi\to\phi_0$. We write arbitrarily

$$\Psi=\phi_0+\chi \quad \text{and} \quad E=E_0+\Delta E, \tag{1}$$

where $H_0\phi_0=E_0\phi_0$. The equation $H\Psi=E\Psi$ then becomes

$$(H_0-E_0)\chi=[\Delta E-H_1](\phi_0+\chi) \tag{2}$$

or using the inverse operator

$$(H_0-E_0)^{-1}\equiv e^{-1} \tag{3a}$$

$$\chi=(1/e)[\Delta E-H_1](\phi_0+\chi). \tag{3b}$$

From Eq. (2) we have

$$\Delta E=E_1+\frac{\langle\phi_0, (H_1-E_1)\chi\rangle}{1+\langle\phi_0, \chi\rangle}, \tag{4}$$

where $E_1=\langle\phi_0, H_1\phi_0\rangle$. The last term is the exact remainder after $\langle\phi_0, H\phi_0\rangle$ and is simplified by the normalization $\langle\phi_0, \chi\rangle=0$, i.e., $\langle\phi_0, \Psi\rangle=1$.

Equations (2) or (3b) can be solved by iterations. To do this it is convenient to write Eq. (2), using (3a), as

$$e\chi=Q[\Delta E-H_1](\phi_0+\chi); \tag{5}$$

Q is the operator, $1-\phi_0\rangle\langle\phi_0$, that projects out the ϕ_0 component of the function on which it acts. Equation (5) is equivalent to Eq. (2) whose right-hand side was already orthogonal to ϕ_0.

Various types of perturbation schemes can now be derived from Eq. (5) depending on how ΔE is treated,

* Part of this work was done by the author at the Department of Chemistry and Lawrence Radiation Laboratory, University of California, Berkeley.

[1] O. Sinanoğlu, Phys. Rev. (to be published); University of California Lawrence Radiation Laboratory Rept. UCRL-9320.

[2] O. Sinanoğlu, Proc. Roy. Soc. (London) (to be published); University of California Lawrence Radiation Laboratory Rept. UCRL-9365.

[3] P. M. Morse and H. Feshbach, *Methods of Theoretical Physics* (McGraw-Hill Book Company, Inc., New York, 1953), Vol. II, pp. 1119–20.

[4] B. F. Gray, J. Chem. Phys. **29**, 276 (1958).

[5] E. A. Hylleraas, Z. Physik. **65**, 209 (1930).

[6] O. Sinanoğlu, Phys. Rev. (to be published); University of California Lawrence Radiation Laboratory Rept. UCRL-9316.

and for each order of χ, i.e., χ_n, lead to equations of the type

$$e\chi_n = Q\mathfrak{F}_m; \tag{6}$$

$\mathfrak{F}_m$ is a known function depending only upon the already determined lower order ($m<n$) wave functions. The role of Q is to ensure that this nonhomogeneous differential equation will have a solution. The existence of such a solution requires[7] the orthogonality of all the solutions of the corresponding homogeneous equation, $e\phi=0$, to the nonhomogeneity, $Q\mathfrak{F}_m$. If E_0 is nondegenerate, the only solution of $e\phi=0$ is ϕ_0; and we have from the definition of Q, $\langle\phi_0, Q\mathfrak{F}_m\rangle=0$. Otherwise the appropriate combinations, ϕ_0^k, of the degenerate eigenfunctions for E_0 must be found to define new $Q^k\mathfrak{F}_m{}^k$'s such that $\langle\phi_0{}^l, Q^k\mathfrak{F}_m{}^k\rangle=0$. Then each ϕ_0^k leads to a different equation, $e\chi_n{}^k=Q^k\mathfrak{F}_m{}^k$.

The RS perturbation series is obtained by substituting λH_1 for H_1

$$\chi=\sum_{n=1}^{\infty}\lambda^n\chi_n \quad \text{and} \quad \Delta E=\sum_{n=1}^{\infty}\lambda^n E_n \tag{7}$$

in Eq. (2). The λ is a *formal* expansion parameter; its role is similar to the role of Q in Eq. (6) and will be discussed later. Equating coefficients of λ^n, one gets

$$e\chi_n=-q\chi_{n-1}+\sum_{k=2}^{n}E_k\chi_{n-k} \tag{8}$$

and from this

$$E_n=\langle\phi_0, q\chi_{n-1}\rangle-\sum_{k=2}^{n-1}E_k\langle\phi_0, \chi_{n-k}\rangle, \tag{9}$$

where

$$q\equiv H_1-E_1.$$

Hylleraas[5] pointed out that Eq. (9) can be reduced much further and that each new order, s, in χ, determines the energy to order $(2s+1)$. To show this, the recurrence relation, Eq. (8), and the self-adjoint property of q, e, and e^{-1} is used; E_n becomes

$$E_n=\langle\chi_1, q\chi_{n-2}\rangle-\sum_{k=2}^{n-1}E_k\{\langle\phi_0, \chi_{n-k}\rangle+\langle\chi_1, \chi_{n-1-k}\rangle\}. \tag{10}$$

Further, from $q\chi_1=E_2\phi_0-e\chi_2$,

$$E_n=\langle\chi_2, q\chi_{n-3}\rangle-\sum_{k=2}^{n-2}E_k\langle\chi_2, \chi_{n-2-k}\rangle$$

$$-\sum_{k=2}^{n-1}E_k\langle\chi_1, \chi_{n-1-k}\rangle-\sum_{k=3}^{n-1}E_k\langle\phi_0, \chi_{n-k}\rangle. \tag{11}$$

In this way one continues to lower χ_{n-3} and raise χ_2. The orders of χ_r and χ_s in the first term of Eq. (11), $\langle\chi_r, q\chi_s\rangle$, are always such that $(r+s+1)=n$. Thus, as we set out to show, if $n=2m+1$, the lowest order of χ from which E_n can be determined is given by $r=s=m$. The normalization of $\phi_0+\chi$ in Eqs. (8) through (11) is arbitrary.

The fact that χ_s determines the energy to the term, E_{2s+1}, follows from the stationary property of $E=\langle\Psi, H\Psi\rangle/\langle\Psi, \Psi\rangle$. A variation in Ψ of the order $\epsilon\Delta\Psi$ affects the energy to order ϵ^2. Thus, suppose Ψ has been approximated by $(\phi_0+\lambda\chi_1+\cdots+\lambda^s\chi_s)$, then the error is

$$\epsilon\Delta\Psi=\Psi-\phi_0-\sum_{n=1}^{s}\lambda^n\chi_n=\sum_{n=s+1}^{\infty}\lambda^n\chi_n$$

$$=\lambda^{s+1}(\chi_{s+1}+\lambda\chi_{s+2}+\cdots) \tag{12}$$

and so $\epsilon=\lambda^{s+1}$. Then the error in energy will be of the order of $\epsilon^2=\lambda^{2s+2}$ and the last term of the energy determined by

$$\Psi_{\text{trial}}=\phi_0+\sum_{n=1}^{s}\lambda^n\chi_n$$

is $\lambda^{2s+1}E_{2s+1}$.

Equations (8), e.g.,

$$e\chi_1+q\phi_0=0 \tag{13}$$

may be solved by a direct method instead of the usual method of expanding χ_1 in the eigenfunctions of H_0. Each χ_n equation may also be replaced[5] by a stationary condition; e.g., for χ_1, Eq. (13) is equivalent to

$$\delta\{2\langle\phi_0, q\chi_1\rangle+\langle\chi_1, e\chi_1\rangle\}=0. \tag{14}$$

This equation may be used to attain E_2 as a minimum with trial functions $\tilde{\chi}_1$. For excited states too, E_2 may be obtained by minimization, provided $\tilde{\chi}_1$ is restricted in the way shown by Sinanoğlu.[6]

For a general χ_n, Eq. (8) is equivalent to

$$\delta\{2\langle\chi_n, q\chi_{n-1}\rangle-2\sum_{k=2}^{n}E_k\langle\chi_n, \chi_{n-k}\rangle+\langle\chi_n, e\chi_n\rangle\}=0, \tag{15}$$

where χ_n is to be varied. Again χ_n may be obtained from Eq. (15) by minimization procedures.

We now relate these properties of the RS perturbation theory to the usual variation method. We shall derive the equations of the RS series given above from the variation method by requiring larger and larger portions of the exact remainder to the energy to be stationary.

RELATION TO THE VARIATION METHOD

The equations of the RS perturbation theory are obtained from the variation method in a quite natural way. The eigenvalue problem $H\Psi=E\Psi$ is equivalent to finding a Ψ such that

$$\delta(\langle\Psi, H\Psi\rangle/\langle\Psi, \Psi\rangle)=0. \tag{16a}$$

[7] See, for example, B. Friedman. *Principles and Techniques of Applied Mathematics* (John Wiley & Sons, Inc., New York, 1957), p. 170.

If Ψ is the lowest state of an irreducible representation, for any trial function, $\tilde{\Psi}$

$$E \leq (\langle \tilde{\Psi}, H\tilde{\Psi} \rangle / \langle \tilde{\Psi}, \tilde{\Psi} \rangle). \tag{16b}$$

The following equation, equivalent to Eq. (2), is obtained when we write $\tilde{\Psi}=\phi_0+\tilde{\chi}$ as a trial function in Eq. (16b),

$$E \leq E_0+E_1+E_R,$$

where

$$E_R[\tilde{\chi}] \equiv \frac{2\langle \phi_0, q\tilde{\chi} \rangle + \langle \tilde{\chi}, e\tilde{\chi} \rangle + \langle \tilde{\chi}, q\tilde{\chi} \rangle}{1+2\langle \phi_0, \tilde{\chi} \rangle + \langle \tilde{\chi}, \tilde{\chi} \rangle}. \tag{17}$$

The equality holds and the last term is stationary when $\tilde{\chi}=\chi$.

In the usual variational procedure one chooses an *arbitrary* $\tilde{\chi}$ and minimizes E_R with respect to some parameters. Instead of this arbitrary procedure, it is desirable to have a systematic way of obtaining a good $\tilde{\chi}$. Since in general it is not possible to solve Eq. (2) directly for χ and make the *entire* E_R stationary, one may inquire instead into the possibility of finding a large *portion* of E_R which would become a minimum for a *definite* $\tilde{\chi}$. This portion of E_R would be stationary and the $\tilde{\chi}$ to make it so would be obtained by solving the Euler equation corresponding to this stationary condition.

One part of E_R in Eq. (17), other than all of E_R, that can be made stationary is $2\langle \phi_0, q\tilde{\chi} \rangle + \langle \tilde{\chi}, e\tilde{\chi} \rangle$. But this is exactly the stationary expression in Eq. (14) and so the desired $\tilde{\chi}$ is the first-order wave function χ_1, of perturbation theory. Thus the condition that part of E_R should be a minimum leads[6] to the Euler equation, $e\chi_1+q\phi_0=0$. The minimum is $\langle \phi_0, q\chi_1 \rangle$ or by Eq. (9), E_2.

If the remaining terms of E_R were negligible, χ_1 would be very close to the exact χ. In any case, χ_1 can be substituted for $\tilde{\chi}$ everywhere in Eq. (17) to obtain an approximation, $E_R^{(1)}$ to the entire E_R. Using Eq. (13)

$$\frac{E_2+\langle \chi_1, q\chi_1 \rangle}{1+2\langle \phi_0, \chi_1 \rangle + \langle \chi_1, \chi_1 \rangle} = E_R^{(1)} > E_R, \tag{18}$$

we thus find that one part of E_R can be used to obtain a definite trial function χ_1 which gives the usual E_2, and a total remainder $E_R^{(1)}$ which should yield a better upper limit to E than $\langle \phi_0, H\phi_0 \rangle$. Equation (10) for $n=2$ and $n=3$ indicates that when $\langle \chi_1, \chi_1 \rangle \ll 1$, Eq. (18) leads to

$$E_0+E_1+E_2+E_3 > E. \tag{19}$$

Also notice that the previous role of the formal expression parameter, λ in Eq. (7), has been to single out that portion of Eq. (17), when minimized, would lead to a solution, χ_1.

The upper limit obtained in Eq. (18) may be improved by continuing the process started above. We go back to E_R in Eq. (17) and this time and the new remainder left after Ψ has been approximated by $\phi_0+\chi_1$.

Let Δ_1 be the error left in χ, and substitute

$$\chi=\chi_1+\Delta_1 \tag{20}$$

in the exact E_R. We use Eq. (13) and Eq. (10) for $n=2$ and 3, clear first the denominator of E_2, then of E_3 and obtain

$$E_R = E_2+E_3 + \frac{2\langle \Delta_1, q\chi_1 \rangle + \langle \Delta_1, (e+q)\Delta_1 \rangle - (E_2+E_3)N + 2E_2\langle \phi_0, \chi_1 \rangle}{1+N}, \tag{21a}$$

where

$$N = 2\langle \phi_0, \chi_1+\Delta_1 \rangle + \langle \chi_1+\Delta_1, \chi_1+\Delta_1 \rangle. \tag{21b}$$

This equation is more useful than the usual perturbation formula. It gives the exact remainder after E_3 and may be used in several ways: the exact Δ_1 minimizes E, so we may use the ordinary variation method at this stage, choose arbitrary trials, $\tilde{\Delta}_1$, and attain the lowest E_R that we can. Or we may seek a systematic way to a good $\tilde{\Delta}_1$ using the same type of approach that led to χ_1. We look for a large portion of the new remainder which can be made stationary. The condition that this portion be stationary should lead to a nonhomogeneous differential equation satisfying the requirements for a solution.[7] This equation will be simplest[1,2] if its homogeneous part consists of $e \equiv H_0-E_0$.

After examining several portions of Eq. (21) one is led to

$$\delta\{2\langle \Delta_1, q\chi_1 \rangle + \langle \Delta_1, e\Delta_1 \rangle - 2E_2\langle \Delta_1, \phi_0 \rangle\} = 0. \tag{22}$$

We denote the solution of this equation by $\Delta_1 \rightarrow \chi_2$; then the corresponding Euler equation is

$$e\chi_2+q\chi_1-E_2\phi_0=0. \tag{23}$$

The solution χ_2 exists because by Eq. (9), $\langle \phi_0, (q\chi_1-E_2\phi_0) \rangle = 0$ for nondegenerate ϕ_0. There appears to be no other portion of Eq. (21) satisfying the conditions mentioned above. Equation (23) is again just the RS equation, i.e., Eq. (8) for $n=2$ which previously had resulted automatically with the aid of λ.

Substituting χ_2 for Δ_1 everywhere in Eq. (21), a second approximation $E_R^{(2)}$ to the remainder is obtained [compare Eq. (18)],

$$E_R^{(2)} \equiv E_2+E_3 + \frac{\langle \chi_2, q\chi_1 \rangle - E_2\langle \chi_2, \phi_0 \rangle + \langle \chi_2, q\chi_2 \rangle - M}{1+N^{(2)}} > E_R, \tag{24}$$

where

$$M \equiv 2E_2\langle \phi_0, \chi_1 \rangle - (E_2+E_3)N^{(2)} + E_2\langle \chi_2, \phi_0 \rangle$$

and $N^{(2)}$ is the same as Eq. (21b) with $\Delta_1=\chi_2$. As in Eq. (18), we again have a remainder more complete than that given by perturbation theory and which yields an upper limit to E. Equation (11) with $n=4$ and $n=5$ indicates that the last term of Eq. (24) consists of E_4 and E_5 with some normalization corrections.

Further remainders and upper limits to the exact E, may be obtained by continuing the above procedure. This time one goes back to Eq. (21), and writes for the exact Δ_1,

$$\Delta_1 \equiv \chi_2 + \Delta_2, \tag{25}$$

defining the new error Δ_2. Then E_R becomes the sum of E_2, E_3, E_4, E_5 and a new remainder in terms of Δ_2. The new remainder, still exact, may be obtained either by minimizing[8] it with respect to trial $\tilde{\Delta}_2$'s, or again, by finding that portion of it which will be stationary and lead to the Eq. (8) for χ_3. In this way one generates the perturbation series, but in addition obtains the remainders after each term.

Thus a very flexible method is obtained. At each step a variation method may be combined with the perturbation method in the ways discussed above. If the scheme converges, closer and closer upper limits to E are obtained, but even when it diverges, the first few terms may yield good approximations to E.

[8] We have been considering mainly lowest states as in Eq. (16b). For excited states, only (16a) applies and minimum principles require orthogonality restrictions[6] on trial functions.

THE JOURNAL OF CHEMICAL PHYSICS VOLUME 34, NUMBER 4 APRIL, 1961

Comparison of Theoretical Calculations on Diatomic Molecules with Experiment

ERNEST R. DAVIDSON*

Chemistry Department, Indiana University, Bloomington, Indiana

(Received September 7, 1960)

A method for the numerical computation of the vibrational-rotational term levels from an arbitrary potential curve is presented. In this method, the potential curve is approximated by a step function and the exact eigenvalues of this latter function are found by an iteration technique. The accuracy of this method is demonstrated by finding the term levels for a Morse potential and for the ground state of H_2.

MOST theoretical calculations on diatomic molecules are based on the Born-Oppenheimer approximation. This reduces the problem to finding first the eigenvalues of an electronic Hamiltonian as a function of internuclear separation, and then the vibrational-rotational energy levels using this function as a potential field for the motion of the nuclei. It has been customary, as a matter of convenience, to omit this last step, and instead, to compare the theoretical potential function with a semiempirical one which reproduces the experimental energy levels. Both esthetically and practically, however, it is better to compute directly the theoretical counterparts of the experimental data so as to leave no intervening step which could mask the origin of the discrepancies. With this in mind, the problem of calculating the expected vibrational and rotational levels directly from a numerical representation of a potential function has been investigated with emphasis on finding a method applicable even when the potential function cannot be approximated accurately by simple standard functions such as the Morse potential.

* Supported in part by a grant from the National Science Foundation and in part by a contract between the AF OSR and Indiana University.

By appropriate substitutions, the problem of finding vibrational and rotational levels of a diatomic molecule[1] can be reduced to the problem of solving the differential equation

$$(d^2S/dR^2)+k[E-V(R)]S=0$$

for $R \geqslant 0$, subject to the boundary conditions $S(0)=0$ and

$$\int_0^\infty S^*SdR < \infty .$$

Here, k is

$$2M_aM_bm_e^{-1}(M_a+M_b)^{-1}$$

and $V(R)$ is given by

$$K(K+1)k^{-1}R^{-2}+Z_aZ_bR^{-1}+U_e(R),$$

where $U_e(R)$ is the electronic energy in Hartree units, and R is the internuclear distance in Bohr radii. If $V(R)$ is approximated by a step function $Q(R)$ defined by

$$Q(R)=Q_n=\tfrac{1}{2}[V(R_{n+1})+V(R_n)]$$

[1] L. Pauling and E. B. Wilson, *Introduction to Quantum Mechanics* (McGraw-Hill Book Company, Inc., New York, 1935), p. 266.

for $R_{n+1} \leqslant R \leqslant R_n$, and the intervals $(R_n - R_{n+1})$ are chosen according to some relation

$$(R_n - R_{n+1}) = \epsilon f(\xi), \qquad R_n \geq \xi \geq R_{n+1},$$

then the resulting differential equation becomes

$$(d^2S/dR^2) + k[E - Q_n]S = 0.$$

This has the general solution

$$S_n = A_n \exp[Rk^{\frac{1}{2}}(Q_n - E)^{\frac{1}{2}}] + B_n \exp[-Rk^{\frac{1}{2}}(Q_n - E)^{\frac{1}{2}}]$$

for $R_{n+1} \leqslant R \leqslant R_n$, but it is more convenient for $E > Q_n$ to use the equivalent form

$$S_n = A_n \cos[Rk^{\frac{1}{2}}(E - Q_n)^{\frac{1}{2}}] + B_n \sin[Rk^{\frac{1}{2}}(E - Q_n)^{\frac{1}{2}}].$$

Hence, from the requirement of continuity of S and dS/dR everywhere, recursion relations for A_n and B_n in terms of A_{n-1} and B_{n-1} are easily obtained and the function $S(E, R)$ is completely determined, for any E, by the values of A_0 and B_0. If R_0 is taken to be infinity and A_0 taken to be zero, then $S(E, R)$ is normalizable.

In principle, the eigenvalues E_v for which $S(E_v, R)$ has v zeros and vanishes at $R = 0$, can be determined by varying E iteratively and evaluating $S(E, R)$. In practice, however, $V(R)$ always has a first- or second-order pole at $R = 0$ so that this scheme cannot be used to determine whether $S(E, 0)$ is zero or not. This difficulty can be avoided by evaluating $S_N(E, R_N)$ for R_N sufficiently small that either S has $(v+1)$ zeros for $R > R_N$ or else S has only v zeros for $R > R_N$ but $(E - Q) < 0$ for $R \leqslant R_N$ and $[S_N(R_N)/S_N'(R_N)] < R_N$. In the former case, it follows from the Sturm separation theorem that $E > E_v$. In the latter case, it follows from $S''/S = k^{-1}(Q - E) > 0$ for $R \leqslant R_N$ that $S(E, R)$ cannot be zero for $0 < R \leqslant R_N$ and hence, that $E < E_v$. With these criteria, upper and lower bounds may be found for E_v which differ by an amount much less than the error introduced by replacing $V(R)$ by $Q(R)$.

The error θ_v in the eigenvalues E_v can be obtained by treating the function $\{V(R) - Q(R)\}$ as a perturbation. The leading term in an expansion of θ in terms of this perturbation is

$$\int_0^\infty \{V(R) - Q(R)\} S_v^2 dR.$$

TABLE I. Eigenvalues of the Morse potential, $V(R) = \exp[-2(R-2)] - 2\exp[-(R-2)]$.

n	E calc	E theory[a]
0	−0.90243	−0.90250
1	−0.72247	−0.72250
2	−0.56254	−0.56250
3	−0.42249	−0.42250

[a] D. ter Haar, Phys. Rev. **70**, 222 (1945).

TABLE II. Values of the electronic energy U_e for the ground state of the hydrogen molecule (Hartree atomic units).

R	U
0	−2.90372
0.8	−2.270175
1.0	−2.124517
1.2	−1.998263
1.3	−1.941554
1.35	−1.914675
1.4	−1.88728
1.41	−1.883648
1.45	−1.863677
1.5	−1.839495
1.6	−1.793438
1.8	−1.710541
2.0	−1.637999
2.2	−1.574465
2.4	−1.518751
2.6	−1.469903
2.8	−1.427099
3.0	−1.38963
3.6	−1.303441
4.0	−1.2641789
6.0	−1.1673302
8.0	−1.1250341
10.0	−1.1000000

For small ϵ this integral is easily shown to be $-c\epsilon^2$, where c is given approximately by

$$\tfrac{1}{8}\int_0^\infty (d^2V/dR^2) S_v^2(R) f^2(R) dR.$$

Hence the leading term in the expansion of θ is negative definite so E_v will in general be too large. Also, the instinctive feeling that $f(R)$ should be small in the regions that $S_v(R)$ is large is verified. For the examples which follow, $f(R)$ was defined implicitly by choosing $(R_{n+1} - R_n)$ as large as possible subject to the conditions $|V(R) - Q(R)| < \epsilon$ and $(R_{n+1} - R_n) \leqslant (R_n - R_{n-1})$. For functions $V(R)$ of the general shape of the Morse potential these conditions lead to a function $f(R)$ with the correct qualitative properties.

The accuracy of this method has been tested by two problems. In the first, $V(R)$ was evaluated from the Morse-type formula

$$V(R) = \exp[-2(R-2)] - 2\exp[-(R-2)],$$

and the differential equation was solved with $k = 100$ and $\epsilon = 0.0075$. As shown in Table I, the maximum error in this case was less than 0.01% in the eigenvalues. With $\epsilon = 0.01$ the maximum error was still less than 0.02%.

Since, for a given potential curve, ϵ determines the number of points R_n, the minimum size of ϵ was limited to about 0.007 D_0^0 by the storage capacity and speed of the IBM 650 on which the computations were performed. With an ϵ of this size no more than 500 intervals are ever used although the exact number of intervals is determined by the value of N such that, for $R = R_N$, the guess E to the eigenvalue E_v can be rejected as too large or too small. The time for a single

TABLE III. Vibrational levels of the ground state of the hydrogen molecule (cm^{-1}).

	Calc.	Exptl.[a]
D_0^0	36 108	36 116.6
Zero point	2177	2170
E_1-E_0	4163	4161
E_2-E_1	3946	3926
E_3-E_2	3714	3695
E_4-E_3	3494	3468
E_5-E_4	3268	3240

[a] G. Herzberg, Can. J. Phys. **37**, 636 (1959).

iteration on E is about 4 min on an IBM 650 tape system. This time varies linearly, for a fixed number of digits in the results, with ϵ^{-1} while the error in the results is proportional to ϵ^2.

In the second problem, the constants appropriate for the hydrogen molecule were used with $U_\epsilon(R)$ given by the two-point interpolation formula

$$U_\epsilon(R)=\exp[\{(\ln U_j)(R_{j+1}-R)/(R_{j+1}-R_j)\}+\{(\ln U_{j+1})(R-R_j)/(R_{j+1}-R_j)\}]$$

for $R_j \leqslant R \leqslant R_{j+1}$. The values of $U=U(R_j)$ shown in Table II were taken from the work[2] of Kolos and Roothaan for $R<4$ and from the work[3] of Hagstrom for $R\geqslant 4$. With $\epsilon=0.001$ and $K=0$, the energy levels given in Table III were obtained.

[2] W. Kolos and C. C. J. Roothaan, Revs. Modern Phys. **32**, 219 (1960).
[3] S. Hagstrom, private communication.

Errors of unknown magnitude remain in the vibrational levels because the Born-Oppenheimer approximation has been used and because the U_j were obtained by the variation method. If it is assumed, however, that the vibrational eigenvalues determined from the U_j given in Table II should agree with experiment, then much of the error in this calculation must be due to the inadequacy of the two-point interpolation formula used for $U_\epsilon(R)$. It would seem from these results that, even with this interpolation formula, this method of solving the differential equation is adequate for finding the energy level spacing to within 0.1% of D_0^0 for any reasonable potential curve $V(R)$.

Numerous other methods are available in the literature for the numerical solution of differential equations. Only one of those, however, is useful for the high-accuracy solution of Sturm-Lionville equations. In that method, the differential operator is replaced by a finite difference operator and the potential function is replaced by a step function. The difference equations for a given E are then solved for a finite interval of the R axis by relaxation techniques and E is varied iteratively. The computer time involved in a solution of the problem by this method of finite differences is comparable in magnitude to the time needed for the method proposed in this paper. A recent paper published after the present work was completed utilized the finite difference method for the vibrational levels of H_2^+.[4]

ACKNOWLEDGMENT

The author wishes to thank Professor Harrison Shull for many helpful criticisms and discussions during the preparation of this paper.

[4] S. Cohen, J. R. Hiskes, and R. J. Riddell, Jr., Phys. Rev. **119**, 1025 (1960).

Second-Order Perturbation Theory of Helium-Like Ions

B. F. GRAY AND R. WHITEHEAD

Royal Technical College, Salford, Lancashire, England

(Received October 11, 1960)

A method for calculating the Coulomb interaction between the electrons to the second order of approximation, due to Kessler, is examined and shown to require modification. This removes the discrepancy between the value obtained by Kessler and that obtained by Hylleraas and Midtdal using a variational method, although only very limited accuracy is obtainable.

I. INTRODUCTION

THREE main methods of attack have been used to treat the problem of the helium-like ion. Of these the variation method has been by far the most successful beginning with the work of Hylleraas[1] and culminating with the extremely accurate work of Kinoshita[2] and Pekeris.[3] However, this work is highly specialized and not easily generalized to other systems except possibly to that of the hydrogen molecule.[4] In fact most of these calculations are specific to helium itself and similar results for two-electron ions with arbitrary nuclear charge can only be obtained by individual calculations in each case.

A more general but slightly less accurate procedure was followed by Hylleraas[5] based on the variation-perturbation approach. The energy for the ground state is assumed to be of the form

$$E=-Z^2+\epsilon_1 Z+\epsilon_2+(\epsilon_3/Z)+\cdots,$$

where $\epsilon_1=\frac{5}{8}$ exactly in atomic units. Rather than attempt to calculate ϵ_2 from the formula

$$\epsilon_2=\sum{}'[v_{1n}{}^2/(E_1{}^0-E_n{}^0)], \tag{1}$$

Hylleraas used a variational method, minimizing the quantity

$$\epsilon_2(F_1')=\int[2F_1'v\phi_1+F_1'H^0F_1'-E_1{}^0(F_1')^2-2\epsilon_1\phi_1F_1']d\tau,$$

where $H_1{}^0\phi_1$ and $E_1{}^0$ are the Hamiltonian, ground-state wave function, and ground-state energy, respectively, of the unperturbed system. Here F_1' is a trial function approximation to F_1, the first-order correction to ϕ_0; $\epsilon_2(F_1')$ is an upper bound to ϵ_2 (see Bethe and Salpeter[6]). Using a 24-parameter trial function, Hylleraas and Midtdal[7] obtained the upper bound for ϵ_2 of -0.157657 a.u. However, the trial function F_1' was of the same analytical form as the purely variational trial function used by the same author, and as such cannot be extended beyond two-electron systems.

An evaluation of ϵ_2 from the infinite series (1) would give more widely applicable results and several attempts have been made in this direction. Matsen and Gerhauser[8] and Gray[9] used the Lennard-Jones approximation, i.e.,

$$\epsilon_2=\sum{}'\frac{v_{1n}{}^2}{E_1{}^0-E_n{}^0}=\frac{1}{E_1{}^0}\sum{}'v_{1n}{}^2+\frac{1}{E_1{}^0}\sum{}'\frac{v_{1n}{}^2E_n{}^0}{E_1{}^0-E_n{}^0}$$

$$=\frac{(v^2)_{11}-v_{11}{}^2}{E_1{}^0}+\left\{\sum{}_1\frac{v_{1n}{}^2E_1{}^0}{E_1{}^0-E_n{}^0}\right\}\Big/E_1{}^0, \tag{2}$$

where it should be a good approximation to neglect the summation if the continuum states are unimportant. These calculations gave $\epsilon_2=-0.31$ a.u., indicating that the continuum states are important, as we might expect.

A method for evaluating ϵ_2 exactly, in closed form, due to Dalgarno and Stewart[10] is, unfortunately, not tractable for the helium-like ions.

Recently Schwartz[11] attempted unsuccessfully to calculate ϵ_2 by analytical means in order to have an exact result by which to judge the variational calculations of Hylleraas. However, he was able to calculate the first-order correction to the one-electron density exactly and compare it with the results from the variation perturbation method.

Finally Kessler in a series of papers[12–14] developed an approximate method of calculating ϵ_2 from the perturbation formula itself and applied it to two-, three-, and four-electron atoms, obtaining the value -0.19 a.u. for two-electron systems, which although the best perturbation value to date, is in serious disagreement with the value -0.16 a.u. obtained by the variation perturbation method. An examination of this method and its possible generalization will form the subject of the rest of this paper.

[1] E. A. Hylleraas, Z. Physik. **54**, 347 (1929).
[2] T. Kinoshita, Phys. Rev. **105**, 1490 (1957).
[3] C. L. Pekeris, Phys. Rev. **115**, 1216 (1959).
[4] H. M. James and A. S. Coolidge, J. Chem. Phys. **1**, 825 (1933).
[5] E. A. Hylleraas, Z. Physik. **65**, 209 (1930).
[6] M. Bethe and E. Salpeter, *Quantum Mechanics of One- and Two-Electron Atoms* (Academic Press, Inc., New York, 1957).
[7] E. A. Hylleraas and J. Midtdal, Phys. Rev. **103**, 829 (1956).
[8] F. A. Matsen and M. Gerhauser, J. Chem. Phys. **23**, 1359 (1955).
[9] B. F. Gray, J. Chem. Phys. **28**, 732 (1958).
[10] A. Dalgarno and A. L. Stewart, Proc. Roy. Soc. (London) **A238**, 269 (1956).
[11] C. Schwartz, Annals of Physics **6**, 156 (1959).
[12] P. Kessler, Compt. rend. **240**, 1058 (1955).
[13] P. Kessler, Compt. rend. **240**, 1314 (1955).
[14] P. Kessler, Compt. rend. **242**, 350 (1956).

TABLE I.

κ	α_κ
1	0.187500000
2	0.178011584
3	0.176988842
4	0.176951420
5	0.177062181
6	0.177179551
7	0.177278693
8	0.177358305
9	0.177421673
10	0.177472336
11	0.177513211
12	0.177546556

II. EXAMINATION OF KESSLER'S METHOD

Kessler splits the infinite series for ϵ_2 into two parts by writing

$$\epsilon_2=\sum_{n=2}^{\kappa}[v_{1n}^2/(E_1^0-E_n^0)]+[\alpha/(E_1^0-E_{\kappa+1}^0)]\sum_{\kappa+1}v_{1n}^2$$

$$=\sum_{n=2}^{\kappa}[v_{1n}^2/(E_1^0-E_n^0)]$$

$$+[\alpha/(E_1^0-E_{\kappa+1}^0)]\{(v^2)_{11}-\sum_{1}^{\kappa}v_{1n}^2\} \quad (3)$$

using matrix summation, i.e.,

$$\sum_{n=1}v_{1n}^2=(v^2)_{11},$$

where

$$(v^2)_{11}=\int\phi_1 v^2\phi_1 d\tau.$$

Kessler then assumes that α is independent of κ and therefore writes, taking $\kappa=1$,

$$\epsilon_2=[\alpha/(E_1^0-E_2^0)][(v^2)_{11}-(v_{11})^2].$$

Further taking $\kappa=6$ he then has two equations for the two unknowns, α and ϵ_2, i.e.,

$$\epsilon_2=[\alpha/(E_1^0-E_2^0)][(v^2)_{11}-(v_{11})^2]$$

$$\epsilon_2=\sum_{n=2}^{6}[v_{1n}^2/(E_1^0-E_n^0)]+[\alpha/(E_1^0-E_7^0)]$$

$$\times[(v^2)_{11}-\sum_{n=1}^{6}v_{1n}^2], \quad (4)$$

which he solves for ϵ_2, not getting the result one would expect for two-electron ions, thus indicating that α is not independent of κ, at least that $\alpha_1\neq\alpha_6$. It is not clear why one should assume α to be independent of κ so it was decided to test the method by application to a known example. It was decided to use the hydrogen atom as treated by Trees[15] as this has much in common with the present problem. In this case the perturbation is $-(1-Z_1)/r$, where Z_1 is the charge on the unperturbed nucleus, i.e., only part of the potential energy is included in the zeroth order and the rest is treated as a perturbation. Using the exact value of ϵ_2 as obtained by Trees we can calculate α exactly as a function of κ. The following results are obtained. (See Table I.)

Here α obviously varies with κ, particularly for small κ, dropping rapidly to a minimum at $\kappa=4$, then rising to a limiting value as $\kappa\to\infty$. Kessler's assumption $\alpha_1\doteq\alpha_6$ is far from justified, the only case which is justifiable being in the neighborhood of the minimum, i.e., $\alpha_3\doteq\alpha_4$. We cannot treat the difference between two values as a direct measure of the constancy of the α's because for large κ *all* differences become small including those between matrix elements and energy denominators. Hence although $\alpha_n\doteq\alpha_{n+1}$ may be true to, say six figures for large enough n, the quantity $v_1^2{}_{,n+1}/E_1^0-E_{n+1}^0$ will be zero to this accuracy and the two equations for ϵ_2 and α are no longer independent, making their solution impossible.

However assuming $\alpha_3\doteq\alpha_4$, gives $\epsilon_2=-0.5025$ a.u. compared with the correct value of $\epsilon_2=-0.5000$ a.u. In a genuine problem one would not know where the minimum lay, and therefore the best values of κ would be unknown. Kessler's values $\alpha_1\doteq\alpha_6$ give 15% error for hydrogen.

It has been possible to find a semiempirical method of detecting the minimum without prior knowledge of ϵ_2, which is very plausible but not rigorous.

We first define a number of finite differences which we will use,

$$\delta_{i,i+1}=\alpha_{i+1}-\alpha_i$$

$$\delta_{i,i+2}{}^2=\delta_{i+1,i+2}-\delta_{i,i+1}. \quad (5)$$

We also have the basic equations

$$\epsilon_2=Y_\kappa+\alpha_\kappa X_\kappa$$

$$\epsilon_2=Y_{\kappa+1}+\alpha_{\kappa+1}X_{\kappa+1}$$

$$\epsilon_2=Y_{\kappa+2}+\alpha_{\kappa+2}X_{\kappa+2}, \quad (6)$$

where

$$X_\kappa=\{(v^2)_{11}-\sum_{1}^{\kappa}v_{1n}^2\}/(E_1^0-E_{\kappa+1}^0)$$

and

$$Y_\kappa=\sum_{1}^{\kappa=1}[v_{1n}^2/(E_1^0-E_n^0)],$$

giving us three equations for four unknowns ϵ_2, α_κ,

[15] R. Trees, Phys. Rev. **102**, 1553 (1956).

$\alpha_{\kappa+1}$, and $\alpha_{\kappa+2}$, where we no longer assume α to be independent of κ. We can replace $\alpha_{\kappa+1}$ and $\alpha_{\kappa+2}$ by $\delta_{\kappa,\kappa+1}$ and $\delta_{\kappa,\kappa+2}{}^2$ giving us

$$\epsilon_2 = Y_\kappa + \alpha_\kappa X_\kappa$$

$$\epsilon_2 = Y_{\kappa+1} + \alpha_\kappa X_{\kappa+1} + \delta_{\kappa,\kappa+1} X_{\kappa+1}$$

$$\epsilon_2 = Y_{\kappa+2} + \alpha_\kappa X_{\kappa+2} + 2\delta_{\kappa,\kappa+1} X_{\kappa+2} + \delta_{\kappa,\kappa+2}{}^2 X_{\kappa+2}, \quad (7)$$

from which we proceed to eliminate ϵ_2 and α_κ, giving us an exact relationship between $\delta_{\kappa,\kappa+1}$ and $\delta_{\kappa,\kappa+2}{}^2$. We can repeat this procedure for various values of κ and use the resulting equations to set up a general relation of the form

$$\delta_{i,i+1} = A_j{}^i \delta_{j,j+2}{}^2 + \beta_j{}^i, \quad (8)$$

where $A_j{}^i$ and $B_j{}^i$ can be determined without knowledge of ϵ_2. In the case of hydrogen we know that $|\delta_{34}|$ is small compared with neighboring values (i.e., minimum in α) and also that $|\delta_{46}{}^2|$ is small compared with neighboring values (inflection in α variation). We might hope that this would be shown in the variation of the $B_j{}^i$, i.e., $|B_4{}^3|$ might be smaller than neighboring values. This is in fact so as inspection of Table II reveals. Hence if we assume that smallness in $|B_j{}^i|$ with respect to its immediate neighbors indicates the position of the minimum and the inflection we can determine ϵ_2 with reasonable (but quantitatively unknown) accuracy. We would suggest that this assumption replace the one of Kessler. We obtain then

$$\alpha_3 = \alpha_4; \qquad \epsilon_2 = -0.5025 \text{ a.u.}$$

$$\delta_{45} = \delta_{56}; \qquad \epsilon_2 = -0.5021 \text{ a.u.}$$

$$\epsilon_2(\text{correct}) = -0.5000 \text{ a.u.}$$

Upon constructing a similar table for two-electron ions, the same phenomenon appears (Table III), indicating again that $\alpha_3 = \alpha_4$ and $\delta_{45} = \delta_{46}$ will give the best results, which are, respectively, $\epsilon_2 = -0.1625$ a.u. and $\epsilon_2 = -0.1621$ a.u. Again we have no idea of the size of the errors, but these results appear to be correct to two figures, that is, in agreement with the variation-perturbation and perturbation methods will give identical results if the latter can be evaluated with greater accuracy. The limiting factor in the present investigation is that we have to use finite differences for a fixed interval of unity.

TABLE II. Values of $B_j{}^i$ for hydrogen.

	δ_{23}	δ_{34}	δ_{45}	δ_{56}
$\delta_{24}{}^2$	−0.00043	−0.00094	−0.0012	
$\delta_{35}{}^2$	+0.00068	−0.00013	−0.00024	
$\delta_{46}{}^2$	+0.00009	+0.0000014	−0.000050	−0.000085
$\delta_{57}{}^2$		+0.000021	−0.0000062	−0.000024
$\delta_{68}{}^2$			+0.0000059	−0.0000045

TABLE III. Values of $B_j{}^i$ for helium-like ions.

	$\delta_{35}{}^2$	$\delta_{46}{}^2$	$\delta_{57}{}^2$
δ_{23}	+0.00015	+0.00015	
δ_{34}	−0.00016	+0.0000056	+0.000047
δ_{45}	−0.00034	−0.000069	+0.0000080
δ_{56}		−0.00011	−0.000016

III. POSSIBLE GENERALIZATIONS OF THE KESSLER METHOD

The problem is essentially to solve the set of n simultaneous equations for $n+1$ unknowns:

$$\begin{aligned}
\epsilon_2 &= Y_1 + \alpha X_1 \\
\epsilon_2 &= Y_2 + \alpha X_2 + \delta X_2 \\
\epsilon_2 &= Y_3 + \alpha X_3 + 2\delta X_3 + \delta^2 X_3 \\
\epsilon_2 &= Y_4 + \alpha X_4 + 3\delta X_4 + 3\delta^2 X_4 + \delta^3 X_4 \\
&\vdots \\
\epsilon_2 &= Y_n + \alpha X_n + (n-1)\delta X_n + \cdots \delta^{n-1} X_n, \quad (9)
\end{aligned}$$

the familiar binomial coefficients appearing, and the $n+1$ unknowns being $\epsilon_2, \alpha, \delta, \delta^2, \cdots \delta^{n-1}$ of which we are really only interested in ϵ_2. We proceed by eliminating all the variables except ϵ_2 and δ^{n-1} which we hope may be negligible. The result is

$$\epsilon_2 = \frac{\begin{vmatrix} a_1 & 1 & & & & \\ a_2 & 1 & 1 & & & \\ a_3 & 1 & 2 & 1 & & \\ a_4 & 1 & 3 & 3 & 1 & \cdots \\ \vdots & \cdots & & & & \end{vmatrix} - \delta^{n-1}}{\begin{vmatrix} b_1 & 1 & & & & \\ b_2 & 1 & 1 & & & \\ b_3 & 1 & 2 & 1 & & \\ b_4 & 1 & 3 & 3 & 1 & \cdots \\ \vdots & \cdots & & & & \end{vmatrix}} \quad (10)$$

$$= |a_n|/|b_n| - \delta^{n-1}/|b_n|, \quad (11)$$

where

$$a_n = Y_n/X_n \quad \text{and} \quad b_n = 1/X_n.$$

The determinants $|a_n|$ and $|b_n|$ are known as recur-

rents[16] and their expansions are given by

$$|a_n| = a_1 - na_2 + \tfrac{1}{2}n(n-1)a_3 + \cdots a_n. \qquad (12)$$

We could conceivably obtain an exact solution to the problem if

$$\lim_{n\to\infty} (\delta^{n-1}/|b_n|) \to 0;$$

δ^{n-1} certainly falls off rapidly for cases where the unperturbed spectrum contains an ionization limit in the discrete part, but it appears that $|b_n|$ also approaches zero, so that in most cases the error term does not vanish. Here $|a_n|$ also becomes zero in the limit, and limiting processes of this kind do not appear a practicable proposition.

An entirely different type of generalization suggests itself upon examination of the values of α in Table I. It will be noticed that to three significant figures, α_3, α_4, $\cdots\alpha_{10}$ are all equal, other values of α differing even to this accuracy. If these α's were strictly equal within this range, then whichever pair we chose to equate would give us the same value of ϵ_2. In fact, whichever pair we equate within this range, we do get reasonable constant values of ϵ_2, i.e., between -0.48 a.u. and -0.52 a.u. (see Appendix). It seems possible then that one might modify the basic equations to the form:

$$\begin{aligned}
\epsilon_2 &= Y_3 + \alpha_3^* X_3 f(3) \\
\epsilon_2 &= Y_4 + \alpha_4^* X_4 f(4) \\
\epsilon_2 &= Y_5 + \alpha_5^* X_5 f(5) \\
&\vdots \\
\epsilon_2 &= Y_{10} + \alpha_{10}^* X_{10} f(10),
\end{aligned} \qquad (13)$$

where $f(\kappa)$ in this case could be chosen as a slowly increasing function of κ by using the criterion that the value of ϵ_2 obtained was independent of the pair of α's chosen within this range. We would then assume that this meant that α_κ^* was really independent of κ over the limited range taken. Further work in this direction is in progress at the moment.

In conclusion it seems very plausible that the ordinary infinite series expression for ϵ_2 will give results in agreement with the perturbation-variation results. It also seems probable that the results of Kessler are about 15% in error due to his unfortunate choice of α_1 and α_6.

ACKNOWLEDGMENTS

The authors wish to thank Dr. P. Kessler for supplying some unpublished numerical information, and Dr. Kerr, Department of Mathematics, Royal Technical College, for the use of computing facilities.

APPENDIX

It is of interest to examine the magnitude of the error in ϵ_2 due to the assumption $\alpha_i = \alpha_j$ as a function of i and j

$$\epsilon_2 = Y_i + \alpha_i X_i$$

$$\epsilon_2 = Y_j + \alpha_j X_j;$$

therefore

$$\alpha_i = [(Y_j - Y_i)/(X_i - X_j)] + [(X_j \delta_{ij}/(X_i - X_j)],$$

and

$$\epsilon_2 = Y_i + X_i[(Y_j - Y_i)/(X_i - X_j)] + [X_i X_j/(X_i - X_j)]\delta_{ij}.$$

We assume that the last term is negligible and obtain

$$\epsilon_2(i,j) = Y_i + [X_i(Y_j - Y_i)/(X_i - X_j)],$$

with an error term $[X_i X_j/(X_i - X_j)]\delta_{ij}$. Hence if we have a range of values of κ where $\epsilon_2(i,j)$ is independent of i and j, or nearly so, we will obtain the smallest errors by choosing i and j from opposite ends of the range, assuming that all the δ_{ij}'s are small. In the hydrogen example we would take (3, 4, 5) and (9, 10, 11) and equate α's across the two sets, thus ensuring that $|X_i - X_j|$ does not become small.

If we take the special case $j = i+1$ we have

$$\epsilon_2 = Y_i + [X_i(Y_{i+1} - Y_i)/(X_i - X_{i+1})] + [X_i X_{i+1}/(X_i - X_{i+1})]\delta_{i,i+1}.$$

Now as the α's approach a limit asymptotically, $\lim_{i\to\infty}(\delta_{i,i+1}) \to 0$ we might under certain conditions make the error term vanish. However for one- and two-electron atoms $1/(X_i - X_{i+1})$ becomes singular sufficiently quickly to prevent this.

A. Muir, *Theory of Determinants*, (The Macmillan Company, New York, 1906).

Microwave Spectrum of *cis* 1-Chloro-2-Fluoroethylene*

JOHN A. HOWE†

Mallinckrodt Chemical Laboratory, Harvard University, Cambridge 38, Massachusetts

(Received August 1, 1960)

The microwave spectrum of *cis* 1-chloro-2-fluoroethylene, CHCl=CHF, has been observed in the 15–25 kMc region for both chlorine species. Rotational constants for $CHCl^{35}CHF$ are $a=16{,}405.9$, $b=3{,}756.05$, and $c=3{,}052.67$ Mc. Agreement of these and other data with values predicted from an assumed structure strongly suggests that the structure can be well represented as a composite of the known vinyl chloride and vinyl fluoride structures. Second-order quadrupole coupling theory is used to afford a direct measurement of χ_{ab}; the nonzero elements of the tensor χ for the Cl^{35} species have the values $\chi_{aa}=-22.46$, $\chi_{bb}=-10.88$, and $\chi_{ab}=\pm 56.7$ Mc. These values show a 4% deviation of the C–Cl bond from cylindrical symmetry.

FOLLOWING the method of Swart,[1] and that of Yakubovchu, *et al.*,[2] a mixture of *cis* and *trans* 1-chloro-2-fluoroethylene was prepared by the following two-step synthesis:

$$CHCl_2CHCl_2+SbF_3 \xrightarrow[Br_2]{SbF_5} CHCl_2CHClF$$

$$CHCl_2CHClF+Zn \longrightarrow CHClCHF.$$

Because of competing side reactions in both steps, the over-all yield was low.

Since all observations were made on the mixture of the two isomers prepared by the foregoing method, it proved impossible to identify any absorption lines as belonging to the *trans* species, the *cis* species giving rise to a very intense and crowded spectrum.

The assumed structure is given in Table I; this structure is based on the work of Kivelson *et al.*[3] on vinyl chloride and on the work of Bak *et al.*[4] on vinyl fluoride. The moments calculated from this structure for the *cis* species are given in Table II. As will be seen shortly, the agreement of these moments with the observed values suggest that the assumed structure is at least approximately correct.

From the assumed structure, it is possible to predict the main features of the microwave absorption spectrum of the *cis* species. These are first, that only *b* type transitions will be important (μ_b being estimated at 1 to 2 *D*), and secondly, that only a few low *J* transitions are to be found in the 15–25 kMc region (two *R* types and the *Q*-type series $J_{0J}\rightarrow J_{1J-1}$). These predictions were experimentally confirmed, the *Q* series being identified by the appearance of the Stark pattern and of the hyperfine quadruplets. The approximate frequency of the $0_{00}\rightarrow 1_{11}$ transition was predicted from the *Q*-type frequencies and assumption of planarity, this line then being found and identified by its hyperfine structure. As further confirmation of the assignment, two components of the $1_{01}\rightarrow 2_{12}$ transition of the Cl^{35} species were observed under low resolution conditions. Although this transition was not observed for the Cl^{37} species, the assignment of the $0_{00}\rightarrow 1_{11}$ transition is corroborated by the agreement of the observed planarity defects for the two species. Of course, the entire assignment is consistent within itself, with the expected hyperfine structure, and with the assumed structure.

TABLE I. Assumed structure.

d	CC	1.333 A	<CCCl	123.6°
d	CCl	1.726	<CCH	123.2°
d	CF	1.348	<CCF	121.0°
d	CH	1.079		

Table III lists the observed frequencies of assigned transitions of *cis* $CHCl^{35}CHF$; also included in this table are transition frequencies calculated from the molecular parameters listed in Table IV. Table V gives similar information for the species *cis*-$CHCl^{37}CHF$. It should be remarked that in some cases it was not possible to measure the frequencies of all of the most prominent components of a multiplet because of overlapping by an adjacent high *J* line.

It is of considerable interest to compare the observed and calculated frequencies given in Table III. With the exception of the $1_{01}\rightarrow 2_{12}$ transition, which was observed under very poor conditions, the mean deviation between calculated and observed frequencies is about 0.06 Mc. However, it will be observed that the $11/2\rightarrow 11/2$ and the $7/2\rightarrow 7/2$ components of the $5_{05}\rightarrow 5_{14}$ transition show a much larger deviation. This

* Financial support of the machine calculations reported in this paper was provided by the U. S. Atomic Energy Commission in conjunction with the Lawrence Radiation Laboratory. The remainder of the work reported herein was supported by a grant extended Harvard University by the Office of Naval Research under contract and by a grant from the California Research Corporation.

† Present address: Chemistry Department, University of California, Berkeley 4, California.

[1] F. Swart, Mem. acad. roy. Belgique **61**, 94 (1901).

[2] A. Y. Yakubovchu *et al.*, Zhur. Obshchei Khim. **24**, 2257 (1954).

[3] D. Kivelson and E. B. Wilson, Jr., J. Chem. Phys. **32**, 205 (1960).

[4] B. Bak *et al.*, Spectrochim. Acta **13**, 120 (1958).

TABLE II. Predicted moments.

	cis-CHClCHF	
	Cl^{35}	Cl^{37}
I_a	31.190 (amu A²)	31.300
I_b	135.254	138.726
I_c	166.444	170.026

deviation arises from a nonnegligible second-order quadrupole coupling term and affords an opportunity to obtain χ_{ab} directly from the observed spectrum.

As is well known, cf. Townes and Schawlow,[5] application of first-order quadrupole coupling theory predicts that the most intense members of the $5_{05}\rightarrow5_{14}$ multiplet are the $\Delta F=0$ transitions and that these form a symmetrical quadruplet. Therefore, if the quantity Δ is defined by $\Delta=\nu(11/2)-\nu(9/2)-\nu(13/2)+\nu(7/2)$, deviation of the value of Δ from zero affords a direct measure of the importance of second- (and higher) order terms, Δ being independent of zero and first-order terms.

From the observed frequencies of Table III, it is calculated that $\Delta=-0.67$ Mc, the large second-order contribution arising because the level 5_{14} lies only 298.2 Mc below the level 4_{22}. Subsequent redetermination of Δ with the aid of the high-resolution spectrometer described by Narath[6] yields the value $\Delta=-0.59$ Mc. By taking the average of these two determinations and by estimating that the uncertainty is likely much less than ±0.14 Mc, an observed value $\Delta=-0.63\pm0.14$ Mc is obtained.

TABLE III. *cis* $CH^{35}ClCHF$.

Transition		ν(Mc) observed	ν(Mc) calculated
$3_{03}\rightarrow3_{12}$	7/2→7/2	15 240.67	15 240.81
	7/2→5/2	15 240.14	15 240.24
	7/2→9/2	15 239.60	15 239.58
	5/2→5/2	15 237.39	15 237.27
	9/2→9/2	15 233.21	15 233.24
	3/2→3/2	15 229.76	15 229.71
$4_{04}\rightarrow4_{13}$	9/2→9/2	16 870.66	16 870.57
	7/2→7/2	16 868.13	16 867.96
	11/2→11/2	16 863.18	16 863.12
	5/2→5/2	16 860.48	16 860.51
$5_{05}\rightarrow5_{14}$	11/2→11/2	19 053.22	19 053.61
	9/2→9/2	19 051.40	19 051.43
	13/2→13/2	19 045.89	19 045.91
	7/2→7/2	19 043.40	19 043.74
$0_{00}\rightarrow1_{11}$	3/2→1/2	19 461.25	19 461.25
	3/2→5/2	19 459.04	19 459.07
	3/2→3/2	19 456.39	19 456.35
$1_{01}\rightarrow2_{12}$	5/2→7/2	25 565.7	25 565.1
	3/2→5/2	25 563.1	25 562.4

[5] C. H. Townes and A. L. Schawlow, *Microwave Spectroscopy* (McGraw-Hill Book Company, Inc., New York, 1955).

[6] A. Narath, thesis, University of California, Berkeley, California, 1960.

TABLE IV. Observed values *cis*-CHClCHF.

	Cl^{35}	Cl^{37}
I_a	30.814 (amu A²)	30.926 (amu A²)
I_b	134.591	138.029
I_c	165.603	169.152
$I_a+I_b-I_c$	−0.197	−0.197
χ_{aa}	−22.46 Mc	−17.31 Mc
χ_{bb}	−10.88	−7.96
χ_{ab}	±56.7	...
k	−0.89465	−0.89911
a	16 405.9 Mc	16 346.6 Mc
b	3756.05	3662.49
c	3052.67	2988.61

With the aid of the matrix elements given by Bragg[7] it is a simple matter to obtain the linear relation between χ_{ab}^2 and Δ, the only additional information required being the value of the matrix element of the direction cosine product $\Phi_{za}\Phi_{zb}$. This value was obtained by the use of a recently completed program for the IBM 704 computer which can compute asymmetric rotor direction cosine elements through $J=11$ and for an arbitrary asymmetry parameter. This procedure yields $\chi_{ab}=\pm56.7$ Mc with a probable error less than ±6 Mc.

The molecule *cis* 1-chloro-2-fluoroethylene is of interest from the standpoint of chemical bonding theory since both the Cl and F lone pair π electrons can interact with the ethylenic π system. In order to test the validity of various models representing this lone pair delocalization, one wishes to obtain from the micro-

TABLE V. *cis*-$CH^{37}ClCHF$.

Transition		ν(Mc) observed	ν(Mc) calculated
$3_{03}\rightarrow3_{12}$	7/2→7/2	15 160.37	15 160.27
	5/2→5/2	15 157.89	15 157.65
	9/2→9/2	15 154.71	15 154.66
$4_{04}\rightarrow4_{13}$	9/2→9/2	16 712.87	16 712.86
	7/2→7/2	16 710.90	16 710.85
	11/2→11/2	16 707.20	16 707.14
	5/2→5/2	16 705.23	16 705.14
$5_{05}\rightarrow5_{14}$	13/2→13/2	18 781.91	18 782.01
	7/2→7/2	18 780.34	18 780.38
$0_{00}\rightarrow1_{11}$	3/2→1/2	19 337.18	19 337.21
	3/2→5/2	19 335.66	19 335.62
	3/2→3/2	19 333.62	19 333.63

[7] J. K. Bragg, Phys. Rev. **74**, 533 (1948).

wave spectrum the dipole moment, the approximate structure, and, as Goldstein[8] has shown, the χ tensor in its principal axis system.

Unfortunately, the presence of quadrupole coupling, with its consequent destruction of M as a good quantum number, renders the quantitative interpretation of Stark effect data difficult. For this reason, no dipole moment can be given here although a preliminary treatment of the Stark effect of the $0_{00} \rightarrow 1_{11}$ multiplet is consistent with a b dipole component of 1.6 D.

If one makes the usual assumption that the χ principal axes coincide with the bond axis system having the z axis coincident with the C—Cl bond axis and the x axis in the plane of the molecule, then, from the above χ elements one obtains $\chi_{zz} = -73.7$ Mc and $\chi_{xx} = 40.3$ Mc with θ, the angle between the a and z axes, being 42°6′. The value of $\chi_{xx} = 40.3$ Mc may be used to obtain a value of δ (see reference 8) of 0.04. A ± 6 Mc uncertainty in χ_{ab} will produce uncertainties of $\pm 18'$ and $\pm .03$ in θ and δ.

A partial check of the δ value may be obtained by using the data for the Cl^{37} species. Using primed quantities to refer to this species, then $\theta' = \theta - \alpha$, where α has the value 20′ and is calculated from the assumed structure. Using this value of θ' with the χ' elements given in Table V, $\delta' = 0.03$ is obtained. Further, it should be noted that the value of θ calculated from the assumed structure is 42° 21′.

[8] J. H. Goldstein, J. Chem. Phys. **24,** 106 (1956).

ACKNOWLEDGMENTS

The author gratefully acknowledges the aid, advice, and encouragement given him by Professor E. B. Wilson, Jr. Further, the author wishes to thank Professor W. D. Gwinn and members of his research group for the use of the high-resolution spectrometer.

THE JOURNAL OF CHEMICAL PHYSICS VOLUME 34, NUMBER 4 APRIL, 1961

Derivation of the Tait Equation and Its Relation to the Structure of Liquids

ROBERT GINELL*

Department of Chemistry, University of Utah, Salt Lake City, Utah

(Received October 12, 1960)

The Tait equation $-(dV/dP) = J/(L+P)$ has been theoretically derived from association theory. It is shown that the constant L, which is temperature dependent should also have a small pressure dependence. From the equation for the constants it is shown how the volume of holes in the liquid can be calculated. The number average degree of association of a liquid is defined and an equation for its determination is given. The general structure of liquids in light of this equation is discussed.

IN a previous paper[1] it was shown, on a geometric basis using association theory, that a liquid whose 1-mers consist of spherically symmetrical particles surrounded by a spherically symmetric force field must contain small asymmetric clusters. Clusters of a similar sort have previously been postulated by Eyring and co-workers[2] in their treatment of the liquid state and also by Bernal[3] who uses the term prenuclei. Such clusters or j-mers as are present in the liquid cannot give rise to crystalline solids very easily, since the formation of nuclei requires the cooperative rearrangement of from 12 to 15 1-mers as a very minimum (homogeneous nucleation). If one bypasses the region where the liquid clusters, ja-mers, are more stable than the crystal clusters, jl-mers, by introducing a seed, then the transformation from liquid to crystal is quite rapid and easy (heterogeneous nucleation). Such a treatment of liquids, however satisfactory qualitatively in giving us an insight into the reasons for nucleation, leaves the picture of the structure of the liquid quite vague; inasmuch as, while it shows that such clusters must exist, it does not show how they are connected. Further, since the explanation involves a model, it is necessarily restricted in its application.

However, association theory enables us to proceed in still another direction and gain other insights, especially into more complex liquids, which together with the geometric approach will ultimately enable us to understand the structure of liquids. The approach in this direction is through the Tait equation, which is a well

* On leave 1960–61; permanent address: Brooklyn College, Brooklyn, New York.

[1] R. Ginell, J. Chem. Phys. **34,** 992 (1961).

[2] H. Eyring, T. Ree, and N. Hirai, Proc. Natl. Acad. Sci. U. S. **44,** 683 (1958); E. J. Fuller, T. Ree, and H. Eyring, *ibid.* **45,** 1594 (1959); C. M. Carlson, H. Eyring, and T. Ree, *ibid.* **46,** 333 (1960); T. R. Thomson, H. Eyring, and T. Ree, *ibid.* **46,** 336 (1960); C. M. Carlson, H. Eyring, and T. Ree, *ibid.* **46,** 649 (1960).

[3] J. D. Bernal, Nature **185,** 68 (1960).

known empirical relationship. This equation[4]

$$-(dV/dP)=J/(L+P) \tag{1}$$

was originally formulated as an empirical law to reproduce the compressibility behavior of water. It was latter applied to many other liquids, e.g., methyl, ethyl, propyl, isobutyl, and amyl alcohols[5]; acetone[5]; ethyl ether[5]; ethyl chloride, bromide, and iodide[5]; carbon disulfide[5]; phosphorus trichloride[5]; benzene[6]; chloro-, bromo-, and nitro-benzene[7]; aniline[7]; ethylene glycol and its aqueous solutions[8]; concentrated aqueous salt solutions,[8] etc. Hirschfelder, Curtiss, and Bird[9] call it the best empirical representation of the equation of state of liquids. Much work has been done on evaluating[6] the coefficients of this equation by Gibson and Loeffler who have also shown that from the equation and a knowledge of the temperature dependence of L (empirically derived) it is possible to obtain[10]

$$(\partial V/\partial T)_P,\ (\partial V/\partial P)_T\ \ (\partial P/\partial T)_V,\ (\partial E/\partial V)_T,$$

and $(\partial C_v/\partial V)_T$.

The parameter J has been found to be a constant independent of temperature[5] at least to about 1000 atm.

It is proposed here to give a theoretical derivation of this equation and from the coefficients derive further insights into the structure of liquids.

We shall start with the equation of state as derived from association theory[11]

$$P/RT=\sum_{i=1}^{m}C_i/(1-\mathfrak{b}/V), \tag{2}$$

where P, R, T, and V have their usual meanings; $\sum_i C_i$ is the sum of the concentrations of all the j-mers present, and $\mathfrak{b}$ is the sum of the excluded volumes of all the various j-mers. We will make here the assumption that the same equation of state will describe both gases and liquids. This assumption is not new and was first made by van der Waals.[12]

Differentiating Eq. (2) with respect to volume at constant temperature, rearranging and substituting Eq. (2) into the derivation, we get

$$dV/dP=\frac{1-(\mathfrak{b}/V)}{RT(d/dV)\sum_{i=1}^{m}C_i+P(d/dV)(\mathfrak{b}/V)}. \tag{3}$$

To evaluate the derivatives we use the relationship from association theory,[13,14]

$$C_j=K_jC_1^j. \tag{4}$$

Therefore

$$(d/dV)\sum_{i=1}^{m}C_i=(d/dV)\sum_{i=1}^{m}K_iC_1^i$$
$$=(\textstyle\sum_i C_i/C_1)(dC_1/dV) \tag{5}$$

from association theory[11]

$$C_1=\sum_{x=1}^{\infty}d_x(\textstyle\sum_i iC_i)^x, \tag{6}$$

where the d_x's are functions of the equilibrium constants as follows:

$$d_1=1$$
$$d_2=-2K_2$$
$$d_3=8K_2^2-3K_3$$
$$d_4=-40K_2^3+30K_2K_3-4K_4.$$

Therefore

$$dC_1/dV=\sum_{x=1}^{\infty}xd_x(\textstyle\sum_i iC_i)^{x-1}(d\sum_i iC_i/dV)$$
$$=[-\sum_{x=1}^{\infty}xd_x(\textstyle\sum_i iC_i)^x/V] \tag{7}$$

since

$$\sum_{i=1}^{m}iC_i=w/M^{(0)}V, \tag{8}$$

where w is the weight of the sample in grams and $M^{(0)}$ is the gram molecular weight of the 1-mer. Hence Eq. (5) becomes

$$\frac{d\sum C_i}{dV}=\frac{\sum iC_i}{C_1}\left(\frac{-\sum xd_x(\sum iC_i)^x}{V}\right); \tag{9}$$

using Eqs. (8) and (6), Eq. (9) becomes

$$d\textstyle\sum C_i/dV=-(w/M^{(0)}V)\cdot V^{-1}$$
$$\cdot[\sum_x xd_x(\sum_i iC_i)^x]/[\sum_x d_x(\sum_i iC_i)^x]$$
$$=-(w/M^{(0)}V)\cdot(1/V)\sum_{x=1}^{\infty}s_x(1/V)^{x-1}$$
$$=-(w/M^{(0)}V)\sum_{x=1}^{\infty}s_x(1/V)^x, \tag{10}$$

where s_x is a function of the coefficients[15] and of $w/M^{(0)}$. The coefficients s_x can be readily evaluated thus. From

[4] P. G. Tait, *Scientific Papers* (Cambridge University Press, New York, 1898), Vol. 2.
[5] A. Carl, Z. physik. Chem. **101**, 238 (1922).
[6] R. E. Gibson and J. F. Kincaid, J. Am. Chem. Soc. **60**, 511 (1938).
[7] R. E. Gibson and O. H. Loeffler, J. Phys. Chem. **43**, 207 (1939); J. Am. Chem. Soc. **63**, 2287 (1941).
[8] R. E. Gibson and O. H. Loeffler, Ann. N. Y. Acad. Sci. **51**, 727 (1949); see also complete bibliography given here.
[9] J. O. Hirschfelder, C. F. Curtiss, and R. B. Bird, *Molecular Theory of Gases and Liquids* (John Wiley & Sons, Inc., New York, 1954).
[10] R. E. Gibson and O. H. Loeffler, J. Am. Chem. Soc. **61**, 2515 (1939).
[11] R. Ginell, J. Chem. Phys. **23**, 2395 (1955).
[12] J. D. van der Waals, Doctoral dissertation, Leiden (1873).
[13] R. Ginell and J. Shurgan, J. Chem. Phys. **23**, 964 (1955).
[14] R. Ginell, Ann. N. Y. Acad. Sci. **60**, 521 (1955).
[15] K. Knopp, *Theory and Application of Infinite Series* (Hafner Publishing Company, New York, 1947).

association theory[11] and Eq. (8)

$$d\sum_{i=1}^{m}C_i/dV=(d/dV)\sum_{x=1}^{\infty}g_x(\sum_i iC_i)^x$$

$$=\sum_{x=1}^{\infty}xg_x(\sum_i iC_i)^{x-1}(d\sum iC_i/dV)$$

$$=-V^{-1}\sum_{x=1}^{\infty}xg_x(w/M^{(0)})^x(1/V)^x. \qquad (11)$$

On equating Eqs. (10) and (11) we have

$$-V^{-1}\sum_{x=1}^{\infty}xg_x(w/M^{(0)})^x(1/V)^x=-(w/M^{(0)}V)\sum_{x=1}^{\infty}s_x(1/V)^x$$

or

$$s_x=xg_x(w/M^{(0)})^{x-1}. \qquad (12)$$

The g coefficients are[11]

$g_1=1$

$g_2=-K_2$

$g_3=4K_2^2-2K_3$

$g_4=-20K_2^3+18K_2K_3-3K_4$,

etc.

Now

$$(d/dV)(\mathfrak{b}/V)=(d/dV)\sum_{i=1}^{m}\mathfrak{b}_iC_i$$

$$=\sum_{i=1}^{m}i\mathfrak{b}_iK_iC_1^{i-1}(dC_1/dV)$$

$$=(\sum_{i=1}^{m}i\mathfrak{b}_iC_i/C_1)(dC_1/dV) \qquad (13)$$

so that using Eqs. (7) and (10)

$$(d/dV)(\mathfrak{b}/V)=-\sum_{i=1}^{m}i\mathfrak{b}_iC_i\sum_{x=1}^{\infty}s_x(1/V)^x. \qquad (14)$$

Substituting Eqs. (11) and (14) into Eq. (3) and rearranging we get

$$-dV/dP=\left[\frac{1-(\mathfrak{b}/V)}{\sum_i i\mathfrak{b}_iC_i\sum_x s_x(1/V)^x}\right]\Big/\left[\frac{(RTw/M^{(0)}V)\sum_x s_x(1/V)^x}{\sum_i i\mathfrak{b}_iC_i\sum_x s_x(1/V)^x}+P\right] \qquad (15)$$

or

$$-dV/dP=\left[\frac{V-\mathfrak{b}}{\sum_i i\mathfrak{b}_iN_i\sum_x s_x(1/V)^x}\right]\Big/\left[\frac{RTw}{M^{(0)}\sum i\mathfrak{b}_iN_i}+P\right]. \qquad (16)$$

Equation (16) is the derived Tait equation with

$$J=(V-\mathfrak{b})/\sum i\mathfrak{b}_iN_i\sum s_x(1/V)^x \qquad (17)$$

and

$$L=RTw/M^{(0)}\sum i\mathfrak{b}_iN_i. \qquad (18)$$

Since at constant temperature L is constant up till 1000 atm, this must mean that $\sum_i i\mathfrak{b}_iN_i$ is at least as constant. $\sum i\mathfrak{b}_iN_i$, which is one of the structural parameters of liquids, is the sum of the excluded volumes for each species multiplied by the number of particles in each species; as such it should not vary too much. It does however vary with temperature.

From Eqs. (13) and (14) we have

$$(\sum_i i\mathfrak{b}_iC_i/C_1)(dC_1/dV)=-\sum_{i=1}^{m}i\mathfrak{b}_iC_i\sum_{x=1}^{\infty}s_x(1/V)^x; \qquad (19)$$

using Eq. (4) and expanding the sum on the right-hand side we have

$$1/V-(1/N_1)(dN_1/dV)=1/V+\sum_{x=2}^{\infty}s_x(1/V)^x \qquad (20)$$

or

$$-d\ln N_1/dV=\sum_{x=2}^{\infty}s_x(1/V)^x. \qquad (21)$$

This shows us that the change in the number of moles of N_1 in the total sample is given by part of the s_x sum. C_1 or N_1 itself can be calculated from Eq. (6), although the series does not converge too rapidly. The fact that

$$\sum_{i=1}^{m}i\mathfrak{b}_iN_i$$

is not truly constant and consequently L is not really constant, is corroborated by the fact that at a higher pressure the equation must be modified.[16] However, till 1000 atm L is constant within experimental error.

From Eqs. (17) and (18) we have

$$\sum i\mathfrak{b}_iN_i=RTw/M^{(0)}L=[(V-\mathfrak{b})/J\sum_x s_x(1/V)^x], \qquad (22)$$

from which

$$(V-\mathfrak{b})=[RTwJ\sum_x s_x(1/V)^x/M^{(0)}L]. \qquad (23)$$

[16] For high-pressure modifications of the Tait equation see J. G. Kirkwood and H. Bethe, Part I OSRD Rept. 588 (Dept. of Comm. No. PB 32182); J. G. Kirkwood and J. M. Richardson, Part III OSRD Rept. 813 (Dept. of Comm. No. PB 32184); J. M. Richardson, A. B. Arons, and R. R. Halverson, J. Chem. Phys. **15**, 785 (1947).

The function $(V-\mathfrak{b})$ is the difference between the total volume and the excluded volume and is equal to the volume of holes in the liquid. That is, in addition to the fractional holes in the structure of the *ja*-mers,[1] which are included in $\mathfrak{b}$, there are additional holes in the liquid structure. As can be seen from the equation, the number of holes will increase with temperature, since L decreases in general with temperature. Very rough calculations seem to show that $\sum_x s_x(1/V)^x$ decreases with temperature, although the decrease is very small. The calculation of the $\sum_x s_x(1/V)^x$ demands a knowledge of the equilibrium constants and of the geometry of the *ja*-mers. The latter has only been carried out for spherical molecules,[1] and hence any exact calculation at this point would be presumptious.

If we substitute Eq. (2) into Eq. (23), we get

$$(w/M^{(0)})/\sum N_i=[L/JP\sum_x s_x(1/V)^x]. \quad (24)$$

In the theory of gases the right-hand side is formally equal to the number average degree of association, Z_n; so that we can say that formally at least

$$Z_n=L/[JP\sum s_x(1/V)^x]. \quad (25)$$

This is an interesting, although a curious equation, since the average degree of association (or equivalently the average molecular weight) is a quantity which is strictly defined only for the gas phase, or for very dilute solutions, where the solute molecules are considered to be a gas and the solvent is considered as viscous space. In the gas phase, the molecule may be defined as that kinetic unit which under a slight impulse moves as a whole. This definition cannot be directly transferred to solutions, since presumably the movement of the solute molecule would involve the movement of a certain amount of solvent. This would really be the definition of the kinetic molecule in solution, i.e., the molecule and its solvated layer. The weight of such a kinetic unit would then be the molecular weight. However, while in the gas phase the average molecular weight as determined by experiment is the average weight of the kinetic unit, in solutions, when using the colligative properties, the solvated layer does not enter. Another definition, more closely related to what is being measured in solution is this: a molecule is that group of atoms around which a continuous surface may be drawn; the surface cutting weaker bonds than those between the atoms included within the group. The molecular weight is then the weight of such a group of atoms. Although this definition is highly inoperational since we do not know too much, with certainty, about the solvated layer, none the less we draw comfort from the fact that molecular weights thus determined agree often with formula weights. Such a definition is not suitable for pure liquids. If we adopt the gas phase definition, then Z_n would define the kinetic unit in the liquid. Presumably this would be the sort of *ja*-mers previously discussed.[1] Surrounding these *ja*-mers would be holes of sizes different from the fractional holes in the *ja*-mer. They might be of molecular size as postulated by Eyring[2] or they might be of various sizes. Looking at Eq. (25) we can see that Z_n will depend strongly on the pressure; an increase in pressure making Z_n smaller. At first sight this is puzzling. The effect of pressure would be first to distort the *ja*-mers. This would in effect force the breaking of bonds, and the information of smaller aggregates. Holes would be squeezed out by the pressure but at the same time more holes would be created by the coalescing of the fractional holes in the collapsing *ja*-mers.

The general picture of a liquid presented then by these functions is one very similar to that of a polycrystalline or mosaic solid except that, while the crystallites in the solid are *jt*-mers, those in the liquid are *ja*-mers. The *ja*-mers are surrounded by defects consisting in the main of 1-mers bound by single bonds or weak bonds to the *ja*-mers and holes. A temperature increase, increases the number of holes, while a pressure increase decreases the average size of the *ja*-mers, creating new holes from the fractional holes in the *ja*-mers while squeezing out some of the defect holes. The mobility of the liquid is due to this high proportion of holes in the liquid. A very rough calculation of the number of holes $(V-\mathfrak{b})$ by Eq. (23) shows that the percentage of holes in water in the temperature range 20°–100°C and pressure range 1–1000 bars lies between 13.5 and 18.3%. Interestingly enough this compares with the figure of 1/7 the volume (=14.3%) derived by Eyring from viscosity work.

Further work is in progress on the exact calculation of some of these quantities, all of which are experimentally derivable. This will give us a much clearer insight into the structure of liquids and especially of particular liquids.

ACKNOWLEDGMENT

I wish to acknowledge the help that the stimulating discussion with Dr. Henry Eyring has given me.

Configuration and Free Energy of a Polymer Molecule with Solvent Interaction

MICHAEL E. FISHER AND BASIL J. HILEY

Wheatstone Physics Laboratory, King's College, London, England

(Received October 24, 1960)

The lattice model of a polymer molecule with excluded volume and nearest-neighbor forces arising from polymer-solvent interaction is investigated by exact numerical calculation for short chains of up to about ten links. Extrapolation to large values of n, the number of links, is shown to be justified and enables the mean configuration, free energy, entropy, and internal energy to be evaluated as functions of the number of links and of temperature for both poor and "super-perfect" solvents. The mean square end-to-end distance is found to vary according to $\langle r_n^2\rangle \approx An^\gamma$, in agreement with Wall *et al.*, but $\gamma=\gamma(\eta)$ is a decreasing function of the nearest-neighbor interaction parameter $\eta=\exp[-V_0/kT]$. For the three-dimensional simple cubic lattice $\gamma(0)\simeq 1.37$, $\gamma(1)\simeq 1.20$ and Flory's theta point, defined by $\gamma=1$, occurs at $\eta\simeq 1.48$. For the two-dimensional square lattice $\gamma(0)\simeq 1.57$, $\gamma(1)\simeq 1.47$, and $\eta\Theta\simeq 2.0$. The fractional variance of the distribution of r_n^2 is found to be appreciably smaller than the corresponding Gaussian value. Numerical data and graphs are presented for the free energy, entropy, and internal energy as functions of η.

I. INTRODUCTION AND SUMMARY

IN extremely dilute solutions of polymers the individual chain molecules are virtually isolated from one another and the thermodynamic and gross physical properties (viscosity, light scattering, etc.) of the solution depend directly on the mean configuration and free energy of a single molecule. The simplest model of a polymer molecule is a freely linked, completely random Gaussian chain[1,2] and this accounts reasonably well for the main features of the experimental observations. The chief difficulty in the way of improving the theory (and testing a more realistic model), however, is the problem of the *excluded volume*. A real polymer molecule cannot intersect itself and this introduces long-range correlations between different parts of the chain which invalidate the simple theory. A central problem is the dependence of the "size" of the molecule (usually characterized by the mean square end-to-end distance) on the degree of polymerization or the number of links n in the model chain. In the absence of excluded volume the chain may be treated as a Markovian random walk[3] and it then follows quite generally that

$$\langle r_n^2\rangle \simeq An, \qquad (n\to\infty). \tag{1}$$

The excluded volume destroys the Markovian nature of the walk and the corresponding behavior is not rigorously known although the mean-square size is certainly increased. The dependence of the free energy and other thermodynamic functions upon the excluded volume is also uncertain. Rigorous solution of these problems would be of considerable theoretical interest since relatively little is known about non-Markovian random walks. Despite a considerable literature[1,2,3] comparatively little progress has been made.

Most direct theoretical attacks have led to perturbation expansions incapable of revealing the behavior for large n (the effective expansion parameter increasing with n). More success has been achieved by numerical studies based on the *quasi-crystalline* or *lattice model* of a polymer molecule. The chain is represented by a random walk which at each step moves from one point of a regular lattice to the next via one of the $q=\sigma+1$ "bonds" radiating from each point. The effect of the excluded volume is represented by preventing the walk from visiting any lattice point more than once.

The numerical methods used to study this model fall naturally into two classes. On the one hand there is the statistical or Monte Carlo approach which has been used extensively by various authors[4,5] and especially by Wall and his collaborators.[6,7] On the other hand the problem may be studied by *exact* numerical calculation and extrapolation. The first attempt along these lines seems to have been made by W.J.C. Orr[8] as early as 1946. More recently Fisher and Sykes[9] have extended and developed this approach using methods which had already proved successful in other branches of statistical mechanics.[10,11] (Mention should also be made of the work of Teramoto and collaborators.[12])

[1] P. J. Flory, *Principles of Polymer Chemistry* (Cornell University Press, Ithaca, 1953), Chap. 14.

[2] R. J. Rubin, J. Chem. Phys. **20**, 1940 (1952); B. H. Zimm, W. H. Stockmayer, and M. Fixman, *ibid.* **21**, 1716 (1953). These papers and that cited in footnote 9 contain many other references to the literature.

[3] E. W. Montroll, J. Chem. Phys. **18**, 734 (1950).

[4] G. W. King, National Bureau of Standards Applied Mathematics Series (U. S. Government Printing Office, Washington, D. C.), No. 12, June 1951; M. N. Rosenbluth and A. W. Rosenbluth, J. Chem. Phys. **20**, 1360 (1952); R. S. Lehman and G. H. Weiss, J. Soc. Ind. Appl. Math. **6**, 257 (1958).

[5] J. M. Hammersley and K. W. Morton, J. Roy. Statist. Soc. **B16**, 23 (1954).

[6] F. T. Wall, L. A. Hiller, and D. J. Wheeler, J. Chem. Phys. **22**, 1036 (1954); F. T. Wall, L. A. Hiller, and W. F. Atchison, *ibid.* **23**, 913 (1955); **23**, 2314 (1955); **26**, 1742 (1957); F. T. Wall, R. J. Rubin, and L. M. Isaacson, *ibid.* **27**, 186 (1957).

[7] F. T. Wall and J. J. Erpenbeck, J. Chem. Phys. **30**, 634 (1959).

[8] W. J. C. Orr, Trans. Faraday Soc. **42**, 12 (1946).

[9] M. E. Fisher and M. F. Sykes, Phys. Rev. **114**, 45 (1959).

[10] C. Domb, Advances in Phys. **9**, 149 (1960).

[11] C. Domb and M. F. Sykes, J. Math. Phys. (to be published).

[12] E. Teramoto, M. Kurata, R. Chujo, C. Suzuki, K. Tani, and T. Kajikawa, J. Phys. Soc. Japan **10**, 953 (1955).

In practice the Monte Carlo method is restricted in accuracy by the inevitable statistical fluctuations, but quite long walks ($n=50$ to 1000) can be sampled. In this way Wall and his co-workers found considerable support for the relation

$$\langle r_n^2\rangle \approx An^{\gamma} \quad (n\to\infty), \tag{2}$$

where γ is significantly greater than unity as against $\gamma=1$ in Eq. (1). Indeed even if (2) is not the rigorously correct asymptotic result (and, of course, no numerical method can *prove* such a conjecture) it now seems fairly clear that a formula of this type is a valid approximation for real finite, polymer molecules. [The proportionality of mean-square size to n^{γ} with $\gamma>1$ was originally suggested, on somewhat inadequate theoretical grounds, by Flory (see work cited in footnote 1) as a basis for interpreting the observed dependence of the viscosity and light scattering of polymer solutions on the molecular weight.]

Wall also found that if c_n is the total number of n step non-self-intersecting random walks (i.e., with excluded volume operative) then

$$c_n \sim \mu^n, \tag{3}$$

where μ is a constant, "the effective coordination number," depending on the lattice. (Wall actually observed that the number of his sample walks was subject to an exponential law of "attrition," but this is equivalent to our statement.) Mathematical support for this result has been provided by Hammersley[6,13] who proved the existence of the limit

$$\lim_{n\to\infty} (1/n)\ \ln c_n = \ln\mu. \tag{4}$$

(This theorem and the strict bounds for μ developed by Frisch, Collins, and Friedman and Fisher[14] and Fisher and Sykes[9] are almost the only rigorous mathematical results available on the problem. The interesting bounds on $\langle r_n^2\rangle$ obtained by Rubin,[2] though almost certainly valid, do not seem to have been established with complete rigour). The results (3) and (4) imply that the free-energy, or entropy per link (or per monomer) of a polymer molecule approaches a limiting value independent of the total length.

On the basis of the Monte Carlo calculations it is impossible to find a more accurate asymptotic expression than (3) for c_n (and, correspondingly, for the free energy). By exact enumeration of the c_n for values of n from 10 to 15, however, Fisher and Sykes[9] discovered strong evidence for a relation of the form

$$c_n \approx Bn^{\alpha}\mu^n \tag{5}$$

with α approximately $\frac{1}{3}$ for all two-dimensional lattices (and about half this for three-dimensional lattices). The estimated values of μ obtained in this way were also considerably more accurate than those based on Monte Carlo calculations with the shorter chains of 50 to 100 steps.[9]

In the present paper we discuss the relation (5) in greater detail using improved extrapolation techniques and further data obtained recently.[15] This yields more accurate estimates for α (which suggest that α is exactly $\frac{1}{3}$ in two dimensions) and establishes that the asymptotic behavior is reliably indicated by the exact results for small n. We then go on to apply the method to the mean-square size. The behavior of the exact values of $\langle r_n^2\rangle$ for the plane square up to $n=10$ and for the simple cubic lattice up to $n=8$ is found to be smooth and supports Eq. (2). The extrapolated estimates for γ agree well with those of Wall.

The distribution of r_n^2 about its mean value is investigated by calculating the fourth moments $\langle r_n^4\rangle$. Extrapolation indicates that the limiting distribution of $\mathbf{r}_n$ differs appreciably from the Gaussian form [which has been assumed by most authors even when accepting (2)]. The fractional variance of r_n^2 for the plane-square lattice is found to achieve only 43% of its Gaussian value while for the simple cubic lattice the figure is approximately 68%.

The model considered above becomes appreciably more realistic if account is taken of the mutual interactions of polymer and solvent. Following Orr[8] these can be included by introducing a Boltzmann factor $\eta=\exp(-V_0/kT)$ for every nearest-neighbor contact of the chain with itself. The energy V_0 measures the energy of a polymer-polymer contact relative to the energies of polymer-solvent and solvent-solvent contacts. (As explained by Orr[8] it is not essential to this model of a polymer molecule in solution to assume that the solvent can be described by the *same* quasi-crystalline lattice as is appropriate to the polymer molecule.)

In an extremely good or "super-perfect" solvent V_0 is positive and large and η tends to zero. In the limit $\eta=0$ polymer-polymer contacts cannot occur and the model reduces to a random walk with no first-neighbor contacts (and no self-intersections). For this case, which is equivalent to an increased excluded volume, the corresponding walks have been enumerated exactly for the plane-square and triangular lattices (up to $n=14$ and $n=12$, respectively) and for the simple cubic lattice (up to $n=10$). The form of expression (5) is found to be still valid but the effective coordination numbers μ (and corresponding limiting free energies per link) are reduced. Furthermore the value of α changes from $\frac{1}{3}$

[13] J. M. Hammersley, Proc. Cambridge Phil. Soc. **53**, 642 (1957).

[14] H. L. Frisch, F. C. Collins, and B. Friedman, J. Chem. Phys. **19**, 1402 (1951). Note that the upper bounds quoted in this paper are incorrect. The lower bounds, however, are quite valid and the method used to derive them forms the starting point for the later developments of Fisher [M. E. Fisher, Discussions Faraday Soc. **25**, 200 (1958)].

[15] B. J. Hiley and M. F. Sykes, J. Chem. Phys. (to be published).

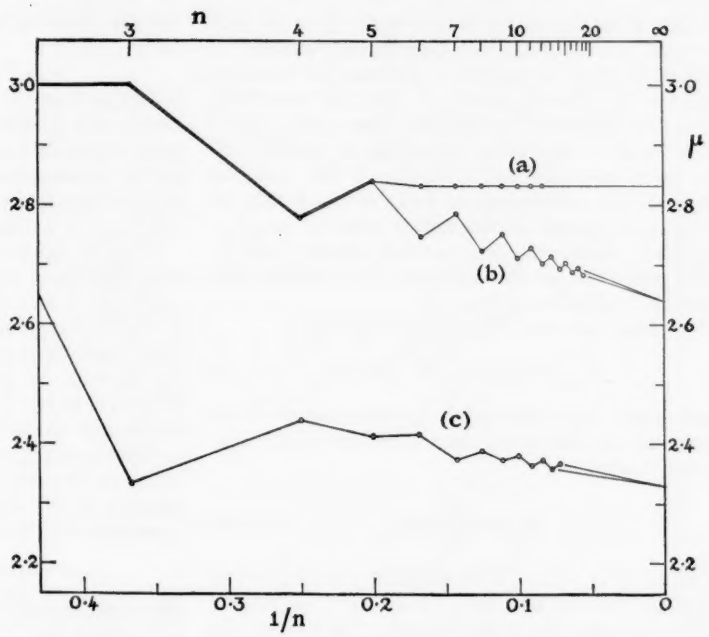

FIG. 1. Plot of the ratios $\mu_n = c_n/c_{n-1}$ vs $1/n$ for walks on the plane-square lattice (a) with only reversals and squares disallowed, (b) with no self-intersections of any order (c) with no self-intersections and no nearest-neighbor contacts.

to about $\frac{1}{8}$ for both the plane-square and plane-triangular lattices.

In order to study the mean-square size and thermodynamic properties more generally over a range of η we have used the analysis of the number of nearest-neighbor contacts in short chains presented by Orr.[8,16] Although this data extends only to eight steps on the plane-square lattice and six steps on the simple cubic it is sufficient, in conjunction with the more extensive data at $\eta=0$ and 1, to justify a preliminary investigation. (Further calculations are planned for larger values of n and for other lattices.) The detailed conclusions drawn are presented in the following sections but for convenience we summarize the main results here.

The mean square end-to-end distance appears to be proportional to n^{γ} in both good solvents ($0 \leq \eta \leq 1$) and poor solvents ($\eta > 1$), but the index γ depends on η, decreasing smoothly with increasing from $\gamma(0) \simeq 1.57$ in two dimensions, and $\gamma(0) \simeq 1.37$ in three dimensions. The existence of Flory's theta-point (at which the excluded volume effect is exactly compensated by favourable polymer-polymer contacts so that γ takes the Markovian value of unity) is clearly indicated in three dimensions (see Fig. 5). It occurs at a temperature determined by $\eta_\theta \simeq 1.48$. The index $\alpha = \alpha(\eta)$ in Eq. (5) also vanishes near this point as would be expected if the walk becomes truly Markovian. The two-dimensional data are less accurate in this region but a theta-point seems to occur at $\eta \simeq 2.0$.

The effective coordination number $\mu(\eta)$ which determines the limiting free energy per link as a function of temperature, rises smoothly with η increasing by about 50% in the range $\eta=0$ to $\eta=2$. The extrapolated values for $\mu(\eta)$ are probably accurate to 1% or better but the internal energy being a derivative of the free energy, cannot be determined with such precision. The entropy reaches a maximum at $\eta=1$ and falls nearly symmetrically by $0.125k$ and $0.14k$ (in two and three dimensions, respectively) as η approaches 0 and 2. The internal energies increase from zero at $\eta=0$ and reach values corresponding to about 0.18 nearest-neighbor contacts per link at $\eta=1$. These values are less than half those predicted by Orr's approximate formulas which are shown to be ill founded.

II. ASYMPTOTIC BEHAVIOR OF NONINTERSECTING WALKS

In this section we discuss the asymptotic behavior of c_n, the number of nonintersecting random walks of n steps, as revealed by the exact values for small n. Techniques for enumerating all walks for the basic excluded volume problem have been discussed by Fisher and Sykes[9] and by Sykes[17] and have been reviewed by Domb.[10] The actual figures for the plane-square, plane-triangular, simple cubic and various other lattices have been tabulated by Fisher and Sykes[9] and additional terms have been given recently by Sykes.[17]

To investigate the behavior of the c_n it is natural to consider the successive ratios

$$\mu_n = c_n/c_{n-1}, \qquad (n=1, 2, 3, \cdots; c_0=1). \quad (6)$$

[16] As explained in Sec. V a slight error has been discovered in this data for chains of eight links.

[17] M. F. Sykes, J. Math. Phys (to be published).

If these ratios approach a limit as $n\to\infty$ then this limit is equal to the "effective coordination number" μ defined by (4).[18] In practice, it is found that when the ratios μ_n are plotted against n^{-1} they lie remarkably close to a straight line of definite slope α which intersects the $n=\infty$ axis at μ_∞. This behavior is illustrated for the plane-square lattice in Fig. 1. The sequence of points (a) corresponds to walks in which only reversals and squares are disallowed[9] while the sequence (b) refers to the complete excluded volume problem. [The points (c) are for walks with first-neighbor contacts also forbidden; see below.]

The linear behavior of μ_n with n^{-1}, namely,

$$\mu_n\simeq\mu_\infty[1+(\alpha/n)], \qquad (n\to\infty) \tag{7}$$

may readily be understood[9,11] by regarding the c_n as coefficients in the power series expansion of the generating function

$$C(z)=\sum_{n=0}^{\infty}c_nz^n. \tag{8}$$

In virtue of (4) $C(z)$ has its singularity nearest to the origin on the real axis at $z=1/\mu$ which will be the radius of convergence of the series (8). The relation (7) implies that the dominant behavior near $z=z_c$ is

$$C(z)\approx K/(1-\mu z)^{1+\alpha}, \tag{9}$$

which in turn yields

$$c_n\approx Bn^\alpha\mu^n \qquad (n\to\infty). \tag{10}$$

Conversely this asymptotic form leads directly to (7) as a first approximation. Series of coefficients very similar to the c_n arise in many other statistical problems, in particular in the Ising model,[9] and the corresponding generating functions often have direct physical significance. The exact solutions available for some of these problems enable one to test the various methods, which we will now discuss, for estimating the asymptotic behavior from the initial sequences.[9,11]

A convenient method for estimating the limiting intercept $\mu_\infty=\mu$ is to calculate successive linear intercepts determined by alternate pairs of ratios μ_n according to

$$\mu_{\text{ext}}=\tfrac{1}{2}[n\mu_n-(n-2)\mu_{n-2}]. \tag{11}$$

(Alternate pairs are used in view of the even-odd oscillation of the ratios which is evident in Fig. 1). The chief uncertainty in this procedure is due to the (unknown) slope of the line (7) and the method tends to be less accurate the larger the value of α, since small irregularities in the μ_n are magnified. As shown by Sykes[15] this difficulty can be alleviated by making an initial estimate of the slope α with the aid of the formula

$$\alpha_{\text{ext}}=n(\mu_n-\mu_{\text{ext}})/\mu_{\text{ext}}, \tag{12}$$

and then forming the modified sequence

$$\mu_n{}^*=\mu_n n/(n+\alpha_{\text{ext}}). \tag{13}$$

It follows from (7) that these ratios will approach the limit μ with a negligible mean slope (ideally zero). The residual even-odd oscillation may be effectively damped out by forming the means $\frac{1}{2}(\mu_n{}^*-\mu_{n-1}{}^*)$. These consequently form a more regular sequence of estimates to μ which can be extrapolated accurately.

Detailed figures and graphs for the plane-square lattice have been given by Hiley and Sykes.[15] The initial estimates for the slope[9] suggest $\alpha\simeq\frac{1}{3}$ and on the scale of Fig. 1 the corresponding sequence of means of (13) is quite level. It may be compared with the sequence (a) for walks in which only reversals and squares are forbidden. In this latter case the problem is completely soluble and the limiting ratio and asymptotic behavior are known exactly and agree closely with the estimates based on the first dozen terms. The estimate for μ obtained in this way from the first 18 terms for the plane-square lattice is

$$\mu\simeq 2.6390\pm 5 \quad \text{(plane square)}.$$

(Here and elsewhere the uncertainty quoted is in the last decimal place.) This result is 2% lower than Wall's initial Monte Carlo estimates based on walks of up to 50 steps[6] but agrees closely with the more recent statistical estimates using walks of up to 800 steps, namely $\mu\simeq 2.6395\pm 15$. (In view of the positive slope α Wall's estimates which are based on log-plots, are expected to be slightly too high).[9] The agreement of these estimates to within 0.02% is strong evidence for the validity of the extrapolation techniques and shows that behavior for large n can be deduced with surprising accuracy from the exact values of the first few reasonably large terms.

Sykes and Hiley[15] also report additional terms for the plane triangular and simple cubic lattices. On the basis of the improved extrapolation techniques the values now estimated are

$$\mu\simeq 4.152\pm 3 \quad \text{(plane triangular)},$$

which confirms the estimate of Fisher and Sykes[9] within closer limits, and

$$\mu\simeq 4.683\pm 7 \quad \text{(simple cubic)},$$

which is slightly lower than the estimate of Fisher and Sykes although within their quoted limits. As yet no new data have been obtained for the body-centered or face-centered cubic lattices but a reexamination of the existing figures along the present lines indicates that the previously published estimates should also be reduced by about 0.15%.

It should perhaps be pointed out that uncertainties specified on these and similar estimates do not in any sense furnish rigorous bounds for the exact result. They represent, rather, reasonable confidence limits

[18] J. M. Hammersley, Phys. Rev. **118**, 656 (1960).

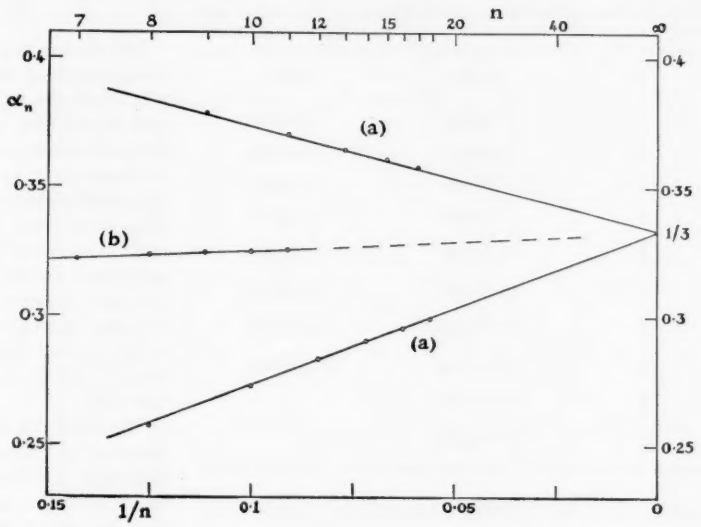

FIG. 2. Estimation of the index α from a plot of α_n vs $1/n$ for walks on (a) the plane-square lattice, (b) the plane-triangular lattice.

based, in the light of experience and known results, on the observed uniformity and consistency of the extrapolations.

General mathematical considerations and examination of comparable exactly soluble problems indicates that the linear behavior of the ratios μ_n with $1/n$ represents the dominant terms in an asymptotic expression for μ_n and leads one to expect the presence of higher terms of order $1/n^2$, $1/n^3$, etc. Thus generalizing (7), we may postulate,

$$\mu_n=\mu_\infty[1+(\alpha/n)+(\beta/n^2)+\cdots], \quad (n\to\infty), \quad (14)$$

where in view of the observed oscillations in the ratios, one must expect odd-even oscillations in the coefficient β (as would arise from a lower order singularity in $C(z)$ on the negative real axis). Clearly there are no really strong theoretical reasons for supposing that terms such as $1/n^{\frac{1}{2}}$, $(\ln n)/n^2$ or $1/n\ln n$ should not occur in (14) but as we will show, the numerical data seem to support the validity of (14). This in turn provides justification for an improved method of estimating the gradient α.

To examine this point suppose that μ_∞ is known precisely. Successive estimates of α based on (12) would, assuming (14), behave as

$$\alpha_n=\alpha+(\beta/n)+\cdots. \quad (15)$$

This implies the linearity of α_n with n^{-1} (neglecting the higher order terms) so that linear extrapolation would lead to an accurate value of α. In practice μ_∞ is not known exactly but one may use an estimated value obtained as described above. If the error in the estimate is $\Delta\mu$ the calculated values of α_n will differ in first order from (15) by an amount

$$\Delta\alpha_n=-(\Delta\mu/\mu_\infty)(1/n)^{-1}-(\Delta\mu/\mu_\infty)\alpha-(\Delta\mu/\mu_\infty)(\beta/n). \quad (16)$$

For large n the first term in this expression becomes important and the calculated values of α_n will curve away hyperbolically from the straight line (15). Conversely the observation of a curvature increasing systematically in one direction indicates an error in the value of μ_{ext} which may thus be adjusted to restore linearity. In this way consistent estimates of α and μ can be obtained simultaneously.

The first 16 values of c_n for the plane-square lattice were analyzed in this way and the results are presented graphically in Fig. 2(a) which is a plot of calculated values of α_n against n^{-1}. The pair of full lines in Fig. 2 have been drawn in accordance with the formula

$$\mu_n=2.6389\{1+\tfrac{1}{3}(1/n)-\tfrac{1}{10}[1+(-)^n5](1/n)^2\}. \quad (17)$$

It will be observed that the fit with the data is remarkably good. For $n>8$ the deviations in α_n never exceed 0.3% while agreement with the μ_n is correspondingly more accurate. As a test the values of c_{17} and c_{18} were predicted *before* their exact calculation had been undertaken. The predicted values based on Fig. 2(a) were (after rounding)

$$c_{17}\simeq 46\ 464\ 800, \qquad c_{18}\simeq 124\ 656\ 700,$$

while the exact values[15] are

$$c_{17}=46\ 466\ 676, \qquad c_{18}=124\ 658\ 732.$$

The errors of the predictions amount to only 4 parts in 10^5 and 1.6 parts in 10^5, respectively.

The coefficients α and β in (17) are simple fractions but if another estimate for μ were used their optimum

TABLE I. Mean square end-to-end distances $\langle r_n^2 \rangle$ for walks with no self-intersections on the plane-square and simple cubic lattices.

n	Square	Cubic
1	1.000000	1.000000
2	2.666667	2.400000
3	4.555556	3.880000
4	7.040000	5.553719
5	9.563380	7.234295
6	12.574358	9.070542
7	15.556169	10.897235
8	19.012846	12.845084
9	22.411359	
10	26.242539	

values would be different. The observed fitting limits are

$$\mu_\infty = 2.6389 \pm 5 \uparrow$$

which is consistent with the estimate quoted above, and, with a corresponding sense as indicated by the arrows,

$$\alpha = 0.333 \pm 5 \downarrow \quad \text{(plane square)}$$

$$\beta_{\text{odd}} = 0.40 \pm 3 \uparrow, \qquad \beta_{\text{even}} = 0.60 \mp 3 \downarrow.$$

In view of these figures it is hard to avoid the conclusion that the exact value of α for the plane-square lattice is $\frac{1}{3}$ as originally conjectured.[9]

Fewer terms are available for the triangular lattice and so these have been analyzed only by assuming the value for μ quoted above. The last five values of α_n calculated in this way are shown in Fig. 2(b). They lie close to a straight line whose extrapolated intercept is almost exactly $\frac{1}{3}$ (actually very slightly less). It is also remarkable that this line deviates by less than 1% from the mean of the two lines (17) which approximate the square lattice results. It seems highly plausible that α is also precisely $\frac{1}{3}$ for the plane triangular lattice and, indeed, has the same value for all related two-dimensional lattices.[9]

The data on the three-dimensional cubic lattices are at present insufficient to justify very detailed analysis. The values of α, however, appear to be the same in each case and certain, differ from those of the two-dimensional lattices. On the basis of the refined estimates for μ we find $\alpha \simeq 0.167 \pm 10$ which suggests that α might be exactly $\frac{1}{6}$ in three dimensions. (Owing to slightly high estimates for the limits μ the values of α estimated originally by Fisher and Sykes for these lattices were rather lower, lying between 0.14 and 0.15.[19])

[19] The limits on the estimates of α quoted by Fisher and Sykes for these lattices did not take full account of the uncertainties in μ.

III. MEAN DIMENSIONS

The rather detailed analyses of c_n, the numbers of nonintersecting walks, made in the previous section establishes the validity of the extrapolation procedures and shows that the smooth trends exhibited by the first half-dozen terms can be expected to continue as the sequence develops. To obtain accurate estimates it is always desirable to have a large number of terms preferably more than 12 but in most cases quite reliable estimates can be obtained (within appropriately wider confidence limits) from the first seven or eight terms. On these grounds it seems worthwhile examining the sequence of exact values of $\langle r_n^2 \rangle$ in a similar way. One might in any case expect $\langle r_n^2 \rangle$ to show smooth behavior as it is an *average* over the complete distribution of $\mathbf{r}_n$.

The exact calculation of the mean square end-to-end distance of nonintersecting walks is discussed in Appendix A where it is shown how the problem may be reduced to something more tractable and reliable than the direct summation of the individual contributions of all allowable walks. By using the methods expounded there we have calculated the first ten values of $\langle r_n^2 \rangle$ for the plane-square lattice and the first eight for the simple cubic lattice. These are presented in Table I. The method applies equally well to other lattices and the calculations could be extended by a few more terms without excessive labor. To calculate a substantially greater number would, however, be rather difficult, especially for three-dimensional lattices, although progress may be possible with the aid of a digital computer.

To analyze the behavior we consider the ratios

$$\nu_n = \langle r_{n+1}^2 \rangle / \langle r_n^2 \rangle, \qquad (n = 1, 2, 3, \cdots). \quad (18)$$

In the case of unrestricted walks, walks with no immediate reversals[20] and other soluble cases a limiting ratio ν_∞ exists and we may expect this to be true also with excluded volume. Since for all these problems

$$n \leq \langle r_n^2 \rangle \leq n^2, \quad (19)$$

the limit must be unity and this is confirmed by a plot of the ratios ν_n against $1/n$. The sequence of points are observed to approach a straight line of slope γ which extrapolates to $\nu_\infty = 1$. The linearity of the ratios with $1/n$ implies as before that

$$\langle r_n^2 \rangle \approx A n^\gamma, \quad (20)$$

which is in agreement with Wall's Monte Carlo calculations.[6,7] Since $\nu_\infty = 1$ a sequence of estimates for the index γ may be calculated from

$$\gamma_n = n(\nu_n - 1). \quad (21)$$

In accordance with the results of the previous section

[20] C. Domb and M. E. Fisher, Proc. Cambridge Phil. Soc. **54**, 48 (1958); see also Appendix A herein.

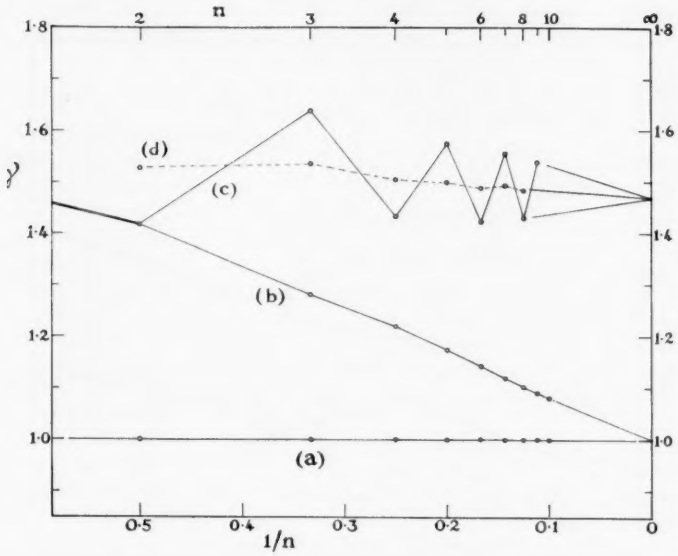

FIG. 3. Successive estimates of γ in the expression $\langle r_n^2\rangle \approx An^\gamma$ for walks of the plane-square lattice (a) with no restrictions, (b) with no immediate reversals (c) with no self-intersections. The sequence (d) is that of the means $\frac{1}{2}(\gamma_n+\gamma_{n+1})$ for case (c).

the series γ_n would also be expected to show a linear variation with $1/n$ and this turns out to be the case.

The sequence of points (a) in Fig. 3 are the values of γ_n for an unrestricted walk on the plane-square lattices; the slope is zero and the limit is $\gamma_\infty=\gamma=1$ as expected. The sequence (b) corresponds to a similar walk but with immediate reversals forbidden.[20] These points lie on a slightly irregular sloping curve which, however, clearly extrapolates to $\gamma_\infty=1$ as on general grounds it must.[3]

Finally the data of Table I for the complete excluded volume problem on the plane-square lattice yield the sequence (c). The points exhibit the characteristic odd-even oscillation about a straight line as observed in the walk ratios μ_n. The amplitude of oscillations can be markedly reduced by forming the means

$$\Gamma_n=\tfrac{1}{2}(\gamma_n+\gamma_{n+1}), \qquad (22)$$

which lie very close to a straight line of small slope and quite well defined intercept [(d) in Fig. 3]. To estimate the limit γ_∞ for the nonintersecting walks we may calculate as in the previous section the extrapolated intercepts defined by successive pairs of points. With an obvious notation we obtain from the γ_n the estimates

$$1.401(4,6) \qquad 1.509(5,7)$$

$$1.452(6,8) \qquad 1.480(7,9),$$

while the means Γ_n yield,

$$1.444(3,5) \qquad 1.459(4,6)$$

$$1.476(5,7) \qquad 1.470(6,8).$$

The average of the last two estimates is 1.473 and we thus adopt as final estimate

$$\gamma=1.47\pm2 \quad \text{(plane square)}.$$

This result may be compared with the results of statistical calculations. Earlier work[4,6] using chains of up to 50 steps led to a value of 1.45 but more recently using an "enriched" sampling technique which generated 1094 walks of 600 steps, Wall and Erpenbeck[7] have obtained the value 1.50. Unfortunately none of these estimates are accompanied by any numerical indication of the statistical deviations or fitting limits. Examination of the published graphs reveals, however, fluctuations of a magnitude which suggests a probable precision of 1 or 2% in the value of γ.[21] Since Wall's latest estimate differs by only 2% from our value (and lies only just outside our confidence limits) the agreement between the two results must be considered very satisfactory.

The data for the simple cubic lattice may be analyzed in the same way and the behavior of the γ_n with $1/n$ is very similar to that of Fig. 3 except that the oscillations are only about two-fifths as large. Extrapolation leads to the estimate

$$\gamma=1.21\pm2 \quad \text{(simple cubic)}.$$

This is based upon fewer terms than were used for the plane-square lattice and is thus somewhat less certain. It agrees closely with the original estimate of 1.22 obtained by Wall[6] and Rosenbluth and Rosenbluth.[4]

[21] Rosenbluth and Rosenbluth (work cited in footnote 4) quote some direct estimates for $\langle r_n^2\rangle$. Their value for $n=8$ differs from the exact result by more than 1% which supports our conclusion regarding probable accuracy. W. H. Stockmayer [Makrmol. Chemie **35**, 54 (1960)] considers that wall and Erpenbeck's data could be fitted equally well with the $\gamma=1.20$ rather than 1.18.

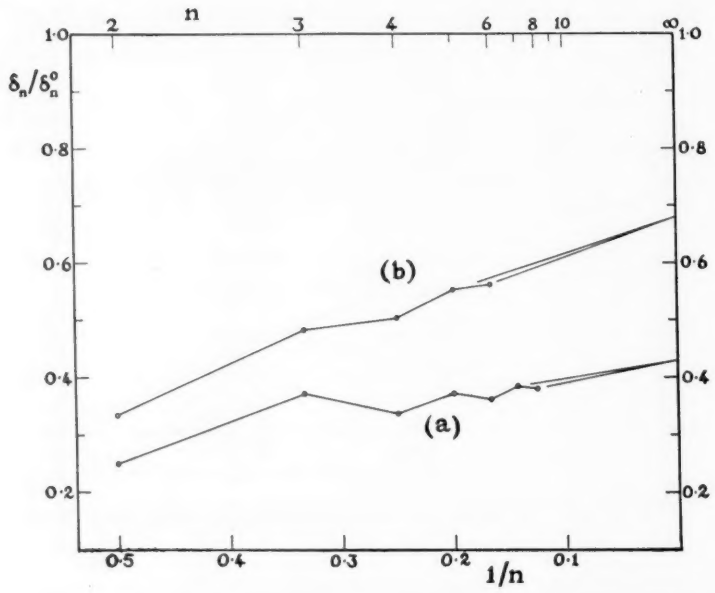

FIG. 4. Plots of δ_n/δ_n^0 the relative fractional variance of r_n^2, for nonintersecting walks (a) on the plane-square lattice and (b) on the simple cubic lattice. (For a Gaussian distribution $\delta_n/\delta_n^0=1$.)

For walks of 50 steps or so the same value applied to the tetrahedral lattice,[6] but the recent work of Wall and Erpenbeck[7] in which walks of 800 steps on the tetrahedral lattice were sampled lead to the lower value 1.18. It is possible that a Monte Carlo result based on longer chains on the simple cubic lattice would also lead to a lower value. The comments made above regarding the statistical errors apply here with equal force but, in any case, the differences between the various estimates amount only to a few percent.[21]

If the value of γ is known, the limiting constant A in (20) may be estimated by extrapolating $\langle r_n^2\rangle/n^\gamma$. In practice the extrapolation may be performed quite accurately but the result is very sensitive to changes in the estimated value of γ. We confine ourselves to reporting the estimate $A=0.87\pm5$ for the plane-square lattice. The uncertainty quoted is almost totally due to the limits of uncertainty in γ. A value of $\gamma=1.45$ leads to $A=0.92$ which agrees closely with the figure given by Rosenbluth and Rosenbluth.[4]

In the limit $n\to\infty$ the distribution of end-to-end distances $\mathbf{r}_n$ becomes Gaussian for an unrestricted random walk and this remains true for restricted walks provided the correlations extend back only a finite number of steps. It is a matter of both theoretical and practical interest to know if this result is still valid for nonintersecting walks. The point may be investigated by studying the behavior of higher moments of the distribution of $\mathbf{r}_n$. To this end we have calculated the exact fourth moments $\langle r_n^4\rangle$ for the plane-square and simple cubic lattices up to $n=8$ and $n=6$, respectively. The values were derived from the detailed data given by Orr[8] which is discussed further in the following sections.

To analyze the behavior we have evaluated the fractional variance of r_n^2, namely,

$$\delta_n=\langle(r_n^2-\langle r_n^2\rangle)^2\rangle/\langle r_n^2\rangle^2$$
$$=\langle r_n^4\rangle/\langle r_n^2\rangle^2-1. \tag{23}$$

For the unrestricted walks it is not difficult to show that

$$\delta_n^0=(n-1)/n \quad \text{(plane square)} \tag{24}$$

and

$$\delta_n^0=2(n-1)/3n \quad \text{(simple cubic)}, \tag{25}$$

which in the limit $n\to\infty$ yield the Gaussian values appropriate to two and three dimensions, respectively. In Fig. 4 the reduced variances δ_n/δ_n^0 have been plotted versus $1/n$ for both lattices. The two sequences of points lie close to definite straight lines (see note added in proof at end of article) which are readily extrapolated to determine the limiting intercepts $\delta_\infty/\delta_\infty^0$. If the limiting distribution were Gaussian $\delta_\infty/\delta_\infty^0$ would be unity but on the basis of Fig. 4 it seems improbable that a Gaussian distribution is approached. We estimate (see note added in proof)

$$\delta_\infty/\delta_\infty^0=0.43\pm2 \quad \text{(plane square)}$$
$$=0.68\pm2 \quad \text{(simple cubic)},$$

which indicates that the effect of the excluded volume is less marked in three dimensions than in two as might be expected.

Significant deviations from Gaussian behavior have also been revealed by Wall and Erpenbeck's studies of the mean internal dimensions and the mean-square

radius of gyration of nonintersecting walks.[22] (These parameters are required in the interpretation of light scattering experiments.)

IV. NEAREST-NEIGHBOR EXCLUSION

As explained in the introduction, a realistic model of a polymer molecule in solution should take into account the forces of interaction between polymer and solvent. The theory should then reveal what effect the interactions have on the number of configurations and the mean size and should predict any changes in the parameters μ, α, and γ. The simplest case, which we examine first, is that of a very good or "super-perfect" solvent in which nearest-neighbor polymer-solvent contacts are energetically so favorable compared to polymer-polymer contacts that the latter never occur. This leads effectively to an increase in the excluded volume since nearest-neighbor contacts as well as self-intersections are now forbidden.[23] This situation also serves as a model for the additional steric hindrances that can arise from bulky side groups attached to the main polymer chain.[23]

We have calculated $c_n(0)$, the exact number of walks subject to these restrictions, for the plane-square and plane-triangular lattices up to 14 and 12 steps, respectively, and for the simple cubic lattice up to 10 steps. These data are presented in Table II. The enumeration was performed, along lines similar to those explained in Appendix A, by subtracting the contributions of higher-order nearest-neighbor contacts and self-intersections from the known number of walks subject only to lower-order restrictions. For this purpose the recurrence relations

$$d_{n+1}=2d_n+d_{n-1} \quad \text{(plane square)}, \tag{26a}$$

$$d_{n+1}=3d_n, \quad \text{(plane triangular)}, \tag{26b}$$

$$d_{n+1}=4d_n+d_{n-1} \quad \text{(simple cubic)}, \tag{26c}$$

were used to generate the number of walks with no nearest-neighbor loops of four steps or less. The first possible nearest-neighbor contacts for these walks occur on the seventh, fifth, and fifth steps, respectively, and are not difficult to enumerate directly with the aid of known data.[9,10]

TABLE II. Values of $c_n(0)$ the number of n steps walks with no nearest-neighbor contacts (or self-intersections) on the plane-square, plane-triangular, and simple cubic lattices.

n	Square	Triangular	Cubic
1	4	6	6
2	12	18	30
3	28	54	126
4	68	162	534
5	164	474	2214
6	396	1398	9246
7	940	4074	38142
8	2244	11898	157974
9	5324	34554	649086
10	12668	100302	2674926
11	29940	290334	
12	71012	839466	
13	167468		
14	396204		

The behavior of the numbers $c_n(0)$ can be analyzed just as in Sec. II to yield estimates of μ and α. The variation of the ratios $\mu_n(0)$ with $1/n$ is again linear as can be seen from the results for the plane-square lattice displayed in Fig. 1(c). The irregularities for small n are slightly more marked but this is not surprising in view of the reduced number of configurations contributing to the total numbers of walks at a given stage. Extrapolation yields the estimates:

$$\mu(0)=2.329\pm 6$$

$$\alpha(0)=0.20\pm 2, \quad \text{(plane square)}$$

$$\mu(0)=2.844\pm 6$$

$$\alpha(0)=0.20\pm 2, \quad \text{(plane triangular)}$$

and

$$\mu(0)=4.050\pm 6$$

$$\alpha(0)=0.15\pm 1 \quad \text{(simple cubic)}.$$

Comparison with the estimates given earlier for walks with allowed nearest-neighbor contacts shows that the effective coordination numbers μ are appreciably reduced by the increased excluded volume. [That this must be so can be shown rigorously by deriving upper bounds for $\mu(0)$ from the recurrence relations (26) and their generalizations.[9,14]] As is to be expected the reduction is greatest for the triangular lattice where it amounts to 31.5%. For the loose-packed square and simple cubic lattice the reductions are only 11.7% and 13.5%, respectively.

A rather less obvious effect is the change in the indices α. Both plane lattices exhibit the *same* marked reduction from $\alpha=\frac{1}{3}$ to $\alpha\simeq\frac{1}{5}$. For the simple cubic lattice only a slight reduction in α is indicated although the numerical values are relatively less certain (see also the results of the next section and Fig. 7). The agreement between the values for the triangular- and plane-square lattices confirms the general impression (obtained from a variety of statistical problems on lat-

[22] F. T. Wall and J. J. Erpenbeck, J. Chem. Phys. **30**, 637 (1959).

[23] Statistical calculations for a walk of this type on the three-dimensional tetrahedral lattice have been performed by F. T. Wall, L. A. Hiller, and W. F. Atchison [J. Chem. Phys. **26**, 1742 (1957)].

TABLE III. Values of $f_{n,t}(r^2)$ (the number of n step walks of square end-to-end distance r^2 with exactly t nearest-neighbor contacts but no self-intersections) on the plane-square net for $n=8$. (The asterisks denote corrections to Orr's figures.)

	t				
r^2	0	1	2	3	4
64	4				
50	64				
40	224				
36	120	48			
34	448	0			
32	280	0			
26	352	352	32		
20	272	544	128		
18	96	288	96		
16	128	240	120	16	
10	144	304	384*	112	
8	56	112	192	80	8
4	40	64	120*	128	16
2	16	80	0	192	16

tices[9,11]) that the nature of the dominant singularity of the generating functions depends primarily on dimensionality and only to a limited extent if at all on the detailed structure of the lattice.

V. MEAN SIZE WITH SOLVENT INTERACTIONS

To investigate the effect of solvent interactions on the mean-square size we consider directly the more general model in which a Boltzmann weighting factor

$$\eta=\exp(-V_0/kT), \tag{27}$$

is introduced for every nearest-neighbor contact of the chain with itself.[8] For a perfect solvent $\eta=1$ and only the excluded volume effect is operative. In a "super-perfect" solvent $0\leq\eta<1$ and the chain will tend to expand due to the effective nearest-neighbor repulsion, while in a poor solvent $\eta>1$ and the chain contracts.

If $f_{n,t}(r^2)$ is the number of nonintersecting walks of n steps which have exactly t nearest-neighbor contacts and a square end-to-end separation r^2 the over-all mean-square size as a function of η is given by

$$\langle r_n^2(\eta)\rangle=\sum_{r^2} r^2\sum_{t=0} f_{n,t}(r^2)\eta^t/\sum_{r^2}\sum_{t=0} f_{n,t}(r^2)\eta^t. \tag{28}$$

To evaluate $\langle r_n^2(\eta)\rangle$ numerically one must know the double distribution $f_{n,t}(r^2)$. The enumeration and classification of the walks needed to determine this distribution is a relatively formidable task once n exceeds 4 or 5. We have not, as yet, endeavored to go further than Orr who in 1946, presented complete results for the plane-square lattice up to eight steps and for the simple cubic lattice up to six steps.[8,24] We have cross checked this data and have discovered one error in the distribution for $n=8$ on the plane-square lattice. (Note that Orr tabulates $\frac{1}{2}f_{n,t}(r^2)$ and that his n denotes the number of "atoms" in the chain. This is one more than the number of links which we denote by n). An impression of the variety of terms arising can be obtained from Table III which shows the corrected distribution for $n=8$.

Using this data we have calculated the sequences of $\langle r_n^2(\eta)\rangle$ for values of η in the range $0\leq\eta<2.5$. Although the number of terms available for extrapolation is rather limited (especially for the simple cubic lattice) it is sufficient to give a fair indication of the variation of the asymptotic behavior with η. Reasonably accurate estimates of the index $\gamma(\eta)$ may be found by following the procedures of Sec. III and being guided by the more accurately known behavior at $\eta=1$.

The results are presented graphically in Fig. 5. (The broken curves indicate the range of uncertainty in the extrapolations.) For the extreme case $\eta=0$ considered in the previous section we find

$$\gamma(0)=1.57\pm6 \quad \text{(plane square)}$$

and

$$\gamma(0)=1.37\pm5 \quad \text{(simple cubic)}.$$

As might be expected these values are significantly higher than at $\eta=1$ where only the normal excluded volume acts. [In any case $\gamma(\eta)$ cannot *decrease* as η decreases.] The result for the simple cubic lattice receives some support from Wall's corresponding calculations for the tetrahedral lattice[23] which yielded the very similar value $\gamma(0)=1.38$. Since, as we noted above, the indices seem to depend primarily on dimension it

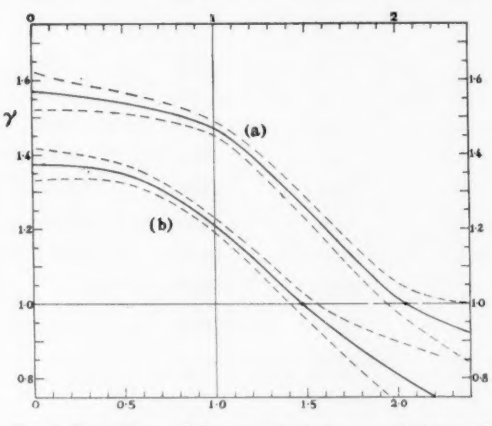

FIG. 5. Dependence of the mean-size index γ on the interaction parameter η for (a) the plane-square lattice and (b) the simple cubic lattice. (The broken curves indicate the range of uncertainty.)

[24] Orr did not discuss the implications of this data for the mean size. His intention to do this appears to have been thwarted by his untimely death.

seems likely that a Monte Carlo calculation for the simple cubic lattice with $\eta=0$ would lead to the same value in agreement with our estimate.[25] We may expect, similarly, that our estimates for other values of η will differ by no more than a few percent from any statistical estimates based on walks of 50 to 1000 steps.

In poor solvents ($\eta>1$) the index γ falls off rapidly indicating appreciable contraction of the chain. In agreement with Flory's arguments[1] our results indicate definitely the existence of a *theta point* at which $\gamma=1$ (so that $\langle r_n^2\rangle$ is proportional n as in a Markovian model). For the three-dimensional simple cubic lattice we find

$$\eta_\Theta=1.48\pm.6 \quad \text{(simple cubic)},$$

corresponding to a theta temperature

$$T_\Theta=[0.26\pm.3](V_0/k) \quad \text{(simple cubic)}.$$

For the plane-square lattice the extrapolations become less reliable when $\eta>1.7$, but we estimate

$$\eta_\Theta=2.04\pm.15,$$

$$T_\Theta=[0.14\pm.2](V_0/k) \quad \text{(plane square)}.$$

The present evidence for the square lattice is not strong enough, however, to disprove the conjecture $\eta_\Theta=\infty$. Physically, values of η exceeding 1.5 or 2.0 are not very significant since polymer molecules in solution then tend to attract one another so that coagulation and eventually phase separation set in. In this case a single chain is no longer a satisfactory model. Theoretically, however, the limit $\eta\to\infty$ is interesting since the chain collapses into a closely packed configuration of a maximum diameter $d^{\frac{1}{d}}n^{1/d}$ where d is the dimensionality of the lattice. For the simple cubic lattice this implies that $\gamma(\infty)\leq\frac{2}{3}$ so that, assuming $\gamma(\eta)$ is a continuous function of η a theta point *must* occur for some finite value of η. In the case of plane lattices we only obtain $\gamma(\infty)\leq 1$ so that a theta point *need not* exist.

In the straightforward "single contact" or lowest-order cluster expansion theory the excluded volume per atom is given by

$$v(T)=\int\{1-\exp[-V(r)/kT]\}d\tau, \tag{29}$$

where $d\tau$ is a volume element. The theta point can then be defined by $v(T_\Theta)=0$. In adapting this theory to the lattice model it seems reasonable to take some account of the two sites in the nearest-neighbor shell of an "atom" of the chain which are completely excluded by the two adjacent atoms in the chain. This leads to the rough theoretical estimate

$$\eta_\Theta\simeq(q+1)/(q-a), \tag{30}$$

with a lying between 1 and 2. If we take $\alpha=1.5$ we obtain for the simple cubic ($q=6$) and plane-square ($q=4$) lattices $\eta_\Theta\simeq1.56$ and $\eta_\Theta\simeq2.0$, respectively. These values correspond quite reasonably with our direct estimates and suggest that the plane-square lattice really does have a theta point at finite η.

VI. THERMODYNAMIC FUNCTIONS

In this section we consider the thermodynamic and statistical properties of the general model or arbitrary η. If

$$c_{n,t}=\sum_{r^2} f_{n,t}(r^2) \tag{31}$$

is the number of n-step nonintersecting walks with precisely t nearest-neighbor contacts, the configurational partition function for a chain of n steps is

$$Q_n(T)=c_n(\eta)=\sum_{t=0}^{\frac{1}{2}(q-2)n} c_{n,t}\eta^t. \tag{32}$$

(The notation $c_n(\eta)$ is consistent with our previous usage.) The upper limit for t derives from the observation that ignoring the unimportant end effects, each point of a chain can be in nearest-neighbor contact with no more than $q-2$ other points of the chain. The effective coordination number $\mu(\eta)$ can be defined, as before, by

$$\ln\mu(\eta)=\lim_{n\to\infty}(1/n)\ln c_n(\eta), \tag{33}$$

and by (32) this is directly related to the limiting free energy per link of a long chain,

$$\Delta F(\eta)=\lim_{n\to\infty}(F_n/n)=-kT\ln\mu(\eta),$$

$$=V_0\ln\mu(\eta)/\ln\eta. \tag{34}$$

The asymptotic relation

$$c_n(\eta)\approx B(\eta)n^{\alpha(\eta)}[\mu(\eta)]^n, \tag{35}$$

which was shown to hold when $\eta=0$ or 1 leads to the general expression

$$F_n(\eta)\approx -kT[n\ln\mu(\eta)+\alpha(\eta)\ln n], \tag{36}$$

for the free energy of a finite chain.[9] Other thermodynamic functions may be derived in the standard way by differentiating the free energy and hence may be calculated if $\mu(\eta)$ and $\alpha(\eta)$ are known.

The mean number of nearest-neighbor contacts per link of a chain of n links is

$$p_n(\eta)=\langle t_n\rangle/n=n^{-1}\sum_{t=0} tc_{n,t}\eta^t/\sum_{t=0} c_{n,t}\eta^t,$$

$$=\eta(\partial/\partial\eta)n^{-1}\ln Q_n(\eta). \tag{37}$$

In a long chain $\langle t_n\rangle$ becomes proportional to n and $p_n(\eta)$ approaches a limit given by

$$p(\eta)=\lim_{n\to\infty} p_n(\eta)=\eta(\partial/\partial\eta)\ln\mu(\eta). \tag{38}$$

[25] It should be noted, however, that Wall found evidence of a lower value of γ for walks of 50 steps or more although it seems possible that this was just a reflection of the statistical uncertainties.

The mean internal energy per link of a long chain is then simply

$$\Delta U(\eta) = V_0 p(\eta) \tag{39}$$

and the limiting entropy per link is given by

$$\Delta S/k = \ln\mu(\eta) - p(\eta)\ln\eta. \tag{40}$$

Some general properties of $\mu(\eta)$ and the thermodynamic functions may be derived theoretically. Thus for small η

$$p(\eta) \approx n g_0 \qquad (\eta \to 0), \tag{41}$$

where, by (37),

$$g_0 = \lim_{n\to\infty} n^{-1}(c_{n1}/c_{n0}). \tag{42}$$

From (38) it then follows that

$$\mu(\eta) \approx \mu(0)(1+g_0\eta), \qquad (\eta \to 0) \tag{43}$$

and from (40),

$$\Delta S/k \approx \ln\mu(0) + g_0\eta|\ln\eta|, \qquad (\eta \to 0). \tag{44}$$

By differentiating (40) and using (38) one derives

$$(\partial/\partial\eta)(\Delta S/k) = -\ln\eta(\partial p/\partial\eta), \tag{45}$$

which implies that the entropy exhibits a maximum at $\eta = 1$, where it has the value $k\ln\mu(1)$.

As $\eta \to \infty$ the mean number of contacts per link tends to an upper bound

$$p(\infty) = \tfrac{1}{2}(q-2), \tag{46}$$

which follows from the argument given for $t_{\max}$. This limit has the values 1 and 2 for the plane-square and simple cubic lattices, respectively. As mentioned in the previous section the behavior for large η is not very relevant to the physics of polymer solutions but as a matter of mathematical interest we record the limiting expression

$$-\Delta F/kT = \ln\mu(\eta) = p(\infty)\ln\eta + \ln\kappa + O(1/\eta), \qquad (\eta \to \infty), \tag{47}$$

$$\Delta S/k = \ln\kappa + O(1/\eta), \quad (\eta \to \infty), \tag{48}$$

where the constant

$$\kappa = \exp[\lim_{n\to\infty} n^{-1}\ln c_{n,t_{\max}}] \tag{49}$$

is the effective coordination number of an infinite, fully, closely packed chain. Orr has estimated that $\kappa \simeq 1.4$ for the plane-square lattice and $\kappa \simeq 1.9$ for the simple cubic lattice.[8]

To make further progress in the evaluation of the thermodynamic quantities one must turn to the numerical data. In Sec. II and IV quite accurate estimates were obtained for $\mu(\eta)$ and $\alpha(\eta)$ at the points $\eta = 1$ and $\eta = 0$. For intermediate and larger values of η the same extrapolation techniques can be used to estimate $\mu(\eta)$ and $\alpha(\eta)$ from the ratios $\mu_n(\eta) = c_n(\eta)/c_{n-1}(\eta)$. We have calculated values of $c_n(\eta)$ from Orr's data.[8] Since the number of terms is relatively limited the accuracy of the estimates is not as high as at $\eta = 1$ and $\eta = 0$. Nonetheless in the range $0 \leq \eta \leq 1.8$ the uncertainties in $\mu(\eta)$ are less than 1%. The results are presented graphically in Figs. 6 and 7. (The broken lines again indicate the confidence limits.)

The effective coordination numbers $\mu(\eta)$ increase smoothly and increasingly rapidly as η increases. The points at which $\mu(\eta) = q-1 = \sigma$ (the value for walks with no reversals) is

$$\eta_\sigma = 1.59 \pm 2 \quad \text{(plane square)},$$
$$= 1.29 \pm 3 \quad \text{(simple cubic)},$$

while the freely linked value, $\mu(\eta) = q$ is reached at

$$\eta_q = 2.7 \pm 1 \quad \text{(plane square)},$$
$$= 2.00 \pm 6 \quad \text{(simple cubic)}.$$

The corresponding theta points (see previous section) fall between η_q and η_σ and the ratios η_q/η_Θ is close to 1.33 for both lattices.

For reasons which seem to have no obvious physical basis the index $\alpha(\eta)$ exhibits a maximum near $\eta = 1$ on the plane-square lattice and near $\eta = 0.5$ on the simple cubic lattice. In the latter case $\alpha(\eta)$ vanishes and changes sign at $\eta_0 = 1.44 \pm 3$ which is rather close to the

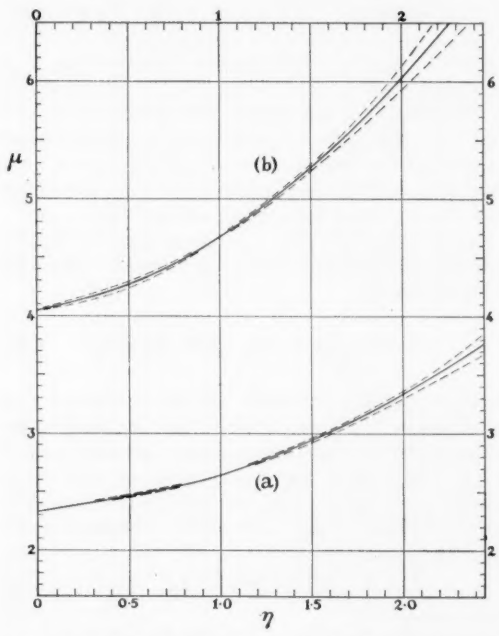

FIG. 6. Variation of the effective coordination number μ with the interaction parameter η for (a) the plane-square lattice and (b) the simple cubic lattice.

theta point 1.48±6. If the walk becomes truly Markovian at the theta-point the relation $\eta_0=\eta_\Theta$ should hold exactly. For the plane-square lattice α seems to vanish before the theta point is reached but the limits of uncertainty are sufficiently great to allow the possibility of coincidence.

The mean number of contacts per link $p(\eta)$ can be estimated through (38) by numerical or graphical differentiation of $\ln\mu(\eta)$ or directly by extrapolating the values of $p_n(\eta)$ vs $1/n$. The results of these two methods agree to within the accuracy attainable, namely about 10%. The estimated behavior of $p(\eta)$ for the plane-square lattice is shown in Fig. 8 [curve (a)]. The values for the simple cubic in the range $0\leq\eta\leq 2$ are very similar but lie some 5 to 10% higher. At $\eta=0$ we find

$$g_0=(\partial p/\partial\eta)_0=0.12\pm 2$$

for both lattices in agreement with Orr.[8] In the physically important region near $\eta=1$ we may write

$$p(\eta)\simeq p(1)+b(\eta-1), \tag{50}$$

where, for the plane-square lattice,

$$p(1)=0.180\pm 6, \qquad b=0.37\pm 4.$$

These values for $p(\eta)$ are considerably lower than those predicted by approximate formulas developed by Orr[8] (who only fitted his data at $\eta=0$ and $\eta\to\infty$). At $\eta=1$ Orr's formulas yield 0.37 for the plane-square lattice and 0.84 for the simple cubic lattice. These results, however, are quite inconsistent with (38) and the accurately known values of $\mu(0)$ and $\mu(1)$. (Orr's formulas for $\mu(\eta)$ are also seriously in error since at $\eta=1$ they predict values of μ exceeding $q-1$ which is clearly impossible.)

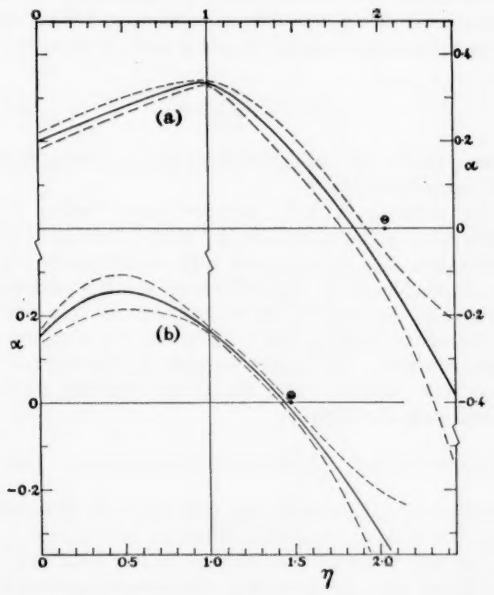

FIG. 7. Dependence of the index α on the interaction parameter η for (a) the plane-square lattice and (b) the simple cubic lattice. Note the vertical displacement between the axes for the two curves. The approximate theta points are indicated by Θ.

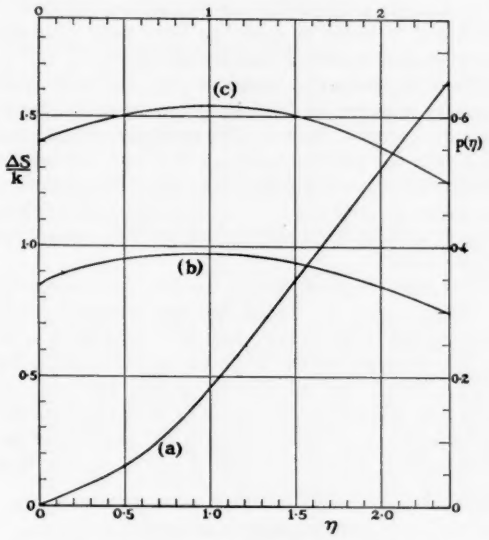

FIG. 8. Variation with η of (a) the limiting number of contacts per link $p(\eta)$ and (b), and (c) the limiting entropy per link for the plane-square and simple cubic lattices, respectively.

Orr seems to have realized that his results might be unreliable in this region since he endeavored to make an independent statistical estimate of $p(1)$ for the plane-square lattice. He obtained a value of 0.42 from a random chain of 3300 links and this seemed in reasonable agreement with the predictions of his formulas. Orr does not give very precise details of the statistical procedure used to generate this random walk but his remarks that "the relative directions of successive links were chosen at random, *blocking configurations being excluded*" suggests that whenever the random walk would have intersected itself the direction of the next step was chosen at random from one of the *remaining* allowable possibilities. Unfortunately this method leads to serious bias in favor of a walk with many contacts. This can be seen intuitively by noting that as the walk is prevented from dying whenever it approaches itself it must continue life in the close vicinity of previously visited sites. It does not seem possible to evaluate exactly what the error will be for large n but detailed calculation for $n=3$, 4, 5, and 6 shows that the expected number of contacts obtained this way are too large by factors of 1.000, 1.250, 1.342 and 1.531, respectively. These figures seem to be approaching a limit greater than 2.0 which suggests that Orr's estimate should be reduced to 0.2 or less. The statistical

data thus gives support to our estimate rather than to Orr's but it would be useful to have more extensive and unbiased statistical calculations for $p(\eta)$.

From the estimated values of $\mu(\eta)$ and $p(\eta)$ quite accurate estimates of the entropy can be made (better than 2% except at large η). The results are represented by curves (b) and (c) in Fig. 8. For both lattices the entropy falls almost symmetrically about the maximum, the values at $\eta=0$ and $\eta=2$ being about $0.125k$ (plane square) and $0.14k$ (simple cubic) per link lower than the maximum.

Note added in proof. Recent machine calculations by C. Domb and J. L. Martin (private communication) have yielded values of $\langle r_n^2\rangle$ and $\langle r_n^4\rangle$ for n up to 12 on the plane-square lattice. When the points representing this additional data are plotted on Fig. 3(c) and (d) (two more points) and on Fig. 4(a) (four more points) they are found to lie very close to our previous extrapolation lines. Our estimates for γ and $\delta_\infty/\delta_\infty{}^0$ are thus confirmed within closer limits.

ACKNOWLEDGMENTS

We are indebted to Dr. M. F. Sykes for assistance with the configurational data and to Professor C. Domb for comments on the manuscript. The interest of Professor J. T. Randall is gratefully acknowledged. One of us (B.J.H.) is indebted to the Department of Scientific and Industrial Research for a maintenance grant.

APPENDIX A

Exact Calculation of the Mean-Square Dimensions of Nonintersecting Walks

If $f_n(\mathbf{r})$ is the *number* of random walks of a specified type which reach the lattice point at $\mathbf{r}$ on the nth step, then the mean square end-to-end distance is defined by

$$\langle r_n^2\rangle = U_n/F_n, \tag{A1}$$

where

$$U_n = \sum_{\mathbf{r}} \mathbf{r}^2 f_n(\mathbf{r}) = \sum_{\text{walks}} \mathbf{r}_n^2, \tag{A2}$$

and

$$F_n = \sum_{\mathbf{r}} f_n(\mathbf{r}). \tag{A3}$$

For the exact calculation of the mean-square size of nonintersecting walks we know (or can find) $F_n=c_n$ the total number of nonintersecting walks, by previous work[9] and so the problem reduces to the determination of U_n, the appropriate square-size sum. To evaluate U_n one could, of course, construct explicitly all possible nonintersecting walks (by drawing or numerical specification) and determine the end-to-end distance for each one in turn. With a high-speed computer this method is probably feasible but with desk machines as n increases above 5 or 6 it rapidly becomes impractical and unreliable.

An alternative method is to compare the nonintersecting walks with a class of walks for which the square-size sum is known in closed form and to correct this by subtracting the unwanted contributions from the (relatively few) walks which do intersect. The more classes of self-intersection that can be excluded by the exact formula the fewer terms need to be removed. On the other hand, the derivation of the formula and its expression, become more involved (see for example, Montroll[3]). The simplest compromise is to use walks in which only *immediate reversals* are forbidden, all higher orders of self-intersection such as triangles and squares being allowed.

For walks with no immediate reversals on a regular lattice of coordination number $q=\sigma+1$ in any number of dimensions it is not difficult to show (see, for example, Domb and Fisher[20] and Flory[26]) that the square-size sum is

$$S_n = \sum_{\text{no reversals}} \mathbf{r}_n^2 = (\sigma+1)(\sigma-1)^2 \times\{[(\sigma^2-1)n-2\sigma]\sigma^{n-1}+2\}. \tag{A4}$$

For the plane-square lattice, for example, this is simply $(8n-6)3^{n-1}+2$. Now the set of walks with no reversals may be divided into disjoint classes in which the *first* self-intersection occurs at $\mathbf{r}_{(l)}$ on the lth step ($l=3, 4, \cdots n$). Each such self-intersection defines a "tadpole" $t(l)$ of l steps, formed of a polygonal head and nonintersecting tail which might be of zero length. As the "no-reversal random walks" proceed beyond the first intersection each tadpole makes a contribution to the square-size sum S_n which must be subtracted. Thus the square-size sum for nonintersecting walks is given by

$$U_n = S_n - \sum_{l=3}^{n} D_n(l), \tag{A5}$$

where $D_n(l)$ is the total contribution to S_n arising from all tadopoles of l steps.

To evaluate $D_n(l)$ for $n>l$ we must consider the addition of a "no-reversal walk" of $n-l$ steps and end separation $\mathbf{r}_{n-l}$ to a tadpole with its intersection at $\mathbf{r}_{(l)}$ formed by an lth step with vector $\mathbf{s}_{(l)}$. It is essential to specify the direction of the tadpole's lth step since if the added random walk commences in the opposite direction along this step it violates the "no-reversal" rule. The over-all square size of the resulting no-reversal walk of n steps is

$$\mathbf{R}_n^2(l) = (\mathbf{r}_{(l)}+\mathbf{r}_{n-l})^2 = \mathbf{r}^2{}_{(l)}+\mathbf{r}_{n-l}{}^2+2\mathbf{r}_{(l)}\cdot\mathbf{r}_{n-l}. \tag{A6}$$

To find $D_n(l)$ we must first sum over all allowable $(n-l)$ step no-reversal walks. Since the first step can be added only in $q-1=\sigma$ ways there are σ^{n-l} possibilities in all and since, by symmetry, the mean-square size is independent of the direction of the first step, each

[26] P. J. Flory, see work cited in footnote 1, p. 414.

direction contributes $S_{n-l}/(\sigma+1)$ to the square-size sum. Thus

$$\sum R_n^2(l)=\sigma^{n-l}\mathbf{r}_{(l)}^2+[\sigma/(\sigma+1)]S_{n-l}+2\mathbf{r}_{(l)}\cdot\sum\mathbf{r}_{n-l}. \tag{A7}$$

But for the bias due to the specified direction of the lth step of the tadpole the last term in this expression would vanish since the mean end-to-end displacement $\langle\mathbf{r}_{n-l}\rangle$ of a symmetric random walk is zero. It follows that the net contribution of this term is minus the mean displacement of a no-reversal walk which starts in the (forbidden) direction $\mathbf{s}_0=-\mathbf{s}_{(l)}$. If the successive step vectors of this biased walk are $\mathbf{s}_1$, $\mathbf{s}_2$, $\mathbf{s}_3$, etc. so that

$$\mathbf{r}_{n-l}=\sum_{t=1}^{n-l}\mathbf{s}_j, \tag{A8}$$

it is quite easy to see[26] that $\langle\mathbf{s}_1\rangle=\mathbf{s}_0/\sigma$, $\langle\mathbf{s}_2\rangle=\mathbf{s}_0/\sigma^2$, $\cdots\langle\mathbf{s}_j\rangle=\mathbf{s}_0/\sigma^j$ which yields

$$\sum\mathbf{r}_{n-l}=\sigma^{n-l}\langle\mathbf{r}_{n-l}\rangle=\sigma^{n-l}\sum_{j=1}^{n-l}\langle\mathbf{s}_j\rangle$$

$$=[(\sigma^{n-l}-1)/(\sigma-1)]\mathbf{s}_0. \tag{A9}$$

On combining these results in (A7) and summing over all tadpoles of order l we obtain $(n\geq l)$

$$D_n(l)=\sigma^{n-l}V_l+[\sigma/(\sigma+1)]S_{n-l}t_l$$

$$+2[(\sigma^{n-l}-1)/(\sigma-1)]C_l, \tag{A10}$$

where t_l is the total number of tadpoles of l steps (including polygonal walks),

$$V_l=\sum_{t(l)}\mathbf{r}_{(t)}^2 \tag{A11}$$

is the square-size sum for tadpoles of order l, and where

$$C_l=\sum_{t(l)}\mathbf{r}_{(t)}\cdot\mathbf{s}_{(t)} \tag{A12}$$

is the algebraic sum of the projections of the last steps of the tadpoles on the vectors spanning their tails.

By means of (A4), (A5) and these last formulas the calculation of the mean-square size of a nonintersecting walk reduces to the determination of the numbers t_l, V_l, and C_l. This represents a comparatively easy configurational problem, which can be solved with the aid of established techniques and known data.[9,10,17] Many partial contributions to the parameters C_l vanish by symmetry. The main difficulty is counting the tadpoles with long tails (i.e., small heads). When necessary this may be simplified by applying in turn to the tails, arguments similar to those used above for the walks. As in the case of evaluating c_n the problem then depends on the number and properties of "dumbbells" and "figure eights" (see Fisher and Sykes[9] and Sykes[17]).

Raman Intensities and the Structure of Some Oxyanions of Group VII*

G. W. CHANTRY AND R. A. PLANE

Department of Chemistry, Cornell University, Ithaca, New York

(Received September 9, 1960)

In order to obtain information concerning bonding and to test a hypothesis concerning the non-existence of BrO_4^-, the absolute intensities and depolarization ratios have been determined for Raman lines of ClO_3^-, BrO_3^-, IO_3^-, IO_4^-, and H_5IO_6. From the data, values of $\bar{\alpha}_{xo}'$ are obtained. These show that ClO_3^- resembles previously studied ions in containing sufficient π bonding to achieve essential electrical neutrality. Values for the other oxyhalides are consistent with this interpretation; however, an independent criterion based on depolarization ratios (which are apparently greater for BrO_3^- and IO_3^- than for ClO_3^-) indicates that there is less π bonding in BrO_3^- and IO_3^- than in ClO_3^-. Since neither criterion can be applied rigorously to the present examples, it is difficult to decide which explanation is correct or wehther the truth lies intermediate between the two extremes.

IN an earlier paper[1] the Raman intensities of the A_1 lines of the oxyanions PO_4^{-3}, SO_4^{-2}, and ClO_4^- were reported and interpreted as supporting the view that the very high-dissociation constant of $HClO_4$ arises from extensive $d_\pi - p_\pi$ double bonding rather than from polarization of the σ bonds. In the course of that paper, it was pointed out that various features which complicate the interpretation of Raman intensity data are absent when an isoelectronic series is studied. Similarly, it might be hoped that the effect of these features would be minimized when attention is restricted to a series of species which, although not isoelectronic, have an identical number of valence electrons. Such a series is the set of oxyanions ClO_3^-, BrO_3, and IO_3^-.

The great interest which attaches to such a series comes from the possibility of bringing the Raman intensity method to bear on a puzzling problem of theoretical chemistry—the fact that, although ClO_4^- and IO_4^- are remarkably stable, BrO_4^- is presumably too unstable to exist. If the presence of extensive multiple bonding confers stability, presumably this feature must be present in IO_4^- yet not in BrO_4^-. An attractive theory of why this might be so is as follows. The contraction of the $3d$ atomic orbitals in a strong field is well known,[2] accounting as it does for the existence of such oddly shaped molecules as ClF_3. This contraction arises from the necessary orthogonality of $3d$ orbitals to s and p orbitals. It follows, therefore, that there is no "spatial" restriction on the value of the constant in the exponential term of the wave function, and that the extent of the contraction depends solely on the magnitude of the field. For the case of ClO_4^-, a structure involving only σ bonds would have a formal charge of $+3$ on the chlorine atom and it is to be expected that the $3d$ orbitals will be strongly contracted and hence able to relieve the charge by taking part in $d_\pi - p_\pi$ double bonding. The case of BrO_4^- is different, however, for here there is the filled $3d$ shell of the bromine atom whose presence imposes "orthogonality" conditions on the contraction of the $4d$ orbitals and it is possible that these orbitals may not be contracted enough to reduce the formal charge on the bromine atom to $+1$. For IO_4^- a new element may enter, for though there will be resistance to the contraction of the $5d$ orbitals, the $4f$ orbitals are available for bonding provided that the field is sufficient to contract them. It is to be hoped that the Raman intensity method would be able to reveal whether or not this state of affairs exists. With this in mind, a study has been made of the Raman intensities of the A_1 lines of ClO_3^-, BrO_3^-, IO_3^-, and IO_4^-.

EXPERIMENTAL

Measurements were made on aqueous solutions of the sodium salts ($NaIO_4$, $NaBrO_3$, and $NaClO_3$) and the potassium salt KIO_3 at concentrations approximately 0.5 M. The spectra were recorded using the Cary Model 81 Raman spectrophotometer. All intensity measurements were made relative to both ClO_4^- and NO_3^- with the exception of those on KIO_3 where the insolubility of $KClO_4$ restricted measurements to be relative to NO_3^- only; the appropriate sodium salt (either $NaClO_4$ or $NaNO_3$) being present in the same solution. This comparison technique was adopted in order to minimize errors due to differences of refractive indices of the various solutions. The observed intensities were corrected for the wavelength dependence of the sensitivity of the instrument in the manner previously described and the absolute intensity scale used was that previously deduced.[1]

The periodate measurements call for special comment, since in general there are several kinds of periodate anion in equilibrium with one another in aqueous solution. This equilibrium has been studied by Crouthamel, Hayes and, Martin[3] as a function of pH. They

* This work was supported by the United States Air Force through the Air Force Office of Scientific Research of the Air Research and Development Command.

[1] G. W. Chantry and R. A. Plane, J. Chem. Phys. **32**, 319 (1960).

[2] D. P. Craig, A. Maccoll, R. S. Nyholm, L. E. Orgel, and L. E. Sutton, J. Chem. Soc. **1954**, 332.

[3] C. E. Crouthamel, A. M. Hayes, and D. S. Martin, J. Am. Chem. Soc. **73**, 82 (1951).

conclude that, at pH 7 the only significant species present is IO_4^-; at pH 1.2 there is an equimolar mixture of IO_4^- and H_5IO_6; at pH values less than this the equilibrium becomes dominated by H_5IO_6. We find, in complete agreement with their observations, that the aqueous solution of $NaIO_4$[pH = approximately 7] shows a spectrum characteristic of a tetrahedral ion with the A_1 line [at 797 cm^{-1}] completely polarized and that as the pH decreases, all four lines of this spectrum decrease in intensity, while a new broad band [at 640 cm^{-1}] appears. In concentrated acid, this band dominates the spectrum and the line at 797 cm^{-1} has all but vanished. It is reasonable, therefore, to attribute the line at 797 cm^{-1} to IO_4^- and that at 640 cm^{-1} to H_5IO_6.

RESULTS AND DISCUSSION

The relative intensities and degrees of depolarization of the A_1 lines of the various species are listed in Table I. The calculation of $\bar{\alpha}_{x0}' = \partial\bar{\alpha}/\partial\nu$ for the trigonal ions is somewhat more complicated than it is for the tetrahedral ones because there are now two A_1 lines which correspond to modes neither of which is pure stretching. In fact, each mode is a mixture of pure stretching and pure bending and the degree of mixing is determined by the normal coordinate transformation matrix £. The calculation of this matrix is straightforward[4] when the vibrational potential energy function for the molecule in question is known, but unfortunately, for trigonal XY_3, the A_1 part of this function involves three unknown constants and since there are only two frequencies we are left with two relationships between three unknowns and the determination of these three is not possible.

If we define six internal coordinates R_1, R_2, R_3 (the lengths of the three bonds X—O) and $R_0\theta_1$, $R_0\theta_2$, $R_0\theta_3$ (the arcs of the three interbond angles) then:

$$2V_{A_1} = F_{11}S_1^2 + F_{12}S_1S_2 + F_{22}S_2^2,$$

where

$$S_1 = \sqrt{3}^{-1}[\Delta R_1 + \Delta R_2 + \Delta R_3]$$

$$S_2 = \sqrt{3}^{-1}[R_0\Delta\theta_1 + R_0\Delta\theta_2 + R_0\Delta\theta_3],$$

and F_{11}, F_{12}, and F_{22} are the three unknown constants. If μ_x denotes the reciprocal of the mass of atom X and if tetrahedral angles are assumed, then the two vibration frequencies are proportional to the square roots of the eigenvalues of the matrix product

$$\begin{bmatrix} \mu_0 + 1/3\mu_x, & -(2\sqrt{2}/3)\mu_x, \\ -(2\sqrt{2}/3)\mu_x, & \mu_0 + 8/3\mu_x, \end{bmatrix} \begin{bmatrix} F_{11}, & F_{12}, \\ F_{12}, & F_{22}, \end{bmatrix}$$

and the normal coordinate transformation matrix is composed of its eigenvectors. If this latter matrix is labeled

$$\mathfrak{L} = \begin{bmatrix} l_{11}, & l_{12}, \\ l_{21}, & l_{22}, \end{bmatrix},$$

then we have

$$\partial\bar{\alpha}/\partial Q_1 = l_{11}(\partial\bar{\alpha}/\partial S_1) + l_{21}(\partial\bar{\alpha}/\partial S_2)$$

$$\partial\bar{\alpha}/\partial Q_2 = l_{12}(\partial\bar{\alpha}/\partial S_1) + l_{22}(\partial\bar{\alpha}/\partial S_2).$$

The derivative with respect to bond length is then given by

$$\partial\bar{\alpha}/\partial\nu = \sqrt{3}^{-1} \cdot (\partial\bar{\alpha}/\partial S_1).$$

A common way of reducing the number of unknowns and rendering the problem soluble is to assume that F_{12} is zero, this approach being generally known as the simple valence force field. Since F_{12} is related to the interaction valence constant connecting stretching and bending, it will be much smaller than the principal constants F_{11} and F_{22} and the approximation is quite good. This method was adopted in the present work for the case of ClO_3^-. The force fields for BrO_3^- and IO_3^- were not investigated owing to the lack of reliable intensity data for the ν_2 vibrations of these molecules. The two potential constants for ClO_3^- are $F_{11} = 6.62 \times 10^5$ d/cm and $F_{22} = 1.84 \times 10^5$ d/cm. It is interesting to observe that F_{11} which is the sum of the bond stretching constant f_r and twice the stretch-stretch interaction constant f_{rr} is somewhat less than the corresponding quantity for ClO_4^- (where it is the sum of f_r and three times f_{rr}), the actual value being 8.24. It is unlikely that the difference is due to the extra f_{rr} although this quantity is known to be positive and of the order of magnitude unity. Perhaps this difference reflects the presumably weaker bonding in ClO_3^- than in ClO_4^-. The £ matrix corresponding to the potential constants derived above is

$$\begin{bmatrix} 0.260934 & 0.061670 \\ -0.178622 & 0.325134 \end{bmatrix}.$$

TABLE I. Raman data.

Species	A_1 Frequency	Relative intensity	$\bar{\alpha}_{x0}'$
ClO_4^-	$\gamma_1 = 935$ cm^{-1}	0.675	1.73 A^2
ClO_3^-	$\gamma_1 = 935$ cm^{-1} $\gamma_2 = 610$ cm^{-1}	0.412 [$\rho = 0.087$] 0.051 [$\rho = 0.280$]	1.39
BrO_3^-	$\gamma_1 = 806$ cm^{-1} $\gamma_2 = 421$ cm^{-1}	1.104 [$\rho = 0.251$] ...[a]	1.95
IO_3^-	$\gamma_1 = 779$ cm^{-1} $\gamma_2 = 390$ cm^{-1}	1.600 [$\rho = 0.269$] ...[a]	2.24
IO_4^-	$\gamma_1 = 797$ cm^{-1}	2.077	2.74
H_5IO_6	"γ" = 640 cm^{-1}	1.872 [$\rho = 0.21$]	1.62[b]

[a] Relative intensity too small for accurate measurement.
[b] See discussion in the text.

[4] Cf. E. B. Wilson, J. C. Decius, and P. C. Cross *Molecular Vibrations*, (McGraw-Hill Book Company, Inc., New York, 1955).

The unit of mass used in deriving this matrix is that of the chemical atomic weight system. The derivatives of the molecular polarizability with respect to the two normal coordinates Q_1 and Q_2 are found from the equation

$$I_p=\frac{KM(\nu_0-\nu_p)^4}{\nu_p[1-\exp(-h\nu_p/kT)]}\cdot 45(\partial\bar{\alpha}/\partial Q_p)^2\cdot[6/(6-7\rho)],$$

where I_p is the observed intensity and the other quantities have been defined in I. The actual values found for ClO_3^- are $\partial\bar{\alpha}/\partial Q_1=0.6278$, $\partial\bar{\alpha}/\partial Q_2=0.1478$ in units complementing to those used for £ and with the unit of derived polarizability being the square angstrom. Finally we have $\partial\bar{\alpha}/\partial S_1=2.405$ A^2 and $\partial\bar{\alpha}/\partial S_2=0.002$ A^2 so that $\partial\bar{\alpha}/\partial\nu_1$ has the value 1.39 A^2. The values of this quantity for BrO_3^- and IO_3^- were calculated assuming that ν_2 was a pure bending mode. Because of the very low intensity of ν_2 this is an excellent approximation and the error introduced is much less than the experimental error. The very small value of $\partial\bar{\alpha}/\partial S_2$ is worthy of comment, for the Wolkenstein intensity theory[5] predicts that this value should be zero. This excellent agreement may be somewhat fortuitous, for a very approximate potential function has been used but nevertheless it does provide evidence that the Wolkenstein theory is at least a good first-order approximation.

With the magnitude of $\partial\bar{\alpha}/\partial r$ for ClO_3^- established it becomes possible to investigate whether it is permissible to compare bonds in molecules of different shapes. In the earlier paper,[1] it was concluded that the series PO_4^{-3}, SO_4^{-2}, and ClO_4^- exhibited an increase of multiple bonding, sufficient to reduce the formal charge on the central atom to unity. The relationship between $\bar{\alpha}_{x0}'$ and bond order is of the form

$$\bar{\alpha}_{x0}'=0.91+(n-1)1.64,$$

where n is the bond order. For ClO_3^- a formal charge of unity leads to a bond order of 4/3 and an expected value $\bar{\alpha}_{x0}'=1.46$ A^2. The agreement between theory and experiment ($\bar{\alpha}_{x0}'=1.39$ A^2) is seen to be good and we can, with more confidence, go on to argue about XO_4^- species from the corresponding XO_3^-.

The increase in $\bar{\alpha}_{x0}'$ in going from ClO_3^- to BrO_3^- would be expected even if the bonds in BrO_3^- are essentially single, for as noted by Woodward and Long,[6] there is a sharp increase in $\bar{\alpha}_{xy}'$ when x changes from the first long period to the second. However, the data listed in Table I do establish that the bonding in BrO_3^- and that in IO_3^- is substantially the same. However, this would be predicted by the electroneutrality principle as well as by that outlined earlier. Furthermore, both theories predict the increase in bond order in going from IO_3^- to IO_4^-. The only way of deciding between the two possibilities, using the intensity data alone, lies in an examination of the sequence H_5IO, IO_3^-, and IO_4^-. The values of $\bar{\alpha}_{x0}'$ for these three species comprise a series similar to that previously discussed for the oxyanions of the elements P, S, Cl. A similar treatment for the oxyiodides shows that experimental values obey (within the experimental error) the relation:

$$\bar{\alpha}_{IO}'=1.60+(n-1)2.10,$$

where n is the bond order obtained by assuming that I carries a +1 charge in each case. Considering that iodine occurs two periods below the elements previously discussed, the increased contributions of both the σ (1.60) and π bonds (2.10) are reasonable. It should, however, be remarked that the value of $\bar{\alpha}_{IO}'$ for H_5IO_6 has been calculated using two assumptions:

(a) that the effect of the five hydrogen atoms surrounding the IO octahedron is negligible,

(b) that all six I—O bonds are equivalent.

Although these assumptions are reasonable, the fact that they have been made must introduce an element of doubt. But, on balance, the evidence from the $\bar{\alpha}_{x0}'$ supports the electroneutrality theory rather than exclusive σ bonds in IO_3^- and hence BrO_3^-.

Further evidence bearing on the nature of the bonding can be obtained from the degrees of depolarization. The total intensity is made up from an isotropic part $[45(\bar{\alpha}_1')^2]$ and an anisotropic part 7 $(\gamma_1')^2$ thus:

$$I_1=K[45(\bar{\alpha}_1')^2+7(\gamma_1')^2],$$

and the degree of depolarization ρ is determined by the relative magnitudes of these two quantities

$$\rho=6(\gamma_1')^2/[45(\bar{\alpha}_1')^2+7(\gamma_1')^2].$$

In terms of the components of the bond polarizability tensor, α_l and α_p (where α_l is the component along the bond and α_p that perpendicular to the bond) $\bar{\alpha}_1'$ is determined by the quantity $(\partial\alpha_l/\partial r+2\partial\alpha_p/\partial r)$ and γ_1' by the quantity $(\partial\alpha_l/\partial r-\partial\alpha_p/\partial r)$. Chantry and Plane have suggested that for single bonds $\partial\alpha_l/\partial r$ is very much larger than $\partial\alpha_p/\partial r$ whereas for multiple bonds which have cylindrical symmetry $\partial\alpha_l/\partial r$ is comparable to $\partial\alpha_p/\partial r$.[7] For the present case (XO_3^- trigonal) this suggestion would predict a small value of γ_1' relative to $\bar{\alpha}_1'$ when multiple bonding is present and consequently a small value of ρ. In passing it should be pointed out that the ordinary double bond as in ethylene does not possess cylindrical symmetry but that this is ensured in the present case by the degeneracy of the two d_π orbitals.

Inspection of Table I shows that ClO_3^- where multiple bonding has been established has a very small ρ whereas BrO_3^- and IO_3^- have much larger values.

[5] M. Wolkenstein, Compt. rend. acad. sci. U.R.S.S. **32**, 185 (1941).

[6] L. A. Woodward and D. A. Long, Trans. Faraday Soc. **45**, 1131 (1949).

[7] G. W. Chantry and R. A. Plane, J. Chem. Phys. **32**, 634 (1960).

This is good evidence in support of the single-bonded picture for these latter two but unfortunately is not conclusive since the band ν_4 (completely depolarized, $\rho=6<7$) is unresolved from ν_3 in all cases and it is just possible that the relative intensity of ν_4 to ν_3 is very much higher in the cases of BrO_3^- and IO_3^- leading to an apparent ρ for ν_1 very much higher than the true value.

In conclusion, both theories agree with part of the observed data but neither with all of it. It is likely, therefore, that due to the assumptions required, the Raman method is unable to determine which is correct. On the other hand, it is also possible that the true state of affairs is a composite; that there is considerable double bonding in BrO_3^-, but that to form BrO_4^- the 4*d* orbitals are unable to contract sufficiently further to reduce the increased charge, whereas in IO_4^- the charge is relieved by participation of the 4*f* orbitals.

THE JOURNAL OF CHEMICAL PHYSICS VOLUME 34, NUMBER 4 APRIL, 1961

Decomposition Rate of Nitric Oxide between 3000 and 4300°K*

E. FREEDMAN† AND J. W. DAIBER

Cornell Aeronautical Laboratory, Buffalo, New York

(Received August 18, 1960)

Time-resolved absorption spectra of shock-heated nitric oxide in the far ultraviolet have been taken using photoelectric detection. The decomposition rate of nitric oxide between 3000 and 4300°K was thereby measured. The initial rate was found to be the sum of the direct dissociation reaction, $NO+Ar\rightarrow N+O+Ar$, with $k=7\times10^{12}\exp(-150\,000/RT)$ liters/mole sec, and the bimolecular reaction, $2\ NO\rightarrow N_2+O_2$, with $k=4.8\times10^{20}T^{-5/2}\exp(-85\,500/RT)$ liters/mole sec.

INTRODUCTION

ON account of its important role in the chemistry of air at elevated temperatures, and in combustion processes involving air, there is a continuing high level of interest in the kinetics of formation and decomposition of nitric oxide.

A number of investigations[1,2] of the mechanisms and rate constants of the decomposition of nitric oxide have been made with reaction ovens or flow tubes where the process is predominantly heterogeneous. Another limitation of these methods is that the maximum temperatures are approximately 2000°K. To avoid these handicaps, Glick *et al.*[3] used the single-pulse shock tube to measure the formation of NO between 2000 and 3000°K. In the present experimental work on the decomposition of NO we utilized a shock tube to heat the NO to a known uniform state with temperatures up to 4300°K, and followed its decomposition by time-resolved spectrophotometric techniques.

By studying the reaction over a wide temperature range, it can be ascertained whether the reaction paths which contribute to the over-all transformation at low temperatures determine the rate of decomposition; or whether new reaction paths which were neglected (or unknown) at low temperatures become dominant at higher temperatures. Also, the wider the temperature range over which the reaction is studied, the better its activation energy can be determined.

THEORY

There are five important reactions involving NO, N_2, and O_2:

Zel'dovich mechanism

$$N_2+O\underset{-1}{\overset{1}{\rightleftharpoons}}N+NO$$

$$NO+O\underset{-2}{\overset{2}{\rightleftharpoons}}N+O_2$$

Dissociation

$$NO+M\underset{-3}{\overset{3}{\rightleftharpoons}}N+O+M$$

Bimolecular

$$2NO\underset{-4}{\overset{4}{\rightleftharpoons}}N_2+O_2$$

Oxygen equilibrium

$$M+O_2\underset{-5}{\overset{5}{\rightleftharpoons}}2O+M.$$

Reactions 1, −2, and 2, −2 were first proposed by

* Supported in part by the AFOSR under contracts.

† Present address: Ballistic Research Laboratories, Aberdeen Proving Grounds, Maryland.

[1] F. Kaufman and L. J. Decker, *Seventh Symposium (International) on Combustion* (Butterworths Publications, Ltd., London, 1959), p. 57.

[2] E. L. Yaun, J. I. Slaughter, W. E. Koerner, and F. Daniels, J. Phys. Chem. **63**, 952 (1959).

[3] H. S. Glick, J. J. Klein, and W. Squire, Cornell Aeronautical Laboratory Rept. No. AD-959-A-1 (September 1957); J. Chem. Phys. **27**, 850 (1957).

Bodenstein[4] and later by Zel'dovich[5] to explain the observed kinetics of NO decomposition at temperatures above 2000°K. This mechanism can lead to various rate equations, depending on which assumptions are introduced. If the usual steady-state assumptions for N and O are made [i.e., $d(\mathrm{N})/dt=d(\mathrm{O})/dt=0$] and, in addition, it is assumed that O atoms are in equilibrium with O_2 molecules, then the initial rate of NO decomposition is[6]

$$d(\mathrm{NO})/dt=-2k_2\mathrm{K}_o(\mathrm{O}_2)^{\frac{1}{2}}(\mathrm{NO}). \qquad (1)$$

Here the back reaction -2 has been ignored; and the equilibrium expression,

$$(\mathrm{O})=\mathrm{K}_o(\mathrm{O}_2)^{\frac{1}{2}},$$

where

$$\mathrm{K}_o=1.3\times10^2\exp(-58\,000/RT)\,(\mathrm{mole/liter})^{\frac{1}{2}}$$

has been used. In addition, it has been assumed that

$$k_{-1}(\mathrm{NO})\gg k_{-2}(\mathrm{O}_2).$$

The rate-controlling reaction for NO *decomposition* is thus reaction (2). An extensive study[3] in a shock tube over the range 2000–3000°K of the *formation* of NO established the controlling reaction to be reaction (1). The rate constant k_1 was found to be

$$k_1=5\times10^{10}\exp(-75\,000/RT)\ \text{liter/mole sec.}$$

Detailed calculations of the formation of NO have been made with the aid of an IBM 704.[7] The assumptions introduced in obtaining the rate equation involving k_1 were investigated. They are the same as the assumptions introduced in the foregoing for the decomposition, except that during formation

$$k_{-2}(\mathrm{O}_2)\gg k_{-1}(\mathrm{NO}).$$

The results indicated that at 3000°K an error of 35% in k_1 results when the measured (NO) vs time curve is fitted by the approximate equation analogous to Eq. (1), namely,

$$d(\mathrm{NO})/dt=2k_1\mathrm{K}_o(\mathrm{O}_2)^{\frac{1}{2}}(\mathrm{N}_2). \qquad (2)$$

The differential equation for the NO concentration can be obtained from Eq. (1) and the mass conservation equation for oxygen. Using [NO] to denote the ratio of instantaneous to initial concentrations, the expression is

$$d[\mathrm{NO}]/dt=-\sqrt{2}\mathrm{K}_ok_2(\mathrm{NO})_0^{\frac{1}{2}}[\mathrm{NO}]\{1-[\mathrm{NO}]\}^{\frac{1}{2}}.$$

This equation can be integrated to give

$$[\mathrm{NO}]=\mathrm{sech}^2\{(1/2\mathrm{NO})_0^{\frac{1}{2}}k_2\mathrm{K}_o t\}, \qquad (3)$$

when t is small (i.e., $t\ll$1msec at 4000°K), then

$$[\mathrm{NO}]\cong1-1/2(\mathrm{NO})_0k_2^2\mathrm{K}_o^2t^2. \qquad (4)$$

This equation is valid only when the assumptions underlying the simplified rate expression, Eq. (1), are satisfied. In reactions involving the formation of NO from O_2 and N_2, O_2 is plentiful, and the assumptions are justified. By using Byron's[8] value for the rate of dissociation of oxygen, for example, it is easily shown that in a typical experiment on the rate of formation of NO, the oxygen atoms and molecules equilibrate in less than 10 μsec. In the case of the decomposition of NO, however, there is no O_2 at the start of the reaction except perhaps as an impurity. Consequently, the steady-state assumption for O is violated, and there can be no equilibrium established between O and O_2 at first. Therefore, for early times, any reactions that can decompose NO faster than the sequence of reactions (1) and (2) will be the dominant ones. Two of these are reactions (3) and (4).

The decomposition of NO by reaction (3) is given by the rate expression

$$d(\mathrm{NO})/dt=-k_3(\mathrm{NO})(\mathrm{M}), \qquad (5)$$

if reactions 2 and -1 are neglected. The rate constant k_{-3} has been measured recently by Wray and Teare,[9,10] (see also Teare and Dreiss[11]). They find

$$k_{-3}=1\times10^{14}T^{-1.5}\ \text{liter}^2/\text{mole}^2\ \text{sec.}$$

Also, they point out that the reaction

$$\mathrm{N+NO\rightarrow N_2+O}$$

has no activation energy, and therefore proceeds extremely rapidly. As a result, measured values of k_3 are actually too large by a factor of two.

The bimolecular reaction path, 4, has been extensively studied at lower temperatures,[1] where it has been found that

$$k_4=1.3\times10^9\exp(-63\,000/RT)\ \text{liter/mole sec.}$$

The experimental temperature range was less than 1600°, and consequently the activation energy cannot be safely employed for extrapolations to high temperatures.

The primary purpose of the present work was to measure the rate constant k_3 and k_4 at higher temperatures.

By considering NO as decomposing by the dissociation reaction and the bimolecular reaction, the rate of change of NO concentration is given by

$$d(\mathrm{NO})/dt=-k_3(\mathrm{NO})(\mathrm{M})-k_4(\mathrm{NO})^2$$

[4] M. Bodenstein, Roczniki Chem. **18**, 374–80 (1938); Chemical Abstracts **33**, 6534[6] (1939).
[5] J. Zel'dovich, Acta Physicochim. U.R.S.S. **21**, 577 (1946).
[6] Norman Davidson, AVCO Research Rept. 32 (June, 1958).
[7] R. E. Duff and N. Davidson, J. Chem. Phys. **31**, 1018 (1959).
[8] S. R. Byron, J. Chem. Phys. **30**, 1380 (1959).
[9] J. D. Teare and K. L. Wray, AVCO Research Note 134 (June, 1959).
[10] K. L. Wray and J. D. Teare, *Abstracts of Papers*, 137th Meeting of the American Chemical Society (April, 1960), p. 37R.
[11] J. D. Teare and G. J. Dreiss, AVCO Research Note 176 (December, 1959).

if reactions 2 and -1 are again neglected. This equation can be written

$$\{(1/(NO)_0\}(d[NO]/dt) = -k_3[NO][Ar] - k_4[NO]^2,$$

where the inert diluent M is taken to be argon and $[Ar] = (Ar)/(NO)_0$. This can be integrated to give

$$[NO] = (k_3[Ar])/\{-k_4 + (k_3[Ar] + k_4) \times \exp(k_3[Ar](NO)_0 t)\}. \quad (6)$$

At small times ($t \ll 10^3$ μsec at 4000°K)

$$1/[NO] = 1 + k_3[Ar](NO)_0 t + k_4(NO)_0 t. \quad (7)$$

If only the dissociation reaction were present, the rate equation (5) could be integrated, and k_3 would be given by

$$k_3 t = -[1/(Ar)]\ln[NO] \cong (1/[NO] - 1)/(Ar).$$

This is the same result as obtained from Eq. (7) with $k_4 = 0$. Likewise, if only the bimolecular reaction were present, the integrated rate equation for k_4 is

$$k_4 t = (1/[NO] - 1)/(NO)_0.$$

This also follows from Eq. (7) when $k_3 = 0$.

Thus, at early times the decrease in NO is that due to the sum of the dissociation reaction and the bimolecular reaction acting independently. This is not true at later times when these reactions are coupled, as shown by Eq. (6). The foregoing mechanisms then provide a path by which the concentration of oxygen can be built up so that the faster Zel'dovich mechanism can become dominant.

EXPERIMENTAL

The shock tube was used to heat mixtures of nitric oxide and argon to high temperatures at known thermodynamic conditions. A beam from a long-duration, low-noise light source was passed through this gas into a spectrograph. A photoelectric readout at selected spectral windows recorded the time history of the radiation, from which the instantaneous concentration of nitric oxide could be found.

The shock tube used in this study is the same tube that was used in previous studies of radiative properties of hot gases.[12,13] The driver gas was helium at pressures from 200 to 800 psia, and the test gas in the driven section was nitric oxide diluted in argon at total pressures varying from 100 to 400 mm mercury. The vacuum pump to each section of the tube had a liquid nitrogen cold trap at its intake to prevent oil vapors from reaching the tube; in addition, the impurity level of the tube was kept to a minimum by thoroughly cleaning the tube after every second run. The pressure level in the tube after pumping was always less than 2 μ of mercury, and the leak rate was about 2 μ/min; consequently, the initial concentration of O_2 was approximately 3×10^{-8} mole/liter.

The nitric oxide employed was a commercial product of high purity. This gas was passed through a soda-lime trap to remove any nitrogen dioxide it might have contained, and was then mixed with argon in separate tanks to prepare mixtures containing 1.5, 5, and 10% (by volume) of nitric oxide in argon. These tanks, which are filled to an initial total pressure of 100 psi, were stored from one to three days after first being filled, so that the gases would thoroughly mix. The argon bath acted as a large heat sink which helped to maintain a nearly constant temperature during the slightly exothermic NO decomposition.

The passage of the shock could readily be detected at various stations along the shock tube by conventional heat-transfer gauges. Four gauges were used and one SLM pressure transducer; these served not only to time the speed of the shock wave, but also to generate synchronizing signals to the various other components of the system. The first heat transfer gauge triggered oscilloscope 1, where the arrival of the shock wave at stations 2, 3, 4, and 5 was displayed on a rasterized sweep. The beam intensity was modulated to produce 10-μsec calibration pips, which aided in the determination of the wave speed from distances along the sweep record. The accuracy in determining the passage time between any two stations was slightly better than two μsec.

The measured wave speed exhibited a slight attenuation and was consequently linearly extrapolated to the end wall. The conditions of the gas behind the reflected shock wave were computed from an IBM program[14] which included vibrational, but not chemical, equilibrium. On account of the attenuation in the wave speed, the error in the time between stations resulted in an uncertainty of ±50°K in the gas temperature behind the reflected shock wave.

The output of the end-wall pressure gauge was displayed on an oscilloscope. This record was only used to determine the length of the testing time and not as a measure of the shock Mach number. The second of the five heat-transfer gauges on the shock tube triggered the lamp. This light source was a xenon lamp, operated by a bank of capacitors totaling 187.5 μf charged to 1400 v. Although the total duration of the flash was approximately 1.1 msec, the light intensity during the first 500 μsec was generally neither constant nor reproducible, while the intensity over the next 600 μsec varied smoothly with time, and was reproducible or correctable to within 3% from one flash to the next. Thus, the signal from the heat-transfer gauge was de-

[12] W. H. Wurster, H. S. Glick, and C. E. Treanor, Cornell Aeronautical Laboratory Rept. No. QM-997-A-2 (September, 1958); J. Chem. Phys. **32**, 758 (1960).

[13] C. E. Treanor, W. H. Wurster, J. W. Daiber, and M. J. Williams, Cornell Aeronautical Laboratory Rept. No. QM-1209-A-2 (April, 1960); J. Chem. Phys. **32**, 758 (1960); J. Qual. Spectroscopy Rad. Transfer **1**, 1961.

[14] We want to thank Dr. R. E. Duff, Los Alamos Scientific Laboratory, Los Alamos, New Mexico, for supplying this program.

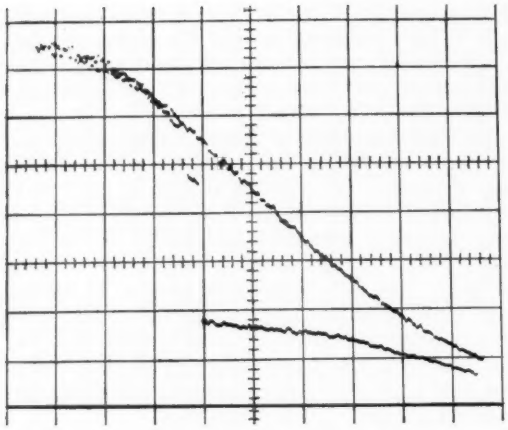

FIG. 1. Spectrophotometric record at 2465 A for run 41. Time increases from left to right with 1 cm being 50 μsec.

layed appropriately so that the flash would start when the shock was still about 500 μsec away from the end-plate, thus permitting the optimum part of the flash to be used for recording data.

The light from the flash lamp was collimated and formed a beam 0.30 mm wide by 5 mm high when passing through the shock tube at a point about 3 mm from the end plate. The beam was then focused on the entrance slit of a Bausch and Lomb medium quartz spectrograph. This spectrograph was fitted with two 931-A photomultiplier tubes mounted in its focal plane. These photomultipliers defined two spectral windows, each of about 20-A width, in the spectrum formed by the instrument. The first was located at 2283 A, where heated oxygen absorbs strongly. The second was at 2465 A, which is in the bandhead of the (0, 2) band of the gamma sequence of nitric oxide. Unfortunately oxygen also absorbs in this region, and in addition there is some absorption from nitric oxide in the first window as well. This complication was allowed for in the data-reduction procedure.

The outputs from the two detectors were led directly to a dual-channel oscilloscope and the display photographed. This oscilloscope was triggered 500 μsec after the flash lamp; hence it displayed only the reproducible part of the flash discussed in the foregoing. Just before each run, a calibration flash was fired, which placed a total transmission line on the photograph.

A number of records of the emission from the lamp were made. It was found that the output was not reproduced from flash to flash, and further, that reproducibility at one wavelength did not ensure reproducibility at other wavelengths. However, these outputs could be made to agree over the entire time of the flash by measuring the intensity ratio, and assuming this scale factor to be constant. A portion of the lamp flash was timed to occur prior to arrival of the incident shock wave (see Fig. 1). Using this measured ratio of initial intensities and assuming it to be constant throughout the run, the incident intensity for the run was constructed from the calibration flash.

DATA REDUCTION

From the photographs of the oscilloscope traces of the photoelectric channel outputs, the ratio of the light intensity after absorption to the initial transmitted light intensity T_i was directly determined (Fig. 2). This ratio depends on the pathlength L, the concentration C^j, and the absorption strength K^j of each chemical species j present,

$$T_i=\exp\{-L(K^1C^1+K^2C^2+\cdots+K^jC^j)\}. \quad (8)$$

In Eq. (8) it is assumed that there is sufficient pressure broadening of the rotational lines so that each vibrational band may be regarded as a continuum. To check whether this was fulfilled, so that meaningful concentration data could be deduced, a plot of measured initial transmission behind the reflected shock wave divided by the density of NO vs temperature was made. If Eq. (8) is valid, a unique curve for all densities would be obtained; within the experimental error, all points did fall on the same curve.

The gamma system of NO consists of "headed" bands and consequently a channel viewing one of the bandheads in absorption gives a measure of the instantaneous population in that vibrational level of the lower electronic state. It has been shown that NO achieves vibrational equilibrium faster than the 3-μsec resolving time,[15] and thus the change in population of a vibrational level is directly proportional to a change in the total concentration of NO. However, as the NO decomposes, oxygen is produced. Oxygen is a continuum absorber over the wavelength interval in the

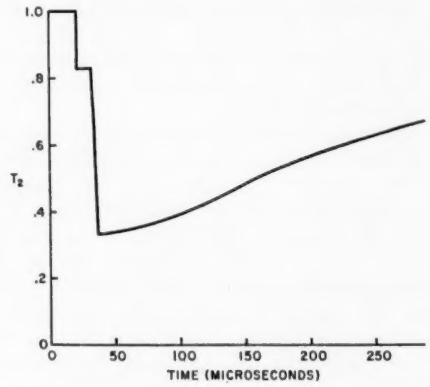

FIG. 2. Ratio of light intensity after absorption to the initial intensity at 2465 A for run 41. The small step at 25 μsec is caused by the incident shock wave.

[15] F. A. Robben, Lockheed Tech. Rept. LMSD–288010 (August, 1959).

present study and will consequently contribute to the absorption in the channel viewing the NO $\gamma(0, 2)$ bandhead. There will also be absorption in this channel due to the tail of the $\gamma(0, 3)$ and possibly parts of other NO bands. Thus, for channel 2 inside the (0, 2) band and channel 1 outside this band the transmissions will be, respectively,

$$\ln(1/T_2) = L\{(\mathrm{NO})_2 K_2^{\mathrm{NO}} + (\mathrm{NO})_x K_x^{\mathrm{NO}} + (\mathrm{O}_2) K^{\mathrm{O}_2}\}$$

$$\ln(1/T_2) = L\{f(\mathrm{NO})_x K_x^{\mathrm{NO}} + g(\mathrm{O}_2) K^{\mathrm{O}_2}\}.$$

The subscripts 2 and x refer to the $\gamma(0, 2)$ and stray NO contributions, respectively. The functions f and g depend only on temperature and are the ratio of the total stray NO absorption and the total oxygen absorption, respectively, in channels 1 to channel 2. The values of g can be found from the absorption measurements in pure oxygen reported in the work cited in footnote 16.

Combining these equations

$$\ln(1/T_2) - (1/g)\ln(1/T_1) = L\{(\mathrm{NO})_2 K_2^{\mathrm{NO}} + (1-f/g)(\mathrm{NO})_x K_x^{\mathrm{NO}}\}.$$

With vibrational equilibrium, the population in any vibrational level is directly proportional to the total NO concentrations,

$$(\mathrm{NO})_2 = h(T)(\mathrm{NO})$$

$$(\mathrm{NO})_x = \mathrm{M}(T)(\mathrm{NO}).$$

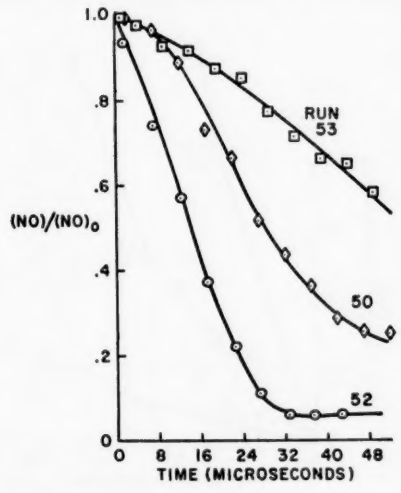

FIG. 3. Time variation of instantaneous to initial NO concentration.

Defining the functions X and F by

$$X(T) = hK_2^{\mathrm{NO}} + (1-f/g)\mathrm{M}K_x^{\mathrm{NO}},$$

$$F = (1/g)\ln T_1 - \ln T_2, \qquad (9)$$

then

$$F/LX = (\mathrm{NO}).$$

The function F was determined from the measured transmissions by means of Eq. (9) and the ratio of the instantaneous concentration of NO to the initial concentration

$$F/F_0 = [\mathrm{NO}]$$

behind the shock wave was found as a function of time, see Fig. 3.

RESULTS

Nine runs were made from which data could be obtained. The measured variation of NO concentration is shown in Table I and the conditions behind the reflected shock wave are summarized in Table II.

If the rate expression Eq. (1) were correct, then [NO] should vary linearly with time squared. As can be seen from Table I, this relationship is not fulfilled at times less than $\sim$20 μsec. This then implies that this simplified rate expression, if not the entire mechanism, does not describe the rate of decomposition for early times. The plots of $-(\ln[\mathrm{NO}])/[\mathrm{A}](\mathrm{NO})_0$ are shown in Fig. 4. Each plot is linear for $\sim$20 μsec, then changes into a rapidly increasing function. At 3000°K, the Zel'dovich mechanism would produce 8×10^{-8} moles/liter of oxygen in 20 μsec, which is comparable with the initial contamination in the tube. On the other hand, the combined reactions (3) and (4) would produce 8×10^{-5} mole/liter of oxygen in the same time. Consequently, it can be concluded that the decomposition of nitric oxide initially proceeds by the parallel dissociation and bimolecular reactions, after which the Zel'dovich reaction becomes dominant. At 5830°K, Wray's calculations[11] on the contribution of reactions indicated that the dissociation reaction would be dominant for the first 2 μsec after which the Zel'dovich mechanism prevails. In contrast with these results, however, Allport[17] has reported briefly experiments that show the Zel'dovich mechanism is always dominant above 1800°K.

The time at which the slope changes in the ln[NO] plots was estimated by eye, then least squares used to find the initial slopes. These slopes are [by Eq. (7)] $m = \{k_3 + k_4/[\mathrm{A}]\}$, and are tabulated in Table II.

The runs for which the percentage of NO was 1.5 ($[\mathrm{A}] = 66$) define a single line which is best represented by

$$m_{66} = 3\times10^9 \exp(-73\,000/RT).$$

The bimolecular reaction rate can then be found for the other relative concentrations. The rate constants

[16] W. H. Wurster and C. E. Treanor, Cornell Aeronautical Laboratory Repr. No. AD-1118-A-10 (December, 1959), AFOSR TN 59-1089.

[17] J. J. Allport, Bull. Am. Phys. Soc. Ser. II **5**, 250 (1960).

TABLE I. Measured concentrations of NO. The entries are 10^4 times the instantaneous concentrations of NO divided by the initial concentration of NO. The time is in microseconds.

Time	Run 41	43	50	52	53	54	56	58	59
2	9935	9486	9915	9371	9937	8538	9865	9736	
7		9581	9702	7396	9747	4883	9424	9737	9465
12	9610	9270	8868	5688	9237	3022		9567	8709
17		8851	7297	3715	9143	1815	9021	9344	8339
22	9280	8419	6652	2174	8718	1180		9274	7836
27		7739	5155	1086	8514	1024	8454	9014	7621
32	8993	7269	4361	609.5	7716	781.8		8729	7284
37		6932	3632	592.3	7128	682.6	7877	8396	7103
42	8646	5880	2873	611.7	6625			8109	6343
47		5031	2530	549.6	6479		7547	7721	5935
52	8220	4575	2501		5831			7427	5588
57							6894		

determined this way are shown in Fig. 5. They are best represented by

$$k_4 = 8.2\times10^9 \exp(-57\,000/RT) \text{ liter/mole sec.}$$

When the low temperature rates of Kaufman and Decker[1] are extrapolated to higher temperatures, it is found that they have to be multiplied by ten to agree with this result.

If instead we combine our results with Kaufman and Decker's, then the two sets of data extend over a range of 3000°, and a more refined representation is possible.

When the collision theory is extended to allow the energies of molecular rotations and vibrations to contribute to the energy of activation, the following expression for the bimolecular rate constant results:

$$k = (Z/s!)(E/RT)^s \exp(-E/RT),$$

TABLE II. Testing conditions. The ratio of (Ar) to (NO) initial is denoted by [Ar]. The rate m is approximately the sum of the bimolecular and dissociation reactions.

Run	T (°K)	$\rho/\rho_0)_{NO}$	[Ar]	m (liters/mole-sec)
41	3010	0.1189	19	3.737×10^4
43	3090	0.4663	9	5.818×10^4
50	3700	0.05427	66	1.280×10^5
52	4062	0.05622	66	3.054×10^5
53	3490	0.02341	66	1.092×10^5
54	4265	0.1478	19	9.049×10^5
56	3125	0.09752	9	1.564×10^5
58	3195	0.04997	66	2.432×10^4
59	3090	0.1742	19	7.267×10^4

while $Z=\alpha D(2\pi RT/M)^{\frac{1}{2}}$, α being the probability of reaction, and D the collision diameter. (See, for example, Fowler and Guggenheim.[18])

The proper value of s is not known in advance. A suitable value can be selected by using the method of least squares to determine the best values of A and E in the equation

$$k = AT^{-s} \exp(-E/RT)$$

and letting s take on the values 0, $\frac{1}{2}$, 1, $\frac{3}{2}$, $\cdots$, in succession. The best fit is thus found at $s=\frac{5}{2}$, which gives

$$k_4 = 4.79\times10^{20} T^{-\frac{5}{2}} \exp(-85\,800/RT) \text{ liter/mole sec,}$$

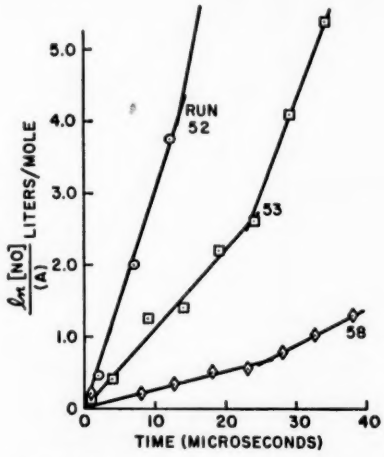

FIG. 4. Correlation curves for the decomposition of NO at small times.

[18] R. H. Fowler and E. A. Guggenheim, *Statistical Thermodynamics* (Cambridge University Press, New York, 1939), p. 505.

or

$$k_4=2.17\times10^7T^{\frac{1}{2}}(E/RT)^3\{(\tfrac{5}{2})!\}^{-1}\exp(-E/RT)$$

with $E=85\,500$ cal/mole.

If the collision radius for NO is taken as 3×10^{-8} cm, then $ZT^{\frac{1}{2}}=3.2\times10^9$ liters/mole sec, which gives $\alpha=0.007$, a low value but still reasonable.[19]

The choice of $s=\frac{5}{2}$ is open to question because it means that all of the internal degrees of freedom are involved (except for two rotational degrees, which are fixed by the requirement of conservation of angular momentum). A value of $s=\frac{3}{2}$ may, therefore, be more plausible. This choice leads to

$$k_4=6.48\times10^7(E/RT)^2\{(\tfrac{3}{2})!\}^{-1}T^{\frac{1}{2}}$$
$$\times\exp(-E/RT)\text{ liter/mole sec}$$

with $E=81\,500$ cal, and $\alpha=0.02$.

The root mean-square deviations for these fittings are 0.13 for $s=\frac{5}{2}$, and 0.20 for $s=\frac{3}{2}$. Therefore, in the absence of unequivocal physical grounds for a selection, we have favored the former.

It is interesting to note that the Hirschfelder rule[20] applied to this reaction gives an activation energy of 87 kcal. Also Zel'dovich[5] and Frank-Kamenetsky[21] found 82 ± 10 kcal.

The rate for the dissociation mechanism can now be extracted from m (see Fig. 6). Following Teare and Wray[9] the rate constant k_3 has been divided by two in order to correct for the occurrence of the much faster

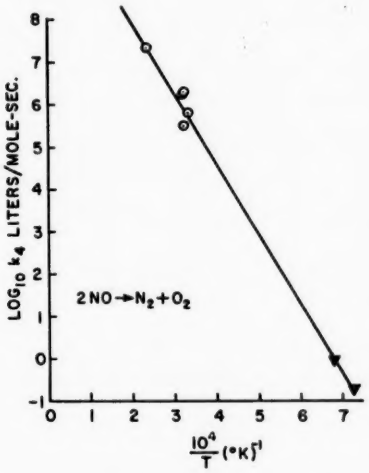

FIG. 5. Bimolecular reaction rate. The filled symbols are the work cited in footnote 1.

[19] *Cf.* S. W. Benson, *The Foundations of Chemical Kinetics* (McGraw-Hill Book Company, Inc., New York, 1960), p. 291, for a list of values of α for other reactions. Note, however, that for $NO+O_3$, $\alpha=0.008$.

[20] J. Hirschfelder, J. Chem. Phys. **9**, 645 (1941).

[21] D. Frank-Kamenetsky, Acta Physicochim. U.R.S.S. **23**, 27 (1947).

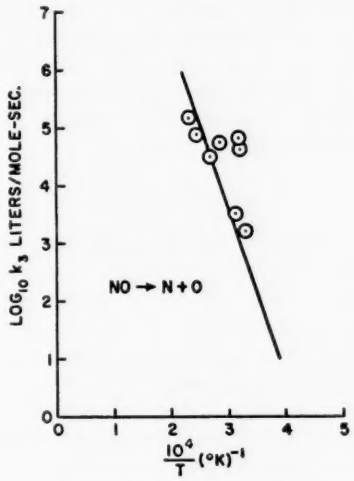

FIG. 6. Dissociation reaction rate. The straight line is given by $2k_3=1.4\times10^{13}\exp\{-150\,000/RT\}$.

reaction $N+NO\rightarrow N_2+O$. This gives

$$k_3=7\times10^{12}\exp(-150\,000/RT)\text{ liters/mole sec.}$$

The activation energy here has been taken to be the heat of formation of NO from its atoms, since the recombination reaction has no activation energy.

From thermodynamic data[22] the equilibrium constant, k_3/k_{-3} can be calculated as

$$k_3/k_{-3}=76.6T^{\frac{1}{2}}\exp(-150\,000/RT)\text{ liters/mole,}$$

which leads to

$$k_{-3}=1\times10^{11}T^{-\frac{1}{2}}\text{ liter}^2/\text{mole}^2\text{ sec.}$$

This value cannot be compared directly with Teare and Wray's result because of the different temperature dependencies that have been used. At 4000°K, where the two determinations should overlap, the results are

$$k_{-3}=1\times10^9\text{ liter}^2/\text{mole}^2\text{ sec}$$

for the present work; and

$$k_{-3}=4\times10^8\text{ liter}^2/\text{mole}^2\text{ sec}$$

for Teare and Wray. In view of the uncertainties involved in the present determination, the agreement is as good as can be expected.

It would be expected that the rate for the Zel'dovich mechanism could now be determined from the measured concentrations. However, the initial mechanisms are producing both oxygen molecules and atoms; for the temperature range of these experiments the relaxation time for the recombination of oxygen atoms is large compared to the time scale of the experiment.

[22] NACA Rept. 1037 (1951), p. 54 [but corrected for the erroneous value of $D(N_2)$ used there].

Consequently, the assumption of oxygen equilibrium is not fulfilled, and therefore the approximate rate expression Eq. (1) is no longer valid. A computational program to reduce the data was not justifiable in view of the limited amount of data available. The data themselves are presented in Table I.

CONCLUSIONS

The decomposition of nitric oxide between 3000 and 4300°K has been shown to proceed by at least three mechanisms. The initial rate is independent of the Zel'dovich reaction because it depends on the concentration of oxygen, which is a product and consequently is of low initial concentration. The bimolecular and the dissociation reactions were separated and the rates determined because they are second and first order, respectively, in NO.

The activation energy for the bimolecular reaction was determined by combining our rates with those of Kaufman and Decker. In this way a wider temperature range is used and the result is more accurate than if the activation energy is determined only over our range or the range of the work cited in footnote 1. The fit determined by least squares gives an activation energy of 85 000 cal so that

$$k_4=2.17\times10^7T^{\frac{1}{2}}(E/RT)^3\{(\tfrac{5}{2})!\}^{-1}\times\exp\{-E/RT\}\ \text{liters/mole sec}$$

over the range $1500°\text{K}<T<4300°\text{K}$.

The rate for the direct dissociation of nitric oxide could not be as accurately determined, because it was the difference between two nearly equal numbers. Consequently, small errors in the measured slopes resulted in large errors in k_3. Approximately,

$$k_3=7\times10^{12}\exp(-150\,000/RT)\ \text{liters/mole sec.}$$

The Zel'dovich reaction dominated the decomposition kinetics after an induction period which decreased with increasing temperature (since all the initial NO concentrations were comparable). However, the rate for this reaction could not be determined, because the oxygen recombination time was long compared to the experimental time and consequently the simplified rate expression could not be used.

ACKNOWLEDGMENTS

We wish to express our appreciation to Dr. Walter H. Wurster, who designed the photoelectric probe; to Dr. Charles E. Treanor, who suggested the method of data reduction; and to Professor S. H. Bauer, of Cornell University, who gave us much valuable advice.

Electronic Paramagnetic Relaxation Times in Potassium-Ammonia and Potassium-Deuteroammonia Solutions*

CLYDE A. HUTCHISON, JR., AND DONALD E. O'REILLY†‡

Enrico Fermi Institute for Nuclear Studies and Department of Chemistry, University of Chicago, Chicago, Illinois

(Received October 13, 1960)

The longitudinal and transverse paramagnetic relaxation times T_1 and T_2 for K-NH_3 and K-ND_3 solutions, have been measured over a range of concentrations and temperatures. T_1 is found to be equal to T_2 at the higher concentrations. At the lower concentrations, the values of T_1 are found to be greater than those of T_2, although at the very lowest concentrations studied they are again approaching each other in value with decreasing molarity. The product of the linewidth at zero rf field by the ratio of temperature to viscosity is found to be constant in both NH_3 and ND_3 over the temperature range studied.

INTRODUCTION

LINEWIDTHS and signal saturation curves for paramagnetic resonance absorptions in solutions of K in liquid NH_3 have been measured previously in this laboratory by Hutchison and Pastor.[1] In the present paper we report a considerable extension of these measurements to include solutions in ND_3 as well as in NH_3 and to include measurements of saturation factor over a range of temperatures and over a wider range of concentrations than those given in the previous work.

EXPERIMENTAL METHODS

The magnetic resonance apparatus including calibrator circuit[2] was essentially the same as that used by Hutchison and Pastor.[1] Measurements of linewidths and signal saturations were made on 10 K-NH_3 samples and 18 K-ND_3 samples at the temperatures, −33.4°, 0.9°, and 25.0°C for the K-ND_3, and −33.2°, 0.8°, and 26.2°C for the K-NH_3 samples. Three samples were not run at all temperatures and a total of 80 sets of data were taken. Each set of data consisted of measurements at a given temperature of (a) linewidth between points of maximum magnitude of slope and (b) signal intensity, at 8 to 15 different rf coil voltages. The measurements were made at a frequency of 7.0×10^6 cps. The coil voltages were measured with a vacuum tube voltmeter which had been calibrated with an absolute electrodynamometer at 100 cps. A voltage supplied at 7.0×10^6 cps with the same amplitude as that of the 100 cps voltage permitted a comparison of the meter response at these two frequencies. The rf voltage measurement was made at the end of the coaxial line outside the cryostat.[1] The corresponding voltage directly across the coil was proportional to the measured voltage V and the ratio of the two was determined experimentally. Accurate measurements of coil and sample geometry permitted the calculation from V of the average rf magnetic field H_1 in the sample.

For each sample at each coil voltage the current in the solenoid supplying the field was adjusted until the maximum deflection of the output meter of the phase-sensitive detection system was obtained on the low-field side of the absorption. The voltage across a calibrated resistor in series with the solenoid was measured as described previously[1] and the static magnetic field was calculated from the solenoid's accurately known dimensions.[1] The static field was then increased so that the phase of the derivative signal shifted by π and the voltage for maximum deflection was again measured. Then the field was reduced to zero and the low-field maximum signal was simulated with the calibrator circuit as described previously.[1] These three measurements were made at a series of coil voltages V beginning at 0.05 v and going up to voltages high enough so that accurate calibration and width measurements were not possible because of the low intensities of the signals.

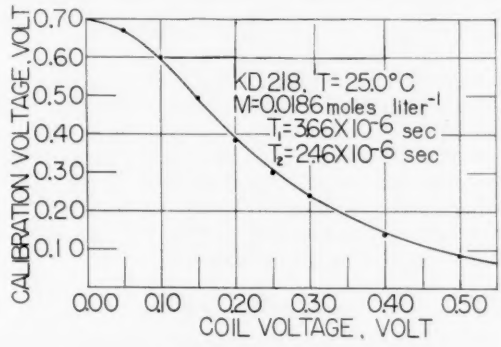

FIG. 1. Calibrator voltage vs coil voltage.

The magnetic field was modulated at a frequency of 49.3 cps with an amplitude sufficiently small so that undistorted first-derivative signals were produced. This modulation system was calibrated by oscilloscopic display of the K-NH_3 resonance with a sweep amplitude

* This research was supported by the U. S. Office of Naval Research.

† Present address: Argonne National Laboratory, Argonne, Illinois.

‡ U. S. Rubber Company Fellow, 1952–1953.

[1] C. A. Hutchison, Jr., and R. C. Pastor, J. Chem. Phys. **21**, 1959 (1953).

[2] G. D. Watkins and R. V. Pound, Phys. Rev. **82**, 343 (1951).

that was large compared with its width, and measurement of the static-field change required to shift the absorption in field by the amount of the sweep.

Figures 1 and 2 show typical examples of the variations of (a) calibrator voltages required to simulate the maximum first derivative signal meter deflections and (b) resonance widths, respectively, with rf coil voltage. In Fig. 2 the width is given as voltage across the resistor in series with the solenoid. The ratio of field strength at the center of the solenoid to voltage across the resistor was 40.81 gauss v^{-1}.

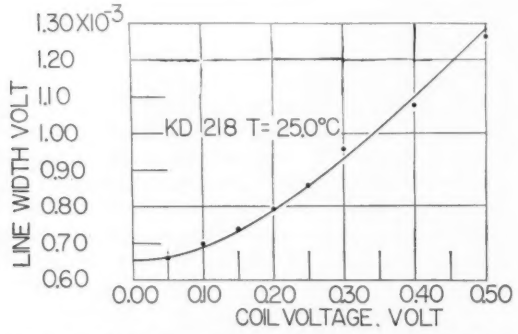

FIG. 2. Width of resonance at maximum slope vs coil voltage. The linewidth is given as voltage across the resistor in series with the solenoid. The ratio of field strength at the center of the solenoid to voltage across the resistor was 40.81 gauss v^{-1}.

Figure 3 shows a typical example of the display of a resonance signal on a recorder chart. Such charts were run for each sample at three or four different values of coil voltage. At intervals the recorder input was switched from the resonance detector output to the voltage across a calibrated resistor in series with the static-field current supply. In this way an accurate plot of signal vs field was obtained.

TREATMENT OF DATA

For a system obeying the Bloch equations[3] the imaginary component χ'' of the susceptibility[1] satisfies the relation,

$$\chi''(H_1, H) = \frac{\frac{1}{2}\chi_0 T_2 \omega_0}{1+(\gamma T_2)^2(H-H_0)^2+\gamma^2 H_1^2 T_1 T_2}, \quad (1)$$

in which H_1 is the magnitude of that rotating component of the magnetic field which is effective in causing magnetic transitions, H is the magnitude of the static polarizing field, χ_0 is the static field susceptibility, ω_0 is the angular frequency of the rf field in a fixed frequency experiment, γ is the magnetogyric ratio of the electron ($\omega_0=\gamma H_0$), T_1 is the longitudinal or spin-lattice relaxation time, and T_2 is the transverse relaxation time.

In the present case the modulation frequency is much

[3] F. Bloch, Phys. Rev. **70**, 460 (1946).

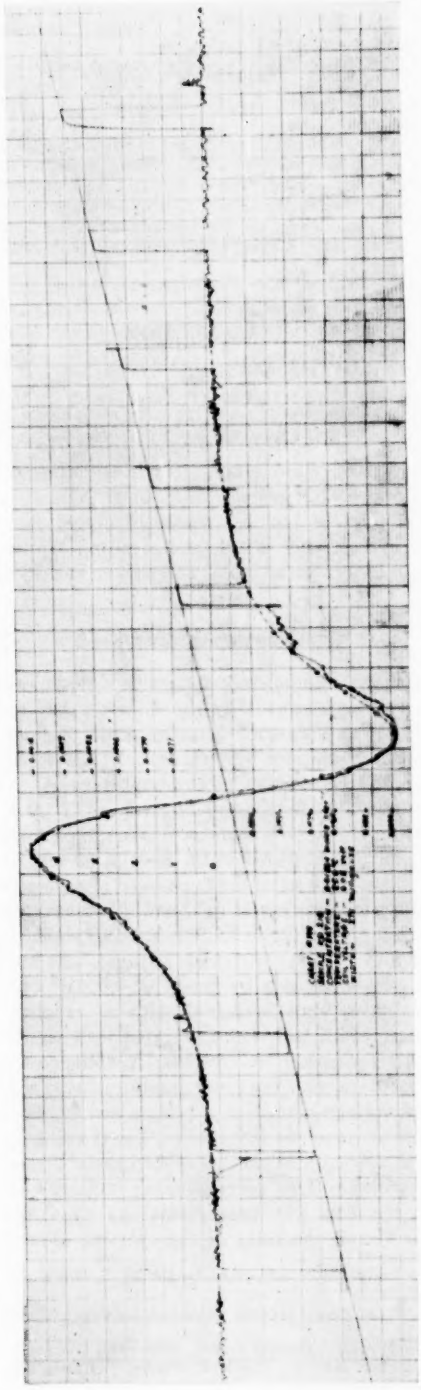
(a)

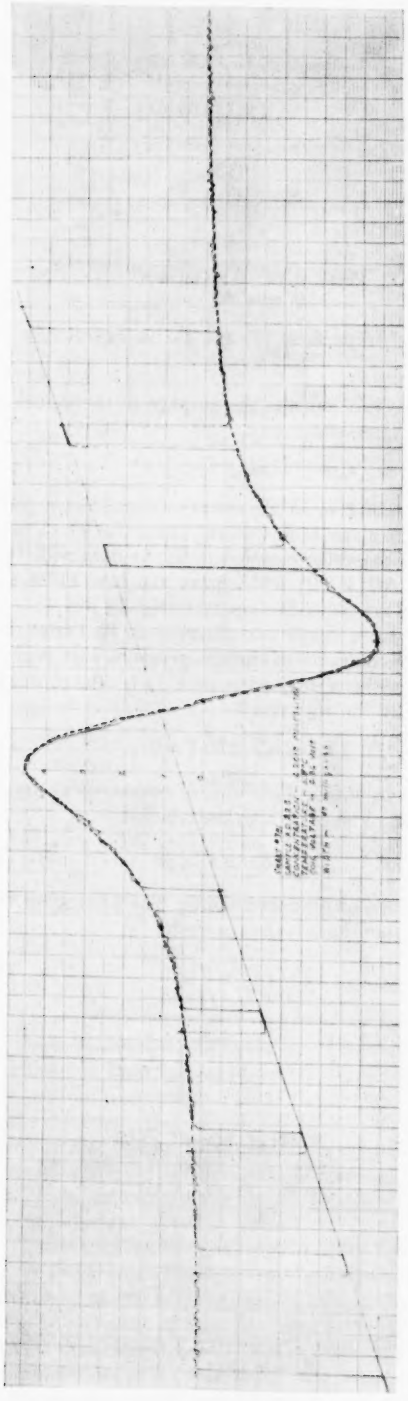

(b)

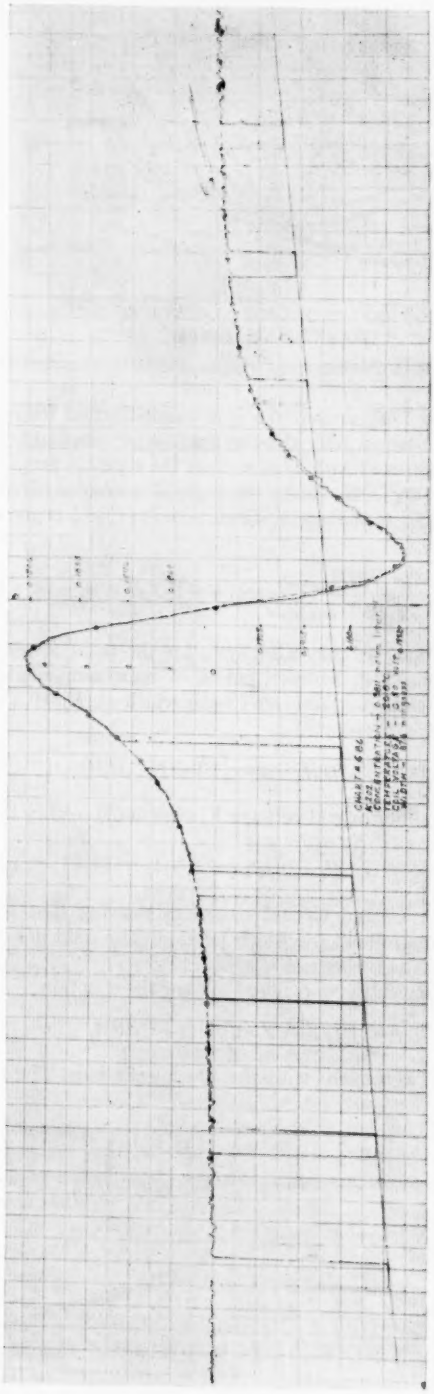

(c)

FIG. 3. Recorder charts. These are typical recorder charts run at coil voltages of 0.05, 0.36, and 0.50 v reading from top to bottom, (a) 0.05 v, (b) 0.36 v, and (c) 0.50 v.

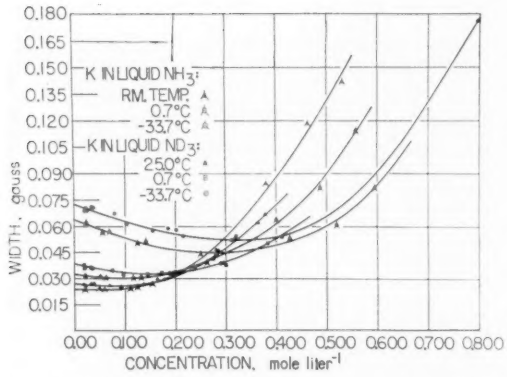

FIG. 4. Width of resonance at maximum slope vs concentration.

less than $1/T_1$ so that the spin magnetization follows the modulation field, and the modulation amplitude is small compared with $1/T_2$ so that the signal is proportional to $\partial\chi''/\partial H$. Hence the ratio of maximum signal at finite H_1 to maximum signal at zero rf field is given by

$$\frac{(\partial\chi''/\partial H)_{\max,H_1}}{(\partial\chi''/\partial H)_{\max,H_1=0}}=\{1+\gamma^2T_1T_2H_1^2\}^{-\frac{1}{2}}. \tag{2}$$

In addition, we may also write for the ratio of resonance linewidth between points of maximum magnitude of slope at finite H_1 to the width at $H_1=0$ the following expression,

$$\Delta H(H_1)/\Delta H(H_1=0)=\{1+\gamma^2T_1T_2H_1^2\}^{\frac{1}{2}}. \tag{3}$$

The calibrator grid voltages V_g were found to obey the relation

$$V_g=C_1/(1+C_2'V^2)^{\frac{1}{2}}, \tag{4}$$

in which C_1 and C_2' are constants showing that the saturation follows the Bloch relation. The solid line in Fig. 1 is the theoretical relation.

The linewidths were found to obey the equation

$$\Delta H(V)/\Delta H(V=0)=(1+C_2V^2)^{\frac{1}{2}}, \tag{5}$$

again in agreement with the Bloch equations. The C_2 used in this relation was the average of the values of C_2 in the expression

$$C_2=[(V_g/C_1)^{-\frac{1}{2}}-1]/V^2 \tag{6}$$

for each of the 8 to 15 measurements made on a given sample at a given temperature. The value of C_1 used in (6) was the value required to fit the data with (4). Values of $\Delta H(V=0)$ which gave the best fit of (5) to the data are plotted vs concentration in Fig. 4.

Since the line shape was observed to be Lorentzian and field fluctuations and inhomogeneities were negligible, the transverse relaxation time T_2 is related to the linewidth by the equation

$$T_2=2/\sqrt{3}\gamma\Delta H(V=0). \tag{7}$$

In order to obtain T_1 it was, of course, necessary to calculate H_1. Values of K in the relation

$$H_1=KV \tag{8}$$

were obtained as described above. The product of the two relaxation times is then given by

$$T_1T_2=C_2/K^2\gamma^2; \tag{9}$$

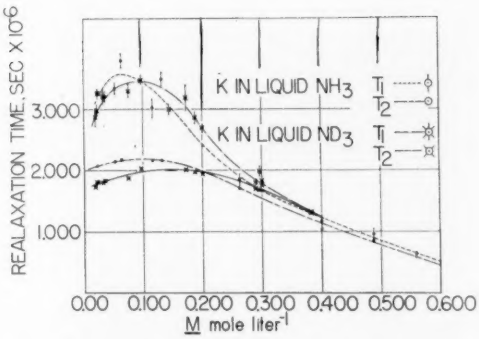

FIG. 6. Relaxation times (T_1 and T_2) vs concentration for K-NH_3, K-ND_3 solutions, 0.8°C.

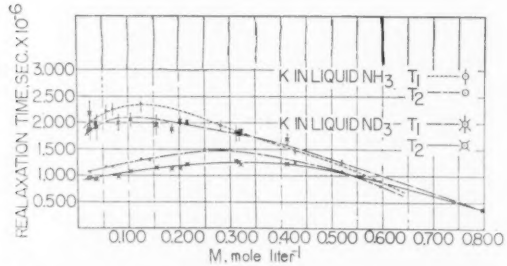

FIG. 5. Relaxation times (T_1 and T_2) vs concentration for K-NH_3, K-ND_3 solutions, −33.4°C.

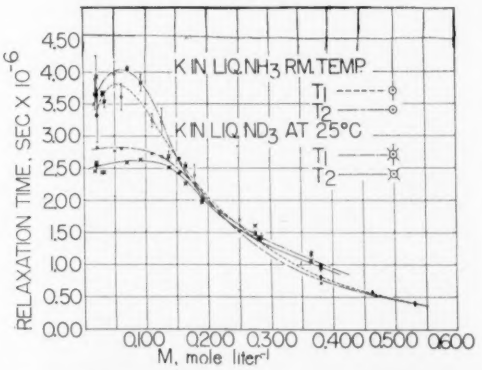

FIG. 7. Relaxation times (T_1 and T_2) vs concentration for K-NH_3, K-ND_3 solutions, 25°C (room temperature).

TABLE I. Relaxation times.

−33.4°C					
K-NH_3			K-ND_3		
M mole l^{-1}	T_1 sec×10^{-6}	T_2 sec×10^{-6}	M mole l^{-1}	T_1 sec×10^{-6}	T_2 sec×10^{-6}
0.020	1.96	1.07	0.020	1.80	0.95
0.050	2.16	1.14	0.050	1.99	0.98
0.100	2.32	1.33	0.100	2.10	1.06
0.200	2.24	1.41	0.200	1.98	1.18
0.300	1.88	1.46	0.300	1.82	1.24
0.400	1.57	1.33	0.400	1.61	1.23
0.600	0.88	0.79	0.600	0.99	0.84
			0.800	0.36	0.36
−0.8°C					
K-NH_3			K-ND_3		
M mole l^{-1}	T_1 sec×10^{-6}	T_2 sec×10^{-6}	M mole l^{-1}	T_1 sec×10^{-6}	T_2 sec×10^{-6}
0.020	3.10	2.06	0.020	2.89	1.77
0.050	3.53	2.13	0.050	3.31	1.86
0.100	3.45	2.18	0.100	3.45	1.98
0.200	2.43	1.99	0.200	2.70	1.97
0.300	1.66	1.54	0.300	1.78	1.69
0.400	1.23	1.13	0.400	1.24	1.22
0.600	0.48	0.44			
25°C					
K-NH_3			K-ND_3		
M mole l^{-1}	T_1 sec×10^{-6}	T_2 sec×10^{-6}	M mole l^{-1}	T_1 sec×10^{-6}	T_2 sec×10^{-6}
0.020	3.31	2.80	0.020	3.60	2.53
0.050	3.81	2.82	0.050	4.02	2.59
0.100	3.42	2.77	0.100	3.74	2.62
0.200	2.06	2.01	0.200	1.98	1.94
0.300	1.24	1.15	0.300	1.36	1.29
0.400	0.74	0.70	0.400	0.95	0.89
0.500	0.47	0.46			

T_1 was then obtained from the relation

$$T_1=(C_2/K^2\gamma^2)/T_2, \tag{10}$$

in which T_2 is given by (7) above.

Values of T_1 and T_2 so obtained are plotted in Figs. 5, 6, and 7. All values of T_1 and T_2 were corrected from the experimental temperatures to the temperatures given in the graphs by graphical interpolations using plots of times vs temperature. Values of T_1 and T_2 read from smooth curves drawn through the experimental points are given in Table I.

The average fractional deviation of the 8 to 15 values of C_2 from their average, was calculated from the measurements on a given sample at a given temperature. The average of these averages for all but three of the 80 runs was 5.1×10^{-2}. The uncertainty in the determination of T_2 was much less than this arising mainly from the error in setting the current to maximum meter deflection. This error in T_2 amounted to approximately 2%. Therefore the uncertainty in T_1 is essentially the same as the uncertainty in C_2 described above, the errors in determining K being very small.

DISCUSSION OF RESULTS

The theoretical discussion of these data will be given in a subsequent paper.[4] The K-NH_3 and K-ND_3 solutions are seen to obey the Bloch[3] equations at the temperatures and concentrations employed in this research.

The linewidths show a minimum with concentration at −33°C which occurs at ∼0.30 M for NH_3. The minimum is still clearly present for ND_3 at 1°C and occurs at ∼0.15 M; for NH_3 there is a shallow minimum at ∼0.10 M. At room temperature, ∼25°C, the minimum is very shallow indeed for ND_3 at ∼0.08 M and for NH_3 occurs at zero concentration. The sharpest

[4] D. E. O'Reilly (to be published).

line observed was for a 0.02 M solution at room temperature where the width was 23×10^{-3} gauss.

Blume[5] has investigated the linewidths and relaxation times of Na-NH_3 solutions by pulse techniques at room temperature only. The $\Delta H(V=0)$ calculated from his T_2 data using (7) has its minimum at zero concentration and the value is $\sim21\times10^{-3}$ gauss. The data of Hutchison and Pastor[1] on Na-NH_3 were quite fragmentary but had given a width of $\sim25\times10^{-3}$ gauss. Blume has suggested that fluctuations in the earth's magnetic field might be responsible for the 20% difference in these results. We do not believe that this explanation can be correct. The linewidths were not determined by slow sweeping through the absorption, but rather as described above. The effect of such fluctuations on the line widths would have been negligible in the procedure employed for their determination which involved repetition of the width measurements at a given coil voltage. In addition, there was no evidence of any fluctuating field of the size required when the resonance was observed on the oscilloscope with a very small time constant.

The viscosities of K-NH_3 solutions have been measured at -33°C, 0°C, and 20°C.[6] It is interesting to note that the six values of $T\Delta H(V=0)/\eta$, where η is the viscosity, at infinite dilution for K-NH_3 and K-ND_3 at three temperatures each average to 53 gauss deg cp^{-1} with an average deviation from the mean equal to 4 gauss deg cp^{-1}. This is in agreement, for a given isotope, with the prediction of the motional narrowing theory of Kaplan and Kittel[7] that the linewidth should vary directly as η/T. But the fact that the same value is obtained in ND_3 as in NH_3 would seem to be in disagreement with their model which attributes the breadth to hyperfine interaction with the H or D nuclei as narrowed by the motion, and would therefore predict much narrower lines in ND_3 than in NH_3 at equal extents of molecular motion, because of the much smaller magnetic moment of the deuteron. This result is, of course, in agreement with the observations of McConnell and Holm[8] from nuclear resonance that the hyperfine interactions are chiefly with the N nuclei.

The absolute values of T_2 found for K-NH_3 in the present work are much lower than those found by Blume[5] for Na-NH_3. We find 2.8×10^{-6} sec at 0.0 M compared with his 3.2×10^{-6} sec, $\sim2.0\times10^{-6}$ sec at 0.2 M compared with ~3.0 and ~1.0 at 0.4 M compared with his ~2.1.

When the values of T_1 and T_2 are compared at various concentrations it will be observed that T_1 is greater than T_2 at low concentrations for all three temperatures. The two times become essentially equal above a certain concentration reaching equality at ~0.5 M at -33°C, ~0.3 M at 1°C and 0.17 M at room temperature, ~25°C. However, although T_2 approaches zero molarity with small slope and its value at infinite dilution is certain, T_1 is seen to be decreasing very rapidly with decreasing molarity at the very lowest concentrations after passing through a maximum in the vicinity of 0.10–0.15 M at -33°C, 0.10 M at 1°C, and 0.06 M at ~25°C. Because of this very sharp drop in T_1 at the lowest concentrations it would appear that the two times might approach equality at infiinte dilution as required by the theory of Bloembergen, Purcell, and Pound[9] for a case such as this in which $\omega\tau_c\ll1$, where ω is the angular frequency of the rf field and τ_c is the correlation time.

The measurements of T_1 by Blume[5] on Na-NH_3 cover the concentration range from ~0.12 M to ~0.43 M and over this range at 24°C he finds $T_1=T_2$ within ±10%. This is in good agreement with our results at room temperature on K-NH_3 and K-ND_3 in so far as the equality is concerned. We have seen before, however, that our absolute values are not in agreement.

A measurement of T_1 for ~0.2 M Na-NH_3 solution presumably at room temperature has been made by Pollak and Norberg.[10] They find the value 2.0×10^{-6} sec for T_1, in excellent agreement with our value for K-NH_3 solution.

ACKNOWLEDGMENT

We thank Edward Bartal for construction of apparatus used in this work.

[5] R. J. Blume, Phys. Rev. **109**, 1867 (1958).
[6] C. A. Hutchison, Jr., and D. E. O'Reilly (to be published).
[7] J. Kaplan and C. Kittel, J. Chem. Phys. **21**, 1429 (1953).
[8] H. M. McConnell and C. H. Holm, J. Chem. Phys. **26**, 1517 (1957).
[9] N. Bloembergen, E. M. Purcell, and R. V. Pound, Phys. Rev. **73**, 679 (1948).
[10] V. L. Pollak and R. E. Norberg, Bull. Am. Phys. Soc. **1**, 397 (1956).

Electron Spin Resonance in a Gamma-Irradiated Single Crystal of Thiodiglycolic Acid*

YUKIO KURITA† AND WALTER GORDY

Department of Physics, Duke University, Durham, North Carolina

(Received August 25, 1960)

The electron spin resonance of a gamma-irradiated single crystal of thiodiglycolic acid was measured at room temperature at 9 kMc. From the analysis of the anisotropy in the spectroscopic splitting factor and in the nuclear hyperfine interaction constants, a model of the free radical

HOOC—CH_2—S—CH—COOH

is proposed. In this free radical, the electron spin density is mainly in a π orbital, about 60% of which is the p orbital of the CH carbon, 2% is the 1s orbitals of the CH_2 hydrogens, and 22% is in the p orbital of the S.

INTRODUCTION

PREVIOUS studies of the electron spin resonance (ESR) of irradiated powders of many organic compounds containing divalent sulfur atoms have shown that compounds R—S—H and R—S—S—R′ give rise to similar patterns spreading toward a higher field than the resonant field strength for DPPH.[1,2] Compounds R—S—R′ give rise to quite different patterns, similar to those observed for the corresponding oxygen analogs. From single crystal studies, the free radical produced in cystine was confirmed to be of the form HOOC—$CHNH_2CH_2\dot{S}$.[3] These facts are explained on the basis of assumptions that irradiation produces R—S· radicals from R—S—S—R′ and R—S—H compounds and that R—S—R′ compounds give a different kind of free radical with a small spin density on the sulfur atom. In an effort to learn the particular structure of the free radical we have examined the ESR of gamma-irradiated single crystals of thiodiglycolic acid (HOOC—CH_2—S—CH_2—COOH).

EXPERIMENTAL PROCEDURE

The single crystals of thiodiglycolic acid were grown from aqueous solution at room temperature by slow evaporation. The crystal is a thin plate with a marked cleavage perpendicular to the largest plane (Fig. 1). A rectangular coordinate system $a'b'c'$ was defined for convenience. The b' axis was selected parallel to the largest plane and the cleavage plane, and the a' axis was selected perpendicular to the cleavage plane. The crystal structure is unknown.

The single crystals were irradiated by a kilocurie cobalt 60 gamma-ray source at room temperature. The ESR of irradiated single crystals was measured at 9.04 kMc for various orientations of the crystal in the magnetic field at room temperature. The ESR spectrometer and the method of measurement were the same as those employed in the previous work.[4]

EXPERIMENTAL RESULTS

The ESR spectra that are observed at most crystal orientations are complex and contain a number of unresolved lines. The unit vector **Z** is taken along the the static magnetic field. The direction cosines (l, m, n) of **Z** with respect to the a', b', c' axes will be used to specify the field orientation. Spectra with **Z**= (l, m, 0) and (l, $-m$, 0) were found to be identical.

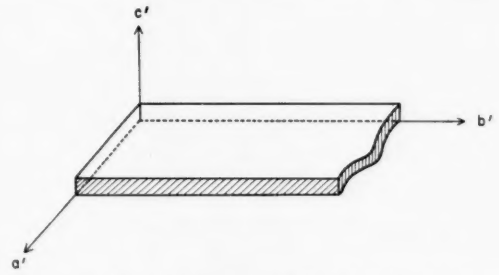

FIG. 1. The crystal form of thiodiglycolic acid and the coordinate axes employed.

Similar symmetry of the spectra between **Z**= (0, m, n) and **Z**= (0, m, $-n$), and between **Z**= (l, 0, n) and **Z**= (l, 0, $-n$) was observed. Therefore, the patterns are consistent with orthorhombic symmetry with the principal axes a', b', c'. In an orthorhombic crystal there are at least four free radicals which are chemically equivalent, but have different orientations. They are related to each other by orthorhombic symmetry. Hence, if the orientation of a free radical with regard to the a', b', c' axes is denoted by (l, m, n), the orientations of others are ($-l$, m, n), (l, $-m$, n), and (l, m, $-n$).[5]

Figure 2 shows the ESR curve at 9 kMc for the

* This research was supported by the United States Air Force through the Air Force Office of Scientific Research of the Air Research and Development Command and by the Office of Ordnance Research, Department of the Army.

† Fellow of the Visiting Research Scientist Program, National Academy of Sciences.

[1] H. Shields and W. Gordy, J. Phys. Chem. **62**, 789 (1958).
[2] G. McCormick and W. Gordy, J. Phys. Chem. **62**, 783 (1958).
[3] Y. Kurita and W. Gordy, J. Chem. Phys. **34**, 282 (1961).
[4] I. Miyagawa and W. Gordy, J. Chem. Phys. **30**, 1590 (1959).
[5] Orientation (l, $-m$, $-n$) is magnetically equivalent with ($-l$, m, n).

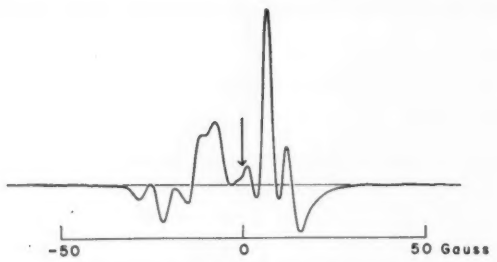

FIG. 2. ESR curve at 9 kMc for the powdered sample of gamma-irradiated thiodiglycolic acid. The curve represents second derivative of the actual absorption curve.

powdered sample of gamma-irradiated thiodiglycolic acid. Figure 3 shows the resonance patterns for the gamma-irradiated single crystal at 9 kMc with the magnetic field along the a', b', and c' axes. All radicals in unit cell must be magnetically equivalent for these three orientations. The patterns for the a' and c' axes are two triplets with relative intensities of 1, 2, 1; 1, 2, 1. The observed patterns can arise from two equivalent or nearly equivalent coupling hydrogen nuclei having a nearly isotropic interaction constant of 5.5 gauss and a third hydrogen nucleus. The patterns for the a', b', and c' axes can be explained in terms of

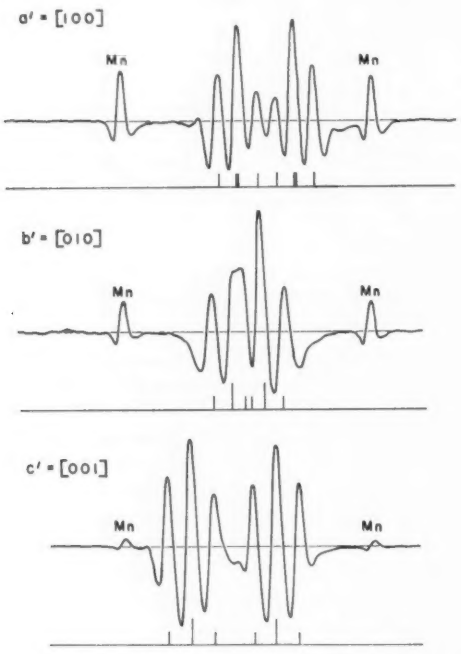

FIG. 3. ESR curves for a gamma-irradiated single crystal of thiodiglycolic acid at 9 kMc for the static magnetic field in the a', b', and c' axes. The bars show the theoretical patterns. The separation between the two Mn markers is 67.6 gauss and the middle point of the two markers corresponds to $g=2.0060$.

the interaction of the third hydrogen of 15.3, 8.1, and 23.2 gauss, respectively. These patterns suggest that the free radical observed in irradiated thiodiglycolic acid is of the form

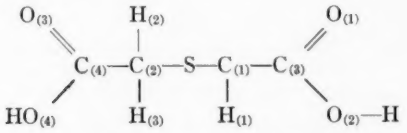

in which $H_{(1)}$ gives rise to a strongly anisotropic nuclear hyperfine interaction (8–23 gauss) while $H_{(2)}$ and $H_{(3)}$ give rise to a small, nearly isotropic nuclear hyperfine interaction (5–6 gauss).

ANALYSIS OF RESULTS

Most of the observed spectra can be accounted for in terms of the following assumptions: (a) The radical giving ESR has the formula above. (b) The unpaired electron is a π electron and mainly on $C_{(1)}$ and S. (c) The radicals are related to one another by a symmetry operation of an orthorhombic crystal. If the direction cosines of a principal element of a free radical are (l, m, n) the direction cosines of a corresponding principal element of other radicals are (l, m, n), $(-l, m, n)$, $(l, -m, n)$, or $(l, m, -n)$. (d) The spin Hamiltonian for the radical is

$$\mathcal{H}=\beta H(g_{zz}S_z+g_{zX}S_X+g_{zY}S_Y)+\sum_{i,j=X,Y,Z}A_{ij}S_i(I_{(1)})_j+A_{(2)}\mathbf{S}\cdot\mathbf{I}_{(2)}+A_{(3)}\mathbf{S}\cdot\mathbf{I}_{(3)} \quad (1)$$

or

$$\mathcal{H}=\mathcal{H}_0+\mathcal{H}', \quad (2)$$

where

$$\mathcal{H}_0=\{\beta Hg_{zz}+(A_{(1)})_{zz}(I_{(1)})_z+A_{(2)}(I_{(2)})_z+A_3(I_{(3)})_z\}S_z \quad (3)$$

$$\begin{aligned}\mathcal{H}'=&\beta H(g_{zX}S_X+g_{zY}S_Y)\\&+(A_{(1)})_{XX}S_X(I_{(1)})_X+(A_{(1)})_{YY}S_Y(I_{(1)})_Y\\&+(A_{(1)})_{XY}\{S_X(I_{(1)})_Y+S_Y(I_{(1)})_X\}\\&+(A_{(1)})_{ZX}\{S_Z(I_{(1)})_X+S_X(I_{(1)})_Z\}\\&+(A_{(1)})_{ZY}\{S_Z(I_{(1)})_Y+S_Y(I_{(1)})_Z\}\\&+A_{(2)}\{S_X(I_{(2)})_X+S_Y(I_{(2)})_Y\}\\&+A_{(3)}\{S_X(I_{(3)})_X+S_Y(I_{(3)})Y\}.\end{aligned} \quad (4)$$

The effects of the nuclear paramagnetic term $g_I\beta_I\mathbf{I}\cdot\mathbf{H}$, neglected in Eqs. (1)–(4), are discussed later. The eigenvalues for $\mathcal{H}_0$ are

$$E_0=[g_{zz}\beta H+(A_{(1)})_{zz}M_1+A_{(2)}M_2+A_{(3)}M_3]M_S, \quad (5)$$

where M_S, M_1, M_2, and M_3 are $\pm\frac{1}{2}$. The contribution E'

from $\mathcal{H}'$ was calculated with second-order perturbation theory. It contains only one significant term

$$E'=\frac{(A_{(1)})_{zx}^2+(A_{(1)})_{zY}^2}{2(A_{(1)})_{zz}}M_1+\text{smaller terms.} \quad (6)$$

The energies of the transitions $\Delta M_S=1$, $\Delta M_1=\Delta M_2=\Delta M_3=0$ are

$$h\nu_0=g_{zz}\beta H+(A_{(1)})_{zz}M_1+A_{(2)}M_2+A_{(3)}M_3+\frac{(A_{(1)})_{zx}^2+(A_{(1)})_{zY}^2}{2(A_{(1)})_{zz}}M_1. \quad (7)$$

The resonant field strength (H) for the line centers of the first-order transition was calculated from the equation

$$H_0=(g_{zz}/g_0)H+(g_0\beta)^{-1}\times\left[(A_{(1)})_{zz}M_1+A_{(2)}M_2+A_{(3)}M_3+\frac{(A_{(1)})_{zx}^2+(A_{(1)})_{zY}^2}{2(A_{(1)})_{zz}}M_1\right] \quad (8)$$

or

$$H-H_0\simeq(H_0/g_0)(g_{zz}-g_0)+(g_0\beta)^{-1}\left[(A_{(1)})_{zz}M_1+A_{(2)}M_2+A_{(3)}M_{(3)}+\frac{(A_{(1)})_{zx}^2+(A_{(1)})_{zY}^2}{2(A_{(1)})_{zz}}M_1\right], \quad (9)$$

where $H_0(=h\nu_0/g_0\beta)$ and g_0 are the resonant field strength and the g factor for DPPH, respectively. The matrix elements of the g factor and $A_{(1)}$ are expressed in terms of the principal values of $g(g_u, g_v, g_w)$ and $A_{(1)}\{(A_{(1)})_x, (A_{(1)})_y, (A_{(1)})_z\}$, as

$$g_{zz}=\sum_{i=u,v,w}g_i\cos^2(i,Z) \quad (10)$$

$$(A_{(1)})_{zz}=\sum_{i=x,y,z}(A_{(1)})_i\cos^2(i,Z) \quad (11)$$

$$(A_{(1)})_{zx}^2+(A_{(1)})_{zY}^2=\sum_{i=x,y,z}(A_{(1)})_i^2\cos^2(i,Z)-\{\sum_{i=x,y,z}(A_{(1)})_i\cos^2(i,Z)\}^2. \quad (12)$$

The observed values of principal elements of g, $A_{(1)}$, and their direction cosines with regard to the $a'b'c'$ system are shown in Table I. The nuclear hyperfine interaction constants for the hydrogen $H_{(1)}$ are in good agreement with those observed for irradiated carboxylic acids[6–10] and with theoretical values for

TABLE I. The principal values of g, $A_{(1)}$, and their direction cosines with regard to the $a'b'c'$ system.

		Direction cosines with regard to the $a'b'c'$ system		
g_u	2.002	0.93	−0.34	0.14
g_v	2.005	0.36	0.78	−0.50
g_w	2.011	0.06	0.52	0.85
$A_{(1)x}$	7	0.34	0.94	0.09
$A_{(1)z}$	16	0.94	−0.33	−0.07
$A_{(1)y}$	23	0.04	−0.11	0.99

$A_{(2)}=A_{(3)}=5.5$ gauss, almost isotropic.

The direction cosines of other radicals are $(-l, m, n)$, $(l, -m, n)$, and $(l, m, -n)$.

σ proton-π electron interaction by McConnell and Strathdee.[11] The principal values for *N*-acetylglycine were found to be 10 gauss along the C—H bond, 17 gauss along the normal to the molecular plane, and 27 gauss in the molecular plane and normal to the C—H bond.[6] These values are in good agreement with the values for $H_{(1)}$ (7, 16, 23 gauss). By comparison of these two sets of values, the z axis is identified to be along the $C_{(1)}$—$H_{(1)}$ bond, the x axis is perpendicular to the $SC_{(1)}C_{(3)}$ plane and the y axis is in the $SC_{(1)}C_{(3)}$ plane and perpendicular to the $C_{(1)}H_{(1)}$ bond. The u axis, the direction of the g (minimum), is found to be almost parallel (12°) to the x axis. This supports the assumption that the unpaired electron is in a π orbital perpendicular to the $SC_{(1)}C_{(3)}$ plane.[12] The magnitude of the isotropic Fermi term $A_{(1)f}$ is obtained from the observed elements by $(A_{(1)x}+A_{(1)y}+A_{(1)z})/3$ to be 15 gauss, which indicates that the electron spin density on $C_{(1)}$ is $15/25=0.60$.[12]

The magnitude of the isotropic Fermi term for $H_{(2)}$ is 5.5 gauss, which leads to the spin density of $5.5/507=0.01$ on $H_{(2)}$. That is the same for $H_{(3)}$. The evaluation of the coupling tensors $A_{(2)}$ and $A_{(3)}$ from the experimental data is not accurate because of the incomplete resolution of the $H_{(2)}$ and $H_{(3)}$ splitting. The dipole-dipole interaction term between a proton H and a point electron spin on an atom X was calculated with the equation[13]

$$A=28\rho_X(3\cos^2\theta+1)^{\frac{1}{2}}/R^3 \text{ gauss}, \quad (13)$$

where R is the magnitude of the vector $X\rightarrow H$ measured in angstroms, θ is the angle between XH and the magnetic field, and ρ_X is the electron spin density considered as concentrated at the center of the atom X. This approximate equation was applied to possible molecular configurations and possible spin density distributions in the free radical. The dipole-dipole interaction term between the proton $H_{(2)}$ ($H_{(3)}$) and the spin density on

[6] I. Miyagawa, Y. Kurita, and W. Gordy, J. Chem. Phys. **33**, 1599 (1960).
[7] I. Miyagawa and W. Gordy, J. Chem. Phys. **32**, 255 (1960).
[8] H. M. McConnell, C. Heller, T. Cole, and R. W. Fessenden, J. Am. Chem. Soc. **82**, 766 (1960).
[9] N. M. Atherton and D. H. Whiffen, Mol. Phys. **3**, 1, 103 (1960).
[10] C. Heller and H. M. McConnell, J. Chem. Phys. **32**, 1535 (1960).
[11] H. M. McConnell and J. Strathdee, Mol. Phys. **2**, 129 (1959).
[12] For the details of the discussion, see footnote 6.
[13] H. Zeldes, G. T. Trammell, R. Livingston, and R. W. Holmberg, J. Chem. Phys. **32**, 618 (1960).

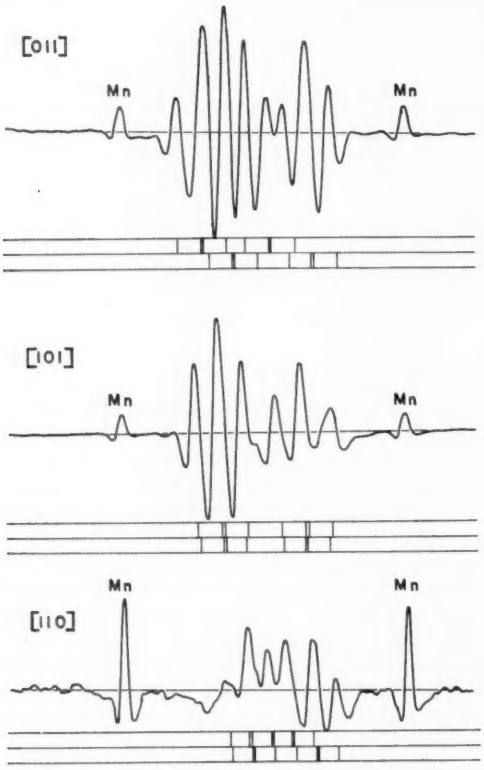

FIG. 4. ESR curves similar to Fig. 3 but for the static magnetic field along the [011], [101], and [110] directions.

$SC_{(3)}OOH$, $H_{(1)}$, and $H_{(3)}(H_{(2)})$ were found to be negligibly small compared with the term between the proton $H_{(2)}(H_{(3)})$ and the spin density on $C_{(1)}$. The latter term was smaller than 2 gauss.

The line centers were calculated from Eq. (9) using the data shown in Table I and from Eqs. (10)–(11) together with $A_{(2)f}=A_{(3)f}=+5.5$ gauss. The calculated line centers were compared with the observed spectra. The sign of the Fermi term in $A_{(2)}$ and $A_{(3)}$ was not determined through this experiment, but the sign of the π-proton isotropic hyperfine interaction has been predicted to be positive.[14] The positions of the line centers shown in Figs. 3 and 4 were calculated for a configuration meeting the following conditions: (a) The free radical is planar and in the yz plane with all trans configuration (Fig. 5). (b) All relevant valence angles are tetrahedral. (c) The $C_{(1)}$—$H_{(1)}$ bond is along the z axis and the $C_{(1)}\cdots C_{(2)}$ distance is along the y axis. (d) $C_{(1)}$—S=$C_{(2)}$—S=1.82 A and C—H=1.11 A.

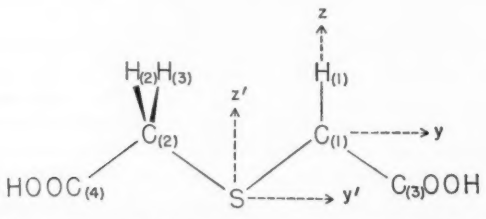

FIG. 5. Diagram indicating reference axes for the free radical.

[14] A. D. McLachlan, Mol. Phys. **1**, 233 (1958).

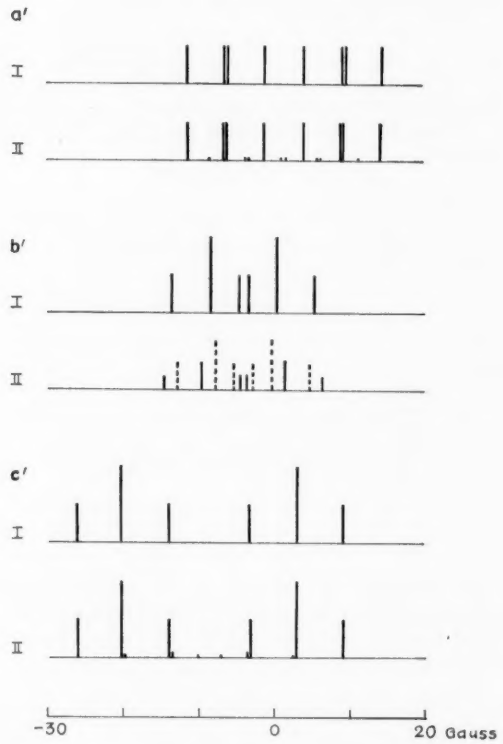

FIG. 6. Comparison of the resonance patterns I, calculated from Eq. (8), and II, calculated including the second order effects for the magnetic field along the a', b', and c' axes. The thick line shows the "outer line" and the broken line shows the "inner line." The relative intensity of the "inner line" to the "outer line" is 0.04 for the a' axis and 0.004 for the c' axis.

Second-order effects observed to give rise to satellite lines in other similar free radicals with

proton coupling[7–9] should be observed here. The effects arise from the off-diagonal elements $(A_{(1)})_{ZX}$ and $(A_{(1)})_{ZY}$, and the nuclear paramagnetic term $g_I\beta_I H(I_{(1)})_Z$ in $\mathfrak{IC}$.[15] The theory for calculating frequencies and relative intensities for these satellites is developed in detail by Miyagawa and Gordy.[7] The

[15] The effect of other terms in $\mathfrak{IC}'$, which can be estimated by a perturbation method, are smaller than 0.1 gauss.

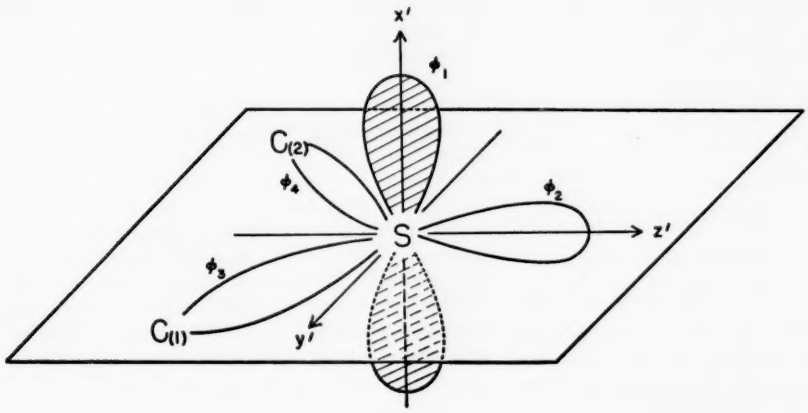

FIG. 7. Diagram indicating the orbitals and reference axes on the S atom.

resonance patterns including second-order effects were calculated from Eqs. (10)–(19) of footnote 7 and Eqs. (10)–(12) in this paper. The results for the orientation of the magnetic field along the a', b', and c' axes are shown in Fig. 6, together with the results calculated from Eq. (9) of this paper. The general features of the patterns are quite similar. The second-order effects are not observed because of the small separation between adjacent lines compared with the width of the individual lines.

Most planar molecules with hydrogen bonding have been found to be in the cleavage plane in the crystal. The u and x axes which are perpendicular to the $SC_{(1)}C_{(3)}$ plane make a small angle of 20° with the a' axis which is perpendicular to the cleavage plane (see Table I). This fact suggests that the free radical is planar and is disposed parallel to the cleavage plane.

It is interesting to compare the ESR data on irradiated thiodiglycolic acid with those on the corresponding oxygen analog. From single crystal studies, the free radical produced in diglycolic acid hydrate was confirmed to be of the form

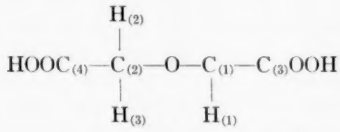

and the principal values of $A_{(1)}$ are 11, 19, and 26 gauss, with $A_{(2)f}=A_{(3)f}=5$ gauss.[16] The g tensor for the oxygen analog has not yet been evaluated accurately, but anisotropy in the g factor is significantly larger for the S compound than for the O compound. This must be due to the difference in the spin-orbit coupling constants of sulfur (382 cm^{-1}) and oxygen (152 cm^{-1})[17] and to the smaller spin density on the O.

[16] Y. Kurita and W. Gordy (to be published).
[17] D. S. McClure, J. Chem. Phys. **17**, 905 (1949).

ELECTRONIC STRUCTURE OF THE FREE RADICAL

From comparison with diglycolic acid hydrate and other compounds in which the spin density is concentrated on O or C atoms, it is evident that the relatively larger anisotropy in the g factor, $g_{max}-g_{min}=0.009$, for HOOC—CH_2—S—CH—COOH is essentially due to the spin density on S. For example, the anisotropy in the g factor for HOOC—$\dot{C}$H—COOH is only one tenth as great, $g_{max}-g_{min}=0.0009$[8] ($g_x=2.0026$, $g_y=2.0035$, $g_z=2.0033$). In our earlier work on a single crystal of cystine dihydrochloride where the spin density was found to be concentrated almost completely on the S, a still larger anisotropy in g was observed. From the anisotropy in the g tensor we shall attempt to estimate the electron spin density on the sulfur atom of the free radical, HOOC—CH_2—S—CH—COOH.

To calculate the spin density on the S of the actual free radical from the g tensor, we need to know the principal g value expected for the idealized contributing structure

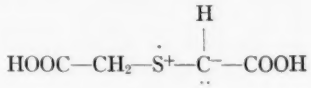

(I)

in which the unpaired electron is entirely on the S, $\rho_S=1$. This structure is of significance because of the comparable electronegativities of S and C, 2.5 each.[18] In our approximate treatment we neglect d-orbital contributions. We assume the unpaired electron to be in pure p orbital and the other occupied orbitals of the valence shell of the S^+ to be equivalent sp_2 hybrids. The orbitals are indicated graphically in Fig. 7 and are chosen as follows:

ϕ_1 is directed along x' and has an unpaired electron,
ϕ_2 is directed along z' and has an unshared pair,

[18] L. Pauling, *The Nature of the Chemical Bond* (Cornell University Press, Ithaca, New York, 1960), 3rd ed., p. 90.

ϕ_3 is directed along S—$C_{(1)}$ and forms a σ bond,
ϕ_4 is directed along S—$C_{(2)}$ and forms a σ bond.

The normalized orbitals are:

$$\phi_1=(3p_{x'})_S \tag{14}$$

$$\phi_2=\sqrt{3}^{-1}(3s)_S+(\tfrac{2}{3})^{\frac{1}{2}}(3p_{z'})_S \tag{15}$$

$$\phi_3=\sqrt{2}\{\sqrt{3}^{-1}(3s)_S-(1/\sqrt{6})(3p_{z'})_S +\sqrt{2}^{-1}(3p_{y'})_S+\psi_{C_{(1)}}\} \tag{16}$$

$$\phi_4=\sqrt{2}^{-1}\{\sqrt{3}^{-1}(3s)_S-(1/\sqrt{6})(3p_{z'})_S -\sqrt{2}^{-1}(3p_{y'})_S+\psi_{C_{(2)}}\}. \tag{17}$$

The configuration of lowest energy will be $\phi_1^1\phi_2^2\phi_3^2\phi_4^2$. We designate its energy as E_1. The other configurations, $\phi_1^2\phi_2^1\phi_3^2\phi_4^2$, $\phi_1^2\phi_2^2\phi_3^1\phi_4^2$, and $\phi_2^2\phi_2^2\phi_3^2\phi_4^1$, which correspond to excited states are designated by E_2, E_3, and E_4, respectively. The bonding electrons have lower energy than the nonbonding pair. The two bonds are equivalent, or approximately so. Thus, $E_1<E_2<E_3=E_4$. The expected g tensor for structure I can be calculated from the above wave functions with the formula of Pryce,[19]

$$g_{ij}=g_f\left\{\delta_{ij}-\lambda\sum_{n=2}^{4}\frac{(\phi_1|L_i|\phi_n)(\phi_n|L_j|\phi_1)}{E_n-E_1}\right\} \tag{18}$$

and the auxiliary relations,

$$L_{x'}|p_{x'})=0,\quad L_{y'}|p_{x'})=-ip_{z'},\quad L_{z'}|p_{x'})=ip_{y'}. \tag{19}$$

The results are:

$$g_{x'x'}=g_f \tag{20}$$

$$g_{y'y'}=g_f\left\{1-(\lambda/12)\left(\frac{8}{E_2-E_1}+\frac{1}{E_2-E_1}+\frac{1}{E_4-E_1}\right)\right\} \tag{21}$$

$$g_{z'z'}=g_f\left\{1-(\lambda/4)\left(\frac{1}{E_3-E_1}+\frac{1}{E_4-E_1}\right)\right\}. \tag{22}$$

Here $g_f=2.0023$ is the g value for the free electron spin and $\lambda=-382$ cm^{-1} is the spin orbit coupling constant.[17] We take the difference in energy of the respective orbitals to be the same as that found for the free radical RS·.[3] Thus,

$$E_2-E_1=15\,000\text{ cm}^{-1}$$

$$E_3-E_1=E_4-E_1\approx 43\,000\text{ cm}^{-1}.$$

These approximations seem justified since the formal charge on the S for the structure I under consideration should lower the energy of all the S orbitals but should not affect their differences in the first-order approximation. These values, with Eqs. (20), (21), and (22) yield

$$g_{x'x'}=2.0023$$

$$g_{y'y'}=2.039$$

$$g_{z'z'}=2.011$$

as the approximate theoretical values for structure I, for which $\rho_S=1$.

For the structure II

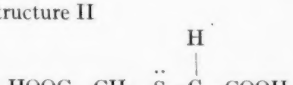

(II)

in which $\rho_S=0$, we can expect principal g values close to those, 2.0026, 2.0033, and 2.0035, found for HOOC—ĊH—COOH.[8] These are so nearly equal that we can for our purposes take g to have the isotropic value of their mean, or 2.003. Thus for the idealized contributing structure II we can expect,

$$g_{x'x'}=g_{y'y'}=g_{z'z'}=2.003$$

with $\rho_S=0$.

The observed values g_w and g_v of Table I for the actual structure must correspond to values of $g_{y'y'}$ and $g_{z'z'}$ for which $0<\rho_S<1$. We assume the spin density ρ_S on the S in the actual structure to be proportional to the deviation in g from the values expected for the idealized structures I and II, or

$$\rho_S=\frac{(g_{y'y'})_{\text{obs}}-(g_{y'y'})_{\rho_S=0}}{(g_{y'y'})_{\rho_S=1}-(g_{y'y'})_{\rho_S=0}}$$

$$=\frac{2.011-2.003}{2.039-2.003}=0.22.$$

Similarly, from the z' components,

$$\rho_S=\frac{2.005-2.003}{2.011-2.003}=0.25.$$

The values are seen to be reasonably consistent, although the one obtained from the z' component is less reliable because of the smaller differences involved. We thus take the estimated value for the spin density on the S as 0.22.

From the isotropic components of the hyperfine structure the spin density on $C_{(1)}$ was found to be 0.60, and that on $H_{(2)}$ and $H_{(3)}$ to be 0.01 each. Assuming that all spin densities observed have the same sign, we have accounted for a total spin density of $0.22+0.60+0.02=0.84$. It is reasonable to assume that the remaining quantity 0.16 obtained by normalizing the total to unity, is largely concentrated on $O_{(1)}$. We can describe this by postulating a contributing structure of form III

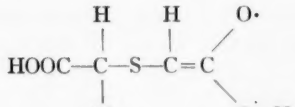

(III)

which would have a weight of about 0.16, or 16%.

[19] M. H. L. Pryce, Proc. Phys. Soc. (London) **A63**, 25 (1950).

Thus the electronic structure of the free radical can be regarded approximately as a hybrid of structures I, II, and III, with the weights 0.22, 0.60, and 0.16, respectively.

An alternative assumption of a negative spin density on the sulfur atom leads to an unreasonably large remaining spin density of $0.60=1+0.22-0.60-0.02$. McConnell and others[20] pointed out that the most likely spot to find a negative spin density is on an atom which has zero spin density in the ground state configuration. For odd alternate radicals, which have carbon atoms of odd number and π electrons of the same number, negative spin densities are produced on alternate carbon atoms. On the other hand, the free radical proposed above is regarded as a system with five atoms (S, $C_{(1)}$, $C_{(3)}$, $O_{(1)}$, $O_{(2)}$) and seven π electrons or with four atoms (S, $C_{(1)}$, $C_{(3)}$, $O_{(1)}$) and five π electrons. In either case all these atoms have nonzero spin density in the ground state configuration. Therefore, the above assumption that all spin densities have the same sign is justified.

The mobile π character of the unpaired electron indicates that the free radical is planar, or approximately planar. If the atoms $C_{(2)}$, S, $C_{(1)}$, and $C_{(3)}$ are planar and have the *trans* configuration indicated in Fig. 5, with the valence angles

$$\angle C_{(2)}SC_{(1)}=\angle SC_{(1)}C_{(3)}=120^\circ$$

the respective coordinates xyz and $x'y'z'$ are expected to be parallel (Fig. 5). The directions of x, y, and z relative to the $a'b'c'$ system of Fig. 1 were derived from the anisotropy in the coupling of $H_{(1)}$, whereas the directions of x', y', and z' are determined from the g tensor, if we identify these coordinates with u, w, and v as described above. The direction cosines for both systems relative to $a'b'c'$ are given in Table I. From them we obtain the relative angles

$$\angle x \text{ to } u=12^\circ$$

$$\angle y \text{ to } w=36^\circ$$

$$\angle z \text{ to } v=36^\circ.$$

Hence we see that the coordinate systems derived in this manner are not exactly parallel. However, the closeness to the parallel configuration is regarded as satisfactory, considering the approximate treatment, the possibility of nonplanarity in the structure, of deviation of the valence angles from 120°, and of experimental error in the measurements.

Nuclear couplings are now commonly used for evaluation of electron spin densities on coupling atoms. So far as we know, the present work represents the first evaluation of the spin density on a given atom from the g tensor. Despite the approximations involved, the method seems to have merit, especially for organic free radicals containing sulfur.

MEASUREMENTS AT HIGHER FREQUENCY

The above results and conclusions are based entirely on measurement at 9.04 kMc. The ESR has also been measured at 28.2 kMc for the crystal orientations with the magnetic field along the a', b', and c' axes. The patterns are identical with those measured at 9.04 kMc. This fact confirms that the patterns in Fig. 3 arise from one free radical and excludes the possibility that the patterns arise from two free radicals each of which gives rise to a triplet. The measurements confirmed the foregoing interpretation of the spectra.

[20] H. M. McConnell and D. B. Chesnut, J. Chem. Phys. **27**, 984 (1957); **28**, 107 (1958); H. M. McConnell and H. H. Dearman, J. Chem. Phys. **28**, 51 (1958), H. M. McConnell, J. Chem. Phys. **28**, 1188 (1958); G. J. Hoijtink, Mol. Phys. **1**, 157 (1958).

Pressure Dependence of the Absolute Catalytic Efficiency of Surfaces for Removal of Atomic Nitrogen

ROBERT A. YOUNG*

University of Washington, Seattle, Washington

(Received January 25, 1960)

By utilizing the nitrogen afterglow to monitor the exponentially decaying nitrogen atom concentration within a closed observation bulb, the low catalytic efficiency of four wall coatings is measured over a large pressure range. The catalytic efficiency of all surfaces is essentially independent of pressure.

INTRODUCTION

MEASUREMENTS of the catalytic efficiency of surfaces for the removal of atomic species have been largely restricted to oxygen and hydrogen; only fragmentary data pertain to atomic nitrogen. The method originated by Smith[1] and used extensively by Linnett[2] has provided the bulk of accurate information concerning surface reaction of atomic oxygen and hydrogen. In this method, as with most methods designed to measure the rate of surface reactions, volume recombination must be kept small. To meet this requirement with the available atom detectors (catalytic probes or Wredge gauges), present methods are limited to low pressures and high fractional atom concentration. These conditions restrict the pressure range over which the catalytic efficiency of surfaces has been measured. We wish to report measurements of the catalytic efficiency of several surfaces for atomic nitrogen over a large pressure range by a technique which utilizes the nitrogen afterglow to monitor the atomic concentration of the reacting gas.

METHOD

Consider a volume V with walls of area S and catalytic efficiency γ, defined as the fraction of atoms colliding with the surface that react. At sufficiently low atom concentrations, the surface reaction rate may be much larger than the volume recombination rate, although, in the case of atomic nitrogen, the afterglow produced by volume recombination will still be detectable. We shall assume that the concentration of atoms is sufficiently small that volume recombination is unimportant relative to surface recombination. When γ is small, such that $L/\gamma \gg R$, where L is the mean free path and R is a typical dimension of the confining volume,[2,3] diffusion will be rapid enough to produce an essentially uniform distribution throughout the volume. The number of atoms striking the wall is $Snv/4$, where n is the number density of atoms, and v is their mean velocity. The equation for the loss of n is then

$$-dn/dt=(Sv\gamma/4V)n=k_s n \tag{1}$$

and

$$n=n_0 \exp(-k_s t). \tag{2}$$

Generally two other loss processes occur which must be added to Eq. (1), i.e., reactions between nitrogen atoms and volume impurities, and diffusion out of the observation region.

Recently, evidence has accumulated indicating that the intensity of the first positive band system of molecular nitrogen excited in active nitrogen is proportional to the square of the nitrogen atom concentration,[4] thus

$$I \propto n^2 \propto \exp(-2k_s t), \tag{3}$$

even when heterogeneous losses predominate. If this relationship remains true at very low atom concentrations, a simple measurement of the decay rate of the afterglow will usually provide enough information to determine k_s, and thus γ.

This method of measuring the catalytic efficiency of surfaces for atomic nitrogen removal has several advantages over more common methods: (a) the surface is subjected to a considerably less reactive atmosphere because of the lower atom concentration needed; (b) a large pressure range is easily covered; (c) the order of the surface reaction is immediately evident from the decay of the afterglow; (d) the atom concentration is selectively observed, thus eliminating other reactive discharge products which may recombine on, and/or transfer energy to, the catalytic surface; (e) absolute measurements of the atom concentration are not needed and the relative efficiencies of two detectors need not be known; (f) the measurement of the atom concentration does not affect in any way their rate of decay; and (g) the diffusion coefficient of the atoms does not need to be known when γ is small.

EXPERIMENTAL

The observation volume V was usually a $\frac{1}{2}$-liter bulb connected to a second 1-liter discharge bulb through a

* Present address: Stanford Research Institute, Menlo Park, California.

[1] W. V. Smith, J. Chem. Phys. **11**, 110 (1946).

[2] J. W. Linnett and D. G. H. Marsden, Proc. Roy. Soc. (London) **A234**, 489, 504 (1956); J. C. Greaves and J. W. Linnett, Trans. Faraday Soc. **54a**, 1323 (1958); **55**, 1338, 1346, 1355 (1959).

[3] S. Kash, Final Report, N6 ONR-2708 (1951), Institute of Geophysics, University of California at Los Angeles.

[4] J. Berkowitz, W. Chupka, and G. B. Kistiakowsky, J. Chem. Phys. **25**, 457 (1956); P. Harteck, R. R. Reeves, and G. Mannella, *ibid.* **29**, 608 (1958).

magnetically operated glass valve made from standard ball joints. This valve prevented diffusion from the observation bulb after it had been filled with the glowing gases.

At high pressures a triggered arc discharge of a 24-μf condenser charged to 4 kv between aluminum electrodes produced a pulse of dissociated gas which easily traveled through 20 cm of 10-mm-diameter tubing and through the glass valve to the observation bulb. At lower pressures the gas was dissociated by a ring discharge, which was produced when a 13-kv spark gap (in series with four turns of wire about the discharge bulb) broke down and discharged a 0.0012-μf capacitor 60 times/sec. The transfer of active nitrogen from the discharge to the observation bulb was due to diffusion.

The afterglow was detected by a photomultiplier whose response was limited to the first positive bands of nitrogen with a Corning colored glass filter. Spectrograms of the afterglow verified this. The photomultiplier output was suitably amplified and applied to a Varian recorder.

The observation bulb was either wrapped with aluminum foil or coated externally with MgO, which increased the light collection efficiency by an order of magnitude.[5] Light radiated by luminescent wall reactions was thus collected as effectively as that due to volume processes. However, negligible surface radiation was observed. This was ascertained by employing two photomultipliers, one highly collimated in such a manner that it discriminated against light emitted or reflected from the walls of the observation bulb. It was experimentally verified that less than 10% of the afterglow light detected by this photomultiplier could have originated on the walls of the bulb. Both detectors behaved identically and their relative response was constant over a pressure range from 0.05 to 1 mm Hg. From this we conclude that luminescent wall reactions are not important in our observation system.

Because of the long decay times involved and the large range of intensities measured, a single pressure run took several hours. Every effort was made to keep the impurity content of the initially mass-spectroscopically pure nitrogen at a low level. The glass system could be pumped below 10^{-6} mm Hg. Under these conditions, a calibrated thermistor vacuum gauge showed a rate of rise of pressure of about 10^{-5} mm Hg/hr. A liquid nitrogen trap was in contact with the gas at all times. With these conditions, consistent decay times have been obtained.

The surface of the observation bulb and the exposed surface of the glass valve were coated as uniformly as possible with the material to be studied. One is limited, of course, to coatings that are more or less transparent. Eicosane (obtained from Eastman Organic Chemicals) was distilled over the surface, while the Teflon coating was baked on the surface from a colloidal dispersion (Du Pont clear finish 852–201). The glass surface was cleaned with dilute hydrofluoric acid, rinsed thoroughly, and dried over phosphorus pentoxide. The metaphosphoric acid coating was investigated in another system with a 2-liter observation bulb. The system could be pumped down to about 3×10^{-5} mm Hg when the surface was coated with eicosane or metaphosphoric acid, and somewhat lower with a Teflon surface.

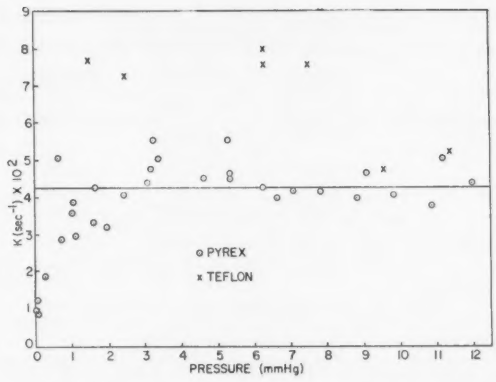

FIG 1. The exponential decay constant of the nitrogen afterglow k as a function of pressure. The loss of nitrogen atoms occurs on the walls of the ½-liter Pyrex observation bulb, before ⊙, and after ×, coating with Teflon.

RESULTS

The light intensity decayed over several orders of magnitude in an accurate exponential manner. There is no doubt that nitrogen atoms are destroyed by a first-order process[6] at the low atom concentrations at which these measurements were made. This conclusion has also been reached by Winkler *et al.*[7]

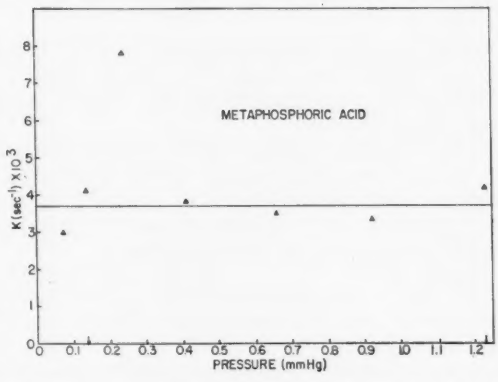

FIG. 2. The exponential decay constant of the nitrogen afterglow k as a function of pressure. The 2-liter observation bulb walls have been coated with deliquescent phosphorous pentoxide.

[5] R. A. Young, J. Opt. Soc. Am. **50,** 627 (1960).

[6] K. Laidler, J. Phys. Chem. **53,** 712 (1949).

[7] R. Back, W. Dutton, and C. Winkler, Can. J. Chem. **37,** 2059 (1959); R. Kelly and C. Winkler, *ibid.* **37,** 62 (1959).

TABLE I. The catalytic efficiency (γ) of four surfaces for oxygen, nitrogen, and hydrogen atoms.

	Oxygen	Nitrogen	Hydrogen
Metaphosphoric acid	12×10^{-5} [b]		2.0×10^{-5} [h]
	10^{-6}–10^{-7} [c]	1.4×10^{-6} [a]	
Glass	2.0×10^{-5} [d]	1.5×10^{-5} [f]	7.5×10^{-5} [i]
	1.2×10^{-4} [e]	3.0×10^{-5} [g]	1.0×10^{-5} [h]
	3.1×10^{-5} [b]	1.7×10^{-5} [a]	1.8×10^{-5} [j]
Teflon	...	2.9×10^{-5} [a]	...

[a] This report.
[b] J. C. Greaves and J. W. Linnett, Trans. Faraday Soc. **55,** 1346 (1959).
[c] P. Harteck, R. R. Reeves, and G. Manella, J. Chem. Phys. **29,** 1333 (1958).
[d] F. Kaufman, Proc. Roy. Soc. (London) **A247,** 123 (1958).
[e] J. W. Linnett and D. G. H. Marsden, Proc. Roy. Soc. (London) **A234,** 489 (1956).
[f] J. T. Herron, J. L. Franklin, P. Bradt, and V. H. Dibeler, J. Chem. Phys. **30,** 879 (1959).
[g] T. Wentink, Jr., J. O. Sullivan, and K. L. Wray, J. Chem. Phys. **24,** 231 (1958).
[h] W. V. Smith, J. Chem. Phys. **11,** 110 (1946).
[i] B. Wood and H. Wise, J. Chem. Phys. **29,** 1416 (1958).
[j] M. Green, K. Jennings, J. Linnett, and D. Schofield, Trans. Faraday Soc. **55,** 2152 (1957).

Figure 1 is a plot of the experimental decay constant k vs the pressure for a clean glass and a Teflon surface. It is seen that for a glass surface, k is independent of pressure over most of the pressure range; there is some indication that a decrease in k occurs as the pressure is reduced below about 1 mm Hg. The fewer data points for a Teflon surface indicate that it is also constant from 1 to 8 mm Hg, with perhaps a significant decrease at pressures above this. First-order volume reactions and diffusion-limited surface reactions are not compatible with the observed pressure independence of k.

In Fig. 2 the exponential decay constant for a metaphosphoric acid surface is plotted against pressure in the 0.1 to 1 mm Hg range. The catalytic efficiency is approximately constant except for one point at 0.25 mm Hg.

Attempts to measure the catalytic efficiency of an eicosane surface were limited by volume reaction; however, the surface catalytic efficiency could not have been greater than 10^{-4}.

Table I contains a summary of the catalytic efficiencies obtained from Figs. 1 and 2. Also included in this table are measurements, from the literature, of the catalytic efficiency for the surfaces used in this study for reactions with oxygen and hydrogen.

DISCUSSION

Linnett and his collaborators[2,8] have proposed different mechanisms for the interaction of atomic oxygen and hydrogen with quartz surfaces. Volume oxygen atoms are considered to react with oxygen atoms naturally present in the glass structure, but in strained lattice positions while volume hydrogen atoms react with hydrogen atoms bound at sites normally occupied by surface OH radicals. In either case the molecule resulting from surface recombination leaves the surface and a gas atom is subsequently sorbed on the vacated site.

On the basis that the catalytic efficiency is determined more by the number of reactive surface sites and less by their particular characteristics, so long as the surface atom is loosely bound, the similar catalytic efficiencies of atomic nitrogen and hydrogen may not be surprising. Because nitrogen is not a normal surface constituent, it probably would interact with the surface by a mechanism similar to that proposed for atomic hydrogen. The nature of the loose bonding of atomic nitrogen to the surface when replacing OH is speculative. However, the similarity between γ for atomic oxygen on the one hand, and γ for atomic nitrogen and hydrogen on the other, is perhaps surprising. One would not expect the number of sufficiently displaced lattice oxygen atoms to correspond simply to the number of hydroxyl radicals replaceable by atomic hydrogen or nitrogen.

The similarity of our results for atomic nitrogen to those for atomic oxygen and hydrogen may imply that the surface reaction mechanism is similar, and that it differs from that previously discussed. Schuler and Laidler[9] have suggested a process for atomic hydrogen surface reactions that may be generalized. This process can be represented as

$$S-X\cdots Y+Y\rightarrow S-X+Y_2$$

$$S-X+Y\rightarrow S-X\cdots Y,$$

where $\cdots$ denotes van der Waals' sorption and — represents an unknown bonding of the impurity X to the surface. The nonspecific nature of van der Waals' sorption is attractive in view of the similar behavior of atomic nitrogen, oxygen, and hydrogen.

[8] M. Green, K. Jennings, J. Linnett, and D. Schofield, Trans. Faraday Soc. **55,** 2152 (1959).
[9] K. Shuler and K. Laidler, J. Chem. Phys. **17,** 1212 (1949).

Measurements of the Diffusion Coefficient of Atomic Nitrogen in Molecular Nitrogen and the Catalytic Efficiency of Silver and Copper Oxide Surfaces

ROBERT A. YOUNG*

Boeing Airplane Company, Seattle, Washington

(Received May 25, 1960)

By utilizing the first positive bands of nitrogen to monitor the decay of atomic nitrogen caused by diffusion to a catalytic surface, the diffusion coefficient of atomic nitrogen in molecular nitrogen has been investigated, leading to a probable value of $280/p$ cm² sec⁻¹. The catalytic efficiency γ of silver and copper oxide surfaces is found to be of the general form $\gamma=a/(bp+c)$, where p is the molecular nitrogen pressure, b and c are constants for each surface, and a is a constant independent of the surface.

INTRODUCTION

THE flux of labile particles lost to a catalytic surface generally depends upon the product of the diffusion coefficient and the catalytic efficiency of the surface for removal of the labile species. Any method which uses this loss to measure the diffusion coefficient must separate these quantities and thus leads to their simultaneous measurement. A new method based on the diffusion loss to a catalytic surface has been proposed to measure the diffusion coefficient and the catalytic efficiency.[1] Its simplicity in the case of atomic nitrogen has also been pointed out.

The diffusion coefficient of atomic nitrogen or hydrogen has not been measured directly and only very recently has this quantity been obtained for atomic oxygen.[2] Likewise, very little has been reported on the catalytic efficiency of metal surfaces for atomic nitrogen removal. Measurements of the catalytic efficiency will be reported for surfaces of silver, copper, and their oxides. The diffusion coefficient measurement of atomic nitrogen will be discussed; since complicating phenomena occur, a probable value is obtained. Because of the newness of the method, and the absence of any measurement of the diffusion coefficient of atomic nitrogen in molecular nitrogen, it is thought advantageous to present these initial results.

METHOD

A rather full discussion of the general method used in making the present measurements has been presented elsewhere,[1] making only a brief resumé necessary. We shall define the catalytic efficiency γ of a surface as the fraction of colliding atoms that react on the surface. The exponential decay time τ of the atom concentration within a volume V, to which is attached a cylindrical diffusion tube of cross-sectional area A containing a catalytic surface of efficiency γ at a distance L from the tube entrance, is found by simple arguments to be

$$\tau=(V/A)[(L/D)+\mu]. \quad (1)$$

In Eq. (1) D is the diffusion coefficient, and $\mu=4/\gamma v$ where v is the mean thermal velocity of the diffusing species at the catalytic surface. By varying the catalyst's position while observing the decay of the atom concentration, one can plot τ vs L and obtain from the slope the diffusion coefficient (as V/A is known) and from the intercept at $L=0$, the catalytic efficiency of the surface. The several conditions necessary for the simple relation (1) to be valid are discussed at length in a previous publication.[1] It is obvious that volume recombination must be unimportant during the measurements of τ for the above analysis to be applicable.

It has been shown that the first positive bands of molecular nitrogen are proportional to the square of the atom concentration in active nitrogen[3]; thus the decay time of the atom concentration can be found by measuring the decay of this band system.

EXPERIMENTAL ARRANGEMENT

The means of producing active nitrogen have been discussed elsewhere.[4] The volume V was a 2-liter bulb isolated from the remainder of the vacuum system by a glass valve. A Pyrex diffusion tube (130 cm long; 2 cm i.d.) was attached to the bulb by a ball joint, and its far end capped with a similar joint after the insertion of the catalytic slug.

The catalytic slug was constructed from a $\frac{1}{4}\times$2-in. carriage bolt over which slipped a Teflon sheath whose diameter was 1 mm less than the inside diameter of the diffusion tube. A circular nut of the catalytic material, with a diameter slightly less than that of the Teflon sheath and with a smooth-faced surface, was screwed onto the bolt to complete the catalytic slug assembly. Catalytic surfaces were changed by replacing the nut. The iron bolt was easily manipulated along the diffusion tube with a large magnitron magnet.

The bulb was coated with metaphosphoric acid to

* Present address: Stanford Research Institute, Menlo Park, California.

[1] R. A. Young, J. Chem. Phys. **33**, 1112 (1960).

[2] S. Krongelb and M. W. P. Strandberg, J. Chem. Phys. **31**, 1196 (1959).

[3] J. Berkowitz, W. Chupka, and G. B. Kistiakowsky, J. Chem. Phys. **25**, 457 (1956).

[4] R. A. Young and K. C. Clark, J. Chem. Phys. **32**, 604 (1960).

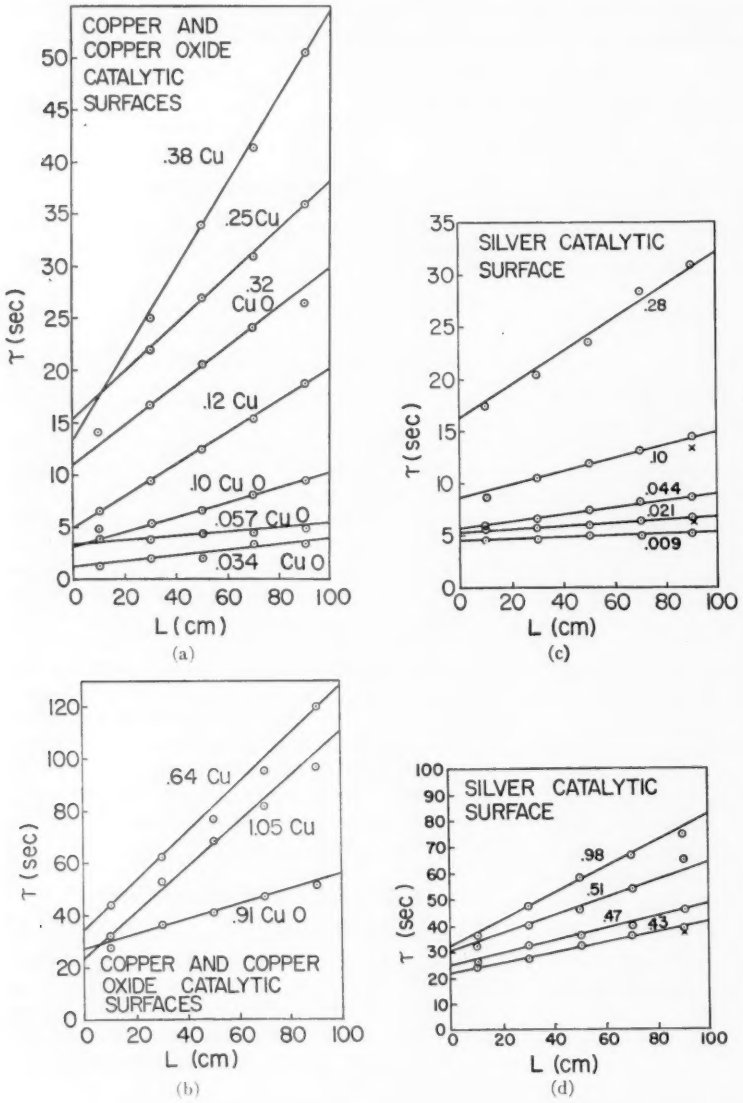

FIG. 1(a)–(d). The experimental decay time of the nitrogen first positive bands in the nitrogen afterglow as a function of the distance L of the catalytic surface from the entrance of the diffusion tube. Each curve label specifies the pressure and the catalytic surface used. The linear dependence of τ on L shown here is predicted by Eq. (1).

reduce losses at the walls.[5] However, it has been our experience that other uncoated surfaces in the vicinity may become affected after some time under vacuum. Therefore, the catalytic efficiencies reported here may not be applicable under different circumstances. The nitrogen was generated from sodium azide and passed through a liquid nitrogen trap. Its pressure was measured to $\pm 1\%$ by a multiplying oil manometer, and the position of the catalytic surface was measured to $\pm \frac{1}{2}$ mm with a meter stick permanently fixed to the diffusion tube.

The observation bulb was coated externally with MgO, which increased the light-collection efficiency by more than an order of magnitude.[6] Light radiated by luminescent wall reactions might be as effectively collected as light due to volume processes. However, auxiliary measurements[5] have shown that negligible surface emission occurred.

Spectrographic examination of the afterglow[4] showed weak NOβ bands, the OI(5577A) auroral green line, weak first positive bands of N_2 in the 5500- to 5600-A region, and fairly strong CN bands in the blue, in

[5] Lord Rayleigh (Strutt), Proc. Roy. Soc. (London) **A151,** 567 (1935); R. A. Young, J. Chem. Phys. **34,** 1292 (1961).

[6] R. A. Young, J. Opt. Soc. Am. **50,** 627 (1960).

addition to the expected strong first positive bands of N_2. A 6655-A RCA photomultiplier and Corning yellow filter (No. 3-69) detected the nitrogen first positive bands; various colored glass and interference filters were used with a 1P21 photomultiplier to detect other radiating systems. Studies of the loss mechanism operative at these low atom concentrations,[4,5] both in this system and in others, indicate that the assumptions necessary in the derivation of Eq. (1) are experimentally true. These measurements show that the catalytic efficiency of the metaphosphoric acid surface is $\approx 10^{-6}$, and that of the Pyrex walls of the diffusion tube is $\approx 10^{-5}$. Diffusion to the catalytic surface generally reduces the time constant of the atom decay compared to its value when the catalytic surface had been removed. The decay times were usually of the order of minutes, while the time for an atom to have moved a mean distance equal to the diameter of the bulb was less than a second. Thus a negligible concentration gradient existed in the bulb. Because of the low catalytic efficiency of the diffusion-tube walls, there was essentially no radial gradient and no loss on its surface. Below about 1 mm Hg, the decay of the first positive bands was generally exponential over at least a factor of 10^3, while the decay was followed over a total intensity ratio of 10^7. The large pressure range (from 0.01 to 1 mm Hg) over which observations were made was limited at the high

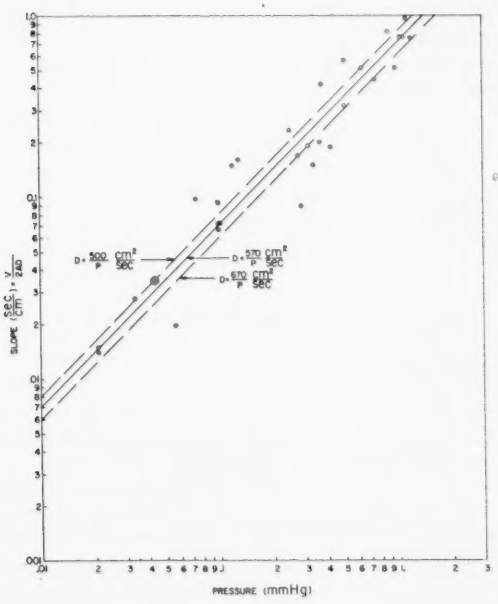

FIG. 2. The log of the slope of curves of τ vs L such as those in Fig. 1 are plotted vs the log of the pressure. Equation (1) relates these slopes inversely to the diffusion coefficient. The dashed lines indicate the curve displacement caused by assuming different diffusion coefficients; the solid line is the best fit. All lines have unit slopes as expected from the pressure dependence of the diffusion coefficient.

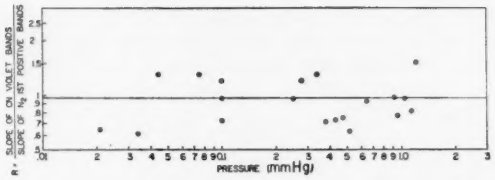

FIG. 3. The log of the ratio of slopes of simultaneous τ vs L curves obtained with detectors responsive to (a) the CN violet bands, and (b) the first positive bands of nitrogen. This ratio is pressure independent with an average value of 0.96 but with considerable scatter.

end because of the presence of recombination at the lowest detected first positive band intensity, and at the low end by the rapidity of decay. For present purposes, no measurements were made below 0.01 mm Hg because the mean free path of the atoms then would approach the dimensions of the diffusion tube, and transport down the tube would become one of molecular flow rather than one of diffusion.

RESULTS

Figures 1(a)-(d) show the degree to which the measured decay times τ are proportional to the position of the catalytic surface L as specified by Eq. (1). There are several experimental effects, which will not be enumerated, that may mask this linear dependence of τ on L. For these reasons data in which τ was not proportional to L were discarded.

Figure 2 is a log-log plot of the slopes of curves like those in Figs. 1(a)-(d) as a function of the total pressure. These slopes are inversely proportional to the diffusion coefficient as Eq. (1) shows. The data in Fig. 2 were taken over a period of several months with three catalytic surfaces; silver, copper, and copper oxide. It is apparent that the results are independent of the catalytic surface as, of course, was expected. Despite the fairly large scatter, the points shown in Fig. 2 lie about a straight line of unit slope. From the measured value of V/A (800 cm), one finds that $D=560p^{-1}$ cm^2 sec.

In Fig. 3 the ratio of the slopes of τ vs L curves are plotted from simultaneous observations of the CN violet band system and the N_2 first positive bands. Despite the several catalytic surfaces used, this ratio remains roughly constant.

Figures 4(a)-(d) are plots of the intercepts τ_0 at $L=0$ for different catalytic surfaces and different observed emission systems vs total nitrogen pressure. The position of the catalytic slug was measured from an arbitrary zero point 17 ± 0.3 cm from the mouth of the diffusion tube. From the measured slope of the τ vs L curves for the first positive band and the known value of V/A, one finds from Eq. (1) that

$$\tau_0=0.70pL_0+4\times10^2\mu, \qquad (2)$$

where L_0 should be the distance from the zero of the

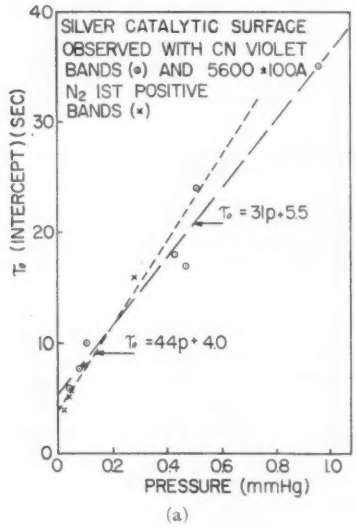

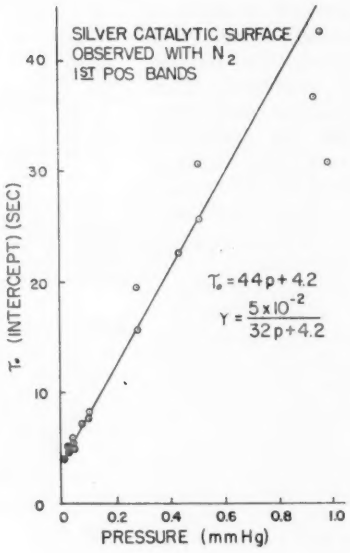

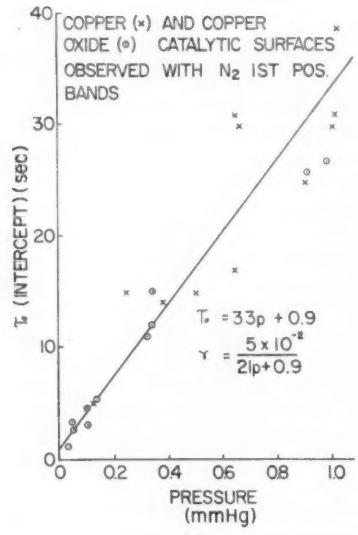

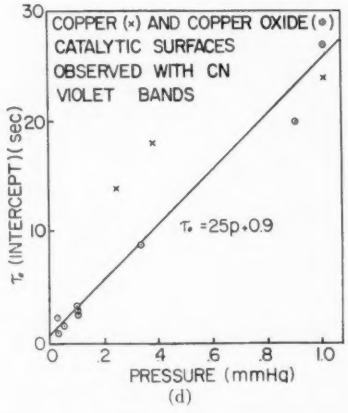

FIG. 4(a)–(d). The intercepts τ_0 of τ vs L curves are plotted against the pressure for various catalytic surfaces and for the emission systems indicated. The catalytic efficiency was computed from Eq. (1) after correction for the displacement of the scale origin from the entrance of the diffusion tube.

position scale to the entrance of the diffusion tube. When L_0 is computed from the curves shown in Figs. 4(a)–(d) (assuming that μ is a constant), it is found to be 2 or 3 times the measured 17 cm, while γ is found to be $1-5\times10^{-2}$. Though the latter is reasonable, the former is not. Such a large discrepancy cannot be attributed to an extension of the diffusion-tube gradient into the spherical volume V of diameter 14 cm. One then concludes that γ is pressure dependent. The data in Figs. 4(a)–(d) imply that

$$\gamma=a/(bp+c). \tag{3}$$

The values of the constants are shown in Table I, only b and c depend upon the surface.

TABLE I. The coefficients a, b, c, in the expression $\gamma=a/(bp+c)$ describing the pressure-dependence of the catalytic efficiency of different surfaces toward atomic nitrogen.

Coefficients	Silver	Copper and copper oxide
a	5×10^{-2}	5×10^{-2}
b	32	21
c	4.2	0.9

DISCUSSION

1. The Catalytic Efficiency for Atomic Nitrogen

The only previous measurement of the absolute catalytic efficiency for atomic nitrogen of a surface used in the present study is that of Lord Rayleigh.[7] He found $\gamma = 2\times10^{-3}$ at 3 mm Hg pressure for a copper oxide surface, which is to be compared with the present measurement of 8×10^{-3}. Willey[8] measured the catalytic efficiency of several metals relative to that of copper (probably copper oxide) at 10 mm Hg and found for a silver surface a ratio of 0.26 or 0.79, depending upon the state of the copper surface. Our measured relative catalytic efficiency for these two surfaces is 0.65. When both the probable variability in surface characteristics and the low precision of the early measurements are considered, these comparisons are quite satisfactory.

Schechter[9] has investigated the recombination of nitrogen atoms on platinum and nickel at high temperatures. The measurements are not in a form from which a catalytic efficiency may be obtained. Willey[8] considers that the surface atoms are chemically bound as nitrides of the surface metal and that the catalytic efficiency is determined by the stability of these nitrides—implying that low stability leads to high catalytic efficiency.

The pressure dependence observed in the present experiments of the (probably) metal oxide surfaces suggests the formation of a protective molecular nitrogen layer over a saturated atomic layer. An inverse pressure dependence of γ, which would approximate that observed at high pressures, would be expected either from a Langmuir treatment of molecular sorption combined with the assumption that $\gamma \propto (1-\theta)$, where θ is the fractional surface coverage, or from reaction rate theory as emphasized by Shuler and Laidler.[10] Alternatively, one may assume that the catalytic action of the surface arises from the production of a nitrogen-containing compound requiring the presence of molecular nitrogen at the surface.

2. The Diffusion Coefficient of Atomic Nitrogen

Though at first glance it appears that Eq. (1) satisfactorily describes the data, the equation is incomplete in that no account is taken of the possible production of reactants at the catalytic surface.

As a schematic approach to the problems that may arise if the catalytic surface generates a reactive species, consider the following situation: (a) Nitrogen atoms diffuse to the catalytic surface and are thus lost from the volume V at a rate that has previously been calculated[1] (b) A second reactive component X is formed at the surface and reacts with N at the rate $\epsilon[N][X]$. However, because of the value of ϵ, and the very low concentrations of reactants present, negligible reaction occurs as the species X diffuses out of the tube into the volume V (c) X is lost only through the reaction considered in (b). Then

$$d[N]/dt = -k[N] - \epsilon[N][X] \tag{4}$$

$$dX/dt = \alpha k[N] - \epsilon[N][X], \tag{5}$$

where α represents the fraction of nitrogen atoms lost at the catalytic surface that produce the component X. Subtracting the above equations, utilizing the experimental fact that $[N]$ decays exponentially, $[N] = [N_0]\exp(-Kt)$, and performing the necessary integration gives

$$[X] = \alpha k/\epsilon \tag{6}$$

$$K = k(1+\alpha). \tag{7}$$

Thus the component X has a fixed concentration at equilibrium and the observed experimental decay rate may differ by the factor $(1+\alpha)$ from that corresponding to τ^{-1} of Eq. (1). Note that the surface can act only as a source or sink for the reactants and that only under these conditions would the observed variation of τ be linear with L. We have been discussing an example of the former; Eq. (1) was derived by considering only the latter.

By its nature α cannot be larger than one, or smaller than zero. The latter case has, of course, been discussed. When $\alpha = 1$, the diffusion coefficient obtained from the slope of τ vs L curves for the first positive bands will be half that previously obtained with $\alpha = 0$, i.e., $D = 280p^{-1}$ cm^2 sec^{-1}. The catalytic efficiencies of the surfaces for atomic nitrogen removal will also be half their former value. This will not materially alter the remarks of the previous section.

Reactions between counterflowing reactants in the diffusion tube have not been considered. Such reactions would be expected to distort the linear gradients in the diffusion tube resulting in a nonlinear dependence of τ on L. A volume reaction which would not destroy the linear gradient would still contribute a term proportional to L^{-1} in the expression for τ. The linearity of our selected experimental curves indicates that this complication is not present. However, reaction within the diffusion tube may be one of the causes for the curvature of some of the rejected data.

Computation of the interaction cross sections is one means of comparing the diffusion coefficient of atomic nitrogen, oxygen, and hydrogen. Because of the limited accuracy of the present measurements, the hard-sphere interaction potential will be used. The diffusion coefficient is given by [11]

$$D_{12} = \frac{2[T^3(M_1+M_2)/2M_1M_2]^{\frac{1}{2}}}{p\sigma_{12}^2}\ \frac{\text{cm}^2}{\text{sec}}, \tag{8}$$

[7] Lord Rayleigh, Proc. Roy. Soc. (London) **A88**, 302 (1913).
[8] E. J. B. Willey, J. Chem. Soc. **1927**, 2188.
[9] A. Schechter, Acta Physicochim. U.R.S.S. **10**, 379 (1939).
[10] K. E. Shuler and K. J. Laidler, J. Chem. Phys. **151**, 1212 (1949).
[11] J. Hirschfelder, C. Curtiss, and B. Bird, *Molecular Theory of Gases and Liquids* (John Wiley & Sons, Inc., New York, 1954).

TABLE II. Collision diameters assuming a ridged-sphere potential.

Collision partners	Collision diameters (in angstroms) Atom-atom Calculated	Atom-atom Experimental	Atom-molecule Calculated	Atom-molecule Experimental	Molecule-molecule Experimental
N, N_2 $\alpha=0$	2.88[e]	0.66[d]	3.26[f]	2.07	3.48[a]
	2.97[g]		3.32[g]		
N, N_2 $\alpha=1$	2.88[e]	2.40[d]	3.26[f]	2.94	3.48[a]
	2.97[g]		3.32[g]		
O, O_2	2.96[e]	2.89[d]	3.40[f]	3.12[b]	3.35[a]
	2.75[g]				
H, H_2	3.38[e]	2.60[d]	2.80[f]	2.49[c]	2.71[c]

[a] J. Hirschfelder, C. Curtiss, and B. Bird, *The Molecular Theory of Gases and Liquids* (John Wiley & Sons, Inc., New York, 1954), p. 545, Table 8, 3-1.
[b] S. Krongelb and M. Strandberg, J. Chem. Phys. **31**, 1196 (1959).
[c] I. Amdur, J. Chem. Phys. **4**, 339 (1936).
[d] Computed from $\sigma_{\text{atom-atom}}=2\sigma_{\text{atom-molecule}}-\sigma_{\text{molecule-molecule}}$.
[e] $\sigma_{\text{atom-atom}}=R_e$ (internuclear separation of diatomic molecule)$+1.8$ as suggested by J. Hirschfelder and M. Eliason, Ann. N. Y. Acad. Sci. **67**, 451 (1957).
[f] $\sigma_{\text{atom-molecule}}=4/3R_e+1.8$, J. Hirschfelder and M. Eliason, Ann. N. Y. Acad. Sci. **67**, 451 (1957).
[g] Calculated using the potentials of J. Vanderslice, E. Mason, and E. Lippincott J. Chem. Phys. **30**, 129 (1959) and J. Vanderslice, E. Mason, and W. Maisch, *ibid.* **32**, 515 (1960) by the method of J. Hirschfelder and M. Eliason, Ann. N. Y. Acad. Sci. **67**, 451 (1957).

where T is the absolute temperature, M_1 and M_2 are molecular weights, σ_{12} is the collision diameter in angstroms, which is the average diameter of the collision partners, i. e., $\sigma_{12}=\frac{1}{2}(\sigma_1+\sigma_2)$, and p is the pressure in mm Hg. Table II shows the results of such calculations.

Despite the failings of the hard-sphere model, particularly when strong attractive valence forces are present, some useful deductions may be made from Table II. One would expect a smaller difference in σ between O and N than between O and H. The inference is that $\alpha=1$. It must be remembered that these cross sections (or collision diameters) refer to nonreactive collisions.

On the basis of estimates of the atom-molecule collision diameters made using a method suggested by Hirschfelder and Eliason,[12] the experimental collision diameters for both nitrogen and oxygen are too small. This estimate may be made either from $\sigma=\frac{4}{3}R_e+1.8$ A where R_e is the equilibrium internuclear separation of the atoms in the diatomic molecule or from the potential for the N–N_2 interaction. If the potential found by Vanderslice *et al.*[13] is used one obtains $\sigma_{N-N2}=3.32$ A, while estimates from the internuclear diatomic separation give 3.26 A. These differ from the experimental value of 2.94 A. Part of this discrepancy is due to the different interaction potentials used in computing σ_{N-N_2}, and part is due to the somewhat arbitrary definition of this quantity when the hard-sphere potential is not used.

3. The CN Bands

One cannot, within the framework of the present theory, rationalize the fact that the τ vs L curves for the CN bands have the same slope but different intercepts from the first positive bands. Thus Eq. (1) can be generalized to the case of two interacting labile species.[1] However, to obtain τ vs L curves of the same slope as when only one component is present, one must also have the same intercept. Neither can one assume that a situation similar to that discussed in the preceding section is occurring: if the light intensity is proportional to $[N][X]$ where X is created on the catalytic surface, the τ vs L curves for this radiation should reflect those of the first positive bands.

The magnitude of the intercept of the CN band curves indicates that the reaction involves a decaying species other than atomic nitrogen. If one assumes this second species to have a decay time independent of L, then the over-all decay time will have a term proportional to L^2, and even if this should be relatively unimportant, both the remaining terms, one proportional to L and one independent of L, differ from the corresponding terms in Eq. (1) by the same factor.

One may approach the problem differently by

[12] J. Hirschfelder and M. Eliason, Ann. N. Y. Acad. Sci. **67**, 451 (1957).
[13] J. Vanderslice, E. Mason, and E. Lippincott, J. Chem. Phys. **30**, 129 (1959).

attempting to determine the most probable excitation mechanism for the CN bands in the present experiments. Hydrogen cyanide is probably the original carbon compound injected into the volume, because it is the major product of atomic nitrogen reactions with stopcock greases.[14] Further reactions of atomic nitrogen with HCN may produce light emission by the process[15]

$$N+HCN\rightarrow(N\cdot HCN] \qquad I$$

$$N+[N\cdot HCN]\rightarrow N_2+CN^*+H. \qquad II$$

The relative importance of reactions I and II compared with others involving C_2N_2 (which are the next alternatives)[15] will depend upon the residual hydrogen concentration because of the reactions[15,16]

$$C_2N_2+H\rightarrow HCN+CN \qquad III$$

$$CN+H_2\rightarrow HCN+H. \qquad IV$$

Since one generally obtains at least one hydrogen atom for each carbon atom liberated through atomic nitrogen reactions with stopcock grease, reactions III and IV will ultimately convert C_2N_2 to HCN, and reactions I and II will then be more important in the present system than reactions with C_2N_2. Even the assumption that the CN bands are excited by reactions I and II does not, however, clarify the experimental results.

[14] C. Haggart and C. A. Winkler, Can. J. Chem. **38,** 329 (1960).
[15] H. Evans, G. Freeman, and C. Winkler, Can. J. Chem. **34,** 1271 (1956).

[16] From the measurements of Haggart and Winkler[17] one would expect a negligible concentration of CN radicals because of their rapid reaction with the metaphosphoric acid coated walls (for which they measure a catalytic efficiency of 0.1). However, their walls, having been exposed to a very different environment from those in the present experiments, may have a different character.
[17] C. Haggart and C. A. Winkler, Can. J. Chem. **37,** 1791 (1959).

THE JOURNAL OF CHEMICAL PHYSICS VOLUME 34, NUMBER 4 APRIL, 1961

Infrared Spectra and Potential Constants of Some Monohaloacetylenes* † ‡

G. R. HUNT AND M. KENT WILSON

Department of Chemistry, Tufts University, Medford 55, Massachusetts

(Received October 13, 1960)

The infrared spectra of gaseous HC≡CF, HC≡CCl, and HC≡CBr and their deutero-compounds have been obtained under prism dispersion between 250 and 3500 cm^{-1}. All five fundamental vibrations have been identified for each of the hydrogen compounds and all but the lower bending mode for each of the deuterated compounds. Potential constants and vibrational amplitudes have been calculated.

INTRODUCTION

THE infrared spectra of HC≡CCl and DC≡CCl have been previously examined by Richardson and Goldstein.[1] These authors were able to identify four of the five fundamental frequencies of each molecule and to calculate the stretching force constants using a simple valence force field. A spectrum of one sample of monofluoroacetylene was given by Middleton and Sharkey,[2] but no spectrum of monobromoacetylene was found in the literature.

The molecular dimensions have been determined by electron diffraction for HC≡CBr,[3] by microwave spectroscopy for HC≡CF,[4] and by both techniques for HC≡CCl.[3,5] All three molecules have the expected linear configuration.

EXPERIMENTAL

Monofluoroacetylene was prepared by passing monofluoromaleic anhydride through a silica-packed column at 650°C.[2] Decomposition of the mercury (II) salt of 1,2-dichloroethylene with aqueous KOH and KCN[6] yielded monochloroacetylene, while monobromoacetylene was obtained directly from 1,2-dibromoethylene with aqueous KOH and KCN.[6] Each compound was collected in a trap cooled with liquid nitrogen and

* Contribution No. 269 from the Department of Chemistry, Tufts University, Medford, Massachusetts.
† This work is part of a program supported by the National Science Foundation.
‡ Presented, in part, at the Ohio State Symposium on Molecular Structure and Molecular Spectroscopy, Columbus, Ohio, June 13–17, 1960.
[1] W. S. Richardson and J. H. Goldstein, J. Chem. Phys. **18,** 1314 (1950).
[2] W. J. Middleton and W. H. Sharkey, J. Am. Chem. Soc. **81,** 803 (1959).
[3] L. O. Brockway and I. E. Coop, Trans. Faraday Soc. **34,** 1429 (1938).
[4] J. Sheridan (private communication, 1960).
[5] A. A. Westenberg, J. H. Goldstein, and E. B. Wilson, J. Chem. Phys. **17,** 1319 (1949).
[6] L. A. Bashford, H. J. Emeleus, and H. V. A. Briscoe, J. Chem. Soc. **1938,** 1358.

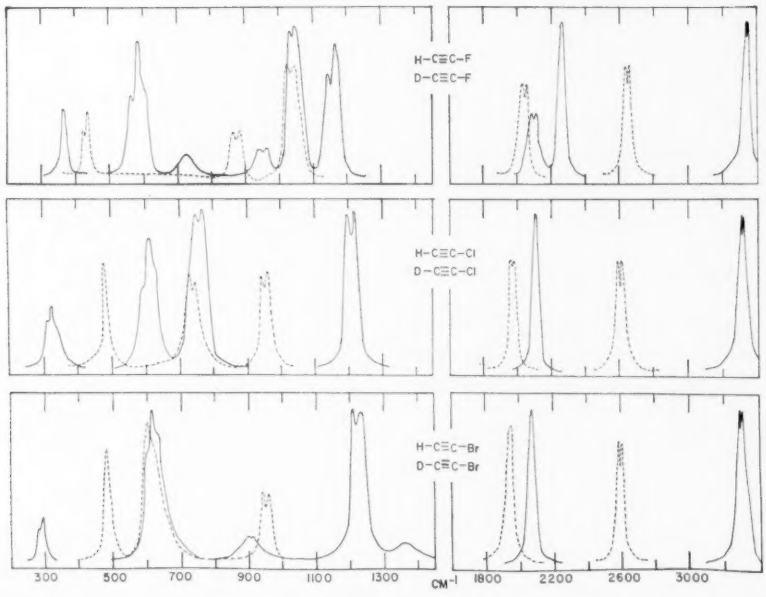

FIG. 1. Infrared spectra of monofluoroacetylene, monochloroacetylene, and monobromoacetylene. The solid curves are for the hydrogen compounds while the dashed curves are for the deuterated species.

purified by repeated bulb-to-bulb distillation until no absorption bands due to impurities could be observed.

The deutero-derivatives of these three compounds were prepared by repeatedly passing the gases through weakly alkaline D_2O and then purified by bulb-to-bulb distillation. About 70% deuteration was easily effected. As liquid monofluoroacetylene is liable to spontaneous decomposition[2] and the chloro- and bromo- compounds react violently with even slight traces of oxygen, no attempt was made to obtain higher enrichment. Because of the simple spectra of the acetylenes, the requisite information was readily obtained from these isotopically impure samples.

The infrared spectra were recorded with Perkin-Elmer model 21 spectrophotometers equipped with CaF_2, NaCl, and CsBr prisms. The spectra were recorded in absorption cells 10 cm in length with CsBr or KBr windows at gas pressures from 1 to 15 cm Hg.

The spectra obtained, replotted on a linear frequency scale, are reproduced in Fig. 1 and the band centers and band assignments for the fundamentals are listed in Table I. The spectra of the chloro-compounds are in essential agreement with those of Richardson and Goldstein.[1]

ASSIGNMENT

A linear molecular consisting of four atoms has seven vibrational degrees of freedom: three nondegenerate stretching modes (σ^+) and two doubly degenerate bending modes (π). All five fundamental frequencies are infrared and Raman active. The assignment of fundamentals is greatly aided by having the series of both heavy and light compounds.

The carbon-hydrogen stretching frequencies, $\nu_1(\sigma^+)$, occur near 3300 cm^{-1}, and move down to about 2600 in the deutero-compounds, while the C≡C stretching vibration, $\nu_2(\sigma^+)$, is found within 150 cm^{-1} of 2100 cm^{-1} for all compounds, as expected. The absorption bands near 1050, 750, and 600 cm^{-1} are assigned as the carbon-halogen stretching frequency $\nu_3(\sigma^+)$ in

TABLE I. Observed fundamental frequencies (cm^{-1}).

Mode of vibration		HC≡CF	DC≡CF	HC≡CCl	DC≡CCl	HC≡CBr	DC≡CBr
CH stretch	ν_1	3355	2645	3340	2612	3325	2600
CC stretch	ν_2	2255	2065	2110	1980	2085	1950
C—halogen stretch	ν_3	1055	1048	756	742	618	606
CCH bend	ν_4	578	439	604	472	618	480
CC—halogen bend	ν_5	367	~364	326	~312	295	~283

the fluoro-, chloro-, and bromo- compounds, respectively. The frequency shift on deuteration for these compounds is small, and further assistance in making these assignments is provided by comparison with the corresponding vibration in the methyl halides, where they occur at 1048,[7] 732,[8] and 611 cm^{-1},[9] and also with the halocyanides, where they appear at 1077,[10] 729, and 580 cm^{-1}.[11]

The carbon-hydrogen bending frequency, $\nu_4(\pi)$, is observed at 578, 604, and 618 cm^{-1} for the fluoro-, chloro-, and bromo- compounds, respectively. Upon deuteration this band decreases by about 130 cm^{-1} in each compound. Such an assignment places the carbon-hydrogen bending vibration and the carbon-bromine stretching vibration coincident in monobromoacetylene. No other bands are observed in this region and the assignment given fits into the consistent pattern for the series. It may also be mentioned that in monoiodoacetylene the C—H bending mode is observed at ~630 cm^{-1} and the C—I stretching frequency is found at ~600 cm^{-1}.[4]

Finally the carbon-carbon-halogen bending frequencies, $\nu_5(\pi)$, are assigned as the lowest frequency bands in the spectra. They are found at 367, 326, and 295 cm^{-1} for the hydrogen compounds, listed in the usual order. The centers of the corresponding bands in the deutero-compounds are not easily located as the bands are weak and in the heavier compounds lie near the limit of the instrument. Thus, the values of $\nu_5(\pi)$ for the chloro- and bromo- compounds, listed in Table I, are those obtained by application of the product rule.[12] The calculated and observed values of the product rule for the σ^+ vibrations, as well as the calculated values for the π vibrations, are listed in Table II. Satisfactory agreement between theory and experiment is noted.

TABLE II. Redlich-Teller product rule.

	HC≡CF, DF≡CF		HC≡CCl, DC≡CCl		HC≡CBr, DC≡CBr	
Mode	Calc	Obs	Calc	Obs	Calc	Obs
Stretches[a]	1.398	1.394	1.402	1.388	1.407	1.394
Bends[b]	1.326	...	1.337	...	1.341	...

[a] For stretching modes: $w_1w_2w_3/w_1^0w_2^0w_3^0=(m_iM/mM_i)^{\frac{3}{2}}$.
[b] For bending modes: $w_4w_5/w_4^0w_5^0=(m_iMI/mM_iI_i)^{\frac{1}{2}}$.

POTENTIAL CONSTANTS

The potential constants were calculated by the *F-G* matrix method.[13] The initial 5×5 matrix is factorized by symmetry into a 3×3 (σ^+) matrix and a 2×2 (π) matrix. The *G* elements are listed in Table III; those for the bending modes were obtained by the method of Ferigle and Meister.[14] The potential constants for the stretching modes were obtained by setting all off-diagonal terms in the *F* matrix equal to to zero and combining the three frequencies of both the heavy and light compounds. The latter procedure is valid only if zero-order frequencies are available. In the absence of such data for the haloacetylenes, anharmonicity corrections were estimated by considering the anharmonicity constants quoted for acetylene and acetylene-d_2 by Allen, Blaine, Plyer, and Tidwell.[15,16] These corrections were made in such a way that the Redlich-Teller product rule was exactly obeyed, and involved increases of about 30 cm^{-1} for the C—H stretch, about 15 cm^{-1} for the C—D stretch, 10 cm^{-1} for the C≡C stretch, and very small corrections, if any, for the C—halogen stretching frequency.

No adjustment was made for anharmonicity in the

TABLE III. *G*-matrix elements.

$$g_{11}=\mu_H+\mu_C$$

$$g_{12}=g_{21}=g_{23}=g_{32}=-\mu_C$$

$$g_{22}=2\mu_C$$

$$g_{33}=\mu_C+\mu_X$$

$$g_{44}=\mu_C\{(1/r_1^2)+[1/(r_1+r_2)^2]+[2/(r_1^2+r_1r_2)]+(1/r_1^2)\}+(\mu_H/r_1^2)$$

$$g_{45}=g_{54}=-\mu_C\{(2/r_2^2)+(1/r_1r_2)+(1/r_2r_3)\}$$

$$g_{55}=\mu_C\{(1/r_3^2)+[1/(r_2+r_3)^2]+[2/(r_2^2+r_2r_3)]+(1/r_2^2)\}+(\mu_X/r_3^2)$$

[7] W. H. Bennett and C. F. Meyer, Phys. Rev. **32**, 888 (1928).
[8] E. F. Barker and E. K. Plyer, J. Chem. Phys. **3**, 367 (1935).
[9] H. D. Noether, J. Chem. Phys. **10**, 664 (1942).
[10] E. E. Aynsley, R. E. Dodd, and R. Little, Proc. Chem. Soc. (London) **1959**, 265.
[11] W. G. Penney and G. B. B. M. Sutherland, Proc. Roy. Soc. (London) **A156**, 654 (1936).
[12] G. Herzberg, *Infrared and Raman Spectra of Polyatomic Molecules* (D. Van Nostrand Company, Inc., Princeton, New Jersey, 1945), p. 231.
[13] E. B. Wilson, Jr., J. Chem. Phys. **9**, 76 (1941).
[14] S. M. Ferigle and A. G. Meister, J. Chem. Phys. **19**, 982 (1951).
[15] H. C. Allen, E. K. Blaine, and L. R. Plyler, J. Research Natl. Bur. Standards **56**, 279 (1956).
[16] H. C. Allen, E. D. Tidwell, and E. K. Plyler, J. Research Natl. Bur. Standards **57**, 213 (1956).

TABLE IV. Adjusted frequencies for stretching modes (cm^{-1}).

HC≡CF	DC≡CF	HC≡CCl	DC≡CCl	HC≡CBr	DC≡CBr
3385	2660	3372	2627	3358	2615
2265	2075	2122	1987	2097	1958
1055	1048	759	742	620	606

TABLE V. Force constants.

	Stretching×10^5 d/cm			Bending×10^{-11} d/cm/rad	
Compound	C—H	C≡C	C—halogen	C≡C—H	C≡C—halogen
HC≡CF DC≡CF	6.2	15.4	8.8	0.135	0.360
HC≡CCl DC≡CCl	6.0	15.8	5.4	0.159	0.345
HC≡CBr DC≡CBr	5.9	15.7	4.6	0.173	0.303

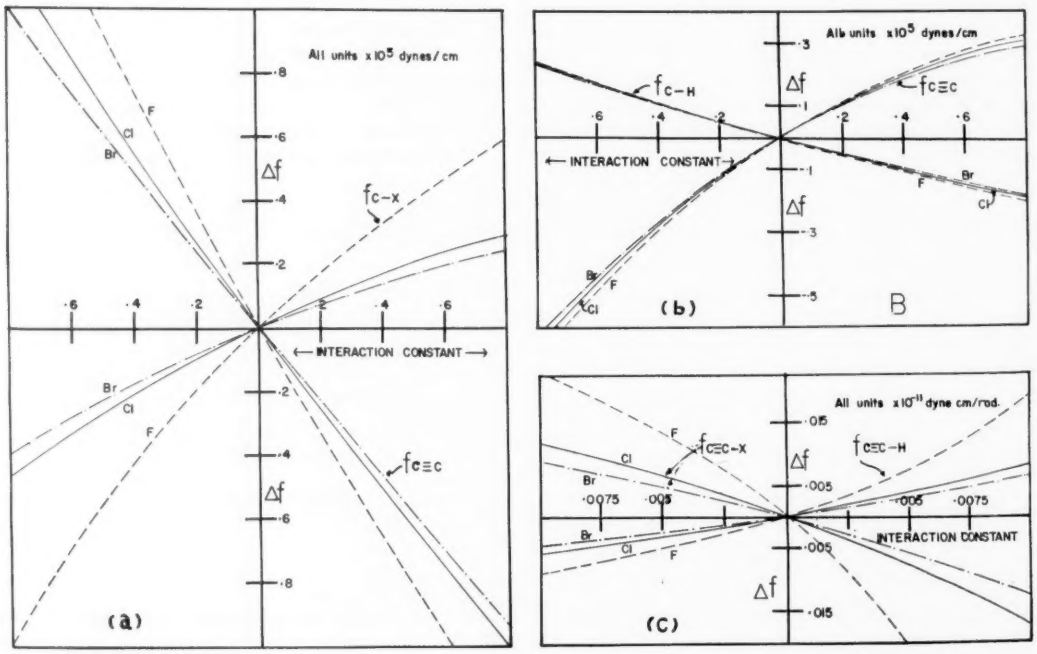

FIG. 2. The effect of the interaction terms on the principal force constants. (a) Interaction between the C-halogen and C≡C stretching modes, (b) interaction between the C—H and C≡C stretching modes, and (c) interaction between the C≡C-halogen and C≡C—H bending modes.

bending frequencies as the lower frequencies in the deuterium compounds were calculated with the aid of the product rule. The numerical values of the adjusted stretching vibrational frequencies actually used in the calculation are listed in Table IV, and the potential constants obtained are listed in Table V. In the absence of correct values for the anharmonicity constants or Coriolis coupling constants, no attempt was made to obtain definite values for the off-diagonal terms in the F matrix. However, in order to gain some indication of the effect on the principal force constants of neglecting these off-diagonal terms, the diagonal terms were calculated by including a range of values separately for each of the interaction constants. The extent of coupling between the C—H and C≡C, and between the C≡C and C—halogen valence vibrations were investigated separately; the matrix element linking the C—H and C—halogen stretching vibrations was kept equal to zero at all times. Results of these calculations for the σ^+ vibrations, as well as those for a similar calculation for the coupling between the two bending vibrations, are shown graphically in Fig. 2. Here the values of the interaction constant are plotted horizontally, while the difference between the value of the principal force constant computed with zero interaction and computed with the given value of the interaction constant, designated as Δf, is plotted vertically. Thus a positive value of Δf indicates a decrease in the principal force constant, while a negative Δf value indicates an increase.

Amplitudes of the various vibrational modes have been calculated using the adjusted frequencies and diagonal force constants. These amplitudes are illustrated in Fig. 3. The amplitudes of stretching modes are magnified 10 times relative to the internuclear distances. The amplitudes of the hydrogen bending modes are magnified 50 times and the other bending modes are enlarged 100 times relative to the internuclear distances.

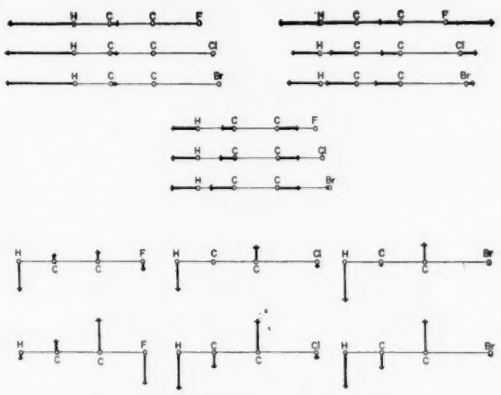

FIG. 3. Vibrational amplitudes. The amplitudes of the stretching modes are amplified 10 times relative to the internuclear distances. The amplitudes of the hydrogen bending modes are magnified 50 times and the other motions in the bending modes are amplified 100 times relative to the internuclear distances.

DISCUSSION

Table VI is a compilation of carbon-carbon, carbon-nitrogen, and carbon-halogen bond distances, and diagonal F-matrix elements for the haloacetylenes and several related molecules. Since the values quoted are for the F-matrix elements, which have different forms for vibrations of different symmetry, rather than for the individual bond stretching constants, f_i, it is difficult to make any direct comparison of these values. If it is assumed, however, that the interaction terms are small relative to the principal force constants, then such comparisons may be useful.

The C—halogen stretching force constants for the monohaloacetylenes are significantly larger than for the corresponding ethyl halides, but are essentially the same as those quoted for the cyanohalides. The C—halogen distances are very much shorter (about 10%) in the monohaloacetylenes than in the ethyl halides, but slightly longer than the corresponding bonds in the halocyanides. In the halocyanides the C≡N bond is lengthened over its value in hydrogen cyanide, and the lengthening is greatest in the case of fluorocyanide and least in bromocyanide. Also, because the carbon-hydrogen bond is most shortened in fluorocyanide, considerable support is given to the view that a double-bonded hybrid $N^-{=}C{=}F^+$ is contributing largely to the structure.[17] This contention is substantiated by the nuclear quadrupole coupling constants for the cyanohalides.[18]

On the other hand, the monohaloacetylenes show no evidence that the C≡C bond length is increased over the value for acetylene itself. In fact, except in the case of monochloroacetylene, where it appears there may be a very slight increase, the monohaloacetylenes exhibit a C≡C distance which appears to be shorter than that in acetylene itself. A similar situation is encountered in diacetylene[19] and dicyanoacetylene,[19] where the C—C bond distance is very much less than is ordinarily ascribed to a single bond, yet the C≡C bond shows no lengthening over that normally associated with a pure triple bond. Likewise, no lengthening of the central bond is observed in the dihaloacetylenes. However, Mulliken[20] has shown that for double bonds involved in conjugation, the best calculations to date indicate that only a very small increase in length is to be expected. This increase is so small as to lie within the experimental uncertainty. It might be pointed out that the C≡C stretching force constants in the monohaloacetylenes are lower than in acetylene, but only

[17] J. Sheridan *et al.*, Nature **185**, 96 (1960).
[18] P. A. Casabella and P. J. Bray, J. Chem. Phys. **28**, 1182 (1958).
[19] G. D. Craine and H. W. Thompson, Trans. Faraday Soc. **49**, 1273 (1953).
[20] R. S. Mulliken, Tetrahedron **6**, 68 (1959).

TABLE VI. Bond lengths (A) and stretching force constants ($\times 10^5$ d/cm) of the monohaloacetylenes and related compounds.

Molecule	X=hydrogen		X=fluorine		X—chlorine		X—bromine	
	C—H dist.	f_{C-H}	C—F dist.	f_{CF}	C—Cl dist.	f_{CCl}	C—Br dist.	f_{CBr}
CH_3CH_2—X	1.107 E*[a]	4.79[b]	1.375 M[e]	5.96[d]	1.777 M[e]	3.64[d]	1.94 M[f]	3.13[d]
CH_2=CH—X	1.071 I*[g]	5.08[h]			1.736 M[i]		1.891 M[j]	
CH_3C≡C—X	1.060 M*[k]	5.18[l]			1.637 M[m]	5.3[l]	1.793 M[n]	4.35[l]
HC≡C—X	1.0587$_o$	5.85[b]	1.275 M[p]	8.8	1.632 M[q]	5.4	1.80 E[r]	4.6
N≡C—X	1.0630[p]	5.80[d]	1.260 M[s]	8.07[t]	1.629 M[u]	5.2[d]	1.790 M[u]	4.2[d]
	C—C dist.	f_{CC}	C—C dist.	f_{CC}	C—C dist.	f_{CC}	C—C dist.	f_{CC}
CH_3CH_2—X	1.536 E[a]	4.50[b]	1.540 M[e]	4.50[b]	1.5508 M[e]	4.50[b]	1.5508 M[f]	4.50[b]
CH_2=CH—X	1.353 I[g]	9.57[b]			1.34 M[i]		1.34 M[j]	
CH_3C≡C—X	1.207 M[k]	15.799[l]			1.2069 M[m]	15.799[l]	1.207 M[n]	15.799[l]
HC≡C—X	1.2054[o]	15.85	1.20 M[p]	15.4	1.211 M[q]	15.8	1.20 E[r]	15.7
N≡C—X	1.1538†[o]	17.9†[d]	1.165 M†[s]	17.5†[t]	1.163 M†[u]	16.7†[d]	1.158 M†[u]	16.9†[d]

CH≡C—C≡CH; C—C dist. 1.379, C≡C dist. 1.205 I[v,19]
CH≡C—C≡N; C—C dist. 1.382, C≡C dist. 1.203, C≡N dist. 1.157 M[v,19]

* Letters refer to method of measurement: E, electron diffraction; I, infrared; M, microwave.
† Refers to N≡C dist. and $f_{N\equiv C}$.

[a] A. Almenningen and O. Bastianson, Acta Chem. Scand. **9,** 815 (1955).
[b] B. L. Crawford and S. R. Brinkley, J. Chem. Phys. **9,** 69 (1941).
[c] J. Kraitchman and B. P. Dailey, J. Chem. Phys. **23,** 184 (1955).
[d] W. G. Penney and G. B. B. M. Sutherland, Proc. Roy. Soc. (London) **A156,** 654 (1936).
[e] R. S. Wagner and B. P. Dailey, J. Chem. Phys. **23,** 1355 (1955).
[f] R. S. Wagner, N. Solimene, and B. P. Dailey, J. Chem. Phys. **23,** 599 (1955).
[g] W. S. Galloway and E. F. Barker, J. Chem. Phys. **10,** 88 (1942).
[h] Footnote 12, p. 184.
[i] J. W. Simmons, Phys. Rev. **76,** 689 (1949).
[j] C. D. Cornwell, J. Chem. Phys. **18,** 1118 (1950).
[k] L. F. Thompson, E. I. Sherrard, and J. Sheridan, Trans. Faraday Soc. **51,** 619 (1955).
[l] A. G. Meister, J. Chem. Phys. **16,** 950 (1948).
[m] C. C. Costain, J. Chem. Phys. **23,** 2037 (1955).
[n] J. Sheridan and W. Gordy, J. Chem. Phys. **20,** 735 (1952).
[o] J. Overend and H. W. Thompson, Proc. Roy. Soc. (London) **A234,** 306 (1956).
[p] J. Sheridan (private communication).
[q] A. A. Westenberg, J. H. Goldstein, and E. B. Wilson, J. Chem. Phys. **17,** 1319 (1949).
[r] L. O. Brockway and I. E. Coop, Trans. Faraday Soc. **34,** 1429 (1938).
[s] J. Sheridan *et al.*, Nature **185,** 96 (1960).
[t] W. J. Orville Thomas, J. Chem. Phys. **20,** 920 (1952).
[u] C. H. Townes, A. N. Holden, and F. R. Merritt, Phys. Rev. **74,** 1113 (1948).
[v] G. D. Craine and H. Thompson, Trans Faraday Soc. **49,** 1273 (1953).

significantly so for fluoroacetylene. From a consideration of the force constants alone, then, it may be argued that the carbon—halogen bond has some double-bond character, and if so, this is greatest in the case of monofluoroacetylene, as one might expect. However, until more information concerning the anharmonicity constants, Coriolis coupling constants, and quadrupole coupling constants for the monohaloacetylenes is available, we do not feel that a quantitative estimate of the double-bond character can be made. We do feel, however, that since stretching the C—halogen bond would favor the single-bonded C—halogen structure, the interaction constant between the C≡C stretch and C—halogen stretch should be positive and probably largest for fluoroacetylene. If such is the case, then the figures quoted in Table V for the zero interaction constant represent minimum values for the C≡C force constants and maximum values for the C—halogen constants. Figure 2(b) indicates that there is no strong coupling between C≡C and C—H stretching motions, as expected, and Fig. 2(c) indicates the same situation for the coupling between the bending modes.

We do not feel that the differences between the C—H stretching force constants in the monohaloacetylenes quoted in Tables V and VI are significant. The values are in the region usually associated with an acetylene system.

ACKNOWLEDGMENTS

The authors wish to thank Professor Paul Doty for the use of a Perkin-Elmer model 21 spectrophotometer equipped with CaF_2 optics, Dr. W. H. Sharkey for the gift of a sample of monofluoromaleic anhydride, and Dr. J. Sheridan for communicating to us preliminary results on HC≡CI and DC≡CI.

An Extended Hole Theory of Liquids

GEORGE E. BLOMGREN

Parma Research Laboratory, Union Carbide Corporation, Parma, Ohio

(Received October 28, 1960)

The hole theory of liquids has been extended to include the effect of all configurations of particles and holes on the partition function. The potential energy of a particle in a cell surrounded by a given number of particles and holes is approximated by a Lennard-Jones and Devonshire-type function appropriate to the given number of neighbors. The partition function is derived on the basis of the model and an expansion procedure is used to simplify the problem of the summation over all configurations of particles and holes. The equation of state is obtained from the partition function and expressed in terms of a reduced volume and temperature, a cell size parameter and known physical constants. Possible extensions of the present theory are discussed.

I. INTRODUCTION

IN the past decade a considerable amount of work has been done on lattice theories of the liquid state. Most of this work has been based on, or given impetus by, the treatment of Kirkwood[1] in 1950 which showed the relationship of the Lennard-Jones and Devonshire[2] (L–JD) free volume theory of liquids to statistical mechanics in terms of well defined approximations. The L–JD theory is based on a model of the liquid in which a regular lattice structure of cells, each containing one molecule, is assumed. Thus, the number of cells is the same as the number of molecules. Further developments[3] proceeding from Kirkwood's analysis have considered the effect of configurations allowing multiple occupation of cells, keeping the number of cells fixed.

Another approach to the theory of liquids relaxed the free-volume theory restriction of the number of cells equal to the number of molecules, but maintained the restriction of single occupancy as a maximum. Thus, this model, introduced by Eyring[4] in 1936, pictures the liquid state as an equilibrium mixture of singly occupied cells and unoccupied cells or "holes" in a regular lattice structure. As has been shown by Hill,[3] this model is capable of giving an exact theory of the liquid state which is independent of the particular lattice geometry chosen, if no approximations are introduced, as long as the cell size is small enough to make multiple occupation unlikely. Unfortunately, it is not possible to solve the problem exactly, due to the difficulties presented by many body interactions and a dependence of any hole theory on the lattice geometry, as well as the cell size, is to be expected.

The hole theory of liquids has been developed historically in much the same way as the free-volume theory. On the basis of the model, several approximations to the partition function were intuitively derived.[5–8] Then a derivation of the partition function, which was based largely on the solution theory of Salsburg and Kirkwood[9] and which defined the approximations inherent in the intuitive developments, was made by Hill.[3] This derivation and subsequent discussion brings into sharp focus one of the essential problems of any lattice-theory approach to the theory of liquids, which is to satisfy the requirement for fluid states that the singlet density or probability of finding a particle at any point within the liquid boundaries be independent of the position of the point. In the free-volume theory this requirement can be satisfied only if multiple occupation of cells is taken into account and a constant density restraint imposed. In the hole theory proceeding from the Hill derivation a constant density restraint poses some difficult problems in the theoretical development. In the theory developed in this paper, no provision is made for the constant density condition and as a result the model resembles a solid somewhat more than a liquid, as do all other current lattice theories. A discussion will be presented, however, showing the direction in which the present theory might be extended to improve the cell density situation.

It should be mentioned that another hole theory has been developed by Mayer and co-workers[10,11] based on a derivation from the grand canonical ensemble. This treatment, however, includes approximations different from those in the present work, as pointed out by Hill,[3] and will not be discussed further.

It should also be mentioned that all the work discussed in this paper is based on classical statistical mechanics.

[1] J. G. Kirkwood, J. Chem. Phys. **18,** 380 (1950).
[2] J. E. Lennard-Jones and A. F. Devonshire, Proc. Roy. Soc. (London) **A163,** 53 (1937).
[3] T. L. Hill, *Statistical Mechanics* (McGraw-Hill Book Company, Inc., New York, 1956), Chap. 8.
[4] H. Eyring, J. Chem. Phys. **4,** 283 (1936).
[5] F. Cernuschi and H. Eyring, J. Chem. Phys. **7,** 547 (1939).
[6] S. Ono, "Memoirs of the Faculty of Engineering," Kyushu Univ. **10,** 190 (1947).
[7] H. M. Peek and T. L. Hill, J. Chem. Phys. **18,** 1252 (1950).
[8] J. S. Rowlinson and C. F. Curtiss, J. Chem. Phys. **19,** 1519 (1951).
[9] Z. W. Salsburg and J. G. Kirkwood, J. Chem. Phys. **20,** 1538 (1952).
[10] J. E. Mayer and G. Careri, J. Chem. Phys. **20,** 1001 (1952).
[11] H. B. Levine, J. E. Mayer, and H. Aroeste, J. Chem. Phys. **26,** 201, 207 (1957).

II. EARLIER HOLE THEORIES

In this discussion of the earlier hole theories,[5–8] the model consists of a face-centered cubic lattice of L spherical cells containing N molecules, subject to the conditions $L \geq N$, single maximum occupancy and intermolecular interactions limited to nearest neighbors.

Following Hill[3] one can derive an approximate configurational partition function from statistical mechanics given by

$$Z = \sum_l \exp\left\{-\frac{[zN - N_{AB}(l)]E(0)}{2kT}\right\} \prod_{i=0}^{z} (v_i)^{N_i(l)}, \qquad (1)$$

where l represents a particular configuration of N molecules in L cells and the summation of l is over all distinct configurations which differ by more than an interchange of the identical molecules; z is the first coordination number which is 12 for a face-centered cubic lattice; $N_{AB}(l)$ is the number of nearest-neighbor pairs with one cell occupied and the other vacant, which depends on the particular configuration, l; $E(0)$ is the pair potential energy of a molecule at the center of its cell and a nearest neighbor which lies with equal probability at any position on a sphere of radius equal to the lattice spacing constant; v_i is the $L-JD$ "free volume" integral for a molecule surrounded by i neighbors averaged over the sphere; $N_i(l)$ is the number of molecules which have i neighbors in the configuration l. To complete the above definitions, the following expressions are given,

$$E(0) = \epsilon(q^{-4} - 2q^{-2}), \qquad (2)$$

where

$$q = v_{\text{cell}}/v_0, \qquad v_0 = r_0^3, \qquad v_{\text{cell}} = a^3/\sqrt{2}, \qquad (3)$$

and ϵ and r_0 are the energy and distance characteristics of the Lennard-Jones intermolecular potential

$$E(r) = 4\epsilon\{(r_0/r)^{12} - (r_0/r)^6\}, \qquad (4)$$

where r is the distance between two spherical molecules.
Further,

$$v_i = 2\pi\sqrt{2} r_0^3 q g_i \qquad (5)$$

$$g_i = \int_0^s y^3 \exp\{-(i/\tau)[q^{-4} l(y) - 2q^{-2} m(y)]\} dy, \qquad (6)$$

where

$$y = r^2/a^2 \qquad (7)$$

$$l(y) = (1 + 12y + 25.2y^2 + 12y^3 + y^4)(1-y)^{-10} - 1 \qquad (8)$$

$$m(y) = (1+y)(1-y)^{-4} - 1 \qquad (9)$$

$$s = (\tfrac{3}{4}\pi\sqrt{2})^{\frac{1}{3}} = 0.30544 \qquad (10)$$

$$\tau = kT/\epsilon \qquad (11)$$

and r is now the distance of the molecule from the center of its cell. The total number of distinct configurations is given by

$$g(L, N) = L!/N!(L-N)!. \qquad (12)$$

The total partition function is given by the product of Eq. (1) and the factor $(2\pi mkT/h^2)^{3N/2}$, which represents the kinetic-energy part of the partition function.

The above notation corresponds closely to that of the work cited in footnote 8. Rowlinson and Curtiss[8] have given a careful analysis of the approximations made in their own and earlier theories[5–7] in the further development of Eq. (1). They point out that all of these theories make the approximation that the dependence of the "free volume" integral v_i on the number of neighbors can be expressed by a linear relation of the form

$$\ln v_i = (z-i)A + iB. \qquad (13)$$

Thus the only essential difference between these four theories lies in the choice of the constants A and B. That any relation of the form of Eq. (13) is poor can be seen from Fig. 1 of the work cited in footnote 8. The reason that the approximation is made is that when Eq. (13) is substituted into Eq. (1), Eq. (1) becomes of the same form as the initial equation of the "quasi-chemical" approximation of Guggenheim and Bethe.[12] Thus, the difficult problem of performing the summation over all configurations can be handled by well-known methods to the accuracy inherent in this approximation.

That the error involved in the linear assumption of Eq. (13) can be avoided and the statistical problem of summing over configurations can be handled for the more general problem by a technique of the same general accuracy as the "quasi-chemical" approach is shown in the next section.

III. THE EXTENDED HOLE THEORY

A. General Treatment

The total number of neighbors of particles for any configuration is given simply by

$$zN = N_{AB}(l) + 2N_{AA}(l), \qquad (14)$$

where $N_{AA}(l)$ is the number of nearest-neighbor pairs of cells, both occupied. The quantity $2N_{AA}(l)$ for the configuration is also given by

$$2N_{AA}(l) = \sum_{i=0}^{z} iN_i(l) = zN - N_{AB}(l). \qquad (15)$$

Therefore, substituting Eq. (15) for $zN - N_{AB}(l)$ into Eq. (1), the result is obtained

$$Z = \sum_l \exp\{\sum_{i=0}^{z} \lambda_i N_i(l)\}, \qquad (16)$$

where

$$\lambda_i = -i(E(0)/2kT) + \ln v_i. \qquad (17)$$

[12] R. H. Fowler and E. A. Guggenheim, *Statistical Thermodynamics* (Cambridge University Press, New York, 1939).

If the different configurations l were to occur with equal probability, Eq. (16) would reduce to the Bragg-Williams approximation (see work cited in footnote 12), which is

$$Z_{\text{B.W.}}=g(L, N)\exp\{\sum_i \lambda_i \bar{N}_i\}, \tag{18}$$

where $g(L, N)$ is defined by Eq. (12) and $\bar{N}_i$ is the unweighted average value of the number of particles with i neighbors. Now, if Eq. (16) is divided by Eq. (18),

$$Z/Z_{\text{B.W.}}=[1/g(N, L)]\sum_l \exp\{\sum_i \lambda_i(N_i(l)-\bar{N}_i)\}. \tag{19}$$

Equation (19) is now in a form suitable to be handled by a technique similar to one developed by Kirkwood[13] for mixtures. Thus, if the departures of $N_i(l)$ from the unweighted average value are not large for the majority of the configurations, the exponential in Eq. (19) can be expanded in a power series of the term in brackets

$$\exp\{\sum_i \lambda_i(N_i(l)-\bar{N}_i)\}=1+\sum_i \lambda_i(N_i(l)-\bar{N}_i)$$
$$+\tfrac{1}{2}\sum_{i,j}\lambda_i\lambda_j(N_i(l)-\bar{N}_i)(N_j(l)-\bar{N}_j)+\cdots. \tag{20}$$

Substituting Eq. (20) into Eq. (19),

$$Z/Z_{\text{B.W.}}=[1/g(N, L)]\sum_l\{1+\sum_i \lambda_i(N_i(l)-\bar{N}_i)\}$$
$$+\tfrac{1}{2}\sum_{i,j}\lambda_i\lambda_j(N_i(l)-\bar{N}_i)(N_j(l)-\bar{N}_j)+\cdots. \tag{21}$$

Now the order of the summation over l and those over i, j, etc., can be interchanged and since λ_i is independent of the configuration l, the result is obtained,

$$Z/Z_{\text{B.W.}}=1+\tfrac{1}{2}\sum_{i,j}\lambda_i\lambda_j(\langle N_iN_j\rangle_{\text{Av}}-\bar{N}_i\bar{N}_j)+\cdots, \tag{22}$$

where $\langle N_iN_j\rangle_{\text{Av}}$ is the unweighted average value of $N_i(l)N_j(l)$. The quantity of interest, however, is the logarithm of the partition function from which the thermodynamic properties may be obtained. Thus, if logarithms of both sides of Eq. (22) are taken and the right hand side expanded, the result is,

$$\ln Z=\lng(N, L)+\sum_i \lambda_i\bar{N}_i$$
$$+\tfrac{1}{2}\sum_{i,j}\lambda_i\lambda_j(\langle N_iN_j\rangle_{\text{Av}}-\bar{N}_i\bar{N}_j)+\cdots, \tag{23}$$

where the expression for $\ln Z_{\text{B.W.}}$ obtained from Eq. (18) has been substituted into Eq. (23). In the present treatment, the approximation has only been carried out to square terms in the λ's. It has been shown, however,[14] that there is a very close correspondence between the "quasi-chemical" approximation and the method of Kirkwood through cubic terms in the interaction energy (which plays a role similar to the λ's in the present theory) in regular solution theory and that for determining the critical temperature of mixing, for example, the largest contribution from correction terms to the Bragg-Williams approximation comes from the square term with higher terms contributing successively smaller corrections (see Table 4.9, work cited in footnote 14).

The method of determining the statistical factors will now be discussed and the lengthy algebra involved will make apparent the reason for stopping with the quadratic term.

B. The Terms $\bar{N}_i$

The unweighted average value of the number of particles with i neighbors $\bar{N}_i$ can be found in the following way. First a configuration of a central particle with i neighbors and $(z-i)$ holes at definite locations is specified, where z is 12. The probability of this configuration is given by the following, where N_h is the number of holes, equal to $L-N$,

$$N[(N-1)/(L-1)][(N-2)/(L-2)]\cdots[(N-i)/(L-i)][N_h/(L-i-1)]\cdots[(N_h-11+i)/(L-12)],$$

since the probability of a particle being at any particular site is given by the number of particles divided by the number of sites available. The number of ways in which the i particles and $(12-i)$ holes can be rearranged to give distinct configurations which differ by more than an interchange of particles is given by the binomial coefficient

$$\binom{12}{i}.$$

Thus, the quantity $\bar{N}_i$ is the product of these two terms,

$$\bar{N}_i=N\binom{12}{i}[(N-1)/(L-1)][(N-2)/L-2)]\cdots[(N-i)/(L-i)][N_h/(L-i-1)]$$
$$\cdots[(N_h-11+i)/(L-12)]. \tag{24}$$

[13] J. G. Kirkwood, J. Chem. Phys. **6**, 70 (1938) and J. Phys. Chem. **43**, 97 (1939).
[14] E. A. Guggenheim, *Mixtures* (Oxford University Press, New York, 1952), Chap. IV.

It is of interest to determine some sum rules for the quantities $\bar{N}_i$. In particular, it can be shown that

$$\sum_i \bar{N}_i = N \tag{25}$$

and

$$\sum_i i\bar{N}_i = 12N[(N-1)/(L-1)]. \tag{26}$$

The first rule Eq. (25) follows from the definition of $\bar{N}_i$ and can also be found by summing the individual terms. The second rule Eq. (26) was found by summing the individual terms and can be shown to be equivalent to the corresponding summation in Kirkwood's theory of mixtures,[13] which is defined as the first moment of the distribution of type B particles around type A particles. In our case we are interested in the distribution of A particles around A particles and a suitable change in the terms $\bar{N}_i$ must be made to show the correspondence.

It should also be noted that the terms $\bar{N}_i$ can be expanded to terms of order unity, all other terms of the order of L^{-1} or smaller, to give

$$\bar{N}_i = N\binom{12}{i}\{(N^i N_h^{12-i}/L^{12}) - \tfrac{1}{2}[i(i+1)](N^{i-1}N_h^{12-i}/L^{12}) - \tfrac{1}{2}[(11-i)(12-i)](N^i N_h^{11-i}/L^{12}) + \tfrac{1}{2}[12(13)](N^i N_h^{12-i}/L^{13}) + O(1/L^2)\}. \tag{27}$$

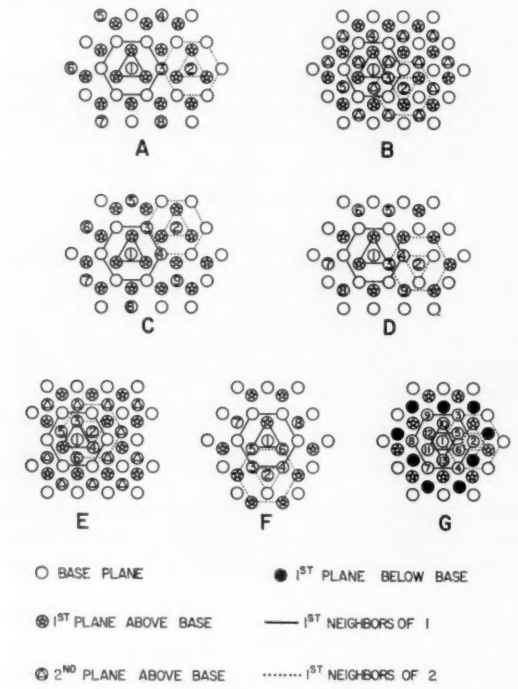

FIG. 1. Face-centered cubic lattice. (A) and (B): 1 and 2 are 4th neighbors (n); 3 is a 1st n site common to 1 and 2; 4–8 are other 4th n sites each having one common 1st n with 1. (C), (D), and (E): 1 and 2 are 3rd n; 3 and 4 are 1st n sites common to 1 and 2; 5–9 other 3rd n sites each having two 1st n in common with 1. (F): 1 and 2 are 2nd n; 3–6 are 1st n sites common to 1 and 2; 7 and 8 are other 2nd n sites each having four 1st n in common with 1. (G): 1 and 2 are 1st n; 3–6 are 1st n sites common to 1 and 2; 7–13 are other 1st n sites each having four 1st n in common with 1.

C. The Terms $(\langle N_i N_j\rangle_{Av} - \bar{N}_i\bar{N}_j)$

To evaluate the terms $(\langle N_i N_j\rangle_{Av} - \bar{N}_i\bar{N}_j)$ it is first necessary to discuss the terms $\langle N_i N_j\rangle_{Av}$ separately. At first it may appear as if some difficulties might be encountered as there will be terms of the order of N^2 occurring in both $\langle N_i N_j\rangle_{Av}$ and the $\bar{N}_i\bar{N}_j$. It will be shown, however, that the terms of order N^2 exactly cancel and only terms of order N and smaller terms, which are of no concern in the present treatment, are left.

The meaning of the term $\langle N_i N_j\rangle_{Av}$ is that the average value is to be obtained for the product of the number of particles with i neighbors and the number of particles with j neighbors. The probabilities can be computed for this case by considering the distributions of neighbors around two particles and including terms for one particle when i is equal to j. This method can be discussed more clearly by the following. Let $\chi_\alpha(i)$ be defined as a quantity which has the value unity if a given particle α has i neighbors and zero otherwise. Then the number of particles with i neighbors in the configuration l is given by

$$N_i(l) = \sum_{\alpha=1}^{N} \chi_{\alpha,l}(i). \tag{28}$$

The average value of N_i is then given by

$$\bar{N}_i = N\langle\chi_1(i)\rangle_{Av}, \tag{29}$$

which is simply another way of expressing the derivation of Eq. (24), where the average value is found from consideration of a given particle, in this case particle 1.

Similarly, for a given configuration l the quantity $N_i(l)N_j(l)$ is given by

$$N_i(l)N_j(l)=\sum_{\alpha,\beta=1}^{N}\chi_{\alpha,l}(i)\chi_{\beta,l}(j). \tag{30}$$

In finding the average value $\langle N_iN_j\rangle_{Nv}$ it is natural to separate the terms on the right-hand side (RHS) of Eq. (30) into terms for which α equals β and those for which α does not equal β. Thus,

$$\langle N_iN_j\rangle_{Nv}=N\langle\chi_1(i)\chi_1(j)\rangle_{Nv}$$
$$+N(N-1)\langle\chi_1(i)\chi_2(j)\rangle_{Nv}. \tag{31}$$

The first term on the RHS of Eq. (31) is evidently zero if i is not equal to j. If i equals j, the probability is simply that which was obtained for the average value $\bar{N}_i$, since in any configuration l if the particle α has i neighbors the weight given by the first term is

$$\chi_{\alpha,l}(i)\chi_{\alpha,l}(i)=1\times1=1,$$

and if the particle does not have i neighbors, the weight is

$$\chi_{\alpha,l}(i)\chi_{\alpha,l}(i)=0\times0=0.$$

Therefore, Eq. (31) can be written

$$\langle N_iN_j\rangle_{Nv}=\bar{N}_i\delta_{ij}+N(N-1)\langle\chi_1(i)\chi_2(j)\rangle_{Nv}, \tag{32}$$

where δ_{ij} is zero if $i\neq j$ and unity if $i=j$. For the second term on the RHS of Eq. (32), two different situations may be distinguished. One in which the two particles under consideration, 1 and 2, have no common nearest neighbors and one in which they have common nearest neighbors. In the first case, the probability may be computed by fixing particle 1 in the lattice and then particle 2 at another lattice site such that 1 and 2 have no common neighbors. A factor $1-[N'/(L-1)]$, where N' is the number of positions with respect to particle 1 in which particle 2 has common neighbors with particle 1, must be introduced into the probability to take account of the reduction of possible locations for particle 2. Then i particles and $(12-i)$ holes are placed around particle 1 and j particles and $(12-j)$ holes are placed around particle 2. The number of distinct ways of placing the neighbors is given by a product of binomial coefficients,

$$\binom{12}{i}\binom{12}{j},$$

so that the average value of $\langle N_iN_j\rangle_{Nv}$ for this case is given by

$$N(N-1)\{1-[(N'/(L-1)]\}\binom{12}{i}\binom{12}{j}\frac{(N-2)\cdots(N-i-j-1)N_h\cdots(N_h-23+i+j)}{(L-2)(L-3)\cdots(L-25)}. \tag{33}$$

By inspection of a face-centered cubic lattice, it can be seen that first-through fourth-neighbor positions with respect to a given particle have common neighbors with the first particle. Of these positions there are 12 first neighbors, 6 second neighbors, 24 third neighbors, and 12 fourth neighbors. The sum of these is 54 which is then the value of N' in the expression (33). The various common neighbor positions must now be treated separately.

Reference to Figs. 1(A) and (B) shows that for a face-centered cubic lattice there are 12 fourth-neighbor positions [three more lie below the base plane in Fig. 1(B)], each having one common nearest neighbor with the central particle. Different probabilities occur for a given i and j depending on whether the common neighbor site [site 3 in Fig. 1(A) and 1(B)] is occupied or vacant. For example, if either i or j is 12, the probability is zero if site 3 is vacant and different from zero if occupied. Thus, there will be two terms in the expression for $\langle N_iN_j\rangle_{Nv}$ for fourth-neighbor positions, one corresponding to site 3 vacant and one to site 3 occupied. The value will also be weighted by the factor $12/(L-1)$, which is the fraction of available sites which are fourth neighbors to the central particle. For this situation there are 23 nearest-neighbor sites which for given i and j may be occupied in two ways which give rise to different probabilities. The fourth-neighbor expression for $\langle N_iN_j\rangle_{Nv}$ then gives

$$N(N-1)[12/(L-1)]\sum_{s=0}^{1}\left[\binom{11}{i-s}\binom{11}{j-s}\frac{(N-2)\cdots(N-i-j+s-1)N_h\cdots(N_h-22+i+j-s)}{(L-2)(L-3)\cdots(L-24)}\right], \tag{34}$$

where it is understood that if either $(i-s)$ or $(j-s)$ is less than zero or greater than 11, the term is zero. The value $s=0$ corresponds to site 3 vacant and $s=1$ to site 3 occupied. The binomial coefficients have an upper index of 11 because the two particles each have 11 independent neighboring sites in which $(i-s)$ and $(j-s)$ particles may be distributed in the number of distinct ways given by the above binomial coefficients.

Figure 1(C), (D), and (E) show the locations of 15 of the 24 third neighbors (the other nine below the plane are not shown) and indicate that all third neighbors have two common nearest neighbors. Similar reasoning to that used in obtaining (34) leads to the expression for $\langle N_iN_j\rangle_{Nv}$ for third neighbors,

$$N(N-1)\binom{24}{L-1}\sum_{r=0}^{2}\binom{2}{r}\binom{10}{i-r}\binom{10}{j-r}\frac{(N-2)\cdots(N-i-j+r-1)N_h\cdots(N_h-21+i+j-r)}{(L-2)(L-3)\cdots(L-23)}, \tag{35}$$

where r is the number of particles on the common neighbor sites, and it is understood that if either $(i-r)$ or $(j-r)$ is less than zero or greater than ten, the term is zero. The binomial coefficient

$$\binom{2}{r}$$

gives the number of distinct configurations arising from r particles on the two common-neighbor sites.

Figure 1(F) shows the location of three of the six second neighbors (the other three lie below the plane). It is evident from the figure that each second neighbor has four common nearest neighbors with the central particle, which leads to the expression

$$N(N-1)\binom{6}{L-1}\sum_{n=0}^{4}\binom{4}{n}\binom{8}{i-n}\binom{8}{j-n}\frac{(N-2)\cdots(N-i-j+n-1)N_h\cdots(N_h-19+i+j-n)}{(L-2)(L-3)\cdots(L-21)}. \tag{36}$$

Again, if $(i-n)$ or $(j-n)$ is greater than eight or less than zero, the term (36) is zero.

Figure 1(G) indicates the location of the 12 nearest neighbors and shows that there are four nearest neighbors common to particles 1 and 2 in addition to the condition that 2 is a nearest neighbor to 1 and vice versa. These conditions give rise to the expression

$$N(N-1)\binom{12}{L-1}\sum_{m=0}^{4}\binom{4}{m}\binom{7}{i-m-1}\binom{7}{j-m-1}\frac{(N-2)\cdots(N-i-j+m+1)N_h\cdots(N_h-19+i+j-m)}{(L-2)(L-3)\cdots(L-19)}. \tag{37}$$

It is understood that if $(i-m-1)$ or $(j-m-1)$ is less than zero or greater than seven, the term (37) is zero. Thus, there is no term for $i=j=m=0$, as expected since we have already specified that the nearest neighbors 1 and 2 are occupied.

Finally, the second term on the RHS of Eq. (32) is given by the sum of the terms (33), (34), (35), (36), and (37). To obtain this result in a form suitable for calculation it will be necessary to reduce these terms to a sum of terms of order N plus terms of order unity or less, but first it is of interest to give two sum rules, which can be found by direct summation of the terms. One is

$$\sum_{i,j=0}^{12}(\langle N_iN_j\rangle_{hv}-\bar{N}_i\bar{N}_j)=N+N[(N-1)/(L-1)](L-55)+12N[(N-1)/(L-1)]+24N[(N-1)/(L-1)]$$
$$+6N[(N-1)/(L-1)]+12N[(N-1)/(L-1)]-N^2=0, \tag{38}$$

where the terms come from the summation of the individual terms given in the above order by the sum over i and j of: the first term on the RHS of Eq. (32), Eq. (33), (34), (35), (36), (37), and the square of Eq. (25). This is the expected result since it is the case of the number of particles with i neighbors independent of λ_i (i.e., λ_i a constant for all i), and all terms beyond the second in the expansion Eq. (23) should vanish. The other sum rule is

$$\sum_{i,j=0}^{12}ij(\langle N_iN_j\rangle_{hv}-\bar{N}_i\bar{N}_j)=\{12N[(N-1)/(L-1)]\{1+11[(N-2)/(L-2)]\}\}$$
$$+\{144N(L-55)[(N-1)/(L-1)][(N-2)/(L-2)][(N-3)/(L-3)]\}$$
$$+\{12N[(N-1)/(L-1)][(N-2)/(L-2)]\{1+143[(N-3)/(L-3)]\}\}$$
$$+\{24N[(N-1)/(L-1)][(N-2)/(L-2)]\{2+142[(N-3)/(L-3)]\}\}$$
$$+\{6N[(N-1)/(L-1)][(N-2)/(L-2)]\{4+140[(N-3)/(L-3)]\}\}$$
$$+\{12N[(N-1)/(L-1)]\{1+26[(N-2)/(L-2)]+117[(N-2)/(L-2)][(N-3)/(L-3)]\}\}$$
$$-\{12N[(N-1)/(L-1)]\}^2, \tag{39}$$

where the order of terms in the curly brackets is the same as in Eq. (38) and the last term is given by the square

of Eq. (26). Simplifying Eq. (39), we get

$$\sum_{i,j} ij(\langle N_iN_j\rangle_{Nv}-\bar{N}_i\bar{N}_j)=24N[(N-1)/(L-1)]+528N[(N-1)/(L-1)][(N-2)/(L-2)]$$
$$+144NL[(N-1)/(L-1)][(N-2)/(L-2)][(N-3)/(L-3)]$$
$$-552N[(N-1)/(L-1)][(N-2)/(L-2)][(N-3)/(L-3)]-144N^2[(N-1)/(L-1)]^2. \quad (40)$$

If we now expand Eq. (40) to order N plus smaller terms of order unity or less, we obtain

$$\sum_{i,j} ij(\langle N_iN_j\rangle_{Nv}-\bar{N}_i\bar{N}_j)=24N(N/L)(N_h/L)^2+O(1). \quad (41)$$

It is to be noted that the terms of order N^2 exactly cancel. Reference to Kirkwood's treatment of mixtures[13] shows that there is an exact correspondence between Eq. (40) and (41) and Kirkwood's result for the second moment of the distribution of particles in a mixture, when suitable adjustment is made of the present treatment to correspond to the case of mixtures. This correspondence represents a check on the accuracy of the algebra up to this point.

The individual terms of Eqs. (32)–(37) can now be expanded to terms of order N and smaller terms of order unity or less than $\bar{N}_i\bar{N}_j$ obtained from Eq. (27) to give

$$\langle N_iN_j\rangle_{Nv}-\bar{N}_i\bar{N}_j=N\left\{\binom{12}{i}(N^iN_h^{12-i}/L^{12})\delta_{ij}\right.$$
$$+\binom{12}{i}\binom{12}{j}[-(i+1)(j+1)(N^{i+j}N_h^{24-i-j}/L^{24})-(12-i)(12-j)(N^{i+j+1}N_h^{23-i-j}/L^{24})+114(N^{i+j+1}N_h^{24-i-j}/L^{25})]$$
$$\left.+12\sum_{m=0}^{4}B_{ijm}+6\sum_{n=0}^{4}C_{ijn}+24\sum_{r=0}^{2}D_{ijr}+12\sum_{s=0}^{1}E_{ijs}+O\left(\frac{1}{L}\right)\right\}, \quad (42)$$

where

$$B_{ijm}=\binom{4}{m}\binom{7}{i-m-1}\binom{7}{j-m-1}\frac{N^{i+j-m-1}N_h^{20-i-j+m}}{L^{19}}$$
$$C_{ijn}=\binom{4}{n}\binom{8}{i-n}\binom{8}{j-n}\frac{N^{i+j-n+1}N_h^{20-i-j+n}}{L^{21}}$$
$$D_{ijr}=\binom{2}{r}\binom{10}{i-r}\binom{10}{j-r}\frac{N^{i+j-r+1}N_h^{22-i-j+r}}{L^{23}}$$
$$E_{ijs}=\binom{11}{i-s}\binom{11}{j-s}\frac{N^{i+j-s+1}N_h^{23-i-j+s}}{L^{24}}. \quad (43)$$

Again it is seen that terms of the order of N^2 exactly cancel.

We return now to Eq. (23) and notice that from the definition of λ_i, Eq. (17), there will be terms of the form $i\bar{N}_iE(0)/2kT$ and $ij(\langle N_iN_j\rangle_{Nv}-\bar{N}_i\bar{N}_j)(E(0)/2kT)^2$ occurring after the summations. Thus, the sum rules Eq. (26) (expanded to terms of the order of N) and (41) can be used to simplify the expression. Substituting Eq. (27) for $\bar{N}_i$ (using only the terms of order N), Eq. (42) for $(\langle N_iN_j\rangle_{Nv}-\bar{N}_i\bar{N}_j)$, the sum rules Eq. (26) and (41), Eq. (17) for λ_i, and Eq. (12) for $g(L, N)$, the result is obtained,

$$\ln Z/N=-A_c/RT=-\ln(N/L)-(N_h/N)\ln(N_h/L)-(6E(0)/kT)(N/L)$$
$$+3[E(0)/kT]^2(N/L)(N_h/L)^2+\sum_{i=0}^{12}A_i\ln v_i+\tfrac{1}{2}\sum_{i=0}^{12}A_i\{-[iE(0)/kT](\ln v_i)+\ln v_i)^2\}$$
$$+\tfrac{1}{2}\sum_{i,j=0}^{12}[\{A_iA_j[-(i+1)(j+1)-(12-i)(12-j)(N/N_h)+114(N/L)]+12\sum_{m=0}^{4}B_{ijm}+6\sum_{n=0}^{4}C_{ijn}$$
$$+24\sum_{r=0}^{2}D_{ijr}+12\sum_{s=0}^{1}E_{ijs}\}\{-[iE(0)/2kT](\ln v_i)-(jE(0)/2kT)(\ln v_i)+(\ln v_i)(\ln v_j)\}]+\cdots, \quad (44)$$

where

$$A_i=\binom{12}{i}(N/L)^i(N_h/L)^{12-i}, \tag{45}$$

where the relation of the configurational Helmholtz free energy A_c with the partition function is indicated.

From the condition that the volume of the liquid is equal to the volume of occupied and vacant cells, and the cell volume definition, Eq. (3), the result is obtained,

$$N/L=v_0q/v, \qquad N_h/L=(v-v_0q)/v, \tag{46}$$

where v is the molecular volume of the liquid. Substituting Eq. (46), (2), and (11) into Eqs. (44) and (45), we get

$$\begin{aligned}-A_c/RT=&-\ln(v_0q/v)-[(v-v_0q)/v_0q)\ \ln[(v-v_0q)/v]-(6/\tau)(q^{-4}-2q^{-2})(v_0q/v)\\&+(3\tau^2)(q^{-4}-2q^{-2})^2(v_0q/v)(v-v_0q/v)^2+\sum_i A_i\ln v_i+\tfrac{1}{2}\sum_i A_i[(-i/\tau)(q^{-4}-2q^{-2})(\ln v_i)+(\ln v_i)^2]\\&+\tfrac{1}{2}\sum_{ij}[\{A_iA_j[-(i+1)(j+1)-(12-i)(12-j)[v_0q/(v-v_0q)]+114(v_0q/v)]+12\sum_m B_{ijm}+6\sum_n C_{ijn}\\&+24\sum_r D_{ijr}+12\sum_s E_{ijs}\}\{(-i/2\tau)(q^{-4}-2q^{-2})(\ln v_j)-(j/2\tau)(q^{-4}-2q)(\ln v_i)+(\ln v_i)(\ln v_j)\}].\end{aligned} \tag{47}$$

It is evident that there is a parametric dependence of Eq. (47) on q, the reduced cell size. Rather than choosing this quantity arbitrarily and keeping it fixed, as was done in some of the earlier hole theories,[5,6] it is possible to find a unique value of q for each set of values of τ and v/v_0, the independent variables, by minimizing the Helmholtz free energy with respect to q. This operation is done by taking the partial derivative of A_c, keeping τ and v/v_0 fixed, setting this quantity equal to zero, and finding the value of q which satisfies this equation. The resulting equation is long and is not shown here, since it is obtained in a straightforward manner. Mayer and Careri[10] have discussed this procedure for a generalized cell theory and indicate that there may be a theoretical difficulty when the L–JD free-volume integrals are used in that a disparity may arise between the mechanical pressure, found from the virial theorem of classical statistical mechanics, and the thermodynamic pressure found from the relation, $p=-(\partial A/\partial V)$. Leaving this problem aside, however, we proceed to compute the thermodynamic pressure and thus the equation of state from

$$pv/kT=-(v/RT)(\partial A/\partial v)_{\tau,q}, \tag{48}$$

where only the configurational part of the Helmholtz free energy need be considered. Carrying out the operation of Eq. (48) gives

$$\begin{aligned}pv/kT=&-(v/v_0q)\ \ln[(v-v_0q/v]+(6/\tau)(q^{-4}-2q^{-2})(v_0q/v)\\&+(3/\tau^2)(q^{-4}-2q^{-2})^2(v_0q/v)[(v-v_0q)/v]\{-[(v-v_0q)/v]+2(v_0q/v)\}\\&+\sum_i A_i\{-i+(12-i)[v_0q/(v-v_0q)]\}(\ln v_i)\\&+\tfrac{1}{2}\sum_i A_i\{-i+(12-i)[v_0q/(v-v_0q)]\}[-(i/\tau)(q^{-4}-2q^{-2})(\ln v_i)+(\ln v_i)^2]\\&+\tfrac{1}{2}\sum_{i,j}[\{A_iA_j\{(i+1)(j+1)(i+j)-(i+1)(j+1)(24-i-j)[v_0q/(v-v_0q)]\\&+(12-i)(12-j)(i+j+1)[v_0q/(v-v_0q)]-(12-i)(12-j)(23-i-j)[v_0q/(v-v_0q)]^2\\&-114(i+j+1)(v_0q/v)+114(24-i-j)(v_0q/v)[v_0q/(v-v_0q)]\}\\&+12\sum_m B_{ijm}\{-(i+j-m-1)+(20-i-j+m)[v_0q/(v-v_0q)]\}\\&+6\sum_n C_{ijn}\{-(i+j-n+1)+(20-i-j+n)[v_0q/(v-v_0q)]\}\\&+24\sum_r D_{ijr}\{-(i+j-r+1)+(22-i-j+r)[v_0q/(v-v_0q)]\}\\&+12\sum_s E_{ijs}\{-(i+j-s+1)+(23-i-j+s)[v_0q/(v-v_0q)]\}\}\{-(i/2\tau)(q^{-4}-2q^{-2})(\ln v_j)\\&-(j/2\tau)(q^{-4}-2q^{-2})(\ln v_i)+(\ln v_i)(\ln v_j)\}].\end{aligned} \tag{49}$$

Other quantities of interest can be obtained by the standard thermodynamic formulas from the expression for the Helmholtz free energy, Eq. (47).

IV. DISCUSSION

A few preliminary calculations have been made using only the Bragg-Williams approximation for the partition function, Eq. (18). It is easy to express the compressibility pv/kT obtained from Eq. (18) in terms of a power series in $(1/v)$ and thus obtain the virial coefficients from the coefficients of powers of $(1/v)$. The second virial coefficient has been evaluated and gives exactly the same result in the high-temperature limit as does the treatment of Rowlinson and Curtiss,[8] i.e.,

$$B(T)=\tfrac{1}{2}Nv_0[36(\xi^{\infty}+1)/\tau]^{1/4}, \tag{50}$$

where

$$\xi^{\infty}=2\int_0^{\infty}y^{\frac{1}{2}}1(y)dy\Big/\int_0^{\infty}y^{\frac{1}{2}}dy=134.8.$$

The value of the coefficient of $\tau^{-1/4}$ differs from the theoretical value of Lennard-Jones[15] by only 15% and the temperature dependence is correctly predicted. At lower temperatures the values of $B(T)$ seem to follow the curve of Rowlinson and Curtiss as nearly as can be determined from the figure in that paper (Fig. 2 in work cited in footnote 8), even though the expressions for $B(T)$ are of different form. These results are encouraging and it is hoped that further calculation using an expansion of Eq. (49) will result in an improvement in the second virial coefficient computation.

The predicted values of the critical constants are a sensitive test for the accuracy of a partition function of the liquid state. So far, no liquid-state theory has accurately predicted all three of these constants (critical temperature, pressure and volume), although the hole theory of Peek and Hill[7] gives reasonably good values for the critical temperature and volume. The equation of state at subcritical temperatures also provides an experimental test of the accuracy of the partition function. Calculations such as the above are currently being performed on the present theory.

All of the current hole theories which have fixed the cell size by minimization of the free energy[7,8,10,11] have resulted in rather large cell sizes and small fractions of holes to molecules. This is unfortunate, since these theories do not allow for multiple occupation of cells and thus considerable error may be introduced. It is possible that the cause of the large cell size is to be found in the density problem of hole theories mentioned in the introduction. By confining the particles to the central region of the cell, a lower free energy is obtained by enlarging the cell than by the introduction of holes. This problem of large cells can be handled by fixing the cell size at some arbitrary, small value for all temperatures and volumes. This procedure, under the present formalism, does nothing to improve the density situation, however. This is because the L–JD smoothing operation removes the orientation effects of the holes and changing the number of neighbors only flattens out the potential energy curve, but has no effect on the relative probability of finding the particle at the cell boundary, to that of finding it at the center. As can be seen from Fig. 2, Chap. VIII of the work cited in footnote 12, a larger cell size has a definite effect of extending the high probability region of the particle toward the cell walls. Apparently the minimization of A with respect to q is improving the density situation while making worse the approximations of the theory.

An alternative to these approaches is to eliminate the L–JD smoothing procedure and deal with the distinct configurations of i particles and $(z-i)$ holes separately. There will still, of course, be configurations with given i which will make the same contribution to the phase integral, e.g., for $i=1$ or 11, all 12 configurations will make the same contribution. This approach could be made without too much difficulty by using the Bragg-Williams approximation for the distribution of particles and constraining the individual neighbors to lie at a fixed distance from the cell center of the central particle and averaging the interaction over the spherical angle formed by the boundaries of the neighbor cell. This should have the virtue of noticeably increasing the particle density near the cell walls. Thus, it is possible that a clear distinction could be made between gas, liquid, and solid phases and that the transitions among them could be predicted.

It should also be mentioned that the present approach should be able to be extended without too much difficulty to the theory of solutions, adsorbed molecules and order-disorder problems in general. It may also be possible to treat transport phenomena using this model of the liquid and extended rate theory expressions, since it has been shown[16] that semiempirical lattice models can give excellent agreement with experiment for viscosity and self-diffusion when combined with absolute rate theory.

V. ACKNOWLEDGMENT

The author wishes to thank Dr. J. A. Pople, National Physics Laboratory, Teddington, Middlesex, England, for his suggestion of the use of the expansion method for treating the statistical problem of particle and hole distribution and for a stimulating discussion regarding the present treatment.

[15] J. E. Lennard-Jones, Proc. Roy. Soc. (London) **A106**, 463 (1924).

[16] G. E. Blomgren, Ann. N. Y. Acad. Sci. **79**, 781 (1960).

Energy Transfer and Quenching Processes in the System Cyclohexane-Benzene-Terphenyl-Oxygen*

A. WEINREB†

Argonne National Laboratory, Argonne, Illinois

(Received August 8, 1960)

A quantitative explanation of the results of Berry and Burton is offered. Some additional results on the effect of oxygen on the fluorescence of terphenyl are included.

IN an article which appeared in 1955, Berry and Burton[1] investigated the fluorescence of solutions of terphenyl in mixtures of benzene and cyclohexane when they were excited by γ radiation. The terphenyl concentration was kept constant (1.58 g/liter) and the intensity was measured as a function of the volume ratio of benzene and cyclohexane. The intensities were determined when the solutions were deoxygenated and when oxygen was introduced at definite pressures. The results are shown in Fig. 1 which is copied from the work cited in footnote 1. In the article the authors indicate an explanation of their results. In collaboration with others[2,3] they have subsequently studied the elementary processes which may account for the results shown in Fig. 1, in particular for the minimum in intensity which appears in all the curves obtained where oxygen was present. The work cited in footnote 2 includes a list of the processes which may occur in the system and an equation which describes the dependence of the fluorescent intensity on these processes. In this article we do not intend to add to the proposed processes, but rather to see what plausible assumptions have to be made in order to explain the results quantitatively. Since the system discussed and several similar systems are of certain importance in radiation chemistry, such an investigation may enable us to draw some conclusions about the processes involved.

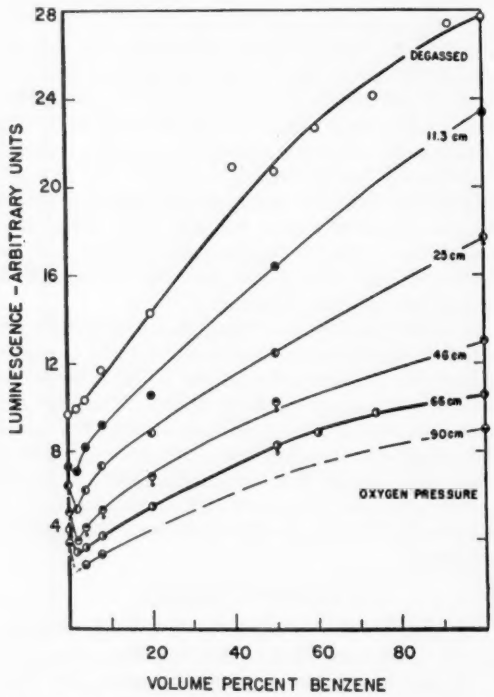

FIG. 1. Effect of oxygen on gamma-induced luminescence of *p*-terphenyl in cyclohexane-benzene solvent.

DEOXYGENATED SOLUTIONS

We consider first the deoxygenated solutions. A numerical examination of the intensity as a function of the concentration of benzene shows that the intensities for the various concentrations can be fairly well described as superpositions of the respective intensities obtained for terphenyl in pure cyclohexane and in pure benzene, if the measured intensities (9.7 and 27.7) are multiplied by the respective volume fractions of cyclohexane and benzene. Hence one is tempted to assume that each solvent transfers its energy to the solute independently. The behavior of the oxygen-containing solutions, however, rules out this interpretation. The increase in the quenching effect of oxygen with decreasing concentration of benzene (which manifests itself most obviously in the minimum at the lowest given benzene concentration) suggests the assumption that a considerable energy transfer from benzene to terphenyl takes place even at the lowest benzene concentration, and that this transfer is affected by the presence of oxygen. This can only be the case if a considerable energy transfer from cyclohexane to benzene takes place even at these low benzene concentrations, since the contribution of the directly excited benzene molecules could not account for such a pronounced effect. This assumption has been made already

* Work performed under the auspices of the U.S. Atomic Energy Commission.

† On leave from the Hebrew University, Jerusalem, Israel.

[1] P. J. Berry and M. Burton, J. Chem. Phys. **23**, 10, 1969 (1955).

[2] M. Burton, P. J. Berry, and S. Lipsky, J. chim. phys. **52**, 657 (1955).

[3] P. J. Berry, S. Lipsky, and M. Burton, Trans. Faraday Soc. **52**, 511 (1956).

in the original article.[1] The assumption of an efficient energy transfer from cyclohexane to benzene, however, necessitates a reconsideration of the results for the deoxygenated solution. If the transfer efficiency at the lowest benzene concentration is appreciable but still much different from its maximum value, one would assume that an increase in concentration would be accompanied by a rather pronounced increase in transfer efficiency, which again would result in an increase of the amount of energy which is transferred from benzene to terphenyl. The intensity would thus be expected to rise much faster with an increase in benzene concentration than is actually observed, and the maximum intensity would be reached at comparatively low concentrations. We are therefore led to the assumption that almost all the energy which can be transferred from cyclohexane to benzene is transferred already at the lowest benzene concentration. As will be seen, this assumption is not entirely correct inasmuch as the transfer efficiency is increased at very high benzene concentrations. The intensity I_B of the solution in pure benzene is given by

$$I_B = A \cdot \epsilon_{BT}(C_O)\eta_B(C_O), \qquad (1)$$

where ϵ_{BT} is the efficiency of energy transfer from benzene to terphenyl and η_B is the quantum yield of terphenyl in benzene, both being functions of C_O, the concentration of oxygen (quencher); A is a constant determined by the experimental conditions.

In the mixed solvents terphenyl can be excited by (a) direct transfer from cyclohexane, (b) transfer from directly excited benzene, and (c) transfer from benzene which has been excited by transfer from cyclohexane. Since even at the lowest concentration of benzene the number of benzene molecules is about 30 times as great as the number of terphenyl molecules, we assume further that process (a) is negligible as compared with the transfer to benzene. This assumption is reasonable if the two transfer processes are not too different. The intensity I in the mixed solutions is then given by

$$I = A[(1-C_B)\epsilon_{CB}(C_O) + C_B]\epsilon_{BT}(C_O)\eta(C_B, C_O), \qquad (2)$$

where ϵ_{CB} is the transfer efficiency from cyclohexane to benzene, C_B is the concentration of benzene, η is the quantum yield of terphenyl (which depends also on the composition of the solvent, i.e., on the concentration of benzene). According to the assumptions made above, ϵ_{CB} is close to its maximum value already at the lowest given benzene concentration or at least reasonably constant for the lower range of the given concentrations. The magnitude of $\epsilon_{CB}(0)$ (i.e., in the absence of oxygen) for the lowest benzene concentration can be found in terms of ϵ_{BT}. From Eqs. (1) and (2) we obtain

$$\epsilon_{CB} = [(I/I_B)(\eta_B/\eta) - C_B]/(1-C_B). \qquad (3)$$

Since η_B/η can be determined by direct excitation of terphenyl with uv, all the magnitudes on the right-hand side of the equation are known and ϵ_{CB} can be determined.

When a solution of 1.6 g/liter terphenyl in pure cyclohexane, in a mixture of equal parts of cyclohexane and benzene ($C_B=0.5$), and in pure benzene are excited by light of wavelength 3130 A which is absorbed by the solute alone, the intensities in arbitrary units are 1.88, 1.74, and 1.64, respectively. The quantum yield of terphenyl in cyclohexane is thus 15% greater than in benzene (i.e., $\eta/\eta_B=1.15$). This may be attributed partly to a genuine change in quantum yield and partly to the difference in the refractive indices of the two solvents, which are given in the work cited in footnote 2 to be 1.50 for benzene and 1.43 for cyclohexane. On the basis of this result and since the differences in intensity are not very great, we assume to a first approximation that the decrease in quantum yield with increasing benzene concentration is proportional to the benzene concentration. Thus substitution of $C_B=0.02$, $I=10.1$,[4] $I_B=27.7$, and $\eta/\eta_B=1.15$ into Eq. (3) yields $\epsilon_{CB}=0.304$. The factor $A\epsilon_{BT}(0)\eta(1, 0)=27.7$ is the measured intensity of the solution in pure benzene. By inserting the value of ϵ_{CB} in Eq. (2) and by changing η according to C_B, we can now compute the intensities for the deoxygenated solutions ($C_O=0$) for the various concentrations C_B. The results are shown in Table I, together with the measured values.

There seems to be rather good agreement between the computed and measured intensities. However, for the two highest benzene concentrations the measured values are higher than the computed ones by a greater amount than could be accounted for by the error in reading the graphs. Several possible explanations of this discrepancy may suggest themselves. On the basis of the scanty experimental evidence, however, the most plausible conclusion from the results seems to be that the assumed constancy of ϵ_{CB} holds only for moderate concentrations of benzene. It would be futile to draw any quantitative conclusions on the change of ϵ_{CB} from the differences between the measured and computed intensities, since we are dealing with differences which are small in comparison to the absolute values, so the accuracy of such a computation would be exceedingly low. An increase in ϵ_{CB} for high values of C_B might mean that in these cases energy is drawn from molecular states of cyclohexane which decay so rapidly that energy transfer can hardly take place at the usual scintillator concentrations. The change in ϵ_{CB} may also be looked at as a solution phenomenon, i.e., a cyclohexane molecule dissolved in benzene may have energy levels which differ slightly from those in pure cyclohexane and thus give rise to different transfer efficiencies.

[4] The accuracy in reading the intensities from the figure in the original article was not better than 4%. However, when through the courtesy of Professor Burton the author got access to part of the data on which Fig. 1 is based, it was found that the differences between the data and the values read from the graphs were very slight.

TABLE I. Intensities for deoxygenated solutions of terphenyl in mixtures of benzene and cyclohexane. The oxygen concentration C_O is in cm Hg, c is the computed intensity, and m is the measured intensity.

C_O \ C_B	0	0.02		0.04		0.08		0.2		0.5		0.74		1.0
	m	c	m	c	m	c	m	c	m	c	m	c	m	m
0	9.7	10.1[a]	10.0	10.5	10.3	11.4	11.6	13.8	14.3	19.4	20.4	23.6	24.9	27.7
11.3	7.4	7.9	7.0	8.3	8.2	9.1	9.2	11.3	11.3					23.6
25	6.6	6.1	5.4	6.5	6.2	7.1	7.3	8.9	9.0					17.9
46	5.4	4.4	3.9	4.7	4.5	5.1	5.4	6.5	7.1					13.0
66	...	3.4	...	3.5	3.5	3.9	4.2	5.0	5.5					10.6

[a] This computed value at the lowest concentration (C_B=0.02) was obtained by assuming that $\epsilon_{CB}(0)=\epsilon_{CT}(0)$, where $\epsilon_{CT}(0)$ is the transfer efficiency from cyclohexane to terphenyl at the given concentration of 1.58 g/liter. Since the computed and measured values are identical within the limits of accuracy, this result would mean that the same amount of energy is transferred from cyclohexane to benzene as to terphenyl in the absence of benzene.

SOLUTIONS CONTAINING OXYGEN

As has been pointed out in Table I of the work cited in footnote 1, the quenching parameter of oxygen is not a constant for all the solutions but changes in a rather peculiar way. On changing from pure benzene to the mixture in which it is most concentrated, the quenching parameter decreases rather sharply and then decreases gradually as the concentration of benzene is decreased. It reaches a minimum at $C_B \equiv 0.2$ and then begins to increase and finally rises rather abruptly at the lowest concentrations of benzene ($C_B < 0.04$). This final rise corresponds to the minimum observed in the intensity curves for all the oxygen-containing solutions. An explanation of the decrease in the quenching constant on changing from pure benzene to the mixtures suggests itself on the basis of the results of the work cited in footnote 2. There it has been found that contrary to the case in benzene solutions, oxygen has no direct quenching effect on terphenyl in cyclohexane. A decrease in the quenching parameter could thus be ascribed, at least qualitatively, to a decrease in the quenching of the terphenyl fluorescence as a consequence of decreasing benzene concentration. However, results obtained by us show that oxygen certainly quenches the fluorescence of terphenyl in cyclohexane also, when it is excited by light of wavelength 3130 A. We assume that this quenching effect takes place also when the fluorescence is excited via energy transfer. The preliminary quenching constant obtained is about 37 liter mole^{-1}. The quenching constant in benzene for excitation by light of wavelength 3130 A was found to be 56 liter mole^{-1} (corresponding to the value of 45±10 given in the work cited in footnote 2). These values are roughly inversely proportional to the respective solubilities of oxygen in cyclohexane and benzene. The change in the composition of the mixtures thus should not greatly affect the influence of oxygen on the quantum yield of terphenyl. This has been verified experimentally by comparing the quenching of the fluorescence of terphenyl in a mixture of equal parts of benzene and cyclohexane with the quenching of solutions in the pure solvents.

A plausible explanation of the change in the quenching constant might be that the assumed proportionality of solubility and volume fraction of the solvents does not hold. However, even a great deviation from this proportionality can hardly account for the observed changes. We tend, therefore, to assume that the quenching action of oxygen on the transfer from benzene to terphenyl is rather abruptly changed by introducing cyclohexane into benzene. Such a change might be understood on the basis of the recent suggestion by Lipsky and Burton,[5] that energy transfer and quenching by oxygen involves a regional arrangement rather than a random distribution of donor and acceptor molecules. Since the quenching parameter is rather constant for benzene concentrations between 50% and 20%, we assume that at C_B=20% benzene may be considered sufficiently diluted so that the values obtained at this concentration represent the quenching effects on the system benzene-terphenyl when it is dissolved in cyclohexane. If no other quenching process were acting, the values for the lower benzene concentrations could be computed by using the quenching parameter obtained from the values at the concentration of 20%. Accepting the preliminary value of 37 liter mole^{-1} as the parameter for the oxygen quenching of terphenyl fluorescence in cyclohexane, we obtain about 126 liter/mole for the corresponding parameter for oxygen quenching of the transfer from benzene to terphenyl. These values have been used in computing the theoretical values given in Table I for the intensities of the quenched solutions. One would say that on the basis of these rather crude assumptions the agreement with the measured values is rather good. For the two higher concentrations of benzene, the computed values are too low at the higher oxygen concentrations. This could be due, at least partly, to Cerenkov radiation,

[5] S. Lipsky and M. Burton, J. Chem. Phys. **31**, 5, 1211 (1959).

which at the low intensities contributes significantly to the measured intensities and which is not quenched. Except for the lowest oxygen concentration, the expected minimum appears at a benzene concentration of about 2%. The computed minima, however, are significantly higher than their measured values. We are thus led to the assumption that at the lowest benzene concentrations an additional quenching mechanism must be acting. This is most probably the quenching of the energy transfer from cyclohexane to benzene, which would be most noticeable at the lowest benzene concentration. In order to compete with energy transfer at these relatively high benzene concentrations, this quenching process must be rather efficient. The magnitude of the quenching parameter may be roughly estimated on the assumption that a Stern-Volmer relation applies to this process. From this estimate one finds that $k_{CO} \approx 6k_{CB}$, where k_{CB} and k_{CO} are the probabilities for energy transfer from cyclohexane to benzene and to oxygen, respectively, for unit molar concentrations of these acceptors. It may be noted that this quenching is exceedingly high at the lowest oxygen concentration. However, this may be expected when we consider that the transfer from cyclohexane to terphenyl suffers a similarly high quenching at the lowest oxygen concentration, as has also been pointed out in the work cited in footnote 3. It may also be that the quenching of the transfer from cyclohexane is "static," at least partially. Recent experiments on the effect of oxygen on the transfer of energy from cyclohexane to diphenyl-oxazole seem to indicate a "static" character for this quenching.

THE JOURNAL OF CHEMICAL PHYSICS VOLUME 34, NUMBER 4 APRIL, 1961

Trimethylene Oxide. II. Structure, Vibration-Rotation Interaction, and Origin of Potential Function for Ring-Puckering Motion*

SUNNEY I. CHAN,† JOHN ZINN,‡ AND WILLIAM D. GWINN

Department of Chemistry, University of California, Berkeley, California

(Received October 19, 1960)

In the previous paper of this series, the microwave spectra of four isotopic species of trimethylene oxide were investigated and the potential function for the puckering of the four-membered ring was determined. Further analysis of the data has now enabled the molecular structure to be calculated. The structural parameters deduced from the rotational constants are: $r(C-C) = 1.549 \pm 0.003$ A, $r(C-O) = 1.449 \pm 0.002$ A, $r(C_\alpha - H_\alpha) = 1.091 \pm 0.002$ A, $r(C_\beta - H_\beta) = 1.100 \pm 0.003$ A, $\angle C_\alpha - C_\beta - C_\alpha = 84°33' \pm 1'$, $\angle C_\alpha - O - C_\alpha = 91°59' \pm 7'$, $\angle C_\beta - C_\alpha - O = 91°44' \pm 3'$, $\angle H_\alpha - C_\alpha - H_\alpha = 110°18' \pm 10'$, $\angle H_\beta - C_\beta - H_\beta = 110°44' \pm 3'$. The alpha-methylene planes are slightly deflected towards the oxygen atom away from the bisectors of the $\angle C_\beta - C_\alpha - O$'s. However, the actual angle of deflection is rather uncertain. Using these structural parameters, models have been constructed to calculate the vibration-rotation interaction due to the ring-puckering vibration. The experimentally observed rotational constant variations were found to be very well reproduced if the out-of-plane bending motion is assumed to follow a curvilinear path without any stretching of the C—C and C—O bonds. The potential function determined in the previous paper is also interpreted in terms of force fields within the molecule.

INTRODUCTION

IN the first paper of this series, the microwave spectra of four isotopic species of trimethylene oxide were reported.[1] In each species, the spectrum was found to contain rotational transitions from excited vibrational states of the ring-puckering mode as satellites to the normal spectrum arising from the ground state. From the relative intensities of these vibrational satellites, the Stark effect of certain lines, and the vibration-rotation interaction associated with the ring-puckering vibration along with the far-infrared data of Danti, Lafferty, and Lord,[2] it was possible to establish the degree of planarity of the four-membered ring and the nature of the potential function for the ring-puckering vibration. It was found that the trimethylene oxide ring is essentially planar but that the ring-puckering potential function did contain a small potential maximum of 35 ± 5 cm^{-1} at the planar configuration. This barrier is so small that the energy of the zero-point vibration is still 8 ± 4 cm^{-1} above the top of the hump. Aside from the barrier, the potential function was found to contain both quadratic and quartic terms. While the quadratic term dominates at the lowest level, the quartic term is predominant for the higher levels studied.

* This research was supported by grants from the Alfred P. Sloan Foundation and the California Research Corporation.

† Kaiser Aluminum and Chemical Corporation Fellow, 1958–1959; National Science Foundation Cooperative Fellow, 1959–1960.

‡ Present Address: Los Alamos Scientific Laboratory, Los Alamos, New Mexico.

[1] S. I. Chan, J. Zinn, J. Fernandez, and W. D. Gwinn, J. Chem. Phys. **33**, 1643 (1960).

[2] A. Danti, W. J. Lafferty, and R. C. Lord, J. Chem. Phys. **33**, 294 (1960).

TABLE I. Effective principal moments of inertia of trimethylene oxide (amu A²).[a]

Vibrational State	I_a	I_b	I_c	$I_a+I_b-I_c$[b]
	Normal trimethylene oxide			
0	41.9701	43.0832	75.1093	9.9440
1	41.9255	43.1126	74.6446	10.3935
2	41.9224	43.1391	74.4632	10.5983
3	41.9179	43.1715	74.2390	10.8504
4	41.9255	43.2132	74.0433	11.0954
	1,1,3,3-Tetradeutero trimethylene oxide			
0	46.3349	56.3176	86.2547	16.3978
1	46.3822	56.2225	85.7657	16.8390
2	46.4199	56.1931	85.5674	17.0456
3	46.4628	56.1584	85.3330	17.2882
	Trimethylene oxide-O^{18}			
0	41.9722	45.1071	77.1272	9.9521
1	41.9367	45.1321	76.6571	10.4117
	β-Monodeutero trimethylene oxide			
0	42.6992	46.8892	78.1750	...
1	42.6542	46.9103	77.7201	...

[a] A conversion factor of 505 538 amu A²/Mc is used in the conversion of the rotational constants to effective moments of inertia.
[b] Experimental uncertainty in $(I_a+I_b-I_c)$ is about 0.001 amu A².

This paper will deal first with the determination of the structure from the experimental rotational constants. The structural parameters so obtained will then be employed to set up models whereby the vibration-rotation interaction associated with the ring-puckering motion will be calculated. The nature of the ring-puckering motion together with the origin of the potential function will finally be discussed in the light of the structural models proposed.

STRUCTURE

The experimental rotational constants of normal trimethylene oxide, 1,1,3,3-tetradeutero trimethylene oxide, trimethylene oxide-O^{18}, and β-monodeutero trimethylene oxide have already been tabulated in Table II in the first paper of this series[1] for various vibrational states of the ring-puckering mode. These give rise to the effective moments of inertia listed in Table I of this paper.

Since the vibration in the ring-puckering mode would be expected to be of fairly large amplitude, the treatment of the effective moments of inertia to yield the structural parameters cannot be exercised without some care. At the same time, while this large amplitude vibration is a complexity in the determination of the structure, it affords the opportunity to test the methods of minimizing the effect of vibration-rotation interaction in structure calculations.

In cases where experimental rotational constants of molecules are available for excited vibrational states, the treatment of the data generally involves an extrapolation to a hypothetical state in which the vibrational energy is zero. The set of rotational constants obtained as a result of this extrapolation supposedly yields a set of structural parameters which are the equilibrium or non-vibrating values. In trimethylene oxide, where we do have the data for excited states of the ring-puckering mode, it appears that a similar treatment may be applicable. However, evidence has already been presented to indicate that the four-membered ring would be bent in such a hypothetical state of zero vibration. In addition, the peculiar zigzagging nature of the rotational constants makes the extrapolation to the nonvibrating state very uncertain. Since all the ring-puckering vibrational levels lie well above the top of the barrier in the potential function, and the molecule is vibrating symmetrically about the planar configuration, it does not seem practical to extrapolate the rotational constants to this puckered state. Not only is it easier, but it is probably more significant in this case to extrapolate the rotational constants to a hypothetical state in which the four-membered ring is planar.

In our preceding paper,[1] we obtained expressions for the three rotational constants of normal trimethylene oxide as functions of the expectation values of Q_1^2 and Q_1^4, where Q_1 is the ring-puckering vibrational coordinate. These expressions yielded the rotational constants for the hypothetical planar molecule. Sufficient data is also available so that a similar treatment may be applied to 1,1,3,3-tetradeutero trimethylene oxide. In view of the fact that the reduced mass of the vibration is somewhat uncertain, the extrapolation of the rotational constants for the tetradeuterated compound is uncertain by as much as 1 Mc. For trimethylene oxide-O^{18} and β-monodeutero trimethylene oxide, where data is only available for two vibrational states, this procedure is no longer applicable. Here, the extrapolation to the hypothetical planar molecule was done by assuming that the correction is proportional to that in normal trimethylene oxide, this proportionality factor being determined by the ratio of the amount of vibration-rotation interaction between the ground and first vibrational levels. If this latter treatment is applied to 1,1,3,3-tetradeutero trimethylene oxide, one obtains extrapolated rotational constants which agree with the ones obtained from the aforementioned numerical fitting to about 1 Mc. This is sufficient accuracy for our present structure determination. As will be discussed later in this paper, it is hoped that with these extrapolations, the major portion of the vibration-rotation interaction due to this large amplitude ring-puckering motion is removed. These extrapolated rotational constants together with their corresponding effective moments of inertia are tabulated in Table II. An uncertainty of about 1 Mc should be attached to the rotational constants of all the species except the normal compound as a result of the uncertainties in the extrapolations. This leads to uncertainties of ~0.001–0.002 in most of the coordinates determined.

The determination of the structure is straightforward. The coordinates of the atoms will be referred to the principal axes coordinate system of the normal species. We shall designate the C—O molecular axis as the X-axis, and the out-of-plane axis, the Z axis. Coordinates of the atoms at the α and β carbon positions are denoted by α and β subscripts.

The effective moments of inertia of the hypothetical planar molecules of normal and tetradeuterated trimethylene oxide combined to yield sets of equations of the type

$$(I_a+I_b-I_c)+\Delta_s=2\sum_i m_i z_i^2. \qquad (1)$$

The Δ's contain zero-point effects due to the vibrations in the other modes. From these equations, we obtain the coordinates of the hydrogens on the α-carbons provided the assumption is made that the Δ's are more or less invariant to isotopic substitution.[3] Since the four α-hydrogens are equivalent in the planar configuration, the coordinates obtained for these atoms are probably "substitution" coordinates in a broader sense.

Since β-monodeutero trimethylene oxide and trimethylene oxide-O^{18} are singly substituted molecules, Kraitchman's equations[4] were used to yield directly the Cartesian coordinates of the β-hydrogens and those of the oxygen atom in the principal-axes system of the normal molecule. This approach yields the substitution coordinates of these atoms. Costain and others have recently speculated that these substitution coordinates minimize the effect of vibration-rotation interaction and that they give structural parameters which are closer to the equilibrium values.[3]

Since spectral data is not available for species with the carbon atoms isotopically substituted, their coordinates can only be calculated by invoking rigid-rotor conditions, that is by assuming that the Δ's are zero in the moment of inertia equations. This approximation probably leads to fairly good effective coordinates for the β-carbon atoms because of their greater mass as compared to that of the hydrogens. The x coordinates of the α-carbons are poorly located on account of their proximity to the principal axis. In the determination of x coordinates of the α- and β-carbons, use is also made of the center of mass condition.

The coordinates of all the atoms in the molecule relative to the principal-axes system of the normal molecule as calculated using the method outlined above are listed in column 1 of Table III. The sign of the x coordinate of the α-hydrogens is not determined from the structure calculations; neither is it evident from the geometry of the molecule since these atoms are so close to the principal axis. However, the positive sign of these coordinates (positive direction of the X axis is pointing towards the β-carbon along the C—O axis) was rejected on the grounds that it leads to a structure with an unreasonably long C—C bond distance of 1.585 A. Furthermore, the negative sign appears reasonable from the viewpoint of structural chemistry insofar as one might expect the repulsions between the hydrogens on the α- and β-methylene groups and the attraction to the oxygen to deflect the α-CH_2 planes away from the bisector of the C—C—O angle in the direction of the oxygen atom. This would be the situation if the negative sign were selected. It should also be pointed out that the very fact that the α-carbons and hydrogens are close to the principal axis is expected to lead to poorly determined x coordinates for these atoms.

TABLE II. Extrapolated rotational constants and effective principal moments of inertia for the hypothetical planar molecule.[a]

A^0	B^0	C^0	I_a^0	I_b^0	I_c^0
Normal trimethylene oxide					
12 031.8	11 739.6	6692.4	42.0168	43.0626	75.5391
1,1,3,3-Tetradeutero trimethylene oxide					
10 919.2	8961.9	5830.1	46.2982	56.4097	86.7117
β-Monodeutero trimethylene oxide					
11 826.4	10 784.9	6432.2	42.7463	46.8745	78.5955
Trimethylene oxide-O^{18}					
12 033.9	11 211.8	6517.9	42.0094	45.0897	77.5621

[a] Rotational constants are in Mc and moments of inertia in amu A^2.

So far only the extrapolated rotational constants have been used in the structural determination. It would of course be most interesting to see how the coordinates would vary if the structural calculations were carried out using the nonextrapolated rotational constants. This would correpond to the neglect of any ring puckering, dynamic or static. This procedure leads to a "structure" for each individual vibrational state. In this case, sufficient data is available so that a complete coordinate determination could be carried out for two vibrational states. Analogous treatment of the rotational constants leads to the coordinates listed in columns 2 and 3 of Table III. Additional excited-state data for the normal species and the tetradeuterated species permitted certain coordinates to be computed for the third and the fourth vibrational states. These are listed in columns 4 and 5 of Table III.

A comparison between columns 1 and 2 of Table III indicates that except for those atoms which lie close to a principal axis, the coordinates obtained using ground-state rotational constants differ from those determined using the extrapolated values by less than 0.005 A. These discrepancies are considered to be surprisingly small insofar as the ring-puckering vibration is expected to be of fairly large amplitude, of the order of 0.06 A for the ground vibrational state and 0.08 A for the first

[3] C. C. Costain, J. Chem. Phys. **29**, 864 (1958).
[4] J. Kraitchman, Am. J. Phys. **21**, 17 (1953).

TABLE III. Coordinates for trimethylene oxide.

Atom	Coordinate	Hypothetical planar state	Ground state	First excited state	Second excited state	Third excited state
			Substitution coordinates			
H_α	x	−0.045	−0.081	−0.112	−0.123	−0.139
		(+0.045)[b]	(+0.081)[b]	(+0.112)[b]	(+0.123)[b]	(+0.139)[b]
	y	±1.665	±1.662	±1.658	±1.656	±1.655
	z	±0.8954	±0.8953	±0.8946	±0.8948	±0.8942
H_β	x	1.752	1.747	1.740	...	...
	y	(0)[a]	(0)[a]	(0)[a]	...	...
	z	±0.9049	±0.9007	±0.8956	...	...
O	x	−1.026	−1.022	−1.018	...	...
	y	(0)[a]	(0)[a]	(0)[a]	...	...
	z	(0)[a]	(0)[a]	(0)[a]	...	...
			Effective coordinates[c]			
C_α	x	−0.019	−0.015	−0.012	...	...
		(−0.068)[b]	(−0.084)[b]	(−0.097)[b]		
	y	±1.042	±1.038	±1.033	±1.032	±1.030
	z	(0)[a]	(0)[a]	(0)[a]	...	...
C_β	x	1.127 (1.126)[b]	1.126 (1.125)[b]	1.125 (1.123)[b]	...	...
	y	(0)[a]	(0)[a]	(0)[a]	...	...
	z	(0)[a]	(0)[a]	(0)[a]	...	...

[a] Assumed because of C_{2v} symmetry.
[b] Rejected alternate solution. See text.
[c] Coordinates calculated by invoking rigid-rotor conditions.

excited state. These amplitudes correspond to a puckering of the ring by 14° and 18°, respectively (dihedral angle between C—C—C and C—O—C planes).

Since the out-of-plane coordinates of both the α- and β-hydrogens were both determined as substitution coordinates, it is possible to evaluate Δ_z of Eq. (1) and to compare it with those calculated by Laurie for other molecules.[5] The value calculated for the hypothetical planar molecule is +0.20 amu A^2. This compares well with values obtained by Laurie. The corresponding values for the ground state and first excited state naturally reflect the ring-puckering motion and the values change sign to −0.20 and −0.70 amu A^2, respectively. Thus the contribution of the ring-puckering vibration to Δ_z is −0.40 amu A^2 for the ground state and −0.90 amu A^2 for the first excited state.

It is also interesting to note some errors which may arise when a substitution coordinate is combined with moment of inertia equations to obtain a second coordinate. If data were available from only normal trimethylene oxide and 1,1,3,3-tetradeutero trimethylene oxide, then it would only be possible to calculate $z_{H\alpha}$ as a substitution coordinate and then to solve for $z_{H\beta}$ in the moment of inertia equation, after neglecting Δ_z. When this is carried out, one obtains results in β-hydrogen out-of-plane distances, of 0.874 A, 0.929 A, and 0.988 A for the hypothetical planar configuration, ground state, and the first excited state, respectively. Since this procedure assigns most of the effects of vibration rotation interaction to the $z_{H\beta}$ coordinate, it results in a greatly exaggerated effect on this distance. This is often done nevertheless, as is done in this paper to evaluate the y coordinates of the α-carbons and the x coordinates of the α- and β-carbons. Here the effect is much smaller because of the heavier mass of the carbon atoms as compared to that of the hydrogens.

Using the coordinates listed in Table III, we have calculated structures of the trimethylene oxide molecule in its hypothetical planar state and in the ground state and first excited state of the ring-puckering mode. The interatomic distances and angles are tabulated in Table IV. The set of structural parameters calculated using extrapolated rotational constants are preferred, since we feel that the discrepancies in the parameters for the ground and first excited states are associated with insufficient consideration of the vibration-rotation

[5] V. W. Laurie, J. Chem. Phys. **28**, 704 (1958).

TABLE IV. Structure of trimethylene oxide.

	Hypothetical planar state	Ground state	First excited state	Preferred structure
$r(C_\alpha-C_\beta)$	1.549 A	1.543 A	1.536 A	1.549±0.003 A
$r(C_\alpha-O)$	1.449 A	1.446 A	1.442 A	1.449±0.002 A
$r(C_\alpha-H_\alpha)$	1.091 A	1.093 A	1.096 A	1.091±0.002 A
$r(C_\beta-H_\beta)$	1.100 A	1.094 A	1.086 A	1.100±0.003 A
$\angle C_\alpha-C_\beta-C_\alpha$	84°33′	84°34′	84°32′	84°33′±1′
$\angle C_\alpha-O-C_\alpha$	91°59′	91°45′	91°30′	91°59′±7′
$\angle C_\beta-C_\alpha-O$	91°44′	91°50′	91°59′	91°44′±3′
$\angle H_\alpha-C_\alpha-H_\alpha$	110°18′	109°57′	109°26′	110°18′±10′
$\angle H_\beta-C_\beta-H_\beta$	110°44′	110°50′	111°3′	110°44′±3′
Angle between α-CH_2 plane and C−C axis	−2°22′[a]	−6°2′[a]	−9°4′[a]	...
Angle between α-CH_2 plane and $\angle C_\beta-C_\alpha-O$ bisector	−30′[a]	−4°14′[a]	−7°20′[a]	...

[a] $C_\alpha-H_\alpha$ towards oxygen atom.

interaction arising from the ring-puckering vibration. However, the set of structural parameters computed using the extrapolated rotational constants still contains uncertainties associated with our inability to consider the vibration-rotation interaction effects of the remaining vibrations. Our preferred structure together with approximate uncertainties in the various parameters are given in the final column of Table IV. The uncertainties cited are well beyond those due to measurements and our method of extrapolation.

The C—C bond in trimethylene oxide (1.549± 0.003 A) appears to be slightly longer than the generally accepted value of 1.543 A for ethane.[6] However, since this latter value may contain an uncertainty of as much as 0.005 A, the margins of error probably overlap, so that one may conclude that, for all practical purposes, the C—C bond length in trimethylene oxide is equal to that in ethane. It is also found to lie within the limits of experimental uncertainty of the value reported for its parent molecule, cyclobutane (1.568 ±0.02 A).[7] It is interesting to note that like the C—C bond in other molecules with four-membered rings the C—C bond in trimethylene oxide does not reflect the bond-shortening effects observed in the corresponding three-membered ring, ethylene oxide (1.472 A).[8] The ∠H—C—H's are also closer to tetrahedral (within a degree) in contrast to a value around 116° found in the three-membered ring.[8] The C—H bond distance of the β-hydrogens obtained here is equal to that reported for ethane (1.102 A)[6] while the corresponding distance for the α-hydrogens is equal to that found in methane (1.092 A).[9]

INTERPRETATION OF THE VIBRATION-ROTATION INTERACTION

The problem of the vibration-rotation interaction in trimethylene oxide may be separated into two distinct parts. In the first paper of this series, the rotational constants were expanded in terms of the expectation values of powers of the ring-puckering vibrational coordinate. There, the coefficients in the expansions were treated as empirical parameters and a study of the variation of the expectation values of Q_1^2 and Q_1^4 with potential functions together with the far-infrared data of Danti, Lafferty, and Lord, led to the quantitative determination of the potential function for the ring-puckering vibration.

The coefficients in these expansions, which were treated as empirical parameters in the determination of the potential function, actually represent the sucessive derivatives of the rotational constants with respect to the vibrational coordinate. As derivatives, they are sensitive to the details of the molecular motion in the molecule during the vibration. An analytical knowledge of these coefficients will therefore provide some understanding about the details of the molecular motion and ultimately the nature of the vibration-rotation interaction. With this idea in mind, these coefficients were investigated.

Trimethylene oxide is unique in that one vibrational mode, the ring-puckering motion, stands out clearly from all the other vibrations. The frequency of this vibration is so low that many levels are populated and

[6] G. E. Hansen and D. M. Dennison, J. Chem. Phys. **20**, 313 (1952).
[7] J. D. Dunitz and V. Schomaker, J. Chem. Phys. **20**, 1703 (1952).
[8] G. L. Cunningham, Jr., A. W. Boyd, R. J. Myers, W. D. Gwinn, and W. I. Levan, J. Chem. Phys. **19**, 676 (1951).
[9] G. G. Shepherd and H. L. Welsh, J. Mol. Spectroscopy **1**, 277 (1957).

pure rotational transitions have been observed for the first five vibrational levels. The vibration-rotation interaction associated with this motion is also unique in that it is impossible to fit the data in the usual form[10] of $B=B_e-\alpha(v+\frac{1}{2})$. The experimental rotational constants when plotted versus the vibrational quantum number show both curvature and zigzagging.

A rigorous treatment of vibration-rotation interaction is straightforward theoretically. The only difficulty is that detailed force functions are required for every vibration of the molecule. The fact that this information is not available except for diatomic and a few triatomic molecules[11–13] and that the execution of this calculation is extremely tedious and lengthy, makes the rigorous approach not only impractical but impossible.

Since the ring-puckering vibration so dominates the data, it seems best to reduce the problem to a one-dimensional one. This simplification neglects all the interactions of this particular vibration with the other modes in the molecule. Since the coefficients in the rotational constant expansions contain not only contributions from the ring-puckering motion alone, but also those arising from the interactions of this particular vibration with the remaining modes, one should consider the following calculations to yield only approximate coefficients for the rotational constant expansions.

The validity of this single-mode approximation, of course, depends on how well it reproduces the experimentally observed variation in the rotational constants. However, since the frequency of this particular vibration is much lower than those of the remaining vibrations, this would be expected to be a reasonable approximation.

If this single-mode approximation is assumed, the average rotational constant for a given vibrational level is simply given by $h/8\pi^2\langle 1/I\rangle$, where $\langle 1/I\rangle$ denotes the corresponding quantum mechanical expectation value of the reciprocal moment of inertia. This is exact for a diatomic molecule, where there is only one vibrational degree of freedom and thus there can be no interactions of the type ignored in the following calculations for the ring-puckering vibration of trimethylene oxide.

The variation in the moment of inertia with ring puckering will be dependent upon the details of the molecular motion. In particular, the general description of the vibrational coordinate is expected to be of some importance, expecially in this case where the vibration is of fairly large amplitude. For the ring-puckering vibration of trimethylene oxide, there are perhaps two ways in which we may describe the general path of the out-of-plane bending motion. The first of these corrresponds to a simple rectilinear motion of all the ring atoms along the out-of-plane axis. Most normal coordinate treatments use a coordinate of this type. The other involves a motion of the ring atoms along a curvilinear path, with no stretching of the bonds in the ring.

These two cases will now be considered individually. In either case, the calculations first consist of the determination of the coordinates of all the atoms in the molecule in terms of the instantaneous out-of-plane displacement. The principal moments of inertia and the rotational constants are then evaluated in the usual way. Corrections for shifts in the center of mass and rotation of the principal axes were made.

The out-of-plane displacement of the ring atoms is referred relative to the average plane defined by the hypothetical planar ring. This average plane is located so that at any instant, the magnitude of the displacements of the oxygen atom and all three carbons from this plane are equal. We shall designate this out-of-plane displacement of the ring atoms as z.

For ease of discussion, the following coordinate system will be set up in the four-membered ring. The Z axis of this coordinate system will be defined such that it is always perpendicular to the average plane referred to above. The X-Y plane coincides with the average plane, with the X and Y areas parallel to the C—O and C—C diagonals, respectively. The hypothetical planar structure as determined from the extrapolated rotational constants is assumed for the molecule at the planar configuration.

Case 1. Simple Rectilinear Motion along the Z axis

In this case, the four-membered ring vibrates under the constraints

$$\delta x_i=0$$
$$\delta y_i=0, \qquad (2)$$

where i denotes a particular atom in the ring skeleton. The kinematics of the hydrogen atoms are as yet not defined. There are, however, probably only two extreme situations which need be considered. In the first of these, the methylene groups move as units such that the hydrogen atoms also satisfy the above constraints (Case 1a). In the other (Case 1b), the motion of the hydrogens is such that each of the methylene angles is bisected by the plane defined at any instant by its carbon atom and the two adjacent atoms in the ring. In neither of these cases, however, are any stretching of the carbon-hydrogen bonds and deformation of the methylene angles assumed to be involved.

With these models, the rotational constant variations depicted in Fig. 1 are obtained. In these plots, the Q_1^2 and Q_1^4 matrix elements for the potential function selected in the previous paper are employed. A reduced mass for the vibration consistent with the model has been used. These reduced masses are 58.0 amu and 97.2 amu for Case 1(a) and Case 1(b), respectively.

[10] C. H. Townes and A. L. Schawlow, *Microwave Spectroscopy* (McGraw-Hill Book Company, Inc., New York, 1955), p. 25.
[11] See work cited in footnote 10, p. 30.
[12] H. H. Nielsen, J. Chem. Phys. **11**, 160 (1943).
[13] J. Pliva, Collection Czechoslov. Chem. Commun. **23**, 777 (1958).

Comparison of the calculated and observed variations indicates that the above models for the ring-puckering motion are probably far from being the actual situation. Whereas rotational constant A increases with the vibrational quantum level experimentally, a large decreasing variation is predicted from these models. The amount of the vibration-rotation interaction in both rotational constants A and B is also calculated to be many orders of magnitude larger than is experimentally observed. Furthermore, rotational constant C is shown to be more or less invariant to the puckering motion, whereas experimentally, the largest vibration-rotation interaction is observed in this rotational constant. Obviously, therefore, the vibration-rotation interaction cannot be explained by a simple rectilinear motion of the ring atoms.

Case 2. Curvilinear Motion

The four-membered ring is here assumed to bend about the C—C and C—O diagonals with no stretching of the C—C and C—O bonds. That is,

$$\delta l_{C-C}=0$$

$$\delta l_{C-O}=0. \tag{3}$$

Each of the methylene angles will be constantly bisected by the plane defined at any instant by its carbon atom and the two adjacent atoms in the ring. As before, we shall assume no stretching of the carbon-hydrogen bonds and no deformation of the methylene angles during the out-of-plane bending motion.

To complete our description of the ring-puckering motion, one additional parameter must be introduced. This parameter must specify the relative amounts of bending about the two diagonals of the four-membered ring and consequently reflects the dissimilarity of the deformation force constants of the ring angles. This parameter ρ is defined by

$$\begin{aligned}\rho&=[\Delta(x_{C\beta})^2/\Delta(y_{C\alpha})^2]\\&\equiv[(x_{C\beta})^2-(x_{C\beta}{}^0)^2]/[(y_{C\alpha})^2-(y_{C\alpha}{}^0)^2]\\&\equiv[\Delta(x_O)^2/\Delta(y_{C\alpha})^2]\\&\equiv[(x_O)^2-(x_O{}^0)^2]/[(y_{C\alpha})^2-(y_{C\alpha}{}^0)^2],\end{aligned} \tag{4}$$

where $x_{C\beta}$, x_O, and $y_{C\alpha}$ represent the instantaneous values of the x coordinates of the β-carbon and the oxygen, and the y coordinate of the α-carbons, respectively; $x_{C\beta}{}^0$, $x_O{}^0$, and $y_{C\alpha}{}^0$ are the corresponding values when the molecule is at its planar configuration; ρ as defined here, has limits of 0 and ∞. The former limit corresponds to the case where the ring simply bends about the C—O axis alone, and the latter to the case where the puckering is a simple bend about the C—C axis. Symmetrical bending will be taken as that case in which ρ is unity.

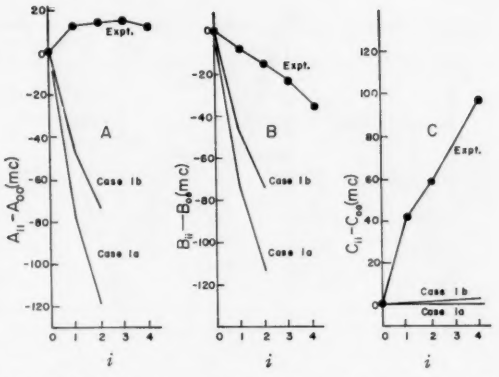

FIG. 1. Rotational constant variations of trimethylene oxide as calculated from models 1(a) and 1(b), plotted against vibrational quantum number.

For convenience, we shall define another parameter ω such that

$$\omega=(1-\rho)/(1+\rho). \tag{5}$$

The limits of ω are -1 and $+1$, with $\omega=0$ corresponding to the situation of symmetrical bending defined above. This definition of ω may now be combined with the geometry of the molecule to yield the following expressions for the coordinates of the ring atoms:

$$\begin{aligned}(x_{C\beta})^2&=(x_{C\beta}{}^0)^2-2(1-\omega)z^2\\(x_O)^2&=(x_O{}^0)^2-2(1-\omega)z^2\\(y_{C\alpha})^2&=(y_{C\alpha}{}^0)^2-2(1+\omega)z^2.\end{aligned} \tag{6}$$

These equations must satisfy the relationships,

$$\begin{aligned}(x_{C\beta})^2+(y_{C\alpha})^2+4z^2&=l_{C-C}{}^2\\(x_O)^2+(y_{C\alpha})^2+4z^2&=l_{C-O}{}^2,\end{aligned} \tag{7}$$

obtained from the geometry of the molecule and the choice of our coordinate system.

The moment of inertia calculations lead to the following rotational constant expansions as a function of ω. These expansions are only carried up to the z^4 term:

$$\begin{aligned}A_{ii}&=11\,999.6\{1+(0.030+1.45\omega)z_{ii}{}^2\\&\quad+(-0.153+0.163\omega+2.14\omega^2)z_{ii}{}^4+\}\\B_{ii}&=11\,707.8\{1+(0.017-1.44\omega)z_{ii}{}^2\\&\quad+(-0.110-0.038\omega+2.11\omega^2)z_{ii}{}^4+\}\\C_{ii}&=6692.2\{1+(1.70-0.020\omega)z_{ii}{}^2\\&\quad+(2.80-0.049\omega+0.046\omega^2)z_{ii}{}^4+\}.\end{aligned} \tag{8}$$

The reduced mass of the vibration consistent with this model is 97.2 amu. Using this reduced mass and the set of matrix elements for the potential function selected earlier, the above rotational constants are

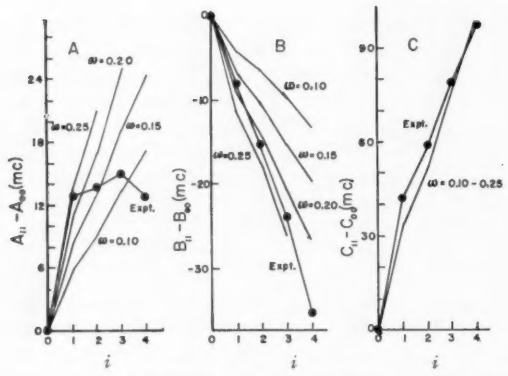

FIG. 2. Rotational constant variations of trimethylene oxide as calculated from model 2, plotted against vibrational quantum number.

plotted versus the vibrational level for several values of ω in Fig. 2.

The best fit to the experimentally observed rotational constant variations is obtained for $\omega \approx 0.20$. While the agreement is by no means perfect, it does reproduce the general variation very nicely. The rotational constant C is very insensitive to the value of ω chosen. The fact that such good agreement is obtained here provides strong justification for the type of molecular motion described in this model.

In Table V, we have tabulated the coefficients of the rotational constant expansions as determined from the numerical fitting in the previous paper and as calculated from the model described here. A comparison between the two sets of values indicates that reasonable agreement is obtained for the second-order coefficients. In view of the complexity of the entire problem, the degree of agreement illustrated here is regarded as quite satisfactory. However, for the fourth-order coefficients, not even qualitative agreement is obtained. There are several possible sources to which we may ascribe the discrepancies. It is clear that the rotational constants are very sensitive to minor changes in the details of the molecular motion. One might expect the detailed motions to change as the amplitude of the vibration increases; ρ and ω are therefore most likely functions of z^2. This would give rise to larger fourth-order coefficients. Additional contributions to both the second-order and fourth-order coefficients should also arise from the interaction of the ring-puckering motion with some of the other lower-lying vibrations, particularly the rocking of the methylene groups and the in-plane deformation of the four-membered ring.

It is important to note that the variations in both rotational constants A and B should be more sensitive to minor details of the molecular motion than should the variation in rotational constant C. For the type of motion described here, where the bending is fairly symmetrical about the two ring diagonals, $\sum_i m_i x_i^2$ and $\sum_i m_i y_i^2$ decrease while $\sum_i m_i z_i^2$ increases with ring puckering. Since $I_a \cong \sum_i m_i y_i^2 + \sum_i m_i z_i^2$ and $I_b \cong \sum_i m_i x_i^2 + \sum_i m_i z_i^2$, the observed rotational constant variations in A and B result from the incomplete cancellations of the changes in $\sum_i m_i x_i^2$ and $\sum_i m_i y_i^2$ by the corresponding change in $\sum_i m_i z_i^2$. The net effect is therefore small so that minor details of the motion can play a more important role in determining the actual variations. For rotational constant C, however, where $I_c \cong \sum_i m_i x_i^2 + \sum_i m_i y_i^2$, the effect is additive, thus giving rise to the large vibration-rotation interaction observed. Here, minor details of the molecular motion should be less important.

Thus, qualitatively at least, the path of the out-of-plane bending motion in trimethylene oxide is one of a curvilinear nature. This result is, of course, not surprising. As will be shown in a latter section, the potential energy associated with this vibration is essentially due to the deformation of the ring angles and to the torsion forces about the C—C and C—O single bonds during the bending motion. Since bending and torsional force constants are small compared to stretching force constants, little stretching of the bonds in the ring skeleton is expected during the vibration.

The very different results obtained with Cases 1 and 2 are striking indeed. In most treatments of vibration-rotation interaction, the initial step is to expand the vibrational motion in terms of the normal coordinates. The coordinates described in Cases 1 and 2 are equally good normal coordinates and are actually equivalent for infinitesimal vibrational displacements. The results of the above considerations very convincingly illustrate the inadequacy of the simple rectilinear motion. It is possible to compensate partially for the improper description of the motion in Case 1 by adding sufficiently large interaction terms so as to mix a small amount of the ring-stretching vibration into the simple rectilinear motion. However, the introduction of such parameters would seem to be artificial and it seems more appropriate to describe the motion in terms of a coordinate system which more closely follows the actual dynamic path of the vibration.

It is probable that the aforementioned effect of path selection on vibration-rotation interaction applies not only to bending motions of the type studied in this problem. The bending motions in linear or nearly linear molecules, the rocking motions of certain groups, for instance, are expected to fall within this category. It is true that for other vibrations, particularly stretching modes, the vibration-rotation interaction is strongly dependent upon the anharmonicities associated with the vibration. However, as has been shown in the previous paper, anharmonicities only determine the finer details of the rotational constant variations for the bending motion considered. Here, it is the path of the motion that decides the sign and the magnitude of the vibration-rotation interaction constants.

Little has been said regarding the so-called Coriolis interactions. So far these interactions have been

TABLE V. Comparison of the coefficients in the rotational constant expansions as obtained from numerical fitting of experimental data and as calculated from model 2.

$(B_{gg})_{ii}=\mathfrak{B}_{gg}{}^{0}+\beta_2{}^{gg}(Q_1{}^2)_{ii}+\beta_4{}^{gg}(Q_1{}^4)_{ii}$[a]

Rotational constant	Zero-order coefficients		Second-order coefficients		Fourth-order coefficients	
	Experiment	Model[b]	Experiment	Model $\omega=0.2$	Experiment	Model $\omega=0.2$
A	12 031.8	12 000	+74.83	+39.4	−29.79	−0.045
B	11 739.6	11 708	−15.66	−32.7	−14.08	−0.041
C	6692.4	6692	+182.3	+117	−31.65	+1.98

[a] Rotational constants are in Mc. The units of Q_1 are amu$^{\frac{1}{2}}$ A.
[b] Rotational constants for hypothetical planar molecule.

assumed to be small so that Wilson and Howard's treatment applies. To the order of approximation carried out by Howard and Wilson,[14] the rotational Hamiltonian is primarily quadratic in the rotational angular momenta. Terms which are quartic in the angular momenta are also involved, but these correspond mostly to centrifugal effects. Neglecting the quartic terms, this rotational Hamiltonian leads to eigenvalues which are given by the equations of King, Hainer, and Cross,[15] namely,

$$W(J,\tau)=[(A+C)/2]J(J+1)+[(A-C)/2]E_\tau(\kappa).$$

The parameters A, C, and κ are, neglecting centrifugal distortion, the same for all rotational levels belonging to a given vibrational state. In the presence of near-vibrational degeneracies, Howard and Wilson's perturbation treatment is no longer valid. Coriolis interaction would then give rise to additional terms in the Hamiltonian which are linear in the rotational angular momenta, and in the presence of which the equations of King, Hainer, and Cross no longer apply. Since the equations have been found to fit all measured transitions with J lower than 10 to within 2 Mc, it is concluded that large Coriolis effects are absent.

The results of this section show that even though the choice between several coordinate systems may be arbitrary as far as normal coordinates are concerned, such a choice is extremely important in the treatment of vibration-rotation interaction. A coordinate system should be selected such that the dynamical path of the vibration will be more nearly coincident with the coordinate chosen.

INTERPRETATION OF THE POTENTIAL FUNCTION IN TERMS OF FORCE FIELDS WITHIN MOLECULE

Aside from a small barrier, the potential function for the ring-puckering motion has been found to contain both harmonic and quartic terms. In particular, the potential function selected is given by

$$V(Q_1)=h\nu_0[0.5\gamma Q_1{}^2+0.08384\gamma^2 Q_1{}^4+1.4\exp(-\gamma Q_1{}^2)],$$
$$\nu_0=93.00\text{ cm}^{-1}. \quad (9)$$

Using a reduced mass of 97.2 amu as calculated for Case 2 in the previous section, one obtains the following potential energy function[16] in terms of the vibrational out-of-plane displacement z(A),

$$V\text{ cm}^{-1}=12\,460z^2+560\,140z^4+130.2\exp(-268.0z^2). \quad (10)$$

In 1945, R. P. Bell[17] suggested that the out-of-plane bending motion in four-membered rings may be quartic in nature. The large quartic term in the above potential function is strong confirmation of this prediction. However, the potential energy function does contain a significant quadratic term. This quadratic term is sufficiently large so that it affects the energy level pattern.

In order to interpret these results, an attempt will be made to obtain a potential function from classical valence forces. The potential energy will be assumed to arise solely from the deformation of the ring angles and the torsional forces about the C—C and C—O bonds.

In the calculations of the strain energy due to angle deformation, the problem arises as to what type of potential should be used to describe the deformation vibration. Since the ring angles here are far from their equilibrium tetrahedral values, one hesitates to use a Hooke's law force. Pliva[13] has recently, in his extensive treatment of vibration-rotation interaction in triatomic molecules, obtained a general potential function for the deformation vibration, which appears to yield reasonable values for cubic and quartic potential constants in bending vibrations of the triatomic molecules studied. The potential as a function of the

[14] E. B. Wilson, Jr., and J. B. Howard, J. Chem. Phys. **4**, 260 (1936).
[15] G. W. King, R. M. Hainer, and P. C. Cross, J. Chem. Phys. **11**, 27 (1943).
[16] Because of a different reduced mass employed, this potential function is slightly different from that previously reported in S. I. Chan, J. Zinn, and W. D. Gwinn, J. Chem. Phys. **33**, 295 (1960). The potential function reported previously, $V(Q_1)=9145z^2+301540z^4+130.2\exp(-196.7z^2)$, is consistent with a reduced mass of 71.3 amu.
[17] R. P. Bell, Proc. Roy. Soc. (London) **A183**, 328 (1945).

deformation angle γ, assumes the form

$$V=\tfrac{1}{2}k\sin\tfrac{1}{2}\phi^e(\sin^2\gamma/\sin\tfrac{1}{2}\phi)[1+b(\sin^2\gamma/\sin^2\tfrac{1}{2}\phi)]; \quad (11)$$

ϕ is the instantaneous valence angle; $\gamma=\phi-\phi^e$, where ϕ^e is the equilibrium value. According to Pliva, b is a small constant of the order of 0.01 for the triatomic molecules studied. k is the usual force constant obtained from zero-order frequencies.

The strain energy due to angle deformation upon the puckering of the ring may then be expanded in a Taylor's series about the angles corresponding to the planar structure. Thus,

$$V \text{ deformation}=\sum_m(\partial V_m/\partial\phi_m)_{\phi m}{}^0\Delta\phi_m + \tfrac{1}{2}(\partial^2V_m/\partial\phi_m{}^2)_{\phi m}{}^0(\Delta\phi_m)^2, \quad (12)$$

where the summation extends over the four ring angles. The evaluation of the derivatives from Pliva's function is tedious but straightforward, and will not be given here. Pliva's deformation potential in the form given by Eq. (11) permits the calculation of all the potential constants in terms of the usual quadratic force constant.

The derivatives in Eq. (12) are evaluated at the configuration of the planar molecule. The $\phi_m{}^0$ are the values of the ring angles at the planar configuration. Since the valence angles are already strained at this configuration, the first derivatives $\partial V_m/\partial\phi_m$ of the deformation potentials evaluated at the planar configuration are different from zero. These give rise to terms in the potential energy which are primarily quadratic in the ring-puckering coordinate. The unstrained equilibrium angles of the $\angle$C—C—C and $\angle$C—C—O's have been calculated from the previously determined methylene angles using the orthogonality relationships[18] for the bond orbitals. The angles are 108° and 109°, respectively. An equilibrium angle of 109° is assumed for $\angle$C—O—C.

The changes in the valence angles with ring puckering were evaluated using the model given in Case 2 of the previous section. The strain energy due to torsional forces about the C—C and C—O single bonds was assumed to be ethane type barriers of the form

$$(V_3/2)(1+\cos3\theta). \quad (13)$$

The torsional barriers used are those for ethane (2800 cal/mole)[19] and methyl alcohol (1070 cal/mole).[20]

The potential function for the out-of-plane motion is now obtained as a function of the out-of-plane displacement z(A). This expression is also a function of ω, the parameter which specifies the relative amounts of bending about the two diagonals of the ring. This parameter has been defined in the previous section. A numerical value for this parameter can now be obtained by minimizing the potential energy with respect to ω, i.e., setting $\partial V/\partial\omega=0$ for all z's.

So far nothing has been said concerning the choice of the quadratic force constants for the deformation of the ring angles. The choice of these quadratic constants is not completely arbitrary. In essence, the following condition must be fulfilled. The planar ring is a rhombus. Given a set of bond lengths, this rhombus may assume a variety of configurations. That configuration which has been assumed by the ring is necessarily one of minimum potential energy, so that at this planar configuration

$$\sum_m(\partial V/\partial\phi_m)_{\phi_m}{}^0\Delta\phi_m{}^0=0. \quad (14)$$

This equation, combined with the conditions

$$\phi^0{}_{C-C-C}+\phi^0{}_{C-O-C}+2\phi^0{}_{C-C-O}=4\pi \quad (15)$$

and

$$l^2{}_{C-C}(1-\cos\phi^0{}_{C-C-C})=l^2{}_{C-O}(1-\cos\phi^0{}_{C-O-C}), \quad (16)$$

yields one relationship that must hold between the force constants. Since three force constants are involved, two will be arbitrary, but the value of the third is restricted by the above condition.

If the bending force constants of the $\angle$C—C—C and $\angle$C—O—C are taken to be 0.8×10^{-11} and 1.0×10^{-11} erg/rad^2, then the value of the $\angle$C—C—O force constant is 1.077×10^{-11} erg/rad^2. Using these quadratic constants and a value of $b=0.01$ for all the valence angles, a value of 0.06 is obtained for ω. This is lower than the value of $\sim$0.20 found empirically in the previous section. It is, however, in the same direction so that the four-membered ring finds it slightly easier to bend about the C—O axis than the C—C axis.

From the calculations outlined above, we obtain the following potential function for the ring-puckering motion of trimethylene oxide,

$$V_{\text{total}}=V_{\text{deformation}}+V_{\text{torsion}},$$

where

$$V_{\text{deformation}}=1.32\times10^5z^2+4.27\times10^5z^4 \text{ cm}^{-1}$$

$$V_{\text{torsion}}=979.4\{1+4(1-3.36z^2+5.59z^4+\cdots)^3-3(1-3.36z^2+5.59z^4+\cdots)\}+374.8\{1+4(1-3.82z^2+7.31z^4+\cdots)^3-3(1-3.82z^2+7.31z^4+\cdots)\} \text{ cm}^{-1}. \quad (17)$$

In order to compare the empirical and calculated potential functions for the ring-puckering motion of trimethylene oxide, these functions are plotted as a function of the out-of-plane displacement in Fig. 3. It is noticed that the curve calculated as outlined above

[18] C. A. Coulson, *Valence* (Oxford University Press, New York, 1952), p. 194.
[19] K. S. Pitzer, Chem. Revs. **27**, 39 (1940).
[20] E. V. Ivash and D. M. Dennison, J. Chem. Phys. **21**, 1804(1953).

(curve A) deviates widely from the experimental curve. An examination of the calculations indicates that the discrepancies arise from the competition between the torsional forces and the deformation strain already present in the planar ring. It is clear from the calculations that in order to obtain a barrier in the potential function it would be necessary either to decrease the slope of the angle deformation potential functions at the points of interest or to increase the torsional barriers of the single bonds. The discrepancy is such that it would be necessary to increase the C—C barrier to around 10 kcal/mole and the C—O barrier to about 4 kcal/mole. Since this is entirely unreasonable, it is thought best to decrease the slopes of the deformation potentials. The curve denoted by B in Fig. 3 was calculated using a $\Sigma_m(\partial V_m/\partial\phi_m)\Delta\phi_m$ of $3.5\times10^4 z^2$, which is about one-fourth that calculated from Pliva's functions. The agreement with experiment is really quite good.

The quadratic term in the angle-deformation strain energy originates from the fact that the valence angles are already strained at the planar configuration. For each valence angle, the contribution is a measure of the slope of the deformation potential at the appropriate strained configuration. This slope is dependent upon the steepness of the potential well for the deformation vibration and the actual degree of strain of the valence angle. It is possible that Pliva's deformation potential is much steeper than the actual situation at the degrees of strain considered. However, even when a parabolic potential function is used, the calculated slope would still be several times too large. Since we are working on the repulsive side of the potential well, the walls should be steeper than that in a harmonic oscillator. The Pliva deformation potential is approximately 20–30% steeper than the parabolic potential function in the regions of interest. This is by no means unreasonable and it is necessary to look elsewhere for an explanation of this discrepancy.

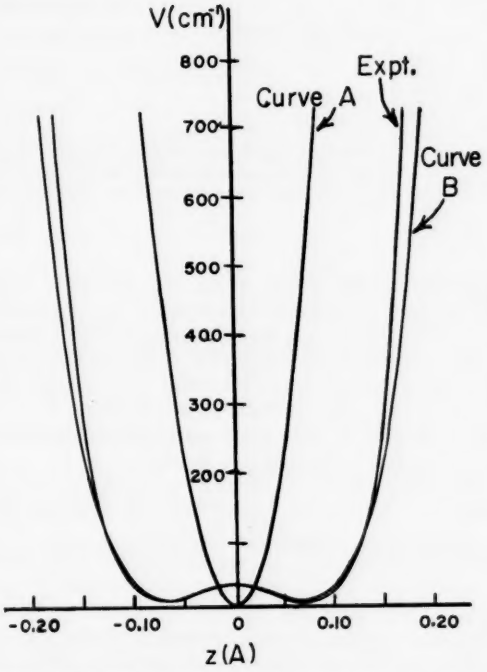

FIG. 3. Empirical and calculated potential functions for the ring-puckering vibration of trimethylene oxide.

The most probable explanation is that the valence angles are not as strained as were assumed in the above calculations. If the degree of strain in the ring angles is diminished by one-third, then the calculated potential function would follow that which is given in Curve B. This implies that the bent bonds in the four-membered ring are not as strained as those which would be calculated using the orthogonality relations of the carbon orbitals alone.

Pi Bonding in Uranyl Ion*

R. LINN BELFORD AND GENEVA BELFORD

The Noyes Chemical Laboratory, University of Illinois, Urbana, Illinois

(Received August 25, 1960)

Overlap integrals were calculated for possible primary bonds of uranyl ion. The $6d\ \sigma$ and π overlaps are about the same and so great that considerable bonding of σd and πd types is indicated. The $5f\ \sigma$ and π overlap integrals are about the same and quite small, but strong σf bonding cannot be ruled out.

PROPERTIES of the uranyl ion (OUO^{++}) have received considerable attention.[1-6] In particular, details of bonding have been the subject of some speculation, especially in connection with the electronic spectra of uranyl compounds and with uranyl salt structures in crystals. Qualitative understanding of the bonding is not difficult. Descriptions can be found in the works cited in footnotes 1 and 3.

Using the uranium $6d$, $5f$ (and $7s$) and the oxygen $2p$ (and $2s$) orbitals, the uranyl ion can form six (or more) bonding orbitals, i.e., $\sigma f(A_{2u})$, $\sigma d(A_{1g})$, two $\pi f(E_{1u})$, and two $\pi d(E_{1g})$ (plus two more if the various s orbitals are used), which accomodate the 12 (or more) valence electrons. Coulson and Lester[4] proposed using some overlap integrals between U Slater orbitals and H $1s$ orbitals as approximate tests of the ability of various molecular orbitals to provide strong bonds, but they devoted their attention particularly to the secondary ligand-to-uranium bonds.

Overlap integrals which we have obtained for the primary uranyl linkage are of some interest in the consideration of possible pi bonding. We performed straightforward numerical integrations (by a two-dimensional Simpson's Rule) using a high-speed digital computer, ILLIAC. To obtain a uranium radical distribution for this purpose, we used the self-consistent-field U^{+6} ion[7] as a core. The radial wave equation, with this core providing the potential, was solved (numerically, by ILLIAC) for $l=3$ (1 node $=5f$), $l=2$ (3 nodes $=6d$), and $l=1$ (7 nodes $=7s$). While the numerical functions so obtained are far from perfect, they should be adequate for our purposes. As one observes in Fig. 1, the Slater $5f$ and $6d$ functions used by Coulson and Lester are roughly similar to ours in the outer regions of the atom. The overlap integrals, $S(l, m)$, were calculated as

$$S(l, m) = \int_0^\infty \int_0^\pi \int_0^{2\pi} Y_l^{-m}(\theta_U, \varphi)\, Y_1^m(\theta_O, \varphi) \times \sin\theta R_{nl}(r_U)\, R_{21}(r_O) r^2 d\phi d\theta dr,$$

where Y's are normalized spherical harmonics, R's are the radial wave functions, and subscripts U or O denote uranium or oxygen atoms. A Hartree-Fock O^- radial function[8] was employed for $R(r_O)$. Results of these integrations are presented in Table I, together with the value derived from each result for the overlap of the uranium orbital with the appropriate combination of orbitals on both oxygen atoms.

TABLE I.

U–O distance		σd	πd	σf	πf
3.15 a_0=1.67 A	U–O	0.175	0.269	0.066	0.075
	(O–U–O)	(0.32)	(0.38)	(0.093)	(0.105)
3.62 a_0=1.92 A	U–O	0.193	0.192	0.052	0.047
	(O–U–O)	(0.27)	(0.27)	(0.073)	(0.069)

The rather surprising outcome of our calculations is that the pi overlap integrals are as large as, sometimes larger than, the corresponding sigma values. To understand this result, we plotted the overlap densities [i.e., the integrand of $S(l, m)$, integrated over ϕ and divided by r] as contour maps; these are shown in Figs. 2 and 3. (The total volume under the mountains of a contour map gives the overlap integral.) Figure 2 shows clearly that while the πd overlap density does not reach as high a value as the σd does, it is spread over a larger volume in space. Also, the angular nodes of the σd function cause its overlap density to be divided into regions of positive and negative values. A partial cancellation therefore reduces the σd overlap integral. The cancellation effect is not a large fraction of the total integral, however; it is not so great as to invalidate our conclusion that πd bonding is likely to be of the same order of magnitude as σd bonding. On the other hand, the low values of the σf overlap integrals may give us a false impression, since it is apparent that the corresponding cancellation effect is here quite large. In such cases, the magnitude of an overlap integral

* This research was aided by a grant from the National Science Foundation.

[1] S. P. McGlynn (privately communicated preprints of papers which are to be published).

[2] R. E. Connick and Z. Z. Hugus, Jr., J. Am. Chem. Soc. **74**, 6012 (1952).

[3] J. C. Eisenstein and M. H. L. Pryce, Proc. Roy. Soc. (London) **A229**, 20 (1955).

[4] C. A. Coulson and G. R. Lester, J. Chem. Soc. **1956**, 3650.

[5] R. L. Belford, J. Chem. Phys. **34**, 318 (1961).

[6] W. H. Zachariasen, Acta Cryst. **7**, 795 (1954).

[7] E. C. Ridley, Proc. Roy. Soc. (London) **A247**, 422 (1958).

[8] D. R. Hartree, W. Hartree, and B. Swirles, Trans. Roy. Soc. (London) **A238**, 229 (1939).

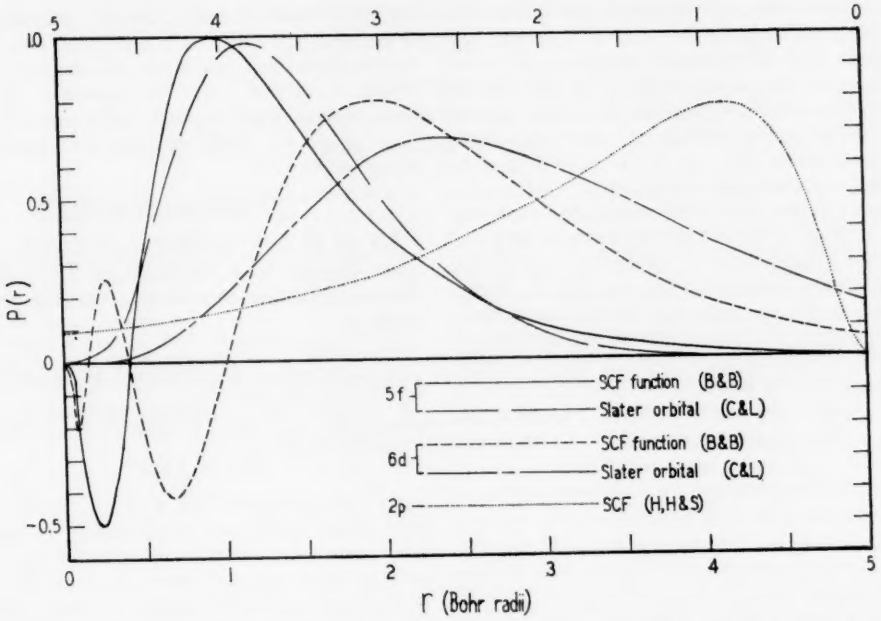

FIG. 1. Comparison of radial wave functions for uranium $5f$ and $6d$, and oxygen $2p$ orbitals. Functions plotted are $rR(r)=P(r)$ (B&B)= Belford and Belford, this work. (C&L)= Coulson and Lester.[4] (HH&S)= Hartree, Hartree, and Swirles.[8] For oxygen, read upper scale.

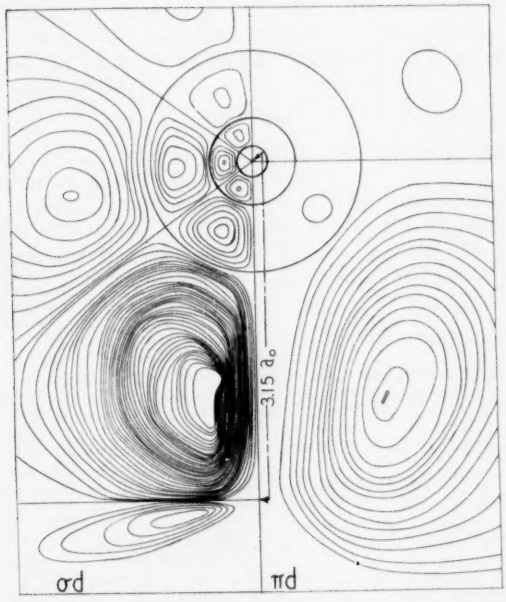

FIG. 2. Contour lines of overlap density of uranium d orbitals with oxygen p orbitals. The vertical coordinate is z and the horizontal coordinate ρ in cylindrical coordinates, both to the same scale. The function plotted is $\int\psi(U)\cdot\psi(o)\cdot\rho d\phi$, i.e., $2\pi\psi(U)\cdot\psi(o)\cdot\rho$. The interval of density is 0.00484. The perfect circles are radial nodes; the straight lines are angular nodes. The sign of the overlap function always changes when a node is crossed.

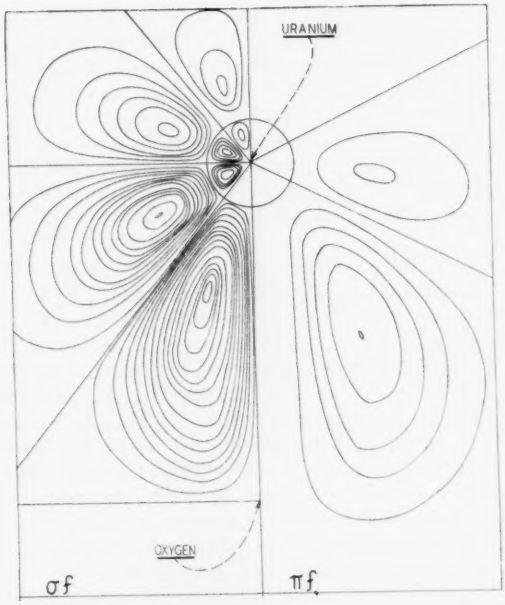

FIG. 3. Contour lines of overlap density of uranium f orbitals with oxygen p orbitals. The interval of density is 0.00748.

may be a poor indicator of bonding possibilities. We are not prepared to judge the point in this case. It is clear, though, that the πf overlap integral is quite small simply because the atomic orbitals do not overlap greatly. We are confident that (in the matter of overlapping) the σ- and πd orbitals are much more likely to form good bonds than the πf. We have reached no such definite conclusion for the σf bond.

Two more points should be mentioned. First, one observes in Figs. 2 and 3 that the presence of radial nodes in our uranium wave functions does not greatly affect the overlap integrals, since most of the overlap occurs outside the last such node. By the same token, the use of oxygen orbitals orthogonalized to the inner shells ($n=1, 2, 3, 4$) of uranium would not change our results drastically. Interference by the $5s$, p, and $6s$, p electrons should have more effect, but the effort involved in our assessing it did not seem to be warranted by the probable returns. Second, the density maps reveal that the electrons in a πd bond would probably be distributed as a pair of very fat doughnutlike charge clouds above and below the equatorial plane, which could interact quite strongly with equatorial ligands. This possibility could account for ligand shifts of uranyl spectra.[9,10]

ACKNOWLEDGMENTS

We are grateful to Professor M. Karplus for helpful discussion and to J. Muirhead, B. Hoffman, and O. Grosz, Jr., for assistance in the calculations and preparation.

---

[9] R. L. Belford, A. E. Martell, and M. Calvin, J. Inorg. & Nuclear Chem. **14**, 169 (1960).

[10] J. Muirhead and R. L. Belford, unpublished work partly reported in the B.S. thesis of J. Muirhead, June, 1960, University of Illinois, Urbana, Illinois.

THE JOURNAL OF CHEMICAL PHYSICS VOLUME 34, NUMBER 4 APRIL, 1961

Molecular Orbital Theory and Hyperfine Splitting in Electron Spin Resonance Spectra of Semiquinones*

GERSHON VINCOW† AND GEORGE K. FRAENKEL

Department of Chemistry, Columbia University, New York, New York

(Received August 17, 1960)

Molecular orbital calculations of the unpaired electron density in a number of semiquinone ions have been made as a function of a range of values of the Coulomb integral α_O for the oxygen atom and the resonance integral β_{CO} between the oxygen atom and the carbon atom. The unpaired electron densities ρ_i were compared with the experimental hyperfine splitting constants a_i arising from the proton bonded to carbon atom i by the use of McConnell's relation $a_i=Q\rho_i$. Excellent agreement is obtained for the proper choice of α_O and β_{CO}. In contrast to most experimental tests of molecular orbital theory, the agreement depends rather critically on the choice of these two parameters. The best values found for the parasemiquinone ions are in the neighborhood of $\alpha_O \cong \alpha_C + 1.2\,\beta_{CC}$ and $\beta_{CO} \cong 1.56\,\beta_{CC}$. The values of $|Q|$ are close to 22.5 gauss. A different set of parameters is needed for the orthosemiquinones. The molecular orbital calculation also fits the experimental splitting constants of the ring protons in the positions meta and para to the methyl group of the tolusemiquinone ion, but there is a large discrepancy at the position ortho to the methyl group. The results of detailed examination of a number of spectra of semiquinone ions are also reported.

I. INTRODUCTION

THE studies of DeBoer and Weissman,[1] and more recently of Symons *et al.*,[2] of the electron spin resonance spectra of aromatic hydrocarbon ions, have shown a remarkable proportionality between the proton hyperfine splitting and the calculated density of the unpaired electron at the carbon atom adjacent to the proton. The unpaired-electron density was calculated by one-electron molecular orbital theory. This proportionality is in accord with the relation proposed by McConnell[3] between the hyperfine splitting constant a_i arising from a proton attached to carbon atom i and the unpaired π-electron density on this carbon atom ρ_i, namely,

$$a_i=Q\rho_i, \tag{1.1}$$

where Q is presumably a constant independent of the molecule or of the proton position.

Theoretical and experimental evidence indicates that Q should be negative.[4,5] The magnitude of Q estimated from the spectrum of the benzene negative ion is $|Q|=22.5$ gauss.[6] For the methyl radical trapped in a solid matrix, the hyperfine splitting is 23 gauss,[7] and McConnell *et al.*,[5] have found $Q=-22$ gauss for trapped malonic acid radicals in a single crystal. Only one other example of a π-electron radical is known in which an estimate of Q can be made without recourse to a calculation of ρ, namely, the recently observed spectrum of the mononegative ion of cyclooctatetraene,[8] for which $|Q|=25.67\pm0.07$. This value may not be comparable with the Q's found for the previously mentioned radicals because the cyclooctatetraenyl radical may not be planar, and even if it were, the C—C bond angle would be 135°.

The results for the univalent positive and negative hydrocarbon ions indicate that there is certainly at least approximate validity to McConnell's expression. The magnitudes of Q's determined from the experimental splitting constants and unpaired-electron densities calculated by means of one-electron molecular orbital theory vary between 26 and 38.[1,2] Within a particular molecule, however, the variation in $|Q|$ is considerably smaller and for all but one molecule studied, is about 15% or less. The variations in $|Q|$ may arise in part from inadequacies in the one-electron molecular orbital theory calculation of unpaired-electron densities.

The density ρ_i in Eq. (1.1) should actually be interpreted as a spin density rather than as an unpaired-electron density,[1] but in a one-electron molecular orbital theory the two densities are the same. It is now well known that the spin density can be negative in odd-alternate hydrocarbon radicals and that these negative densities arise at protons attached to carbon atoms for which the molecular orbital theory with neglect of configuration interaction would predict nodes in the unpaired-electron density. A molecular orbital theory calculation with neglect of configuration interaction cannot be expected to give reasonable results for radicals similar to the odd-alternate hydrocarbons,

* This research was supported in part by the U. S. Air Force through the Office of Scientific Research.

† National Science Foundation Predoctoral Fellow. Present address: California Institute of Technology, Pasadena, California.

[1] E. de Boer and S. I. Weissman, J. Am. Chem. Soc. **80**, 4549 (1958).

[2] A. Carrington, F. Dravnieks, and M. C. R. Symons, J. Chem. Soc. **1959**, 947.

[3] H. M. McConnell, J. Chem. Phys. **24**, 632 (1956).

[4] H. M. McConnell and D. B. Chesnut, J. Chem. Phys. **28**, 107 (1958).

[5] H. M. McConnell, C. Heller, T. Cole, and R. S. Fessenden, J. Am. Chem. Soc. **82**, 766 (1960).

[6] T. R. Tuttle, Jr. and S. I. Weissman, J. Am. Chem. Soc. **80**, 5342 (1958); S. I. Weissman, T. R. Tuttle, Jr., and E. de Boer, J. Phys. Chem. **61**, 28 (1957).

[7] C. K. Jen, S. N. Foner, E. L. Cochran, and V. A. Bowers, Phys. Rev. **112**, 1169 (1958); B. Smaller and M. S. Matheson, J. Chem. Phys. **28**, 1169 (1958); C. F. Luck and W. Gordy, J. Am. Chem. Soc. **78**, 3240 (1956); W. Gordy and C. G. McCormick, *ibid.* **78**, 3243 (1956).

[8] T. J. Katz and H. L. Strauss, J. Chem. Phys. **32**, 1873 (1960).

TABLE I. Experimental splitting constants.

Semiquinone ion derived from	Equivalent proton positions[i]	Splitting constant (gauss)
(1) Hydroquinone[a]	$\alpha=(2,3,5,6)$	2.368±0.001
(2) Catechol[b]	$\alpha=(4,5)$	3.65±0.04
	$\beta=(3,6)$	0.95±0.04
(3) 1,4-Naphthoquinone[c]	$\alpha=(2,3)$	3.23±0.01
1,4-Naphthalenediol[d]	$\gamma=(5,8)$ or $\delta=(6,7)$[j]	0.513±0.005[m]
	$\gamma=(5,8)$ or $\delta=(6,7)$[j]	0.655±0.005[m]
(4) 9,10-Anthraquinone[e]	$\alpha=(1,4,8,11)$ or $\beta=(2,3,9,10)$[j]	0.962±0.005[m]
	$\alpha=(1,4,8,11)$ or $\beta=(2,3,9,10)$[j]	0.550±0.007[m]
(5) o-Phenanthrenequinone[f,g]	[k]	1.66±0.01[n]
	[k]	0.38±0.04[n]
(6) Pyrogallol[h]	$\alpha=5$	5.41±0.02
	$\beta=(4,6)$	0.96±0.02
(7) Quinizarin[g]	$\alpha=(2,3)$[l]	2.60±0.02
	$\beta=(8,11)$	0.49±0.02
	$\gamma=(9,10)$	0.49±0.02

[a] See footnotes 10 and 14; produced by atmospheric oxidation in alkaline alcoholic solution.
[b] See footnote 12 and R. H. Hoskins, J. Chem. Phys. **23,** 1975 (1955); produced by atmospheric oxidation in alkaline alcoholic solution.
[c] Produced by reduction with glucose in alkaline alcoholic solution.
[d] Produced by atmospheric oxidation in alkaline alcoholic solution.
[e] Produced by reduction with sodium dithionite in alkaline alcoholic solution.
[f] See footnotes 13 and 14; produced by reduction with glucose in alkaline alcoholic solution.
[g] See footnote 12; produced by reduction with metallic zinc in alkaline solution of water, ethanol, acetone or mixtures thereof.
[h] See footnote 12 and R. H. Hoskins and B. R. Loy, J. Chem. Phys. **23,** 2461 (1955); produced by atmospheric oxidation in alkaline alcoholic solution.
[i] See Fig. 1 for numbering of positions.
[j] Identification of proton positions with splittings has not been made.
[k] See text.
[l] Assigned by analogy with 1,4-naphthosemiquinone ion.
[m] Corrected for overlap.
[n] Overlap corrections required but not made.

but the results for the even-alternate hydrocarbon radicals indicate that large errors in this latter type of compound are unlikely.

The purpose of the present investigation was to extend the comparison between molecular orbital calculations of unpaired-electron density and experimental splitting constants to the semiquinone ions. Two parameters must be introduced into such a calculation: the Coulomb integral for a $2p_z$ oxygen orbital α_O and the resonance integral between a carbon $2p_z$ orbital and an oxygen $2p_z$ orbital, β_{CO}. Preliminary calculations indicated that the ratios of calculated unpaired-electron densities at different positions in a semiquinone ion, and also the values of $|Q|$, depend markedly on the choice of these two parameters. We therefore proceeded to make a systematic calculation of such ratios and $|Q|$ values over a reasonable range of α_O and β_{CO} for a number of different compounds. The spectra of several compounds were also reinvestigated in order to obtain reliable values of splitting constants.

Molecular orbital calculations on semiquinone ions have been made previously by Bersohn[9] to explain the splitting in the methyl group protons of the methyl-substituted *p*-benzosemiquinone ions with results which are in excellent agreement with experiment. On the other hand, the spectra of the methyl- and chloro-substituted *p*-benzosemiquinone ions show a variation in ring-proton splitting on substitution of methyl groups or chlorine atoms which is much larger than could be accounted for by these calculations in conjunction with Eq. (1.1). In order to avoid the difficulties apparent with substituted semiquinones, the present discussion is concerned primarily with the unsubstituted radicals. One calculation has been made, however, for a methyl-substituted semiquinone ion, and is included in Sec. V.

II. EXPERIMENTAL

The details of the electron spin resonance spectra of the semiquinone ion radicals under consideration in the present work are summarized in Table I. Methods of preparation of the radicals and the techniques employed to study the hyperfine spectra are described elsewhere.[10]

A. 1,4-Naphthosemiquinone Ion

Wertz[11] and Adams *et al.*[12] observed a 15-component hyperfine spectrum composed of a triplet with splitting constant 3.22±0.03 gauss, in which each component is further split into a quintet with splitting constant 0.57±0.03 gauss. This spectrum is consistent with the interpretation that the protons at positions 2 and 3 (see Fig. 1) give rise to the larger splitting and that the 5, 6, 7, and 8 protons are equivalent and give rise to the smaller splitting.

The 1,4-naphthosemiquinone ion was reexamined in the present work under conditions of low radical concentration, low microwave power, and good magnetic-field homogeneity.[10] Each of the quintets previously reported was further resolved into a group of nine components, the intensity ratios of which are consistent with the interpretation of two groups of two equivalent protons each.

The fully resolved spectrum consists of 27 hyperfine components in the approximate intensity ratios

1:2:2:1:4:1:2:2:1:2:4:4:2:8:2:4:4:2:1:2:2:1:4:1:2:2:1.

Values of the three hyperfine splitting constants are reported in Table I.

[9] R. Bersohn, J. Chem. Phys. **24,** 1066 (1956).
[10] B. Venkataraman, B. G. Segal, and G. K. Fraenkel, J. Chem. Phys. **30,** 1006 (1959).
[11] J. E. Wertz and J. L. Vivo, J. Chem. Phys. **24,** 479 (1956).
[12] M. Adams, M. S. Blois, Jr., and R. H. Sands, J. Chem. Phys. **28,** 774 (1958).

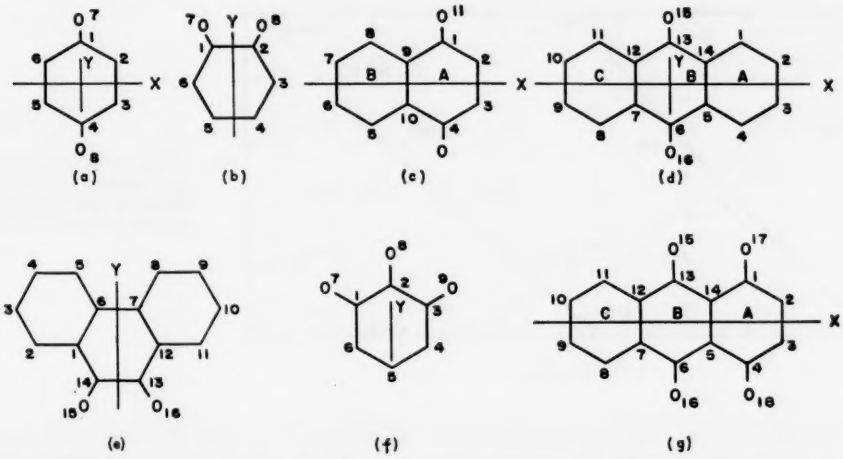

FIG. 1. Structural formulas: (a) *p*-Benzosemiquinone, (b) *o*-Benzosemiquinone, (c) 1,4-Naphthosemiquinone, (d) 9,10-Anthrasemiquinone, (e) *o*-Phenanthrenesemiquinone, (f) Pyrogallolsemiquinone, (g) Quinizarinsemiquinone.

Assignment of the splitting constant with the value 3.23 gauss to the two protons on ring *A* was made on the basis of the spectrum observed on reduction of 2,3-dichloro-1,4-naphthoquinone. The spectrum consists of a single unresolved component with a half-width at half-maximum absorption of approximately $\frac{1}{2}$ gauss, and no chlorine hyperfine splitting was observed.[10] The other two splitting constants cannot be assigned to a particular pair of protons on ring *B* without further evidence.

Corrections for overlap of component lines, as described by Venkataraman,[10,13] were applied to certain measured spacings in order to obtain the reported splitting constants. The overlap correction for 1,4-naphthosemiquinone ion (and also for 9,10-anthrasemiquinone ion, see the following) is only 0.002 gauss and is therefore small compared to the measured spacings.

B. 9,10-Anthrasemiquinone Ion

Adams *et al.*[12] have observed a 13-line hyperfine spectrum of a radical produced by reduction of anthraquinone, but offered no interpretation of the spectrum. In the present work, a hyperfine spectrum has been observed which shows more resolved components than reported by Adams *et al.*, and is consistent with the spectrum predicted from the following model of the 9,10-anthrasemiquinone ion radical.

There are two sets of four equivalent protons each (see Fig. 1). Let us assume that the splitting constant for one set a_1 is approximately twice that for the other set a_2, i.e., $a_1=2a_2+\delta$ where $|\delta|<a_2$. A 25-line hyperfine spectrum would be obtained with predicted intensity ratios of: 1:4:4:6:16:4:6:24:1:24:16:4:36:4:16:24:1:24:6:4:16:6:4:4:1. The hyperfine spacings taken from the central component (relative intensity 36) as origin would be $\pm\delta$, $\pm(a_2+\delta)$, $\pm a_2$, $\pm(2a_2+2\delta)$, $\pm(2a_2+\delta)$, $\pm 2a_2$, $\pm(3a_2+2\delta)$, $\pm(3a_2+\delta)$, $\pm(4a_2+2\delta)$, $\pm(4a_2+\delta)$, $\pm(5a_2+2\delta)$, $\pm(6a_2+2\delta)$.

The observed spectrum is in agreement with these predictions of spacings and relative intensities, and the splitting constants (corrected for overlap) are listed in Table I. The splittings cannot be assigned to definite proton positions without further evidence.

C. *o*-Phenanthrenesemiquinone Ion

This spectrum has been observed by Venkataraman[13,14] and measured by Adams *et al.*[12] It consists of an overlapped quintet each component of which is further split into another highly overlapped quintet of components and is thus consistent with two groups of four equivalent protons each. There are four groups each consisting of two equivalent protons in this radical (see Fig. 1). The observed spectrum can probably be accounted for if the four groups consist of two pairs in each of which the splittings are nearly equivalent, and if the splitting of one set of four protons is considerably different from that of the other set. The deviation from equivalence would account in a large measure for the overlapped appearance of the spectrum. Since overlap corrections were not mentioned by Adams *et al.*, and presumably were not applied, the splitting constants for this radical cannot be considered to be as quantitatively valid as those cited for the other compounds.

D. Quinizarinsemiquinone Ion

In principle free radicals can be produced both by oxidation and reduction of quinizarin. Quinizarin was reduced, in the present work, using sodium dithionite

[13] B. Venkataraman, thesis, Columbia University, New York, 1955.

[14] B. Venkataraman and G. K. Fraenkel, J. Am. Chem. Soc. 77, 2707 (1955).

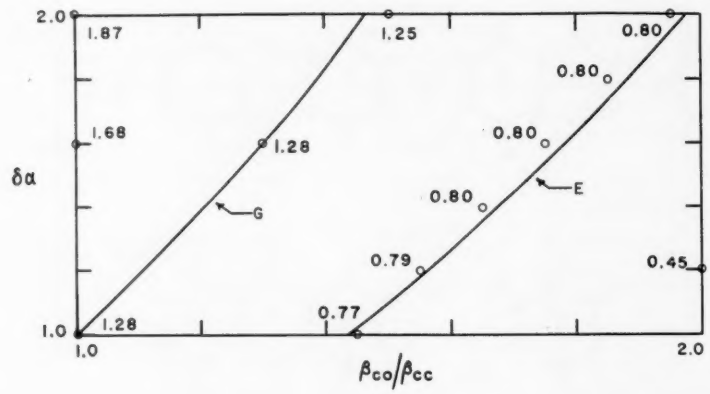

FIG. 2. 1,4-Naphthosemiquinone ion: Contour plot of representative values of the calculated unpaired-electron density ratio ρ_γ/ρ_δ.

in alkaline alcoholic solution, and the hyperfine spectrum observed is consistent with that reported by Adams *et al.*,[12] who did not specify whether the radical observed was formed by oxidation or reduction.

III. MOLECULAR ORBITAL CALCULATIONS

One-electron molecular orbital theory calculations[15] were performed using the Hückel approximation for the free radicals listed in Table I. Energy eigenvalues and eigenfunctions were computed using various sets of values of the molecular orbital theory parameters for the oxygen atoms, namely the Coulomb integral α_O and the carbon-oxygen resonance integral β_{CO}. Calculations were made with an IBM 650 computer, using 30 or more sets of parameters for the *p*-benzosemiquinone ion, 1,4-naphthosemiquinone ion, and the 9,10-anthrasemiquinone ion; 23 sets for the *o*-benzosemiquinone ion; and about 10 sets each for the remainder of the free radicals. The wave functions were used to compute unpaired-electron densities ρ_i and, by means of Eq. (1.1) and the experimental splitting constants a_i, values of $|Q|$ for each proton position. Detailed results, such as the wave functions of the unpaired electron, computed values of odd-electron densities, and computed values of $|Q|$, are tabulated elsewhere.[16]

Some representative results are presented below; others are cited, where pertinent, in the discussion section. The data can be portrayed graphically by means of contour plots. The first contour plot, Fig. 2, will serve as an example. The coordinate axes of these plots are $\delta\alpha=(\alpha_O-\alpha_C)/\beta_{CC}$ and β_{CO}/β_{CC}, where α_C and β_{CC} are the Coulomb and resonance integrals for carbon, respectively. The value of one of the calculated quantities for a particular choice of the parameters $\delta\alpha$ and β_{CO}/β_{CC} is written beside the point defined by this pair of parameters. In Fig. 2, the calculated quantities plotted are ratios of odd-electron densities of the γ to the δ protons in 1,4-naphthosemiquinone ion. These densities are designated ρ_γ/ρ_δ, and the γ, δ notation is defined in Table I. If a large number of points is plotted, it becomes evident that many points have the same value of this ratio. These points could be connected with a continuous curve, and this curve is termed a contour of ρ_γ/ρ_δ. The various contours do not seem to intersect; in a few instances there is more than one contour of the same value. The values of ρ_γ/ρ_δ and, hence, of the contours of ρ_γ/ρ_δ, vary continuously with changes in $\delta\alpha$ and β_{CO}/β_{CC}.

The values of $\delta\alpha$ and β_{CO}/β_{CC} included in the contour plots are in the range $1\leqq\delta\alpha\leqq 2$ and $1\leqq(\beta_{CO}/\beta_{CC})\leqq 2$. These values span the range of oxygen parameters commonly used in the literature.[9,17] In order to test the choice of ranges, a number of calculations have been made using sets of values outside these limits. In general, using Eq. (1.1), poor agreement between experiment and the calculated quantities was obtained, thus justifying the ranges of oxygen parameters selected in the present work.

Figure 3 is a contour plot of representative values of the ratio of odd-electron densities for the α and β protons of 9,10-anthrasemiquinone ion, designated ρ_α/ρ_β. A typical plot of the values of $|Q|$ is presented in Fig. 4, which is a contour plot of representative values of $|Q|$ for the α- and β-position protons of 9,10-anthrasemiquinone ion, designated $|Q_\alpha|$ and $|Q_\beta|$. Each doublet of values is listed in a vertical column beside the point to which it corresponds, with $|Q_\alpha|$ at the top. In this compound, ambiguity arises in the assignment of the observed splitting constants to proton positions, and, for simplicity, only one set of the possible values of $|Q|$ has been plotted (see Sec. IV).

[15] C. A. Coulson and H. C. Longuet-Higgins, Proc. Roy. Soc. (London) **A191**, 39 (1947); C. A. Coulson, Quart. Revs. (London) **1**, 144 (1947); E. Hückel, Z. Physik **70**, 204 (1931).

[16] G. Vincow, thesis, Columbia University, New York, 1959.

[17] (a) R. D. Brown, Quart. Revs. (London) **6**, 63 (1952); (b) M. G. Evans, J. Gergely, and J. de Heer, Trans. Faraday Soc. **45**, 312 (1949); (c) C. A. Coulson, *ibid.* **42**, 106 (1946); (d) B. Pullman and A. Pullman, *Results of Quantum Mechanical Calculations of the Electronic Structure of Biochemicals* (Univ. of Paris, Institute de Biologie Physico-Chimique, Paris, 1957). (Report under U.S. Public Health Service, National Cancer Institute, Grant No. 3073).

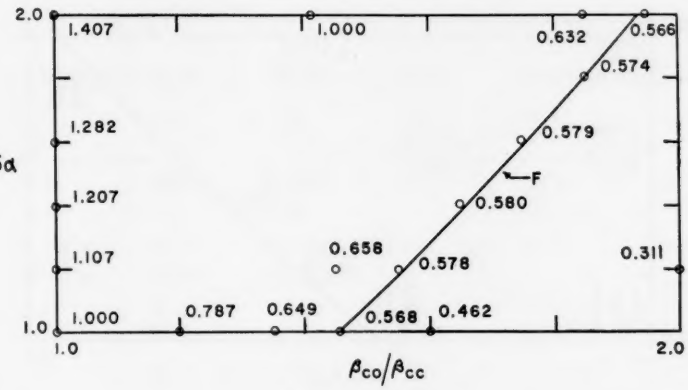

FIG. 3. 9,10-Anthrasemiquinone ion: Contour plot of representative values of the calculated unpaired-electron density ratio ρ_α/ρ_β.

Figure 5 is a contour plot of representative values of $|Q|$ for protons in the α, γ, and δ position of 1,4-naphthosemiquinone, designated $|Q_\alpha|$, $|Q_\gamma|$, and $|Q_\delta|$, respectively.

Figure 6 is a contour plot of representative values of the ratio of odd-electron densities for the α and β protons of *o*-benzosemiquinone ion, ρ_α/ρ_β.

Selected values of the data are collected in Table II. For the *o*-phenanthrenesemiquinone ion, only average values of the calculated quantities for two sets of protons have been tabulated; $\rho_{\beta\beta}$ is the average of ρ_β and ρ_β, and $\rho_{\gamma\epsilon}$ is the average of ρ_γ and ρ_ϵ. The calculations show that ρ_β and ρ_β are roughly equal, and also that ρ_γ and ρ_ϵ are roughly equal. The unpaired-electron density at the first set is larger than at the second. This result is in agreement with the appearance of the spectrum, and the splitting constants can therefore be interpreted as averages arising from two sets of pairs of protons. The Q's are calculated from the average densities and the appropriate experimental splitting constant. For the quinizarinsemiquinone ion, the observed splitting is an average resulting from all the protons in ring C (see Fig. 1), and therefore the only parameters listed for ring C in Table II are an average of the β and γ protons. In principle, two free radicals could be obtained from the oxidation of pyrogallol, one containing nine π electrons and the other containing 11. The calculations show that the wave function of the unpaired electron in the nine π-electron radical has a node in the 5 position and therefore this radical should not produce a large splitting in the 5 position. Since a large splitting is observed at the 5 position, we conclude that the spectroscopically observed radical contains 11 π electrons, and only the calculations for this radical are reported in Table II.

IV. DISCUSSION

A. Parasemiquinones

The first part of the analysis of the molecular orbital calculations will be made by comparing the computed results with the splitting constants of the three parasemiquinone ions for which accurate experimental data is available. These radicals are the *p*-benzosemiquinone ion, the 1,4-naphthosemiquinone ion, and the 9,10-anthrasemiquinone ion. The rings which are not attached to oxygen atoms (ring A in the 1,4-naphthosemiquinone ion, and rings A and C in the 9,10-anthrasemiquinone ion, see Fig. 1) would be expected to be closely analogous to the rings of the hydrocarbon radical ions. Splittings calculated for these adjacent rings from molecular orbital wave functions with the aid of

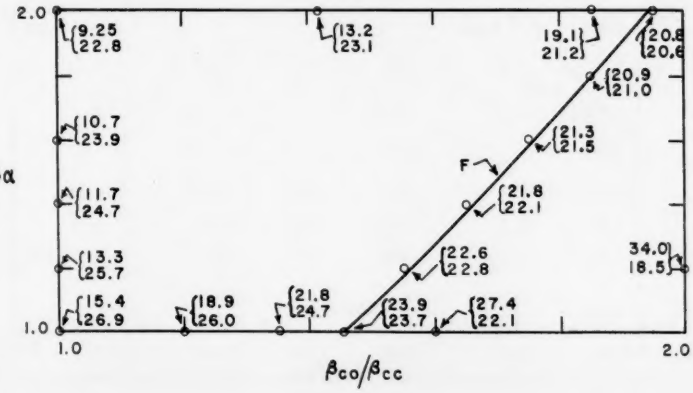

FIG. 4. 9,10-Anthrasemiquinone ion: Contour plot of representative values of $|Q_\alpha|$ and $|Q_\beta|$. Each doublet of values is listed vertically beside each point, with $|Q_\alpha|$ at the top.

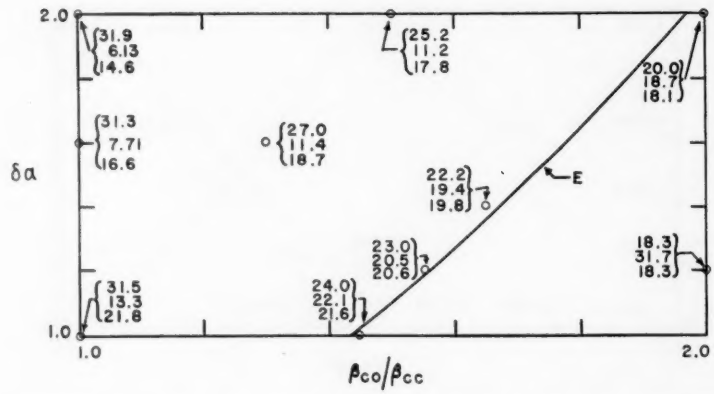

FIG. 5. 1,4-Naphthosemiquinone ion: Contour plot of representative values of $|Q_\alpha|$, $|Q_7|$, and $|Q_8|$. Each triplet of values is listed in a vertical column beside each point in the order $|Q_\alpha|$, $|Q_7|$, $|Q_8|$, with $|Q_\alpha|$ at the top.

McConnell's relation, Eq. (1.1), would therefore be expected to be in rather close agreement with the experimental results provided the parameters α_O and β_{CO} for the oxygen atom are properly chosen. The contour plots of the theoretical ratio of odd-electron densities in the adjacent rings are given in Figs. 2 and 3, and we are interested in finding those contours which possess values in closest agreement with the experimental ratio of splittings. Such contours should indicate the best values of the two oxygen parameters.

Before proceeding, however, the ambiguity in the assignment of the experimental splittings to proton positions in the 1,4-naphthosemiquinone ion and the 9,10-anthrasemiquinone ion must be considered in detail. We assert that the larger of the two splittings arises from the 6 and 7 positions in the 1,4-naphthosemiquinone ion, and from the 2, 3, 9, and 10 positions in the 9,10-anthrasemiquinone ion. The evidence for this choice is as follows:

(1) *Contours of theoretical ratio of odd-electron densities in adjacent ring*

The experimentally determined ratio of the splitting constants for positions 5 (or 8) and 6 (or 7) in the 1,4-naphthosemiquinone ion is 0.78 ± 0.01 or its reciprocal, 1.28 ± 0.02; and for the 1 (or 4, 8 or 11) and 2 (or 3, 9 or 10) positions in the 9,10-anthrasemiquinone ion the ratio is 0.572 ± 0.007 or its reciprocal, 1.75 ± 0.02. The contours which show the best agreement with the experimental ratio of splittings, if the above assignment is correct, are desginated E and F, respectively, in Figs. 2 and 3. The contour which shows the best agreement for the opposite assignment in the 1,4-naphthosemiquinone ion is G. It is an approximate contour since a large number of points were not calculated for the region of the $(\delta\alpha, \beta_{CO}/\beta_{CC})$ plane in the neighborhood of G. The contour showing the best agreement for the opposite assignment in the case of the 9,10-anthrasemiquinone ion is designated H and is not represented in Fig. 3 because it lies outside the plotted range. One point on H lies on the line $(\beta_{CO}/\beta_{CC})=1.0$ at a point considerably above $\delta\alpha=2.5$, and other contour points for $(\beta_{CO}/\beta_{CC})>1.0$ correspond to even larger values of $\delta\alpha$. It is evident from the figures that E and F would be practically superimposable curves on a joint contour plot combining Figs. 2 and 3, whereas G and H would be widely divergent on such a plot.

(2) *Contours of theoretical ratio of odd-electron densities between different rings*

The experimental ratios of the splitting in ring B of the 1,4-naphthosemiquinone ion to the splittings in

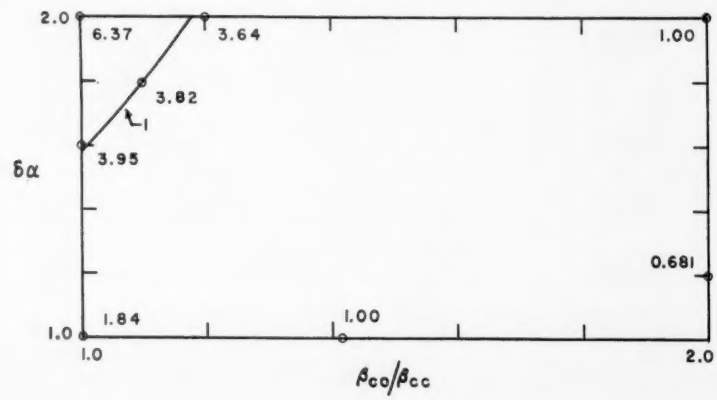

FIG. 6. *o*-Benzosemiquinone ion: Contour plot of representative values of the calculated unpaired-electron density ratio ρ_α/ρ_β.

TABLE II.

		p-Benzo-semiquinone	1,4-Naphthosemiquinone		9,10-Anthrasemiquinone		*o*-Benzosemiquinone	
$\delta\alpha$	$\frac{\beta_{CO}}{\beta_{CC}}$	$\lvert Q_\alpha \rvert$	$\frac{\rho_\alpha}{\rho_\beta}$	$\lvert Q_\alpha \rvert$	$\frac{\rho_\alpha}{\rho_\beta}$	$\lvert Q_\alpha \rvert$	$\lvert Q_\alpha \rvert$	$\lvert Q_\beta \rvert$
1.000	1.000	30.3	3.41	31.5	1.000	15.4	40.8	19.5
1.000	1.400							
1.000	1.414	23.7	4.38	24.5	0.596	23.1	36.5	9.50
1.000	1.450	23.2	4.45	24.0	0.568	23.9		
1.000	1.600	21.4	4.67	22.0	0.462	27.4	34.2	7.38
1.000	2.000						30.3	4.93
1.200	1.550	22.1	4 41	23.0	0.578	22.6		
1.400	1.650	21.2	4.38	22.2	0.580	21.8		
1.600	1.000		2.61	31.3	1.282	10.7	29.9	30.7
1.600	1.750	20.5	4.38	21.6	0.579	21.3		
1.800	1.100						28.6	28.4
1.800	1.850	19.8	4.37	21.0	0.574	20.9		
2.000	1.000	26.9	2.26	31.9	1.407	9.25	25.4	42.1
2.000	1.200	25.4					27.8	26.3
2.000	1.400							
2.000	1.414	23.6	3.29	26.2	1.000	13.2	29.3	17.4
2.000	1.950	19.3	4.38	20.5	0.566	20.8		
2.000	2.000	18.9	4.46	20.0	0.534	21.6	29.1	7.6

		o-Phenanthrenesemiquinone			Pyrogallolsemiquinone			Quinizarinsemiquinone		
$\delta\alpha$	$\frac{\beta_{CO}}{\beta_{CC}}$	$\frac{\rho_{\beta\delta}}{\rho_{\gamma\epsilon}}$	$\lvert Q_{\beta\delta} \rvert$	$\lvert Q_{\gamma\epsilon} \rvert$	$\frac{\rho_\alpha}{\rho_\beta}$	$\lvert Q_\alpha \rvert$	$\lvert Q_\beta \rvert$	$\frac{\rho_\alpha}{\rho_{\beta\gamma}}$	$\lvert Q_\alpha \rvert$	$\lvert Q_{\beta\gamma} \rvert$
1.000	1.000	4.44	40.2	40.8	141	58.7	1470	3.00	31.4	17.8
1.000	1.400	2.68	45.4	27.9	113	53.8	1080	4.39	22.6	18.7
1.000	1.414									
1.000	1.450									
1.000	1.600				30.2	47.8	2560	4.94	19.5	18.1
1.000	2.000	0.766	53.1	9.31	15.4	51.4	140	5.57	15.2	16.0
1.200	1.550									
1.400	1.650									
1.600	1.000	4.87	28.1	31.3	20.8	39.6	146	2.22	33.6	14.0
1.600	1.750									
1.800	1.100									
1.800	1.850									
2.000	1.000	4.81	24.0	26.4	12.7	32.0	72	1.89	34.9	12.4
2.000	1.200	4.86	27.7	30.8	24.4	36.8	159	2.44	30.7	14.1
2.000	1.400				69.4	40.4	498	3.05	26.8	15.4
2.000	1.414									
2.000	1.950									
2.000	2.000	2.28	38.7	20.2	53.7	39.5	376	4.75	18.2	16.3

ring A, the adjacent ring, are 4.93 ± 0.05 and 6.30 ± 0.06. According to the above assignment, the ratio 6.30 would correspond to the 5 and 8 positions, and the theoretical ratios of odd-electron densities for the values of α_O and β_{CO} corresponding to contour E differ from this number by only about 10%. With the opposite assignment, the experimental ratio for these positions would be 4.93, and the theoretical odd-electron density ratio, which must now be computed along contour G, differs from the experimental value by about 50%.

(3) *Contours of* $|Q|$

Figure 4 is a contour plot of values of $|Q_\alpha|$ and $|Q_\beta|$ for the 9,10-anthrasemiquinone ion, and the curve labeled F is the contour of constant odd-electron density ratio taken from Fig. 3. All the $|Q|$ values along curve F are close to $|Q|=22.5$. A similar contour plot of $|Q_\alpha|$, $|Q_\gamma|$, and $|Q_\delta|$, for the naphthosemiquinone ion (Fig. 5) also shows that along curve E the $|Q|$ values are close to $|Q|=22.5$. Along G and H, the contours of odd-electron density consistent with the alternative assignment, the values of $|Q|$ differ considerably from 22.5. For example, in the naphthosemiquinone ion, the values of $|Q|$ along curve E are approximately $|Q_\alpha|=20$–24, $|Q_\gamma|=18$–22, and $|Q_\delta|=18$–22; along curve G, $|Q_\alpha|=25$–30, $|Q_\gamma|=14$–17, and $|Q_\delta|=14$–17. In the anthrasemiquinone ion, the range of values of $|Q_\alpha|$ and $|Q_\beta|$ along F is 21–24; along curve H they are less than 12.

The assignment has not been demonstrated conclusively, but strong evidence has been adduced in its behalf. This assignment will be assumed in the remainder of the discussion.

If we now assume that McConnell's proportionality relation, Eq. (1.1) is correct, then the best values of α_O and β_{CO} will be among those lying on the contour of theoretical odd-electron densities which is in best agreement with the value of the experimental ratio of the splittings, namely, contours E and F in Figs. 2 and 3, respectively.

If one assumes further that the correct value of $|Q|$ for any aromatic CH group lies in a small range about $|Q|=22.5$, then one can obtain ranges for the best values of $\delta\alpha$ and β_{CO}/β_{CC} from an examination of the values of $|Q|$ along curves E and F. One such set of values is given in Fig. 4. Thus, the best values of α_O and β_{CO} consistent with the results of molecular orbital theory and McConnell's proportionality relationship, when applied to the adjacent rings of the 1,4-naphthosemiquinone ion and the 9,10-anthrasemiquinone ion, lie along or very close to contours E and F, and a reasonable range to take is $1.0\leqq\delta\alpha\leqq1.4$ and $1.45\leqq(\beta_{CO}/\beta_{CC})\leqq1.65$. Other quantities were calculated using this best range of oxygen parameters: (1) For the p-benzosemiquinone ion, it was found that $|Q|=21$–23; (2) For the theoretical ratio of odd-electron densities in the 2 (or 3) position to the 6 (or 7) position in the 1,4-naphthosemiquinone ion ρ_α/ρ_β a value was obtained which differs from the experimental ratio of splittings by -9.5% to -11.1%.

If the one-electron molecular orbital theory were an exact theory, the values of α_O and β_{CO} at the point of intersection of contours E and F would be the best values of the oxygen parameters for calculations on semiquinone free radicals. Such values of these parameters are $\alpha_O=\alpha_C+1.2\beta_{CC}$ and $\beta_{CO}=1.56\beta_{CC}$. Since the contours E and F are almost parallel, and the two compounds from which they are derived, the 1,4-naphthosemiquinone and 9,10-anthrasemiquinone ions, are quite similar, the point of intersection is not precisely located and a quite different point of intersection might be obtained if data were available for different compounds. Nevertheless, in spite of the uncertainties concerning the point of intersection and the fundamental inexactness of the theory, it is of interest to examine the values of the other quantities calculated under the assumption that this is the best set of parameters: (1) The value of the theoretical ratio of odd-electron density of the 2 (or 3) position to the 6 (or 7) position in the 1,4-naphthosemiquinone ion, ρ_α/ρ_δ, differs from the experimental ratio of splittings by -10.3%. (2) The values of the Q's for this radical are $|Q_\alpha|=22.3$, $|Q_\gamma|=20.7$, and $|Q_\delta|=20.6$. (3) The values of the Q's for the 9,10-anthrasemiquinone ion are $|Q_\alpha|=22.8$ and $|Q_\beta|=22.7$. (4) The value of $|Q|$ for the p-benzosemiquinone ion is $|Q|=22.0$.

The quinizarinsemiquinone ion is also a parasemiquinone. The theoretical (averaged) ratio of the odd-electron densities (see Sec. III) for values of α_O and β_{CO} in the region close to curves E and F (see Figs. 2 and 3) differs from the experimental ratio of splittings by about 15%. The approximate ranges of $|Q|$ along curves E and F are $|Q_\alpha|=19$–22.5 and $|Q_{\beta\gamma}|=16$–19. These results are in approximate agreement with the results obtained for the other parasemiquinones.

Some comment is perhaps in order about a value of (β_{CO}/β_{CC}) in the range 1.5–1.6. Coulson[17e] has estimated this ratio by assuming that 2β is given by the difference in single-bond and double-bond energies,[18] so that

$$(\beta_{CO}/\beta_{CC})=[E(\text{C—O})-E(\text{C=O})]/[E(\text{C—C})-E(\text{C=C})].$$

Using the values tabulated by Pitzer,[19] namely, E(C—O)=79, E(C=O)=173, E(C—C)=80.5, and E(C=C)=145, one obtains $(\beta_{CO}/\beta_{CC})=1.46$, in surprisingly good agreement with the value found in the present work. On the other hand, the resonance integrals should be at least roughly determined by the overlap integrals, and by interpolating in the tables of Mulliken *et al.*,[20]

[18] J. E. Lennard-Jones, Proc. Roy. Soc. (London) **A158**, 280 (1937).

[19] K. S. Pitzer, *Quantum Chemistry* (Prentice-Hall, Inc., Englewood Cliffs, New Jersey, 1953), p. 170.

[20] R. S. Mulliken, C. A. Rieke, D. Orloff, and H. Orloff, J. Chem. Phys. **17**, 1248 (1949).

one finds, assuming a C—O bond length of 1.33 A, that the ratio of overlap integrals is $(S_{CO}/S_{CC})=0.7$. In other words, these considerations imply that β_{CO} should be less, not greater, than β_{CC}. Similarly, Adrian,[21] in a study of the quadrupole spectrum of cyanuric chloride, found that the carbon-nitrogen resonance integral β_{CN} would fit his data best if it had the value of $\beta_{CN}=0.7\beta_{CC}$, while the ratio of overlap integrals is 0.78.

The foregoing analysis for the parasemiquinone ions indicates that the one-electron molecular orbital theory, in conjunction with Eq. (1.1), is in excellent agreement with experiment, and only small departures are found from the value of $|Q|=22.5$.

B. Orthosemiquinones

We now turn to a discussion of the two orthosemiquinones, the *o*-benzosemiquinone and the *o*-phenanthrenesemiquinone ions. In the former, there is no ambiguity in the assignment of the experimental splitting constants to the proton positions, but in the latter the spectrum is not well resolved and, in addition, there is no experimental evidence for choosing any particular assignment. The ratio of the two splitting constants for the *o*-benzosemiquinone ion is 3.84 ± 0.16; and for the *o*-phenanthrenesemiquinone ion it is 4.4 ± 0.4.[22] The approximate contour of the theoretical ratio of odd-electron densities for the *o*-benzosemiquinone ion giving the best agreement with the experimental ratio of splittings is designated *I* in Fig. 6. Contour *I* is clearly not in agreement with contours *E* and *F* of Figs. 2 and 3. The values of $|Q_\alpha|$ and $|Q_\beta|$ along contour *I* are very similar and range from 27.5 to 30. All other contours show differences, some of them large, between the values of $|Q_\alpha|$ and $|Q_\beta|$ (see Table II). For the *o*-phenanthrenesemiquinone ion, only two sets of (averaged) calculated and experimental quantities can be used (see Sec. III), and again the theoretical ratio of (averaged) odd-electron densities which is in best agreement with the experimental ratio of splittings is in the general region of contour *I*, Fig. 6. Uncertainty in the value of the experimental ratio prevents one from making a stronger comparison. Values of the averaged *Q*'s, $|Q_{\beta\beta}|$ and $|Q_{\gamma\epsilon}|$ (defined in Sec. III), are also closest to 22.5 and to each other in the region of the plot around contour *I*. The similarity between the results for these two compounds indicates that there may be general agreement for all orthosemiquinone ions, but the best values of the oxygen parameters for these compounds are different from the best values for the parasemiquinone ions, and the $|Q|$'s for the ortho compounds are somewhat larger than the $|Q|$'s for the para compounds.

This difference between the best oxygen parameters for the ortho and para compounds implies that the molecular orbital parameters of an oxygen atom are affected by the presence of a second oxygen atom ortho to the first. This effect may be a general phenomenon, and in particular it might be expected that any group ortho to an oxygen atom would require the use of different oxygen parameters from those appropriate in the absence of an ortho-substituted group.

One other unsubstituted radical, the pyrogallolsemiquinone ion, was investigated. It contains three oxygen atoms, and the results obtained are in disagreement with those of both the orthosemiquinones and the parasemiquinones. In fact, there are no values of α_O and β_{CO} in the range under consideration in the present study for which the predicted ratio of odd-electron densities is within a factor of two of the experimental ratio of splittings. One value calculated exceeds the experimental ratio by a factor of about 100, and the values of $|Q_\alpha|$ and $|Q_\beta|$ for this point are 45.7 and 4440, respectively.

The pyrogallolsemiquinone ion is the only radical studied in the present investigation which is an odd-alternate radical, and therefore one would expect that negative spin densities might play an important role.[4] Let us first consider only those valence-bond structures of the 11-electron dinegative ion of pyrogallolsemiquinone in which the two negative charges are on the two most distant oxygen atoms (positions 7 and 9 in Fig. 1). Insofar as the position of the unpaired electron is concerned, such structures are analogous to the structure of the phenoxy radical, and there are no structures in which the odd electron appears at positions 4 and 6, the positions meta to the "phenoxy" oxygen. The simplest theories for these structures would thus predict no unpaired-electron density and no splitting arising from protons at positions 4 and 6. A more refined calculation should, however, give negative spin densities at these positions.

In the present case, simple structures can also be written which place the unpaired electron at positions 4 and 6, although these structures do not cause maximum separation of the two negative charges. There should thus also be a small positive spin density at these positions. The molecular orbital calculations indicate an odd-electron density at these positions, but since the theory does not take into account electron repulsion, it is likely that the calculated results have too large a contribution from structures with the two negative charges near to each other, and thus too large a positive spin density results from the calculation.

The positive and negative spin densities at positions 4 and 6 should thus tend to cancel each other, with the net density being negative, and there should be a very small splitting arising from the protons at these positions. The experimental splitting in the 4 or 6 posi-

[21] F. J. Adrian, J. Chem. Phys. **29**, 1381 (1958).

[22] An interesting numerical sidelight to the agreement among the orthoquinones is the fact, as yet unexplained, that the ratio of splitting constants for all orthosemiquinones investigated to date is about 4. The ratio is 3.84 ± 0.16 for *o*-benzosemiquinone ion, 4.4 ± 0.4 for *o*-phenanthrenesemiquinone ion, and 4.1 ± 0.3 for acenaphthosemiquinone ion.[12]

TABLE III. Tolusemiquinone ion.

α	β_{CO}/β_{CC}	a_3	a_5	a_6
1.000	1.000	1.98	2.52	2.30
1.000	1.450	2.11	2.44	2.36
1.600	1.750	2.11	2.44	2.35
2.000	1.950	2.11	2.46	2.37

tions is only 0.95 gauss and is much smaller than the splitting arising from negative spin density positions in the odd-alternate perinaphthenyl[23] and allyl[24] radicals. The discrepancies between the ratios calculated by one-electron molecular orbital theory and the experimental results can thus be qualitatively understood. In addition, the value of $|Q|$ for the proton in the 5 position is quite high, but it is not unreasonable, in view of the results for the orthosemiquinone ions, that three adjacent oxygen atoms should require a set of oxygen parameters which is at even higher values of $\delta\alpha$ and lower values of β_{CO}/β_{CC} than is needed for the orthosemiquinone ions.

V. TOLUSEMIQUINONE ION

Preliminary investigations of the extension of the present work to substituted semiquinone ions have been made by performing calculations on the tolusemiquinone ion. The experimental splitting constants[14] for the protons at positions 3, 5, and 6, respectively, are 1.764 ± 0.001 gauss, 2.537 ± 0.002 gauss, and 2.462 ± 0.002 gauss. The numbering system in Fig. 1 for *p*-benzosemiquinone has been used with the methyl group at position 2. Bersohn's study of the methyl-group proton hyperfine interaction[9] made use of the molecular orbital theory of hyperconjugation. He used the parameters $\delta\alpha=1.0$, $(\beta_{CO}/\beta_{CC})=1.0$, and two values of β_1, the resonance integral coupling the methyl group to the ring, namely $(\beta_1/\beta_{CC})=0.70$ and $(\beta_1/\beta_{CC})=0.93$, as well as the standard parameters used by Crawford and Coulson in their treatment of hyperconjugation.[25] Bersohn found that the value $(\beta_1/\beta_{CC})=0.93$ gave better agreement with experiment than did 0.70.

In the present work, the wave functions of the tolusemiquinone ion have been calculated for a range of oxygen parameters in the same manner as for the other semiquinones. The methyl-group parameters chosen were those of Crawford and Coulson,[25] and also a set of parameters used by Pullman.[26] The latter are: $\delta\alpha_{CX}=-0.1$, $\delta\alpha_X=-0.2$, and $\beta_{CX}=2\beta_{CC}$, where X is the pseudo-atom notation for the H_3 atoms. Both values of β_1 used by Bersohn were employed.

The methyl group parameters of Crawford and Coulson and of Pullman give essentially identical results, and the results for $(\beta_1/\beta_{CC})=0.93$ are in better agreement than those for the value 0.70. Some of the results obtained with $(\beta_1/\beta_{CC})=0.93$ and the Crawford-Coulson parameters are given in Table III. In the table, the quantities a_3, a_5, and a_6 are the splittings in gauss for protons at positions 3, 5, and 6, respectively. These were obtained, for each set of oxygen parameters, by multiplying the corresponding $|Q|$ for the *p*-benzosemiquinone ion by the calculated unpaired-electron densities at the appropriate positions in the tolusemiquinone ion.

The calculated splittings predict the correct sequence of the magnitudes of the experimental splitting constants. The magnitudes of a_5 and a_6 for $\delta\alpha=1.0$ and $(\beta_{CO}/\beta_{CC})=1.45$ are proportional to the experimental splittings within less than 0.5%, and differ from the experimental splittings by about -5% each. The agreement, for these positions, with McConnell's proportionality relation, Eq. (1.1), is excellent. The 5% difference between calculated and experimental splittings, which is a measure of the agreement for $|Q|$, is comparable to the actual difference between the splittings at these two positions, and therefore the agreement for $|Q|$ cannot be considered to be good in terms of distinguishing the small differences required for this type of problem.

The predicted value of a_3, the splitting for the position ortho to the methyl group, is much higher than the experimental splittings for all sets of parameters used. A possible explanation for this large discrepancy in the value of $|Q|$ at the ortho position is that the methyl group perturbs the σ-bonding orbitals of the group adjacent to it considerably and those of the meta and para much less. Such a perturbation would result in a large change in the value of $|Q|$ at the ortho position. Alternatively, the methyl group might cause a large change in the spin density at the ortho position, and perhaps both effects occur. At present, one must conclude that the theory is not sufficiently precise to use experimental splitting constants as a means of calculating spin densities in aromatic molecules containing substituents.

VI. CONCLUSIONS

The use of McConnell's relation, Eq. (1.1), gives excellent agreement between the experimental splitting constants and the unpaired-electron densities calculated by molecular orbital theory in the unsubstituted semiquinone ions, provided the two molecular orbital theory parameters for the oxygen atoms are properly chosen. The agreement between theory and experiment, in contrast to most types of experimental comparisons with molecular orbital theory, depends quite critically on the proper choice of these parameters. Different sets of parameters are needed for the parasemiquinones and the orthosemiquinones, and in

[23] H. M. McConnell and H. H. Dearman, J. Chem. Phys. **28**, 51 (1958).
[24] E. L. Cochran (private communication).
[25] C. A. Coulson and V. A. Crawford, J. Chem. Soc. **1953**, 2052.
[26] B. Pullman (private communication).

particular,

$$|\alpha_{CO}|_{ortho} > |\alpha_{CO}|_{para}$$

$$|\beta_{CO}|_{ortho} < |\beta_{CO}|_{para}.$$

This result indicates that substituents ortho to each other may have an influence on the unpaired-electron distribution which requires a choice of parameters that is different from the parameters appropriate when the groups are not adjacent as, for example, when they are para to each other. The $|Q|$ values for the parasemiquinones are in better agreement with a value of $|Q| = 22.5$ gauss than are the $|Q|$ values for the ortho compounds.

The pyrogallolsemiquinone ion spectrum does not fit the unpaired-electron density distribution calculated by molecular orbital theory, but the spectrum is in qualitative accord with the distribution that would be expected for an odd-alternate hydrocarbon with contributions from both positive and negative spin densities.

The ring protons in the tolusemiquinone ion at positions meta and para to the methyl group are in good accord with Eq. (1.1), but the ring proton ortho to the methyl group has a considerably smaller splitting than would be predicted by the molecular orbital calculations. Additional factors must clearly be taken into account to obtain the proper theoretical description for substituted compounds.

ACKNOWLEDGMENTS

We are indebted to Professor Richard Bersohn for suggesting many interesting aspects of the present work and for innumerable helpful discussions. Computer service was obtained from the IBM Watson Scientific Computing Laboratories of Columbia University.

Reaction of Nitrogen Atoms with Ozone*

MEI CHIO CHEN AND H. AUSTIN TAYLOR

Nichols Chemistry Laboratory, New York University, New York

(Received August 19, 1960)

The reaction of ozonized oxygen and active nitrogen at room temperature has been shown to produce, almost exclusively, nitrous oxide. Rate measurements in a flow system have been analyzed as involving a primary reaction $N+O_2 \rightarrow NO+O_2$. Accepting present values for the specific rates of subsequent reactions of nitric oxide, the rate of the primary reaction is found to be 10^{10} ml/mole sec. This is several orders faster than the reaction of nitrogen atoms and oxygen molecules and many orders faster than the three-body recombination of atomic nitrogen and atomic oxygen, substantiating the Barth-Kaplan suggestion of the probable source of nitric oxide in the upper atmosphere.

IN order to explain the characteristics of the upper atmosphere, especially the ionosphere, detailed knowledge is necessary of the possible reactions, in an atmosphere containing oxygen and nitrogen. It has been demonstrated that nitric oxide is present at heights below 100 km and its ionization could be responsible for the D layer. Barth and Kaplan[1] considered the reaction of nitrogen atoms with ozone, to produce nitric oxide and oxygen, as having a significant rate, particularly at night when the ozone concentration increases. It was thought advisable to study the reaction with a full realization of the possible further reactions of nitric oxide under laboratory conditions, in an effort to deduce the kinetics of the primary reaction.

EXPERIMENTAL

Nitrogen

Linde tank nitrogen was purified by passage through activated copper[2] supported on Fuller's earth at about 200°C, magnesium perchlorate and ascarite. Alternatively Mathieson tank nitrogen, 99.996% pure was passed through magnesium perchlorate and ascarite.

Ozonized Oxygen

Mathieson tank oxygen, extra-dry grade, 99.6% pure, after passage through magnesium perchlorate and ascarite, was passed through an ozonator[3] comprising three units, each of which consisted of two concentric glass tubes. In the inner tube lead rods in dilute sulfuric acid acted as one electrode. The three units were immersed in a large tank of dilute sulfuric acid which acted as the other electrode through a large copper plate immersed in the acid. The oxygen flowed through the space between the two concentric tubes under a discharge of from 5000 to 10 000 v.

Active nitrogen was produced after the manner of Winkler.[4] A V-shaped discharge tube of 20 mm Pyrex tubing was 120 cm in length including the electrode compartments. The electrodes were heavy aluminum cylinders 24 cm in length. The discharge was operated by a 110–5000-v transformer which fed through a diode rectifier (Raytheon 866–A–GAA) and a 2000-ohm resistance into two condensers in parallel, each 4 μf, 6000 v (Aerovox No. 3). The discharge tube, whose walls were poisoned with phosphoric acid, was connected through the base of the V by a 20 cm length of 20 mm in diam tubing to the reaction vessel of approximately 500 ml volume. The product-receiving trap was 40 cm in length, 35 mm o.d. with a side-tube connecting with a conventional high-speed mercury diffusion pump system. The trap was detachable through a ground-glass joint and its contents could be isolated by two stopcocks. The trap carried a platinum coil which could be heated electrically to decompose excess ozone before the product analysis was made by a mass spectrometer.

For a run, purified nitrogen from a reservoir of 10-liter capacity, maintained at approximately 1 atm pressure, was passed through a metal diaphragm needle valve and calibrated flowmeter and entered the discharge tube near each of the electrodes. The pressure was measured by means of a dibutyl phthalate manometer. When the nitrogen flow was slow, no difficulty was experienced in maintaining constancy of flow. At fast rates, deviations of several millimeters out of 20-cm flowmeter fluid, occurred. This was corrected by passing nitrogen continuously through a flow control into the reservoir. When the power for the discharge was turned on, the yellow afterglow was visible in the discharge tube, down through the reaction vessel and into the receiver. The afterglow intensity in the reaction vessel was measured by a photomultiplier tube (1 P 21), through a Corning 1–56 filter with maximum transmittance around 5200 A, in terms of the deflections of a Rubicon galvanometer. In addition, titration of the atoms with nitric oxide was made.[5]

* This work has been supported by the Geophysics Research Directorate of the Air Force Cambridge Research Center.

[1] C. A. Barth and J. Kaplan, *The Threshold of Space* (Pergamon Press, New York, 1957), p. 7.

[2] F. R. Meyer and G. Rouge, Zeit. angew. Chem. **52**, 637 (1938).

[3] A. L. Herme, J. Am. Chem. Soc. **51**, 2677 (1929).

[4] P. A. Gartaganis and C. A. Winkler, Can. J. Chem. **34**, 1457 (1956).

[5] P. Harteck, R. R. Reeves, and G. Manella, J. Chem. Phys. **29**, 609 (1958).

Pure oxygen was passed into the reaction vessel from a 10-liter reservoir through a metal diaphragm needle valve, ozonator, and flowmeter, in that order. The desired flow rate could be attained in 1 or 2 sec., but constancy of flow required about ½ min.

Runs were of 1-hr duration, timed from the first introduction of oxygen to its stopping, always prior to the cessation of the nitrogen flow. The receiver was immediately isolated by its stopcocks and the liquid nitrogen surrounding it removed. When the receiver had warmed to room temperature, a current was passed through the platinum coil sufficient to make it dull red for 1 sec. Frequently a small explosion accompanied the ozone decomposition. The products were then ready for mass-spectrometric analysis.

The concentration of ozone was determined in blank runs, that is, without the nitrogen flow or with the nitrogen flow but without the nitrogen discharge. The presence of nitrogen without the discharge made no detectable difference. At the end of the run, as soon as the liquid nitrogen was removed from the receiver, about 100 ml of acidified KI solution were drawn into the receiver which was shaken to facilitate reaction. The receiver was then opened to the air and the contents were titrated with 0.01 N $Na_2S_2O_3$ solution.

The mass-spectrometric analysis of mixtures of N_2O,NO and NO_2 is not easy due to the oxidation of the ion-source filament.[6] In earlier runs, with low nitrogen atom and higher ozone concentrations, the product gases were slightly brown-colored showing the presence of NO_2 and analyses were erratic. With higher nitrogen atom and lower ozone concentrations, no color was perceptible. With rhenium in place of the carbon filament and lower ozone concentrations, consistent analyses were achieved even without conditioning of the filament. The gases used for calibration were prepared and purified according to the directions of Nightingale *et al.*[7] To reduce the concentration of nitrogen and oxygen in the products, these were frequently pumped off at liquid nitrogen temperature before analysis.

RESULTS AND DISCUSSION

Table I shows the nitrogen atom flow rate as a function of the nitrogen flow rate interpreted from the nitric-oxide titration and checked by the afterglow intensity.

TABLE I. Nitrogen atom flow rates.

N_2 M/min$\times 10^4$	N M/min$\times 10^4$
0.40	0.52
1.12	0.80
3.76	1.28
7.36	1.76
8.64	2.00
13.8	2.60
17.4	3.00

TABLE II. Ozone production.

O_2 M/min$\times 10^4$	O_3 M/min$\times 10^7$
0.40	1.80
0.65	3.11
0.80	1.90
0.85	3.83
0.90	1.94
1.15	2.24
1.40	5.10
1.45	4.20
1.55	3.92
1.85	5.53
2.00	5.68
2.10	5.38

Table II presents similar calibration data for ozone production as a function of oxygen flow.

Almost the only product of the reaction was nitrous oxide. Occasionally, traces of nitrogen dioxide were found but nitric oxide was never observed. At constant ozone concentration, the rate of production of nitrous oxide was first order in the nitrogen atom concentration. At constant nitrogen atom concentration, the rate was roughly first order in ozone. For the relation

$$d[N_2O]/dt = k[N][O_3], \qquad (1)$$

the concentrations of the various species were taken as the ratios of the flow rates of each species in mole sec^{-1} to the total volume flow in ml sec^{-1}, the latter after making due allowance for the nitrogen dissociation and the oxygen association but neglecting the volume change occurring during reaction. The rate of reaction was taken as the concentration of nitrous oxide divided by the "contact" time calculated as the ratio of the reaction volume to the total volume flow rate. This is, therefore, an apparent contact time and again disregards the volume change occurring due to reaction. Since the contact time, so calculated, averaged less than 1 sec, the neglect of the volume change is justifiable. The values of k, so calculated, were approximately constant for constant ozone runs but showed considerable variation for the constant nitrogen atom runs. It was apparent that nitrous oxide was being produced by reaction other than that of ozone and nitrogen atoms. The above scheme obviously neglects the reaction of nitrogen atoms with oxygen, a reaction frequently demonstrated during the course of this work by making a run without energizing the ozonator. It was further demonstrated, however, that in these latter runs, there was always some back diffusion of oxygen into the nitrogen discharge and the reaction thus measured was not simply that of nitrogen atoms and oxygen molecules. At constant nitrogen atom concentration, the relative amounts of ozone and oxygen vary and this could cause the variation in the value of k, noted above.

[6] R. A. Friedel, Anal. Chem. **25**, 1314 (1953).
[7] R. E. Nightingale, A. R. Downie, D. L. Rotenberg, Bryce Crawford, Jr., and R. A. Ogg, Jr., J. Phys. Chem. **58**, 1047 (1954).

TABLE III. Reaction of N atoms with ozone.

Run	Flow rate M/min$\times10^{+4}$ N_2	Flow rate M/min$\times10^{+4}$ O_2—O_3	Pressure mm Hg N_2	Pressure mm Hg O_2—O_3	Products N_2O M/min$\times10^{+7}$	Products NO_2 M/min$\times10^{+7}$	t sec	k_1 ml/$M\times10^{-10}$
1	1.0	1.10	0.14	0.16	7.75	0.18	1.00	0.51
2	1.2	0.95	0.16	0.15	4.45	1.1	1.08	0.42
3	1.4	0.75	0.18	0.12	7.37	0.17	1.08	1.10
4	1.4	1.4	0.18	0.19	8.37	0.18	1.00	0.29
5	1.4	3.7	0.18	0.38	19.4	0.53	0.87	0.35
6	1.5	2.2	0.19	0.27	12.9	0.33	0.94	0.50
7	1.5	2.9	0.19	0.32	17.5	0.28	0.90	0.60
8	2.0	2.1	0.23	0.25	9.86	4.5	0.93	0.81
9	3.7	1.1	0.35	0.16	16.0	0.32	0.86	1.19
10	5.1	0.8	0.44	0.13	9.91	1.6	0.85	0.68
11	5.3	0.85	0.45	0.14	6.53	4.0	0.89	2.04
12	5.3	1.2	0.45	0.17	19.6	0	0.81	0.89
13	5.9	1.1	0.48	0.16	19.8	0.03	0.79	1.39
14	6.1	0.40	0.49	0.075	9.27	0.94	0.87	1.81
15	6.3	0.40	0.50	0.075	8.30	4.9	0.87	1.53
16	6.5	1.8	0.51	0.23	20.8	0.62	0.76	0.84
17	7.1	1.3	0.54	0.18	19.1	2.5	0.78	1.16
18	7.1	2.3	0.54	0.27	38.1	6.2	0.73	1.69
19	7.2	0.4	0.54	0.075	10.5	1.7	0.84	1.85
20	7.5	0.8	0.56	0.13	19.4	0.93	0.79	2.12
21	7.8	1.2	0.57	0.17	22.6	0.25	0.76	0.95
22	7.8	1.3	0.57	0.19	23.2	0.27	0.76	1.05
23	8.3	1.2	0.59	0.17	26.2	0	0.75	1.17
24	8.5	1.2	0.60	0.17	16.2	0.72	0.74	0.91
25	8.8	1.0	0.61	0.15	16.2	0.23	0.75	1.15

Assuming that the primary reaction is $N+O_3\rightarrow NO+O_2$ (1), since the alternative $N+O_3\rightarrow NO_2+O$ disobeys the spin conservation rule, it has been demonstrated by Harteck and Dondes[8] and by Kistiakowsky and Volpi[9] that the following reactions are possible and likely:

$$N+O_2\rightarrow NO+O \quad (2)$$

$$N+NO\rightarrow N_2+O \quad (3)$$

$$O+NO\rightarrow NO_2 \quad (4)$$

$$O+NO_2\rightarrow NO+O_2 \quad (5)$$

$$N+NO_2\rightarrow 2NO \quad (6)$$

$$N+NO_2\rightarrow N_2O+O \quad (7)$$

$$N+NO_2\rightarrow N_2+O_2 \quad (8)$$

$$NO+O_3\rightarrow NO_2+O_2. \quad (9)$$

That almost the only product observed is nitrous oxide, simply reflects the relative slowness of its reaction in this system. Its absence in the upper atmosphere results from its photochemical instability. Since nitric oxide was not observed among the products and the traces of NO_2 found are not sufficiently reliable due to the error in its mass-spectrometric analysis, to warrant any other conclusion, it has been attempted as a reasonable approximation to treat NO, NO_2, and O as transient intermediates. The application of the stationary-state principle to the series of reactions is only manageable if cognizance is taken of the accepted rates of reactions (2) to (9) and negligible terms are dropped. Such a procedure is more reasonable than the omission of one or more reactions entirely. The following values of the rate constants have been used: $k_2=2\times10^7$; $k_3=1.6\times10^{12}$; $k_4=10^{13}$; $k_5=10^{12}$; $k_6=3\times10^{10}$; $k_7=1.8\times10^{10}$; $k_8=1.2\times10^{10}$; $k_9=10^7$, the units being moles, ml, and sec. It serves no useful purpose to reproduce the details of the algebraic analysis. Suffice that to the approximation stated, the rate of N_2O production is given by the equation $d[N_2O]/dt=(0.080k_1[O_3]+1.77\times10^6[O_2])[N]$.

The calculation of k_1 involves taking the difference between the observed rate of N_2O production and the $[O_2][N]$ term. Occasionally a run was made for which the latter term was larger than the rate of N_2O production observed. It is certain therefore, that the values of k_1 will be minimal values. Table III gives the significant data for 25 runs. It may be noted that the reactions $NO_2+O_3=NO_3+O_2$ and $O_3+O=2O_2$ have not been included in the above scheme. The former should lead to N_2O_5 which, though sought, was never observed, while the rate of the latter under the prevailing conditions is 3×10^7 which is slow in comparison with (4) and (5). Both reactions appear to be too slow to be significant.

The average value of k_1 is 1×10^{10} ml/M sec. This is of the order of the specific rates of reactions (6), (7), and (8) which is not unreasonable for a comparable

[8] P. Harteck and S. Dondes, J. Chem. Phys. **29**, 234 (1958).
[9] G. B. Kistiakowsky and G. G. Volpi, J. Chem. Phys. **27**, 1141 (1957).

oxidation process. The rate is several orders faster than the nitrogen atom reaction with oxygen molecules and many orders faster than the three-body combination of atomic nitrogen and atomic oxygen. It would thus appear to be the most probable source of nitric oxide in the atmosphere.

THE JOURNAL OF CHEMICAL PHYSICS VOLUME 34, NUMBER 4 APRIL, 1961

Interaction Potentials of Simple Nonpolar Molecules with Graphite

A. D. CROWELL AND R. B. STEELE

Department of Physics, University of Vermont, Burlington, Vermont

(Received November 7, 1960)

The interaction and zero-point energies of Ne, A, Kr, Xe, and CH_4 molecules near a semi-infinite graphite lattice at the potential minimum have been calculated using lattice sums of a (6–12) potential with empirically determined potential constants and have been compared with recent experimental data. The significance of the results with respect to the possible role of charge-transfer no-bond mechanism for these systems is briefly discussed and it is concluded that dispersion forces alone are sufficient to account for the interaction energy.

I. INTRODUCTION

THERE have been a number[1–5] of attempts to calculate the interaction energy of nonpolar atoms and molecules with a semi-infinite graphite lattice assuming that the interaction between an individual pair of atoms, one in the molecule and the other a carbon atom in the graphite, could be represented by a potential of the form $u(r) = -A[r^{-6} - (r_0^6/2)r^{-12}]$. Lattice sums of $u(r)$ were then calculated for varying distances z of the atoms above the basal plane to determine the interaction energy. More elaborate calculations, including contributions to the dispersion energy from the dipole-quadrupole and quadrupole-quadrupole interactions and using an exponential repulsive term, have been reported by Kiselev and co-workers.[6] The results of these determinations have not been in particularly good agreement, but they are all of about the same order of magnitude and while generally less than the experimental values, indicate that the dispersion energy at least accounts for a large portion of the total energy of interaction.

Recently Tuck[7] has suggested that the interaction of the inert gases with charcoal is due only to a charge-transfer no-bond mechanism as developed by Mulliken[8] and applied to the interaction of gases with metals by Matsen *et al.*[9] and by Brodd.[10] In discussing these calculations Gundry and Tompkins[11] have pointed out that Tuck's results ignore the dispersion contribution entirely, and that if the charge-transfer no-bond interaction does play a role in the interaction of inert gases with graphite, this interaction must be added to the contribution from the dispersion energy, as had been previously recognized by Mignolet.[12]

Attributing the difference between experimental values (Chackett and Tuck[13]) and the results of lattice summations of a (6–12) potential (Crowell[3]) to charge-transfer interaction, Gundry and Tompkins[11] have estimated the surface potentials of the inert gases on graphite and have shown that they are of the same order of magnitude as the surface potentials of these gases on tungsten as observed by the field emission microscope (Gomer[14] and Erlich and Hudda[15]). As an alternate, Gundry and Tompkins examine the possibility that these surface potentials may be due to simple electrostatic polarization of the adatoms, and they conclude that the experimental results may be adequately accounted for by either theory.

Traditionally the interactions between a simple nonpolar low boiling point molecule with a nonionic adsorbent, such as graphite, have been assumed to be of the London dispersion type plus a repulsive potential, evaluated by a lattice summation method. The lack of

[1] R. M. Barrer, Proc. Roy. Soc. (London) **A161**, 476 (1937).
[2] A. D. Crowell and D. M. Young, Trans. Faraday Soc. **49**, 1080 (1953).
[3] A. D. Crowell, J. Chem. Phys. **26**, 1407 (1957).
[4] E. L. Pace, J. Chem. Phys. **27**, 1341 (1957).
[5] A. V. Kiselev, *Proceedings Second International Congress of Surface Activity* (Butterworths Scientific Publications, Ltd., London, 1957), Vol. II, p. 168.
[6] N. N. Avgul, A. A. Isirikyan, A. V. Kiselev, I. A. Lygina, and D. P. Poshkus, Izvest. Akad. Nauk. S.S.S.R.; Otdel Khim. Nauk. **1957**, 1314.
[7] D. G. Tuck, J. Chem. Phys. **29**, 724 (1958).
[8] R. S. Mulliken, J. Am. Chem. Soc. **74**, 811 (1952).
[9] F. A. Matsen, A. C. Makrides, and N. Hackerman, J. Chem. Phys. **22**, 1800 (1954).
[10] R. J. Brodd, J. Phys. Chem. **62**, 54 (1958).
[11] P. M. Gundry and F. C. Tompkins, Trans. Faraday Soc. **56**, 846 (1960).
[12] J. C. P. Mignolet, J. Chem. Phys. **21**, 1298 (1953).
[13] K. F. Chackett and D. G. Tuck, Trans. Faraday Soc. **53**, 1652 (1957).
[14] R. Gomer, J. Chem. Phys. **29**, 443 (1958).
[15] G. Ehrlich and F. G. Hudda, J. Chem. Phys. **30**, 493 (1959).

TABLE I. Values of the constants A and r_0 in the expression $u(r) = -A[r^{-6}-(r_0^6/2)r^{-12}]$ for interaction between like atoms and the values of A and r_0 for interactions between the gas molecules and carbon.

Molecule	A (like atom) (erg A^6)$\times 10^{12}$	r_0 (like atom) A	A (gas-carbon) (erg A^6)$\times 10^{12}$	r_0 (gas-carbon) A
C	23.9	3.81	...	...
Ne	10.0	3.16	15.4	3.49
A	111	3.87	51.6	3.84
Kr	191	4.04	67.6	3.92
Xe	496	4.46	109	4.14
CH_4	115	4.22	52.5	4.02

agreement with experiment was usually attributed to the limitations in the determinations of the dispersion and repulsive energies, but not in the basic mechanism of interaction. The work of Tuck[7] and Gundry and Tompkins[11] raises the question as to the fundamental nature of the interaction, and it is therefore of considerable importance to know the best possible values which can be calculated from the assumption that the interaction is due to dispersion and repulsive energies only. The determination of an energy of interaction employing lattice sums of $u(r)$ requires knowledge of the potential constants A and r_0. In the case of inert gases and graphite, A has usually[2,3,5,6] been calculated from the Kirkwood-Muller formula and r_0 has been chosen by requiring the potential to have a minimum at some more-or-less arbitrarily chosen distance z_0 from the basal plane, such as the arithmetic mean between the interlaminar spacing of the graphite and the interatomic spacing in the crystal of the adsorbate. Since the Kirkwood-Muller equation gives results which compare with experiment only approximately even in the case of interaction between inert gas atoms, and the interaction potential at the minimum varies rapidly with z_0, the values of the interaction energies can be made to vary by a factor of two or three while keeping the assumptions well within the limits of plausibility. The results may further be modified by including the higher multipole interactions. In any case, the uncertainties in employing the above methods for choosing A and, in effect r_0 render highly questionable a comparison between the results of calculation and experiment to closer than an order of magnitude. Thus before the respective roles of dispersion and charge transfer mechanisms can be evaluated, it is important to determine the best value possible for dispersion interactions alone.

II. CALCULATIONS

In order to avoid the uncertainties inherent in calculating A from the Kirkwood-Muller or similar formula and in assigning an arbitrary value to z_0, the authors have calculated values of A and r_0 for the interaction between an external molecule and a carbon atom in graphite from the corresponding constants for the interaction between pairs of like atoms. These constants were in turn taken as those values which were found by fitting (6–12) potentials to the physical properties of the gas molecules by Mason and Rice[16] and to the properties of graphite by Crowell.[17] The second and third columns of Table I give the values of A and r_0 for pairwise interactions between the like atoms listed in the first column. The constants A and r_0 for the interaction between a carbon atom (constants A_c and r_{0c}) and a gas molecule (constants A_g and r_{0g}) were determined by $A=(A_cA_g)^{\frac{1}{2}}$ and $r_0=\frac{1}{2}(r_{0c}+r_{0g})$. The values of A and r_0 thus found are shown in columns four and five.

If the graphite lattice is represented by a set of planes with a uniform distribution σ atoms per unit area separated by a distance d and the contributions to Σr^{-12} from all but the surface plane are neglected, the energy of interaction $\phi(z)$ of an external molecule located at a distance z from the surface is given by[3,18]

$$\phi(z)=\Sigma u(r)=-(A\pi\sigma/12d^4)\times[\psi^{(3)}(x)-(r_0/d)^6(12/10)x^{-10}], \quad (1)$$

where $x=z/d$ and $\psi^{(n)}(x)$ is defined as $\psi^{(n)}(x)=(d^{n+1}/dx^{n+1})\ln x!$.[19] The functions $\psi^{(n)}(x)$ have been tabulated by H. T. Davis[20] for values of n from 1 to 4.

The value of z_0 for which $\phi'(z_0)=0$ is given by

$$-12(r_0/z_0)^6=x_0^5\psi^{(4)}(x_0). \quad (2)$$

The values of x_0 for which we are interested are between about 0.9 and 1.1, for which interval $x_0^5\psi^{(4)}(x_0)$ is nearly constant and equal to -25.0, giving the

TABLE II. Values of z_0, the equilibrium distance from the surface, $\phi(z_0)$, the interaction energy at the potential minimum ϵ_0 the zero-point energy, $U_0=\phi(z_0)+\epsilon_0$, the internal energy at absolute zero temperature, and $U_{0\text{exp}}$, taken from the results of Sams, Constabaris, and Halsey[21] for a 4–10 potential.

Gas	z_0 (A)	$-\phi(z_0)$ (erg/atom $\times 10^{12}$)	ϵ_0 (erg/atom $\times 10^{12}$)	$-U_0$ (cal/mole)	$-U_{0\text{exp}}$ (cal/mole)
Ne	3.09	0.0670	0.00478	913	734
A	3.40	0.156	0.00463	2163	2142
Kr	3.48	0.187	0.00345	2621	2806
Xe	3.66	0.247	0.00290	3457	3720
CH_4	3.56	0.184	0.00760	2560	...

[16] E. A. Mason and W. E. Rice, J. Chem. Phys. **22**, 843 (1954).
[17] A. D. Crowell, J. Chem. Phys. **29**, 446 (1958).
[18] A. D. Crowell, J. Chem. Phys. **22**, 1397 (1954).
[19] The writers are grateful to Dr. Sydney Ross for pointing out that the definition of $\psi^{(n)}(x)$ given in previous papers, $\psi^{(n)}(x)=(d^n/dx^n)\ln\Gamma(x)$, is incorrect.
[20] H. T. Davis, *Tables of Higher Mathematical Functions* (Principia Press, Inc., Bloomington, Indiana, 1933).

convenient relationship

$$z_0 = 0.885 r_0. \tag{3}$$

The values of $\phi(z_0)$, the potential minimum, is given by

$$\phi(z_0) = -(A\pi\sigma/12d^4)[\psi^{(3)}(x_0) + (x_0/10)\psi^{(4)}(x_0)], \tag{4}$$

which can be expressed as

$$\phi(z_0) = -(A\pi\sigma/12z_0^4)[x_0^4\psi^{(3)}(x_0) + (x_0^5/10)\psi^{(4)}(x_0)]. \tag{5}$$

Since in the neighborhood of $x_0 = 1$, $x_0^4\psi^{(3)}(x_0)$ is also very nearly constant and is equal to 6.49, Eq. (5) becomes

$$\phi(z_0) = -(\tfrac{1}{3})A\pi\sigma z_0^{-4} \tag{6}$$

within a few percent for the values of z_0 for the cases in question.

The values of z_0 from Eq. (3) and of $\phi(z_0)$ from Eq. (6) are given in Table II together with ϵ_0, the zero-point energy for vibrations normal to the surface, for the inert gases and methane. Also included in Table II are values of $U_0 = \phi(z_0) + \epsilon_0$ in column five determined from columns three and four and values of U_0 exp, determined experimentally by Sams, Constabaris, and Halsey[21,22] by the virial coefficient method.

In this method the departure of the gas in the presence of the adsorbent from ideal behavior is attributed to the interactions of the gas molecules at the surface. At low pressures interactions between gas molecules can be neglected and a virial analysis gives the potential parameters of an assumed potential interaction between a single gas molecule and the adsorbent. Sams *et al.*[21] have examined the interactions of Ne, A, Kr, and Xe with a highly graphitized carbon black (P33,2700°) and have presented results for (3–∞), (3–9), (3–12), and (4–10) Lennard-Jones potential models. As the analysis in this paper leads to the conclusion that the (4–10) model is most closely in accord with the results of a lattice summation, the results[21] for this potential are included in Table II.

III. DISCUSSION

The results shown in Table II represent in the writers' opinion close to the best values possible for the interaction between these simple nonpolar molecules and a graphite lattice obtainable using a lattice summation of a (6–12) potential. While in the cases of Ne, Kr, and Xe these results do not differ much from those obtained earlier,[3] the important case of A, which previously differed significantly from the experimental values, as noted by Sams *et al.*,[21] is now seen to be in excellent agreement with experiment. Furthermore the results of this investigation are not subject to many of the objections against the previous calculations.

The problem posed by the discrepancy between the results in Table II and the experimental results of Chackett and Tuck[13] which has been attributed in whole[7] or in part[11] to charge-transfer no-bond interactions appear to the writers to be accounted for in the experimental situations. Chackett and Tuck[13] reported results for a charcoal which was certainly porous and did not necessarily possess a graphite structure. The highly graphitized carbon of Sams *et al.*[21] seems to be much closer to the conditions of the theoretical model. Considering the uncertainties inherent in the calculations, it would seem that the agreement between the last two columns of Table II is sufficiently good to lead to the conclusion that the dispersion forces alone are enough to account for the interactions, and that it is unnecessary to introduce either charge-transfer no-bond forces or classical polarization effects.

ACKNOWLEDGMENT

The authors wish to express their thanks to the Research Corporation for funds for a graduate fellowship held by Mr. Steele during the course of this study.

[21] J. R. Sams, G. Constabaris, and G. D. Halsey, J. Phys. Chem. (to be published).

[22] The authors are grateful to Dr. Sams, Dr. Constabaris, and Dr. Halsey for furnishing a preprint of their paper.

Eigenfunctions for Integer and Half-Odd Integer Values of J Symmetrized According to the Icosahedral Group and the Group C_{3v}

A. G. McLellan

Physics Department, University of Canterbury, Christchurch, New Zealand

(Received October 6, 1960)

Eigenfunctions of J^2 for $J=0, \frac{1}{2}, 1\cdots 8$, have been obtained and tabulated which are symmetrized according to the icosahedral group and the group C_{3v}, in terms of eigenfunctions of J^2 and J_z, referred to a fivefold axis of rotation as the z axis. The functions are symmetrized according to C_{3v} in such a way that the symmetry operation of a $2\pi/3$ rotation is represented by a diagonal matrix. The results have been applied to calculate the anisotropic magnetic splitting factors for the doublet states arising from the above symmetry.

I. INTRODUCTION

JUDD[1] has discussed the possibility that the appropriate symmetry in the double nitrates of the rare earth elements is dominantly that of the icosahedral group P which is to a relatively small extent modified to the symmetry of its subgroup C_{3v}. For the full examination of the possibilities of this assumption, it is desirable to know the eigenfunctions of J^2 symmetrized according to these groups. That is, the $|J_z\rangle$, $J_z = -J, \cdots +J$, transform irreducibly according to the representation D_J of the rotation group (more strictly, of its double group), but transform in general reducibly according to P. The representation D_J of P is reducible to $\Sigma a_i\Gamma_i$, where the Γ_i are irreducible representations of P, and the a_i may be a positive integer or zero. This reduction is tabulated by Judd.[1] To obtain eigenfunctions symmetrized according to P (or its double group), linear combinations of the $|J_z\rangle$ must be obtained which transform irreducibly according to each of the Γ_i occurring in the reduction of D_J. When the symmetry group C_{3v} is taken into account, one must further symmetrize the eigenfunctions which transform according to Γ_i so that they form bases which transform irreducibly according to those irreducible representations γ_α of C_{3v} which occur in $\Gamma_i \rightarrow \Sigma\omega_\alpha\gamma_\alpha$.

Such symmetrized eigenfunctions are of value when the effect of the crystal field, with the above symmetry, is taken into account. To a first approximation a level J is split into levels designated by the Γ_i to which D_J reduces, the corresponding eigenfunctions being those which transform according to the appropriate Γ_i and the degeneracy being the dimensions of Γ_i. Under the influence of a component of the crystal field of symmetry C_{3v}, the level Γ_i splits further into levels determined by the γ_α to which Γ_i reduces, the degeneracy again being the dimensions of γ_α and the eigenfunctions those symmetrized according to γ_α. Actually, C_{3v} has only one- and two-dimensional representations and in the case of odd numbers of electrons, Kramer's theorem leads to degeneracies of two always, i.e., the pair of one-dimensional representations appropriate in this case form a doublet. Judd[1] has tabulated the reduction of the Γ_i to the γ_α and his labeling of representations is followed in this paper.

When referred to such eigenfunctions, the matrices of crystal fields, which have the symmetry in question, take their simplest form. Such functions may be used also to calculate simply the magnetic splitting factors of the energy levels.

2. METHOD OF OBTAINING THE SYMMETRIZED EIGENFUNCTIONS

To obtain this type of eigenfunction, projection operators must be used (see, e.g., Koster[2]). The icosahedral group contains 60 elements, but the application of the projection operator is simplified if the projection operates on a $|J_z\rangle$, referred to the fivefold axis as the z axis, and with the representation matrices of the irreducible representations Γ_i chosen so that in each the matrix corresponding to a rotation of $2\pi/5$, about the z axis is diagonal.

The icosahedral group may be generated from three elements A, B, and C, where A represents the $2\pi/5$ rotation about an axis which passes through the centres of two opposite vertices of the icosahedron, B represents a π rotation about an axis perpendicular to that of A and passing through the midpoints of two opposite edges of the icosahedron. C represents the similar π rotation whose axis is perpendicular to that of B. B and C obviously commute.

The elements of P may be represented by[3]

$$P=K+CK+ACK+A^2CK+A^3CK+A^4CK, \quad (1)$$

where $K=H+BH$, and H is the cyclic subgroup of order 5 generated by the element A. The projection operation on an arbitrary function ϕ is represented by

$$\phi_{ij}{}^{\alpha}=\sum_s D_{ij}{}^{\alpha *}(s)s\phi, \quad (2)$$

[1] B. R. Judd, Proc. Roy. Soc. (London) **A241**, 122 (1957).

[2] G. F. Koster, M. I. T. Solid State and Molecular Theory Group, Tech. Rept. No. 8 (1956).

[3] A. Speiser, *Die Theorie der Gruppen von Endlicher Ordnung* (Dover Publications, New York, 1937).

where the summation is over all elements s of the group; $D_{ij}^{\alpha *}(s)$ is the complex conjugate of the ij element of the representation matrix $D^{\alpha}(s)$ of the element s in the αth irreducible representation of the group. The resulting functions ϕ_{ij}^{α} then transform invariantly according to this irreducible representation as follows,

$$s\phi_{ij}^{\alpha}=\sum_{i'}D_{i'i}^{\alpha}(s)\phi_{i'j}^{\alpha}. \tag{3}$$

That is, for a given j one obtains a basis for the irreducible representations. The bases for different j values may or may not be orthogonal to each other. In the case where ϕ is $|J, J_z\rangle$ and it is operated on by the projection operator for a Γ_i which is contained once only in D_J, the nonzero bases for different j values will be the same, apart perhaps from a phase factor dependent on j only.

In what follows A is represented by a diagonal matrix of the form $\delta_{\alpha,\beta}\exp(2\pi i\alpha/5)$ in all Γ_i and D_J, and the convention is used that the rows and columns of matrices in each Γ_i and D_J are numbered by the integer or $\frac{1}{2}$-integer α which occurs in the exponent of the diagonal element of the corresponding representation matrix of A, which lies in the respective row or column. For example in Γ_3, α is $-2, 0, 2$, i.e., the representation of A in Γ_3 is given by

$$a^{(3)}=\begin{pmatrix} e^{-4\pi i/5} & 0 & 0 \\ 0 & 1 & 0 \\ 0 & 0 & e^{4\pi i/5} \end{pmatrix}, \tag{4}$$

hence the rows and columns of any other matrix in this representation are numbered -2, 0, $+2$. Then it is easily shown that the result of projecting a $|y\rangle$ on to a Γ_α is given by

$$\phi_{ij}^{\alpha}(y)$$

$$=\sum_{x}\{5c_{i,j}^{(\alpha)*}C_{x,y}^{J}+5d_{i,j}^{(\alpha)*}D_{x,y}^{J}+b_{i,j}^{(\alpha)*}B_{x,y}^{J}\}|x\rangle$$

$$+\delta_{i,j}|y\rangle, \tag{5}$$

where $c^{(\alpha)}$, $d^{(\alpha)}$, $b^{(\alpha)}$ are the matrix representations of C, BC, B, respectively, in Γ_α; C^J, D^J, B^J are the matrix representations of these group elements in D_J; $\phi_{ij}^{\alpha}(y)=0$, unless $y=j$ (mod 5), and the summation is over values of $x=i$ (mod 5). Where a certain Γ_α occurs twice in D_J, and this is the highest "multiplicity" in the values of J considered ($J=0, \frac{1}{2}, 1, \cdots 8$), two values of y, y_1, and y_2, must be chosen so that the resulting bases are independent. One is chosen as a basis say ϕ_{ij}^{α}, and the following independent basis is constructed which is orthogonal to the chosen basis

$$\phi_{ij_2}^{\alpha}(y_2)-a\phi_{ij_1}^{\alpha}(y_1),$$

where

$$a=[\phi_{ij_1}^{\alpha}(y_1)\cdot\phi_{ij_2}^{\alpha}(y_2)]. \tag{6}$$

Here both original bases must be normalized to unity. In practice, these two bases may not be the correct zero-order eigenfunctions when the J level is split by a field of icosahedral symmetry, the correct linear combinations of these must be found by diagonalizing the crystal field matrix referred to these two bases. That is, this matrix, when referred to these two (arbitrary) bases, will in general depend on 3 parameters λ, μ, ν in the following form, using submatrices

$$\begin{pmatrix} \lambda E^{(\alpha)} & \nu E^{(\alpha)} \\ \nu^* E^{(\alpha)} & \mu E^{(\alpha)} \end{pmatrix}, \tag{7}$$

where $E^{(\alpha)}$ is the unit matrix in Γ_α, λ, μ being real. Where Γ_α occurs once the crystal field matrix is simply a real multiple of $E^{(\alpha)}$.

3. DETAILS OF THE REPRESENTATIONS

Representations of Γ_2 and Γ_3 are obtained from Speiser[3] in the form:

$$\begin{matrix} & A & & & B & \\ \Gamma_2: & \begin{pmatrix} \epsilon^{-1} & & \\ & 1 & \\ & & \epsilon \end{pmatrix}; & & \begin{pmatrix} 0 & 0 & -1 \\ 0 & -1 & 0 \\ -1 & 0 & 0 \end{pmatrix}; & \end{matrix}$$

$$C$$

$$5^{-\frac{1}{2}}\begin{pmatrix} \beta & -\sqrt{2}i & \alpha \\ \sqrt{2}i & 1 & \sqrt{2}i \\ \alpha & -\sqrt{2}i & \beta \end{pmatrix}; \tag{8a}$$

$$\begin{matrix} & & & & & \\ \Gamma_3: & \begin{pmatrix} \epsilon^{-2} & & \\ & 1 & \\ & & \epsilon^{2} \end{pmatrix}; & & \begin{pmatrix} 0 & 0 & -1 \\ 0 & -1 & 0 \\ -1 & 0 & 0 \end{pmatrix}; & \end{matrix}$$

$$5^{-\frac{1}{2}}\begin{pmatrix} -\alpha & \sqrt{2}i & -\beta \\ -\sqrt{2}i & -1 & -\sqrt{2}i \\ -\beta & \sqrt{2}i & -\alpha \end{pmatrix}, \tag{8b}$$

where $\epsilon=\exp(2\pi i/5)$, $\alpha=(5^{\frac{1}{2}}-1)/2$, $\beta=-(5^{\frac{1}{2}}+1)/2$. Now the matrices of Γ_2 are equivalent to those of D_1, according to which x, y, z transform and by a simple transformation they can be put into the form of the real orthogonal matrices which give the actual transformations of x, y, z when the coordinate axes are rotated according to the physical operations which the group

elements represent, i.e.,

$$A=\begin{pmatrix}1 & 0 & 0\\ 0 & \cos 2\pi/5 & -\sin 2\pi/5\\ 0 & \sin 2\pi/5 & \cos 2\pi/5\end{pmatrix};\quad B=\begin{pmatrix}-1 & 0 & 0\\ 0 & 1 & 0\\ 0 & 0 & -1\end{pmatrix};$$

$$C=5^{-\frac{1}{2}}\begin{pmatrix}1 & -2 & 0\\ -2 & -1 & 0\\ 0 & 0 & -5^{\frac{1}{2}}\end{pmatrix}, \tag{9}$$

where rows and columns are lettered in the order z, x, y. That is, A represents a $2\pi/5$ rotation about the z axis, B a π rotation about the x axis. The axis of C is easily determined to have the direction-cosines $1_x=0$, $1_y=-\alpha(1+\alpha^2)^{-\frac{1}{2}}$, $1_z=(1+\alpha^2)^{-\frac{1}{2}}$. A rotation in 3 dimensions corresponds to two unitary transformations in spinor space, one of which is the negative of the other, and we may without loss of generality represent A, B, and C by the matrices

$$\begin{pmatrix}a & -b^*\\ b & a^*\end{pmatrix}=\begin{pmatrix}\cos(\phi/2)-i1_z\sin(\phi/2), & -(1_y+i1_x)\sin(\phi/2)\\ (1_y-i1_x)\sin(\phi/2), & \cos(\phi/2)+i1_z\sin(\phi/2)\end{pmatrix}, \tag{10}$$

where ϕ is the angle of rotation and 1_x, 1_y, 1_z the direction-cosines of the axis of rotation. The negative of these matrices will represent the elements A', B', C' of the double group. To obtain the matrix representations of A, B, and C in D_J, the following equation is used (see for example Wigner[4]),

$$D_{\mu'\mu}^{J}=\sum_k(-1)^k\frac{[(J+\mu)!(J-\mu)!(J+\mu')!(J-\mu')!]^{\frac{1}{2}}}{(J-\mu'-k)!(J+\mu-k)!k!(k+\mu'-\mu)!}\times a^{J-\mu'-k}a^{*J+\mu-k}b^k b^{*k+\mu'-\mu}, \tag{11}$$

$D_1\rightarrow\Gamma_2$ and the representation of Γ_2 in (8) agrees with the representation obtained from (11), $D_2\rightarrow\Gamma_5$ and thus the representation of Γ_5 is determined. A representation for Γ_4 is obtained from the fact that $D_3\rightarrow\Gamma_3+\Gamma_4$, the basis of Γ_3 was obtained by projection, a suitable unitary transformation completely reducing D_3 was easily found, and hence a representation of Γ_4 obtained. Thus the matrices of the single-valued representations of P were obtained. The matrices of the double-valued representations were found in a similar manner.

In employing the projection operators, y in (5) was when possible chosen to be $\pm J$, in this case only the outermost column of the matrices of D_J was required and these are the simplest to calculate from (11). The eigenfunctions symmetrized according to the icosahedral group are obtained as linear combinations of the eigenfunctions of J^2 and J_z in the form

$$|\Gamma_\alpha,\beta_\alpha)'=\sum_{J_z}f_{\beta_\alpha,J_z}^{(\alpha)'}|J,J_z\rangle \tag{12}$$

$$A|\Gamma_\alpha,\beta_\alpha)'=\exp(2\pi i\beta_\alpha/5)\,|\Gamma_\alpha,\beta_\alpha)', \tag{13}$$

where the summation is over values of $J_z=\beta_\alpha$ (mod 5). For example for Γ_3, β_3 can take the values -2, 0 $+2$.

With the representations obtained from (11), it was found that

$$\theta|\Gamma_\alpha,\beta_\alpha)'=\pm|\Gamma_\alpha,-\beta_\alpha)', \tag{14}$$

where θ is the time-reversal operator and where the $+$ and $-$ occur alternatively as β_α ran over the allowed values. For convenience in arriving at Kramer's pairs when the eigenfunctions are symmetrized to C_{3v}, the representations and bases were transformed as follows,

$$|\Gamma_\alpha,\beta_\alpha)=i^{|\beta\alpha|}|\Gamma_\alpha,\beta_\alpha)',\quad (J\text{ integer})$$
$$=i^{v_\alpha-|\beta\alpha|}|\Gamma_\alpha,\beta_\alpha)',\quad J\tfrac{1}{2}\text{-odd integer}), \tag{15}$$

where v_α is the dimension of Γ_α. This resulted in

$$\theta|\Gamma_\alpha,|\beta_\alpha|)=|\Gamma_\alpha,-|\beta_\alpha|), \tag{16}$$

and the bases then become

$$|\Gamma_\alpha,\beta_\alpha)=\sum_{J_z}f_{\beta\alpha,Jz}^{(\alpha)}|J,J_z\rangle. \tag{17}$$

It should be remarked here that the convention taken for a Kramer's pair is that of Elliott and Stevens[5]

$$\theta|J,J_z\rangle=(-1)^{J+J_z}|J,-J_z\rangle \tag{18}$$

rather than that of Wigner,[4] where the exponent of -1 in (18) is taken to be $J-J_z$. Wigner's form arises from the fact that the Pauli matrix S_y is defined as (see p. 158 of footnote 4)

$$S_y=\begin{pmatrix}0 & i\\ -i & 0\end{pmatrix}, \tag{19}$$

which is the complex conjugate of the matrix usually taken. Equation (19) has the effect that S_x+iS_y changes the spin-function for $S_z=+\frac{1}{2}$ into that for $S_z=-\frac{1}{2}$.

In Table I are given the matrices representing C in the representations Γ_α of the double group of P, according to which the $|\Gamma_\alpha,\beta_\alpha)$ transform, and in Tables II and III are tabulated the coefficients $f_{\beta\alpha,Jz}^{(\alpha)}$ which define the $|\Gamma_\alpha,\beta_\alpha)$, normalized to unity for

[4] E. P. Wigner, *Group Theory and Its Application to Quantum Mechanics* (Academic Press, Inc., New York, 1959), p. 164.

[5] R. J. Elliott and K. W. H. Stevens, Proc. Roy. Soc. (London) **A218**, 553 (1953).

TABLE I.

Γ_α	β_α	$C^{(\alpha)}$
Γ_2	-1 0 $+1$	$5^{-\frac{1}{2}}\begin{bmatrix} \beta & -\sqrt{2} & \alpha \\ -\sqrt{2} & 1 & -\sqrt{2} \\ \alpha & -\sqrt{2} & \beta \end{bmatrix}$
Γ_3	-2 0 $+2$	$5^{-\frac{1}{2}}\begin{bmatrix} -\alpha & \sqrt{2} & -\beta \\ \sqrt{2} & -1 & \sqrt{2} \\ -\beta & \sqrt{2} & -\alpha \end{bmatrix}$
Γ_4	-2 -1 $+1$ $+2$	$5^{-\frac{1}{2}}\begin{bmatrix} -1 & -\alpha & -\beta & -1 \\ -\alpha & 1 & 1 & -\beta \\ -\beta & 1 & 1 & -\alpha \\ -1 & -\beta & -\alpha & -1 \end{bmatrix}$
Γ_5	-2 -1 0 $+1$ $+2$	$(1/5)\begin{bmatrix} \beta^2 & -2\beta & 6^{\frac{1}{2}} & -2\alpha & \alpha^2 \\ -2\beta & \alpha^2 & -6^{\frac{1}{2}} & \beta^2 & -2\alpha \\ 6^{\frac{1}{2}} & -6^{\frac{1}{2}} & -1 & -6^{\frac{1}{2}} & 6^{\frac{1}{2}} \\ -2\alpha & \beta^2 & -6^{\frac{1}{2}} & \alpha^2 & -2\beta \\ \alpha^2 & -2\alpha & 6^{\frac{1}{2}} & -2\beta & \beta^2 \end{bmatrix}$
Γ_6	$-1/2$ $+1/2$	$(2-\alpha)^{-\frac{1}{2}}\begin{bmatrix} -i & \alpha \\ -\alpha & i \end{bmatrix}$
Γ_7	$-3/2$ $+3/2$	$(2-\alpha)^{-1}\begin{bmatrix} -i\alpha & -1 \\ 1 & i\alpha \end{bmatrix}$
Γ_8	$-3/2$ $-1/2$ $+1/2$ $+3/2$	$(2-\alpha)^{-3/2}\begin{bmatrix} i & -\sqrt{3}i\alpha & \sqrt{3}\alpha^2 & \alpha^3 \\ -\sqrt{3}i\alpha & -i\alpha^2 & 1 & \sqrt{3}\alpha^2 \\ -\sqrt{3}\alpha^2 & -1 & i\alpha^3 & \sqrt{3}i\alpha \\ -\alpha^3 & -\sqrt{3}\alpha^2 & \sqrt{3}i\alpha & -i \end{bmatrix}$
	$-5/2$ $-3/2$ $-1/2$ $+1/2$ $+3/2$ $+5/2$	$(2-\alpha)^{-5/2}\begin{bmatrix} -i & 5^{\frac{1}{2}}i\alpha & -(10)^{\frac{1}{2}}i\alpha^2 & (10)^{\frac{1}{2}}\alpha^3 & 5^{\frac{1}{2}}\alpha^4 & \alpha^5 \\ 5^{\frac{1}{2}}i\alpha & -5^{\frac{1}{2}}i\alpha^2 & -(10)^{\frac{1}{2}}i\alpha^3 & (10)^{\frac{1}{2}}\alpha^2 & 5^{\frac{1}{2}}\alpha^3 & 5^{\frac{1}{2}}\alpha^4 \\ -(10)^{\frac{1}{2}}i\alpha^2 & -(10)^{\frac{1}{2}}i\alpha^3 & 5^{\frac{1}{2}}i\alpha^2 & 5^{\frac{1}{2}}\alpha^3 & (10)^{\frac{1}{2}}\alpha^2 & (10)^{\frac{1}{2}}\alpha^3 \\ -(10)^{\frac{1}{2}}\alpha^3 & -(10)^{\frac{1}{2}}\alpha^2 & -5^{\frac{1}{2}}\alpha^3 & -5^{\frac{1}{2}}i\alpha^2 & (10)^{\frac{1}{2}}i\alpha^3 & (10)^{\frac{1}{2}}i\alpha^2 \\ -5^{\frac{1}{2}}\alpha^4 & -5^{\frac{1}{2}}\alpha^3 & -(10)^{\frac{1}{2}}\alpha^2 & (10)^{\frac{1}{2}}i\alpha^3 & 5^{\frac{1}{2}}i\alpha^3 & -5^{\frac{1}{2}}i\alpha \\ -\alpha^5 & -5^{\frac{1}{2}}\alpha^4 & -(10)^{\frac{1}{2}}\alpha^3 & (10)^{\frac{1}{2}}i\alpha^2 & -5^{\frac{1}{2}}i\alpha & i \end{bmatrix}$

TABLE II.

J	α	J_z / β_α	$NF_{\beta\alpha,Jz}^{(\alpha)}$ $\beta_\alpha-10$	$\beta_\alpha-5$	β_α	$\beta_\alpha+5$	N
1	2	0			i		1
		1			-1		1
2	5	0			1		1
		1			i		1
		2			-1		1
3	3	0			i		1
		2		$-\sqrt{2}$	$-\sqrt{3}i$		$5^{\frac{1}{2}}$
	4	1			1		1
		2		$\sqrt{3}$	$-\sqrt{2}i$		$5^{\frac{1}{2}}$
4	4	1		$-8^{\frac{1}{2}}i$	$-7^{\frac{1}{2}}$		$(15)^{\frac{1}{2}}$
		2		1	$-(14)^{\frac{1}{2}}i$		$(15)^{\frac{1}{2}}$
	5	0			1		1
		1		$-7^{\frac{1}{2}}$	$-8^{\frac{1}{2}}i$		$(15)^{\frac{1}{2}}$
		2		$(14)^{\frac{1}{2}}i$	-1		$(15)^{\frac{1}{2}}$
5	2	0		$7^{\frac{1}{2}}$	$6i$	$7^{\frac{1}{2}}$	$5\sqrt{2}$
		1		$-7^{\frac{1}{2}}i$	$\sqrt{3}$		$(10)^{\frac{1}{2}}$
	3	0		3	$-7^{\frac{1}{2}}i$	3	5
		2		$\sqrt{2}$	$-\sqrt{3}i$		$5^{\frac{1}{2}}$
	5	0		$-i$	0	i	$\sqrt{2}$
		1		$-\sqrt{3}$	$7^{\frac{1}{2}}i$		$(10)^{\frac{1}{2}}$
		2		$-\sqrt{3}i$	$\sqrt{2}$		$5^{\frac{1}{2}}$
6	1	0		$7^{\frac{1}{2}}i$	$-(11)^{\frac{1}{2}}$	$7^{\frac{1}{2}}i$	5
	2	0		1	0	-1	$\sqrt{2}$
		1		$(11)^{\frac{1}{2}}i$	$-(33)^{\frac{1}{2}}$	$6^{\frac{1}{2}}i$	$5\sqrt{2}$
	4	1		$6^{\frac{1}{2}}i$	$2\sqrt{2}$	$(11)^{\frac{1}{2}}i$	5
		2		2	$-i$		$5^{\frac{1}{2}}$
	5	0		$-(11)^{\frac{1}{2}}i$	$-2(7)^{\frac{1}{2}}$	$-(11)^{\frac{1}{2}}i$	$5\sqrt{2}$
		1		$3\sqrt{3}$	$-i$	$-(22)^{\frac{1}{2}}$	$5\sqrt{2}$
		2		i	-2		$5^{\frac{1}{2}}$
7	2	0		$2(6)^{\frac{1}{2}}$	$(77)^{\frac{1}{2}}i$	$2(6)^{\frac{1}{2}}$	$5(5)^{\frac{1}{2}}$
		1		$\sqrt{3}i$	$-2(11)^{\frac{1}{2}}$	$(78)^{\frac{1}{2}}i$	$5(5)^{\frac{1}{2}}$
	3	0		$-(77)^{\frac{1}{2}}$	$4(6)^{\frac{1}{2}}i$	$-(77)^{\frac{1}{2}}$	$5(10)^{\frac{1}{2}}$
		2		$7(7)^{\frac{1}{2}}$	$(14)^{\frac{1}{2}}i$	$-(143)^{\frac{1}{2}}$	$10(5)^{\frac{1}{2}}$
	4	1		$-(286)^{\frac{1}{2}}i$	$-(78)^{\frac{1}{2}}$	$-(11)^{\frac{1}{2}}i$	$5(15)^{\frac{1}{2}}$
		2		$2(26)^{\frac{1}{2}}$	$-3(13)^{\frac{1}{2}}i$	$(154)^{\frac{1}{2}}$	$5(15)^{\frac{1}{2}}$
	5	0		$-i$	0	$+i$	$\sqrt{2}$
		1		4	$(33)^{\frac{1}{2}}i$	$-(26)^{\frac{1}{2}}$	$5\sqrt{3}$
		2		$(11)^{\frac{1}{2}}i$	$-3(22)^{\frac{1}{2}}$	$(91)^{\frac{1}{2}}i$	$10\sqrt{3}$
8	3	0		1	0	-1	$\sqrt{2}$
		2	$-4(7)^{\frac{1}{2}}i$	$(39)^{\frac{1}{2}}$	$-(286)^{\frac{1}{2}}i$	$3(7)^{\frac{1}{2}}$	$10(5)^{\frac{1}{2}}$
	4	1		$(14)^{\frac{1}{2}}i$	$-(22)^{\frac{1}{2}}$	$-(39)^{\frac{1}{2}}i$	$5\sqrt{3}$
		2	$-2(26)^{\frac{1}{2}}i$	$2(42)^{\frac{1}{2}}$	$(77)^{\frac{1}{2}}i$	$-(26)^{\frac{1}{2}}$	$5(15)^{\frac{1}{2}}$
	5	0		$-2(77)^{\frac{1}{2}}i$	$-3(26)^{\frac{1}{2}}$	$-2(77)^{\frac{1}{2}}i$	$5(34)^{\frac{1}{2}}$
		1		$-(1001)^{\frac{1}{2}}$	$4(13)^{\frac{1}{2}}i$	$-(66)^{\frac{1}{2}}$	$5(51)^{\frac{1}{2}}$
		2	$-(3179)^{\frac{1}{2}}$	$(3003)^{\frac{1}{2}}i$	$(182)^{\frac{1}{2}}$	$(11)^{\frac{1}{2}}i$	$5(255)^{\frac{1}{2}}$
	5	0		$3(13)^{\frac{1}{2}}i$	$-2(154)^{\frac{1}{2}}$	$3(13)^{\frac{1}{2}}i$	$5(17)^{\frac{1}{2}}$
		1		$-2\sqrt{3}$	$-(23)^{\frac{1}{2}}i$	$-(182)^{\frac{1}{2}}$	$5(17)^{\frac{1}{2}}$
		2		$-i$	$(66)^{\frac{1}{2}}$	$-(273)^{\frac{1}{2}}i$	$2(85)^{\frac{1}{2}}$

positive values of β_α; for positive values of β_α

$$f_{-\beta\alpha,-J_z}{}^{(\alpha)} = (-1)^{J+J_z} f_{\beta\alpha,J_z}{}^{(\alpha)*}. \tag{20}$$

The matrices representing A and B are given by

$$a_{\beta\alpha,\beta\alpha'}{}^{(\alpha)} = \exp\,(2\pi i\beta_\alpha/5)\,\delta_{\beta\alpha,\beta\alpha'}$$

and

$$b_{\beta\alpha,\beta\alpha'}{}^{(\alpha)} = b^{(\alpha)}\delta_{\beta\alpha,-\beta\alpha'}, \tag{21}$$

where $b^{(\alpha)} = -1$ for Γ_2, Γ_3, Γ_4; $+1$ for Γ_5; $+i$ for Γ_6, Γ_7, Γ_9; $-i$ for Γ_8.[6]

[6] The author is grateful to the referee for bringing to his notice a paper entitled "The spherical harmonics with the symmetry of the icosahedral group" by N. V. Cohan, Proc. Cambridge Phil. Soc. **54**, 28 (1958). In this paper symmetrized spherical harmonics are obtained up to the 15th order. The coefficients of this paper when account is taken of phase convention and normalization should agree with those of Table II for the single valued representations of the icosahedral group.

TABLE III.

J	α	J_z / β_α	$N\mathcal{F}_{\beta_\alpha,J_z}^{(\alpha)}$ $\beta_\alpha-10$	$\beta_\alpha-5$	β_α	$\beta_\alpha+5$	N
1/2	6	1/2			i		1
3/2	8	1/2			-1		1
		3/2			i		1
5/2	9	1/2			$-i$		1
		3/2			-1		1
		5/2			i		1
7/2	7	3/2		$-\sqrt{3}i$	$-7^{\frac{1}{2}}$		$(10)^{\frac{1}{2}}$
	9	1/2			$-i$		1
		3/2		$-7^{\frac{1}{2}}i$	$\sqrt{3}$		$(10)^{\frac{1}{2}}$
		5/2		7	i		$5\sqrt{2}$
9/2	8	1/2		$-7^{\frac{1}{2}}i$	$3\sqrt{2}$		5
		3/2		$(21)^{\frac{1}{2}}$	$2i$		5
	9	1/2		$-3\sqrt{2}$	$7^{\frac{1}{2}}i$		5
		3/2		$-2i$	$-(21)^{\frac{1}{2}}$		5
		5/2		-2	$-i$		$5^{\frac{1}{2}}$
11/2	6	1/2		$(77)^{\frac{1}{2}}$	$(66)^{\frac{1}{2}}i$	$7^{\frac{1}{2}}$	$5(6)^{\frac{1}{2}}$
	8	1/2		$-4\sqrt{2}i$	$-(21)^{\frac{1}{2}}$	$(22)^{\frac{1}{2}}i$	$5\sqrt{3}$
		3/2		$-\sqrt{2}$	$-\sqrt{3}i$		$5^{\frac{1}{2}}$
	9	1/2		$-\sqrt{3}$	$(14)^{\frac{1}{2}}i$	$-(33)^{\frac{1}{2}}$	$5\sqrt{2}$
		3/2		$\sqrt{3}i$	$\sqrt{2}$		$5^{\frac{1}{2}}$
		5/2		3	$4i$		5
13/2	6	1/2		$\sqrt{2}$	$(11)^{\frac{1}{2}}i$	$2\sqrt{3}$	5
	7	3/2		$(26)^{\frac{1}{2}}i$	$(13)^{\frac{1}{2}}$	$(11)^{\frac{1}{2}}i$	$5\sqrt{2}$
	8	1/2		$7i$	$-(22)^{\frac{1}{2}}$	$-3(6)^{\frac{1}{2}}i$	$5(5)^{\frac{1}{2}}$
		3/2		$(11)^{\frac{1}{2}}$	$2(22)^{\frac{1}{2}}i$	$(26)^{\frac{1}{2}}$	$5(5)^{\frac{1}{2}}$
	9	1/2		$(66)^{\frac{1}{2}}$	$-4\sqrt{3}i$	$(11)^{\frac{1}{2}}$	$5(5)^{\frac{1}{2}}$
		3/2		$-7\sqrt{2}i$	3	$(143)^{\frac{1}{2}}$	$5(10)^{\frac{1}{2}}$
		5/2		-1	$-3i$		$(10)^{\frac{1}{2}}$
15/2	8	1/2		$3i$	$-(77)^{\frac{1}{2}}$	$(39)^{\frac{1}{2}}i$	$5(5)^{\frac{1}{2}}$
		3/2		1	$(33)^{\frac{1}{2}}i$	$(91)^{\frac{1}{2}}$	$5(5)^{\frac{1}{2}}$
	9	1/2		$4(273)^{\frac{1}{2}}$	$(429)^{\frac{1}{2}}i$	$-23(7)^{\frac{1}{2}}$	$10(85)^{\frac{1}{2}}$
		3/2		$-(91)^{\frac{1}{2}}i$	$(3003)^{\frac{1}{2}}$	$34i$	$5(170)^{\frac{1}{2}}$
		5/2	$-11\sqrt{3}i$	$-(1001)^{\frac{1}{2}}$	$-3(1001)^{\frac{1}{2}}i$	$-47\sqrt{3}$	$10(170)^{\frac{1}{2}}$
	9	1/2		$8(11)^{\frac{1}{2}}$	$-9(7)^{\frac{1}{2}}i$	$(429)^{\frac{1}{2}}$	$10(17)^{\frac{1}{2}}$
		3/2		$(33)^{\frac{1}{2}}i$	1		$(34)^{\frac{1}{2}}$
		5/2	$-7(1001)^{\frac{1}{2}}i$	$-99\sqrt{3}$	$43\sqrt{3}i$	$(1001)^{\frac{1}{2}}$	$50(34)^{\frac{1}{2}}$

4. SYMMETRIZATION WITH RESPECT TO P AND C_{3v}

The irreducible representations Γ_α of P are in general reducible with respect to C_{3v}, i.e.,

$$\Gamma_\alpha \rightarrow \sum_i \mu_i \gamma_i, \tag{22}$$

where the γ_i are the irreducible representations of C_{3v}. In order to obtain eigenfunctions symmetrized according to P and C_{3v} one must obtain those linear combinations of the $|\Gamma_\alpha, \beta_\alpha)$

$$|\Gamma_\alpha, \gamma_i, \beta_i) = \sum_{\beta\alpha} g_{\beta\alpha,\beta_i}^{(\alpha,i)} |\Gamma_\alpha, \beta_\alpha), \tag{23}$$

which transform irreducibly according to one of the γ_i of C_{3v} in (22). These functions are again obtained by applying the projection operators for the γ_i to the functions $|\Gamma_\alpha, \beta_\alpha)$. In this work, the representations γ_i are chosen so that the threefold rotations are represented by diagonal matrices. The two-dimensional representations γ_3 and γ are generated by

$$\begin{matrix} & C_3 & & \sigma_v & \\ \gamma_3: & \begin{pmatrix} e^{-2\pi i/3} & 0 \\ 0 & e^{2\pi i/3} \end{pmatrix} & & \begin{pmatrix} 0 & 1 \\ 1 & 0 \end{pmatrix} & \\ \gamma_6: & \begin{pmatrix} e^{-i\pi/3} & 0 \\ 0 & e^{i\pi/3} \end{pmatrix} & & \begin{pmatrix} 0 & i \\ i & 0 \end{pmatrix}, & \end{matrix} \tag{24}$$

where C_3 is the $2\pi/3$ rotation, and σ_v the reflection in a plane containing the axis of C_3. By reference to the icosahedral group, C_3 is taken to be the $2\pi/3$ rotation A^3CA^3 and σ_v to be ωB where ω is the parity. Thus the reflection plane of σ_v is the YOZ plane of the previously chosen co-ordinate system. The direction-cosines of the axis of C_3 are easily shown to be

$$\begin{aligned} m_x &= 0, \qquad m_y = \sin\phi = 2\alpha/\sqrt{3}(2-\alpha)^{\frac{1}{2}}, \\ m_z &= \cos\phi = (1+\alpha)/\sqrt{3}(2-\alpha)^{\frac{1}{2}}, \end{aligned} \tag{25}$$

TABLE IV.

α	i	ω	β_i	β_α	$N_{g_{\beta\alpha,\beta i}{}^{(\alpha,i)}}$	N
1	1	+1	0	0	1	1
2	1	−1	0	−1	$-\sqrt{2}$	$[3(2-\beta)]^{\frac{1}{2}}$
				0	$-\beta^2$	
				1	$-\sqrt{2}$	
	3	±1	+1	−1	$2\cos(2\pi/15)$	$[3(2-\alpha)]^{\frac{1}{2}}$
				0	$-\sqrt{2}\alpha$	
				1	$2\cos(8\pi/15)$	
3	1	−1	0	−2	$-\sqrt{2}$	$[3(2-\alpha)]^{\frac{1}{2}}$
				0	$-\alpha^2$	
				2	$-\sqrt{2}$	
	3	±1	+1	−2	$2\cos(\pi/15)$	$[3(2-\beta)]^{\frac{1}{2}}$
				0	$\sqrt{2}\beta$	
				2	$-2\cos(4\pi/15)$	
4	1	+1	0	−2	$-5^{\frac{1}{2}}$	$(30)^{\frac{1}{2}}\alpha$
				−1	$-(3\alpha-1)$	
				1	$(3\alpha-1)$	
				2	$5^{\frac{1}{2}}$	
	2	+1	0	−2	1	$[2(2-\beta)]^{\frac{1}{2}}$
				−1	β	
				1	β	
				2	1	
	3	±1	+1	−2	$1-2\cos(2\pi/15)$	$[3\{5-5^{\frac{1}{2}}\cos(\pi/15)\}]^{\frac{1}{2}}$
				−1	$5^{\frac{1}{2}}-2\cos(\pi/15)$	
				1	−1	
				2	$1-2\cos(4\pi/15)$	
5	1	+1	0	−2	α	$(15/2)^{\frac{1}{2}}$
				−1	$-\beta$	
				0	$(3/2)^{\frac{1}{2}}$	
				1	$-\beta$	
				2	α	
	3	±1	+1	−2	$-\cos(\pi/15)$	$(15)^{\frac{1}{2}}/2$
				−1	$-\cos(2\pi/15)$	
				0	$(3/2)^{\frac{1}{2}}$	
				1	$-\cos(8\pi/15)$	
				2	$\cos(4\pi/15)$	
	3	±1	+1	−2	$4\beta-3+12\cos(4\pi/15)-4\cos(2\pi/15)-2\cos(7\pi/15)$	$15/\sqrt{3}$
				−1	$4\alpha-3-12\cos(7\pi/15)-4\cos(4\pi/15)-2\cos(\pi/15)$	
				0	0	
				1	$4\alpha-3+12\cos(2\pi/15)+4\cos(\pi/15)+2\cos(4\pi/15)$	
				2	$4\beta-3-12\cos(\pi/15)+4\cos(7\pi/15)+2\cos(2\pi/15)$	

that is, it lies in the plane of the axes of A and C. The coefficients $g_{\beta\alpha,\beta i}{}^{(\alpha,i)}$ which define the functions $|\Gamma_\alpha, \gamma_i, \beta_i)$, where β_i is defined by

$$C_3|\Gamma_\alpha, \gamma_i, \beta_i) = \exp^{2\pi\beta_i\, i/3}|\Gamma_\alpha, \gamma, \beta_i) \qquad (26)$$

are tabulated in Tables IV and V. The reduction of the $\Gamma_\alpha(\alpha=1, 2, 3, \text{and } 5)$ depends on the parity, i.e., if γ_1 occurs for a certain parity, γ_2 will occur instead for the opposite parity. Where γ_3 and γ_6 occur twice in the reduction, two arbitrary orthogonal bases are given.

TABLE V.

α	i	ω	β	β_α	$N g_{\beta\alpha,\beta_\alpha}^{(\alpha,i)}$	N
6	6	±1	$+1/2$	$-1/2$	$-\alpha i$	$[\alpha^2+4\cos^2(7\pi/15)]^{\frac{1}{2}}$
				$1/2$	$2\cos(7\pi/15)$	
7	6	±1	$+1/2$	$-3/2$	i	$\frac{1}{2}[2[2+2\cos(7\pi/15)-\cos(\pi/15)]]^{\frac{1}{2}}$
				$3/2$	$1+2\cos(7\pi/15)$	
8	4	±1	0	$-3/2$	$(1+i\omega\alpha^2)\exp(-i\omega\phi/2)$	$[6(3-4\alpha)]^{\frac{1}{2}}$
				$-1/2$	$\sqrt{3}\alpha^2\exp(-i\omega\phi/2)$	
				$1/2$	$-\omega\sqrt{3}\alpha^2\exp(-i\omega\phi/2)$	
				$3/2$	$-\omega(1+i\omega\alpha^2)\exp(-i\omega\phi/2)$	
	6	±1	$+1/2$	$-3/2$	$-(\sqrt{3}/2)\alpha^2 i$	
				$-1/2$	$\sqrt{3}\alpha^2 i\sin(2\pi/15)$	
				$1/2$	$-\sqrt{3}\alpha\sin(\pi/15)$	
				$3/2$	$3\sin(\pi/5)-\sin(2\pi/5)-\sin(4\pi/15)$	
9	4	±1	0	$-5/2$	$5^{\frac{1}{2}}(1+i\alpha^2\omega)\exp(-i\omega\phi/2)$	$3(10)^{\frac{1}{2}}\alpha$
				$-3/2$	$(\beta+i\alpha^2\omega)(1+i\alpha^2\omega)\exp(-i\omega\phi/2)$	
				$-1/2$	$\sqrt{2}(\beta-i\omega)(1+i\alpha^2\omega)\exp(-i\omega\phi/2)$	
				$1/2$	$\sqrt{2}\omega(\beta-i\omega)(1+i\alpha^2\omega)\exp(-i\omega\phi/2)$	
				$3/2$	$\omega(\beta+i\alpha^2\omega)(1+i\alpha^2\omega)\exp(-i\omega\phi/2)$	
				$5/2$	$5^{\frac{1}{2}}\omega(1+i\alpha^2\omega)\exp(-i\omega\phi/2)$	
	6	±1	$+1/2$	$-5/2$	$-\sqrt{3}i\alpha^5$	
				$-3/2$	$2(5)^{\frac{1}{2}}i\alpha^4\sin(2\pi/15)$	
				$-1/2$	$2(10)^{\frac{1}{2}}i\alpha^3\sin(\pi/15)$	
				$1/2$	$2(10)^{\frac{1}{2}}\alpha^2\sin(4\pi/15)$	
				$3/2$	$2(5)^{\frac{1}{2}}\alpha\sin(7\pi/15)$	
				$5/2$	$\sqrt{3}+10\alpha^2\sin(\pi/15)$	
	6	±1	$+1/2$	$-5/2$	$[10\alpha^2\sin(\pi/5)-\sqrt{3}(1+a\alpha^5)]i$	
				$-3/2$	$-2(5)^{\frac{1}{2}}i\alpha(1-a\alpha^3)\sin(2\pi/15)$	
				$-1/2$	$2(10)^{\frac{1}{2}}i\alpha^2(1+a\alpha)\sin(\pi/15)$	
				$1/2$	$-2(10)^{\frac{1}{2}}\alpha^2(\alpha-a)\sin(4\pi/15)$	
				$3/2$	$+2(5)^{\frac{1}{2}}\alpha(a+\alpha^3)\sin(7\pi/15)$	
				$5/2$	0	

The following identities are easily proved and are used to reduce the size of the tables,

$$g_{\beta\alpha,+1}^{(\alpha,3)}=\omega b^{(\alpha)}g_{-\beta\alpha,-1}^{(\alpha,3)}$$

$$g_{\beta\alpha,0}^{(\alpha,1)} \text{ for parity } \omega = g_{\beta\alpha,0}^{(\alpha,2)} \text{ for parity } -\omega,$$

$$|\Gamma_\alpha, \gamma_5, 0) \text{ for parity } \omega = |\Gamma_\alpha, \gamma_4, 0) \text{ for parity } -\omega,$$

$$g_{\beta\alpha,+\frac{1}{2}}^{(\alpha,6)} = (\omega b^{(\alpha)}/i)g_{-\beta\alpha,-\frac{1}{2}}^{(\alpha,6)}. \qquad (27)$$

It will be observed from the Tables IV and V, using (16) and (27) that the bases of γ_3, γ_4, γ_5, and γ_6 are such that

$$\theta|\Gamma_\alpha, \gamma_3, +1) = \omega b^{(\alpha)}|\Gamma_\alpha, \gamma_3, -1)$$

$$\theta|\Gamma_\alpha, \gamma_5, 0) = \omega|\Gamma_\alpha, \gamma_4, 0)$$

$$\theta|\Gamma_\alpha, \gamma_6, +\tfrac{1}{2}) = (\omega b^{(\alpha)}/i)|\Gamma_\alpha, \gamma_6, -\tfrac{1}{2}). \qquad (28)$$

TABLE VI.

J	μ	ν	$g_{\parallel}/g$	$g_{\perp}/g$	$(\alpha;i)$
1			2		(2;3)
2			$2\lvert 1-3\sin^2\theta\rvert$		(5;3)
3			3.75		(4;3)
4			6.25		(4;3)
			$(8/3)\lvert 1-3\sin^2\theta\rvert$		(5;3)
5			5		(2;3)
			$\lvert 1-3\sin^2\theta\rvert$		(5;3)
6			1		(2;3)
			7.5		(4;3)
			$\lvert 1-3\sin^2\theta\rvert$		(5;3)
7			4		(2;3)
			10		(4;3)
			$(10/3)\lvert 1-3\sin^2\theta\rvert$		(5;3)
8			10		(4;3)
			...		(5;3)
1/2			1	2	(6;6)
3/2			1	2	(8;6)
			3	0	(8;4,5)
5/2	1	0	3	0	(9;4,5)
			$\lvert\cos\theta+2\sqrt{2}\sin\theta-2\rvert$	$(1/2)\lvert 3+\cos\theta+2\sqrt{2}\sin\theta\rvert$	(9;6)
7/2	0	1	3	0	(9;4,5)
			$(1/6)\lvert 9-\cos\theta-16\sqrt{2}\sin\theta\rvert$	$(1/6)\lvert 12+4\cos\theta+\sqrt{2}\sin\theta\rvert$	(9;6)
9/2	$-117/35$	$-20/7$	9/5	18/5	(8;6)
			27/5	0	(8;4,5)
			$(849)^{\frac{1}{2}}/5$	0	(9;4,5)
			$(1/15)\lvert 43\cos\theta-14\sqrt{2}\sin\theta-36\rvert$	$(1/30)\lvert 7\cos\theta-86\sqrt{2}\sin\theta+21\rvert$	(9;6)
11/2	25/7	24/7	11/3	22/3	(6;6)
			1/3	2/3	(8;6)
			1	0	(8;4,5)
			$(41)^{\frac{1}{2}}$	0	(9;4,5)
			$\lvert 2+2\sqrt{2}\sin\theta-3\cos\theta\rvert$	$(1/2)\lvert 3-6\sqrt{2}\sin\theta+\cos\theta\rvert$	(9;6)
13/2	$-44/35$	$-15/7$	5	10	(6;6)
			7/5	14/5	(8;6)
			21/5	0	(8;4,5)
			$(401)^{\frac{1}{2}}/5$	0	(9;4,5)
			$(1/10)\lvert 9\cos\theta-32\sqrt{2}\sin\theta+7\rvert$	$(1/10)\lvert 24+8\cos\theta-9\sqrt{2}\sin\theta\rvert$	(9;6)
15/2	...	...	17/5	34/5	(8;6)
			51/5	0	(8;4,5)
			...	0	(9;4,5)
			...	...	(9;6)

In Table V, the quantity a is defined as

$$a=\sqrt{3}\alpha^5/[\sqrt{3}+10\alpha^2\sin(\pi/5)]. \tag{29}$$

5. APPLICATIONS TO THE CALCULATION OF MAGNETIC SPLITTING FACTORS

For the case of the crystal field with the symmetry previously described, the energy levels become singlets or doublets, the doublets being designated by $(\Gamma_\alpha, \gamma_3)$ for integer J, $(\Gamma_\alpha, \gamma_4, \gamma_5)$, $(\Gamma_\alpha, \gamma_6)$ for $\frac{1}{2}$ odd integer J. These doublets may be split on the application of a magnetic field, the magnitude in general being dependent on the relative direction of he magnetic field. The splitting is determined by $g_{\parallel}$ and $g_{\perp}$, where the Zeeman splitting Δ is given by $g_{\parallel}\beta H$, for the field parallel to the threefold axis of symmetry, and $g_{\perp}\beta H$, for the field perpendicular to the threefold axis, β being the Bohr magneton. Using the notation of Elliott and Stevens,[5] the splitting factors are given by

$$g_{\parallel}=2\lvert\langle+\rvert L_z+2S_z\rvert+\rangle\rvert=2g\lvert\langle+\rvert J_z\rvert+\rangle\rvert$$
$$g_{\perp}=2\lvert\langle+\rvert L_x+2S_x\rvert-\rangle\rvert=2g\lvert\langle+\rvert J_x\rvert-\rangle\rvert, \tag{30}$$

if the states $\lvert+\rangle$ and $\lvert-\rangle$ describing the doublet are chosen so that L_z+2S_z is diagonal with respect to them. If the states are not so chosen, $g_{\parallel}$ and $g_{\perp}$ are twice the positive eigenvalues of the matrices of L_z+2S_z and

L_z+2S_z, respectively. For Russell-Saunders coupling g is the Landé splitting factor.

If $\Gamma_i\times\Gamma_2\times\Gamma_i$ contains the identity representation once, and this is the case for all Γ_i except Γ_3 and Γ_7, where the identity representation is not contained at all, and Γ_9 where it is contained twice, then the ratio $g_\perp/g_\parallel$ is the same for all the values of J for which the particular doublet state $(\Gamma_\alpha, \gamma_j)$ exists. Further, in this case, the ratio of the values of $g_\parallel$ (or $g_\perp$) is equal to the ratio of any two corresponding elements of $(J, \Gamma_\alpha|\mathbf{J}|J, \Gamma_\alpha)$, and the simplest element to take is $(J, \Gamma_\alpha, \beta_\alpha|J_z'|J, \Gamma_\alpha, \beta_\alpha)$, where J_z' is the component of $\mathbf{J}$ in the direction of the fivefold axis. Such matrix elements are easily calculated using Tables II and III. The splitting factors are calculated for the smallest J value where the doublet occurs, by elementary methods or by using Tables II–IV to calculate the matrix elements of

$$J_z=J_y'm_y+J_z'm_z$$
$$J_x=J_x', \tag{31}$$

where J_z', etc., refer to the coordinate system used previously with the fivefold axis as the z axis, and J_x, J_z refers to a coordinate system with the threefold axis as z axis and the same x axis as in the former system. It should be noted that for the γ_4, γ_5 doublets the states γ_4 and γ_5 do not generally yield a diagonal matrix for J_z. In Table V, these states have been given so that J_z is diagonal with respect to the two states $|\gamma_4\rangle \pm|\gamma_5\rangle$ for the smallest J values where the particular doublet occurs.

For (Γ_7, γ_i) doublets no first-order splitting occurs. For (Γ_9, γ_i) doublets, since the identity representation is contained twice in $\Gamma_9\times\Gamma_2\times\Gamma_9$, it may be shown[7] that for a given value of J

$$(J, \Gamma_9|\mathbf{J}|J, \Gamma_9)=\mu(\tfrac{5}{2}, \Gamma_9|\mathbf{J}|\tfrac{5}{2}, \Gamma_9)$$
$$+\nu(\tfrac{7}{2}, \Gamma_9|\mathbf{J}|\tfrac{7}{2}, \Gamma_9), \tag{32}$$

for corresponding matrix elements; μ and ν may be determined from Table III, by evaluating (32) for diagonal elements of J_z' with respect to the $|J, \Gamma_9, \beta_9\rangle$.

In the case of (Γ_5, γ_3) and (Γ_9, γ_6), γ_3 and γ_6 occur twice in Γ_5 and Γ_9, respectively. In these cases the splitting factors will depend on an angle parameter θ, which determines the correct mixture of the two independent bases for these representations of C_{3v}. In the final analysis θ will depend on the actual form of the crystal field.

In Table VI are tabulated $g_\parallel/g$, $g_\perp/g$ for the doublets (Γ_α, γ) as well as μ and ν of Eq. (32). $g_\perp$ for all γ_3 doublets is zero.

If spin-orbit interaction is taken into account and the $|J, J_z\rangle$ states are expressed in normalized form as

$$|J, J_z\rangle=\sum_{L,S}\rho_{JLS}|S, L, J, J_z\rangle, \tag{33}$$

then it is easily seen that for these states

$$g=\sum_{LS}g_{J,L,S}|\rho_{JLS}|^2, \tag{34}$$

where $g_{J,L,S}$ is the Landé splitting factor for the Russell-Saunders state J, L, S. Wybourne[8] has recently calculated the composition of the electronic states of Nd^{3+} and Er^{3+}, and from his data corrected Landé splitting factors may be easily calculated using (34). For example, for the ground state of Nd^{3+}, the g thus corrected is 1.008 times the Landé factor for the $^4I_{9/2}$ Russell-Saunders ground state. However, a much greater effect on g occurs in the excited states.

ACKNOWLEDGMENTS

The author is grateful to Dr. W. A. Runciman and Dr. B. G. Wybourne for many interesting discussions from one of which the topic of this work arose.

[7] B. R. Judd, Proc. Phys. Soc. (London) **A75**, 330 (1959).

[8] B. G. Wybourne (to be published).

Concentration Dependence of Polymer Chain Configurations in Solution

HIROMI YAMAKAWA

Department of Textile Chemistry, Kyoto University, Kyoto, Japan

(Received July 12, 1960)

On the basis of the theory of fluids and of the fashion prevailing in the statistical thermodynamics of dilute chain polymer solutions, the segment distribution functions are formally derived as a power series in concentration. The mean-square radius of gyration and end-to-end distance at finite concentrations are calculated by using the general equations derived and introducing the modified random flight model. Evaluation is carried out up to the linear term in concentration. The coefficients of the linear terms are obtained as a power series in the excluded volume parameter, and also appropriate closed forms for those are proposed, which might be properly applied to good solvent systems. The results show that the polymer chain dimension decreases with increasing concentration. Then the concentration-dependent term in the intramolecular intensity function in light scattering is evaluated. It is pointed out that the separation of this term and the intermolecular correlation leads to the possibility of estimation of the polymer chain dimension at finite concentrations by light-scattering measurements. Finally, the Huggins constant k' in the viscosity-concentration relation is phenomenologically calculated. The concentration dependence of polymer chain dimensions proves to explain satisfactorily the effect of solvent power on the k' constant.

I. INTRODUCTION

SOME years ago, Flory[1] deduced from a statistical consideration of the excluded volume effect of polymer chain that if a solvent is polymeric in athermal polymer solutions, the linear-expansion factor of polymer chain approaches unity; in other words, a polymer molecule situated in a medium consisting of other polymer molecules of the same kind, or in a medium of unlike polymer molecules with which it mixes athermally, will behave just like an unperturbed ideal chain. We may suggest from Flory's deduction that the polymer chain dimension decreases with increasing concentration, and understand that such a behavior of polymer chain is obviously due to the mutual cancellation of intramolecular and intermolecular volume effects.

Recently, in the paper of Kawai and his co-workers,[2] Krigbaum has derived, by the lattice model treatment, a theoretical expression for the linear expansion factor of polymer chain such that it decreases rapidly with increasing concentration. This result has been employed by Kawai *et al.*[2] to explain an anomalous viscosity behavior; that is, an upswing of the viscosity at very low concentrations.[3] In the present view, however, it seems unlikely that the anomalous viscosity behavior arises from a sudden change of the dimension or tangling of polymer coils with concentration.[4] Indeed, the theoretical treatment of the viscosity by Kawai[2] is very ambiguous, and moreover we are apprehensive that the concentration dependence of polymer chain dimension itself might have been overestimated in the Krigbaum theory.[2] Thus, the primary object of this paper is to derive an expression for the polymer chain dimension at finite concentrations from a more rigorous statistical-mechanical standpoint, and then to deal with the related solution properties.

As in the previous treatment of dilute polymer solutions[5–8] the method of gas theory seems to be more direct and convenient than the lattice model for the present purpose, which reduces to the evaluation of the distribution function for segments of the same molecule at finite concentrations. Now it is known that according to DeBoer[9,10] and Mayer and Montroll[11] the molecular or radial distribution functions for gases may be written as a power series in the density, the coefficients being expressed in terms of modified cluster integrals at zero density. Mayer and McMillan[12,13] also have proposed another method of expanding the difference between the potentials of average force, related to the molecular distribution functions, at different activities in powers of the activity difference, where the coefficients are again functions of the reference activity. Thus, by analogy with the case of gases or fluids, in Sec. II we derive expressions for the molecular and segment distribution functions as a series expansion in the concentration of solute polymers, in which the coefficients can be calculated from a knowledge of the potentials of average force at zero concentration. The similar treatment of the two-body distribution function has been made first by Zimm[14] and recently by Flory and Bueche[15] for the evaluation of the square term in con-

[1] P. J. Flory, J. Chem. Phys. **17**, 303 (1949).
[2] T. Kawai and K. Saito, J. Polymer Sci. **26**, 213 (1957) (with an Appendix by W. R. Krigbaum).
[3] Many references on the anomalous viscosity behavior have been cited in Kawai's paper[2] and will not be recounted here.
[4] S. Claesson, Makromol. Chem. **35**, 75 (1960).
[5] H. Yamakawa and M. Kurata, J. Phys. Soc. Japan **13**, 78 (1958).
[6] H. Yamakawa, J. Phys. Soc. Japan **13**, 87 (1958).
[7] M. Kurata, H. Yamakawa, and E. Teramoto, J. Chem. Phys. **28**, 785 (1958).
[8] M. Kurata and H. Yamakawa, J. Chem. Phys. **29**, 311 (1958).
[9] J. DeBoer and A. Michels, Physica **6**, 97 (1939).
[10] J. DeBoer, Repts. Progr. Phys. **12**, 305 (1949).
[11] J. E. Mayer and E. Montroll, J. Chem. Phys. **9**, 2 (1941). See also T. L. Hill, *Statistical Mechanics* (McGraw-Hill Book Company, Inc., New York, 1956), Chap. 6.
[12] J. E. Mayer, J. Chem. Phys. **10**, 629 (1942).
[13] W. G. McMillan and J. E. Mayer, J. Chem. Phys. **13**, 276 (1945).
[14] B. H. Zimm, J. Chem. Phys. **16**, 1093 (1948).
[15] P. J. Flory and A. M. Bueche, J. Polymer Sci. **27**, 219 (1958).

centration in the equation of the reciprocal intensity of light scattering from polymer solutions. In Sec. III, following the general development we calculate the mean square radius of gyration and the mean square end-to-end distance of polymer chain at finite concentrations, and discuss their initial dependence on the concentration in detail.

It is obvious that the concentration dependence of polymer chain dimensions has influence to some extent on the solution properties such as the light scattering and viscosity. In Sec. IV we examine this effect on the intramolecular intensity function. Albrecht[16] and Flory and Bueche[15] have recently evaluated the intermolecular correlation in light scattering; that is, the angular dependence of the second virial term. These two effects, intramolecular and intermolecular correlations, are superimposed on the second term. Therefore, the separation of them would enable us to estimate the polymer chain dimension at finite concentrations, though up to the linear term in concentration, by light scattering measurements. This problem also will be considered. In Sec. V we deal with the Huggins constant k'[17] in the viscosity-concentration equation. It is well known that the k' constant is not only correlated to the intermolecular hydrodynamic interaction,[18] but also affected by many other complicated, probably thermodynamic, factors as discussed by Eirich, Cragg, and others.[19,20] Evidently one of them is the intermolecular thermodynamic interaction, that is, the concentration dependence of polymer chain dimensions mentioned above. Thus, in part with the aim of reexamining whether the anomalous viscosity behavior originates from this effect or not, we calculate the k' constant taking into account thermodynamic as well as hydrodynamic interactions phenomenologically.

Although all the coefficients of the linear terms in concentration are first derived as a series expansion in the excluded volume parameter as in the previous treatment,[5-8] we attempt to write them in appropriate closed forms.

II. MOLECULAR AND SEGMENT DISTRIBUTION FUNCTIONS AT FINITE CONCENTRATIONS

Suppose a solution of volume V and concentration c in grams per unit volume, in which identical linear chain polymers, each composed of $N+1$ segments, are dispersed in a continuous medium and the $N+1$ segments of the sth polymer molecule are attached numbers $0_s, 1_s, \cdots, N_s$ from one end to the other. For simplicity, we denote the total, external and internal, coordinates of n polymer molecules by $(1, 2, \cdots, n)$, and the differential volume element, by $d(1, 2, \cdots, n)$.

Now we begin by introducing the molecular distribution functions $F_n(c, 1, 2, \cdots, n)$ defined by the statement that in an infinite system of concentration c,

$$V^{-n}F_n(c, 1, 2, \cdots, n)d(1, 2, \cdots, n)$$

is the probability of observing a set of n polymer molecules $1, 2, \cdots, n$ in the configuration element $d(1, 2, \cdots, n)$ at the coordinates $(1, 2, \cdots, n)$ irrespective of the coordinates of the remaining molecules. These distribution functions are normalized (strictly for $V\to\infty$) as

$$V^{-n}\int F_n(c, 1, 2, \cdots, n)d(1, 2, \cdots, n)=1, \qquad (1)$$

and related to the potentials $W_n(c, 1, 2, \cdots, n)$ of average force exerted on the n molecules by the equation

$$F_n(c, 1, 2, \cdots, n)=\exp[-W_n(c, 1, 2, \cdots, n)/kT], \qquad (2)$$

where k is the Boltzmann constant and T the absolute temperature.

We consider the problem of expanding the function $F_1(c, 1)$ in powers of c and expressing the coefficients in terms of the functions $F_n(c, 1, 2, \cdots, n)$ at $c=0$. For simplicity, $F_n(c, 1, 2, \cdots, n)$ and $W_n(c, 1, 2, \cdots, n)$ at $c=0$ are abbreviated to $F_n(1, 2, \cdots, n)$ and $W_n(1, 2, \cdots, n)$, respectively, hereafter. According to the method of the grand-canonical ensemble developed by Mayer and McMillan,[12,13] the difference between the potentials of average force at different activities $x+y$ and x may be expressed as a power series in the activity difference y, the coefficients being functions of the original activity x. Choosing the infinitely dilute solution as the reference state specified by x and changing the variables from y to c, we can immediately obtain[21]

$$W_1(c, 1)-W_1(1)=-kT\sum_l h_{1,l}(1)(N_0c/M)^l + kT\sum_l lB_l(N_0c/M)^{l-1}. \qquad (3)$$

Here N_0 is Avogadro's number and M is the polymer molecular weight. The function $h_{1,l}(1)$ is defined as

$$b_{1,m}(1)=mb_mh_{1,1}(1)+\sum_{l\geq 2}^{m}h_{1,l}(1)(\partial b_m/\partial B_l), \qquad (4)$$

where b_m and $b_{1,m}(1)$, generally $b_{n,m}(1, 2, \cdots, n)$, are the cluster integrals of the first and second kinds, and B_n is the irreducible integral.[22] These integrals in Eq. (4) involve integrals over the coordinates of the solute polymers and the integrands are functionals of the distribution functions at zero concentration.

[16] A. C. Albrecht, J. Chem. Phys. **27**, 1014 (1957).
[17] M. L. Huggins, J. Am. Chem. Soc. **64**, 2716 (1942).
[18] See, for example, J. Riseman and R. Ullman, J. Chem. Phys. **19**, 578 (1951).
[19] F. Eirich and J. Riseman, J. Polymer Sci. **4**, 417 (1949).
[20] L. H. Cragg and C. C. Bigelow, J. Polymer Sci. **16**, 177 (1955).
[21] See Eqs. (43), (56), and (59) of the work cited in footnote 12 and also Eqs. (58) and (72) of the work cited in footnote 13.
[22] For the definitions of these integrals see the works cited in footnotes 12 and 13.

From Eqs. (2) and (3), we obtain

$$F_1(c,1) = F_1(1)\exp\{\sum_{l\geq 1}[h_{1,l}(1)-(l+1)B_{l+1}](N_0c/M)^l\}, \quad (5)$$

which is expanded as follows,

$$F_1(c,1) = F_1(1)[1+F_{11}(1)c+F_{12}(1)c^2+\cdots], \quad (6)$$

with

$$F_{1n}(1) = \sum_{m_l}{}_{(\Sigma lm_l=n)}\prod_l[H_{1,l}(1)\cdot(N_0/M)^l]^{m_l}/m_l! \quad (7)$$

$$H_{1,l}(1) = h_{1,l}(1)-(l+1)B_{l+1}. \quad (8)$$

On the other hand, the osmotic pressure π may be expanded in the form,

$$\pi/RT = c/M+A_2c^2+A_3c^3+\cdots. \quad (9)$$

The relation between A_n, the nth virial coefficient, and B_n reads

$$A_n = -(n-1)N_0^{n-1}B_n/M^n. \quad (10)$$

Therefore, from the definitions[12,13] of the cluster and irreducible integrals and from Eqs. (4), (7), (8), and (10), we obtain for the first few $F_{1n}(1)$

$$F_{11}(1) = \frac{N_0}{MF_1(1)}\int g_2(1,2)d(2)+2A_2M, \quad (11)$$

$$F_{12}(1) = \frac{N_0^2}{2M^2F_1(1)}\int g_3(1,2,3)d(2,3) + \frac{4N_0A_2}{F_1(1)}\int g_2(1,2)d(2)+2(A_2M)^2+\tfrac{3}{2}A_3M, \quad (12)$$

where

$$A_2 = -\frac{N_0}{2VM^2}\int g_2(1,2)d(1,2), \quad (13)$$

$$A_3 = -\frac{N_0}{3VM^3}\int g_3(1,2,3)d(1,2,3)+4A_2^2M, \quad (14)$$

$$g_2(1,2) = F_2(1,2)-F_1(1)F_1(2), \quad (15)$$

$$g_3(1,2,3) = F_3(1,2,3)-F_2(2,3)F_1(1)-F_2(1,3)F_1(2) - F_2(1,2)F_1(3)+2F_1(1)F_1(2)F_1(3). \quad (16)$$

It is easy to see that Eq. (6) with (11) and (12) satisfies the normalization condition (1). In fact, the second term on the right-hand side of Eq. (3) is independent of the coordinates of the solute molecule and thus serves to normalize the function $F_1(c,1)$.

Next we consider the distribution function $P(c,\mathbf{R}_{ij})$ of the vector distance $\mathbf{R}_{ij}$ between segments i and j of molecule 1 at concentration c. It is possible to write in terms of the molecular distribution function given above

$$P(c,\mathbf{R}_{ij}) = V^{-1}\int F_1(c,1)d(1)/d\mathbf{R}_{ij}, \quad (17)$$

where the symbol $d(1)/d\mathbf{R}_{ij}$ indicates that the integration extends over all coordinates of molecule 1 at constant $\mathbf{R}_{ij}$. By using Eq. (6) in Eq. (17), $P(c,\mathbf{R}_{ij})$ may be written as

$$P(c,\mathbf{R}_{ij}) = P(\mathbf{R}_{ij})+P_1(\mathbf{R}_{ij})c+P_2(\mathbf{R}_{ij})c^2+\cdots, \quad (18)$$

with

$$P(\mathbf{R}_{ij}) = v^{-1}\int F_1(1)d(1)/d\mathbf{R}_{ij},$$

$$P_n(\mathbf{R}_{ij}) = v^{-1}\int F_1(1)F_{1n}(1)d(1)/d\mathbf{R}_{ij}. \quad (19)$$

In the case of $i=0$ and $j=N$, Eq. (18) with (19) gives the distribution of the end-to-end vector $\mathbf{R}$ at concentration c. In this paper, consideration is limited to terms linear in c, the coefficient of which is given, from Eqs. (11) and (19), by

$$P_1(\mathbf{R}_{ij}) = (N_0/VM)\int g_2(1,2)d(1,2)/d\mathbf{R}_{ij} + 2A_2MP(\mathbf{R}_{ij}). \quad (20)$$

Before proceeding further, some remarks are to be given concerning the nature of the distribution functions thus far obtained. The distribution functions given by Eqs. (6) and (18) are strictly true only in the case for which the activity of the solvent is kept constant in going from zero concentration to concentration c, that is, the osmotic condition holds. It may be understood that Eqs. (6) and (18) give the distribution functions at the standard atmospheric pressure plus the osmotic pressure. Therefore, under the ordinary condition of constant pressure the pressure correction must be made for these equations by amount of the osmotic pressure. However, this correction may generally be neglected for polymers of high molecular weight, as is discussed in the next section. Thus we start at Eq. (18) with (20).

Now the problem is to evaluate $P_1(\mathbf{R}_{ij})$, which can be performed by the procedure analogous to that of evaluating the second virial coefficient.[6,8] Equation (18) with (20) involves no approximations except the pressure correction mentioned above. For further development pairwise additivity of the potential $W(\mathbf{R}_{kl})$ of average force between the segments is assumed, and moreover the potential $W(\mathbf{R}_{kl})$ is assumed to be of such a short-range nature that it vanishes except in the region of sufficiently small $\mathbf{R}_{kl}$. Although an explicit functional form for $W(\mathbf{R}_{kl})$ has been adopted in the previous treatment,[5-8] any such function can be used

provided its short-range nature is preserved.[23] Following the procedure of Fixman[24] and Albrecht,[25] we may therefore write $g_2(1, 2)$ as

$$g_2(1,2)=F_1(1)F_1(2)\{\prod_{k_1,k_2}[1-\beta\delta(\mathbf{R}_{k_1k_2})]-1\}, \quad (21)$$

where $\delta(\mathbf{R})$ is a three-dimensional Dirac delta function and β is a binary cluster integral defined by

$$\beta=\int\{1-\exp[-W(\mathbf{R})/kT]\}d\mathbf{R}. \quad (22)$$

Equation (21) leads to a power series in β, the terms of which correspond to intermolecular contacts. Similarly $F_1(1)$ and $F_1(2)$ take forms of an expansion whose terms represent intramolecular contacts. It is known that intramolecular contacts are affected by intermolecular contacts; or in other words, the linear expansion factor of each of two molecules in contact is somewhat different from that of isolated molecule.[5,26] In this paper, for the sake of mathematical simplicity, however we treat the intramolecular contacts and hence intramolecular volume effect implicitly by introducing a random-flight model which has an effective step length modified by the linear-expansion factor at zero concentration. This point will be discussed in Sec. VI. Then the integral in Eq. (20) may be written in the form

$$\begin{aligned}(N_0/VM)\int g_2(1,2)d(1,2)/d\mathbf{R}_{ij}&=-(N_0\beta/M)[\sum_{k_1,k_2}P_0(\mathbf{R}_{ij})_{k_1k_2}\\&-\beta\sum_{k_1,k_2}\sum_{l_1,l_2}P_1(0_{l_1l_2},\mathbf{R}_{ij})_{k_1k_2}\\&+\beta^2\sum_{k_1,k_2}\sum_{l_1,l_2}\sum_{m_1,m_2}P_2(0_{l_1l_2},0_{m_1m_2},\mathbf{R}_{ij})_{k_1k_2}-\cdots],\end{aligned} \quad (23)$$

where

$$P_{s-1}(0_{l_1l_2},0_{m_1m_2},\cdots,\mathbf{R}_{ij})_{k_1k_2}=V^{-1}\int F_1(1)F_1(2)\prod_{s\text{ pairs}}\delta(\mathbf{R}_{k_1k_2})d(1,2)/d\mathbf{R}_{ij}, \quad (24)$$

which represents a conditional probability that, when an initial contact between segments k_1 and k_2 exists, there also exist $(s-1)$ additional contacts between segments l_1 and l_2, m_1 and m_2, $\cdots$, and so on, while segments i and j of molecule 1 are separated by the vector distance $\mathbf{R}_{ij}$.

On the other hand, using the present notations and taking the development equivalent to Eq. (23), we may write the second virial coefficient as

$$\begin{aligned}A_2=(N_0N^2\beta/2M^2)[1-\beta N^{-2}&\sum_{k_1,k_2}\sum_{l_1,l_2}P_1(0_{l_1l_2})_{k_1k_2}\\&+\beta^2N^{-2}\sum_{k_1,k_2}\sum_{l_1,l_2}\sum_{m_1,m_2}P_2(0_{l_1l_2},0_{m_1m_2})_{k_1k_2}-\cdots],\end{aligned} \quad (25)$$

where

$$P_{s-1}(0_{l_1l_2},0_{m_1m_2},\cdots)_{k_1k_2}=\int P_{s-1}(0_{l_1l_2},0_{m_1m_2},\cdots,\mathbf{R}_{ij})_{k_1k_2}d\mathbf{R}_{ij}. \quad (26)$$

Combining Eq. (23) with (25) and noting that

$$P_0(\mathbf{R}_{ij})_{k_1k_2}=P(\mathbf{R}_{ij}), \quad (27)$$

we obtain for $P_1(\mathbf{R}_{ij})$

$$\begin{aligned}P_1(\mathbf{R}_{ij})&=(N_0M\beta/M_0^2)\\&\times\{\beta N^{-2}\sum_{k_1,k_2}\sum_{l_1,l_2}[P_1(0_{l_1l_2},\mathbf{R}_{ij})_{k_1k_2}-P_1(0_{l_1l_2})_{k_1k_2}P(\mathbf{R}_{ij})]\\&-\beta^2N^{-2}\sum_{k_1,k_2}\sum_{l_1,l_2}\sum_{m_1,m_2}[P_2(0_{l_1l_2},0_{m_1m_2},\mathbf{R}_{ij})_{k_1k_2}\\&-P_2(0_{l_1l_2},0_{m_1m_2})_{k_1k_2}P(\mathbf{R}_{ij})]+\cdots\},\end{aligned} \quad (28)$$

where M_0 is the molecular weight of a segment. The single contact term vanishes in $P_1(\mathbf{R}_{ij})$, and hence the distribution function $P(c, \mathbf{R}_{ij})$ to the single contact approximation is independent of concentration through the linear term in c.

The problem which remains is to evaluate the conditional probabilities and the indicated multiple summations in Eq. (28). To do this, we put

$$P(\mathbf{R}_{ij})=[3/2\pi(j-i)a^2\alpha_0^2]^{\frac{3}{2}}\times\exp[-3\mathbf{R}_{ij}^2/2(j-i)a^2\alpha_0^2] \quad (29)$$

to the present model already mentioned, where a is a link length of the segments and α_0 is the linear expansion factor at zero concentration. The evaluation of the conditional probabilities can be carried out by the well-established method,[6,24,27,28] and the results are not given here. In addition, each cluster diagram representing the intermolecular contacts in $P_1(\mathbf{R}_{ij})$ is of the same type as each appearing in the second virial coefficient.[29] Now we need not obtain the final expression for $P(c, \mathbf{R}_{ij})$, but its second moment $\langle R_{ij}^2\rangle$ given by

$$\langle R_{ij}^2\rangle=\int\mathbf{R}_{ij}^2P(c,\mathbf{R}_{ij})d\mathbf{R}_{ij}. \quad (30)$$

Hence, after performing the above integration, we evaluate the indicated multiple summations.

[23] W. H. Stockmayer, Makromol. Chem. **35**, 54 (1960).
[24] M. Fixman, J. Chem. Phys. **23**, 1656 (1955).
[25] A. C. Albrecht, J. Chem. Phys. **27**, 1002 (1957).
[26] E. F. Casassa, J. Chem. Phys. **31**, 800 (1959).
[27] S. Chandrasekhar, Revs. Modern Phys. **15**, 1 (1943).
[28] Ming Chen Wang and G. E. Uhlenbeck, Revs. Modern Phys. **17**, 323 (1945).
[29] See Fig. 1 of the work cited in footnote 8.

III. POLYMER CHAIN DIMENSIONS AT FINITE CONCENTRATIONS

Radius of Gyration

First we derive the mean square distance $\langle R_{ij}^2\rangle$ between segments i and j, from Eqs. (18), (28), (29), and (30), as follows,

$$\langle R_{ij}^2\rangle=(j-i)a^2\alpha_{0,ij}^2(1-2J_1c+\cdots), \tag{31}$$

where[30]

$$\alpha_{0,ij}^2=1+\tfrac{4}{3}z\{(8/3)\mu^{\frac{1}{2}}-4(\lambda+\mu)^{\frac{1}{2}}-4(\mu+\nu)^{\frac{1}{2}}+\mu$$
$$-(8/3)\mu^{-1}[\lambda^{\frac{3}{2}}+\nu^{\frac{3}{2}}-(\lambda+\mu)^{\frac{3}{2}}-(\mu+\nu)^{\frac{3}{2}}]\}-\cdots \tag{32}$$

with

$$z=\beta(3/2\pi a^2)^{\frac{3}{2}}(M/M_0)^{\frac{1}{2}}, \tag{33}$$

$$\lambda=i/N, \qquad \mu=(j-i)/N, \qquad \nu=(N-j)/N. \tag{34}$$

The coefficient J_1 also involves a power series in z, the coefficients of which are the sums of functions of the relative positions of segments i, j, l_1, l_2, etc. over these indices except i and j and hence become functions of i and j. On replacing the summations by integrations, this reads, to the double contact approximation,

$$J_1=(N_0M\beta/M_0^2)[(\sum_{s=1}^{4}\gamma_s)(z/\alpha_{0,ij}^2)+0(z^2/\alpha_{0,ij}^6)], \tag{35}$$

with

$$\gamma_1=\mu^{-1}\int_0^1\int_0^\mu(1-S)(\mu-x_2)x_2^2(S+x_2)^{-5/2}dSdx_2, \tag{36}$$

$$\gamma_2=\mu^{-1}\int_0^1\int_0^\lambda\int_0^\mu(1-S)x_2^2(S+x_1+x_2)^{-5/2}dSdx_1dx_2, \tag{37}$$

$$\gamma_3=\mu^{-1}\int_0^1\int_0^\mu\int_0^\nu(1-S)x_2^2(S+x_2+x_3)^{-5/2}dSdx_2dx_3, \tag{38}$$

$$\gamma_4=\mu\int_0^1\int_0^\lambda\int_0^\nu(1-S)(S+x_1+x_3+\mu)^{-5/2}dSdx_1dx_3. \tag{39}$$

The integrals γ_1 to γ_4 correspond to the $B_{21}(f)$, $B_{21}(e)$, $B_{21}(d)$, and $B_{21}(b)$ types of contact in Fig. 1 of the work cited in footnote 8, respectively, where the segments in intramolecular contact may be thought of as segments i and j in this case. As λ, μ, and ν, the variables x_1, x_2, and x_3 represent the number fractions of segments separating the first and second, second and third, and third and fourth segments among four segments i, j, l_1, and m_1 in each type, respectively, and S represents that separating segments l_2 and m_2. These integrals can be evaluated straightforwardly, but the result is not given here because of its tedious length.

[30] See Eq. (C.4) of the work cited in footnote 7.

Now the mean square radius of gyration $\langle S^2\rangle$ can be calculated by the well-known formula

$$\langle S^2\rangle=N^{-2}\sum_{i<j}\langle R_{ij}^2\rangle. \tag{40}$$

Using Eqs. (31) to (39) in Eq. (40) and again replacing summations by integrations, we obtain

$$\langle S^2\rangle=\tfrac{1}{6}Na^2\alpha_{0,S}^2(1-2K_1c+\cdots), \tag{41}$$

where[31]

$$\alpha_{0,S}^2=1+(134/105)z-\cdots, \tag{42}$$

$$K_1=(N_0M\beta/M_0^2)\Big[6(z/\alpha_{0,S}^3)\int_0^1\int_0^{j/N}\mu$$
$$\times\sum_{s=1}^{4}\gamma_s d(j/N)d(i/N)+0(z^2/\alpha_{0,S}^6)\Big]$$
$$=(N_0M\beta/M_0^2)[0.1025(z/\alpha_{0,S}^3)+\cdots]. \tag{43}$$

End-to-End Distance

Putting $i=0$ and $j=N$ in Eq. (31), we can immediately obtain the mean square end-to-end distance $\langle R^2\rangle$, but in this case we evaluate the coefficient of the linear term in c to the triple contact approximation. The result reads

$$\langle R^2\rangle=Na^2\alpha_0^2(1-2I_1c+\cdots), \tag{44}$$

where

$$\alpha_0^2=1+\tfrac{4}{3}z-\cdots, \tag{45}$$

$$I_1=(N_0M\beta/M_0^2)[\sigma_1(z/\alpha_0^3)-(\sigma_{21}+2\sigma_{22})(z/\alpha_0^3)^2+\cdots], \tag{46}$$

with

$$\sigma_1=\int_0^1\int_0^1(1-L)(1-S)L^2(L+S)^{-5/2}dLdS, \tag{47}$$

$$\sigma_{21}=\int_0^1\int_0^1\int_0^L\int_0^S(1-L)(1-S)$$
$$\times[(L^2-Lx_1+Sx_1)x_1+L(L-2x_1)y_1]$$
$$\times[(L+S-x_1-y_1)(x_1+y_1)]^{-5/2}dLdSdx_1dy_1, \tag{48}$$

$$\sigma_{22}=\int_0^1\int_0^1\int_0^L\int_0^S(1-L)(1-S)$$
$$\times[(L^2-Lx_1+Sx_1)x_1+(L^2-x_1^2)y_1]$$
$$\times[(L+S-x_1-y_1)(x_1+y_1)+x_1y_1]^{-5/2}dLdSdx_1dy_1. \tag{49}$$

The integrals σ_1, σ_{21}, and σ_{22} correspond to the B_{20}, $B_{30}(a)$, and $B_{30}(b)$ types of contact in Fig. 1 of the

[31] The numerical coefficient of $(z/\alpha_{0,s}^3)$ in Eq. (43) is correctly $(4/3465)(1028\times2^3-1365)$.

work cited in footnote 8. The variables x_i (for molecule 1) and y_i (for molecule 2) have the same meaning as in the integrals γ_1 to γ_4 except that segments i and j are not concerned in the present case, and the sums $(x_1+x_2+\cdots)$ and $(y_1+y_2+\cdots)$ are replaced by L and S, respectively, in each group.[25] The numerical values for these integrals are obtained as follows,

$$\sigma_1=(8/315)(76\times 2^{\frac{1}{2}}-103)=0.1138,$$
$$\sigma_{21}=(1/27)(224-69\pi)=0.2678,$$
$$\sigma_{22}=0.202, \tag{50}$$

where σ_{22} was evaluated graphically after the reduction to a single integral. Hence, I_1 leads to

$$I_1=(N_0M\beta/M_0^2)[0.1138(z/\alpha_0^3)-0.672(z/\alpha_0^3)^2+\cdots]. \tag{51}$$

Discussion

Since the equations derived here are given as a form of a double-power series in z and c, their applicability, of course, will be limited to the very narrow region of the vicinity of the Θ temperature and of low concentrations. However, it is possible to get some information about the general behavior of polymer chains at finite concentrations from these equations. As is easily seen from Eqs. (43) and (51), the coefficients K_1 and I_1 become zero at the Θ temperature at which β vanishes, and take the positive values at the other temperatures provided z is small. Hence Eqs. (41) and (44) predict that the polymer chain dimension is independent of concentration at $T=\Theta$ as expected from Eqs. (20) and (21), whereas it decreases with increasing concentration at $T\neq\Theta$ provided z is small. We may expect from this fact that the linear expansion factor α as a function of c approaches unity with c and the chain tends to behave asymptotically as an unperturbed chain. It is obvious that this is due to the mutual cancellation of intramolecular and intermolecular volume effects. Furthermore, by a comparison of Eq. (43) with (51), I_1 is seen to be greater than K_1, and hence the end-to-end distance decreases more rapidly with concentration than the radius of gyration does. It is already known that the linear expansion factor at zero concentration for the former is greater than that for the latter above the Θ temperature.[5,32] Therefore, the non-Gaussian character of a chain will disappear with concentration. This seems to be a reasonable aspect. On the other hand, below the Θ temperature, the polymer chain dimension still decreases and moreover the non-Gaussian character becomes remarkable with concentration.

At this stage, let us recall the pressure correction pointed out in Sec. II. As is shown in Appendix A, this correction following the McMillan and Mayer theory[13] leads to the introduction of an additional term K_1^* or I_1^* into the coefficient of the linear term in c, where K_1^* and I_1^* may be expressed in terms of a binary cluster integral β^* between the polymer segment and solvent molecule.[33] If β^* vanishes simultaneously with β at the Θ temperature, the above statement remains unchanged; otherwise, the polymer chain dimension will depend, to some extent, on concentration even at the Θ temperature. In general, however, K_1^* is a magnitude of the order of K_1/N^2 at any other temperature, and similarly I_1^*, of I_1/N^2. Hence the pressure correction may be neglected except at the Θ temperature provided the polymer molecular weight is very high, and further discussion is still based upon Eqs. (41) and (44) with (43) and (51).

Now we turn to the problem of writing K_1 and I_1 in appropriate closed forms. For convenience, we first consider the latter. As is seen from Eq. (20), I_1 may be split into two parts:

$$I_1=(N_0M\beta/2M_0^2)[h_1(z/\alpha_0^3)-h(z/\alpha_0^3)] \tag{52}$$

with

$$h_1(z/\alpha_0^3)=1-2.637(z/\alpha_0^3)+8.38(z/\alpha_0^3)^2-\cdots, \tag{53}$$

$$h(z/\alpha_0^3)=1-2.865(z/\alpha_0^3)+9.73(z/\alpha_0^3)^2-\cdots. \tag{54}$$

Here $h(z/\alpha_0^3)$ is a z series appearing in the expression for the second virial coefficient.[5,8,25] According to Stockmayer (S),[23,25] Orofino and Flory (OF),[34] and Casassa and Markovitz (CM),[35] $h(z/\alpha_0^3)$ may be written in the closed forms[36]

$$h(z/\alpha_0^3)^{S}=1/(1+2.865z\alpha_0^{-3}), \tag{55}$$

$$h(z/\alpha_0^3)^{OF}=\ln(1+5.73z\alpha_0^{-3})/5.73z\alpha_0^{-3}, \tag{56}$$

$$h(z/\alpha_0^3)^{CM}=[1-\exp(-5.73z\alpha_0^{-3})]/5.73z\alpha_0^{-3}. \tag{57}$$

Comparing the two z series (53) and (54), we suggest that $h_1(z/\alpha_0^3)$ may be written in similar closed forms differing from Eqs. (55) to (57) only in the corresponding numerical coefficients. Thus, although the procedure is somewhat artificial, we obtain for the closed expression for I_1

$$I_1=A_2M\varphi(z/\alpha_0^3), \tag{58}$$

with

$$\varphi(z/\alpha_0^3)=h_1(z/\alpha_0^3)/h(z/\alpha_0^3)-1, \tag{59}$$

which, corresponding to Eqs. (55) to (57), may be

[32] B. H. Zimm, W. H. Stockmayer, and M. Fixman, J. Chem. Phys. **21**, 1716 (1953). See also Eqs. (42) and (45).

[33] In Mayer's treatment of ionic solutions, the pressure correction has been made thermodynamically for the activity coefficient. See J. E. Mayer, J. Chem. Phys. **18**, 1426 (1950).

[34] T. A. Orofino and P. J. Flory, J. Chem. Phys. **26**, 1067 (1957).

[35] E. F. Casassa and H. Markovitz, J. Chem. Phys. **29**, 493 (1958).

[36] The constant 5.73 in Eqs. (56) and (57) has been chosen so that the expansion coefficients of the linear term in (z/α_0^3) may coincide with the correct value 2.865 in Eq. (54).

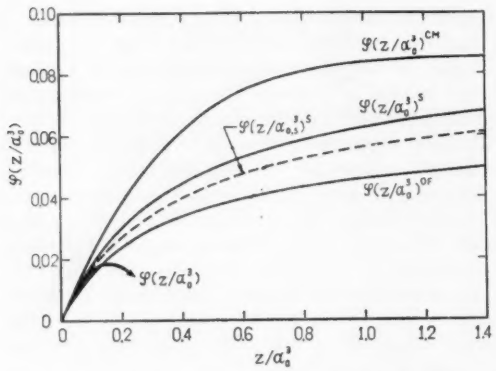

FIG. 1. The coefficients φ as functions of z/α_0^3. Full curves: for the mean square end-to-end distance. Broken curve: for the mean square radius of gyration. Heavy curve: the rigorous expansion (63).

written as

$$\varphi(z/\alpha_0^3)^{S}=0.2276z\alpha_0^{-3}/(1+2.637z\alpha_0^{-3}), \tag{60}$$

$$\varphi(z/\alpha_0^3)^{OF}=1.086\cdot\frac{\ln(1+5.274z\alpha_0^{-3})}{\ln(1+5.730z\alpha_0^{-3})}-1, \tag{61}$$

$$\varphi(z/\alpha_0^3)^{CM}=1.086\cdot\frac{1-\exp(-5.274z\alpha_0^{-3})}{1-\exp(-5.730z\alpha_0^{-3})}-1. \tag{62}$$

These three functions are plotted in Fig. 1 for positive values of z/α_0^3. They are seen to be monotonically increasing functions of z/α_0^3. For comparison, in the figure is also given the rigorous expansion derived from Eqs. (52) to (54) and (58)

$$\varphi(z/\alpha_0^3)=0.2276(z/\alpha_0^3)[1-3.04(z/\alpha_0^3)+\cdots]. \tag{63}$$

On the present basis, it is clear that K_1 takes a form analogous to Eq. (58) with (60), (61), or (62). For example, by adjusting the numerical coefficients, $\varphi(z/\alpha_{0,s}^3)^{S}$ is obtained, from Eq. (43), as follows,

$$\varphi(z/\alpha_{0,S}^3)^{S}=0.2050z\alpha_{0,S}^{-3}/(1+2.660z\alpha_{0,S}^{-3}), \tag{64}$$

which is also plotted in Fig. 1.

In addition, it can be easily shown that the above closed expressions for $\varphi(z/\alpha_0^3)$ and $\varphi(z/\alpha_{0,S}^3)$ have the following asymptotic values, irrespective of their types,

$$\lim_{z\alpha_0^{-3}\to 0}\varphi(z/\alpha_0^3)=0, \qquad \lim_{z\alpha_0^{-3}\to\infty}\varphi(z/\alpha_0^3)=0.0863, \tag{65}$$

$$\lim_{z\alpha_{0,S}^{-3}\to 0}\varphi(z/\alpha_{0,S}^3)=0, \qquad \lim_{z\alpha_{0,S}^{-3}\to\infty}\varphi(z/\alpha_{0,S}^3)=0.0771. \tag{66}$$

In this connection, we discuss the asymptotic behavior of $\varphi(z/\alpha_0^3)$ for large z from a more rigorous standpoint. Albrecht[25] has exactly evaluated the contribution of a special type of intermolecular clusters to the z series $h(z/\alpha_0^3)$ and given a semiquantitative discussion of the asymptotic behavior of the second virial coefficient. Similar consideration is possible for the new z series $h_1(z/\alpha_0^3)$ in Eq. (52) or (59). That is, the two z series may be written in the forms,

$$h(z)=\sum_{k=1}^{\infty}2C_k(-z)^{k-1}, \tag{67}$$

$$h_1(z)=\sum_{k=1}^{\infty}2D_k(-z)^{k-1}. \tag{68}$$

Here, the factor α_0^3 has been dropped for simplicity. The coefficients C_k and D_k result from a *ladder* type of clusters, such as B_{20}, $B_{30}(a)$, $B_{40}(a)$, etc. in Fig. 1 of the work cited in footnote 8, only, and are given by

$$C_k=\int\cdots\int_{\substack{0\le\sum x_i=L\le 1\\ 0\le\sum y_i=S\le 1}}(1-L)(1-S)\prod_{i=1}^{k-1}[(x_i+y_i)^{-1}dx_i dy_i]dLdS \tag{69}$$

$$D_k=\int\cdots\int_{\substack{0\le\sum x_i=L\le 1\\ 0\le\sum y_i=S\le 1}}(1-L)(1-S)[1-L+\sum_{i=1}^{k-1}x_i y_i(x_i+y_i)^{-1}]\times\prod_{i=1}^{k-1}[(x_i+y_i)^{-1}dx_i dy_i]dLdS, \tag{70}$$

where the meaning of the variables is the same as in Eqs. (47) to (49). As is shown in Appendix B, replacing C_k and D_k by the respective asymptotic values C_k^* and D_k^* for large k, we find

$$\lim_{z\alpha_0^{-3}\to\infty}\varphi^*(z/\alpha_0^3)=0.1457. \tag{71}$$

Although the individual asymptotic values of $h(z)$ and $h_1(z)$ so obtained are not reliable, the above value for $\varphi(z)$ itself might be nearly correct because of the cancellation of errors for $h(z)$ and $h_1(z)$. It is of interest that the values in Eqs. (65) and (71) are not so far from each other. In either case, the coefficient I_1 may be expected to be at most of the order of one-tenth of A_2M. Thus we may conclude that the initial concentration dependence of the polymer chain dimension is of the lower order, though not negligible, than that of the reduced osmotic pressure ($\pi M/RTc$).

Finally we make a brief comparison of the present theory with Krigbaum's.[2] On rewriting his result with the equation[1,37] $\alpha_0^5-\alpha_0^3=(\frac{4}{3})z$, his φ function may be expressed as

$$\varphi(z/\alpha_0^3)^{K}=4z\alpha_0^{-3}/(3+10z\alpha_0^{-3}). \tag{72}$$

For the treatment of the viscosity, Kawai[2] has made a modification of the Krigbaum theory.[38] In this case, the φ function may be written as

$$\varphi(z/\alpha_0^3)^{KK}=\tfrac{2}{3}[1-(1+\tfrac{4}{3}z\alpha_0^{-3})^{-\frac{1}{2}}]. \tag{73}$$

[37] W. H. Stockmayer, J. Polymer Sci. **15**, 595 (1955).
[38] See Eq. (3) of the work cited in footnote 2.

It is easily seen that Eqs. (72) and (73) take the asymptotic values 0.4 and 0.667 for large z, respectively. The intermediate values of these functions are plotted in Fig. 2, where the result by the present theory (61) is also shown for the sake of comparison. It follows from this that the initial concentration dependence has been overestimated in the Krigbaum theory. In Sec. V, we shall refer again to this point in connection with the viscosity.

IV. APPLICATION TO LIGHT SCATTERING

There exist no available experimental data which are to be compared with the present theory. This seems to be due to the fact that the method for the determination of the polymer chain dimension at finite concentrations by light scattering measurements has not yet been established. In this section, we consider this problem. Before doing so, we show that the second virial term in the reciprocal intensity function depends on scattering angle θ owing to the concentration dependence of the intramolecular scattering function as well as to the intermolecular correlation introduced by Albrecht[16] and Flory and Bueche.[15]

For the present purpose, the intensity $I(c, \theta)$ of excess scattering at angle θ per unit volume from a solution of concentration c must be written as

$$Kc/I(c, \theta) = 1/MP_1(c, \theta) + 2A_2Q_2(\theta)c + \cdots, \quad (74)$$

where K is a constant and $Q_2(\theta)$ is the intermolecular correlation function.[15,16] The intramolecular intensity function at concentration c, $P_1(c, \theta)$ may be expressed as

$$P_1(c, \theta) = N^{-2} \sum_{i_1, j_1} \int P(c, \mathbf{R}_{i_1 j_1}) \exp(\mathbf{S}\cdot\mathbf{R}_{i_1 j_1}) d\mathbf{R}_{i_1 j_1}, \quad (75)$$

$$\mathbf{S} = 2\pi i\mathbf{s}/\lambda,$$

where $\mathbf{s}$ is the difference between unit vectors in the directions of the incident and scattered lights and λ is the wave length of the light in the medium. It is easily seen from Eq. (75) that $P_1(c, \theta)$ can readily be obtained by using $\langle R_{i_1 j_1}^{2m} \rangle$ at concentration c in the currently used $P_1(0, \theta)$. Therefore, remembering that[14]

$$P_1(0, \theta) = 1 - \tfrac{1}{3}u + \cdots, \quad (76)$$

$$u = 2\pi^2 s^2 N a^2 \alpha_{0,S}^2/3\lambda^2, \quad (77)$$

and using Eqs. (40) and (41), we obtain for $P_1(c, \theta)$ at small c and θ

$$P_1(c, \theta) = P_1(0, \theta) + \tfrac{2}{3}K_1 uc + \cdots. \quad (78)$$

Equation (74) may then be rewritten as

$$Kc/I(c, \theta) = 1/MP_1(0, \theta) + 2A_2Q(\theta)c + \cdots, \quad (79)$$

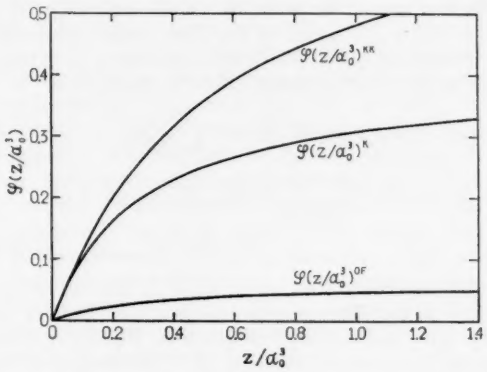

FIG. 2. Comparison of the present theory (61) with Krigbaum's.

where

$$Q(\theta) = Q_2(\theta) - Q_1(\theta), \quad (80)$$

$$Q_1(\theta) = K_1 u/3A_2M + 0(u^2) = 0.0683u(z/\alpha_{0,S}^3) + \cdots. \quad (81)$$

The second line of Eq. (81) has been obtained by the substitution of Eq. (43); $Q_1(\theta)$ is a new function which represents the effect of intramolecular interference on the second virial term, and vanishes on letting θ approach zero. On the other hand, $Q_2(\theta)$ is given by[15,16]

$$Q_2(\theta) = P_2(\theta)/P_1^2(0, \theta) \quad (82)$$

with

$$P_2(\theta) = \frac{\sum_{i_1, i_2} \int g_2(1, 2) \exp(\mathbf{S}\cdot\mathbf{R}_{i_1 i_2}) d(1, 2)}{N^2 \int g_2(1, 2) d(1, 2)} \quad (83)$$

and has already been evaluated as[16]

$$Q_2(\theta) = 1 - 0.296u(z/\alpha_{0,S}^3) + \cdots \quad (84)$$

to the same model and approximation as in the present treatment. Therefore, we obtain, from Eqs. (80), (81), and (84),

$$Q(\theta) = 1 - 0.364u(z/\alpha_{0,S}^3) + \cdots. \quad (85)$$

The effect of intramolecular interference is seen to make a contribution of about 20% to the linear term of $Q(\theta)$. This is not negligible.

Now we consider the problem of separating $Q_1(\theta)$ and $Q_2(\theta)$. To do this, we first attempt to write the coefficients of u in $Q_1(\theta)$ and $Q_2(\theta)$, which are expressed as a series expansion in z, in closed forms. This may readily be done for the former through K_1

$$Q_1(\theta) = u\varphi(z/\alpha_{0,S}^3)/3, \quad (86)$$

where $\varphi(z/\alpha_{0,S}{}^3)$ is given by closed expressions like Eqs. (60) to (62), e.g., by Eq. (64). Similar treatment is possible for $Q_2(\theta)$. To do this, expanding the g function as in Sec. II we rewrite $P_2(\theta)$ in the form

$$P_2(\theta)=h^{-1}(z/\alpha_{0,S}{}^2)\sum_{i_1,i_2}\int[N^{-4}\sum_{j_1,j_2}P_0(\mathbf{R}_{i_1i_2})_{j_1j_2}-\beta N^{-4}\sum_{j_1,j_2}\sum_{k_1,k_2}P_1(0_{k_1k_2},\mathbf{R}_{i_1i_2})_{j_1j_2}+\cdots]\times\exp(\mathbf{S}\cdot\mathbf{R}_{i_1i_2})d\mathbf{R}_{i_1i_2}, \quad (87)$$

where $P_{s-1}(0_{k_1k_2}, 0_{i_1i_2}, \cdots, \mathbf{R}_{i_1i_2})_{j_1j_2}$ are the conditional probabilities similar to functions defined by Eq. (24), and $h(z/\alpha_{0,S}{}^3)$ is given by Eq. (54). If we expand the exponential in Eq. (87), the integral of the first term just gives $h(z/\alpha_{0,S}{}^3)$. Therefore, Eq. (87) leads to

$$P_2(\theta)=1-(2\pi^2s^2/3\lambda^2)h^{-1}(z/\alpha_{0,S}{}^3)\sum_{i_1,i_2}\int\mathbf{R}_{i_1i_2}{}^2\times[N^{-4}\sum_{j_1,j_2}P_0(\mathbf{R}_{i_1i_2})_{j_1j_2}-\beta N^{-4}\sum_{j_1,j_2}\sum_{k_1,k_2}P_1(0_{k_1k_2},\mathbf{R}_{i_1i_2})_{j_1j_2}+\cdots]d\mathbf{R}_{i_1i_2}+\cdots \quad (88)$$

up to the term of s^2. On using the results obtained by Albrecht,[16] Eq. (88) may be written as

$$P_2(\theta)=1-2uh_2(z/\alpha_{0,S}{}^3)/3h(z/\alpha_{0,S}{}^3)+\cdots \quad (89)$$

with

$$h_2(z/\alpha_{0,S}{}^3)=1-2.421(z/\alpha_{0,S}{}^3)+\cdots. \quad (90)$$

The $h_2(z/\alpha_{0,S}{}^3)$ is a second new function similar to h and h_1.

Thus, an alternative form for $Q_2(\theta)$ is obtained, from Eqs. (76), (82), and (89), as follows,

$$Q_2(\theta)=1-\tfrac{2}{3}u\psi(z/\alpha_{0,S}{}^3)+\cdots \quad (91)$$

with

$$\psi(z/\alpha_{0,S}{}^3)=h_2(z/\alpha_{0,S}{}^3)/h(z/\alpha_{0,S}{}^3)-1. \quad (92)$$

Following the same procedure as that used on going from Eq. (59) to Eq. (60), (61), or (62), we can find closed expressions for $\psi(z/\alpha_{0,S}{}^3)$. For example, in the case of the Orofino and Flory type, this reads

$$\psi(z/\alpha_{0,S}{}^3)^{\mathrm{OF}}=1.184\cdot\frac{\ln(1+4.842z\alpha_{0,S}{}^{-3})}{\ln(1+5.730z\alpha_{0,S}{}^{-3})}-1, \quad (93)$$

which takes the asymptotic value 0.1836 for large z.

Finally, we rewrite Eq. (79), by using Eqs. (86) and (91), in the form

$$Kc/I(c,\theta)=M^{-1}[1+\tfrac{1}{3}u(1-2K_1f_z{}^{-1}c+\cdots)+\cdots]+2A_2c+\cdots, \quad (94)$$

where

$$f_z=\varphi(z/\alpha_{0,S}{}^3)/[\varphi(z/\alpha_{0,S}{}^3)+2\psi(z/\alpha_{0,S}{}^3)]. \quad (95)$$

The factor f_z as a function of $z/\alpha_{0,S}{}^3$ can be calculated by using the appropriate closed forms for φ and ψ given above. As is easily seen from Eq. (94), we can estimate the quantity $(1-2K_1f_z{}^{-1}c)$ and hence $2K_1f_z{}^{-1}c$ from the slope of the curve of Kc/I vs $\sin^2(\theta/2)$ by the angular variation method in light scattering measurements. On the other hand, if the values of z and $\alpha_{0,S}$ are known, the value of f_z is determined. Therefore, when multiplied by this factor, the quantity $2K_1f_z{}^{-1}c$ so obtained, just yields the concentration-dependent term in the mean square radius of gyration. Of course, the radius of gyration at zero concentration can be estimated by the usual method. Thus, the evaluation of the polymer chain dimension at finite concentrations would be experimentally possible.

The method presented here is limited to the evaluation up to the linear term in concentration, and moreover is incomplete even in this limited region inasmuch as the factor f_z given by Eq. (95) is not exact and its choice is not unique. However, the theoretical procedure itself is consistent with the chain statistics developed in the preceding sections. In this sense, we shall elsewhere attempt the actual analysis of experimental data.

V. APPLICATION TO VISCOSITY

The viscosity coefficient $\eta(c)$ of the polymer solution of concentration c may be expressed as a power series in c

$$\eta(c)=\eta(0)[1+[\eta]c+k'[\eta]^2c^2+\cdots], \quad (96)$$

where $[\eta]$ is the intrinsic viscosity and k' is the Huggins constant.[17] As already mentioned, the k' constant depends on various kinds of intermolecular interaction. In the present treatment, we concern ourselves only with the two factors: the intermolecular hydrodynamic interaction and the concentration dependence of polymer chain dimensions. As to the former, a number of attempts along the hydrodynamic theory has already been presented.[18,39–41] As has been pointed out by Saito,[42] however, the calculation of k' based on the Stokes approximation in hydrodynamics is always followed by an improper integral which is evaluated to be of different values according to different ways of integration. This is physically unreasonable and the values of k' so obtained[43] have no great significance. Therefore, we must await the calculation to the Oseen approximation instead of the Stokes one[42]—a very troublesome task. Thus, apart from the rigorous hydrodynamic consideration, we attempt a phenomeno-

[39] E. Guth and R. Simha, Kolloid-Z. **74**, 266 (1936).
[40] R. Simha, J. Research Natl. Bur. Standards **42**, 409 (1949).
[41] N. Saito, J. Phys. Soc. Japan **5**, 4 (1950).
[42] N. Saito, J. Phys. Soc. Japan **7**, 447 (1952).
[43] For example, Riseman and Ullman[18] have obtained the value 0.6 for k' in the case of chain polymer solutions.

logical treatment equivalent to the procedure proposed by Brinkman.[44]

Now we consider the *intrinsic viscosity* $[\eta]_c$ at concentration c, which may be well defined as the relative increase of the viscosity per unit concentration on adding the solute polymers to the solution of concentration c. It satisfies the differential equation,

$$d\eta(c)/dc=\eta(c)[\eta]_c. \tag{97}$$

In the limit of $c=0$, Eq. (97) is nothing but the equation defining $[\eta]$. It may be expected that $[\eta]_c$ is proportional to the effective hydrodynamic volume of the polymer at concentration c provided c is small. For convenience, we assume, therefore, that $[\eta]_c$ is proportional to the third power of the radius of gyration at concentration c. It may then be written, by using Eq. (41), in the form

$$\begin{aligned}[\eta]_c&=[\eta](1-2K_1c+\cdots)^{\frac{3}{2}}\\&=[\eta](1-3K_1c+\cdots).\end{aligned} \tag{98}$$

Integrating Eq. (97) after the substitution of Eq. (98), we obtain

$$\eta(c)=\eta(0)\exp[[\eta](c-\tfrac{3}{2}K_1c^2+\cdots)], \tag{99}$$

which is expanded as follows,

$$\eta(c)=\eta(0)[1+[\eta]c+\tfrac{1}{2}([\eta]^2-3K_1[\eta])c^2+\cdots]. \tag{100}$$

Comparing Eq. (100) with (96), we find[45]

$$\begin{aligned}k'&=\tfrac{1}{2}(1-3K_1/[\eta])\\&=\tfrac{1}{2}[1-3(A_2M/[\eta])\varphi(z/\alpha_0s^3)].\end{aligned} \tag{101}$$

The first and second terms on the right-hand side of Eq. (101) result from the hydrodynamic interaction and the concentration dependence of polymer chain dimensions, respectively.

Since the second term in Eq. (101) vanishes at $z=0$, the k' constant takes a value near 0.5 for small z (poor solvent system). On the other hand, it is known that the dimensionless quantity $A_2M/[\eta]$ takes a value of about 1.5 for large z.[46] Further, as has been shown in Sec. III, the asymptotic value of φ for large z is 0.0771 if closed forms such as Eq. (64) for φ are assumed, or 0.1457 if the evaluation is carried out by considering a special type of clusters. Hence, the k' constant takes a value of about 0.2 ± 0.1 for large z (good solvent system). In other words, k' would vary from 0.5 to 0.2 with increasing solvent power. This prediction is in semiquantitative agreement with the experimental results, and also consistent with the equation derived recently by Bhatnagar *et al.*[47] on the basis of the theory of rate processes.

In this connection, we must refer to the anomalous viscosity behavior. On adopting the asymptotic value of φ derived by Krigbaum[2] [Eq. (72) or (73)], it is quite likely that the k' constant takes a negative value. This means that the reduced viscosity decreases initially with increasing concentration, and indeed may serve to explain the anomalous viscosity behavior. Such an apparently favorable situation, of course, comes from the overestimation of Krigbaum's φ itself; and, according to the present theory, k' is always positive. Hence, it seems unlikely that the change of polymer chain dimensions with concentration may well interprete the anomalous viscosity behavior.

VI. CONCLUDING REMARKS

We have investigated theoretically the concentration dependence of various properties of chain polymer solutions, i.e., the two-body problems except the second virial coefficient on the basis of the theory of fluids and of the fashion prevailing in the statistical treatment of dilute polymer solutions.

The essential problem is to deal as well with the segment distribution functions as with the case of the second virial coefficient. This has been done to give a rigorous series expansion in the parameter z on the assumption of the random flight model, the step length of which is modified by the linear expansion factor at zero concentration. As has already been discussed, the modified random flight model, i.e., the uniform expansion model, fails to explain the properties of an isolated molecule such as the intrinsic viscosity on account of the non-Gaussian character of a chain.[5,7,8] It is incorrect also in the case of the two-body problems, because the linear expansion factor of each of two molecules in contact is somewhat different from α_0 for an isolated molecule.[6,26] However, the behavior of the z series appearing in A_2, I_1, K_1, etc. is mainly governed by the way by which the segment distribution functions are approximately factorized,[6,8,26] but is not greatly affected by introducing the present model. It seems quite natural that the intramolecular volume exclusion has only indirect influence on the two- body problems. Indeed, this statement may be manifested by examining the expansion coefficients of A_2, e.g., the triple contact term.[48] If we use α_0, that is, the uniform expansion model, the Flory and Krigbaum model yields $2.704z^2$ for the triple contact term, and for the rigorous random flight model, $15.46z^2$. If we take into account the correlation between the intramolecular and intermolecular contacts, the latter yields $18.51z^2$. Therefore, the present assumption would be acceptable as a first approximation. It must be noted, however,

[44] H. C. Brinkman, J. Chem. Phys. **20**, 571 (1952). See also N. Saito, *High Polymer Physics* (in Japanese; Shokabo, Tokyo, 1958), Chap. 6.

[45] If we start at a difference-equation[44] in place of the differential equation (97), an additional term $v_2/[\eta]$ appears in the bracket of Eq. (101), where v_2 is the specific volume of the polymer. This term is negligible compared to others.

[46] See, for example, Table II of the work cited in footnote 34.

[47] H. L. Bhatnagar, A. B. Biswas, and M. K. Gharpurey, J. Chem. Phys. **28**, 88 (1958).

[48] See Eqs. (B. 28), (B. 31b), and (B. 32) of the work cited in footnote 8.

TABLE I. Numerical values of the integral I_n.

n	I_n Eq. (B4)	Eq. (B6)	Eq. (B7)	% Error Eq. (B6)	Eq. (B7)
1	0.2929	0.2973	0.3031	1.5	3.5
2	0.1427	0.1451	0.1459	1.7	2.2
5	0.02657	0.02702	0.02679	1.7	0.8
6	0.01627	0.01653	0.01637	1.6	0.6
9	0.004112	0.004172	0.004125	1.5	0.3
10	0.002657	0.002693	0.002664	1.4	0.2
13	0.0007465	0.0007557	0.0007477	1.2	0.2
14	0.0004941	0.0005001	0.0004948	1.2	0.1
17	0.0001467	0.0001482	0.0001468	1.0	0.0

that the error caused by this approximation may be diminished by using α_{02} in place of α_0 according to Casassa.[26]

The closed expressions for the z series presented here may be expected to give good approximations for good solvent systems, though the derivation is very arbitrary. On the contrary, however, it is difficult to obtain the closed expression for the c series. A more detailed discussion of the behavior of polymer chains at finite concentrations would have to await the evaluation of the next higher term in c, and hence of the third virial coefficient which has not thoroughly been investigated—the three-body problem. It must be remarked here that the third virial term, derived by Zimm[14] and Flory and Bueche,[15] in the reciprocal intensity function is still incomplete inasmuch as they have ignored the concentration dependence of the distribution function $F_1(1)$ which is involved in both of $P_1(\theta)$ and $g_2(1, 2)$.

A confirmation of the present theory will become possible by a comparison of Eq. (41) with the *observed* value obtained by the procedure proposed in Sec. IV. The validity of approximate closed expressions for A_2 has already been shown by comparison with experiment.[8,23,35] The closed expressions for $h_1(z)$ and $h_2(z)$ introduced here must still be checked experimentally, since it is impossible mathematically. In this connection, the light-scattering measurement is now in progress in Kyoto.

It must be repeated that the concentration dependence of polymer chain dimensions serves to explain the effect of solvent power on the Huggins constant, but not the anomalous viscosity behavior as has recently been discussed by Claesson.[4] The interpretation of the anomalous viscosity behavior itself is beyond the scope of the present paper, and hence we have left it untouched.

Finally it must be stated that work on the concentration dependence of the end-to-end distance along similar lines has recently been carried out by Kotin.[49] His leading term corresponding to the first power of c agrees with the first term of Eq. (51) aside from the omission of the symmetry factor of two. The qualitative conclusions concerning the concentration effect are quite similar to those of the present work.

[49] L. Kotin, Doctoral thesis, Harvard University (1960).

ACKNOWLEDGMENTS

The author wishes to express his appreciation to Professor Ichiro Sakurada for stimulating discussions and encouragement. Thanks are also tendered to Professor Ei Teramoto for his critical reading of this manuscript, and to Professor Michio Kurata for his advice and kind help with publication.

APPENDIX A

Pressure Correction for the Chain Dimension

For convenience, we consider only the case of the end-to-end distance. According to the McMillan and Mayer theory,[13] the extra term $F_{11}^*(1)$, which is to be added to the coefficient $F_{11}(1)$ in Eq. (6) on account of the pressure correction, may be written in the form

$$F_{11}^*(1) = (N_0/M)[B_{1,1_s} - h_{1,1_s}(1)], \qquad \text{(A1)}$$

with

$$B_{1,1_s} = V^{-1}\int [F_2(1, 1_s) - F_1(1)F_1(1_s)]d(1, 1_s), \quad \text{(A2)}$$

$$h_{1,1_s}(1) = F_1^{-1}(1)\int [F_2(1, 1_s) - F_1(1)F_1(1_s)]d(1_s). \qquad \text{(A3)}$$

Here, the suffix s indicates the quantities for the solvent; $B_{1,1_s}$ is the *second virial coefficient* between the polymer and solvent molecules.

Hence, the corresponding additional term $P_1^*(\mathbf{R})$ in the distribution function $P(c, \mathbf{R})$ may be written, with taking into account $F_1(1_s) = 1$, as

$$P_1^*(\mathbf{R}) = P(\mathbf{R})(N_0/VM)\int [F_2(1, 1_s) - F_1(1)]d(1, 1_s)$$

$$-(N_0/VM)\int [F_2(1, 1_s) - F_1(1)]d(1, 1_s)/d\mathbf{R}. \quad \text{(A4)}$$

Expanding the integrands just as in $P_1(\mathbf{R}_{ij})$ and performing the integrations over the coordinates, we obtain

$$P_1^*(\mathbf{R}) = -(N_0\beta^*/M_0)$$

$$\times \{\beta^* N^{-1}\sum_{i<j}[P_1(0_{ij}, \mathbf{R}) - P_1(0_{ij})P(\mathbf{R})] + \cdots\}, \quad \text{(A5)}$$

where β^* is a binary cluster integral between the polymer segment and solvent molecule, and the functions $P_1(0_{ij}, \mathbf{R})$ and $P_1(0_{ij})$ are conditional probabilities similar to those used in text.

Finally we can easily obtain for the corrected mean square end-to-end distance in place of Eq. (44)

$$\langle R^2\rangle = Na^2\alpha_0^2[1-2(I_1+I_1^*)c+\cdots], \quad \text{(A6)}$$

where

$$I_1^* = -(2Na^2\alpha_0^2)^{-1}\int \mathbf{R}^2 P_1^*(\mathbf{R})\,d\mathbf{R}$$

$$= -(N_0\beta^*/2M)[\tfrac{4}{3}(z^*/\alpha_0^3)+\cdots], \quad \text{(A7)}$$

$$z^* = \beta^*(3/2\pi a^2)^{\frac{1}{2}}N^{\frac{1}{2}}. \quad \text{(A8)}$$

Roughly speaking, I_1^* is a magnitude of the order of one-N^2th of I_1 except at vanishing z. Therefore, the former may be neglected compared to the latter in general, provided M is large.

APPENDIX B

Asymptotic Behavior of the Function φ for Large z

The integral (69) has been evaluated by Albrecht.[25] Similarly the integral (70) can be evaluated. The results read

$$C_k = 2^{k+2}\pi^{(k-2)/2}[(k^2+3)I_{k-1}-(k-1)2^{-(k-1)/2}]/(k+1)(k+3)\Gamma(k/2), \quad \text{(B1)}$$

$$D_k = 2^{k+1}\pi^{(k-2)/2}[k(k^4+12k^3+50k^2+4k+77)I_{k-1}$$
$$-(k-1)(k^3+12k^2+55k+16)2^{-(k-1)/2}]/3k(k+1)(k+3)(k+5)\Gamma(k/2), \quad \text{(B2)}$$

where

$$I_n = \int_0^{1/4\pi} \sin^n\theta\, d\theta. \quad \text{(B3)}$$

The integral I_n is evaluated to

$$I_{2p+1} = \frac{(2p)!!}{(2p+1)!!}\left[1-2^{-\frac{1}{2}}\sum_{r=0}^{p}\frac{(2p-2r-1)!!}{(2p-2r)!!}2^{-(p-r)}\right],$$

$$I_{2p} = \frac{(2p-1)!!}{(2p)!!}\left[\frac{\pi}{4}-\sum_{r=0}^{p-1}\frac{(2p-2r-2)!!}{(2p-2r-1)!!}2^{-(p-r)}\right], \quad \text{(B4)}$$

as n is odd or even, where

$$(2m)!! = (2m)(2m-2)\cdots 4\cdot 2,$$

$$(2m+1)!! = (2m+1)(2m-1)\cdots 3\cdot 1.$$

Now we consider the asymptotic forms of C_k and D_k for large k by introducing an approximate formula for I_n. As is seen from Eqs. (69) and (70), C_k and D_k must satisfy the inequality,

$$C_k > D_k > 0 \quad \text{for all } k. \quad \text{(B5)}$$

Approximating I_n by the equation,

$$I_n \simeq (n+1)^{-1}2^{-(n+1)(n+2)/2(n+3)}, \quad \text{(B6)}$$

Albrecht has derived the asymptotic form of C_k. However, the approximation (B6) is unavailable for the present problem, because it breaks down the condition (B5) in the asymptotic limit of large k. Thus, we must use a better approximation for I_n than Eq. (B6). It was found to be

$$I_n \simeq (n+1)^{-1}2^{-n/2}\exp[-2/(2n+11)]. \quad \text{(B7)}$$

For the sake of comparison, the errors by Eqs. (B6) and (B7) are tabulated together with the correct and approximate values of I_n for several n in Table I.

Then substituting Eq. (B7) into Eqs. (B1) and (B2) and letting k become sufficiently large, we find

$$C_k^* = \frac{4\cdot 2^{\frac{1}{2}}(2\pi)^{k/2}}{\pi\Gamma(k/2+3)} - \frac{143\cdot 2^{\frac{1}{2}}(2\pi)^{k/2}}{48\pi\Gamma(k/2+4)}, \quad \text{(B8)}$$

$$D_k^* = \frac{337\cdot 2^{\frac{1}{2}}(2\pi)^{k/2}}{144\pi\Gamma(k/2+3)} + \frac{1909\cdot 2^{\frac{1}{2}}(2\pi)^{k/2}}{576\pi\Gamma(k/2+4)}. \quad \text{(B9)}$$

The values of $2C_2^*$ and $2D_2^*$ are 3.068 and 2.988, respectively, whereas the respective correct values are 2.865 and 2.637. The agreement is surprisingly good even for small k.

We discuss the asymptotic behavior of the function φ by replacing C_k and D_k by C_k^* and D_k^*. The series (67) and (68) then become

$$h^*(z)=\sum_{k=1}^{\infty}2C_k^*(-z)^{k-1}, \tag{B10}$$

$$h_1^*(z)=\sum_{k=1}^{\infty}2D_k^*(-z)^{k-1}. \tag{B11}$$

By using Eqs. (B8) and (B9), Eqs. (B10) and (B11) may be rewritten in the form

$$h^*(z)=16\pi^{-\frac{1}{2}}S_1(x)-(143/12)\pi^{-1}S_2(x), \tag{B12}$$

$$h_1^*(z)=(337/36)\pi^{-1}S_1(x)+(1909/144)\pi^{-\frac{1}{2}}S_2(x) \tag{B13}$$

with

$$S_1(x)=\sum_{k=1}^{\infty}(-x)^{k-1}/\Gamma(k/2+3),$$

$$S_2(x)=\sum_{k=1}^{\infty}(-x)^{k-1}/\Gamma(k/2+4), \tag{B14}$$

$$x=(2\pi)^{\frac{1}{2}}z,$$

since $h^*(z)$ and $h_1^*(z)$ are absolutely convergent. It can be shown that the series S_1 and S_2 have the sums,

$$S_1(x)=\tfrac{1}{2}x^{-1}-(4/3)\pi^{-\frac{1}{2}}x^{-2}+x^{-3}-2\pi^{-\frac{1}{2}}x^{-4}+x^{-5}(1-\mathrm{Erfc}x\cdot\exp x^2), \tag{B15}$$

$$S_2(x)=\tfrac{1}{6}x^{-1}-(8/15)\pi^{-\frac{1}{2}}x^{-2}+\tfrac{1}{2}x^{-3}-(4/3)\pi^{-\frac{1}{2}}x^{-4}+x^{-5}-2\pi^{-\frac{1}{2}}x^{-6}+x^{-7}(1-\mathrm{Erfc}x\cdot\exp x^2), \tag{B16}$$

where $\mathrm{Erfc}x$ is a complementary error function. The $S_1(x)$ and $S_2(x)$ are seen to have the asymptotic forms,

$$S_1(x)=\tfrac{1}{2}x^{-1}+0(x^{-2}), \tag{B17}$$

$$S_2(x)=\tfrac{1}{6}x^{-1}+0(x^{-2}) \tag{B18}$$

for large x. Therefore, we find

$$\lim_{z\to\infty}h^*(z)=433/72\cdot 2^{\frac{1}{2}}\pi z, \tag{B19}$$

$$\lim_{z\to\infty}h_1^*(z)=5953/864\cdot 2^{\frac{1}{2}}\pi z, \tag{B20}$$

which lead to

$$\lim_{z\to\infty}\varphi^*(z)=0.1457. \tag{B21}$$

Since we have considered only a special type of clusters and further replaced the coefficients C_k and D_k by their asymptotic forms, the values given by Eqs. (B19) and (B20) are of course inexact. However, the value given by Eq. (B21) may be expected to be near the true one because of the cancellation of approximations for $h(z)$ and $h_1(z)$.

High-Temperature Absorption of Carbon Dioxide at 4.40 μ*

MARTIN STEINBERG AND WILLIAM O. DAVIES

Physics Research Division, Armour Research Foundation, Chicago, Illinois

(Received November 2, 1960)

The absorption of carbon dioxide-nitrogen mixtures at 4.40 μ was examined over a temperature range of 1200 to 2100°K for optical densities of 0.10 to 0.40 atm-cm. The test gas was elevated to desired temperatures by shock compression. Properties of the test gas were determined by measurement of initial concentrations and shock wave velocities. Absorption was observed as a diminution of source beam intensity monitored with a rapid response infrared detector and displayed on an oscilloscope. Beer's law was found to be applicable over the range of temperature and concentration studied. Absorption coefficients calculated from Beer's law plots reached a maximum of 3.0 atm^{-1} cm^{-1} at about 1400°K, and were independent of total pressure from 0.26 to 1.05 atm. The absorption was also measured over a wavelength interval of 4.37 to 4.6 μ. The results of this investigation are compared to the existing theoretical and experimentally determined absorption data.

INTRODUCTION

ALTHOUGH the infrared absorption spectrum of carbon dioxide has been fairly extensively investigated at ordinary temperatures, few measurements of high temperature absorptivities have been made. With increasing temperature and population of higher vibrational states the number of possible transitions in absorption and the complexity of the absorption increase markedly. Some determinations of infrared absorption have been carried out in furnaces and furnace heated jets at temperatures up to 1390°K.[1-7] The use of flames to study carbon dioxide optical properties at still higher temperatures suffers from thermal and concentration gradients, possible lack of thermodynamic equilibrium, and interference by bands of other species.

In a study of the oxidation of carbon monoxide behind shock waves we have had occasion to measure the absorption of carbon dioxide-nitrogen mixtures at 4.40 μ at temperatures up to 2100°K. The shock tube permits the ready attainment of higher temperatures than can be readily reached in furnaces, without the disadvantages of flames. The recent development of sensitive rapid-response infrared detectors now permits the application of the shock tube to the study of infrared absorptivities and emissivities of hot gases.

EXPERIMENTAL

Shock Tube

The gas mixtures used in the study were heated by shock compression in a simple, uniform-bore shock tube. The tube is constructed of 3 in. i.d. seamless steel tubing, and has a honed and chrome plated bore. A 5-ft driver section rides on tracks to facilitate opening and closing the tube. The test chamber is 15 ft long and is composed of two 5-ft, one 3-ft, and one 2-ft flanged sections. All flanged joints are sealed with *O* rings. Cellulose acetate or aluminum diaphragms are clamped between the driver and test sections to separate the driver and test gases. Diaphragms are ruptured by a spring-actuated needle which runs the length of the driver section. A pair of flat calcium fluoride windows 0.50 in. in diam and 0.375 in. thick are mounted tangent to the bore of the tube 2 ft from the downstream end on opposite sides of the test chamber. The window ports are also sealed with *O* rings.

Both chambers are evacuated to a few microns Hg with a mechanical pump. The test section is further evacuated to about 10^{-4} mm Hg with a consolidated MCF-300 oil-diffusion pump. Low pressures are measured with a Consolidated Pirani gauge and a Miller cold-cathode ionization gauge.

Helium is used as the driver gas at initial pressures up to 800 psig. Mixtures of carbon dioxide and nitrogen are prepared and stored in 50-liter Pyrex flasks. Matheson "bone-dry grade" carbon dioxide (99.8% minimum purity) is condensed at −195°C and the bulb is evacuated to remove noncondensable impurities. The bulb temperature is then raised to −78.5°C and the carbon dioxide is distilled into the storage flask to the desired partial pressure. Nitrogen for the mixture is passed through a trap at −195°C to remove condensable impurities. A Wallace and Tiernan 0–60 mm Hg differential pressure gauge (model FA-141) and 0–760 mm Hg dial manometer (model FA-145) are used to measure pressures of the synthetic mixtures and initial test gas pressure in the shock tube. The gauges were periodically checked against a mercury manometer. The gas mixtures were allowed to stand at least 24 hr before use to ensure complete mixing.

Upon diaphragm rupture, high-pressure helium expands into the test section generating a shock wave which compresses and heats the carbon dioxide-

* This research was sponsored by the Aeronautical Research Laboratories of the Air Force Research Division.

[1] E. F. Daly and G. B. B. M. Sutherland, *Third Symposium on Combustion and Flame and Explosion Phenomena* (Williams & Wilkins, Baltimore, Maryland, 1949), p. 530.

[2] J. H. Taylor, W. S. Benedict, and J. Strong, J. Chem. Phys. **20**, 528 (1952).

[3] R. H. Tourin, J. Chem. Phys. **20**, 1651 (1952); Natl. Bur. of Standards (U. S.) Circ. No. **523**, 87 (1954).

[4] J. H. Taylor, W. S. Benedict, and J. Strong, J. Chem. Phys. **20**, 1884 (1952).

[5] R. H. Tourin, *Technical Report No.* 258 (The Warner and Swasey Company, May, 1954).

[6] R. H. Tourin, and P. M. Henry, AFCRC-TR-60-203 (The Warner and Swasey Company, December, 1959).

[7] D. K. Edwards, J. Opt. Soc. Am. **50**, 617 (1960).

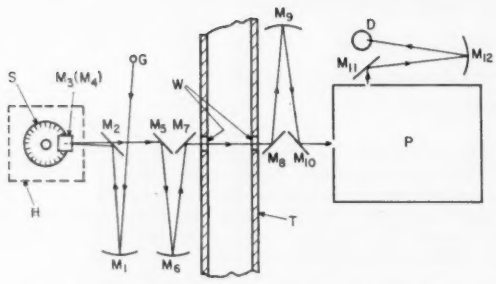

FIG. 1. Optical system. G = globar source, M = mirror, S = sector wheel, H = chopper housing, W = window, T = shock tube, P = monochromator, D = detector.

nitrogen mixtures. The temperature T_2 and pressure P_2 developed behind the shock is dependent on the initial pressure P_1 in the test section and the pressure ratio across the diaphragm. The initial temperature is about 298°K. Because of the nonideality of diaphragm rupture, shock velocities were measured to accurately determine the conditions behind the shock waves. Using the conservation relations for mass, momentum, and energy, T_2 and P_2 are readily calculated from P_1, T_1, the shock velocity, and the heat capacity of the test gas. The theory and use of the shock tube has been adequately treated and will not be repeated here.[8,9]

Shock Velocity

Shock velocities are determined from measurements of shock transit time between two velocity stations using thin film platinum gauges to sense shock passage.[10,11] The gauges are located 375 and 750 mm upstream of the windows. Narrow films of Hanovia bright platinum No. 5 were painted and fired on glass blanks between hermetically sealed electrical contacts in the surface. The gauges were sealed flush with the shock tube wall. The films, about 1 mm wide and 5 mm long, had resistances of about 70 ohms. A constant current of about 40 ma was passed through the film. On shock passage over the film the temperature and resistance increase and fast rise outputs of a few millivolts are amplified 1000× and used to start and stop a Berkeley model 7260 microsecond time interval meter. Shock velocities over the 375-mm interval can be measured with a $\frac{1}{2}$% accuracy corresponding to about a 1% uncertainty in the temperature behind the shock.

Optical System

The spectrophotometer system for absorption measurements behind the shock waves is drawn in Fig. 1. The drawing attempts to show a plan view. Light from the globar source is focused via mirrors M_{1-3} on the slits of a high-speed chopper in a protective aluminum housing. The chopper is used to modulate the transmitted beam at about 50 kc/sec so as to allow absorption measurements in the presence of emission from the hot carbon dioxide. The sector wheel, 4 in. in diam with 120 slots 1 mm wide and 1 cm deep, is made of a high-tensile aluminum alloy. The wheel is driven in a horizontal plane at about 25 000 rpm by an air motor (Onsrud, $\frac{1}{2}$ hp). Helium is flushed through the chopper housing to reduce air drag which would slow the chopper to about 14 000 rpm.

Mirror M_3 passes the beam down through the sector wheel to M_4 below the wheel. The slits on the sector are imaged at the center of the shock tube via M_{4-7}. Vertical slits, 2 mm wide, on the shock-tube windows limit the beam width and time resolution behind the shocks. The transmitted light along with the emitted light is brought to focus via M_{8-10} on the inlet slit of a Perkin-Elmer model 98 monochromator with a CaF_2 prism. The output from the monochromator is focused on the detector via M_{11-12}. The detector is a Texas Instrument M-2035 indium atimonide photovoltaic cell, sealed in a Dewar for operation at −195°C. The cell has an active area of 0.0177 cm², a noise equivalent input of 1.3×10^{-9} w/cm², with a maximum time constant of 0.2 μsec. The detector linearity was checked up to flux densities of 2 mw/cm² which includes the range used in the study. The amplitude of the modulated signal was independent of chopping rate up to the maximum of 50 kc, indicating that the response time of the detector was adequate for the study.

A toroidal transformer having a band pass from 10 kc to 1 Mc is used to amplify the 50-kc modulated signal and suppress the relatively slowly varying thermal-emission signal. The output from the transformer is amplified (100×) with a Tektronix 121 amplifier and displayed on a Tektronix 545 oscilloscope. Traces are recorded with a DuMont 2620 oscilloscope camera. The amplified output of one of the velocity gauges triggers a time delay in the oscilloscope. The delay is set to start the sweep a short time before shock arrival at the window so as to allow transmission measurements slightly before shock compression.

RESULTS

The object of the study was to obtain absorption coefficients of CO_2 at high temperatures which could then be used to monitor CO_2 concentrations behind shock waves. Some absorption measurements were made on cold CO_2 (5% CO_2 in N_2) at 4.26 μ in the shock tube. With no CO_2 in the shock tube and a spectral slit width of 0.054 μ, atmospheric CO_2 absorption attenuated source intensity by 75%. Taking a value of 0.026% for the atmospheric CO_2 concentration[12] the optical

[8] E. L. Resler, S. C. Lin, and A. Kantrowitz, J. Appl. Phys. **23**, 1390 (1952).

[9] S. S. Penner, F. Harshbarger, and V. Vali, in *Combustion Researches and Reviews* (Butterworths Scientific Publications, Ltd., London, 1957), p. 134.

[10] A. J. Chabai and R. J. Emrich, J. Appl. Phys. **26**, 779 (1955).

[11] J. Rabinowicz, M. E. Jessey, and C. A. Bartsch, J. Appl. Phys. **27**, 97 (1956).

[12] R. M. Goody, *The Physics of the Stratosphere* (Cambridge University Press, New York, 1954).

density of CO_2 in the 300-cm optical path external to the shock tube was about 0.078 atm cm. Measurements of absorption at room temperature by total optical depths up to 0.25 atm cm in the tube plus atmosphere showed departures from a linear Beers law plot below 0.078 atm cm. At elevated temperatures the 4.3 μ band extends to longer wavelengths. In order to avoid the complication introduced by atmospheric CO_2 absorption measurements were initiated at 4.40 μ just outside of the atmospheric absorption band.

The absorption of CO_2 at 4.40 μ was determined over a temperature range of 1200 to 2100°K for CO_2 partial pressures of 10 to 40 mm Hg behind the shocks. A 5% mixture of CO_2 in N_2 was used for the study. The absorption path through the shock tube is 7.62 cm. The optical densities varied from 0.10 to 0.40 atm cm with total pressures ranging from 0.26 to 1.05 atm. The monochromator slit width was 0.5 mm corresponding to a spectral slit width of 0.054 μ. Figure 2 is a typical oscilloscope trace. The amplitude of the modulated signal is proportional to the transmitted intensity. The bottom envelope of the trace would be a measure of the emission intensity from the hot gas were it not for the toroidal transformer. The amplitude of the modulated signal before shock compression is a measure of the incident intensity I_0 since cold CO_2 in the tube or atmosphere does not absorb at 4.40 μ. The amplitude after shock compression is a measure of the transmitted intensity I. On shock arrival at the window section the CO_2 is heated and the amplitude decreased to a new level. The constancy of the transmitted intensity behind the shock is evidence for the attainment of equilibrium.

Some shocks were passed through nitrogen and air to check for 4.40-μ absorption by possible impurities in the hot shocked gas. The transmission signal remained unchanged on shock passage. The possible effect of the heated sector wheel contributing to the modulation of the transmission signal was also checked. The light from the globar was suddenly interrupted and the amplitude of the modulated transmission signal went to zero.

Absorption was determined as a function of CO_2 pressure at several temperatures. As it was not possible to produce repeatedly a given temperature behind the shock waves, a spread of as much as ± 25°K was obtained in some of the series about the central temperature. The results were examined by plotting $\ln I_0/I$ against CO_2 partial pressures in the hot shocked gas. Some representative plots are given in Fig. 3. The data in all cases is fit by straight lines through the origin indicating the applicability of Beer's law,

$$I = I_0 \exp(-kpL),$$

where k is the average absorption coefficient over the spectral slit width in atm^{-1} cm^{-1}, p the CO_2 partial pressure in atmospheres, and L the path length (7.62 cm). The absorption coefficients along with their standard deviations σ_k, obtained by a least-square treatment of the data, are given in Table I.

The variation of absorption coefficient with temperature is shown in Fig. 4. The variation of absorption with wavelength was determined at $1220° \pm 30$°K over the range from 4.37 to 4.46 μ (Fig. 5). The absorption

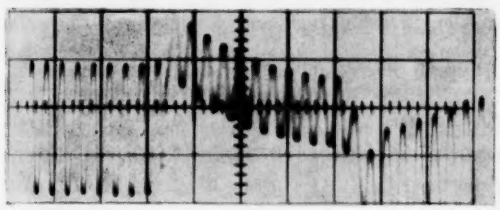

FIG. 2. Oscilloscope trace of transmitted intensity. Shock velocity = 1.96 mm/μsec through 5.0% mixture of CO_2 in N_2. $P_1 = 16.0$ mm Hg, $P_2 = 576$ mm Hg, $T_2 = 1880$°K. Sweep time = 50 μsec/cm.

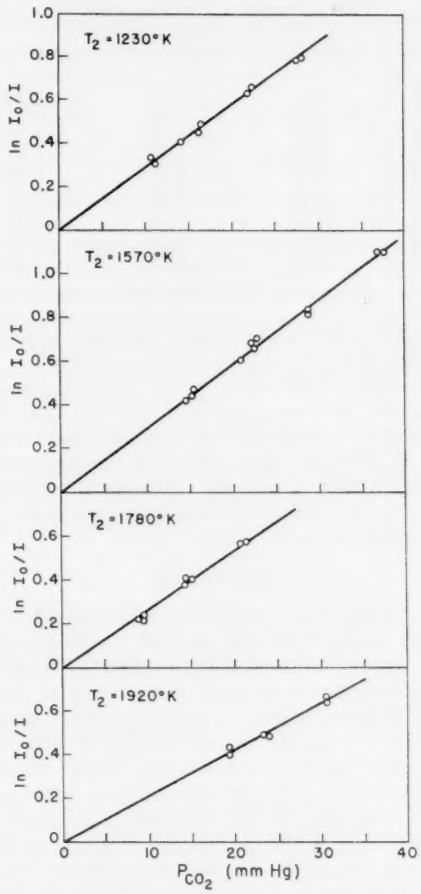

FIG. 3. Beer's law plots for CO_2 absorption at 4.40 μ and $T_2 =$ 1230, 1570, 1780, and 1920°K.

TABLE I. Absorption coefficients of hot CO_2.

T_2(°K)	ΔT_2(°K)	k(atm^{-1} cm^{-1})	σ_k(atm^{-1} cm^{-1})
1230	±8	2.91	0.09
1435	±15	3.06	0.17
1530	±10	2.92	0.08
1535	±15	2.80	0.07
1570	±10	2.98	0.10
1780	±23	2.73	0.16
1905	±30	2.41	0.10
1920	±10	2.27	0.06
2060	±20	2.14	0.05
2065	±35	2.19	0.09

coefficient at 4.37 μ is essentially the same as at 4.40 μ and then decreases with increasing wavelength.

The effect of slit width on the apparent absorption coefficients was determined at 4.40 μ and 1520±20°K for an optical density of 0.28 atm cm. The results are listed in Table II. The decrease in the calculated absorption coefficient with the 1.00-mm slit is consistent with the variation of the absorption coefficient with wavelength shown in Fig. 5.

DISCUSSION

The absorption coefficients reported above are average values over the spectral bandwidth. From Table II it can be seen that absorption coefficient measurements at 4.40 μ are independent of spectral slit width below 0.054 μ. At the temperatures employed here there is considerable overlapping of lines in the CO_2 vibrational-rotational spectrum. Neill[13] found the absorption of continuum radiation by hot CO_2 at 2000°K was approximately the same as the absorption of radiation from CO_2 at the same temperature as the absorbing sample. Tourin and Henry report that the 4.40-μ absorption by 1.67 atm cm of CO_2 at 1273°K and a total pressure of 100 mm Hg is essentially independent of spectral slit width from 0.008 to 0.021 μ.[6] They further show the 4.40-μ absorption by 0.84 atm cm of CO_2 at 1273°K is approximately independent of total pressure above 0.2 atm. Thus it appears that the spectral absorption coefficient of hot CO_2 is a slowly varying function of wavelength and may be approximated at 4.40 μ by the average values reported here.

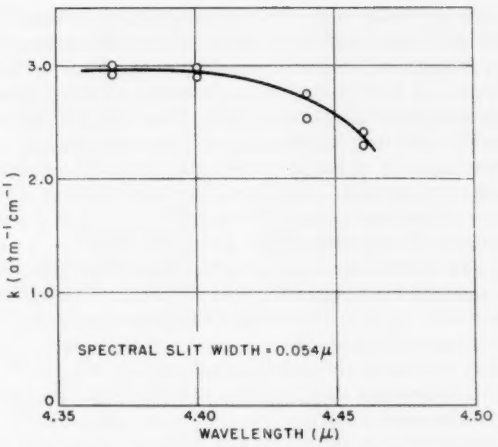

FIG. 5. Absorption coefficients of CO_2 at 1220°K.

There are few data with which the present results can be directly compared. Tourin measured the absorption of CO_2 in a furnace from 300 to 1273°K.[5,6] He obtained a coefficient of about 1.0 atm^{-1} cm^{-1} from a Beers law plot for 4.40-μ absorption at 1273°K which compares with a value of 2.9 atm^{-1} cm^{-1} in the present study. Tourin worked at densities above 0.8 atm cm. However, this does not account for the discrepancy between the measurements. In the present study the temperature and density are constant along the optical path except for a cool thin boundary layer on the shock tube wall and windows. Under the conditions of the study the boundary layer is less than 0.12 cm thick,[14] small compared with the 7.62-cm path through the tube. The temperature profile in the furnace measurements was not reported. The experimental system and procedure in the current study has been carefully reexamined and measurements have been repeated under various conditions that might conceivably account for the discrepancy. Checks of test gas purity, possible leaks, stray light, detector linearity, wavelength calibration, and possible errors in deter-

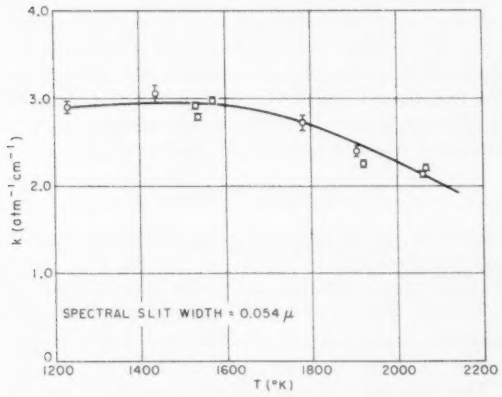

FIG. 4. Absorption coefficients of hot CO_2 at 4.40 μ.

TABLE II. Effect of slit width on absorption measurements.

Slit width (mm)	0.3	0.5	1.00
Spectral slit width (μ)	0.033	0.054	0.105
k(atm^{-1} cm^{-1})	2.86±.02	2.89±.07	2.72±.04

[13] H. W. Neill, J. Opt. Soc. Am. **49**, 505 (1959).

[14] H. Mirels, National Advisory Committee for Aeronautics, Report TN-3712, May, 1956.

mination of temperature and density all confirm the present data.

Plass[15] has recently calculated the spectral emissivity of CO_2 over the 4.3-μ band from 300° to 2400°K. The conditions of the present study correspond to his weak line approximation[16] in which

$$\epsilon = 1 - \exp(-Su/d),$$

where ϵ is the spectral emissivity, S is the line strength, d is the line spacing, and $u = pL$ is the optical density. Thus we see that $S/d = k$. Experimental and theoretical absorption coefficients are listed in Table III.

Plass' calculated value for S/d is in good agreement with the experimental data at 1200°K. He also predicts a maximum in the 4.40-μ absorption at about 1400°K which is confirmed by the experimental results. However, the calculated values of S/d fall off rapidly with increasing temperature above 1400°K and there is poor agreement between the experimental and theoretical results at 1800°K. Plass used the harmonic oscillator approximation to find the electric moment matrix elements necessary for the calculation of line strengths. The validity of the approximation decreases with increasing temperature and population of higher vibrational states.

TABLE III. Comparison of experimental and theoretical absorption coefficients at 4.40 μ.

T(°K)	k atm^{-1} cm^{-1}	S/d atm^{-1} cm^{-1}
1200	2.90	2.50
1800	2.70	0.56

[15] G. N. Plass, J. Opt. Soc. Am. **49**, 821 (1959).
[16] G. N. Plass, J. Opt. Soc. Am. **50**, 868 (1960).

ACKNOWLEDGMENTS

The authors wish to acknowledge the assistance of David Gast in the study, and thank Dr. G. N. Plass for his helpful comments.

THE JOURNAL OF CHEMICAL PHYSICS VOLUME 34, NUMBER 4 APRIL, 1961

Reflectance Spectra of Terbium Oxides in the Range Tb_2O_3 to Tb_4O_7†

F. VRATNY*

Department of Chemistry, Purdue University, West Lafayette, Indiana

(Received October 3, 1960)

The diffuse reflectance spectra of terbium oxides (TbO_x) have been studied in the composition range $1.5 \leqslant x \leqslant 1.75$ from 300 to 1500 mμ. An ultraviolet cutoff was observed at about 325 mμ. A general decrease in reflectance was observed for an increase in the oxygen to metal ratio. A band was also noted in the 380 to 400-mμ region.

THE reflectance spectra of terbium oxides have been studied as part of a general program involving the nonstoichiometric properties of metallic oxides. A previous paper in the series[1] has considered the spectra of the praseodymium oxide system, PrO_x in the composition range $1.5 \leq x \leq 1.83$. In the present investigation, information is presented for the terbium oxide system TbO_x, where x may be in the composition range $1.50 \leq x \leq 1.75$. This oxide system has received very little attention; however, it may be speculated by comparison to the praseodymium oxide system that these oxides may exhibit rather interesting solid-state properties.

EXPERIMENTAL

The terbium oxide used in this study was obtained from the Lindsay Chemical Company and had a purity of greater than 99.9%. The nonstoichiometric compositions were prepared by heating Tb_4O_7 under various conditions of pressure, temperature, and time. The composition $TbO_{1.75}$ (Tb_4O_7) was obtained by the air oxidation of terbia. The sample was heated to 750°C for 1 hr and then cooled slowly to room temperature. The composition $TbO_{1.53}$ was obtained at a temperature of 800°C and a pressure of $\sim 1 \times 10^{-2}$ mm Hg within a 15-min period. The lower oxides were obtained within periods of $\frac{1}{2}$ to 20 hr at a pressure of $\sim 1 \times 10^{-5}$ mm Hg and a temperature of 980°C. The sesquioxide $TbO_{1.50}$ was obtained by reduction in hydrogen at 980°C. In all cases, the final composition was established by means of a previously described technique.[2] The compositions thus obtained are accurate for the lower oxides to about 0.002 stoichiometric units, and to about 0.005 for the higher oxides. In general, the method of sample preparation should preclude the possibility of large inhomogeneities within the oxide

* Present address: Bell Telephone Laboratories, Murray Hill, New Jersey.

† This work was supported by the Lincoln Laboratories, an organization of the Massachusetts Institute of Technology, with the joint support of the Army, Navy, and Air Force.

[1] F. Vratny, J. Inorg. & Nuclear Chem. (to be published).

[2] F. Vratny, Anal. Chim. Acta **21**, 579–83 (1959); Anal. Chim. Acta, (to be published, 1961).

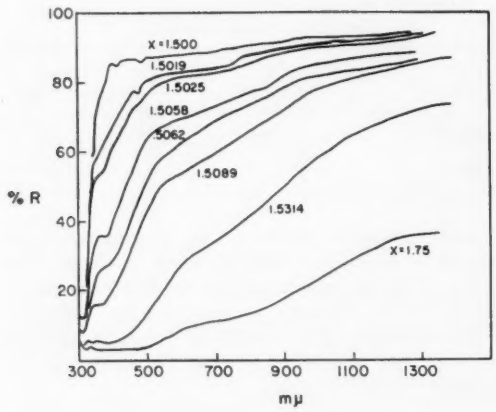

FIG. 1. Reflectance spectra of TbO_x in the region 300 to 1500 mμ, ordinate: mμ, abscissa: % R.

sample. However, microscopic composition variation could exist in excess of the above figures of accuracy.

The powdered samples, as obtained from the preparation were immediately pressed in aluminum planchets and the spectra observed by means of a Beckman DU spectrophotometer with a reflectance attachment. The intensities were referred to magnesium carbonate U.S.P. as a reference standard. A photomultiplier tube was used in the visible region of the spectrum. The measurement technique has otherwise been previously described.[3] From previous experience it is felt that the reflectance intensities are accurate to about 1%.[3,4]

RESULTS AND DISCUSSION

The reflectance spectra of the terbium oxides are reproduced in Figs. 1 and 2. From these figures, it may be seen that terbia exhibits a rather pronounced ultraviolet cutoff at 320 mμ. A reflectance band is also evident at ~380 mμ, with lesser bands at 410 and 480 mμ. Further, the reflectance of terbia decreases most rapidly in the composition range $TbO_{1.5}$ to $TbO_{1.53}$ and then declines until the stable phase $TbO_{1.75}$ is reached, see Fig. 3. This change is most apparent in the lower-wavelength region. It should also be noted that the spectra of terbia may be analyzed in terms of segments having a discrete slope. The most pronounced, as mentioned above, is the extremely sharp ultraviolet cutoff at ~380 mμ. The next slope occurs in the region from 400 to 600 mμ with yet another slope in the region from 600 to 1100 mμ. The latter family of slopes breaks up into two slopes for the higher oxide $TbO_{1.75}$.

In the reflectance spectra of single crystals, it is possible to employ this type of information to obtain the variation of n and k as a function of the wavelength. This may be accomplished if one realizes that if $|R|^{\frac{1}{2}}$, the absolute value of the square root of the reflected intensity, and θ the phase of the intensity, are known as a function of the frequency, then n and k may be obtained.[5] Due to the Kramers-Kronig relation, one can obtain r, the complex amplitude of reflection, from the absolute value of the reflectance amplitude $|r|$, and θ the phase.[6] The phase θ can be obtained from a knowledge of $|r|$ as a function of frequency.[6,7]

For powdered samples, however, a number of difficulties are encountered in using this type of approach

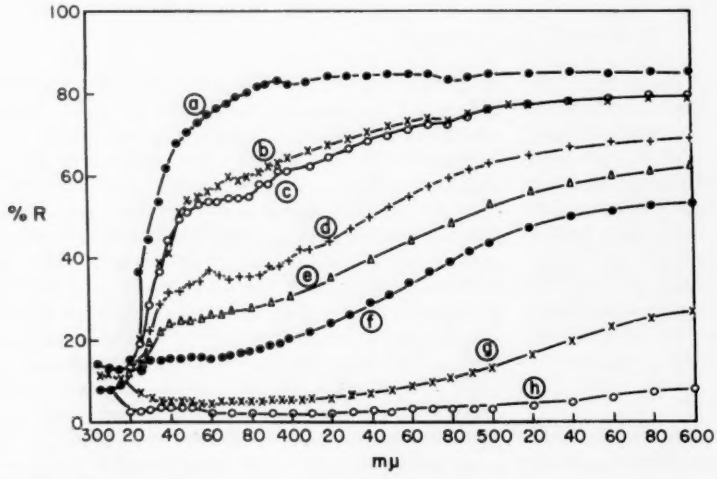

FIG. 2. Reflectance spectra of TbO_x in the region 300 to 600 mμ, ordinate: mμ, abscissa: % R. X in TbO_x (a) 1.500, (b) 1.5019, (c) 1.5025, (d) 1.5058, (e) 1.5062, (f) 1.5089, (g) 1.5314, (h) 1.75.

[3] R. B. Fisher and F. Vratny, Anal. Chim. Acta **13**, 588 (1955).
[4] "Spectrophotometry, 200 to 2000 mμ," Natl. Bur. Standards (U. S.) Circ. No. 484.
[5] T. S. Moss, *Optical Properties of Semiconductors* (Butterworths Scientific Publications, Ltd., London, 1959), p. 25.
[6] F. C. Johoda, Phys. Rev. **107**, 1261 (1957).
[7] H. W. Bode, *Network Analysis and Feedback Amplifier Design* (D. Van Nostrand Company, Inc., Princeton, New Jersey, 1957), Chap. 15.

to obtain n and k. A number of these difficulties are discussed by Johnson[8] who found that n and k are interdependent functions of the particle size of the powder. In a limited range he was able to analytically obtain k if R, n and d, the diameter of the particle were known. Although the data presented here are not directly amenable to this type of interpretation in terms of n and k, it is possible to indicate as a result of the above type of analysis the approximate positions of maxima in k. Such maxima will occur on the low-wavelength side, or slightly before the center of a given line segment. The exact position is dependent upon the phase contribution from other regions of the spectrum. In general, the greater the slope, the smaller the relative contribution from other regions of the spectrum and thus, the nearer the maximum in k will appear at the midpoint of the slope segment. The data presented below are based on this midpoint approximation.

In Fig. 4, data are presented for the change in energy at the midpoint of a given slope segment as a function of composition of TbO_x. It is to be noted that the ultraviolet cutoff in the 325-mμ region remained constant within experimental limits of 3.74 ± 0.01 ev throughout the composition range up to $TbO_{1.53}$. At a composition of $TbO_{1.53}$ the slope segment was no longer noted.

The second line segment (Band II) in the 400–600 mμ region was observed to have a changing midpoint with composition from about 3.4 to 2.2 ev. For the composition $TbO_{1.75}$, this band was nearly unobservable. The third line segment (Band III) found in the 600- to 1100-mμ region was noted to change regularly from 1.8 to 1.4 ev for the composition progression $TbO_{1.5}$ to $TbO_{1.75}$. For the higher oxide, $TbO_{1.75}$ it was found that this segment consisted of two discrete slopes

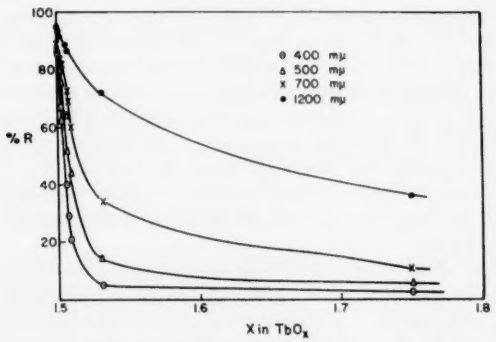

FIG. 3. Change in the reflectance of TbO_x at various wavelengths: ○−400 mμ, Δ−500 mμ, ×−700 mμ, ●−1200 mμ, ordinate: X in TbO_x, abscissa: % R.

[8] P. D. Johnson, J. Opt. Soc. Am. **42**, 978 (1952).

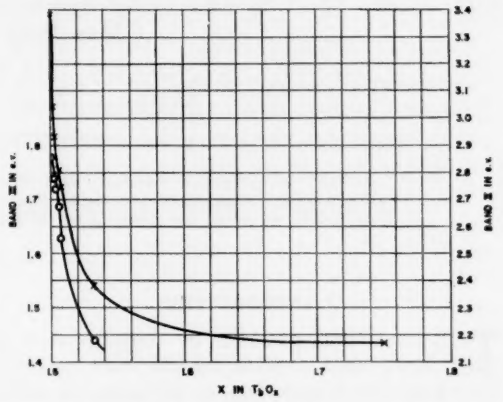

FIG. 4. Change in the position of k maximum (midpoint approximation) as a function of composition Band II (400–600 mμ), and Band III (600–1100 mμ). Ordinate: X in TbO_x, abscissa: left−position of Band III in ev; right−position of Band II in ev; × for Band II, ○ for Band III.

with a k maximum at ~1.63 and 1.17 ev, respectively. The lower energy spectrum was not investigated.

Although conclusive x-ray data are not available for the terbium oxide system, it has been reported that reduction of terbia in an atmosphere of hydrogen leads to cubic terbium sesquioxide.[9] The similarity of terbia to the praseodymium oxide system would lead one to speculate on the structural properties of terbia on the basis of that of praseodymia. In this regard, it should be noted that both a cubic and a hexagonal sesquioxide exist at room temperature. Further, a pronounced phase change occurs at the composition $PrO_{1.53}$ and must result in a significant alteration in the band structure of the oxide. The similarity is most evident in the spectra of the two oxides which exhibit an extreme alteration in the spectral characteristics in this composition range.

A number of significant dissimilarities are to be noted between the two oxide systems; inner electron transitions are most prominent in praseodymia and are not observed in terbia. Terbia does not seem to exhibit low energy band characteristics as does praseodymia which exhibits a reflectance band at ~1 ev. Finally, the alteration in the maxima in k in terbia appears to progress from higher to lower energy as a function of increasing oxygen stoichiometry with an energy gap of ~3.74 ev for the sesquioxide, and changing interband transitions for the nonstoichiometric compositions. This picture is further complicated for the higher oxide $TbO_{1.75}$ with the occurrence of additional bands at ~1.63 and 1.17 ev.

[9] D. M. Gruen, W. C. Koehler, and J. J. Katz, J. Am. Chem. Soc. **73**, 1475 (1951).

Cubic-Field Splitting and Cubic-Symmetry Orthonormal Sets of Wave Functions for J Manifolds (J Half-Integer)

R. PAPPALARDO

Bell Telephone Laboratories, Inc., Murray Hill, New Jersey

(Received October 21, 1960)

Energy level splittings of manifolds characterized by half-integer values of J have been derived in the case of a cubic crystal potential containing fourth- and sixth-order terms. Orthonormal sets of wave functions in cubic symmetry are tabulated for the same manifolds.

1. INTRODUCTION

THE absorption spectrum of single crystals of yttrium gallium garnet doped with erbium has been studied at room temperature, at 78°K, and at 4.2°K. This material is suitable for maser operation in the 7-mm region. The experimental results and the discussion of the spectrum will be reported soon. In general, a good agreement was found between the predicted position of the multiplet components of the free ion and the experimental position of the various groups of lines. In particular, the $^4I_{13/12}$ multiplet component predicted by Wybourne[1] at 6775 cm^{-1} (and never reported before, as far as we know) has been found centered at 6700 cm^{-1}.

In order to interpret the fine structure of each multiplet component of Er^{3+}, we calculated the splitting of the various J manifolds (J half-integer) due to a crystalline potential of cubic symmetry and containing fourth- and sixth-order terms in the f-electron coordinates. Crystal field mixing of levels with different J has been neglected in the present calculation.

2. OUTLINES OF CALCULATIONS

(a) The axial matrix elements of the crystal potential have been tabulated by Stevens,[2] using the formalism of the operator equivalents. The matrix element of the nonaxial component of the crystal potential can be obtained using Wigner's three-vector product formula.[3] A correlation between the results of the two different methods can be obtained evaluating some of the matrix elements using both methods.[4] The relevant secular equations for J manifolds ($J=15/2$ to $J=5/2$) have been constructed and can be solved analytically without too much toil. From Bethe's work[5] one knows the degeneracy of the roots of the secular equations to be expected for the various manifolds. This gives a good check on the correctness of the results obtained besides the obvious check of the diagonal-sum rule. Furthermore the results of the analytical solution of the various secular equations have been checked constructing appropriate orthonormal bases (in cubic symmetry) for the various J manifolds and evaluating directly the crystal field splittings using these "zero-order" wave functions.

(b) In the absence of strong crystal-field mixing of levels with different J, orthonormal sets of wave functions labeled by J and transforming according to the double-valued representations of the cubic group, can be obtained using suitable transformation matrices. The coefficients of such matrices are given by[6]

$$D^{(J)}(\{\alpha\beta\gamma\})_{M'M} = \sum_{\chi}(-1)^{\chi}\frac{[(J+M)!(J-M)!(J+M')!(J-M')!]^{\frac{1}{2}}}{(J-M'-\chi)!(J+M-\chi)!\chi!(\chi+M'-M)!} \times e^{iM'\alpha}\cos^{2J+M-M'-2\chi}\tfrac{1}{2}\beta\sin^{2\chi+M'-M}\tfrac{1}{2}\beta e^{iM\gamma}, \quad (1)$$

where α, β, and γ are the three Euler angles defining each cubic group operation. In the derivation of this formula Wigner[3] uses a left-hand coordinate system and Euler angles characterizing rotations around the Z, X', Z'' axes. A modification of this formula for the choice of a right-handed coordinate system and for the rotational sequence Z, Y', Z'' is given, e.g., by Rose.[7] One can easily prove that in the particular case of cubic symmetry and for double-valued representations, the results obtained for the appropriate linear combinations of ψ_{J,M_J} functions [Table VI(b) and following tables] are identical, either using a left-handed coordinate system and the rotational sequence Z, X', Z'' or using the right-handed coordinate system, both with the choice of rotations Z, X', Z'' or with the sequence Z, Y', Z''.

(c) Analogous sets of wave functions for J manifolds, (J integer), have been given by Satten and Margolis.[8] When a given J manifold contains a certain representation Γ_i of the cubic group only once, then the basis wave functions obtained will have universal validity, because they simply depend on the transformation

[1] R. G. Wybourne, J. Chem. Phys. **32**, 573 (1960).
[2] K. W. H. Stevens, Proc. Phys. Soc. (London) **A65**, 209 (1952).
[3] B. L. Van der Waerden, *Gruppentheoretischen Methode in der Quantenmechanik S. 70* (Springer-Verlag, Berlin, 1932).
[4] R. Pappalardo and D. L. Wood, J. Chem. Phys. **33**, 1734 (1960).
[4] R. Pappalardo and D. L. Wood, J. Chem. Phys. **33**, 1734 (1960).
[5] H. Bethe, Ann. Physik **3**, 133 (1929).
[6] E. Wigner, *Gruppentheorie und ihre Anwendung auf die Quantenmechanik der Atomspektren* (Friedrich Vieweg und Sohn, Brauschweig, Germany, 1931).
[7] M. E. Rose, *Elementary Theory of Angular Momentum* (John Wiley & Sons, Inc., New York, 1957).
[8] R. A. Satten and J. S. Margolis, J. Chem. Phys. **32**, 573 (1960).

TABLE I. Matrix elements of the cubic potential (3) for a $J=15/2$ manifold.

$\langle \pm 15/2 \mid V_4^0+V_6^0 \mid \pm 15/2\rangle = 273\lambda_{15/2}+65\mu_{15/2}$

$\langle \pm 13/2 \mid V_4^0+V_6^0 \mid \pm 13/2\rangle = -91\lambda_{15/2}-117\mu_{15/2}$

$\langle \pm 11/2 \mid V_4^0+V_6^0 \mid \pm 11/2\rangle = -221\lambda_{15/2}-39\mu_{15/2}$

$\langle \pm 9/2 \mid V_4^0+V_6^0 \mid \pm 9/2\rangle = -201\lambda_{15/2}+59\mu_{15/2}$

$\langle \pm 7/2 \mid V_4^0+V_6^0 \mid \pm 7/2\rangle = -101\lambda_{15/2}+76\mu_{15/2}$

$\langle \pm 5/2 \mid V_4^0+V_6^0 \mid \pm 5/2\rangle = 23\lambda_{15/2}+45\mu_{15/2}$

$\langle \pm 3/2 \mid V_4^0+V_6^0 \mid \pm 3/2\rangle = 129\lambda_{15/2}-25\mu_{15/2}$

$\langle \pm 1/2 \mid V_4^0+V_6^0 \mid \pm 1/2\rangle = 189\lambda_{15/2}-75\mu_{15/2}$

$\lambda_{15/2}=60[(7/18)(Ze^2\alpha_s/R^5)]\beta_{15/2}\langle r^4\rangle$

$\mu_{15/2}=13860(Ze^2\alpha_s'/9R^7)\gamma_{15/2}\langle r^6\rangle$

$\langle \pm 15/2 \mid V_4^{\pm 4}+V_6^{\pm 4} \mid \pm 7/2\rangle = (7\times 13\times 15)^{\frac{1}{2}}(\lambda_{15/2}-5\mu_{15/2}$

$\langle \pm 13/2 \mid V_4^{\pm 4}+V_6^{\pm 4} \mid \pm 5/2\rangle = (7\times 13\times 15)^{\frac{1}{2}}(\lambda_{15/2}-3\mu_{15/2})$

$\langle \pm 11/2 \mid V_4^{\pm 4}+V_6^{\pm 4} \mid \pm 3/2\rangle = (11\times 39)^{\frac{1}{2}}(5\lambda_{15/2}-7\mu_{15/2})$

$\langle \pm 9/2 \mid V_4^{\pm 4}+V_6^{\pm 4} \mid \pm 1/2\rangle = (77)^{\frac{1}{2}}(15\lambda_{15/2}-3\mu_{15/2})$

$\langle \pm 7/2 \mid V_4^{\pm 4}+V_6^{\pm 4} \mid \mp 1/2\rangle = (3\times 77)^{\frac{1}{2}}(10\lambda_{15/2}+6\mu_{15/2})$

$\langle \pm 5/2 \mid V_4^{\pm 4}+V_6^{\pm 4} \mid \mp 3/2\rangle = (15)^{\frac{1}{2}}(42\lambda_{15/2}+42\mu_{15/2})$

In the particular case of $Er^{3+}(^4I_{15/2})$ and for $L-S$ coupling,[a]

$$\beta_{15/2}=2/(11\times 15\times 273)=0.445\cdot 10^{-4}$$

$$\gamma_{15/2}=8/(7\times 9\times 121\times 169)=0.621\cdot 10^{-5}$$

[a] See footnote 2.

TABLE II. Matrix elements of the cubic potential (3) for a $J=13/2$ manifold.

$\langle \pm 13/2 \mid V_4^0+V_6^0 \mid \pm 13/2\rangle = 143\lambda_{13/2}+143\mu_{13/2}$

$\langle \pm 11/2 \mid V_4^0+V_6^0 \mid \pm 11/2\rangle = -77\lambda_{13/2}-319\mu_{13/2}$

$\langle \pm 9/2 \mid V_4^0+V_6^0 \mid \pm 9/2\rangle = -132\lambda_{13/2}-11\mu_{13/2}$

$\langle \pm 7/2 \mid V_4^0+V_6^0 \mid \pm 7/2\rangle = -92\lambda_{13/2}+227\mu_{13/2}$

$\langle \pm 5/2 \mid V_4^0+V_6^0 \mid \pm 5/2\rangle = -13\lambda_{13/2}+185\mu_{13/2}$

$\langle \pm 3/2 \mid V_4^0+V_6^0 \mid \pm 3/2\rangle = 63\lambda_{13/2}-25\mu_{13/2}$

$\langle \pm 1/2 \mid V_4^0+V_6^0 \mid \pm 1/2\rangle = 108\lambda_{13/2}-200\mu_{13/2}$

$\lambda_{13/2}=60[(7/18)(Ze^2\alpha_s/R^5)]\beta_{13/2}\langle r^4\rangle$

$\mu_{13/2}=2160(Ze^2\alpha_s'/9R^7)\gamma_{13/2}\langle r^6\rangle$

$\langle \pm 13/2 \mid V_4^{\pm 4}+V_6^{\pm 4} \mid \pm 5/2\rangle = (5\times 11\times 13)^{\frac{1}{2}}(\lambda_{13/2}-21\mu_{13/2})$

$\langle \pm 11/2 \mid V_4^{\pm 4}+V_6^{\pm 4} \mid \pm 3/2\rangle = (11)^{\frac{1}{2}}(15\lambda_{13/2}-161\mu_{13/2})$

$\langle \pm 9/2 \mid V_4^{\pm 4}+V_6^{\pm 4} \mid \pm 1/2\rangle = (22)^{\frac{1}{2}}[15\lambda_{13/2}-(91/2)\mu_{13/2})]$

$\langle \pm 7/2 \mid V_4^{\pm 4}+V_6^{\pm 4} \mid \mp 1/2\rangle = (6)^{\frac{1}{2}}[35\lambda_{13/2}+(147/2)\mu_{13/2}]$

$\langle \pm 5/2 \mid V_4^{\pm 4}+V_6^{\pm 4} \mid \mp 3/2\rangle = (5)^{\frac{1}{2}}(42\lambda_{13/2}+196\mu_{13/2})$

TABLE III. Matrix elements of the cubic potential (3) for a $J=11/2$ manifold.

$\langle \pm 11/2 \mid V_4^0+V_6^0 \mid \pm 11/2\rangle = 66\lambda_{11/2}+22\mu_{11/2}$

$\langle \pm 9/2 \mid V_4^0+V_6^0 \mid \pm 9/2\rangle = -54\lambda_{11/2}-62\mu_{11/2}$

$\langle \pm 7/2 \mid V_4^0+V_6^0 \mid \pm 7/2\rangle = -66\lambda_{11/2}+22\mu_{11/2}$

$\langle \pm 5/2 \mid V_4^0+V_6^0 \mid \pm 5/2\rangle = -26\lambda_{11/2}+50\mu_{11/2}$

$\langle \pm 3/2 \mid V_4^0+V_6^0 \mid \pm 3/2\rangle = 24\lambda_{11/2}+8\mu_{11/2}$

$\langle \pm 1/2 \mid V_4^0+V_6^0 \mid \pm 1/2\rangle = 56\lambda_{11/2}-40\mu_{11/2}$

$\lambda_{11/2}=60[(7/18)(Ze^2\alpha_s/R^5)]\beta_{11/2}\langle r^4\rangle$

$\mu_{11/2}=3780[(1/9)(Ze^2\alpha_s'/R^7)]\gamma_{11/2}\langle r^6\rangle$

$\langle \pm 11/2 \mid V_4^{\pm 4}+V_6^{\pm 4} \mid \pm 3/2\rangle = (11\times 30)^{\frac{1}{2}}(\lambda_{11/2}-7\mu_{11/2})$

$\langle \pm 9/2 \mid V_4^{\pm 4}+V_6^{\pm 4} \mid \pm 1/2\rangle = (42)^{\frac{1}{2}}(5\lambda_{11/2}-13\mu_{11/2})$

$\langle \pm 7/2 \mid V_4^{\pm 4}+V_6^{\pm 4} \mid \mp 1/2\rangle = (210)^{\frac{1}{2}}(3\lambda_{11/2}+\mu_{11/2})$

$\langle \pm 5/2 \mid V_4^{\pm 4}+V_6^{\pm 4} \mid \mp 3/2\rangle = \sqrt{2}\,(35\lambda_{11/2}+63\mu_{11/2})$

properties of the manifold. If this does not happen, the wave functions belonging to the same representations will mix and the modality of mixing will depend on the detailed values of the matrix elements of the crystal potential. In that case, in order to obtain a suitable orthonormal set for the given J manifold, it will be necessary to use standard perturbation calculation methods for degenerate levels. The *reduced secular equation* to be solved is

$$\| H_{ik}-\Delta_{ik}E_i \| = 0, \tag{2}$$

$i, k=1, 2, 3, \cdots, n$ (where n is the number of times a given representation Γ_j is contained in the manifold in question; H_{ik} are the matrix elements of the crystal potential between states defined by the wave functions which transform according to Γ_j; Δ_{ik} are the overlap

TABLE IV. Matrix elements of the cubic potential (3) for a $J=9/2$ manifold.

$\langle \pm 9/2 \mid V_4^0+V_6^0 \mid \pm 9/2\rangle = [(7\times 18)/5]\lambda_{9/2}+24\mu_{9/2}$

$\langle \pm 7/2 \mid V_4^0+V_6^0 \mid \pm 7/2\rangle = -[(7\times 22)/5]\lambda_{9/2}-88\mu_{9/2}$

$\langle \pm 5/2 \mid V_4^0+V_6^0 \mid \pm 5/2\rangle = -[(7\times 17)/5]\lambda_{9/2}+80\mu_{9/2}$

$\langle \pm 3/2 \mid V_4^0+V_6^0 \mid \pm 3/2\rangle = [(3\times 7)/5]\lambda_{9/2}+48\mu_{9/2}$

$\langle \pm 1/2 \mid V_4^0+V_6^0 \mid \pm 1/2\rangle = [(7\times 18)/5]\lambda_{9/2}-64\mu_{9/2}$

$\lambda_{9/2}=60[(7/18)(Ze^2\alpha_s/R^5)]\beta_{9/2}\langle r^4\rangle$

$\mu_{9/2}=630(Ze^2\alpha_s'/9R^7)\gamma_{9/2}\langle r^6\rangle$

$\langle \pm 9/2 \mid V_4^{\pm 4}+V_6^{\pm 4} \mid \pm 1/2\rangle = (14)^{\frac{1}{2}}(3\lambda_{9/2}-60\mu_{9/2})$

$\langle \pm 7/2 \mid V_4^{\pm 4}+V_6^{\pm 4} \mid \mp 1/2\rangle = (14)^{\frac{1}{2}}(5\lambda_{9/2}-12\mu_{9/2})$

$\langle \pm 5/2 \mid V_4^{\pm 4}+V_6^{\pm 4} \mid \mp 3/2\rangle = (21)^{\frac{1}{2}}(5\lambda_{9/2}+32\mu_{9/2})$

TABLE V.[a] Matrix elements of the cubic potential (3) for manifold with $J=7/2$ and $J=5/2$.

$J=7/2$	$J=5/2$
$\langle \pm 7/2 \mid V_4^0+V_6^0 \mid \pm 7/2\rangle = 7\lambda_{7/2}+6\mu_{7/2}$	$\langle \pm 5/2 \mid V_4^0+V_6^0 \mid \pm 5/2\rangle = \lambda_{5/2}$
$\langle \pm 5/2 \mid V_4^0+V_6^0 \mid \pm 5/2\rangle = -13\lambda_{7/2}-30\mu_{7/2}$	$\langle \pm 3/2 \mid V_4^0+V_6^0 \mid \pm 3/2\rangle = -3\lambda_{5/2}$
$\langle \pm 3/2 \mid V_4^0+V_6^0 \mid \pm 3/2\rangle = -3\lambda_{7/2}+54\mu_{7/2}$	$\langle \pm 1/2 \mid V_4^0+V_6^0 \mid \pm 1/2\rangle = 2\lambda_{5/2}$
$\langle \pm 1/2 \mid V_4^0+V_6^0 \mid \pm 1/2\rangle = 9\lambda_{7/2}-30\mu_{7/2}$	$\langle \pm 5/2 \mid V_4^{\pm 4}+V_6^{\pm 4} \mid \mp 3/2\rangle = (5)^{\frac{1}{2}}\lambda_{5/2}$
$\langle \pm 7/2 \mid V_4^{\pm 4}+V_6^{\pm 4} \mid \mp 1/2\rangle = (35)^{\frac{1}{2}}(\lambda_{7/2}-18\mu_{7/2})$	
$\langle \pm 5/2 \mid V_4^{\pm 4}+V_6^{\pm 4} \mid \mp 3/2\rangle = \sqrt{3}(5\lambda_{7/2}+42\mu_{7/2})$	
$\lambda_{7/2}=60[(7/18)(Ze^2\alpha_s/R^5)]\beta_{7/2}\langle r^4\rangle$	$\lambda_{5/2}=60[(7/18)(Ze^2\alpha_s/R^5)]\beta_{5/2}\langle r^4\rangle$
$\mu_{7/2}=210(Ze^2\alpha_s'/9R^7)\gamma_{7/2}\langle r^6\rangle$	$\mu_{5/2}=0$

[a] See also R. Pappalardo and D. L. Wood, J. Chem. Phys. **33**, 1734 (1960).

integrals for these same wave functions and E_i the eigenvalues of the crystal potential. The E_i values obtained from Eq. (2) should coincide with the roots of the $(2J+1)\times(2J+1)$ secular equation. After that the determination of the mixing coefficients is straightforward.

3. CHOICE OF THE CRYSTAL POTENTIAL

The crystal field potential of cubic symmetry for eightfold coordination of point charges (which is the rare-earth ion coordination in the garnets[9] can be written as[4,8,10]

$$V_{\text{cub}}=V_4^0+(V_4^4+V_4^{-4})+V_6^0+(V_6^4+V_6^{-4})$$
$$=V_{\text{cub}}^{(4)}+V_{\text{cub}}^{(6)}, \quad (3)$$

with

$$V_4^0=\sum{}_{1\,8}^{7}\frac{Ze^2\alpha_s}{R^5}[35z^4-30z^2r^2+3r^4] \quad (4)$$

$$V_4^4+V_4^{-4}=\sum{}_{3\,6}^{3\,5}\frac{Ze^2\alpha_s}{R^5}[(x+iy)^4+(x-iy)^4] \quad (5)$$

$$V_6^0=\sum\frac{Ze^2\alpha_s'}{9R^7}[231z^6-315r^2z^2+105r^4z^2-5r^6]$$

$$=\sum 16\frac{Ze^2\alpha_s'}{9R^7}(4\pi/13)^{\frac{1}{2}}Y_6^0r^6 \quad (6)$$

$$V_6^4+V_6^{-4}$$

$$=\sum\frac{Ze^2\alpha_s'}{9R^7}[-\tfrac{21}{2}(11z^2-r^2)\{(x+iy)^4+(x-iy)^4\}]$$

$$=\sum-\frac{Ze^2\alpha_s'}{9R^7}(4\pi/13)^{\frac{1}{2}}8(14)^{\frac{1}{2}}(Y_6^4+Y_6^{-4})r^6, \quad (7)$$

where Ze is the charge on the nearest neighbors, α_s and α_s' are screening constants, R is the distance of the nearest neighbors, and $\sum$ is the sum over the f electrons. The matrix elements of the potential (3) are given in the following tables in terms of the splitting factors λ_J and μ_J, which are related, via multiplicative constants, to the Stevens-Judd[2,11] operators β_J and γ_J (or $\langle SLJ\,||\beta||\,SLJ\rangle$ and $\langle SLJ\,||\gamma||\,SLJ\rangle$). These operator equivalents are the transformation coefficients from the $LSJM_J$ scheme to the "zero-order" scheme nlm_lm_s and are accordingly the only quantities affected by any breakdown of the $L-S$ coupling. Their detailed values will depend on the *parentage* of the particular J manifold considered. In particular, in Russell-Saunders coupling, if the values of the Stevens-Judd operator equivalents are known for a given value of J, then the corresponding values pertaining to the remaining components J' of the same multiplet can be

[9] S. Geller and M. A. Gilleo, J. Chem. Phys. Solids **3**, 30 (1957); Phys. Rev. **110**, 73 (1958).

[10] W. Low, Phys. Rev. **109**, 265 (1959).

[11] B. R. Judd, Proc. Roy. Soc. (London) **A241**, 414 (1957); J. P. Elliott, B. R. Judd, and W. A. Runciman, *ibid.* **A240**, 509 (1957).

TABLE VI(a). An orthonormal set of "zero-order" wave functions for a cubic-symmetry potential is given by the following linear combinations of wave functions $\psi_{J,MJ}$ belonging to the $J=15/2$ manifold. See text for relative phase of Γ_a and Γ_b (also Γ_c and Γ_d).

$$\Gamma_6: \quad \begin{bmatrix} (1/24)[(13\times15)^{\frac{1}{2}}\psi_{15/2}+3(7)^{\frac{1}{2}}\psi_{7/2}+3(33)^{\frac{1}{2}}\psi_{-1/2}+(21)^{\frac{1}{2}}\psi_{-9/2}] & (\Gamma_{6a}) \\ (1/24)[(13\times15)^{\frac{1}{2}}\psi_{-15/2}+3(7)^{\frac{1}{2}}\psi_{-7/2}+3(33)^{\frac{1}{2}}\psi_{+1/2}+(21)^{\frac{1}{2}}\psi_{9/2}] & (\Gamma_{6b}) \end{bmatrix}$$

$$\Gamma_7: \quad \begin{bmatrix} (1/24)[-(33\times7)^{\frac{1}{2}}\psi_{13/2}-(5\times39)^{\frac{1}{2}}\psi_{5/2}+3(13)^{\frac{1}{2}}\psi_{-3/2}+(33)^{\frac{1}{2}}\psi_{-11/2}] & (\Gamma_{7a}) \\ (1/24)[-(33\times7)^{\frac{1}{2}}\psi_{-13/2}-(5\times39)^{\frac{1}{2}}\psi_{-5/2}+3(13)^{\frac{1}{2}}\psi_{3/2}+(33)^{\frac{1}{2}}\psi_{11/2}] & (\Gamma_{7b}) \end{bmatrix}$$

$$\Gamma_8^{(i)} \ (i=1,2,3): \quad \begin{bmatrix} a_{1i}[-(7/72)^{\frac{1}{2}}\psi_{15/2}+(65/72)^{\frac{1}{2}}\psi_{-9/2}]+a_{2i}[-(21/86)^{\frac{1}{2}}\psi_{13/2}+(65/86)^{\frac{1}{2}}\psi_{7/2}]+a_{3i}[-(33/40)^{\frac{1}{2}}\psi_{7/2}+(7/40)^{\frac{1}{2}}\psi_{-1/2}] & (\Gamma_{8a}) \\ \cdots \text{ same, with } M\rightarrow -M \cdots & (\Gamma_{8b}) \\ b_{1i}[-(11/50)^{\frac{1}{2}}\psi_{-3/2}+(39/50)^{\frac{1}{2}}\psi_{-11/2}]+b_{2i}[(1/8)^{\frac{1}{2}}\psi_{13/2}+(7/8)^{\frac{1}{2}}\psi_{-11/2}]+b_{3i}[(3/8)^{\frac{1}{2}}\psi_{5/2}+(5/8)^{\frac{1}{2}}\psi_{-3/2}] & (\Gamma_{8c}) \\ \cdots \text{ same, with } M\rightarrow -M \cdots & (\Gamma_{8d}) \end{bmatrix}$$

In the particular case of $Er^{3+}(^4I_{15/2})$ the following values of the constants are obtained, for the fourth-order potential (4) and (5):

$a_{11}=-0.1624$	$a_{12}=-1.5351$	$a_{13}=-1.3093$
$a_{21}=0.4881$	$a_{22}=-0.4625$	$a_{23}=0.5012$
$a_{31}=-0.8958$	$a_{32}=0.5136$	$a_{33}=0.8952$
$b_{11}=0.1437$	$b_{12}=-0.3171$	$b_{13}=-0.9249$
$b_{21}=-1.9548$	$b_{22}=2.148$	$b_{23}=-0.8848$
$b_{31}=1.3054$	$b_{32}=-0.2565$	$b_{33}=0.3518$

For the sixth-order component of the potential (6) and (7), one obtains:

$a_{11}=-0.0248$	$a_{12}=1.3291$	$a_{13}=0.4627$
$a_{21}=1.0295$	$a_{22}=-0.464$	$a_{23}=-0.4437$
$a_{31}=-0.0807$	$a_{32}=-0.9225$	$a_{33}=-1.534$
$b_{11}=0.9139$	$b_{12}=-1.1153$	$b_{13}=1.1871$
$b_{21}=-1.9968$	$b_{22}=1.1487$	$b_{23}=-0.5653$
$b_{31}=-0.8518$	$b_{32}=-1.4906$	$b_{33}=-0.1839$

TABLE VI(b). Energy level splitting for $J=15/2$, using the zero-order wave functions of Table VI(a), and the matrix elements of Table I.

$\langle\Gamma_6 \mid V_{cub} \mid \Gamma_6\rangle = 296\lambda_{15/2}-40\mu_{15/2}$	
$\langle\Gamma_7 \mid V_{cub} \mid \Gamma_7\rangle = -26\lambda_{15/2}-312\mu_{15/2}$	
$\langle\Gamma_8^{(1)} \mid V_{cub}^{(4)} \mid \Gamma_8^{(1)}\rangle = 266.26\lambda_{15/2}$	Corresponding coefficients a_{1i} and b_{1i}[a]
$\langle\Gamma_8^{(2)} \mid V_{cub}^{(4)} \mid \Gamma_8^{(2)}\rangle = -141.44\lambda_{15/2}$	Corresponding coefficients a_{2i} and b_{2i}
$\langle\Gamma_8^{(3)} \mid V_{cub}^{(4)} \mid \Gamma_8^{(3)}\rangle = -258.86\lambda_{15/2}$	Corresponding coefficients a_{3i} and b_{3i}
$\langle\Gamma_8^{(1')} \mid V_{cub}^{(6)} \mid \Gamma_8^{(1')}\rangle = 274.15\mu_{15/2}$	Corresponding coefficients a_{1i} and b_{1i}
$\langle\Gamma_8^{(2')} \mid V_{cub}^{(6)} \mid \Gamma_8^{(2')}\rangle = 64.003\mu_{15/2}$	Corresponding coefficients a_{2i} and b_{2i}
$\langle\Gamma_8^{(3')} \mid V_{cub}^{(6)} \mid \Gamma_8^{(3')}\rangle = -162.01\mu_{15/2}$	Corresponding coefficients a_{3i} and b_{3i}

[a] A correlation between the (i) label splittings and the (i') label splittings can only be made on the basis of the similarity of the set of coefficients a_{ki} (and b_{ki}) of Table VI(a).

TABLE VII(a). Orthonormal basis for $J=13/2$ in cubic symmetry. For the Γ_7 and Γ_8 species, linear combinations of the expressions in square brackets must be taken. The values of the coefficients in the particular case of the potential (3) are given.

Γ_6:
$$\begin{bmatrix} \frac{1}{4}[-(11)^{\frac{1}{2}}\psi_{9/2}+\sqrt{2}\psi_{1/2}-\sqrt{3}\psi_{-7/2}] \\ \frac{1}{4}[-(11)^{\frac{1}{2}}\psi_{-9/2}+\sqrt{2}\psi_{-1/2}-\sqrt{3}\psi_{+7/2}] \end{bmatrix}$$

$\Gamma_7^{(1)}$:
$$\begin{bmatrix} a_{11}\{[1/2(43)^{\frac{1}{2}}][-(55)^{\frac{1}{2}}\psi_{13/2}+2(13)^{\frac{1}{2}}\psi_{5/2}+(65)^{\frac{1}{2}}\psi_{-3/2}]\}+a_{12}\{[1/2(31)^{\frac{1}{2}}][-7\psi_{5/2}+2(5)^{\frac{1}{2}}\psi_{-3/2}+(55)^{\frac{1}{2}}\psi_{-11/2}]\} \\ \cdots \text{ same, with } M\rightarrow -M \cdots \end{bmatrix}$$

$\Gamma_7^{(2)}$:
$$\begin{bmatrix} b_{11}\{[1/2(43)^{\frac{1}{2}}][-(55)^{\frac{1}{2}}\psi_{13/2}+2(13)^{\frac{1}{2}}\psi_{5/2}+(65)^{\frac{1}{2}}\psi_{-3/2}]\}+b_{12}\{[1/2(31)^{\frac{1}{2}}][-7\psi_{5/2}+2(5)^{\frac{1}{2}}\psi_{-3/2}+(55)^{\frac{1}{2}}\psi_{-11/2}]\} \\ \cdots \text{ same, with } M\rightarrow -M \cdots \end{bmatrix}$$

$\Gamma_8^{(1)}$:
$$\begin{bmatrix} c_{11}\{[1/(5)^{\frac{1}{2}}][\sqrt{3}\psi_{1/2}+\sqrt{2}\psi_{-7/2}]\}+c_{12}\{[1/(14)^{\frac{1}{2}}](-\sqrt{3}\psi_{9/2}+(11)^{\frac{1}{2}}\psi_{-7/2})\} \\ \cdots \text{ same, with } M\rightarrow -M \cdots \\ d_{11}\{[1/2(53)^{\frac{1}{2}}][(143)^{\frac{1}{2}}\psi_{13/2}+2(5)^{\frac{1}{2}}\psi_{5/2}+7\psi_{-3/2}]\}+d_{12}\{[1/2(5)^{\frac{1}{2}}][(5)^{\frac{1}{2}}\psi_{5/2}-2\psi_{-3/2}+(11)^{\frac{1}{2}}\psi_{-11/2}] \\ \cdots \text{ same, with } M\rightarrow -M \cdots \end{bmatrix}$$

$\Gamma_8^{(2)}$
$$\begin{bmatrix} e_{11}\{[1/(5)^{\frac{1}{2}}][\sqrt{3}\psi_{1/2}+\sqrt{2}\psi_{-7/2}]\}+e_{12}\{[1/(14)^{\frac{1}{2}}][-\sqrt{3}\psi_{9/2}+(11)^{\frac{1}{2}}\psi_{-7/2}]\} \\ \cdots \text{ same, with } M\rightarrow -M \cdots \\ f_{11}\{[1/2(53)^{\frac{1}{2}}][(143)^{\frac{1}{2}}\psi_{13/2}+2(5)^{\frac{1}{2}}\psi_{5/2}+7\psi_{-3/2}]\}+f_{12}\{[1/2(5)^{\frac{1}{2}}][(5)^{\frac{1}{2}}\psi_{5/2}-2\psi_{-3/2}+(11)^{\frac{1}{2}}\psi_{-11/2}]\} \\ \cdots \text{ same, with } M\rightarrow -M \cdots \end{bmatrix}$$

Values of the coefficients for the fourth-order component of the potential (3), namely, $v_{cub}^{(4)} = v_4^0 + v_4^4 + v_4^{-4}$, are given by:

$a_{11}=0.982$	$a_{12}=0.265$
$b_{11}=-0.1668$	$b_{12}=0.97$
$c_{11}=-0.2158$	$c_{12}=1.455$
$d_{11}=0.061$	$d_{12}=-0.9927$
$e_{11}=-1.187$	$e_{12}=0.4868$
$f_{11}=3.1603$	$f_{12}=0.123$

For $V_{cub}^{(6)}$ one has:

$a_{11}=0.392$	$a_{12}=0.9596$
$b_{11}=-0.929$	$b_{12}=0.290$
$c_{11}=-1.0804$	$c_{12}=1.052$
$d_{11}=0.7636$	$d_{12}=0.6942$
$e_{11}=0.5388$	$e_{12}=0.5927$
$f_{11}=-0.6508$	$f_{12}=0.7204$

TABLE VII(b). Energy level splittings for $J=13/2$, using the appropriate "zero-order" set of wave functions.[a]

$$\langle \Gamma_6 \mid V_{\text{cub}} \mid \Gamma_6 \rangle = -162\lambda_{13/2}+80\mu_{13/2}$$
$$\langle \Gamma_7^{(1)} \mid V_{\text{cub}}^{(4)} \mid \Gamma_7^{(1)} \rangle = 125\lambda_{13/2}$$
$$\langle \Gamma_7^{(2)} \mid V_{\text{cub}}^{(4)} \mid \Gamma_7^{(2)} \rangle = -55\lambda_{13/2}$$
$$\langle \Gamma_8^{(1)} \mid V_{\text{cub}}^{(4)} \mid \Gamma_8^{(1)} \rangle = -109\lambda_{13/2}$$
$$\langle \Gamma_8^{(2)} \mid V_{\text{cub}}^{(4)} \mid \Gamma_8^{(2)} \rangle = 155\lambda_{13/2}$$
$$\langle \Gamma_7^{(1')} \mid V_{\text{cub}}^{(6)} \mid \Gamma_7^{(1')} \rangle = -837.87\mu_{13/2}$$
$$\langle \Gamma_7^{(2')} \mid V_{\text{cub}}^{(6)} \mid \Gamma_7^{(2')} \rangle = 885.43\mu_{13/2}$$
$$\langle \Gamma_8^{(1')} \mid V_{\text{cub}}^{(6)} \mid \Gamma_8^{(1')} \rangle = -377.8\mu_{13/2}$$
$$\langle \Gamma_8^{(2')} \mid V_{\text{cub}}^{(6)} \mid \Gamma_8^{(2')} \rangle = 313.8\mu_{13/2}$$

[a] See footnote a of Table VI(b).

TABLE VIII(a). Orthonormal basis for $J=11/2$ in cubic symmetry.

Γ_6:
$$\begin{bmatrix} (1/4\sqrt{3})[(7)^{\frac{1}{2}}\psi_{9/2}-(6)^{\frac{1}{2}}\psi_{+1/2}+(35)^{\frac{1}{2}}\psi_{-7/2} \\ (1/4\sqrt{3})[(7)^{\frac{1}{2}}\psi_{-9/2}-(6)^{\frac{1}{2}}\psi_{-1/2}+(35)^{\frac{1}{2}}\psi_{7/2}] \end{bmatrix}$$

Γ_7:
$$\begin{bmatrix} (1/4\sqrt{3})[-(15)^{\frac{1}{2}}\psi_{11/2}+(22)^{\frac{1}{2}}\psi_{3/2}+(11)^{\frac{1}{2}}\psi_{-5/2}] \\ \cdots M\rightarrow -M \cdots \end{bmatrix}$$

$\Gamma_8^{(1)}$:
$$\begin{bmatrix} a_{11}\{(1/\sqrt{3})[-\psi_{3/2}+\sqrt{2}\psi_{-5/2}]\}+a_{12}\{[1/(26)^{\frac{1}{2}}][(11)^{\frac{1}{2}}\psi_{11/2}+(15)^{\frac{1}{2}}\psi_{-5/2}]\} \\ \cdots M\rightarrow -M \cdots \\ b_{11}\{[1/(13)^{\frac{1}{2}}][(6)^{\frac{1}{2}}\psi_{9/2}+(7)^{\frac{1}{2}}\psi_{+1/2}]\}+b_{12}\{[1/(6)^{\frac{1}{2}}][-(5)^{\frac{1}{2}}\psi_{9/2}+\psi_{-7/2}] \\ \cdots M\rightarrow -M \cdots \end{bmatrix}$$

$\Gamma_8^{(2)}$:
$$\begin{bmatrix} c_{11}\{(1/\sqrt{3})[-\psi_{3/2}+\sqrt{2}\psi_{-5/2}]\}+c_{12}\{[1/(6)^{\frac{1}{2}}][-(5)^{\frac{1}{2}}\psi_{9/2}+\psi_{-7/2}]\} \\ \cdots M\rightarrow -M \cdots \\ d_{11}\{[1/(13)^{\frac{1}{2}}][(6)^{\frac{1}{2}}\psi_{9/2}(7)^{\frac{1}{2}}\psi_{1/2}]\}+d_{12}\{[1/(6)^{\frac{1}{2}}][-(5)^{\frac{1}{2}}\psi_{9/2}+\psi_{-7/2}]\} \\ \cdots M\rightarrow -M \cdots \end{bmatrix}$$

Values of the coefficients for $V_{\text{cub}}^{(4)}$ of the potential (3):

$a_{11}=-0.8826$	$a_{12}=1.271$
$b_{11}=1.2657$	$b_{12}=0.694$
$c_{11}=0.9212$	$c_{12}=0.120$
$d_{11}=1.071$	$d_{12}=0.120$

Same, for $V_{\text{cub}}^{(6)}$:

$a_{11}=-1.265$	$a_{12}=0.9001$
$b_{11}=-0.9008$	$b_{12}=0.1482$
$c_{11}=0.154$	$c_{12}=0.8971$
$d_{11}=0.9011$	$d_{12}=1.2661$

TABLE VIII(b). Energy level splitting for $J=11/2$, using the "zero-order" set of wave functions of Table VIII(a).

$$\langle \Gamma_6 \mid V_{cub} \mid \Gamma_6 \rangle = -84\lambda_{11/2}+16\mu_{11/2}$$
$$\langle \Gamma_7 \mid V_{cub} \mid \Gamma_7 \rangle = 44\lambda_{11/2}+176\mu_{11/2}$$
$$\langle \Gamma_8^{(1)} \mid V_{cub}^{(4)} \mid \Gamma_8^{(1)} \rangle = 77.2\lambda_{11/2}$$
$$\langle \Gamma_8^{(2)} \mid V_{cub}^{(4)} \mid \Gamma_8^{(2)} \rangle = -57.2\lambda_{11/2}$$
$$\langle \Gamma_8^{(1')} \mid V_{cub}^{(6)} \mid \Gamma_8^{(1')} \rangle = -136.55\mu_{11/2}$$
$$\langle \Gamma_8^{(2')} \mid V_{cub}^{(6)} \mid \Gamma_8^{(2')} \rangle = 40.55\mu_{11/2}$$

TABLE IX(a). Orthonormal basis for $J=9/2$ in cubic symmetry.

Γ_6:
$$\begin{bmatrix} [1/2(6)^{\frac{1}{2}}][3\psi_{9/2}+(14)^{\frac{1}{2}}\psi_{1/2}+\psi_{-7/2}] \\ \cdots M\rightarrow -M \cdots \end{bmatrix}$$

$\Gamma_8^{(1)}$:
$$\begin{bmatrix} a_{11}[\psi_{9/2}]+a_{12}[\psi_{-3/2}] \\ a_{11}[\psi_{-9/2}]+a_{12}[\psi_{+3/2}] \\ b_{11}\{[1/(15)^{\frac{1}{2}}][-\psi_{1/2}+(14)^{\frac{1}{2}}\psi_{-7/2}]\}+b_{12}\{[1/(10)^{\frac{1}{2}}](-\psi_{9/2}+3\psi_{-7/2})\} \\ \cdots M\rightarrow -M \cdots \end{bmatrix}$$

$\Gamma_8^{(2)}$:
$$\begin{bmatrix} c_{11}[\psi_{3/2}]+c_{12}[\psi_{-3/2}] \\ \cdots M\rightarrow -M \cdots \\ d_{11}\{[1/(15)^{\frac{1}{2}}][-\psi_{7/2}+(14)^{\frac{1}{2}}\psi_{-7/2}]\}+d_{12}\{[1/(10)^{\frac{1}{2}}](-\psi_{9/2}+3\psi_{-7/2})\} \\ \cdots M\rightarrow -M \cdots \end{bmatrix}$$

Values of the coefficients, for $V_{cub}^{(4)}$ of the potential (3).

$a_{11}=0.4889$	$a_{12}=0.872$
$b_{11}=1.5397$	$b_{12}=2.494$
$c_{11}=-0.872$	$c_{11}=0.4885$
$d_{11}=-1.143$	$d_{12}=0.1586$

Same, for $V_{cub}^{(6)}$:

$a_{11}=0.7443$	$a_{12}=0.6675$
$b_{11}=-2.4665$	$b_{12}=2.412$
$c_{11}=-0.6677$	$c_{11}=0.7446$
$d_{11}=0.3773$	$d_{12}=0.6426$

TABLE IX(b). Energy level splitting for $J=9/2$ using the "zero-order" set of wave functions.

$$\langle \Gamma_6 \mid V_{cub} \mid \Gamma_6 \rangle = 32.9\lambda_{9/2}-256\mu_{9/2}$$
$$\langle \Gamma_8^{(1)} \mid V_{cub}^{(4)} \mid \Gamma_8^{(1)} \rangle = 17.04\lambda_{9/2}$$
$$\langle \Gamma_8^{(2)} \mid V_{cub}^{(4)} \mid \Gamma_8^{(2)} \rangle = -36.7\lambda_{9/2}$$
$$\langle \Gamma_8^{(1')} \mid V_{cub}^{(6)} \mid \Gamma_8^{(1')} \rangle = 211.5\mu_{9/2}$$
$$\langle \Gamma_8^{(2')} \mid V_{cub}^{(6)} \mid \Gamma_8^{(2')} \rangle = -83.5\mu_{9/2}$$

obtained using the relations[11]:

$$\langle SLJ'\|\beta\|SLJ'\rangle = \beta_{J'} = (-1)^{J-J'}(2J'+1)/(2J+1) \times\left[\frac{(2J'-4)!(2J+5)!}{(2J'+5)!(2J-4)!}\right]^{\frac{1}{2}} \frac{W(LJ'LJ';\ S4)}{W(LJLJ;\ S4)} \langle SLJ\|\beta\|SLJ\rangle.$$

$$\langle SLJ'\|\gamma\|SLJ'\rangle = (-1)^{J-J'}(2J'+1)/(2J+1) \times\left[\frac{(2J'-6)\cdot(2J+7)}{(2J'+7)\cdot(2J-6)}\right]^{\frac{1}{2}} \cdot \frac{W(LJ'LJ';\ S6)}{W(LJLJ;\ S6)} \times\langle SLJ\|\gamma\|SLJ\rangle, \quad (8)$$

where $W(LJLJ;\ Sk)$ are Racah's coefficients.[12]

4. RESULTS

(a) In Tables I–V the matrix elements of the potential (3) and the energy level splitting of the various manifolds are listed in terms of the splitting factors λ_J and μ_J. The manifolds with $J=\frac{3}{2}$ and $J=\frac{1}{2}$ have been omitted, since they are not affected in first order by cubic-symmetry potentials. Also the orthonormal sets of wave functions to be used as "zero-order" sets in perturbation calculations, are given in Tables VI(a)–X(b). For the sake of brevity we omitted the label J in the expression of the matrix elements of the potential $\langle J, M_J|V_{\text{cub}}|J, M_J'\rangle$ and also in writing the linear combinations of ψ_{J,M_J} functions.

We may remark that the knowledge of the actual form of the crystal-field eigenfunctions is useful in the interpretations of the spectrum of the rare-earth ions in garnets, especially if one introduces rhombic-symmetry components of the potential as perturbations on a predominant cubic potential.

A pair of wave functions (Γ_a and Γ_b) pertains to each Γ_6 and Γ_7 representation of the cubic group. Each Γ_b function is obtained from the corresponding Γ_a by changing in the $\psi_{J,M}$ the M values into $-M$. This satisfies the group requirements but leaves undefined the relative phase of Γ_a and Γ_b. A convenient phase relationship can be fixed using[13] an operation of the group to generate Γ_b from Γ_a. Such operation is the reflection σ on the (xz) plane. Then[14]

$$\sigma\psi_{J,M}=(-1)^{M-J+\Sigma l_k}\psi_{J,-M}. \quad (9)$$

In general the phase factor will depend on the l values and on the number of electrons (in the present consideration such number is odd). For this reason the phase factor has been omitted in the tables for the sake of generality, but it will be useful to express it in the detailed treatment of tetragonal and orthorhombic symmetry.[13]

Similar considerations will apply to the two pairs of wave functions Γ_a, Γ_b and Γ_c, Γ_d pertaining to each Γ_8 representation.

(b) The formalism used in the present case for a potential of the form (3) can easily be adapted to the case of octahedral and tetrahedral symmetry, simply by

TABLE X(a). Orthonormal basis for $J=7/2$ and $5/2$ in cubic symmetry.[a]

$J=7/2$

Γ_7:
$$\begin{bmatrix} \frac{1}{2}(\sqrt{3}\psi_{5/2}-\psi_{-3/2}) \\ \frac{1}{2}(\sqrt{3}\psi_{-5/2}-\psi_{+3/2}) \end{bmatrix}$$

Γ_8:
$$\begin{bmatrix} (7/12)^{\frac{1}{2}}\{\psi_{7/2}-[5/(35)^{\frac{1}{2}}]\psi_{-1/2}\} \\ (7/12)^{\frac{1}{2}}\{\psi_{-7/2}-[5/(35)^{\frac{1}{2}}]\psi_{+1/2}\} \\ \frac{1}{2}(\psi_{5/2}+\sqrt{3}\psi_{-3/2}) \\ \frac{1}{2}(\psi_{-5/2}+\sqrt{3}\psi_{3/2}) \end{bmatrix}$$

Γ_6:
$$\begin{bmatrix} (5/12)^{\frac{1}{2}}\{\psi_{7/2}+[7/(35)^{\frac{1}{2}}\psi_{-1/2}\} \\ [5/12)^{\frac{1}{2}}\{\psi_{-7/2}+[7/(35)^{\frac{1}{2}}\psi_{1/2}\} \end{bmatrix}$$

$J=5/2$[b]

Γ_7:
$$\begin{bmatrix} [1/(6)^{\frac{1}{2}}][\psi_{5/2}-(5)^{\frac{1}{2}}\psi_{-3/2}] \\ [1/(6)^{\frac{1}{2}}][\psi_{-5/2}-(5)^{\frac{1}{2}}\psi_{3/2}] \end{bmatrix}$$

Γ_8:
$$\begin{bmatrix} \psi_{1/2} \\ \psi_{-1/2} \\ [1/(6)^{\frac{1}{2}}][(5)^{\frac{1}{2}}\psi_{3/2}+\psi_{-3/2}] \\ [1/(6)^{\frac{1}{2}}][(5)^{\frac{1}{2}}\psi_{-3/2}+\psi_{3/2}] \end{bmatrix}$$

[a] See footnotes 4 and 15.
[b] See footnotes 4 and 13.

TABLE X(b). Energy level splitting[a] for $J=7/2$ and $J=5/2$.

$J=7/2$:

$$\langle\Gamma_7|V_{\text{cub}}|\Gamma_7\rangle=-18\lambda_{7/2}-72\mu_{7/2}$$
$$\langle\Gamma_8|V_{\text{cub}}|\Gamma_8\rangle=2\lambda_{7/2}+96\mu_{7/2}$$
$$\langle\Gamma_6|V_{\text{cub}}|\Gamma_6\rangle=14\lambda_{7/2}-120\mu_{7/2}$$

$J=5/2$:

$$\langle\Gamma_7|V_{\text{cub}}|\Gamma_7\rangle=-4\lambda_{5/2}$$
$$\langle\Gamma_8|V_{\text{cub}}|\Gamma_8\rangle=2\lambda_{5/2}$$

[a] See footnote 4.

[12] G. Racah, Phys. Rev. **62,** 438 (1942).
[13] A. D. Liehr, J. Phys. Chem. **64,** 43 (1960).
[14] E. Fick and G. Joos, *Handbuch der Physik*, edited by S. Fugge (Springer-Verlag, Berlin, 1957), Vol. 28, 234.
[15] C. Kittel and J. M. Luttinger, Phys. Rev. **73,** 172 (1948).

altering the multiplicative constants present in the expression of the potential and implicitly contained in λ_J and μ_J.

An analogous procedure will apply when the potential is due not to point-charges, but to electric dipole moments (e.g., in aquocomplexes).

ACKNOWLEDGMENTS

The writer wishes to thank Dr. A. D. Liehr for valuable criticism of the manuscript, Dr. D. L. Wood for interesting discussions, and Miss M. A. Lounsberry of the Computing Center for the numerical solution of some of the reduced secular equations.

THE JOURNAL OF CHEMICAL PHYSICS VOLUME 34, NUMBER 4 APRIL, 1961

Derivation of Interelectronic Screening Parameters from Statistical Considerations*

ROBERT P. BAUMAN AND JAMES P. CONSIDINE†

Polytechnic Institute of Brooklyn, Brooklyn, New York

(Received July 1, 1960)

A model for helium and two-electron ions has been found in which assumptions similar to that of the Bohr model for the hydrogen atom lead to ionization energies and atomic radii in agreement with observed values and values calculated by the Hartree-Fock method, respectively. An effective screening potential is found by quasi-classical statistical arguments. The angular momentum of each electron is fixed at one unit and the two electrons constrained to move on the same sphere. The interelectronic distance is assumed to follow an exponential distribution expressed in terms of the Coulombic repulsion. When the distance between electrons is then fixed at its most probable value according to this distribution function, no adjustable parameters remain. The method can be extended to excited states.

THE Bohr model for the hydrogen atom was an important early breakthrough in attempts to understand matter at the submicroscopic level. Although it failed to provide quantitative answers for atoms with more than one electron, and has subsequently been superseded by the methods of quantum mechanics, it did provide a picture that most workers still find helpful and has strongly influenced subsequent discussions of atomic structure. It seems possible that an extension of the Bohr model to atoms with more than one electron might provide some additional insight into atomic structure and methods of calculating atomic properties.

I. EMPIRICAL REGULARITIES

The periodicity of ionization energies, in agreement with the Periodic Table, is generally recognized and often cited. Also, the drop in ionization energy with increasing atomic number for each group (e.g., Li, Na, K, etc.) is easily explained in terms of the increasing size of the atom. Not so easily explained is the nearly linear dependence of the ionization energies on the "effective nuclear charge," or "kernel charge." Consideration of this regularity, explained in greater detail below, suggested that a suitable first-approximation treatment of polyelectron atoms might be found that could give a more physical picture of the cause of this simple relationship. The goal of calculating ionization energies for atoms with several electrons has not yet been reached, but the two-electron system has yielded to a modified Bohr-type calculation.

In Fig. 1, ionization energies are plotted against atomic number. It will be observed that the value for helium is slightly less (by 2.6 ev) than twice the value for hydrogen. If the lithium atom and beryllium atom are considered as one-electron and two-electron systems with "kernels" of charge one and two, respectively, then it seems reasonable that the ionization energy for beryllium also should be slightly less (by 1.5 ev) than twice that of lithium. This is continued for each pair of elements of the first and second groups. It will be noted that the deviation from linearity is essentially that found in most ions (and molecules) when electrons move from equivalent orbitals into the same orbital, that is, about 1 to 3 ev.

The electrons added to form the atoms boron, carbon, and nitrogen go into separate orbitals and follow an exactly linear dependence on atomic number. Extrapolation of this line indicates an apparent effective kernel charge of about 2.6 for boron, indicating that the screening of $2s$ electrons for $2p$ electrons is less effective than that of $1s$ electrons for $2s$ and $2p$ electrons. The ionization energies for oxygen, fluorine, and neon also fall on a straight line but this is displaced downward, as might be expected on the grounds that these electrons are going into occupied orbitals. The patterns described are repeated up to the transition elements. For these a charge is added to the nucleus and a compensating

* From a thesis by James P. Considine submitted in partial fulfillment of requirements for the degree of Doctor of Philosophy at the Polytechnic Institute of Brooklyn.

† National Science Foundation Predoctoral Fellow, 1958–1960.

charge is added to the inner electronic shell, giving little or no change in the ionization energy for the outermost electron.

Second and third ionization energies follow a pattern which is equivalent to that for first ionization energies (see Fig. 2). The relatively high values obtained for the effective kernel charge for p electrons could be interpreted as poor shielding of these from the nucleus by the inner s electrons or as an indication of the existence of a linear correction term that should be applied to all p electrons.

The difficulty in calculating ionization energies lies, of course, in the uncertain value to be assigned to the electron-electron repulsion energies, or screening constants. If such repulsion energies could be ignored, ionization energies would be proportional to the square of the atomic number; if shielding were "perfect," the ionization energy would be constant, independent of atomic number. The nearly linear dependence is apparently inexplicable in terms of present models and approximations.

II. MODEL FOR HELIUM GROUND STATE

In selecting a model for the helium atom it was felt important that only quantities that could be given a direct physical interpretation be employed. The Bohr atom was selected as the most promising starting point for satisfying this criterion. Accordingly, each electron was constrained to move at a fixed distance r from the nucleus and the angular momentum of each electron was fixed at the value $h/2\pi$. The total potential energy of the atom is written

$$-V=2Ze^2/r-e^2/\beta r, \tag{1}$$

where β is a parameter relating the interelectronic distance to the nucleus-electron distance. Equation (1) is meant to signify that the two electrons move on the circle with radius r in unison, separated by the distance βr; but the equation can also be interpreted as assuming the screening charge $(1/2\beta)$ for both electrons. The object of the present investigation is the theoretical derivation of a value for β by introducing certain quasi-classical statistical arguments which serve to substitute for certain aspects of the wave character of quantum mechanics.

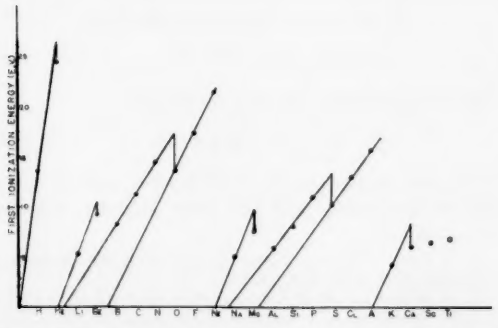

FIG. 1. First ionization energies plotted against atomic number.

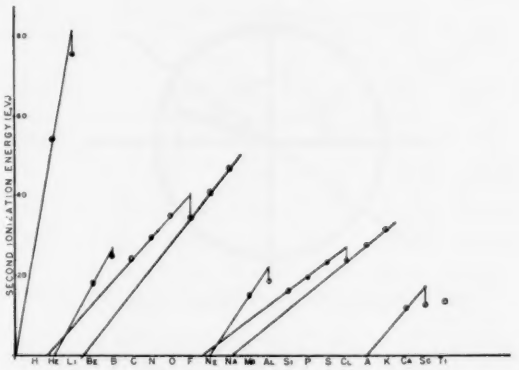

FIG. 2. Second ionization energies plotted against atomic number.

From the virial theorem

$$E=-\bar{T}=\tfrac{1}{2}\bar{V} \tag{2}$$

and from the restriction on the angular momentum

$$P=mvr=\hbar, \tag{3}$$

one can write for each electron,

$$\tfrac{1}{2}mv^2=P^2/2mr^2=\hbar^2/2mr^2=e^2a_0/2r^2, \tag{4}$$

and for the atom

$$\bar{T}=e^2a_0/r^2=\tfrac{1}{2}e^2(2Z-1/\beta)/r=-\tfrac{1}{2}\bar{V}$$

or

$$r=a_0(Z-1/2\beta), \tag{5}$$

where a_0 is the Bohr radius, $\hbar^2/me^2$. The ionization energy can therefore be expressed as

$$\begin{aligned}\text{I.E.}&=[\tfrac{1}{2}(2Z-1/\beta)^2-Z^2]e^2/2a_0\\&=[2(a_0/r)^2-Z^2]e^2/2a_0,\end{aligned} \tag{6}$$

since the ionization energy is the difference between the total energy of the two-electron atom and that of the one-electron atom, the latter being just $-Z^2e^2/2a_0$.

The parameter β may be specified in terms of the angle θ formed by the radius vectors to the two electrons, as indicated in Fig. 3. If the electrons were at opposite poles of the sphere, β would be 2. If there were no repulsive energy, the average value of $1/d$ would be $1/r$ and thus β would be unity. The actual value of β must fall between these limits. (A value of 1.8660 would give an ionization energy for helium twice that for hydrogen.)

One can imagine the quantities r and θ to be subject to small variations about their most probable values. The variables r, θ, and ϕ may then be considered as almost independent, or "nearly closed."[1] The proba-

[1] L. D. Landau and E. M. Lifshitz, *Statistical Physics* (Addison-Wesley Publishing Company, Boston, Massachusetts, 1958), pp. 2–7, 110–111.

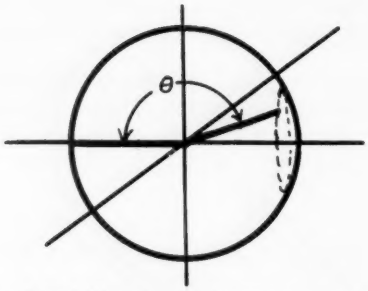

FIG. 3. Definition of angle θ between vectors r_1 and r_2.

bility for any set of values is the product of probabilities, or the log of the probability is the sum of logs of the individual probabilities and must be a linear function[2] of the energy [which is uniquely related to the angular momentum through Eq. (4)]. These conditions lead to an exponential distribution function. That is, the value of the angle θ should follow a distribution function of the form

$$F(\theta) = \exp-\left\{\frac{e^2/r[2(1-\cos\theta)]^{\frac{1}{2}}}{V_0}\right\}d\tau, \qquad (7)$$

where the "volume element" $d\tau$ is the element of surface area $2\pi r^2 \sin\theta d\theta$. The most probable value of θ is found by differentiating this distribution function and θ is then assumed fixed at this most probable value $\hat{\theta}$. The quantity V_0 is taken as the most probable potential energy of interaction $e^2/\beta r$ where $\beta=[2(1-\cos\hat{\theta})]^{\frac{1}{2}}$. Then

$$F(\theta) = \exp-\left\{\frac{e^2/r[2(1-\cos\theta)]^{\frac{1}{2}}}{e^2/r[2(1-\cos\hat{\theta})]^{\frac{1}{2}}}\right\}2\pi r^2\sin\theta \qquad (8)$$

$$F'(\theta) = 2\pi r^2\left\{\cos\theta-\frac{\sin^2\theta[2(1-\cos\theta)]^{\frac{1}{2}}}{[2(1-\cos\theta)]^{\frac{1}{2}}}\right\} \times \exp\left[\frac{-(1-\cos\hat{\theta})^{\frac{1}{2}}}{(1-\cos\theta)^{\frac{1}{2}}}\right] \qquad (9)$$

TABLE I. Ground-state energies and radii.

Ion	r/a_0 calc	r/a_0 lit	I.E. calc	I.E. obs
He^0	0.592	0.592	23.45	24.58
Li^+	0.372	0.372	74.8	75.6
Be^{++}	0.271	0.271	154.2	153.8
F^{+7}	0.115	0.115	954.3	953.6

[2] If the problem is nearly separable, then the total energy is the sum of the energies associated with the various coordinates, whereas the probability is the product of the respective probabilities, L. D. Landau and E. M. Lifshitz, *Statistical Physics* (Addison-Wesley Publishing Company, Boston, Massachusetts, 1958), pp. 10–13. See also E. B. Wilson, Ann. Math. **10,** 129–166 (1909).

and, letting $\cos\hat{\theta}=y$, $F'(\hat{\theta})=0$, one obtains

$$3y^2-2y-1=0. \qquad (10)$$

Under these assumptions the value of β is calculated to be $(8/3)^{\frac{1}{2}}=1.632$, corresponding to $\cos\hat{\theta}=-\frac{1}{3}$. This value of β can be inserted into Eq. (6) to find the ionization energy, or into Eq. (5) to find the radius r. Values obtained for the ground states of He, Li^+, Be^{++}, and F^{+7} are shown in Table I, along with the observed ionization energies[3] and the radii calculated from Hartree-Fock equations[4] or by the approximation of Morse, Young, and Haurwitz.[5]

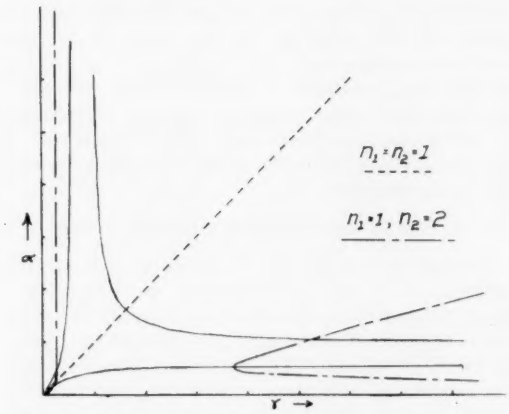

FIG. 4. Loci of solutions to Eqs. (13) and (15) for $Z=2$.

III. MODEL FOR EXCITED STATES

An excited state for the helium atom is obtained from the model given for the ground state by allowing the radii of the orbits of the two electrons to take on different values, determined by the conditions that for each electron the angular momentum is $n\hbar$ where n is the integer representing the principal quantum number of that electron.

It is convenient to introduce the following notation. The radii of the circular orbits are designated r_1 and r_2, with $r_1 \leqslant r_2$; the interelectronic distance is $d=\alpha r_2=\gamma r_1$. The kinetic energy for each electron is

$$T_i=\tfrac{1}{2}mv_i^2=P_i^2/2mr_i^2=n_i^2\hbar^2/2mr_i^2 =n_i^2e^2a_0/2r_i^2. \qquad (11)$$

The potential energy for each electron is

$$V_i=-Ze^2/r_i+e^2/2d. \qquad (12)$$

Since each electron moves, with fixed T and V, in the field of the nucleus and the other electron, one can

[3] C. E. Moore, "Atomic Energy Levels," Natl. Bur. Standards U. S. Ann. Rept. Circ. **467,** 1949.

[4] W. S. Wilson and R. B. Lindsay, Phys. Rev. **47,** 681 (1935).

[5] P. M. Morse, L. A. Young, and E. S. Haurwitz, Phys. Rev. **48,** 948 (1935).

apply the virial theorem for each electron. This gives the condition, when the equations for the two electrons are combined,

$$\gamma/\alpha=(n_2^2/n_1^2)\{[Z-(2\gamma)^{-1}]/[Z-(2\alpha)^{-1}]\}. \quad (13)$$

The distribution function takes the form

$$D(\theta)\sim \sin\theta \exp-\left\{\frac{e^2/r_1[1+(\gamma/\alpha)^2-2(\gamma/\alpha)\cos\theta]^{\frac{1}{2}}}{e^2/r_1[1+(\gamma/\alpha)^2-2(\gamma/\alpha)\cos\theta]^{\frac{1}{2}}}\right\}. \quad (14)$$

Setting $\partial D/\partial\theta=0$ one obtains, after algebraic manipulation,

$$\alpha^4+\gamma^4+3\alpha^4\gamma^4-4\alpha^2\gamma^4-4\alpha^4\gamma^2-2\alpha^2\gamma^2=0. \quad (15)$$

The locus of points satisfying this equation is shown in Fig. 4. If a similar plot is made for Eq. (13), for given values of Z, n_1, and n_2, the intersections of these curves give the solutions. For example, if $n_1=n_2$ Eq. (13) gives the straight line $\alpha=\gamma$ and the only intersection is at the point $\alpha=\gamma=(8/3)^{\frac{1}{2}}$ as found above. Calculated values for radii and ionization energies are shown in Table II, compared with observed ionization energies[3] and radii calculated by the approximation of Morse, Young, and Haurwitz.[5]

TABLE II. Excited-state energies and radii.

	$1s(r/a_0)$		$2p(r/a_0)$		I.E.	
Ion	calc	lit	calc	lit	calc	obs
He^0	0.525	0.500	2.622	3.90	2.87	3.37
He^0	..	...	2.361	2.3(5)	5.907	5.743
Li^+	0.345	0.334	1.58	1.95	13.57	13.42
Be^{++}	0.257	0.250	1.13	1.30	31.00	31.96
F^{+7}	0.113	0.111	0.469	0.503	220.6	216.1

IV. DISCUSSION

The model described can have no more validity than the Bohr model for the hydrogen atom, with which it has certain features in common.[6] On the other hand, the results appear too consistently close to the true values to be attributed to coincidence or lack of sensitivity of the calculations. Certain very obvious difficulties exist, as in the simplest Bohr picture, which could probably be removed by considering precessing elliptical orbits with relativistic (spin) corrections.

The primary value in the model is not concerned with the ultimate accuracy that might be achieved for simple problems that have been or can be calculated quite exactly by current methods, but rather with the possibility that such a classical representation may suggest better first-order approximations for polyelectron systems to be treated by quantum mechanics.

[6] A statistical model based on very different assumptions, applicable to heavy atoms, has been described by L. H. Thomas, Proc. Cambridge Phil. Soc. **23**, 542 (1927) and E. Fermi, Z. Physik **48**, 73 (1928), and recently extended by S. Golden, Phys. Rev. **110**, 1349 (1958).

Pressure Dependence of Fluorescence Spectra

DAVID J. WILSON AND BARBARA NOBLE

Department of Chemistry, University of Rochester, Rochester, New York

AND

BETTY LEE

Computing Center, University of Rochester, Rochester, New York

(Received October 10, 1960)

The pressure dependence of the fluorescence spectra of molecules in the gas phase is calculated for two models; one involving a strong collision mechanism for transferring vibrational energy, the other involving a stepwise collision mechanism. The fluorescence spectra of the two models show very marked differences at pressures between the low pressure region of resonance fluorescence and the high pressure limit.

I. INTRODUCTION

THE currently accepted qualitative explanation of the pressure dependence of unimolecular reactions was proposed almost 40 years ago by Christiansen[1] and Lindemann.[2] A short time earlier, Stern and Volmer introduced the presently accepted mechanism accounting for the pressure dependence of fluorescence and of quantum yields.[3] Both of these theories involve the idea that energy is transferred to and from the internal degrees of freedom of the reactant molecules by collisions of these molecules with a "heat-bath" of gas molecules, either reactants or reactants, and added inert gases. Subsequent work has emphasized the importance of vibrational energy in these processes.

The details of the energy transfer process are therefore of some interest in the analysis of fluorescence spectra and of rate data on photochemical and unimolecular reactions. One might have expected that the nature of this collisional activation and deactivation mechanism could be at least qualitatively elucidated by studying the pressure dependence of unimolecular rate constants. It was found that such was most definitely not the case; collisional vibrational transition probabilities of widely differing functional form led to log-log plots of rate constant vs pressure which were experimentally indistinguishable.[4,5] All of the details of the collisional processes are washed out in the averaging which occurs when one studies a unimolecular decomposition under conventional conditions.

We felt that perhaps the dependence of photochemical quantum yields on pressure might be helpful in gaining insight into these collision processes, which involve molecules in high vibrational energy states. However, the recent calculations of Porter and Connelly[6] demonstrate most convincingly that, to quote these authors, "To decide whether or not unimolecular theory can be used to interpret photodissociation requires very precise experimental data, more precise than is available at present."

The emphasis placed by many photochemists on the study of fluorescence[7] in connection with photochemical work led us to think about the pressure dependence of fluorescence spectra, originally considered by Stern and Volmer.[3] We considered two quite different sets of collisional vibrational transition probabilities, and calculated the intensities of the lines of the fluorescence spectra of these models as functions of pressure. This paper includes a brief discussion of mechanism and notation, descriptions of the two models used, a word on the computer program employed, and conclusions.

II. MECHANISM

The probable steps in photochemical processes in gases have been discussed in detail by Noyes, Porter, and Jolley.[7] The computational requirements for solving the general equations were beyond the capacities of the budget and computer available, so we simplified the mechanism as much as possible without destroying the salient features of the pressure dependences of the fluorescence spectra. In particular, we considered only a single excited electronic state with its associated vibrational levels; we thereby neglected the possibility of singlet-triplet transitions. We also neglected internal conversion, by means of which levels of the excited electronic state are depopulated by some process which results in neither fluorescence nor chemical reaction. (This last restriction could be removed without difficulty.)

The mechanism considered is the following:

$$A_p \rightarrow A_n^* \qquad I_{pn} \tag{1}$$

$$A_1^* + M \rightarrow A_m^* + M \qquad a_{lm} \tag{2}$$

$$A_m^* \rightarrow \text{Products} \qquad c_m \tag{3}$$

$$A_m^* \rightarrow A_q + h\nu_{mq} \qquad d_{mq}; \tag{4}$$

[1] J. A. Christiansen, thesis, Reaktion-Kinetiske Studier, Copenhagen (1921).
[2] F. A. Lindemann, Trans. Faraday Soc. **17**, 598 (1922).
[3] O. Stern and M. Volmer, Physik Z. **80**, 183 (1919).
[4] F. P. Buff and D. J. Wilson, J. Chem. Phys. **32**, 677 (1960).
[5] D. J. Wilson, J. Phys. Chem. **64**, 323 (1960). See this paper for earlier references on the problem of energy transfer in unimolecular reactions.
[6] G. B. Porter and B. T. Connelly, J. Chem. Phys. **33**, 81 (1960).
[7] See, for example, W. A. Noyes, Jr., G. B. Porter, and J. E. Jolley, Chem. Revs. **56**, 49 (1956), and many of the references cited therein.

A_r represents a reactant molecule in the rth vibrational level of the ground electronic state; A_i^* represents a reactant molecule in the ith vibrational level of the excited electronic state; I_{pn} is the number of quanta of light absorbed per unit volume per unit time which induce the transition (1); M represents a heat-bath molecule, assumed to be in thermal equilibrium[8]; a_{lm}, c_m, and d_{mq} are the microscopic rate constants for the processes with which they are associated; ν_{mq} is the frequency of the light emitted in step (4); and h is Planck's constant.

The concentrations of reactant molecules in the various vibrational levels of the excited electronic state are then given by the following set of linear differential equations

$$d[A_m^*]/dt=\sum_p I_{pm}+\sum_h a_{nm}[M][A_n^*] - (\sum_n a_{mn}[M]+c_m+\sum_q d_{mq})[A_m^*]. \quad (5)$$

(We assume that the concentration of electronically excited reactant is negligible compared to $[M]$.)

If the illumination is steady and of moderate intensity (i.e., we exclude flash photolysis, chopped light, or steady illumination of extremely high intensity), the first summation in (5) depends only on the reactant studied, the temperature, and the light source used; it will be essentially constant for reactions run to only a small percent conversion of reactants to products. Under these conditions we can also make the steady-state approximation that $d[A_m^*]/dt=0$.[4,6] Equations (5) are thereby reduced to a set of linear algebraic equations which can readily be solved by standard methods.

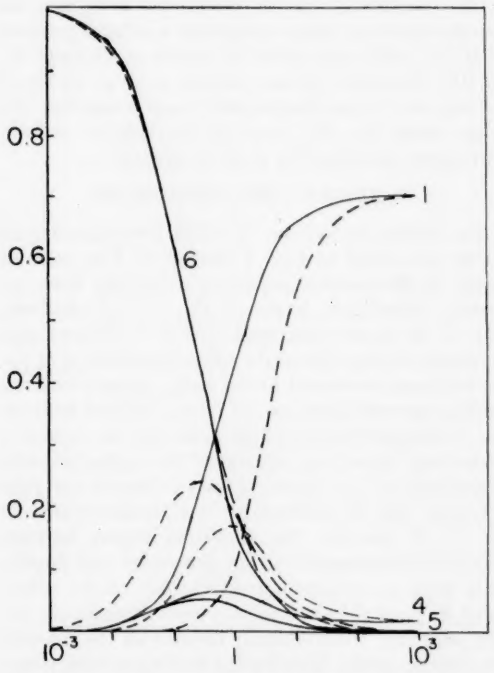

FIG. 1. Strong and weak collision mechanisms, $s=1$, $I_{06}=1$, 8 levels, $\rho=0.3$. Vertical scale is fluorescence intensity, horizontal scale is reduced pressure.

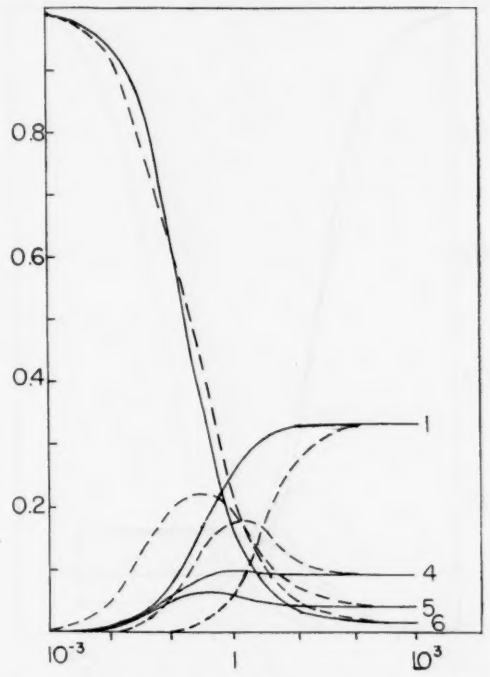

FIG. 2. Strong and weak collision mechanisms, $s=3$; other parameters are the same as in Fig. 1.

III. MODELS

The quantities I_{pm} were given the value zero for all transitions except $A_0 \rightarrow A_v^*$; by linear combination of solutions obtained for various values of v, one can obtain the solution for any distribution of the I_{pm}. The c_m were computed by Kassel theory[9] as $c_m=c\cdot g_s(m-i^*)/g_s(m)$, where $g_s(k)=(k+s-1)!/k!(s-1)!$ is the degeneracy of the kth energy level of the set of s identical, coupled harmonic oscillators used to represent a reactant molecule, and i^* is the lowest vibrational level for which chemical reaction can occur. The vibrational energy levels of the model were assumed equally spaced, with a Boltzmann factor $\rho=\exp(-h\nu_{\text{vib}}/kT)$. The quantities d_{mq} were assumed independent of m and given the value $d\delta_{q0}$, where

$$\delta_{q0}=1, \quad q=0$$
$$=0, \quad q\neq 0.$$

[8] H. S. Johnston, J. Chem. Phys. **20**, 1103 (1952).

[9] L. S. Kassel, *Kinetics of Homogeneous Gas Reactions* (Chemical Catalog Company, New York, 1932).

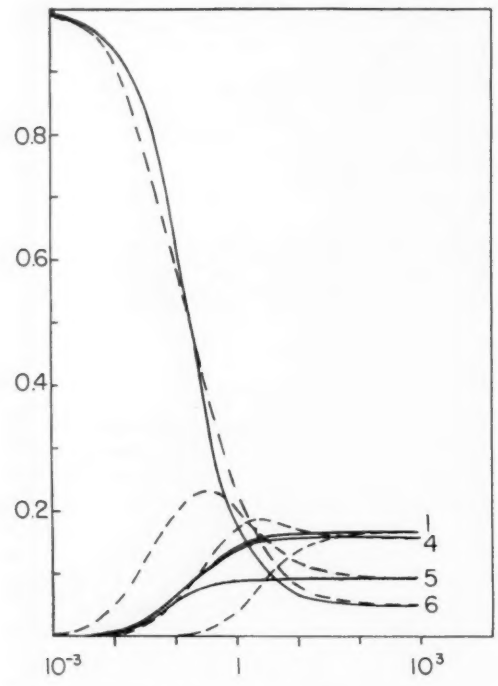

FIG. 3. Strong and weak collision mechanisms, $s=5$; parameters are the same as in Fig. 1.

This assumption is essentially that of ignorance, uniformly distributed; there is, of course, nothing to preclude the insertion of better values should they become available.

For the first model, the collisional vibrational transition rate constants $a_{m,m-k}$ were set equal to a constant a; the $a_{m,m+k}$ are then defined by the requirement of microscopic reversibility as $a_{m,m+k}=ag_s(m+k)\rho^k/g_s(m)$. This corresponds to a "strongly coupled" collisional mechanism similar to that used by Kassel,[9] Slater,[10] and others.[11]

The a_{mn} used in the second model were those used by Buff and Wilson earlier[4]; they are a generalization to s-oscillator systems of the Landau-Teller transition probabilities[12] used by Montroll, Shuler, Nikitin, Mahan, and others.[13] These a_{mn} are defined as

$$a_{n,n+1}=a(n+s)$$

$$a_{n,n-1}=a\cdot n$$

$$a_{n,k}=0, \quad k\neq n\pm 1.$$

This corresponds to a weakly coupled collision mechanism in which vibrational activation and deactivation are a stepwise process involving the transfer of no more than one vibrational quantum per collision.

We felt that these two types of collisional vibrational transition rates should bracket those actually occurring in physical systems. If the fluorescence spectra obtained from these two models differed sufficiently from each other, one might attempt to get high-resolution fluorescence spectra at quite low pressures, from which information about collisional vibrational transition rates of highly excited levels could be obtained.

IV. COMPUTATIONAL DETAILS

A computer program capable of handling up to 20 vibrational levels in the excited electronic state was written for the IBM 650 computer of the University of Rochester Computing Center. The program was designed to handle both models, and permitted us to vary the relative contributions from steps (3) and (4) over the entire range from fluorescence only to photochemical decomposition only. The linear algebraic equations resulting from Eqs. (5) were solved by the method of successive elimination; rounding-off errors were negligible in all the results considered here, but this method cannot be extended to systems involving many more than 20 levels.

The quantity I_{0n} was set equal to one in all runs, and calculations were made in terms of a reduced pressure, $a[M]/d$, which was varied by powers of ten from 10^{-3} to 10^{3}. The ratio c/d was defined as γ, so that $\gamma=0$ corresponds to pure fluorescence; large γ together with large values for the range of the reduced pressure correspond to essentially pure decomposition.

V. RESULTS AND CONCLUSIONS

The results for systems in which fluorescence alone occurs are shown in Figs. 1 through 5. The quantum yields of fluorescence involving transitions from the various vibrational levels of the excited electronic state to the single vibrational level of the ground state are plotted as functions of the reduced pressure, $a[M]/d$. Dotted lines correspond to the weak, stepwise collision mechanism; solid lines, to the strong collision mechanism. It is apparent that, if the molecules are excited to moderately high-lying vibrational levels, the pressure dependences of the spectra of the two models are quite different; this is particularly well demonstrated in Fig. 5. In general, the transition region between resonance fluorescence (at low pressures) and fluorescence from an equilibrium distribution of the vibrational levels of the electronically excited molecules (at high pressures) is considerably broader for the stepwise deactivation model. If excitation is to a low-lying vibrational level, the differences between the two models are less marked. (Compare Figs. 2 and 4.) Both of these conclusions are qualitatively what one would intuitively expect. A comparison of Figs. 1 through 3 in-

[10] N. B. Slater, *Theory of Unimolecular Reactions* (Cornell University Press, Ithaca, New York, 1959).
[11] See, for example, H. S. Johnston and J. R. White, J. Chem. Phys. **22**, 1969 (1954).
[12] L. Landau and E. Teller, Physik. Z. Sowjetunion **10**, 34 (1936).
[13] See the work cited in footnote 5 for a listing of these papers.

dicates that variation in molecular complexity (determined by s) does not affect these conclusions appreciably.

In connection with the appearance of these curves, it should be noted that, in contradiction to a statement by Porter and Connelly,[14] the distribution of molecules among the vibrational levels of the excited electronic state approaches that at equilibrium as the pressure increases. This will be true even if chemical reaction, singlet-triplet conversion, internal conversion, or any other *pressure-independent* processes are considered in addition to those analyzed here. A simple proof follows.

Let **a** be the matrix of collisional vibrational transition rate constants; **c** the matrix of fluorescence rate constants d_{0i}, reaction rate constants c_i, etc., so that $c_{ii}=d_{0i}+c_i+\cdots$; **A**, the vector representing the concentrations $[A_i^*]$; $[M]$, the heat-bath molecule concentration; and **Y** the vector representing the I_{0i}. Then, with the steady-state assumption, we have $(\mathbf{a}[M]+\mathbf{c})\mathbf{A}=\mathbf{Y}$, so that $(\mathbf{a}+\mathbf{c}/[M])\mathbf{A}=\mathbf{Y}/[M]$. As $[M]$ becomes large, this equation approaches the form $\mathbf{aA}=0$, for which the only physically pertinent solution is the equilibrium distribution.

The work of Boudart and Dubois[15] on the fluorescence yield of β-naphthylamine vapor in the presence of foreign gases[16] suggests rather strongly that a stepwise collisional deactivation of vibrational energy levels is operative in this system. It should be noted, however, that the collisional mechanism proposed by these authors is correct only in the limit as the temperature approaches absolute zero; elsewhere it violates microscopic reversibility. The expression they used for the rate constant for a unimolecular process (internal conversion) taking place in a molecule having a specified internal energy is in agreement with the expressions derived by Kassel[9] and Slater[10] only over a rather limited range of vibrational energies. These facts may cast some doubt on the authors' subsequent interpretation. (The use of microscopic rate constants developed to describe decomposition of vibrationally activated molecules to describe internal conversion is highly speculative at the present time, we believe.)

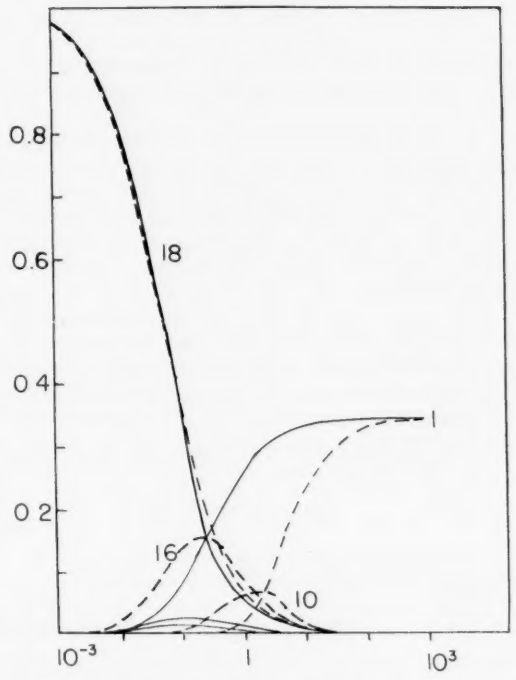

FIG. 5. Strong and weak collision mechanisms, $s=3$, $I_{0,18}=1$, 20 levels, $\rho=0.3$.

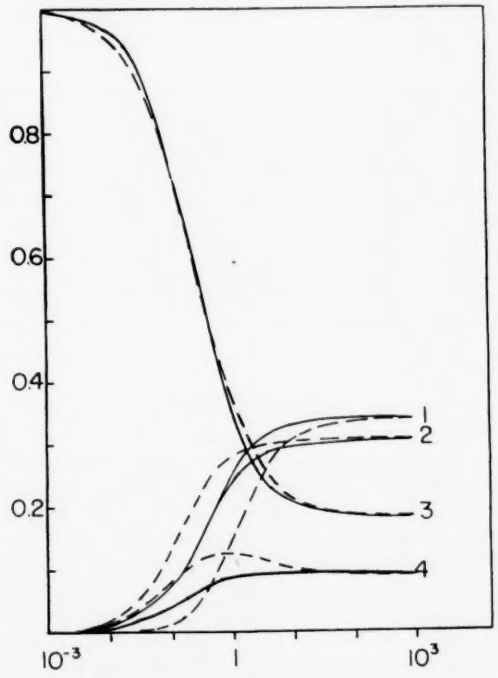

FIG. 4. Strong and weak collision mechanisms, $s=3$, $I_{03}=1$, other parameters are the same as in Fig. 1.

The same comments can be made with regard to Dubois' recent paper on the photolysis of biacetyl.[17] In addition, his statement that "when a molecule contains very little or no excess (over thermal) vibrational energy in its excited state, as is achieved by exciting near the 0–0 transition, the pressure effect on the primary quantum yield ϕ is negligible..." is in

[14] See p. 82 of work cited in footnote 6.

[15] M. Boudart and J. T. Dubois, J. Chem. Phys. **23**, 223 (1955).

[16] The fluorescence of this compound in the vapor phase was first reported by Neporent; see B. S. Neporent, Zhur. Fiz. Khim **24**, 1219 (1950).

[17] J. T. Dubois, J. Chem. Phys. **33**, 229 (1960).

general incorrect; unless no vibrational energy is necessary for the reaction to occur, ϕ will increase with increasing pressure under these circumstances, since collisional activation is now required in order for reaction to occur.

It is interesting to note that Boudart and Dubois find support for a stepwise deactivation process in β-naphthylamine (a conclusion with which we are inclined to agree), while Rabinovitch and his co-workers[18] find what we regard as equally strong evidence for a strong collisional deactivation mechanism for "hot" *sec*-butyl radicals.

Runs made with $\gamma=1.0$ and 10.0 reaffirmed the findings of Porter and Connelly that the pressure dependence of quantum yields is not a useful source of information about collisional activation and deactivation; plots of quantum yield vs pressure were very similar in shape for the two types of collisional mechanism.

These results indicate that attempts to obtain fluorescence spectra of extremely high resolution at low pressures would, if successful, prove most instructive in determining the nature of collisional vibrational energy transfer processes involving highly excited vibrational energy levels. The difficulties of making such measurements are formidable, and we know of no data currently available of sufficient resolution and taken at sufficiently low pressures to be compared with our findings.[19]

ACKNOWLEDGMENT

We are indebted to the Research Corporation for a grant supporting this work.

[18] R. E. Harrington, B. S. Rabinovitch, and M. R. Hoare, J. Chem. Phys. **33**, 744 (1960).

[19] See, for example, the remarks of Neuberger and Duncan in connection with nitrogen dioxide. D. Neuberger, thesis, The University of Rochester, 1953; D. Neuberger and A. B. F. Duncan, J. Chem. Phys. **22**, 1693 (1954).

THE JOURNAL OF CHEMICAL PHYSICS VOLUME 34, NUMBER 4 APRIL, 1961

$n\rightarrow\pi^*$ Electronic Transition in Pure Alkali Nitrate Melts*

G. PEDRO SMITH AND CHARLES R. BOSTON

Metallurgy Division, Oak Ridge National Laboratory,† Oak Ridge, Tennessee

(Received October 19, 1960)

The lowest-energy transition ($n\rightarrow\pi^*$) of the nitrate ion was found to shift in energy and intensity in a systematic way over the series of molten alkali nitrates from $LiNO_3$ through $CsNO_3$. The energy E of the band maximum varied in a linear way with the cationic radius. At 365°C (extrapolated for $CsNO_3$) E in electron volts was given by $(3.81+0.33/r_0)$, where r_0 is the cationic radius (Ahrens) in A. The temperature dependence dE/dT was of the order of -10^{-4} ev/deg and increased in magnitude with increasing cationic $1/r_0$. The f number (oscillator strength) decreased steadily along the series of alkali nitrates from 4.1×10^{-4} for $LiNO_3$ down to 0.86×10^{-4} for $RbNO_3$ and then rose again to 1.0×10^{-4} for $CsNO_3$. The thermal coefficient $(1/f)(df/dT)$ was in the range of 10^{-4} to 10^{-3} deg^{-1}. The bandwidth changed by only a small amount for changes either in cation or in temperature. The origin of the observed shifts was considered in terms of interionic cohesive forces by application of the Franck-Condon and conservation of energy principles to a localized transition in a classical ionic melt. Digital computer procedures for profile analysis were described whereby an absorption band may be separated from an overlapping absorption edge.

I. INTRODUCTION

An electronic molecular transition frequently occurs at a somewhat different energy when the molecule is dissolved in different solvents as, for example, in the well-known "solvent shifts" of $n\rightarrow\pi$ and $\pi\rightarrow\pi$ transitions. Presumably this effect of solvent on the absorption spectrum of a solute arises because of a change in the interaction between the solute molecules and their solvent environment in going from the ground state to the excited state. Some of the importance of this phenomenon lies in the expectation that, when it is better understood, it may become a tool for making direct measurements of intermolecular interactions. In systems of importance to chemistry and allied sciences, solute-solvent interactions are commonly too complex for *a priori* quantum mechanical analysis and significant theoretical understanding rests to a great extent on initial experimental disclosure of the relative importance of different molecular parameters. In the case of spectral "solvent shifts", the limited theoretical progress stems largely from the experimental discovery of instances in which the transition energy of a solute changes in a systematic way when certain molecular properties of the solvent are changed in a systematic way. However, examples of such systematic changes

* Presented in part at the 11th Annual Summer Symposium of the Division of Analytical Chemistry of the American Chemical Society in Schenectady, New York, June, 1958.

† Operated by the Union Carbide Corporation for the U. S. Atomic Energy Commission.

are of limited variety so that further empirical disclosures of systematic behavior are an essential prelude to theoretical advances.

The preponderance of work on the spectral shifts of internal molecular transitions (as distinguished, for example, from charge transfer to solvent and $d \rightarrow d$ transitions) has been done with organic molecules and has been attributed in different instances to permanent dipole forces, dispersion forces, hydrogen bonding, and repulsive overlap forces.

The present work is an extension of the solvent-shift type of phenomenon to ion-ion interactions in molten salts, and reports a systematic shift in transition energy for an internal transition of a molecule anion which accompanies a systematic change from one cation to another. Other spectral parameters were also checked for systematic changes and interesting results are described for the oscillator strength.

The lowest-energy transition of the nitrate ion gives rise to a weak absorption band in the neighborhood of 300 mμ which has been assigned to the excitation of a lone-pair, nonbonding electron (n orbital) on oxygen into an antibonding π orbital (π^* orbital) of the nitrate ion, that is, an $n \rightarrow \pi^*$ transition. This is a characteristic transition for ortho-oxyanions.[1]

Spectral profiles of the molten alkali nitrates were measured at several temperatures over a wavelength range of approx 250 to 360 mμ. The lowest-energy band was found to be overlapped by the edge of a much stronger band and the amount of this overlap was deduced through a quantitative analysis of the shape of the spectrum. From this analysis the parameters of the lowest-energy band were computed. The band energy and the f number were found to change from one alkali nitrate to another in a way which was systematic and which could be correlated with differences in cation size. This behavior is attributed to the effect which cation force fields have on the change in electron distribution which is characteristic of an $n \rightarrow \pi^*$ transition. The shift in band energy is empirically analogous to the "blue-shift" effect which polar solvents have on the $n \rightarrow \pi^*$ transition in organic solutes.[2]

II. EXPERIMENTAL

A. Materials

The lithium, sodium, and potassium nitrates were reagent grade. The best obtainable rubidium and cesium nitrates were supplied by the Fairmount Chemical Company and the Maywood Chemical Works, respectively. All of the nitrates were first recrystallized and then oven dried at 140°C. The optical cells were loaded in air with approx 5 g of material. Since these compounds do not react readily with small amounts of water, it was possible to carry out the final dehydration in the optical cells by bubbling dry argon through the melt for about 1 hr.

[1] S. P. McGlynn and M. Kasha, J. Chem. Phys. **24**, 481 (1956).
[2] J. W. Sidman, Chem. Rev. **58**, 689 (1950).

B. Apparatus

The spectrophotometer used in this work was a Cary model 11MS modified for high-temperature work. The instrumentation for the measurement and control of temperature was more than adequate to ensure an accuracy and control within 0.5°C. Melts were kept under an argon atmosphere. Short path lengths were obtained by use of precision, fused-silica inserts. The spectrophotometer and cells have been described.[3] The various misalignment errors usually associated with the use of inserts in work with aqueous solutions were studied by forcing an insert into positions of misalignment with a fused nitrate in the cell and then measuring the absorbance curve. Such errors were very small, presumably, because geometric restrictions limited considerably the amount of misalignment and because the fused nitrates have refractive indexes[4,5] close to that of fused silica.

C. Path Length

The spectral profiles which are reported here were obtained at two path lengths for each nitrate except $RbNO_3$. One path length was chosen so that band maxima lay in the absorbance range of 1.5 to 2.7. The other path length was shorter by a factor of 2 to 3.5 and was used to extend the spectra along a terminal absorption edge. This extension was not considered necessary for $RbNO_3$. The path lengths were as follows: 19.1 and 60.4 μ for $LiNO_3$, 60.4 and 115 μ for $NaNO_3$, 60.4 and 212 μ for both KNO_3 and $CsNO_3$, and 212 μ for $RbNO_3$. Additional data were obtained at other path lengths for the purpose of estimating errors in the extinction coefficient.

The well-known difficulties of determining such short path lengths with useful accuracy are tersely summarized by Kelly and Svensson.[6] In the present work, path-length calibrations were made mechanically by measuring the thickness of the insert and the inside dimensions of the cell (at several points) by means of several different precision micrometer devices, each involving different sources of error, and by absorption measurements using the Bouguer-Lambert Law. The results fell within a precision of 1%.

The absorption measurements for calibration purposes were made at 370.0 mμ using K_2CrO_4 solutions up to 0.06M in 0.05N aqueous KOH. The extinction coefficients for somewhat less concentrated K_2CrO_4 in aqueous NaOH solutions (rather than KOH) are known to be slightly concentration dependent.[7] However, the authors made measurements at 7 to 13 path lengths for each of four solutions ranging from 0.004339 to 0.06045M in K_2CrO_4 and 0.05N in KOH. Within the

[3] C. R. Boston and G. P. Smith, J. Phys. Chem. **62**, 409 (1958).
[4] H. Bloom and D. C. Rhodes, J. Phys. Chem. **60**, 791 (1956).
[5] O. H. Wagner, Z. physik. Chem. **131**, 409 (1928).
[6] J. W. Kelly and G. Svensson, J. Phys. Chem. **62**, 1076 (1958).
[7] G. Kortüm, Z. physik. Chem. **B33**, 243 (1936).

precision of the measurements (about 0.5%), no significant trend was found and the average extinction coefficient of 4842 liters/mole-cm at 370.0 mμ was only 0.6% greater than the value reported by Gibson[8] for 0.0002060M K_2CrO_4 in 0.05 N KOH.

D. Nitrite Interference

Special attention was given to the possibility of spectral interference from the nitrite ion, since this substance, a product of the thermal decomposition of the nitrate ion, absorbs in the near ultraviolet. The nitrite ion in fused nitrate solution was found to have an absorption minimum in the neighborhood of the lowest-energy nitrate band and an absorption maximum at approx 360 mμ where the fused nitrates are substantially transparent. Thus, inasmuch as all spectral measurements included the 360 mμ region, it was possible to detect the presence of nitrite ions before they became concentrated enough to affect appreciably the nitrate spectrum.

Nitrate melts were subjected to thermal treatments which were more severe than those involved in the spectral measurements. These melts were then cooled, dissolved in water, and analyzed for nitrite by a colorimetric method which involved the formation of an aminoazo complex. The concentration of nitrite ions in these melts was found to be only a few parts per million which is well below anything of spectral significance.

E. Correction for Light Losses

The quantity which was measured was $\log(I_1/I_2)$, where I_1 was the intensity incident on the absorption cell and I_2 was the intensity transmitted through the absorption cell. In order to obtain the *internal absorbance* A_i of the molten nitrate layers it was necessary to correct for light losses due to reflections at interfaces and due to absorption by the silica in the cell walls and insert. A detailed numerical computation of the magnitudes of these light losses, together with auxiliary measurements, showed that the necessary corrections could be made accurately by using as a reference a silica plate at the same temperature as the sample and of a thickness equal to the combined thicknesses of the two cell walls and insert. This simple method of correction was made possible by the fortuitous closeness of the refractive indexes of silica and the fused nitrates.[4,5] The corrections were small (about 0.03 absorbance units at 300 mμ) and varied only slightly with temperature. Computations for reflective losses at a single interface were based on the Cauchy-Beer formula. Of the several infinite series required to describe first-order multiple reflections from a system of six successive interfaces, only one, that for the two air-silica interfaces, gave a sensible correction.

[8] K. S. Gibson, *National Bureau of Standards Circular 484* (U. S. Government Printing Office, Washington, 1949).

F. Molar Extinction Coefficient

Spectra were obtained as chart recordings which were corrected for light losses, as discussed above, to give the internal absorbance $A_i(\lambda)$ as a continuous function of wavelength. Light absorption was attributed to the nitrate ion and, hence, the molar extinction coefficient $\epsilon(\lambda)$ was obtained from the relation $\epsilon(\lambda)=A_i(\lambda)/Mb$, where b is the path length in centimeters and M the concentration of nitrate ions in moles per liter.

Molar concentrations were determined from the following empirical equations in which t is the temperature in °C and the units of M are moles per liter: $M(LiNO_3)=27.88-0.00806t$, $M(NaNO_3)=25.00-0.00825t$, $M(KNO_3)=20.87-0.00725t$, $M(RbNO_3)=18.86-0.00658t$, $M(CsNO_3)=16.82-0.0058t$. These equations are based on extensive, precision density measurements made by G. F. Petersen of this Laboratory.

The reproducibility of $A_i(\lambda)$ was about 0.3% or else 0.003 absorbance units, whichever was greater. Absolute values of ϵ at band maxima were to within about 5% with the primary uncertainty residing in the path length.

III. GENERAL CHARACTERISTICS OF MOLTEN NITRATE SPECTRA

Figure 1 shows typical molten-nitrate spectra plotted as $\log\epsilon$ vs λ. The points marked off at 2 mμ intervals represent data used in a numerical profile analysis described below. The spectra in Fig. 1 are for $LiNO_3$ at 273°C, represented by circles; $NaNO_3$ at 314°C, represented by triangles; and $CsNO_3$ at 425°C, represented by squares. The shaded symbols represent data taken with the short path length cells which are referred to above.

In keeping with the notation of Rhodes and Ubbelohde[9] the band whose maximum is shown in Fig. 1 will be numbered **II**. This is the lowest-energy electronic band. The next band, of which only the absorption edge appears in Fig. 1, will be numbered **I**.

The spectra shown in Fig. 1 are mild variations of the characteristic spectrum of the nitrate ion in non-fused-salt media. The maximum of band **II** has generally been found in the neighborhood of 300 mμ with an extinction coefficient between 6 and 12 liters/mole-cm depending on the solvent composition. The maximum of band **I** has not often been measured, but in dilute aqueous solutions it has been reported[10,11] at approx 200 mμ with an extinction coefficient of 12 000 liters/mole-cm, and in crystalline potassium nitrate[11] at between 200 and 220 mμ with an absorption constant only 20 times greater than that of band **II**.

Some characteristic features of molten nitrate spectra are listed in Table I. The coordinates of the

[9] E. Rhodes and A. R. Ubbelohde, Proc. Roy. Soc. (London) **A251**, 156 (1959).

[10] G. Scheibe, Ber. deut. chem. Ges. **59**, 1321 (1926).

[11] I. Maslakowez, Z. Physik **51**, 696 (1928).

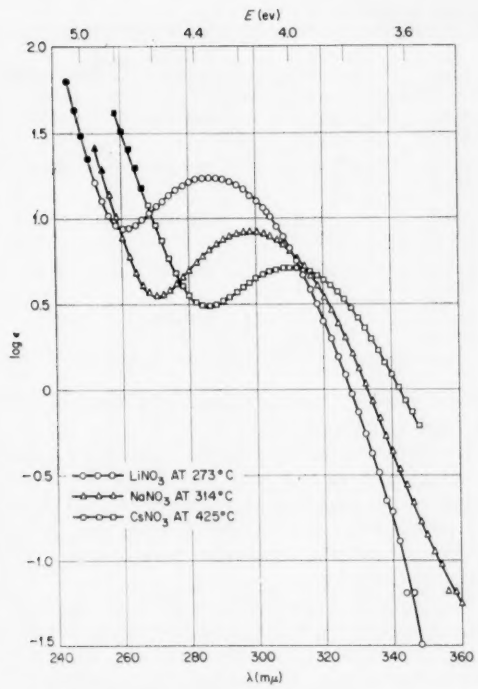

FIG. 1. Typical spectra of molten alkali nitrates in the neighborhood of the lowest-energy absorption band. The logarithm of the molar extinction coefficient (liters/mole-cm) is plotted on a linear wavelength scale with the corresponding photon energy in ev shown at the top of the graph. The spectra shown are for $LiNO_3$ at 273°C, represented by circles; $NaNO_3$ at 314°C, represented by triangles; and $CsNO_3$ at 425°C, represented by squares. The open symbols represent data taken with "long" path length cells while the filled symbols represent data taken with "short" path length cells. The sizes of long and short path length cells, which were different for different nitrates, are specified in the text.

maximum of band **II** are stipulated by ϵ_{max} and λ_{max}. The positions of the long wavelength edges of bands **I** and **II** are given, respectively, by the wavelength λ_I at which $\epsilon(\lambda)$ for band **I** equals ϵ_{max}, and by the wavelength λ_{II} at which $\epsilon(\lambda)$ for band **II** equals $\epsilon_{max}/2$.

The spectral range over which precise $\epsilon(\lambda)$ values could be determined are given under λ *Range* and the molar extinction coefficient at the short wavelength end of this range is denoted ϵ^*. Table I, together with Fig. 1, provides a survey of the influence which cation and temperature have on the grosser features of the nitrate spectrum.

The wavelength of the maximum of band **II** was determined as the limit at the maximum of the midpoints of a sequence of chords drawn across the band parallel to the wavelength axis. The precision was 0.1 to 0.2 mμ (order of 10^{-3} ev).

All available data on E_{max} are collected in Fig. 2. It will be seen that the temperature dependence of E_{max} is so small that it can be ascertained only in a very approximate way. The trend is such that dE_{max}/dT is negative, very roughly of the magnitude of -10^{-4} ev/deg (-2 cal/deg) and becomes a smaller negative number over the series from $LiNO_3$ to $CsNO_3$. The data for $CsNO_3$ are particularly limited and the formal extrapolation to 365°C, which is shown by a dashed line in Fig. 2 and used later, could be in error by 0.005 ev or more.

Differences in melting points and differences in rates of decomposition among the nitrates at higher temperatures preclude the possibility of measuring precise spectra for all of the nitrates over substantially the same temperature range.

IV. PREVIOUSLY MEASURED SPECTRA OF MOLTEN ALKALI NITRATES

In 1916, Schaefer[12] determined the ultraviolet spectrum of molten KNO_3 with results which compare well with those described here. (The "log mm" scale used by Schaefer equals $-\log\epsilon$ plus an unknown constant.) In 1957, Sakai[13] reported wavelength values for absorption edges of $RbNO_3$, $CsNO_3$, and NH_4NO_3 from room temperature to above their melting points. His values for molten $RbNO_3$ and $CsNO_3$ correspond to the energy values of the edge of band **I** given in Table I. This is in accord with the very short path length of 0.5 μ which he used. Sundheim and Greenberg[14] measured absorption edges of a large number of fused salts including the nitrates of lithium and potassium. The wavelength values which they report for these nitrates lie far out on the low-energy side of band **II** as will be

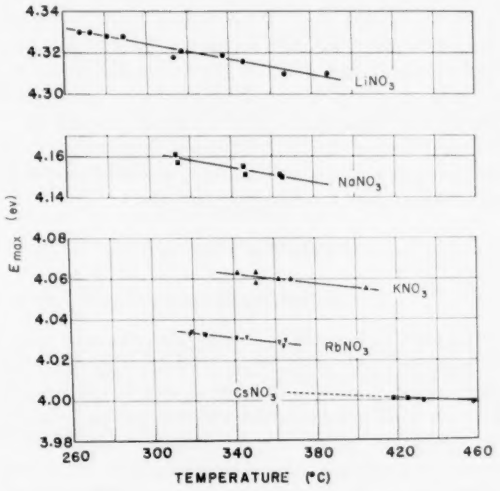

FIG. 2. Effect of temperature on the energy of the maximum of band **II**, E_{max}. The dashed line extrapolates the data for $CsNO_3$ to 365°C.

[12] K. Schaefer, Z. anorg. allgem Chem. **97**, 285 (1916).
[13] K. Sakai, J. Phys. Chem. **61**, 1131 (1957).
[14] B. R. Sundheim and J. Greenberg, J. Chem. Phys. **28**, 439 (1958).

TABLE I. Characteristics of selected spectra.

Melt	Temp. (°C)	ϵ_{max} (liter/mole-cm)	λ_{max} (mμ)	λ_{II} (mμ)	λ_{I} (mμ)	λ Range (mμ)	ϵ^* (liter/mole-cm)
$LiNO_3$	273	17.30	286.4	306.6	251.7	244–348	62.7
	367	16.70	287.7	309.5	257.4		
$NaNO_3$	314	8.37	298.3	317.3	259.5	252–360	25.5
	365	8.38	298.8	318.7	262.7		
KNO_3	342	4.78	305.2	324.7	266.8	258–360	16.8
	405	4.87	305.8	326.1	271.2		
$RbNO_3$	318	4.44	307.4	326.0	266.8	262–360	8.75
	365	4.45	307.9	327.3	270.1		
$CsNO_3$	425	5.12	309.9	330.0	275.3	258–348	41.1
	458	5.08	310.1	330.4	278.0		

seen by a comparison of their λ_0 values with the λ_{II} values in Table I. This agrees with the fact that they worked at a path length of 2000 μ. Rhodes and Ubbelohde[9] measured ultraviolet spectra of thin films of $LiNO_3$, $NaNO_3$, and KNO_3 in both the crystalline and molten states. From their plots, the coordinates of the maximum of band **II** may be estimated fairly well for a melt of $LiNO_3$ and rather roughly for a melt of $NaNO_3$. Assuming that they calculated the "absorption constant" as A_i/d rather than the frequently used quantity $2.303\ A_i/d$, we estimate that their values for the maximum of band **II** agree approximately with those reported here in Table I.

The profile analysis which will be described requires that band **I** be much stronger than band **II**. The data of Rhodes and Ubbelohde support this requirement for melts of $NaNO_3$ and KNO_3 but not for melts of $LiNO_3$. They report that band **I** for molten $LiNO_3$ at 264°C peaks at about 740 cm^{-1} which is only a little higher than the maximum of band **II**. In contrast with this, the measurements described here followed the absorption edge of band **I** at 273°C up to an A_i/d of about 1600 cm^{-1} (see ϵ^* in Table I) and at this point the edge was rising at a rate which was only a little slower than exponential. (See the following sections.)

V. PROFILE ANALYSIS

A. Profile Models

Inasmuch as band **II** is overlapped by band **I**, it was necessary to devise a procedure for separating the bands in the region of overlap in order to specify the spectral parameters of the transition associated with band **II**. The procedure which was followed was to construct numerical models of $\epsilon(\lambda)$ functions and to adjust parameters in these models so as to obtain a "best" fit with the experimentally measured $\epsilon(\lambda)$ functions. The models were chosen to be the sum of two functions, one of which could be identified with band **I** and the other with band **II**. In order to permit the use of numerical methods, the continuous experimental $\epsilon(\lambda)$ functions were digitized at 2 mμ intervals so as to obtain approx 50 points per spectrum. Such digitized points are shown in Fig. 1.

It will be necessary to discuss extinction coefficient functions both on a λ scale and on an E scale. For simplicity the following notation will be used. If $\epsilon(E)$ is a profile model on a uniform E scale, then the same model on a uniform λ scale, that is, $\epsilon(1240/\lambda)$, will be designated $\bar{\epsilon}(\lambda)$.

A qualitative examination of plots of $\log\epsilon$ vs E or vs λ, such as shown in Fig. 1, provides clues to a proper choice of profile models. For all of the nitrates, the long-λ edge of band **II** is essentially parabolic so that the band shape is essentially Gaussian. This is to be expected from previous studies of the profiles of bands without significant overlap.[15] On the other hand, the edge of band **I**, beyond the range within which overlap affects it, is almost linear with a very slight curvature. Thus, whatever the complete shape of band **I** may be, the segment of it which was measured can be approximated quite well by an exponential function. These qualitative considerations lead one to seek a suitable Gaussian function to represent band **II** combined with a suitable exponential function to represent band **I**.

Two models were selected for close study. Each consisted of the sum of a Gaussian function ϵ_{II}, identified with band **II**, and an exponential function ϵ_I, identified with the edge of band **I**. The first model, to be referred to as the Kuhn-Braun model,[16] was of the form

$$\epsilon(E) = \epsilon_0 \exp\{-[(E-E_0)/\theta]^2\} + \exp(aE-b), \quad (1)$$

and the second, to be referred to as the Lowry-Hudson model,[17] was of the form

$$\bar{\epsilon}(\lambda) = \epsilon_0 \exp\{-(\lambda-\lambda_0/\sigma)^2\} + \exp(w-v\lambda). \quad (2)$$

In these models, ϵ_0 and E_0 or λ_0 are the coordinates of the maximum of ϵ_{II} and are to be distinguished from ϵ_{max} and E_{max}, the coordinates of the maximum of the composite function $\epsilon(E)$. The constants θ and σ are

[15] C. K. Jörgensen, Acta Chem. Scand. **8**, 1495 (1954).
[16] W. Kuhn and E. Braun, Z. physik. Chem. **B8**, 281 (1930).
[17] T. M. Lowry and H. Hudson, Phil. Trans. Roy. Soc. London **A232**, 117 (1933).

TABLE II. Profile analysis with Lowry-Hudson model.

Melt	Temp. (°C)	ϵ_0 (liters/mole-cm)	λ_0 (mμ)	σ (mμ)	v (mμ^{-1})	w	δ (liters/mole-cm)	f ($\times 10^{-4}$)	λ Range (mμ)
$LiNO_3$	273	17.29	286.2	24.34	0.1829	48.73	0.048	3.98	248–348
	367	16.56	288.0	26.14	0.1568	42.83	0.076	4.05	252–352
$NaNO_3$	314	8.33	298.0	23.62	0.1587	43.22	0.048	1.713	256–360
	347	8.32	298.5	24.09	0.1521	41.79	0.053	1.738	258–360
	365	8.32	298.8	24.39	0.1493	41.22	0.057	1.742	258–360
KNO_3	342	4.75	305.2	23.66	0.1515	41.91	0.037	0.933	258–360
	368	4.78	305.5	24.00	0.1450	40.42	0.038	0.950	258–360
	405	4.81	306.0	24.57	0.1394	39.25	0.041	0.973	262–360
$RbNO_3$	318	4.41	306.8	23.15	0.1524	42.09	0.038	0.838	262–360
	341	4.46	307.3	23.51	0.1503	41.77	0.035	0.849	264–360
	365	4.41	307.6	23.83	0.1427	39.93	0.032	0.857	266–360
$CsNO_3$	425	5.07	310.2	24.68	0.1307	37.46	0.039	1.005	262–348

bandwidth constants, although each has a different physical significance because θ is on an E scale and σ is on a λ scale. The constants (a, b) and (w, v) describe the exponential extrapolation of band **I** on E and λ scales, respectively.

The digitized data were fitted to these profile models so as to minimize the sum of the squares of the residuals by methods developed by Dr. D. A. Gardiner and coded for digital computer by Mrs. G. J. Atta. (Both are members of the Mathematics Panel of this Laboratory.) Two methods of fitting were tested.

First was the *generalized Newton method*. The model was expanded in a Taylor's series about initial guesses of the parameters. Then the model was linearized by dropping second-order and higher terms. The experimental values (about 50 points in all cases) were substituted into the linearized model and a least-squares solution obtained. This gave corrections to the initial guesses of the parameters. The resultant first-corrected parameters were used for an iteration. This procedure was continued until successive iterations gave sums of the squares of the residuals which differed by no more than a few parts in 10^8. Convergence was tested over the series of iterations and was always satisfactory.

Second was *Garwood's method*.[18] This differed from the generalized Newton method in that the model was linearized by expanding its first derivative about initial guesses of the parameters and dropping terms above first order. Computations which used Garwood's method proved to be slower than those which used the generalized Newton method and did not lead to better estimates of the parameters.

The same computing procedures were used on profile models which consisted of the sum of two Gauss functions. However, the calculations did not converge in a satisfactory way and such models were abandoned. This behavior is presumed to have arisen from the fact that the edge of band **I** departed from an exponential function by only a slight amount.

[18] F. Garwood, Biometrika **32**, 48 (1941).

Profile studies also were made in which the shape of $\epsilon(E)$ was estimated by the functions proposed by Mead[19] and Jörgensen.[15] Mead's function did not give much better results than the Kuhn-Braun model, while Jörgensen's function gave results comparable with the Lowry-Hudson model.

Intensity considerations for a band are conveniently presented in terms of an integrated photon cross section. The empirical f number (oscillator strength) is used here for this purpose as defined by the relation

$$f = 2.303\times 10^{11}(\mathbf{m}/\pi\mathbf{e}hN_0)\int \epsilon(E)\,dE$$

$$= 3.483\times 10^{-5}\int \epsilon(E)\,dE, \quad (3)$$

where **m** and **e** are, respectively, the mass and charge of the electron, h is Plank's constant, N_0 is Avogadro's number, and the integration is taken over all sensible intensity of band **II**. When $\epsilon_{II}(E)$ functions from Eqs. (1) and (2) are substituted into Eq. (3) one obtains for the Kuhn-Braun model

$$f = 6.173\times 10^{-5}\theta\epsilon_0, \quad (4)$$

and for the Lowry-Hudson model

$$f = 0.07653(\epsilon_0\sigma/\lambda_0^2)\sum_{r=0}^{\infty}(\sigma/2\lambda_0)^r[(2r+1)!/r!]. \quad (5)$$

Convergence of the series in Eq. (5) depends on the ratio of σ to $2\lambda_0$. For the spectra reported here, this ratio was always in the neighborhood of 0.04 and the series converged very rapidly.

B. Results of Profile Analysis

Twelve spectra were fitted to both the Lowry-Hudson and the Kuhn-Braun profile models. Results for the Lowry-Hudson model are listed in Table II and a representative selection of results for the Kuhn-Braun model are listed in Table III. Both tables give

[19] A. Mead, Trans. Faraday Soc. **30**, 1052 (1934).

TABLE III. Profile analysis with Kuhn-Braun model.

Melt	Temp. (°C)	ϵ_0 (liters/mole-cm)	E_0 (ev)	θ (ev)	a (ev^{-1})	b	δ (liters/mole-cm)	f ($\times 10^{-4}$)
$LiNO_3$	273	17.41	4.340	0.3474	8.09	37.0	0.28	3.73
$NaNO_3$	347	8.33	4.159	0.3171	7.27	32.4	0.11	1.630
KNO_3	368	4.79	4.066	0.3056	7.76	34.3	0.08	0.903
$RbNO_3$	341	4.42	4.043	0.2960	7.85	34.8	0.08	0.808
$CsNO_3$	425	5.03	4.002	0.3034	7.24	31.0	0.06	0.942

values for the five parameters in the models, the standard deviation δ of the residuals, and the f number. Both models were fitted over the same wavelength ranges and these are listed in Table II.

The Lowry-Hudson model gives a significantly better fit than the Kuhn-Braun model. For all of the spectra, the standard deviation for the Kuhn-Braun model was 1.6 to 5.8 times as great as that for the Lowry-Hudson model. A correspondingly large divergence was found for the 95% confidence limits on the parameters for band **II** and on the f number. Values of the f number estimated by the Lowry-Hudson model are from 4–10% (average approx. 6%) above those estimated by the Kuhn-Braun model and will be taken as being more nearly correct. Values of λ_{max}, λ_I, and λ_{II} in Table I differ from those obtained from the Lowry-Hudson model by no more than 0.6 mμ and generally by much less. Values of ϵ_{max} in Table I differ by no more than the standard deviation from those computed by substituting λ_0 for λ in the Lowry-Hudson model.

An important consequence of fitting a linearized model to the data by the least-squares criterion is that the model lies first above and then below the data in a cyclic fashion. Because of this cycling, the least-squares criterion causes even a moderately poor model, such as the Kuhn-Braun profile, to give a moderately good fit.

The profile analyses show that band **II** has a Gaussian shape which is skewed toward higher energies. It is now generally recognized that smooth electronic bands nearly always have a near-Gaussian shape. Although it is often assumed that the Gaussian is symmetrical on an E scale, a skewness of the magnitude and direction reported here has been found for other electronic bands.[15,16] The Lowry-Hudson band profile is an approximate representation of the positive skewness (on an E scale) of band **II** and has the advantage over Jörgensen's function for curve fitting purposes of having a minimum number of parameters to be adjusted. It should be emphasized that no special meaning is attached to the fact that this profile is symmetrical on a wavelength scale.

VI. EMPIRICAL REGULARITIES

The primary facts to be deduced from the experimental data incorporated in Fig. 2 and Table II are the influence which temperature at the 600°K level and a molten-salt environment free of complex-forming cations have on the lowest-energy transition of the nitrate ion. A cursory scan of the data reveals that the effect which a 10% change in absolute temperature has on the parameters of band **II** is in every instance so small that it can be ascertained only in a rather approximate way. In contrast, the effect of changing from one alkali nitrate to another is substantial in all but a few instances. Of these environmental effects, the most striking is the systematic way in which the energy of the maximum of band **II** decreases over the series from $LiNO_3$ through $CsNO_3$.

It has long been recognized that very high concentrations (the order of 2 to 10M) of cations of noble-gas electron configurations will shift the lowest-energy band of the nitrate ion relative to its position in dilute aqueous solution.[20] The ratio of water molecules to cations in such solutions is sufficiently small to ensure that there will be many cation-anion pairs separated by no more than a single water molecule. Katzin[21] used t-butyl alcohol as a solvent so as to produce a high degree of ion clustering and thereby obtain direct cation-anion contact. He found that polyvalent cations of noble-gas configurations, such as Al^{3+} were more effective than Li^+ in shifting band **II** to higher energies and pointed out that the shift was "a function of electrostatic charge and effective ionic radius."

In a molten alkali nitrate, two simple forms of structural order can be recognized. First, the nitrate ion does not depart greatly from the D_{3h} symmetry of the isolated ion. The most convincing evidence for this comes from Raman measurements on molten nitrates.[22,23] Thus, it is possible to regard the spectral effects produced by changing from one alkali nitrate to another as perturbations of the molten-salt environment on the properties of an isolated nitrate ion. Second, the nitrate ion is surrounded by a "cage" or nearest-neighbor shell of alkali cations, which is deeply penetrated by nitrate anions because of their large relative size. That is, the alkali nitrates behave like "normal" ionic

[20] H. v. Halban and J. Eisenbrand, Z. physik. Chem. **132**, 401 (1928).
[21] L. I. Katzin, J. Chem. Phys. **18**, 789 (1950).
[22] E. F. Gross and V. A. Kolesova, Akad. Nauk. S.S.S.R. Pamyati S. I. Vavilova **1952**, 231.
[23] W. Bues, Z. physik. Chem. **10**, 1 (1957).

melts for the usual reasons of coulombic attraction and repulsion. Furthermore, radial distribution functions obtained from x-ray scattering measurements[24] on molten $NaNO_3$ and KNO_3 show that crystal radii persist in the melt. Thus, the cationic crystal radius is a meaningful parameter in the melt despite the fact that the precise distribution of cation-anion distances is unknown.

The correlation between the transition energy of band **II** and the reciprocal of the cation radius proves to be quantitatively simple as illustrated by Fig. 3. Of the various energy parameters which were determined, E_{max} (see Table I and Fig. 2) gives the best estimate of the mean transition energy of band **II** for two reasons. First, E_{max} may be determined with greater precision than the profile analysis parameter E_0; and, second, E_{max} intrinsically differs from the energy of the maximum of band **II** by a very small amount because the slope of $\epsilon_f(E)$ is very small at E_{max}.

The values of E_{max} in Fig. 3 are chosen at 365°C from Fig. 2. All of the nitrates except $CsNO_3$ were studied at a temperature near 365°C. The data for $CsNO_3$ were extrapolated to 365°C along the dashed line shown in Fig. 2. Values of the ionic radii in A are the crystal radii given by Ahrens.[25]

The correlation between E_{max} and $1/r_0$, shown in Fig. 3, is represented with fair accuracy by a straight line. The quantitative simplicity of this correlation is somewhat surprising since the crystal radii of the cations are only an approximate measure of their "effective" size in a melt. The straight line which is shown in Fig. 3 is given by the relation $E_{max}=3.81+0.33/r_0$ where r_0 is in A. The effect of temperature on E_{max} is shown in Fig. 2 and was discussed above. In brief, dE_{max}/dT corresponds to small thermal motions (-2 cal/deg), and an increase in temperature decreases the effect which cations have in shifting the band energy.

The f number of band **II** increases as a smoothly accelerating function of $1/r_0$ for all of the nitrates except $CsNO_3$, as shown in Table II. The f number for $CsNO_3$ lies slightly above the f numbers for $RbNO_3$ and KNO_3. The thermal coefficient $(1/f)(df/dT)$ amounts to about 10^{-4} to 10^{-3} deg^{-1} in all cases.

The width of band **II** is notable for its relative insensitivity to change from one alkali nitrate to another except for a small increase in going from $NaNO_3$ to $LiNO_3$. The bandwidth on an E scale is conveniently measured by the ratio of the f number to ϵ_0. This ratio is in the range of 1.9 to 2.1×10^{-5} at all temperatures for all of the alkali nitrates except $LiNO_3$. For $LiNO_3$ the ratio is about 2.4×10^{-5}. For each nitrate the bandwidth increases by a small amount with increasing temperature. This thermal broadening is almost universal for smooth electronic bands at elevated temperatures and undoubtedly arises from phonon-photon interactions.

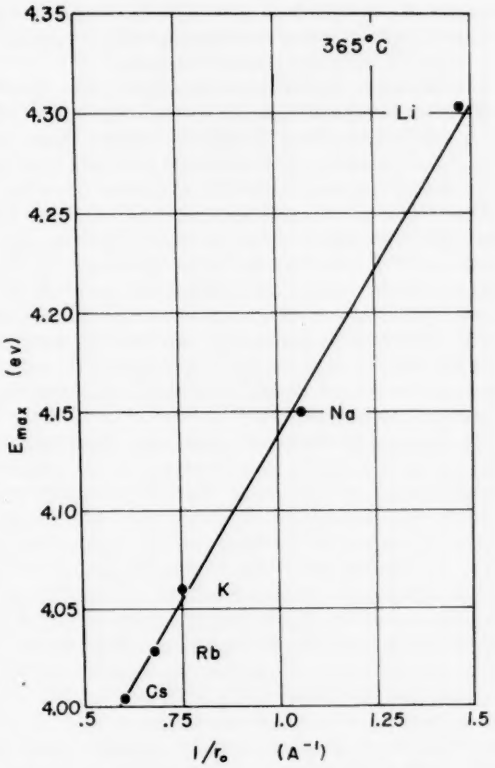

FIG. 3. The energy of the maximum of band **II**, E_{max}, at 365°C as a function of the reciprocal of the cationic radius, r_0. Values of r_0 are the crystal radii of Ahrens. The value of E_{max} for $CsNO_3$ is extrapolated to 365°C from measurements at higher temperatures.

VII. DISCUSSION OF RESULTS

A. Band-Energy Considerations

The electronic assignment of the lowest-energy nitrate band in terms of the linear combination of atomic orbitals (LCAO) molecular-orbital treatment has been discussed by Walsh,[26] McGlynn and Kasha,[1] Friend and Lyons,[27] and Sayre.[28] These treatments agree on the origin of the excited electron as an essentially lone-pair, nonbonding orbital on oxygen (n-type orbital) and on its destination as an antibonding π orbital spread over the molecule ion (π^* type orbital), that is, an $n\rightarrow\pi^*$ type of transition. There were several points of disagreement among these authors, one of which was the choice of electronic symmetry species for the excited state. In terms of the D_{3h} point-group symmetry of the isolated, nonvibrating ion, Sayre

[24] V. I. Danilov and S. Ia. Krasnitskii, Doklady Akad. Nauk. S.S.S.R. **101**, 661 (1955).
[25] L. H. Ahrens, Geochim. et Cosmochim. Acta. **2**, 155 (1952).
[26] A. D. Walsh, J. Chem. Soc. **1953**, 2301.
[27] J. A. Friend and L. E. Lyons, J. Chem. Soc. **1959**, 1572.
[28] E. V. Sayre, J. Chem. Phys. **31**, 73 (1959).

assigned the transition as $A_1' \rightarrow E'$, which is symmetry allowed, while the other authors assigned the transition as $A_1' \nrightarrow A_1''$, which is symmetry forbidden.

An empirical regularity which characterizes $n \rightarrow \pi^*$ transitions in organic molecules is the effect which solvents of progressively increasing polarity have in progressively shifting an $n \rightarrow \pi^*$ band for a solute molecule toward higher energies.[2] Superficially, this polar-solvent "blue-shift" effect appears to be paralleled by the blue-shift effect which cations of progressively increasing $1/r_0$ have on the $n \rightarrow \pi^*$ transition for the nitrate ion in molten salts. However, many of the known polar-solvent blue shifts occur in hydroxylic media where the band-shifting mechanism involves stabilization of n type electrons in the ground state by hydrogen bonding.[29] Clearly, this mechanism does not apply to alkali nitrate melts.

The nitrate ion blue-shift must arise from ion-ion interaction forces. The dominant forces are overlap repulsion and coulomb forces. As will be pointed out in more detail, overlap repulsion may well be an important factor in the blue-shift mechanism; however, the dependence of blue-shift on cationic $1/r_0$ or, including Katzin's observations, on cationic charge-to-radius ratio Z/r_0 suggests that Coulomb forces play a dominant role in shifting the transition energy. Working from existing data, one cannot distinguish separate contributions of overlap and Coulomb forces, but one can set up a model in which these forces occur in separate, additive terms and thereby examine from a theoretical view the way in which atomic parameters are involved in the Coulomb contribution alone.

The melt will be regarded as a classical ionic medium in the sense that its cohesive energy[30] U is assumed to arise from pairwise ion-ion interactions. That is, for a melt consisting of ions numbered 1 through m,

$$U = \tfrac{1}{2} \sum\nolimits^{0} [\phi_{ij}(\mathbf{r}_i, \mathbf{r}_j) + \gamma_{ij}(\mathbf{r}_i, \mathbf{r}_j)], \tag{6}$$

where $\sum^0$ is the summation over all i and j from one through m but excluding terms for which $i=j$; ϕ_{ij} is the coulomb potential energy between the ith and jth ions, a function of the vector coordinates $\mathbf{r}_i$ and $\mathbf{r}_j$ over the spaces of the ith and jth ions, respectively, and γ_{ij} is the overlap potential energy between the ith and jth ions. The electronic polarization of one ion by its neighbors will be neglected so that the electronic transition $n \rightarrow \pi^*$ will be regarded as localized on individual nitrate ions.

Let the melt, containing m ions, be irradiated with a pulse of photons over the bandwidth of the $n \rightarrow \pi^*$ transition so as to excite m' nitrate ions into the Franck-Condon, metastable excited state with the absorption of a total photon energy $m'E$. Number the excited nitrate ions 1 through m'. Denote the cohesive energy of the melt with these ions in the excited state as U' and the corresponding Coulomb and overlap terms as ϕ_{ij}' and γ_{ij}', respectively. From the Franck-Condon principle plus the restriction on electronic polarization, it follows that $(\phi_{ij}' - \phi_{ij})$ and $(\gamma_{ij}' - \gamma_{ij})$ are zero when neither i nor j equals one through m'. Thus, the change in cohesive energy which accompanies light absorption is

$$U' - U = \sum_{i=1}^{m'} \sum_{j=1}^{m}{}^{*} (\phi_{ij}' - \phi_{ij} + \gamma_{ij}' - \gamma_{ij}), \tag{7}$$

where the asterisk * signifies that terms for which j is 1 through m' are divided by 2 and terms for which j equals i are excluded.

The Coulomb potential energy

$$\sum_j{}^{*} \phi_{ij}'$$

due to the interaction of the ith excited nitrate ion with the rest of the ions in the melt is given more explicitly by the relation

$$\sum_j{}^{*} \phi_{ij}'(\mathbf{r}_i, \mathbf{r}_j) = \mathbf{e} \int \rho_i'(\mathbf{r}_i) V_i(\mathbf{r}_i) dv_i, \tag{8}$$

where $\mathbf{e}$ is the unit of electronic charge, ρ_i' is the charge-density function over the ith excited nitrate ion, V_i is the Coulomb potential which all of the other ions exert over the space of the ith ion, dv_i is a volume element in the ith ion, and the integration is over the space of the ith ion. The charge-density function ρ_i' may be expressed as the sum of four delta functions for the nuclear charges *minus* the electron-density function $|\psi_i'|^2$, where ψ_i' is the total electronic eigenfunction of the ith excited ion. The Coulomb potential V_i is given by the relation

$$V_i(\mathbf{r}_i) = \sum_{j=1}^{m}{}^{*} (\mathbf{e}/D) \int \frac{\rho_j(\mathbf{r}_j)}{|\mathbf{r}_j - \mathbf{r}_i|} dv_j, \tag{9}$$

where D is an effective dielectric constant, ρ_j is the charge-density function for the jth ion, and the volume integral is taken over the space of the jth ion.

The ground-state term $\sum_j{}^{*} \phi_{ij}$ in Eq. (7) is expressed by an equation like Eq. (8) in which ρ_i' is replaced by the ground-state charge-density function ρ_i which contains the ground-state electron-density function $|\psi_i|^2$. The Coulomb potential V_i for the ground state is slightly different from that for the excited state since the latter contains the charge-density functions of $m'-1$ excited nitrate ions. However, this will be ignored because the total number of nitrate ions $m/2$ is enormously greater than m'.

---

[29] G. J. Brealey and M. Kasha, J. Am. Chem. Soc. **73**, 5332 (1951).

[30] N. F. Mott and R. W. Gurney, *Electronic Processes in Ionic Crystals* (Oxford University Press, New York, 1948), 2nd ed., pp. 1–10.

It is convenient to introduce the notation

$$\Delta\Phi = \sum_{i=1}^{m'} \sum_{j=1}^{m}{}^{*}(\phi_{ij}' - \phi_{ij}), \tag{10a}$$

$$\Delta\Gamma = \sum_{i=1}^{m'} \sum_{j=1}^{m}{}^{*}(\gamma_{ij}' - \gamma_{ij}), \tag{10b}$$

where $\Delta\Phi$ is, by definition, the total change in Coulomb potential energy which accompanies the transition and $\Delta\Gamma$ is the corresponding total change in overlap energy. Substituting Eq. (8) for the excited-state terms and a like expression for the ground-state terms into Eq. (10a) and applying the Franck-Condon principle, one obtains

$$\Delta\Phi = -\mathbf{e}\sum_{i=1}^{m'} \int \{ |\psi_i'(\mathbf{r}_i)|^2 - |\psi_i(\mathbf{r}_i)|^2 \} V_i(\mathbf{r}_i) dv_i. \tag{11}$$

If one does an energy balance on the photon-absorbing process which was described above and neglects a small change in thermal energy, then one obtains for $m'E$ the total photon energy absorbed,

$$m'E = U' - U + m'E_\infty, \tag{12}$$

where $m'E_\infty$ is the transition energy of m' nitrate ions separated to infinity. Combining Eqs. (8), (11), and (12), and defining $E = m'E/m'$, one obtains

$$E - E_\infty = (1/m')(\Delta\Phi + \Delta\Gamma), \tag{13}$$

where $E - E_\infty$ must be regarded as an average over a distribution of configurational states. Now, consider two alkali nitrates each with a different species of cation C_1^+ and C_2^+, respectively. Denoting the energy terms for each nitrate by appropriate superscripts and recognizing that E_∞ is the same for both nitrates, one obtains from Eq. (13)

$$E^{(1)} - E^{(2)} = (1/m')[\Delta\Phi^{(1)} - \Delta\Phi^{(2)} + \Delta\Gamma^{(1)} - \Delta\Gamma^{(2)}]. \tag{14}$$

A qualitative statement of the experimental observation is that if $r_0^{(1)}$ and $r_0^{(2)}$ are the ionic radii of C_1^+ and C_2^+, respectively, then the experimental shift $E^{(1)} - E^{(2)}$ has the same sign as $1/r_0^{(1)} - 1/r_0^{(2)}$. Equation (14) relates this observation to the average change in interaction energy between the melt and the nitrate ions, and Eqs. (9) and (11) relate the Coulomb part of this change to atomic parameters.

From this point onward one should deal with the difference $\Delta\Phi^{(1)} - \Delta\Phi^{(2)}$ of Eq. (14) rather than the "absolute" $\Delta\Phi$ of Eq. (13) because certain terms which occur in $\Delta\Phi$, and which are difficult to evaluate, approximately cancel in $\Delta\Phi^{(1)} - \Delta\Phi^{(2)}$. However, the remaining discussion is very qualitative and much is gained in notational simplicity by dealing directly with $\Delta\Phi$.

The qualitative dependence of $\Delta\Phi$ on the cationic charge-to-radius ratio Z/r_0 follows from Eq. (9). [Equations (8) and (9) involve no special assumptions as to the net charges on the ions.] The contribution made by a shell of ions about the ith nitrate ion to the gradient in V_i decays very rapidly as the diameter of the shell of ions increases. Consequently, the major contribution comes from the nearest-neighbor shell, and as one changes from one nitrate to another the major change in the nearest-neighbor shell is the change in the species of cation. The Coulomb potential due to a cation of rare-gas configuration is essentially the same as that of a point charge so that the integral in Eq. (9) may be replaced by $Z/|\mathbf{r}_j - \mathbf{r}_i|$, where $\mathbf{r}_j$ is the fixed vector to the cation nucleus and $\mathbf{r}_i$ ranges over the volume of the nitrate ion. It follows that the potential close to a cation is approximately scaled according to Z/r_0. It is a maximum at cation nuclei and passes through minima along lines which interconnect cation nuclei. The presence of intervening neighbor anions suppresses these minima. The net potential V_i has an average positive value because nitrate is negative.

The $n \rightarrow \pi^*$ transition shifts charge density from the neighborhood of oxygens to the neighborhood of nitrogens with a conservation of total charge. Consequently, it is possible to divide the space of a nitrate ion into two regions, one around nitrogen and the other around oxygens such that the volume integral of $|\psi_i'|^2 - |\psi_i|^2$ has some positive value α over the space around nitrogen and has the corresponding negative value $-\alpha$ over the space around oxygens. Thus, for purposes of qualitative discussion, choose $|\psi_i'|^2 - |\psi_i|^2$ to be a step function with the value α over a region around nitrogen and the value $-\alpha$ over a region around oxygens. In like manner choose V_i to be a similar step function with the value $V_i^{(\mathrm{ox})}$ over the region around oxygens and $V_i^{(\mathrm{N})}$ over the region around nitrogen. Substituting these functions into Eq. (11) one obtains

$$\Delta\Phi/m' = -(\mathbf{e}\alpha/m')\sum_{i=1}^{m'}[V_i^{(\mathrm{N})} - V_i^{(\mathrm{ox})}]. \tag{15}$$

According to this expression the relative magnitudes of $V_i^{(\mathrm{N})}$ and $V_i^{(\mathrm{ox})}$ determine whether the Coulomb forces of the melt contribute toward a blue shift ($\Delta\Phi$ positive) or toward a red shift ($\Delta\Phi$ negative). The experiments say that $\Delta\Phi$ is positive.

Elementary electronic considerations[31] are sufficient to show that nitrogen-oxygen bonds on the nitrate ion in its ground state are polarized in such a direction that the charge around oxygens (electrons plus nuclei) is more negative than the charge around nitrogen. Therefore, the lowest-energy melt configurations will tend to be those in which nitrogen-oxygen bonds lie along directions in which $V_i^{(\mathrm{ox})}$ is greater than $V_i^{(\mathrm{N})}$. According to Eq. (15), this is the condition for a coulomb contribution to a blue shift. At a sufficiently low temperature such configurations will predominate. In a melt, of course, there will be configurations which are not energetically favorable and their increasing prevalence with increasing temperature will be manifest

[31] L. Pauling, *The Nature of the Chemical Bond* (Cornell University Press, Ithaca, N. Y., 1945), 2nd ed., p. 346.

in band broadening and in a decreasing contribution of the Coulomb potential to a blue shift. The observed thermal shift for all nitrates is of the order of -10^{-4} ev/deg (-2 cal/deg) which corresponds to the energy of small thermal motions.

The foregoing considerations describe in terms of a classical model the way in which Coulomb interaction forces in a simple melt can contribute to a localized anion transition. The application of the model to alkali nitrate melts involves uncertainties concerning the direction of the external Coulomb field. However, a possible basis is suggested for supposing that this direction is such as to correlate the contribution of the Coulomb interaction forces with the observed influence of cationic Z/r_0 and temperature.

Repulsive overlap forces decay rapidly with interionic distance so that they may be considered as existing only between nearest-neighbor ions. The $n\rightarrow\pi^*$ transition involves a net expansion of the nitrate charge cloud because of the occupancy of an antibonding orbital in the excited state. Most of this expansion probably occurs in the neighborhood of nitrogen. Consequently, collision between nitrate nitrogen and a neighbor ion results in an increase in overlap upon transition with a consequent increase in repulsive overlap energy of the system $\Delta\Gamma$ and a blue shift in transition energy.

B. Band-Intensity Considerations

The simplest basis for explaining the observed increase in f number with cationic $1/r_0$ over the series from $RbNO_3$ through $LiNO_3$ is in terms of the $A_1'\nrightarrow A_1''$ assignment mentioned in the preceding section. The forbidden character of this transition is presumably relaxed in part by coupling with appropriate vibrations and in part by an asymmetric external coulomb-potential V_i [see Eq. (9)] which modifies the D_{3h} point-group symmetry of the nuclear-charge field. Clear experimental evidence for the latter effect and its proper dependence on cationic Z/r_0 for ions of rare-gas configurations is given by Raman studies of the broadening and splitting of the doubly degenerate valence frequency ν_3 in nitrate melts.[22,23]

The origin of the small decrease in f number in going from $CsNO_3$ to $RbNO_3$ is unknown.

VIII. CONCLUDING REMARKS

Certain molecular electronic transitions are quite sensitive to the environment of the light-absorbing molecule. The importance of this phenomenon is the expectation that it may become a tool for making direct measurements of intermolecular interactions. At the present time the theoretical analysis of this phenomenon is sufficiently formidable so that progress is keyed to the experimental disclosure of correlations between changes in spectral parameters and corresponding changes in molecular parameters of the environment. The work described here extends these considerations to molten salts.

Systematic changes are reported in the lowest-energy transition of the nitrate ion over the series of molten alkali nitrates. The most striking of these systematic changes is the almost linear correlation between band energy and the reciprocal of the cationic radius. Another, less simple, correlation is reported between the empirical f number and the cationic radius. The procurement and analysis of these data were made possible by advances in the technique of molten-salt spectrophotometry and in the technique of numerical profile analysis.

A classical theoretical model is advanced in an endeavor to account for the experimental observations in terms of the cohesive forces between a nitrate ion and neighboring ions in a melt.

ACKNOWLEDGMENTS

We express our thanks to G. F. Petersen and W. M. Ewing of the Metallurgy Division who made many preliminary calculations by laborious manual procedures, also to Mr. Petersen for the density data, to Dr. D. A. Gardiner and Mrs. G. J. Atta of the Mathematics Panel for developing machine methods for numerical profile analysis, and to Dr. H. C. Schweinler of the Solid State Division for criticisms of theoretical ideas and for encouragement.

Ionization Potentials of Multiply Charged Krypton, Xenon, and Mercury

F. H. DORMAN AND J. D. MORRISON

Division of Chemical Physics, C.S.I.R.O. Chemical Research Laboratories, Melbourne, Australia

(Received September 9, 1960)

The determination of threshold potentials for multiple ionization processes is shown to depend on the threshold law assumed for these processes. Further support has been obtained for the previously proposed nth power rule for n-fold ionization by electron impact, and limits have been set to the values of the thresholds for multiple ionization in the rare gases and mercury.

INTRODUCTION

INTEREST in the physics of hot plasmas calls for quantitative data on the higher ionization potentials of the elements. For the lower members of the periodic table, many of the values of these ionization potentials are known with precision, but conspicuous gaps still appear in the table for some of the higher members.[1] Those higher ionization limits which have been determined have not been observed directly, since they lie in the x-ray region of the spectrum, and they have been deduced from spark or stellar spectra in the visible and near ultra-violet. The values found depend on numerous correlations and assignments of terms, and the difficulty of interpreting the spectra of complex atoms accounts for the lack of data concerning their ionization potentials.

Electron impact methods, in conjunction with a mass analyzer, provide a means of singling out and studying these processes of higher ionization in a direct manner. In practice, the determination of the ionization thresholds is not a perfectly straightforward matter. With increasing degree of ionization, the cross-section for the processes become progressively less, and in addition the ionization probability curves seem to approach the energy axis in a more and more slowly asymptotic manner. Nevertheless, the threshold energies for some processes of multiple ionization by electron impact were measured by Tate and Smith,[2] Bleakney,[3] and Smyth.[4]

Recent experimental work by the present authors[5] and others[6] has favored the view that the probability for the occurrence of a process of direct n-fold ionization induced by electron impact varies above the threshold as the nth power of the excess energy. These findings support the theoretical arguments of Wannier.[7] Almost simultaneously, Fox has claimed that while the process $He+e \rightarrow He^{2+}+3e$ obeys a square law, his data for n-fold ionization in the other rare gases are better interpreted by assuming linear threshold laws in all cases.[8] The disagreement between the two sets of findings will be shown to involve large errors in the determined threshold energies.

DISCUSSION AND RESULTS

It is plain that, if the nth power rule is correct, the methods of determining the threshold energy which have been applied to processes of direct single ionization need not necessarily give correct results for those of multiple ionization. To achieve accuracy in the determination of the thresholds, it is desirable to use a method which takes into account the form of the ionization probability curve for some distance above the threshold, rather than one like the vanishing current (V.C.) method, which depends on one or two points at the very foot of the curve. The differential method of interpretation[9] has a sound theoretical justification, but for processes where the degree of ionization is greater than two, the experimental scatter makes it impracticable. A very simple alternative, assuming that the probability of ionization $p(E)$ for a few volts above the threshold E_e is related to the energy E by an expression of the form $p(E)=K(E-E_e)^n$, is to plot the nth root of $p(E)$. This is not a very sensitive method for detecting the presence of higher excited states of ions, nor can it be used to identify the threshold law when n is large. This last point may be important, in that the efficiency curve for production of an n-charged ion need not necessarily be made up by the sum of only nth power curves. The method does have the advantage of being very little affected by scatter in the experimental points.

The low relative cross sections for processes of multiple ionization have the result that when the nth roots are plotted against the energy E, an extrapolation has to be made to obtain the threshold on the energy axis. This extrapolation ranges from 2 ev for a 3-charged ion to 30 ev for a 6-charged ion. Such a long extrapolation as the latter requires that the nth power

[1] C. E. Moore, "Atomic Energy Levels," Natl. Bur. Standards Circ. (U. S.) No. 467 (1959).
[2] J. T. Tate and P. T. Smith, Phys. Rev. **46**, 773 (1934).
[3] W. Bleakney, Phys. Rev. **35**, 139 (1930).
[4] H. D. Smyth, Revs. Modern Phys. **3**, 347 (1931).
[5] F. H. Dorman, J. D. Morrison, and A. J. C. Nicholson, J. Chem. Phys. **31**, 1335 (1959); J. D. Morrison and A. J. C. Nicholson, *ibid.* **31**, 1320 (1959).
[6] V. H. Dibeler and R. M. Reese, J. Chem. Phys. **31**, 282 (1959); M. Krauss, R. M. Reese, and V. H. Dibeler, J. Research Natl. Bur. Standards **63A**, 201 (1959).
[7] G. H. Wannier, Phys. Rev. **100**, 1180 (1956).
[8] R. E. Fox, *Advances in Mass Spectrometry* (Pergamon Press, New York, 1959), p. 397; J. Chem. Phys. **33**, 200 (1960).
[9] J. D. Morrison, J. Appl. Phys. **28**, 1409 (1957).

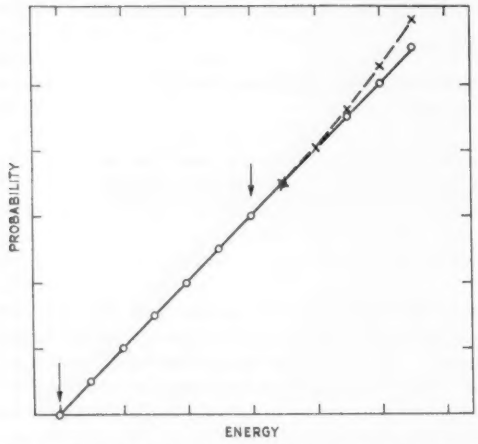

FIG. 1. Plots of the fourth root of the sum of two fourth power curves with (a) equal probabilities (circles) and (b) the upper curve ten times as probable as the lower (crosses). The thresholds of the two curves are indicated by arrows.

law hold over a range of as much as 40 ev from threshold. The presence of higher levels of the ion would tend to make the extrapolated threshold too high, while the gradual decrease in gradient which occurs in all ionization efficiency curves at higher energies might make the extrapolated value too low. The first of these sources of error can be shown to be insignificant when n is equal to or greater than 4. Figure 1 illustrates the fourth root of a curve made up by the sum of two fourth power curves with thresholds as indicated. The break is indistinguishable, and the error in finding the first threshold is negligible. The second source of error can be minimized by carrying out the extrapolation only when the experimental points in the nth root curve lie on a straight line for a range of at least a few volts.

Autoionization has been shown to contribute significantly to the production of singly-charged ions.[10] Such processes may also occur in the formation of multiply-charged ions, for example there is some evidence for cascade Auger processes in the multiple ionization of xenon by high-energy particles.[11] For such processes, it would be predicted that the resulting n-fold ionization would have a probability curve of lower than nth power. If such processes occur close to the threshold for direct n-fold ionization, the nth root plot may indicate a threshold which is lower than the correct value.

It may be considered therefore that the nth root extrapolation sets a definite lower limit to the value for the ionization threshold, and this limit is the correct value if the nth power rule is applicable. Because of the low cross section for processes of 3- and higher-fold ionization, the energy at which ion current is first detected sets, in all cases, a definite upper limit to the ionization potential, regardless of the threshold law.

In view of the disagreement with the findings by Fox, further confirmation has to be obtained of the fact that the nth power rule holds for n-fold ionization. The method of plotting the nth root of the ionization efficiency curves will be justified both by the linearity of the curves, and by the agreement of the thresholds found with available spectroscopic data. The experimental work was carried out mainly using a 5-in. radius 180° single-focussing mass spectrometer (the CEC 21.103), some of the curves being measured also with a 12-in. radius 60° sector instrument. An oxide cathode was used as a source of electrons, and the effective half-width of their energy distribution was determined to be 0.3 ev from the shape of the second differential I.E. curve for He^+. The energy scales were calibrated using the known values of the thresholds for the singly charged ions.

The nth root curves obtained for doubly and triply charged argon, krypton, and mercury, are shown in Figs. 2, 3, and 4. All of the curves and also the corresponding curves for xenon, are straight lines within experimental error, for at least 5 ev above threshold. The values of the thresholds are listed in Table I for comparison with the spectroscopic ionization potentials.

The agreement is good for the doubly charged ions, but poor for Kr^{3+} and Xe^{3+}. The disagreement for the latter may not be a serious objection, in that the spectroscopic values for the triply charged ions are estimates. It has to be admitted that the values obtained by Fox for Kr^{3+} and Xe^{3+} agree well with the present spectroscopic figures.

The nth root plots for 4-charged mercury, and for 4-, 5-, and 6-charged krypton are shown in Figs. 4 and

TABLE I.

Ion	Threshold potential: nth root extrapolation	Threshold potential: Spectroscopic[a]
Ar^{2+}	43.3	43.38
Kr^{2+}	38.1	38.56
Xe^{2+}	33.5	33.33
Hg^{2+}	29.0	29.18
Ar^{3+}	84.0	84.28
Kr^{3+}	73.3	75.46
Xe^{3+}	64.8	65.5
Hg^{3+}	63.5	63.38

[a] See footnote 1.

[10] F. H. Dorman, J. D. Morrison, and A. J. C. Nicholson, J. Chem. Phys. **32**, 378 (1960); J. D. Morrison, H. Hurzeler, M. G. Inghram, and H. Stanton, *ibid.* **33**, 821 (1960).

[11] E. H. S. Burhop, *The Auger Effect and Other Radiationless Transitions* (Cambridge University Press, New York, 1952).

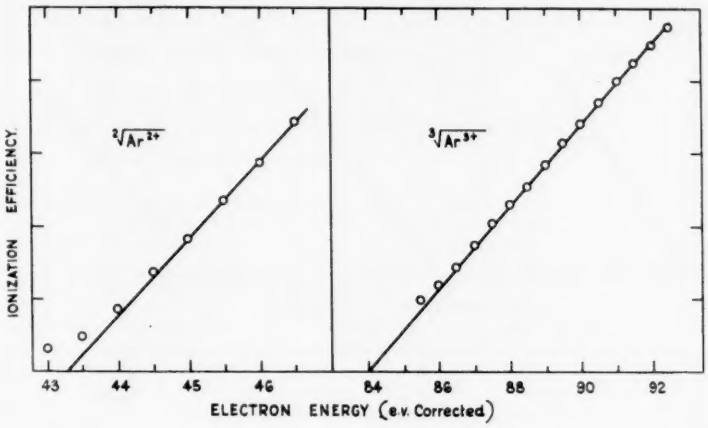

FIG. 2. Plots of the square and cube roots of the ionization efficiencies for Ar^{2+} and Ar^{3+}, respectively.

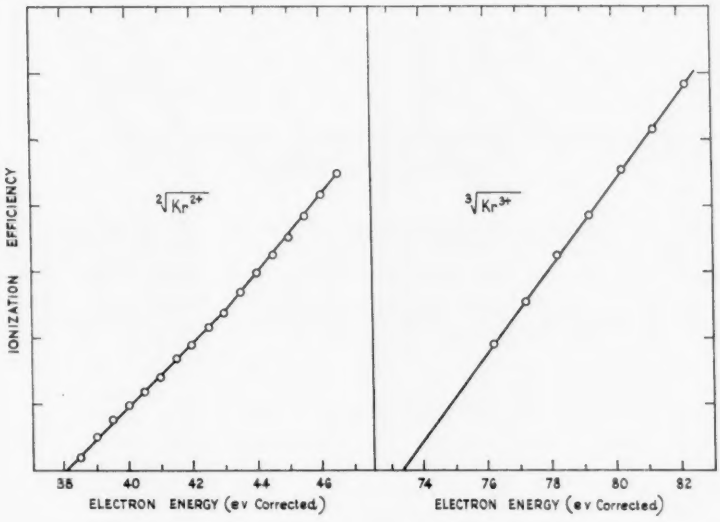

FIG. 3. Plots of the square and cube roots of the ionization efficiencies for Kr^{2+} and Kr^{3+}, respectively.

TABLE II.

Degree of charge	Krypton			Xenon			Mercury		
	*n*th root extrapolation	Direct extrapolation	Fox[8]	*n*th root extrapolation	Direct extrapolation	Fox[8]	*n*th root extrapolation	Direct extrapolation	Bleakney[3]
1	**14.0**	**14.0**		**12.1**	**12.1**		**10.4**	**10.4**	
2	38.1±0.1	38.5	38.45	33.5±0.2	33.3	33.3	29.0±0.2	29.8	30.2
3	73.3±0.2	77	75.6	64.8±0.5	65.4	66.2	63.5±0.5	68.5	71.4
4	118±1	130	146.6	107±1	111	110	113±1	122.5	144
5	181±2	195	217.5	160±1	171	170	158±2	175	227.5
6	275±10	310	350	218±1	246	255	225±10	300	...

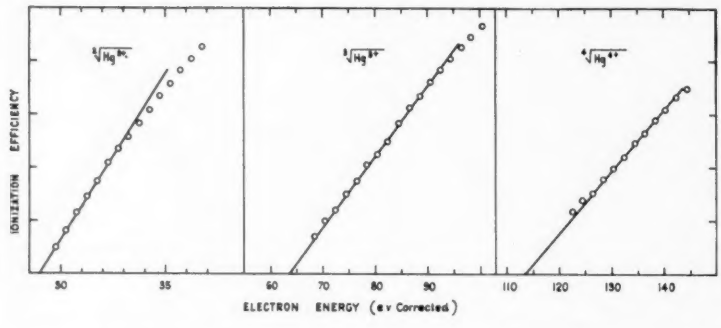

FIG. 4. Plots of the square, cube, and fourth roots of the ionization efficiency curves for Hg^{2+}, Hg^{3+}, and Hg^{4+}, respectively.

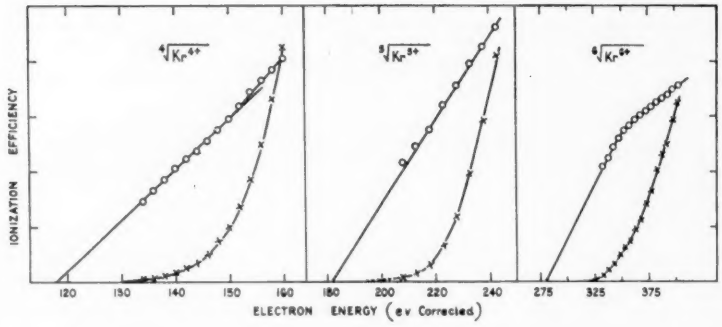

FIG. 5. Direct ionization efficiency curves (crosses) and nth root plots (circles) for 4-, 5-, and 6-charged krypton.

5. The curves for xenon have been recorded previously.[2] In all cases except Kr^{6+}, the nth root curves are reasonably good straight lines over the first few volts, and the uncertainty in the extrapolations to threshold is small. The direct I.E. curves, which are also shown in the figures, may be extrapolated to the energy axis to set definite upper limits to the ionization thresholds. Many of these values are lower than the estimates made by previous workers. All of the values found are collected in Table II.

Transient Measurements of Photochemical Processes in Dyes. I. The Photosensitized Oxidation of Phenol by Eosin and Related Dyes*

L. I. GROSSWEINER AND E. F. ZWICKER

Department of Physics, Illinois Institute of Technology, Technology Center, Chicago, Illinois

(Received September 6, 1960)

Irradiation of the fluorescein dyes in their visible absorption bands excites metastable triplet states which decay by the bimolecular reaction of triplet molecules. A rapid reaction of phenol with triplet eosin is shown by the retardation of the rate of aerobic photobleaching and an acceleration of the rate of triplet disappearance. The primary photochemical reaction between phenol or phenolate ion with the triplet dye produces a phenoxy free radical and a reduced dye free radical, which disappear in second-order processes. Numerical values are given for the rate constants of several elementary reactions. The competition between physical quenching and charge-transfer chemical reaction can be explained by spin-conserving processes.

I. INTRODUCTION

FLUORESCEIN and its halogenated derivatives are active photosensitizers of chemical reactions. Visible light absorbed by the dye induces chemical reaction of the solvent or added solute. The dye may either be dehalogenated, permanently bleached or remain unchanged. Investigations of the continuous photobleaching of the fluorescein dyes have shown that the contributing reactions are complex and depend on the specific reaction conditions. For example, aqueous eosin is photobleached only when oxygen is present, while ethanolic eosin is photobleached only when oxygen is excluded.[1,2] However, evacuated solutions of eosin in mixtures of water and ethanol are dehalogenated by irradiation.[3] Many workers have proposed and given evidence for photosensitization mechanisms involving long-lived states. A summary and bibliography of work prior to 1957 is given by Reid.[4] Most experimental results can be qualitatively explained with elementary processes proposed by Oster and Adelman[5,6] and Imamura and Koizumi.[2,3,7] Their conclusions most pertinent to our work can be summarized as follows: (a) in aqueous solutions the primary attack of oxygen is on an excited state of the dye of some 10^{-5} sec lifetime and presumably the lowest triplet state, and (b) various organic compounds such as ethanol, acetone, allyl thiourea, etc., react with triplet dye, reducing it to an unstable free radical. Our results support the conclusions from the continuous irradiation work in the main, although they conflict with the mechanism of radiationless decay of triplet dye assumed by these workers.[2,5]

Our interest in phenol as a photosensitized reductant is based on earlier flash photolysis work which showed that the irradiation of phenol solutions with ultraviolet light produces a transient substance, which was identified as the protonated phenoxy free radical.[8–10] The same species is produced when aqueous eosin and phenol mixtures are irradiated under conditions where only eosin absorbs light.[11] This paper reports additional flash spectroscopy measurements on dye-phenol solutions, flash bleaching results with photoelectric detection and some steady photobleaching experiments.

II. EXPERIMENTAL DETAILS

A. Flash Spectroscopy

The basic flash photolysis methods used were similar to those previously reported.[12,13] Two 30-cm fused-silica lamps with molybdenum electrodes and filled with xenon to 5 cm Hg were used in a parallel arrangement. A 35-μsec light flash was excited by a 20-μf capacitor charged to 10 kv. The spectroflash lamp was a 12 mm by 10 cm Vycor glass heavy-wall capillary tube with tungsten electrodes and filled with xenon to 2 cm Hg. It was excited by a 2-μf capacitor at 9 kv and gave a 20-μsec light flash with a continuous spectrum from 220 to 800 mμ. The flash lamps were fired in series with open air gaps and the timing controlled by the delaying sweep of a Tektronix type 545 oscilloscope. A Vycor glass irradiation cell was located between the two main flash lamps inside a polished aluminum reflector. The sample was contained inside a 25-cm-long inner cylinder which could be evacuated to 10^{-6} mm Hg. A concentric outer chamber held solutions to filter the incident light. Spectra were taken on a Hilger

* Supported by the U. S. Atomic Energy Commission.

[1] M. Imamura, J. Inst. Polytech. Osaka City Univ. **5**, 85 (1956).

[2] M. Imamura and M. Koizumi, Bull. Chem. Soc. Japan **29**, 899 (1956).

[3] M. Imamura and M. Koizumi, Bull. Chem. Soc. Japan **29**, 914 (1956).

[4] C. Reid, *Excited States in Chemistry and Biology* (Butterworths Scientific Publications, Ltd., London, 1957).

[5] G. Oster and A. H. Adelman, J. Am. Chem. Soc. **78**, 913 (1956).

[6] A. H. Adelman and G. Oster, J. Am. Chem. Soc. **78**, 3977 (1956).

[7] M. Imamura, Bull. Chem. Soc. Japan **30**, 249 (1956).

[8] L. I. Grossweiner, J. Chem. Phys. **24**, 1255 (1956).

[9] L. I. Grossweiner and W. A. Mulac, Radiation Research **10**, 515 (1959).

[10] L. I. Grossweiner and E. F. Zwicker, J. Chem. Phys. **32**, 305 (1960).

[11] L. I. Grossweiner and E. F. Zwicker, J. Chem. Phys. **31**, 1141 (1959).

[12] G. Porter, Proc. Roy. Soc. (London) **A200**, 284 (1950).

[13] L. I. Grossweiner and M. S. Matheson, J. Phys. Chem. **61**, 1089 (1957).

TABLE I. The quenching of dye fluorescence by phenol and phenolate ion.

Dye solution[a]	pH	Quenching constant (M^{-1})
27 μM fluorescein	8	13.3±0.5
27 μM fluorescein	12	19.9±0.5
14 μM eosin	8	22.3±0.9
14 μM eosin	12	13.2±0.6
140 μM eosin	4	22.3±0.5
57 μM erythrosin	8	3.1±0.3
57 μM erythrosin	12	5.3±0.5
100 μM rose bengal	8	6.0±0.6
100 μM rose bengal	12	11.0±0.5

[a] Air-saturated, 25°C.

E498 (medium) quartz prism spectrograph, with 0.15- to 0.35-mm slit widths. The wavelength on each plate was calibrated with a low-pressure mercury arc spectrum. The maximum error in the wavelength region of interest was 0.5 mμ, which is much smaller than the width of any of the absorption bands measured. Photographic density was measured with a Leeds and Northrup recording photoelectric microphotometer. The photographic plates, usually Kodak 103–F, 103–O and I–L, were calibrated with a Hilger seven-step neutral filter.

B. Flash Bleaching

Transmission changes after flash irradiation were followed with a Hilger E720 photoelectric scanning unit on the spectrograph. The light source was an Edgerton FX-1 flashtube with a 1-in. gap and excited at 100 wsec. The incident light uniformly irradiated a long face of a 1 by 1 by 4-cm Pyrex glass cell. Transmission changes were monitored through the perpendicular faces with a 6-v "automobile headlight" lamp. The 1P28 photomultiplier signal was directly coupled to a Tektronix type 545 oscilloscope and photographed with a Dumont type 299 camera. Vertical linearity was checked with Bausch and Lomb neutral density filters which were calibrated on a Beckman DU spectrophotometer. The time scale was checked with a Tektronix type 180 A time-mark generator. Useful measurements were possible from 100 μsec to any longer time and the sensitivity was better than 0.001 optical density.

C. Fluorescence and Continuous Photobleaching

Fluorescence quenching and photobleaching of dye solutions were measured with a simple apparatus in the same cell used for flash bleaching. The solutions were irradiated with a 6-v tungsten lamp while the light transmission in the main absorption band was measured with a 929 phototube. The fluorescence was measured with a 1P28 photomultiplier through a narrow slit near the front face of the cell and perpendicular to the incident beam. Spectral isolation of the incident and fluorescent light was effected with Corning bandpass and Farrand interference filters.

D. Chemicals

The commercial dyes used were Fluorescein (2-$NaOCOC_6H_4C$:C_6H_3-3-(:O)OC_6H_3-6-ONa), National Aniline, C.I.No. 766; Eosin Y (2′, 4′, 5′, 7′-tetrabromofluorescein), National Aniline, C.I.No. 768; Erythrosin B (2′, 4′, 5′, 7′-tetraiodofluorescein), Matheson Coleman and Bell, C.I.No. 773; Rose Bengal (2′, 4′, 5′, 7′-tetraiodo-3,6 dichlorofluorescein), Matheson Coleman and Bell, C.I. No. 779. The phenol was Merck, reagent grade. It was found that air-saturated solutions of dye and phenol slowly decompose in the dark and all solutions were mixed immediately before their use.

III. RESULTS

A. Quenching of Dye Fluorescence by Phenol

The quenching of dye fluorescence was measured in air-saturated solutions from 0.002 to 0.3 M phenol. No significant differences were observed in several runs with solutions evacuated to 10^{-5} mm Hg. Measurement at *p*H 8 in citric acid-Na_2HPO4 buffer showed the quenching action of phenol on basic eosin, and measurement at *p*H 12 in Na_3PO_4 showed the quenching action of phenolate ion on basic eosin. A run with 0.0001 M HCl checked the effect of phenol on acidic eosin. The other dyes were measured at *p*H 8 and *p*H 12. In all cases the Stern-Volmer equation was accurately followed over the range of phenol concentrations. The quenching constants [the quantity $k_6/(k_1+k_2)$ in Eq. (4)] are summarized in Table I. Their magnitude

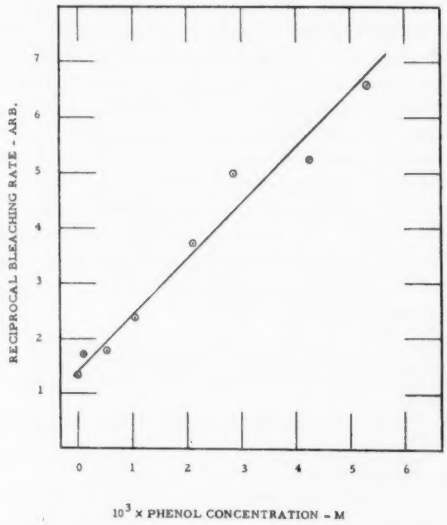

FIG. 1. Retardation of aerobic photobleaching of 6 μM eosin by phenol.

TABLE II. Transient spectra from the flash irradiation of phenol-dye mixtures.

Solution	*p*H	Transient bands[a]			
5 μM fluorescein+0.01 M phenol	6.8	359(s, vb)	399(w, n)	382(w, n)	
6 μM eosin+0.01 M phenol	6.8	369(vs, vb)	399(vs, n)	382(w, n)	
5 μM erythrosin+0.01 M phenol	6.8	373(s, vb)	399(s, n)		
4 μM rose bengal+0.01 M phenol	6.8	376(w, vb)	399(w, n)		
6 μM eosin+0.01 M phenol	7.4	369(w, vb)	399(vs, n)		
6 μM eosin+0.01 M phenol	8.9	405(vs, vb)		382(w, n)	
6 μM eosin+0.01 M phenol	11.8	405(vs, vb)		382(w, n)	
0.001 M phenol[b]	7		399(vs, n)	382(s, n)	368(w, n)

[a] Wavelength of peak in mμ. The first symbol inside the brackets indicates the relative intensity: vs—very strong, s—strong, w—weak; the second symbol indicates the width of the band: vb—very broad, n—narrow.
[b] Taken with unfiltered flash irradiation.

indicates that phenol and phenolate ion are "strong" quenchers and probably act through a diffusion-controlled process.

B. Photobleaching of Air-Saturated Eosin Solutions

Imamura[7] found that the retardation of the rate of aerobic photobleaching of aqueous eosin could be correlated for different additives with

$$(1/\phi)=(1/\phi_0)+K(A)/(H_2O), \qquad (1)$$

where ϕ is the quantum yield photobleaching, ϕ_0 is the quantum yield for photobleaching of pure aqueous solution, and K is a constant for each additive A. We performed similar experiments with phenol added to air-saturated eosin solutions. To eliminate *p*H changes due to phenol, the solutions were maintained at *p*H 7.5 with 0.1 M K_2HPO_4-KH_2PO_4 buffer. Check runs with unbuffered solutions and with *p*H 8 citric acid-Na_2HPO_4 and *p*H 8 NaOH-KH_2PO_4 showed no effect of added buffer salts on the photobleaching rate of air-saturated eosin. Figure 1 shows that the bleaching retardation by phenol agrees with Eq. (1). To compare these results with the compounds measured by Imamura,[7] we can calibrate our system with the quantum yield for photobleaching of air-saturated eosin at 30°C which is 2.7×10^{-4}.[1] In the units of Eq. (1), K for phenol is 1.5×10^{3}. This may be compared to 1.5×10^{2} for ethanol, 0.7×10^{3} for methanol, and 2.3×10^{3} for acetone.[7] It is apparent that the reaction between excited eosin and phenol is some 10^{3} times faster than the aliphatic alcohols.

C. Flash Spectroscopy of Dye and Dye-Phenol Solutions

The flash spectra were taken with 0.03% ferric ammonium citrate in the outer chamber of the 25-cm cell, limiting absorption to wavelengths above 350 mμ. Spectra of pure air-free dye solutions taken 10 to 100 μsec after flash irradiation show a considerable transient bleaching of the visible absorption bands, attaining 50% for high-flash lamp energies. Air-saturated solutions do not photobleach. Since there is a negligible permanent decomposition per flash for air-saturated solutions, it is clear that the primary action of oxygen is to quench the triplet state of the dye. A diffuse transient absorption spectrum with very broad bands near 400 and 580 mμ is present whenever eosin is temporarily photobleached. This is believed to be absorption by triplet eosin. It is consistent with the low temperature absorption spectrum of fluorescein under strong cross-illumination,[14] and one would not expect any other species than the triplet to absorb strongly above the main visible bands of eosin. A triplet absorption spectrum was detectable for erythrosin in the same spectral regions as eosin, but the resolution was too low for determination of the wavelength shift. A triplet spectrum was not observed for fluorescein or rose bengal.

It was previously reported that irradiation of eosin and phenol solutions with visible light produces the same transient species as the irradiation of phenol alone with ultraviolet light.[11] Analogous results for other dye-phenol mixtures are summarized in Table II. In air-free, slightly acidic solutions each transient spectrum taken shortly after irradiation shows a strong bleaching of the dye, the identical phenol transient spectrum, and a broad absorption band in the near ultraviolet. The peak positions of the latter shift towards longer wavelength in the same order as the visible absorption bands of the respective normal dye. They are believed to be the reduced dye free radicals, $DH\cdot$. For eosin, which was investigated in most detail, the $DH\cdot$ band is very weak at *p*H 7.4 and is replaced at higher *p*H by an intense band at 405 mμ. This band was distinguished from the triplet by its much higher intensity, narrower width, the absence of an associated longer wavelength absorption, and the fact that it was

[14] G. N. Lewis, D. Lipkin, and T. T. Magel, J. Am. Chem. Soc. **63**, 3005 (1941).

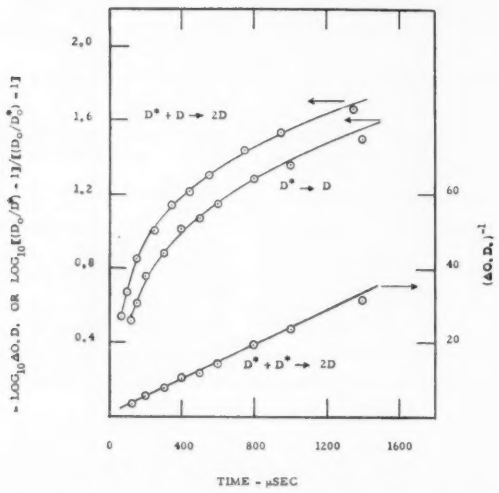

FIG. 2. Disappearance of triplet eosin by first-order deactivation, triplet-triplet reaction, and triplet-singlet reaction.

never observed when phenol was absent. It is believed to be due to the dissociated reduced dye free radical $(D\cdot)^-$. The situation is analogous to the spectra of the durosemiquinone free radicals in acidic and alkaline media as reported by Bridge and Porter.[15] The transient spectra are not obtained when oxygen is present, further evidence that the reaction of phenol is with the triplet dye. To summarize, the transient spectra obtained with eosin are the weak triplet bands near 400 and 580 mμ, the reduced dye free radical $DH\cdot$ at 369 mμ and the reduced dye radical-ion $(D\cdot)^-$ at 405 mμ.

The phenol transient spectrum was first assigned by Grosswiener and Mulac[9] and later by the present authors[10] to the phenol radical cation. Recent work of Land and Porter[16] shows that the doubly protonated durosemiquinone radical has a pK near -1. It would be surprising if this radical and the phenoxy radical have such widely different acidities in aqueous solution. However, the phenol transient spectrum in question was not observed in gas phase flash photolysis of phenol[17] and no other spectrum is obtained in strongly acid media[18] supporting the original assignment. We cannot resolve this question at present and shall refer to the transient species as the phenoxy radical, which may either be neutral or protonated. There is every indication from preliminary kinetic measurements that the free radicals observed are already in acid-base equilibrium. We conclude that the primary photochemical act in basic solution is an electron transfer from phenolate ion to triplet dye. In neutral and acid solution we cannot distinguish between electron and hydrogen transfer.

D. Flash Bleaching of Dye Solutions

Because of the very short lifetime of excited singlet dye and negligible permanent decomposition in air-free solutions, we may assume that the instantaneous concentration of bleached dye after flash irradiation is equal to the concentration of triplet dye. The following relationship holds between the concentration of triplet dye and the photoelectric transmission signal,

$$-\Delta(\text{O.D.}) = (\epsilon_D - \epsilon_{D^*})\, LD^* = \log_{10}(V/V_s), \qquad (2)$$

where D^* is the molar concentration of triplet dye, ϵ_D and ϵ_{D^*} are the molar extinction coefficients of normal and triplet dye, respectively, L is the optical path length, V_s is the initial photoelectric signal, and V is the instantaneous photoelectric signal. (In this paper we use the same symbol to represent the chemical species in reaction equations and the molar concentration of that species in rate equations.) For measurements at the peak of the dye absorption bands, the absorption contribution of the triplet dye was ignored.

Irradiation of eosin solutions with filters interposed between the flash lamp and cell showed that most of the transient bleaching is due to light absorption in the 516-mμ band. For example, considerable bleaching occurs with a Corning C.S. no. 3-70, which transmits only above 500 mμ. There was no evidence that the "dimer band" near 490 mμ behaves differently than the 516 mμ band. The extent of bleaching with a Corning C.S. no. 7-59 filter, which transmits from 300–480 mμ, is consistent with the light absorption in that wavelength region.

The triplet dye may be deactivated in any of three ways, ignoring quenching by impurities: first-order interaction with the surroundings, bimolecular collisions between triplet dye molecules, and bimolecular collisions between triplet and normal dye molecules. The integrated rate equations for the elementary processes are

$$D^* \rightarrow D \qquad D^* = D_0^* \exp(-kt) \qquad (3a)$$

$$D^* + D^* \rightarrow 2D \qquad (D^*)^{-1} = (D_0^*)^{-1} + kt \qquad (3b)$$

$$D^* + D \rightarrow 2D$$

$$[(D_0/D^*) - 1] = [(D_0/D_0^*) - 1] \exp(kD_0 t), \qquad (3c)$$

where D_0 is the initial concentration of normal dye and D_0^* is the concentration of triplet dye at some arbitrary short time after the light flash. Figure 2 shows the application of the above equations to flash bleaching of air-free eosin at pH 7.5. There is good agreement only with Eq. (3b). The analysis of numerous flash bleaching recovery curves showed good agreement with a bimolecular quenching reaction of triplet dye;

[15] N. K. Bridge and G. Porter, Proc. Roy. Soc. (London) **A244**, 276 (1958).
[16] E. J. Land and G. Porter, Proc. Chem. Soc. (London) to be published.
[17] G. Porter and F. J. Wright, Trans. Faraday Soc. **51**, 1469 (1955).
[18] G. Porter, private communication.

representative data is summarized in Table III. The absolute rate constant was obtained from the slope of the $(\Delta O.D.)^{-1}$ vs t plot, in each case, by means of Eq. (2) and neglecting the optical absorption by the triplet at the peak of the dye absorption, where the measurements were made. A bimolecular process is consistent with recent measurements of the decay of triplet anthracene,[19] chlorophylls,[20,21] and porphyrins.[22] It might be noted that Bridge and Porter[15] found only first-order decay of duroquinone triplets in liquid paraffin, so that this mechanism is not universally operative. The triplet eosin decay was also measured by transmission measurements at 405 mμ. [This wavelength was chosen for convenient correlation with other work done with a mercury arc monitoring lamp, and has no relationship to the eosin $(D\cdot)^-$ band which coincidentally peaks at 405 mμ.] The slope of the second-order decay curve, Fig. 3, and the rate constant obtained from Fig. 2 give an extinction coefficient for triplet eosin at 405 mμ of $3.8\times10^4\pm20\%$.

TABLE III. Rate constants for bimolecular decay of triplet dye.

Solution[a]	pH	Slope ($\times10^{-4}$)	ϵ_D ($\times10^{-4}$)[b]	Rate constant ($M^{-1}sec^{-1}$)
27 μM fluorescein	11.8	7.5	4.1	3.1×10^9
15 μM eosin	11.8	2.3	8.3	1.9×10^9
11 μM erythrosin	11.8	7.2	6.2	4.5×10^9
10 μM rose bengal	11.8	6.8	6.7	4.6×10^9
5 μM eosin	3.9	16.9	7.6	1.3×10^{10}
5 μM eosin	4.7	16.9	7.6	1.3×10^{10}
12 μM eosin	7.5	2.2	8.3	1.8×10^9
5 μM eosin	11.8	2.1	8.3	1.7×10^9

[a] Degassed to 10^{-5} mm Hg and measured in 1-cm-long cell.
[b] As measured on Beckman DU spectrophotometer for actual solutions.

The addition of phenol to evacuated eosin solutions causes two changes in the bleaching recovery curves; there is a permanent loss of dye at the end of each irradiation and the rate of return of coloration is accelerated near the beginning of the process. At the higher phenol concentrations transmission measurements at 405 mμ show that the eosin triplet is completely quenched before 100 μsec, and yet the dye return requires some 2000 μsec. This shows that the triplet has not simply been quenched to normal dye but instead has been converted into another product. Transmission measurements at 399 mμ show the strong transient absorption of the phenoxy radical and at 369 mμ the transient absorption of $DH\cdot$. These transients both decay by second-order processes. Thus, phenol must rapidly react with triplet eosin (competing with bimolecular decay of the triplet) and then a product of this reaction must decay by a process which returns normal dye. The obvious reactions are analogous to those proposed by earlier continuous irradiation experiments, $D^*+C_6H_5OH\rightarrow DH\cdot+C_6H_5O\cdot$; $DH\cdot+DH\cdot\rightarrow DH_2+D$. There is also a possibility of direct back-reaction between the product radicals, $DH\cdot+C_6H_5O\cdot\rightarrow D+C_6H_5OH$. Our present results do not

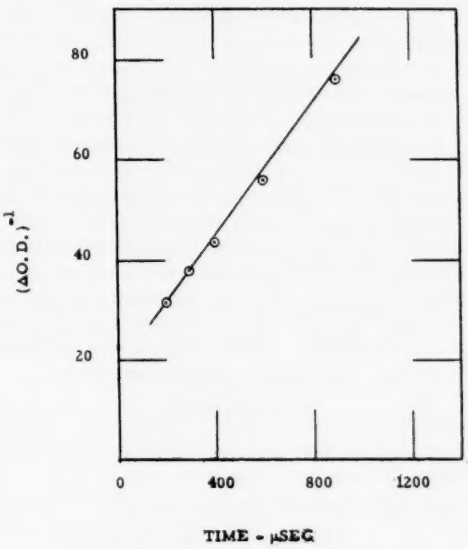

FIG. 3. Disappearance of triplet eosin at 405 mμ as a second-order process.

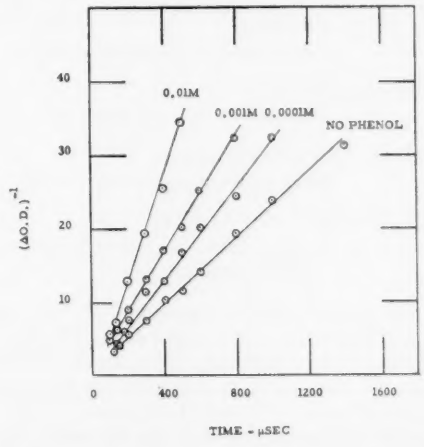

FIG. 4. Effect of phenol on the bleaching recovery rate of 12 μM eosin.

[19] H. Linschitz and L. Pekkarinen, J. Am. Chem. Soc. **82**, 2411 (1960).
[20] R. Livingston, J. Am. Chem. Soc. **77**, 2179 (1955).
[21] H. Linschitz and K. Sarkanen, J. Am. Chem. Soc. **80**, 4826 (1958).
[22] L. Pekkarinen and H. Linschitz, J. Am. Chem. Soc. **82**, 2407 (1960).

make it possible to determine whether this last reaction is significant.

A reasonable correction for the amount of weakly absorbing permanent products can be made by assuming that the concentration of $DH\cdot$ is equal to (D_0-D_f-D) where D_0 is the initial dye concentration, D_f is the permanent loss of dye, and D is the instantaneous dye concentration. This makes a relatively small error at the beginning of recovery where the total amount of bleached dye is much greater than the ultimate loss and becomes exact towards the end of recovery. Figure 4 shows the optical densities calculated in this way plotted as second-order processes. The recovery of dye remains second order, even at high phenol concentrations, in agreement with the mechanism presented.

IV. DISCUSSION

A sequence of elementary reactions pertinent to the above results is:

$D+$ light$\rightarrow D'$
Optical excitation of singlet dye;

(1) $D'\rightarrow D$
fluorescence of excited singlet dye;

(2) $D'\rightarrow D^*$
internal conversion to triplet;

(3) $D^*+D^*\rightarrow D+D$
nonradiative decay of triplet;

(4) $D^*+O_2\rightarrow D+O_2$
oxygen-quenching of triplet;

(5) $D^*+O_2\rightarrow$ products
attack of oxygen on triplet;

(6) $D'+C_6H_5OH\rightarrow D+C_6H_5OH$
phenol-quenching of excited singlet;

(7) $D^*+C_6H_5OH\rightarrow DH\cdot+C_6H_5O\cdot$
attack of phenol on triplet;

(8) $DH\cdot+DH\cdot\rightarrow DH_2+D$
dismutation of reduced dye;

(9) $DH\cdot+O_2\rightarrow D+HO_2\cdot$
oxidation of reduced dye;

(10) $C_6H_5O\cdot+C_6H_5O\cdot\rightarrow$ products
disappearance of phenoxy radical;

(11) $C_6H_5O\cdot+DH\cdot\rightarrow D+C_6H_5OH$
back-reaction of reduced dye and phenoxy radical.

The rate of reaction 2 was measured by Oster and Adelman.[5,6] Reactions 4, 5, 8, and 9 are proven by the work of Imamura and Koizumi.[1-3,7] Our results show the importance of reactions 3, 6, and 7, but do not distinguish between reactions 10 and 11. As previously noted, reaction 3 is in disagreement with the first-order decay of the triplet previously assumed and leads to different steady-state rate equations. The distinction should be evident in the dependence of the rate of photobleaching on light intensity. A linear relationship has been reported,[1,5] but it is not known whether this was examined at very low solute concentrations where the square-root intensity-dependence of reaction 3 is strongest.

The rate equations of these elementary reactions can be applied to our results. (a) Fluorescence quenching by phenol:

$$(F_0/F)=1+k_6C/(k_1+k_2), \tag{4}$$

where F and F_0 are the experimental fluorescence intensities in the presence and absence of phenol, respectively, and C is the phenol concentration. This is the well-known Stern-Volmer equation, where $(k_1+k_2)^{-1}$ is the total lifetime of the excited singlet state. Oster and Adelman[5] found that (k_1/k_2) is 9.80 for eosin. Applying this quantity and Brody's experimental value for the fluorescent lifetime of eosin of 1.6 mμ sec,[23] our measured quenching constant gives a value for k_i of 1.5×10^{10} M^{-1} sec^{-1}; (b) retardation of aerobic photobleaching: We can neglect reaction 3 for air-saturated solutions and also reaction 6 at moderate phenol concentrations. This leads to the following dependence of photobleaching quantum yield on phenol concentration,

$$(\phi_0/\phi)=1+k_7C/(k_4{}^0+k_5{}^0), \tag{5}$$

where

$$\phi_0=k_5{}^0k_2/(k_1+k_2)(k_4{}^0+k_5{}^0);$$

ϕ and ϕ_0 are the quantum yields for aerobic photobleaching in the presence and absence of phenol, respectively, and the superscript 0 indicates the product of the rate constant and the oxygen pressure in air-saturated solution. Using Imamura's quantum yield quoted above, we find that (k_5/k_4) equals 0.0029 and applying this to the slope of Fig. 1 gives a value for (k_i/k_4) of 0.19. Thus, the rate of reaction of phenol with triplet eosin is only about 20% slower than for oxygen-quenching; (c) flash bleaching of eosin-phenol solutions: The rate-constant of reaction 3 obtained from the data of Fig. 2 is 1.9×10^9 M^{-1} sec^{-1}. The minimum value of (k_8+k_{11}) from the data of Fig. 4 is 6×10^8 M^{-1} sec^{-1}. We cannot evaluate whether k_8 or k_{11} is more important, and work in progress is directed toward this end. The observation that 0.01 M phenol entirely quenches the eosin triplet leads to a maximum value for k_7 of 10^7 M^{-1} sec^{-1}, and therefore from the above, to a maximum value for k_4 of 10^8 M^{-1} sec^{-1}. Finally, measurements of the disappearance of the phenoxy radical at pH 7.5 give a bimolecular rate constant of 3×10^8 M^{-1} sec^{-1}, assuming an extinction coefficient for $C_6H_5O\cdot$ of 10^4.

These results show that there is a rapid chemical reaction between phenol or phenolate ion with the triplet state of the fluorescein dyes and no evidence of "physical quenching." At higher pH the primary act

[23] S. S. Brody, Rev. Sci. Instr. **28**, 1021 (1957).

is almost certainly an electron transfer from phenolate ion to triplet dye

$$C_6H_5O^- + D \rightarrow C_6H_5O\cdot + (D\cdot)^-.$$

It is pertinent to consider why this takes place to the exclusion of physical quenching. Porter and Wright[24] have ascribed the quenching of triplets by paramagnetic compounds to spin-conserving processes. A different mechanism which is valid for diamagnetic quenchers as well has been proposed by Linschitz and Pekkarinen.[19] They suggest that the potential energy surface of the triplet-quencher complex crosses that of a charge-transfer complex at small separation and that the latter mixes with the ground state of the singlet-quencher complex. Although neither model is directly applicable to charge-transfer chemical reaction in aqueous solution, it is interesting to examine the alternative processes, limiting discussion to spin-conserving reactions,

$$^3D^* + {}^1P^- \rightarrow {}^1D + (^3P^-)^* \qquad \text{physical quenching,}$$

$$^3D^* + {}^1P^- \rightarrow (^2D\cdot)^- + {}^2P\cdot \qquad \text{charge-transfer.}$$

A very rough estimate of the relative energies can be made from available spectral data. The difference between $^3D^*$ and ^1D from the eosin solution phosphorescence is 1.9 ev.[25] From the absorption spectrum of phenolate ion (probably an electron-transfer process) we estimate the difference between $^1P^-$ and $^2P\cdot$ as 4.3 ev. Assuming that $(^3P^-)^*$ is the phosphorescent state of phenol, the energy above the ground state is 3.5 ev.[25] Finally, we can estimate $(^2D\cdot)^-$ by assuming that the transferred electron fills the dye molecular orbital vacated by excitation of the triplet at the energy of the lowest allowed absorption of eosin, which is -2.4 ev. We find that charge transfer from phenolate ion to triplet phenol requires 0.0 ev, while physical quenching is endothermic by 1.6 ev. It is doubtful whether energy changes in internal modes or due to hydration would alter the qualitative result.

[24] G. Porter and M. R. Wright, J. chim. phys. **705**, (1958).

[25] P. Pringsheim, *Fluorescence and Phosphorescence* (Interscience Publishers, Inc., New York, 1949).

V. CONCLUSIONS

1. Irradiation of aqueous fluorescein dyes in their visible absorption bands excites metastable triplet states; for eosin, the triplet absorption spectrum shows weak maxima near 400 and 580 mμ, with an extinction coefficient of $3.8\times10^4\pm20\%$ M^{-1} cm^{-1} at 405 mμ.

2. The dye triplets disappear in bimolecular quenching reactions between triplet molecules, with rate constants from 2 to 5×10^9 M^{-1} sec^{-1} for the different basic dyes; the bimolecular rate for acidic eosin is some ten times larger.

3. Flash irradiation of dye-phenol solutions produces transient absorption spectra of the reduced dye free radicals ($DH\cdot$) and a free radical from phenol which is either the neutral or protonated phenoxy free radical. For eosin, the $DH\cdot$ absorption maximum is at 369 mμ; above *pH* 8 this spectrum is replaced by that of $(D\cdot)^-$ with a maximum at 405 mμ.

4. Although phenol quenches the fluorescence of excited singlet eosin with a bimolecular rate constant of 1.5×10^{10} M^{-1} sec^{-1}, a reduction of eosin is much more probable in the reaction of triplet eosin with phenol. The bimolecular rate constant for reduction of triplet eosin by phenol is 0.19 times that for quenching of triplet eosin by oxygen. Another indication of the efficient reaction of triplet eosin with phenol is that the rate of retardation of the photobleaching of aerated eosin by phenol is about 10^3 larger than for aliphatic alcohols and ketones. The favorable energetics of the triplet eosin-phenol reaction are consistent with a spin-conserving process.

ACKNOWLEDGMENT

The authors wish to thank Professor F. F. Cleveland of this department for the use of the Leeds and Northrup microphotometer in the Spectroscopy Laboratory.

Heat Capacities and Thermodynamic Functions of ZrH_2 and ZrD_2 from 5 to 350°K and the Hydrogen Vibration Frequency in ZrH_2†

HOWARD E. FLOTOW AND DARRELL W. OSBORNE

Argonne National Laboratory, Argonne, Illinois

(Received October 17, 1960)

The heat capacities of ZrH_2 and ZrD_2 were measured in an adiabatic type calorimeter from 5 to 350°K. X-ray analyses showed the hydrides consist of a single face-centered tetragonal phase. The data for both compounds below 11°K were found to fit the equation $C_v=9.8\times10^{-4}T+464.6(T/\theta)^3$ cal deg^{-1} mole^{-1}, where $\theta=311.4$, and this equation was used to extrapolate the heat capacities below 6°K. Between 20 and 100°K the C_p of ZrD_2 averages 1% lower than that of ZrH_2 but above 110°K the C_p of ZrD_2 becomes increasingly greater than that of ZrH_2. At 298.15°K the heat capacities and thermodynamic functions calculated from the data are $C_p=7.396\pm0.015$ cal deg^{-1} mole^{-1}, $S^\circ=8.374\pm0.02$ cal deg^{-1} mole^{-1}, $H^\circ-H_0^\circ=1284.1\pm2$ cal mole^{-1}, and $(F^\circ-H_0^\circ)/T=-4.067\pm0.01$ cal deg^{-1} mole^{-1} for ZrH_2, and 9.631 ± 0.019, 9.168 ± 0.02, 1474.4 ± 3, and -4.223 ± 0.01, respectively, for ZrD_2. The free energy of formation of ZrH_2 at 298.15°K is -30.9 ± 2 kcal mole^{-1} and that of ZrD_2 is -31.2 ± 2. On the assumption that the difference in the heat capacity between the two isotopic compounds arises from a triply degenerate hydrogen vibration, it was found that the difference in the temperature range 100 to 350°K could be satisfactorily fitted by the difference between two Einstein heat capacity functions with a frequency of 1190 ± 30 cm^{-1} for ZrH_2 and $1190/\sqrt{2}$ cm^{-1} for ZrD_2. This result is compared with the optical lattice vibration frequency found by neutron scattering experiments.

INTRODUCTION

ZIRCONIUM reacts with hydrogen to form a continuous range of compositions up to ZrH_2. These hydrides seem to be metallic compounds, as evidenced by their electrical conductivity,[1] which is comparable to that of zirconium metal, and by their metallic luster. The phase diagram has been outlined for temperatures between 25 and 900°C on the basis of equilibrium hydrogen pressures,[2–11] x-ray diffraction data,[12–23] and heat content measurements.[24] At room temperature over the composition range Zr to $ZrH_{1.44}$ there are two phases, α-Zr (hexagonal close-packed) and δ-hydride (face-centered cubic). From $ZrH_{1.44}$ to $ZrH_{1.6}$ there is a single phase, the δ-hydride; from $ZrH_{1.6}$ to $ZrH_{1.7}$ there are two phases, the δ-hydride and the ε-hydride (tetragonal); and from $ZrH_{1.7}$ to ZrH_2 there is only one phase, the ε-hydride. These composition limits were taken from a recent review article by Libowitz.[11]

There are no published experimental values for the heat capacities of zirconium hydrides below 0°C. Douglas and Victor[25] have reported mean heat capacities which were derived from their heat content data for five compositions of ZrH_x ($x=0.324$, 0.556, 0.701, 0.999, and 1.071) from 0 to 900°C. This paper presents determinations of the heat capacities of the isotopic hydrides ZrH_2 and ZrD_2 from 5 to 350°K.

From neutron scattering experiments[26–29] it is known that zirconium hydride has an optical lattice vibration; the frequencies 1049 and 1105 cm^{-1} have been reported for $ZrH_{1.5}$ and 1129 cm^{-1} for $ZrH_{1.8}$. In this mode of vibration the hydrogen atoms are vibrating nearly

† Based on work performed under the auspices of the U. S. Atomic Energy Commission.

[1] P. W. Bickel, Atomic Energy Commission Research and Development Report NAA-SR-4173, January, 1960. (Available from the office of Technical Services Department of Commerce, Washington 25, D. C. Price $0.50.)

[2] A. Sieverts and E. Roell, Z. anorg. u. allgem. Chem. **153**, 289 (1926).

[3] M. N. A. Hall, S. L. H. Martin, and A. L. G. Rees, Trans. Faraday Soc. **41**, 306 (1945).

[4] S. L. H. Martin and A. L. G. Rees, Trans. Faraday Soc. **50**, 343 (1954).

[5] R. K. Edwards, P. Levesque, and D. Cubicciotti, J. Am. Chem. Soc. **77**, 1307 (1955).

[6] E. A. Gulbransen and K. F. Andrew, J. Metals **7**, 136 (1955).

[7] C. E. Ells and A. D. McQuillan, J. Inst. Metals **85**, 89 (1956–57).

[8] M. W. Mallett and W. M. Albrecht, J. Electrochem. Soc. **104**, 142 (1957).

[9] L. D. LaGrange, L. J. Dykstra, J. M. Dixon, and U. Merten, J. Phys. Chem. **63**, 2035 (1959).

[10] J. R. Morton and D. S. Stark, Trans. Faraday Soc. **56**, 351 (1960).

[11] G. G. Libowitz, J. Nuclear Materials **2**, 1 (1960).

[12] G. Hägg, Z. physik. Chem. (Leipzig) **B11**, 433 (1931).

[13] J. Fitzwilliam, A. Kaufmann, and C. Squire, J. Chem. Phys. **9**, 678 (1941).

[14] R. E. Rundle, C. G. Shull, and E. O. Wollan, Acta Cryst. **5**, 22 (1952).

[15] E. A. Gulbransen and K. F. Andrew, J. Electrochem. Soc. **101**, 474 (1954).

[16] C. M. Schwartz and M. W. Mallett, Trans. Am. Soc. Metals **46**, 651 (1954).

[17] W. Trzebiatowski and B. Stalinski, Roczniki Chem. **30**, 691 (1956).

[18] D. A. Vaughan and J. R. Bridge, J. Metals **8**, 528 (1956).

[19] V. V. Sof'ina, Z. M. Azarkh, and N. N. Orlova, Soviet Phys. Cryst. **3**, 544 (1958).

[20] H. L. Yakel, Jr., Acta Cryst. **11**, 46 (1958).

[21] D. Whitwham, M. A. Huber, and J. Hérenguel, Acta Met. **7**, 65 (1959).

[22] P. Azou and P. Bastien, Compt. rend. **249**, 1105 (1959).

[23] O. T. Maliuchkov and B. N. Finkel'stein, Doklady Akad. Nauk S.S.S.R. **127**, 822 (1959).

[24] T. B. Douglas, J. Am. Chem. Soc. **80**, 5040 (1958).

[25] T. B. Douglas and A. C. Victor, J. Research Natl. Bur. Standards **61**, 13 (1958).

[26] I. Pelah, C. M. Eisenhauer, D. J. Hughes, and H. Palevsky, Phys. Rev. **108**, 1091 (1957).

[27] A. Andresen, A. W. McReynolds, M. Nelkin, M. Rosenbluth, and W. L. Whittemore, Phys. Rev. **108**, 1092 (1957).

[28] W. L. Whittemore and A. W. McReynolds, Phys. Rev. **113**, 806 (1959).

[29] A. D. B. Woods, B. N. Brockhouse, M. Sakamoto, and R. N. Sinclair (Atomic Energy of Canada Ltd., Chalk River, Ontario), to be published.

independently, with the zirconium atoms remaining essentially stationary, and therefore the frequency should be lowered in the corresponding deuterium compound by a factor of approximately $1/\sqrt{2}$. If the contributions of the acoustic modes and of the electrons to the heat capacity are the same in ZrH_2 and ZrD_2 the difference in the heat capacities of these compounds is due to this change in the optical frequency upon isotopic substitution, and it should be possible to determine the hydrogen vibration frequency from the heat capacity measurements. We have found that the difference in the measured heat capacities of ZrH_2 and ZrD_2 as a function of temperature can be fit by the difference between two Einstein heat capacity functions with characteristic frequencies $\tilde{\nu}=1190$ cm^{-1} and $1190/\sqrt{2}$ cm^{-1}, respectively, which we consider to be the hydrogen and deuterium vibration frequencies.

SAMPLES

The ZrH_2 and ZrD_2 samples were prepared on a high vacuum line by direct reaction of zirconium metal with hydrogen and deuterium, respectively, at 1-atm pressure and at a temperature of about 400°C. Purified hydrogen and deuterium gases were generated by the thermal decomposition of UH_3 and UD_3, respectively. After the reaction was complete the samples were gradually cooled to room temperature over a period of 4 hr and then the unreacted gas was evacuated.

The hydrogen or deuterium content was determined by two independent methods. One measurement was obtained from the difference in weight between the zirconium metal and the hydrided metal. This gave $H/Zr=2.003\pm0.004$ and $D/Zr=2.001\pm0.004$. The second measurement was obtained by thermally decomposing a known amount of the sample at 1000°C and measuring the total volume of gas evolved. This gave $H/Zr=2.001\pm0.004$ and $D/Zr=1.998\pm0.004$. The composition of the samples used for this experiment can be represented within experimental error by the formulas $ZrH_{2.000}$ and $ZrD_{2.000}$, if no correction is made for the small amount of hydrogen present in the deuterium. The deuterium gas, obtained from General Dynamics Company, assayed 99.65 atom % D and 0.35 atom % H. The gas from a thermally decomposed portion of ZrD_2 gave the same isotopic analysis.

Spectrographic analyses showed the samples to contain amounts of impurities equal to the following in parts per million: Ag, 0.2; Al, 15; B, 0.1; Cr, 4; Cu, 100; Fe, 200; Ni, 4; and Pb, 2. The following elements were looked for but were not detected (the numbers indicate the limits of sensitivity in parts per million): As, 50; Ba, 20; Be, 1; Bi, 1; Ca, 100; Ce, 200; Co, 1; Dy, 100; Er, 20; Eu, 10; Gd, 100; Hf, 200; Ho, 100; K, 20; La, 20; Li, 1; Lu, 20; Mg, 1; Mn, 1; Mo, 100; Na, 1; Nb, 50; Nd, 100; P, 50; Pr, 200; Rb, 20; Sb, 1; Sc, 10; Si, 100; Sm, 400; Sn, 5; Sr, 100; Ta, 500; Tb, 100; Ti, 100; Tm, 100; V, 20; W, 200; Y, 5; Yb, 5; Zn, 50. Chemical analysis of the zirconium metal from which the hydrides were prepared showed 19, 38, 170, and 10 parts per million for N, O, C, and halogens, respectively. The ZrH_2 was found to contain 100 parts per million oxygen, which indicates that no appreciable oxidation occurred during the preparation of the samples. The samples were always handled in a vacuum or in a helium atmosphere to prevent oxidation, although this precaution was probably not necessary at room temperature. Direct chemical analysis of the ZrH_2 for zirconium gave $97.72\pm0.03\%$ while the calculated percentage of zirconium on the basis of the formula ZrH_2 is 97.84%. From these analyses, it is estimated that the ZrH_2 and ZrD_2 samples contain not more than 0.1% total impurities.

Portions of the samples were ground in a mortar to a fine powder and examined by x-ray diffraction. Both were found to consist of a single tetragonal phase. The lattice constants found for the ZrH_2 at 25°C are $a_0=4.981\pm0.01$ A, $c_0=4.451\pm0.01$ A for a face-centered tetragonal lattice with four molecules per unit cell or $a_0=3.522\pm0.01$ A, $c_0=4.451\pm0.01$ A for the equivalent body-centered tetragonal lattice with two molecules per unit cell, in agreement within experimental error with the values reported in the literature.[12,14–17,19–21,23] The lattice constants found for ZrD_2, which have not been reported previously, are $a_0=4.972\pm0.01$ A, $c_0=4.447\pm0.01$ A for a face-centered tetragonal lattice. The densities calculated from these values of the lattice constants are 5.61 g/cc for ZrH_2 and 5.75 g/cc for ZrD_2.

The samples were in the form of small irregular pieces which varied in size from about 0.1 to 3 mm on an edge. The masses used for the calorimetric measurements were 81.3712 g of ZrH_2 and 87.0048 g of ZrD_2. The calorimeter also contained 8.7×10^{-4} moles of helium.

APPARATUS

The heat capacity measurements were made using an adiabatic calorimeter and apparatus which have been described in previous publications from this Laboratory.[30,31] The temperature was measured with a platinum resistance thermometer which has been calibrated on the International scale above 90°K and on the scale of the National Bureau of Standards[32] between 14 and 90°K. Below 14°K the scale was obtained by fitting the equation $R=A+BT^2+CT^5$ to the resistance at the boiling point of liquid helium, the resistance at 14°K and dR/dT at 14°K. It is believed that the temperature scale agrees with the thermodynamic scale within 0.1° from 4 to 14°K, within 0.03° from 14 to 90°K and within 0.05° from 90 to 350°K.

---

[30] E. F. Westrum, Jr., J. B. Hatcher, and D. W. Osborne, J. Chem. Phys. **21**, 419 (1953).

[31] D. W. Osborne and E. F. Westrum, Jr., J. Chem. Phys. **21**, 1884 (1953).

[32] H. J. Hoge and F. G. Brickwedde, J. Research Natl. Bur. Standards **22**, 351 (1939).

TABLE I. Heat capacity of ZrH_2, mol. wt. = 93.24; 0°C = 273.15°K.

T °K	C_p cal deg^{-1} mole^{-1}	T °K	C_p cal deg^{-1} mole^{-1}
Series I		Series III	
6.87	0.0119	57.30	1.965
9.60	0.0230	62.42	2.254
11.54	0.0358	67.98	2.548
13.64	0.0548	74.12	2.846
15.30	0.0740	81.24	3.172
17.20	0.1006	89.14	3.489
19.12	0.1348		
20.96	0.1738	Series IV	
22.63	0.2156	89.50	3.502
24.48	0.2702	98.52	3.802
26.68	0.3424	107.49	4.064
		117.18	4.308
Series II		127.61	4.538
6.51	0.0105	138.07	4.734
8.34	0.0165	148.30	4.905
10.23	0.0264	158.34	5.055
12.14	0.0406	168.19	5.194
14.17	0.0609	178.09	5.327
16.22	0.0869	188.08	5.462
18.26	0.1190		
20.24	0.1582	Series V	
22.25	0.2060	186.63	5.445
24.25	0.2626	196.67	5.583
26.17	0.3248	206.59	5.725
28.09	0.3936	216.40	5.870
30.10	0.4735	226.27	6.022
32.90	0.5988	236.14	6.183
36.27	0.7643	245.92	6.356
39.76	0.9507	255.66	6.535
43.63	1.168	265.42	6.722
47.99	1.422	275.27	6.919
52.99	1.716	285.24	7.122
58.27	2.020	295.39	7.336
		305.52	7.557
		315.61	7.782
		325.79	8.012
		335.94	8.240
		345.42	8.470

HEAT CAPACITIES AND THERMODYNAMIC FUNCTIONS

The experimental values of the heat capacity of ZrH_2 and ZrD_2 are presented in chronological sequence in Tables I and II, respectively. A small correction for the finite temperature increment was made to the values in Tables I and II by adding $-(d^2C_p/dT^2)(\Delta T)^2/24$ to the measured mean heat capacity. No correction was applied for the presence of 0.35 atom % H in the deuterium used to prepare ZrD_2. (The estimated correction is only 0.009 cal deg^{-1} mole^{-1} at 350°K and even less at lower temperatures.)

Figure 1 is a plot of the heat capacities of ZrH_2 and ZrD_2 as a function of temperature. It can be seen that up to 100°K the heat capacities are nearly equal, and that at higher temperatures the heat capacity of ZrD_2 becomes increasingly greater than that of ZrH_2. This behavior will be discussed in the next section.

The values of the heat capacity for ZrH_2 given in Table III and for ZrD_2 given in Table IV were read from smooth curves drawn through the experimental points. The probable error of these results is considered to be 5% at 5°K, 1% at 14°K, and 0.2% above 30°K. These curves were also used to obtain the heat capacity values needed to calculate the thermodynamic functions given in Tables III and IV. In these tables S° is the entropy, H° is the enthalpy or heat content, and F° is the Gibbs free energy of the compounds in the standard state; H_0° is the enthalpy at 0°K.

The data below 11°K were fitted to an equation of the form used for the heat capacity of a metal at low temperatures,

$$C_v = \gamma T + 464.6(T/\theta)^3 \text{ cal deg}^{-1} \text{ mole}^{-1}, \quad (1)$$

where γT is the electronic heat capacity and the term in T^3 is the lattice contribution. This equation, with $\gamma = 9.8 \times 10^{-4}$ cal deg^{-2} mole^{-1} and $\theta = 311.4$°K, fits the experimental heat capacities of both ZrH_2 and ZrD_2 below 11°K with an average deviation of 1% and was used to extrapolate the heat capacities below 6°K. In this temperature region, it can be assumed that $C_p = C_v$.

TABLE II. Heat capacity of ZrD_2, mol. wt. = 95.24; 0°C = 273.15°K.

$\bar{T}$ °K	C_p cal deg^{-1} mole^{-1}	$\bar{T}$ °K	C_p cal deg^{-1} mole^{-1}
Series I		Series III	
6.22	0.0097	55.70	1.851
8.29	0.0168	57.48	1.953
10.12	0.0260	62.96	2.260
12.06	0.0395	69.00	2.575
14.05	0.0595	75.47	2.886
16.00	0.0830	82.57	3.206
18.01	0.1141	90.41	3.516
20.06	0.1530	99.11	3.810
22.10	0.2003	Series IV	
24.32	0.2616	95.08	3.679
26.79	0.3414	103.46	3.947
29.37	0.4377	112.97	4.225
32.10	0.5537	122.93	4.495
35.20	0.7002	133.00	4.752
38.47	0.8678	143.07	5.002
41.63	1.041	152.98	5.250
45.69	1.270	163.13	5.511
50.51	1.551	173.43	5.784
55.47	1.838	183.56	6.062
Series II		193.47	6.344
5.97	0.0092	203.27	6.636
7.99	0.0160	213.00	6.931
10.07	0.0256	222.85	7.235
12.14	0.0404	233.14	7.556
14.12	0.0602	Series V	
16.05	0.0836	235.80	7.643
18.00	0.1139	245.49	7.960
20.00	0.1517	255.57	8.284
22.04	0.1990	265.69	8.609
24.24	0.2593	275.80	8.931
26.56	0.3333	285.93	9.251
29.16	0.4294	296.08	9.567
32.17	0.5569	306.22	9.884
35.36	0.7079	316.37	10.197
38.76	0.8836	326.57	10.491
42.37	1.082	336.73	10.781
46.30	1.305	345.85	11.029
50.76	1.565		

It is interesting to compare the γ and θ for ZrH_2 and ZrD_2 with those reported for zirconium metal. Wolcott[33] found $\gamma = 7.25 \times 10^{-4}$ cal deg^{-2} mole^{-1} and $\theta = 304$ to 277 in the temperature range 5 to 11°K. Estermann, Friedberg, and Goldman[34] found $\gamma = 6.92 \times 10^{-4}$ cal deg^{-2} mole^{-1} and $\theta = 265°$. The fact that Eq. (1) fits the heat capacities at low temperatures with a γ not greatly different from that found for zirconium metal is another indication of the metallic nature of the hydrides.

HYDROGEN VIBRATION FREQUENCIES

It is known that in ZrH_2 and ZrD_2 each hydrogen atom is surrounded by four equidistant zirconium atoms.[14] The latter are located at the corners of a tetrahedron that differs from a regular tetrahedron by a compression of approximately 10% along one of the twofold axes. ZrH_2 and ZrD_2 have a distorted fluorite structure, which is tetragonal rather than cubic because of the compression along one axis. On the other hand, the δ-hydride phase, which is present for H/Zr or D/Zr ratios of less than 1.7, is face-centered cubic, and in this phase presumably each hydrogen atom is surrounded by four zirconium atoms at the corners of a regular tetrahedron.

There are two types of vibration of the lattice, the acoustic and the optical modes. The acoustic modes are those in which the zirconium atoms and hydrogen atoms are vibrating in phase, and these give rise to a Debye-like contribution to the heat capacity. In the optical modes the hydrogen atoms vibrate against the zirconium atoms but because of the great disparity between the masses the zirconium atoms remain essentially stationary. It should be a good approximation to consider each hydrogen (or deuterium) atom as vibrating essentially independently in a potential well provided by the zirconium atoms and to regard the oscillations as harmonic. The symmetry at each hydrogen site is such that in ZrH_2 and ZrD_2 there should be a doubly degenerate frequency and a nondegenerate frequency. The optical vibrations according

[33] N. M. Wolcott, Phil. Mag. **2**, 1246 (1957).
[34] I. Estermann, S. A. Friedberg, and J. E. Goldman, Phys. Rev. **87**, 582 (1952).

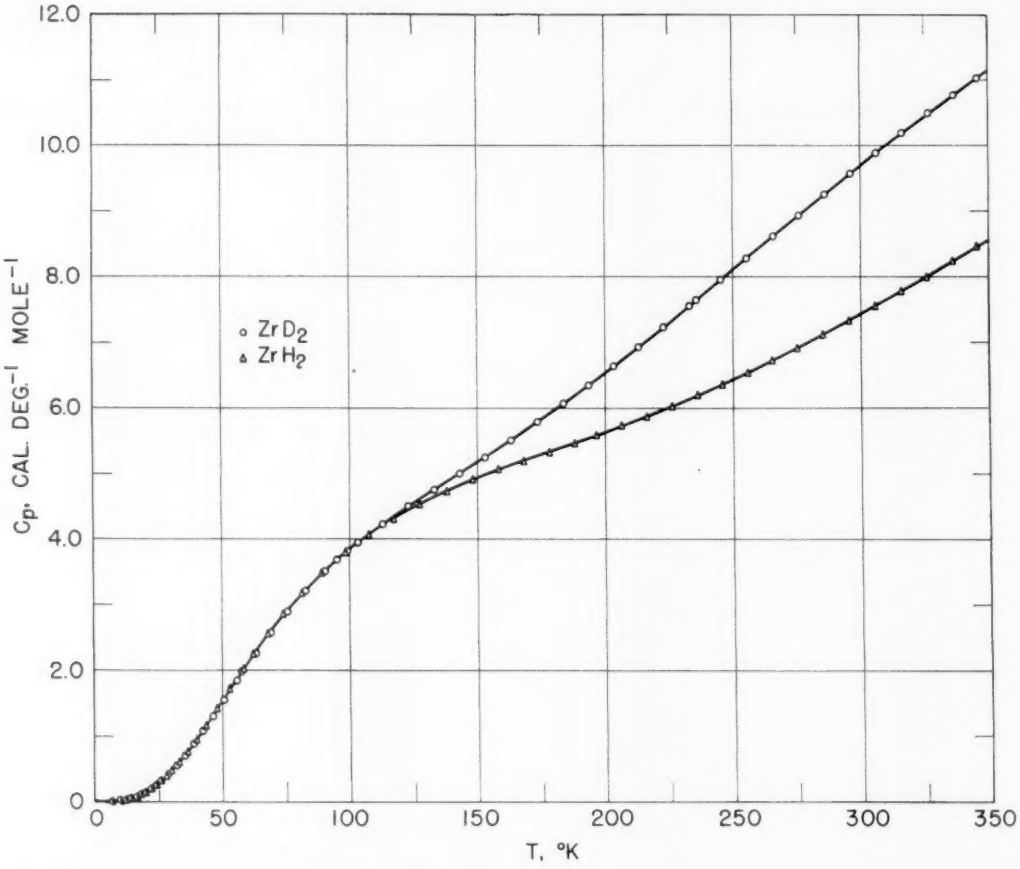

FIG. 1. Heat capacities of ZrH_2 and ZrD_2.

to this model should consist of $2N$ modes per g atom of H with a fundamental frequency ν_0 and N modes with a fundamental frequency ν_1, where N is the Avogadro number. Actually there is some coupling of the hydrogen vibrations, which spreads each optical frequency into a narrow band of frequencies. In the δ-hydride because of the higher symmetry at each hydrogen site there should be $3N$ optical modes per g atom of H, all with nearly the same frequency.

The heat capacity of ZrH_2 is given by Eq. (2),

$$C_p=(C_p-C_v)+\gamma T+F(T)+4E(u_0)+2E(u_1), \quad (2).$$

in which γT is the electronic contribution, $F(T)$ is the contribution of the acoustic modes, $E(u_i)$ is the Einstein heat capacity function for one degree of freedom,

$$E(u_i)=Ru_i^2 \exp u_i(\exp u_i-1)^{-2} \quad (3)$$

and $u_i=h\nu_i/kT=hc\tilde{\nu}_i/kT$. We assume that the effect of substituting D for H has little effect on the first three terms of Eq. (2) and that the effect on the Einstein functions is to reduce each frequency ν_i to $\nu_i/\sqrt{2}$. That the first assumption is fairly good can be seen by examining the heat capacities in Tables III and IV below 100°K, where the contribution of the Einstein functions can be neglected. The heat capacity of ZrH_2 in the range 20 to 100°K averages approximately 1% higher than that of ZrD_2, a difference which we believe to be appreciably larger than our experimental error, but the maximum difference is only 0.024 cal deg^{-1} mole^{-1}. If the mass of the zirconium atoms is considered to be infinite, the hydrogen vibration frequency is reduced when deuterium is substituted by the ratio $\nu_H/\nu_D=(m_D/m_H)^{\frac{1}{2}}=(2.0142/1.0079)^{\frac{1}{2}}=(1.9984)^{\frac{1}{2}}$. Although it is not possible to make an exact calculation for the three dimensional crystal it is probably sufficiently accurate for the present purposes to take $\nu_H/\nu_D=\sqrt{2}$.

The difference in the heat capacities is then given by Eq. (4),

$$\Delta C_p=C_p(ZrD_2)-C_p(ZrH_2)$$
$$=4E(u_0/\sqrt{2})-4E(u_0)+2E(u_1/\sqrt{2})-2E(u_1). \quad (4)$$

TABLE III. Thermodynamic functions of ZrH_2.

T °K	C_p cal deg^{-1} mole^{-1}	$S°$ cal deg^{-1} mole^{-1}	$H°-H_0°$ cal mole^{-1}	$(H°-H_0°)/T$ cal deg^{-1} mole^{-1}	$-(F°-H_0°)/T$ cal deg^{-1} mole^{-1}
5	0.0068	0.0055	0.015	0.0029	0.0026
10	0.0252	0.0149	0.087	0.0087	0.0062
15	0.0706	0.0326	0.313	0.0209	0.0117
20	0.1528	0.0631	0.853	0.0426	0.0205
25	0.2863	0.1105	1.927	0.0771	0.0334
30	0.469	0.1781	3.795	0.1265	0.0516
35	0.700	0.2672	6.702	0.1915	0.0757
40	0.964	0.3776	10.85	0.2713	0.1063
45	1.246	0.5073	16.37	0.3638	0.1435
50	1.540	0.6538	23.33	0.4667	0.1871
60	2.117	0.9860	41.64	0.6940	0.2920
70	2.648	1.353	65.54	0.936	0.417
80	3.116	1.738	94.40	1.180	0.558
90	3.519	2.129	127.64	1.418	0.711
100	3.848	2.517	164.52	1.645	0.872
110	4.130	2.898	204.45	1.859	1.039
120	4.374	3.268	247.00	2.058	1.210
130	4.586	3.626	291.82	2.245	1.381
140	4.768	3.973	338.60	2.419	1.554
150	4.930	4.308	387.11	2.581	1.727
160	5.078	4.630	437.16	2.732	1.898
170	5.219	4.943	488.65	2.874	2.069
180	5.354	5.245	541.52	3.008	2.237
190	5.490	5.538	595.74	3.135	2.403
200	5.630	5.823	651.33	3.257	2.566
210	5.775	6.101	708.35	3.373	2.728
220	5.925	6.373	766.84	3.486	2.887
230	6.082	6.640	826.87	3.595	3.045
240	6.250	6.903	888.52	3.702	3.201
250	6.430	7.161	951.91	3.808	3.353
260	6.617	7.417	1017.1	3.912	3.505
270	6.812	7.670	1084.3	4.016	3.654
280	7.014	7.922	1153.4	4.119	3.803
290	7.221	8.172	1224.6	4.223	3.949
300	7.435	8.420	1297.9	4.326	4.094
310	7.656	8.667	1373.3	4.430	4.237
320	7.880	8.914	1451.0	4.534	4.380
330	8.110	9.160	1530.9	4.639	4.521
340	8.342	9.406	1613.2	4.745	4.661
350	8.579	9.651	1697.8	4.851	4.800
273.15	6.875	7.750	1105.8	4.048	3.702
298.15	7.396	8.374	1284.1	4.307	4.067
	±0.015	±0.02	±2	±0.01	±0.01

This equation can be fitted to the experimental data between 100 and 350°K if one takes $\tilde{\nu}_0=\tilde{\nu}_1=1190$ cm^{-1}. A comparison of the experimental and calculated values is given in Table V. The average magnitude of the deviations of ΔC_p calculated from Eq. (4) from the experimental values is 0.03 cal deg^{-1} mole^{-1}. Taking into account the fact that the estimated probable error in the experimental ΔC_p is about 0.01 cal deg^{-1} mole^{-1} at 100°K and 0.03 cal deg^{-1} mole^{-1} at 350°K as well as the assumptions implicit in Eq. (4), we estimate that the probable error in the hydrogen frequency is 30 cm^{-1}. The result that an adequate fit can be obtained with $\nu_0=\nu_1$ indicates that the environment of the hydrogen atoms is nearly isotropic, in spite of the compression of the fluorite structure along one axis.

The hydrogen vibration frequency found from this analysis of the heat capacity curves, 1190±30 cm^{-1}, may be compared with the results of neutron scattering experiments. By observation of the energy distribution of scattered slow neutrons that had exchanged energy with the lattice vibrations Pelah, Eisenhauer, Hughes, and Palevsky[26] found that $ZrH_{1.5}$ has an optical vibration with an energy of 0.130 ev, corresponding to $\tilde{\nu}=1049$ cm^{-1}. From the effect of temperature on the intensity of the slow neutrons scattered by the first optical level of $ZrH_{1.5}$. Andresen, McReynolds, Nelkin, Rosenbluth, and Whittemore[27] also determined the energy of the level to be 0.130±0.005 ev. Whittemore and McReynolds[28] have deduced from the variation of the total neutron cross section with energy that the first optical level in $ZrH_{1.5}$ is at 0.137 ev or 1105 cm^{-1}. Further, no significant change in this energy was found in the composition range $ZrH_{1.2}$ to $ZrH_{1.9}$.[35] Recently Woods, Brockhouse, Sakamoto, and Sinclair,[29] employing the beryllium detector technique, have found the first optical level in $ZrH_{1.8}$ to be at 0.140 ev or 1129 cm^{-1}.

[35] A. W. McReynolds, M. S. Nelkin, M. N. Rosenbluth, and W. L. Whittemore, *Proceedings of the Second United Nations International Conference on the Peaceful Uses of Atomic Energy* (United Nations, Geneva, 1958), Vol. 16, p. 297.

TABLE IV. Thermodynamic functions of ZrD_2.

T °K	C_p cal deg^{-1} mole^{-1}	$S°$ cal deg^{-1} mole^{-1}	$H°-H_0°$ cal mole^{-1}	$(H°-H_0°)/T$ cal deg^{-1} mole^{-1}	$-(F°-H_0°)/T$ cal deg^{-1} mole^{-1}
5	0.0068	0.0055	0.015	0.0029	0.0026
10	0.0252	0.0149	0.087	0.0087	0.0062
15	0.0705	0.0326	0.313	0.0209	0.0117
20	0.1518	0.0629	0.850	0.0425	0.0204
25	0.2823	0.1099	1.914	0.0766	0.0333
30	0.463	0.1765	3.756	0.1252	0.0513
35	0.690	0.2644	6.622	0.1892	0.0752
40	0.950	0.3732	10.71	0.2678	0.1054
45	1.230	0.5012	16.16	0.3590	0.1422
50	1.520	0.6456	23.03	0.4605	0.1851
60	2.096	0.9740	41.12	0.6854	0.2886
70	2.624	1.338	64.78	0.925	0.413
80	3.093	1.719	93.39	1.167	0.552
90	3.500	2.108	126.43	1.405	0.703
100	3.838	2.494	163.16	1.632	0.862
110	4.140	2.875	203.08	1.846	1.029
120	4.417	3.247	245.89	2.049	1.198
130	4.675	3.611	291.36	2.241	1.370
140	4.925	3.966	339.37	2.424	1.542
150	5.175	4.315	389.86	2.599	1.716
160	5.430	4.657	442.88	2.768	1.889
170	5.691	4.994	498.48	2.932	2.062
180	5.964	5.327	556.75	3.093	2.234
190	6.244	5.657	617.78	3.251	2.406
200	6.537	5.984	681.68	3.408	2.576
210	6.838	6.311	748.56	3.565	2.746
220	7.146	6.636	818.48	3.720	2.916
230	7.456	6.960	891.49	3.876	3.084
240	7.780	7.284	967.67	4.032	3.252
250	8.105	7.609	1047.1	4.188	3.421
260	8.426	7.933	1129.8	4.345	3.588
270	8.746	8.257	1215.6	4.502	3.755
280	9.063	8.581	1304.7	4.660	3.921
290	9.378	8.904	1396.9	4.817	4.087
300	9.688	9.227	1492.2	4.974	4.253
310	10.003	9.550	1590.7	5.131	4.419
320	10.302	9.872	1692.2	5.288	4.584
330	10.588	10.194	1796.7	5.444	4.750
340	10.870	10.514	1904.0	5.600	4.914
350	11.144	10.833	2014.0	5.754	5.079
273.15	8.847	8.359	1243.3	4.552	3.807
298.15	9.631	9.168	1474.4	4.945	4.223
	±0.019	±0.02	±3	±0.01	±0.01

The value $\tilde{\nu}=1190$ cm^{-1} for ZrH_2 agrees with the results of Woods, Brockhouse, Sakamoto, and Sinclair[29] and of Whittemore and McReynolds[28] within the experimental uncertainties of the measurements. The value of 1049 cm^{-1} obtained[26,27] for $ZrH_{1.5}$ appears to be somewhat low. It is possible, however, that although the neutron scattering studies[35] did not detect a shift in the hydrogen vibration frequency as a function of hydrogen concentration in the range $ZrH_{1.2}$ to $ZrH_{1.9}$ there may be a frequency shift as the fully hydrided composition ZrH_2 is approached.

TABLE V. A comparison of ΔC_p obtained from the experimental values in Tables III and IV with ΔC_p calculated from Eq. (4), with $\tilde{\nu}_0=\tilde{\nu}_1=1190$ cm^{-1}.

T °K	$\Delta C_{p(\text{exp})}$ cal deg^{-1} mole^{-1}	$\Delta C_{p(\text{calc})}$ cal deg^{-1} mole^{-1}
100	−0.01	0.01
150	0.24	0.23
200	0.91	0.86
250	1.68	1.65
300	2.25	2.26
350	2.56	2.61

ENTHALPIES OF FORMATION AND FREE ENERGIES OF FORMATION OF ZrH_2 AND ZrD_2

If the difference in zero-point energies between ZrH_2 and ZrD_2 arises solely from the difference in the zero-point energies of H atom and D atom vibrations then,

$$\Delta H_0° = (H_0°)_{ZrH_2} - (H_0°)_{ZrD_2} = 3.5hc\tilde{\nu}_H[1-(1/\sqrt{2})]. \quad (5)$$

For $\tilde{\nu}_H$ equal to 1190 cm^{-1} the value of $\Delta H_0°$ is 2989 cal mole^{-1}. This value was combined with the zero-point energies and enthalpies for hydrogen and deuterium[36] and with the enthalpies for ZrH_2 and ZrD_2 taken from Tables III and IV to calculate the difference in the

[36] H. W. Woolley, R. B. Scott, and F. G. Brickwedde, J. Research Natl. Bur. Standards **41**, 379 (1948).

enthalpies of formation of ZrH_2 and ZrD_2 at 298.15°K, with the result shown in Eq. (6);

$$(\Delta H_f^\circ)_{ZrH_2} - (\Delta H_f^\circ)_{ZrD_2} = 1014 \text{ cal mole}^{-1}. \quad (6)$$

The free energy of formation of ZrH_2 at 298.15°K calculated from the enthalpy of formation of ZrH_2 reported by Sieverts, Gotta, and Halberstadt[37] (−40.5 kcal mole^{-1}), the entropy of hydrogen,[38] the entropy of zirconium,[38] and the entropy of ZrH_2 given in Table III is −30.9 kcal mole^{-1}. The uncertainty in this value is about 2 kcal mole^{-1} due almost entirely to the inaccuracy in the heat of formation of ZrH_2, which was calculated from heat of combustion data obtained with Zr and ZrH_2 containing several percent impurities. If, in accordance with Eq. (6), the enthalpy of formation of ZrD_2 is taken as −41.5 kcal mole^{-1}, the free energy of formation of ZrD_2 at 298.15°K is −31.2 kcal mole^{-1}.

[37] A. Sieverts, A. Gotta, and S. Halberstadt, Z. anorg. u. allgem. Chem. **187**, 159 (1930).
[38] G. B. Skinner and H. L. Johnston, J. Am. Chem. Soc. **73**, 4549 (1951).

ACKNOWLEDGMENTS

The authors acknowledge the help of Joseph Taguè, who assisted with the measurements, and are grateful to Mrs. Elizabeth Sherry for the x-ray analyses. Also the authors are indebted to the spectrographic and analytical groups of the Chemistry Division for their assistance in evaluating the purity of the samples and to the Chemical Engineering Division for providing the zirconium metal. Finally, the authors thank Dr. B. M. Abraham for helpful discussions.

THE JOURNAL OF CHEMICAL PHYSICS VOLUME 34, NUMBER 4 APRIL, 1961

Complex Cyclotron Resonance in Dilute Gases

R. L. COLLINS

Phillips Petroleum Company, Bartlesville, Oklahoma

(Received September 22, 1960)

An X-band electron spin resonance spectrometer has been used to analyze the products of an electrodeless discharge in flowing gases at low pressure. During a search for polyatomic free radical fragments, a multiple signal was found near $g = 2.0000$. Three poorly resolved peaks were found for a variety of paraffins and olefins, while methane, ammonia, methylamine, and sulfur dioxide yielded doublets. The structure was best resolved at low pressure. The spacing of the peaks increased with ESR microwave power. Evidence is presented that the signal is caused by cyclotron resonance of photo-ionized electrons. It is suggested that this multiple resonance is more apparent than real, and arises from either a velocity-dependent capture process or from dephasing of electrons upon collision with gas molecules.

I. INTRODUCTION

THE production of free radicals in flowing gaseous systems by an electrical discharge has been known for some time. R. W. Wood[1] first showed that hydrogen atoms could be pumped out of a glow discharge in hydrogen, and that they could be carried a considerable distance before they recombined. Atomic free radicals which have been produced by electrical discharge and examined by electron spin resonance (ESR) include hydrogen,[2] oxygen,[3] and nitrogen.[4] ESR measurements indicate the presence of these atoms in their ground electronic states and readily determine their abundances. An attempt has been made to detect and identify polyatomic free radicals from various gases passed through a 2450 Mc electrodeless discharge. A very strong resonance was observed near $g = 2.0000$ for many of these gases. The multiple structure which appeared at low pressure prevented immediate identification as cyclotron resonance of electrons. The detailed investigation of this resonance forms the basis of this paper.

[1] R. W. Wood, Proc. Roy. Soc. (London) **A97**, 455 (1920).
[2] R. Beringer and M. A. Heald, Phys. Rev. **95**, 1474 (1954).
[3] E. B. Rawson and R. Beringer, Phys. Rev. **88**, 677 (1952).
[4] M. A. Heald and R. Beringer, Phys. Rev. **96**, 645 (1954).

II. EXPERIMENTAL

The ESR spectrometer operates near 10 kMc. The operating frequency is determined by the cavity plus specimen. The cavity is of the reflection type, and includes an adjustable iris for matching purposes. The loaded Q of the cavity is about 350. Up to 40 mw are dissipated in the cavity, hence the power level within the cavity is 14 w diminished by the attenuator setting. The cavity is constructed of Fiberglas with a thin internal silver plating. Field modulation at 20 kc is applied with external coils. Since phase-sensitive detection is employed, the displayed spectra represent the derivative of the absorption spectra. The magnet is water-cooled and has pole pieces 12 in. in diameter

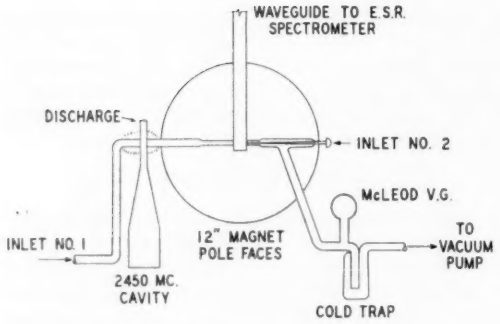

FIG. 1. Arrangement of glassware in ESR spectrometer.

spaced 3 in. apart. The general arrangement of the gas-handling system and of the electrodeless discharge is sketched in Fig. 1. The discharge is powered by a 2450-Mc 100-w Raytheon microtherm diathermy unit. The discharge cavity is based on a design by the free radical group of the Bureau of Standards.

The ESR cavity operates in the TE_{102} mode. The broad face is normally aligned parallel to the pole faces in such a way that the microwave magnetic-field vector is perpendicular to the field of the electromagnet. This position is illustrated in Fig. 2(a). Cyclotron resonance depends upon having the microwave electric vector perpendicular to the field of the electromagnet. Thus it is "twice forbidden" in the configuration of Fig. 2(a), since the microwave electric field is parallel to the dc magnetic field and the sample is placed in a region of zero microwave electric-field intensity. Small departures from ideal geometry are expected since the cavity has access holes and since the specimen introduces a susceptibility discontinuity. Also, the electric field is strictly zero only along a plane midway between the cavity ends, whereas the specimen has finite thickness and so encounters nonzero electric fields.

Several experiments were performed with the cavity oriented as shown in Fig. 2(b). The microwave electric field is perpendicular to the dc magnetic field and the possibility of cyclotron resonance is enhanced. An attempt was made to place the sample in the region of maximum electric field (one quarter of the way from the end of the cavity), but this degraded the cavity Q excessively.

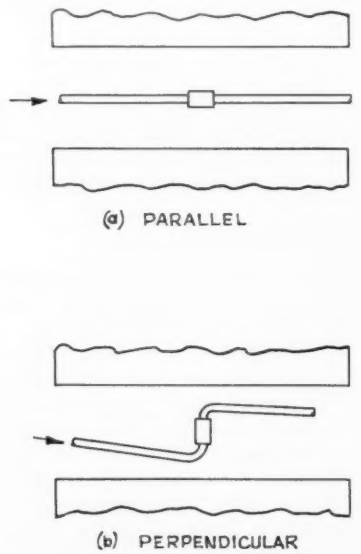

FIG. 2. Cavity arrangements within electromagnet.

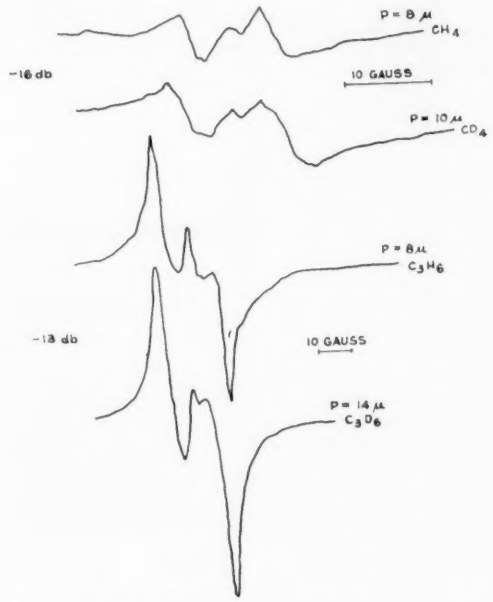

FIG. 3. Multiple resonances in ordinary and deuterated hydrocarbons.

The hydrocarbon gases used were Phillips research grade, and the other gases were purchased from the Matheson Company and are of high purity.

III. RESULTS

A broad strong line near a "g" value of 2.0000 was found for a number of gases. The signal was strongest at about 0.03 mm Hg pressure. At higher pressure, it weakened and broadened. Lower pressure led to a sharpening and, in many gases, the appearance of a two or three line "structure".

Methane and propylene gave, respectively, two and three line spectra at the lowest pressure at which the discharge could be operated (Fig. 3). The species responsible for the signal was identified as arising from photolysis, since a simple bend in the tubing between discharge and analyzing cavity eliminated the signal.

The frequency of the light causing the resonance was measured by inserting loosely fitting windows in place of the bend. A lithium fluoride window 0.88 mm thick with cutoff at 1100 A reduced the signal by a factor of 40. A fused silica window 2 mm thick with cutoff at 1600 A reduced the signal by a factor of 800.

To determine the necessity of a flowing gas stream, the reactant was introduced through inlet number two (Fig. 1) with inlet number one closed. The signal intensity increased slightly. The decomposition products of hydrocarbons in an electrical discharge include a resin which builds up on the walls of the discharge area. The resin conducts electricity and tends to put out the discharge. Also, small "carbon arcs" occur between fractured portions of the resin and these local hot spots lead to premature glass breakage. Helium, which does not foul the discharge zone, was tried at inlet number one to provide the vacuum ultraviolet light for photolysis. The reactant gas still flowed through inlet number two. This proved quite effective, and multiple resonances (doublets) were obtained with methane, ethane, ethylene, propane, propylene, propyne, ammonia, and methylamine. A single line was obtained for sulfur dioxide, and no resonance was found for hydrogen and carbon tetrachloride.

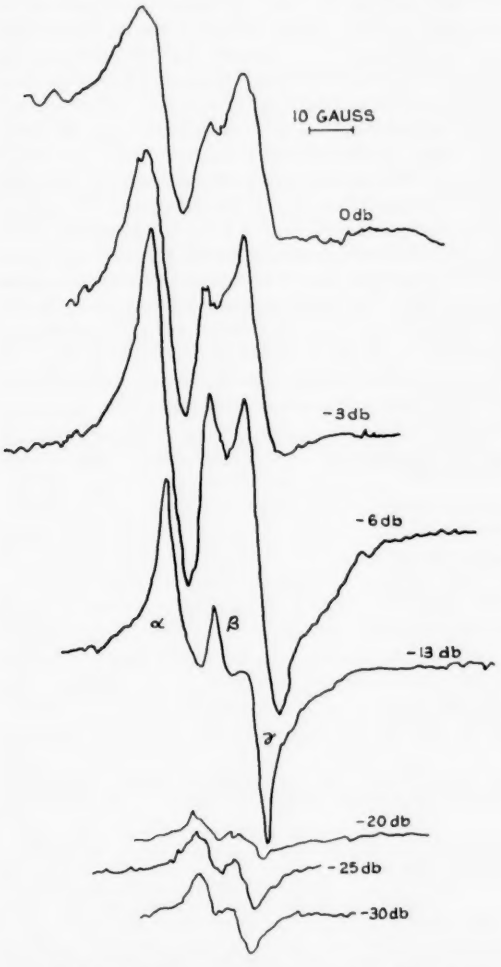

FIG. 4. Effect of microwave power level upon multiple structure of propylene.

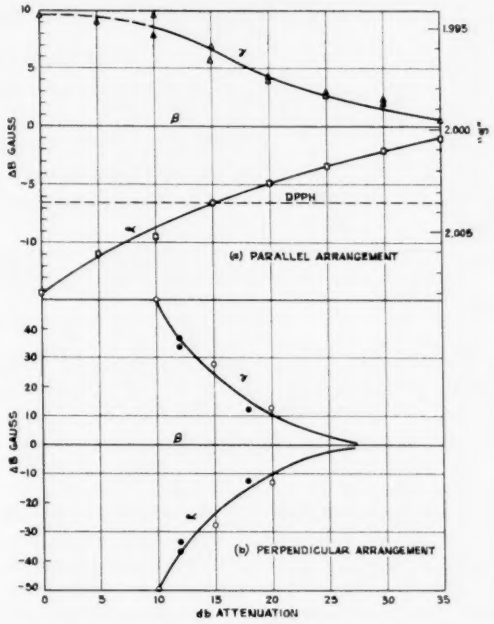

FIG. 5. Effect of microwave power on structure and "g" value for propylene.

The helium flow was eliminated in an attempt to achieve lower pressures and, hence, better resolution. The indicated pressure was reduced from 30–50 μ to the 10 μ range. A doublet was still found for methane and a triplet was found for propylene, *n*-butane, isobutylene, *cis*-butene-2, and 1,3-butadiene.

To determine whether the reaction leading to this triple line was homogeneous or occurred on the Pyrex surface, a ball of Pyrex wool was affixed to the end of inlet number two within the ESR cavity. No difference was found.

To guard against the triplet arising from an instrumentation artifact, the modulation frequency was dropped from 20 kc to 10 kc with no change in the spectrum.

The possibility that the structure arose from a magnetic interaction between one or more protons and the photo-excited electrons was considered and rejected, since deuterium substitution produced no change in the signal from methane and propylene (see Fig. 3).

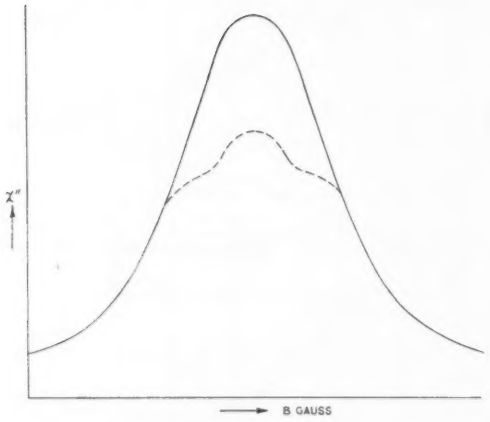

FIG. 6. Possible origin of structure.

Saturation measurements on the resonance resulting from propylene indicated that the ESR power level strongly affected the nature and spacing of the structure (Fig. 4). The spacing of the outer components α and γ clearly increased with increasing ESR power. This spacing is plotted in Fig. 5 for the normal (parallel) arrangement. Similar runs were made with the cavity turned to the "perpendicular" position shown in Fig. 2(b). Comparable intensity of the resonance was observed, despite the large loss of light intensity caused by the bend. In fact, a bend so reduced the intensity that no signal was observed for the "normal" position. The spacing of the outer components of the resonance varied more rapidly with microwave power in this configuration, as shown in the second graph of Fig. 5. The "g" value of the central component β is 1.9999 ± 0.0002 relative to powdered α,α-diphenyl-β-picryl hydrazyl with assumed g value 2.0036.[5] "Saturation" occurred only above the power at which the onset of the line-broadening effect began.

IV. DISCUSSION

Abundant evidence has been presented that the resonance observed is caused by cyclotron resonance of photo-ionized electrons. It is far from clear where the structure arises. Arguments based upon magnetic coupling are readily refuted by the lack of a change in structure when deuterium is substituted for hydrogen. A classical argument of reasonable plausibility is that the electrons are accelerated by the cyclotron action to some critical velocity. At this velocity, they are either removed by some capture process which reduces the total electron population or they suffer dephasing collisions which effectively reduce the number of electrons in correct phase relation to extract energy from the microwave field. Either of these mechanisms might lead to an absorption curve of the type shown in Fig. 6, where the solid curve is that expected for a constant concentration of electrons undergoing cyclotron resonance and the dashed curve shows the effect of removing some of the electrons upon reaching a critical velocity. A derivative of the dashed curve would obviously display three peaks. A change in the capture process might simply "eat a hole" in the center of the curve, and the derivative curve would have two peaks. This explanation is consistent with the wider separation of the outer peaks at higher power level, in that the critical velocity is attained somewhat farther away from the center of the resonance. Unfortunately, very little is known about the interaction between slow electrons and hydrocarbon molecules.

[5] D. J. E. Ingram, *Spectroscopy at Radio and Microwave Frequencies* (Butterworth Scientific Publications, Ltd., London, 1955), p. 205.

THE JOURNAL OF CHEMICAL PHYSICS VOLUME 34, NUMBER 4 APRIL, 1961

Expected Square of the Length of Isotactic Vinylic Hydrocarbon-Type Chains

VICTOR E. MEYER* AND JACK B. KINSINGER

Kedzie Chemical Laboratory, East Lansing, Michigan

AND

PAUL M. PARKER

Physics Department, Michigan State University, East Lansing, Michigan

(Received October 17, 1960)

The mean square length of long isotactic vinylic hydrocarbon-type chains is calculated. The Markov chain formalism is employed for this calculation. The problem of excluded volume is not considered.

I. INTRODUCTION

TOBOLSKY[1] has shown that Markov chain formalism[2] can be used for the calculation of the mean square length of chain structures. Specifically, Tobolsky extended the work of Eyring[3] to take into account the effect of hindered rotations on the expected square of the end-to-end length of unperturbed polymethylene chains. M. V. Volkenstein[4] has reviewed the rotational matrix approach to this problem and gives appropriate equations for the various stereoregular polymers. The respective mean square lengths are expressed as functions of the averages of the sine and cosine of the rotational angle ϕ.

In the present communication, we consider an isotactic molecule containing $n+1$ backbone carbon atoms connected by n vector bonds of constant and equal length and of tetrahedral valence angle. Each bond has rectangular vector components $(X^{(i)}, Y^{(i)}, Z^{(i)},)$ $i=0, 1, 2, \cdots, n-1$. For simplicity of calculation, the magnitude of each component is taken to be unity. If l_0 is the actual bond length, the calculated mean square length must therefore, as the last step of the calculation, be scaled by the factor $l_0^2/3$.

Each vector bond is thus represented by one of the eight combinations $(\pm 1, \pm 1, \pm 1)$ and successive bonds differ only in the change of *one* algebraic sign.[5]

In the isotactic vinylic chain it is possible to distinguish between two different types of bond. The distinction[6] is made between the clockwise sequence of attached atoms about the asymmetric carbon atoms. For example, if the asymmetric carbon atom C_i is viewed from the direction of $\mathbf{M}_{i-1}$, the clockwise sequence of attached atoms is: H, C_{i+1}, *R*. Now if the same asymmetric carbon atom is viewed from the direction of $\mathbf{R}_i$, the clockwise sequence of attached atoms is: H, *R*, C_{i-1}, or the counterclockwise sequence is H, C_{i-1}, *R*. Thus, although each bond is between a methylene carbon atom and an asymmetric carbon atom, because of the differences in relative orientation of the bonds to their asymmetric carbon atom the isotactic vinylic chain is in fact composed of two alternating types of bond as is indicated in Fig. 1. If the $\mathbf{R}_i$ bond is in position (1, 1, 1) and $\mathbf{M}_{i+1}$-bond is in position (1, 1, −1), then the probability of occurrence of the $\mathbf{R}_{i+2}$-bond in a (1, 1, 1) position is taken to be *A*; in a (−1, 1, −1) position it is taken to be *B*; and in a (1, −1, −1) position it is taken to be *C*. These correspond to the *trans* and two *gauche* conformations (Fig. 2), respectively, with, of course, $A+B+C=1$. The conformations and positions of *B* and *C* will be reversed depending on whether one is dealing with a macromolecule of (*d*) or (*l*) configuration. Therefore, care must be taken to consider the molecule as depicted in Fig. 1, and in particular the number sequence of the subscripts on the backbone carbon atoms must be rigorously observed. To be definite, the molecule is selected such that when the above mentioned three bonds are in the *trans* conformation, the pendant *R* group of carbon atom C_{i+2} lies in the (1, −1, −1) position. If the above three bonds are in the *trans* conformation, then the $\mathbf{M}_{i+3}$-bond has probabilities *a*, *b*, and *c* of being found in positions (1, 1, −1), (−1, 1, 1), and (1, −1, 1), respectively. The probabilities *a*, *b*, and *c* correspond to the *trans* and the two *gauche* conformations (Fig. 3) in that order; and $a+b+c=1$. Thus, in general, we have that *A*, *B*, and *C* refer to $\mathbf{R}-\mathbf{M}-\mathbf{R}$ three-bond combinations; and *a*, *b*, and *c* refer to $\mathbf{M}-\mathbf{R}-\mathbf{M}$ three-bond combinations.

If the chain commences with an $\mathbf{R}$ bond, the end-to-end length is the magnitude of

$$\mathbf{h}_R=\mathbf{R}_0+\mathbf{M}_1+\mathbf{R}_2+\mathbf{M}_3+\cdots, \tag{1}$$

and if the chain commences with an $\mathbf{M}$ bond, the end-to-end length is the magnitude of

$$\mathbf{h}_M=\mathbf{M}_0+\mathbf{R}_1+\mathbf{M}_2+\mathbf{R}_3+\cdots. \tag{2}$$

* Supported in part by a grant from the Research Corporation, and in part by a National Science Foundation Summer Fellowship.

[1] A. V. Tobolsky, J. Chem. Phys. **31**, 387 (1959).

[2] W. Feller, *An Introduction to Probability Theory* (John Wiley & Sons, Inc., New York, 1957), 2nd ed., pp. 338–349, 380–385.

[3] H. Eyring, Phys. Rev. **39**, 746 (1932).

[4] M. V. Volkenstein, J. Polymer Sci. **29**, 441 (1958).

[5] A. V. Tobolsky, R. E. Powell, and H. Eyring, in *The Chemistry of Large Molecules*, edited by R. E. Burk and O. Grummitt (Interscience Publishers, Inc., New York, 1943), Chap. 5.

[6] S. Lifson, J. Chem. Phys. **29**, 811 (1958).

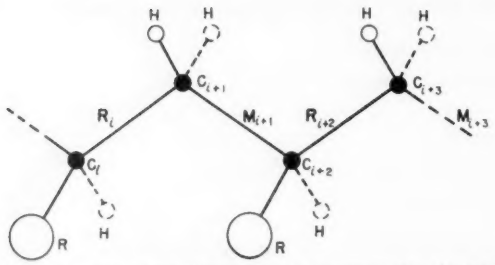

FIG. 1. Planar zigzag illustration of a segment of an isotactic macromolecule.

The *a priori* probabilities of occurrence of these two situations we assume to be one-half for each of the two cases. Then the over-all mean square length for both situations will be $(\mathbf{h}^2)_{Av}$ and

$$(\mathbf{h}^2)_{Av}=\tfrac{1}{2}(\mathbf{h}_R\cdot\mathbf{h}_R)_{Av}+\tfrac{1}{2}(\mathbf{h}_M\cdot\mathbf{h}_M)_{Av}. \tag{3}$$

If end effects are neglected

$$(\mathbf{M}_i\cdot\mathbf{R}_{i+j})_{Av}=(\mathbf{M}_{i+k}\cdot\mathbf{R}_{i+j+k})_{Av},$$

$$(\mathbf{R}_i\cdot\mathbf{M}_{i+j})_{Av}=(\mathbf{R}_{i+k}\cdot\mathbf{M}_{i+j+k})_{Av};$$

with this, (3) can be arranged in the form

$$(\mathbf{h}^2)_{Av}=\tfrac{1}{2}[3n+2\sum_{j=1}^{n-1}(n-j)\,(\mathbf{R}_0\cdot\mathbf{N}_j)_{Av}]$$

$$+\tfrac{1}{2}[3n+2\sum_{k=1}^{n-1}(n-k)\,(\mathbf{M}_0\cdot\mathbf{N}_k)_{Av}], \tag{4}$$

where $\mathbf{N}_j=\mathbf{R}_j$ for j even, $\mathbf{N}_j=\mathbf{M}_j$ for j odd, $\mathbf{N}_k=\mathbf{R}_k$ for k odd, and $\mathbf{N}_k=\mathbf{M}_k$ for k even.

We define L_j as the expected value of the scalar product term occurring in (4), i.e.,

$$L_j=E\{X^{(0)}X^{(j)}+Y^{(0)}Y^{(j)}+Z^{(0)}Z^{(j)}\}, \tag{5}$$

and hence

$$(\mathbf{h}^2)_{Av}=\tfrac{1}{2}[3n+2\sum_{j=1}^{n-1}(n-j)\,L_j]_R$$

$$+\tfrac{1}{2}[3n+2\sum_{k=1}^{n-1}(n-k)\,L_k]_M=\tfrac{1}{2}(E_R+E_M), \tag{6}$$

where in this expression L_j pertains to terms for which $(X^{(0)}, Y^{(0)}, Z^{(0)})$ is an **R** bond, and L_k pertains to terms for which $(X^{(0)}, Y^{(0)}, Z^{(0)})$ is an **M** bond.

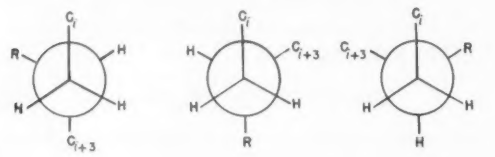

FIG. 2. Newman projections of $\mathbf{R}_i-\mathbf{M}_{i+1}-\mathbf{R}_{i+2}$ bond sequence in the *trans* and two *gauche* conformations.

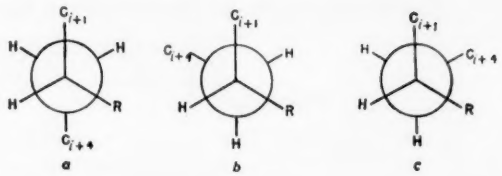

FIG. 3. Newman projections of $\mathbf{M}_{i+1}-\mathbf{R}_{i+2}-\mathbf{M}_{i+3}$ bond sequences in the *trans* and two *gauche* conformations.

We now choose our coordinate system such that $(X^{(0)}, Y^{(0)}, Z^{(0)})=(1, 1, 1)$, in which case

$$L_j=E\{X^{(j)}+Y^{(j)}+Z^{(j)}\}, \tag{7}$$

and clearly $L_0=3$. However, $(X^{(0)}, Y^{(0)}, Z^{(0)})=(1, 1, 1)$ may still be either an **M** bond or an **R** bond.

II. THE PROBABILITY MATRIX

Now, $X^{(j)}+Y^{(j)}+Z^{(j)}$ may have, in general, (a) the possible numerical values $+3$, -3, $+1$, -1; (b) reference to either an **M** bond or an **R** bond; and (c) if it has the numerical value $+1$, it may arise either from $(X^{(j)}, Y^{(j)}, Z^{(j)})=(-1, 1, 1)$, or from $(1, -1, 1)$, or from $(1, 1, -1)$ and we denote these three cases as 1_1, 1_2, 1_3, respectively. According to this scheme there are then 16 distinct classification cases of $X^{(j)}+Y^{(j)}+Z^{(j)}=U_j$. We may imagine affixed to U_j the proper subscripts or superscripts to make the U_j symbol as definite as is needed under the above classification.

In the manner of Tobolsky, we consider now the sequence of pairs (U_0U_1), (U_1U_2), (U_2U_3), $\cdots$, $(U_{n-1}U_n)$. Each member of this sequence is a state in the sense of the Markov formalism and the sequence of pairs forms a Markov chain. Considering all possible

TABLE I. The 48 states of the isotactic vinylic chain. The remaining twenty-four states are numbered from 25–48 in the order above and with M and R interchanged.

State	U_j	U_{j+1}	State	U_j	U_{j+1}
1	$R\ 3$	$M\ 1_3$	13	$R\ -1_1$	$M\ 1_2$
2	$R\ 3$	$M\ 1_2$	14	$R\ -1_1$	$M\ 1_3$
3	$R\ 3$	$M\ 1_1$	15	$R\ -1_1$	$M\ -3$
4	$M\ 1_3$	$R\ -1_1$	16	$R\ -1_2$	$M\ 1_1$
5	$M\ 1_3$	$R\ -1_2$	17	$R\ -1_2$	$M\ 1_3$
6	$M\ 1_3$	$R\ 3$	18	$R\ -1_2$	$M\ -3$
7	$M\ 1_2$	$R\ -1_3$	19	$R\ -1_3$	$M\ 1_2$
8	$M\ 1_2$	$R\ -1_1$	20	$R\ -1_3$	$M\ 1_1$
9	$M\ 1_2$	$R\ 3$	21	$R\ -1_3$	$M\ -3$
10	$M\ 1_1$	$R\ -1_3$	22	$M\ -3$	$R\ -1_2$
11	$M\ 1_1$	$R\ -1_2$	23	$M\ -3$	$R\ -1_3$
12	$M\ 1_1$	$R\ 3$	24	$M\ -3$	$R\ -1_1$

U_j's under our classification, we find that there are 48 possible states (i.e., possible pairs of U_j's) for the molecule under consideration. These 48 states are catalogued in Table I; the notation is self-explanatory. The resulting 48 by 48 probability matrix is more elaborate than need be, and the 48 states can be combined to give only 16 states of distinct Markovian character. We relabel our states from 1–16 and show the relation of the relabeled states to the original states in Table II.

The matrix of transition probabilities P in terms of the relabeled 16 states is shown in Fig. 4. It is clear that states 1–8 and states 9–16 constitute "closed sets."

If we denote the kth power of P by P^k and its matrix elements by $p_{ij}^{(k)}$, then

$$L_k=3p_{9,9}^{(k)}+(p_{9,10}^{(k)}+p_{9,11}^{(k)}+p_{9,12}^{(k)})-3p_{9,13}^{(k)}+(p_{9,14}^{(k)}+p_{9,15}^{(k)}+p_{9,16}^{(k)}), \quad (8)$$

and

$$L_j=3p_{11}^{(j)}-(p_{12}^{(j)}+p_{13}^{(j)}+p_{14}^{(j)})-3p_{15}^{(j)}+(p_{16}^{(j)}+p_{17}^{(j)}+p_{18}^{(j)}). \quad (9)$$

For convenience, we denote the complete matrix of transition probabilities (Fig. 4) by

$$P=\begin{bmatrix}0 & S & 0 & 0\\ T & 0 & 0 & 0\\ 0 & 0 & 0 & V\\ 0 & 0 & U & 0\end{bmatrix}. \quad (10)$$

III. SPECIAL CASE OF THE POLYMETHYLENE CHAIN

We calculate first the expected square length for the special case when $A=a$, $B=C=b=c=\frac{1}{2}(1-a)$. This is the case considered by Tobolsky. The P matrix (10) assumes the simpler form

$$P=\begin{bmatrix}0 & S & 0 & 0\\ S & 0 & 0 & 0\\ 0 & 0 & 0 & V\\ 0 & 0 & V & 0\end{bmatrix}=\begin{bmatrix}P_R & 0\\ 0 & P_M\end{bmatrix}. \quad (11)$$

Because of the occurrence of two closed sets, the P_R matrix and its powers can be considered separately from the P_M matrix and its powers. We have

$$P_R{}^j=\begin{bmatrix}S^j & 0\\ 0 & S^j\end{bmatrix} \quad \text{for } j \text{ even}, \quad (12)$$

and

$$P_R{}^j=\begin{bmatrix}0 & S^j\\ S^j & 0\end{bmatrix} \quad \text{for } j \text{ odd}; \quad (13)$$

$P_R{}^0$ is of course, the eight by eight unit matrix. Similar expressions hold for P_M and its powers.

First, we wish to compute the expression in the first square brackets of (6). We have L_j given by (9). If we denote the matrix elements of S^j by $s_{ij}^{(j)}$, then, because of (12) and (13) L_j can be written as

$$L_j=-3s_{11}^{(j)}+(s_{12}^{(j)}+s_{13}^{(j)}+s_{14}^{(j)}), \quad \text{for } j \text{ odd}, \quad (14)$$

and

$$L_j=3s_{11}^{(j)}-(s_{12}^{(j)}+s_{13}^{(j)}+s_{14}^{(j)}), \quad \text{for } j \text{ even}. \quad (15)$$

Since S^j preserves for all j the stochastic property that

$$s_{11}^{(j)}+s_{12}^{(j)}+s_{13}^{(j)}+s_{14}^{(j)}=1, \quad (16)$$

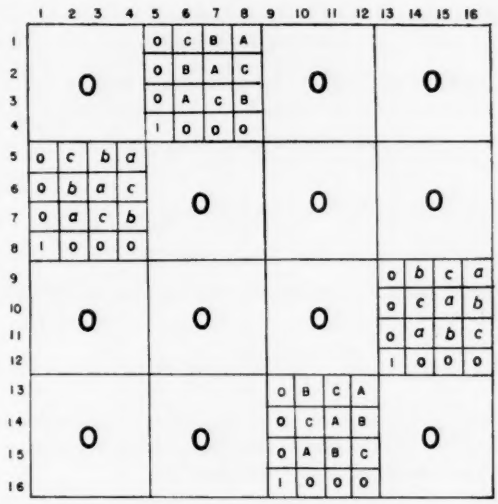

FIG. 4. The matrix of transition probabilities P.

TABLE II. Relation of the relabeled states to the original states for the isotactic vinylic chain. The remaining eight states (states 9–16) are obtained from the original states 25–48 by a similar scheme in analogous order.

Relabeled state			
Number	Value		Original state number
1	3	1	1, 2, 3
2	−1	1	13, 17, 20
3	−1	1	14, 16, 19
4	−1	−3	15, 18, 21
5	−3	−1	22, 23, 24
6	1	−1	4, 7, 11
7	1	−1	5, 8, 10
8	1	3	6, 9, 12

we have that

$$L_j=(-1)^j(4s_{11}^{(j)}-1) \tag{17}$$

for all j. Therefore, the expression that we seek can be written as

$$\begin{aligned}E_R&=-3n+2\sum_{j=0}^{n-1}(n-j)(-1)^j(4s_{11}^{(j)}-1)\\&=-3n-2n\sum(-1)^j+2\sum(-1)^jj\\&\qquad+8\sum(-1)^j(n-j)s_{11}^{(j)}.\end{aligned} \tag{18}$$

Upon evaluating the first two summations of (18) we obtain

$$E_R=\begin{Bmatrix}-4n\\-4n-1\end{Bmatrix}+8\sum_{j=0}^{n-1}(-1)^j(n-j)s_{11}^{(j)}, \tag{19}$$

where the upper value in the curly bracket applies when n is even, and the lower value applies when n is odd.

The remaining sum of (19), viz.,

$$m_{11}=\sum(-1)^j(n-j)s_{11}^{(j)}, \tag{20}$$

is the element in row one and column one of the *matrix* summation

$$M=\sum(-1)^j(n-j)S^j \tag{21}$$

or

$$\begin{aligned}M=n(1-S+S^2-S^3+\cdots)\\+(1-2S+3S^2-4S^3+\cdots)S\\\mp S^{n+1}(1-2S+3S^2-4S^3+\cdots).\end{aligned} \tag{22}$$

The three series shown in (22) are infinite series; the upper sign applies when n is even, the lower sign applies when n is odd. Equation (22) can now be written in the form

$$M=n(1+S)^{-1}+[(1+S)^2]^{-1}S\mp S^{n+1}[(1+S)^2]^{-1} \tag{23}$$

if we assume the existence of the needed inverses. The inverses, however, do exist, since $\det(1+S)\neq 0$, except in the extreme case for which $a=1$, $b=c=0$. This case can, of course, he handled by a more elementary approach. Furthermore, barring this extreme case, convergence of the infinite matrix series of (23) is assured, since all elements of S^j are less than unity (except for the smallest few values of j which is immaterial for convergence).

It remains then to find the element in row one and column one of M of (23) and this element will represent the needed summation term (20). The first two terms of (23) can be handled by standard matrix algebra techniques. In the third term of (23), we approximate S^{n+1} for large n by $\lim_{n\to\infty}S^n$. This approximation can be found with ease,[2] and is

$$\lim_{n\to\infty}S^n=K, \tag{24}$$

where K is a four by four matrix all of whose elements are equal to $\frac{1}{4}$. No further difficulties are encountered in constructing m_{11} and we subsequently find

$$E_R=n\frac{(2+6a)}{(1-a)}-\frac{(a+3)(5a-1)}{(1-a)^2}+\tfrac{1}{2} \tag{25}$$

for reasonably large n, viz., sufficiently large so that (24) is a good approximation.[7]

The expression in the second square brackets of (6) can be found in a similar manner from P_M and gives a result identical with (25). Hence we have immediately that

$$(\mathbf{h}^2)_{Av}=n\frac{(2+6a)}{(1-a)}-\frac{(a+3)(5a-1)}{(1-a)^2}+\tfrac{1}{2}. \tag{26}$$

The first term of (26) is identical with Tobolsky's leading term and the entire expression (26) represents a conveniently simple approximation to Tobolsky's exact result.

To find the mean square length, $(\mathbf{h}^2)_{Av}$ must, of course, be multiplied by $l_0^2/3$.

IV. THE ISOTACTIC VINYLIC CHAIN

We now return to the general P matrix (10). It is again possible to consider separately

$$P_R=\begin{bmatrix}0&S\\T&0\end{bmatrix} \tag{27}$$

and

$$P_M=\begin{bmatrix}0&V\\U&0\end{bmatrix}. \tag{28}$$

We shall seek only the leading term of $(\mathbf{h}^2)_{Av}$ that arises in this more general case.

A straightforward application of the method of calculation given above for the more restricted P matrix generates, for this more general problem, matrix inverses of the form $(1-ST)^{-1}$. These inverses, however, do not exist since $\det(1-ST)\equiv 0$, and the calculation gives, in fact, an element m_{11} which has the indeterminate form of type $0/0$.

To avoid this difficulty it is necessary to set

$$P_R=\begin{bmatrix}0&K\\K&0\end{bmatrix}+\begin{bmatrix}0&S'\\T'&0\end{bmatrix}, \tag{29}$$

where K is defined in (24) and $S'=S-K$, $T'=T-K$. Observing that $K^n=K$ for all positive n; that the sum of the elements of any row or column of S' or T' is equal to zero; and that this null property is preserved for any product matrix formed from T' and S', we find that

$$P_R^2=P_RP_R=\begin{bmatrix}K&0\\0&K\end{bmatrix}+\begin{bmatrix}S'T'&0\\0&T'S'\end{bmatrix} \tag{30}$$

$$P_R^3=P_RP_R^2=\begin{bmatrix}0&K\\K&0\end{bmatrix}+\begin{bmatrix}0&S'T'S'\\T'S'T'&0\end{bmatrix}, \tag{31}$$

[7] The limiting term, viz., the third series of (23) has the value $\mp(1/16)$ in the approximation (24). It thus removes the odd-even ambiguity of (19).

and so on; P_R^0 is, of course, the unit matrix of order eight.

As before, L_j is given by (9). The K matrix gives *no* contribution to L_j. Therefore, for purposes of computing E_R we may write

$$P_R^0=1, \qquad P_R^1=\begin{bmatrix}0 & S'\\ T' & 0\end{bmatrix}, \qquad P_R^2=\begin{bmatrix}S'T' & 0\\ 0 & T'S'\end{bmatrix}, \quad \cdots, \tag{32}$$

and, in general,

$$P_R^j=\begin{bmatrix}0 & Q^{(j)}\\ Q^{(j)\prime} & 0\end{bmatrix} \quad \text{for } j \text{ odd}, \tag{33}$$

and

$$P_R^j=\begin{bmatrix}Q^{(j)} & 0\\ 0 & Q^{(j)\prime}\end{bmatrix} \quad \text{for } j \text{ even}, \tag{34}$$

and the meaning of $Q^{(j)}$ is clear from the context. We note that $Q^{(j)}$ for all positive j has the property that each of its rows and columns sums to zero. Upon denoting the elements of $Q^{(j)}$ by $q_{ij}^{(j)}$ we find that

$$L_j=(-1)^j 4q_{ii}^{(j)}, \qquad j\neq 0. \tag{35}$$

Therefore

$$E_R=-3n+2\sum_{j=0}^{n-1}(n-j)\,L_j=3n+8\sum_{j=1}^{n-1}(-1)^j(n-j)\,q_{11}^{(j)}. \tag{36}$$

The leading term of the summation in (36) is

$$m_{11}'=\sum_{j=1}^{n-1}(-1)^j n q_{11}^{(j)}, \tag{37}$$

which is the element in row one and column one of the matrix sum

$$M'=n\sum_{j=1}^{n-1}(-1)^j Q^{(j)} \tag{38}$$

or

$$M'=n(-S'+S'T'-S'T'S'+\cdots), \tag{39}$$

which we approximate by an infinite series. Now,

$$n^{-1}M'=-S'+S'T'(1-S'+S'T'-\cdots) \tag{40}$$

$$n^{-1}M'=-S'+S'T'(1+n^{-1}M'), \tag{41}$$

and upon solving for M', we secure

$$M'=n(1-S'T')^{-1}(S'T'-S'). \tag{42}$$

Now the needed inverse does exist. The construction of m_{11}' is a straightforward but laborious task. After m_{11}' is found, E_R follows readily.[8] We find that

$$E_R=(n/D)[8(AB+AC+BC)(ab+ac+bc) +4(Ab+Ac+Bc)(Ab+Ac+Cb)+\Delta], \tag{43}$$

where

$$D=(ab+ac+bc)(B^2+BC+C^2) +(AB+AC+BC)(b^2+bc+c^2) \tag{44}$$

and

$$\begin{aligned}\Delta=&\,2(A^2+B^2+C^2)(a^2+b^2+c^2)-2(Aa+Bb+Cc)^2\\ &+(Ab-Ba)(Bb+Cb-3Bc)\\ &+(Ac-Ca)(Bc+Cc-3Cb)\\ &+(Bc-Cb)(Bb-Cc+2Bc-2Cb)\\ &+2(BCa^2-A^2bc).\end{aligned} \tag{45}$$

We note that upon setting $A=a$, $B=C=b=c=\frac{1}{2}(1-a)$, we have that $\Delta=0$, and the remaining terms of (43) reduce readily to the leading term of (26).

Comparison of P_M with P_R shows that E_M can be obtained from E_R by making the following interchanges in E_R: A with a, B with c, and C with b. With E_M and E_R known, $(\mathbf{h}^2)_{Av}$ follows from (6) and we find

$$(\mathbf{h}^2)_{Av} =4n\frac{(1-\sigma^2)(1-\Sigma^2)+2\sigma^2\Sigma^2-2(\alpha^4+\beta^4+\gamma^4)}{(1-\sigma^2)(B^2+BC+C^2)+(1-\Sigma^2)(b^2+bc+c^2)}, \tag{46}$$

where

$$\begin{aligned}\sigma^2&=a^2+b^2+c^2\\ \Sigma^2&=A^2+B^2+C^2\\ \alpha^4&=(A^2-BC)(a^2-bc)\\ \beta^4&=(B^2-AC)(b^2-ac)\\ \gamma^4&=(C^2-AB)(c^2-ab).\end{aligned} \tag{47}$$

To find the mean square length, $(\mathbf{h}^2)_{Av}$ must be multiplied by $l_0^2/3$.

The problem of excluded volume is obviously not considered in any of our calculations.

[8] A better approximation to E_R can be found in principle by adding to the E_R given by (43) the element in row one and column one of 16 $S'T'[(1-S'T')^2]^{-1}(S'-1)+8(1-S'T')^{-1}S'$. The resulting E_R in that case would be of the order of approximation that corresponds to the one in our result for the special case of Sec. III.

Luminescence during Annealing and Phase Change in Crystals*

NOYE M. JOHNSON AND FARRINGTON DANIELS

Department of Chemistry, University of Wisconsin, Madison, Wisconsin

(Received March 9, 1960)

The accepted definition of thermoluminescence is the thermal release of trapped electrons with accompanying optical transition. This interpretation presupposes an exposure to ionizing radiation in order to fill the electron traps. Other processes such as mechanical stress and chemical reaction can also serve to excite electrons, as observed in triboluminescence and chemiluminescence. It is proposed that some instances of luminescence during heating are produced by physical processes other than the release of previously trapped electrons. Evidence for this is provided by the correlation of certain glow-curve peaks with crystalline annealing, decomposition, and polymorphic transition. Measurements of annealing and polymorphic changes were made through x-ray diffraction. Attempts to interpret the thermal or radiation history of geological specimens by thermoluminescence must account for both radiation-induced and radiation-independent forms of light generation.

INTRODUCTION

THERMOLUMINESCENCE is ordinarily induced by irradiating a crystal at a suitably low temperature. The irradiation excites electrons which may become trapped at various imperfections. Subsequent heating of the crystal releases these electrons as thermoluminescence. However, unusual cases of thermoluminescence have been noted where certain crystals become thermoluminescent because of compression or rapid crystallization.[1] The process of grinding has also been found to induce thermoluminescence in calcite[2] and glass.[3] The trapped-electron concept was employed to explain the stress-induced forms of thermoluminescence, however, with a difference in mechanism for electron excitation.[1] Mechanical processes were assumed to substitute for irradiation under certain circumstances.

Newer data now suggest a different interpretation for stress-induced thermoluminescence. Some cases of high-temperature thermoluminescence may be associated with the annealing of lattice strains instead of the thermal release of trapped electrons. Other solid state reactions such as polymorphic transition and crystal decomposition can also produce luminescence which may be confused with radiation-induced thermoluminescence.

Triboluminescence

Luminescence during crystal deformation, usually grinding, has long been known as triboluminescence. This phenomenon is quite common in organic and inorganic compounds. In a survey of 1883 materials, about 50% of the inorganic and 30% of the organic crystals could be made to triboluminesce.[4] In the usual case of triboluminescence, an external mechanical force works on the crystal and part of this disrupting energy is transformed into light quanta. Evidently, the deforming stresses may occasionally be concentrated on individual atoms in sufficient magnitude to excite them.

The fact of this charge separation is confirmed by the grinding of triboluminescent crystals between the plates of a condenser. Triboluminescent intensity was found to be directly proportional to the electric potential induced during grinding.[4] Excited electrons may also be produced within crystals by plastic deformation without shear or rupture. In certain crystals, dislocation loops and vacancies may excite valence electrons during their translation in plastic flow.[5] The transient electric current thus generated is called the "Tyler effect". As an immediate cause, therefore, triboluminescence may be considered a consequence of triboelectricity. The triboluminescence of many crystals is characterized by N_2 spectra, i.e., an external electric discharge through air between or along cleaved crystal faces. In crystals which are efficient phosphors the electronic energy may be dissipated within the lattice as normal fluorescence. The pulverizing of radiation-colored crystals results also in another form of triboluminescence. Examples and references to the various types of triboluminescence are discussed by Wick.[6]

Chemiluminescence

The phenomenon of chemiluminescence is a form of light emission usually associated with strongly exothermic reactions.[7] The photon energy of chemiluminescence is probably derived from the energy released during chemical reaction. Crystalloluminescence[7] is another effect closely related to both triboluminescence and chemiluminescence. During the sudden precipitation of certain crystals from solution, notably strontium bromate, a luminescent glow may be observed. The

* Presented in part at the International Union for Pure and Applied Chemistry, Munich, August 1959, abstracted in Angew. Chem. **72**, 45 (1960).

[1] E. J. Zeller, J. L. Wray, and F. Daniels, J. Chem. Phys. **23**, 11, 2187 (1955).

[2] R. E. Nyswander and B. E. Cohn, Phys. Rev. **36**, 1257 (1930).

[3] A. Debenedetti, Nuovo cimento **7**, 251 (1958).

[4] G. Gross, I. N. Stranski, and G. Wolff, Z. Elecktrochem. **59**, 346–350 (1955).

[5] D. Fishbach and A. Nowick, J. Phys. Chem. Solids **5**, 302 (1958).

[6] F. G. Wick, J. Opt. Soc. Am. **29**, 10, 407 (1939).

[7] E. J. Bowen, *Chemical Aspects of Light* (Clarendon Press, Oxford, England, 1946).

generation of photons may be attributed here to movement of microcrystalline parts similar to that which occurs in triboluminescence.

EXPERIMENTAL METHOD

Thermoluminescence Instrumentation

The system used for measuring thermoluminescence[8,9] is essentially composed of: (1) a nichrome-ribbon heating element upon which the sample is placed, (2) a variable transformer to regulate the heating rate, (3) a photomultiplier tube mounted in a light-tight box, (4) a combination ac rectifier-amplifier, (5) a rapid tracing recorder. The photomultiplier tube is an RCA–1P21–S4 with maximum response in the blue-violet. The recorder is a Sanborn, model 127, equipped with a built-in dc amplifier, model 126B. Use of large samples, rapid heating and strong amplification adapt this apparatus for the detection of low-level thermoluminescence.

Heating-Annealing Technique

The equipment employed heated the powdered sample from room temperature to incandescence in a few seconds. A standard temperature-time curve was established for the loaded furnace by means of crayons of known melting point (Fig. 1). When at the standard voltage setting, furnace temperature rose nearly linearly at first and then leveled off at about 450°C.

Sample volume and geometric distribution were controlled by using powdered samples placed in piles on the nichrome heating ribbon with the help of small molds. Because of rapid one-sided heating, uniform sample temperatures were not realized. However, the manner of heating was reproducible and consequently glow curves for specific samples were readily duplicated. A thermoluminescence run could be arrested at any stage (temperature) by turning off the furnace and quickly removing the sample. To determine the extent of annealing during heating, a sequence of samples was taken at progressively longer intervals (higher temperatures) after the start of the furnace. These powder samples were later x rayed to determine line profile broadness.

Sample Preparation

Crystals of the material to be tested for stress-induced luminescence were ground in a mechanical mortar for about 15 min and passed through a 325 Tyler equivalent (44 μ) screen. To activate radiation-induced thermoluminescence the samples were placed in gelatin capsules and exposed to a Co^{60} gamma-ray source. After irradiation, samples were kept at dry-ice temperature to prevent thermoluminescent leakage. Powders to be run for thermoluminescence were packed into a 78-mm³ circular mold of 1 mm depth. Also a 78-mm³ powder holder was built for use in a x-ray diffractometer. A representative part of all sample material was x rayed after grinding to ascertain purity and polymorphic constitution. Since x rays induce thermoluminescence, the x-ray tested portion of a sample was not used to study annealing luminescence.

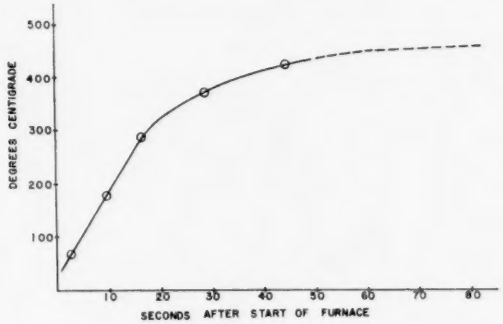

FIG. 1. Standard heating curve.

X-Ray Instrumentation

X-ray powder patterns and line profiles were recorded using a Norelco x-ray unit with Geiger-counter diffractometer and circuit panel. Nickel-filtered copper radiation was used from a power-stabilized tube. For the measurement of line broadening a scan rate of 1/8° (2θ)/min was utilized, and 1° divergence and 0.006-in. receiving slits. Powder samples were uniformly packed in a holder of 1 mm depth. The same scale factor and time-constant settings were used for each member of an annealing series.

X-Ray Techniques

The sharpness of an x-ray powder pattern depends on the size and perfection of the scattering crystals and inherent instrumental factors. Below a critical size, crystallite smallness and the presence of imperfections tend to broaden the x-ray powder pattern. The broadness of a diffraction line may be used to indicate the state of internal strain and the size of the aggregate sample crystallites. Consequently, for detecting annealing or recrystallization through various stages of thermoluminescence, certain x-ray line profiles were compared for broadness. Generally, the higher Bragg angle reflections are more susceptible to line profile broadening. The highest-angle strongest lines were therefore used whenever possible. Because calcite has no suitable high-angle lines, a strong low-angle line (202) was utilized instead.

A useful measure of line broadness is the Laue integral breadth, which is the ratio of area under the line profile to the maximum height of the profile. Integrated

[8] W. F. Ammentorp, Master's thesis, University of Wisconsin (1957).

[9] N. M. Johnson, W. F. Ammentorp, and F. Daniels, Am. Mineralogist (to be published).

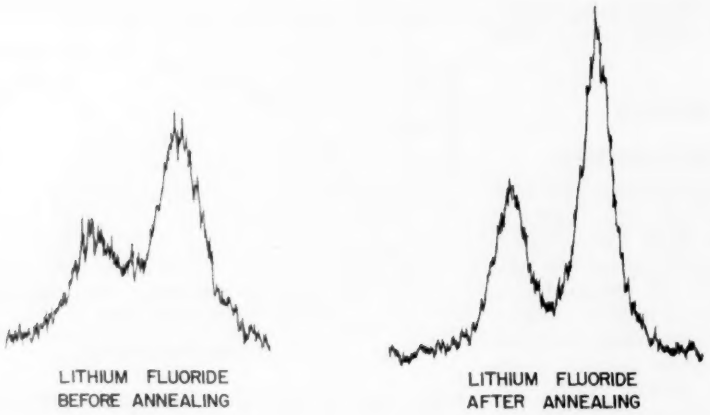

FIG. 2. Effect of thermal annealing on the 422 Bragg reflection of strained lithium fluoride ($K_{\alpha 1}$ and $K_{\alpha 2}$).

intensities were determined by planimetry from a smoothed diffractometer trace. Background intensity was eliminated by joining the background level on each side of the peak. Maximum intensities were measured in millimeters from the smoothed line profile. The broadness parameter was then a composite of intrinsic and instrumental factors expressed in arbitrary relative units.

The broadness parameters for individual samples were found reproducible to within a few percent.

EXPERIMENTAL RESULTS

Luminescence During Annealing

When crystals are crushed or plastically deformed, strains are introduced into the lattice which take the form of various imperfections. Paterson[10] has found that deformed calcite may store up to 12 cal/g as internal strain.

In general terms, annealing is defined as any process which reduces internal strain and surface energy. The driving force of annealing is the release of strain energy during recrystallization and repair. Generally, the smaller and more defective the crystals, the lower will be the annealing temperature.

Grinding-induced thermoluminescence in calcite and glass has been previously noted. A test of 78 different solids showed that several other materials possess this property to varying degrees as listed in Table I. The only requirement for inducing thermoluminescence in crystals of these materials is to deform them by grinding or pressure. Light is emitted later when the strained crystals are heated.

TABLE I. Representative materials showing grinding-induced thermoluminescence.

Strong
$CaCO_3$ (calcite); CaF_2; LiF
Moderate
Al_2O_3; $CaSO_4$; K_2SO_4; SiO_2 (quartz)
Weak
BaS; $CaSiO_3$; Li_2CO_3; ZnS (sphalerite)

[10] M. S. Paterson, Phil. Mag. **4**, 451 (1959).

X-ray diffraction patterns of strained crystals taken before and after heating showed that some annealing was produced by the heating. An example of this annealing in strained lithium fluoride is shown in Fig. 2. In a series of progressively sampled thermoluminescence runs, the temperature interval of annealing as determined from x-ray line profiles was found to coincide with the interval of luminescence as shown in Figs. 3 and 4. It is suggested that the movement of dislocations and the migration of vacancies produces photons, probably in a manner similar to triboluminescence. The thermal annealing of metastable lattice imperfections, other than color centers, makes this possible. As the experiment was arranged, the sample temperature never exceeded 500°C (Fig. 1). As this temperature was approached, annealing leveled off

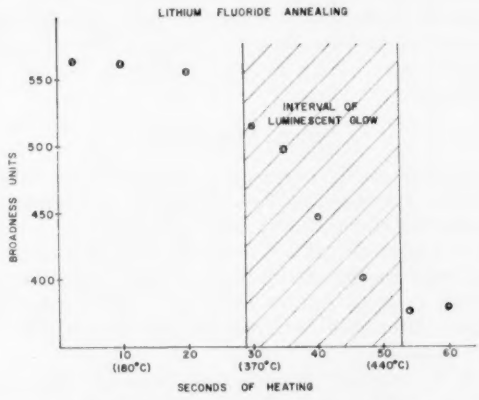

FIG. 3. Annealing and thermoluminescence of strained calcite (Mallinckrodt). Broadness derived from 202 reflection.

and the luminescent glow also ceased (Figs. 3 and 4). With higher furnace power settings, higher temperatures were attained and annealing was found to continue above 500°C; however, any associated luminescence was obscured by strong black body incandescence.

Gilman and Johnston[11] conclude that annealing of radiation-damaged lithium fluoride begins about 300°C. In our study, annealing of mechanically-damaged lithium fluoride was found to start near 370°C. Griggs *et al.*,[12] have found that annealing recrystallization of deformed calcite begins at 500°C, which is considerably higher than indicated here. However, Griggs *et al.* used mainly microscopic techniques to determine the extent of recrystallization. Recovery and repair at the atomic scale was not comprehensively studied by them, and this may account for their higher annealing temperature. As indicated by x-ray diffraction-pattern changes, incipient annealing of finely ground calcite begins about 340°C. The exact temperature depends on the degree of grinding and the rate of heating employed.

Luminescence During Polymorphic Transition

At normal temperatures and pressures, calcium carbonate may crystallize either as orthorhombic aragonite or trigonal calcite. The calcite structure is the stable form, but aragonite may persist metastably. At temperatures above 400°C, however, the aragonite structure rapidly changes to the stable calcite form. Coincident with this transition, a luminescence glow may be observed. Figure 5 shows that the temperatures at which the transition occurs, as determined by x ray, and the temperatures at which light is emitted are the same.

The aragonite-to-calcite transition involves large changes in cell dimensions, readjustments in atomic coordination and bond distances. It is classified as the most severe type of solid-solid transformation.[13] Conveniently, the aragonite-to-calcite transition occurs at a temperature below strong incandescence and therefore the associated luminescence is readily detected. Since the reorganization takes place with practically no heat change, it is not chemiluminescence in the usual sense. The energy available to reorganize the crystal structure may occasionally be localized and converted into excited electrons and the emission of photons.

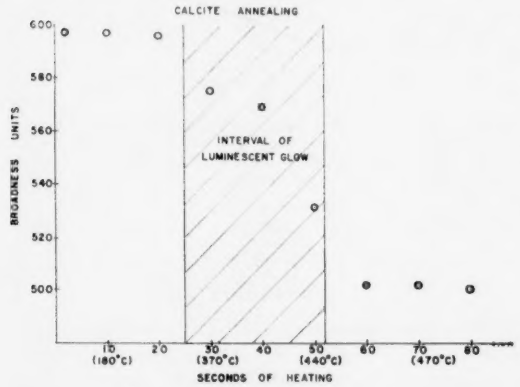

FIG. 4. Annealing and thermoluminescence of strained lithium fluoride (Chemical Commerce Co.). Broadness derived from 422 reflection.

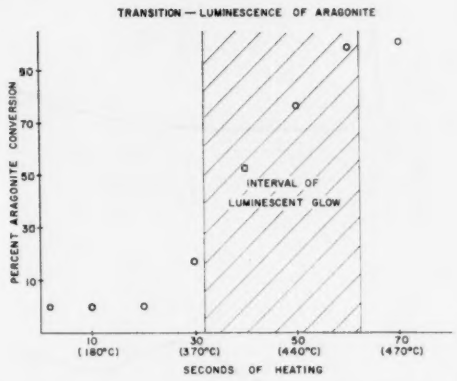

FIG. 5. Aragonite-calcite polymorphic transition and luminescence.

Radiation-Induced Thermoluminescence

To demonstrate the basic differences between them, the glow curves of radiation-induced thermoluminescence were compared with the glow curves of stress-induced luminescence in equivalent materials. In the samples of calcite (Mallinckrodt) used for this study the radiation-induced thermoluminescence produced sharper lower-temperature peaks than stress-induced luminescence. The distribution of annealing-luminescence over a wide temperature range is particularly distinctive as shown by the glow curves in Fig. 6. A similar relationship in glow curves was found for lithium fluoride between radiation and stress thermoluminescence. The color of stress-induced luminescence was found to be the same as radiation-induced thermoluminescence, at least within the limits of visual inspection.

The annealing-luminescence of spectrographically pure calcite crystals also showed that trapped electrons are not involved. No thermoluminescence could be detected in a chemically pure calcite sample (Johnson and Matthey) after 50 000 r of Co^{60} gamma irradiation. At least in the temperature range studied, the electron storage capacity of this particular calcite was negligible. Nevertheless, the calcite crystals showed pronounced

[11] J. J. Gilman and W. G. Johnston, J. Appl. Phys. **29**, 877 (1958).

[12] D. T. Griggs, M. S. Paterson, H. C. Heard, and F. J. Turner, Geol. Soc. Am. Mem. **79**, 21 (1960).

[13] M. J. Buerger, *Phase Transformations in Solids* (John Wiley & Sons, Inc., New York, 1951).

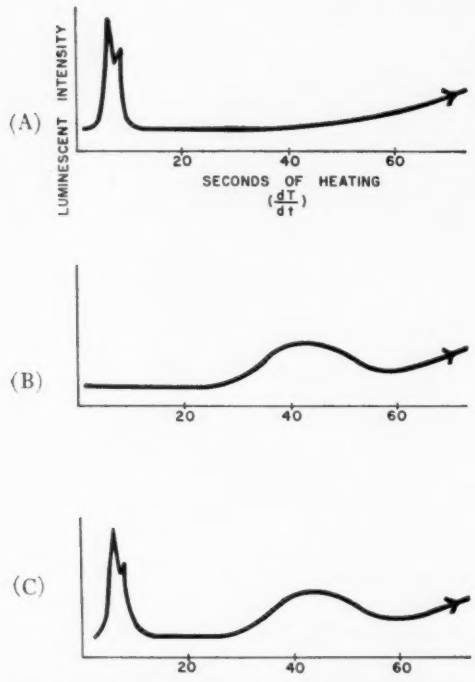

FIG. 6. Schematic glow curves of Mallinckrodt calcite (A) after 50 000 r Co^{60} radiation, no grinding (B) after grinding, no irradiation (C) after 50 000 r Co^{60} radiation plus grinding.

grinding-induced thermoluminescence. Annealing luminescence of calcite is evidently independent of chemical purity and electron storage capacity. Annealing luminescence can occur in calcite even when radiation-induced thermoluminescence cannot. This fact demonstrates the fundamental difference in mechanism between the two forms of luminescence. In these experiments the broad glow zone at 340–450°C in calcite is a function of internal strain rather than trapped electrons.

Experiments in this laboratory have shown that aragonite has no high-temperature radiation-induced thermoluminescence.[14] Many different mineral and laboratory-grown crystals of aragonite were found devoid of radiation-thermoluminescence even after extended exposure to gamma radiation. The only radiation-thermoluminescence in these samples was traced to calcite contamination. The amount of transition luminescence in aragonite was found to be independent of radiation dosage.

TABLE II. Materials showing low temperature decomposition luminescence or decrepitation-luminescence.

Strong
CaO; $Ca(OH)_2$; $NaHCO_3$; $ZnCO_3$
Weak
$Al(OH)_3$; $CaSO_4 \cdot 2H_2O$; $KHCO_3$; $KClO_4$; $MgClO_4$

[14] N. M. Johnson, J. Sediment. Petrol. **30**, 305 (1960).

Luminescence During Decomposition

The thermal decomposition or decrepitation of crystals may also be accompanied by light emission.[15] During this research, several materials were found to exhibit such reactions. Out of 24 thermal decompositions tested, those recorded in Table II showed luminescence. The movement and disruption of crystal parts attending breakdown can apparently occasionally excite electrons into optical transitions (Fig. 7).

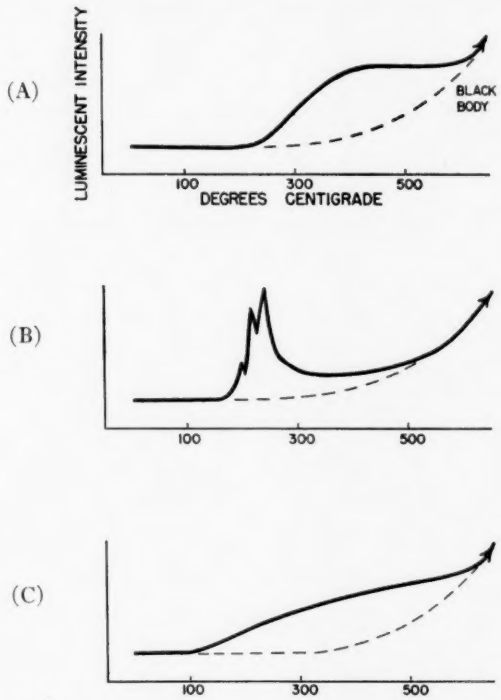

FIG. 7. Schematic glow curves without irradiation (A) decomposition-luminescence of sodium bicarbonate, (B) decrepitation-luminescence of potassium perchlorate, and (C) decomposition-luminescence of zinc carbonate.

DISCUSSION

It has been demonstrated that thermoluminescence may occur in a variety of materials without previous exposure to x rays or other ionizing radiation. The cause of this luminescence upon heating is associated with the processes of crystalline annealing, chemical decomposition, or phase change. This luminescence may be explained by analogy with triboluminescence, chemiluminescence, and crystalloluminescence.

[15] J. Ewles, Trans. Faraday Soc. **35**, 119 (1939).

Luminescence within a crystal implies that some form of energy is being transformed into optical photons. The usual mechanism is through the radiative transition of electrons which are displaced by high-energy particles, electromagnetic waves or by the action of mechanical stress upon the atoms of the crystal. The annealing of strains, polymorphic changes, or decomposition induced by heating, all may produce local areas of mechanical stress within a crystal. Relatively small stresses may be involved in this process when considered over the whole volume of the crystal. However, such stresses may occasionally be concentrated at favorable sites and give rise to luminescence, as for example, triboluminescence.

This investigation has indicated that the mechanism of stress-induced luminescence upon heating is quite different from that of radiation-induced thermoluminescence. The former is a function of the stress-strain history of the crystal and the latter depends upon the accumulation of trapped electrons. Both structural annealing and release of trapped electrons are accomplished by sufficient heating. A thermoluminescence glow curve may contain luminescence from either or both of these sources.

When a geological interpretation is given for the natural thermoluminescence of rocks and minerals, consideration must be given to both forms of luminescence. For example, the age estimation of minerals,[16] limestones,[17] lavas, and archeological ceramics[18] from natural thermoluminescence, assumes that this luminescence is derived only from the traces of uranium present in the sample. The time required to accumulate the observed thermoluminescence is calculated from the radioactivity of the mineral and its calibrated thermoluminescence sensitivity.

The work described here emphasizes the fact that annealing luminescence may be induced by the grinding of the sample or by stresses experienced during the geological history of the crystal. This luminescence may tend to confuse the age estimates based only on radiation-induced thermoluminescence. Lavas and pottery appear to have little annealing luminescence,[17] but limestones may have considerable amounts. In order to distinguish between the luminescence induced by stress and that induced by radiation, efforts might be directed toward annealing crystal strain without disturbing trapped electrons. This might be accomplished by ultrasonic or infrared treatments.

It is important to prepare minerals for thermoluminescence tests in such a way that stress-induced luminescence is avoided. For satisfactory age determinations, it will be necessary to find ways to compensate for annealing-luminescence which may be introduced by the preparation procedures or by geological forces during the history of the mineral.

ACKNOWLEDGMENTS

The authors are pleased to acknowledge support of this research by the Atomic Energy Commission and the Research Committee of the University of Wisconsin with funds from the Wisconsin Alumni Research Foundation. They also thank Dr. O. C. Simpson, Dr. P. H. Yuster, and Dr. S. W. Bailey for reviewing this manuscript.

[16] F. Daniels, C. A. Boyd, and D. F. Saunders, Science **117**, 343 (1953).

[17] E. J. Zeller, J. L. Wray, and F. Daniels, Bull. Am. Assoc. Petrol. Geologists **41**, 121 (1957).

[18] G. C. Kennedy, Sci. News Letter **79**, 10, 149 (1959), and private written communications.

Extreme Pressures. II. Volume-Temperature Relationship for Gases*

LEONARD S. LEVITT

Department of Chemistry, Stevens Institute of Technology, Hoboken, New Jersey

(Received August 24, 1960)

It is found, using Bridgman's data for H_2O, N_2, and Ar, that the V-T isobars, though curved at medium pressures, become good straight lines at the same higher pressures for which the isothermal relation $p=Ce^{B/V}$ begins to hold (above 1000 kg/cm² for gases, and above 4000 for liquids). Aside from the surprising linear variation of V with T under these extreme conditions, the most remarkable feature of the V-T plots is the apparent convergence of all the isobars (for a given gas) to a common intercept on the V coordinate (at 0°K). The isobars for gases therefore can be represented by the equation, $V=V_0+a_pT$, where V_0 is the incompressible molar volume of the substance at 0°K. Eliminating a_p for two different temperatures at constant pressure gives an exact V-T relation for high pressures comparable to Charles' law,

$$V_2=V_1(T_2/T_1)+V_0(1-T_2/T_1).$$

The slope a_p of the isobars decreases with increasing pressure, and it is found that $a_p\simeq R'/p$, where R' is a new gas constant for high pressures, which at first increases somewhat with pressure, and reaches the same *limiting* value of $\frac{3}{2}R$ at 6000 atm for both N_2 and Ar.

INTRODUCTION

IN the previous article[1] it was shown that experimental pressure-volume data at constant temperature and extreme pressures (from 10^3 to 10^5 atm) are represented accurately by the equation

$$p=C\exp(B/V) \tag{1}$$

or

$$\ln(p_2/p_1)=B(1/V_2-1/V_1), \tag{2}$$

where B and C are constants characteristic of a particular gas, liquid, or solid. This relation holds well for gases above 1000 atm, for liquids above 4000 atm, and for solids above 25 000 atm.[1]

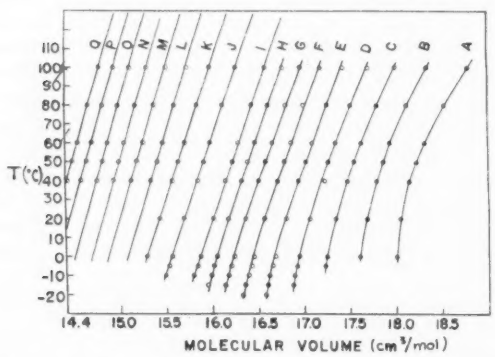

FIG. 1. T-V isobars for 1 mole H_2O at various pressures to 12 000 atm: A, 1 atm; B, 500; C, 1000; D, 1500; E, 2000; F, 2500; G, 3000; H, 3500; I, 4000; J, 5000; K, 6000; L, 7000; M, 8000; N, 9000; O, 10 000; P, 11 000; Q, 12 000 atm.

In the present paper we show that the temperature-volume relation at constant pressure for substances under extreme pressures is likewise a surprisingly simple one.

T-V ISOBARS

In Fig. 1 are presented T-V plots for water at various constant pressures from 1 to 12 000 atm. The data are from Bridgman's work.[2] It is apparent that the T-V isobars are quite curved in the region of lower pressures, but gradually straighten out at higher pressures, becoming excellent straight lines at 4000 atm and above.[3] It is to be noted that this is also the pressure at which the p-V isothermal equation [Eq. (1)] begins to hold.[1] Similar isobaric plots of Bridgman's data[4] are given for nitrogen[5] and for argon in Figs. 2 and 3, respectively. It is seen that good straight lines are obtained with these gases at pressures as low as 2000 atm.

Aside from the surprising linear variation of V with T under these extreme conditions, the most remarkable feature of the $T-V$ plots is the apparent convergence of all the isobars, for a given substance, to a common intercept on the V coordinate at (or very near) absolute zero.[6] At constant high pressures, therefore, the T-V

* This paper was presented before the Vancouver Meeting of the American Physical Society, August 28, 1958.

[1] L. S. Levitt, J. Phys. Chem. **58**, 573 (1954); Bull. Am. Phys. Soc. Sec. II, **3**, 340 (1958); **4**, 376 (1959).

[2] P. W. Bridgman, J. Chem. Phys. **3**, 597 (1935).

[3] A linear variation of V with T at extreme pressures was also observed recently for high molecular weight hydrocarbons [W. G. Cutler, R. H. McMickle, W. Webb, and R. W. Schiessler, J. Chem. Phys. **29**, 727 (1958)].

[4] P. W. Bridgman, Proc. Am. Acad. Arts Sci. **70**, 20 (1935).

[5] The experimental data of M. Benedict [J. Am. Chem. Soc. **59**, 2224 (1937)] for N_2 also plot linearly in this pressure region.

[6] The data for water are at much higher temperature than for the gases, and it is difficult to extrapolate the isobars to absolute zero. It is apparent that the lines are converging, but it seems that they will converge at a temperature considerably below 0°K. For this reason, what follows in this paper will apply strictly to gases only. (There do not appear to be any temperature-variable high-pressure data for solids in the literature).

relation for gases can be represented by the equation

$$V = V_0 + a_p T, \tag{3}$$

where V_0 is the molar volume of the substance at 0°K, and $a_p = (\partial v/\partial T)_p$. It should be noted from the slopes of the isobars that a_p decreases with increasing pressure.

RELATION TO VAN DER WAALS' b

Since V_0 is apparently independent of pressure (or nearly so), this quantity represents essentially an "incompressible volume" at absolute zero, and must be related to the quantity b in the van der Waals equation of state. Table I gives a comparison of V_0 with b for the substances under discussion. The values of V_0 appear to be about two-thirds the value of the corresponding b.

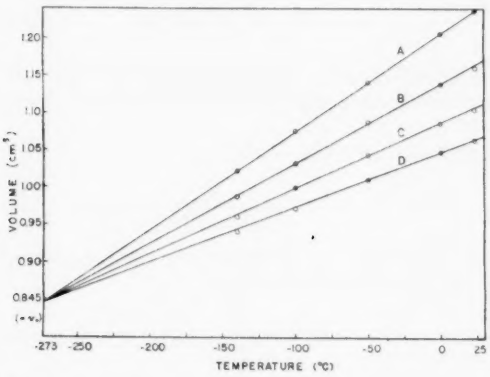

FIG. 2. T-V isobars for 1 g N_2 at various high pressures: A, 3000 atm; B, 4000;, C, 5000;, D, 6000 atm.

A NEW CHARLES' LAW FOR HIGH PRESSURE

Along any isobar, a_p is a constant, and the volume is given by Eq. (3). For two different temperatures the respective volumes are

$$V_1 = V_0 + a_p T_1$$

$$V_2 = V_0 + a_p T_2. \tag{4}$$

Eliminating a_p from Eqs. (4) gives a simple volume-temperature relation comparable to Charles' law, and permits the calculation of the volume at one temperature from knowledge of the volume at any other temperature, without any knowledge of the pressure [so long as the pressure is in the high range where Eq. (3) is valid]. Thus

$$T_2/T_1 = (V_2 - V_0)/(V_1 - V_0) \tag{5a}$$

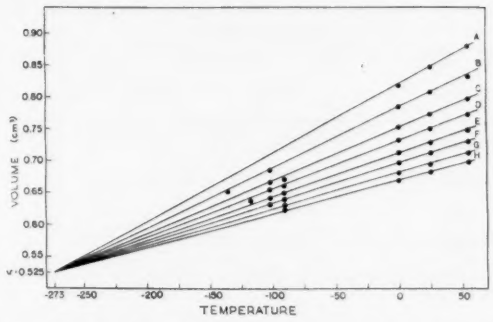

FIG. 3. T-V isobars for 1 g Ar at various high pressures: A, 2000 atm; B, 2500; C, 3000; D, 3500; E, 4000; F, 4500; G, 5000; H, 5500 atm.

or

$$V_2 = V_1(T_2/T_1) + V_0(1 - T_2/T_1). \tag{5b}$$

Without the second term Eq. (5b) is identical to Charles' law. It is interesting to compare Eq. (5a) with the isobaric form of the van der Waals equation,

$$T_2 = T_1[(V_2 - b)/(V_1 - b)] + (a/R)(V_2 - b) \times (1/V_2^2 - 1/V_1^2). \tag{6}$$

It is easily shown that, at extreme pressures, the second term in Eq. (6) becomes negligible by comparison with the first, thus leaving an expression identical to Eq. (5a) if b is taken equal to V_0.

"GAS CONSTANT" AT HIGH PRESSURE

As was noted above, a_p is a function of pressure, decreasing with increasing pressure. Such a decrease in $(\partial V/\partial T)_p$ is required by thermodynamics,[7] since this derivative is mathematically equal to $-(\partial S/\partial p)_T$, and the decrease in entropy caused by increasing pressure at constant temperature cannot exceed the total entropy of the substance at that temperature. As a first conjecture, we can assume a_p is simply inversely proportional to p, and define a new constant R' such that $a_p = R'/p$. In Tables II and III we show for N_2 and Ar, respectively, the measured slopes a_p of

TABLE I. Comparison of V_0 with van der Waals' b. The values of V_0 appear to be about two-thirds the value of the corresponding b.

Substance	b (cm³)	V_0 (cm³)
Nitrogen	39.1	23.7
Argon	32.2	21.0

[7] P. W. Bridgman, *The Physics of High Pressure* (G. Bell and Sons, London, 1949), p. 175.

TABLE II. The slope a_p for N_2 at various pressures, and the calculation of R'.

p (atm)	a_p (cc/mol deg)	R' (liter atm/mol deg)
3000	0.037	0.11
4000	0.030	0.12
5000	0.024	0.12
6000	0.020	0.12

the isobars at various pressures, and the product $pa_p(=R')$. It is seen that R' is reasonably constant, increasing somewhat with pressure, and apparently reaching the same *limiting* value of around 0.12 liter atm/mol deg in the case of both gases.

SOME THERMODYNAMIC RELATIONS AT HIGH PRESSURE

The total decrease in entropy due to increased pressure is given by

$$-\Delta S=\int_0^p (\partial V/\partial T)_p dp=R'\int_0^p (dp/p)=R'\ln(p_2/p_1), \tag{7}$$

which is nearly identical to the isothermal expression for an ideal gas, $-\Delta S=R\ln(p_2/p_1)$. It should be remarked that R' has the same dimensions as the gas constant R, but its limiting numerical value for high pressures is equal to about $\frac{3}{2}R$. On combining Eq. (2) with Eq. (7), we obtain

$$-\Delta S=R'B(1/V_2-1/V_1). \tag{8}$$

Since $(\partial V/\partial T)_p=R'/p$, it follows that $(\partial^2 V/\partial T^2)_p=0$ for gases at high pressures, and does not become negative between 3000 and 4000 atm, as is thought[8] to be the case with liquids. This also implies that at high pressures C_p ceases to decrease with rising pressure and apparently becomes independent of the pressure,

$$(\partial C_P/\partial p)_T=-T(\partial^2 V/\partial T^2)_p=0. \tag{9}$$

The difference between the heat capacity at constant pressure and that at constant volume for gases at extreme pressures is found to be

$$C_p-C_V=-T\frac{(\partial V/\partial T)_p^2}{(\partial V/\partial p)_T}=-T\frac{(R'/p)^2}{(-V^2/Bp)}$$
$$=[(R')^2BT/pV^2]. \tag{10}$$

[8] See work cited in footnote 7, pp. 136–137.

Since the right-hand member of Eq. (10) is always a positive quantity, then even though C_p decreases at first with increasing pressure, reaching a lower limiting value at high pressure [Eq. (9)], it always remains larger than C_V.

It should be noted that the van der Waals equation gives a quite different result for C_p-C_V at high pressures, namely,

$$C_p-C_V=(2a/RT^2)[p+(a/V^2)]+[p(V-b)/T],$$

which predicts that the difference gets continually larger with increasing pressure.

The isobaric thermal expansion β is defined as

$$\beta=(1/V)(\partial V/\partial T)_p \tag{11a}$$

and this is found, for gases at extreme pressures, to be simply

$$\beta=(1/V)(R'/p)=R'/pV. \tag{11b}$$

Differentiation of Eq. (11b) with respect to p gives the decrease in thermal expansion with increasing pressure,

$$-d\beta/dp=(R'/p^2)(1/V-1/B)$$
$$=(R'/pV)(1/p-V/Bp). \tag{12a}$$

Since $R'/pV=\beta$, and $V/Bp=\alpha$, the compressibility,[1] Eq. (12a), is equivalent to

$$-d\beta/dp=\beta(1/p-\alpha) \tag{12b}$$

or

$$-(d\ln\beta/dp)=1/p-\alpha=(1/p)(1-V/B). \tag{12c}$$

It is interesting to compare this expression with that

TABLE III. The slope a_p for Ar at various pressures, and the calculation of R'.

p (atm)	a_p (cc/mol deg)	R' (liter atm/mol deg)
2000	0.043	0.086
2500	0.038	0.093
3000	0.033	0.10
3500	0.030	0.11
4000	0.027	0.11
4500	0.025	0.11
5000	0.023	0.12
5500	0.021	0.12

obtained previously[1] for the change of α with p, namely,

$$-(d\ln\alpha)/dp=1/p+\alpha=(1/p)(1+V/B), \qquad (13)$$

from which it is obvious that α decreases more rapidly with increasing pressure than does β, this behavior being what is theoretically expected, and the same as that found by Bridgman for liquids and solids.[9] In fact $(d\beta/dp)$ becomes zero when $V=B$.

Finally, we obtain the following expression for the decrease of thermal expansion with increasing temperature, at extreme pressures, by differentiating Eq. (11b) with respect to T,

$$-d\beta/dT=(R')^2/p^2V^2+[(R')^2B/p^2V^3]$$

$$=(R'/pV)^2(1+B/V)=\beta^2(1+B/V). \qquad (14)$$

In a forthcoming paper we shall discuss the pressure coefficient, the internal energy, and the internal pressure, and shall attempt to derive the complete equation of state for gases at extreme pressures.

[9] See work cited in footnote 7, p. 172.

Letters to the Editor

THE Letters to the Editor section is subdivided into three parts entitled Communications, Comments and Errata, and Notes. These three sections are all subject to the same limitations on length. The textual material of each Letter is limited to a number of words equal to 950 minus the following; (a) 200 words for each average-sized figure; (b) 50 words for each displayed equation; (c) 7 words for each line of table including headings and horizontal rulings. No proof will be sent to the authors of "Communications" and "Comments and Errata." Proof will be sent to the authors of "Notes." The publication charge for Letters is $30 per page, with a minimum of $30 per Letter, If honored, the Institution will be entitled to 100 reprints without covers. See issues of May–September, 1957, for descriptions of categories.

Communications

Open- and Closed-Shell SCF Method for Conjugated Systems*†‡

O. W. ADAMS AND P. G. LYKOS

Division of Chemistry and Chemical Engineering, Armour Research Foundation of the Illinois Institute of Technology and the Department of Chemistry, Illinois Institute of Technology, Chicago 16, Illinois

(Received December 14, 1960)

ROOTHAAN[1] and Huzinaga[2] have extended the LCAO-MO-SCF method of Roothaan[3] for closed-shell systems to include open-shell systems. We have concerned ourselves with the lowest singlet, doublet, and triplet states of conjugated systems within the pi-electron approximation[4] and have prepared for the UNIVAC 1105 computer an automatic general program for handling open-shell systems for which the total energy can be expressed in the form

$$E=2\sum_k H_k+\sum_{kl}[2J_{kl}-K_{kl}]+f\{2\sum_m H_m+f\sum_{mn}[2aJ_{mn}-bK_{mn}]+2\sum_{km}[2J_{km}-K_{km}]\}.$$

The definitions of the various terms in this equation are exactly the same as those given by Roothaan.[1] The LCAO-MO-SCF method as programmed for the 1105 is similar to that of Roothaan[1] except that we take cognizance of no symmetry and accordingly we find it convenient to normalize each of the MO's to unity. Also we work within the assumption of zero differential overlap.[5]

The **F** matrix is expressed in the form

$$\mathbf{F}=\mathbf{H}+2\mathbf{J}_c-\mathbf{K}_c+2\mathbf{J}_0-\mathbf{K}_0+\mathbf{D}_t\mathbf{B}+\mathbf{B}\mathbf{D}_t-\mathbf{B},$$

where $\mathbf{B}=(2\alpha\mathbf{J}_0-\beta\mathbf{K}_0)$ with $\alpha=(1-a)/(1-f)$ and $\beta=(1-b)/(1-f)$. The matrix $\mathbf{D}_t$ is the total density matrix.

Within zero differential overlap the elements of the various matrices contributing to **F**−**H** are:

$$J_{C,pp}=\sum_k J_{k,pp}=\sum_k\sum_s C_{sk}^2(pp|ss)$$

$$K_{C,pq}=\sum_k K_{k,pq}=\sum_k C_{pk}C_{qk}(pp|qq)$$

$$J_{O,pp}=f\sum_m J_{m,pp}=f\sum_m\sum_s C_{sm}^2(pp|ss)$$

$$K_{O,pq}=f\sum_m K_{m,pq}=f\sum_m C_{pm}C_{qm}(pp|qq)$$

$$D_{T,pq}=\sum_k C_{pk}C_{qk}+f\sum_m C_{pm}C_{qm}$$

$$J_{C,pq}=J_{O,pq}=0.$$

Here *kl*, *mn*, and *ij* are indices which run over the closed-shell, open-shell or both open- and closed-shell orbitals, respectively, and *f* is the fractional occupancy of the open shells.

Lefebvre[6] has used a perturbation approach for handling open-shell SCF problems and concerned himself with the lowest singlet and triplet states of *trans*-butadiene. The MO's which he obtained from the triplet-state problem did not differ greatly from the MO's which characterized the lowest singlet state MO's suggesting that separate optimization of the LCAO-MO vectors does not lead to significantly different results.

The symmetry of *trans*-butadiene is sufficiently high that not many degrees of freedom are left for this difference to manifest itself. Accordingly we have selected for a test problem for our general program the perturbed *trans*-butadiene that results when an $sp^2\pi$ nitrogen atom is substituted for a terminal $sp^2\pi$ carbon atom, say carbon atom number 4.

The results which obtain for the singlet ground state and for the lowest triplet state are given in Table I.

TABLE I. SCF results for perturbed *trans*-butadiene.

Coefficients	Singlet ground state	Lowest triplet state
C_{11}	0.427	0.667
C_{21}	0.517	0.692
C_{31}	0.520	0.257
C_{41}	0.529	0.098
C_{12}	0.561	0.226
C_{22}	0.480	0.090
C_{32}	−0.344	−0.514
C_{42}	−0.581	−0.822
C_{13}	0.535	0.288
C_{23}	−0.409	−0.068
C_{33}	−0.543	−0.776
C_{43}	0.502	0.557
C_{14}	0.465	0.648
C_{24}	−0.581	−0.713
C_{34}	0.562	0.260
C_{44}	−0.361	−0.062

We observe that the two sets of MO's are quite different. A more complete discussion of the method employed here and of the basis of the choice of parameters[7] will be given in a subsequent paper. That paper will also include calculations on aromatic and *N*-heteroaromatic systems.[8]

* Part of a thesis by O. W. Adams, submitted to the Illinois Institute of Technology, 1960, in partial fulfillment of the requirements for the Ph.D. degree.

† This research was supported in part by a grant to the Illinois Institute of Technology from the National Science Foundation.

‡ We wish to thank the Illinois Institute of Technology for the generous contribution of UNIVAC 1105 computer time.

[1] C. C. J. Roothaan, Revs. Modern Phys. **32**, 179 (1960).
[2] S. Huzinaga, Phys. Rev. **120**, 866 (1960).
[3] C. C. J. Roothaan, Revs. Modern Phys. **23**, 69 (1951).
[4] P. G. Lykos and R. G. Parr, J. Chem. Phys. **24**, 1166 (1956).
[5] R. Pariser and R. G. Parr, J. Chem. Phys. **21**, 466, 767 (1953).
[6] R. Lefebvre, *Calcul Des Fonctions D'Onde Moleculaire* (International Colloquium at the National Center of Scientific Research, Paris, 1958), p. 95.
[7] Part of a thesis by O. W. Adams submitted to the Illinois Institute of Technology, 1960, in partial fulfillment of the requirements for the Ph.D. degree.
[8] B. Grabe, Arkiv Fysik **17**, 97 (1960) and J. R. Hoyland and L. Goodman, Symposium on Molecular Structure and Spectroscopy, The Ohio State University, Columbus, June 13–17, 1960, have used the open-shell SCF method of Roothaan for odd-electron aromatic systems. As brought out explicitly by Grabe and by private communication to one of us (P.G.L.) from Professor Goodman, similar differences are noticed in comparing the ground state of the ion with the ground state of the parent aromatic system.

Far-Infrared Bands of Some Crystals with Strong Hydrogen Bonds

D. Hadži*

Mellon Institute, Pittsburgh 13, Pennsylvania

(Received January 18, 1961)

PREVIOUS investigations[1,2] have shown the occurrence of two OH stretching bands near 3000 cm^{-1} in the infrared spectra of certain solids containing very strong hydrogen bonds. This was attributed to the splitting of vibrational energy levels due to proton tunnelling. Evidence for such proton motion was also obtained from nuclear magnetic resonance studies.[3] As a further step in this work far-infrared spectra have now been measured in the range 500–100 cm^{-1} for solid potassium, rubidium, and ammonium dihydrogen phosphates, potassium dihydrogen arsenate, silver trihydrogen periodate, potassium hydrogen di-(*p*-nitrobenzoate), and phenylphosphinic acid. The hope was to find bands due to the direct transitions between the split zero level of the OH oscillator $\nu_{0+} \rightarrow \nu_{0-}$ (see Fig. 1). The first five substances are of particular interest because of their ferroelectric properties.

TABLE I.

	Δ_0 (cm^{-1})	$\Delta\nu_{OH}$ (cm^{-1})
KH_2PO_4	123	360
RbH_2PO_4	121	350
KH_2AsO_4	130	380
Phenyl phosphinic acid	145	400
KH di-(*p*-nitrobenzoate)	151	400

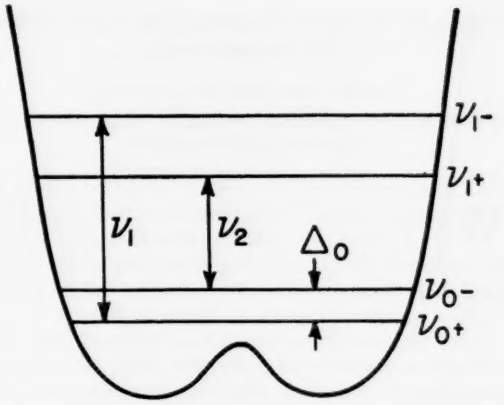

FIG. 1. Schematic representation of the infrared transitions in a double-minimum potential field ($\Delta\nu_{OH} = \nu_1 - \nu_2$).

The observed frequency differences between the two OH stretching bands are given in Table I ($\Delta\nu_{OH}$, from the works cited in references 1 and 2). They indicate that bands due to the $\nu_{0+} \rightarrow \nu_{0-}$ transition will be in the range 100–160 cm^{-1}. In fact, we have found bands in this region with five of the above mentioned substances (Δ_0 in the table). They do not appear with the deuterated analogs, probably being shifted below 100 cm^{-1}. It was not possible to find them there with the instrument used. The large shift makes the assignment to the mentioned transition more probable than the alternative assignment to some lattice modes. The fact that the substances showing a larger $\Delta\nu_{OH}$ have larger Δ_0 too is also significant. The detection of bands was particularly difficult with the group of ferroelectrics which exhibits very strong absorption extending from above 500 cm^{-1} to below 200 cm^{-1}. The low-frequency slope of this absorption may have covered the bands of the other two substances so that they could not be observed.

The author is indebted to Dr. Foil A. Miller for interest in this work and for the facilities put at his disposal. The work was supported by the National Science Foundation.

* On leave from the University of Ljubljana, Ljubljana, Yugoslavia.

[1] R. Blinc and D. Hadži, Mol. Phys. **1**, 391 (1958).
[2] D. Hadži and A. Novak, *Infrared spectra of, and hydrogen bonding in, some acid salts of carboxylic acids* (University of Ljubljana, Yugoslavia, 1960).
[3] R. Blinc and D. Hadži, Spectrochim. Acta **16**, 852 (1960).

Open-Shell Wave Functions for Conjugated Hydrocarbons*

J. R. HOYLAND† AND LIONEL GOODMAN

Whitmore Chemical Laboratory, The Pennsylvania State University, University Park, Pennsylvania

(Received January 25, 1961)

WE have extended our earlier work on deformation of π- and σ- type orbitals[1] to include reminimization of open-shell states. The procedure is the open-shell SCF method devised by Roothaan[2] and applied to the π electrons in conjugated hydrocarbons.

This communication is chiefly concerned with the changes in the π-MO's upon ionization, capture, or excitation of a π electron. The π-electron approximation is assumed, along with the assumptions of differential overlap[3] and deformation of orbitals.[1] Utilizing Roothaan's[2] definitions, the matrix $\mathbf{F}$ for an open-shell system is given by $\mathbf{F}=\mathbf{H}+2\mathbf{J}_T-\mathbf{K}_T-(2\alpha\mathbf{J}_0-\beta\mathbf{K}_0)+\mathbf{SD}_T\mathbf{Q}+\mathbf{QD}_T\mathbf{S}$. In the framework of the π-electron approximation and differential overlap, and for the open-shell orbitals normalized to $\frac{1}{2}$, $\mathbf{S}$ becomes the unit matrix

$$\left[S_{pq}=\int\chi_p^*(1)\chi_q(1)d\tau(1)=\delta_{pq}\right],$$

$$J_{T,pq}=\delta_{pq}\sum_r D_{T,rr}(rr\,|\,pp),$$

$$J_{0,pq}=\delta_{pq}\sum_r D_{0,rr}(rr\,|\,pp),$$

$$K_{T,pq}=D_{T,pq}(pp\,|\,qq),$$

and

$$K_{0,pq}=D_{0,pq}(pp\,|\,qq).$$

TABLE I. SCF molecular orbitals for naphthalene.[a]

Species	Molecular orbitals[b,c]	q_1[d]	q_2[d]	q_9[d]
Ground state	$\psi_1=0.3007\Phi_1+0.2589\Phi_3+0.4303\Phi_5$	0.0904	0.0670	0.1852
	$\psi_2=0.2720\Phi_2+0.4196\Phi_6$	0.0740	0.1761	0
	$\psi_3=0.3992\Phi_6+0.2081\Phi_7+0.3075\Phi_8$	0.1594	0.0433	0.0946
	$\psi_4=0.0141\Phi_1+0.3737\Phi_2-0.4693\Phi_3$	0.0002	0.1397	0.2202
	$\psi_5=0.4196\Phi_9+0.2720\Phi_{10}$	0.1761	0.0740	0
	$\psi_6=0.4196\Phi_4-0.2720\Phi_5$	0.1761	0.0740	0
	Total charge density	1.0000	1.0000	1.0000
Positive ion	$\psi_1=0.2963\Phi_1+0.2161\Phi_2+0.4806\Phi_3$	0.0878	0.0467	0.2310
	$\psi_2=0.2697\Phi_4+0.4210\Phi_5$	0.0727	0.1772	0
	$\psi_3=0.3987\Phi_6+0.1804\Phi_7+0.3420\Phi_8$	0.1590	0.0325	0.1170
	$\psi_4=0.0533\Phi_1+0.3972\Phi_2-0.4229\Phi_3$	0.0028	0.1578	0.1788
	$\psi_5=0.4313\Phi_9+0.2529\Phi_{10}$	0.1860	0.0640	0
	Total charge density	0.8306	0.8924	1.0536
Negative ion	$\psi_1=0.3009\Phi_1+0.2772\Phi_2+0.4065\Phi_3$	0.0905	0.0768	0.1652
	$\psi_2=0.2539\Phi_4+0.4307\Phi_5$	0.0645	0.1855	0
	$\psi_3=0.4003\Phi_6+0.2136\Phi_7+0.2972\Phi_8$	0.1602	0.0456	0.0883
	$\psi_4=-0.0323\Phi_1+0.3757\Phi_2-0.4644\Phi_3$	0.0010	0.1412	0.2157
	$\psi_5=0.4214\Phi_9+0.2691\Phi_{10}$	0.1776	0.0724	0
	$\psi_6=0.4307\Phi_4-0.2539\Phi_5$	0.1855	0.0645	0
	Total charge density	1.1731	1.1075	0.9384
Lowest energy triplet state	$\psi_1=0.2994\Phi_1+0.2428\Phi_2+0.4503\Phi_3$	0.0896	0.0590	0.2028
	$\psi_2=0.2288\Phi_4+0.4446\Phi_5$	0.0523	0.1977	0
	$\psi_3=0.4004\Phi_6+0.1832\Phi_7+0.3349\Phi_8$	0.1603	0.0336	0.1122
	$\psi_4=0.0017\Phi_1+0.3968\Phi_2-0.4302\Phi_3$	0	0.1575	0.1851
	$\psi_5=0.4446\Phi_9+0.2288\Phi_{10}$	0.1977	0.0523	0
	$\psi_6=0.4446\Phi_4-0.2288\Phi_5$	0.1977	0.0523	0
	Total charge density	1.0000	1.0000	1.0000

[a] The numbering system for naphthalene is that used by C. M. Moser, [J. chim. phys. **54**, 24 (1955)], i.e., 9, 10 are junction positions, 1 and 2 are the α and β positions, respectively.

[b] The MO's are written in terms of the following symmetry orbitals:

$$\Phi_1=(X_1+X_4+X_5+X_8),\quad \Phi_2=(X_2+X_3+X_6+X_7),\quad \Phi_3=(X_9+X_{10}),\quad \Phi_4=(X_1+X_4-X_5-X_8),\quad \Phi_5=(X_2+X_3-X_6-X_7),$$
$$\Phi_6=(X_1-X_4-X_5+X_8),\quad \Phi_7=(X_2-X_3-X_6+X_7),\quad \Phi_8=(X_9-X_{10}),\quad \Phi_9=(X_1-X_4+X_5-X_8),\quad \Phi_{10}=(X_2-X_3+X_6-X_7).$$

[c] Only those orbitals which are occupied are listed. For the ground state, the completion orbital Φ_6 is given for comparison purposes.

[d] Charge orders, i.e., $q_i=C_i^2$.

Here $D_{T,pq}=\sum_i c_{pi}c_{qi}^*$, i running over both closed- and open-shell orbitals, and $D_{0,pq}=\sum_m c_{pm}c_{qm}^*$, with m running over the open-shell orbitals only. In the case of one open-shell orbital and a closed-shell core (doublet), or a triplet arising from the excitation of an electron in a closed-shell molecule, $\alpha=0$ and $\beta=-2$.

Recently Grabe[4] has carried out open-shell calculations on systems of biochemical interest utilizing the Roothaan method. Other formulations for construction of open-shell configurational wave functions in conjugated systems, are those of Lefebvre[5] and Pople and Nesbet,[6] the latter being an approximate procedure. The calculations reported here (and those of Grabe[4]) are exact in the sense that the wave functions are eigenfunctions of the correct Hartree-Fock Hamiltonian within the π-electron approximation[7] plus deformation and parameter assumptions.

The SCF π-MO's for (1) the singlet ground state, (2) doublet positive ion, (3) doublet negative ion, and (4) lowest energy triplet excited configuration of naphthalene, are given in Table I. The ground-state calculations were made by closed-shell SCF theory[8] with a set of assumptions equivalent to those made in the open-shell computations. It is seen by inspection that the MO's of the open-shell species differ significantly from those of the ground state.[9] Similar results are obtained for 11 other conjugated hydrocarbons. These calculations lead to the conclusion that open-shell configurational wave functions constructed from ground-state MO's are reasonable approximations to the true wave function. However, reminimization of the open-shell state becomes important when the charge distribution is considered (e.g., see naphthalene charge densities at position 9 in Table I; where excess ***negative charge*** is predicted in the ***positive ion*** and a ***positive charge*** predicted in the ***negative ion***).

A detailed discussion of the calculations reported here will be published in the near future.

* Presented at the Sanibel Island, Florida Institute for Quantum Chemistry and Solid-State Physics, January 2–13, 1961.

† National Science Foundation Predoctoral Fellow 1959–1961.

[1] J. R. Hoyland and L. Goodman, J. Chem. Phys. **33**, 946 (1960).

[2] C. C. J. Roothaan, Revs. Modern Phys. **32**, 179 (1960).

[3] R. Pariser and R. G. Parr, J. Chem. Phys. **21**, 466 (1953); **21**, 767 (1953).

[4] B. Grabe, Arkiv Fysik **17**, 97 (1960).

[5] R. Lefebvre, J. chim. phys. **54**, 168 (1957); H. Brion, R. Lefebvre, and C. Moser, *ibid.* **54**, 363 (1957); R. Lefebvre, *Calcul des Fonctions D'Onde Moleculaire* (International Colloquium at the National Center of Scientific Research, Paris, 1958), p. 95.

[6] J. A. Pople and R. K. Nesbet, J. Chem. Phys. **22**, 571 (1954).

[7] Adams and Lykos have communicated that they have carried out open-shell SCF calculations on a perturbed *trans*-butadiene system.

[8] C. C. J. Roothaan, Revs. Modern Phys. **23**, 69 (1951).

[9] Caution must be used in interpreting the changes in the MO's since Roothaan's method determines these uniquely only up to two unitary transformations which transform MO's of the same symmetry among themselves in the closed and open sets separately. Thus the changes in the B_{1u} MO's ψ_3 and ψ_4 in Table I cannot be absolutely interpreted.

Electron Nuclear Double Resonance in Irradiated Organic Crystals

T. Cole, C. Heller, and J. Lambe

Scientific Laboratory, Ford Motor Company, Dearborn, Michigan

(Received February 15, 1961)

We here report the observation of electron nuclear double resonance (ENDOR)[1] in irradiated single crystals of succinic acid.[2] In succinic acid ENDOR lines corresponding to the hyperfine splitting of the radical $HOOC\dot{C}HCH_2COOH$ were observed and in addition depolarization[3] ENDOR was also observed.

Single crystals were prepared and irradiated as previously described.[2,4] Lines in the electron magnetic resonance were observed at 4.2°K under partial saturation[1] with a conventional EMR spectrometer employing 5-kc field modulation and phase-sensitive detection. Radio-frequency energy was supplied to a small wire loop surrounding the crystal by a Hewlett Packard 606 signal generator and broad-band rf amplifier. The rf power was amplitude modulated at 3 cps while sweeping the frequency from 10 to 75 Mc. Sweeping the rf through an ENDOR line caused a modulation in the intensity of the EMR signal. This 3-cps modulation was observed with a mechanical synchronous detector. ENDOR spectra for succinic acid were observed both parallel and perpendicular to the crystalline b axis.

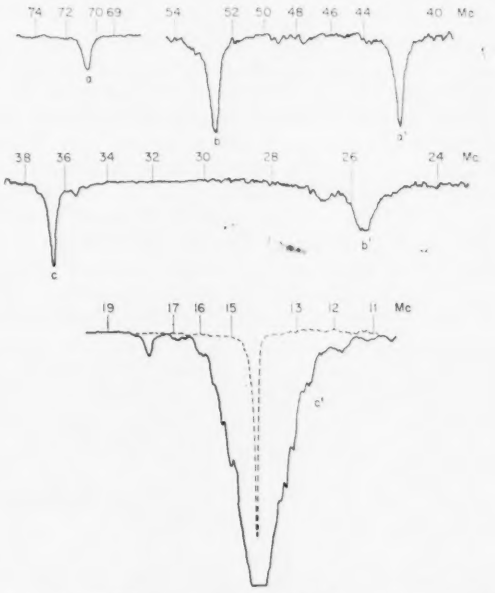

FIG. 1. ENDOR spectrum of $(HOOC)\dot{C}HCH_2(COOH)$ with the magnetic field along the b axis. Lines labeled C and C' are due to the CH proton; b, b' and a, a' are due to the CH_2 protons. The intense line at 14.2 Mc which partially obscures C' is due to depolarization ENDOR. The dotted spectrum indicates a 100-fold reduction in rf power.

For these orientations the two molecules in the unit cell are magnetically equivalent.[2]

A typical ENDOR spectrum for succinic acid is shown in Fig. 1. Linewidths are in the range of 0.2 to 0.5 Mc. Linewidths in the EMR spectrum,[2] on the other hand, are in the range of 6 to 9 Mc. There are three pairs of strong lines in the upper two lines of the spectrum. Pairs a, a' and b, b' are due to the two CH_2 protons while the pair c, c' is due to the CH proton. Pairs a, a' and b, b' vary over a range of less than 15% in frequency as the magnetic field is rotated relative to the crystal axis system while c, c' shows a much larger angular anisotropy.

The hyperfine splitting Δ_i for proton i in the EMR spectrum of the free radical is related to the two ENDOR frequencies ν_i and ν_i' of that proton by

$$\Delta_i=\nu_i+\nu_i'. \tag{1}$$

The difference between ν_i and ν_i' is approximately twice the nuclear Zeeman frequency of 14 Mc. Splittings for the "forbidden"[4] ($\Delta m_I=\pm 1$) hyperfine transitions are

$$\Delta_i=|\nu_i-\nu_i'|. \tag{2}$$

Preliminary calculations of Δ_i based on ENDOR frequencies appear to be in general agreement with the values obtained from conventional EMR.[2]

In addition to the six lines mentioned above we note also a very intense line at 14.2 Mc surrounded by a number of weak satellites. This strong line is due to the depolarization of protons distant from the paramagnetic center.[5] The time required for recovery of the EMR signal after removal of the rf is of the order of 100 sec for the distant proton line while that for the intramolecular protons is 0.01 to 0.1 sec. This distant ENDOR appears to be very similar to the effect noted for distant aluminum nuclei in ruby.[3] The basic mechanism of the effect is that microwave power causes a dynamic polarization of distant nuclei which is removed by rf energy at the Laramor frequency of these nuclei. Satellite lines near the distant proton line correspond to hyperfine splittings of the unpaired electron by neighboring protons which are too small (less than 4 Mc) to be resolved in conventional EMR. Distant or depolarization ENDOR has also been observed in irradiated malonic acid.[4] This line shows the same relaxation characteristics as the distant ENDOR line in succinic acid.

Work is now in progress on the detailed calculation of the hyperfine tensors from ENDOR data.

[1] G. Feher, Phys. Rev. **103**, 500 (1956).
[2] C. Heller and H. M. McConnell, J. Chem. Phys. **32**, 1535 (1960).
[3] J. Lambe, N. Laurance, E. C. McIrvine, and R. W. Terhune, Phys. Rev. (to be published).
[4] H. M. McConnell, C. Heller, T. Cole, and R. W. Fessenden, J. Am. Chem. Soc. **82**, 766 (1960).
[5] A. Abragam and W. G. Proctor, Compt. rend. **246**, 2253 (1958).

Comments and Errata

Dissociation Energies of Diatomic Molecules*

E. R. Lippincott, R. Schroeder,† and D. Steele

Department of Chemistry, University of Maryland, College Park, Maryland

(Received December 14, 1960)

In a discussion of dissociation energies of diatomic molecules G.R. Somayajulu[1] has used the relation

$$k_e r_e/D=\text{constant}, \tag{1}$$

to relate the force constant k_e, dissociation energy D_0, and equilibrium distance r_e. He comments that a suitable potential function might be expected to lead to this relation but then states "It appears, however, that the potential functions so far proposed do not lead to this result." We wish to point out that this relation may be derived from the previously proposed[2] function;

$$V=D_e[1-\exp(-n\Delta r^2/2r)][1+af(r)], \tag{2}$$

where n=constant of Eq. (1), $\Delta r=r-r_e$, a=constant, and $f(r)$ is a function such that $f(r)=0$ as $r\rightarrow\infty$ and $f(r)=\infty$ as $r\rightarrow 0$. Relation (1) has been used to correlate and predict dissociation energies of diatomic molecules and bond energies of bonds in polyatomic molecules.[2-4] Somayajulu's results are in essential agreement with our earlier calculations on diatomic molecules except where more recent data has been available. We also have used this relation to show that a value of 170 kcal/mole is favored for the heat of sublimation of graphite.[4] The main difference between our use of this relation and that of Somayajulu is that he assumed a characteristic value for the constant of Eq. (1) for different sequences of molecules, whereas we evaluated this constant from ionization potentials by means of an empirical rule.

It should be pointed out that relation (1) is not valid for excited states of diatomic molecules in that Somayajulu's sequence constants cannot be used without modification. We have derived some relations from a consideration of the proposed function (2) which enable one to calculate dissociation energies of excited states from the equivalent of (1) through the use of r_e and vibrational frequencies for the excited states.[5] Some results are given in Table I for O_2 for which the relations are particularly good.

The working equation is

$$D_e(\text{ev})=\frac{1.8387\times 10^{-6}b^2\mu\omega^4 r^{11/2}[1-\frac{5}{4}a(x)]^2}{\omega_x^2 r_x^{-7/2}}, \tag{3}$$

where a is the parameter a of Eq. (2), $a(x)$ is the value

of this parameter for the ground state of the molecule, μ is the reduced mass in atomic units, ω_x and r_x refer to the vibrational frequency and bond length of the ground state of the molecule in cm^{-1} and A, respectively, and b is a constant defined by the form of $f(r)$. Here b is equal to 1.065 for all molecules excepting hydrogen for which it takes the value 1.16. The parameter a is given by

$$a=\frac{1}{6B_e^2/\alpha\omega+\frac{5}{4}}. \tag{4}$$

The parameter has been shown to be periodic within the periodic table.[5] For an heteronuclear molecule the $a(x)$ is given satisfactorily as the mean of the $a(x)$ for the constituent elements.

Finally it should be pointed out that the potential function (2) is not the only one which will allow a derivation of relation (1). Actually there are several families of functions which give this relation but (2) is the only one which gives (1) and at the same time gives a usable correlation of anharmonicity, force constant, dissociation energy, and bond lengths.

TABLE I. Calculation of dissociation energies of excited states of O_2 from ω_e and r_e.

State	ω_e	r_e	D_e obs	D_e calc
$X^3\Sigma_g^-$	1580.36 cm^{-1}	1.2074 A	5.220 ev	5.02 ev
$a^1\Delta_g$	1509.3	1.2155	4.13	4.48
$b^1\Sigma_g^+$	1432.69	1.2267	3.58	3.55
$B^3\Sigma_u^-$	700.36	1.604	1.00	0.96
$^1\Sigma_u^-$	650.49	1.597	0.67	0.69

* This work has been supported in part by the Office of Ordnance Research, U. S. Army.

† Present address: Department of Chemistry, Southwestern Louisiana University, Lafayette, Louisiana.

[1] G. R. Somayajulu, J. Chem. Phys. **33**, 1541 (1960).
[2] E. R. Lippincott, J. Chem. Phys. **21**, 2070 (1953); E. R. Lippincott and R. Schroeder, *ibid.* **23**, 1131 (1955); E. R. Lippincott, D. Steele, and P. Caldwell, *ibid.* (to be published).
[3] J. Pliva, Collection Czechoslov. Chem. Commun. **23**, 777, 1839, 1846, 1852 (1958).
[4] E. R. Lippincott and R. Schroeder, J. Am. Chem. Soc. **78**, 5171 (1956).
[5] D. Steele and E. R. Lippincott (unpublished).

Dissociation Energies of Diatomic Molecules*

G. R. SOMAYAJULU

Department of Chemistry and Lawrence Radiation Laboratory, University of California, Berkeley 4, California

(Received January 9, 1961)

IT is gratifying to note that Lippincott's function[1] (which we have unfortunately overlooked) leads to the relation

$$k_e r_e/D=n, \tag{1}$$

and at the same time satisfies the conditions desirable of a good potential function. Empirically, we have found[2] that n is approximately constant for sequences of similar diatoms in the ground state. Lippincott and Schroeder[3] use bond-dissociation energies of polyatomic molecules to conclude that n is constant for bonds of any type between two given atoms. Thus n should be constant for different types of bonds between similar atoms such as O, S, Se, and Te. It is found[2] that the first members of sequences of similar diatoms have different n values. Also the same value of n cannot be used for the ground state and excited electronic states. The relationship[3] between n and ionization potentials of the bonded atoms would seem more reasonable if valence-state ionization potentials were used. The resulting variation of n with valence state would explain the difference between the value of n for ground and excited states.

We may also point out that bond energy, bond length, and force constant are related[4,5] by the expression

$$k_e r_e^2/E=\beta, \tag{2}$$

where E is the bond energy, and β is a constant for bonds of any type and of any order between two given atoms in their normal valence states. Relation (2) follows from the function[6]

$$U=ar^{-m}-br^{-n}, \tag{3}$$

and also from a number of other functions.[7]

The results which illustrate the validity of relation (3) for the S—S bonds have been presented in Table I.

TABLE I.

Bond	Molecule	k_e(md/A)	r_e(A)	E(kcal/mole)	β
S=S	S_2	4.959	1.889	101.46	0.1744
S—S	H_2S_2	2.60	2.05	62.65	

The S—S bond energy of 62.65 kcal/mole was calculated from Eq. (3). A value of 63 kcal/mole for E(S—S) may be obtained from the heats of atomization[8] of H_2S_n-type molecules and also from the heat of atomization[9] of gaseous S_8. Similar results confirming the validity of relation (2) have been obtained in a number of cases.

For bonds between two given atoms, relations (1) and (2) lead to the simple result that

$$Dr_e/E=\beta/n=\text{constant}. \tag{4}$$

It appears, however, that there are a few cases where the bond energies are approximately equal to bond dissociation energies. Obviously, in such cases relation

(4) leads to the absurd result that r_e=constant for different types of bonds between two given atoms. Even otherwise, we have not found much evidence to support relation (4). In view of this, we are hesitant to recommend relations (1) and (4) for different types of bonds between two given atoms. On the other hand, we expect relation (1) to hold for similar bonds with constant bond type in polyatomic molecules (e.g., CH_3—F, CH_3—Cl, CH_3—Br, and CH_3—I).

We have used[5] relation (3) and also a method based on valence-state energies of atoms to obtain the bond energies of various types of CC, CH, CO, CS, and CN bonds. On the basis of these energies, we have found little evidence in favor of resonance in classical molecules such as 1,3-butadiene, methyl acetylene, etc. We have also found that the strengths of heteropolar bonds, explained by Pauling[10] on the basis of ionic-covalent resonance, can be successfully explained in terms of strengths of hybrid orbitals.

We wish to take this opportunity to correct an error that has been found in Eq. (8) of our paper on dissociation energies of diatomic molecules.[2] Equation (8) should read as $k_e r_e^2/D_e = mn$.

My thanks are due Professor Leo Brewer for his kind interest in this work.

* Work performed under the auspices of the U. S. Atomic Energy Commission.

[1] E. R. Lippincott, J. Chem. Phys. **21**, 2070 (1953).
[2] G. R. Somayajulu, J. Chem. Phys. **33**, 1541 (1960).
[3] E. R. Lippincott and R. Schroeder, J. Am. Chem. Soc. **78**, 5171 (1956).
[4] J. J. Fox and A. E. Martin, J. Chem. Soc. **1939**, 884.
[5] G. R. Somayajulu (unpublished).
[6] G. B. B. M. Sutherland, Proc. Indian Acad. Sci. **8**, 341 (1938).
[7] Y. P. Varshni, Revs. Modern Phys. **29**, 664 (1957).
[8] F. Feher and G. Winkhaus, Z. anorg. u. allgem. Chem. **292**, 210 (1957).
[9] G. B. Guthrie, D. W. Scott, and G. Waddington, J. Am. Chem. Soc. **76**, 1488 (1954).
[10] L. Pauling, *The Nature of the Chemical Bond* (Cornell University Press, Ithaca, New York, 1960), 3rd ed.

On the Structure of Ferric Chloride Solutions*

C. L. Standley and R. F. Kruh

Department of Chemistry, University of Arkansas, Fayetteville, Arkansas

(Received February 15, 1960)

We have reviewed Brady's diffraction study[1] of ferric chloride solutions and do not believe that the results "indicate in a straightforward way the octahedral ligand cage" for Fe^{3+}. Moreover, Brady's accounting for the entire first maximum in the radial distribution function (RDF) by assigning six chlorine neighbors to only half the irons, practically ignores the other half. The literal $FeCl^{++}$ Brady suggests (as one possibility) is unreasonable in view of solvation, and any reasonable species would make a substantial contribution to the first maximum in the RDF. This defect suggests that his model is incorrect, and further measurements in hydrochloric acid solution lead to a more satisfactory picture involving the tetrahedral coordination of iron by chlorine.

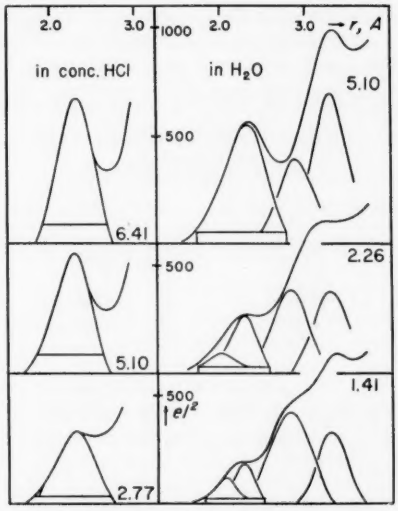

FIG. 1. Portions of the radial distribution curves for ferric chloride solutions. The figures by each curve show the molality. The area beneath the horizontal lines within the peaks at 2.3 A is that deducted for the hydrogen-chlorine interactions. A calculated peak for four chlorine neighbors per iron is drawn under the first maximum for each of the hydrochloric acid solutions and the 5.1 molal water solution. For the dilute water solutions the first maximum is resolved in terms of iron-water (at 2.0 A) and iron-chlorine (at 2.3 A) interactions as described in the text. The calculated maxima indicated at 2.8 and 3.3 A are for four water neighbors per water and six water neighbors per chlorine and are intended only to illustrate the possible magnitude of their contributions to the second maximum.

Measurements[2] were made on the following:

1.41 molal $Fe_{0.023}Cl_{0.070}(H_2O)_{0.907}$

2.26 molal $Fe_{0.035}Cl_{0.106}(H_2O)_{0.858}$

5.10 molal $Fe_{0.067}Cl_{0.201}(H_2O)_{0.732}$

2.77 molal $Fe_{0.036}Cl_{0.108}(HCl)_{0.142}(H_2O)_{0.720}$

5.10 molal $Fe_{0.061}Cl_{0.184}(HCl)_{0.086}(H_2O)_{0.669}$

6.41 molal $Fe_{0.074}Cl_{0.223}(HCl)_{0.057}(H_2O)_{0.646}$.

Intensity was corrected for background, polarization, absorption, and incoherent scattering. The radial distribution curves include the contribution of hydrogen to the average electron density, and we have corrected the area of the first peak (at 2.3 A) for the hydrogen-chlorine interactions associated with the hydration of chloride ions. For this we assume an average of from eight to ten hydrogens per chloride ion, and the total

areas and net areas are 80, 140, 310 and 58, 100, 240 el² for the 1.41, 2.26, and 5.10 molal solutions; and 160, 295, 340 and 130, 220, 265 el² for the 2.77, 5.10, and 6.41 molal solutions. Areas expected[3] for Fe—Cl, Fe—H_2O, H_2O—H_2O, and Cl—H_2O pairs are 440, 200, 60, and 130 el².

For all the solutions the first maximum occurs at from 2.25 to 2.30 A, the expected separation for an iron-chlorine pair. The area per iron atom in the hydrochloric acid solutions is virtually constant (3600 el²) and corresponds to 4.1 chlorine neighbors per iron. In the water solutions the area per iron approaches this value with increasing concentration; the values are 2500, 2850, and 3600 el². This suggests that the ion $FeCl_4^-$ is the principal ion in the hydrochloric acid solutions and that four-coordination also occurs in concentrated water solution. In the water solution, however, this would require the sharing of some chlorines between irons, and the number density of chlorines is great enough to permit this.

For the 1.41 and 2.26 molal solutions the position of the maximum (at 2.3 A) makes extensive coordination with water unlikely. If we assume that the iron still has four neighbors, we get 1.7 and 2.8 chlorines per iron, the balance being water, and corresponding components are shown in Fig. 1. Although the situation in these two solutions is uncertain we believe that for the other solutions, the data strongly support four-coordination of iron by chlorine.

The second main peak (at 3.3 A), which might be expected to give information as to whether the coordination is square or tetrahedral (or octahedral) contains predominantly water-water and water-chlorine interactions, as it does in KCl and LiCl solutions.[4] Even though it must also contain contributions from chlorine-chlorine interactions, its location at nearly $2.3\times\sqrt{2}$ may be misleading, since Brady takes it as proof of octahedral coordination. As it is he has not allowed for the substantial water-water interaction in this peak, so the agreement between calculated (290 el²) and "observed" (300 el²) areas for chlorine-chlorine is dubious. Most probably the coordination is tetrahedral, but the RDF cannot confirm this.

This review shows that the structural information given by diffraction measurements on this system is limited and that Brady's proposal of $FeCl_6^{3-}$ octahedra and his suggestions involving Fe_2Cl_6 and $FeCl_4^-$ mixtures are less straightforward than alleged. The interpretation we make is less detailed, but it has the advantage of consistency with other findings[5–7] as well as that of accounting for the nearest neighbors of all of the iron.

* The support of the U. S. Atomic Energy Commission is gratefully acknowledged.

[1] G. W. Brady, J. Chem. Phys. **29**, 1371 (1958).

[2] See P. C. Sharrah, J. I. Petz, and R. F. Kruh, J. Chem. Phys. **32**, 241 (1960) for description of apparatus.

[3] J. Waser and V. Schomaker, Revs. Modern Phys. **25**, 671 (1953).

[4] G. W. Brady and J. T. Krause, J. Chem. Phys. **27**, 304 (1957); G. W. Brady, *ibid.* **28**, 464 (1958).

[5] E. Rabinowitch and W. H. Stockmayer, J. Am. Chem. Soc. **64**, 335 (1942).

[6] H. L. Friedman, J. Am. Chem. Soc. **74**, 5 (1952).

[7] D. E. Chalkley and R. J. P. Williams, J. Chem. Soc. **1955**, 1920.

Mayer's Ensembles of Maximum Entropy

ANDREW D. MCLACHLAN* AND ROBERT A. HARRIS†

Conant Chemical Laboratory, Harvard University, Cambridge 38, Massachusetts

(Received December 12, 1960)

MAYER'S theorem[1] about the ensembles of maximum entropy has a very simple proof, depending on Lagrange's undetermined multipliers. In this note we shall for simplicity treat only a closed system of N particles. Let us then find the N-particle distribution function W_N which makes S [Eq. (1)] a maximum, subject to the conditions that w_n for some $n<N$ is given [Eq. (2)], and W_N is normalized [Eq. (3)] (w_n also determines $w_{n-1}\cdots w_0$);

$$S=-k/N!\int^{(N)} W_N \log W_N dv. \tag{1}$$

$$w_n(1\cdots n)=1/(N-n)!\int^{(N-n)} W_N dv, \tag{2}$$

$$1=1/N!\int^{(N)} W_N dv. \tag{3}$$

Here $\int^{(m)}$ stands for the integral over the last m particles.

First, if P is any permutation of $1\cdots N$, the symmetrized function $1/N!\sum_P W_N(1_P\cdots N_P)$ has at least the entropy of W_N, as $-x\log x$ is a convex function of x; so that the W_N which we seek must be a symmetric function of 1, 2, $\cdots N$. All variations of W_N must also be symmetric, of the form

$$\Delta W_N(1\cdots N)=1/N!\sum_P \delta W_N(1_P\cdots N_P),$$

where δW_N is an arbitrary function. Equation (3) can be eliminated from the variational problem by a single Lagrangian multiplier α, but Eq. (2) implies an infinite number of constraints, one for each set of points (1, 2, $\cdots n$); one must introduce a different multiplier $\beta_n(1, 2, \cdots n)$ for each set, with β_n a symmetric function of 1, 2, $\cdots n$. These multipliers must

make the coefficient of δW_N in δ's vanish, so that

$$(1+\log W_N)+\alpha+\sum_P \beta_n(1_P\cdots n_P)=0, \qquad (4)$$

and W_N is therefore a product of terms which involve at most n particles at a time, and all the higher correlation functions[1] ϕ_{n+m} vanish. This is Mayer's result. To derive Eq. (4) we convert the condition that $\delta w_n(1'\cdots n')=0$ into an integral over N particles,

$$\int^{(N)} \delta W_N[\sum_P \delta(1_P-1')\cdots\delta(n_P-n')]dv=0. \quad (5)$$

[The delta functions in (5) select the region of N-particle phase space where particles are simultaneously at the points $1'\cdots n'$]. Then, to see that the numbers $\beta_n(1'\cdots n')$ correspond to the finite number of multipliers used in a variation problem with a finite number of constraints, we may make the following transition. Start with phase space divided into cells i, and let $W_N(i)$ be the average of W_N over each cell. The modified variation problem, with $\sum_i$ for $\int^{(N)}$ and a finite number of cells, may certainly be solved by Lagrange's multipliers. As the size of the cells tends to zero we obtain Eq. (4) in the limit. Equation (4) implies only that S is stationary, but the second-order change of S is proportional to

$$-\int^{(N)} (\delta W_N)^2/W_N\cdot dv,$$

and is negative definite.

As Mayer pointed out, the correlation functions ϕ_0, ϕ_1, $\cdots\phi_n$ corresponding to the maximum entropy ensemble $W_N\{n\}$ determined by w_n are not unique, since, for example, ϕ_0 may be absorbed into ϕ_1. However, *if the maximum entropy ensemble $W_N\{n\}$ is uniquely determined by w_n* we can also choose ϕ_0, ϕ_1, $\cdots$ uniquely. Since w_n determines w_0, w_1, $\cdots w_{n-1}$ there is a unique series of maximum entropy ensembles $W_N\{0\}=1$, $W_N\{1\}$, $\cdots$ fixed by them, with entropies $S_0>S_1\cdots>S_n$. Now since $\log W_N$ can be calculated from the ϕ's, we choose them successively so that ϕ_0 gives $W_N\{0\}$; ϕ_0 and ϕ_1 together give $W_N\{1\}$; and so on. Each additional ϕ_m introduces an additional degree of correlation, and reduces the entropy further by

$$k/m!\int^{(m)} w_m\phi_m dv.$$

We thus have a systematic way of dividing the entropy of a closed system into contributions from higher and higher order correlations. In thermal equilibrium all ϕ_n vanish for $n>2$, and we may generally expect higher order ϕ's to be small even when equilibrium is disturbed; so $W_N\simeq W_N\{2\}$, or the entire distribution is largely determined by the pair distribution function.

The proof that $W_N\{n\}$ is unique is rather simple. Let W' and W'', with entropies S', S'' ($S'\leq S''$) be two maximum entropy ensembles consistent with a given w_n. Now consider the combined ensemble $W(\lambda)=(1-\lambda)W'+\lambda W''$ which also has the same w_n. First we readily prove that $S(\lambda)\geq(1-\lambda)S'+\lambda S''$, so that $\partial S/\partial\lambda\geq(S''-S')\geq 0$. But since W' is a maximum entropy ensemble, $\partial S/\partial\lambda=0$ and so $S'=S''$. Now consider $S(\lambda)$ again, with $S'=S''$. Since $S(\lambda)\geq S'=(1-\lambda)S'+\lambda S'$ and $\partial S/\partial\lambda=0$ we deduce that $\partial^2 S/\partial\lambda^2\geq 0$; but the second derivative is equal to

$$-k/N!\int^{(N)} (W'-W'')^2 W'\cdot dv$$

and is negative unless $W'=W''$. Hence W is uniquely fixed by w_n.

We thank Professor Mayer for sending us his forthcoming paper,[1] with independent but similar versions of some of these proofs.

* Junior Fellow, Society of Fellows, Harvard University.
† Harkness Fellow of the Commonwealth Fund, 1959–61.

[1] J. E. Mayer, J. Chem. Phys. **33**, 1484 (1960); **34**, 0000 (1961).

Notes

Second Virial Coefficient of Boron Trifluoride*

C. J. G. Raw

Department of Chemistry, Saint Louis University, St. Louis, Missouri

(Received December 5, 1960)

THE second virial coefficients of mixtures of boron trifluoride and nitrogen have been determined[1] at 30°C, but no data on the temperature dependence of the second virial coefficient of pure boron trifluoride seems to have been reported in the literature. In this note, a study of the temperature dependence is presented to supplement the existing investigations[2,3] of intermolecular forces in boron trifluoride.

The apparatus used in this series of measurements has been described previously.[1] The basic principle of the method was the accurate determination of the pressure when a given mass of the gas was compressed or expanded through several stages at a constant temperature. The volume of each compression or expansion stage had been previously determined by a technique involving the weighing of mercury. The boron trifluoride used in these experiments was drawn from a cylinder supplied by the Matheson Company, and was purified by vacuum distillation in the usual way. Measurements were made at temperatures in the range 20°–70°C. These temperatures were held constant to ±0.05°C, and were measured on a calibrated mercury thermometer. At each temperature, a series of six or seven successive determinations were made, and the

mean values of the resulting second virial coefficients $B(T)$ are recorded in Table I, together with the average error for the series of measurements at each temperature.

Using the method of calculation based on the statistical-mechanical theory of the equation of state outlined by Hirschfelder, Curtiss, and Bird,[4] we may evaluate the intermolecular potential parameters from the experimental results of Table I, assuming that the

TABLE I. Second virial coefficients of boron trifluoride.

T (°K)	293.2	303.2	313.2	323.2	343.2
$B(T)$ (cm³ mole⁻¹)	−105.1	−98.0	−89.7	−82.0	−71.2
Av error	5.4	6.1	5.6	5.5	5.8

nonpolar pseudospherical boron trifluoride molecule has an intermolecular force field well represented by the Lennard-Jones model. According to this model, the potential energy of interaction of a pair of molecules separated by a distance r is $\phi(r)=4\epsilon[(\sigma/r)^{12}-(\sigma/r)^{6}]$, where ϵ is the depth of the potential well and σ is the separation when $\phi=0$. The two parameters are usually reported as ϵ/k (in °K; k=Boltzmann's constant) and σ (in A). This model has already proved satisfactory in accounting for the viscosity of boron trifluoride.[2,3] Potential parameters computed from the gas viscosity and from the polarizability by the method of Brandt,[5] are compared in Table II with the values obtained using the second virial data reported in Table I.

From Table II, it is clear that the Lennard-Jones potential is a quite adequate representation of the molecular interactions in gaseous boron trifluoride.

TABLE II. Lennard-Jones (12, 6) potential parameters for boron trifluoride.

	Second virial coefficient	Gas viscosity	Polarizability
ϵ/k (°K)	178	170[2]; 178[3]	179[3]
σ (A)	4.38	4.27[2]; 4.22[3]	4.12[3]

This fact, together with the magnitude of the error involved in the experimental determination of $B(T)$, shows that there is little point in the consideration of more complicated models for the interaction potential.

* Part of this work was done while the author was at the University of Natal, South Africa.

[1] G. L. Brooks and C. J. G. Raw, Trans. Faraday Soc. **54**, 972 (1958).

[2] C. J. G. Raw, J. South African Chem. Inst. **7**, 20 (1954).

[3] J. C. McCoubrey and N. M. Singh, Trans. Faraday Soc. **53**, 877 (1957).

[4] J. O. Hirschfelder, C. F. Curtiss, and R. B. Bird, *Molecular Theory of Gases and Liquids* (John Wiley & Sons, Inc., New York, 1954).

[5] W. Brandt, J. Chem. Phys. **24**, 501 (1956).

"Sub-Threshold" Photocurrents of High-Quantum Yield in 9,10-Dichloroanthracene*

A. BREE† AND W. G. SCHNEIDER

Division of Pure Chemistry, National Research Council, Ottawa, Ontario, Canada

(Received November 14, 1960)

THE fundamental question of how charge carriers are produced in organic crystals has not yet received a satisfactory explanation, mainly because it has not proved possible to locate and take measurements on a "conduction level." In general the threshold of photoconduction in these crystals has been found to coincide with the band edge of a bound exciton state. On the other hand the apparent band-gap energy indicated by measurements of the thermal activation energy of semiconduction is ordinarily much smaller than the photoconduction threshold. However, this interpretation of the thermal activation energies may be questioned, since it is possible they would be largely dominated by effects arising from electrode barriers,[1] surface states,[2] or trapping and impurity centers.[3] In this connection the present observations of photocurrent response peaks in single crystals of 9,10-dichloroanthracene at lower energies than the first exciton level are of considerable interest, and may ultimately lead to a characterization of the corresponding crystal levels.

Reagent grade 9,10-dichloroanthracene was purified by chromatography through alumina and recrystallization from petroleum ether. Single-crystal samples were grown from chloroform solution or from the melt in a Bridgeman furnace. The surface photocurrent i_s was studied as a function of the incident light intensity L and the applied field strength E. In agreement with an earlier result,[4] i_s was proportional to $L^{0.86}$ and increased at a slightly faster rate than E. A typical photocurve, representing the response of the crystal to an equal number (10^{10}) of incident photons/second at all wavelengths (E=2.5 v/cm) is shown in Fig. 1(b); for purposes of comparison the crystal and solution absorption spectra are shown in Fig. 1(a). All measurements were made on the well-developed (010) face in which the fast optical direction α was about 5° from the needle axis a and the medium optical direction β was normal to α. The absorption band in spectral region I ($\bar{\nu}>23\,500$ cm^{-1}) marks the presence of the first bound exciton state. The photocurrent peaks coincide with the absorption peaks and in air or oxygen are very much increased over their vacuum value—a behavior quite analogous to that observed in anthracene.[5] The photocurrents in regions III ($\bar{\nu}<16\,000$ cm^{-1}) and in the intermediate spectral region II have no counterpart in the anthracene photocurve and they occur with an increased quantum efficiency Q of at least one order of magnitude over that observed in

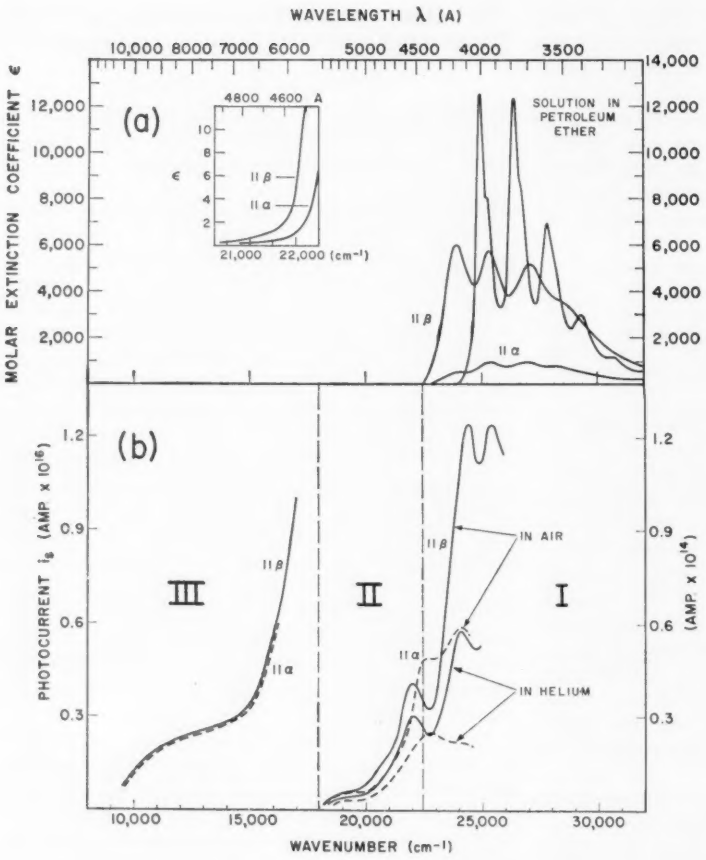

FIG. 1. (a) Absorption spectrum of 9,10-dichloroanthracene (solution and monocrystal). Insert at left is an enlargement of the absorption edge. (b) Spectral response of photocurrent in 9,10-dichloroanthracene monocrystal corrected for equal number of incident photons. The photocurrent scale at the right applies to regions I and II ($\nu > 18\,000$ cm^{-1}), while the scale at the left applies to region III ($\nu < 18\,000$ cm^{-1}). Full curves correspond to incident light polarized along the β direction of the crystal, dotted curves along the α direction.

region I; Q is defined as being the number of electrons produced in the external measuring circuit when $E=1$ v/cm for each *absorbed* photon. On account of the ambiguity in estimating the number of absorbed photons per second in a spectral region having no absorption maxima corresponding to the observed photocurrent peaks, only a lower limit can be found for Q in region II. Values of the molecular extinction coefficient ϵ were chosen from the smooth curve [see inset, Fig. 1(a)], which is evidently the tail of the absorption system at 4170 A; at 5300 A ϵ was 0.1, the error of measurement. Thus Q has the value 10^{-8} electron cm/photon v at the photocurve peaks in region I (under vacuum conditions), while in region II it has the value 10^{-7} electron cm/photon v. The photocurrents in region III were not generated by stray light within the double monochromator since the uncorrected photoconductivity response curve reproduced, in wavelength and intensity, the strong emission lines near 8300, 8900, and 9900 A of an Osram XB0-1001 high-pressure xenon light source.[6]

Some observed differences in behavior of i_s in spectral regions I and II (e.g., observed rise times and the effect of oxygen) may be explained on the basis of the different distribution of charge in the sample resulting from different depths of light penetration. In region III, i_s rose to a maximum value in about 20 sec and then slowly decreased. The original curve was retraced only if the crystal was irradiated with light in regions I and II. Thus, the process of free carrier production in 9,10-dichloroanthracene is to be associated with the spectral regions I and II—presumably the energy absorbed into the bound exciton state in region I degrades into a "conduction level" in region II. The currents in region III are thought to be generated by the release of trapped charge in the crystal bulk. The nature of such traps, having an apparent vertical depth of about 1.2 ev, remains obscure. Since the phenomena of conductance and fluorescence are extremely sensitive to trace impurity, this work is being investigated further on samples obtained by zone refining, and other techniques, and on "doped" samples

in an effort to determine the role played by impurity molecules.

* Contribution from the Division of Pure Chemistry, National Research Council. Issued as NRC No. 6215.

† National Research Council Post-doctorate Fellow 1957–59. Present address: William Ramsay and Ralph Forster Laboratories, University College, London, England.

[1] N. F. Mott and R. W. Gurney, *Electronic Processes in Ionic Crystals* (Clarendon Press, Oxford, England, 1940), p. 168.
[2] J. Bardeen, Phys. Rev. **71**, 717 (1947).
[3] F. J. Bryant, A. Bree, P. E. Fielding, and W. G. Schneider, Discussions Faraday Soc. **28**, 48 (1959).
[4] E. Boch, J. Ferguson, and W. G. Schneider, Can. J. Chem. **36**, 507 (1958).
[5] L. E. Lyons, A. Bree, and G. C. Morris, *Proceedings of the 1957 Conference on Carbon* (Pergamon Press, New York), p. 87.
[6] F. J. Bryant (unpublished result).

Spectrum and Radius of OH^- in Solution

JOSHUA JORTNER, BARUCH RAZ, AND GABRIEL STEIN

Department of Physical Chemistry, Hebrew University, Jerusalem, Israel

(Received June 7, 1960)

ELECTRON affinities[1] and ionic radii[2] of anions in solution can be calculated from their absorption spectra. We now investigated the hydroxyl ion, the size of which in aqueous solution is not accurately known. The ionic radius of OH^- in crystals cannot be directly obtained from the investigation of the structure of solid hydroxides[3]; effective radii of 1.32–1.84 A were obtained, depending on the cation.

The absorption spectrum[4] of OH^-_{aq} was accurately determined at several temperatures, using a Hilger Uvispek spectrophotometer fitted with a special fused silica prism, and checked for absence of stray light effects to 188 mμ; λ_{max} was determined to an accuracy of 0.15 mμ by the method of means.[2b,5] Solutions were prepared in the absence CO_2 from A.R. KOH, triply distilled water saturated with N_2, diluted and transferred to closed fused silica cells. Figure 1 shows the effect of temperature; $d(h\nu_{max})/dT = 14.5$ cm^{-1} deg^{-1}.

From the relations[2]

$$h\nu_{max} = E_X - L_X + 0.77e^2/r_0 - 1.58 \text{ ev} \qquad (1)$$

and

$$K = -d(h\nu_{max})/dT = (0.77e^2/r_0^2)(dr_0/dT), \qquad (2)$$

using $E_{OH} = 2.17$ ev[6] and $L_{OH} = 0.27$ ev,[7] the mean ionic cavity radius $r_0(OH^-_{aq})$ at 30°C = 1.78 A; $dr_0/dT = 0.52\times10^{-3}$ A deg^{-1}. In these calculations the known equilibrium value of the electron affinity was used instead of the required vertical value; r_0 is the equivalent radius of the (presumably nonspherical) cavity occupied by the ion.

For I^-_{aq}, $dr_0/dT = 0.93\times10^{-3}$ A deg^{-1}. These results are consistent with Latimer's assumption[8] of a linear correlation between ionic radii in solution and their

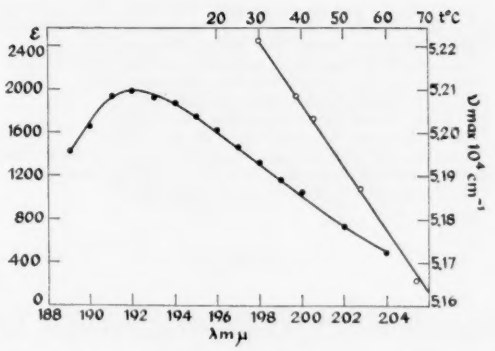

FIG. 1. Full circles: the spectrum of OH^-_{aq} at 43°C; open circles: ν_{max} as a function of temperature.

temperature coefficients. The radius r_0 represents [2a] the cavity at the disposal of the ion at a certain temperature. The intensity distribution along the absorption band may be assumed to be due to different apparent ionic radii. For I^-_{aq} it was shown [2b] that K the temperature coefficient, decreases when passing from the band onset to shorter wavelengths. From the linear dependence between K and $h\nu$ at constant T, $h\nu(K=0)$ gave a value of effective radius about equal to the crystallographic radius of I^-. Similarly for OH^-, in Fig. 2 $h\nu$ vs K is plotted at the band onset ($\epsilon=5$), band halfwidth, and band maximum. Lines for different temperatures yielded on extrapolation $h\nu(K=0) = 5.77\times10^4$ cm^{-1}. From Eq. (1), $r = 1.63$ A, corresponding to the virtual limit for the shrinking of the ionic cavity.

The oscillator strength of OH^-_{aq}, $f = 4.31\times10^9 \epsilon_{max}\Delta\nu$; ϵ_{max} being $\sim2\times10^3$ we obtain $f = 0.04$.[9] This value fits the correlation[10] between ionic radius and oscillator strength for anions in solution, based on the investigation of the halide series.

[1] J. Jortner, G. Stein, and A. Treinin, J. Chem. Phys. **30**, 1110 (1959).
[2] (a) G. Stein and A. Treinin, Trans. Faraday Soc. **55**, 1086 (1959); (b) *ibid.* p. 1091.

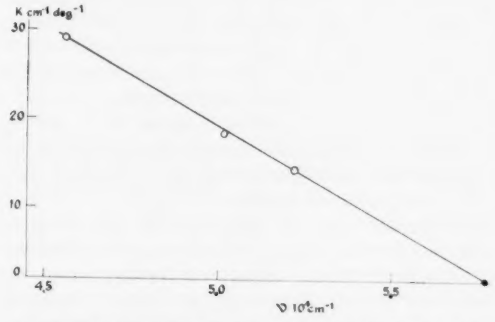

FIG. 2. The temperature coefficient K as a function of ν along the absorption band. Open circles: experimental values at 30°C. Full circle: extrapolated value of ν for $K=0$.

[8] J. D. Bernal and H. D. Megaw, Proc. Roy. Soc. (London) **A151**, 384 (1934); A. F. Wells, *Structural Inorganic Chemistry* (Oxford University Press, New York, 1950), p. 415.
[4] H. Ley and B. Arends, Z. physik Chem. **B6**, 240 (1929).
[5] G. Scheibe, Ber. deut. chem. Ges. **58**, 586 (1925).
[6] H. O. Pritchard, Chem. Revs. **52**, 529 (1953).
[7] P. Gray, Trans. Faraday Soc. **55**, 708 (1959).
[8] W. M. Latimer, J. Chem. Phys. **22**, 91 (1955).
[9] See *Chemical Applications of Spectroscopy*, edited by W. West (Interscience Publishers, Inc., New York, 1957), Chap. I.
[10] J. Jortner and A. Treinin (to be published).

Transitions between Different Forms of Ice

R. H. Beaumont,* H. Chihara,* and J. A. Morrison

Division of Pure Chemistry, National Research Council, Ottawa, Canada

(Received December 8, 1960)

Under special conditions (deposition from the vapor onto a surface at low temperatures) ice can be prepared in forms other than the ordinary hexagonal crystal. One of these, a cubic crystalline form, has been studied by both electron[1,2] and x-ray[3] diffraction techniques. A second form, which gives only diffuse diffraction halos, has been variously described as vitreous, amorphous, or microcrystalline. Its transparent glassy appearance[4] suggests, however, that it is best viewed as vitreous. The transitions from one form to another have been examined by different methods including simple calorimetry,[4–6] but estimates of the transition temperatures vary (see Fig. 8 of the work cited in footnote 1). Also, it has been suggested[3] that the formation of the cubic phase is sensitive to the nature of the substrate upon which the ice is deposited.

Preparatory to an extensive calorimetric study of the ice system, we have investigated the transitions between the different forms of ice using x-ray diffraction and simple thermal analysis with the object of establishing their reproducibility. Although different apparatus was used for each set of experiments, the conditions of deposition of the ice were kept as similar as possible. The results show that vitreous ice transforms cleanly to cubic ice over the temperature range 140°–156°K with an energy release of approximately 12 cal/g. The cubic ice in turn transforms into hexagonal ice over a wider temperature range beginning at about 200°K. No release or absorption of energy was detected in the latter transition, but the method used would not have "seen" energies less than about 1.5 cal/g.

The thermal analyses were carried out using an experimental arrangement similar to that of de Nordwall and Staveley.[6] Water vapor was brought into the calorimeter vessel (immersed in liquid nitrogen), which was a thin-walled copper cylinder, through a heated German silver tube. During the analysis the vessel was heated by maintaining a constant temperature head between it and a surrounding thermal shield. When ice, which had been deposited, at a slow enough rate, was heated up, an exothermic change took place between 140° and 156°K. The shapes of the heating curves were much like those found by de Nordwall and Staveley (Fig. 2 of work cited in footnote 6). The energies were, however, somewhat higher. For rates of deposition less than 0.01 g/cm² hr, the resulting energies were reproducible and the average of six separate measurements was 12 cal/g with an average deviation of 2 cal/g. At deposition rates higher than this, the energy was smaller and in some cases not detectable. From this we conclude that at high deposition rates the temperature of the deposit exceeded the transition temperature.

For the x-ray measurements a simple low-temperature vacuum camera was used, which could be attached to the goniometer head of a Norelco diffractometer equipped with a copper target. The camera was made from a brass cylinder and had two beryllium windows on its cylindrical side. The specimen holder was a lead-covered copper plate supported on a German silver tube. The plate was cooled by means of a copper rod which ran through the tube and into liquid nitrogen in a Dewar flask. Water vapor was brought in through a second tube with a funnel at its end directed at the specimen holder. After deposition of the water the camera was sealed off. With this arrangement the specimen holder was the coldest point in the camera. The temperature was measured with a copper-constantan thermocouple soldered to the holder.

The two crystalline modifications were distinguished by means of the diffraction lines (220) and (311) for cubic ice and (11.0), (10.3), and (11.2) for hexagonal ice. As long as the temperature of the holder was kept below 135°K during the deposition (deposition rate less than 0.04 g/cm² hr), no distinct diffraction lines were apparent.[7] When the deposit was warmed slowly (~0.5°/min), the characteristic lines of cubic ice appeared rather suddenly at about 150°K, and their intensities increased with time, reaching a maximum within a few minutes. With continued heating the deposit remained cubic until a temperature of about 200°K was reached. At this point the (10.3) line of the hexagonal phase could just be distinguished. Its intensity increased slowly in the temperature region 200° to 240°K. On several occasions deposits were cooled down again but there were no indications that the transformations reversed.

We conclude from the foregoing results that the transitions in ice show sufficient reproduciblity and consistency to merit a more detailed study. It is also apparent that the temperature of deposition is the important parameter, which suggests that uncontrolled variation of temperature may have been the cause of the different estimates of transition temperatures recorded previously. The agreement between the

x-ray and thermal analyses, which involved different substrates, indicates that the formation of vitreous or cubic ice by deposition from the vapor does not depend critically upon the structure or condition of the substrate.

We should like to thank Dr. Z. S. Basinski for the loan of the x-ray diffractometer.

Note added in proof. Since this note was submitted for publication, another paper describing x-ray measurements on the different forms of ice has appeared [L. G. Dowell and A. P. Rinfret, Nature **188**, 1144 (1960)]. The results contained therein differ somewhat from the results given here. In particular, Dowell and Rinfret find the transitions beginning at rather lower temperatures. While the general experimental arrangements were similar, our camera was used under vacuum and theirs with a small pressure of permanent gas in it. The resulting greater heat leak in their system could lead to an underestimate of the temperatures of the transitions, but it is difficult to make a quantitative assessment of the effect.

* National Research Council Postdoctorate Fellow, NRC No. 6213.

[1] M. Blackman and N. D. Lisgarten, Proc. Roy. Soc. (London) **A239**, 93 (1957).
[2] K. Shmaoka, J. Phys. Soc. Japan **15**, 106 (1960).
[3] F. V. Shallcross and G. B. Carpenter, J. Chem. Phys. **26**, 782 (1957).
[4] L. Staronka, Roczniki Chem. **19**, 201 (1939).
[5] J. A. Pryde and G. O. Jones, Nature **170**, 685 (1952).
[6] H. J. de Nordwall and L. A. K. Staveley, Trans. Faraday Soc. **52**, 1061 (1956).
[7] When deposited at temperatures above 135°K, the diffraction pattern of the deposit showed the lines of the cubic phase.

Electron Spin Resonance Studies of Some Quinone Reactions*

D. C. Reitz,† J. R. Hollahan, F. Dravnieks, and J. E. Wertz

School of Chemistry, University of Minnesota, Minneapolis, Minnesota

(Received November 21, 1960)

A number of semiquinone radicals exhibit hyperfine spectra which can be interpreted only by one assuming that the original quinone or hydroquinone has been altered chemically in the process of semiquinone formation.[1,2] In alcoholic solutions *p*-benzosemiquinone is unstable; the original five-line spectrum decays in a matter of minutes, and a narrower, more complex signal is observed.[2] Gutowsky and co-workers[1] have interpreted several such spectra in terms of structures involving the coupling of two quinone molecules. Coupled products of type I and II were suggested for hydroquinone oxidation, while compounds of type III presumed to be formed on quinone reduction.

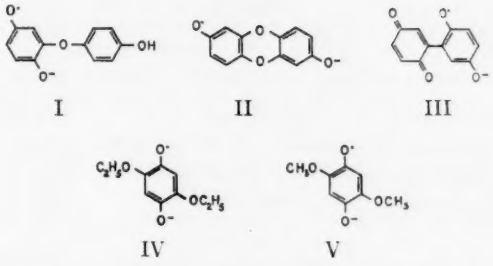

In order to explain the pattern and the breadth of the spectra in terms of coupled products they found it necessary to invoke fast transfer of the unpaired electron between both phenyl rings of the molecules. This would then reduce the ring proton splittings from about 2 gauss to 1 gauss. The possibility of simple alkoxyl attack on the ring was rejected by them because of the small over-all width of the spectrum. It was assumed that the ring proton splittings of alkoxyl substituted semiquinones would not be appreciably different from those of unsubstituted semiquinones. (Methyl-[3] and chlorosubstituents[4] do not appreciably reduce the ring proton splittings.)

In connection with an investigation of the reaction products of *p*-benzoquinone,[5] we have made some observations which prove that alkoxyl attack does occur in alcoholic solvents and we show that if a coupled product does form, spin exchange between the two halves is slow.

Observations reported in this note were made either by autoxidation of hydroquinones or reduction of quinones with glucose. No qualitative differences were found for the two procedures, and the measured coupling constants agreed within experimental error. The concentrations of quinone or hydroquinone were of the order of 0.01 to 0.03 *M*. Unless 10% aqueous NaOH is specified, the solvent was either methanol with sodium methylate or ethanol with sodium ethylate. The concentration of sodium in these solutions was 0.2 to 0.7 *M*. Methoxy-substituted compounds were observed in methanol, and ethoxy compounds in ethanol. The concentration of radicals produced was of the order of 10^{-4} mole/liter.

We have also observed the hfs of 2,5-diethoxysemiquinone (IV) and 2,5-dimethoxysemiquinone (V).[6] The splitting constants for the various protons are listed in Table I. The spectra obtained from a solution of *p*-benzoquinone in ethanol or methanol (after disappearance of the original five-line spectrum) have exactly the same splittings and *g*-values as IV or V, respectively. The spectrum of IV is very similar to the spectra of several halogen substituted semiquinones in ethanol reported earlier.[1] The ring proton splittings of IV and V are about eight times smaller than in unsubstituted benzosemiquinone. Therefore alkoxyl attack

TABLE I.

Parent compound	Splitting constants: Ring	Alkoxyl	g value
Hydroquinone	2.40		2.00483
2,5-Dimethoxyhydroquinone	0.28	0.96	2.00454
2,5-Diethoxyhydroquinone	0.35	1.06	2.00456
Dihydroquinone	0.92 0.45 0.1		2.00445

on halogen-substituted quinones cannot be rejected as Gutowsky and co-workers did because of the small line breadth of the ESR spectrum of the products.

We have also prepared an authentic sample of III.[7] In 10% NaOH solution, III exhibits a spectrum of eight lines of equal intensity. This spectrum is identical in all details with the spectra obtained from either hydroquinone or quinone in 10% NaOH. The spectrum is very different from that obtained from a solution of hydroxyhydroquinone in 10% NaOH. The splittings and g values are listed in Table I.

The simplest explanation of the spectrum of III (provided it has not undergone further chemical reaction) is that spin exchange between the two halves of the molecule is slow, and that the eight lines originate from the three nonequivalent protons on one-half of the molecule. This is analogous to the situation existing in the *bis*-triarylmethyl biradicals[8] and in 4,4′-dinitrodiphenylether negative ion[9] and is not in accord with the conclusions of Gutowsky and co-workers.

In alcoholic solution III exhibits hfs which indicate that alkoxyl attack has occurred. We have not as yet interpreted these results, but these spectra are entirely different from the spectra obtained from *p*-benzoquinone in alcohol.

In view of the identity of the ESR spectra of semiquinone compounds of known structure with the spectra of secondary semiquinones formed by solvent attack or coupling, the structures of the latter group would appear to be established.

Interpretations of spectra of a variety of secondary semiquinones will be published elsewhere.

* This research was supported in part by the Air Force Office of Scientific Research, Aeromedical Section.

† Present address: Radiation Physics Laboratory, DuPont Experimental Station, Wilmington, Delaware.

[1] D. H. Anderson, P. J. Frank, and H. S. Gutowsky, J. Chem. Phys. **32**, 196 (1960).
[2] J. L. Vivo, Ph.D. thesis, University of Minnesota, Minneapolis 14, Minnesota (1955); J. L. V. Acrivos (unpublished).
[3] B. Venkataraman, B. G. Segal, and G. K. Fraenkel, J. Chem. Phys. **30**, 1006 (1959).
[4] J. E. Wertz and J. L. Vivo, J. Chem. Phys. **23**, 2441 (1955).
[5] J. E. Wertz, D. C. Reitz, J. R. Hollahan, and F. Dravnieks (to be published).
[6] Y. Matsunaga and C. A. McDowell, Can. J. Chem. **38**, 1158 (1960).
[7] W. J. Hale and C. A. Robertson, J. Am. Chem. Soc. **39**, 692 (1908).
[8] D. C. Reitz and S. I. Weissman, J. Chem. Phys. **33**, 700 (1960).
[9] A. Moscowitz, D. C. Reitz, and S. I. Weissman (unpublished observation).

Dispersion of Lattice Waves in Copper

S. K. JOSHI AND M. P. HEMKAR
Physics Department, The University, Allahabad 2, U. P., India

(Received January 9, 1961)

AN *a priori* calculation of the lattice vibrational properties of metals presents great difficulties because of the presence of the conduction electrons. The initial attempts were restricted to the use of central forces alone.[1–3] Later a number of models[4–8] were advanced in which the electron gas was considered and taken account of in various approximate ways. With the availability of the information on the dispersion relation [i.e., the relation $\nu=\nu_s(q)$ between the frequency ν, the wave vector q and the polarization s of a phonon], through the experiments on both the diffuse scattering of x rays[9–12] and the inelastic scattering of neutrons by lattice vibrations,[13] it is possible to make a comparative study of the various theories. Horton and Schiff[14] thought it premature to compare the dispersion curves deduced from Bhatia's theory and the theory of Born and Begbie with those deduced from the diffuse x-ray scattering experiments of Jacobsen[10] on copper, because the results of the x-ray method are vitiated by the serious errors due to Compton and multiphonon scattering. Recently Cribier *et al.*[15] have plotted the dispersion curve for the longitudinal lattice waves propagating in [110] direction for copper from their experiments on slow neutron scattering, and it is not surprising that their results are not in agreement with the results of Jacobsen from x-ray measurements. As the slow neutron scattering method is more reliable, it is worthwhile to compare the dispersion relations deduced from the various theories with the neutron-scattering experiments. It is for these longitudinal vibrations studied by Cribier *et al.* that the effect of electron gas becomes prominent and the applicability of the Born-von Karman theory is doubtful.

The dispersion curves for copper for the longitudinal waves propagating in [110] direction for the various theories are plotted in Fig. 1 together with the experimental results by x-ray and neutron scattering methods. In the calculations after the theory of Bhatia and of de Launay the values of the elastic constants are taken from the measurements of Overton and Gaffney.[16] The values refer to a temperature of 290°K and are

$$c_{11}=16.875\times10^{11}\ \mathrm{d/cm^2}$$

$$c_{12}=12.158\times10^{11}\ \mathrm{d/cm^2}$$

$$c_{44}=\ 7.568\times10^{11}\ \mathrm{d/cm^2}.$$

For the calculation of the other two dispersion curves the force constants given by White[17] and by Jacobsen were used. The value of the density was taken as 8.95 g/cm³ and the nearest-neighbor distance as 2.557 A. It is clear from the plot that the theory of Bhatia gives

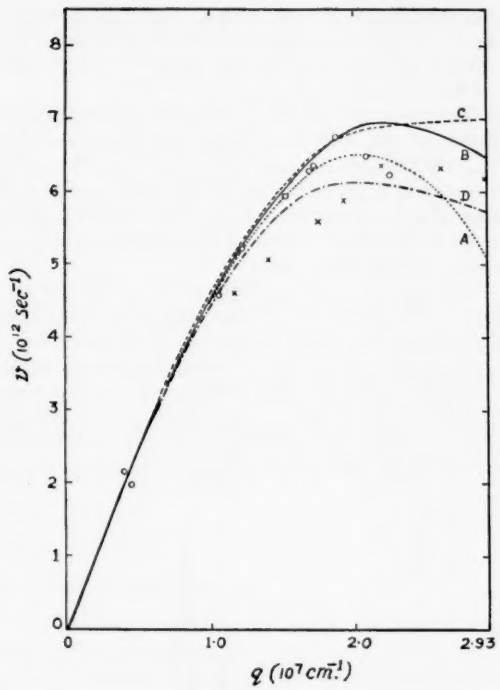

FIG. 1. Dispersion curves for longitudinal waves propagating in [110] direction in copper for various theoretical models. Curves A and B represent the theories of Bhatia and de Launay, respectively. The curves C and D are computed from the force constants given by White and Jacobsen, respectively. The experimental results of Cribier *et al.* from the neutron scattering are shown as circles and Jacobsen's experimental results by the x-ray method are shown by crosses.

much better agreement with the neutron scattering experiment, throughout the whole range of wave vectors, than the other theories. More detailed experimental investigations on dispersion relations in other directions with slow neutron scattering method are desirable for this and other noble and alkali metals to make a decisive comparison possible.

The authors are deeply indebted to Professor K. Banerjee for his interest in the investigation.

[1] P. C. Fine, Phys. Rev. **56**, 355 (1939).
[2] W. V. Houston, Revs. Modern Phys. **20**, 161 (1948).
[3] R. B. Leighton, Revs. Modern Phys. **20**, 165 (1948).
[4] E. Bauer, Phys. Rev. **92**, 58 (1953).
[5] G. Leibfried and W. Brenig, Z. Physik **134**, 451 (1953).
[6] J. de Launay, J. Chem. Phys. **21**, 1975 (1953); **22**, 1676 (1954).
[7] A. B. Bhatia, Phys. Rev. **97**, 363 (1955).
[8] A. B. Bhatia and G. K. Horton, Phys. Rev. **98**, 1715 (1955).
[9] C. B. Walker, Phys. Rev. **103**, 547 (1956).
[10] E. H. Jacobsen, Phys. Rev. **97**, 654 (1955).
[11] R. E. Joynson, Phys. Rev. **94**, 851 (1954).
[12] H. Curien, Acta Cryst. **5**, 392 (1952).
[13] L. S. Kothari and K. S. Singwi, *Solid State Physics*, edited by F. Seitz and D. Turnbull (Academic Press, Inc., New York, 1959), Vol. 8, p. 109.
[14] G. K. Horton and H. Schiff, Phys. Rev. **104**, 32 (1956).
[15] D. Cribier, B. Jacrot, and D. Saint-James, J. phys. radium **21**, 69 (1960).
[16] W. C. Overton, Jr., and J. Gaffney, Phys. Rev. **98**, 969 (1955).
[17] H. C. White, Phys. Rev. **112**, 1092 (1958).

Note Concerning Ruby Maser-Type Hamiltonians*

PAUL M. PARKER

Department of Physics, Michigan State University, East Lansing, Michigan

(Received December 14, 1960)

THE energy eigenvalues of the spin Hamiltonian[1]

$$\mathcal{H}_S = g_{\|}\beta H_z S_z + g_\perp \beta (H_x S_x + H_y S_y) + D[S_z^2 - \tfrac{1}{3}S(S+1)], \quad (1)$$

with spin quantum number $S=\frac{3}{2}$ has been the subject of a number of recent numerical calculations.[2-4] In this note we wish to point out that there exist simple relationships in closed form between the eigenvalues of Eq. (1) and the physical constants in Eq. (1).

If θ is the angle between H and the crystalline symmetry axis, and ϕ is the azimuth of H, then

$$\mathcal{H}_S' = \mathcal{H}_S/2D = 2x\cos\theta S_z + y\sin\theta[S_+\exp(-i\phi) + S_-\exp(+i\phi)] + \tfrac{1}{2}[S_z^2 - \tfrac{1}{3}S(S+1)], \quad (2)$$

where $x = g_{\|}\beta H/4D$, $y = g_\perp \beta H/4D$, and $2D$ is the zero applied-field splitting of the two Kramers doublets, $M_s = \pm\frac{3}{2}$, $M_s = \pm\frac{1}{2}$.

The matrix elements of Eq. (2) in the S^2, S_z diagonal representation are found with ease, and application of the method of energy moments[5] to Eq. (2) yields

$$W_1^2 + W_2^2 + W_3^2 + W_4^2 = 20x^2\cos^2\theta + 20y^2\sin^2\theta + 1, \quad (3)$$

$$W_1^3 + W_2^3 + W_3^3 + W_4^3 = 12(2x^2\cos^2\theta - y^2\sin^2\theta), \quad (4)$$

where the W_i's are the eigenvalues of Eq. (2). Of course $W_1+W_2+W_3+W_4=0$ since the representation is traceless.

If it is assumed that $x=y$, i.e., if $g_{\|}=g_\perp$, then Eqs. (3) and (4) become

$$W_1^2 + W_2^2 + W_3^2 + W_4^2 = 20x^2 + 1, \quad (5)$$

$$W_1^3 + W_2^3 + W_3^3 + W_4^3 = 12x^2(3\cos^2\theta - 1). \quad (6)$$

A spot check of eigenvalues cited by Stahl-Brada and Low[2] showed their numerical results to be in agreement with Eqs. (5) and (6). Users of the Stahl-Brada and Low energy tables should be aware that for all entries a decimal point should be placed after the third digit, although this is not stated explicitly.

The relationships given in this note serve as a convenient check on energy eigenvalues obtained from machine calculations. Also, if for given H and θ enough

transitions can be observed to infer all four W_i's, the relationships given will be of use in data analysis.

* This investigation was supported in part by the Air Force Office of Scientific Research (ARDC) under contract.

[1] B. Bleaney and K. W. H. Stevens, Repts. Progr. in Phys. **16**, 108 (1951).

[2] R. Stahl-Brada and W. Low, Nuovo cimento Suppl. **15**, 290 (1960).

[3] E. O. Schulz-DuBois, Bell System Tech. J. **33**, 271 (1959).

[4] W. S. Chang and A. E. Siegman, Stanford Electronics Laboratories, Stanford, California, Tech. Rept. No. 156-2.

[5] P. M. Parker and L. C. Brown, Am. J. Phys. **27**, 509 (1959).

Nuclear Magnetic Resonance Spectrum of the Triphenylcarbonium Ion*

R. S. Berry,† R. Dehl, and W. R. Vaughan

Department of Chemistry, University of Michigan, Ann Arbor, Michigan

(Received December 15, 1960)

THE relative order of the chemical shifts in the ring spectrum of the triphenylcarbonium ion was estimated by Moodie, Connor, and Stewart[1] and measured by us[2] from appropriately deuterated species. The chemical shifts which we originally reported are essentially correct: $\delta_{\text{para-ortho}}=0.525$ ppm and $\delta_{\text{para-meta}}=0.355$ ppm. However, the coupling constants were in error. We have reevaluated the latter by the method of total reproduction of the NMR spectrum, based on the complete solution of the secular equation for the system AB_2C_2. The calculations followed the general procedure used by Schneider, Bernstein, and Pople[3] for pyridine, an AB_2X_2 spectrum. Our spin wave functions and Hamiltonian matrix elements were identical to those used in the pyridine case, except for the inclusion of a few additional off-diagonal matrix elements, made necessary by the removal of the X approximation for AB_2X_2.

Table I is a list of the additional nonvanishing matrix elements for AB_2C_2 in the spin wave notation of Schneider, Bernstein, and Pople.[3]

The diagonalization of the submatrices of the complete Hamiltonian and the computation of line intensities were performed on an IBM 704 computer for several sets of trial coupling constants, using the measured relative chemical shifts. Line intensities were calculated for each of the 110 transitions allowed by the selection rule $\Delta F_z=\pm 1$, where F_z is the total z component of angular momentum of a given spin wave function. In order to approximate the general appearance of an NMR spectrum, we drew a smooth curve through points which were evaluated by (1) plotting a Lorentz curve about each of the computed transition intensities, using a single value of T_2 estimated from the experimental linewidths and, (2), adding up the contributions from all 110 curves at small regular intervals over the span of the spectrum. The experimental 60-Mc spectrum of triphenylcarbonium is shown in Fig. 1(a), together with the calculated spectrum [Fig. 1(b)] which was judged a best fit after several trial sets of parameters.

The value used for T_2 was 0.4 sec, and the chemical shifts in cps were as follows: $J_{om}=8.2$, $J_{om'}=0.5$, $J_{mp}=8.0$, $J_{op}=1.2$, $J_{mm'}=1.7$, $J_{oo}=1.2$. The primes are used to denote a proton on the opposite side of the ring; $J_{om'}$ is very small and could be negative, but the signs of the other J's are all apparently positive, and correct within ± 0.5 cps.

The relative chemical shifts of the ortho and meta protons are the reverse of those estimated by O'Reilly and Leftin,[4] but their alternative assignments are in good agreement with ours. A complete spectral calculation identical to that of Fig. 1(b), except for the reversal of the meta and ortho shifts, yields quite a different spectrum [Fig. 1(c)] which does not agree well with the observed one. Using these authors' calculations for the

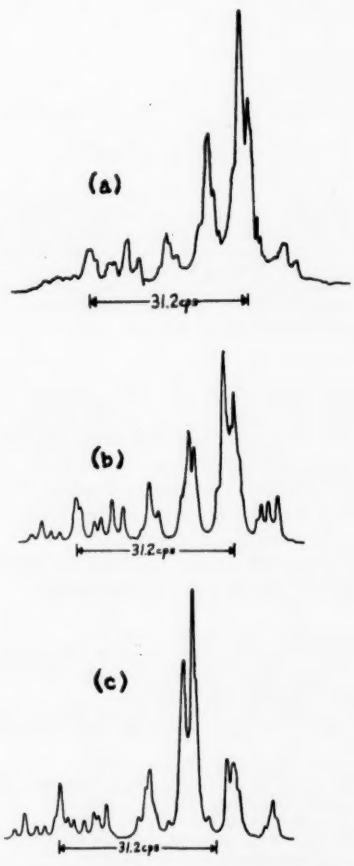

FIG. 1. (a) 60-Mc NMR spectrum of the triphenylcarbonium ion. (b) Calculated 60-Mc spectrum. (c) Calculated 60-Mc spectrum with ortho and meta chemical shifts reversed.

TABLE I. Off-diagonal matrix elements of the AB_2C_2 Hamiltonian not included in the AB_2X_2 approximation.

Symmetric	Antisymmetric[1,11]
$(1s_{\frac{1}{2}} \mid H \mid 2s_{\frac{1}{2}}) = (4s_{\frac{1}{2}} \mid H \mid 6s_{\frac{1}{2}})$	$(1a_{\frac{1}{2}} \mid H \mid 2a_{\frac{1}{2}})$
$= (1s_{-\frac{1}{2}} \mid H \mid 3s_{-\frac{1}{2}})$	$= (3a_{\frac{1}{2}} \mid H \mid 4a_{\frac{1}{2}})$
$= (2s_{-\frac{1}{2}} \mid H \mid 3s_{-\frac{1}{2}}) = \frac{1}{2}(J_{om} + J_{om'})$	$= (1a_{-\frac{1}{2}} \mid H \mid 2a_{-\frac{1}{2}})$
$(1s_{\frac{1}{2}} \mid H \mid 3s_{\frac{1}{2}}) = (1s_{\frac{1}{2}} \mid H \mid 4s_{\frac{1}{2}})$	$= (1a_{-\frac{1}{2}} \mid H \mid 2a_{-\frac{1}{2}})$
$= (3s_{-\frac{1}{2}} \mid H \mid 6s_{-\frac{1}{2}})$	$= \frac{1}{2}(J_{om} - J_{om'})$
$= (1s_{-\frac{1}{2}} \mid H \mid 3s_{-\frac{1}{2}}) = 1/\sqrt{2}\, J_{op}$	$(1a_{\frac{1}{2}} \mid H \mid 4a_{\frac{1}{2}})$
$(1s_{\frac{1}{2}} \mid H \mid 3s_{\frac{1}{2}}) = (3s_{\frac{1}{2}} \mid H \mid 5s_{\frac{1}{2}})$	$= (2a_{\frac{1}{2}} \mid H \mid 4a_{\frac{1}{2}})$
$= (2s_{-\frac{1}{2}} \mid H \mid 4s_{-\frac{1}{2}})$	$= (1a_{-\frac{1}{2}} \mid H \mid 3a_{-\frac{1}{2}})$
$= (4s_{-\frac{1}{2}} \mid H \mid 6s_{-\frac{1}{2}}) = 1/\sqrt{2}\, J_{om}$	$= (1a_{-\frac{1}{2}} \mid H \mid 4a_{-\frac{1}{2}})$
$(2s_{\frac{1}{2}} \mid H \mid 6s_{\frac{1}{2}}) = (3s_{\frac{1}{2}} \mid H \mid 6s_{\frac{1}{2}})$	$= \frac{1}{2} J_{op}$
$= (1s_{-\frac{1}{2}} \mid H \mid 4s_{-\frac{1}{2}})$	
$= (1s_{-\frac{1}{2}} \mid H \mid 5s_{-\frac{1}{2}}) = \frac{1}{2} J_{op}$	
$(1s_{\frac{1}{2}} \mid H \mid 2s_{\frac{1}{2}}) = (2s_{\frac{1}{2}} \mid H \mid 5s_{\frac{1}{2}})$	
$= (2s_{-\frac{1}{2}} \mid H \mid 5s_{-\frac{1}{2}})$	
$= (5s_{-\frac{1}{2}} \mid H \mid 6s_{-\frac{1}{2}}) = 1/\sqrt{2}\, J_{om'}$	

ring-current contribution to the chemical shifts, we suggest that the discrepancy may be resolved by asuming the slightly larger value of 1.2 A for the effective van der Waals radius of hydrogen, which increases the average inclination angle of the benzene rings to about 30° from the horizontal.

* Supported in part by a grant from the University of Michigan Cancer Research Institute.

† Present address: Sterling Chemistry Laboratory, Yale University, New Haven, Connecticut.

[1] R. B. Moodie, T. M. Connor, and Ross Stewart, Can. J. Chem. **37**, 1402 (1959).
[2] R. Dehl, W. R. Vaughan, and R. S. Berry, J. Org. Chem. **24**, 1616 (1959).
[3] W. G. Schneider, H. J. Bernstein, and J. A. Pople, Can. J. Chem. **35**, 1487 (1957).
[4] D. E. O'Reilly and H. P. Leftin, J. Phys. Chem. **64**, 1555 (1960).

Intrinsic Viscosity of Stiff Chains

ROBERT ULLMAN AND A. MUZYKA

The Institute for Polymer Research, Department of Chemistry, and Department of Mathematics, Polytechnic Institute of Brooklyn, Brooklyn, New York

(Received November 21, 1960)

THE intrinsic viscosity of a solution of partially coiled polymer molecules is being investigated by us using a procedure developed by Burgers[1] and extended by Kirkwood and Riseman.[2] The coiling of the polymer molecules is described by the chain statistics of Hermans and Ullman.[3] In this treatment, two parameters are important, the length n and a quantity λ which is large when the chain is tightly coiled and is small when the chain becomes straight. Specifically, if θ is the angle a tangent to the chain makes with an arbitrary axis, λ is one quarter of the average square change in θ per unit of chain (see p. 958 of the work cited in footnote 3).

The formal treatment is similar to that of Kirkwood and Riseman, the solution of the problem depending on an inhomogeneous integral equation of the Fredholm type. The result may be written

$$[\eta] = -(N/100M_0\eta_0\epsilon)\int_0^n \langle(\mathbf{R}_{0l}\cdot\mathbf{e}_y)(\mathbf{F}_l\cdot\mathbf{e}_x)\rangle_{Av}dl$$

$$= (\zeta N/1200M_0\eta_0\lambda^2)F(\lambda n), \quad (1a)$$

$$\langle(\mathbf{R}_{0k}\cdot\mathbf{e}_y)(\mathbf{F}_l\cdot\mathbf{e}_x)\rangle_{Av} = (-\zeta\epsilon/6)\langle\mathbf{R}_{0k}\cdot\mathbf{R}_{0l}\rangle_{Av}$$

$$-(\zeta/6\pi\eta_0)\int_0^n \langle(\mathbf{R}_{0k}\cdot\mathbf{e}_y)(\mathbf{F}_s\cdot\mathbf{e}_x)\rangle_{Av}\langle 1/R_{ls}\rangle_{Av}ds, \quad (1b)$$

where $[\eta]$ is the intrinsic viscosity; η_0 is the solvent viscosity; ζ is the friction constant per unit length; ϵ is the shear gradient of flow; M_0 is the molecular weight per unit length; $\mathbf{R}_{0k}$ and $\mathbf{R}_{0l}$ are vectors from the mass to positions k and l units distance along the chain; $\mathbf{F}_l$ is the force exerted on the solvent by an element of the chain at l; $\mathbf{e}_x$ and $\mathbf{e}_y$ are unit vectors in the x and y direction.

The $\langle\mathbf{R}_{0k}\cdot\mathbf{R}_{0l}\rangle_{Av}$ is easy to calculate, but $\langle 1/R_{ls}\rangle_{Av}$, the kernel of the integral equation, is not. In our treatment it is approximated by the formula

$$\langle 1/R_{ls}\rangle_{Av} = [1/\langle R_{ls}^2\rangle_{Av}]^{\frac{1}{2}}G(\lambda\,|1-s\,|) \quad (2)$$

$$\langle R_{ls}^2\rangle_{Av} = |l-s\,|/\lambda - (1/2\lambda^2)[1-\exp(-2\lambda\,|l-s\,|)],$$

where G varies from 1.00 to 1.38 as the particle changes from a rod to a coil form.

It is easy to show that if λ is allowed to approach zero, Eq. (1a) assumes the form obtained previously for the rodlike molecule,[4,5] and as λ becomes large, the solution is essentially similar to the result obtained for the random coil.[2]

From Eq. (1a), one can recognize that the intrinsic viscosity may be considered as a product of two functions, one of which depends on λ the stiffness parameter and the other on the product of the stiffness parameter and chain length. Multiplying by n^2 in the numerator and denominator, the intrinsic viscosity may also be expressed as a product of n^2 and a function of the stiffness parameter times chain length.

The Fredholm equation [Eq. (1b)] which applies to the stiff chain model cannot be solved in terms of known functions as could the problems of the works cited in footnotes 2, 4, and 5. Instead, numerical computations are being used to obtain a solution. A serious difficulty is encountered because of the mathematical singularity in the kernel of the integral equation.

The kernel $\langle 1/R_{ls}\rangle_{kl}$ must necessarily approach $1/|l-s|$ as l approaches s. If this is substituted in Eq. (1b), no solution exists. The procedure adopted by us is the introduction of a cutoff in the kernel as was done earlier.[4,5] That is, $1/|l-s|$ is replaced by zero for $|l-s|<K$, where K is a somewhat arbitrary selected constant. This is justifiable on physical grounds because of the finite thickness of the polymer chain. The effect of this procedure on the results of the calculation is not yet known.

[1] J. M. Burgers, *Second Report on Viscosity and Plasticity* (North-Holland Publishing Company, Amsterdam, 1938), Chap. 3.
[2] J. G. Kirkwood and J. Riseman, J. Chem. Phys. **16**, 565 (1948).
[3] J. J. Hermans and Robert Ullman, Physica **18**, 951 (1952).
[4] J. Riseman and J. G. Kirkwood, J. Chem. Phys. **18**, 565 (1950).
[5] J. G. Kirkwood and P. L. Auer, J. Chem. Phys. **19**, 281 (1951).

Thermal Expansion of Metals

S. S. MITRA

Department of Physics, Ontario Research Foundation, Toronto, Canada

AND

S. K. JOSHI

Department of Physics, The University, Allahabad, India

(Received December 5, 1960)

STARTING from the Debye equation of state for solids, it was shown[1] by Grüneisen that the linear thermal expansion coefficient,

$$\alpha=(\chi C_v/3V)\gamma, \tag{1}$$

where χ, V, and C_v are, respectively, compressibility, volume, and specific heat at constant volume, and Grüneisen constant $\gamma=-d\ln\nu/d\ln V$.

On introducing a force constant f associated with the eigenfrequency ν, one obtains

$$\alpha=-(1/18)(\chi C_v/Nc r_0^2)(1/f)(df/dr)_{r=r_0}, \tag{2}$$

where r is the nearest-neighbor distance and c is the packing factor, such that $V=Nc r^3$. The force constant f and its first derivative are given by

$$f=(1/N)(d^2U/dr^2)_{r=r_0} \tag{3}$$

$$df/dr=(1/N)(d^3U/dr^3). \tag{4}$$

Expressions (3) and (4) can be easily evaluated if the energy of the crystal U is known as a function of r. In case of metals, the problem of calculating the effective potential energy from first principles is an extremely difficult one. However, there have been attempts[2,3] to use certain phenomenological potentials to represent and predict some of the metallic properties. Slater[4] has suggested the use of the Morse potential function to approximate the internal energy of a metal,

$$U=E_0\{\exp[-2\epsilon(r-r_0)]-2\exp[-\epsilon(r-r_0)]\}; \tag{5}$$

E_0 represents the latent heat of vaporization and ϵ is a potential parameter that can be evaluated from the

TABLE I. Coefficient of linear expansion of metals. (All data refer to room temperature.)

Structure	Metal	C_v cal/deg mole[a]	$a\times10^8$ cm[b]	$\chi\times10^{12}$ d^{-1} cm^2 [c]	E_0 kcal/mole[c]	$\alpha\times10^6$ calc (Eq. 8)	$\alpha\times10^6$ exptl[d]
bcc	α Cr	5.43	2.8845	0.62	80	12.9	7.5
	Cs	5.94	6.05	71.4	18.8	100.5	97
	α Fe	5.26	2.8665	0.60	97	11.3	11.7
	K	5.93	5.344	36.4	22.6	80.3	83
	Li	5.36	3.5087	8.9	36.5	53.1	45
	Mo	5.38	3.150	0.37	155	8.9	5.2
	Na	5.87	4.2906	15.9	26.0	69.3	71
	Rb	5.94	5.709	53.0	18.9	99.3	
	Ta	5.81	3.3026	0.49	185	6.6	6.6
	W	5.50	3.1648	0.33	201	5.2	4.6
fcc	Ag	5.79	4.086	1.0	69	15.8	18.9
	Al	5.41	4.0495	1.37	74.4	16.8	23.6
	Au	5.87	4.0781	0.59	82	11.3	13.9
	α Ca	5.79	5.57	5.8	46	29.1	22.5
	Cu	5.57	3.6147	0.73	81	14.4	17.0
	Ir	5.69	3.8389	0.28	165	5.8	6.5
	Ni	5.28	3.5239	0.54	101	10.9	12.5
	Pb	5.93	4.9496	2.42	46	23.1	28.8
	Pd	5.70	3.8902	0.54	93	10.6	11.6
	Pt	5.78	3.9237	0.37	122	7.6	8.9
	β Rh	5.55	3.8044	0.37	138	7.2	8.4

[a] Calculated from Debye formula given in *American Institute of Physics Handbook* (McGraw-Hill Book Company, Inc., New York, 1957), p. 4-44.
[b] See footnote a, p. 2-48.
[c] See Kittel,[1] p. 99.
[d] W. B. Pearson, *A Handbook of Lattice Spacings and Structures of Metals and Alloys* (Pergamon Press, New York, 1958), p. 123.

measured values of compressibility by

$$1/\chi = (1/9Ncr_0)(d^2U/dr^2)_{r=r_0} = 2\epsilon^2 E_0/9Ncr_0. \quad (6)$$

On combining Eqs. (2)–(6), one obtains for the coefficient of linear expansion of metals

$$\alpha = (C_v/2)(\chi/2NcE_0r_0^3)^{\frac{1}{2}}. \quad (7)$$

Now, for the bcc structures, $c=4/3\sqrt{3}$ and the axial length $a=2r_0/\sqrt{3}$; therefore,

$$\alpha = (C_v/2)(\chi/NE_0a^3)^{\frac{1}{2}}. \quad (8a)$$

In the case of the fcc structures, $c=1/\sqrt{2}$ and $a=\sqrt{2}r_0$; consequently,

$$\alpha = (C_v/2)(2\chi/NE_0a^3)^{\frac{1}{2}}. \quad (8b)$$

The calculated values of α from relations (8a) and (8b) along with their experimental values are presented in Table I. The agreement is remarkably good considering the limitations of the theory, viz., (i) use of Debye equation of state, and (ii) use of the Morse potential function to approximate the internal energy of a cubic metal.

[1] C. Kittel, *Introduction to Solid-State Physics* (John Wiley & Sons, Inc., New York, 1956), p. 154.
[2] L. A. Garifalco and V. G. Weizer, Phys. Rev. **114**, 687 (1959).
[3] H. Cole, IBM J. Research Develop. **3**, 126 (1959).
[4] J. C. Slater, *Introduction to Chemical Physics* (McGraw-Hill Book Company, Inc., New York, 1939), p. 452.

Heat Capacity of Antiferromagnetic $CuCl_2 \cdot 2H_2O$ in the Spin Wave Region*

R. G. PETERSEN
Department of Physics, University of California, Berkeley, California
AND
NORMAN E. PHILLIPS
Department of Chemistry and Lawrence Radiation Laboratory, University of California, Berkeley, California

SPIN wave theory predicts a T^3 temperature dependence for the magnetic heat capacity of an isotropic antiferromagnet. The presence of anisotropy modifies this result to give an exponential temperature dependence at temperatures that is small compared with the geometric mean of the exchange and anisotropy energies.[1] $CuCl_2 \cdot 2H_2O$ was chosen as an example in which to look for these effects because the anisotropy field and the T^3 lattice heat capacity are both known. We have so far been unable to obtain a single crystal large enough for the measurement but report here some preliminary results obtained with a compressed polycrystalline sample. The relatively long thermal equilibrium times encountered in this sample may have introduced systematic errors below 0.3°K. Temperature measurements were based on an extrapolation of the susceptibility of copper potassium sulfate from above

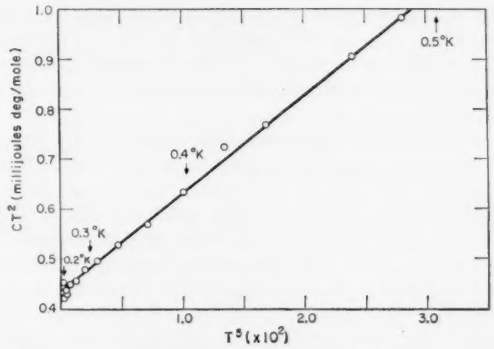

FIG. 1. The total heat capacity C of $CuCl_2 \cdot 2H_2O$. Higher temperature points show a positive deviation from the straight line and are omitted in this plot.

1°K according to a Curie-Weiss law. The experimental results are shown in Figs. 1 and 2.

Nakamura[2] has shown that, in the long wavelength limit, the frequencies $\omega_i(k)$ of the spin wave modes in an orthorhombic antiferromagnet are related to their propagation vectors k by an expression of the form

$$\omega_i(k) \cong 2z\,|\,J\,|\,S[bk^2+2\alpha_i]^{\frac{1}{2}} \quad i=1,2, \quad (1)$$

in which b, z, J, and S are, respectively, a structure factor, the number of nearest neighbors, the exchange integral, and the spin. Here α_1 and α_2 are proportional to the antisotropy fields and can be deduced from the antiferromagnetic resonance frequencies or the critical fields for flipping of the spins. Eisele and Keffer[1] have shown that for $CuCl_2 \cdot 2H_2O$, Eq. (1) gives, at temperatures small compared with T_c(4.3°K), a magnetic heat capacity C_M which satisfies

$$C_M/RT^3 = (2\pi^2/3)(k_B/2z\,|\,J\,|\,S)^3 C_M'(T,\alpha_1,\alpha_2), \quad (2)$$

in which k_B is Boltzmann's constant and R is the molar gas constant. The C_M' is strongly temperature depend-

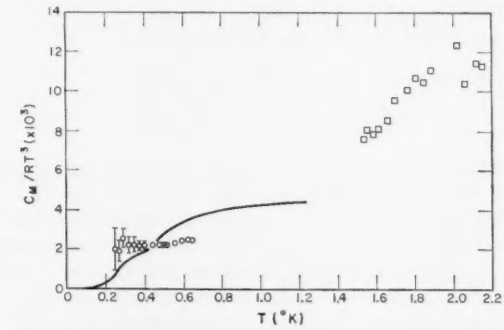

FIG. 2. The magnetic heat capacity C_M of $CuCl_2 \cdot 2H_2O$. The indicated errors correspond to an estimated error of 2% in the total heat capacity. The points designated by squares are from the measurements of Friedberg (see the work cited in footnote 3). The solid curve represents the calculation of Eisele and Keffer (see the work cited in footnote 1).

ent at low temperatures but approaches unity for $kT \gtrsim 2z|J|S(2\alpha)^{\frac{1}{2}}$; C_M/RT^3 predicted by Eq. (2) is shown as the solid curve in Fig. 2; J/k_B is taken as 5.4°K to give order of magnitude agreement with the experimental result.

Below 0.55°K the total heat capacity can be resolved into components varying as T^{-2} and T^3, as shown in the figures. The lattice heat capacity[3] accounts for 7% of the T^3 term leaving $2.25\times10^{-3}RT^3$ for C_M and 5.25×10^{-5} RT^{-2} for nuclear alignment effects. The latter part probably arises principally from the magnetic hyperfine interaction between the copper nuclei and the electron spins. Upper limits of 132 Mc/sec and 142 Mc/sec are thus established for the separation of the levels of Cu^{63} and Cu^{65}, respectively.

The T^3 temperature dependence for C_M is not in agreement with Eq. (2). Apart from the possibility of an unexpectedly large error in the T^{-2} term or of particle size effects, the discrepancy may arise from the phenomenological way in which anisotropy is treated in spin wave calculations. A similar situation exists with respect to the parallel susceptibility of MnF_2. Griffel and Stout[4] have observed the T^2 temperature dependence, predicted by spin wave theory for an isotropic antiferromagnet,[5] at temperatures for which the anisotropy should have brought about a more rapid temperature variation.[1]

* Supported in part by the National Science Foundation and in part by the U. S. Atomic Energy Commission.

[1] J. A. Eisele and F. Keffer, Phys. Rev. **96**, 929 (1954).
[2] T. Nakamura, Progr. Theoret. Phys. (Kyoto) **7**, 539 (1952).
[3] S. A. Friedberg, Physica **18**, 714 (1952).
[4] M. Griffel and J. W. Stout, J. Chem. Phys. **18**, 1455 (1950).
[5] R. Kubo, Phys. Rev. **87**, 568 (1952).

X-Ray Diffraction Study of Liquid Mercury-Indium Alloys*

YOUNG SOO KIM,† C. L. STANDLEY,‡ R. F. KRUH, AND GLEN T. CLAYTON

Departments of Physics and Chemistry, University of Arkansas, Fayetteville, Arkansas

(Received November 22, 1960)

IN an attempt to detect independent distributions in binary liquid metals, we have studied the mercury-indium system. In contrast to our study of lead-bismuth,[1] which was treated as monatomic, we expected that differences in radii and in atomic number would produce a splitting in the first peak of the radial distribution function, or at least a prominent shoulder on it. The expectation was unfulfilled, and this note is to report that the first maximum in each of the several distribution functions is practically symmetrical and can be accounted for by assuming the same pair distribution exists over the entire composition range.

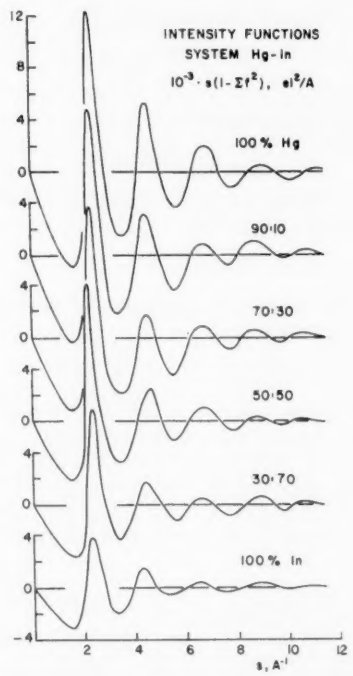

FIG. 1. Intensity functions in electron units. Compositions are in atom percents.

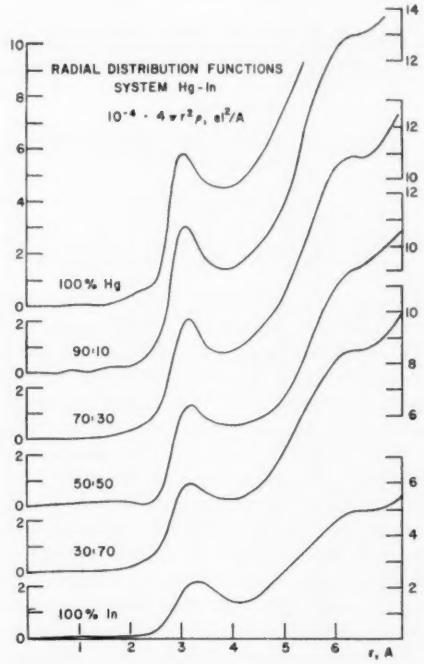

FIG. 2. Distribution functions. Compositions are in atom percents.

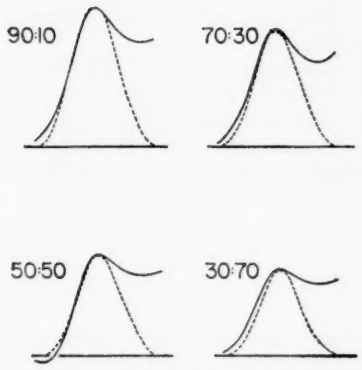

FIG. 3. Superposition of calculated and observed first maxima in distribution functions for binary melts. The mercury-mercury, mercury-indium, and indium-indium contributions to the calculated maximum are centered at 3.15, 3.22, and 3.30 A, respectively.

The liquids studied had mole fractions of 1.0, 0.9, 0.7, 0.5, 0.3, and 0.0 in mercury. The temperatures were 23°, 24°, 24°, 24°, 140°, and 175°; and the densities 13.54, 12.76, 11.68, 10.28, 9.01, and 7.03 g/cm^3, respectively.

Figures 1–3 show the intensity functions, the distribution functions, and the fit of the first maxima with a sum of calculated contributions. The intensity functions were modified by a sharpening factor before Fourier inversion, and the same sharpening factor was compensated for in calculating the peak contributions expected for mercury-mercury, mercury-indium, and indium-indium pairs.[2]

The peaks in Fig. 3 are calculated on the assumption of a random superposition of these pairs, and are given by

$$n[x_{\mathrm{Hg}}{}^2 T_{\mathrm{Hg-Hg}}(r)+2x_{\mathrm{Hg}}x_{\mathrm{In}}T_{\mathrm{Hg-In}}(r)+x_{\mathrm{In}}{}^2 T_{\mathrm{In-In}}(r)],$$

where $T(r)$ is the peak shape expected for the indicated atom pair and where a common number of nearest neighbors, $n=7.8$, is assumed. Each $T(r)$ is centered at the sum of the appropriate atom radii. The close agreement between calculated and observed maxima indicates, within the limited resolution of the distribution function, a random participation of atoms in a common distribution. This seems reasonable since the coordination numbers for pure mercury and pure indium are both about 8, and the distribution curves, as well as the intensities, are much the same except for scale.

* The support of the U. S. Atomic Energy Commission is gratefully acknowledged.

† Taken in part from master's thesis, University of Arkansas, 1961.

‡ Taken in part from master's thesis, University of Arkansas, 1959.

[1] P. C. Sharrah, J. I. Petz, and R. F. Kruh, J. Chem. Phys. **32**, 241 (1960). Experimental methods are given here.

[2] J. Waser and V. Schomaker, Revs. Modern Phys. **25**, 671 (1953).

Decomposition of Dimethyl Carbonate on Quartz*

M. H. J. WIJNEN

Radiation Research Laboratories, Mellon Institute, Pittsburgh, Pennsylvania

(Received November 16, 1960)

WHILE studying the photolysis of dimethyl carbonate we observed that increasing amounts of dimethyl ether were produced with increasing temperatures. These results could not be reconciled with the formation of dimethyl ether through recombination of methyl and methoxy radicals as observed in other studies.[1] The possibility of dimethyl ether formation by thermal decomposition of dimethyl carbonate was, therefore, investigated. Thermal decomposition experiments were carried out in a cylindrical quartz reaction vessel normally employed for photochemical investigations. Internal diameter of the cell was 4.8 cm, length 12 cm.

Observed as reaction products were CO_2, CH_3OCH_3, and occasionally CH_3OH. Methanol was observed only in experiments following previous admittance of air to the cell even though the cell had been evacuated for some time before the start of the experiment. The appearance of methanol coincided with an increased production of carbon dioxide. It seems, therefore, probable that methanol and in part carbon dioxide were formed by hydrolysis of dimethyl carbonate with traces of water left behind in the cell after evacuation of the air.

Data obtained for the production of dimethyl ether at various temperatures, pressures, and contact times are given in Table I.

The data obtained at 209° and at 232°C show clearly that a threefold change in initial pressure does not cause any variation in the rate of dimethyl ether production. The apparent zero order of this reaction indicates that even at the lowest pressure used in our investigation, the quartz surface is completely covered. It is also interesting to point out that the admittance

TABLE I. Thermal decomposition of dimethyl carbonate on quartz.

Temp °C	Initial pressure molecules/cc $\times 10^{-17}$	Time sec	CH_3OCH_3 moles $\times 10^8$	k CH_3OCH_3 moles/sec $\times 10^{10}$
257	6.56	320	64.7	20.2
232	6.50	320	27.8	8.7
232	2.27	300	27.8	9.3
209	6.85	1465	57.5	3.9
209	6.50	305	12.0	3.9
209	6.91	584	17.9	3.1
209	3.56	1205	46.7	3.9
209	6.55	1166	53.4	4.6
209	2.11	1200	46.7	3.9
147	2.48	3600	10.8	0.3
147	6.63	3552	11.7	0.3

of small amounts of formaldehyde to the cell caused a considerable drop in the rate of dimethyl ether production. Only prolonged evacuation at 260°C restored the quartz surface to its original state. The data at 209°C also indicate that within the limits of our investigation no retardation by the reaction products is observed. It is thus possible to calculate the true activation energy for the production of dimethyl ether from the obtained data for the apparent rate constant. Such calculations give a value of 17 ± 1 kcal for the thermal decomposition of $(CH_3O)_2CO$ into CH_3OCH_3 and CO_2.

It may be interesting to point out that a minimum Arrhenius factor may be calculated assuming that the cell surface is covered by a monlayer of ester and that the surface reaction is unimolecular. Accepting 20 A^2 as cross section of the ester molecule, such a calculation yields an Arrhenius A factor of about 10^5 sec^{-1}.

The decomposition of dimethyl carbonate into CH_3OCH_3 and CO_2 is similar to the decomposition of formic acid into H_2 and CO_2, where activation energies of 24 to 31 kcal have been obtained[2] depending on the nature of the surface. It should be pointed out that we have observed a similar reaction with diethyl carbonate which thermally decomposes on quartz to form diethyl ether and carbon dioxide. In this case, however, an additional reaction was observed producing ethylene, ethanol, and carbon dioxide.

The author wishes to express his sincere thanks to J. A. Guercione for carrying out the experiments described in this note.

* This investigation was supported, in part, by the U. S. Atomic Energy Commission.

[1] M. H. J. Wijnen, J. Chem. Phys. **27**, 710 (1957); **28**, 271, 393 (1958).

[2] C. N. Hinshelwood, *Kinetics of Chemical Change* (Oxford University Press, New York, 1947), p. 218.

Site of Protonation in Methyl Formate*

GIDEON FRAENKEL†

Gates and Crellin Laboratories of Chemistry, California Institute of Technology, Pasadena, California

(Received December 19, 1960)

WHILE it is well known from structural studies[1] and thermochemical evidence[2] that esters undergo considerable resonance stabilization (I), there has been no measurement of the barrier to rotation about the

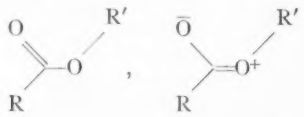

(I)

C_{CO}–C_{OR} bond in esters and no experiment to determine the basic site.

Dipole measurement studies[3] establish open-chain esters to assume the *trans* configuration (I). The existence of a rapid equilibrium between the two possible rotational isomers [reaction (1)], has been suggested from ultrasonic relaxation[4,5] measurements;

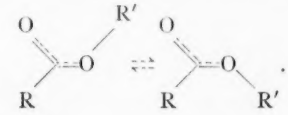

(1)

Methyl formate is one of the few compounds in which NMR proton spin coupling across oxygen and two carbon atoms,

is large enough to observe. The value is 1.25 cycles. This may be ascribed to the 25% double-bond character of the central C_{CO}—O_{OR} bond in the molecule, see (I). On the other hand, in trimethylorthoformate which has only single bonds sp^3 we have found that the CH, CH_3 proton coupling constant is less than 0.05 cps.

Empirically it is found that only in unsaturated molecules such as olefins, aromatic compounds, acetylenes,[6] and amides,[7] are long-range coupling constants, over more than three bonds, large enough to observe. Since the main contribution to the coupling constants comes from the Fermi contact interaction[8] and if the coupling is carried mainly by s electrons,[9] as in aromatic molecules, increasing the s character of C—H bonds should result in larger coupling constants. This has been confirmed for B″—H coupling constants.[10] Hence for N,N-dimethylformamide,[7] N-methylformamide,[7] and methyl formate, the formyl-methyl proton coupling constants owe their large values to the partial double bond character of the central C_{CO}—N or C_{CO}—O_{OR} bond in the molecule.

It is possible to differentiate between the two modes of pronation of methhl formate (II) and (III), by examining the NMR spectra of this ester

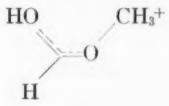

(II)

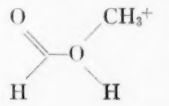

(III)

dissolved in very strong acids: Protonation on carbonyl oxygen (II) would yield a spectrum very similar to that of pure methyl formate. On the other hand, protonation on alcoxy oxygen (III), would cause free rotation, excluding the resonance contribution (IV), about the C_{CO}—O_{OR}^+ bond. Hence the formyl-methyl proton coupling constant would be too small to observe

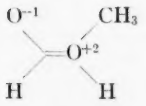

(IV)

by analogy to trimethylorthoformate. Thus for the case of slow proton exchange on alcoxy oxygen in (II) we expect the methyl resonance to consist of a doublet, separation 6 cps due to CH_3, OH proton coupling. Fast proton exchange on alcoxy oxygen would yield a single sharp line for the methoxy protons. Similar arguments may be applied to locating the site in methyl formate most basic to boron trifluoride.[11]

The formyl-methyl proton coupling constants for methyl formate under different conditions are listed in Table I.

Although methyl formate decarbonylates in 100% sulfuric acid it was possible to observe the J_{CH,CH_3} before decomposition became evident. The methoxy proton resonance of a solution of methyl formate in 100% sulfuric acid consists of a doublet, separation 0.8 cps due to CH_3 of methyl formate, and a single peak 0.133 ppm to higher field due to CH_3 in methyl sulfate. The latter peak increases in intensity with time while the doublet decreases. After about 30 min at 30° an equilibrium solution remains, 90% of the methyl formate having decomposed to methyl sulfate and formyl sulfate. The formyl proton resonance of protonated methyl formate was not clearly resolved but is of the correct size to accommodate a 1,3,3,1 quartet, separation 0.8 cps. On the high-field side of this band is the sharper proton resonance assigned to CH in formyl sulfate; a line with an identical chemical shift to the latter appears in the NMR spectra of solutions of 100% sulfuric acid containing only dissolved carbon monoxide. Similar results have been found for 100% D_2SO_4 solutions of methyl formate.

Newman showed from cryoscopic measurements that methyl *p*-nitrobenzoate was monoprotonated[12] in 100% sulfuric acid. This implies that methyl formate is also monoprotonated in this medium. According to the criteria outlined above, the results establish that methyl formate protonates chiefly on carbonyl oxygen. The same conclusion applies to the binding of boron trifluoride to methyl formate since the complex shows only the normal formyl-methyl proton coupling and no boron proton interactions. In all these species the methyl-formyl proton coupling constants are so similar that it may be assumed that the degree of double-bond character in the C_{CO}—O_{OR} bond is not appreciably altered compared to that of pure methyl formate in contrast to the results found for amides.[7]

TABLE I. J_{CH,CH_3} in methyl formate under different conditions, 29°, 60 Mc.

Medium	Concentration, *M*	J_{CH,CH_3} cps
Pure methyl formate	...	1.25
5*M* HB in glacial acetic acid	0.4	1.00
70% $HClO_4$	0.4	1.15
100% H_2SO_4	0.4	0.80
100% D_2SO_4	0.4	0.90
Pure BF_3-methyl formate	...	1.00
Me_2SO_4	0.2	1.1
CCl_4	0.2	1.2

* Supported in part by the U. S. Public Health Service.

† Present address: Chemistry Department, The Ohio State University, Columbus, Ohio.

[1] R. F. Kurl, Jr., J. Chem. Phys. **30,** 1529 (1959).
[2] G. W. Wheland, *Resonance in Organic Chemistry* (John Wiley & Sons, New York, 1955), p. 99.
[3] K. J. B. Marsden and L. E. Sutton, J. Chem. Soc. **1936,** 1383.
[4] J. Karpovitch, J. Chem. Phys. **22,** 1767 (1954).
[5] D. Tabuchi, J. Chem. Phys. **28,** 1014 (1958).
[6] L. M. Jackman, *Applications of NMR Spectroscopy* (Pergamon Press, New York, 1959), p. 85.
[7] A. Berger, A. Loewenstein, and S. Meiboom, J. Am. Chem. Soc. **81,** 62 (1959); G. Fraenkel and C. Franconi, *ibid.* **82,** 4478 (1960).
[8] M. Karplus and D. M. Anderson, J. Chem. Phys. **30,** 6 (1959); M. Karplus, *ibid.* **30,** 11 (1959).
[9] H. McConnell, J. Chem. Phys. **30,** 126 (1959); G. A. Williams and H. S. Gutowsky, *ibid.* **30,** 717 (1959).
[10] W. D. Phillips, M. C. Muller, and E. L. Muetterties, J. Am. Chem. Soc. **81,** 4498 (1959).
[11] M. Waloff and S. Sugden [J. Chem. Soc. **1932,** 1492] describe the preparation of the methyl formate-BF_3 adduct.
[12] M. S. Newman, H. G. Kuivila, and A. B. Garrett, J. Am. Chem. Soc. **67,** 704 (1945).

Molecular Structure of Diphenylethers

HIROSHI SHIMIZU

Faculty of Pharmaceutical Sciences, the University of Tokyo, Tokyo, Japan

AND

SHIZUO FUJIWARA AND YONEZO MORINO

Department of Chemistry, Faculty of Science, the University of Tokyo, Bunkyo-ku, Tokyo, Japan

(Received October 31, 1960)

THE conformation of diphenylether and its *o,o'*-disubstituted derivatives has not yet been determined. From the measurement of dipole moment, three different structures have been proposed. Smyth and Walls[1] proposed a structure in which the two benzene rings are perpendicular to the plane of the oxygen valence angle, $\theta=\phi=90°$ in Fig. 1, and the rings oscillate at room temperature about this position. Sutton and Hampson[2] proposed a coplanar structure, at the suggestion of Pauling, which is stabilized by the resonance via the lone-pair orbital on the oxygen atom, $\theta=\phi=0°$. According to the suggestion of Morino, Higasi and Uyeo[3] proposed a structure of perpendicular

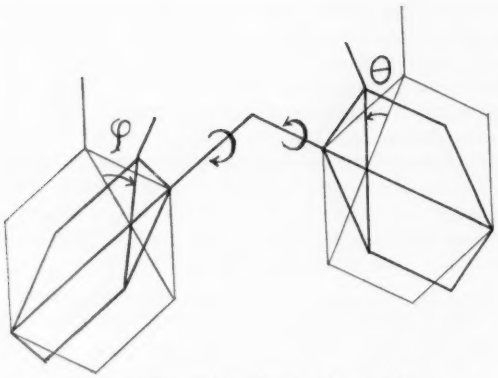

FIG. 1. The conformation of diphenylether.

type in which the two rings are placed at nonequivalent positions, $\theta=0°$ and $\phi=90°$.

The NMR spectrum at 56.4 Mc of the methyl protons of 2,2′-dimethyldiphenylether which is shown in Fig. 2 was observed by us at 25°C. The spectrum is composed of two lines of equal intensity separated by about 1.35 ± 0.07 cps. Since the magnitude of the spin-spin couplings between the methyl protons and the ring protons is negligible, the appearance of the doublet suggests that the two methyl groups are placed at nonequivalent positions in the molecule, being restricted with respect to the rotation about the C—O bonds. This fact is consistent with the conclusion obtained from the infrared spectrum[4] of this compound and from the x-ray analysis[4] of 2,2′-diiododiphenylether. By the nonequivalence of the two rings, the structures of Smyth and Walls (the Symth model) and of Sutton and Hampson (the Pauling model) are to be abandoned.

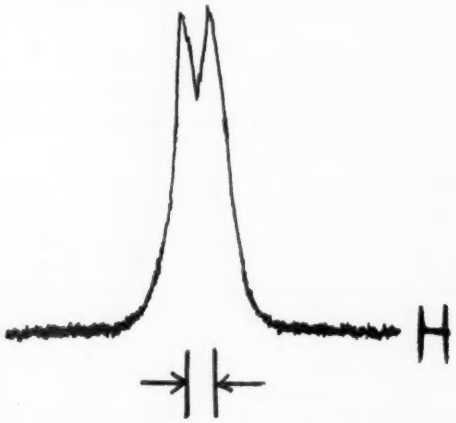

FIG. 2. The NMR spectrum of methyl protons of 2,2′-dimethyldiphenylether.

The NMR spectrum of diphenylether was also observed, in a mixture (1:1 in volume ratio) with carbontetrachloride. The spectrum is composed of a number of lines split by the chemical shifts and spin-spin couplings between the ring protons, the range of the splitting being about 30 cps, about the same magnitude as that of phenol. Assuming the values for the bond lengths and the valence angle, C—C=1.39 A, C—O=1.40 A, C—H=1.08 A, and $\angle COC=120°$, one can estimate the magnitude of the magnetic shielding by the neighboring ring current[5] at each proton of diphenylether. The values of the chemical shift between the most and the least shielded protons are (a) the Smyth model: 15 cps ($-0.25\sim0.0$ ppm), (b) the Pauling model: 60 cps ($-1.10\sim-0.06$), and (c) the Morino model: 85 cps ($-0.17\sim+1.30$). The comparison with the experimental data indicates that the Morino model does not also fit, since the magnitude of the expected shift for that model cited above[6] is far larger than the experimental. More extensive and detailed investigations on this subject are now being carried out by the authors, I. Yamaguchi, and N. Hayakawa; results will be reported in this Journal in the near future.

[1] C. P. Smyth and W. S. Walls, J. Am. Chem. Soc. **54**, 3230 (1932).
[2] L. E. Sutton and G. C. Hampson, Trans. Faraday Soc. **31**, 945 (1935).
[3] K. Higasi and S. Uyeo, Bull. Chem. Soc. Japan **14**, 87 (1939).
[4] H. Shimizu, M. Katayama, and Y. Morino, J. Chem. Phys. (to be published).
[5] C. E. Johnson and F. A. Bovey, J. Chem. Phys. **29**, 1012 (1958).
[6] This value refers to the shift between chemically equivalent protons attached to the 2 and 5 carbon atoms in the same benzene ring.

Ground-State Wave Functions for Linear Molecules

ENRICO CLEMENTI

Laboratory of Molecular Structure and Spectra, Department of Physics, University of Chicago, Chicago, Illinois

(Received January 12, 1961)

A SYSTEMATIC study of the wave functions for linear tri- and tetraatomic molecules is in progress at the University of Chicago. Here we report the LCAO-MO-SCF wave functions for the $^1\Sigma_g^+$ ground states of the molecules C_3, N_3^-, NO_2^+, and HF_2^-. Slater-type AO's (STO's) are used as basis set. The STO orbital exponents used were the best free atom values[1] except for C_3, where best-limited LCAO[2] ζ values for C_2 were adopted.

McLean's program[3] for the Univac Scientific 1103 A was used in the computations. The coefficients of the STO's and the orbital energies are given in Tables I and II for the occupied σ_g and σ_u MO's. Table III

TABLE I. Coefficients and orbital energies for σ_g MO's.[a]

Molecule	$1s+1s$	$2s+2s$	$2p-2p\sigma$	$1s(M)$	$2s(M)$	ϵ (a.u.)
	0.7046	0.0124	0.0028	0.0180	−0.0083	−11.2576
	0.0130	0.0052	0.0019	−0.9958	−0.0306	−11.1845
C_3	−0.1108	0.3256	0.1626	−0.1930	0.5492	−1.0451
	−0.1228	0.6522	−0.3779	0.1018	0.5322	−0.4738
	0.0022	−0.0043	−0.0024	0.9966	0.0182	−15.5324
	0.7047	0.0123	0.0047	−0.0030	−0.0098	−15.1689
N_3^-	−0.1018	0.2871	0.1469	−0.1992	0.5992	−1.1266
	0.1309	−0.6670	0.3232	−0.1026	0.4890	−0.2662
	0.7051	0.0094	0.0028	0.0004	−0.0056	−21.3281
	−0.0001	0.0028	0.0013	−0.9970	−0.0142	−16.5455
NO_2^+	−0.1196	0.4139	0.1577	−0.1654	0.4868	−2.0957
	−0.1288	0.6400	−0.2889	0.1370	−0.6275	−1.2676
	0.7049	0.0095	0.0011	−0.0037		−25.5756
HF_2^-	0.1659	−0.6563	−0.0380	−0.1714		−0.9895
	0.0545	−0.2898	0.4971	0.5163		−0.1792

[a] The coefficients in Tables I–III are for symmetry orbitals. The AO for the middle atom is indicated by (M).

TABLE II. Coefficients and orbital energies for σ_u MO's.[a]

Molecule	$1s-1s$	$2s-2s$	$2p\sigma+2p\sigma$	$2p\sigma(M)$	ϵ (a.u.)
	0.7049	0.0111	0.0036	0.0031	−11.2575
C_3	−0.1436	0.4737	0.1664	−0.4296	−0.8875
	−0.0910	0.5128	−0.4522	0.3785	−0.4316
	0.7048	0.0127	0.4961	0.0065	−15.1690
N_3^-	−0.1394	0.3845	0.1243	−0.5403	−0.8876
	−0.0934	0.5721	−0.4252	0.4527	−0.1790
	0.7051	0.0103	0.0035	0.0060	−21.3283
NO_2^+	0.1441	−0.4896	−0.1351	0.3892	−1.9582
	−0.0934	0.5311	−0.4284	0.5023	−1.1239
	0.7051	0.0085	0.0005		−25.5754
HF_2^-	−0.1786	0.7310	0.0115		−0.9264
	0.0004	−0.0027	0.7124		−0.1169

[a] See footnote a in Table I.

lists the orbital energies and STO coefficients for the occupied π_u and π_g MO's. The z axis is chosen to point in the same direction for all three atoms. The internuclear distances for neighboring atoms were taken as 1.28,[4] 1.12,[5] 1.15,[6] and 1.13 A[7] for C_3, N_3^-, NO_2^+, and HF_2^-, respectively (these molecules have $D_{\infty h}$ symmetry).

TABLE III. Coefficients and orbital energies for π_u and π_g MO's.[a]

Molecule	$2p\pi\pm2p\pi$	$2p\pi(M)$	MO	ϵ (a.u.)
C_3	0.3813	0.6272	π_u	−0.4012
N_3^-	0.3412	0.7035	π_u	−0.3498
	0.7147		π_g	0.0700
NO_2^+	0.4131	0.6515	π_u	−1.1904
	0.7095		π_g	−0.8814
HF_2^-	0.7059		π_u	0.0294
	0.7083		π_g	0.0409

[a] See footnote a in Table I.

The total energy in atomic units is −113.08754, −162.54219, −202.90110, and −198.28264 for C_3, N_3^-, NO_2^+, and HF_2^-, respectively.

We are extending these calculations to C_4, C_2N_2, OCN^-, and SCO. In addition, we are studying ways to improve our wave functions with an extended set. From preliminary results it appears that inclusion of valency and Coulombic polarization[8] (by including $3d\pi$ and $3d\sigma$ STO's in the basis set) is important.

[1] C. C. J. Roothaan, University of Chicago Tech. Rept. LMSS (1955).
[2] B. J. Ransil, Revs. Modern Phys. **32**, 245 (1960).
[3] A. D. McLean, J. Chem. Phys. **32**, 1595 (1960).
[4] See K. S. Pitzer and E. Clementi, J. Am. Chem Soc. **81**, 4477 (1959), for references and ground state assignment.
[5] J. F. Llewellyn and F. E. Whithmore, J. Chem. Soc. **15**, 881 (1947).
[6] E. Grison, K. Eriks, and J. L. de Fries, Acta Cryst. **3**, 290 (1950).
[7] S. W. Peterson and H. A. Levy, J. Chem. Phys. **20**, 704 (1952).
[8] It is my pleasure to thank Professor R. S. Mulliken for several stimulating discussions on this point.

Proton Magnetic Resonance Spectrum of Diketene

DONALD W. MOORE

Michelson Laboratory, U. S. Naval Ordnance Test Station, China Lake, California

(Received January 9, 1961)

DIKETENE has been investigated by nuclear magnetic resonance[1,2] and single crystal x-ray diffraction[3] and is postulated to have the 3-buteno-β-lactone structure (Fig. 1), but high-resolution NMR spectra have not been reported. We have determined chemical shifts and spin-coupling constants for the 40-Mc proton spectrum of vacuum-distilled diketene, and feel that these data further confirm the proposed structure.

The spectrum shown in Fig. 2 was obtained using the pure liquid in a spinning 5-mm sample tube. The chemical shifts are referred to tetramethylsilane as an internal

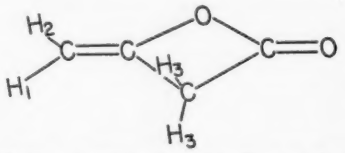

FIG. 1. Diketene molecular structure, H_1 and H_2 are in the plane of the ring.

standard. Assignment of the H_1 and H_2 multiplets was based upon the observed spin-coupling between these protons and the ring CH_2 group. These values agree surprisingly well with the values of 1.9 and 1.3 cps given by Alexander[4] for the corresponding interactions in butene-1. The measured coupling values are: $J_{12}=3.92\pm0.03$ cps, $J_{13}=1.82$, $J_{23}=1.34$.

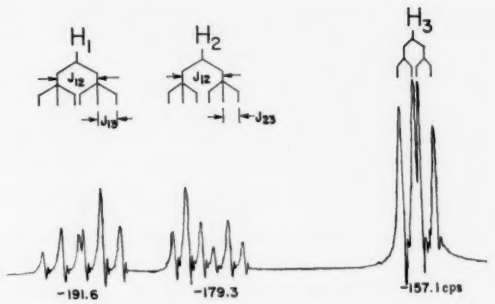

FIG. 2. Forty-Mc NMR spectrum of diketene. Chemical shifts referred to tetramethylsilane.

The small long-range interactions are as expected for alkyl-substituted ethylenic systems, but the geminal H_1–H_2 coupling is comparatively large, usually being 1–2 cps in ordinary compounds. This may be interpreted according to the theoretical predictions of Gutowsky, Karplus, and Grant[5] as arising from a decrease of the H_1—C—H_2 bond angle, which apparently reflects the bond strain of the adjacent ring carbon where the C—C—O angle is only 91°.

The relatively small range of chemical shifts involved is as expected, the weak shielding of the ethylenic protons being almost equaled by the unshielding of the methylene protons in the lactone ring.

[1] P. T. Ford and R. E. Richards, Discussions Faraday Soc. **19**, 230 (1955).
[2] A. R. Bader, H. S. Gutowsky, G. A. Williams, and P. E. Yankwich, J. Am. Chem. Soc. **11**, 2385 (1956).
[3] M. I. Kay and L. Katz, Acta. Cryst. **11**, 897 (1958).
[4] S. Alexander, J. Chem. Phys. **28**, 358 (1958).
[5] H. S. Gutowsky, M. Karplus, and D. M. Grant, J. Chem. Phys. **31**, 1278 (1959).

THE JOURNAL OF CHEMICAL PHYSICS

Bonnal Coordinate Treatments and
Chlorides and Phosphoryl Fluo

NMR Spectra of Propyl Derivatives

Proton Chemical Shifts for the Alkyl Po

Calculation of Complex Equilibrium with

Changes in the Electronic Transitions of
Substituted Cyclic Polyenes

Changes in the Electronic Transitions of
Theory to Substituted Benzenes

Millimeter Wave Absorption and Mo
H. Ray Hilton, Jr.

Influence of the Molecular Environment

Thermoelectric Power of Silver Halides

Wave Functions and Correlation Ene

Anisotropic Hyperfine Interactions in the

Microwave Spectrum, Structure, Dipole

Analysis of the Absorption Spectrum and

Tests for Chemisorption of Nitrogen on

Three-Dimensional H_2-MO Model

Proton Magnetic Resonance Studies of

Approach to Thermodynamic Equilibrium

Theoretical Metastable Transition Pro

The SPO (Split p-Orbital) Method

Relation of Perturbation Theory to

Comparison of Theoretical Calculations

Second-Order Perturbation Theory

Microwave Spectrum of *cis* 1-Chloro

Derivation of the Tait Equation and Its

Configuration and Free Energy of a Poly

Raman Intensities and the Structure of

Decomposition Rate of Nitric Oxide between

Electronic Paramagnetic Relaxation Times

Electron Spin Resonance in a Gamma-Irradiated

Pressure Dependence of the Absolute Catalytic

Measurements of the Diffusion Coefficient of
Silver and Copper Oxide Smokes

Infrared Spectra and Potential Constants of

An Extended Hole Theory of Liquids

Energy Transfer and Quenching Processes in the

Trimethylene Oxide. II. Structure, Thermodynamic
Motion

Pt Bonding in Dioxyl Ion

Molecular Orbital Theory and Hyperfine

Reaction of Nitrogen Atoms with Ozone

Interaction Potentials of Simple Hydrogen